DAGOMYS,
city of SOCHI
June 25 – July 1,
2007

INTERNATIONAL SOCIETY of
CONDENSED MATTER NUCLEAR SCIENCE
RUSSIAN PHYSICAL SOCIETY
NUCLEAR SOCIETY of RUSSIA
COMMITTEE on BALL LIGHTNING PROBLEMS
at RUSSIAN ACADEMY of SCIENCE

on Condensed Matter Nuclear Science

ICCF-13

PROCEEDINGS

INTERNATIONAL SOCIETY on
CONDENSED MATTER NUCLEAR SCIENCE
RUSSIAN PHYSICAL SOCIETY
NUCLEAR SOCIETY of RUSSIA
COMMITTEE on BALL LIGHTNING PROBLEMS
at RUSSIAN ACADEMY of SCIENCES

PROCEEDINGS
of the
13th INTERNATIONAL CONFERENCE
on
CONDENSED MATTER NUCLEAR SCIENCE (ICCF-13)

DAGOMYS, city of SOCHI
June 25 – July 1, 2007

Editor: Yuri Bazhutov

Moscow – 2008

DDC 539.17+811.111

PROCEEDINGS of the 13th INTERNATIONAL CONFERENCE on CONDENSED MATTER NUCLEAR SCIENCE (ICCF-13). DAGOMYS, city of SOCHI, June 25 – July 1, 2007
Moscow, MATI, 11.06.2008 – 4.5 ed. p.

© Erzion Center, 2008

ISBN 978-5-93271-436-2

LOCAL PROGRAM COMMITTEE

Kuz'min R.N. (Editor-in-chief), DSc, Physical and Mathematical Sciences;
Bazhutov Yu.N. (Deputy Editor-in-chief), PhD, Physical and Mathematical Sciences;
Goryachev I.V. (Scientific Secretary), DSc, Technical Sciences;
Baranov D.S. PhD, Physical and Mathematical Sciences;
Bychkov V.L. DSc, Physical and Mathematical Sciences;
Gareev F.A. DSc, Physical and Mathematical Sciences;
Karyaka V.I. PhD, Physical and Mathematical Sciences;
Lipson A.G. PhD, Physical and Mathematical Sciences;

Nikitin F.I. DSc, Physical and Mathematical Sciences;
Rodionov B.U. DSc, Physical and Mathematical Sciences;
Vlasov A.N. DSc, Physical and Mathematical Sciences;
Samsonenko N.V. PhD, Physical and Mathematical Sciences;
Savvatimova I.B. PhD, Technical Sciences.

Editor: Yuri Bazhutov
Technical Editing by Marina Berkova & Vladimir Starostin
Corrector: Alexander Sedov

Format 60x84/8. Offset printing 300 copies.

Publisher Center MATI, Tsiolkovsky Moscow Technical University,
14 Bernikovskaya quay, 109240, Moscow, Russia

PREFACE

Short History of the ICCF Conferences

The International Conferences on "CONDENSED MATTER NUCLEAR SCIENCE» originate from the notorious press-conference in March 1989 at the University of Utah where Martin Fleischmann and Stanley Pons announced about their experiments with electrolyzing heavy water resulted in registration of excess heat yield. Since their interpretation of the phenomenon observed related it to a possibility of running nuclear reactions at normal temperature which contradicted to the system of academic nuclear physics knowledge this discovery agitated the whole worldwide scientific community and actually initiated a new direction in modern physics – Condensed Matter Nuclear Science.

The new direction got supported by a great number of research groups and qualified researchers in more than 30 countries and in some of the countries those research activities immediately got state support as well as participation of small and medium business and sometimes also funding from the part of big business groups.

It can not be said that the optimistic expectations of fast solving energy problems based on the newly discovered physical principles have already been justified. But at the same time it should not be ignored the fact that the process of developing those research efforts with implementation of a wide variety of different methods now has resulted in appearing strong belief in that a new field of scientific activities has opened before modern science with quite reasonable expectation of finding not only new solutions of a number of fundamental problems about origination and interaction of matter and energy in the Universe but also development of a number of breakthrough technologies that would make capable to provide noticeable influence on the global technical civilization. Even nowadays a number of research groups pass from laboratory investigations of the phenomena of low energy nuclear reactions in condensed matter towards developing practically valuable technologies and technical projects. Evident recognition by the business community takes place regarding the commercial perspectives of implementing the results of scientific achievements in this field.

The present Conference is the 13th international forum in this new field of science. According to the opinion of the Organizing Committee the main subjects and goals of the Conference should incorporate consolidation of the results obtained by the scientists of many countries in investigating the physical phenomenon with the achievements in some other fields of science and technology such as nuclear engineering, mechanical engineering, electrical engineering, laser science and engineering, material science, nano-technology, bio-technology, etc. for the sake of fast solving valuable application problems.

The special aspect of the ICCF13 is that according to the tradition of the Russian National annual conferences the scope of the problems to be considered incorporates also the theoretical and experimental research related to the phenomena of nuclear transmutations not only in condensed matter but also in gaseous and plasma media which relates to another important problem of modern science – the nature and likely implementation of Ball Lightning phenomenon.

We believe that the physics of low energy nuclear reactions in condensed matter will take one of the leading roles among the brand new directions of developing science and technology in XXI century. The future shall definitely come! It is just crucial not to fall behind with realization of it reality and importance!

The following topics were discussed in the conference:

- **Analysis and Diagnostic Techniques)AD)**
- **Processes in Gaseous and Plasma Media (GP)**
- **Excess Heat and Related Nuclear Products (HP)**
- **Innovative Engineering and Projects (IP)**
- **Materials and Conditions (MC)**
- **Nuclear Transmutation (NT)**
- **Social, Political and Philosophical Issues (SP)**
- **Theoretical Models and Result Interpretation (TM)**

INTERNATIONAL ADVISORY COMMITTEE (IAC)

Yuri Bazhutov, IZMIRAN RAS, Russia, IAC Chairman, (ICCF-13 chairman);
Jean Paul Biberian, University of Marseilles Luminy, France, (ICCF-11 chairman);
Tullio Bressani, Dept. di Fisica Sperimentale, Universita di Torino, Italy;
Francesco Celani, INFN, Frascati, Italy;
William Collis, ISCMNS Secretary;
Igor Goryachev, Russian Research Center "Kurchatov Institute", Russia;
Antonella De Ninno, ENEA, Frascati, Italy;
Peter Hagelstein, MIT, USA (ICCF-10 chairman);
Yasuhiro Iwamura, Mitsubishi Heavy Industries, Japan;
Jirohta Kasagi, Laboratory for Nuclear Science, Tohoku University, Japan;
Xing Zhong Li, Tsinghua University, China (ICCF-9 chairman);
Andrei Lipson, Institute of Physical Chemistry, RAS, Moscow, Russia;
Michael McKubre, SRI International, USA (ICCF-3 chairman);
George Miley, Fusion Studies Laboratory, University of Illinois, USA;
Ken-ichiro Ota, Dept of Energy and Safety Engineering, Yokohama, Nation. Univ., Japan;
Nikolai Samsonenko, People Friendship University, Russia;
Francesco Scaramuzzi, ENEA, Frascati (retired), Italy, (ICCF-8 chairman);
Mahadeva Srinivasan, BARC (retired), India;
Edmund Storms, Lattice Energy, LLC, USA;
Akito Takahashi, Osaka University, Japan, (ISCMNS President, ICCF-12 chairman).

LOCAL ORGANIZING COMMITTEE

Bazhutov Yu.N. (Chairman), Institute of Terrestrial Magnetism, Ionosphere and Radiowave Propagation, Russian Academy of Sciences (IZMIRAN), Erzion Center;
Samsonenko N.V. (Deputy Chairman), Department of Theoretical Physics, Russian Peoples Friendship University, Moscow;
Mozzhegorov A.A. (Deputy Chairman), Representative of Local Business Community;
Goryachev I.V. (Scientific secretary), Russian Research Center "Kurchatov Institute";
Savvatimova I.B. (Executive secretary), Scientific and Industrial association "LUCH";
Berkova M.D. (Web Site Editor), Institute of Applied Mechanics, RAS;
Stakhanova I.G. (Web Site Co-editor), IZMIRAN, Russian Academy of Sciences;
Starostin V.A. (Web Site Co-editor), Russian Research Center "Kurchatov Institute";

Committee members:

Baranov D.S., Institute for High Temperatures, Russian Academy of Sciences;
Bychkov V.L., Department of Physics, Lomonosov Moscow State University,
Famina N.V. Moscow Technical University (MADI);
Kornilova A.A. Department of Physics, Lomonosov Moscow State University,
Nikitin A.I., Institute of Energetic Problems of Chemical Physics, RAS;
Sarkisov V.I. Firm "Svitaks".

Sponsors of the ICCF-13

Andrew Mozzhegorov, private Russian Sponsor;
International Society of Condensed Matter Nuclear Science;
Steve Krivit, private American Sponsor, Senior Editor of "New Energy Times" Internet magazine;
"Dagomys" Health Improvement Complex at Russian President Department

Resolution of the 13th International Conference on Condensed Matter Nuclear Science (ICCF-13)

The 13th International Conference on Condensed Matter Nuclear Science (ICCF-13) was held in the city of Sochi ("Dagomys" Health Improvement Complex at Russian President Department, Dagomys settlement) during June 25 through July 1, 2007.

The Conference was arranged by the ICCF-13 Local Organizing Committee in accordance with presentation of Russian Coordinating Committee on the Problems of Cold Nuclear Transmutation & decision of the International Advisory Committee (IAC). It was held under the auspices of International Society of Condensed Matter Nuclear Science, Russian Physical Society, Nuclear Society of Russia and Committee on the Problems of Ball Lightning at Russian Academy of Sciences.

Conference organization, edition of the "Program and Abstracts" & Proceedings of the ICCF-13 and also partial financial support of several ICCF-13 participants were provided by sponsorships of private Russian Sponsor Andrew Mozzhegorov, International Society Condensed Matter Nuclear Science & private American Sponsor Steve Krivit, "New Energy Times" Internet magazine Senior Editor.

Totally 80 scientists and specialists took part in the Conference including 46 persons from Russian Federation and 34 foreign representatives from United State of America (12), Japan (5), Israel (5), France (4), Great Britain (2), Italy (3), India (1), Ukraine (1) and Kazakhstan (1).

Russia was presented from different regions: Moscow – 23 representatives, Moscow region (Dubna – 2, Podolsk – 3, Troitsk -1), Ryazan – 1, Krasnodar region (Sochi – 2, Armavir – 2), Leningrad region, Gatchina – 2, Novosibirsk – 1, Tomsk – 3, Ufa – 1, Nizhniy Novgorod region, Sarov – 2, Rostov region, Volgodonsk – 3.

At the ICCF-13 opening participants were welcomed by President of Russian Physical Society Vitaliy Mikhailin, Russian ICCF-13 Sponsor Andrey Mozzhegorov, Deputy General Director of "Dagomys" Health Improvement Complex at Russian President Department Valeriy Shkuratov, President of the International Society Condensed Matter Nuclear Science Akito Takahashi and International Advisory Committee member Mahadeva Srinivasan.

Vladimir Bychkov, on behalf of Vitaliy Mikhailin, the President of the Russian Physical Society, granted with certificates of honorable members of Russian Physical Society the following foreign CMNS scientists (D.Nagel, F.Celani, J.Kasagi, M.Srinivasan, A.Takahashi, J.Fisher, M.McKubre, J.Dash, S.Chubb and P.Hagelstein).

Executive Secretary of the International Society Condensed Matter Nuclear Science William Collis awarded 2 Russian Scientists, Alexander Karabut & Andrey Lipson, by Giuliano Preparata Medal.

75 reports were presented and considered at the Conference, including 45 oral reports & 30 poster reports. Most of them (47) based upon the results of experimental investigations, 25 reports were theoretical works included in the "Theoretical Models & Results Interpretation

session (TM)" and 3 Reviews was in the field of "Social, Political & Philosophical Issues (SP)". 7 of those presentations were dedicated to the problems of "Analysis & Diagnostic Techniques (AD)", 12 – to "Processes in Gaseous & Plasma Media (GP)", 13 – to "Excess Heat & Related Nuclear Products (HP)", 7 – to "Innovative Engineering & Projects (IP)", 3 – to "Materials & Conditions (MC)" and 5 presentations were dedicated to the problems of "Nuclear Transmutation (NT)". Though sometimes such division turned out to be definitely conditional since the subject of those reports related to both problems simultaneously.

Among all those experimental reports dedicated to Cold Nuclear Transmutation there were evidenced regular registration of Excess Heat, Nuclear Products (neutron fluxes, generation of Tritium, X-radiation and gamma-radiation), transmutation of nuclei, various structural changes in solid and liquid substances & etc.

In the experimental reports presented on the problems of Cold Nuclear Transmutation implementation of different methods of initiating the processes of Cold Fusion was shown which is typical for Russian & foreign investigations. There were implemented as usual electrolysis, so electrolysis with gas discharge (both on cathode and on the anode), glow discharge, hydrodynamic & ultrasonic cavitations, electrical blast of metal wires and others.

In the 25 theoretical reports relating to Cold Nuclear Fusion a wide variety of original simulation author models was presented. Within the frames of some of those models new structures of substances & elementary particles were proposed based on strong theoretical understanding.

The reviews presented relating to the problems of Cold Nuclear Transmutation turned out to be very interesting and informative as well as the presentation about the mission and role of the international Society of Scientists on the problems of Cold Nuclear Transmutation (ISCMNS) in innovation input of Science & Business Community that arise their common activities & success.

In the conclusion of the Conference all ICCF-13 participants unanimously expressed their opinion about the reasonability to continue investigations of the problems of Cold Nuclear Transmutation, publishing of ICCF-13 Proceeding this year and supported the proposal of the International Advisory Committee to hold next 14th International Conference on the Problems of Cold Transmutation of Nuclei of Chemical Elements (ICCF-14) in next 2008.

Editor: Dr. Yuri N. Bazhutov,
Chairman ICCF-13,
Dagomys, Sochi, Russia,
June 2008.

ICCF-13 Review

Steven Krivit,
"New Energy Times" Internet magazine Senior Editor.

This report reviews a few of the highlights from the 13th International Conference on Condensed Matter Nuclear Science, held in June at Dagomys, Sochi, Russia. It is by no means a complete and full report of the excellent work performed by this research community.

Many of the Russian scientists share a strong cross-disciplinary interest in the subject of ball lightning, as well as low energy nuclear reactions. As a result, both subjects were included in the formal program. However, ball lightning does not fall within the subject matter covered by *New Energy Times*.

Yuri Bazhutov (Russian Academy of Sciences), Igor Goryachev (Kurchatov Institute), Nikolay Samsonenko (People's Friendship University), Irina Savvatimova (Federal State Unitary Enterprise) and others put an amazing amount of energy into the conference and pulled off a very effective meeting.

Bazhutov opened the conference with a formal welcome, and Goryachev provided an inspiring vision for the conference.

"Our Russian television has been stating that the city of Sochi is a possible site for the 2014 Winter Olympics," he said, "and that Sochi is the gateway to the future. I am sure that our ICCF-13 conference here at Dagomys, Sochi will be the gateway to the future."

The audience was honored to receive welcome addresses by several individuals, including Vladimir Bychkov, on behalf of Vitaliy Mikhailin, the president of the Russian Physical Society, as well as a private individual, Andrey Mozzhegorov, who helped sponsor the conference.

Mozzhegorov was initially inspired to contribute to the conference as a result of a question one of his daughters asked him. She knew that he was an advocate for science and technology, but she was aware that such progress has contributed to many ecologically unfavorable situations around the world. She asked him what he could do to apply science and technology to help make the world better.

Sometime after that, Mozzhegorov heard about the CMNS research community and began to look into the area. Mozzhegorov is not a scientist; he is an attorney and formerly a fighter pilot for the Russian military.

He was impressed with the CMNS researchers; he noted that they often explored beyond the limits of the ordinary and practiced out-of-the-box thinking. He found this inspiring. Likewise, the CMNS found his and his wife Olga's participation inspirational.

ICCF-13 Audience: Left to right: Pierre Clauzon, Yuri Bazhutov, Irina Savvatimova, Fangil Gareev. Photo: S. Krivit

This link will provide access to the program, abstracts and other conference information. Very few papers were distributed at the meeting. *New Energy Times* has obtained a few of them and will provide links within this report.

The proceedings may take a year or two to publish; therefore, readers who would like further details are encouraged to check online at Edmund Storms and Jed Rothwell's www.LENR.org library for uploaded papers/presentations, or contact the authors directly.

At times, barriers existed to obtaining papers or more complete details on the presentations. Sometimes, these barriers were the result of language difficulties; sometimes, these apparently were the result of proprietary commercial interests that led the researchers to keep important details under wraps.

A significant, paradoxical trend continues; as more commercial funding is coming into the field, researchers are engaging in less open exchange, outside of those researchers who share information within their collective business partnerships.

Many of the researchers use the term "cold fusion" in their presentations despite the fact that the underlying mechanism(s) is (are) still in dispute. The wisdom of such decisions, or old habits, seems uncertain because the speculative historical term has a tendency to confuse observers of the field who otherwise might regard the rigorous experimental findings with greater respect.

Despite the fact that no breakthrough announcements were delivered at the Sochi conference, the fact that excess heat and anomalous nuclear products continue to be reported, year after year, are a testament to the truth and likely significance of these novel effects of nature.

Preparata Medal Award Winners

Andrei Lipson receives Preparata Award from Francesco Celani. Photo: S. Krivit

Alexander Karabut receives Preparata Award from William Collis. Photo:S. Krivit

The condensed matter nuclear science community has awarded prizes to its members for outstanding achievements dating to 1993, when the "Truffle Prizes" were first awarded by the Italian automotive group Fiat.

Those prizes eventually were replaced by the Preparata Medal, in honor of Italian physicist Giuliano Preparata. The production of the current set of medals was sponsored by the Fondazione Cassa di Risparmio di Asti, part of a local banking institution whose mission is to further scientific search, education, the arts, and culture.

This year's prizes were awarded to Russian scientists Andrei Lipson of the Russian Academy of Sciences and Alexander Karabut with Federal State Unitary Enterprise "Luch."

John Dash, Wu Shou Zhang and Hideo Kozima Report Excess Heat

John Dash, professor emeritus of physics, with the Low Energy Nuclear Laboratory at Portland State University, and Wu Shou Zhang, with the Institute of Chemistry at the Chinese Academy of Sciences, described by Dash as a calorimetrist, theoretical physicist, and excellent experimentalist, reported a confirmation of a LENR phenomena that has been observed for many years; as the temperature of the electrolyte is permitted to go (or brought) to higher temperatures, the excess heat effect is amplified.

This effect also is referred to as positive feedback: the more heat that exists within the cell, the more likely excess heat is to occur.

Zhang and Dash report that "best results are obtained when the electrolyte temperature is close to the boiling point."

Italian researcher Giuliano Mengoli explicitly noted this effect in his paper "Calorimetry Close to the Boiling Temperature of the D2O/Pd Electrolytic System."

Zhang and Dash used isoperibolic calorimetry and Seebeck envelope calorimetry concurrently, and the results of each method agreed with the other.

They reported that they "were able to obtain excess heat output from 12 consecutive samples" in the multimilliwatt range with a confidence level of five sigma. They also reported the anomalous "presence of silver on the palladium surface after electrolysis in heavy water."

During the mid-1990s, mass flow calorimetry was a favored choice of LENR researchers as a reaction to critics' reluctance to accept results from isoperibolic calorimetry, which is highly complex and relatively inaccessible to nonspecialists.

Mass flow is far simpler, and critics claimed they would not accept excess heat claims from mass flow calorimetry. After such results were obtained, critics subsequently came up with additional objections to avoid the uncomfortable hypothesis of excess heat.

But mass flow calorimetry had and has a significant disadvantage. The circulating flow has a tendency to keep the experiment cool and unfortunately inhibit optimal results.

As a consequence of this limitation, resuming the use of isoperibolic calorimetry may now be more useful for researchers. When combined with a secondary envelope-type calorimetry system, the results become notably rigorous.

Dash et al. state in one of their papers, "Since the discovery of excess heat in 1989, the reproducibility has been a difficult problem. Our results suggest a reason why Fleischmann and Pons and other groups observed excess heat using Dewar-type electrolytic cells and isoperibolic calorimetry, but some groups using mass-flow calorimetry had difficulty detecting excess heat, or the reproducibility was very poor.

"The reason is that the latter method involves a low temperature, semi-isothermal measurement. The temperature difference between the electrolytic cell and the water flowing during electrolysis is very small. Therefore, this system has to be stimulated by various methods, e.g., high input power, laser irradiation etc. Even then, the reproducibility is still low because the cell temperature is not high enough."

Dash et al. reported periodic excess heat bursts in the 0.5 Watt range and bursts of up to 2 watts, as Dash reported to *New Energy Times* during a follow-up interview.

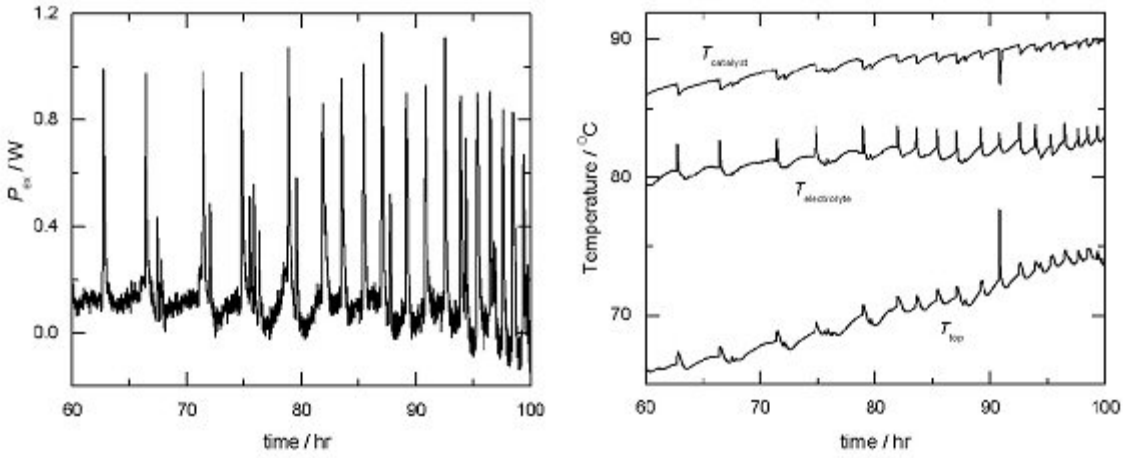

Heat bursts and corresponding temperatures during electrolysis

New Energy Times spoke with Dash about another anomalous observation from his team. Dash uses thin cold-rolled palladium foils for his cathodes, and these cause interesting effects. Soon after the electrolysis begins, within minutes, the cathode develops an unusual bend visible to the naked eye.

"That by itself turned me on to this in 1989," Dash said. "How can this happen? It's opposite of what you'd expect because the side facing the anode has a higher current density and if you form the hydride, it involves an expansion. But this result says that it involves a contraction on that side. So there's a big mystery."

Dash interpreted the bursts as mini-explosions, similar to that reported by researchers in China (Zhang and co-workers), Japan (Mizuno), and France (Biberian).

"It busted their cells," Dash said. "I think in all the cases, they were open cells so there would not have been a pressure buildup. In our experiments, it appears we are getting explosions, but they are controllable explosions. When you drive your car, that's what you're getting, controllable explosions, and that's what we need here." Dash also explained that they place their Seebeck envelope calorimeter within another box to isolate it thermally from the room environment. They found this was necessary to obtain optimal results. However, he states, researchers who have controlled room temperature environments wouldn't need the secondary enclosure.

They also reported experiments using mass and gamma ray spectroscopy indicating anomalous isotopic abundances and unexpected elements. "The changes in isotopic abundance and the occurrence of unexpected elements can be explained," Dash wrote, "if thermal neutrons are produced during electrolysis and during glow discharge."

Excess Heat Reported by Clauzon

Pierre Clauzon, a former nuclear engineer who designed the cores for fast breeder reactors, reported 30 percent excess heat in a series of plasma electrolysis experiments that he claims was 100 percent repeatable in his lab. Measurements were made using a steam calorimeter at the Laboratoire de Sciences Nucléaires in Paris.

Clauzon exemplified the persistence of many of the CMNS researchers, saying of himself, a Frenchman, "the frog will never give up."

Excess Heat Reported by Celani

Francesco Celani, a physicist with the Italian National Institute of Nuclear Physics, reported results of an Arata-style double-wall structure experiment using palladium nano-powders, though the specific details of his claims were difficult to follow.

Karabut Reports Excess Heat Interpretation

Alexander Karabut, with Federal State Unitary Enterprise "Luch," presented data showing an experiment which yielded 300 watts output as a result of an unusually high energy source. *New Energy Times* was unable to obtain copies of his presentation; however, we spoke with him afterward to learn more details.

We learned that Karabut's presentation was his own theoretical treatment of data from an experiment performed around 1994 by another group of Russian researchers.

Karabut explained to *New Energy Times* that the spectacular results that he reported at ICCF-13 were not based on his own data but were those of the other group. He says that their results confirm his ideas. Unfortunately, Karabut said, all but one of the six or seven members of that group are dead. Karabut hopes to repeat their experiment himself in the near future.

Toyota Replication of Mitsubishi Transmutation

After many years of absence from the field, Toyota has re-emerged on the CMNS scene through the work of Tatsumi Hioki, Naoko Takahashi and Tomoyoshi Motohiro at Toyota Central Research and Development Laboratories Inc. in Nagakute, Aichi, Japan.

The researchers have attempted to replicate the Yasuhiro Iwamura deuterium gas permeation experiment performed at Mitsubishi Heavy Industries. The Toyota team reported an experiment that showed mildly positive evidence of the low energy nuclear transmutation of cesium into praseodymium.

Nagel Reports on LENR Reaction Rates

David Nagel, a research professor at George Washington University, presented a paper on reaction rates for low energy nuclear reactions at surfaces. In this paper, he reviewed the effects on surface phenomena as observed with regard to the Letts-Cravens laser effect, the Arata/Zhang palladium-black material, and the Iwamura transmutation experiments. He also made note of an experiment performed by Edmund Storms in which he reversed the polarity of the electrodes and observed anomalous behavior including excess heat.

Nagel referred to the fourth paper (in pre-print) by Allan Widom and Lewis Larsen that gives estimates and an expression for reaction rates of10E12 to 10E14 reactions/second/cm2.

Nagel's review also displayed a perspective of the various material geometries and the range of their effects when going from millimeter to micrometer to nanometer scales.

He made his best attempt to quantify the characteristics of power generation but admitted that a complete, comprehensive analysis was out of reach because of too many unknown parameters.

He pleaded to the experimentalists, "Measure or estimate your total surface area," and to the theoreticians, "Provide values for the reaction rates per area."

China Institute of Atomic Energy Contributes Paper

Songsheng Jiang of the China Institute of Atomic Energy contributed a paper, along the lines of work by Steven E. Jones (formerly of Brigham Young University), reporting evidence for naturally occurring fusion in the earth.

Lipson on H/D Loading

Andrei Lipson (Russian Academy of Sciences) et al. presented new research on the use of single-wall carbon nanotubes to enhance the diffusion of deuterium/hydrogen into palladium. He also reported a rigorous method of particle detection using CR-39 detectors which indicated 3.0 MeV (DD) protons and high energy alphas in a repeatable experiment.

Lipson et al. also took a comprehensive look at nuclear signatures in CMNS experiments and reported findings and particle energies from glow discharge experiments recorded with the use of CR-39 detectors and metal filters.

Exploding Wire Experiments

Two Russian groups, one from the Ryazan State Radio Engineering University and another from the Russian Federal Nuclear Center, reported results from exploding wire experiments; however, the significance and conclusions are difficult to understand. A.N. Vlasov, from Ryazan, reported that the wire was vaporized in the course of the explosion.

Bazhutov Reports Neutrons, Tritium

Yuri Bazhutov presented several papers, but one particular experiment that he reported stood out. He reported that "large neutron yield reached a value of 10E6 neutrons per second with correlated tritium yield value ~ 10E11 in heavy water & much less in light water" in his paper "Neutrons, Gamma-Rays & Tritium Diagnostic at Electrolysis with Anode Gas Discharge in Water Solution."

Alexander Koldamasov's Hydraulic-Electrostatic Device

Two years ago, *New Energy Times* first reported the work of Alexander Koldamasov, brought to Edmonton, Canada, by Hyunik Yang. Yang partnered with Patrick Cochrane and his Innovative Energy Solutions Inc. business partners in an attempt to develop the Koldamasov method into a commercial product. They didn't do so well. They took a few million dollars from small private investors, produced nothing and ended up in bankruptcy.

A default judgment was issued on Aug. 29 in Clark County, Nev., district court against Ronald Foster, Patrick Cochrane and Frederick Dornan with compensatory damages of $15 million and punitive damages of $45 million.

Real science and potentially viable technology may be behind Innovative Energy Solutions Inc.'s failed attempt, but the lesson to learn here, as always, is caveat emptor, and watch out for the snake oil.

Yang has continued with his attempts to develop the method into a commercial product with a few deep-pocket private investors, and he has kept very quiet since his unfortunate experience in Edmonton. Yang has not appeared at any CMNS conference since the 2005 conference in Yokohama, Japan.

New Energy Times was able to speak with Koldamasov during the Sochi meeting and learn a great deal about the background of this work.

List of ICCF-13 participants in collective photo (from left to right)

1. **Gennady Schelkunov,**
2. **Aleksey Roussetski,**
3. **Nikolai Bakumtsev,**
4. **Gennady Shabanov,**
5. **Akito Takahashi,**
6. **Alexander Koldomasov,**
7. **Vladimir Vysotskii,**
8. **Anatoly Shestopalov,**
9. **Nikolai Samsonenko,**
10. **Irina Savvatimova,**
11. **Fangil Gareev,**
12. **Natalie Famina,**
13. **Boris Sokolovsky,**
14. **Alexander Vlasov,**
15. **Yuri Bazhutov,**
16. **Victor Sharkov,**
17. **Tatiana Bakumtseva,**
18. **Dmitry Sinyapkin,**
19. **Andrei Mozzhegorov,**
20. **Olga Mozzhegorov,**
21. **Boris Rodionov,**
22. **Francesco Celani,**
23. **Gennady Tarasenko,**
24. **Michael McKubre,**
25. **Scott Chubb,**
26. **Mahadeva Srinivasan,**
27. **Ivan Chernov,**
28. **Jirota Kasagi,**
29. **Andrei Lipson,**
30. **Igor Goryachev**
31. **Pierre Clauzon,**
32. **Tomoyoshi Motohiro,**
33. **Vladimir Starostin,**
34. **Michael Melich,**
35. **Marina Belyaeva,**
36. **William Collis,**
37. **Tatsumi Hioki,**
38. **John Dash,**
39. **Nicolas Armanet,**
40. **Alla Kornilova,**
41. **Vasili Velikodny,**
42. **Patric Wettin,**
43. **Dmitri Afonichev,**
44. **Yuri Laptev,**
45. **Mikio Fukuhara,**
46. **David Nagel,**
47. **Peter Mobberley,**
48. **Susan Mobberley,**
49. **Elena Sergeeva,**
50. **Yuri Sinyapkin,**
51. **Dmitri Baranov,**
52. **Vladimir Bychkov.**

CONTENTS

Page

PREFACE ….…….. 3

Short History of the ICCF Conferences ……..…… 3

International Advisory Committee …….. 4

Local Organizing Committee & Sponsors …… 5

Resolution of the Conference ……. 6

ICCF-13 Review by Steven Krivit ……. 8

Collective photo ……... 16

CONTENTS ……. 17

ANALYSIS AND DIAGNOSTIC TECHNIQUES (AD) ……. 25

New Results On Cosmic Ray Erzions Search Received on the Scintillation Spectrometric Telescope "Doch-4m" during (2001-2006)
Yu.N. Bazhutov, Yu.V. Kozlov, V.P. Martemyanov,E.V. Pletnikov, A.A. Sabelnikov, V.A. Starostin, V.G. Tarasenkov, E.V. Turbin, V.N. Vyrodov …… 26

A Steam Calorimeter for the Study of he Abnormal Excess Heat Observed During Mizuno-Type Experiments
P. Clauzon- J.F. Fauvarque, G. Lallevé- G. Le Buzit ……. 41

Setup for Measuring of Energy Balance at Interaction of Metals and Hydrogen Isotopes Gas at High Temperatures and Pressures
V.A. Kirkinskii , A.I. Khmelnikov …… 43

Tritium Released from Interior's Earth: Evidence for Natural Nuclear Fusion
Songsheng Jiang ……. 47

Plasma-Electrochemical Transformation of Electric Energy in Heat by Water Electrolyte
Velikodny V.Yu.. Gavrilov S.V., Grishin V.G., Popov Yu.A. ……... 48

Pulse Electric Breakdown of The Distilled Water at Micron Interelectrode Distances
I.V.Goryachev , V.I.Karyaka , M.M.Martynyuk , N.V.Samsonenko …… 53

Excitation of Hydrogen Subsystem in Metals by External Influence
I. P. Chernov,yu. M. Koroteev, V. M. Silkin, Yu. I. Tyurin …… 63

PROCESSES IN GASEOUS AND PLASMA MEDIA (GP) …….. 72

Characteristics of X-Ray Emission from Solid-State Cathode Medium in Electric Discharge Systems
A. B. Karabut …….. 73

Classical Cold Synthesis. Whether It Exists?
A.G. Krivshich, G.D. Shabanov, B.Yu. Sokolovsky, O.M. Zherebtsov …… 74

The Nature of Ball Lightning
G.D. Shabanov, A.G. Krivshich, B.Yu. Sokolovsky, O.M. Zherebtsov …… 75

Ball Lightning Observation Properties (Modern Analysis)
V. L. Bychkov, D.V. Bychkov ……... 76

Unipolarly Ball Lightning Theory
V. L. Bychkov, D.V. Bychkov ……... 86

Modern Realization of Laboratory Ball Lightnings (Modern Analysis)
V. L. Bychkov, D.V. Bychkov ……... 94

The Possibilities for the Formation of the Ordered Plasma Structures in Nature.
A. I. Nikitin, A. M. Velichko, T. F. Nikitina ……. 115

Researches of Interaction of Long –Living Plasma Formations with Supersonic Stream and Barrier
V.A.Bityurin, V.Yu.Velikodny, I.A.Samuolis, E.B.Kolesnikov, V.V.Popov …….. 127

Classical Approaches to Anomalous and Geophysical Phenomena: Methodological Aspects and Physical Matter of Transmutation Phenomenon
V.L. Bychkov, B.S. Grevtsov, V.A. Krivitsky, V.V. Nizovtsev …….. 139

Experimental Researches of Electrical Explosion of the Wire Spiral Turned in the Torus and Dipped in Water
A.N.Vlasov, B.I.Kolotilin, S.A.Kolesnikov, A.B.Manoshkin, V.V.Panin ……. 147

On Issue of Spatial Distribution of Electrical Explosion Products of Single Wire
Yu.T.Sinyapkin, D.Yu.Sinyapkin …….. 153

Globe Lightning: Modeling and Application
G.P. Schelkunov, I.M. Olikhov …… 154

EXCESS HEAT AND RELATED NUCLEAR PRODUCTS (HP) …… 155

Neutrons, γ–Rays & Tritium Diagnostic at Electrolysis with Anode Gas Discharge in Water Solutions
Yu.N.Bazhutov, V.Yu.Velikodny, V.G.Grishin, [A.V.Eremeev], V.V.Popov, A.D.Rumyantsev, Yu.A.Sapozhnikov, N.I. Khokhlov, A.P.Koshelev, V.A.Starostin …… 156

Excess Heat During Diffusion of Deuterium through Palladium
Jean-Paul Biberian and Nicolas Armanet …….. 170

High Temperature Deuterium Absorption in Palladium Nano-Particles.
Francesco Celani, A. Spallone, E. Righi, G. Trenta, V. Andreassi, A. Marmigi, P. Quercia, G. Cappuccio, D. Hampai, P. Marini, V. Di Stefano, M. Nakamura, F. Todarello, E. Purchi, A. Mancini, U. Mastromatteo, F. Falcioni, M. Marchesini, P. Di Biagio, P.G. Sona, F. Fontana, L. Gamberale, D. Garbelli ……... 181

Excess Heat Reproducibility and Evidence of Anomalous Elements after Electrolysis in Pd|D_2O+H_2SO_4 Electrolytic Cells
W.-S. Zhang and J. Dash ……. 202

Heat Measurements and Surface Studies of Pd Wires after Being Exposed to A H2 Gas-Loading System Irradiated with a Yag Frequency Doubling Laser
J.Tian, L H Jin, B J Shen, Q S Wang, J Dash …….. 217

Excess Heat Power Registration in High Voltage Electrolysis and Discharge Systems
A. B. Karabut ……. 225

Development of Multi-Purpose Installations for Energy Generation by Way of Cold Nuclear Synthesis
A.I.Koldamasov, N.J.Bakumtsev ……. 237

Evidence for Condensed Matter Enhanced Nuclear Reactions in Metals with a High Hydrogen Solubility
Andrei G. Lipson, Alexei Roussetski, George H. Miley …….. 248

Replication of Energetics Heat and Tritium Production
M. McKubre, F. Tanzella, V. Violante, C. Sibilia, T. Zilov, I. Dardik …… 269

The Fleischmann-Pons Effect
M. C. H. McKubre …….. 270

Bursts of Count Rate of Beta-Radioactive Sources during Long-Term Measurements
A.G. Parkhomov …….. 279

The Analyses of Test Data of Cavitation Heat-Generator of «TMK-25» Type
A.V. Pinaev ……..... 291

Decay in Tungsten Irradiated by Low Energy Deuterium Ions
Irina Savvatimova, Gennady Savvatimov, Alla Kornilova ……. 295

Calorimetry in PT/K_2CO_3/PD Light Water Electrolysis System
J.Tian, L H Jin, B J Shen, C Y Wang, J W Guo 309

Excess Heat While Saturation of Titanium by Deuterium and Air Mixture.
S.A. Tsvetkov …… 311

Calorimetric Results of ENEA Cooperative Experiments
V. Violante, F. Sarto, E.Castagna, C. Sibilia, M.Bertolotti, R. Li Voti, G.Leahu, M. McKubre, F. Tanzella, K.Grabowski, G.Hubler, D. Knies, T. Zilov, and I. Dardik …… 312

Large Change in Isotopic Ratio of Li with Anomalous ^{6}LIH Formation by Light Water Electrolysis
H. Yamada and S. Nagao …… 324

Report on Electrolysis Experiments at Energetics Technologies
I. Dardik, T. Zilov, H. Branover, A. El-Boher, E. Greenspan, B. Khachaturov, V. Krakov, S. Lesin, A.Shapiro and M. Tsirlin …… 325

Precision Measurement of Excess Energy in Electrolytic System Pd/D/H_2SO_4 and Inverse-Power Distribution of Energy Pulses VS. Excess Energy
H. Kozima[1,2], W.-S. Zhang[2,3], and J. Dash…… 348

INNOVATIVE ENGINEERING AND PROJECTS (IP) …… 359

A Flow Calorimeter for Glow Discharge Experiments
R. F. Cantwell, S.S. Booth, M.L. Mcconnell …… 360

Purposeful Synthesis of Chemical Elements and Ecologically Pure Mobile Sources of Energy
V.A. Krivitsky, F.A. Gareev ……. 361

Inspection Method to Check Quality of Nuclear Transmutation Media
B.U.Rodionov, M.S.Godin, I.B. Savvatimova …….. 372

Cold Fusion Heaters
Talbot A. Chubb ……... 390

Chemical Transformations on a Basis of Electrical Discharge
Tarasenko G.V. …… 398

Cyclonic – Cavitational Generator
M.D. Berkova, V.Y. Velikodny, V.G. Grishin, V.V. Popov, A.A Bykov …… 399

Plasma Technologies in Ecological Problems
M.D.Berkova, A.A.Bykov, V.Yu.Velikodny, V.P.Vorotilin, V.G.Grishin, Yu.V.Dobrynetc, O.V.Krychenko, L.K Nikitenko, V.V Popov, E.N Rychagov, B.N.Tolkunov …… 409

Advanced Projects of Energy Generating Units
I.V.Goryachev, I.N.Goryacheva …….. 420

MATERIALS AND CONDITIONS (MC) …… 438

Surface Plasmons Excitation on Metal and Metal Hydride Surfaces
E.Castagna, V. Violante, C.Sibilia, F. Sarto ……... 439

Interplay Between Deuteron and Host Atoms in Metal Deduced from Low-Energy Beam Experiments
H. Yonemura, Y. Ishikawa and J. Kasagi 440

Novel Highly D-Loaded/High D-Diffusivity Nanostructured Materials on the Pd Substrate As a Potential Media to Enhance Low Energy Nuclear Reactions
A.G. Lipson, A.S Roussetski, B.F. Lyakhov, E.I. Saunin, D.M. Sakov, A.Yu.Tsivadze …….. 446

Luminescence of Micro-Bubbles from Liquids
Kuzmin R., Serov P. …… 460

NUCLEAR TRANSMUTATION (NT) ……..… 461

Surface Studies after Loading Metals with Hydrogen and/or Deuterium
J. Dash and D.S. Silver …… 462

Transmutation Reactions Induced by D_2 Gas Permeation through Pd Complexes (Pd/CaO/Pd)
Y. Iwamura, T. Itoh, N.Yamazak, S.Kuribayashi, Y.Terada, T.Ishikawa, A.Kishida, K.Fukutani,D.Sekiba, M.Wilde, S.Ogura, H.Yamashita, M.Matsumoto, T.Okano, H.Matsuzaki, H.Yonemura, J.Kasagi, T.Nebiki, T.Narusawa ……. 476

Investigation of Memory Phenomena in Water and Study of Isotopes Transmutation in Growing Biological Systems Containing Activated Water
Vladimir I.Vysotskii, Alla A.Kornilova, Alexandr B.Tashyrev …… 477

Resonant Tunneling in Glow Discharge Experiments
David Y. Chung and James Lindesay* …… 498

Creation of More Light Elements in Tungsten Irradiated by Low-Energy Deuterium Ions
Irina Savvatimova …… 505

XPS Study on Surface Layer Elements of Pd/CaO Multilayer Complex with and without Deuterium Permeation
Tatsumi Hioki, Naoko Takahashi, Tomoyoshi Motohiro …… 518

SOCIAL, POLITICAL,AND PHILOSOPHICAL ISSUES (SP) …… 529

From Cold Fusion to Low Energy Nuclear Reactions: 2007 Review
Steven B. Krivit …… 530

From Cold Fusion towards Nuclear Transmutation – Probable Alternative for Nuclear Power Engineering (Glance from Russia)
Igor Goryachev, Yu.Bazhutov ……. 534

Preparata Medal Lecture - A Tribute to Giuliano Preparata, a True Pioneer in Cold Fusion Theory
George H. Miley …….. 548

THEORETICAL MODELS AND RESULT INTERPRETATION (TM) ……. 549

Resonance Transfer of Neutron from Deuteron – Mechanism of Low Energy Nucleus Reactions in Metals
D.D. Afonichev 550

Condensed Matter Nuclear Effects under Platonic Symmetry
Akito Takahashi …….. 554

Deuterons-to-Helium-4 Channels
Akito Takahashi ……... 569

Effective Electrical Charge in Disordered Semiconductors
D. Alexandrov …….. 579

Possible Generation of Neutrons Bursts in Framework of Erzion Model & Their Possible Registration
Yu.N. Bazhutov …… 581

Essence of Erzion Model
Yu.N. Bazhutov …… 585

Progress on Phonon Exchange Models for Excess Heat in Metal Deuterides
Peter L. Hagelstein and Irfan U. Chaudary …… 590

Roles of Approximate Symmetry and Finite Size in the Quantum Electrodynamics (QED) of Deuteron (D)-D Fusion in PDD
Scott R. Chubb ……. 607

The Interactions of Erzions with Natural Isotopes
William Collis ……. 621

Use of a Quantum Mechanical Tunneling Model to Explain the Glow Discharge Characteristic I-V Curve
David y. Chung, Thomas K.T. Hsieh, Frank Senftle ……... 628

Fundamental Interactions and Their Relative Contribution to the Nuclear Reactions at Low Energies
N.V. Samsonenko ……. 637

On the Possibility of the Dineutron Existence and the Difficulties of It's Experimental Detection
N.V. Samsonenko, S.L.Doubkov …… 638

Theory of Cold Nuclear Transmutation
Mikio Fukuhara …….. 639

New Discovery: Quantization of Atomic and Nuclear Rest Masses and Self-Organization of Atoms and Nuclei
F.A. Gareev, G.F. Gareeva, I.E. Zhidkova ……. 653

Calculation of Tunneling Probability for the Strongly Screened Coulomb Barrier, and Check-up of Probability of WKB Approach
A.I. Goncharov, V.A. Kirkinskii, V.V. Samovolik …… 661

Anomalous Nuclear Reactions Created by Torsion Field within Electrochemical Systems
Xingliu JIANG and Lijun HAN …… 665

Polyneutron Theory
John C. Fisher ……. 666

About the Features of Lepton Terletski Quadriga in Electromagnetic Vacuum
L.I.Kholodov, I.V.Goryachev ……... 669

Estimation of Geofusion Probability
V.A. Kirkinskii ……. 685

Physics of the Cold Fusion Phenomenon
Hideo Kozima …….. 690

The Extended Micro Hot Fusion Scenario
Rainer W. Kühne ……. 704

Graviatoms with Leptons and Mesons
Yu. P. Laptev, M. L. Fil'chenkov** and S. V. Kopylov* …… 709

Selective Resonant Tunneling Model for Lattice Confined Deuterons
Xing Z. Li, Qing M. Wei, Bin Liu …… 714

Photon/Phonon-Aided Low-Energy Nuclear Reactions in Condensed Matter
A.Meulenberg and K.P.Sinha ……. 715

Cluster Reactions in Lenrs
George H. Miley, Andrei Lipson, Nie Luo, Heinz Hora, and Prajakti Joshi Shrestha ……... 716

Issues for Charged-Particle and X-Ray Emission in Lenr Experiments
George H. Miley, Lawrence P.G. Forsley, Pamela A. Mosier-Boss …….. 717

Phenomenological Model of Low Energy Element Transmutation and Element Distribution in Transmutation Products.
G.V. Mishinsky, V.D. Kuznetsov 718

Rates for Low Energy Nuclear Reactions at Surfaces
David J. Nagel 738

Powers, Materials and Radiations from Low Energy Nuclear Reactions on Surfaces
David J. Nagel 739

The Conception of Nuclear Forces in Field Physics
O.N. Repchenko 756

Nuclear Transmutations at Meteorology
B.U. Rodionov, O.G. Kudryavtzev, V.V. Botvinovsky 757

Fundamental Interactions and Their Relative Contribution to the Nuclear Reactions at Low Energies
N.V. Samsonenko 765

On the Possibility of the Dineutron Existence and the Difficulties of It's Experimental Detection
N.V. Samsonenko, S.L.Doubkov 766

Cold Nuclear Fusion Mechanism at Crack Tip Spearhead Located Deep under the Ground
A.V.Shestopalov 767

Many-Body Effects of Bose Particle System in Solid
Ken-ichi Tsuchiya, Shigeru Sasasbe, Masao Ozaki 777

Possible Catalysis of Nuclear Transmutations at Electronic Screening of Nucleus Charges in the Dense Low-Temperature Plasma of the Powerful Pulsing Induction Discharge
A.N. Vlasov 778

Form of Nuclear Fusion in Solid Crystals
Norio Yabuuchi, Akito Takahashi 793

List of ICCF-13 Participants 803

Author Index 813

Analysis and Diagnostic Techniques (AD)

NEW RESULTS on COSMIC RAY ERZIONS SEARCH RECEIVED on THE SCINTIILLATION SPECTROMETRIC TELESCOPE "DOCH-4M" during (2001-2006)

Yu.N. Bazhutov*, Yu.V. Kozlov, V.P. Martemyanov**, E.V. Pletnikov***, A.A. Sabelnikov**, V.A. Starostin**, V.G. Tarasenkov**, E.V. Turbin**, V.N. Vyrodov****

Terrestrial Magnetism and Radio Propagation Institute (IZMIRAN), Troitsk, Moscow region, **E-mail: bazhutov@izmiran.ru*
***Russian Science Center «Kurchatov Institute», Moscow*
****State Technical University (MAI), Moscow*

In the framework of cosmic ray Erzions search program on the scintillation spectrometric telescopes "Doch-4M" running during (2001-2006) it is received the new results of season variations of the high ionization cosmic ray component. For the first time it was observed in cosmic rays the large variations (A~30%), practically independent on zenith orientation of the telescope "Doch-4M" axis. These events nature is discussed using their classification by character types of events depended on the number of charged particles passed through the outer plastic scintillation environment. It was received the abnormal absorption dependence of the studied high ionization cosmic ray component in the passive absorber (lead & polyethylene) placed above the telescope. These new unusual results, contradicted orthodox cosmic ray physics as on variations so on absorption dependence, are analyzed in framework of Erzion model.

1. Introduction

In 1999 on a telescope «Doch-4» in MADI the first results on detection in Cosmic Rays of new stable heavy charged particles - Erzions [1-4] have been received. After that, for check of the fact of detection of new particles in Cosmic Rays the telescope has been automated and has worked continuously in a line with the personal computer already on the territory RRC Kurchatov Institute as a telescope «Doch-4a» since July 2001 till May 2002 with an inclination of its axis to the south on 18° (T_a=242.7 day). Then the telescope has been modernized by addition to it of an environment from plastic scintillators (PS) from above ("Roof"), from below ("Bottom") and from the sides ("Tire cover") with corresponding labels (R, B, C) impulses developed on the oscillogram at simultaneous operation PS with a telescope. In such mode the modernized telescope «Doch-4m1» has worked since June 2002 till March 2003 (T_{m1}=234.4 day) with a vertical arrangement of its axis. Further the same modernized telescope has been inclined to the south, on 43° and in such position it has worked from May till September 2003 as «Doch-4e» (T_e=152.5 day). Then it has been returned in vertical position and in such mode has worked till August 2004 as «Doch-4m2» (T_{m2}=247,7 day). After repair ADC from January till July 2005 it has worked as «Doch-4m3» (T_{m3}=139,8 day) and after repair of the controller since August 2005 till February 2006 - as «Doch-4m4» (T_{m4}=118,1 day). Thus, for 5 years of continuous operation of a telescope «Doch-4m» in the personal computer it is saved up the richest peak material (~5,000,000 events with the digitized shape of impulses from crystals CsI and NaI) from charged

components of Cosmic Rays (including showers) with total "alive" time - T_{Σ}~1220 day for various corners of their arrival ($0° < \theta < 60°$) from a vertical for the south. For 5 years of continuous work of a telescope in the set forth above modes daily [7,8] and season variations of the account of events in the field of registration of the high ionization [9]. For finding-out of the nature high ionized components of the Cosmic Rays selected and analyzed in telescope Doch-4m, additional studying absorption curve of high ionized components on the same installation with addition above a telescope of a canopy with passive substance of an absorbent from lead and polyethylene has been fulfilled.

2. Installation and modes of its operation

The design of a telescope of installations «Doch-4m» (fig.1) completely corresponds to their progenitress - to installation «Doch-4», worked in MADI in 1999 [1-4] and is vertical coaxial scintillation telescope consisting of thin crystal CsI (∅63x0,35 mm^2) from above and thick crystal NaI (∅150x100 mm^2) from below a telescope. Difference of installation «Doch-4a» consists only in new automatic registration of synchronizing amplitudes of signals of crystals CsI and NaI, by their numbering and a conclusion to a personal computer (PC) by means of a 2 channel ADC - LA-n10, built in the PC.

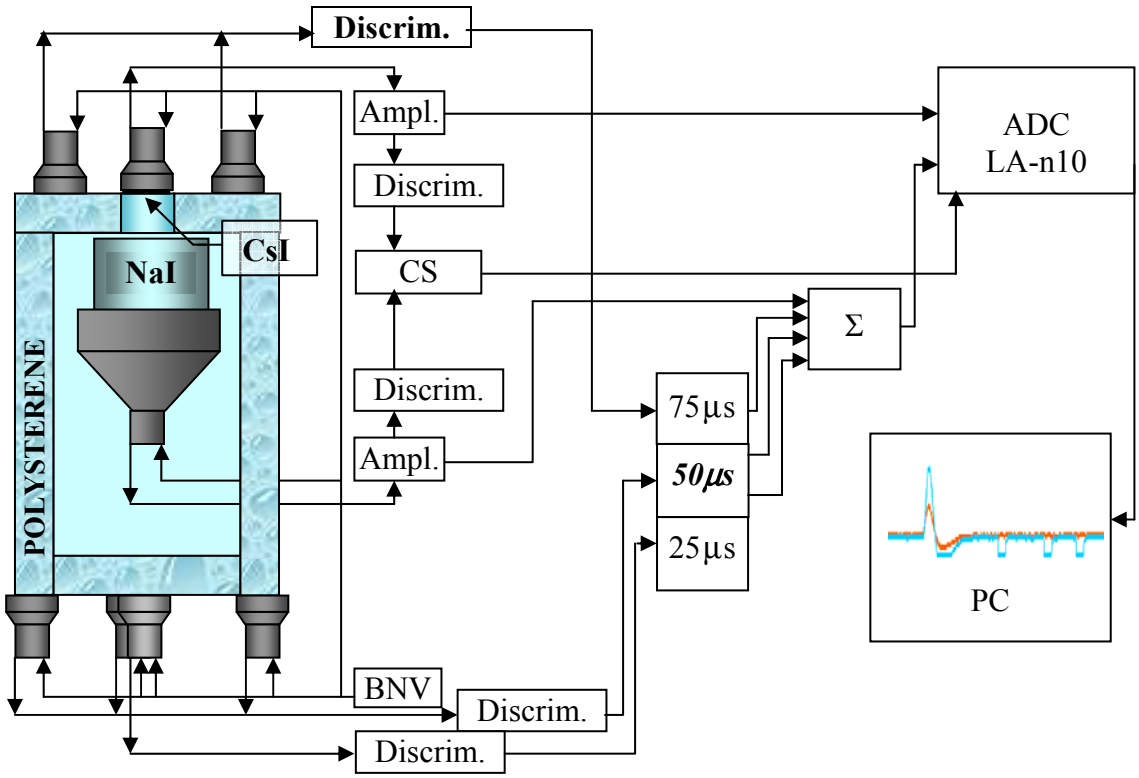

Fig.1. The block scheme of installations «Doch-4m»

In the subsequent operating modes of installation «Doch-4m» the "shirt" from standard polystyrene plastic scintillation detectors (PSD) has been added to 2 crystal telescope: from above a telescope (a label-K), from below (a label-D) and around of it (a label-P). The label is developed at simultaneous occurrence of a signal in a telescope and any of PSD (time of coincidence T_c=1 μs) and summarized with a corresponding delay on a signal from crystal NaI. Thresholds of discrimination at all 3 PSD are set such effectively to select signals from passage through a crystal of a single relativistic charged particle of Cosmic Rays (muon-μ, as a rule). Amplitudes in crystals of telescope CsI and NaI also are normalized to the amplitude corresponding μ signal (1μ) and measured at processing in these normalized values (1μ). For this purpose both at preliminary adjustment and at the subsequent regular control over stability of work of a telescope spectrums of amplitudes from space μ in crystals CsI and NaI in the chosen area of channels of the analyzer of amplitudes (AA) by their change by means of a high voltage of a feed of photomultipliers of corresponding crystals are removed. Besides, the control over stability of the crystals CsI and NaI work was provided by the constant control over the crystals intensity. For this purpose thresholds of their discriminators were established at a level 1,5μ on sharp parts of a spectrum of amplitudes of the crystal that at 10% change of operating intensity of the crystal to feel change of amplification of its path at a level of 3%. On fig.2 the characteristic oscillogram of signals of crystals CsI and NaI with corresponding (K, D, P) the detained labels on a signal from crystal NaI is presented. In figures 3 and 4 characteristic are presented 1μ spectrums from crystals CsI and NaI. On fig.5 diagrams on a regular basis controllable weekly intensities works accordingly PSD, crystals CsI and NaI and their concurrences defining frequency of operation of a telescope for last period of its work “Doch-4m4” are presented. Apparently from diagrams, for half year an interval of work of installation of intensities change on all to 4-th channels of registration are within the limits of several percent ($\Delta J/J < 10\%$), as our level of stability on intensity, with corresponding it to a level of stability on amplitude - $\delta A = (\Delta A/A) <$defines 3%.

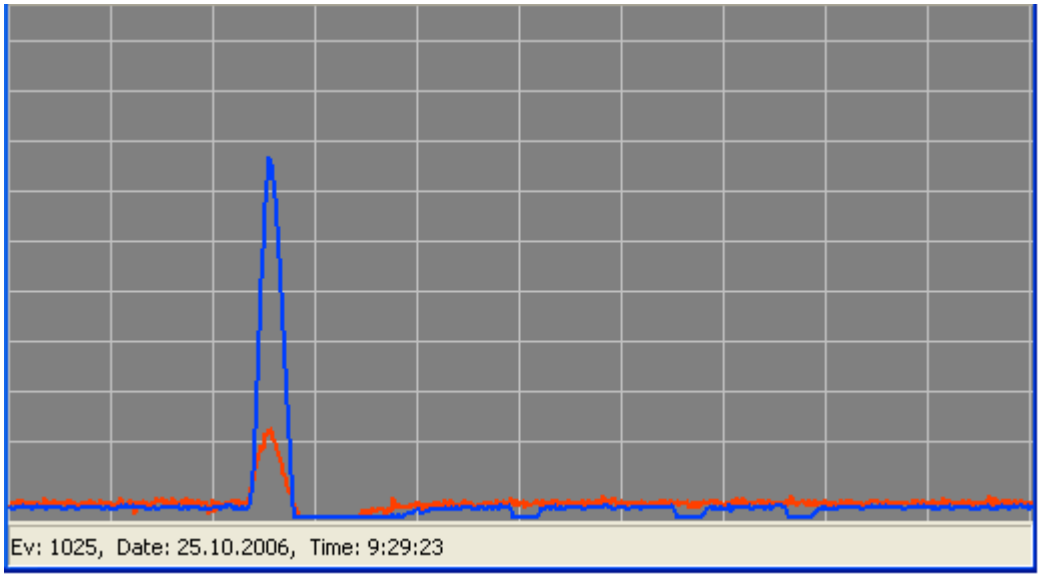

Fig. 2. ADC LA-n10 oscillogram from CsI and NaI crystals.

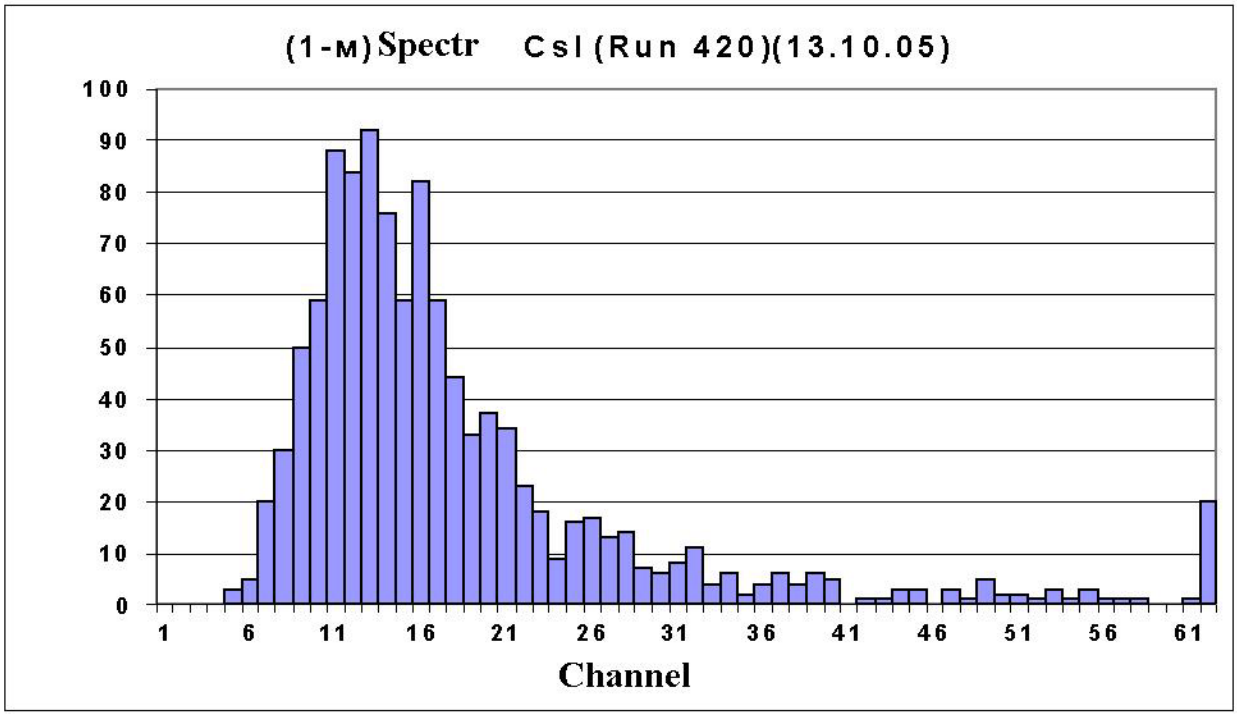

Fig. 3. CsI (1-m) amplitude spectrum

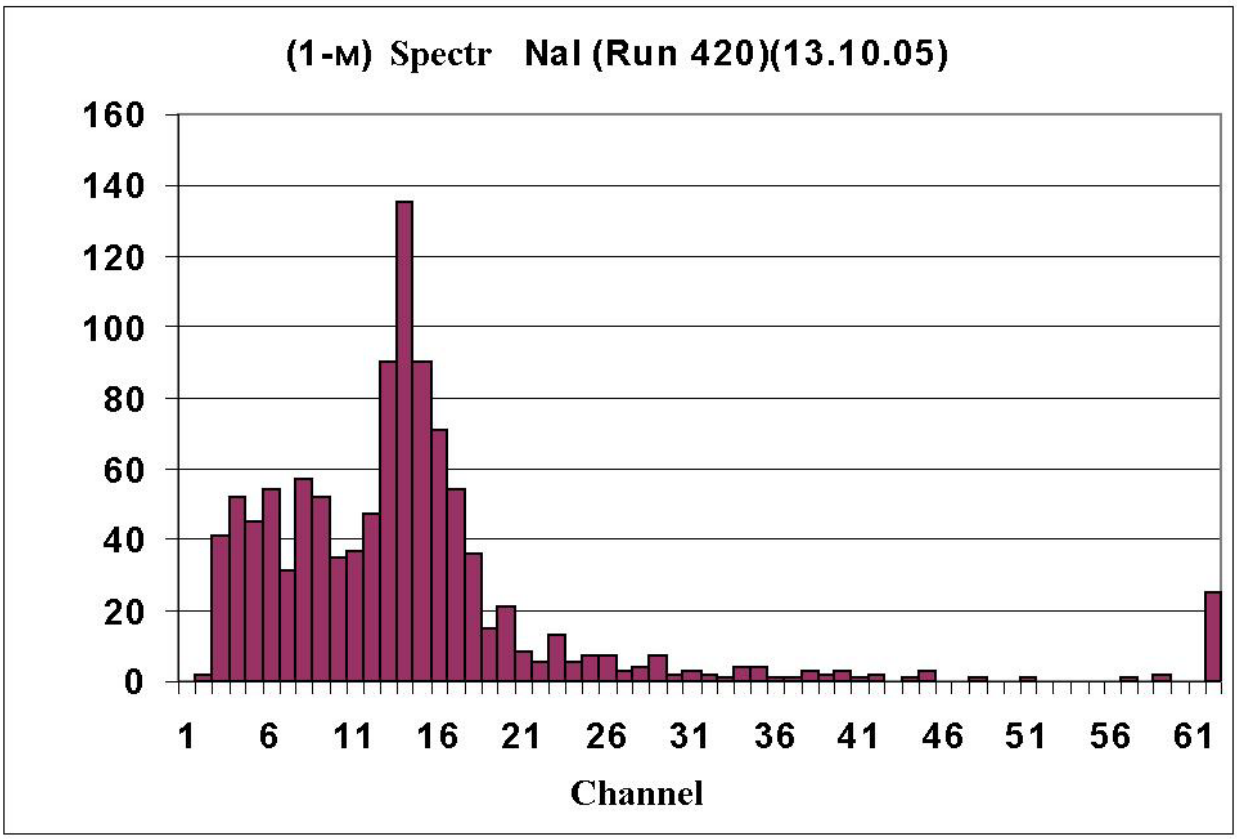

Fig. 4. NaI (1-m) amplitude spectrum

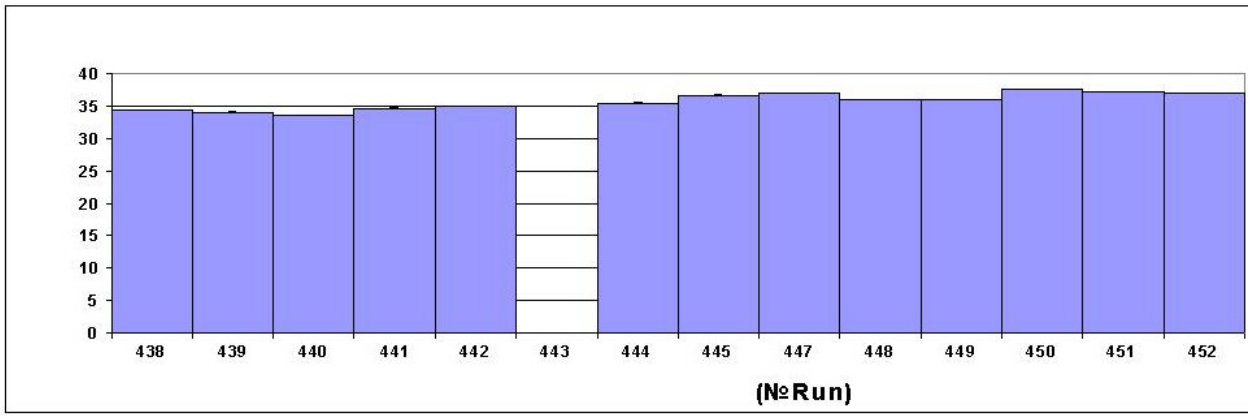

Fig. 5. Diagram of PSD weekly intensities (Hz).

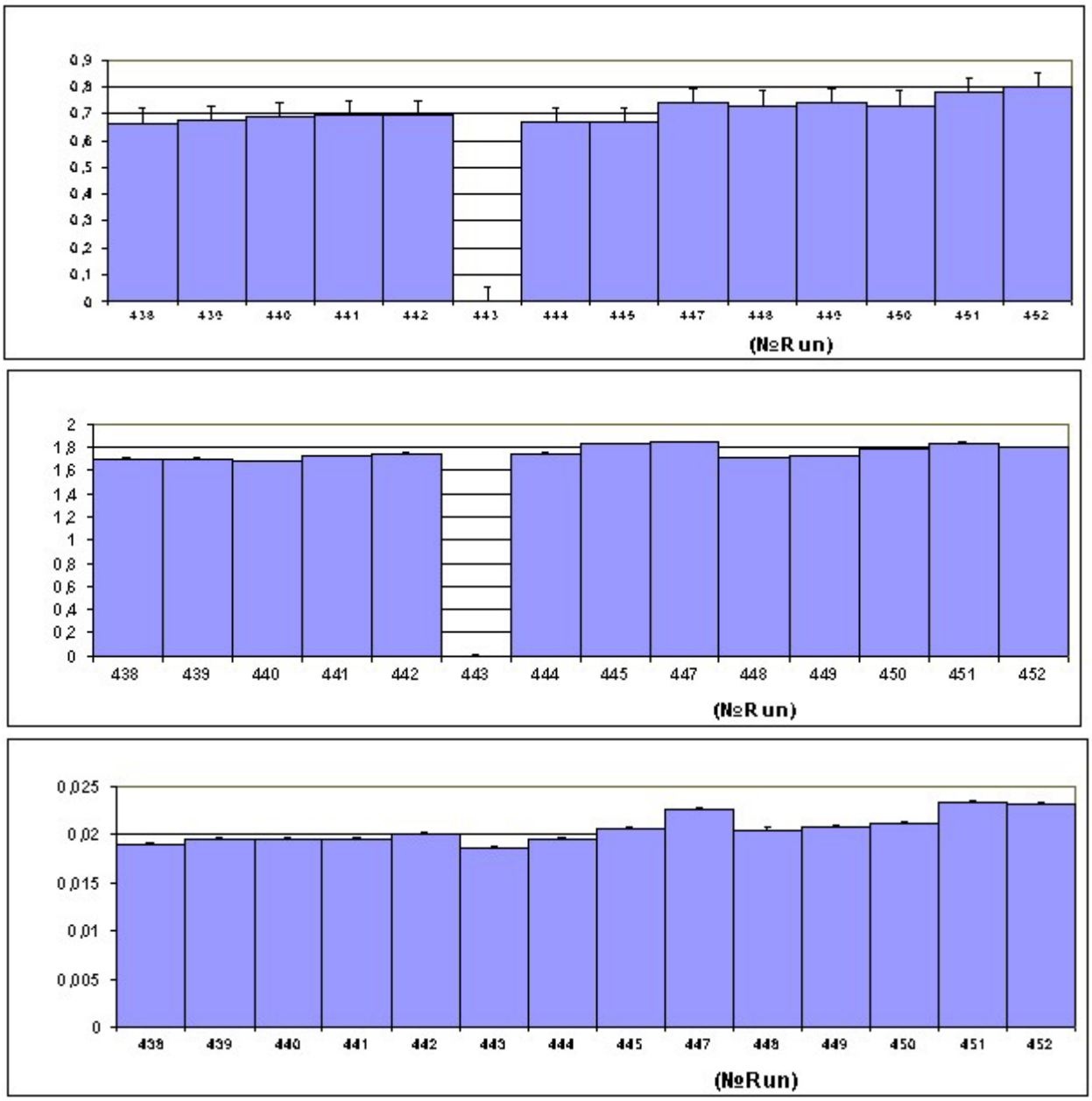

Fig. 6. Diagram of CsI and NaI and their concurrences weekly intensities (Hz).

3. The received results on variations

As for search massive Erzions we were interested only greater amplitudes of signals from crystals CsI and NaI, caused high ionized no relativistic charged particles. At the subsequent processing the saved up events with amplitude in both crystals exceeding ~10 multiple amplitude relativistic cosmic muons (10μ) were selected only. In table 1 there are presented: time intervals for various operating modes of a telescope «Doch-4m» (a, m1, e, m2, m3, m4), numbers of the selected events inside of these intervals and corresponding them intensity. On fig.7 the intensities histogram of the selected events inside of these any intervals is presented.

Table 1. Selected events with high amplitude (10μ) for various operating modes of the telescope "Doch-4m"

Opera-ting modes	Start time	End time	Sum Time	Number of Selected Events	Intensity	Standard Deviation
			(days)	(events)	(events/day)	(events/day)
A	25.07.01	29.05.02	254,55	333	1,31	0,07
M1	14.06.02	06.03.03	239,89	259	1,08	0,07
E	06.03.03	02.09.03	166,51	250	1,5	0,09
M2	02.09.03	10.08.04	247,67	183*(x2)	1,48	0,11
M3	18.01.05	12.07.05	139.76	216*(0,844)	1,54	0,11
M4	30.08.05	08.02.06	118,13	165	1,4	0,11

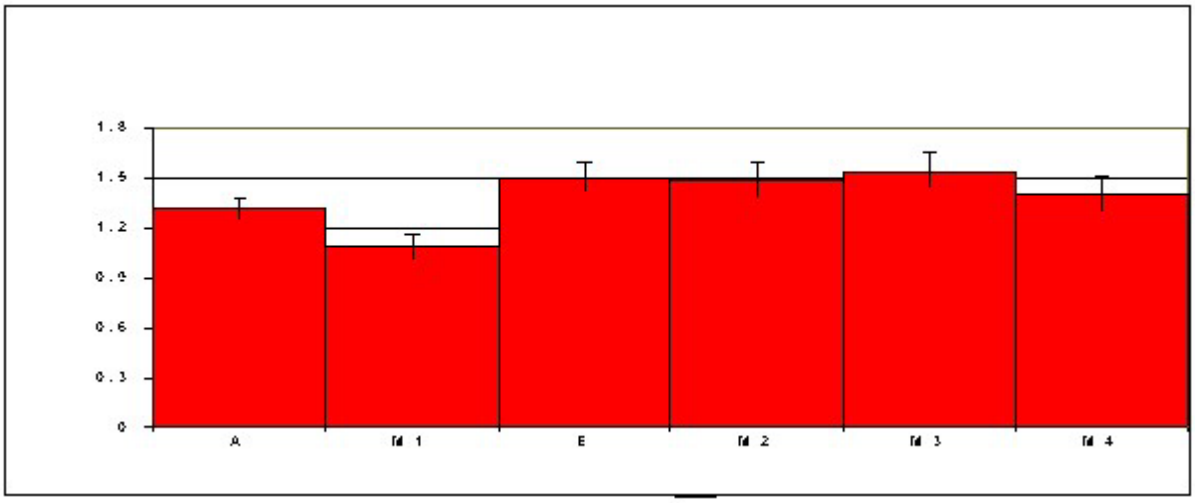

Fig.7 Selected (10μ) events intensities for various operating modes of a telescope "Doch-4m"

From the presented histograms and the table 1 it is visible, that intensity of the selected events with the high ionization for various operating modes of a telescope approximately (that is within the limits of 2-3 Standard Deviation) coincides with each other. Besides as all the periods of a telescope work in various modes were compared with a year, all of weekly intensities for all 5 years of work of a telescope have been averaged for reduction of a statistical error. In table 2 and on fig.8,9 results weekly intensities for all 5 years of a telescope work are presented.

Table 2. Selected (10μ) events weekly intensities for all 5 years of a telescope work

№\ Year	2001	2002	2003	2004	2005	2006	Σ (J)	Number	< J >
week	evs/day	evs/day	evs/day	evs/day	evs/day	evs/day		weeks	evs/day
1		1,4	1,5	1,4		1,7	6	4	1,5
2		1,2	1	1,4		1,7	5,3	4	1,3
3		1,2	1,6	2,2	1,2	1,3	7,5	5	1,5
4		1	1,2	2,2	1,4	1,6	7,4	5	1,5
5		1,3	1,4		1,2	0,9	4,8	4	1,2
6			0,8		1,2	3,3	5,3	3	1,8
7		1,5	0,9		2,6		5	3	1,7
8		1,9	1,4		2,2		5,5	3	1,8
9		1,8	0,8	3,4	1,9		7,1	4	1,8
10		1,8		0,8	1,9		4,5	3	1,5
11		1,8	2	1,4	1,7		6,9	4	1,7
12		1,6	2,2	1,8	2		7,6	4	1,9
13		1,2	2,6	1,8	1,4		7	4	1,8
14		1,2	1		1		3,2	3	1,1
15		1,2	1,9		2		5,1	3	1,7
16			1,7	1,8	1,1		4,6	3	1,5
17		2,1	2	2,2	1,3		7,6	4	1,9
18		2,1	3,2	1,6	1		7,9	4	2
19		1,2	1,1	1,6	1		4,8	4	1,2
20		1,7	2,4		1,1		5,2	3	1,7
21			2	1,4	1,1		4,5	3	1,5
22			1	1,2	1,1		3,3	3	1,1
23			1,4	1,6	1		4	3	1,3
24		1	1,7	1,6	0,6		4,9	4	1,2
25		2,3	1,7	1,2	0,6		5,8	4	1,4
26		1,7		1,2	1,7		4,6	3	1,5
27		1,1			1,1		2,2	2	1,1
28		1,5	2	1,8			5,3	3	1,8
29		0,5	1,3	2,2			4	3	1,3
30	2	1	1,3	0,8			5,1	4	1,3
31	0,8	1,2	0,9	1,2			4,1	4	1
32	2	0,9	2,1	1,6			6,6	4	1,6
33	1,3		0,6				1,9	2	1
34		1,4	0,9				2,3	2	1,2
35		1	1,4				2,4	2	1,2
36	1,2	1,1	1,4				3,7	3	1,2
37	0,8						0,8	1	0,8
38	0,6	0,8	0,8				2,2	3	0,7
39	0,5	0,3	1,8				2,6	3	0,9
40	0,7		0,8		0,4		1,9	3	0,6
41	0,7	0,7	1,2		0,7		3,3	4	0,8
42	0,7	1	1,4		0,9		4	4	1
43	0,9	1,1	1,8		0,7		4,5	4	1,1
44	1,9	0,8			1,3		4	3	1,3
45	1	0,8	0,8		0,9		3,5	4	0,9
46	0,7	1,2	0,8		1,7		4,4	4	1,1
47	1,4	1	0,6		1,6		4,6	4	1,1
48	1,4				0,8		2,2	2	1,1
49	0,8				1,3		2,1	2	1
50	1,4	0,7	2,4		2,3		6,8	4	1,7
51	1,4	1,6	0,6		1,1		4,7	4	1,2
52	1,2	1,5	1,4				4,1	3	1,4

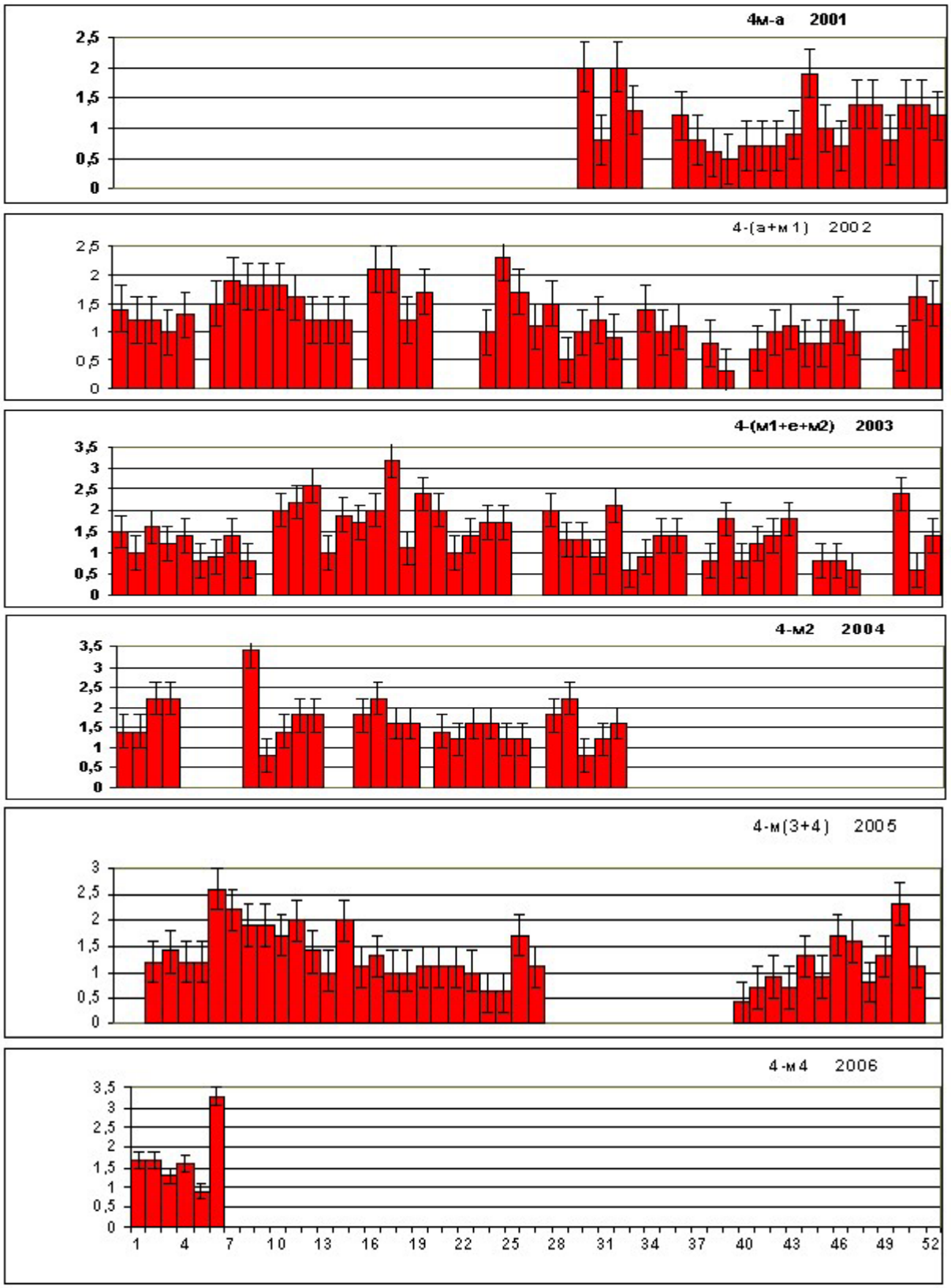

Fig.8. Weekly intensities for all 5 years of a telescope“Doch-4m” operation

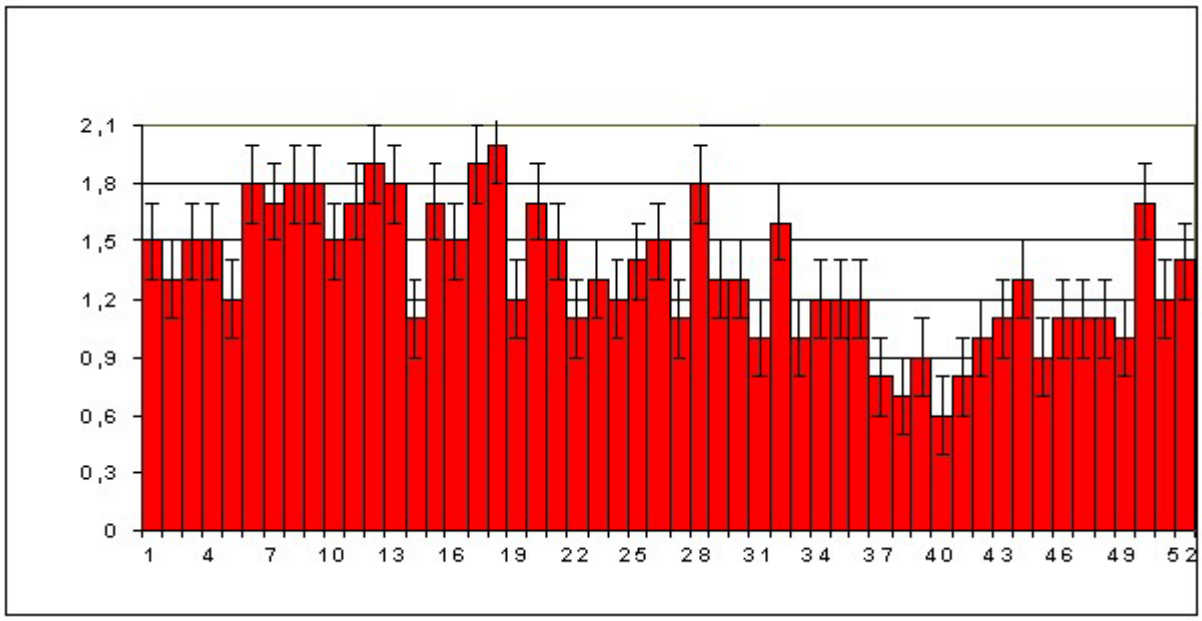

Fig.9. Sum weekly intensities for all 5 years of a telescope"Doch-4m" operation

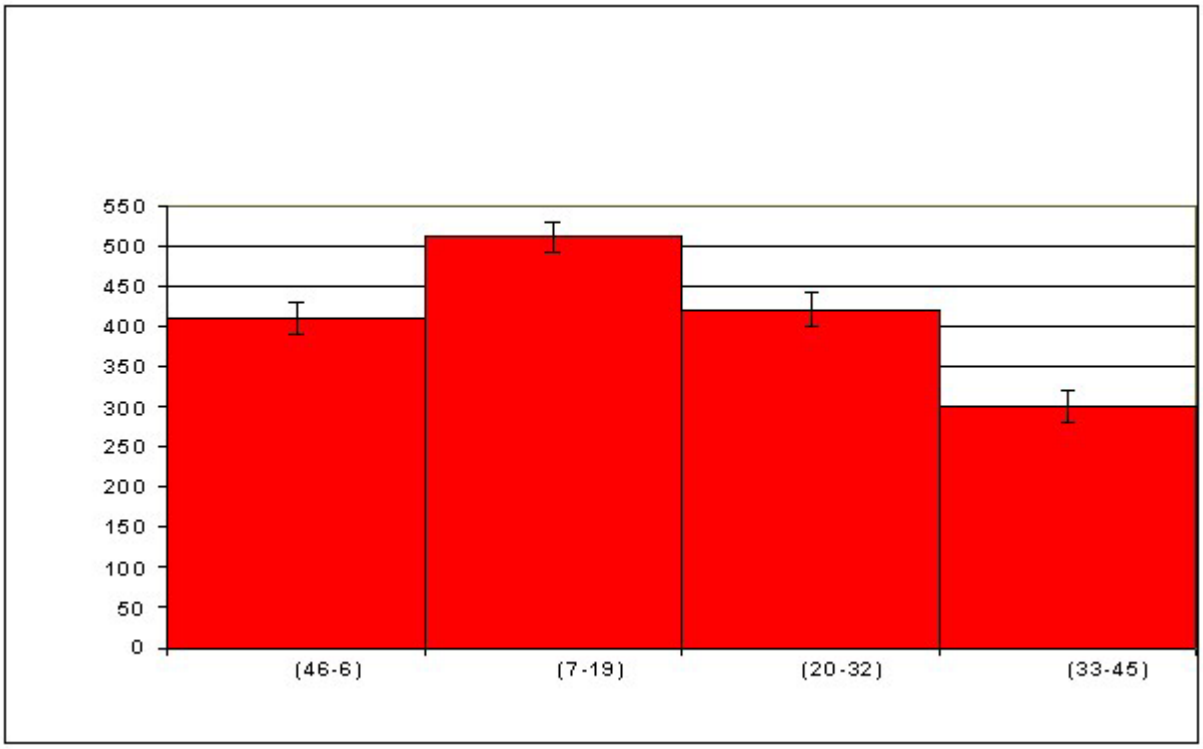

Fig.10. Sum season numbers of selected (10μ) events for various operating modes of a telescope "Doch-4m" during 5 years (2001-2006)

Table 3. Sum season numbers of selected (10μ) events for various operating modes of a telescope "Doch-4m" during 5 years (2001-2006)

Season	**(№ week)**	**Winter (46-6)**	**Spring (7-19)**	**Summer (20-32)**	**Autumn(33-45)**
Σ for 5 years	(events number)	410	510	420	300

From the presented histograms on fig. 8 & 9 and tables 2 it is visible, that annually in September-October considerably (~30 %) decrease intensity high ionized components of Cosmic Rays and as increases in March-April. For display of this effect by most statistically provided image all year (52 weeks) has been broken into 4 seasons, to each equal 13 weeks. In each season for all 5 years of work of a telescope there was an average intensity for this season which then was multiplied by effective 44 weeks as a full operating time of a telescope for all 5 years of its work were equaled to 176 weeks. Received thus effective season number of events is presented in table 3 and on the histogram fig.10. From the presented values ΔN (Spring-autumn) = (510-300) = (210 +/-28,5) (7,3 σ); ΔN (Summer-winter) = (420-410) = (10 +/-29,5) (0,34 σ) is visible, that effective number of the selected events for years and winter seasons coincide within the limits of a standard deviation (σ) while their values in the spring and differ on 7,3 standard deviation in the autumn. Thus, statistically convincing proof for the first time the found out effect of season variations for high ionized components of Cosmic Rays with amplitude of variations - (A~30 %) is received. Earlier we had been received results on the same strong daily variation same high ionized components of Cosmic Rays on telescope “Doch-4a” at an inclination of its axis on the south on 18 [7-8].

4. The received results by the nature high ionized components of Cosmic Rays

The nature of these components a priori is not absolutely clear to us. Therefore, that it is better to understand it, we shall analyze other performances of these selected events registered on our telescope. First of all we use the information received on a telescope about support of the core energy losses in crystals of telescope CsI and NaI by signals of its environment from plastic scintillators (PSD). For this purpose it is used data about labels of support (K,P,D) basic signals CsI and NaI. In figure 11 distribution of the selected events on their various support in a shirt surrounding a telescope from 3 types PSD is presented: from above ("Roof"), from below (the “Bottom”) and from sides ("Tire cover") with corresponding labels (K,P,D). When there is no a signal of support in one of PSD is an event concerns to type - CN.

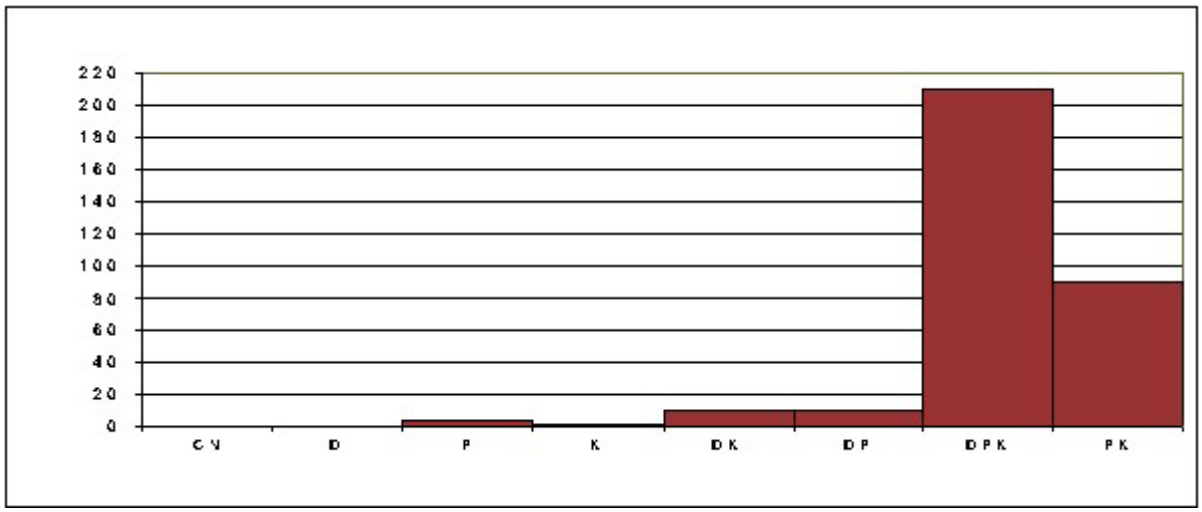

Fig.11. Distribution of the selected (10μ) events on their various support in a shirt surrounding a telescope consisted from 3 types PSD (K,P,D)

Apparently from Fig.11, events of type (K,P,D) make a great bulk of these events in all modes «Doch-4m», that specifies the strong support by secondary charged particles of selected events with the high ionization in CsI and NaI detectors of a telescope.

Let's consider one more important performance of selected events – correlation dependence of amplitudes CsI and NaI detectors of a telescope. On Fig.12 such dependence where on an abscissa axis the amplitude of crystal CsI is postponed, and on an axis of ordinates - amplitude of crystal NaI in terms of channels ATSP (10 channel corresponds to amplitude 1м) is presented.

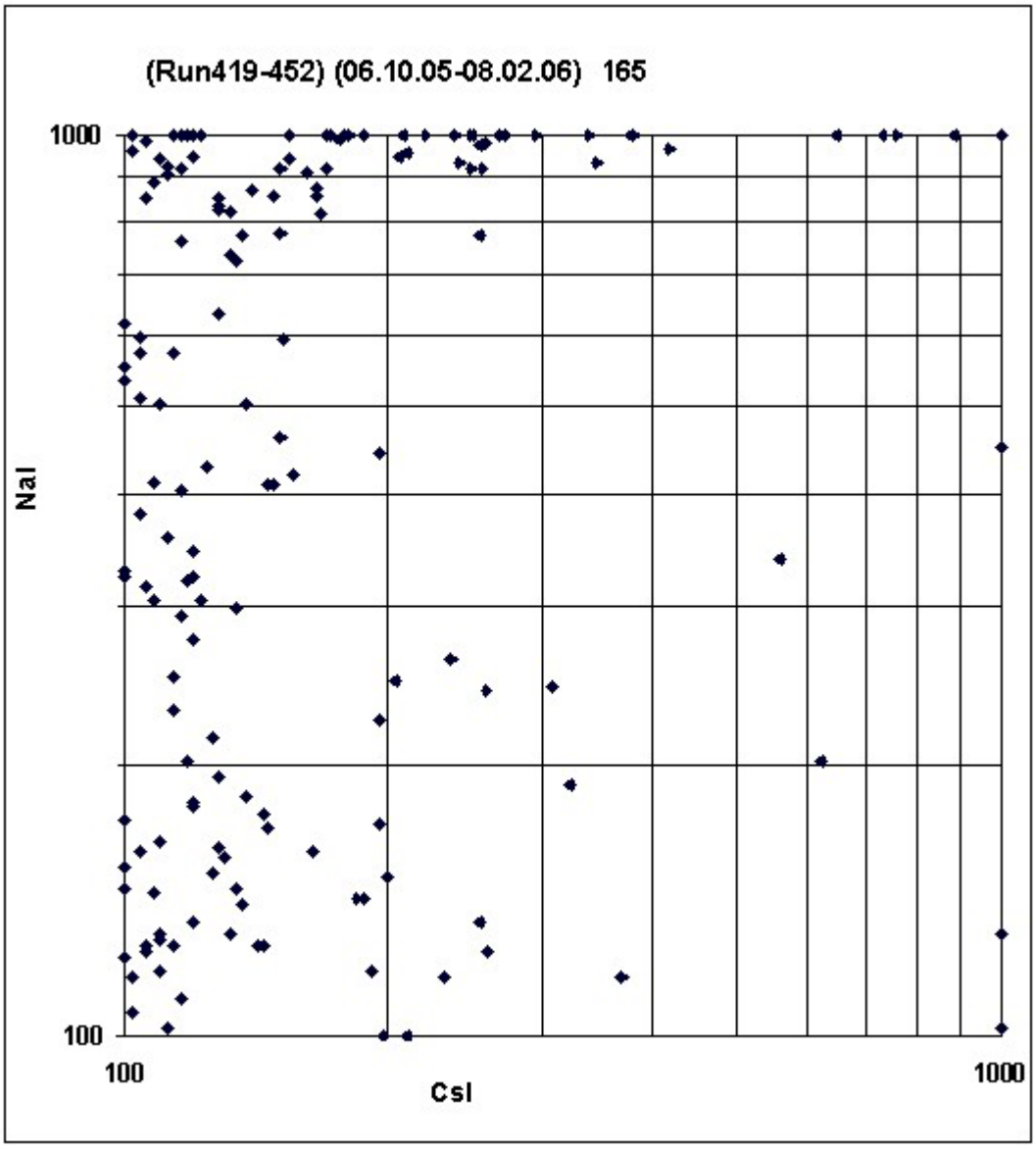

Fig.12. Correlation dependence of amplitudes CsI and NaI detectors of a telescope «Doch-4m» for selected (10μ) events

From figure it is visible, that amplitudes at all do not correlate with each other as should be for single charged high ionizing particles. Moreover, of this distribution and previous performances of the strong support secondary particles develop impression about the nature of

these events as hadron splitting of nuclei with generation of "stars" and the big number of the secondary particles consisting of evaporation nucleons and easy nuclei and π & K - mesons. This version corresponds also to energy loss quantity in crystal NaI equivalent for a level 10μ-100μ to value 1-10 GeV. The number of shower particles at such energy is equivalent to 3-10 charged particles that also corresponds to the histogram of supported selected events.

With such version of analyzed events, we have been carried out additional researches on a telescope «Doch-4m» on measurement of a curve of absorption studied high ionization components of Cosmic Rays. For this purpose above a telescope at height ~1meter the canopy has been built on which the passive lead absorbent by thickness up to 200 g/cm^2 and the area (1x1,5)m^2 along directions (East-West) has been placed. In table 4 and on Fig.13 the received results for 4 months of work of a telescope (25.04-22.08).07 with various thickness of a lead absorbent above a telescope are presented.

Table 4. Absorption of high ionization Cosmic Rays components in lead

h	№ Run	Date	Time	Events	Intensity	Standard deviation
(g/см2)			(days)	number	(events / day)	(events / day)
0	445 - 452	07.12.05 - 08.02.06	57,95	99	1,71	0,17
40	485 - 488	(01 - 22).08.06	20,91	56	2,68	0,36
80	470 - 474	(25.04 - 18.05).06	22,79	54	2,37	0,32
120	483 - 484	(11.07 - 01.08).06	20,98	27	1,29	0,25
200	475 - 482	(18.05 - 11.07).06	47,83	51	1,07	0,15

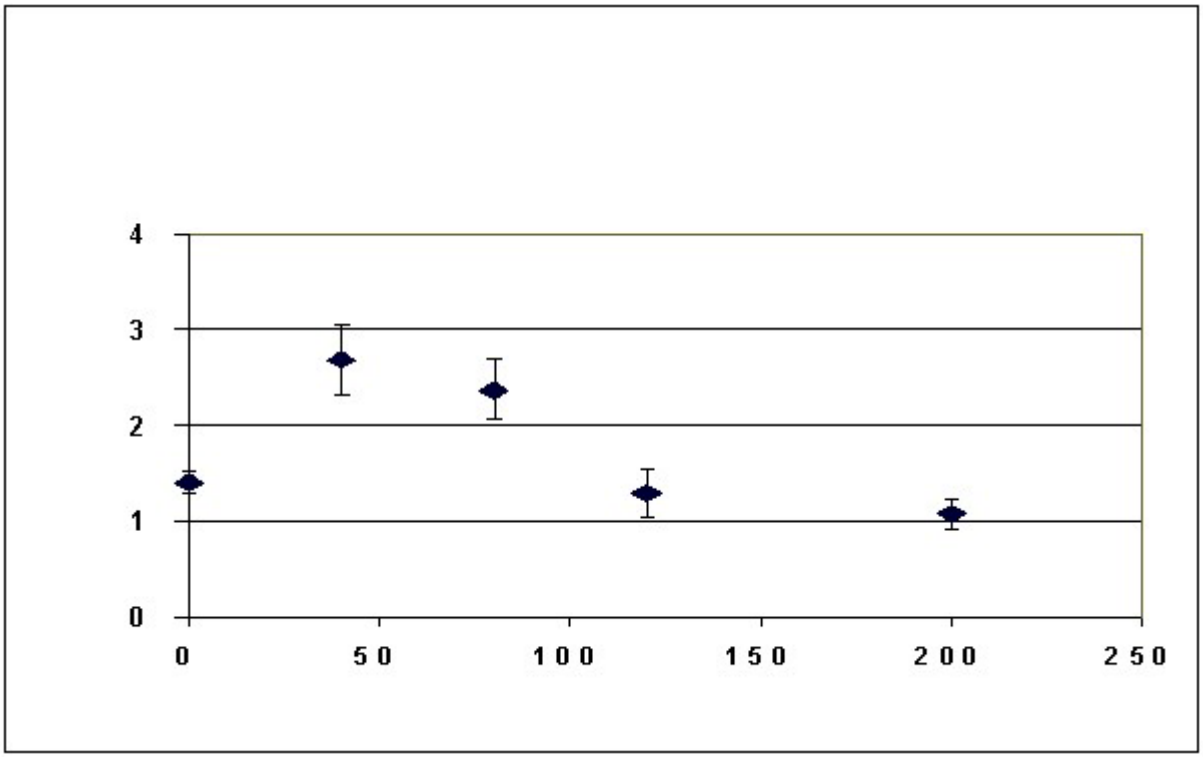

Fig.13. Absorption dependence of high ionization Cosmic Rays components in lead

Then the same has been repeated with polyethylene instead of lead. In table 5 and on Fig.14 the received results for 4.5 months of work of a telescope (12.09.06-23.01.07) with various thickness of a polyethylene absorbent above a telescope are presented.

Table 5. Absorption of high ionization Cosmic Rays components in polyethylene

h	№ Run	Date	Time	Events	Intensity	Standard deviation
(g/cm^2)			(days)	number	(events/day)	(events/day)
0	419 - 452	07.12.05 - 08.02.06	118,13	165	1,41	0,11
15	491 - 502	(12.09 - 29.11).06	77,7	138	1,78	0,15
30	503 - 517	(29.11 - 26.12).06	21,1	46	2,2	0,3
60	518 - 519	26.12.06 - 23.01.07	22,9	68	2,96	0,36

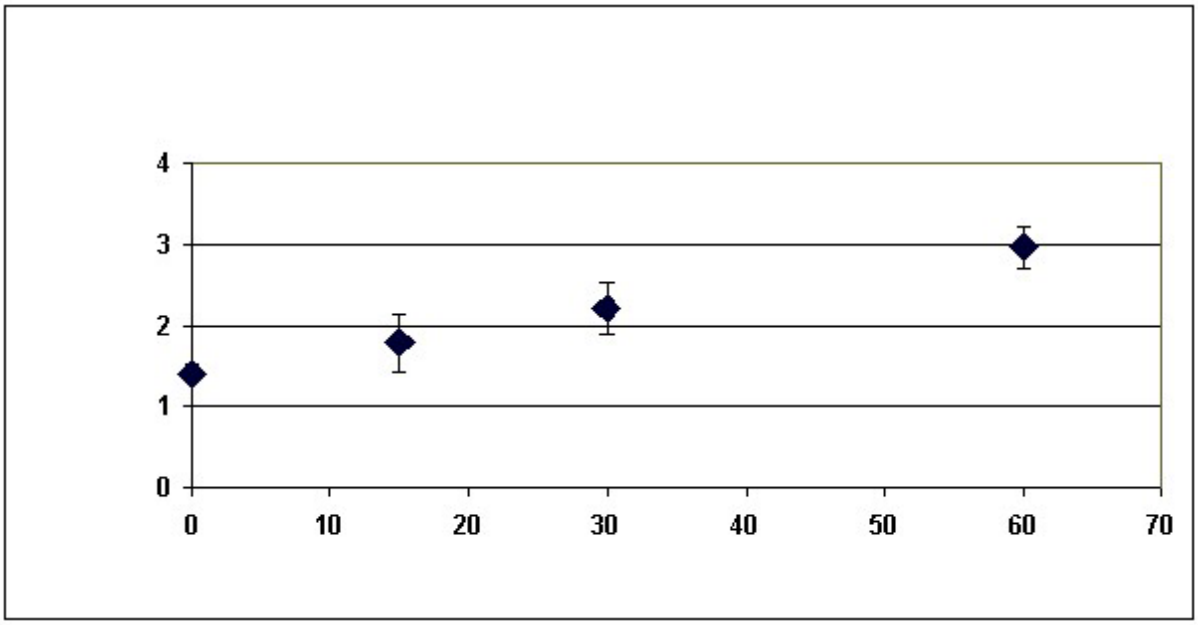

Fig.14. Absorption dependence of high ionization Cosmic Rays components in polyethylene received on a telescope «Doch-4m»

From Fig.13,14 it is visible, that both with heavy, and with an easy absorbent down to thickness of 60 ú/sm2 there is an increase in intensity, that is additional generation high ionization components of Cosmic Rays to its subsequent absorption in lead with length of absorption L_{Pb}=(150+/-15) g/cm^2. It is impossible to explain this feature generation of showers in an absorption of hadron Cosmic Rays component (nucleons or, π & K - mesons), splitting of nuclei in crystal NaI. First, length of absorption in lead for nucleons L_N = (280 +/-10) g/cm^2 and for mesons it is even more, and, secondly, they should not give growth of intensity of such events, but only its absorption. Within the framework of Erzion models these results have a simple and natural explanation by splitting nuclei in crystal NaI basically by Enions (E_N) with energy E (E_N) ~10GeV. Then transpiration nucleons in a return hemisphere

can create high (10μ) ionization in crystal CsI, and secondary shower particles (n~10) at such energies) together with evaporation nucleons and nuclei which can create high (10m) ionization in crystal NaI. Neutral Erzions (E_0), the main component of the Erzion component of secondary Cosmic Rays, also can create such splitting of nuclei, but their full cross-section of splitting should be much less, than for Enions because of additional resonance channels of their interaction with nuclei Na and I, completely absent for E_0. For the same reason and length on absorption in lead for secondary Enions, generated by primary neutral Erzions in the same place, appears almost in 2 times less (150 g/cm^2 instead of 280 g/cm^2), than for usual hadrons (high energy protons or neutrons), including neutral Erzions.

Conclusion

Thus, to published before the information [7-8] about observation large daily variations (A~50 %) for high ionizing component of Cosmic Rays now for 5 years of continuous operation of the telescope «Doch-4m» we may enough convincingly (7,3 σ) to add the same great (A~30 %) it's season variation. Both daily and season variations of Cosmic Rays on neutron monitors or muon's telescopes as much as possible reach amplitude of variations (1-2) %, but not (30-50) % as in our case. Therefore these our new results, including also the received dependence of absorption in lead for this components, can't be explained within orthodox physics of Cosmic Rays and it demands the introduction of new hypotheses for their interpretation. However, all these received results easily and naturally can be explained by presence in primary space radiation of solar negative Erzions (J_E~10^{-6}см-2с-1стер-1) and neutral Erzions (J_E~10^{-6}см$^{-2}$с$^{-1}$стер$^{-1}$) of the galactic origin directed mainly from the Virgo constellation (the center of a conglomeration of the nearest galaxies). Negative Erzions with impulse P_E~50GeV/C and energy E_E~6GeV traveling from the Sun are deviated by magnetic field of the Earth on a angle close to 90º and come in near vertical direction on a telescope in the evening in Spring for 56º parallels of an arrangement of Moscow [5,6]. For neutral Erzions also spring position of an orbit of the Earth is optimum for a direction to the Virgo constellation, the most active area of the Universe in the field of the nearest galaxies conglomeration for sources of radiations in radio, x-ray and γ- ray ranges. In other season probably more significant influence on Cosmic Ray neutral Erzions by solar wind or others unknown while factors of Solar influence, stronger inside of an orbit of the Earth. The first indications on an opportunity of existence of 2 natures of Erzions sources (solar origin and galactic), for the first time have been received on installation «Doch-4a» at registration in the winter daily distribution of events from high ionization components of Cosmic Rays of 2 peaks (evening - a solar origin and morning - galactic) [7,8].

References

1. Bazhutov Yu.N. // "Disclosure of new stable heavy charged particles in Cosmic Rays". Web-site: XXX.LANL.GOV/abs/hep-ex/9908053;
2. Bazhutov Yu.N. // "Observation of new stable massive charged particles in Cosmic Rays". Moscow. VINITI. 1999. №2872-B99;
3. Bazhutov Yu.N. // "Disclosure of Erzions in Cosmic Rays as Hypothetic Catalyze of Cold Nuclear Transmutation". RCCNT-7 Proceeding. Moscow. 2000. p. 47-57.
4. Bazhutov Yu.N. // "Registration of new stable heavy charged particles in cosmic rays". Proc. 27th ICRC. Hamburg. 2001. V. 1. P. 1517.

5. Bazhutov Yu.N. // “Registration of Erzions in Bubble Chamber «SKAT»». RCCNT-8 Proceeding. Moscow. 2001. p. 63-69.
6. Bazhutov Yu.N., Borog V.V., Simakov O.P. // «Experiment Project on Erzions Search in Solar Cosmic Rays by Ground Muon Hodoscope». RCCNT-8 Proceeding. Moscow. 2001. p. 70-75.
7. Bazhutov Yu.N., Vyrodov V.N., Kozlov Yu.V. etc. // “Monitoring Results of Solar Erzions on the “Doch-4a” Telescope”. RCCNT-9 Proceeding. Moscow. 2002. p. 26-37.
8. Bazhutov Yu.N., Kozlov Yu.V., Kumantseva Yu.A. et al. // Abs. 18th EuCRSym. Moscow. 2002. HE22P.
9. Bazhutov Yu.N., Kozlov Yu.V., Martemyanov V.P. et al. // “Results of New Stable Massive Charged Particles Search in Cosmic Rays on the Spectrometric Scintillation Telescopes “Doch-4m””. RCCNT-11 Proceeding. Moscow. 2004. p. 18-24.

This work was supported by RFBR
№ 01-02-16117

A STEAM CALORIMETER FOR THE STUDY OF THE ABNORMAL EXCESS HEAT OBSERVED DURING MIZUNO-TYPE EXPERIMENTS

P. Clauzon- J.F. Fauvarque, G. Lallevé- G. Le Buzit

CNAM Electrochimie Industrielle

We have given in YOKOHAMA at the ICCF12 conference the results of a study on abnormal excess heat observed during MIZUNO-type experiments (1). These electrolyses were carried out in a beaker under quite strong voltages (300-350 volts). The measurements of vaporised water weights gave us thermal energies and the indications of a UNIGOR wattmeter gave us the amounts of the electric consumption.

However, the possible loss of electrolyte in tiny droplets, the eventual storage and de-storage of thermal energy and maybe false indications of the wattmeter in severe conditions for the current and the voltage have been raised as possible artefacts being able to give suspicions on our experimental conclusions. In the new device described here after, a steam calorimeter, the possible loss of electrolyte droplets and the storage and de-storage of thermal energy are measured and taken into account. Their influence is negligible. Moreover, the measurement of the thermal heat given by a resistance in series with the electrolysis experiment showed us that the UNIGOR wattmeter gave consistent results within 2% accuracy.

Our experiments have confirmed the coming out of abnormal excess heat. Energy out over energy in ratio (COP) gives us reproducible results around 1.3. This device thus seems to be suitable for more detailed studies to elucidate the MIZUNO mystery. We present finally some ideas for the future experimental program.

(1) “Abnormal excess heat observed during MIZUNO-type experiments” by J.F. FAUVARQUE- P.P. CLAUZON- G.J-M. LALLEVE (CNAM – Paris). Paper presented at YOKOHAMA ICCF12 Conference in November 2005.

Experimental Scheme

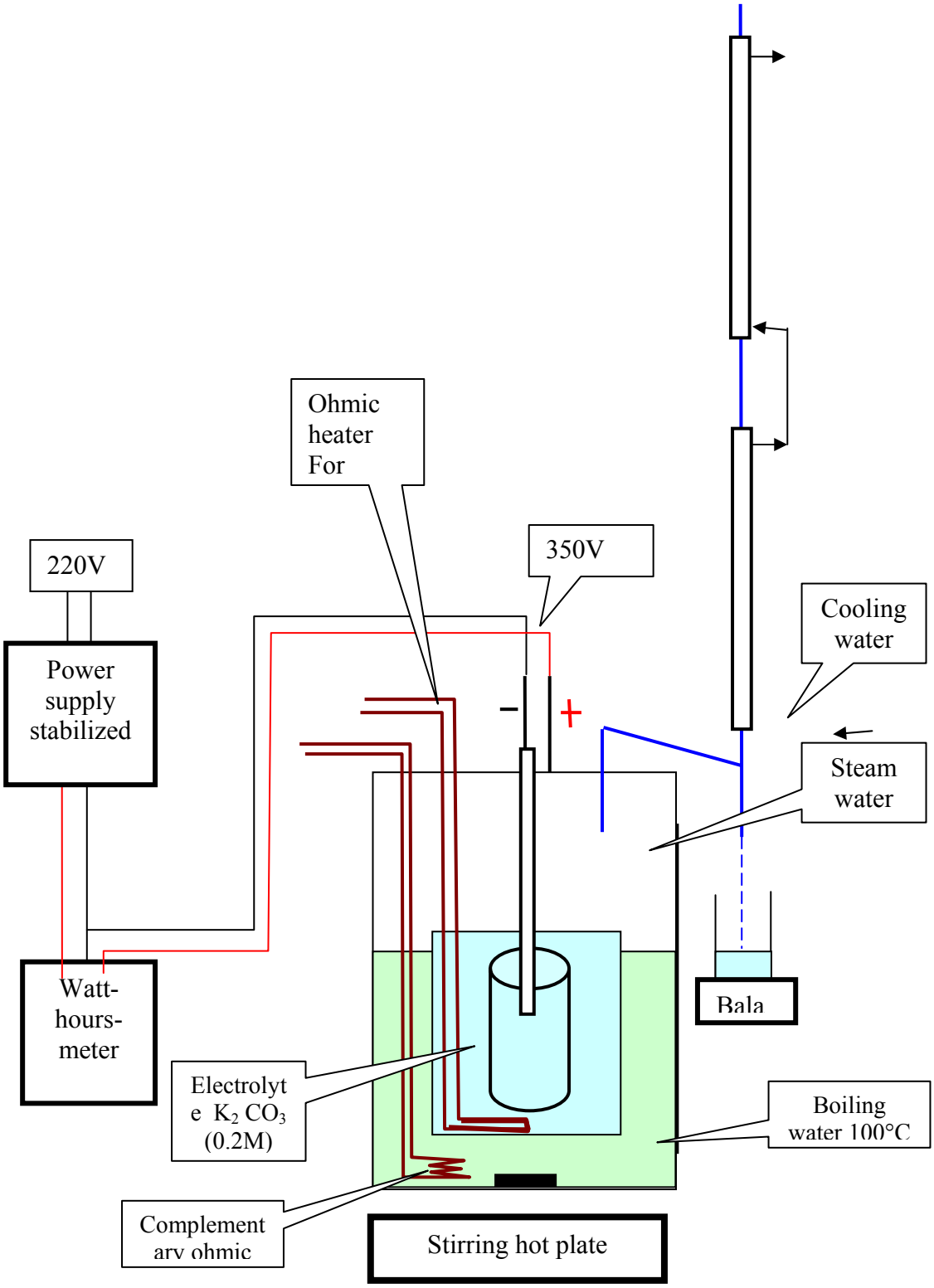

SETUP FOR MEASURING OF ENERGY BALANCE AT INTERACTION OF METALS AND HYDROGEN ISOTOPES GAS AT HIGH TEMPERATURES AND PRESSURES

V.A. Kirkinskii , A.I. Khmelnikov

Institute of Geology and Mineralogy, Siberian Branch of the Russian Academy of Sciences, Novosibirsk, prospect Acad. Koptyuga 3, Russia
E- mail: kirkinsk@uiggm.nsc.ru

The setup was designed for investigation of fusion reactions in gas - solid systems at temperatures up to 1000 K and pressures up to 5 MPa. The reactor is designed as two coaxially positioned steel tubes. The inner tube has a closed bottom. The external tube has thread and autoclave valve. On the outer tube of the reactor a heat exchanger is mounted, thermally insulated from outside. A fine grained palladium powder was placed into the reactor. The reactor is connected to a vacuum pump through a drainage-type vacuum valve and a receiver. Resistance furnaces are placed in the inner tube of the reactor. The electric energy input is measured by watt - hour meter of active energy with an accuracy of ±0.5%. The energy output is calculated on the heat capacity and mass of water, which has passed through the heat exchanger. Two operating modes were used: stationary and circling. The error in the measurement of the released energy is ±1.5%. Results of preliminary determination of energy balance at interaction of palladium and deuterium are presented.

A setup was designed for investigation of fusion reactions in gas - solid systems at temperatures up to 1000 K and pressures up to 5 MPa. It is based on our patents [1 - 4].
A scheme of the setup is shown on the fig. 1.

The reactor is designed as two coaxially positioned steel tubes. The inner tube in outer diameter 40.2 mm has a closed bottom. The external tube in internal diameter 56.7 mm has thread and an autoclave valve. The tubes were welded at one end through a steel washer. The working reactor capacity is nearly 300 cm^3.

On the outer tube of the reactor a heat exchanger is mounted thermally insulated from outside by layers of asbestos and isocyanate foam. The cooling distilled water is fed from the thermostat through thick-walled rubber hoses with incorporated thermocouple elements connected to measure the temperature difference of the water entering and exiting the heat exchanger.

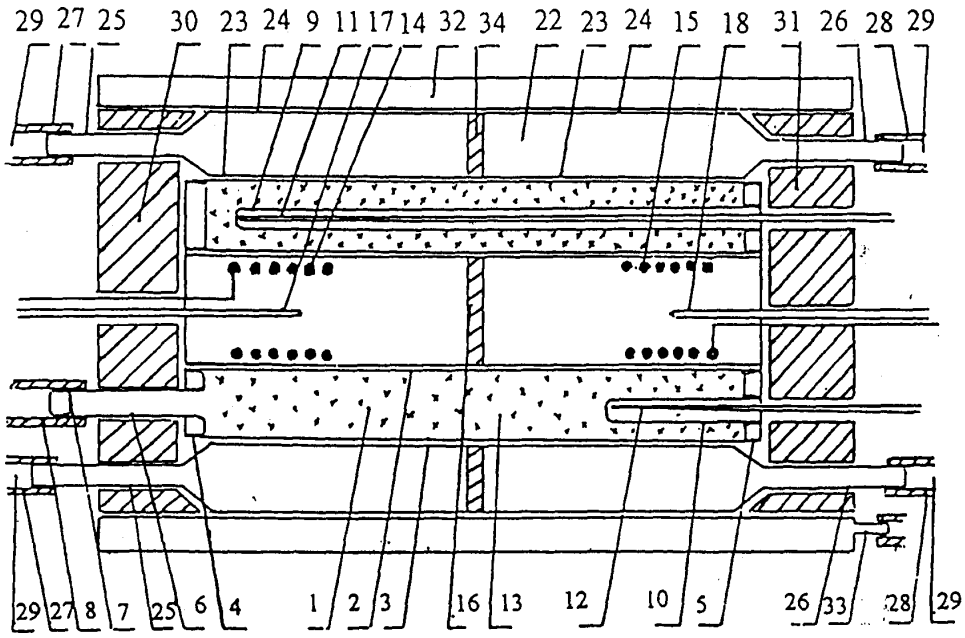

Figure 1. Scheme of the setup for measuring of energy balance.

Notations: 1-reactor, 2-internal tube, 3-outer tube, 4,5-seals, 6-through nipple, 7-fiilter, 8- high pressure line, 9,10-pockets, 11,12-thermocouples, 14,15-resistive heaters, 16-screen, 17,18-thermocouples, 22-heat exchanger, 23-internal tube of heat exchanger, 24- outer tube of heat exchanger, 25,26-nipples, 27,28- connecting hoses, 29-heat carrier (water), 30,31-covers, 32-heat insulator, 33-through nipples, 34-partition.

A fine grained palladium powder with particle size 30-100 nm was placed into the reactor. In another series of runs we used a granulated powder of γ-Al_2O_3 with great surface (more than 100 m^2/g) on which small palladium crystals (size 20 - 30 nm) were deposited (7 % from Al_2O_3 weight).

After charging the reactor with the working substance the tightening copper ring was plastically deformed through an obturator by means of a packing nut. The reactor is connected to a vacuum pump through a drainage-type vacuum valve and a receiver. The reactor vacuum treatment is performed until the pressure was less than 1Pa. Then the necessary quantity of deuterium gas produced by chemical interaction of lithium with heavy water (99.9 % D_2O) was fed into the reactor, and the latter was hermetically sealed with a high-pressure needle valve.

Resistance furnaces are placed in the inner tube of the reactor. The electric energy input is measured by watt-hour meter of active energy "Mercury 200" (exclusive the energy consumed by a transformer) with an accuracy of ±0.5%.

The output energy Q_{out} was determined on the formula:

$Q_{out} = C_t$ *·m * (t_{out} - t_{in}),

where: t_{in} - temperature of the water entering into the heat exchanger,

t_{out} - temperature of the water exiting from the heat exchanger,

C_t - heat capacity of the water at temperature (t_{in} + t_{out}) / 2,

m- water mass passed trough the heat exchanger during a run.

The difference in the temperatures of the water flowing into the heat exchanger and out of it was measured every 10 seconds and was averaged over the experience time.

An error of determination of output energy is put together from the error of determination of water mass passed trough the heat exchanger, the error of heat capacity estimation and the error of temperature difference determination by the differential thermocouple.

The total mass of the water having passed through the heat exchanger is measured by weighting with an accuracy of ±0.5%. The error of heat capacity determination depends on a small temperature drift of the water entering into the heat exchanger (not more than ± 0,5%) and comes to only ±0.05%. The error of temperature difference determination by the chromel-alumel differential thermocouple was determined in run series using mercury thermometer having the error ±0.05% and equals ±0.13%. The integer root-mean square error received by summing of all errors equals ±1.5%.

The experiments were performed on our theoretical computation of probability of deuteron interaction in the crystal structure of palladium deuteride [5 - 7] and on the suggested methods for its intensification [1 - 4].

Energy balance was measured at the interaction of a fine grained palladium powder with gaseous deuterium at temperatures up to 700^{o}C at pressures up to 600 kPa with the help of developed setup and method. More than 200 runs were conducted at constant temperatures and at circling by a temperature rise and its reduction to the initial level. It was shown that in comparison with runs at the same pressures of air, argon and usual hydrogen reproducible energy outputs take place, measuring 20-30 % from the input energy. That is more than tens times exceeds the integer root-mean square error of our measurements. High excessive energy outputs, hermetically sealed reactor, stationary and circling regimes of experiments exclude any chemical cause of the energy excess.

Ranges of temperatures and pressures were found most favorable to excessive energy output, a dependence of the last one was found also from preparation method of palladium and from other factors. After a repeated check-up of these experiments a detailed description of their results will be published elsewhere.

Such a setup can be manufactured with much greater reactor volume and energy output trough increasing of its length and diameter. The relative excessive energy output is expected will also grow. The developed method of balance energy measuring can be used for optimization and characterization of heat generators, which will be built on the base of the created setup.

Reverences

1. V.A. Kirkinskii, Method and device for producing energy and obtaining tritium, helium and free neutrons, *International patent application* PCT/RU93/00174, G21 B1/00 G21 G4/02, Number of international publication WO 94/03902, 17.02.94, 30 p.

2. V.A. Kirkinskii, Method of producing of free neutrons*, Patent of the Russian Federation* № 2056656, Bulleten "Izobretenija, towarnie znaki", March 20, №8, part II, 267-268 (1996).
3. V.A. Kirkinskii, A.I. Khmelnikov, Ustroistwo dlja poluchenija energii Power producing device, *Patent of the Russian Federation* № 2195717, Bulleten "Izobretenija, towarnie znaki" №56, December 2002.
4. V.A. Kirkinskii, A.I. Khmelnikov, Power producing device, *International patent application* PCT/RU02/00336, G21 B1/00, Number of international publication WO 03/0019576 A1, 06.03.2003, 30 p.
5. V.A. Kirkinskii, Yu.A. Novikov, *Theoretical modeling of cold fusion,* Novosibirsk, Novosibirsk State University, 105 p.(2002).
6. V.A. Kirkinskii V.A., Yu.A Novikov, "A new approach to theoretical modelling of nuclear fusion in palladium deuteride", *Europhysics Letters*, **46**, No.4, 448-453 (1999).
7. V.A. Kirkinskii V.A., Yu.A Novikov Yu.A., "Modelling of dynamic screening effects in solid state", *Europhysics Letters*, **67,** No.3, 362-368 (2005).

This work is supported by RFBR (grant No 05-05-64930).

TRITIUM RELEASED FROM INTERIOR'S EARTH: EVIDENCE FOR NATURAL NUCLEAR FUSION

Songsheng Jiang

China Institute of Atomic Energy, P O Box 275(49), Beijing 102413 China

*** E-mail: ssjiang@iris.ciae.ac.cn**

Abstract

Detection of tritium in the Earth's interior is a key to explore natural nuclear fusion in deep Earth. Mantle helium isotopes and other volatiles will be released to the some of volcanic crater lakes. The ability of volcanic lakes to store magmatic gases can be used to detect mantle degassing. In this paper we demonstrate the observation of mantle tritium in the volcanic lakes. The excess ^{3}H and ^{3}He have been observed at the bottom of two volcanic lakes, Lakes Nemrut and Laacher. The excess helium isotopes are confirmed to be from the mantle. The excess ^{3}H in the both lakes might also originate from mantle source. To our knowledge, this is the first time to report a positive result on searching for tritium released from deep Earth. The "mantle tritium" concentrations are estimated to be 3.7 ± 1.1 TU in Lake Nemrut and >1.0 TU in Lake Laacher.

PLASMA-ELECTROCHEMICAL TRANSFORMATION OF ELECTRIC ENERGY IN HEAT BY WATER ELECTROLYTE

Velikodny V.Yu.. *Gavrilov S.V., Grishin V.G., *Popov Yu.A.

Institute of Applied Mechanics of RAS, Moskow, Russia
**Moscow Engineering Physics Institute (State University), Russia*

The laboratory of physical and chemical hydrodynamics is being engaged in development of plasma-electrochemical (PEC) technology during 7 years and, certainly, arising thus fundamental problems. Authors had been declared an opportunity of transformation of electric energy in heat in water electrolytes with transformation factor more then 1 [1]. During the development of «porous electrolyte» production technology [2] the optimum of electromagnetic and hydrodynamic fields interaction comprehensible to practical use has been found. In development of ballast water sterilization [3] «rectified effect» is received, allowing to generate the pseudo-stationary electric discharge (which authors suggest to name «volumetric-diffussive») for industrial needs. As a result authors register the application for invention [4] of ultraeconomic steamgenerator. The main reason of basic researches of plasma-electrochemical behavior of water electrolytes was the application right at the end of the XX-th century [5,6] about «supper heat» reception in such processes, besides various radiating effects are observed [7,8]. Therefore the above-state technological development of authors were necessarily accompanied by calorimetric and radiation appreciations. On the basis of the saved up experimental and theoretical data the model «the plasma-electrochemical water transformer of electric energy in heat» (BT) (which block-scheme is presented on fig. 1) is created. The scheme consists of the input block of electric energy (БВВЭ), the block of its transformation to energy of PEC-reaction (БПЭХ) and the block of thermal energy leading out (БВТЭ). By means of БВВЭ electric power from a municipal network (a pressure and ~ 220, 380 or 660 V) moves in BT by a phase to «cathode» and by «zero» to «anode», by means of БПЭХ on «cathode» «E.D.Zykov´s plasma closed spheroid» is formed (which authors suggest to name «plasmadynamic reactor») [9], enveloping «cathode», and by means of БВТЭ thermal energy is led out from BT in the form of saturated water vapor.

On the 13th March 2007 the model of a patented steamgenerator GAME - 3/4 (the application №2006143833 from 12.12.2006) has was tested. The model is presented on fig. 2 and it is a thermos established on balance (SW – 10) with a limit of weighting of 10 kg with error ±5 g. Thermos is filled with 3 kg of water with margin error ±5 g. The temperature of water in thermos is measured by device DT – 830C with thermocouple. The model joins in the municipal electric network (~220 V) for 15 minutes. Vapor development by model begins in an interval of time of 30 seconds after voltage, the formation of plasmadynamic reactor is proved by the sharp failing of current and characteristic sound claps.

In the first 15 minutes the temperature of water has been risen from 19 up to 66 degrees of Celsius, vapor was produced - 95 g and the transformation factor, calculated with formulas (see Fig. 3), was equal - 1,16.

After the short break which has gone on calculation, the second switching on was made, and in the second 15 minutes the temperature of water has been risen from 61 up to 102 degree of Celsius, vapor was produced 335 g and the factor of transformation has grown up to 1,37.
After the next short break the third switching on was made and in the third 15 minutes the temperature of water has risen from 89 up to 102 degrees of Celsius, vapor was developed 665 g, and the factor of transformation has grown up to 1,48.

The fourth switching on was made without interruption, only after switching-off the temperature in the natural order has lowered down to 100 degrees of Celsius. The fourth switching on for 15 minutes has given quantity of vapor 825 g and factor of transformation - 1,73. On the Fig. 3 the report of measurement and dependence of transformation factor from the start water temperature is presented.

On the Fig. 4 the outline for making pre-production model GAME - 3 / 4 is presented.

References

1. *V.Yu.Velikodny, V.G.Grishin*. Plasmadynamic generation of hydrogen in natural water. Proc. 11-th Russian Conf.on Cold Nuclear Transmutation of Chemical Elements and Ball Lightning.Dagomys,28 sept-5 Oct. 2003,M.,2004, p.25-36.
2. *V.Yu.Velikodny, V.G.Grishin*. Plasmadynamic forming of D_2-Li mixure for microbubble synthesis. Proc. 13-th Russian Conf.on Cold Nuclear Transmutation of Chemical Elements and Ball Lightning.Dagomys, 11 sept-18 Sept. 2005, M., 2006,p.176-186.
3. *V.Yu.Velikodny, V.G.Grishin A.D.Davydov, A.V.Eremeev, L.K.Nikitenko*. Plasma-electrochemical way of sewage treatment. Proc. 14-th Russian Conf. on Cold Nuclear Transmut. of Chemical Elements and Ball Lightning. Dagomys, Sept 2006, M., 2007.
4. *V.G.Grishin, A.D.Davydov*. Plasmadynamic reactor for neutralization of protons and Deutrons in natural water. Proc. 9-th Russian Conf. on Cold Nuclear Transmutation of Chemical Elements.Dagomys, 30 Sept-7 Oct 2001, M., 2002,p.106-114.
5. *E.D.Zykov, V.N.Scherbak*. Plasmachemotronic synthesis extremely energy saturated electrolytic substances in water solution of electrolytes. Proc. 7-th Russian Conf. on Cold Nuclear Transmutation of Chemical Elements. Dagomys, 27 Sept-2 Oct 1999, M., 2000, p.58-67.
6. *F.M.Kanaryov*. Water-the new source of energy. Krasnodar, Kuban State Agrarian University, 1999, 154p.
7. *T.Mizuno, T.Ohmori, T.Akimoto et.al*. // Probability of neutron and heat emission from Pt electrode induced by discharged in the alkakine solution. Fusion technology, 1997, vol.31, h210-215.
8. *Yu.N.Bazhutov, S.N.Yashin*. Regular reproduced radiating effects at electrolysis with gas discharge. Proc. 6-th Russian Conf. on Cold Nuclear Transmutation of Chemical Elements. Dagomys, 28 Sept-3 Oct 1998, M., 1999, p.24-33.
9. *V.G.Grishin, I.L.Klykov, S.V.Kopernik, N.V.Schavruk*. Anodic electrical discharge in electrolyte. Scientific session of MEPhI-2003, M., 2003, vol.4, p.119-121.

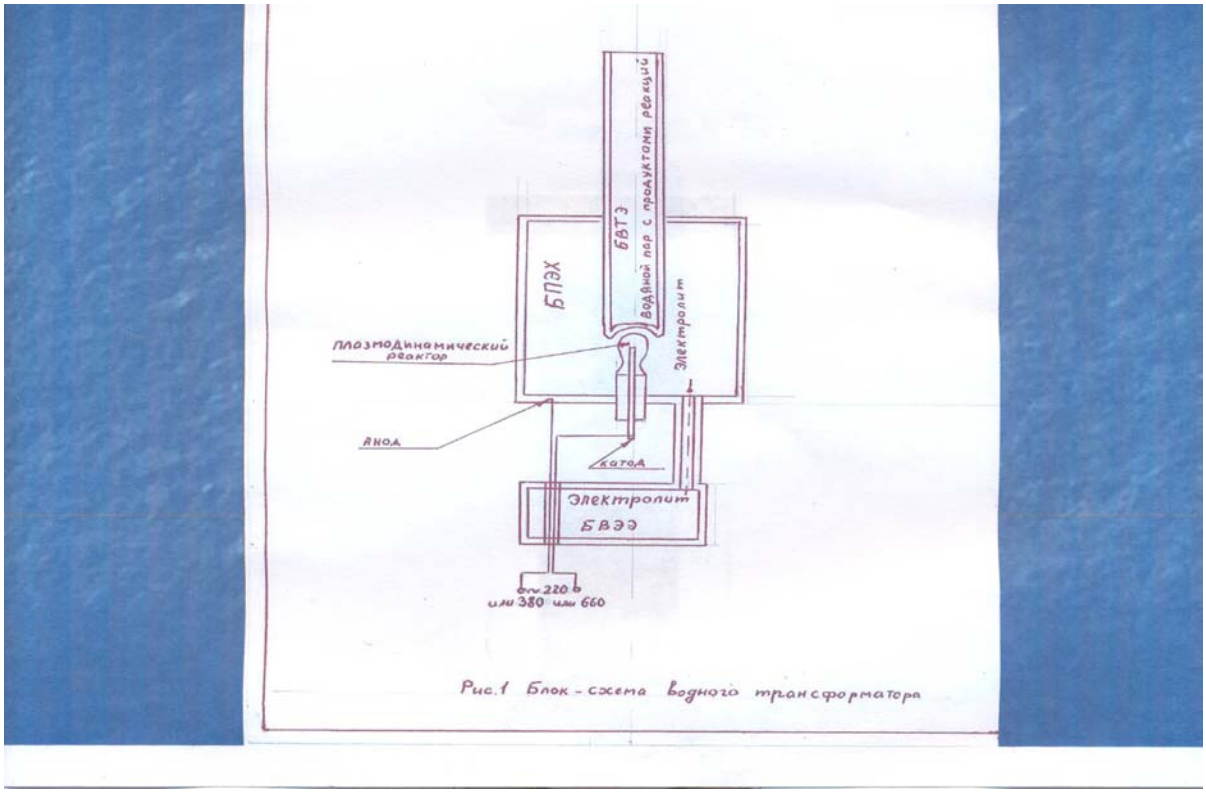
БПЭХ
БВТЭ
Водяной пар с продуктами реакций
Электролит
Плазмодинамический реактор
Анод
Катод
Электролит БВЭЭ
~ 220 в или 380 или 660
Рис.1 Блок-схема водного трансформатора

Fig. 1.

Рис. 2

Fig. 2.

$t_{начальная}$ воды	$t_{конечная}$ воды	$M_{выработанного}$ пара	$E_{электроэнергии}$	$Q_{тепловой}$ энергии	$K_{преобразования}$
19 °C	66 °C	0,095 кг	0,194 кВт ч	806,39кДж	1,16
$Q_{воды}$=3 кг х 47град х 4,19 кДж/кг.град=				590,79 кДж	$K_{пр} = \frac{806,39}{0,194 \cdot 3600} = 1,155$
$Q_{пара}$=0,095 кг х 2269 кДж/кг =				215,6 кДж	
61 °C	102 °C	0,335кг	0,256кВт ч	1259,12 кДж	1,37
$Q_{воды}$=2,905 кг х 41град х 4,19 кДж/кг.град=				499,00 кДж	$K_{пр} = \frac{1259,12}{0,256 \cdot 3600} = 1,366$
$Q_{пара}$=0,335 кг х 2269 кДж/кг =				760,12 кДж	
89 °C	102 °C	0,665кг	0,310кВт ч	1648,89 кДж	1,48
$Q_{воды}$=2,507 кг х 13град х 4,19 кДж/кг.град=				140,00 кДж	$K_{пр} = \frac{1648,89}{0,310 \cdot 3600} = 1,478$
$Q_{пара}$=0,665 кг х 2269 кДж/кг =				1508,89 кДж	
100 °C	102 °C	0,825кг	0,303кВт ч	1888,00 кДж	1,73
$Q_{воды}$=1,905 кг х 2град х 4,19 кДж/кг.град=				16,00 кДж	$K_{пр} = \frac{1888,00}{0,303 \cdot 3600} = 1,731$
$Q_{пара}$=0,825 кг х 2269 кДж/кг =				1872,00 кДж	

1. Потребляемая электрическая мощность (максимальная) – 12 кВт
2. Производительность по пару (максимальная) – 30 кг пара /час
3. Максимальное давление пара (потребителю) – 2,0 МПа
4. Максимальная температура пара (потребителю) – 200°С
5. Габаритные размеры установки: 600 × 600 × 1200 мм
6. Масса установки – не более 50 кг

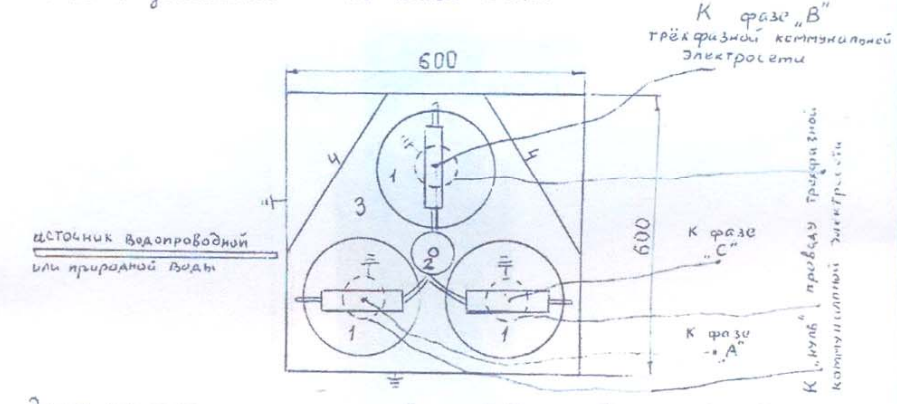

Эскиз контура установки – вид сверху. Вид спереди см. Лист 2

1. Модуль парогенератора мощностью 4 кВт – всего 3 штуки
2. Паровлагоотделитель – пар, вырабатываемый модулями поступает в один поз.2
3. Питатель водой, работающий за счет энергии вырабатываемого пара
4. Панель приборов контроля и регулирования работы установки

Fig. 3.

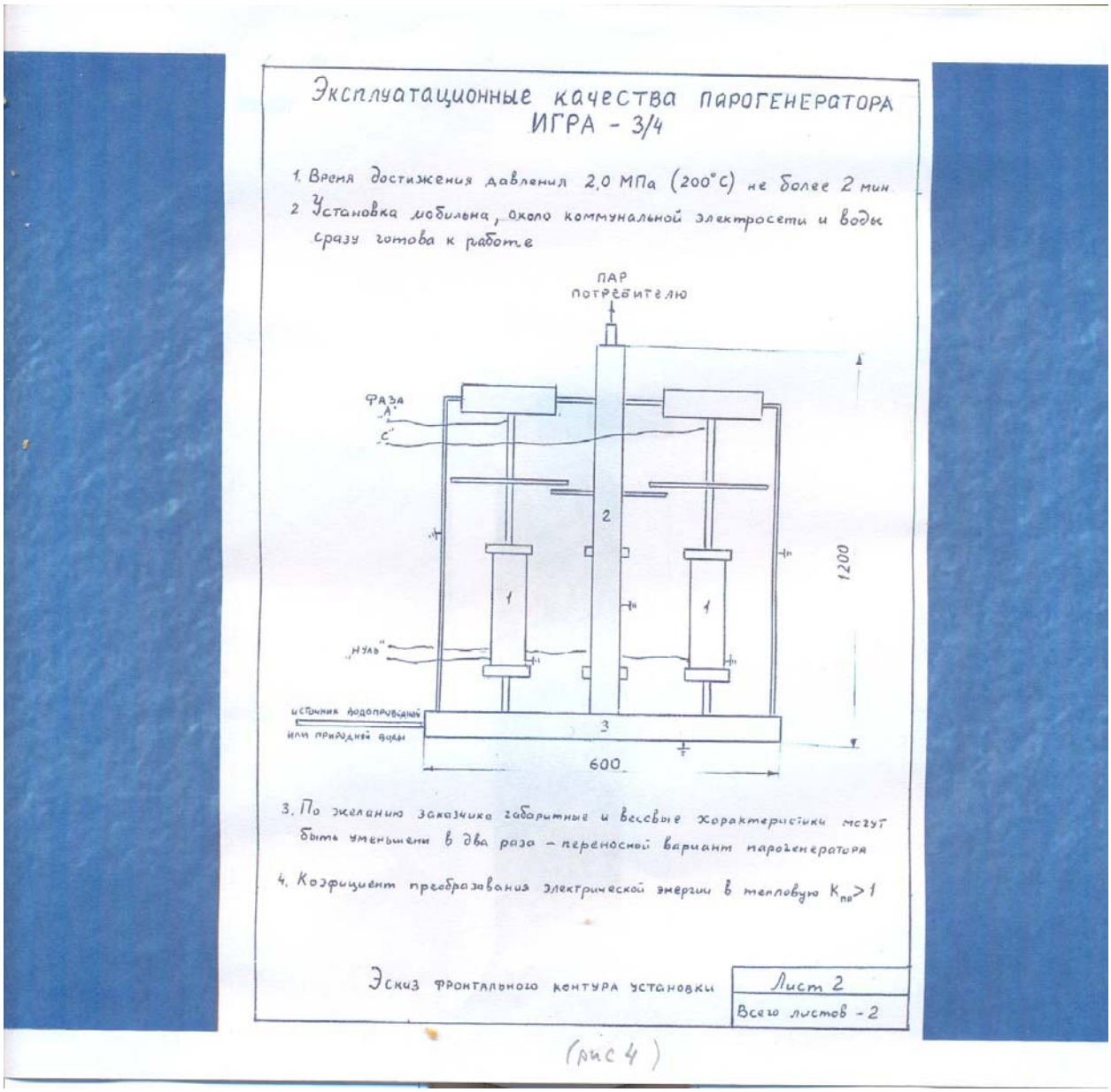
Эксплуатационные качества ПАРОГЕНЕРАТОРА
ИГРА - 3/4
1. Время достижения давления 2,0 МПа (200°С) не более 2 мин
2 Установка мобильна, около коммунальной электросети и воды сразу готова к работе
ПАР ПОТРЕБИТЕЛЮ
ФАЗА "А"
"С"
2
1
1
1200
"НУЛЬ"
ИСТОЧНИК ДОДОПРИВОДНОЙ ИЛИ ПРИРОДНОЙ ВОДЫ
3
600
3. По желанию заказчика габаритные и весовые характеристики могут быть уменьшены в два раза - переносной вариант парогенератора
4. Коэфициент преобразования электрической энергии в тепловую $K_{пв} > 1$
Эскиз фронтального контура установки
Лист 2
Всего листов - 2
(рис 4)

Fig. 4

PULSE ELECTRIC BREAKDOWN OF THE DISTILLED WATER AT MICRON INTERELECTRODE DISTANCES

I.V.Goryachev *, V.I.Karyaka **, M.M.Martynyuk **, N.V.Samsonenko **

** Russian Research Center "Kurchatov Institute ", Moscow*
*** Peoples' Friendship University of Russia, Moscow*

Abstract

Fast energy input in deuterated metal edges at their electric explosion in heavy water can lead to stimulation of nuclear reactions of deuterium synthesis owing to processes of the spinodal decay, homogeneous and spark cavitation. In the experiments there were determined the conditions for electric breakdown in distilled water, necessary for realization of electric explosion of deuterated titanic edge 10 microns of radius: interelectrode distance ≤10 microns, intensity of the electric field at the edge $\geq 10^5$ *V /cm*, duration of the electric pulse – several microseconds, time of the increase of electric tension before breakdown $\approx 5 \cdot 10^{-7}$ s. These electric characteristics correspond to the "bubbles" mechanism of breakdown of the interelectrode distance in liquid. In experiments the neutron emission due to the nuclear reactions of synthesis was not found out. The researchers came to the conclusion, that microexplosive mechanism of breakdown is more favorable for stimulation of nuclear processes. In this case under action of electrons emission from the cathode the phase explosion of the edge occurs, followed by a shock wave, explosive bubbles formation and their cavitations in deuterated titan. Conditions, for realization of phase explosion of the edge are rigid enough: time of pulse increase - no longer than 10^{-8} s, electric field intensity - some tens megavolts on centimeter. To achieve these parameters it is necessary to raise he electric field intensity for several orders by increasing the sours tension or the use of an interelectrode liquid with small dielectric permeability.

Introduction

Researches of electric explosions of conductors with the purpose to stimulate the nuclear reactions, including reactions of synthesis of deuterium nuclei, was carried out in many laboratories since the middle of the last century. The review of these researches is presented in [1, 2]. The scientists failed to reach the essential results in the investigations. In our experiments on electric explosion of titanic conductors, saturated by deuterium [3, 4], the neutron emission as a cause of nuclear reactions was not discovered. In these experiments the amount of energy managed to be put in the conductor before its destruction was essentially below the value, necessary for occurrence of local rise in temperature, sufficient for the beginning of the nuclear reactions. For further researches in this direction the analysis of physical processes has been lead [1, 2], which has specified the following possible

mechanisms, causing the local rise in temperature and promoting thus the stimulation of nuclear reactions.

Spinodal decay of the unstable liquid phase. If the time of intensive heating of a liquid in the boundary of thermodynamic stability is short enough, it is possible to enter the area of an unstable phase for which the factors of thermodynamic stability are negative. In these conditions the elasticity and thermal capacity of the unstable phase are negative: at isothermal expansion its pressure increases, and at isobaric heat removal its temperature raises. The surface tension for a unstable liquid phase is equal to zero, therefore the formation of vapor germs, limited by physical interface, is impossible. These features define the character of decay of the unstable phase known under the name of *spinodal decay*. At development of this process it is formed the continuous non-uniform structure, consisting of small compressed and extending elements without phase borders between them. As the thermal capacity of the unstable phase is negative, its factor of temperature conductivity $\Theta = \lambda / \rho \cdot C_P$ is negative too (λ - factor of heat conductivity, ρ - density, C_P - specific heat). From the equation of heat conductivity it follows, that temperatures differences, which have locally arisen in an unstable phase, do not disappear and exponentially accrue, until the system will not leave the area of instability. Thus, during the spinodal decay appear the "hot points".

Homogeneous cavitation. Researches have shown that during the conductor heating by the current impulse, the conductor liquefies, and in a liquid condition can be overheated significantly above a boiling point. At the approach to the spinodal the explosive mechanism of homogeneous formation and growth of vapor germs comes into effect that is the reason of explosion. Some of these germs grow, and others collapse, owing to what the intensive cavitational process arises (*homogeneous cavitation*). During the germs collapses there is a sharp increase of pressure and temperature of gas in it (for example, of deuterium). The ultraspeed metal heating is necessary for increase of intensity of this process. According to estimations [5], for a germ in the water, filled by air at T_0 = 300K, the values of parameters are equal: $P_{\max}$ = 7,8·10^8 bar, $T_{\max}$ = 3,7·10^6 K. In work [6] it is shown, that values of the maximal pressure and temperature in the germs of cavitation can be still above.

Spark cavitation. During the electric explosion of a metal conductor in *liquids* the "hot points ", besides homogeneous cavitation in the liquid metal, can arise due to the *spark cavitation*. At electric explosion of micro edges on the cathode there are local extractions of energy about 10^{-5} J in the volume of 10^{-9} cm^3 during 3 nanoseconds. There is a shock wave in the liquid thereof, and the cavities are formed, filled with the metal vapor. The cavities extend up to the maximal radius, and then make the decreasing vibrations. There is a warming of the gas, containing in the cavity, at each of its compression. Such mechanism of development of the *spark cavitation* proves to be true by experimental researches.

In work [1] it is shown, that the processes of occurrence of the centers of sharp local rise in temperature are easier for carrying out during the electric explosion of metal edges *in a liquid*. The mechanism of electric explosion of the edge is similar to electric explosion of the conductors; it is defined by the phase explosion of overheated liquid metal. The development of D,D-reactions in places of occurrence of " hot points " is possible, if the metal edges are saturated by deuterium. As these "points" arise at substance compression, the density of substance can be above normal density of the condensed substance ($n > 10^{23}$ cm^{-3}). The lower temperature for D,D-reaction ignition is required in the dense substance, as the height of Coulomb's barrier decreases with growth of nuclei concentration. During electric explosion of the deuterated edges the conditions for "hot points " occurrence and D,D-reaction

development are more favorable in the case of electric impulses of short duration (less than 1 microsecond). For stimulation of nuclear reactions the physical processes at explosion of metal edges should pass as follows. At submission of impulses of electric tension the micro edges of the deuterated cathode blow up under action of the current of autoelectronic emission. During the deuterated metal explosion the "hot points" appear owing to development of homogeneous and spark cavitation, and also during spinodal decay of an unstable phase. In the "hot points" D,D-reaction of nuclear synthesis starts. These processes can repeat continuously, as the new edges are formed after the explosion. The ultra disperse metal powder with particles of 10-20 nanometers in size is formed during the explosion, and in contact with cathode promote the development of additional microexplosions. To prove the fact of D,D-reaction it is necessary to measure the additional heat, due to this reaction, to register the output of D,D-reactions products: neutrons, helium-3 and tritium, and carry out the researches to reveal the new isotopes, which can arise at neutrons absorption by nuclei.

Experimental installation

To investigate the electric explosion of metal edges, the experimental installation has been created, the basic scheme and its design is presented on fig.1, 2. The discharge chamber K (fig.3) is filled by distilled water. The cathode consists of several titan edges (the sample of the edge see fig.4), the plane anode is made of titan. Electric impulses are periodically formed by means of the R-C discharge contour. The capacity C discharge through resistance R while the circuit is switch on by the spark interrupter B. Impulses of electric tension, arising on resistance R during the discharge, feed the electrodes of the chamber.

In experiments it is necessary to create near the edge the electric field of high intensity (more than 10^5 *V /cm*), and to have short impulses (less than 1microsecond) of big power and high electric tension. It imposes rigid restrictions on value of L, C and R. Capacity C should be sufficiently big to provide conditions for the spinodal decay at explosion of an edge, i.e. to put into area of explosion enough energy. In experiments C is equal to 0.1 microfarads. The inductance L of the scheme should be minimally possible. It means that the sizes of installation should be minimized. The appearance of the discharge chamber made of teflon is represented on fig.3. External diameter of the bottom part of the chamber is equal to 38mm. The edge cathode was made from the titanic wire 0,5 mm in diameter at its slow extract from the water solution of nitric acid with fluoric ammonium. The radius of the edge has the sizes of 3-8 micron (fig .4). Saturation of samples by deuterium was performed in the gas phase by technique stated in [3]. Deuterium absorption was estimated on pressure reduction in the chamber after the sample saturation. The duplicating measurements of absorption were made, based on weight change of the samples after their saturation. The titanic edges saturated by deuterium up to 60 nuclear percent were used in the experiments.

On fig.5 the oscillogram of discharge current is presented, the electric tension on the capacity - 3 *kV,* the value of resistance *R* is equal to zero, i.e. the circuit resistance is created only by wires of the scheme. The discharge represents typical decreasing vibration on which signals of electromagnetic noise are imposed. At *R = 4 ohm* the discharge becomes non periodic, but close to critical (fig.6). The tension maximum on resistance *R* reaches 1, 5 *kV*, the current is equal to 375 *A*.

Experimental results and their discussion

Realization in practice the ideas for electric explosion of the edges stated in [1], is connected with essential technical complexities. At submission of the impulse tension up to 10 kV of magnitude the breakdown of interelectrode water interval did not occur even at millimetric edge - anode distances. Unsuccessful also there was an attempt to carry out the discharge using the cathode from ultradisperse powder, received at electric explosion of titan wire in water. The analysis of experiments has specified essential distinction between conditions of electric explosion of conductors and explosion of edges in a liquid. In the first case the conductor initially closes the electrodes, forming steady electric contact. In case of the edges between the cathode and the anode there is a layer of liquid, which renders basic influence on process of formation of the electric discharge. In this case the mechanism of the discharge significantly depends on intensity of an electric field at the edge and time of the increase of electric tension. Mechanisms of discharge initiation in a liquid at a pulse discharge are studied in work [7]. Their essence consists in the following:

1) Electrothermal mechanism. The current provoked by a high voltage causes a liquid warming, especially in areas near the electrodes, where the field intensity is maximal. There is a liquid boiling, the ionization of bubbles, filed by vapor and gas, and formation of the plasma channel. This mechanism is realized at great values of product of specific electro conductibility by duration of tension.

2) ‘’Bubbles’’ mechanism. At this ignition mechanism of the discharge a main role play bubbles of gas, the sizes of (1-100) micron, existing on electrodes and in a liquid (optical supervisions show, that in the distilled filtered water permanently exist bubbles of micron sizes in quantity $(10^3 - 10^4)cm^{-3}$). The discharges in a bubble arise at achievement of the breakdown tension. After the discharge the field in the bubble decreases owing to shielding of the external field by the charges, which have settled on bubble walls. It causes decreasing or termination of the ionization processes. Action of the electric field on the settled charges leads to the bubble elongation, and to the charges movement deep into the liquid. The discharge ignition in the liquid will occur, when field intensity near the bubble pole will reach the critical value, and the avalanche duplication of electrons or the molecules autoionization in the liquid will begin. Bubbles mechanism of discharge ignition in water is carried out, when duration of tension impulse is equal to (1-100) microseconds and field intensity is of the order of 10^6 V/cm.

3) Microexplosive mechanism. The field intensity of nearby 10^7 V/cm of magnitude provokes the electron emission from the cathode into the liquid, fast local warming of the liquid, formation of a shock wave, the ionization of bubbles, and formation of the plasma channel. The basic condition for realization of this mechanism of discharge initiation - a high tension of the field near the electrodes and tension impulses of nanosecond durations.

4) Ionization mechanism. In this case the origin of plasma channel occurs directly due to the shock ionization of molecules of a liquid by the electrons or autoionization of molecules in the strong electric field . The realization of this mechanism of discharge ignition is possible if the field intensity is of the order of 10^8 V/cm and the impulse duration is less than 10^{-8} s.

At millimetric distances between electrodes in the experiments the fields intensity at the edge was nearby $2 \cdot 10^4 V/cm$ and its average values in the interelectrode interval was approximately $1 \cdot 10^3 V/cm$. These field values were insufficient for realization of water breakdown on mechanisms 2), 3) and 4). On the electrothermal mechanism breakdown could not occur, as time of an impulse in experiments (nearby 1microsecond) was to short.

The use of the ultradisperse powder, received at electric explosion in water of titanic wire, also has not solved the problem. Mass-spectrometer analysis (fig. 7) has shown in the powder presence of a plenty of oxygen. The titan -oxygen ratio in the powder shows, that titan contains in the form of Ti_3O_4, i.e. chemical compound $Ti_2O_3 \cdot TiO$, where titan is two and three valent. The titan oxides are not conductors. It is impossible to restore them to the metallic titan in the hydrogen atmosphere or in vacuum even at temperature of the order of thousand degrees. We failed to saturate this powder with deuterium using the saturation technology for titanic wire.

It is obvious, that for the purposes of stimulation of nuclear processes the most perspective is the area of parameters corresponding to microexplosive or ionization mechanism of breakdown. Conditions, for realization of these mechanisms of breakdown of a liquid rigid enough: time of increase of an impulse - no more than ten nanoseconds, intensity of the electric field at an electrode - some tens megavolt on centimeter. At lower values of parameters the breakdown of a liquid occurs on bubbled or electrothermal mechanisms, apparently, poorly effective for stimulation of nuclear processes. Hence, for success of the further researches in this direction it was necessary to increase the intensity of an electric field at the edge almost by three orders, and also to reduce time of increase of the impulse. In the further experiments this problem was solved by reduction of interelectrode distance. For this purpose in the design of the discharge chamber have been made changes: the top electrode has been established on the micrometric screw, allowing the adjustment of the interelectrode distances in a micron range. The chamber had two glass windows, allowing to measure interelectrode distance under a microscope. Also the value of resistance R has been increased. In this case the time of tension increase has become shorter, and electrode tension has rised.

The breakdown of the plane-edge distance was possible to carry out at the field tension on capacity ≈ 3 kV and the interelectrode distance near 10 microns. Under these conditions the field intensity at the edge reached the values of 10^5 *V/cm* and increased at interelectrode distances less than 10 microns. Time of the tension increase up to the maximal value is approximately equal to $5 \cdot 10^{-7} s$. These values of parameters correspond to the liquid breakdown on bubbles mechanism. Breakdown was accompanied by the bright flash observed through the windows. At the breakdown the resistance of the discharge chamber sharply decreased, shunting resistance R, owing to what the non periodic discharge passed in the mode of decreasing vibrations. After breakdown the part of metal (nearby 10^{-6} g) was pulled out from the edge, increasing the edge radius approximately 5 times, thus the interelectrode distance has extended for two orders. Thereof at submission of repeated tension impulses the breakdown of the interelectrode distance did not occur. For recurrence of experiment the replacement of the edge was required.

In experiments the neutron measurements have been lead near the discharge chamber during 0, 5 milliseconds after submission of the tension impulse (the technique of neutron measurements is stated in [8]). Two blocks from 10 proportional He^3 counters surrounded by paraffin moderator were used for neutrons registration. According to the measurements lead with use of the calibrated Cf^{252} source of neutrons, general efficiency of neutron measurements has been estimated in 3 %. Neutron measurements have not registered the signals testifying the D, D- reaction at the edge explosion. In the further it is planned to lead experiments with the use of heavy water instead of ordinary one. In this case the reactions of deuterium synthesis are possible not only in the titanic samples, but also in the liquid.

For stimulation of nuclear reactions of deuterium synthesis, as the carried out researches have shown, it is necessary to increase the field intensity up to several tens megavolt by centimeter, the time of the pulse increase should be reduced to tens

nanoseconds. Probably, the field augmentation by increase of the tension on the capacity is more suitable. In this case it will be possible to extend the interelectrode distance that can affect efficiency of the cavitational processes in the liquid volume. For increase of the field intensity in the chamber it is possible to use, instead of water, a liquid with smaller dielectric permeability, for example, deuterated acetone or others liquid dielectrics.

References

1. Martynyuk M.M., Kravchenko N.JU. Reaction of nuclear synthesis in mesophase substance during electric explosion. The applied physics (Russian), 2003, 1, p.79-90.
2. Martynyuk M.M. Phase transitions at pulse heating. Moscow, Publishing house RUDN.1999, 332 p.
3. Karyaka V.I., Martynyuk M.M., Samsonenko N.V. Experimental search of nuclear effects at thermocycling of deuterated titan and electric explosion of titanic samples. Bulletin RUDN. Series Physics, 2002, №10 part.1, p. 109-112.
4. Goryachev I.V., Karyaka V.I., Samsonenko N.V., Kholodov L.I. Analysis of element structure of titanic samples before and after electric explosion. Proc. of the 12-th Russian Conf. on Cold transmutation of nuclei of chemical elements. (Dagomys, Sochi, 2004),p.137-146.
5. Walton A. J., Reynolds G. T. // Advances in Physics. 1984. V. 33, №6, p. 595.
6. Kravchenko., Martynyuk M.M // Bulletin RUDN. Series Physics, 2000. №8, p.118.
7. Ushakov V.Ya. Breakdown of liquids at pulse tension. Tomsk, Publishing house of scientific and technical literature, 2005.
8. Dougar-Jabon V.D., Karyaka V.I., Samsonenko N.V. Study of the Neutron and γ-Emission From the Palladium-Deuterium System in the Process of the Transformation of the Crystalline Structure. Proc.of the 8 Inter. Conf. on Cold Fusion. Italy, 2000, p.219-224.

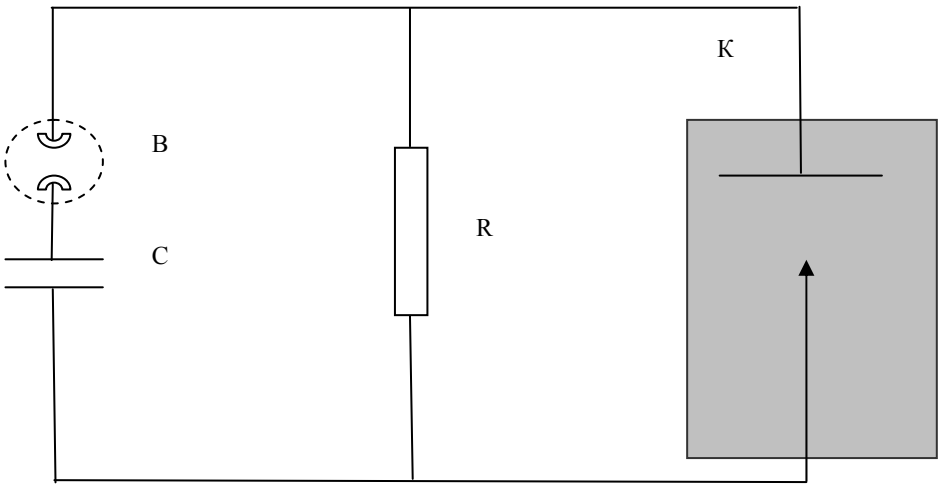

Fig.1.The basic scheme of experimental installation. B – spark vacuum discharger, K-discharge chamber, C-capacity, R- discharge resistance

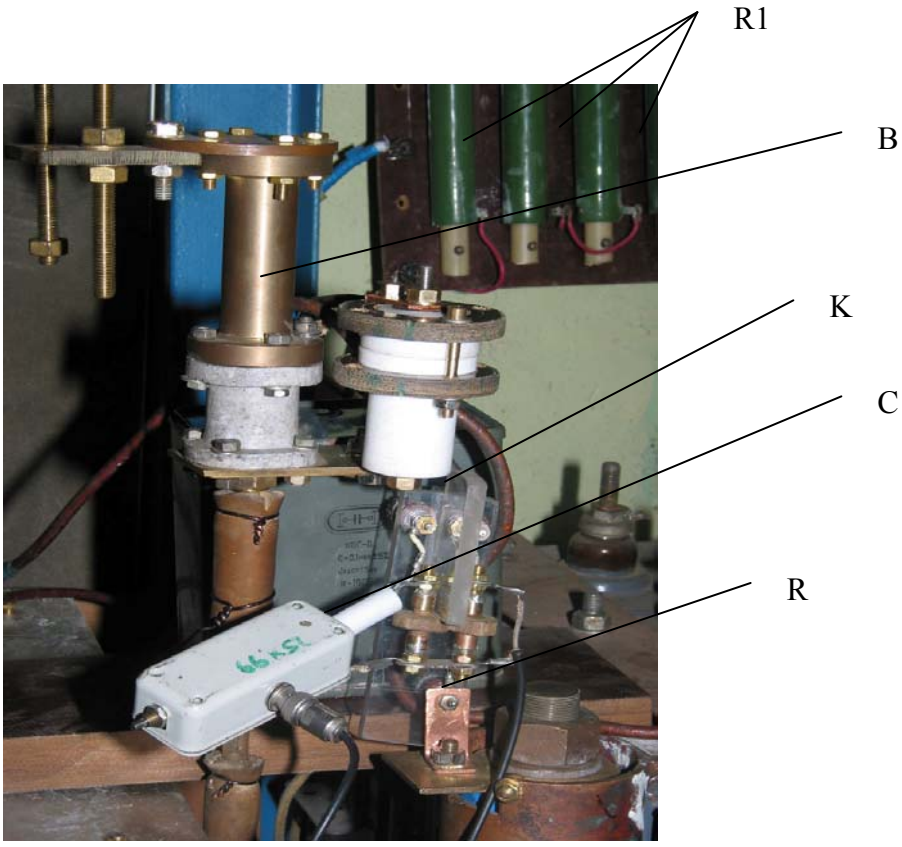

Fig.2. Experimental installation. R1-charge resistance, B – spark vacuum discharger, K-discharge chamber, C-capacity, R- discharge resistance

Fig.3. The discharge chamber

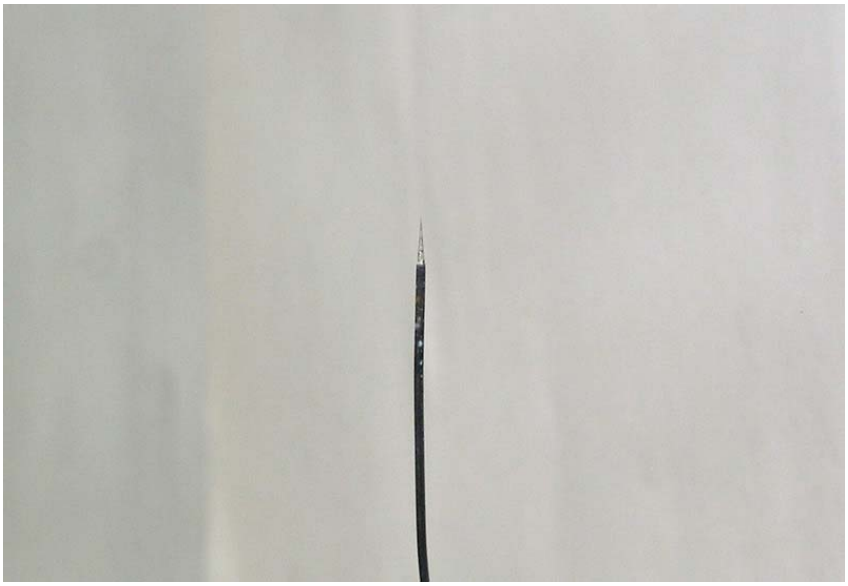

Fig.4. The edge made of a titanic wire

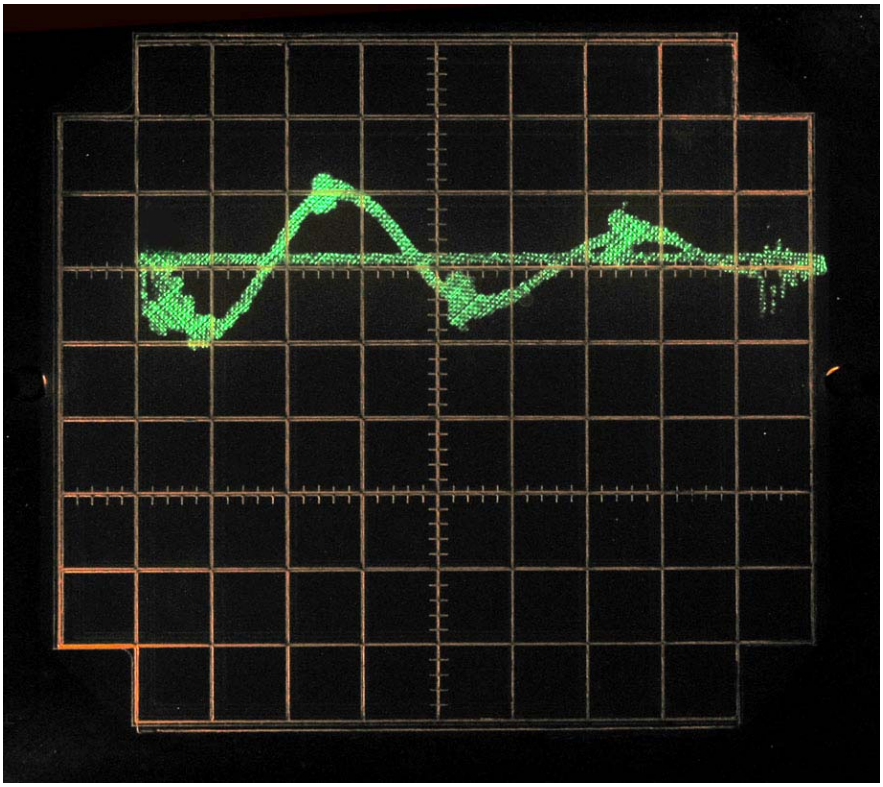

Fig.5. Current at the capacity discharge. Decreasing vibrations at small resistance R. One big horizontal division corresponds to 0, 5 microseconds.

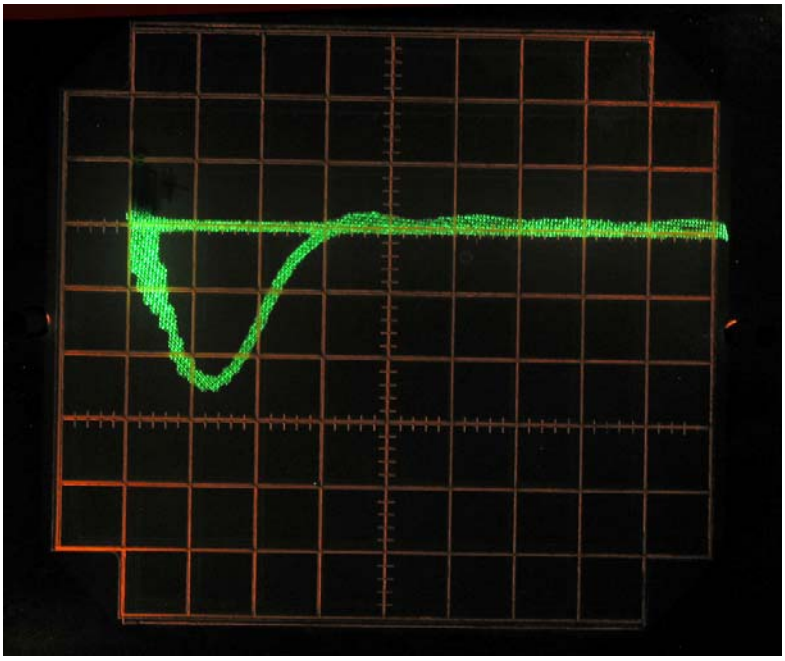

Fig.6. Current at the capacity discharge in non periodic mode. *R = 4 ohm*. One big horizontal division corresponds to 0, 5 microseconds.

	atomic % (before explosion)	atomic % (after explosion)
C	0,022	0,024
O	0,0000	57,25
F	0,0005	0,0050
Na	0,0097	0,10
Mg	0,0005	0,024
Al	0,0068	0,041
Si	0,011	0,049
P	0,012	0,0014
S	0,0204	0,0037
Cl	0,0024	0,0088
K	0,0023	0,11
Ca	0,0089	0,16
Ti	99,7475	42,21
V	0,0005	0,0003
Cr	0,0093	0,0065
Mn	0,0017	0,0010
Fe	0,115	0,059
Ni	0,0005	0,0022
Co	0,0146	0,0002
Cu	0,01	0,0048
Zn	0,0041	0,016

Fig.7. The analysis of deuterated titanic sample: sample before and after electric explosion in water.

EXCITATION OF HYDROGEN SUBSYSTEM IN METALS BY EXTERNAL INFLUENCE

I. P. Chernov[1],Yu. M. Koroteev[2], V. M. Silkin[1,3], Yu. I. Tyurin[1]

[1]*Tomsk Polytechnic University, Tomsk, Russia*
[2]*Institute of Strength and Materials Science, Russian Academy of Sciences, Tomsk, Russia*
[3]*Donostia International Physics Center, San Sebastian, Spain*

Abstract

The experimental results which point out to the existence of the hydrogen subsystem in solids and a possibility of its excitation by external influence are described. Occupying the equivalent positions inside host metal, hydrogen forms its own subsystem inside a crystal lattice and has vibration frequencies lying outside the phonon spectrum of a crystal. Under the external energy input (for instance by means of radiation) there occurs an excitation of vibrations of the hydrogen subsystem. The following facts point out to this: intensive migration, diffusion and release of hydrogen isotopes from metals at low temperature; super linear dependence of H, D release from metals on the electron current density and H, D concentration; H and D release from the whole volume of samples during the irradiation process by focused electron beam; H and D release in both molecular and atomic forms.

Introduction

Hydrogen in metals is very important technical and scientific problem. The technical problem is related to the negative influence of hydrogen on the mechanical properties of metals. Hydrogen produces different types of defects, cracks, and sample embitterment. Hydrogen is a lightest element and possesses high mobility in solids; hence metal-hydrogen systems present a special scientific interest for the study. Pons and Fleshman have initiated a great interest to the problem of hydrogen in metals in the connection of a so-called “cold nuclear fusion”. Numerous investigations have demonstrated that saturation of metals by hydrogen at electrolysis or in a glow discharge can lead to the excess heat, X-rays emission, change of isotopic and mass composition of metals. However all these processes, as a rule, are uncontrolled, realized spontaneously and their mechanism is unknown. One of the reasons of this is insufficient knowledge about the influence of an electrolytic medium and glow discharge on the behavior of hydrogen dissolved in solids.

In present report we discuss a new phenomena “Excitation of hydrogen subsystem in metals by external influence”, which helps us to understand the above enumerated processes.

Experimental results

Systematic investigations of influence of hydrogen and radiation (accelerated ions and electrons, X-rays, gamma- quantum) on metals properties have shown [1-4] the next: hydrogen atoms occupy regular positions in the crystal lattice forming their own hydrogen subsystem; the hydrogen subsystem is able to accumulate the external energy; the absorbed energy is distributed inside the hydrogen subsystem and, as a result, the hydrogen atoms kinetic energy is much higher than that of the matrix atoms.

The following experimental findings point out to the existence of the hydrogen subsystem in solids and on the possibility of its excitation by external radiation.

1. *Intensive migration, diffusion and release of hydrogen isotopes from metals at low temperatures.*

The hydrogen migration and release from metals caused by the accelerated ions was explored by the elastic recoil detection method. This method allows us to study the hydrogen migration in the sample irradiated by accelerated ions. Fig. 1 shows the change of hydrogen concentration in 12Cr18Ni10Ti stainless steel versus the radiation flux of the 12 MeV N^{14} ions for three depths x=50, 100, and 200 nm. In all layers the hydrogen concentration decreases in the process of irradiation. Similar results were obtained on other metals. A large yield of H atoms cannot be explained by the nuclear collision of H with nitrogen nuclei since the number of collisions calculated from the Rutherford cross-section is 10^8 times less than the corresponding experimental value.

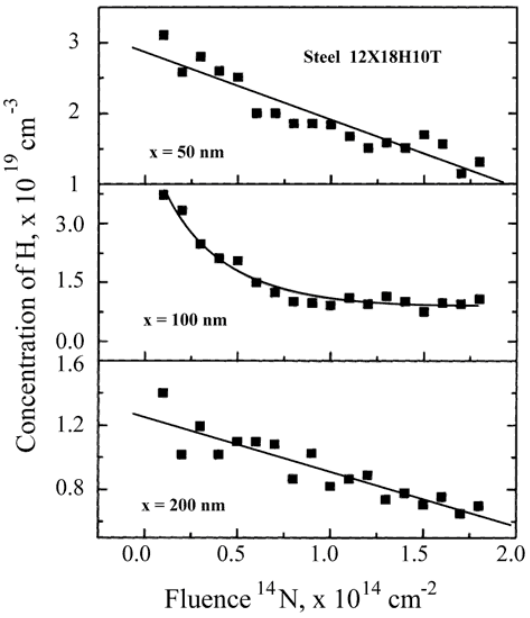

Fig.1. Hydrogen concentration dependence at different depths x on the N^{14} dose.

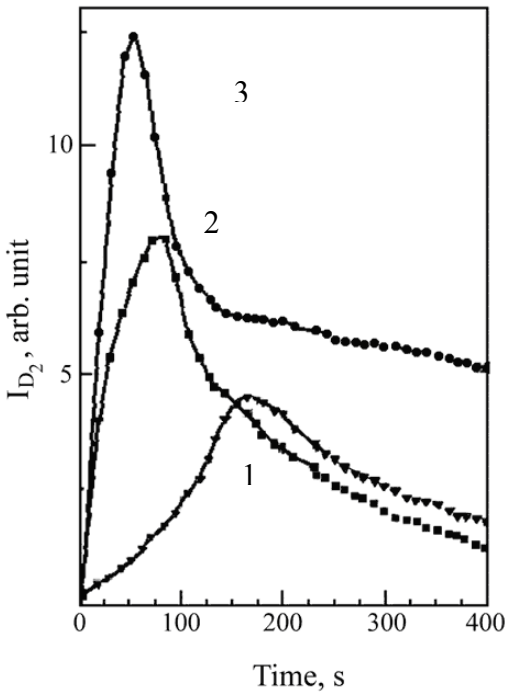

Fig.2. Intensity of deuterium release from stainless steel under the electron beam irradiation (U=20keV). 1: I=50 μA; 2: I=100 μA; 3: I=150 μA.

The hydrogen migration and release under the irradiation by the accelerated electrons and X-rays were studied in a high vacuum installation. This installation includes a programmed heating unit, a vacuum cell connected to a mass-spectrometer and an electron gun with energy of 10-100 keV. Metal samples were saturated with deuterium electrolytically. Loading with deuterium made possible to study the gas release alone, separating it from uncontrollable hydrogen presence in the vacuum system. In the process of radiation exposure the sample temperature was measured by a thermocouple. Under the electron beam influence U of 20 keV energy and the current I=50 μA, 100 μA, and 150 μA, the intensive release of deuterium from the stainless steel takes place (Fig. 2). The maximums of deuterium release rate at accelerated electrons irradiation are observed at the times of 150s, 60s, and 45s for I=50 μA, I=100 μA, I=150 μA, respectively. During these measurements, the temperature of the external side of samples in the electron beam area was not risen more than 60^0C, and on the rear side than 40^0C. In the absence of an electron beam the equilibrium release of hydrogen was not observed at these temperatures.

2. *Super linear dependence of H, D release from metals on the electron current density and H, D concentration.*

Dependence of H, D release from stainless steel and niobium on electron current density is shown on Figs. 3*a* and 3*b*. This dependence reveals that the collective interaction between the radiation and the hydrogen subsystem exists.

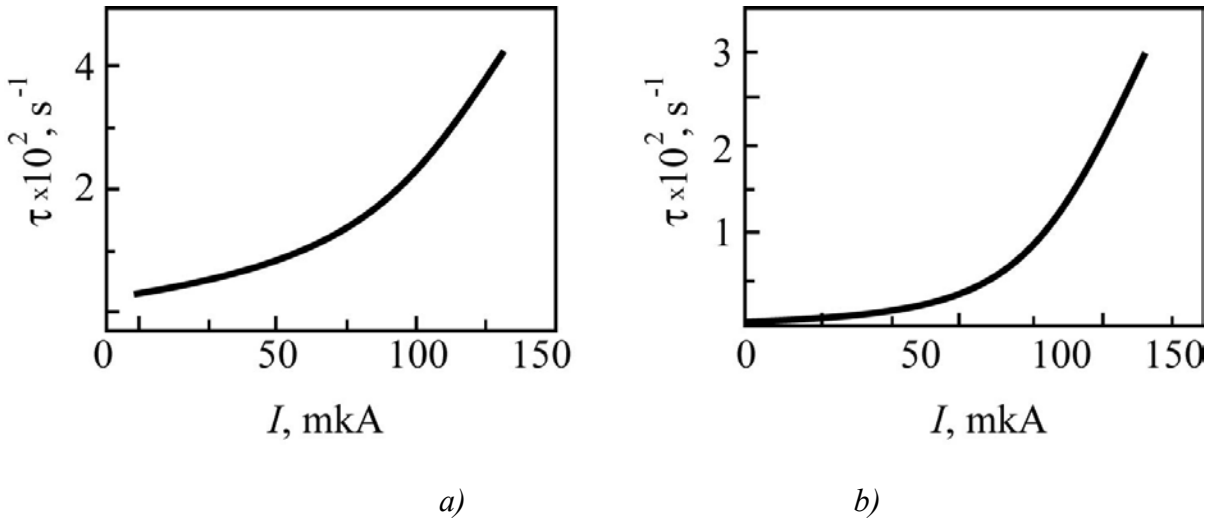

Fig. 3. Dependence of D release from *a)* stainless steel and *b)* niobium on the electron current density, I.

3. Hydrogen isotopes release from the whole volume of samples during the irradiation process by focused electron beam..

Hydrogen isotope release from the metals was studied at the simultaneous application of an electron beam and a linear heating. The area of the sample irradiated by the electron beam is 0,20 cm^2 that is much smaller than the total sample area (2-4 sm^2).

The linear heating along with the electron beam effect was accompanied by the maximum hydrogen release shift into the low temperature region (Fig. 4). This shift is 80°C in stainless steel; 125°C in niobium, and 65°C in palladium.

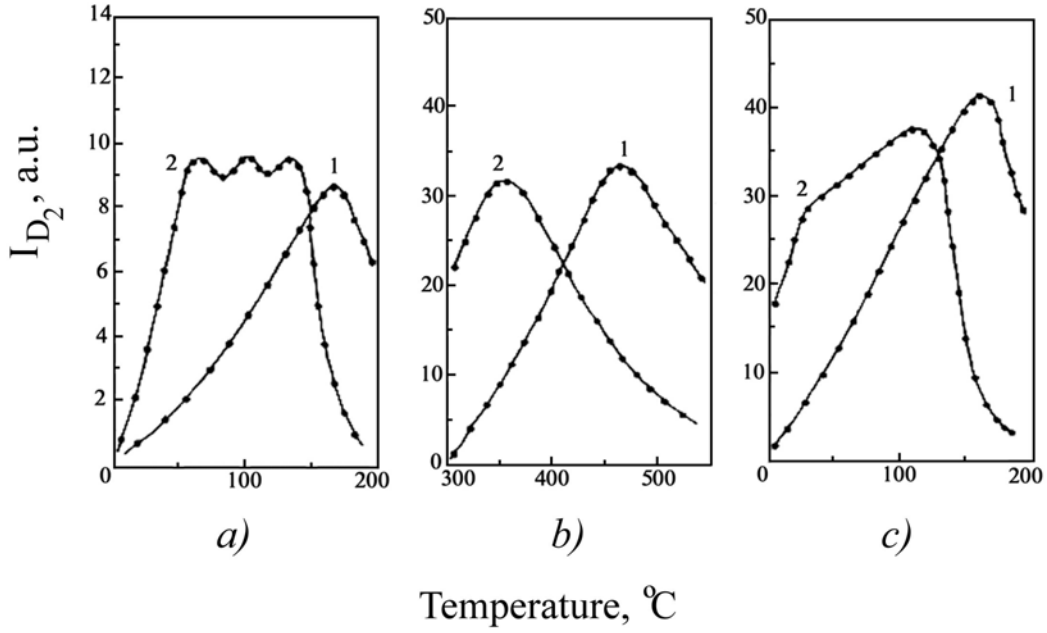

Fig. 4. Deuterium release from stainless steel (*a*), Nb (*b*) and Pd (*c*) versus the linear heating with the speed of 0,4 °C/s: *1* – without electron beam; *2* – with electron beam; *E* = 20 keV. The current I is *a)* 100 μA, *b*) 50 μA, and *c)* 20 μA.

4. Hydrogen isotopes release in both atomic and molecular forms.

The presence of released atomic hydrogen was measured by special dye-staff, which is sensitive to hydrogen in atomic form. The measuring method is based on the bleach effect of organic pigments placed on a catalytic substrate. Atomic hydrogen bleaches a dye-staff changing its color from red to white, while molecular hydrogen does not affect the dye-staff color. The bleach of the dye-staff is more effective when the longer is the hydrogen exposure and the greater its concentration. The bleach of the pigment by D and H atoms allows "to observe" the intensity distribution of atom release along the surface. The experimental scheme is presented in Fig. 5.

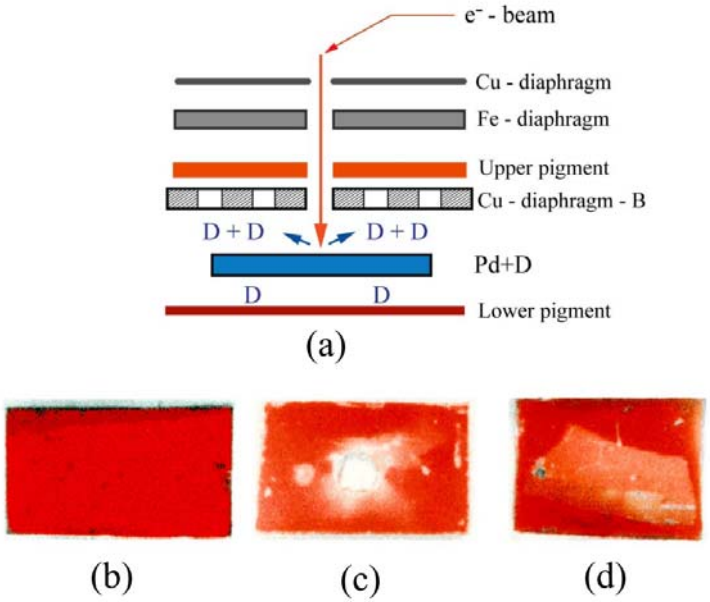

Fig. 5. The arrangement of the diagram and pigments at the Pd film irradiated by an electron beam: (a) the scheme of the experiment; (b) initial pigment; (c) a state of the upper pigment after irradiation; (d) a state of the lower pigment after irradiation.

In this experimental setup the copper and iron diaphragms form the e-beam. The second copper plate with holes was placed between Pd and the dye-staff. The whole "sandwich" was tightly pressed in order to avoid a lateral clearance between the Pd film and the plates. Measurements have shown that atomic hydrogen most intensively released under the direct effect of the electron beam (Fig. 5c). In addition, a weak release of D and H atoms was observed from the opposite side which was not exposed to the electron beam. This resulted in the appearance of the bleach region in the dye-staff in the form of the Pd sample (Fig. 5d). The bleach area in the dye-staff on the rear side of the Pd sample was uniform throughout the whole surface in its contact with Pd and had no peculiarities at the point opposite to the electron beam entrance. The uniform bleach of the dye-staff on the rear (not irradiated) side showed that D and H atom release is not connected with the thermal heating of Pd at the point of electron beam effect. The temperature on both the lower and upper sides of the irradiated thin (d ~ 0,15mm) Pd sample was practically the same, which was maintained by the thermocouples placed on the upper and lower sides of the sample. In our experiments it did not exceed 60-100°C.

The most important finding is that the hydrogen releases from metal not only in a molecular, but also in an atomic form. Moreover, the electron beam directly affecting only locally the sample excites the whole internal hydrogen subsystem.

Electron structure of the palladium hydrogen system

Unexpected observation here is that hydrogen diffusion is stimulated by ionizing radiation (accelerated electrons and ions, X-rays). It is known that ionizing radiation loses its energy in the process of collision with sample electrons producing exciting electron subsystem. Lifetime of these processes in metal is very small (10^{-15} - 10^{-16} s) and it is not clear how the energy from the electron subsystem is transferred to the hydrogen subsystem.

To answer these questions it is necessary to study the modification of the host electronic structure of metals by the presence of hydrogen. With this purpose the electronic structure of a pure Pd crystal in the FCC lattice and the Pd-H system in which the hydrogen atoms occupy octahedral sites have been calculated using the self-consistent linearized augmented-plane wave method. The *ab initio* calculations were performed within the local-density-functional approximation, using the Hedin-Lundqvist exchange-correlation potential. The valence states were treated in a scalar-relativistic approximation, while the core states were treated fully relativistic. Using thus obtained band structure the imaginary part of the dielectric function ε_2 in the energy range $\hbar\omega$ <18 eV has been calculated within the constant matrix element approximation.

Fig. 6 shows the calculated electronic densities of states for pure Pd and PdH. From comparison of the band structures of the pure Pd and Pd-H systems one can note the following characteristic modification of the pure Pd electronic structure upon hydrogen absorption:

- the filling of the *s* - band of palladium by the electrons of dissolved hydrogen;
- the lowering of the bottom of the conduction band due to hybridization of *s* states of hydrogen with *s*, *p*, and *d* states of Pd atoms;
- an upward shift of the Fermi level relative to the top of the *d* Pd band which results in a decrease of the electronic density of states of the system at the Fermi level.

It can be also seen from Fig. 6 that the presence of hydrogen in Pd lattice results in a pseudogap in the electronic spectrum of the Pd-H system lying the energy around ~4 eV. The presence of this pseudogap in the electronic spectra of the Pd-H systems indicates the appearance of a covalent component of the bond between palladium and hydrogen atoms in addition to the metallic bond characteristic of the pure palladium. It is known that in crystals with a covalent bonding a lifetime of electronic excitations is longer than in pure metals. Hence during this longer time hydrogen is capable to start to migrate.

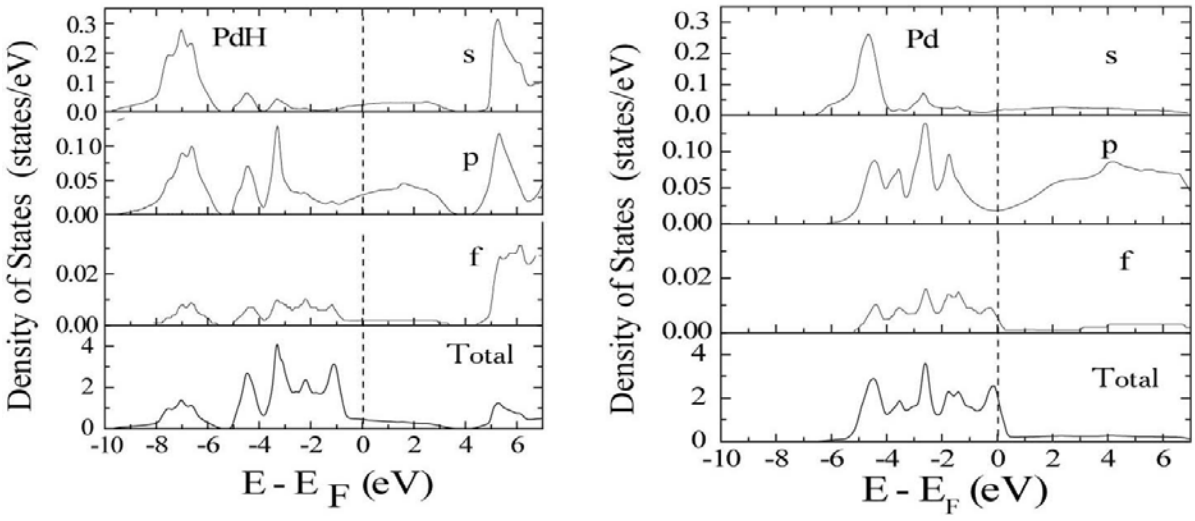

Fig. 6. Calculated partial and total electron densities of state for Pd and PdH.

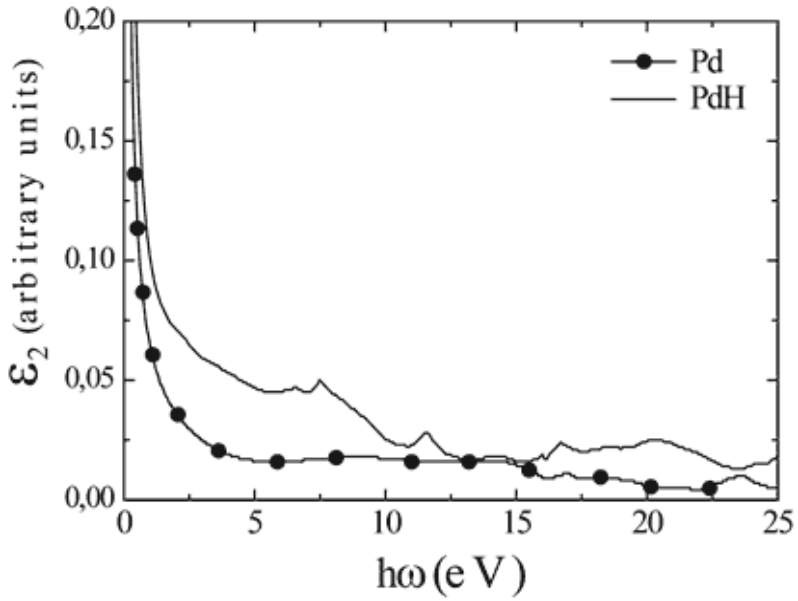

Fig. 7. Imaginary part of dielectric function ε.

Fig. 7 shows the calculated imaginary part of the dielectric function, $\varepsilon_2(\hbar\omega)$. From the figure it is seen that the presence of the hydrogen in the palladium significantly enhances the value of the dielectric function $\varepsilon_2(\hbar\omega)$ in the energy range from ~1.5 eV up to ~7 eV. This fact leads to the increase in absorption of the external influence energy by the metal-hydrogen system. Thus, one can conclude that the features of the electronic structure of the metal-hydrogen system can lead under the irradiation influence to the following effects:

- increase of lifetimes of the one-electron excitations due to the local character of the metal-hydrogen bonds;
- increase in absorption of the irradiation energy by the crystal due to the appearance of an additional electronic density localized in the vicinity of the hydrogen atoms.

At the next step we have studied the peculiarities of collective electronic excitations in metal–hydrides taking as an example the Pd–H system. Our calculations show that in both

pure Pd and PdH a large number of peaks is observed in the excitation spectra in agreement with existing energy loss experiments. Fig. 8 shows the dominant plasmon peak dispersions in the pure Pd and Pd–H systems. One can see that dominant plasmon energy in the Pd–H system is lower than in the pure Pd case.

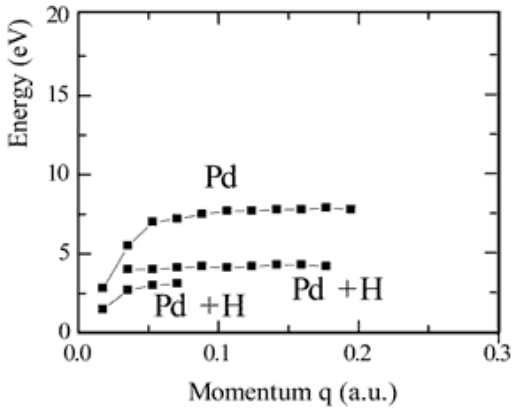

Fig. 8. Dispersions of the low energy dominant collective electronic excitations in Pd and PdH.

This fact indicates that probability of excitation of plasmons in Pd–H system increases in comparison with the pure Pd case. Hence one can suggest that in the process of ionizing irradiation large-scale oscillations of the electronic density are possible in the Pd–H system at lower energy. As a result, strong local electric fields can appear inside the crystals (Fig. 9) in which hydrogen atoms could be accelerated.

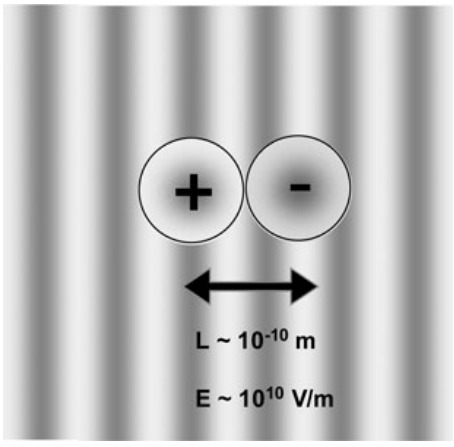

Fig. 9. Possible local electric fields inside a crystal due to plasmon excitation.

Hydrogen subsystem is able to be excited under a glow discharge. Hydrogen atoms in plasma have energy sufficient to excite plasmons in metal. Excitation of the hydrogen subsystem at electrolysis process takes place in a result of slam of hydrogen babbles. Slam of babbles is accompanied by emission of the low energy photons. Excitation probability can be increased in the case of draw of hydrogen babbles to a cathode. It can realized for instance by using of the porous films (example, nucleus filters).

Conclusion

During occupation of the regular positions inside a metal, hydrogen forms its own subsystem inside a crystallographic lattice of a host metal which has vibration frequencies lying above the phonon spectrum of a crystal. Under the input of energy, for instance, by means of radiation, electrolysis process, and glow discharge hydrogen subsystem can be excited. Non-equilibrium vibrations of the hydrogen subsystem are long-lived on the time scale of electronic relaxations in metals. Therefore, the diffusion of hydrogen can be stimulated by absorption of not only the energy of thermal vibrations kT, but also by the energy of non-equilibrium vibrations of hydrogen $\hbar\omega$ which exceeds kT. In the process of ionizing irradiation large-scale oscillations of the electronic density are possible in the Pd–H system at lower energy. As a result, strong local electric fields can appear inside the crystals in which hydrogen atoms could be accelerated. Excited hydrogen subsystem in metals is a specific medium, a high density and low temperature plasma, in which some exothermal chemical and nuclear processes can occur.

References

1. *I.P. Chernov, Yu.I. Tyurin,* J. Nucl Mater 233–237, 1118–22 (1996).
2. *I.P. Chernov, Yu.I.Tyurin*, Ju.P. Cherdantzev, Int. J. Hydrogen Energy 24, 359–62 (1999).
3. *I.P.Chernov, Yu.I.Tyurin*, Report of Russian Academy of Science 367 (3), 328–32 (199).
4. *I.P.Chernov, Yu.I.Tyurin*, Int. J. Hydrogen Energy 27, 829-837 (2002).

Processes in Gaseous and Plasma Media (GP)

CHARACTERISTICS OF X-RAY EMISSION FROM SOLID-STATE CATHODE MEDIUM IN ELECTRIC DISCHARGE SYSTEMS

A.B.Karabut

FSUE "LUCH" 24 Zheleznodorozhnaya St, Podolsk,
Moscow Region, 142100, Russia.
Tel. (095) 5508129; Fax (095) 5508129;
***E-mail** 7850.g23@g23.relcom.ru*

Experimental results on X-ray emission characteristics from the cathode material in the high-current Glow Discharge are presented. The X-ray emission ranging 0.6 – 10.0 keV and more with the dose rate up to 0.01 J/s has been registered. The X-ray spectra were registered on a film with the curved mica crystal X-ray spectrometer. The spectrum is registered both as bands of the continuum with energies ranging 0.6 - 4.0 keV and as spots resulting from the emission of series of high-density monoenergetic X-ray beams (with energies of 0.6 - 10.0 keV) characterized by small angular divergence. The energetic position within the above spectrum range is dependent upon the cathode material used (specific for a given cathode material) and looks similar to characteristic X-ray spectra.

The obtained results were the direct experimental evidence of existing the excited metastable energy levels with the energy of 0.6-10.0 keV in the solid of the cathode sample. Hypothetically, the mechanism of forming the metastable energy levels with the energy of 0.6-10.0 keV in the solid was caused by exciting the electron inner levels of the solid atom shells when bombarding the cathode surface by plasma ions. Hypothetically, the inverse medium population with the energy of 0.6-10.0 keV was created in the volume of separate crystals having the sizes of 0.1-0.01 mm.

CLASSICAL COLD SYNTHESIS. WHETHER IT EXISTS?

A.G. Krivshich, G.D. Shabanov, B.Yu. Sokolovsky, O.M. Zherebtsov

***E-mail**: kriv@pnpi.spb.ru,discharge@gtn.ru,boris@pnpi.spb.ru*

Ectons and explosive emission of electrons play a fundamental role in various types of electric discharges. Based on these concepts we have verified the results of the recent works that assumed existence of so-called "cold nuclear transmutation of chemical elements" and “cold synthesis” in particular. The results of those works are disputable and not evident. This relates to the empirical approach they used while “cold synthesis” requires high precision of parameters that is difficult to achieve in practice.

We show the problems related to the empirical approach and consider that “cold synthesis” ("cold nuclear transmutation of chemical elements") is actually Coulomb synthesis. By analogy with the recently introduced Coulomb explosion we suggest to change the notion of "cold synthesis" to “Coulomb synthesis”.

THE NATURE OF BALL LIGHTNING

G.D. Shabanov, A.G. Krivshich, B.Yu. Sokolovsky, O.M. Zherebtsov

E-mail: ***discharge@gtn.ru,kriv@pnpi.spb.ru, boris@pnpi.spb.ru***

We want to perform the laboratory ball of lightning (LBL). LBL is a hollow body; it has free like charges (negative charge) inside itself. LBL doesn't have free positive charges. LBL and natural ball of lightning have the identical mechanism of formation and of its lifetime. BL forms when the leader of a streak lightning stops (lightning stroke doesn't exist). The statistical data on ball of lightning in our hypothesis corresponds to the same data on streak lightning. The performed data confirmed by experimental way:

1. G.D. Shabanov // Technical Physics Letters. 2002. V28. №2. P164.
2. N.G. Shabanova, G.D. Shabanov // New Energy Technologies. 2004. №4 (19). P71.
3. G.D. Shabanov, B.Yu. Sokolovsky // Plasma Physics Reports. 2005. V31. №6. P512.
4. a) G.D. Shabanov, O.M. Zherebtsov //Proceedings of the 10-th Russian Conference on Cold Nuclear Transmutation of Chemical Elements and Ball Lightning. Dagomys, City of Sochi. 29.09-06.10.2002 (M: 2003). (RCCNT & BL-10). P285. b) N.G. Shabanova, G.D. Shabanov // RCCNT & BL-11. 2003 (M: 2004). P269. c) G.D. Shabanov, O.M. Zherebtsov // RCCNT & BL-11. 2003 (M: 2004). P279.
5. G.D. Shabanov, A.G. Krivshich, B.Yu. Sokolovsky, O.M. Zherebtsov //Proceedings 9th International Symposium on Ball Lightning (ISBL-06), 16-19 August 2006, Eindhoven, The Netherlands. P202.

BALL LIGHTNING OBSERVATION PROPERTIES
(Modern analysis)

V. L. Bychkov[1], D.V. Bychkov[2]

[1] *Physics Department, M.V.Lomonosov Moscow state, 119992, Leninskie Gory, Moscow, Russia*
E-mail: *bychvl@orc.ru*
[2] *Moscow institute of textile industry, Moscow, Russia*

Abstract

A review of observation data on ball lightning (BL) and their discussion is presented. Anew consideration of BL properties such as surface temperature and energy is given. New observations are represented, which show that BL could be warm and even hot object. Undertaken analysis shows that part of BL represents high-energy objects with hot surface. Traces left by BL speak about a possibility of thermal and electric impact of BL.

1. Introduction

Main set of ball lightning (BL) observation data had been gathered in a period from 60-ies to 90-ties of 20th century. Many investigators put efforts in collection of BL data including M.T. Dmitriev [1,2], S.Singer, I.M.Imyanitov [3], I.P.Stakhanov [4], A.I.Grigor'ev [5], G. Egeli [6], A. Keul, et al. They had collected large amount of data reflecting different manifestations of this object. However, analysis of these data did not give a complete picture of this phenomenon at that time.

M.T. Dmitriev, A.I.Grigor'ev, G. Egeli and S.I. Stepanov [7] considered BL as high energy possessing object. But I.P.Stakhanov [4] and B.M. Smirnov [8] after him thought that BL possesses moderate energy of density ~1-30 J/cm^3, M. Stenhoff [9] later came to the same conclusion.

M.T. Dmitriev considered BL surface as a hot substance in plasma state [1,2]. V.A.Saranin considered BL as charged ball, which surface consists of hot melted substance, however his work [10] was hard-to-reach and was out of the discussion. I.P.Stakhanov thought that BL surface is rather cold and is not higher than 500-600 K, however one can find in his book [4] several cases description of people burnt by BL (see below). These data did not change his opinion about BL temperature. B.M. Smirnov [8] has the same opinion.

Since books [4,8,9] were more accessible than references [1,2, 5-7], then namely positions of these books authors became mostly disseminated, and they lead to a result that an interest to BL as to an object with high energy was significantly dropped down in the end of 20-th century. And a concept that BL is low energy, rather cold, light, insignificantly electrically

charged formation became popular, several different theories or sooner hypothesis could describe these features [4,8], and BL became only a curious object.

At the same time most interesting BL features regularly appearing in BL observation descriptions came out of these theories field of vision, for example BL blowing out from socket couplers [11], coiling of fire filaments to fire balls [5], BL transformation to pancake, disc, tape and back into ball form [4,5,12], BL impact on jewelry [11]. BL with complex surface structure [12], branches and jets ejecting from the surface [13], etc., practically fell out theoretical analysis.

Fig. *Ball lightning photo made by V.L. Bychkov during a thunderstorm 31.05.2007, 5.30 AM, observation time1-1.5 s.*

Statistical analysis made in last decade of 20-th century [14-17] insignificantly enlarged BL features picture, it was connected with clarification of average BL properties on a basis of large set of observations. It had shown that increase of air humidity and electric field value lead to decrease of BL observation lifetime, and electric field influence is secondary effect with respect to humidity. This showed that BL can be charged formation; in this case it is sensitive to increase of humidity and electric field value.

BL color distribution correlation analysis [16] accounted 18 factors, which could influence perception of BL 6 main colors. Correlation coefficients for all these factors but four proved to be in 95% confidence interval with correlation coefficients from 0,903 to 1 for random sampling. Four factors were: observations in September, observations before thunderstorm and in nighttime, and observations of decaying BL. Number of observations in these four cases (factors) was considerably smaller than at other factors. This result was unexpected since BL color is its most important feature according to [8], which allows to conclude about BL.

Radiation losses logarithm via BL volume logarithm obtained on a basis of non parametric analysis proved to be different for different ways of BL disappearance.

Dispersion analysis of reference [15] had shown that a factor of BL location (indoors or outdoors) proves to be substantial for such BL parameters as a diameter, lifetime and radiated power: BL distribution over colors does not depend on their location.

Statistical analysis showed that exploding BL have the maximum specific energy and the smallest radiation ability. To the contrary BL becoming dim posses maximum radiation ability and the smallest specific energy. Decaying BL represent the intermediate case. BL that appear indoors are secondary with respect to outdoor BL. These results agree with conclusions made in [7].

It followed from analysis of these works that BL could be heterogeneous or composite formations with luminescent surface.

Investigations in a field of BL information collection were slowly continuing during last two decades [9, 11-20], they were developed to collection of new observations, statistical treatment of earlier collected BL observation cases [21] and more precise analysis of earlier obtained results.

The goal of this paper is attraction attention to some BL observation properties, which did not attracted special attention by a number of reasons or were forgotten.

2. BL energy

We have to emphasize that a number of BL manifests high-energy content [20]. In [4, observation case №35] was described an event of BL burning out a hole in metallic seat in an airplane. Estimate of metal melting and evaporation made by the author of this paper with a help of the observation data from [4] showed high energy density $W \approx 520$ MJ/m^3 (the author of [4] most probably used a value of BL diameter at BL energy density evaluation but not those of its radius, so he got a value by 8 times smaller). Estimate of BL energy density made on a basis of BL making a hole in window glass event [4, №30] gives $W \approx 100$ MJ/m^3, but it was considered in [4] as too high without any discussion. At that in [4] was expressed an idea that BL takes away charges induced on surfaces of different subjects during a thunderstorm, and then it transports charges realizing high energy effects. Sooner this opinion was based on energy estimates of BL energy density W~90 MJ/m^3 accounting for ionization, dissociation and probable chemical reactions in air. G.Egeli [6] came to a conclusion that BL has extremely high energy density $W > 10^3$ MJ/m^3 basing on high energy BL impact on subjects in Hungary. Analogous conclusions there were made in [7,20,22,23] basing on traces left by BL and polymer-composite theory.

3. BL thermal effects

It is usually different to separate thermal and electrical BL effects from observation, since impacts take place simultaneously . We represent below observations[2, 28], which are infallible proof of BL hot surface. These are some data from [2]. A bright ball attacked mountaineers in a tent. Its size was 5-7 cm, observation time was 10 s, the ball was hissing. Holes in sleeping-bags and on people bodies had appeared in places of BL touching. Holes in clothes and sleeping-bags corresponded to affected part of a body. There were 5 observers, one of them perished. Affections: burns of 2nd – 4th degree with covering 12 % of body surfaces.

In an article [28] doctors describe curing of burns gotten by a father and his daughter after BL hit them. The daughter had gotten burns of 2nd and 3rd degree of a hand, back and neck.

Curing was typical for the burns gotten at fires. Doctors came to the conclusion that BL had burned people, but an electric current had also hit the father, who had lost consciousness.

BL explosion took place [4, №5], which had led to appearance of charred spot on a floor, at that an observer had gotten burns on his foot. This can be explained by an impact of hot pieces of exploded BL on a man's body.

There is another case showing that BL can represent a hot or melted substance. The observer is M.V. Lozovsky (interview of 1994 when he was a student), an event of middle of July 1983-1984 . Settlement Voronovo near Moscow when the observer was 8 y.o. "It was in the second part of the day at 17-17.30. A thunderstorm with shower and lightnings had started. There was a strong wind, air temperature was 22°-23° C. My grandmother and I were returning from a forest. Suddenly in green round meadow we had seen a ball of 20-22 cm diameter at a distance 15 m from us. It was moving over a spiral-type trajectory. It was rotating: after touching of the earth it moved for 5 cm. It resembled a clew of woolen threads. The base red clew was covered by blew threads. Intensity of luminosity was as of 120 W incandescent lamp. We had become scared and quickly went away. Next day we had seen that the meadow surface was burnt out, its color had become brown-black."

In [4, №103] is described that an observer had collected fallen leaves at BL explosion in a crown of a tree "…small round or slightly elongated holes with charred edges had appeared (in the leaves). The leaves had been partially burnt around, part of a leave surface became thinner and shrinked. They had the appearance as if they were for a moment blown by a hot air from a campfire."

Six events in [9] also indicate thermal BL impact on subjects and people.

In Table 1 one can see newly analyzed observations with respect to BL thermal impact.

Table1. Events connected with BL thermal impact.

Effect	**Number of cases**	**percentage , %**
[4] Burns, fires, melts	Total number of events in collection 1293 Number of events described in [4] 120	4.9% 21 %
[5] body burns, fires	383	17%
[20] fires, melts	58	28%
[6] fires, melts, water heating	281	>25%

In the Table 1 one can see 4.9 % - often used number of thermal effects out of 1293 events collected by I.P. Stakhanov. We also represent the percentage of "hot" BL, which can be singled out from observation descriptions of [4]. In Table 1 we also represent the percentage of "hot" BL from different sources where detailed BL impact effects had been described. Our analysis have shown that it was "hot" in ~25% of events where it was near an observer or left traces on subjects, which it touched.

This great difference of statistical data indicates necessity of BL information additional collection on thermal and electrical traces left by BL. In particular it is most interesting to analyze events of BL penetration through glasses without their visible damage or at creation of unnoticeable holes in them.

In [20] one can find an observation, in which BL "penetrated through a glass" of a window leaving traces in a form of small holes.

Analogous observation was made by a professor of mechanics P.A. Zhilin and his wife I.A. Zhilina. It was in 1972 (interview of 2003). Lithuania, Laftyushniki settlement. July, evening 20.00-20.30. Thunderstorm conditions, but without raining, observation in a village house. "Luminescent object (a ball) of 8-12 cm diameter unexpectedly had appeared in a closed room. It moved firstly along a wall,

then over a ceiling. It covered the room perimeter of ~ 16 m. Suddenly it hit a bulb on a ceiling. Slight crackle has been sounded and the luminescence faded out in a form of blew splashes. Observation time was about 1 s. The bulb was transformed into a sieve uniformly covered with holes of 0.1-0.2 mm diameter."

Appearance of small holes in the glass at BL interaction speaks about mutual impact of temperature and electric charge on amorphous glass material, which separating into phases is dependent on electric field and temperature.

There are many questions about BL propagation through holes in glasses. Existing theory [29] speaks that if BL is a liquid ball with a surface non-interacting with a glass then it can flow through the hole under a pressure drop realized on both sides of the glass. The questing is: Why BL does not interact with the walls? The answer to this question can be connected with creation of a plasma layer over BL surface, in which electrons and ions create additional pressure at high values of E/N parameter (E is electric field strength near BL surface, N is neutral molecules density in this layer), which can be realized at high gas temperature of the layer.

A following observation also leads to BL image as of the "hot" object [13]. The event had took place 5 September 1995 during a day. " I (female) was doing something at the table at a distance of 2 m from a window, which was opened for about 10 cm. Suddenly something made me to put my head. I had seen (at a distance of 3,5 m from the window) lighting and maybe sparkling but not blinding ball. It was as if motionless hanging in the room space. It had disappeared after 1 s. Then deafening thunder clap had sounded, and a shower had started right after it.

Ball edges were quite determined, not smooth but slightly fuzzy. Its whole surface was as boiling. It consisted of hazardously located "hills" with brightly expressed peaks and deepenings between them. Jets were ejected from the ball in all directions, mostly continuing its radiuses. The whole system had different tints of metallic steel in the condition of pale-pink and white heating. The ball in general was intense-pink but not dark-pink. Peaks were more dark pink and spaces between them were sooner white. The ball diameter was about 35 cm, the distance between peaks was about 3 cm. Jets had forms of tubes, or cylinders to be more exact. Their length was different, up to 15-20 cm, and their diameter was about 5 mm. Near places of origination they sooner white, at ends – dark-pink, especially the longest. These jets acted as fountains in the gravitation field. Few of them, the longest, sharply changed their direction after reaching maximum height, and in a form of drops fell down on the ball surface. The distance between points of jet outlet from the ball was about 5-10 cm."

Such descriptions are rather often, for example there are 3 such descriptions in [13,18]. Represented data show that it is necessary to be cautious with conclusions about "cold " BL of books [4, 8-9].

Observations of BL blowing out of electric plugs and electron devices also lead to consideration BL as a hot object. One can find 3 new descriptions of this phenomenon in [13,18].

Observer S. Evdokimov (male). Winter, End of 1960, winter. Leningrad. **"**There was one window in the room. A massive socket was located on a wall to the right from the window. It was made of clay covered with white glaze. Cloth isolation on wires going to it was old, sparks appeared at taking a plug out of the socket.

Once in the evening I had to take a plug out of the socket. It was difficult to do it for sometime because the plug was densely sitting in the socket. Finally I had pulled it out, put it on a table and turning back had stood still. A bubble resembling a soap bubble was slowly blowing out of the socket. The bubble had separated from the socket when its diameter had reached 40 cm. It got up for 10 cm and hanged. Its color was alike the soap bubble color. The difference was that there was milk whitish tint besides bluish colors. White spot occupied a small place on a bubble, but they were constantly moving with respect to each other. Something alive was pulsating in the hanging bubble, as if some

vibration process took place in it. Concentric circles of non-regular form were located near the milk-whitish spots. Their color varied from pale-blue (near the spot) to dark bleu (fare from the spot). The bubble did not give any sound. It did not have a smell. It was transparent. By a form it resembled irregular sphere. Its form was changing in small ranges constantly. This ball radiated soft scattered light. Suddenly the bubble made several vibrations around a vertical axis, stood motionless for a moment and then smoothly had flown directly to the third finger of my right hand. I was not scared at that time and did not make any motion. The bubble had smoothly touched my third finger, was "pieced through" by my finger for a length of a nail, and quickly decreasing in volume had disappeared without any sound. I had felt warmth in the finger, which was flowing from the hand to the whole body (but my head), and then it had disappeared. I had gone out of numbness. My hands and feet were slightly trembling."

Analogous observation was made by V.B. Medvedev in 1985. During a day without a thunderstorm a ball of 15-18 cm diameter had been blown out of the socket of a radio transmitter. The observer also felt heat inside his palm when he touched the ball. Later made device investigation later had shown some insignificant melting of metallic parts inside it.

4. Properties of BL substance

Questions about uniqueness of BL substance directly side with questions about BL surface properties. For example in reference [4, №18] one can find a following unique event. "V.A. Bobrin associated professor from Khabarovsk city met BL in July of 1954, in the evening, before a thunderstorm, when he went hunting. It was about 20-25 cm in a diameter, white, it was moving horizontally copying a relief of an area. When it was at a distance of 15 m he made a shot into it from a scatter-gun. There was no effect after this; the ball had slightly shaken. BL went out of vision field after about 40 s, it had covered about 40 m."

A principle conclusion was made on a base of this unique observation in [4]: BL represents a gaseous matter, and its density is approximately equal to air density.

We represent now an observation of another observer. In the end of June 1972 a student of engineering specialty V.N. Nezamaikin went hunting near Dnepr river, near a settlement Kopos, Ukraine (interview of 1992). A sky was clear, there were no thunderstorm or atmospheric precipitation. When he was on an open place on a high bank of Dnepr river he suddenly had seen a glowing object at 7 m from him in rushes. It had been a ball of 10 cm in a diameter, it was of bright bleu color shining as an incandescent lamp of 100 or 200 W. BL was motionless hanging over a sedge, at a height of 60-70 cm over the earth. Its substance dense in appearance was unsteady vibrating resembling a soap bubble.

Without thinking for a long time the student made a case - shot into it. The ball size had been increased by one and a half times, after that it fell in pieces with a clap. Its unsymmetrical ragged form pieces became dim near water surface. The event lasted a minute or a minute and a half.

It follows from this description that BL was heavier then air, because its separate pieces were falling down, besides one can see description of its material extinguishing, as if it was a burning object.

Now let us consider a following observation of a professor R.N. Kuzmin (63 y.o. during the observation, an interview of 2002). Moscow. End of June 1997. Before a thunderstorm. Time-14.30. Leninsky prospect, a bridge over a railway line.

BL unexpectedly had passed by faces of observers (he was with his wife) at a distance of 15 cm. They had stopped and saw a bleu jelly-fish with slight yellow tint, its diameter was 10-12 cm. It resembled a living thin. A motion of a film was going over BL surface, its color tints were changing as on a soap bubble. No heat was felt from BL, a film was half-transparent. BL had flown behind hand-rail of the bridge and had descended to the railway. Then it goes out of the field of vision. The following

observation had shown that a discharge between electromagnetic brake shoe of the trolleybus and the current carrying wire had originated a white ball. The ball had separated from the place of origination, grew a little and had repeated the previous observation. BL smoothly flew over the hand-rail, descended and exploded almost without a sound in 1-2 meters from the earth surface with shaft of sparks. The size of the shaft had been larger then a meter in a diameter. BL had slightly decreased in sizes before the explosion, it had grown red, and dark core had appeared inside it.

Analogous observation of 40 cm BL appearance in a place of the trolley-pole connection with the wire is represented in [18 №6].

These two observations depict BL in a form of a ball, appearing in the place of the contact but not a lump of interknitted metallic threads as it was supposed in [8]. So also in this case detailed observations lead to another picture of the phenomenon. They have to be accounted for analysis in frames of BL observations total set and they have not excluded from it as it was recommended in [8].

5. To a question of BL meeting with airplanes

We had analyzed 73 meetings of luminous objects (LO) with airplanes in our work [29], 49 cases corresponded to the data of military pilots. Analysis of [33] had shown that inter-cloud discharges appear mainly from September to May, at the same time BL are observed mainly from May to September. Our correlation analysis had shown that main part of LO had been observed by pilots from September to May. Only in 18 cases out of 73 it was possible to affirm that there were BL. So the number of reliable cases is much smaller than it is accepted to think.

Questions connected with large sized LO, which follow airplanes during hours are attributed to LO of rainbow type [30]. These LO are formed at the Sun or Moon rays reflection from plane ice crystals in the atmosphere. These questions had been investigated in details in connection with crashes of airplanes [30]. Conception that pilots perceive optical effects but not real BL correspond to skeptical estimates of tremendous drag force $W \sim 10^4$ N [31], which has overcome 10 m diameter BL following a jetliner.

6. Rare BL properties.

Let us enumerate BL properties for which analysis it is necessary to additionally collect observation data and undertaking of laboratory experiments.

1. Rolling of BL up in a ball from a thread or a bar [5, №.22-23.], [4, №77,79]. Such known cases can be in principle explained if one supposes that BL is a melted charged thread. A behavior of melted tin leads to this idea. Additional laboratory experiments with unipolarly charged melts are required for clarification of the charge role.

2. Processes of BL blowing out of wires and plugs. Cases [4,№77; 11] and represented above require undertaking of experiments of plugs in conditions of high electric field overloading.

3. Magnetic BL properties. There is shortage of an information represented in [11] and description of a unique case of BL metallic subjects magnetization [33] for explanation of this phenomenon. However there is such a capability of subjects magnetization by electrically charged melted bubble [10].

4. BL capability of human body drag [11], displacement of metallic sheets [34] and of other subjects requires an additional information about thunderstorm conditions, presence of

thunderclouds, metallic roofs and other metallic subjects and their impact on moving objects. Inductive charging of metallic objects in a field of thundercloud can lead to observed effects of electrical nature.

5. Consider effects of disappearance of rings and bracelets [3,11] from hands of people. One of the latest cases was desribed by http://www.ufo.lv (ufolats). 10.06.06 O. Andreev , 42 year old, Rizhskyi gulf, near Yaunkemeri. Near 16.00 pm.

After bathing he was going out on the shore. Suddenly (by his wife' words) near him flew bright yellow-orange ball, of tennis ball size. Strong crash sounded. Andreev fell down with face in the sand. He did not lose consciousness, but was strongly inhibited, consciousness was scattered. When he was turned over his face was covered with soot.

People bathing in the gulf at that time felt noticeable current shock.

He was hospitalized. Before the event he had a golden chain on this neck, which had disappeared after this. A finger thick trace of burn left on his body. (On the photo one can see thin trace on his body widening near near his neck.) He was in the shock state with injuries of heels and genitals. After two days he returned home without serious consequences.

Represented example poses more questions than answers.

There is a shortage of existing information for analysis of such phenomena. In particular there is absence of an information about psychological state of observers. One can not exclude the following: observers can feel short time pain at electrical or thermal BL impact on metallic subjects (rings and bracelets), in conditions of psychological stress they put of these metallic subjects from their hands, and later they forget about their own actions. 8^{-th} case described in [11] leads to this supposition. The killed girl at supposed contact with BL got a ring burn on a place of a ring, but the ring had disappeared. It means that heating of metallic subjects on a men's body takes place during interaction with BL and also the burn of the body takes place.

7. Conclusions

Represented data allow to look afresh at the problem of BL. Our analysis shows that part of BL represent highly energetic objects with hot surface. Traces left by BL speak about thermal and electric impact possibility.

Data on BL blowing out and making holes in glasses can be result of BL surface high temperature and poorly investigated mechanisms of charged melts interaction with different substances (for example with glasses).

Statistics of BL meeting with airplanes is not so large as it accepted to think. At analysis of airplane meeting with anomalously long-lived objects one has to account for realization of optical illusions.

Analysis of observations shows a necessity of BL interaction with different subjects cases continuing collecting, and especially of left traces. In this case it becomes possible to get some numerical characteristics on BL properties.

Let us emphasize two facts that essentially complicate solution of BL problem. The first one is impossibility to use the single observation feature. We have demonstrated to what contradictory conclusions they lead. The second one is difficulty of observer's interview undertaking: witnesses usually give their information only once, it is a problem for an investigator to make them repeat their interview.

References

1) Dmitriev, M.T., Bakhtin, B.I., Martynov, V.I.., Zhurnal Tekhnicheskoi Fiziki . 1981. V.51. №. 12. P. 2567;
2) Dmitriev, M.T., Lakshin, A.M., Morozov, S.S., Ortopediya, travmotologiya I protezirovanie. 1986. №11. P**.** 66.
3) Imyanitov, I., Tikhii, D., *Behind scientific laws.* Moscow. Atomizdat. 1980.
4) Stakhanov, I.,P., *About physical nature of ball lightning.* Moscow. Energoatomizdat.1985.
5) Grigor'ev, A.I., *Fiery killers.* Yaroslavl. Debiut. 1990.
6) Egely., G. *Hungarian ball lightning observation.* Budapest: Centr. Research. Inst. Physics. Hung. Acad. Sci. KFKI-1987-10/D. 1987.
7) Stepanov, S.I., Zhurnal Tekhnicheskoi Fiziki . 1990. V.60. №.2. P. 211.
8) Smirnov, B.M., *A problem of ball lightning.* Moscow. Nauka. 1988.
9) Stenhoff, M., *Ball lightn*ing. New-York: Kluwer Academic/Plenum Publishers 1999.
10) Saranin, V.A., *Ball lightning model.B.A.* Perm, Glazov, 1986. Dep. VINITI 11.11.86. №7696-B86.
11) Likhosherstnykh, G.U., *in Collection of works Ball lightning in a laboratory.* Eds. R.F. Avramenko, V.L. Bychkov, A.I. Klimov, O.A.Sinkevich. Moscow. Khimia. 1994.
12) Grigor'ev, A.I., Grigor'eva, I.D., Shiryaeva, S.O*., In Collection of works Plasma chemistry.* Ed. Prof. B.M. Smirnov. Energoatomizdat. 1993. № 17. P. 218.
13) Bychkov, V.L., et al., *in Collection of works of 10-th Russian conference on cold nuclear transmutation of chemical elements and ball lightning,* Dagomys, city of Sochi, September 29 –October 6 2002.. Moscow.: 2003. P. 109.
14) Amirov, A.Kh., Bychkov, V.L Physica Scripta 1994. V. 50. P. 93.
15) Amirov, A.Kh., Bychkov, V.L. Physica Scripta 1994. V.50. P. 588.
16) Amirov, A.Kh., Bychkov, V.L. Physica Scripta. 1995.V.52. P. 222.
17) Amirov, A.Kh., Bychkov, V.L. Physica Scripta. 1996. V.53. N.2. P. 252.
18) Bychkov,V.L., Bychkov, D.V., Sedov, YuB., *Collection of works of 11-th Russian conference on cold nuclear transmutation of chemical elements and ball lightning,* Dagomys, city of Sochi, September 28 – October 5. 2003. Moscow.: 2004. P 244.
19) Grigor'ev, A.I., Shiryaeva, S.O., Grigor'ev, O.A., Kuzmitchev, Yu.B*., in Collection of works of 10-th Russian conference on cold nuclear transmutation of chemical elements and ball lightning,* Dagomys, city of Sochi, September 29 –October 6 2002.. Moscow.: 2003. P. 154.
20) Abrahamson, J., Bychkov, A.V., Bychkov, V.L. Phil. Trans. Roy. Soc. 2002. V.360. №.1790. P. 11.
21) Stakhanova, I.G., *Observational properties of ball lightning.* IZMIRAN. Preprint №5 (1148). Moscow. 2002.
22) Bychkov, V.L., Bychkov, A.V., Vasiliev, M.N., Klimov, A.I. J. Meteorology U.K. 1996. V.21. №206. P. 77.
23) Bychkov, V.L. Physica Scripta. 1994. V. 50. P. 591.
24) Singer, S. *The nature of ball lightning* . Moscow.Mir.1973.
25) Barry, J.D, *Ball lightning and bead lightning.* Moscow. Mir.1983.
26) Kozlov, B.N., Doklady AN SSSR 1978. V.238. P.61.
27) Wittman, A., Nature. 1971. V.232. 625. P.
28) Selvaggi, G., Monstrey, S., Von Heimburg, D., et al. Annals of plastic surgery. 2003. V.50. N.5. P. 541.

29) Amirov, A.Kh., Bychkov, V.L. *On the ball lightning interaction with airplanes*. Proc. 6-th Intern. Symp. on Ball Lightning. 23-26. August. 1999. University of Antwerp. Antwerp Belgium. P. 34.
30) Gaidukov, N.I., Zhurnal Tekhnicheskoi Fiziki . 1992. V.62. №.2. P. 27.
31) *Menzel, D.H., Flying saucers.* Moscow. Inostrannaya literature publishers. 1962.
32) Brylev, G.B., Gashina, S.B., Evteev, B.F., Kamaldina, I.I., *Characteristics of electrically active zones in strato-type clouds* . Leningrad. Gidrometeoizdat. 1989.
33) Leonov, R.A., *A mystery of ball lightning.* Moscow. Nauka. 1965.
34) Nikolaev, G.V.*, Scientific vacuum.* Tomsk. Kursiv. 1999.

UNIPOLARLY BALL LIGHTNING THEORY

V. L. Bychkov[1], D.V. Bychkov[2]

[1]*Physics Department, M.V.Lomonosov Moscow state,*
119992, Leninskie Gory, Moscow, Russia
E-mail: ***bychvl@orc.ru***
[2] *Moscow institute of textile industry, Moscow, Russia*

Abstract

Ball lighting (BL) theory was proposed earlier by the author. It is a generalization of earlier presented theories of V.A. Saranin and the author of this work. According to this model creation of melted bubble type substance and its unipolar charging take place during thunderstorms by strike of linear lightning into earth and other different objects of inorganic and organic origination that can be melted. At high electric field in the ground atmospheric layer and high electrical (mainly negative) charge of this object there appears a capability of this object to levitate. This object explosion is connected with its combustion in air after its heating by plasma on its surface to temperatures of ignition. Electro-hydrodynamic instabilities on its surface can lead to appearance of droplets and filaments on it and to facilitation of ignition. Specific energy of this object proves to be high and it is in agreement with observations. In frames of this model one can explain observed lifetime of BL, its explosion and collapse.

8. Introduction

The problem of ball lightning (BL) continues to attract attention of scientists since there is no final experiment on its modelling. Collection and analysis of BL observations has allowed to single out aspects that should be explained by BL theory. These are estimated high BL energy density of some objects $\sim 10^3 \cdot$MJ m^{-3}, its long lifetime and its ability to levitate [1-3]. BL appears in summer period when thunderstorms take place and interaction of linear lightning with different materials leads to BL appearance according with observations. This object can have hot surface. So developed theory has to include the possibility of different materials for BL framework, its high energy, high values of electric field on its surface, its long lifetime and ability to levitate.

Experiments [4-6] have shown that it is possible to experimentally produce long-lived luminous formations analogous to natural BL both of organic and inorganic origin. They represented melted and burning objects created in plasmas with the lifetime determined by combustion processes in air. Their surfaces were hot. So they showed the possibility of hot BL.

Our previous analysis allowed us to propose one type of BL as an object with a bubble-type structure [7,8], which material is organic, inorganic or composite charged melt. This model includes features of theories [9-11] of BL as melted unipolarly weakly charged object and develops it.

9. Model

The possibility of BL existence follows from the fact that linear lightning leader and the return stroke are unipolarly charged objects and they can transfer energy directly and inductively to the substances.

BL appearance. There is a possibility for BL appearance in the result of the unipolar linear lightning stroke into any material; heating and melting of this material and its charging. (In this paper we will not consider inductive BL creation first considered in [11]). BL in this case can be a sphere or a bubble of melted material. In the case of bubble appearance inside a plug it can go outside through the holes. An isolation pressure layer protects its surface from the contact with the walls.

The electric field at BL surface is determined by the charge density passed from the linear lightning discharge to the melt. Results obtained by us in [9] showed that a gas discharge develops on BL surface, it heats this surface (during $1\text{-}10^2$ s) to the temperature of the ignition, then the object destruction takes place. BL lifetime in [9] was accepted to be equal to the time of the BL surface heating up to the temperature of the surface destruction (for organic dielectrics it corresponds to heating by ~100 K) or its ignition. Heating of surfaces for ~300 K starting from the melting temperature is enough for ignition both of organic and inorganic substances. The theory [9] gave reasonable agreement with experiments and observations. BL lifetime of several seconds is possible even at very large values of electric field on BL surface up to $\sim 30 \cdot E_{br}$ (E_{br} -breakdown field in air $\sim 3 \cdot 10^6$ V/m). This point is included unchanged to the theory of unipolarly charged BL. Existence of plasma creates some pressure increase in the layer $P = P_0\left(1 + \frac{N_e T_e + N_i T_i}{N \cdot T}\right)$, where N_e, N_i, N - respectively concentrations of electrons, ions and neutrals in the layer and T_e, T_i, T are their temperatures which protects BL surface from direct interaction with objects.

At burning such BL disappears during very short time (with respect to heating) and high energy BL leave burning or melt traces that give average energy density $\sim 10^3 \cdot$ MJ m^{-3} and higher.

At definite charge on BL surface and high thunderstorm electric field (including electric fields of the Earth and the cloud or their combination) BL would levitate. This follows from the fact that high thunderstorm electric fields of $\sim 3 \cdot 10^3$ V/m were detected [11]. The second fact confirming this is that: usually soil consists of 50% of SiO_2 [12], samples of SiO_2 can accumulate high values of electrical charge [13] (with creation of electric fields over them of$\sim 10^7$ V/m and higher). So at linear lightning multiple strokes to some region on earth there is a realization possibility of extremely high electric fields over it by accumulating of charges from these strokes.

Ignition and the combustion of the BL material in air leads to energy release, at that the estimates show that the ignition of the polymer material melt and of the inorganic material melt takes place at heating for approximately the same temperature value (300-400 K) starting from the melting point.

Evident equations corresponding to this model are (in SI units system):

$$q_{surf} = 4\pi\varepsilon\varepsilon_0 E_{surf} \cdot R_{sph}^2 , \quad (2)$$

$$q_{surf} E_{exe} \approx m_{sph} \cdot g , \quad (3)$$

$$m_{sph} = W_{spec} \cdot \frac{4}{3}\pi R_{sph}^3 / \Delta U_{comb} , \quad (4)$$

$$\rho = \frac{m_{sph}}{\frac{4}{3}\pi R_{sph}^3} = \frac{W_{spec}}{\Delta U_{comb}} \quad (5)$$

here q_{surf} – is the electric charge on the sphere surface, E_{surf} – is the electric field on the sphere surface, $E_{ext} = E_{earth} + E_{cloud}$ – is the environmental electric field, R_{sph}, m_{sph}, -raduis and mass of the sphere, ΔU_{comb}~(2-4)·10^7 J/kg – typical combustion release energies of substances (Al, Si, paraffin), g – gravitation constant, $\varepsilon\varepsilon_0$ – dielectric constant of the air, W_{spec}– BL specific energy, ρ - effective density of the object. (2) - equation for electric field on BL surface. (3) – equilibrium equation of electric and gravitation forces. (4) – equation for BL material mass necessary to provide required energy during the combustion. (5)-equation for BL effective density.

Basing on (2)-(3) one can find the following equation

$$W_{spec} = \frac{3\varepsilon\varepsilon_0 E_{surf} E_{ext} \Delta U_{comb}}{g R_{sph}} , \text{ or } W_{spec} \approx \frac{(0.5-1)\cdot 10^{-4} E_{surf} E_{ext}}{R_{sph}} , \text{ J/m}^3 \text{ for the given } \Delta U_{comb}.$$

For explanation of the flying object appearance possibility with energy density of about 10^3 MJ/m^3, it is necessary to suppose the presence of anomaly large electric fields on the object surfaces at very large thunderstorm fields. For example, at E_{surf}~10^8 V/m, E_{ext}~10^5 V/m one has

$$W_{spec} \approx \frac{(0.5-1)\cdot 10^9}{R_{sph}} , \text{ J/m}^3; \ \rho = \frac{25}{R_{sph}} , \text{ kg/m}^3,$$

i.e. large objects of the melt and disperse composition satisfy these results.

Estimates also show that electric energy of considered objects is much smaller than their chemical energy.

BL certainly can exist at the violation of equations (2)-(4), in this case they will not posses many unique properties.

Works devoted to charged melted balls and bubbles [9-10,14,15] show, that separation of particles from them and the appearance of elongated structures on their surface is advantageous from the point of view of the energy minimum. Experiments with the unipolarly charged ball covered with the liquid dielectric (octol) [15], showed the appearance of threads finishing by the small balls on its surface, BL with analogous surfaces are well documented [16]. We also obtained such threads on the surface of metallic melted luminous balls in our experiments [4].

From the point of view of the presented theory the objects obtained in experimental works represented variants of BL as melted burning objects and they were analogous to the natural BL .

BL disappearance. Let us discuss a question about a type of BL elimination. BL becoming dim can be equated with burning of BL material without an explosion. Its

separation into pieces can be the manifestation of electrostatic instabilities. Let us consider Bl collapse and explosion.
For this purpose we consider BL as a bubble with charged liquid surface. In equilibrium the following equation is valid for it [11]:

$$P_{vap} + P_{gas} + \frac{kQ^2}{8 \cdot \pi \cdot R^4} = P_{atm} + \frac{4\alpha}{R}. \qquad (6)$$

Here P_{vap}, P_{gas} describe vapor and gas pressure inside a cavity of the bubble. At that their sum can be either higher than the atmospheric pressure or smaller it with respect to conditions of formation. The third term from the left describes BL surface stretching due to electric charges, $k = 1/(4\pi \cdot \varepsilon \varepsilon_0)$. P_{atm} is the atmospheric pressure, the last term from the right corresponds to Laplace pressure, where α - is a coefficient of surface tension.

If BL surface is heated then P_{vap}, and P_{gas} values can rise and lead to variation of BL radius. In the case of molecular gas in the cavity one can show

$$P_{vap} + P_{gas} = P_{\text{int}\,0} \cdot (T / T_0) \cdot (R_0 / R)^3, \qquad (7)$$

here P_{int0} , T_0, R_0 are respectively initial pressure inside a sphere, initial temperature and initial radius of the bubble.

Let us consider now different situations using the fact that $P_{atm} >> \frac{4\alpha}{R}$ for materials like iron, aluminum, silicon and paraffin, by which we model BL substance at typical sizes.

Let the ball was created so that $P_{vap} + P_{gas} << P_{atm}$, then its radius is determined as

$$R \approx \left(\frac{kQ^2}{8 \cdot \pi \cdot P_{atm}} \right)^{1/4}. \qquad (8)$$

One can see from this equation that the radius decreases at loosing of electric charge by the bubble in the result of streaming or breakdown, so the collapse of the object takes place.

Let the ball was created so that the initial pressure in it was close (by its value) to the external value (blowing out of the object) $P_{vap} + P_{gas} \approx P_{atm}$, then its initial radius is determined by the equation

$$R \approx \left(\frac{kQ^2}{32 \cdot \pi \cdot \alpha} \right)^{1/3} = \frac{32 \cdot \pi \cdot \alpha \cdot k}{E^2}, \qquad (9a)$$

note that,

$$R \approx \left(\frac{kQ^2 \cdot (T / T_0)^k}{32 \cdot \pi \cdot \alpha_0} \right)^{1/3}, \qquad (9b)$$

since usually $\alpha = \alpha_0 \cdot (T_0 / T)^k$

In Table 1 one can see values of BL radiuses obtained by (9a) at different electric field values on BL surface. These values reasonable agree with observed radiuses of BL.

Table 1. BL radiuses for different materials (9b)

R (m)\E	Fe	Al	Si	glass	paraffin
E=10^6 V/m	1,7 m	0,8 m	0,8 m	0,12 m	0,04 m
E=$3 \cdot 10^6$ V/m	0,18 m	0,09 m	0,09 m	0,013 m	0,004 m
E=10^7 V/m	0,017 m	0,008 m	0,008 m	0,0012	0,00045 m

Now let us consider BL explosion possibility, for example, when the surface of BL is heated in the result of gas discharge development over it so that it can be ignited. At that in (7) we consider that the temperature inside BL and on its surface rises as $T \sim T_0 \cdot \exp(t/\tau_{ign})$, where τ_{ign} is ignition time. Then form (6), (7) one can get the following equation: $P_{\text{int}0} \cdot \exp(t/t_{ign}) \cdot (R_0/R)^3 \approx 4\dfrac{\alpha}{R_0}\left(\dfrac{R_0}{R}\right)$

or

$$R \sim \exp(t/(2 \cdot \tau_{ign})), \qquad (10)$$

BL radius rises sharply, this leads to its destruction.

Appearence of small melted particles due to electrostatic instabilities of BL surface facilitates ignition and accelerates combustion of disperse material on BL surface and also to its explosion.

10. Examples

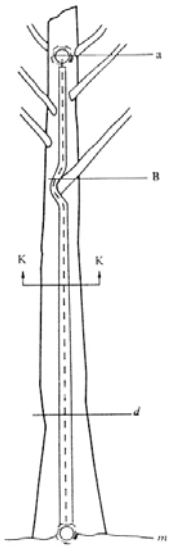

Let us consider two examples of presented model application.

The first one is connected with BL observation in Novosibirsk in 1996 [15]. BL had been appeared on a pine-tree at a height of about 12 m. Then in descended down, almost directly. At that it created a furrow, which width was about 5 mm at the top and 50 mm near the ground, see Fig.1. Then it moved and covered about 62 m and exploded in the end. At that its total observation time was about 8-9 s (we represent only necessary data for our analysis)

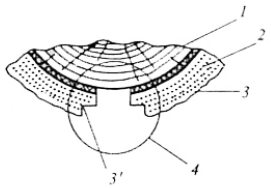

Fig.1. *BL traces on a pine-tree [15].*

Before our analysis we have to mention that a theory of vapor explosion created by linear lightning and BL was delivered in [16]. According to it electric field of the lightning creates electric current in water, Joule heating takes place, which heats water to vaporization, and vapor pressure brakes the tree surface.

We also consider this reason for BL bark destruction. We account for [17] that water in trees moves upward exactly under the bark, so namely there should be destructions (see Fig.1). Also one has to note that water in trees is purified, due to its transportation through

molecular membranes of a root system [17]. So its electrical conductivity is close to those of distilled water.
Let us determine electric field strength on a surface of BL, at which evaporation of water takes place under the bark and causes the vapor explosion.

$$W_v \approx \lambda_v \cdot \rho \cdot V \,, \tag{11}$$

here λ_v- is specific water vaporization heat, $\lambda_v \approx 2{,}26 \cdot 10^5$ J/kg, ρ-water density, V-volume occupied by water.
Electrical energy going for water vaporization is:

$$W_e \approx \sigma \cdot E^2 \cdot V \cdot \tau \,, \tag{12}$$

here E – is electric field strength on BL surface, σ - is water electrical conductivity, $\sigma \approx 5 \cdot 10^{-4}$ S/m is average value of distilled water conductivity, τ - time of BL interaction with water in the layer under a bark, for estimates we take $\tau \approx$ 1,5 s proportionally to the covered distance. Combining (11) and (12) one has:

$$E \approx \sqrt{\frac{\lambda_v \cdot \rho}{\sigma \cdot \tau}} \,, \tag{13}$$

inserting data into (13) one obtains $E \sim 1{,}7 \cdot 10^6$ V/m.

This result shows electrical field strength about breakdown field strength of air in normal conditions, this is in agreement with presented model.

Let us consider the second example of BL blowing out from a socket. In Fig.2 one can see a consequence of BL blowing out from a socket [18].

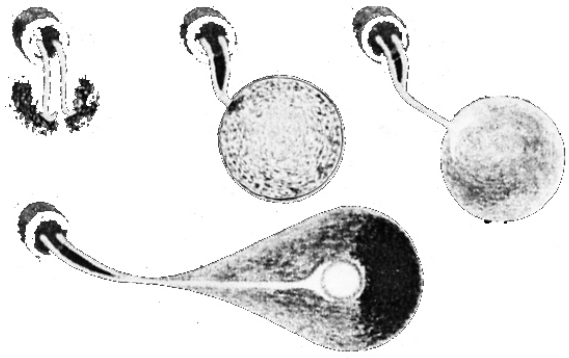

Fig.2 *A consequence of BL blowing out from the socket [18].*

In Fig.3 we represent this consequence accounting for processes taking place with a bubble created inside the socket, see Fig.3a, which we obtained on a basis of equations (6)-(9). Appearance of a bubble takes place in the socket at a overloading voltage in the electrical circuit: melting and charging of some material piece (wire, solder material, composite material of a socket) takes place inside the socket, there appears a charged liquid drop, then at

motion in the result of cavitation it transforms into the charged bubble [19]. It is covered with a plasma layer, so there is no direct contact with the walls of the socket.

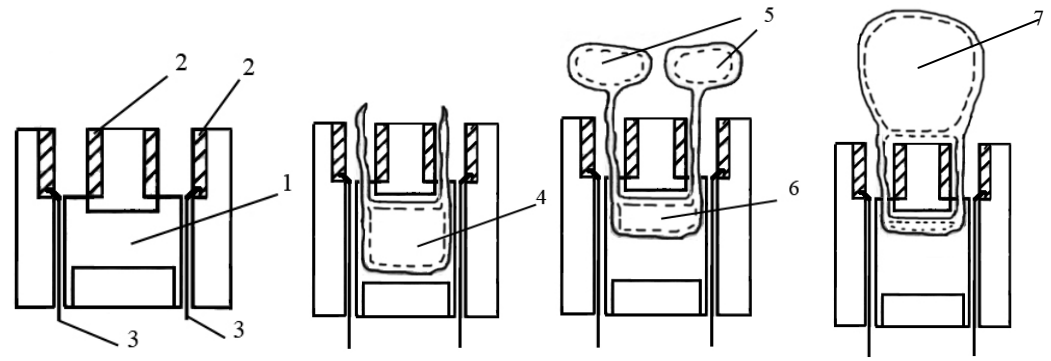

Fig.3a **Fig.3b** **Fig.3c** **Fig.3d**

***Fig3**. BL blowing out process.*
1-a cavity, 2-conducting cylinders, 3-wires, 4-charged internal bubble, 5-outside bubbles, 6- decreased internal bubble, single bubble.

If the internal bubble volume is greater than those of the cavity inside the socket then it begins to propagate outside through the holes in the socket, Fig.3b.

Charges in the melted – conductive material are concentrated at edges of the structure, so there (7), (9) appear conditions for outside local bubbles appearance on these edges, Fig.3c. Electric field conditions creating plasma are improved on a surface of outside bubbles, their temperature rises due to joule heating of plasma layer and the conductivity rises. Charges begin to flow to these outside bubbles from the internal bubble, so the size of the internal bubble decreases.

Processes of plasma joule heating on the surface of the outside bubbles continue to rise their temperature and sizes (9b), Fig. 3d. Being melted (liquid) large outside bubbles coalesce at touching with producing of single large outside sphere. Since the temperature of the sphere is the highest all the charges penetrate to it, and internal bubble disappears and its connecting part closes.

11. Conclusions

Development of unipolarly charged melted structure BL theory has been made. In frames of presented model one can explain BL lifetime, its capability to blow out of holes of sockets, BL explosion and collapse, impact on some materials (wood).

We did not consider penetration through windows in this work. Explanation of rare BL properties for penetration through window panes without visible destruction require additional analysis of observation reports, properties of melted glasses and formulation of new experiments.

Considered approach allows to explain a number of BL properties in frames of the same model

12. Acknowledgment

We thank A.I. Nikitin for helpful discussion and useful critics. Namely his critics made us reconsider the polymer BL theory and to pass from it to BL theory as unipolarly charged sphere.

References

1) Stakhanov, I.P.*On physical nature of ball lightning*. Moscow. Energoatomizdat. 1985.
2) Abrahamson, J., Bychkov, A.V., Bychkov, V.L. Phil. Trans. Roy. Soc. **360**. N. 1790. 97. 2002.
3) Grigoriev, A.I. *Fiery killers*. Yaroslavl . Debyut. 1990.
4) Emelin, S.E. , Semenov, V.S., Bychkov, V.L. , Belisheva, N.K., and Kovshik, A.P.. Tech. Phys.**42**. 269. 1997.
5) Bychkov, V.L., Bychkov, A.V. and Timofeev, I.B. Tech. Phys. 2004. **74**. 128.
6) Bychkov,V.L., Gridin,A.Yu., Klimov, A.I. Teplofizika Vysokikh Temperatur (High Temperature in English edition). **32**. 190. 1994.
7) Bychkov, V.L., *In Proceedings of 8-th international Symposium on Ball lightning,* 3-6 August, 2004, National Central University Chung-li, Taiwan, P.64-69.
8) Bychkov, V.L. Khimicheskaya Fizika. 2006, V.25, N.3, P.63-71.
9) Amirov, A.Kh., Bychkov, V.L. and Bobkov, S.E. Physica Scripta. **54**. 13. 1998.
10) Saranin, V.A. *Equilibrium of liquids and its stability.* Moscow. Institute of computer investigations Publishers. 2002.
11) Saranin ,V.A. Perm, Glazov, 1986.-Dep. In VINITI 11.11.86, №7696-B86
12) Anderson, F.J., Freier, G.D. J. Geophys. Res. **78**.N.27. 6359. 1973.
13) Abrahamson, J. and Dinniss, J. Nature. **403**, 519, 2000.
14) *Electrets*. Ed. G.M. Sessler. NY. Springer-Verlag. 1980.
15) Pudovkin, A.K. *Ball lightning in Novosibirsk Akadem gorodok.* Uspekhi Fizicheskikh Nauk. 1996.V.166. N.11. P.1253-1254.
16) Saranin, V.A. Teplofizika Vysokhikh Temperatir. 1999. N.37. N.1. P.31-36.
17) Mineev, A.. *in Physics and biology*. Ed. V.A. Tikhomirova and A.I. Chernoutsan. Moscow. Buerau Kvantum. 2001.
18) Likhosherstnykh, G.U. Tekhnika Molodezhi. 1983. N.3 P. 38-43.
19) Yuriev B.N. *Experimental aerodynamics.* Glavnaya Redaktsya Aviatsionnoi Literatury. Moscow-Leningrad. 1936.

MODERN REALIZATION OF LABORATORY BALL LIGHTNINGS (Modern analysis)

V. L. Bychkov[1], D.V. Bychkov[2]

[1] *Physics Department, M.V.Lomonosov Moscow state, 119992, Leninskie Gory, Moscow, Russia*
E-mail: ***bychvl@orc.ru***
[2] *Moscow institute of textile industry, Moscow, Russia*

Abstract

Experiments on creation of autonomous long-lived luminescent formations - artificial ball lightnings (ABL) have been considered. These are experiments on ABL realization in electric discharge conditions, creation of fireballs from metallic vapors at closing of powerful batteries contacts, creation of ABL at application of pulsed and brush discharges in mixture of air with organic gases or organic aerosol, creation of structures in conditions of material vaporization at presence of discharge electric field. Experiments with plasma streams are under a discussion, namely, experiments on creation of relatively short lived ABL, on ABL creation at presence of metallic or organic components in the stream. Analysis of experiments shows a complicated character of origination and elimination of ABL gasdynamic or plasma chemical nature, when processes of oxidation and destruction in air can take place.

1. Introduction

A notion “long-lived luminescent object” or artificial ball lightning (ABL) appeared in the second part of the 20-th century in a course of different discharge plasmas investigations [1-6].

Anomalously long life time (luminescent time) of these objects with respect to time of their realization by a discharge source or typical time of plasma elimination at atmospheric conditions (elimination of plasma in recombination processes considered in [8]) is the feature of these objects.

Autonomous is another feature of the luminescent formations, i.e. their capability to move in space keeping their form, size and color during time compared with their lifetime. By these properties they are analogous to natural ball lightnings (BL) [8-9].

ABL are different from St. Elms fires namely by the autonomous nature, since St. Elms fires are usually attached to charges surfaces, or charged drops [10]. Such feature is absent in the case of plasma objects generated by microwave radiation [11-12] or non-oriented contours [13]. We also limit our discussion by experiments at atmospheric pressure or close to it.

2. ABL generation in electric discharge conditions

2.1. To historically first experimental approach one can attribute creation of fireballs made by Plante in 19-th century. He obtained luminescent balls of many types [16,14] with battery of accumulators and electrodes over/ in water vessel. In Fig.1. is represented Plante experimental scheme.

In Fig. 3a and 3b one can see ball-type formations created by different scientific teams [17, 18]. Essence of the design consists in the following. A copper electrode in a form of a ring is on the bottom of the vessel filled by water, it is connected by isolated bus-bar with positive pole of the battery. Negative pole of the battery is connected with the electrode located in the center of the vessel near the water surface and is directed up wards to air. A quartz tube surrounds this cylindrical electrode made of coal, copper or aluminum, it is higher than it and higher than water surface by 3-5 mm. The capacity battery is of 0,6 mF and is charged up to 5,5 kV. The central electrode is moistened by a drop of water for generation of ABL. A luminescent formation appears with sharp bang at quick closing of the discharger, it is transformed in a spherical object.

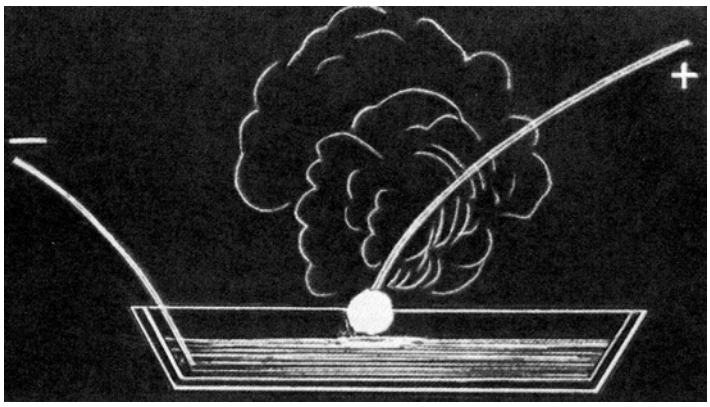

Fig.1.*Appearance of luminescent object [16] at application of the liquid as negative electrode and metallic rod as the positive electrode.*

Analogous experiments [17-19] made with modern powerful capacities are called "Gatchinskyi" discharge. In Fig.2 one can see a design of the set up.

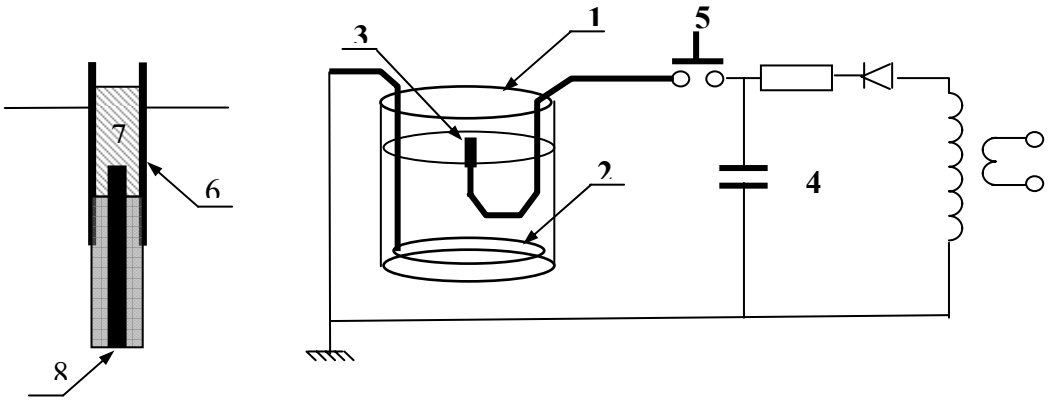

Fig.2. *Set up of "Gatchinskyi" discharge 1 – Polyethylene vessel. 2 – ring electrode. 3 – central electrode. 4 – Capacity battery of 0.6 mF. 5 –discharger. 6 – quartz tube. 7 – coal or metallic electrode 8 – copper bus-bar.*

Fig.3a *A luminescent formation from [17].*

In Fig. 3a and 3b one can see ball-type formations created by different scientific teams [17, 18]. Essence of the design consists in the following. A copper electrode in a form of a ring is on the bottom of the vessel filled by water, it is connected by isolated bus-bar with positive pole of the battery. Negative pole of the battery is connected with the electrode located in the center of the vessel near the water surface and is directed up wards to air. A quartz tube surrounds this cylindrical electrode made of coal, copper or aluminum, it is higher than it and higher than water surface by 3-5 mm. The capacity battery is of 0,6 mF and is charged up to 5,5 kV. The central electrode is moistened by a drop of water for generation of ABL. A luminescent formation appears with sharp bang at quick closing of the discharger, it is transformed in a spherical object.

Fig.3b. *A luminescent formation from [18]*

One can think that water plays a principle role in this experiment, however appearance of ABL was observed in these experiments at closing of contacts far from water vessel. It means that the object formation is connected with energy release in the electrode zone accompanied with generation of burning material (hydrogen in case of vessel with water due to discharge release in and over water or melting and erosion of electrodes) in air. Cylindrical walls of the vessel can easily generate a vortex of burning material.

Luminescent balls were observed in the experiment [20]. They were formed at explosion of thin metallic wire (of Cu, Ni, Ti) in plastic miniature bath filled with a flammable mixture. A hole for outlet of electric explosion products was in the bath. ABL sizes reached 5-6 cm and its lifetime was 2-3 s. The objects transformed in vortex rings on the last stage of their existence analogous to those observed in [17-19], see Fig. 4.

Fig.4. *Vortex ring on the last stage of the object existence (diameter is 25 cm) [20].*

Analogous structures are observed at flowing of streams from plasma generators (see below). In reference [3] their formation is connected with development of Kelvin –Helmholts instability. Main differences of these objects from natural ball lightnings are their vortex form and low decay without a bang or explosion.

2.2. To the second direction one can attribute formation of balls out of metallic vapor plasma at closing of powerful electric batteries contacts [22-23], and also ball generations at closing of electric wires in air and in water [22]. Sizes of ABL reached several cm and their lifetime tens part of the second. Brightness temperature corresponded to temperature of vaporization and oxidation of a metal.

Luminescent balls of 2-4 mm diameter and the lifetime of 2-5 s were obtained in [22] at short-circuit by two electrodes in water. The balls resembled drops of melted metal burning in air. After cooling they represented metallic spheres 2 mm diameter with traces of oxides on the surface in a form of thin hair.

In reference [21] luminescent balls of 10-15 cm size and the lifetime up to 5 ms appeared after explosion of titanium foils in cuvettes with water. Hey were over the cuvettes covered with vacuum seal. Energy put to 8 cuvettes with titanium foils (with sizes $50\mu m \times 1$ cm $\times$ 5 cm) was 50 kJ and the pulse duration was 60 μs. In Fig.5 one can see a scheme of the experiment. In Fig.6 one can see the last stage of the object existence. The luminescence during the object lifetime changed from pure diffuse type to those filled by glowing particles. This allows to speak about the condensation processes going in metallic plasma, which penetrated through the seal.

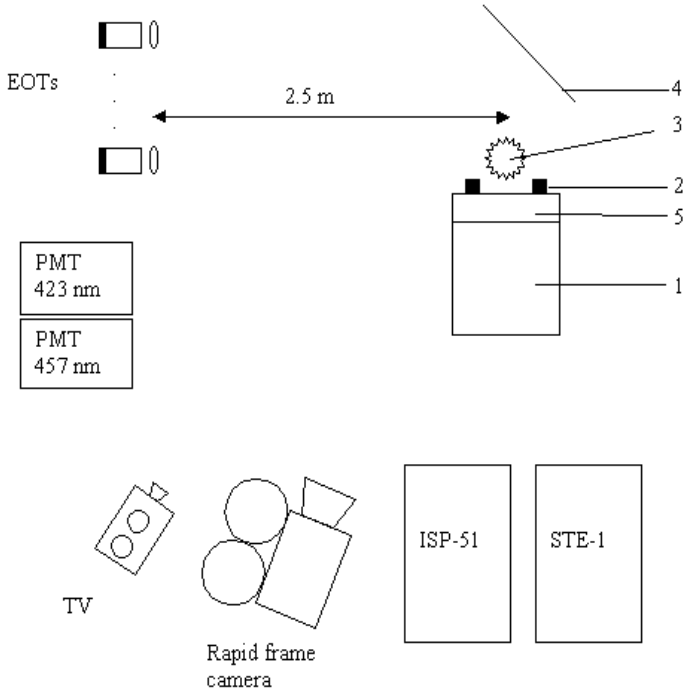

Fig.5 *A scheme of diagnostics set up [21]: 1- Torus; 2.High-voltage lead-ins; 3.Ball-like plasma formation; 4. Mirror; 5. Dielectric cover*

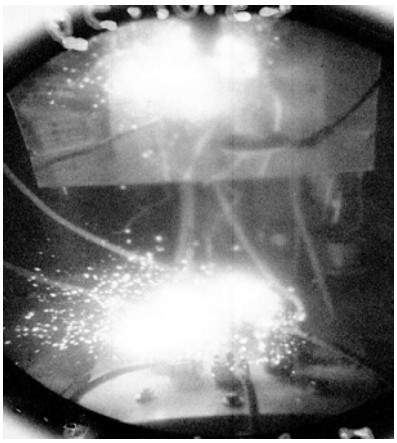

Fig. 6. *Luminescence filled by glowing particles [21].*

2.3. The third direction is creation of ABL with the lifetime from some ms to several seconds at application of pulsed and brush discharges in mixtures of air with organic gases or organic aerosol [24-26] or at destruction of metallic electrode's material [27] in discharge afterglow.

The brush discharge in [24] was ignited in the bath of 4 m^3 volume filled with air at presence of aerosol particles p-xylene-azo-β-naphtol in it with their portion 15 mg/m^3. The discharge color was initially greenish blue. Then a sphere of 20 cm diameter was formed in the center of the chamber, its color was 20 cm, it consisted of large particles. Analysis of these particles under the microscope showed that they represented long chains of small particles up to 10^3 units in each.

One can find descriptions of experiments with the pulsed discharge in air with propane admixture (with inter electrode voltage of 10 kV and energy in the pulse ~ 250 J) in [14]. Air pressure was the atmospheric one, volumetric propane concentration was 1,4-1,8 %, it is smaller than the concentration necessary for inflammation of the mixture. In the result yellow-green ball appeared, which lifetime was 1-2 s.

In [14-15] one can find description of Nauer experiments [29] on creation of luminescent balls at gas discharge in air with admixture of hydrogen and hydrocarbons such as methane, propane and benzene in concentrations somewhat smaller than those necessary for inflammation of mixtures. The greatest effect was observed at application of benzene. Bright luminescent balls were observed even at presence of tiny traces of it in the discharge chamber. At explanation of experiments authors in this work made a supposition that the glow appears on the tangle of thin threads, produced at benzene combustion. At that the luminescence was considered as result of organic matter combustion.

In [30] a red ball of 5 mm diameter was observed. It flew between two electrodes, one of which was a metallic net and another - a rod. Electrode gap with potential difference of 40 kV was poured on from above by artificial rain. Suddenly a formless leave separated from the net, then on a distance of 15 mm it had transformed to the right ball of red color. It continued to move over the force line and soundless disappeared without reaching the second electrode.

The ball in opinion of the authors had appeared on a basis of a lump of aerosol, because tests of the smoke generator were made at the place of the experiment the day before. The luminescence was explained by appearance of the conductivity of threads flying in air at their watering. Presence of electric current leads to glowing of threads in points of their contact or appearance of gas discharges between threads. According to the authors ball lightning appearance is the result of luminescence of organic carbonized thread tangles.

In reference [25], which ideologically continued [14], the pulsed discharge in air was created between the copper electrodes, see Fig.7, which were at a distance of 3 mm. At that the discharge voltage was changed in range 8-10 kV, and energy in the pulse was 350 J. Discharge chamber had sizes 150 × 120 × 150 cm. The principle scheme of the circuit is represented in Fig.8. At ethane content of 2.1% in air sometimes one could observe appearance of a red ball with a diameter up to ~ 4 cm with lifetime 0,3 s. An object of white color and 3 cm diameter was observed in the discharge afterglow during 0.8 s at addition of 100 cm^3 of cotton fibers to the gas mixture. Appearance of luminescent objects were observed four times in the mixture consisting of ethane 2,7 % and 100 cm^3 cotton fibers processed into small particles. Once a diameter of such an object was 5 см, and its lifetime after switching off the discharge pulse was 2 s.

According to the author's opinion, appearance of the balls took place in experiments at concentrations of flammable mixtures lower than required for inflammation threshold. One can not exclude a possibility of presence of excited or dissociated molecules in air in discharge conditions, which could change ignition characteristics [28].

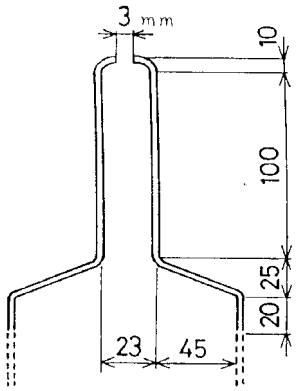

Fig. 7. *Typical appearance of electrodes [25].*

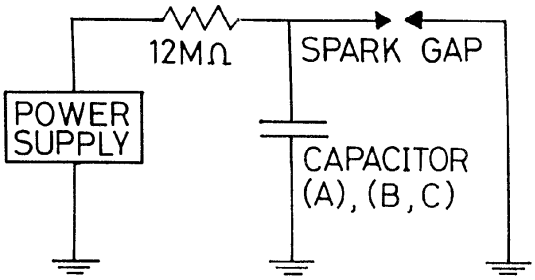

Fig. 8. *Principle electrical scheme of the experiment [25].*

In reference [31] was made analysis of anomalously long afterglow of the high frequency discharge (with frequency $7.5 \cdot 10^7$ Hz) in air [27], which reached 1 s in the experiment. The conclusion of [31] was that fractal clusters play essential role in the luminescence; they were formed in metallic vapors appearing on electrodes.

Streamer discharges were used in [26] for generation of ABL in [26], they were created by high frequency Tesla generator at the frequency of 67 kHz. At that the mean power delivered to the high voltage electrode was 3,2 kW. A set up of N. Tesla was recreated in [26] in smaller size. It was experimentally established that a large number of hydrocarbon and metallic particles evaporated from the electrode appear during the discharge development. Their maximum number was observed in the small near electrode region, strong electric fields (with electric fields of 10-20 kV/cm) appeared in the same region. ABL appeared near the high voltage electrode, as is "from nowhere", because they were absent at previous frames of video recoding, so their formation time was about τ_{cr}=40 ms. ABL had different colors: red, yellow, bleu and white; their lifetime reached 2 s and size 1-5 cm. In the end of the existence they often exploded with loud bang, this effect we have to specially mark. Best results were realized when the high-voltage electrode was covered by wax or charred wood.

N Tesla [32] had realized fireballs by himself, their sizes reached several centimeters. The high-voltage electrode in his case was covered with the isolation made of natural rubber and a layer of graphite powder was between the electrode and the isolation. Therefore particles of metal, soot, carbon and polymer evaporated from the electrode could take part in complicated processes of structure formation and combustion.

ABL were obtained in [33] at breakdown of birch wood in the discharge at atmospheric pressure in the flask of pyrex glass when a piece of wood was places between the lead

electrodes. A hole of 0,2 mm surrounded by cracks had appeared at the ball interaction with the flask wall. Red-blue balls of 5-10 mm diameter (two cases of appearance during 450-500 acts of breakdown). In [33] was expresses an idea about a lignin (component of wood) as a basis for creation of natural BL at linear lightning stroke into a tree.

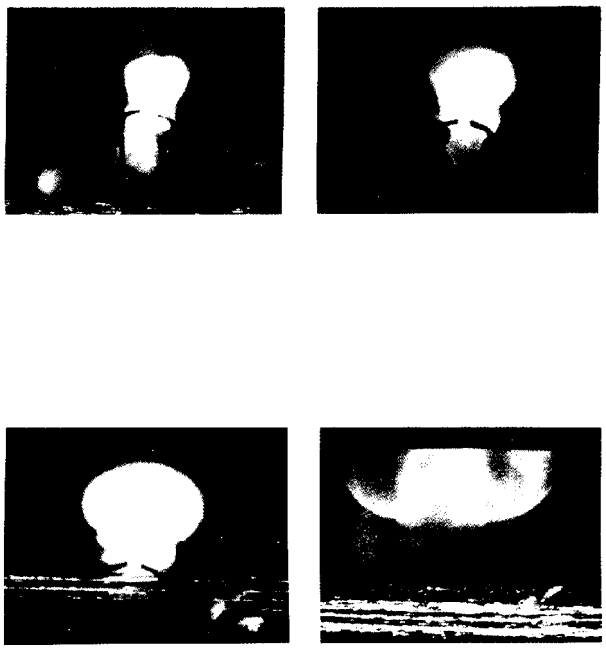

Fig.9. *Typical forms of fireballs in the experiment [25].*

To the same direction one can attribute experiments on closing of electrical circuits by conductors covered by charcoal or water layers. In [34] in such experiments were obtained ABL with sizes 9-12 mm and the lifetime from 30 ms to 0,8 s.

In Fig 10 one can see a scheme of electric circuit from [34] and in Fig.11. ABL obtained in this experiment.

Works [24, 26, 33] made essential impact on appearance of BL model [35]. BL in this model is considered as a tangle of polymeric chains, rolled up in tangles. These tangles are created at destruction of plants or gathered from organic dust, they also can be formed at destruction of isolation materials of organic origination at short circuit in domestic electrical devices. The aggregation process is analogous to those considered in [8] leads to fractal structure growth. Ions appearing in air during linear lightning activity charge this structure, which capability to keep them is high.

2.4. To the fourth direction one can attribute investigations of structures generation in conditions of materials evaporation at presence of discharge electric field.

One of the first works in this direction was reference [36] of Podmoshenskyi team. Formation of thread type conglomerates was observed at explosion of thin wires or foils of tungsten at pressure 100-760 Torr and pulsed put of energy up to 50 J (the explosion was realized by the capacity discharge). Thickness of the conglomerate micro threads was 20-30 nm. Results of these experiments were connected in [37] with a possibility of BL formation of aerosol particles analogous to the investigated.

Idea expressed in [36,37] was a basis for works of Smirnov [8], in which a hypothesis was expressed that BL framework can be a fractal aggregate gathered of solid particles charged in external electric field.

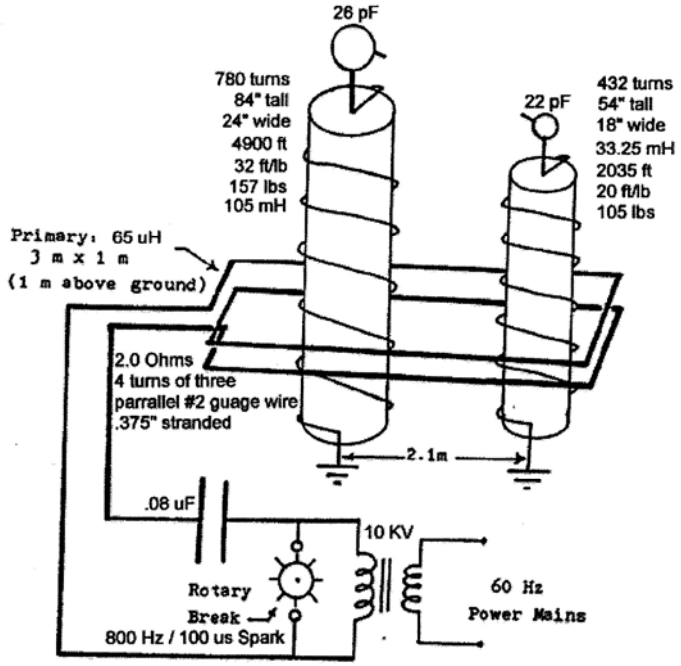

Fig.10. *Developed in [26] N.Tesla set up*

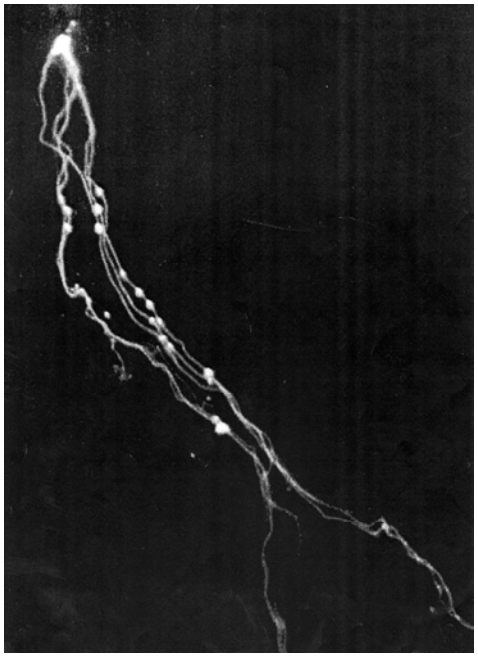

Fig.11*. Fireballs in experiments [26]*

Formation of aerogel structures from fractal aggregates was investigated in works [38-39]. Appearance of fractal aggregates with a density ~7 g/m^3 was observed at ruby laser radiation pulses action on titanium surface in external electric field. . Pulse energy was about 70 J and duration10^{-3} s, electric field was varied from 100 to $1{,}5 \cdot 10^3$ V/cm. It is considered that these aggregates are formed at vapor condensation with creation of small single particles (1-10 nm size) and following their coagulation, at that the aggregate with fractal dimension $D = 1.82$ is formed. Formation of visible macroscopic structure was the result of these processes. Authors came to the conclusion that such a structure can be a framework of BL consisting of particles created at linear lightning stroke into an obstacle.

Reference [40] is devoted to fractal cluster growth in gas phase features. It is shown in it that fractal aggregates of metals can be formed at combustion of metals (magnesium in particular) in the arc discharge in air. At that the ionization level of the medium at high temperature, T > 1000 K, makes visible influence on the structure of growing aggregates. Reference [41] is devoted to origination of the spherical tangle of silicon, Si, nano particles. It was based on experiments on investigation of the pulsed discharge breakdown to the soil, at power put E~$4{,}5 \cdot 10^4$ J. At that it was considered that particles of silicon oxide, SiO_2, are present in the soil. Creation of nano particles Si/ SiO / SiC takes place at discharge interaction with organic components of the soil composition in the place of energy release.

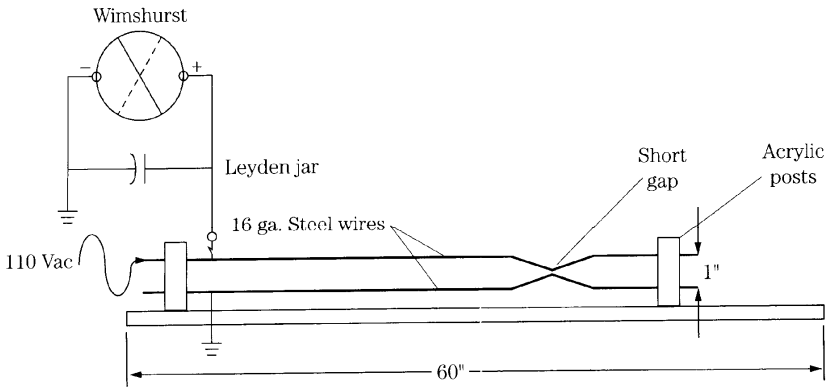

20-13 Electrostatic ac hybrid circuit.

***Fig. 12**. Electric circuit for creation of luminescent ABL [34].*

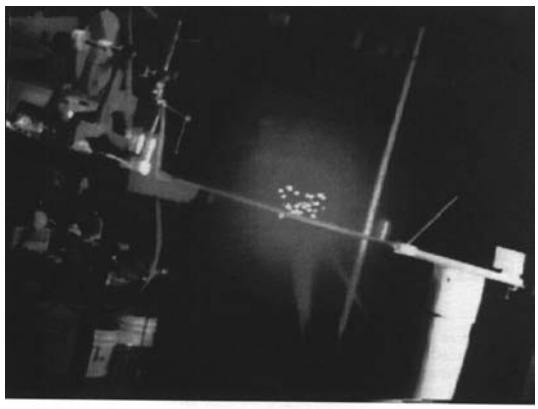

***Fig.13.** ABL with sizes 9-12 mm and the lifetime from 30 ms to 0,8 s in experiment [34].*

Conducted experiments [41] showed that indeed the polymeric threads can be formed under the discharge action. Chains of 25-125 nm length consisting of spheres 5-70 nm diameter were created at propagation of the powerful discharge through the soil (at put in energy E~23 kJ) containing 12,5 % of silicon. Shortly lived luminescent vortex rose over the interaction area. In Fig.12-13 one can see the experimental scheme and the vortex from [41].

We have to note that appearance of different structures also takes place in plasmas of high frequency discharges at presence of organic components in gases. For example in [42] was observed formation of structures with the size up to 3 mm at generation of thin films in the discharge in Freon -318 at pressure P=25-75 Pa. They resembled interknitted chains with thickness of 10-20 μm.

Arc between 6-7 electrodes was ignited [43], electrodes were placed over the generatrix of the ring and the electrode in the center of the ring. The arc existed about 0,5 s, then heated luminescent area rose and formed a spheroid configuration with size of several cm. Its lifetime reached 0,5 s.

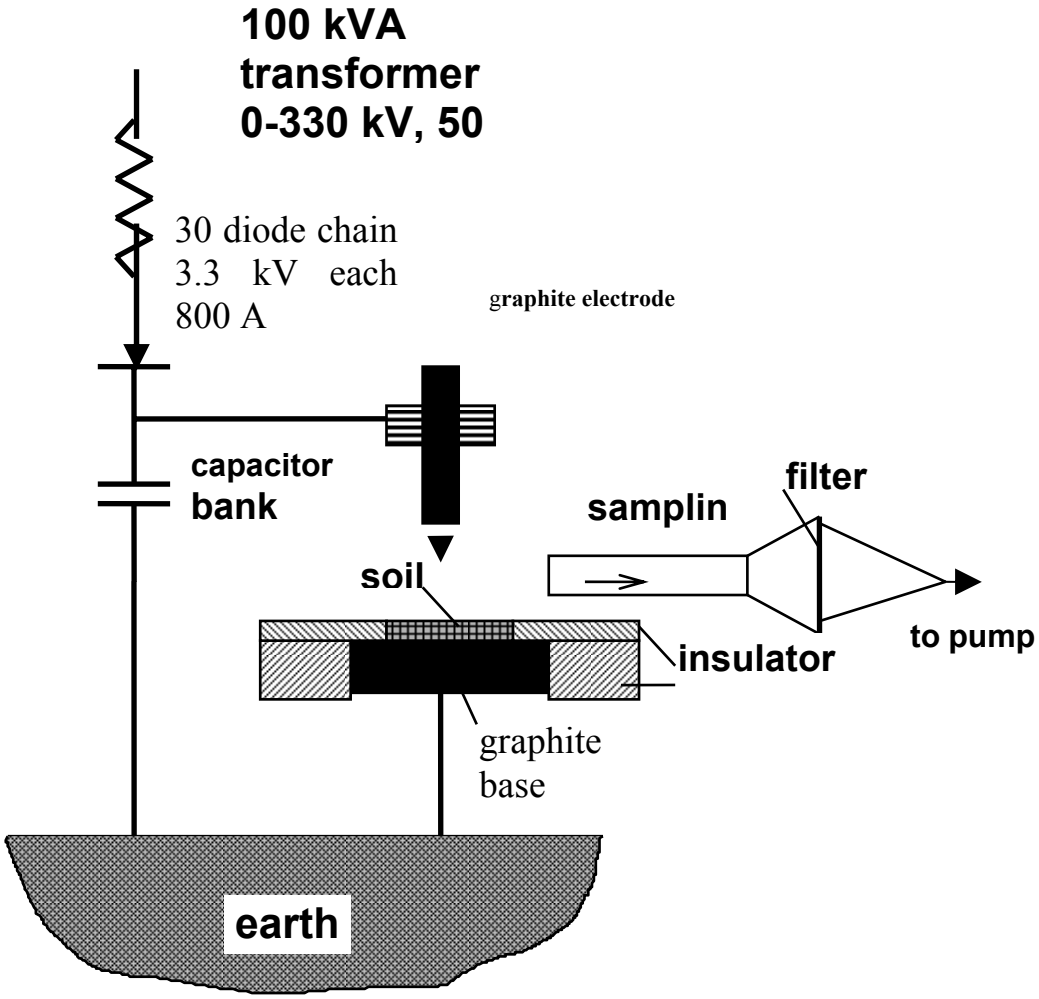

Fig. 14. *Experimental scheme of [41]*

Thus experiments with gas discharges show the possibility of appearance of the luminescent structures, ABL, conglomerates and fractal clusters of organic and inorganic origination. At that one can suppose that some of them are hot, or burning particles and structures created in air plasmas, since all the experiments were carried out in air at typical discharge temperatures, at which processes of oxidation and combustion are easily take place [28].

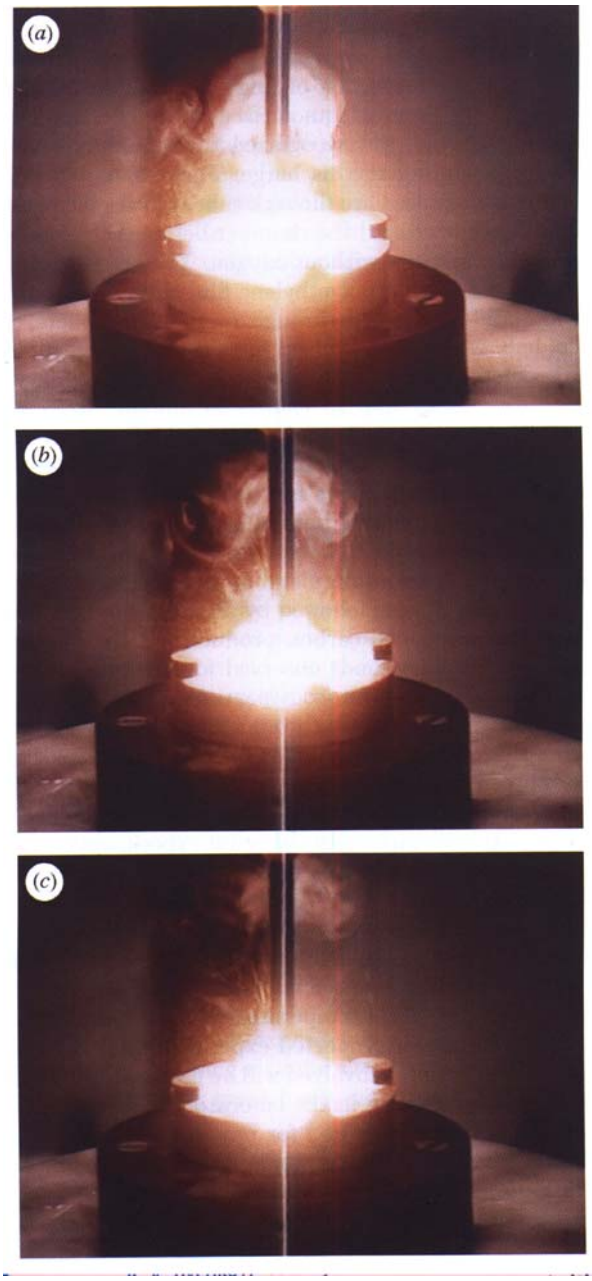

Fig.15. *Appearance of the luminescent vortex from [41]*

3. Experiments with plasma jets

Experiments on creation of ABL were undertaken at application of different types of pulsed plasma injectors in the range of put in energy 10^2 to 10^5 J [1-3].

3.1. To the first group we attribute experiments on creation of relatively shortly lived ABL. At pulsed plasma injection to air took place creation of plasma structures of different forms – spheroid (at specific energy put Q>1 kJ/cm^3 into the channel of the plasma generator) [1-3], toroid (at at specific energy put Q Q~0,51 kJ/cm^3 into the channel of the plasma generator) [1-3], cylindrical [1,4-7] and others with typical sizes 10-40 cm and the lifetime up to 0,1-1 s. At that the time of energy put was varied from 10 μs to 10 ms. A typical value of temperature in initial stage of ABL existence was 7000-10000 K. Initial concentration of electrons was 10^{16} - 10^{17} cm^{-3} .

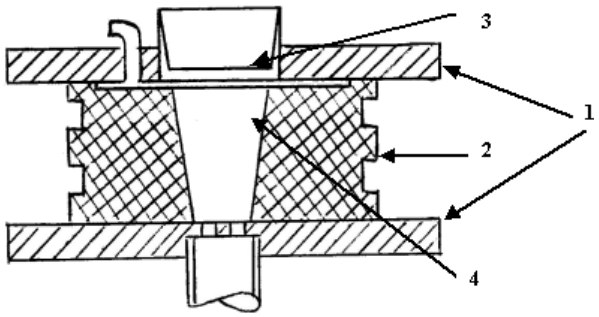

Fig.16*. The plasma generator appearance. 1- electrodes; 2- dielectric body; 3- the hole covered with Mylar; 4- plasma generator chamber. Energy putted into the discharge is 0-20 kJ. Quasi-period of the discharge current is T=65 μs, the maximum current* I_{max}*=250 kA, initial pressure in generator chamber 0.1-3 atm* [1, 3].

In Fig.16 one can see the plasma generator for producing of ABL in [1, 3]. The spherical object is represented in Fig. 17. In [1-3] were studied spectra of plasma radiation and their temporary evolution.

Fig. *17. The mush-room configuration of the plasma jet [1,3].*

It was shown that the ABL spectra at their late stages of existence corresponds to the radiation of solid carbon particles and particles of metal oxides, and as well to the radiation of burning organic materials.

3.2. To the second group one can attribute experiments on creation of ABL at inserting of metallic or organic components to the stream. Organic glass [1,4,45], kaprolon [1-3] and different organic materials of natural origination – wax, paraffin, colophony with natural filling agents, wood, lignin, etc. [6,7,46,47] were used as plasma forming materials. Metallic wires were also located in the plasma generator's channel for generation of ABL [48]. Injection of the discharge products was made into air, liquid nitrogen [7], and also to air saturated with vapors of organic materials [46-47].

The size of the torch increased by several times and its lifetime for ~10 ms (with respect to the torch from organic glass channel) at injection of the discharge material from the wax and paraffin capillaries [7,46]. The corresponding experiments [49] showed that particles coming out of the plasma generator change their properties with respect to the character of interaction with the obstacle and its feature. Thus polymeric tangles and treads were formed at injection of discharge products from the wax capillary to the liquid nitrogen [7,48].

In references [50,51] was undertaken the investigation of erosive and arc discharge plasmas injection to the liquid nitrogen. Appearance of luminescent balls up to 4 mm size and the lifetime of the glow of several seconds (~ 5 s) was observed in some experiments.

In reference [45] particles of charcoal or cotton wool were located in the channel of the plasma generator made of organic glassв (up to 10 units) with 0,1 mm diameter or 50-100 μm metallic particles. In case of hydrocarbon particles aggregates with rose luminescence with size up to 0,7 cm flew out of the channel at the discharge, after that they were shining for several seconds. They were descending slowly. After their extinction one could find white aggregates of organic glass resembling snow flakes, and charred aggregates as well.

Explosive creation of the luminescent regions with sizes 10-30 cm and the lifetime about parts of a second was realized at the distance 30-100 cm from the injector in experiments on the plasma generation in the channel with metallic particles [45, 48]

Yellow red balls 3-5 mm diameter were created at interaction of the plasma stream with the lead wire. Appearing on a flat surface they made high jumps and left traces as after drops of melted metal. After cooling the surface of the balls was covered by the tread type clusters of lead oxide, SnO_2, of 50 μm length.

Structures of the fractal types with length up to 3 cm and width of several millimeters and fractal dimension D=1.8 ± 2 appeared at interaction of the plasma jet with lead wire. These structures were highly elastic during first minutes then they became fragile and were quickly destroyed.

The next experimental type described in [45] was on the meeting point of electric discharge and plasma dynamic formulation. It can be attributed to creation of regions with plasma conditions analogous to those, which are realized at linear lightning stroke to the soil or at explosion in the closed space area, see Fig.18.

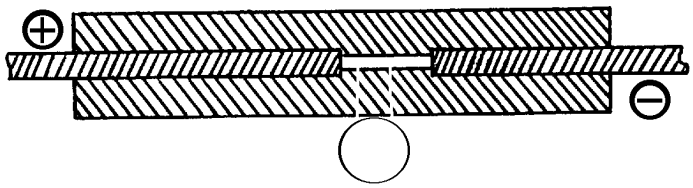

Fig.18*. creation of ABL in the closed discharge volume.*

The discharge or plasma were created in the closed volume, see Fig.18., then the created luminescent formation, consisting of mixture of vapor plasma, particles of electrode material melt and ionized air went outside through the specially prepared hole, or the hole broken through in the tube due to pressure rise during the discharge development.

The lifetime of such formations reached 5-7 seconds. They exploded after hitting an obstacle, leaving traces as from multi-layered object with melted core. Sometimes it was possible to find their remains, which resembled oxidized metal shells. This was one of a few experiments when there was an explosion of ABL.

Luminescent Formations of 10 mm diameter were obtained in [48] in the closed tube of polyethylene. Pressure increased in the tube at the discharge, the tube swelled up, its wall became thinner and the luminescent balls leaked out through it.

This direction had a development in works [46,47]. It was discovered in these experiments that different ABL structures were formed at application of organic plasma forming materials and at injection of plasmas into air saturated with organic vapors.

In Fig.19 one can see a principle scheme of the experimental circuit, in Fig.20 – a scheme of the capillary discharge (capillary plasma generator). In Fig.21 is represented a scheme of experiments with vapors.

Plasma jet from the plasma generator passed over a cuvette keeping melted paraffin or wax at undertaking of these experiments. At that the plasma generator energy of about 200j was delivered to the gas mixture during ~6-8 ms. Video recording had showed that spheroid or mushroom type formations, see Fig.22, were formed immediately after the "shoot" over the cuvette and rose up, their size was 10-20 cm and temperature T ~1500 - 2000 K (as was estimated by their rising velocity), they existed up to 0,5 s.

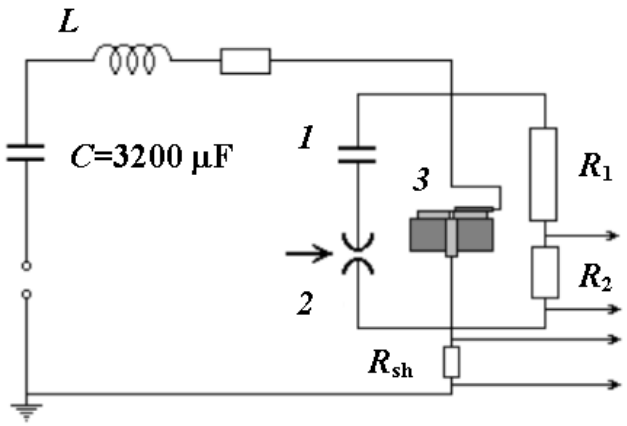

Fig. 19: *Principle scheme of experiments with erosive discharge (capillary plasma generator). 1-capacity storage, 2 – discharger, 3- capillary plasma generator, R_1, R_2 - resistances of the voltage divider, R_{sh}- the current shunt.*

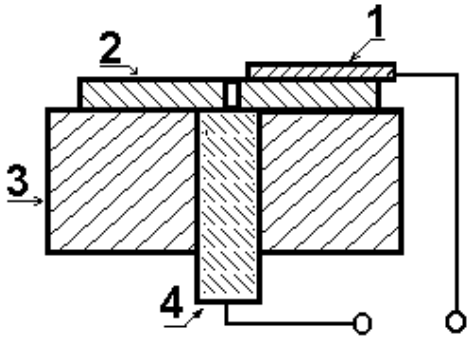

Fig.20. *Erosive discharge (capillary plasma generator): 1,4- electrodes, 2-a dielectric plate with a capillary(discharge chamber), 3- plasma generator bed (of organic glass)*

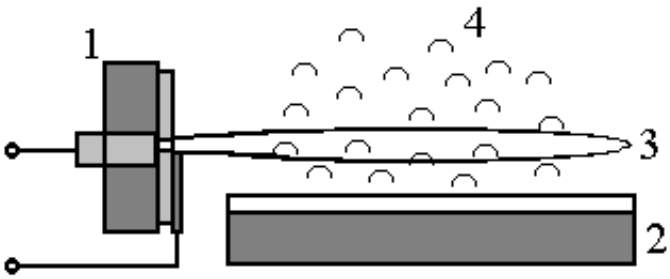

Fig.21. *A scheme of experiments with application of the erosive plasma generator: 1- capillary plasma generator, 2- a cuvette with melted wax, 3- plasma region, 4-vapors of wax.*

Luminescent objects in experiments [46,47] were created by the plasma stream, they appeared over the cuvette with melted wax and paraffin even 10 minutes after stopping of the cuvette heating. Such a long time of vapors high concentration existence proved to be unexpected, this shows that in real conditions gaseous hydrocarbons can be accumulated in some places. Quite probable that luminescence of balls in Barry experiments with organic gases [14] was connected with these processes. Appearance of such objects allows to explain a nature of the luminescent objects, which lead to summer forest fires and are observed in coniferous forest in clear weather [50].

Fig.22 *Combustion of light fraction of wax vapors in result of interaction with plasma stream. A size of thee luminescent area ~ 10 cm.*

In another experimental series [46,47] with use of the capillary of 1- 2 mm made in the material of complex organic mixture consisting of paraffin, colophony and milled wood with average sizes of the "seed" 1×0,3×0,3 mm (volumetric proportions of the mixture were 1:1:3) were obtained luminescent objects with typical visible size 1-2 cm and the lifetime 1-2 s. Such ABL is represented in Fig.23. Several times it was possible to find remains of these ABL. They were investigated with electron microscope. Electron microscopy showed their polymer fractal-porous structure.

These ABL practically completely copied descriptions of BL motion. They unexpectedly appeared from the channel of the plasma generator, usually 30 ms after the plasma flow. Visually they unexpectedly disappeared though the movie showed their gradual starvation during 0,3-0,4 s. In reference [53] experimentally and theoretically was shown that analogous

in sizes and the lifetime objects were observed at burning of small particles of wood with sizes ~1-2 mm. Such particles could be formed in this experiment at erosion of the channel wall and then they ignited.

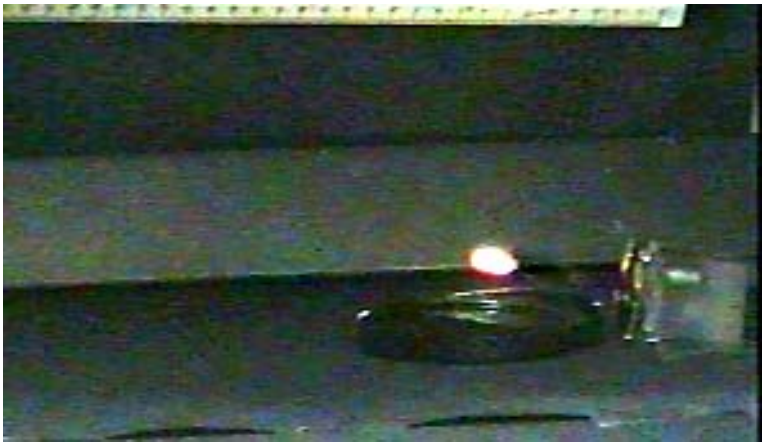

Fig.23 *Typical ABL obtained with a help of the capillary plasma generator. (16-th frame)*

Long lived luminescent formation with a form close to the spherical (plasma vortex) and sizes 30-35 cm and the lifetime about 2 s was formed at explosion of round metallic diaphragm of the plasma gun by powerful current pulse (I_{max}~10-12 κA, U~80 V, pulse time ~ 80 ms) at put in energy about 10 kJ [54] .

Experiments with jets show that complex gasdynamic configurations are formed in experimental conditions;: eroded material of electrodes and walls comes into their composition. Complicated processes of these particles oxidation in air (combustion) determine their luminescence time. It should be marked that energy put into the channel is usually large with respect to the thermal, so the character of processes in highly excited material of eroded material of electrodes and walls of the device can be essentially different from the equilibrium.

New results

Recently several works devoted to ABL generation have been published. In reference [55] indicated that G.Fussmann (M.Plank institute for Plasma Physics)and colleagues (Humbolt University) simulated the effect of lightning strike on a vessel of water. They inserted two electrodes into a large beaker filled with water, with one electrode surrounded by a ceramic tube. Using a powerful capacitor bank they then passed a current of about 60 A and energy of 8 kJ through the water. This caused the water within the tube to evaporate. The result was a plasma formation that hovered over the water for about 0.3 s after the current was switched off. Indeed in this experiment were repeated experiments of Plante and their development in works [17-19] in a new form. Unfortunately the authors of these experiments have forgotten to mention the routes of their experiment.

In work [56] authors generated fireballs by exposing silicon, glass and alumina to concentrated microwave beam. By melting and vaporizing the material they firstly formed a column and then a fire ball . This object did not last long – about 30-40 ms after the power source was turned off.

In work [57] authors sandwiched a peace of silicon 0.3 mm thick between two electrodes and applied a voltage 0f 20-25 V. They then raised the top electrode, thereby creating an electrode arc from which luminous spheres the size of table-tennis balls flew in all directions. They last for up to 8 s. However, these fireballs are not a perfect mach with natural BL since they are not as large, or do not freely (although they do bounce around, sometimes reaching heights of 20 cm). Their formation match to the theory [58] where BL is considered as charged structure with hot melted surface.

In work [59] a comparably long lifetime of ABL due to introduction of flammable material which is a material of electrodes to the non – stationary discharge was achieved; this increases the time of the afterglow to several parts of the second. It can be realized by closing and opening of electrodes with high erosion, such as copper, aluminum and coal. At that one can observe a tendency of the plasma to form a spherical configuration. In Fig. 24 one can see ABL appearing at closing –opening of the coal electrodes at the discharge parameters: current about 25 A, 50 Hz, 380 V through the resonance series vibrator circuit with characteristic resistance R_c~16 Ω.

In the end of this section we have to note also results of the work [60], where long-lived ABL with life time of 0.24 s was obtained at passing of the current of 1200 A through a spiral rolled-up in tore. Here we see melting, evaporating and ignition of the spiral metallic material. At that its form impacts its combustion features.

5. Conclusions

Reviewed experiments show a complicated character of origination and elimination of ABL objects both gasdynamic and plasma chemical nature

ABL can appear in gasdynamic conditions at formation of plasma or vortex structures, in this case they have gasdynamic nature and means of their creation and conditions of their existence are understood in principle. Д

Analysis of experiments demonstrates also existence possibility of ABL on a basis of heterogeneous structures (mixture of a gas with solid or melted components) or ABL with solid framework. They are formed at the destruction both organic polymeric materials and inorganic materials , such as Si, SiO or SiC. In the plasma conditions these ABL can be highly excited and represent non-equilibrium electrically charged structures and melts that combust in air.

Fig.24 *Two stages of ABL realization [59] : to the left – generation of the fire ball between coal electrodes; to the right - after glow lasting during 1 s*

Fig.25. *Electric explosion of wire spiral rolled –up in tore, t=0.24 s of its existence [60].*

References

1. *Ershov A.P., Timofeev I.B., Chuvashev S.N.* // Teplofizika Vysokikh Temperatur. 1990. V.28. № 3. P. 583.
2. *Aleksandrov A.F., Isaev K.Sh., Chernikov V.A.* // Teplofizika Vysokikh Temperatur. 1990. V.28.. № 5. P. 833.
3. *Alexandrov A.F., Chernikov V.A., Chuvashev S.N., et.al.* Long-lived plasma formations in air// AIAA-99-4977. 9-th Int. Space Planes and Hyper. Syst. and Technol. Conf. 1-4 Nov. 1999. Norfolk. USA. 12. P.
4. *Avramenko R.F., Bakhtin B.I., Nikolaeva V.I., et. Al. //Zhournal Tekhnicheskoi Fiziki*. 1990. V.60, №12. P. 73.
5. *Avramenko R.F., Nikolaeva V.I., Poskacheeva L.P. //* Collection of works Ball lightning in a laboratory. Eds. *Avramenko R.F.,* Bychkov V.L., Klimov A.I., Sinkevich O.A. Moscow. Khimiya. 1994. P. 15.
6. *Bychkov V.L., Gridin A.Yu., Klimov A.I.* //Ibidem. C. 66.
7. *Bychkov V.L., Gridin A.Yu., Klimov A.I.* // Teplofizika Vysokikh Temperatur. 1994. V. 32. №. 2. P. 190.
8. *Smirnov B.M. Ball lightning problem. Moscow. Nauka.* 1988.
9. *Stakhanov I.P. About physical nature of ball lightning.* Moscow. Energoatomizdat. 1985.
10. *Grigor'ev A.I., Sinkevich O.A.* // *Zhournal Tekhnicheskoi Fiziki*. 1984. V.54. № 12. P. 1276.
11. *Brovkin V.G., Kolesnichenko Yu.F.* // *Zhournal Tekhnicheskoi Fiziki*. 1984.V.64. № 2. P. 194.
12. *Shibkov V.M., Aleksandrov A.F., Kuzovnikov A.A.* // Collection of works Ball lightning in a laboratory. Eds. *Avramenko R.F.,* Bychkov V.L., Klimov A.I., Sinkevich O.A. Moscow. Khimiya. 1994. P. 136.
13. *Shakhparonov I.M.* //Ibidem. P. 184.
14. *Barry J.* Ball lightning and bead lightning. Moscow.: Mir.1983.
15. *Singer S. The nature of ball lightning.* Moscow.: Mir.1973.
16. *Plante G.* Electric phenomena in atmosphere. S-t- Petersburg V. Bezobrazov press. 1891.
17. *Shabanov G.D.* // Pis'ma v Zhurnal Tekhnicheskoi Fiziki, 2002. V. 28. №. 4. P. 81.
18. *Emelin S.E., Pirozerskyi A.L., Egorov A.I. e. al.* // Works of. 9-th Russian Conf. on Cold Transm. Nuclei of Chem. Elements and Ball Lightning. Dagomys. Sochi. 29 September- 6 October 2002. Moscow. 2002. P. 240.

19. *Egorov A.I., Stepanov S.I.* //Preprint PIYAF -2004 № 2558. Gatchina. 2004..
20. Kuz'min R.N., Miskinova N.A., Shvilkin B.N.// Khimicheskaya Fizika.2006.. 25. №3. P.90-93.
21. *UrutskoevL.I., Liksonov V.I., Tsynoev V.G.* // Prikladnaya Fizika. 2000. № 4. P. 83.
22. *Dijkhuis G.C.* // Nature.1981. V. 284. P. 150.
23. *Golka R. K.* // J.Geophys.Res. 1994. V.99. P. 10 679.
24. *Cawood, W., Patterson H.S.* // Nature. 1931. V.128. P.637.
25. *Ohtsuki, Y.H., Ofuruton H.* // Il Nuovo Cimento. 1990. V. 13C. P. 761.
26. *Corum K.L., Corum J.F.* // Uspekhi Fizicheskikh Nauk. 1990. V. 160. № 4. P. 47.
27. *Powell J.R., Filkenstein D.*//American Scientist. 1970. V.58. P. 262.
28. *Ardelyan N., Bychkov V., Gromov V., et al.* //Proc.341 15-th Intern. Conf. on MHD Energy Conv. and 6-th Intern. Workshop on Magnetoplasma aerodyn. Moscow. May 24-27. 2005. Vol.1. P. 341.
29. *Nauer H.*//Z. Angew. Phys. 1953. Bd.5. № 12. S. 441.
30. *Voitsekhovskyi B.V., Voitsekhovskyi M.B.* // Doklady Akademii Nauk SSSR. 1986. V.287. P. 331.
31. *Smirnov B.M.*// Int. J. Theor. Phys. 1993. V.32. P.1453.
32. *Tesla N.* Colorado Springs Notes 1899-1900. Beograd.: Nolit. 1978. 437 P.
33. *Slyusarev N.M.* // Ball lightning. Ed. Prof. Smirnov B.M. Moscow. IVTAN. 1990. P. 18.
34. *Ford R.A.* Home made lightning. McGraw-Hill. N.Y. 2001. 228 P.
35. *Bychkov V.L.* //Physica Scripta. 1994. V. 50. P. 591
36. *Aleksandrov V.Ya., Borodin I.P., Kirichenko E.V., Podmoshenskyi I.V.* // Zhurnal Tekhnicheskoi Fiziki. 1982. V.52. № 4. P. 818.
37. *Aleksandrov V.Ya., Golubev E.M., Podmoshenskyi I.V.* // Zhurnal Tekhnicheskoi Fiziki.. 1982. V.52. № 10. P. 1987.
38. *Lushnikov A.A., Negin A.E., Pakhomov A.V.* // Chem. Phys. Lett. 1990. V.175. №1-2. P. 138.
39. *Lushnikov A.A., Negin A.E., Pakhomov A.V.* // Ball lightning. Ed. Prof. Smirnov B.M. Moscow. IVTAN. 1990. P. 11.
40. *Mikhailov E.F., Vlasenko S.S., Kiselev A.A.* // Fizika Plasmy. 1995. V.21. №5. P. 442.
41. *Abrahamson J., Dinniss J.* // Nature. 2000. V. 403. P. 519.
42. *Vinogradov G.K., Imanbaev G.Zh., Polak L.S., et al.*. // Khimia Vysokikh Energii.. 1983. V. 17. P. 372.
43. *Alexeff I., Parameswaran S.M., Thiyagarajan M., et al.* //IEEE Trans. Plasma Science. 2004. V.32. N.3. P. 1378.
44. *Alexandrov A.F., Bychkov V.L., Ershov A.P., et al.* // Proc.8-th Inter. Symp. on Ball Lightning. 3-6 August 2004. Nat. Centr. University Chung-li. Taiwan. P. 111.
45. *Emelin S.E., Semenov V.S., Bychkov V.L. et al.* // Zhurnal Tekhnicheskoi Fiziki. 1997. V.67. №.1. P. 19.
46. *Bychkov A.V., Bychkov V.L., Timofeev I.B.* //Abstracts. 7-th Int. Symp. on Ball Lightning. 26-29 July. 2001. University of Missouri. St.Louis. Missouri. P. 16.
47. *Bychkov V.L., Bychkov A.V., Timofeev I.B.*// Zhurnal Tekhnicheskoi Fiziki. 2004. V.74. № 1. P. 128.
48. *Emelin S.E.,Pirozerskyi A.L., Skvortsov G.E.et al.*. // Works of. 9-th Russian Conf. on Cold Transm. Nuclei of Chem. Elements and Ball Lightning. Dagomys. Sochi. 29 September- 6 October 2002. Moscow. 2002. P. 252.
49. *Bychkov V.L., Klimov A.I., Babaev V.G.,et al.* // Izvestiya A N. Ser. Fizicheskaya V.60. №2. P. 112.

50. *Taylor A.R.* Forest fire. Yearbook of science and technology. N.Y.: McGraw-Hill. 1974. 201 P.
51. *Klimov A.I., Mel'nichenko D.M., Sukovatkin N.N.* // Collection of works Ball lightning in a laboratory. Eds. *Avramenko R.F.,* Bychkov V.L., Klimov A.I., Sinkevich O.A. Moscow. Khimiya. 1994. P.72.
52. *Dimitrov S.K., Zhdanov S.K., Kirko D.L. et al.* //Ibidem. P. 79.
53. *Konev E.V.* Physical grounds of plant materials combustion. Novosibirsk. Nauka. 1977.
54. *Kunin V.N., Pleshivtsev V.S., Furov L.V.* // Teplofizika Vysokikh Temperatur. 1997. V.35. №. 63. P.866.
55. *Cartlidge E.* // Physics world. 2007.05. P. 35.
56. *Dikhtyar V.*, Jerby E.// Phys. Rev.Lett.2006. v.96. P. 045002.
57. *Pavão A., Paiva G., Vascocelos E.A. et al.* // Phys. Rev.Lett.2007. v.98. P. 048501.
58. B*ychkov V.L., Bychkov D.V.* //Ball lightning as unipolarly charged object with hot surface. Proc. 9-th Intern. Sympos. on ball lightning. (ISBL-06) 16-18 August 2006. Eindhoven University of Technology. Eihdhoven, the Netherlands. P. 26-32.
59. *Emelin S.A., Pirozerskyi A. L.*//Khimicheskaya fizika. 2006. V. 25. №3, P. 83.
60. Vlasov A.I., Vlasov A.A. // Proc. 9-th Intern. Sympos. on ball lightning. (ISBL-06) 16-18 August 2006. Eindhoven University of Technology. Eihdhoven, the Netherlands. P.234

THE POSSIBILITIES FOR THE FORMATION OF THE ORDERED PLASMA STRUCTURES IN NATURE.

A. I. Nikitin, A. M. Velichko, T. F. Nikitina

Institute for Energy Problems of Chemical Physics, Russian Academy of Sciences
Moscow, Russia
E-mail: anikitin@chph.ras.ru

In the second half of the 20th century due to the works by I.R. Prigozhin and his school one could come to perceive that self-organization of the matter is possible in open thermodynamic systems (far from their equilibrium) along with the formation of microscopic structures. In nature ball lightning appears to be regarded as an example of such an orderly plasma structure. It was reported to carry electric charges, to be particularly energetic and to exist for a rather long time. This raises the questions of special interest of what can prevent the fast recombination of charges, in which form the energy is stored in ball lightning, what forces confine the electric charges to the bounded region of a space, what is the mechanism of its radiation. In recent years the model of ball lightning has been developed by the authors, in which it is considered as a heterogeneous structure composed of energy core and dielectric shell. The core is a system of electrons and protons moving in vacuum. Electrons move in a circle drifting in the crossed electric and magnetic fields, and protons, generating the magnetic field, revolve around electron ring: they are maintained in orbit with the electric field, produced by the charge of the ring. The total number of protons in the system exceeds the number of electrons therefore the energy core has a non-compensated positive charge. Like any plasmoid the core couldn't be confined by its own magnetic field and expands radially. This expansion of the core is retarded by the bubble-shaped shell, which tends to shrink under the action of non-uniform electric field of the core. The stability of the system is kept by the equality in value of two forces, expanding and shrinking the shell. The energy in the system is stored in the form of kinetic energy of protons and the energy of the core's electric field. The radiation of ball lightning may be associated with a synchrotron emission of relativistic electrons. In nature the discussed ordered plasma system may be formed in the vicinity of the linear lightning channel as a result of vacuum cavity rise, separation and acceleration of the charges, the loss of the part of negative charge and production of the shell by water drops.

1. Introduction

In the open dissipative thermodynamic system the development of self-organization process is possible [1]. The typical example of such a system is the Earth's atmosphere, which obtains the low-entropy energy of the Sun's light emission. In the real atmosphere non-uniformities of different scale arise – pressure jumps, winds, whirlwinds, hurricanes. Some of them live some seconds, while the other may exist some weeks. Plasma, which may be regarded as uniform only in the average, in fact in the scale of microscopic lengths and short time intervals is a mosaic of vortices, waves and ordered flows of particles. It is not improbable, that among

these creations the structures with rather long lifetime may exist. According to observations, some features of ball lightning may be explained by the presence of electric charges in its substance. Because of this it is possible, that the substance of ball lightning may represent a certain form of highly-ordered plasma.

Since the nature has, undoubtedly, found a method for creation of such type of plasma, it is worthwhile to try to find a related method of ball lightning producing in laboratory. In this search two different ways are possible. One may make the experiments with electric discharge in air, varying experimental conditions (energy, voltage and form of current pulse, composition and humidity of gas etc.) in the hope, that eventually he will find empirically the conditions, analogous to conditions of ball lightning creation in nature. However, it may be turned out, that this way is very long and very expensive. Moreover, this way is not necessarily successful, because always doubts remain whether all minor details, which may turn out to be crucial, are taken into account in organization of discharge. Because of this the other way is considered as more preferential: to try to "guess" the structure of long-living plasma creation and to focus the experiment on the producing of such object. It is precisely this approach to study of ball lightning structure that is proposed in this paper.

2. Dynamic electrical capacitor

A dynamic electrical capacitor, as it is called, is regarded to be a basic element of ball lightning substance [2 – 4]. This system resembles an atom, as though it is "turned inside out": in the central part of this capacitor the electrons are placed, and positive ions (protons) rotate around them (see Fig. 1). The prototype of this system is a hydromagnetic capacitor, invented in the fifties of the twentieth century [5]. It comprises a plasma, placed in radial symmetric electric field and normal to it magnetic field. In the crossed fields the separation of electrons and positive ions and their drift in circles of different radius proceeds. The centrifugal force of ions is transferred to the coils, generating the magnetic field. In this case the force, stretching winding of the coils, is compensated by elastic force of the coil material. The discussed dynamic capacitor differs from hydromagnetic capacitor in that its magnetic field H is created due to motion of protons and not by the external coils. Under the action of this magnetic field

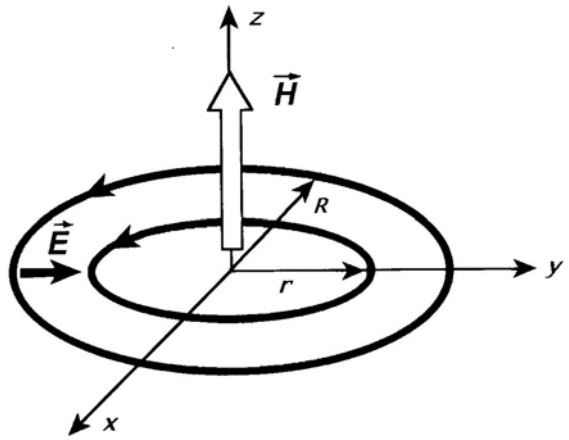

Fig. 1. *The diagram of charges movement in dynamic electrical capacitor. The inner ring is composed of electrons, and the outer – of protons.*

and normal to it radial electric field $\boldsymbol{E}$, acting in the gap between electrons' and protons' orbits, electrons are drifting with a velocity [6]:

$$\boldsymbol{v}_d = [\boldsymbol{EH}] / \mu_o H^2. \quad (1)$$

Here μ_o is a magnetic constant, $\mu_o = 1.2566 \cdot 10^{-6}$ *H*/m. In order that the electrons rotate in a circle, the condition must be fulfilled [7, P. 75]:

$$H \geq (\varepsilon_o/\mu_o)^{1/2} E. \quad (2)$$

Here ε_o is an electric constant, $\varepsilon_o = 8.8542 \cdot 10^{-12}$ F/m. Substituting condition (2) in formula (1), we find that the velocity of electron must be near the light velocity:

$$v_d \leq E/\mu_o H = (\mu_o \varepsilon_o)^{-1/2} = 2.998 \cdot 10^8 \text{ m/s}.$$

Moving in a circle, the electrons will execute oscillations along the direction of electric field with the amplitude [8, P. 44]:

$$b = 2mE/e\mu_o^2 H^2. \quad (3)$$

One can see that the amplitude is proportional to the mass of electron *m* and its charge *e*. It is worth noting that if we would try to "make" an analogous system of protons, located inside, and outside electrons, then the amplitude of radial oscillations of protons would be in 1836 times greater. So, in this case the creating of dynamic system with a small gap between the charges' orbits, and, consequently, with a large strength of electric field *E*, would be impossible.

In the flat system, shown in Fig. 1, generated by protons' motion magnetic field in the place of electron ring location has a radial component, directed outward from the ring axis. This component of magnetic field will create a force, causing electrons to leave the orbit's plane [2, 3]. For the opposite case to take place, the radial component of magnetic field must be directed toward the axis of the ring. This may be done, if magnetic field near the plane of electrons' orbit will have a "barrel-like" configuration (which is used for axial focusing of charged particles orbits in cyclotron and betatron [9, 10]). The required configuration of the field may arise if protons due to Coulomb repulsion will leave the orbit's plane and will move in numerous orbits,

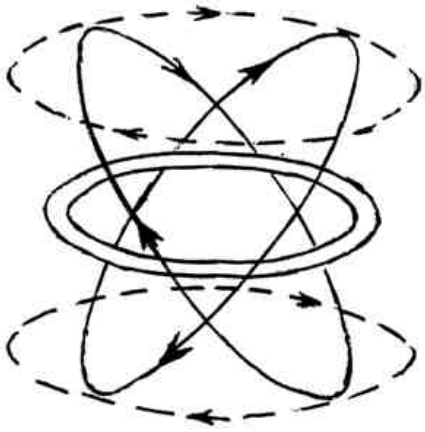

Fig. 2. *A view of protons orbits in dynamic capacitor.*

inclined at different angles to the plane of electron's ring (see Fig. 2). So, our system of charges may look like a sphere with truncated poles, filled with proton's orbits, a ring of electrons, moving with near-light velocity, being located inside this sphere. To estimate characteristics of this system let us replace it with a cylindrical capacitor with outer electrode of radius R, equal to radius of proton's orbit, and with internal radius r, equal to radius of electrons' ring. To be specific, let radius R be 0.5 cm, r = 0.35 cm, and cylinder's height h = 0.5 cm. Capacitance of this condenser is $C = (2\pi\varepsilon_o h) / \ln(R/r) = 0.78\cdot10^{-12}$ F. Let energy W_e of electric field of this capacitor be 100 J, then a potential difference on its electrodes is $U = (2W_e /C)^{1/2} = 1.6\cdot10^7$ V, an average electric field strength is $E = U / (R - r) = 1.07\cdot10^{10}$ V/m, and its charge is $Q = CU = 1.25\cdot10^{-5}$ C. It should be noted that the found value of electric field strength is in $3\cdot10^3$ times larger than the value, when electric breakdown of air occurs, $E_{br} = 3\cdot10^6$ V/m. Because of this the sole insulator in our capacitor may be only a fine vacuum. Let the motion of proton in orbit of radius R is provided by electric field E. From the condition of equality of the force $F_e = eE$ and centrifugal force $F_c = (m_p v_p^2)/R$, we find proton's velocity $v_p = (eER /m_p)^{1/2} = 7.15\cdot10^7$ m/s. (When the relativistic corrections are considered, we obtain $v_p = 7.05\cdot10^7$ m/s). Here m_p is proton's mass, $m_p = 1.673\cdot10^{-27}$ kg, and $R = 5\cdot10^{-3}$ m. Frequency of the proton rotation in an orbit $f_p = v_p/2\pi R = 2.244\cdot10^9$ s^{-1}. With the total charge of protons Q_p' equal to the total charge of electrons Q_e and on the assumption that orbits of protons lay in the same plane, the current, generated by protons' motion, is $I' = Q_p' f_p = Q_e f_p = 2.8\cdot10^4$ A, and magnetic field intensity in the centre of electron orbit is $H' = I'/2R = 2.8\cdot10^6$ A/m. As it was mentioned above, for suppressing of electrons' drift in radial direction the condition $H \geq (\varepsilon_o/\mu_o)^{1/2}E = 2.654\cdot10^{-3}E$ must be fulfilled. At $E = 1.07\cdot10^{10}$ V/m there should be $H \geq 2.84\cdot10^7$ A/m. The found value H is ten times greater than the value H', obtained for electrically neutral system of charges. To increase magnetic field strength up to required value, one must suppose that the number of protons (and, correspondingly, their total charge) is ten times larger than the number of electrons. As a result we come to the conclusion that the dynamic electrical capacitor with the above estimated parameters may exist, if the total charge of protons will be equal to $Q_p = 10Q_p' = 1.25\cdot10^{-4}$ C. So the capacitor as a whole will have non-compensated positive charge $Q = Q_p - Q_e = 1.125\cdot10^{-4}$ C. According to formula (3) the amplitude of radial oscillations of electrons at $E = 1.07\cdot10^{10}$ V/m and $H = 2.84\cdot10^7$ A/m is $b \leq 10^{-4}$ m, that is lower than inter-electrode gap $R - r = 1.5\cdot10^{-3}$ m in 15 times. Kinetic energy of protons with total charge $Q_p = 1.25\cdot10^{-4}$ C is equal to $W_p = (Q_p m_p v_p^2)/2e = 3.34\cdot10^3$ J. This energy is 33.4 times higher than electrical energy of capacitor W_e = 100 J, therefore it is possible to consider that energy of this dynamic electrical capacitor is basically stored in the form of kinetic energy of protons.

The "constructed" system of moving charges is unstable against radial expansion. Indeed, since the electrons' ring is constrained by the pressure of magnetic field, generated by protons motion, this ring in its turn "press" on protons, trying to increase radiuses of their orbits. If the magnetic field was created by the external coils (as it takes place in the hydromagnetic capacitor), then this pressure was be taken by material of coils. In our case we have no any "rigid" coils, so their function must be taken up by some other element of our construction. As such an element a shell of any dielectric (for instance, of water), separating the charges from atmosphere, may appear. Previously we implicitly assumed the presence of this shell since we considered that the motion of charges takes place in vacuum. As a force, shrinking the vacuum cavity, located inside the shell, and, correspondingly, the system of charges, moving inside the cavity, may be the force of atmospheric pressure. So for the shell with inner radius R = 6.2 cm (which volume is 1 liter) the force of atmospheric pressure is $F_a = P_a\cdot4\pi R^2 = 4.83\cdot10^3$ N. (Here $P_a = 10^5$ N/m^2). According to virial theorem [11], the kinetic energy W_k of particles, constrained in container of volume V, which is compressed by a pressure P, can

not exceed a value $W_k = 3PV$. So in the volume $V = 10^{-3}$ m^3 at $P = P_a$ one can carry particles, the total kinetic energy of which is no more than 300 J, and energy density is below $\rho_E = 3 \cdot 10^5$ J/m^3. There are evidences for observing of ball lightning with energy density $6 \cdot 10^8$ - $6 \cdot 10^9$ J/m^3 [12 – 14]. This set us to assume, that the substance of ball lightning (if its basic energy is kinetic energy of particles) is compressed by the other forces, which strength exceeds the atmospheric pressure by some orders. According to above reasoning the energetic core of ball lightning (the dynamic capacitor) has the excess electric charge. This must add to the force, stretching the shell due to motion of particles, the extra force, caused by Coulomb repulsion of the charges of the same sign. Fortunately, just the availability of this non-compensated charge imparts to shell properties, casing it to shrink towards the centre. In the strong electric field of the core a polarization of molecules in the shell must proceed. On the inner surface of the shell the charges, which sign is opposite to the sign of the core, will be gathered, and on its outer surface the charges will be gathered, which sign coincides with the sign of the core. In non-uniform electric field of the central charge a force, shrinking the shell, must arise. The value of this force is proportional to gradient of electric field and to dipole moment of the shell (product of surface charge on shell thickness). As will be shown below, this force is quite sufficient to constrain inside the shell the charged core with density of kinetic energy up to $2.3 \cdot 10^{10}$ J/m^3.

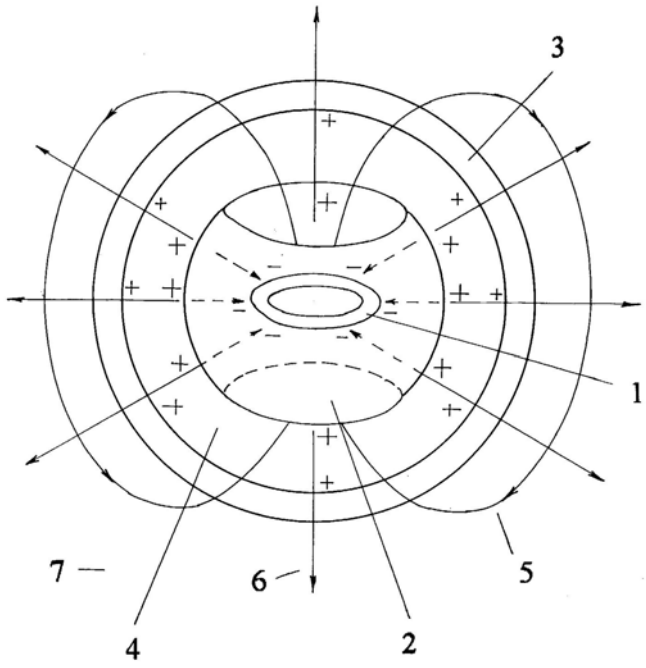

Fig. 3. *The structure of ball lightning with one-element power core. 1 – electrons' ring; 2 – protons; 3 – shell; 4 – vacuum; 5 – magnetic field; 6 – electric field; 7 – atmosphere.*

In the light of the preceding ball lightning may appear as an object shown in Fig. 3. Here the single dynamic capacitor is located inside the shell. In environment this object will behave as an electric monopole with positive charge and as magnetic dipole. Due to continuous losses of charge by the energetic core the shell is also positively charged. This insures reflection from it at collisions of the parts of power core, as well as of a whole core. (The last must lead to producing of sound). The other configuration, presented in Fig. 4, is also possible. In this case the core consists of large number of small dynamic capacitors. Magnetic fields of the neighbour

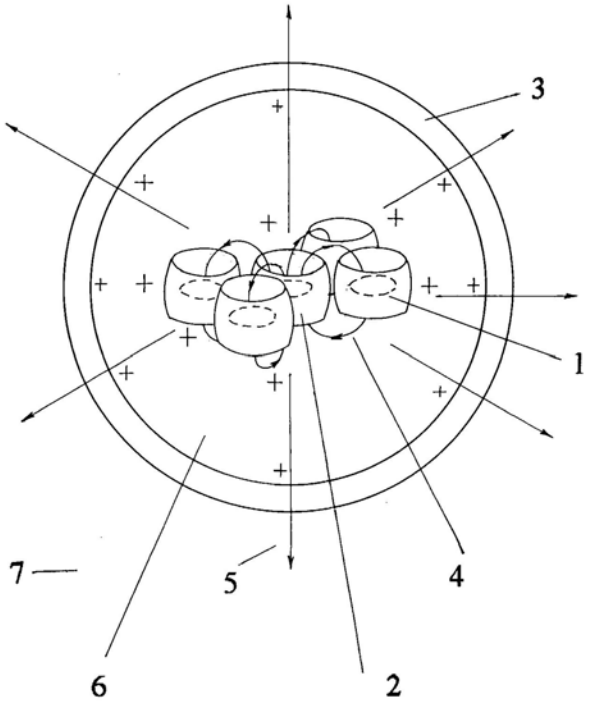

Fig. 4. *The structure of ball lightning with multi-element power core. 1 – electrons' ring; 2 – protons; 3 – shell; 4 – magnetic field; 5 – electric field; 6 – vacuum; 7 – atmosphere.*

capacitors are closed on each other, because of this for configuration with multi-element core the outer magnetic field must be weak. The estimates show, that when values of total kinetic energy of protons and radiuses of shells are equal, the pressure of the core on the shell for two configurations turns out to be approximately equal. Because of this one may analyse the simple configuration, shown in Fig. 3, with certainty that the results are also true for the more complex multi-element configuration [15, 16].

3. Properties of the electrodynamic model of ball lightning

The developed thermodynamic system has unusual properties. In spite of the fact that it possesses large energy, it is highly ordered, so its entropy may be rather low. If entropy S is interpreted as a function, proportional to logarithm of number of states, occupied by the system, $S = k_B \ln N$ (here k_B is Boltzman constant), one can see, that, on the one hand, the system of the moving charges is located in a small part of volume of cavity inside shell, and, on the other hand, spectra of allowed values of energy for electrons and protons are very narrow [17]. Besides, the temperature of this system $T = dW/dS$ (here W is an energy of the system), characterizing the degree of randomness of particles motion, is also low. If motion of charges proceeds without collisions and they are uniformly distributed along the length of orbit, the temperature T may be sufficiently lower than room temperature. An analogy to this may be given by the situation in supersonic flows of gas, where in spite of large velocity of molecules motion along the axis of jet, the velocity of their random motion in the direction, perpendicular to the axis, turns out to be low and it is characterized with a low temperature [18]. The circumstances indicated above (high order, absence of collisions, low temperature) is a decisive factor in the process of reflection of power core from the walls of the charged shell. According to Gauss theorem [19], a charge, localized inside the shell, is free of forces. Because of this the force, preventing the core from approaching to the shell, arises only at

their close contact in the moment of collision. This force occurs due to local deformation of a part of the shell and the shell's tendency to eliminate this deformation. Since the velocity of orbital motion of proton at the moment of reflection is directed almost at a tangent to the shell surface, the shell experiences only that part of the proton's pulse, which is caused by expanding of its orbit in radial direction. The value of this part of the proton's pulse is in many orders lower than the total pulse of proton. Moreover, the transmitted pulse can not exceed the large, but finite value, depending on total mass of protons, their velocity, radii of orbits and Coulomb repulsion of charges. In contrast to this constraining of non-ordered system of particles (for instance, of randomly moving charges) inside of the shell, in principle, is impossible. Indeed, among these charges one always can find a small part of very fast particles, which can not be reflected by the shell. Moreover, at a thermal equilibrium the losses of these rapid particles in this system will be steadily replenished.

According to the aforesaid, ball lightning comprises a system of expanding core of moving charges and of shrinking dielectric shell, this system is at dynamic equilibrium. One of the forces, stretching the shell, is a centrifugal force F_{cf} of protons, which move with velocity v_p in an orbit of radius R (which is assumed to be equal to the inner radius of the shell):

$$F_{cf} = M_p v_p^2 / R = 2W_p / R. \tag{4}$$

Here M_p is the total mass of protons, and W_p is the kinetic energy of protons. The energy W_p can be taken as the energy of ball lightning. The second force, stretching the core (and correspondingly the shell) is the force F_{el}, caused by Coulomb repulsion of charges and by magnetic field, generated by the moving protons. Let us assume, that in the creation of this force only a non-compensated part of total charge $Q = Q_p - Q_e$ takes part. The value of this force is [20, P. 46]:

$$F_{el} = kQ^2 / 8\pi\varepsilon_o R^2, \tag{5}$$

where $k = (1 + \beta^2)L / \pi$, $\beta = v_p/c$, c is light velocity, $L = \ln[16R / (a_r + a_z)]$, a_r and a_z are radial and axial half-axes of proton's ring section. (Here we conventionally assume that protons move in one plane). When $v_p = 1.5 \cdot 10^8$ m/s then $1 + \beta^2 = 1.25$. If $a_r + a_z = 0.1R$, $L \approx 5$ and $k \approx 2$.

The force F_{sh}, shrinking the shell in radial direction, is proportional to the dipole moment of the shell (product of surface charge density σ and wall thickness a), to the gradient of electric field, which is created by the charge Q, located inside the shell, and to the area of the shell's surface:

$$F_{sh} = \sigma a \cdot \text{grad}\, E \cdot 4\pi R^2 = -4\sigma a Q / \varepsilon_o (2R + a). \tag{6}$$

Here in calculation of gradient of E the radius is taken as $R + a/2$, and the surface charge density may be assumed to be $\sigma = 1.6$ C/m^2. The second force, shrinking the shell, is an atmospheric pressure force:

$$F_a = -P_a \cdot 4\pi R^2. \tag{7}$$

Here $P_a = 10^5$ N/m^2. Because the action of F_a becomes significant only at large values of R, when $R >> a$, in formula (7) $R + a$ is replaced with R. The condition of equilibrium of the shell is the balance of all the forces, acting on it:

$$F = F_{cf} + F_{el} + F_{sh} + F_a = \frac{2W_p}{R} + \frac{kQ^2}{8\pi\varepsilon_o R^2} - \frac{4\sigma a Q}{\varepsilon_o (2R + a)} - 4\pi P_a R^2 = 0. \tag{8}$$

Assuming that the volume of the shell is constant and that increase of shell's radius takes place only due to work of the forces, extending the power core, and taking the derivative dF/dR (near $F = 0$), one can see that at any values of k, Q, a and R this derivative is negative. This means, that equilibrium of the shell in respect to variation of radius is stable [21].

In Fig. 5 the dependencies of the shell wall thickness a on power core charge Q, constructed with the formula (8), for inner radius R = 3 cm, k = 2 and kinetic energy of protons W_p from 1 to 10^7 J, are shown. One can see, that at $W_p > W_{p,cr}$ = 16.96 J curves of function $a(Q)$ have a minimum. One can find the minimum value of thickness a_m and corresponding value of charge Q_m from formula (8) at condition $da/dQ = 0$:

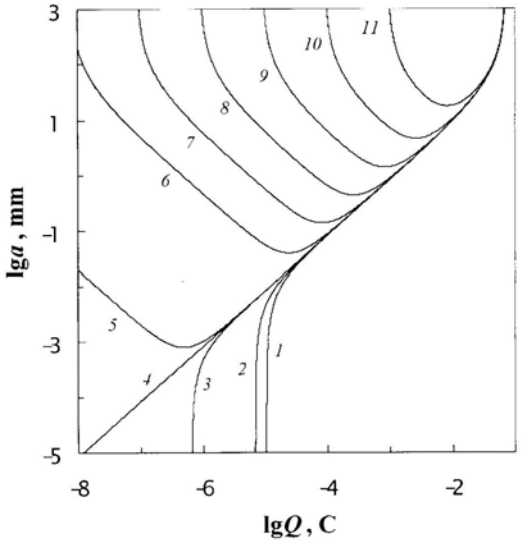

Fig. 5. *The dependence of shell wall thickness a for ball lightning with inner shell's radius R = 3 cm on the charge Q of power core for the values of kinetic energy of protons W_p equal to 1 J (curve 1), 10 J (2), 16.9 J (3), 16.9646 J (4), 17 J (5), 10^2 J (6), 10^3 J (7), 10^4 J (8), 10^5 J (9), 10^6 J (10) and 10^7 J (11).*

$$Q_m = [16\pi\varepsilon_o R(W_p - 2\pi P_a R^3)]^{1/2}, \tag{9}$$

$$a_m = \frac{2R\varphi}{1-\varphi}, \tag{10}$$

where $\varphi = [k\varepsilon_o(W_p - 2\pi P_a R^3) / 16\pi\sigma^2 R^3]^{1/2}$. With small radius R and large W_p one can neglect the second term in round brackets of formulae (9) and (10). As a result, assuming k = 2, we obtain:

$$a_m = \frac{2R\xi}{R^{3/2} - \xi}, \tag{11}$$

where $\xi = (W_p\varepsilon_o / 8\pi\sigma^2)^{1/2}$. From condition $dV_{en}/dR = 0$ we can find the value of inner shell radius $R_{m,v}$ when its volume V_{en} is minimal, $R_{m,v} = 2.57\ \xi^{2/3}$. Most probably, that ball lightning with large energy is created in conditions of scarcity of water, from which its shell is built. Because of this the parameters of "compact" ball lightning are of special interest. The calculated parameters of such ball lightning with kinetic energy of protons from 10^4 J to 10^{10} J are shown in Fig.6. Here the mean energy density of ball lightning is $\rho_E = W_p / (4/3)\pi(R + a)^3 = 2.3\cdot10^{10}$ J/m^3. One can see that volume of shell for the "compact" ball lightning, which energy is larger than 10^9 J, becomes extremely big (hundreds of cubic decimeters), this means that their existence in nature is unlikely. The points indicate values of outer radius and energy for the observed high-energetic ball lightning: "English lightning" [12], "Ukraine lightning" [13], "Khabarovsk lightning" [14, 22] and "Yerevan lightning" [23]. One can see a good agreement between the measured and calculated values. The cases, when energy of natural ball lightning appeared to be more than calculated energy, may be explained by the fact that

kinetic energy of protons (which is assumed to be equal to energy of ball lightning) is actually only a part of this energy. In some cases up to half of ball lightning energy may be contained in electric and magnetic fields.

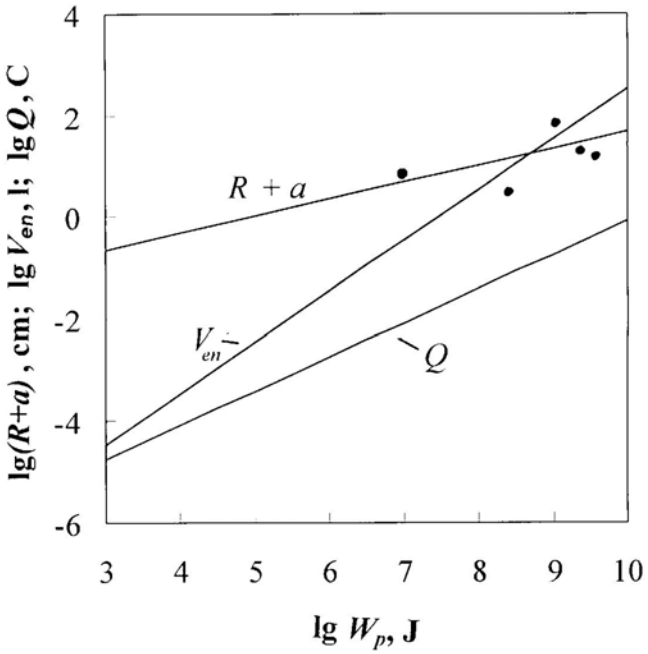

Fig. 6. *The dependencies on W_p – kinetic energy of protons – of outer radius of ball lightning R + a, shell's volume V_{en} and power core charge Q for the case of minimal volume of the shell. The points are the values of outer radius for observed ball lightning with measured energy: 10 MJ [12], 260 MJ [13], 1000 MJ [14], 2300 MJ [22] and 4000 MJ [27].*

4. The peculiarities of behavior of ball lightning

The main conclusion from the aforesaid is the fact that in positively charged plasma at high pressure long-term existence of highly-ordered structures, consisted of moving ions and electrons, is possible. Lifetime of these structures depends on the rate of energy losses. Since in these structures the electrons, moving with near-light velocities in round orbits, are present, the main channel of energy losses is the synchrotron emission of electrons. The estimations show that if the energy of the electrons appears to be sufficient for the maximum of synchrotron radiation intensity to fall in the middle of the spectrum of visible radiation (λ_{max} = 500 nm) the rate of energy losses due to radiation of electrons becomes very high, and the energy of ball lightning could be spent out in 10^{-2} s. But if there were a large number of electrons evenly distributed over an orbit, due to interference the radiation of one electron will be absorbed by another electron, and hence the rate of energy losses by the ensemble of the electrons will be drastically decreased [2, 3, 16]. This hypothesis provides an explanation for the long duration of ball lightning radiation, which has been observed to last up to several minutes.

The non-compensated charge of ball lightning allows one to interpret the observed cases of electrification by ball lightning of nearby objects as well as the peculiarities of its motion. The occurrence has been described, when a ball lightning with 10 cm diameter appeared at a distance of 1 m from the girl's head and lifted her 20 cm long hairs [24]. The experiments with electrostatic machines show that for the hairs of a human to be lifted his potential must be not less than U = 300 kV [25] and the electric field at the roots of hairs (with the head's radius r_h = 0.1 m) must be $E_h = U_h/r_h = 3\cdot10^6$ V/m. The charge Q of ball lightning inducing at a distance r = 1 m the field $E_h = 3\cdot10^6$ V/m is $Q = 4\pi\varepsilon_0 r E_h = 3.33\cdot10^{-4}$ C. With such a value of the charge the electric field intensity at a surface of ball lightning with 5 cm radius appears to

be $E_{bl} = 1.2 \cdot 10^9$ V/m, that in 400 times exceeds the breakdown voltage of air $E_{br} = 3 \cdot 10^6$ V/m. But in spite of such a high intensity of field no arc discharge occurs, since the energetic core of ball lightning carrying this charge is separated from the atmosphere with a good insulator – vacuum gap. A small number of charges, penetrating through this gap, accelerating in the electric field induced by the ball lightning core and electrifying gas, give rise to a corona discharge near the surface of ball lightning. The existence of the corona discharge allows explaining the cases of ball lightning levitation over conducting surfaces [26].

The analysis of the photo of ball lightning trace performed in [27] allowed a conclusion that ball lightning had a positive charge of $7.7 \cdot 10^{-5}$ C. During the thunderstorm the electric field in the vicinity of the Earth's surface may increase up to $E_{st} = 10^5$ V/m and the field vector under the cloud is usually directed from the Earth to the cloud [28]. The force acting in that field on the charge $10^{-4} – 10^{-3}$ C comprises $F_{el} = QE_{st} = 10 – 100$ N. This means that such a field is able to lift to the cloud a ball lightning of mass from 1 to 10 kg. The case has been known when ball lightning has lifted to the air a laboratory magnet of mass about 1 kg [13, P.72]. This can be explained by the arrangement of elementary magnets inside ball lightning core under the action of the magnet's field, thus evolving the core into magnetic dipole. And the lifting force was provided by the interaction of ball lightning electric charge with the electric field of the Earth. The stability of the dimensions of ball lightning throughout its lifetime, noted by many observers, may be attributed to the correlation between the rate of energy losses to radiation and the rate of the loss of electric charge from ball lightning [16]. If the rate of the charge flow from the ball lightning shell is determined only by the conductivity of the atmosphere λ_a, a decrease in charge will be described by the equation

$$Q = Q_0 \exp(-\lambda_a t/\varepsilon_0). \qquad (12)$$

The characteristic time of decrease of charge in e times $\tau_e = \varepsilon_0/\lambda_a$ can be used for the estimation of the average lifetime of ball lightning. At $\lambda_a = 3.5 \cdot 10^{-14}$ $(\Omega \cdot \text{m})^{-1}$ [29] $\tau_e = 253$ s. At the instant of its birth under the action of linear lightning discharge ball lightning resembles a flat system, shown in Fig.1, with the dimensions approximately equal to the inner diameter of vacuum cavity, inside which its formation takes place [16, 30, 31].

It is thermodynamically advantageous for the large current ring to be divided into a large number of small rings. Such a fragmentation of rings can be provided by a deformation of a large ring like its curling into a figure of eight. There is reason to think that the process of fragmentation ends when the diameter of an elementary dynamic capacitor approaches to several mm. Such a "low scaling" of the core's structure allows to explain the observations when ball lightning took the shape of a filament or a tape and then changed its shape in the passage through the narrow splits and small orifices.

Problems are experienced in the discussed model (as well as in all the models of ball lightning, where it is considered to be a material object) with the explanation of the passage of ball lightning through the undamaged glass. One possibility is that due to the heating of the glass area in a high electric field [32] the structure of the glass changes, and thus the glass gains the capacity to pass through itself small elements of ball lightning core [33]. The other possibility presumes the death of ball lightning on one surface of the glass and its re-birth on the opposite surface due to the transmission of high-frequency energy through the glass and inducing of magnetic field pulse leading to separation and acceleration of charges in the ball lightning core [16, 34].

5. Conclusion.

The described plasma creation as a structure of moving protons and electrons (with the excess of protons), which expansion is restricted by dielectric shell, allows to explain with a minimum of assumptions almost all of the features of the observed ball lightning. As in any theoretical model the problems arise upon the explanation of some exotic peculiarities of ball lightning, for example, of its capacity to pass through the window panes, leaving them undamaged, or of the absence of the breakdown at the conditions when the electric field on the surface of ball lightning is many times higher than the electric field of air breakdown. But all these difficulties seem to be surmounted without a necessity of essential changes in the basic model of ball lightning.

References

1. *G. Nicolis, I. Prigogine*. Self-organization in non-equilibrium systems. New York: John Wiley, 1977.
2. *A. I. Nikitin*. Electrichestvo. 1998. N. 11, P. 14 – 23. (In Russian).
3. *A. I. Nikitin*. Electrical Technology Russia. 1998. N. 4, P. 70 – 85.
4. *A. I. Nikitin*. Proc. 6th Intern. Symp. on Ball Lightning. 1999. Antwerp, Belgium, P. 91 – 95.
5. *O. Anderson, W. R. Baker, A. Bratenahl et al*. J. Appl. Phys. 1959. V. 30, N. 2, P. 188 – 196.
6. *L. A. Artsimovich*. Elementary physics of plasma. Moscow: Atomizdat, 1969. (In Russian).
7. *L. D. Landau, E. M. Lifshits*. The field theory. Moscow: Fizmatgiz, 1960. (In Russian).
8. *L. A. Artsimovich*. The controllable thermonuclear reactions. Moscow: Fizmatgiz, 1961. (In Russian).
9. *L. A. Artsimovich, S. Yu. Luk'ianov*. The movement of charged particles in electric and magnetic fields. Moscow: Nauka, 1978. (In Russian).
10. *V. A. Moskalyov*. Betatrons. Moscow: Energoatomizdat, 1981. (In Russian).
11. *D. Finkelstein, J. Rubinstein*. Phys. Rev. A. 1964. V. 135, N. 2A, P. A390 – A396.
12. *B. L. Goodlet*. J. Inst. Elect. Eng. 1937. V. 81, P. 1.
13. *I. Imianitov, D. Tikhi*. Beyond the border of lows of science. Moscow: Atomizdat, 1980. (In Russian).
14. *M. T. Dmitriev, B. I. Bakhtin, V. I. Martynov*. Zhurnal Technicheskoy Fiziki. 1981.V. 51, N. 12, P. 2567 – 2572. (In Russian).
15. *A. I. Nikitin*. Electrichestvo I Zhizn'. 2000. N. 2, P. 22 – 27. (In Russian).
16. *A. I. Nikitin*. Khimicheskaya Fizika. 2006. V. 25, N. 3, P. 38 – 61. (In Russian).
17. *Ch. Kittel*. Thermal physics. New York: John Wiley, 1969.
18. *G. N. Abramovich*. An applied gas dynamics. Moscow: Nauka, 1976. (In Russian).
19. *S. G. Kalashnikov*. Electricity. Moscow: Nauka, 1985. (In Russian).
20. *V. P. Sarantsev, E. A. Perel'stein*. Collective acceleration of ions by the electron rings. Moscow: Atomizdat, 1979. (In Russian).
21. *A. I. Nikitin*. Electrichestvo. 2004, N. 3, P. 29 – 36. (In Russian).
22. A. Batygin, I. Mosin. Newspaper "Pravda". Moscow. 1989, N. 220 (25939), P. 6. (In Russian).
23. *V. V. Balyberdin*. Samolyotostroenie i Tekhnika Vozdushnogo Flota. Kharkov. 1965, N. 3, P. 102 – 104. (In Russian).

24. *G. U. Lihosherstnyh*. Ball Lightning in Laboratory. Eds. R. F. Avramenko, V. L. Bychkov, A. I. Klimov and O. A. Sinkevich. Moscow: Khimia, 1994, p.222. (In Russian).
25. *R. A. Ford*. Homemade Lightning. New York: McGraw-Hill, 2002. P.179.
26. A. I. Nikitin, I. O. Leipunsky, T. F. Nikitina. Proc. 9th Intern. Symp. on Ball Lightning. 2006. Eindhoven, Netherlands. P. 139-147.
27. *A. I. Nikitin, A. M. Velichko, A.V. Vnukov, T. F. Nikitina*. Proc. 9th Intern. Symp. on Ball Lightning. 2006. Eindhoven, Netherlands. P. 148-156.
28. *M. A. Uman*. Lightning. New York: McGraw-Hill, 1969.
29. *J. A. Chalmers*. Atmospheric electricity. Oxford: Clarendon, 1949.
30. *A. I. Nikitin.* Electrichestvo. 2000, N. 3, P. 16 – 23. (In Russian).
31. *A. I. Nikitin*. Proc. 6th Intern. Symp. on Ball Lightning. 1999. Antwerp, Belgium. P. 85 – 90.
32. *A. I. Nikitin, V. L. Bychkov, T. F. Nikitina, A. M. Velichko*. Khimicheskaya Fizika. 2006. V.25. N.4. P.98 - 105. (In Russian).
33. *E. Cartlidge*. Seeking to Solve the Mistery of Ball Lightning. Physics World. 2007. May. P. 35 - 38.
34. *A. I. Nikitin.* Journ. of Russian Laser Research. 2004. V. 25. N. 2. P. 169 – 191.

RESEARCHES OF INTERACTION OF LONG–LIVING PLASMA FORMATIONS WITH SUPERSONIC STREAM AND BARRIER

•[1] V.A.Bityurin, V.Yu.Velikodny, I.A.Samuolis, E.B.Kolesnikov, V.V.Popov

[1] Scientific Association for High Temperatures of RAS, Moscow, Russia
•Institute of Applied Mechanics of RAS, Moscow, Russia

The theoretical substantiation of an opportunity of long-living plasma formations receiving is presented. Installation on the basis of the erosion discharge is created. Long-living plasma formations have been received. Two modes have been realized. The first one is long-living plasma formations in the form of spherical objects itself. And the second - breakdown in the form of beaded lightning.

Introduction.

Even in N. Tesla's pioneer experimental works it was marked, that the plasma containing products of erosion of electrodes, or products of condensation from specially evaporated wax substrate has a number of unique properties. In particular, big time of life was marked (~ 0,1-1 sec) these plasma formations. Subsequently these results were repeatedly repeated in a plenty experimental works (see, for example [1,2]), where alongside with long time of life the received plasma formations other interesting features were marked also (for example, splitting front of a shock wave, realization of more potentials in front (SW), resulting in this physical object. In theoretical works [3-5] for the first time on the basis of the complex approach, combining the decision of system of kinetic equations Boltzmann's and Poisson's and the decision the equations multitemperature, multivelocity gas dynamic's charged particles, the description shock waves structure in low ionized ionic cluster or dusty plasma is given, able to arise as a result of erosion electrodes or substrates. In these works a lot of "abnormal" properties was predicted and the effects inherent in such environment. We shall note, that such plasma differs from usual that, What the majority electrons in it is connected, that is the condition is satisfied $n_e << n_{i-} \le n_{p-} \le n_{i+}$ (where n_e – concentration electrons, $n_{i\pm}$ - concentration it is positive and negatives charged ions, $n_{p\pm}$ - concentration it is positive or negatives charged clusters, nano-particles, microparticles). The major result received in [3-5], is the prediction of effects " energy cumulating", i.e. an opportunity of transfer of the big kinetic energy (100 keV - 10 MeV and more), concentrated in clusters or the motes, to separate ions, electrons. And one of these effects is realized on "macro level" in result Divisions of charges in front UV, and the second at "micro level" as a result of collision кластеров, having a dispersion on the sizes and weights at distribution UV. The first it is in detail described earlier in [6].

Realization of the given effects can result in breakdown, or intensive to course of physical and chemical processes in front of a shock wave depending on it parameters and parameters of plasma, that in turn can significantly affect the start of chain avalanche processes [6] it was shown [3-6], that front shock wave in such environment can act as an effective chemical reactor. In to work [4] on the basis of the decision of system of kinetic Boltzmann's equations together with by equation Poisson's for lines of special cases it was shown, that front of a shock wave in low ionized ionic clusters plasma has strongly pronounced multiscale structure. It is possible to allocate zones fast $\delta_1 \le 10\lambda_1$ and one - two zones $\delta_2 \le 100\lambda_1$, $\delta_3 \le 10^3 \div 10^4 \lambda_1$ slow change of parameters, where δ_i - the characteristic size λ_1 - length of free runaway electrons. Partials temperatures and speeds components of environment essentially differ in all zones. On the basis of results [4] for the description of structure of front in low ionized clusters plasma authors was the complex approach combining the decision of system of the Boltzmann's equations is developed and applied for a zone of fast change of parameters and use of results of these decisions as boundary and entry conditions, for the equations multitemperature, multivelocity gas dynamic the charged particles together with equations chemical kinetics for zones of slowly varied parameters. It has enabled to describe structure of front of a shock wave in complex chemically reacting environments, 50 chemical reactions including more and the big number of components. It was received [6], that presence of an impurity of the charged microparticles or clusters in ionic reacting to plasma can result in reduction (on the order and more) time of an induction of lines the chain reactions which are of great importance for practical appendices. It is known [7], that clusters depending on temperature can have a charge of different polarity. In [3-4] it was shown, that for cases in which clusters or microparticles have positive polarity, electrons are accelerated in front. For cases, in which clusters or microparticles have negative polarity, electrons are braked and collected ahead of front. Depending on a charge clusters can to be realized current of plasma with essentially distinguished physical processes.

I. Model cumulating energy at collision clusters.

Within this year the base physical model of transfer with big probability of kinetic energy from system of many particles (clusters, fullerenes, nanotubes) to separate electrons, ions [7-10] is formulated. The essence of model is, that clusters with a dispersion on weights and diameter have in a zone transnational nonequilibrium in front SW strongly distinguished speeds. At speed distributions SW some kilometers per one second at the moment of collision clusters in to zone translational nonequilibrium of SW electrons an external environment of heavy atoms, components cluster, make a start, and nucleus on inertia continue to approach. In result the significant local division of charges generating strong electric field is realized. In this field "free" electrons can be accelerated and to get energy $E \cong E_t N_t^{2/3}$, where E_t - energy of a heavy nucleus, N_t -number heavy atoms in cluster. Therefore electron can pass to higher power level in atom, a component cluster, and then owing to transition in the basic condition can be generated radiation (in ultraviolet, vacuum ultraviolet) [11], or there can be an ionization cluster with emission "hot" electron. Effective temperature (in keV), got " average electron " in cluster at its collision with another cluster or with a wall due to the mechanism collective interaction, it is defined on semiempirical to the formula:

$$T_{ef} = \frac{2}{3}\frac{E}{N}\left(0.316 + 0.5\exp(-0.5(\frac{N_0}{N})^{2/3})N^{2/3}\right) \quad , \quad (1.1)$$

where E - energy cluster in keV, N- number of molecules in cluster; N_0 -number of molecules (or atoms) in cluster for which the exit of the excited products is maximal.

The formula (1.1) is received at processing experimental data [17] on excitation electronic levels of atoms of carbon in clusters at their collision with each other in to zone transnational nonequilibrium in front of a shock wave. In a basis of a conclusion (1.1) The physical model, consisting that cluster is considered as is put cvaziparticles with effective weight $m_{ef} = m_c N^{2/3}$, (N - number of atoms or molecules in cluster depending on a level of its organization, m_c - weight of atoms or molecules, forming cluster) and effective section $\sigma_{ef} = \pi d_c^2 N^{2/3}$ (d_c - diameter of atom or molecules). Probability of that the particle -electron will receive the energy concentrated in cvaziparticles, it is defined under the formula $W = \exp\left(-\alpha(\frac{N_0}{N})^{2/3}\right)$, where $\alpha = \gamma n_a^{-2/3}$ - semiempirical constant, in which n_a - number of atoms in a molecule. Size N_0 is function of kinetic energy cluster, structure and its internal structure and it is determined from experiment. Thus the size $\frac{E}{N}$ in (1.1) represents the energy, falling one atom or a molecule in a cluster. In calculations are accepted the following values of constants $\gamma \approx 1$, $\beta \approx 1$. A multiplier at exponent a member $\alpha N^{2/3}$ characterizes average energy cvaziparticles. Basically with a sufficient degree the formula (1.1) can be submitted to accuracy as

$$T_{ef} \cong \frac{2E}{3N}\left(\frac{1}{n_a} + (\frac{N}{n_a})^{2/3}\exp(-(\frac{N_0}{n_a N})^{2/3})\right) \quad , (1.2)$$

where for cluster, consisting of molecules, N - number of molecules in it; n_a - number of atoms in to molecule, for a case cluster, having nuclear structure, N - number of atoms, and $n_a = 1$. The effective temperature is defined from a ratio with [14]

$$\left\langle v\sigma(T_{ef})\right\rangle_{eq} = \left\langle v\sigma\right\rangle_{neq} \quad , (1.3)$$

Where $\langle\ \rangle_{eq}$ - expression for a constant of speed of process in " equilibrium conditions ", $\langle\ \rangle_{neq}$ - expression for a constant of the speed, caused by nonequilibrium effects.

II. Structure of a shock wave cluster ionic plasma.

Front of a shock wave in lowionezed ionic cluster plasma (with negatively charged cluster) consists of three characteristic zones: two zones slow change of parameters and a zone of fast change of parameters. Certainly, division of area of current into these three zones only conditionally, as width of these zones can it essential varies depending on parameters of a mix and a stream. Therefore in the general case it is necessary to solve system of kinetic Boltzmann's equations in common with Poisson's equation for all area of current, what for

multicomponent $N \geq 5$ the reacting environment now represents practically not solving a problem. In the given work flows of medium are considered at such parameters of a mix of a stream, at which probably above-stated simplification. In a forward part of front- δ_2, where concentration electrons increased, compensating a superfluous positive charge, and a back part δ_3 fronts, where concentration clusters slowly leaves on equilibrium value, the description is conducted on the basis of the equations of multitemperature, multivelosity gas dynamics of charged particles [5,6]:

$$\frac{\partial n_s}{\partial t} + \frac{\partial n_s u_s^{\alpha}}{\partial r_{\alpha}} = \frac{1}{2} \sum_{a,b,c} \left(k_{ab} n_a n_b - k_{ds} n_d n_s \right) \tag{2.1}$$

$$\rho_s \frac{du_s^{\nu}}{dt} + \frac{\partial}{\partial r_{\beta}} p_s^{\beta\nu} - e_s n_s E^{\nu} = \Delta Q_s^{\nu} \tag{2.2}$$

$$\frac{3}{2} n_s k \frac{dT_s}{dt} + p_s^{\beta\alpha} \frac{\partial u_s^{\alpha}}{\partial r_{\beta}} + \frac{\partial q_s^{\alpha}}{\partial r_{\alpha}} = \Delta Q_s^{ll} \tag{2.3}$$

$$\operatorname{div} \mathbf{E} = \frac{1}{\varepsilon_0} \sum_s n_s e_s \tag{2.4}$$

where n_s, u_s, T_s – partial concentration, speed, temperature; $p_s^{\beta\nu}$ - pressure tensor; $p_s^{\beta\nu} = \delta^{\beta\nu} p_s - \sigma_s^{\beta\nu}$; p_s - partial pressure; $\sigma_s^{\beta\nu}$ - viscous stress tensor; q_s^{α} - thermal stream; $m_{si} = \frac{m_s m_i}{m_s + m_i}$, m_i - weight of particle; ρ_s - partial density; e_s - charge of particle; k_{sd} – velocity constant of non-elastic process:

$$\Delta Q_s^{\nu} = \sum_{s \neq \tau} m_{s\tau} n_s n_{\tau} \Omega_{s\tau}^{(1.1)} (u_{\tau} - u_s) \xi_{s\tau} \tag{2.5}$$

$$\begin{aligned} \Delta Q_s^{ll} = & \sum_{s \neq \tau} m_{s\tau} n_s n_{\tau} \Omega_{s\tau}^{(1.1)} \left[\frac{3k(T_{\tau} - T_s)}{m_s + m_{\tau}} \xi_{1s\tau} + u_{s\tau}^2 \xi_{s\tau} \right] + \\ & + \frac{1}{2} \sum_{a,b,d} \left(\mu_{ba} E_{ba} n_b n_a k_{ba} - \mu_{ds} E_{sd} n_s n_d k_{ds} \right) \end{aligned} \tag{2.6}$$

where $\Omega_{sd}^{(1.1)}$ - Chapman-Kalugin omega integral, E_{sd} - a threshold of energy of activation non-elastic processes. References and expressions for other functions and the parameters which are included in (2.1)-(2.6) are given in [5,6]. In the field of fast change of parameters $\delta_1 \leq 10\lambda_1$, the description is conducted on to basis of system of kinetic Boltzmann's equations together with Poisson's equation:

$$\mathbf{v}_s \frac{df_s}{d\mathbf{x}} + \frac{e_s \mathbf{E}}{m_s} \frac{\partial f_s}{\partial \mathbf{v}_s} = \sum_{\tau} \iiint [f_s' f_{\tau}' - f_s f_{\tau}] |g| \sigma(\chi, y) d\Omega d^3 V_{\tau} \tag{2.7}$$

$$\frac{dE}{dx} = \sum_i \frac{n_i e_i}{\varepsilon_0} \tag{2.8}$$

where E - intensity of an electric field, g - relative speed, $d\Omega$ - corporal corner $\sigma(\chi, y)$ - section of collisions, $\mathbf{v}_s$ - molecular speed of a particle ε_0 - electric constant. Owing to

littlest width of this zone δ_1, in it has time to react only small, but a final share of particles, from the common number. Therefore influence physical and chemical transformations on movement of environment in this zone (as a first approximation) it is possible to neglect. It is reflected in the equations (2.7) in which members are omitted, responsible for physical and chemical transformations. It is essentially only influence of environment on physical and chemical transformations. This influence is taken into account in dependence k_{sd} from functions of distributions, received from (2.7):

$$k_{sd} = \int f_s(x, \mathbf{v}_s) \cdot f_\beta(x, \mathbf{v}_s) \cdot P_{sd}^{ab} \sigma(g, \chi) |g| d\Omega d^3 V_\alpha d^3 V_\beta .$$

.

Then the values received thus k_{sd} are substituted in souses members in the equations of dissolubility. In more detail with a technique of the decision of a problem in this se it is possible to familiarize in work [8]. The description of movement of low ionized plasmas in forward part of front is probably on the basis of the joint decision (2.1) - (2.8) by the method of consecutive approximations. The width of front of a forward part of a wave can vary in wide limits depending on initial concentration electrons. Further we shall be to consider a case $\delta_2 \geq \delta_1$. In this case it is possible to apply the reception used in [8]. As a first approximation influence of physical and chemical transformations on movement environments as a whole it is possible to neglect. Taking into account only influence of movement of environment on physical and chemical transformations (that is depth of transformation though is small, but it is final). At it the quantity of the reacted particles is enough to render essential influence on start of chain reactions. In view of the afore said, from (2.1) - (2.8) for the description movements electrons, neutral particles, ions, clusters for a forward zone of front δ_2 and zones of fast change of parameters we have the following equations and expressions:

$$\frac{dP_e}{dx} = -eEn_e \qquad (2.9)$$

$$T_e = \left(\frac{n_e}{n_{1e}} \right)^{2/3} T_1 \qquad (2.10)$$

$$\frac{dE}{dx} = \frac{1}{\varepsilon_0} \left(-n_e e + ez_i n_{1i} f(x) + ez_p n_{1p} \right) \qquad (2.11)$$

$$f(x) = \frac{1}{1+e^{Bx}} + \frac{u_1}{u_2} \frac{e^{Bx}}{1+e^{Bx}} \qquad (2.12)$$

where $P_e = n_e k T_e$ - partial pressure of electrons; n_{1e}, n_{1i}, n_{1p} - concentration electrons, ions, clusters in an accumulating stream, accordingly; z_i, z_p - charging numbers of ions and clusters; f (x) - the function describing change of concentration of ions and the neutral gas-carrier, it is received on the basis of the analysis of the decision (2.7), (2.8) [5,6] and results of work [9]; u_1 - speed of a stream on $-\infty$, u_2, T_2 - speed and temperature of a stream behind a zone of fast change of parameters (u_2, T_2 - speeds and are not equal to temperature $u_{+\infty}$, $T_{+\infty}$, where all mix is in balance). Expressions for u_2, T_2 and a way of their reception are given in [5,6]. Size B which is included in (2.12) $B = 4/\delta$, $s = 4\lambda_1/\delta = 0.8 \div 1.2$ (see [9]). The decision systems of the equations (2.9) - (2.12) it is

possible numerically. To start integration by one of numerical methods is necessary to find the analytical decision systems in vicinity special points on $(-\infty)$. The analytical decision is searched standard way by linearization (2.9) - (2.12) and rejection nonlinear members in ε vicinities special points. In result we have:

$$\psi = c_1 e^{\sqrt{A}t} + \frac{Az}{A - s^2} e^{st} \qquad (2.13)$$

where, $A = \frac{3}{5}\frac{\kappa_e n_{1n} e^2 \lambda_1^2}{\varepsilon_1 k T_{1e}}$, $z = z_i \kappa_i \left(\frac{u_1}{u_2} - 1 \right)$, $\kappa_e = \frac{n_{1e}}{n_{1n}}$, $\kappa_i = \frac{n_{1i}}{n_{1e}}$, n_{1n} - concentration neutral particles in an accumulating stream, e - a charge electron, $t=x/\lambda_1$, λ_1 - length of free run, $n_e/n_{1e}=1+\psi$. Prominent feature (13) is that in expression for concentration electron's the constant c_1 enters unknown beforehand. And, as sizes T_e and E behind area of fast change of parameters of current are beforehand unknown, and their values $T_e(+\infty), E(+\infty)$ are known only in balance behind front, the equation (2.9)-(2.12) it is necessary to integrate together with full system (2.1) - (2.4) (for a zone slow change of parameters of current δ_3), using results (2.9) - (2.12) in quality of boundary conditions for (2.1) - (2.4). The decision (2.9) - (2.12) together with (2.1) - (2.4) is searched by a method of shooting. As a result of the decision of a problem on structure of a shock wave in low ionized ionic cluster plasma (in this case were considered negatively charged clusters) the effect of "superbulldozer" is predicted. Essence of effect is, what in low ionized ionic clusters to plasma ($n_{1e} << n_{1i_\pm} \sim n_{1p_\pm} << n_{1n}$, , where n_{1e} – concentration of electrons, $n_{1i_\pm}$– concentration of ions of different polarity, $n_{1p_\pm}$ -concentration clusters, n_{1n} - concentration of the neutral gas - carrier) electrons as "would be raked up" by front of a shock wave during it's propagation. Concentration electrons can increase by some orders ($n_e \sim n_i$) depending on that as far as its initial concentration n_e is small. In limiting cases compression of electrons in a forward part of a shock wave δ_2 can occur as adiabatic, and izotermical depending on parameters of environment and a stream. For practical appendices the greatest interest represents a case adiabatic compression, as thus the temperature electrons essentially grows, that is accompanied intensive physical and chemical processes. Interesting feature given effect that electrons speed is practically equal to speed of distributions of a shock wave. In this case the wave transfers not only a pulse and energy, but also small weight. Calculations of distribution shock were carried out waves for model low ionized ionic cluster plasmas, which parameters are given in table 2.1.

Table 2.1

n	1	2	3	4
κ_1	10^{-6}	10^{-8}	10^{-8}	10^{-7}
R	1	1	0.42×10^{-5}	4×10^{-6}
$\tilde{d}$	10	10	0.14	36
z	1	1	-1	-10

where serial numbers N=1.2 - designate positively charged ions, N=3- electrones, N=4 - clusters, $\kappa_i = \frac{n_i}{n_{1n}}$ - the relation of concentration of the charged particles to concentration of the gas - carrier; $R = \frac{m_i}{m_n}$; $\widetilde{d} = \frac{d_i}{d_n}$ - the relation of effective diameters the charged particles to effective diameter of the gas - carrier, z_i - charging numbers. Number Max of propagation of shock wave M=3.1. In figures 2.1 and 2.2 in different scales change of concentration is submitted electrons in front of a shock wave $\frac{n_e}{n_{1e}}$, where x – coordinate λ_1 - length free run in an accumulating stream. From figures it is visible, that electrons concentration in front SW it is increased practically by two order. The width of a forward part of front for electrons is $\delta_2 \sim 40\lambda_1$. For comparison in figure 2.3 change dimensionless is submitted concentration $\frac{n-1}{n_2-1}$ from $\frac{x}{\lambda_1}$ the gas - carrier and ions (a curve 1), clusters (a curve 2). From figure 2.3 it is visible well defined two - wave structure δ_1 - a zone fast changes of parameters of a stream δ_3 - a zone of slow change of parameters of a stream.

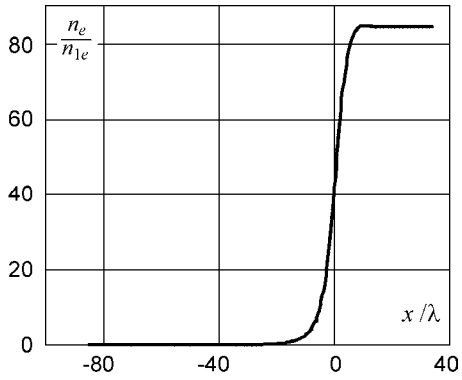

Fig 2.1

Change of relative concentration electrons in a zone forward nonequilibrium in front of a shock wave (the reduced scale).

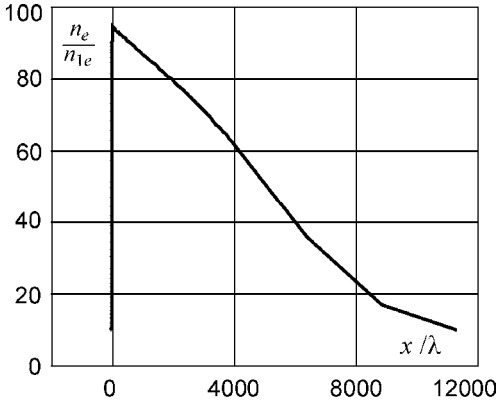

Fig. 2.2

Change of relative concentration electrons in a zone forward nonequilibrium in front of a shock wave (the increased scale).

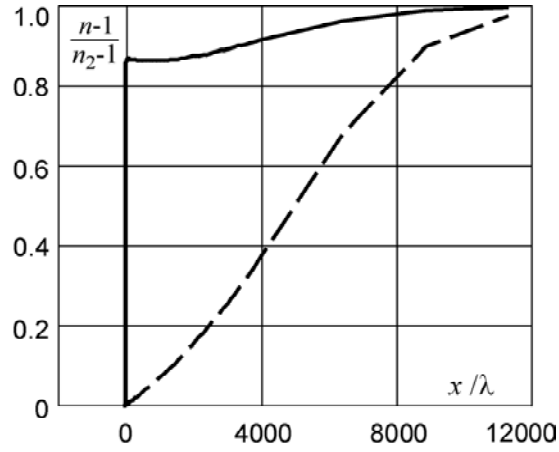

Fig. 2.3

Change relative concentrations $\frac{n_i - 1}{n_2 - 1}$ neutral gas of the carrier (continuous Curve) and charged clusters (the shaded curve) in a zone forward nonequilibrium in front of a shock wave.

In figure 2.4 change of the given temperature electrons $\frac{T_e - 1}{T_2 - 1}$ is submitted in front of a shock wave. From figure it is visible, that electrons (at parameters mixes, the data in table 2.1) are compressed practically adiabatic. Temperature of electrons in a point of a maximum surpasses equilibrium behind front in 35 times.

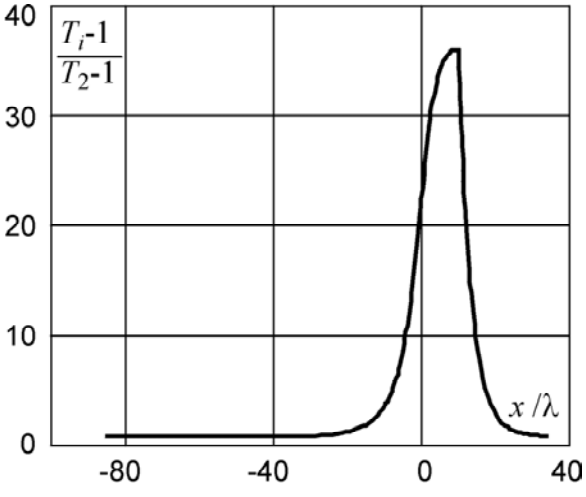

Fig. 2.4

Change relative partial temperatures electrons in a zone translational nonequilibrium in front of a shock wave.

In figure 2.5 change of potential in front of a shock wave (V) is submitted. Prominent feature of the received result is presence of a maximum Potential in the front, the mark of size of a field caused by change [6].

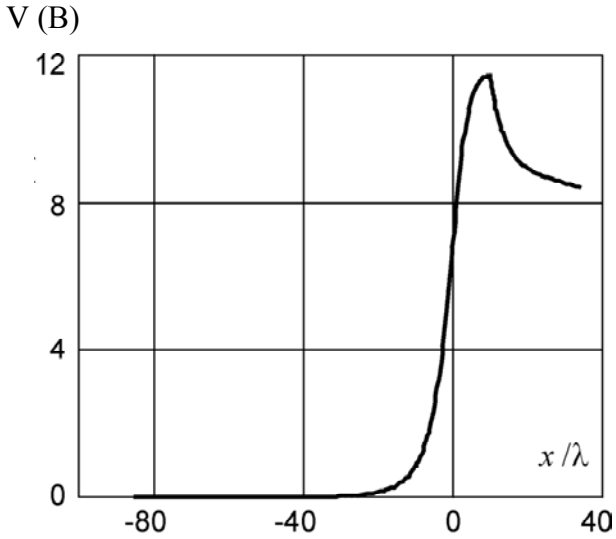

Fig. 2.5

Change of potential in a zone translational nonequilibrium in front shock waves.

Let's note, that presence of potential in size in 12 V means, that charged particles (electrons) can have temperature ~ 100 000 K (if not to take into account it's decrease due to non-elastic collisions). Really, as follows from fig. 2.4, the maximal temperature electrons ~ 18000 K. In it the effect is shown gasdynamic cumulative energy on "macrolevel". Equilibrium temperature of a mix behind front of a shock wave at M=3.1, T_{eq}=820 K.

Stronger effects of division and gasodynamic cumulation of energy are realized at the effusion of ionic cluster plasma from Laval's nozzle.

1. Experimental researches of long-living plasma formations receiving.

For long-living plasma formations receiving the idea of erosion discharge first realized in Tesla's works has been used. Later this idea was realized in some works [12]. For realization of erosion discharge wax was used. One of the anodes was greased by wax partly. Wax as well was the electrode safeguard (its metal part) from intensive erosion. As a working medium the supersonic stream of air and fine-dyspersated drops of electrolyte of high concentration was used. It gave us an opportunity to realize breakdown in a significant discharge space ~ 1м at small voltage 600 – 800V and to receive with high probability long-living plasma formations. The basic idea lays in installation copies the processes occurring in the nature during appearance of fireballs. There is a precision linear discharge in a small space. As a result of wax evaporation from the anode and its subsequent condensation in supersonic gas-drop stream, clusters are formed and balls of biological polymer (wax). Owing to greater mobility electrons stick to these wax formations. Positive ions are carried away by a supersonic stream. Significant division of a charge is formed. Similar processes are realized in shock waves.

The basic diagram of installation is presented on Fig.3.1.

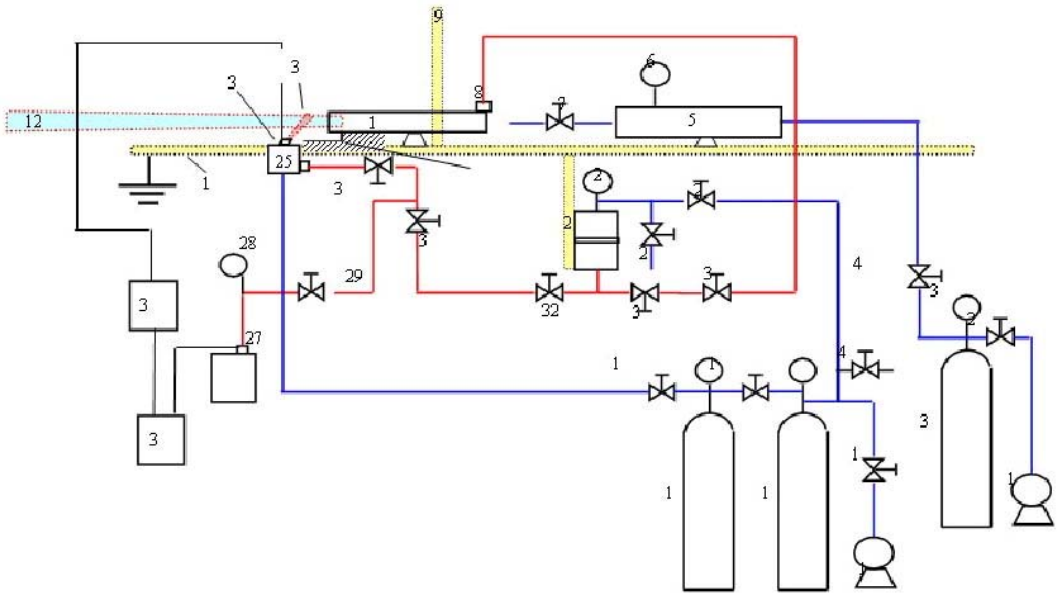

Fig. 3.1

1.Compressor. 2. Stop-cock. 3. Receiver with the manometer. 4. Stop-cock. 5. Collector. 6. Manometer. 7. Stop-cock. 8. Sprayer for atomizing of the main fuel part. 9. Protection screen. 10. Laval nozzle transforming to the supersonic channel. 11. A step modeling the flame stabilizing zone. 12. Gas-drop torch. 13. Working table. 14. Compressor. 15. Stop-cock. 16. Receiver with the manometer for supercharging of the fuel tank. 17. Stop-cock. 18. Stop-cock. 19. Receiver with the manometer. 20. Stop-cock. 21. Discharging cock. 22. Fuel tank manometer. 23 The fuel tank for fuel delivery to the Laval nozzle. 24. Drive-valve for air discharging through the bubblier. 25. Bubblier. 26. The fuel tank for fuel delivery to the bubblier. 27. Submerged pump. 28. Manometer. 29. Shut-off valve. 30. Drive-valve. 31. Escape valve. 32. Closing cock. 33. Closing cock. 34. Drive-valve. 35. Spaying-igniting device. 36. Control panel. 37. High voltage source. 38. Anode. 39. Porous fuel stream. 40. Discharging cock.

General view of installation

Fig. 3.2

Work of installation in a mode of receiving of long-living plasma formations is shown on Fig. 3.3 and 3.4.

Fig. 3.3

Fig. 3.4

Linear breakdown is presented in Fig. 3.3. In Fig. 3.4 basic discharge has disappeared. There is only long-living plasma formation. In Fig. 3.5 the discharge in a mode of realization of breakdown in the form of beaded lightning is presented. In Fig. 3.6 the oscillogram of the charges getting on the metal screen is presented.

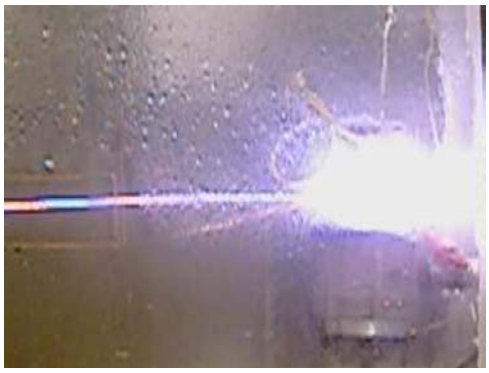

Fig. 3.5

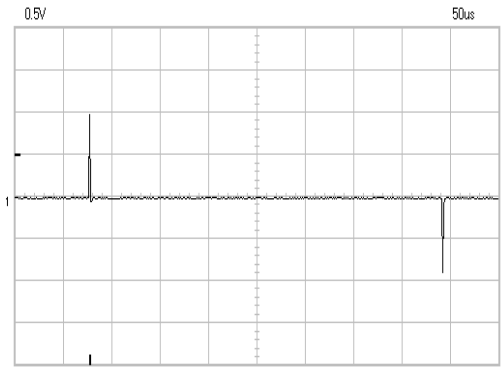

Fig. 3.6

According to stated by us before model not compensated positive charge of the ions getting on the metal screen, is fixed by the first impulse. The negative one – by the second impulse Fig. 3.6.

Conclusions.

1. Structure of a shock wave in low ionized ionic cluster plasma with negatively charged clusters qualitatively differs from structure of shock wave in this plasma (at presence positively charged clusters):

a) in a case of negatively charged clusters electrons are braked, and their concentration is sharply increased in front;

b) in a case of positively charged clusters electrons are accelerated, and their concentration is reduced in front.

2. At compression electrons modes as adiabatic compression and isothermal compression depending on parameters of medium and stream can be realized.
3. Electrons in front move practically with speed of shock wave distribution, the wave transfers thus not only a pulse, energy, but also mass. Character of distribution of electron compression wave reminds a lonely wave- soliton.
4. Installation for realization of long-living plasma formations is created.
5. Long-living plasma formations have been got.

References:

1. File Ball in a Laboratory. Collection of Papers. Chemistry, 1994, 256p.
2. *A.Klimov, V.Nikolaeva. R.Avramenko*. Development of Plasma Aerodynamics Russia. // In: Prospective on 2nd Workshop on Magneto-and Plasma-Aerodynamics for Aerospace Application, IVTAN, Moscow, April 5 - 7, 2000, p.30-33.
3. *Velikodnyi V.Yu., Bityurin V.A.* On structure of a plane shock wave in weakly ionized plasmas // Nonequilibrium processes and their applications. IV Int. Sch.-Seminar. Minsk. 1998. P.72-75.
4. *Velikodnyi V.Yu., Bityurin V.A*. Shock nave structure in ionic plasma. // Ac. Of Sc. Reports, 1998, v.361, No.3, p.325-328 (in Russian).
5. *V.Yu. Velikodnyi, V.A.Bityurin*. Shock wave structure in long-lived plasma formations // In: Prospective on 2nd Workshop on Magneto-and Plasma-Aerodynamics for Aerospace Application, IVTAN, Moscow, April 5 - 7, 2000, p.301-306.
6. *J.T.Lineberry, V.Yu. Velikodnyi, V.A.Bityurin.* Influence of Charged Nano-Particles on Shock Wave Structure. Chain Reaction Initiation in Shock Wave Front in Cluster Ionic Plasma // AIAA 2001-0638, 39th AIAA Aerospace Sciences Meeting and Exibit, 8-11 January 2001, Reno, Nevada, 6p.
7. *V.M.Smirnov*. Process in cluster plasma and cluster bunches(beams) // Letters in JETPh, Vol.68, Is.10, p. 741-746.
8. *Velikodnyi V.Yu., Bityurin V.A.* The effect of translational nonequilibrium on the kinetic of physicochemical conversions in the shock wave front // Chem. Phys. Reports. 1997, vol.16, No.19, p.1521-1531.
9. *Struminskij V.V., Velikodnyi V.Yu*. Structure of shock waves // Dok of the USSR, 1982, Vol.266, № 1, p. 28-31.

CLASSICAL APPROACHES TO ANOMALOUS AND GEOPHYSICAL PHENOMENA: METHODOLOGICAL ASPECTS AND PHYSICAL MATTER OF TRANSMUTATION PHENOMENON

V.L. Bychkov[*], B.S. Grevtsov[**], V.A. Krivitsky[***], V.V. Nizovtsev[****]

[*] *M.V. Lomonosov Moscow state university, Vorobjevy Gory, MSU, Physics department, Moscow 119992,* ***E-mail:*** *bychvl@orc.ru*
[**] *Moscow aircraft institute.*
[***] *International university 'Dubna', Applied geophysics department, Moscowskaja obl., Dubna, University St. 19, 141980*
[****] *M.V. Lomonosov Moscow state university, Worobjevy Gory, MSU, Soil science department, Moscow 119992*

Methodological introduction

The problem of a transmutation still does not find public appreciation and is out of scientific understanding range. Naturally one can doubt in cogency and repeatability of experimental prove of the transmutation possibility, however, results accumulated in geology on this question unambiguously indicate a frailty of atoms composing our planet.

According to the concept of hot planet origination, the Earth was formed of a portion of proto-element magma dropped by the Sun at some definite evolution stage. A spectra of chemical elements originated from abyssal material was determined by the geological conditions, in which initial magma of young planet dissociated to different element compositions. It is revealed in the correlation between the type of geological structures and composition of rocks.

A question about an age of chemical elements on the earth surface and para-genesis of minerals and, hence, chemical elements in the earth's crust had emerged as far back as in beginning of XIX-th century. Geologists in XX-th century starting from V.I. Vernadski repeatedly indicated necessity of most attentive attitude to this problem, however in fact physicists prohibited its development. Modern physics and cosmogony are nowadays unready to discuss geochemical problems in scientific terms.

Really, what is the pre-chemical material of magma? Why its dispersion takes place? Why separation of a Sun magma portion (later it can be a planet or another celestial body) results in generation of nuclei and chemical elements? How to explain rock element composition dependence on conditions, in particular, rock formation process dynamics?

Laboratory experiments also bring up no smaller number of questions. The transmutation in the laboratory is observed in conditions of processes such as mass and energy transport, current pulse, discharge or explosion. However, modern physics knows little about nucleons and nuclides under extreme conditions of acceleration. It is suffice to say that relativistic effects do not have physical explanation.

Thus a deficit of necessary physical knowledge does not allow a discussion the transmutation in laboratories or in nature in the scientific terms arguments "for" or "against".

Problems of micro-particle's structure and stability

Natural processes of chemical elements generation and laboratory transmutation processes have common aspect. The lithosphere element composition depends on nuclei stability, but in laboratory conditions processes are determined by the nuclei or nucleons instability. So questions of atomic particle genesis, structure and stability gain the fundamental character in the discussed problem.

These questions are out of modern physics competence range. So we will rely on classical ether-dynamical paradigm lost in the course of scientific revolution in the beginning of XX-th century. Till then questions about of the substrate, genesis and structure of elementary particles were brought in science. Classical tradition goes back to works of N. Malebranche (1638–1715), J. Bernoulli (1667–1748) and W. Thomson (1824–1907). In XX – th century it invisibly existed near the mainstream of the modern science and had an appreciable development[1-2].

Electromagnetic stochastic physical vacuum in terms of the classical approach is the turbulent ether with typical pulsation velocity of about of light speed. The turbulization of the cosmic ether medium come of the cascade decay of galactic and metagalactic scale vortices, as it was proved by W. Nernst[3]. Under the hypothesis of W. Thomson[4], atoms are formed from the ether substrate and represent vortex structures with large store of flow energy (rest energy).

Structure module of elementary particles

By analogy with α-extended model of nuclei put forward by William D. Harkins[5], one may speculate that elementary particles have the module structure too. The previously derived models indicate that it is the electron in different energy states turns out the structure module of all the elementary particles. True, mesons are the structure module for nucleons, but the former ones are of the electron-type structures too.

After William Thomson[6] and William Sutherland[7] we model the electron in a form of ether knotted vortex thread. A knot is taken to mean a space curve gomeomorthic to the circle[8]. In Fig.1 one can see two versions of a simple or trefoil knot. Let the right-handed trefoil knot (a) corresponds to the positron in the topological sense, the left-handed knot (b) – to the electron.

The cardinal question for our theme is these structures stability. Such particles are unstable at absence of energy infeed due to finite viscosity of the ether substrate. It is axiomatic that turbulence by itself pointed to some viscosity of ether. It follows from hydrodynamics that there is a possibility of this type structures existence; in the turbulence theory they are called the coherent structures. The last ones spontaneously appear and exist in the turbulent medium absorbing pulsations**[9].** To illustrate a vorticity at large amplitudes organizes itself in a form of tubes, even though the turbulence is globally homogeneous and isotropic[10].

a b c

Fig.1. *Knots and linkage of two vortex lines: right-handed trefoil knot (a); the left-handed knot (b); linkage of vortex lines (c). A figure from the work of W.Thomson[6] was used at the knots «a» and «b» construction. Arrows indicate the vorticity direction in the vortex line.*

In a similar way the stability of structures outlined in figures is sustained by the ether turbulent pulsations. So, atomic particles, being the primary dissipative structures of the material reality, continuously absorb pulsations of the ether-vacuum, transforming them into heat, which is displayed in the microwave cosmic radiation with the temperature of 2,7 K.

A knotted tread can be imagined as coiling on imaginary tore (Fig. 2) Large radius of the vortex tore is Compton wave-length $\lambda_c = \hbar/m_0c$ that equals to $3{,}86\cdot10^{-13}$ m in the case of electron. Using solution of vortex thread vorticity viscous diffusion equation and the Biot-Savart law for a velocity field of the trefoil knot one can obtain current lines in different moments of dimensionless time. This time is defined as a ratio of typical size of a structure and typical velocity of flows. In case of considering structures these parameters are Compton wavelength and light velocity *c*.

A self-induction due to a local curvature brings about an axial flow. One can see in Fig.3 that an element of a liquid runs about a torus, it means an existence of the axial velocity. At that velocities in points 1, 2 and 3 are 6.0 s, 13.0 s and 4,s respectively for $t = 0.1$ and λ being 90% of maximal (external) radius of the torus (see Fig.2).

Angular moment of this flow is spin $\hbar/2$. Aspden[11] was the first to establish this fact. Thus elementary

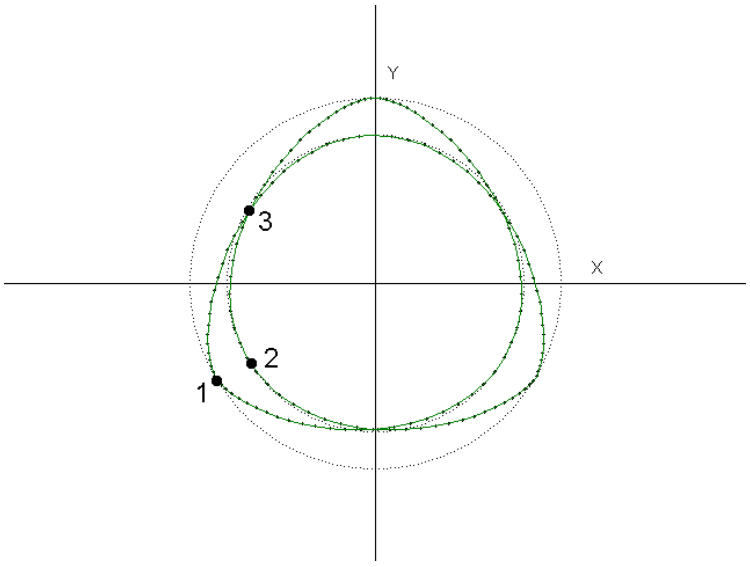

Fig. 2. *A trefoil on a tore (dashed line).*

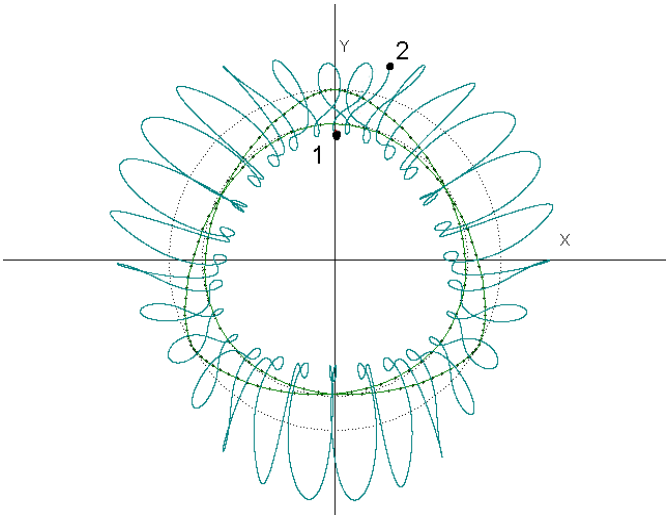

Fig. 3. Current lines between points 1 and 2.

particles are ring-type swirl[12] flows with azimuth (spin) and meridian components of flows. The meridian flow is responsible for particle transfer, which discussed below.

Tectonic–chemical correlations

One can easily understand that for existence of atomic particles some level of pulsation volume density is necessary. If the cosmic medium is the source for the turbulent pulsations then one has to expect decrease of their density in the Earth's interior, so stable existence of nuclear particles and nuclides turns out to be impossible at some depth.

The theory of vortex dynamics allows estimation of the pulsation dynamic pressure distribution in the Earth. Earlier it has been proved that regular component of the solar system kinematics is controlled by the currents of aether[13]. In particular, rotation of our planet and revolution of its satellite is maintained by the vortex drive of the cosmo-chemical genesis[14]. the planet is in a center of a vortex structure that has a form of a cocoon. H.K.Moffat[15] had called these vortex structures as vortons. In first approximation one can suppose that the core of the vortex ($r < r_1$, where r_1 – is the Earth radius) has a solid body rotation with peak velocity approximately equal to the first orbital velocity at the Earth. In nature, vortex cores are recognized as the centers of tornadoes[16]. Vortex velocity distribution outside the core ($r > r_1$) has a form $v = K\, r^{-1/2}$, where K – some constant.

Then the pressure in the core is[17]:

$$p_c = P_0 - c_0\, K^2\, \frac{(3\, r_1^2 - r^2)}{2\, r_1^3}, \qquad r < r_1$$

The pressure outside the Earth ($r > r_1$) is

$$p_p = P_0 - c_0\, K^2\, \frac{1}{r}, \qquad r > r_1$$

here ρ_0 is the density of the ether, P_0 is the pressure at infinity (Fig. 3). The pressures are all negative, i.e., below the ambient pressure at large r, and hence are of particular interest in connection with gravitation problems.

Using approach of Lord Kelvin [18] and accounting optic radiation power limiting value of modern quantum generators ($3.4 \cdot 10^{14}$ J/m^3) one obtains density of turbulent ether $3.7 \cdot 10^{-3}$ kg/m^3 .

Basing on the accounted one can make a supposition that a scenario of magma dispersion at its raising to the earth surface is essentially determined by the circumstance that the ether-vacuum volume density of pulsations depends on depth of the earth horizon and nature of enclosing and overlying strata. Then space dynamics of nucleons and nuclei isolation from magma at its rising motion in the lithosphere and the earth crust depends on definite geological situation.

Victor A. Ambartsumyan[19] supposed that proto-element magma in the earth core represents a condensate with a density close to the density of nuclei. We suppose that magma has meson-nucleon composition. Structural stability of elementary particles composing magma is apparently ensured by collective interactions and does not depend on a level of ether-vacuum turbulent pulsations in the Earth nucleus.

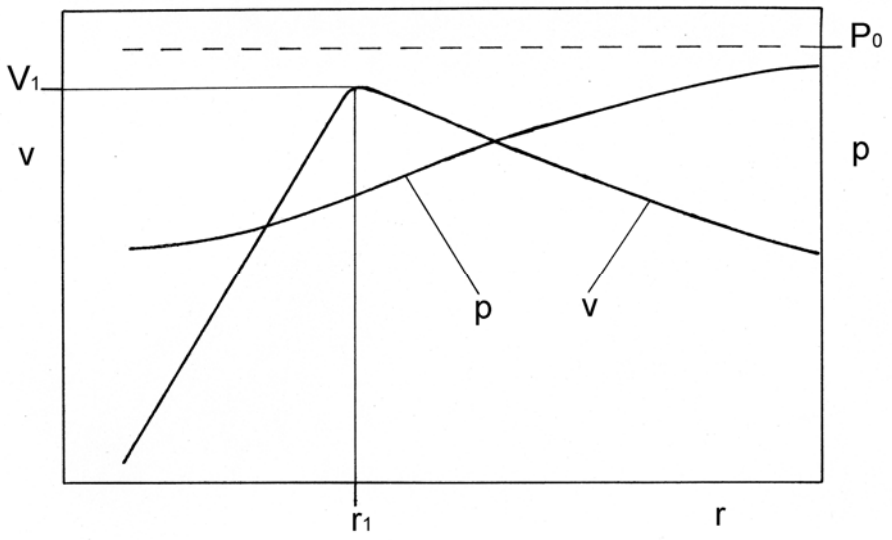

Fig. 4. *Distribution of flows azimuth velocity* ***(v)*** *vortex drive and pulsations pressure (p) in the Earth ($r < r_1$) and its vicinity ($r > r_1$). V_1 is the first cosmic velocity.*

On stability of vortex particles

Let us consider now why is the stability distorted at excitation of bounded or acceleration of free elementary particle. This is important for understanding of transmutation processes in laboratory conditions. Let us show that energy change of a particle is accompanied by its structural reconstructions, at which its decomposition or formation of a new type particle is possible.

It is experimentally proved for electron that translation energy increase in range of five orders of magnitude is accompanied by strict inverse proportional change of the particle size (Fig.4). The correlation between the particle size and its energy testifies to the reconstruction of the particle structure at variation of its energy.

Particle energy increase at photon absorption or acceleration by electric field is interpreted pure kinematically in modern physics. At that the inverse proportion between energy and size has not yet found the explanation. Let us open its physical matter.

W.Sutherland[7] in 1901 studying nature of hydrogen atom line spectra supposed convergent series of lines correspond to successive looping of knots on the ring structure of electron. Each next knot brings in smaller put in to electron energy than the previous one.

As of now, simple linkage of two vortex rings of intensity I_1 and I_2 or self linkage (looping) of the vortex thread (Fig.1) is in hydrodynamics characterized by the structure parameter $K = I_1 I_2$, which is quadratic invariant of localized motion[20]. Here I_i is intensity or circulation of a thread (see Fig. 6). K by its implication is kinetic energy ("rest" energy) of localized dynamic structure. Increase of energy from the morphological point of view means appearance of additional knots in the particle structure.

Let us now consider the correlation between the size of the particle and its velocity. The primary role in this dependence belongs to the velocity according to modern physics, i.e. namely the acceleration for some reason causes reduction of the particle sizes. The subordination in realty is reverse: looping of the electron ring causes its acceleration (Fig.5).

Increase of a number of knots on a thread causes not only reduction of external sizes of the particle structure but also increase of meridian velocity of flows in the toroid and, as a result, increase of forward movement velocity. Translation velocity in ordinary vortex ring is determined by the ring sizes and its intensity I (Fig. 6, a).

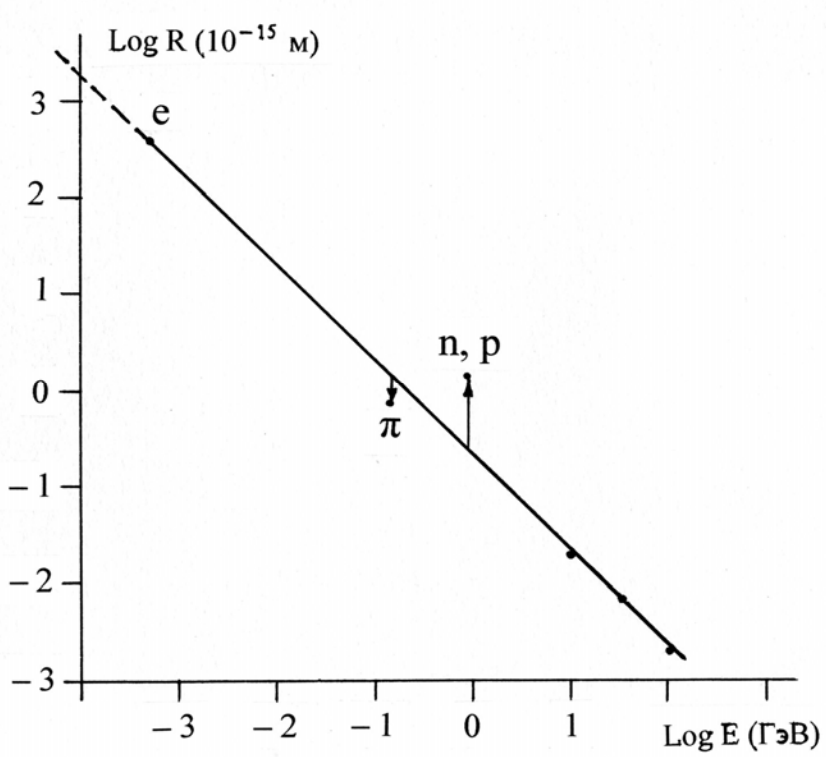

Fig. 5. *A correlation between electron energy and size: positions of electron (e), nucleons (n, p) and pion (π) are shown by dots. Dashed portion of the line corresponds to bound electron.*

$$v = I\,(\eta - 1/4)/4\pi R, \qquad I = 2\pi r V, \qquad \eta = \ln(8R/r).$$

A direction of the translation velocity v coincides with a direction of flows on the ring axis (V_0 - velocity) induced by the meridian velocities V. Effective value of the velocity V increases at looping of the vortex tread (Fig. 6, b), that leads to acceleration of the structure.

This takes place, in particular, at absorption of knots from an accelerating field by the particle. In future we will consider electric field turbulent structure.

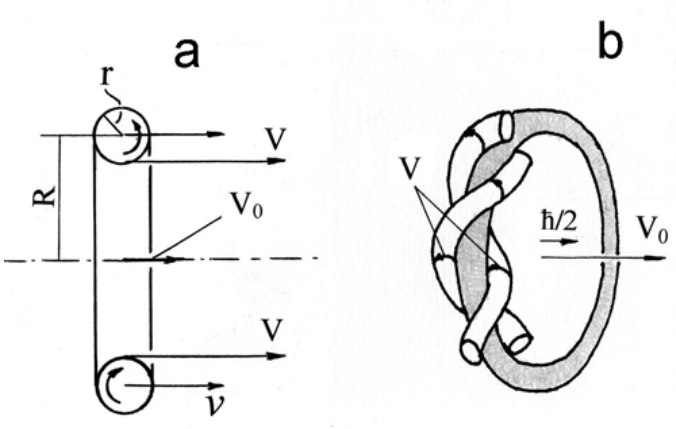

Fig. 6. *Flows in the vortex ring (a) and in the fragment of right-handed knot with multiple linkage (b): V – meridian velocity of flows; V_0 –flow velocity in the ring center induced by the flow V; v – translation motion velocity of the ring. The fragment for visual demonstration is winded over the imaginary tore (shown grey)*

Pulse and, even better, cyclic accelerations of vortex structures in the experiments on transmutation apparently lead to decrease of their stability due to variation of particle sizes and complicated processes of structure relaxation in conditions of turbulent medium pulsations variable gradients. It is not inconceivable that transmutation in modes of pulsed processes in bases namely on this effect. The transmutation at passing of pulsed currents through melts witnesses about a possibility of nucleon stability control by imposing of variable electromagnetic fields. It is important to emphasize that structural reconstructions at that take place at the scale level of nucleons but not nuclides.

Conclusions

The interior of the Earth is nature laboratory of nuclei synthesis, there processes of magmatic meson-nucleon condensate dispersion constantly take place with formation of nuclides and atoms. A separation of super heavy proto-nuclei is determined by a level of turbulent pulsations background level depending on depth, thus a spectrum of generated chemical elements is determined by geodynamical conditions.

Transmutation in laboratory conditions is possible in the decay of strictly speaking nucleons, but not nuclei of stable elements. Dissipative nature of elementary particles and their dependence of condition of ether-vacuum speak in favor of this.

Owing to historical reasons, vortex models of elementary particles and their genesis, proto-nuclei magmatic substrate of chemical elements in the Earth core and heavy nuclei separation from it, following paragenesis of chemical elements – all these models and hypothesizes proved to be out of XX-century science interests. So it is not surprising that the experimental results on transmutation defy scientific interpretation and cause distrust.

References

1. *Wolf E.* 1954. “Optics in terms of observable quantities”, *Nuovo Cim.*, 12, 884–888.
2. *Bourret R.C.* 1960. “Coherence properties of blackbody radiation”, *Nuovo Cim*., 18, 347–356.
3. *Nernst, W.* 1921. *Das Weltgebaüden im Licht der neueren Forschung,* Springer Verlag, Berlin, S. 5, 32, 40.
4. *Thomson, W*. 1867. “On the vortex atoms”, *Phil. Mag. Ser. 4*, 34, 15–24.
5. *Harkins, W.D*. 1931. “Periodic system of atomic nuclei and the principle of regularity and continuity of series”, *Phys. Rev. A,* 38, 1270–1288.
6. *Thomson, W*. 1869. “On vortex motion”, *Trans. R. Soc. Edinburgh*, 25, 217–260.
7. *Sutherland W*. 1901. “The cause of the structure of spectra”, *Phil. Mag. Ser. 6,* 2, No. 9, 245–274.
8. *Moffat H.K.* 1969. “The degree of knottedness of tangled vortex lines”, *J. Fluid Mech.* 35, 117–129.
9. *Hussain, A.K.M.F.* 1986. “Coherent structures and turbulence”, *J. Fluid Mech.*, 173, 303–356.
10. *Sreenivasan, K.R.* 1999. “Fluid turbulence”, *Rev. Mod. Phys.* 71, s383–s395.
11. *Aspden, H.* 1969. *Physics without Einstein.* Sabberton Publications, England, 63.
12. *Gupta, A.K., Lilley, D.G., Syred, N*. 1984. *Swirl flows.* Abacus Press, § 1.1.
13. *Nizovtsev, V.V*. 2002. “On substances formation in the solar system vortex”, *Proc. 9-th Russ. Conf. Cold Nuclear Transmutation of Chemical Elements, Sochi-Moscow*, 249–256.
14. *Nizovtsev, V.V., Bychkov, V.L.* 2005. “Shear streams in the shells of the Earth. Geodynamics and geomagnetism”, *Proc. 12-th Russ. Conf. Cold Nuclear Transmutation of Chemical Elements Nuclei, Sochi-Moscow*, 254–272 (in Russ.).
15. *Moffat, H.K.* 1986. “On the existence of localized rotational disturbances which propagate without change of structure in an inviscid fluid”, *J. Fluid Mech.,* 173, 289–302.
16. *Lugt, H.J.* 1983. *Vortex flow in nature and technology.* John Wiley & Sons, New York, 203–224.
17. *Prandtl, L.* By Tietjens, O.G. 1934. *Fundamentals of Hydro- and Aeromechanics.* N.Y.–L., 213–214.
18. *Thomson, W*. 1854. “Note on the possible density of the luminiferous medium and on the mechanical value of a cubic mile of sunlight”, *Phil. Mag.* 9, 28–33.
19. *Ambartsumyan, V.A.* 1960. *Works*. Armenian Acad. Sci. Press, Erevan. Vol. 2, 178–185 (in Russ.).
20. *Moffat, H.K.* 1990. “Structure and stability of solutions of the Euler equation: a lagrangian approach”, *Phil. Trans. R. Soc. L. A.*, 333, 321–342.

EXPERIMENTAL RESEARCHES OF ELECTRICAL EXPLOSION OF THE WIRE SPIRAL TURNED IN THE TORUS AND DIPPED IN WATER

A.N.Vlasov, B.I.Kolotilin, S.A.Kolesnikov, A.B.Manoshkin, V.V.Panin

The Ryazan State Radio Engineering University, Russia
E-mail:anv@fulcra.ryazan.ru

Abstract

Attempt of an explanation is undertaken of extremely large lifetime of the plasmoids gained at electrical explosion of wire spirals turned in a torus. The guess of developing of a powerful induction discharge through gases under action of back front of an impulse of an induction of the toroidal magnetic field created by a wire spiral at the moment of its fracture is considered. At a qualitative level the analysis of physical processes of input of electromagnetic energy in the discharge is carried out, it is shown that at electrical explosion of the wire spiral turned in a torus its magnetic field may be grasped in part by shaped toroidal current stratum. Calculation of quantity of a current of the spiral necessary for formation of a current layer in a plasmoid is carried out; the lifetime shaped magnetohydrodynamical configurations is appreciated.

1. Introduction

Electrical explosion of a wire [1], including in air [2], is of interest from the point of view of studying dynamic processes in plasma. The previous experiments with electrical explosions of the wire spirals turned in a torus [3] have shown that the lifetime of gained plasmoids is much higher in comparison with the plasmoids gained at electrical explosions of wires with other configurations. The probable reason of this phenomenon is presence of a powerful toroidal magnetic field inside a spiral before its explosion, but that stability of plasmoids provided with a shaped ring vortex is not excluded. Revealing of the mechanism is of interest from the point of view of a potential opportunity transmutation nucleus of chemical elements at electrical explosion of the wire spirals turned in the torus, as if the toroidal magnetic field promotes pinch of a lifetime of gained plasmoids thus the toroidal current layer with extremely high density of an electric current should be shaped. In this case the opportunity of electronic screening of charges of nucleus down to nuclear gauges is not excluded. Dipping of the wire spirals turned in the torus in water essentially changes parameters of electrical explosion that allows revealing new properties of this process and establishing the possible mechanism of occurring processes.

2. Experimental effects.

The principle of operation of the experimental installation, fig. 1, is based on a charge of condenser battery ***C*** through switch ***S1*****,** and then the discharge of this battery through switch ***S2*** and wire spiral ***W***.

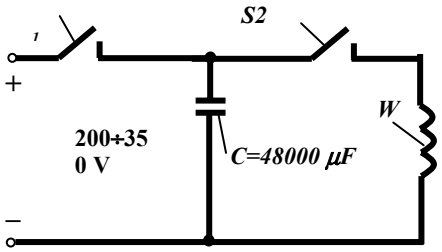

Fig. 1. *The simplified schema of the experimental installation.*

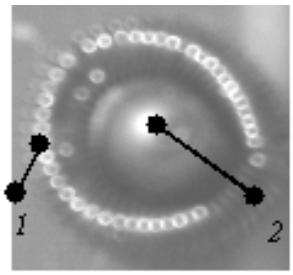

Fig. 2*. Replaceable cartridge with the wire spiral turned in the torus* ***1*** *and the shaper of a plasma vortex* ***2****.*

Wire spiral ***W*** was disposed on replaceable cartridge, fig. 2, and contained 60 coils of a copper wire in diameter of 0.5 mm, small radius of a torus r had the size about 2 mm, major radius of a torus R had the size of 8 mm.

At experiments through a spiral the current near *1 kA* was passed; approximately through *1 ms* after switching on of a voltage there was an explosion and the plasmoid was formed, fig. 3.

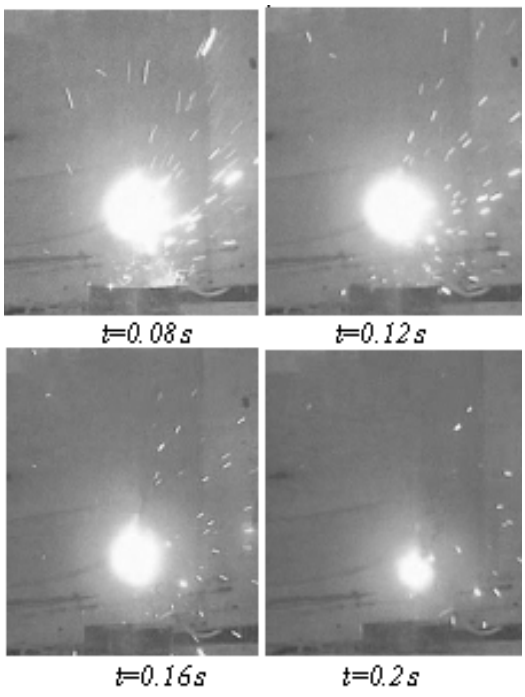

Fig. 3. *Consecutive pictures of one of the generated*

The lifetime of plasmoids in some experiments achieved values about one second and on the average on the order surpassed a lifetime of the plasma formations gained in check experiments at electrical explosions of the linear spirals and wires of other configurations with the same mass of metal.

3. Principles of formation of plasmoid

One of explanations it is an abnormal large lifetime of gained plasmoids the guess of development of the powerful induction discharge may serve at action of a unipolar impulse [4] at the moment of fracture of a spiral. It is the first base principle of formation of long-lived plasmoids.

The second principle streams from definition of powerful discharges through gases. As a powerful discharge through gases understand such discharge, at which in the discharge channel of radius R and a discharge current i creates magnetic pressure p_m comparable with gas dynamic pressure of plasma carrier gas p_g:

$$p_g \cong p_m = \mu_0 i^2 \big/ \left(8\pi^2 R^2\right). \tag{1}$$

Here μ_0 is magnetic constant.

The relation (1) serves as a reference point for forecasting quantity of a necessary current impulse i in a plasmoid.

The third principle concerns a question of stabilization of the discharge. Inductions discharges (H-discharges), as is known [5], based the phenomenon of an electromagnetic induction and are widely used in generators of the dense low-temperature plasma - high-frequency plasma generators. The main constructive moment of these devices is tangential delivery of gas [5]. Stabilization of the pulsing ***H*-**discharge by the vortex stream promotes pinch of a lifetime of gained plasmoids.

4. Entrapment of a magnetic field

As the wire spiral ***1*** is turned in a torus (fig. 4) as at a gear transmission of an electric current (which direction is shown by pointers on a spiral (fig. 4)) creates the strong toroidal magnetic field. After a heating and transpiration of a spiral material the ring gas vortex ***2*** is shaped (it is provided by a construction cartridge), and inside this vortex at sharp wane of a toroidal magnetic field the current ring ***3*** with the frozen toroidal magnetic field ***4*** may be induced, and this field is a part of initiating created field inside the spiral. The ring with a current supported in equilibrium pressure of outside gas is known, it may be equilibrium magnetohydrodynamical configuration [6].

The wire spiral turned in a torus can be viewed as an initial winding of transformer ***T*** (fig. 5), and the shaped plasmoid can be viewed as aggregate of a secondary winding of transformer ***T*** with loading ***Z***.

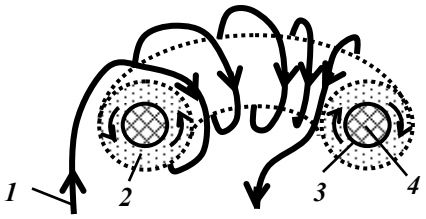

Fig. 4. *Scheme of formation of a plasmoid.*

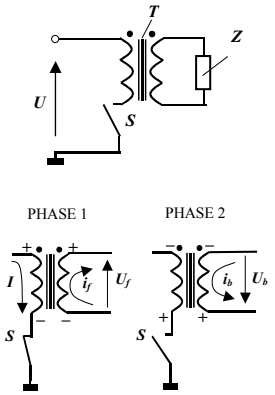

Fig. 5. *Dual circuit of pumping-over of energy in a plasmoid and two phases of this process.*

Process of transferring of magnetic field energy from a blowing up wire spiral to a current ring can be divided into two phases [4].

PHASE 1: switch ***S*** is locked, (fig. 5) that corresponds to delivery of a voltage on a wire spiral. In this case the current ***I*** of an initial winding of transformer linearly accrues and in transformer ***T*** energy in the shape of a magnetic field collects. In a secondary winding thus voltage $\boldsymbol{U_f}$ is induced, which may create a small current $\boldsymbol{i_f}$.

PHASE 2: switch ***S*** is unlocked, (fig. 5) that corresponds to explosion in a wire spiral. In this case the self-induction overturns polarity of a voltage on transformer ***T***, in a secondary winding voltage $\boldsymbol{U_b}$ is induced and in loading ***Z*** (a current ring) the current $\boldsymbol{i_b}$ acts (transmits a part of the reserved energy of a magnetic field of the wire spiral turned in a torus).

Quantity of current impulse amplitude of the spiral at the moment of its explosion should be such that magnetic pressure (1) was reached in view of entrapment coefficient ξ of initial magnetic field:

$$\xi = i_b / (I_m N), \tag{2}$$

where i_b is amplitude of a current of a plasmoid at explosion of a spiral, I_m is quantity of a current of a spiral before its explosion, N is number of coils of a spiral.

With the account (1) and (2) at $\xi \approx 0.4$ and atmospheric pressure ($p_g = 1 \cdot 10^5, Pa$) the current of a spiral can be estimated by means of relations:

$$I_m = \frac{B}{N} \cdot 2R, \tag{3}$$

$$B = (\pi/\xi)\sqrt{2 p_g / \mu_0} \approx 3 \cdot 10^6, \quad A/m. \tag{4}$$

For a case of the carried out experiments took place $R = 0.008\, m$ and $N = 60$. Calculation under formulas (3) and (4) gives value for a current of a spiral $I_m \approx 8 \cdot 10^2\ A$ that well corresponds to experimental data.

5. Hypotheses on a toroidal current layer

After explosion of the wire spiral turned in a torus non-stationary processes of interaction of squeezed electro conductive medium with a magnetic field begin to be arisen. In these requirements the phenomenon of the T-layer [7] may arise and develop. In a viewed case the toroidal magnetic field in magnetohydrodynamical configuration begins to work as the magnetic pump extorting plasma from space, engaged as a magnetic field, as at the initial

moment it was happened $p_m \geq p_g$. In effect the toroidal current layer [8] (see fig. 4 - a ring with a current) may be generated.

Conductance of plasma in a toroidal current layer should surpass copper conductance a million times that large enough lifetime of a magnetohydrodynamical configuration was provided. It is possible only at relativistic velocities of electrons, as section of a Coulomb scattering of electrons on ions in inverse proportion to a quadrate of energy of electrons. On assessments of works [8] energy of electrons may reach a level about unities *MeV*, and a lifetime of a plasmoid τ thus may be appreciated under the formula

$$\tau = \sigma_\tau r^2 . \qquad (5)$$

Here $\sigma_\tau \approx 1 \cdot 10^5$, s/m^2, and r is small radius of a torus of a current layer. Experimental data quite satisfactorily correspond to effects of evaluations under the formula (5).

Thus, the guess of development of the powerful induction discharge at electrical explosion of the wire spiral turned in a torus looks quite justified, that allows to hope for an opportunity of formation of long-lived current layers for getting of extremely high densities of a current in plasma. It is possible that in this case probably effective screening of charges of nucleus in a layer of the relativistic electrons and electron-catalyzed fusion may be implemented.

6. Experimental results with dipping spirals in water

Dipping of the wire spirals turned in the torus in water essentially changes parameters of electrical explosion that allows revealing new properties of this process and establishing the possible mechanism of occurring processes.

On fig. 6 are shown a picture of oscillation of a plasmoid at electro explosions of the spiral dipped in water. Apparently the gas vortex that was not observed at electrical explosions of spirals without water in this case is shaped of the first photo at electrical explosion. From the subsequent photos it is visible, that the sizes of a plasmoid it is much less, than at usual electrical explosions without water. The lifetime of plasmoids is approximately same, as well as dry spirals.

t=0.067 s ***t=0.133 s*** ***t=0.200 s*** ***t=0.267 s*** ***t=0.333 s***

Fig. 6. *Consecutive pictures of one of the generated plasmoids.*

On fig. 7 oscillograms of voltages and currents of a chain of the discharge, gained are shown at oscillation of a plasmoid at electro explosions of spirals without water, and at dip in water. As it visual, oscillograms essentially differ. It most probably speaks a different heat capacity of a surrounding medium at electrical explosion of spirals.

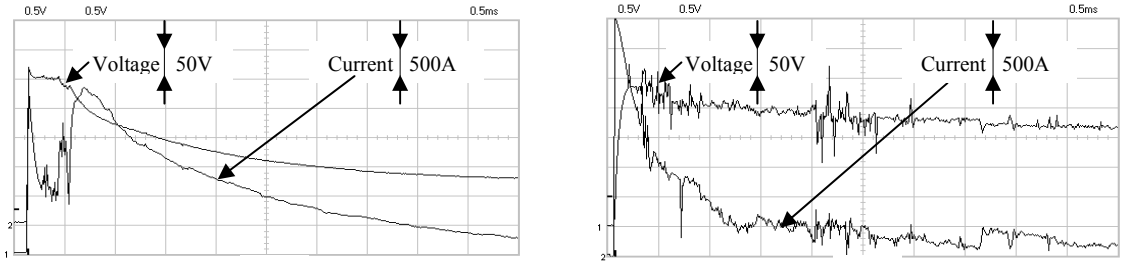

a) **b)**

Fig. 7. *Oscillograms: a) Without water; b) With the water*

7. Conclusion

Thus, the guess of development of the powerful induction discharge at electrical explosion of the wire spiral turned in a torus looks quite justified, that allows to hope for an opportunity of formation of long-lived current layers for getting plasmoids. The water doesn't promote the lifetime of plasmoids but it can be useful for forming gas vortex for current layer.

References

1. Exploding wires. Edited by W.G. Chace and H.K. Moore. Plenum Press, Inc., New York. Chapman & Hall, Ltd., London. 1959.
2. *Tkachenko S.I., Barishpol'tsev D.V., Ivanenkov G.V. at al.* Modeling of the processes accompanying electrical explosion of thin wires in air [In Russian] // Physics of extreme states of substance. Edited by V.E. Fortov et al. Ghernogolovka. 2007. P.65-67.
3. *Vlasov A.N., Kolesnikov S.A., Manoshkin A.B*. On features of electrical explosion of the wire spiral turned in a torus [In Russian] // Theses of reports on XXII international conference "Action of intensive streams of energy on substance". Edited by V.E. Fortov et al. Elbrus, Ghernogolovka. 2007. P.192-193.
4. *Vlasov A.N., Vlasov D.A., Kisselev Yu.V*. Features of the induction discharge at unipolar pulsing feed [In Russian] // News of Academy of Sciences. Physical series. 2003. V. 67. No. 9. P.1241-1243.
5. *Rajzer Yu.P.* Physics of gas discharge. [In Russian]. The Science, Moscow. 1987.
6. *Shafranov V.D.* On equilibrium magnetohydrodynamical configurations [In Russian] // JETP. 1957. V. 33. No 3 (9). P.710-722.
7. *Tikhonov A.N., Samarin A.A., Zaklyazminsky L.A. etc*. Nonlinear effect of formation of itself supported high-temperature electro conductive layer of gas in non-stationary processes of magneto hydrodynamics [In Russian] // Reports of Academy of Science of the USSR. 1967. V. 173. No. 4. P.808-811.
8. *Vlasov A.N.* Possible formation of a toroidal current layer during a spark discharge // Sov. Phys. JETP. 1990. V. 70 (2). P.259-262. ©American Institute of Physics (1990).

ON ISSUE OF SPATIAL DISTRIBUTION OF ELECTRICAL EXPLOSION PRODUCTS OF SINGLE WIRE

Yu.T.Sinyapkin, D.Yu.Sinyapkin

Russian Federal Nuclear Center – VNIIEF, Sarov, Russia,
E-mail: ***mailbox@ntc.vniief.ru***

Investigations of multi-wire liner systems, being carried out both in Russia and in foreign laboratories, the main goal of which creation of high-power pulsed x-ray source of magajoule range, are stalled due to recently discovered phenomena, impeding adiabatic self-constriction process. First of all this is heterogeneous absorption of electric energy on Z and X by a single wire and appearance of "kern" regime. Finally this leads to appearance of azimuth and axial heterogeneities at the end of a shell convergence, disturbing adiabatic regime. That is why it is impossible to get continuous (solid) plasma shell. Taking into account general gas-dynamic regularities we considered that large heterogeneities on the liner finish are consequences of small heterogeneities, i.e. their reasons are associated with the processes taking place on the start in the single wire. This work is devoted to investigation of this issue. It was preferable for us to study spatial mass distribution of exploding wire. Complexity and high cost of the equipment for spatial and time measurements lead us to creation of a method, called AUTOGRAPHY. Its main idea lies in absorption of scattered plasma-cluster-drop fragments with the target, located around the wire (a). Patterns obtained with this were densitometered (b) and, based on the results, we made a conclusion on a structure of mass spatial distribution of exploded wire, homogeneity of its scattering.

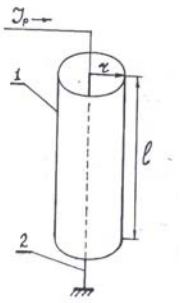

а)

б)

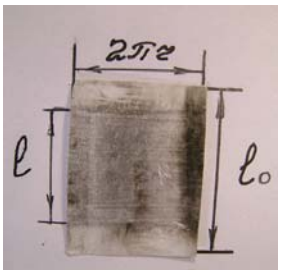

в)

г)

Experimental facility for multi-variant studies consisted of pulsed power source, based on lines with distributed parameters, hermetically sealed chamber for samples fastening, evacuation and gas filling unit of a discharger and the chamber, complex of measurement equipment to record electric parameters of the wire explosion process, and also instruments to control charging voltage and pressure in the discharger and working chamber. Results of experimental research have good reproducibility and make it possible to affirm that scattering products of electrical explosion of the single wire have a structure of successively located, relatively to the wire axis, self-organized toroidal-vortex formations from plasma-cluster fragments. Multiple investigation results showed that the structure is sensitive to experimental conditions and depends on wire material, its length, diameter and surface clarity, type and pressure of surrounding air, current and voltage of the power source.

GLOBE LIGHTNING: MODELING AND APPLICATION

G.P. Schelkunov, I.M. Olikhov

CJSC SPE "Gamma",
E-mail: ***gammaf@mail.ru***

We assume different periods of solving globe lightning problem, which are revelation of its nature and creation of generating plasmoid-models mechanism.
We suppose here a new device project, which enable some more valid experiments.

Excess Heat and Related Nuclear Products (HP)

NEUTRONS, γ−RAYS & TRITIUM DIAGNOSTIC AT ELECTROLYSIS WITH ANODE GAS DISCHARGE IN WATER SOLUTIONS

Yu.N.Bazhutov[1], V.Yu.Velikodny[2], V.G.Grishin[2], [A.V.Eremeev[2]], V.V.Popov[2], A.D.Rumyantsev[3], Yu.A.Sapozhnikov[4], N.I. Khokhlov[5], A.P.Koshelev[6], V.A.Starostin[7]

[1]IZMIRAN, [2]IPRIM RAS, [3]SRIDevice, [4]Chem. Dep. of MSU, [5]Karpov SRPCI, [6]Research Automation Institute, [7]RRC Kurchatov Institute
bazhutov@izmiran.ru

It was fulfilled series of experiments of electrolysis with anode gas discharge. Voltage was (100−1000)V. Current amplitude was (1−10)A. Heavy water concentration in electrolyte was (0,017−30)%. Possible addition of Lithium & Potassium in electrolyte was (0−20) %. Titanium or Nickel plates were used for cathode; Gold or Tungsten was used for anode. For received results there were used following diagnostic methods: 1) γ-spectrometer based on low background pure Ge detector (120 ml) & NaI(Tl) scintillation detector (Ø63x63 mm^2 first and then Ø150x100 mm^2); 2) Tritium liquid scintillation diagnostic in electrolyte (sensitivity ~ 0.1 Bq/ml); 3) Neutron flux diagnostic (sensitivity ~ 2 n/cm^2s). Received results of regular reproducibility of neutrons & tritium generation were corresponded to the Erzion model predictions. Large neutron yield reached value ~ 10^6 neutrons per second with correlated tritium yield value near ~ 10^{11} Tritium atoms. Control experiment predicted in framework of Erzion model suppressed neutron yield down to zero.

Introduction

In materials of 9-th and 10-th Russian Conferences on Cold Nuclear Transmutations 2 works [1,2] which have stimulated carrying out of this experiment have been published. In first of them [1] by method of γ-spectrometry during plasma electrolysis of solution LiOH−D_2O in a cell with the Pd cathode and the Tungsten anode the induced radioactivity was revealed. In the same place it has been shown, that among lines of a spectrum of the induced activity there is such which together with a spectrum view; intensity and a half-life time correspond to the isotope Ta^{183} decay. In the 2-nd of them [2], with enough similar plasma technique of high-voltage electrolysis on the W anode (7M KF, 50% D_2O) there were observed reproduced strange turbidity of water in an external cooling contour of a cell from the anode side. Both these results have been quantitatively interpreted in the report [2], as consequence with Erzion model [3−5]. This work is continuation previous [2], but with addition of a lot of new methods of nuclear diagnostics: 1) a gamma-spectrometry of a cell with help of the scintillation NaI(Tl)-detector (Ø63x63mm^2) (Background ~ 100Hz) and the dosimeter "Sosna" (Background ~ 0,1μR/h), 2) liquid scintillation diagnostics of Tritium in an electrolyte (the Level of the Background ~ 0.1Bq/ml), 3) diagnostics of neutrons generation by radiometer (the Level of the Background ~ $2n/cm^2s$).

Statement of the experiment

As the present experiment is continuation and development of the previous experiment [2] it is natural, that in it the old electrolytic cell was used (Fig.1). It consists of a bake able glass cap with working volume 500 ml, closed by a teflon cover with several apertures for an output formed vapors and gases (the open cell) and input in its volume of a mercury thermometer and the metal anode and cathode. The cathode (50x70x2 mm^3) has been completely plunged into an electrolyte and has been made from the porous titanium or nickel. The anode was screwed in the end of a steel core potential wire (Ø6x260 mm^2) with the adjusting screw and fell with its help under a surface of an electrolyte on the depth defining a current in installation. As the anode were used either gold «bullet» by weight of 5g and with purity of 99,99 %, or conic Tungsten tip (Ø3-5mm) had weight of 10g. The control over temperature of an electrolyte was carried out by means of a standard mercury thermometer. As electrical power brought to a cell during the experiment was about kW, the cell was located inside of a secondary contour of water cooling with a forced circulation of water through buffer volume 50l. A secondary contour was executed in the form of a standard glass aquarium (12x17x38 cm^3). The principle of action of an electrolysis with a discharge through gases on the anode (a plasma electrolysis) is in details described by us in the previous work [2], where it U−I curve was presented. We worked in this experiment always in the field of a plateau of this performance, switching on or off at once the chosen voltage, creating thus plasma formation around of the anode with a powerful luminescence. The electrical source of a cell was carried out in the first 4 series by means of standard industrial manufacturing device VSA-111B. Since 5-th series, we used a self-made source of the voltage using 2 phases of a network Voltage (220 V), passed through autotransformers and through the 4 diodes bridge scheme with or without using of capacitive filters, as well as in industrial source VSA-111B. Above a cell the system of the forced extract was starting with vapors and gases outgoing from cell. In last series of experiment, since 10-th, a working cell together with an aquarium of cooling have been placed in steel boxing (~17x25x45cm^3) with a face glass window (~15x23cm^2) for shielding from radio noises of a measuring system and the best hermetic sealing from alkalis vapors (see Fig.2).

The system of nuclear diagnostics consisted of several detectors and measurement systems. For measurement of the neutron flux generated in a cell due to prospective Erzion-nuclear catalytic transmutations of nuclei, radiometer with special head, adjusted onto registration of thermal neutrons with switched measurement ranges of a neutron flux was used standard industrial manufacturing up to: 100, 1000, 10000 and 100000 ($n/s \cdot cm^2$) and accordingly by division of a scale of measurement: 4, 40, 400 and 4000 ($n/s \cdot cm^2$). On Fig.1 and Fig.2 the special radiometer head is to the left of a cell, resting the detecting end face in shielding boxing or a cooling aquarium. The measuring part of the device is carried from installation on the distance ~1,5 m. The special radiometer head and device are earthed on special grounding.

At the near left corner of an aquarium the "Sosna" dosimeter is located to act as the additional operative control over a radiation doze on the edge of installation. The basic measurements of γ-radiation from working installation were made by means of scintillation crystal NaI(Tl) (Ø63x63 mm^2 first, and then Ø150x100 mm^2), placed in 5cm lead cover "small house" with the sizes of an external contour - (30x30x30 cm^3) for reduction of a background (Fig.1 and 2). Distance from an end face of a crystal up to an aquarium was ~10cm. Signal from photoelectron multiplayer of detector NaI(Tl) after preliminary amplification acted on an input 1024-channel analyzer, built inside of a Personal Computer (Fig.2). For set in advance time exposition in each series of measurements, energy spectrums

up to ~2 or ~10 MeV before electrolysis (background), during (effect) and after it (posteffect) were measured. Up to each series of measurements and after it from an electrolyte there were done control castings and were brought then onto 2 independent liquid scintillation installations for measurement of Tritium accumulation to the Moscow State University and to the Karpov Institute.

Results of the experiments.

As a result of this experiment executed from July 20 2005, 12 independent series with various electrolytes and anodes have been fulfilled which results are presented in table 1. Before each series all detectors preliminary got trained. Then the background γ-spectrum was received on crystal NaI with certain time of an exposition on the amplitude analyzer. After such preliminary preparation on electrodes of a cell the running voltage switched on, and every minute there were written down values of: 1) running time, 2) temperature of an electrolyte in a cell 3) running voltage, 4) running current, 5) indications of a dosimeter and 6) radiometer RUP-1 neutron flux indications. In parallel during the same time the amplitude spectrum from crystal NaI was typed on the analyzer. After end of time of an exposition the voltage on a cell was switched off and also a current stopped. Then the spectrum of amplitudes from crystal NaI (post effect) in current of same time of an exposition was again typed. Unfortunately, in one of series it has not been gained significant excess in values of spectrums of "effect" or "post effect" above background spectrums (see fig.7).

Apparently from table 1 where average values of all removed in each series of experiment of parameters are presented, in first 4 series we worked with the gold anode and a low running voltage (<100B). In these series it has not been registered neither thermal neutrons, nor an accumulation of Tritium. After full dissolution in an electrolyte in the 4-th series of a gold anode tip we have replaced it by tungsten and have simultaneously involved a self-made source of a voltage for reception of higher voltage that follows from predictions of Erzion model and experiments - prototypes [1,2]. And, apparently from table 1, registration of the significant flux of thermal neutrons under indications of radiometer RUP-1 at once has begun and in 5-th series outside 3 statistical errors the accumulation of Tritium has been registered. Unfortunately, in the subsequent 2 series (6-th and 7-th) where also in an electrolyte there was a heavy water, the accumulation of Tritium has not proved to be true. But in all subsequent series the even greater flux of thermal neutrons (see fig. 3-7 & tables 2-6) was registered even. For check of this fact check experiment (11-th series) with such composition of chemical substances in an electrolyte that according to Erzion model [3-5] there was no absolutely a generation of neutrons has been specially put. By the way, all the previous compositions of electrolytes were chosen according to Erzion model [3-5] so that generation of neutrons was as much as possible observed. And so neutrons completely were none in 11-th series of check experiment, although the basic electro technical parameters of the experiment (a current and a voltage) have remained approximately the same. Besides since 10-th series to reduce possible influence radio engineering noises onto radiometer RUP-1, an aquarium of cooling with the electrolytic cell where there was a discharge through gases and plasma on a surface of the anode was formed, has been placed in steel boxing with a glass face window. However, it essentially has not affected onto indications of radiometer RUP-1. On the basis of all above-stated it is possible to hope, that RUP really registered neutrons, instead of radio noise from a discharge through gases. And nevertheless, the final answer in this occasion will be given with our subsequent experiments, because this devise registration may be coursed by creation of initial Erzion-nuclei reaction chains in organic scintillation of

neutron radiometer. But if we really registered neutrons in 9-th series we have gained the maximal output of neutrons in a cell of ~10^6 neutrons per second. And from 5-th series where the operating time of Tritium (T) has been registered, follows, that the ratio of an output of Tritium ($\sum T \sim 10^{12}$) to an integrated output of neutrons ($\sum n \sim 10^7$) makes the factor K = (T/n) 10^5, that corresponds on an order of magnitude, the values gained in experiments on Cold Nuclear Transmutations, instead of in thermonuclear reactions, where K~1. Besides the gained results of experiment are in the full consent with predictions of Erzion model [3-5] at the choice of a composition of an electrolyte, the anode material and also running voltage.

In the conclusion we express gratitude in experiment assistance to Baranov D.S., Kazyonov A.J., Karasyov B.V., [Kosarev V.B.], Krychenko O.V., Lupatov V.M. and Nikitenko L.K.

References

1. Zelenskij V.F., Poljashenko R.F., «Production of an isotope $_{73}Ta^{183}$ during a pulsing electrolysis of solution LiOH-D_2O in a cell with Pd cathode and the tungsten anode». Proceedings of 9-th Russian Conference on cold nuclear transmutations of chemical elements, (Dagomys, Sochi, 30 Sep. - 7 Oct., 2001), Moscow, 2002, pp.46-54.
2. Bazhutov Yu.N., Grishin V.G., [Nosov V.N.] «Electrolysis with a discharge through gases on the anode ». Proceedings of 10-th Russian Conference on cold nuclear transmutations of chemical elements and a fireball, (Dagomys, Sochi, 29 Sep. - 6 Oct., 2002), Moscow, 2003, pp.19-26.
3. Bazhutov Yu.N., Vereshkov G.M. «New stable hadrons in space beams, their theoretical interpretation and a possible role in catalysis of cold nuclear synthesis», Preprint 1, CSRIM, 1990.
4. Bazhutov Yu.N., Vereshkov G.M., Kuksa V.I. «About an opportunity of existence new stable hadrons - hypothetical catalysts for cold nuclear transmutations», Proceedings of 3-d Russian Conference on cold nuclear fusion, Moscow, 1996, pp. 157-201.
5. Bazhutov Yu.N., [Kuznetsov A.B.], Pletnikov E.V. “Spectroscopy of Erzion catalytic nuclear transmutations". Preprint # 1 SRC FTP «Erzion»,1993, CSRIM, 1-172.

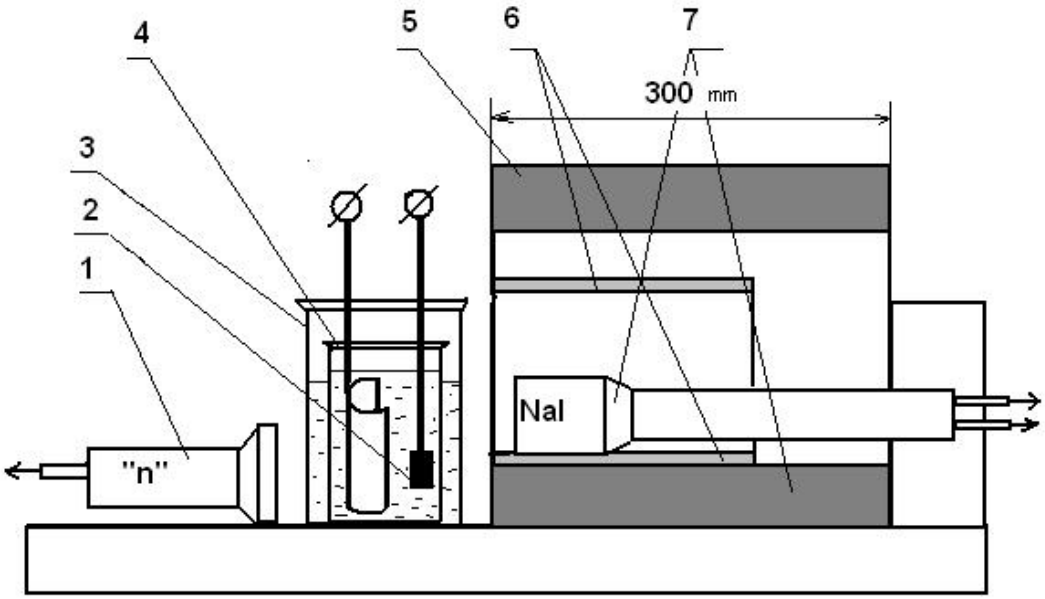

Fig.1. The experimental installation scheme.

1 *– detector of neutrons flux,* ***2*** *–gold or tungsten anodes (S ~1 cm^2), cathode - the porous titanium (S~30 cm^2),* ***3*** *– glass aquarium with cooled water (~7 l),* ***4*** *– glass electrolytic cell (500 ml),* ***5*** *– external lead shield - small house from standard modules,* ***6*** *– internal (additional) lead shield of the gamma rays detector, 7 – the detector of gamma-radiations (standard crystal NaI (Tl) 63x63 mm^2)*

Fig.2. The experimental installation view.

Thermal neutrons flux (n/cm^{2}s) on a wall of an aquarium in 5 series (Anode–W, Cathode–Ti) (2.2M–LiOH; 15%–D_2O).Tritium production–(1.8+/-0.5) Bk/ml

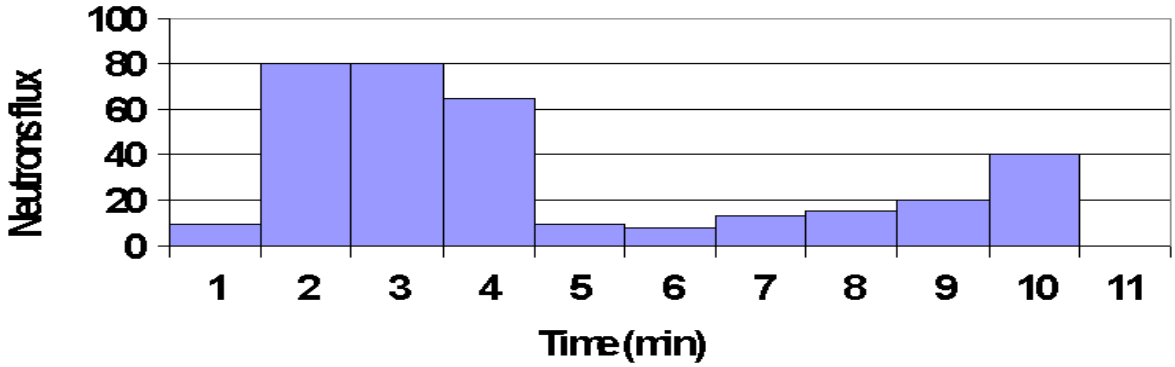

Electric current at electrolysis with the discharge on the tungsten anode in 5 series of experiment

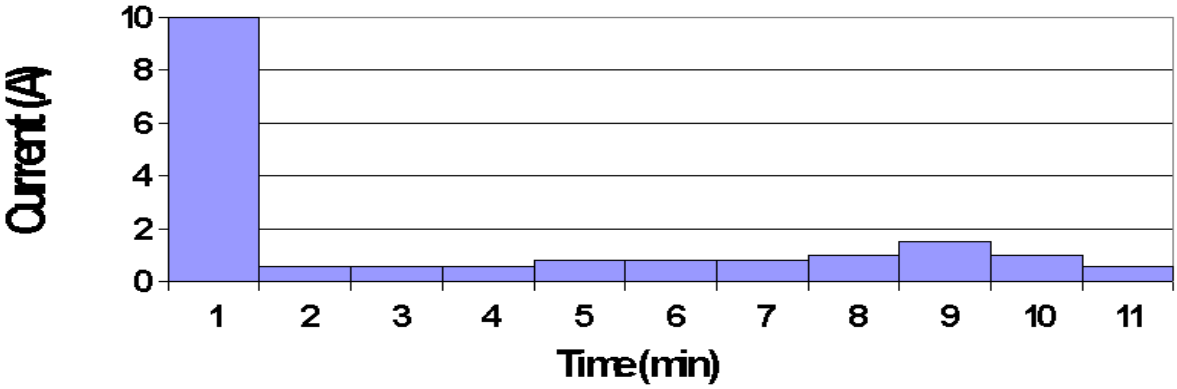

Doze rate of a dosimeter "Pine" in 5 series

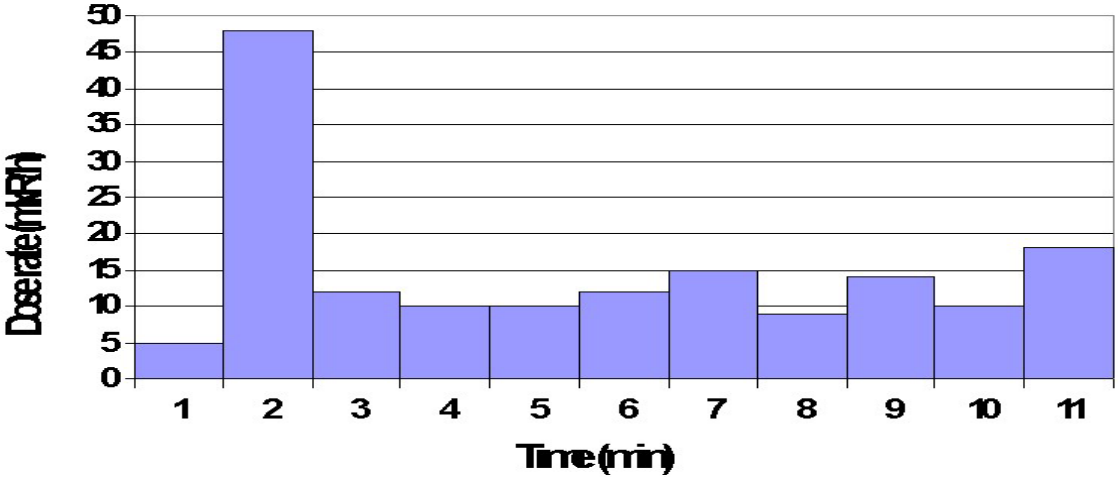

Fig.3. The 5-th experimental series results.

Thermal neutrons flux (n/cm^{2}s) on a wall of an aquarium in 6-th series (Anode–W, Cathode–Ti) (2.2M–LiOH; 15%–D_2O) Tritium production up to – (2.4+/-1.5) Bk/ml

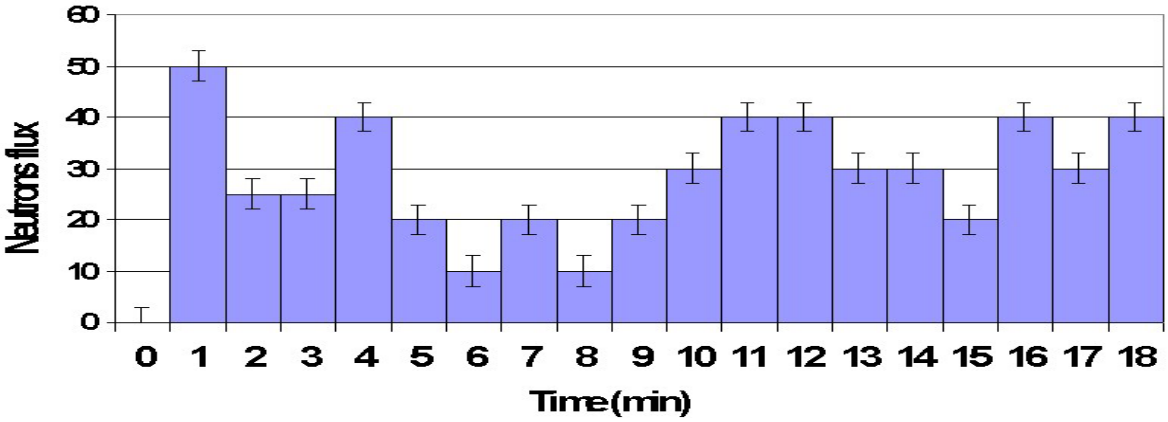

Electric current at electrolysis with the gas discharge on the tungsten anode in the 6-th series of experiment

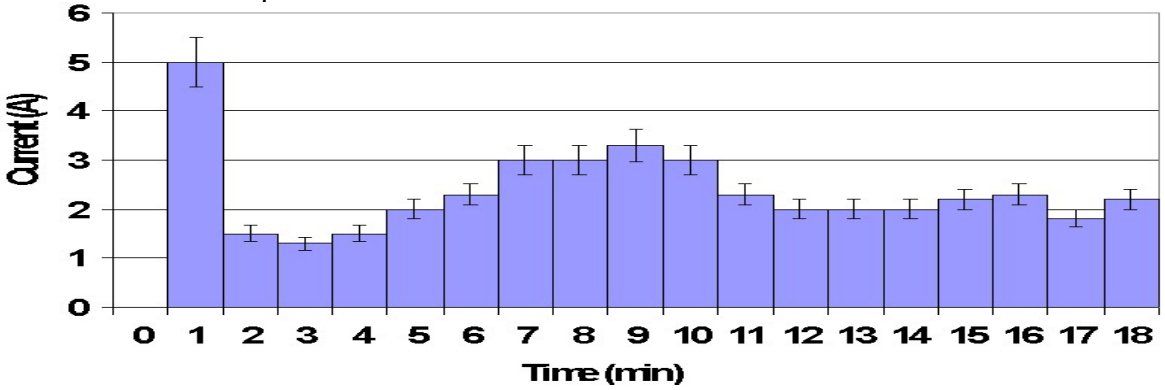

Doze rate of a dosimeter "Pine" in the 6-th series

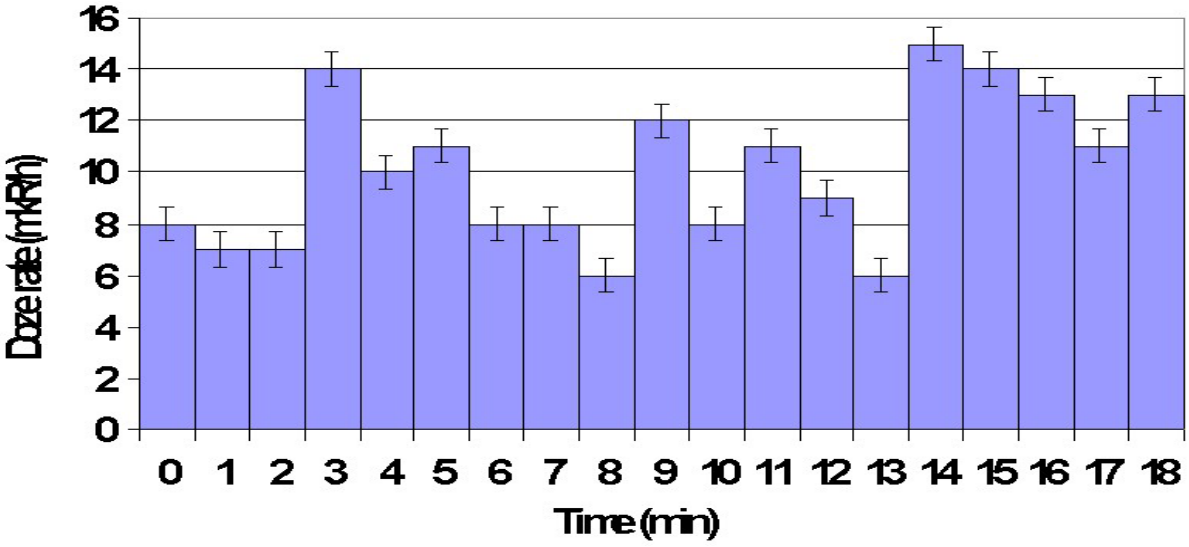

Fig.4. The 6-th experimental series results.

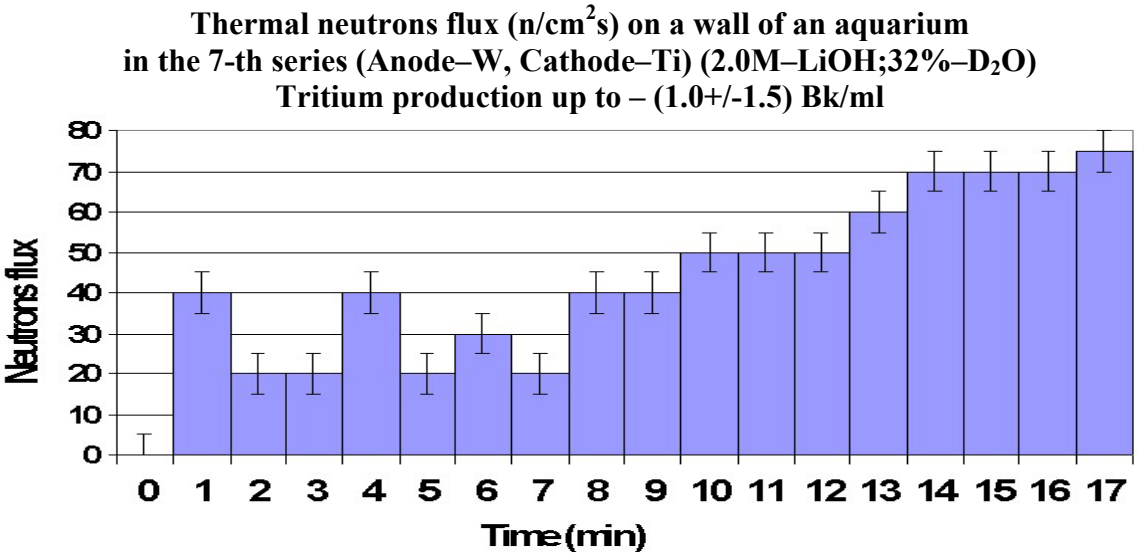

Electric current at an electrolysis with the discharge on the tungsten anode
In the 7-th series of experiment

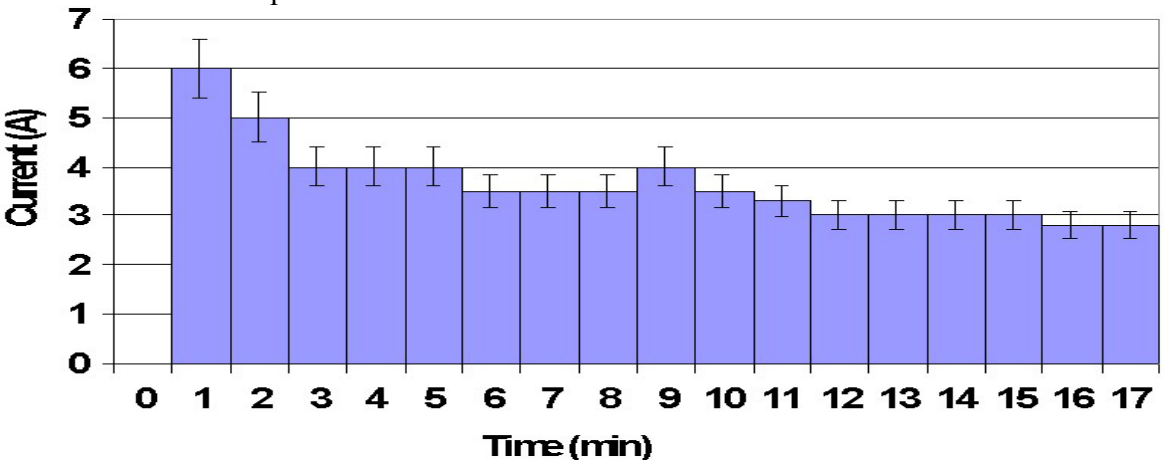

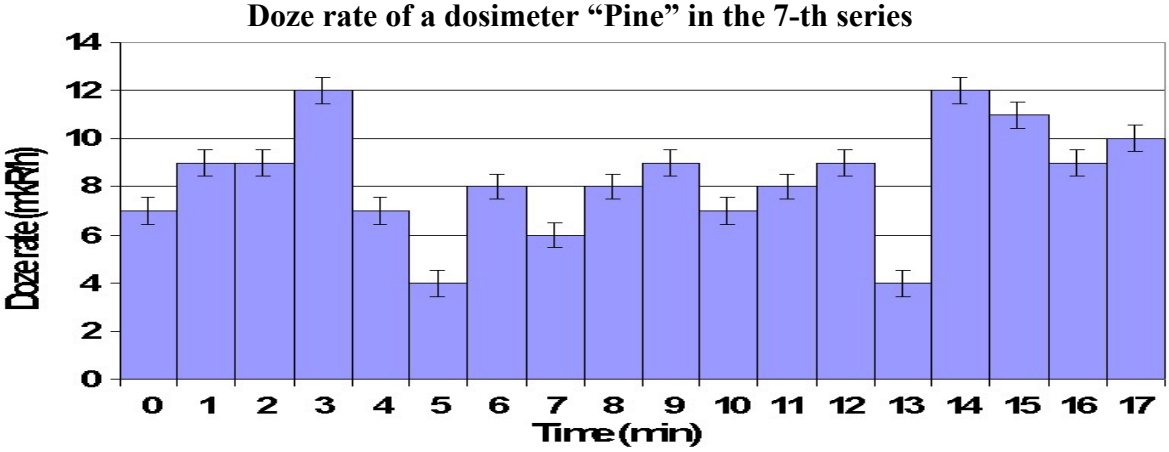

Fig.5. The 7-th experimental series results.

Thermal neutrons flux (n/cm^{2}s) on a wall of an aquarium
In the 8-th series (Anode–W, Cathode–Ti) (10.0M–NaOH)
Tritium production–(?) Bk/ml

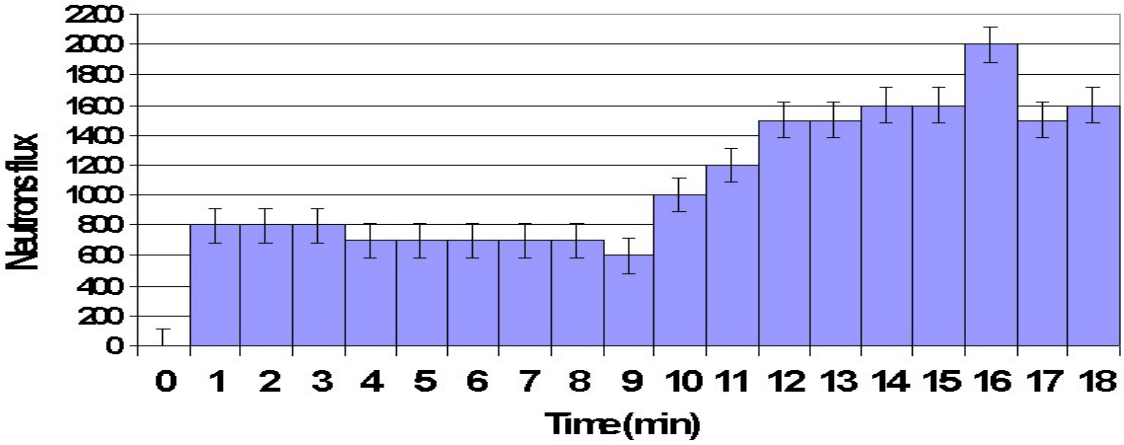

Electric current at electrolysis with the discharge on the tungsten anode in the 8-th series of experiment

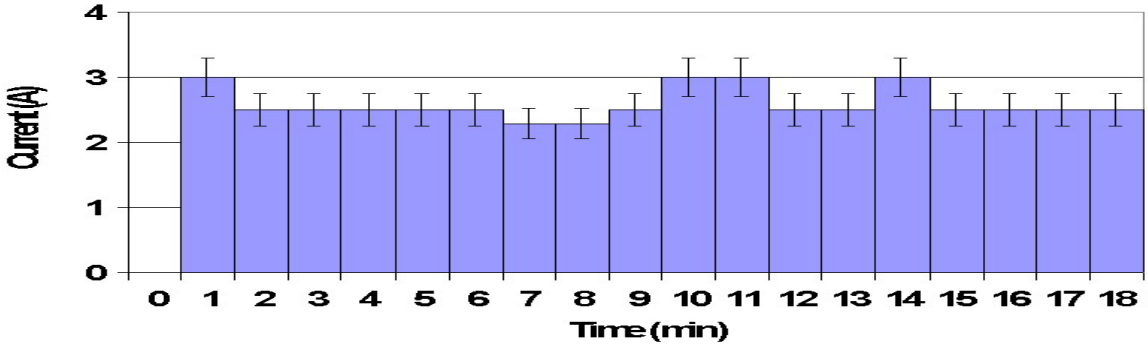

Doze rate of a dosimeter "Pine" in the 8-th series

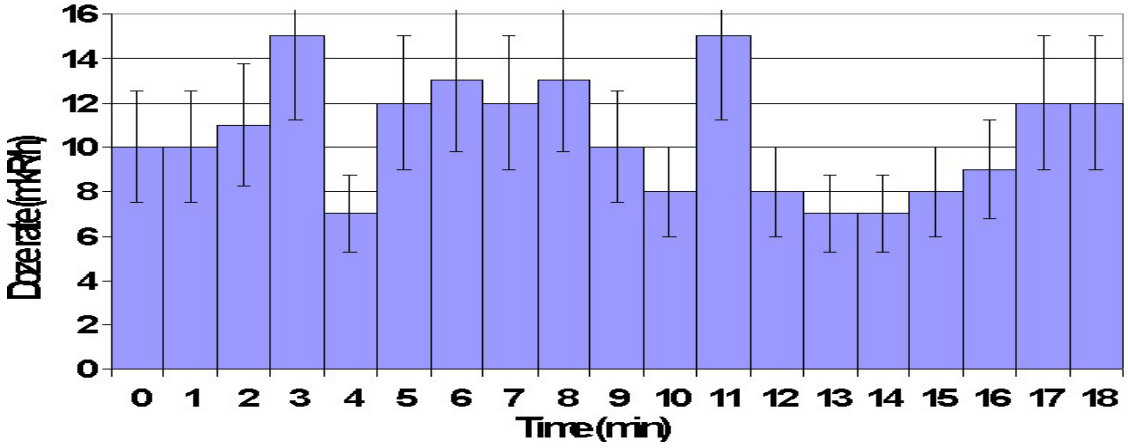

Fig.6. The 8-th experimental series results.

Thermal neutrons flux (n/cm^{2}s) on a wall of an aquarium in 9-th series (Anode–W, Cathode–Ti) (10.0M–NaOH) Tritium production–(0.4+/-0.5) Bk/ml

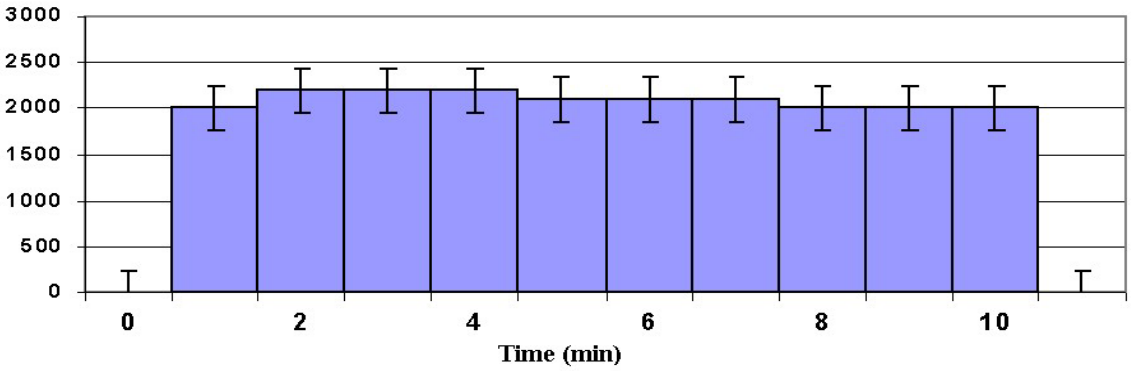

Values of amplitude γ-spectrums of "effect" & “background” spectrums in the crystal NaI (T=3000s, background spectrums is red)

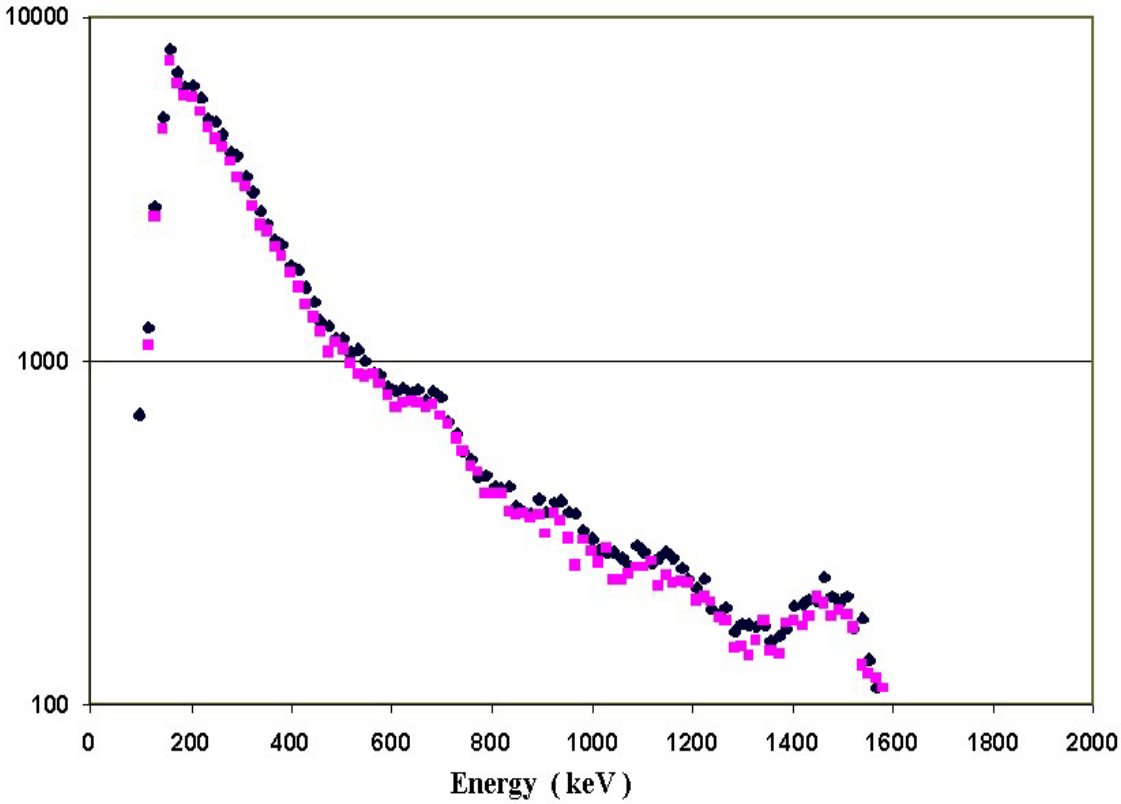

Fig.7. The 9-th experimental series results.

Table 1. Experimental data from all 12 series.

№ Series	Electrolyte	Anode	Δt (min)	<U> (V)	<I> (A)	<W> (W)	Neutrons 1/(cm^2 s)	Doze rate (μR/h)	T/max (^{0}C)	Tritium (Bk/ml)
1	10M- NaOH	Au	60	90	2,22	200	0	9,3 +/- 0,4	81	-0,5 +/- 0,5
2	0,15M-Li_2CO_3 (5%D_2O)	Au	60	90	1,85	168	0	9,8+/-0,4	73	-2,9 +/- 30
3	10M- $LiNO_3$ (5%D_2O)	Au	59	89	2,33	207	0	9,4+/-0,4	79	-30 +/- 30
4	15M-LiCl (25%D_2O)	Au	54	90	2,84	256	0	9,4+/-0,4	94	?
5	2,2M-LiOH (15%D_2O)	W	11	368	1,63	500	8-80	14,8 +/- 1,2	80	1,8 +/- 0,5
6	2,2M-LiOH (15%D_2O)	W	18	344	2,37	820	10-50	10,3 +/- 0,7	99	-0.5 +/- 0,5
7	2M-LiOH (32%D_2O)	W	17	333	3,64	1210	20-75	8,3 +/- 0,7	96	-0.5 +/- 0,5
8	10M-NaOH	W	18	340	2,58	880	600-2000	10,5 +/- 0,7	95	?
9	10M-NaOH	W	10	340	2,1	505	2000-2200	?	93	0,4 +/- 0,5
10	10M- NaOH	W	32	330	1,28	420	200-2000	9,9 +/- 0,6	95	?
11	1,3M-$FeSO_4$*7H_2O	W	34	330	1,67	550	0	8,1+/-0,5	88	-0,2 +/- 0,5
12	10M- NaOH	W	4	330	5	1650	80-400	11+/-3	70	?

Table 2. Experimental results from the 5-th series

Time (min)	Voltage (V)	Current (A)	Power (kW)	Flux (n/cm^{2}s)	Doze rate (μR/h)	Temperature (^{0}C)
1	250	10	2,5	10	5	56
2	380	0,5	0,2	80	48	62
3	380	0,5	0,19	80	12	64
4	380	0,5	0,19	65	10	64
5	380	0,8	0,304	10	10	64
6	380	0,8	0,304	8	12	66
7	380	0,8	0,304	13	15	70
8	380	1	0,38	15	9	74
9	380	1,5	0,57	20	14	78
10	380	1	0,38	40	10	80
11	380	0,5	0,19	0	18	80

Table 3. Experimental results from 6 series

Time (min)	Voltage (V)	Current (A)	Power (W)	Flux (n/cm^{2}s)	Doze rate (μR/h)	Temperature (^{0}C)
0	0	0	0	0	8	20
1	250	5	1250	50	7	62
2	350	1,5	525	25	7	83
3	350	1,3	455	25	14	84
4	350	1,5	525	40	10	88
5	350	2	700	20	11	91
6	350	2,3	805	10	8	96
7	350	3	1050	20	8	97
8	350	3	1050	10	6	98
9	350	3,3	1155	20	12	99
10	350	3	1050	30	8	98
11	350	2,3	805	40	11	96
12	350	2	700	40	9	96
13	350	2	700	30	6	95
14	350	2	700	30	15	94
15	350	2,2	770	20	14	93
16	350	2,3	805	40	13	93
17	350	1,8	630	30	11	93
18	350	2,2	770	40	13	93

Table 4. Experimental results from the 7-th series

Time (min)	Voltage (V)	Current (A)	Power (W)	Flux (n/cm^2s)	Doze rate (μR/h)	Temperature (^0C)
0	0	0	0	0	7	20
1	330	6	1980	40	9	55
2	330	5	1650	20	9	64
3	330	4	1320	20	12	72
4	330	4	1320	40	7	87
5	330	4	1320	20	4	95
6	330	3,5	1155	30	8	96
7	330	3,5	1155	20	6	96
8	330	3,5	1155	40	8	96
9	335	4	1340	40	9	96
10	335	3,5	1173	50	7	96
11	335	3,3	1106	50	8	96
12	335	3	1005	50	9	96
13	335	3	1005	60	4	96
14	335	3	1005	70	12	96
15	335	3	1005	70	11	96
16	335	2,8	940	70	9	96
17	335	2,8	940	75	10	96

Table 5. Experimental results from the 8-th series

Time (min)	Voltage (V)	Current (A)	Power (W)	Flux (n/cm^2s)	Doze rate (μR/h)	Temperature (^0C)
0	0	0		0	10	22
1	340	3	1020	800	10	92
2	340	2,5	850	800	11	92
3	340	2,5	850	800	15	91
4	340	2,5	850	700	7	91
5	340	2,5	850	700	12	90
6	340	2,5	850	700	13	91
7	340	2,3	780	700	12	91
8	340	2,3	780	700	13	91
9	340	2,5	850	600	10	91
10	340	3	1020	1000	8	91
11	340	3	1020	1200	15	91
12	340	2,5	850	1500	8	92
13	340	2,5	850	1500	7	91
14	340	3	1020	1600	7	94
15	340	2,5	850	1600	8	94
16	340	2,5	850	2000	9	95
17	340	2,5	850	1500	12	95
18	340	2,5	850	1600	12	95

Table 6. Experimental results from the 9-th series

Time (min)	Voltage (V)	Current (A)	Power (kW)	Flux (n/cm^{2}s)	Doze rate	Temperature (^{0}C)
0	0	0	0	0	?	21
1	340	3,7		2000	?	40
2	340	3		2200	?	50
3	340	3		2200	?	60
4	340	2		2200	?	70
5	340	2		2100	?	80
6	340	1,5		2100	?	85
7	340	1,5		2100	?	90
8	340	1,4		2000	?	93
9	340	1,4		2000	?	93
10	340	1,4		2000	?	93
11	0	0		0	?	93

EXCESS HEAT DURING DIFFUSION OF DEUTERIUM THROUGH PALLADIUM

Jean-Paul Biberian and Nicolas Armanet

Département de Physique, Faculté des Sciences de Luminy, Université d'Aix-Marseille II,
163 Avenue de Luminy, 13288 Marseille cedex 9, France.
***Email:** jpbiberian@yahoo.fr, armanetnicolas@hotmail.com*

Abstract

We have developed a mass flow calorimeter enabling us to measure accurately excess heat production during deuterium diffusion through the walls of palladium tubes. The experiment consists usually of a palladium tube 10 cm long, 2mm outer diameter with 200 µm thick walls, and closed at one end. Deuterium gas is introduced in the tube at various pressures, and temperatures and diffuses out through the walls of the tube. The tube, heated by a resistor, is positioned inside a reactor cell which is a small vacuum chamber. The reactor cell is positioned inside a second vacuum chamber. The outer walls of the vacuum chamber are water cooled. Thermal energy is determined by measuring inlet and outlet temperatures and water mass flow. The energy yield of this calorimeter is 95-98 % depending on input power.

We study the influence of deuterium pressure, tube temperature, various metal powders placed inside the tube, and metal deposited on the external surface of the tube. Our best result so far is an excess heat of 3 Watts with an input power of 47 Watts using an oxidized palladium tube filled with palladium powder. We propose a model involving reactions between D+ and D to explain our experimental results.

1. Introduction

Since the announcement of the discovery of Cold Fusion by Stan Pons and Martin Fleischmann (1) in 1989, researchers have tried all kinds of ways to reproduce and improve the experiment. Most work has been done by electrochemical means with solid electrodes in order to reproduce the original results. There are at least two major limitations to electrolysis in view of obtaining high energy outputs with little input power. On one hand electrochemistry in aqueous solutions and atmospheric pressure limits the cell temperature to 100 °C, and on the other hand lot of input energy is spent to dissociate water. There are

certainly solutions to avoid these limitations, for example electrolysis with molten salts, or water at high pressure. However these technologies are difficult to implement in an ordinary laboratory.

More and more people are trying alternative solutions. One of them is the use of deuterium gas instead of heavy water. There are several advantages to that choice; one of the most important one is the fact that operations are feasible at much higher temperatures, and it is very likely that nuclear reactions in solids increase with increasing temperatures.
Most researchers have chosen solid metal electrodes as Pons and Fleischmann (1). However several experiments have been realized with either thin films or metal powders. Certainly the most interesting work has been produced by Arata and Zhang (2) with their DS cathode where a hollow palladium cathode is filled with palladium nano powder. They show large excess heat production when using heavy water and no excess heat with ordinary water. They have also measured production of helium-4 during these runs (3). Recently the same authors have developed an alternative technique to obtain similar results applying high pressures of deuterium gas on the outside of a palladium tube filled with palladium nano powder. With this new design there is no energy spent to dissociate water and temperature can be larger than with an electrolytic design.

Another interesting result has been obtained by Li et al. (4). They observed excess heat when deuterium gas flows through a palladium foil. Interestingly, back in 1989, Fralick et al. (5) reported a similar experiment when they loaded an hydrogen gas purifier with deuterium, and then pumped it out. They observed a temperature rise with deuterium versus no temperature variation with hydrogen.

All these results indicate that diffusion of deuterium through palladium produces excess heat.

A weak point of Arata (2), Li (4) and Fralick (5) experiments is the lack of accurate calorimetry. In all three cases temperatures are measured, that clearly indicate excess heat, but no absolute value of the heat produced is given. Therefore we decided to build a calorimeter capable of doing experiments similar to the above, whilst keeping its capacity of good calorimetry.

This paper gives preliminary results of diffusion of deuterium through palladium. They show interesting features that need confirmation.

2 - Experimental setup

The main idea behind our calorimeter design is the use of a mass flow calorimetric method so that no calibration is necessary. Its design has been improved over time and it can be described in two different designs described below.

2.1 - First design

Figure 1 shows a view of the first system. The vacuum chamber is a stainless steel cylinder 7 cm in diameter and 50 cm long. It is surrounded by a second stainless steel envelope where 30°C water circulates at a constant flow rate of 180 ml/min. In and out temperatures of water

are measured with two calibrated thermistors. A palladium tube closed at one end usually 10 cm long and 2 mm in outer diameter is welded on a 6 mm diameter stainless steel rod which is attached to a 6 mm diameter stainless steel tube with a Swagelok® fitting (figure 2). A thermocouple is inserted inside the stainless steel tube up to the center of the palladium tube when it is empty, and to its edge when it is filled with palladium powder from Goodfellow 80-180 nm. Therefore for a given heating power the measured temperatures differ according to the position of the thermocouple. The first value is closer to reality than the second one. Also because of the heat losses by conduction and non uniform heating, the temperature of the palladium tube is not uniform along the tube.

The palladium tube is heated by radiation with a Thermocoax resistor wrapped around it using DC current. Four stainless steel concentric reflectors are positioned around the resistor in order to minimize heat losses by radiation. Input heat applied to the resistor is dissipated mainly by radiation and is collected by the water cooled envelope. However part of the heat is lost by conduction through the 6 mm stainless steel tube attached to the palladium tube and also through the metal flange which holds the electric feedthroughs and the various pumping tubes.

A major flaw of this design is the fact that when deuterium gas diffuses out of the palladium tube, pressure inside the vacuum chamber increases. This also occurs when we purposely close the valve of the vacuum chamber towards the pumping system and let the pressure rise inside the vacuum chamber. Under these circumstances heat is transferred from the heater not only by radiation, but also by conduction and convection. This has been solved in the second design of the equipment described in the next section.

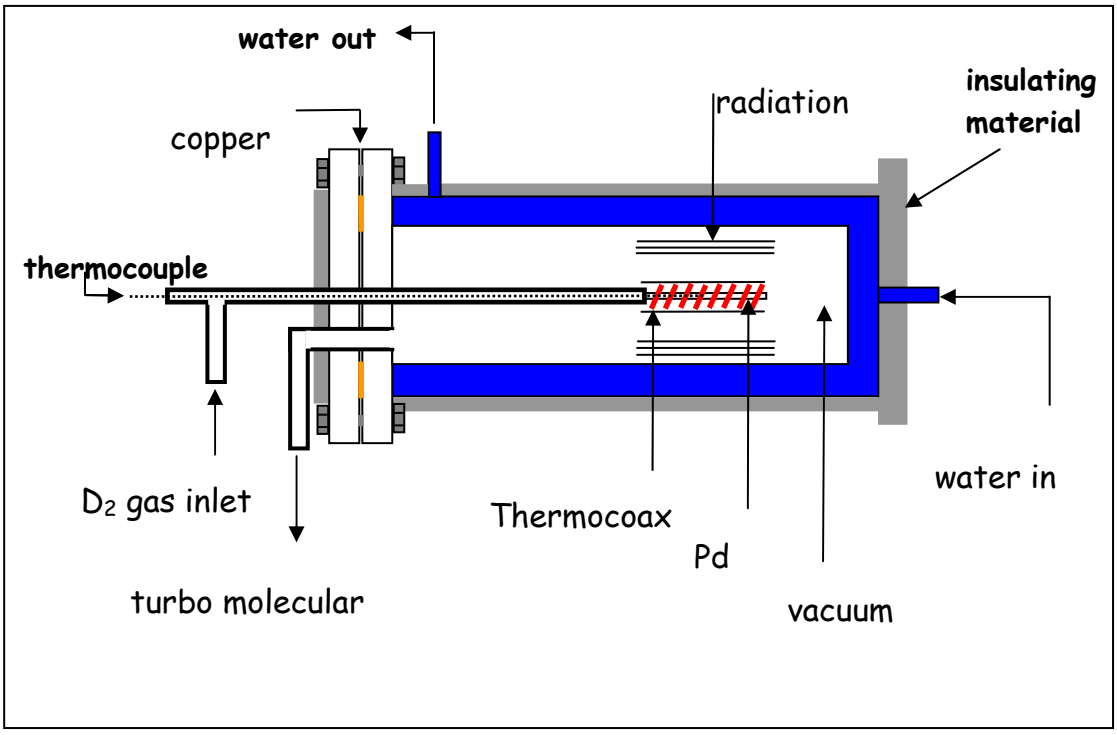

Figure 1

First design of the mass flow calorimeter

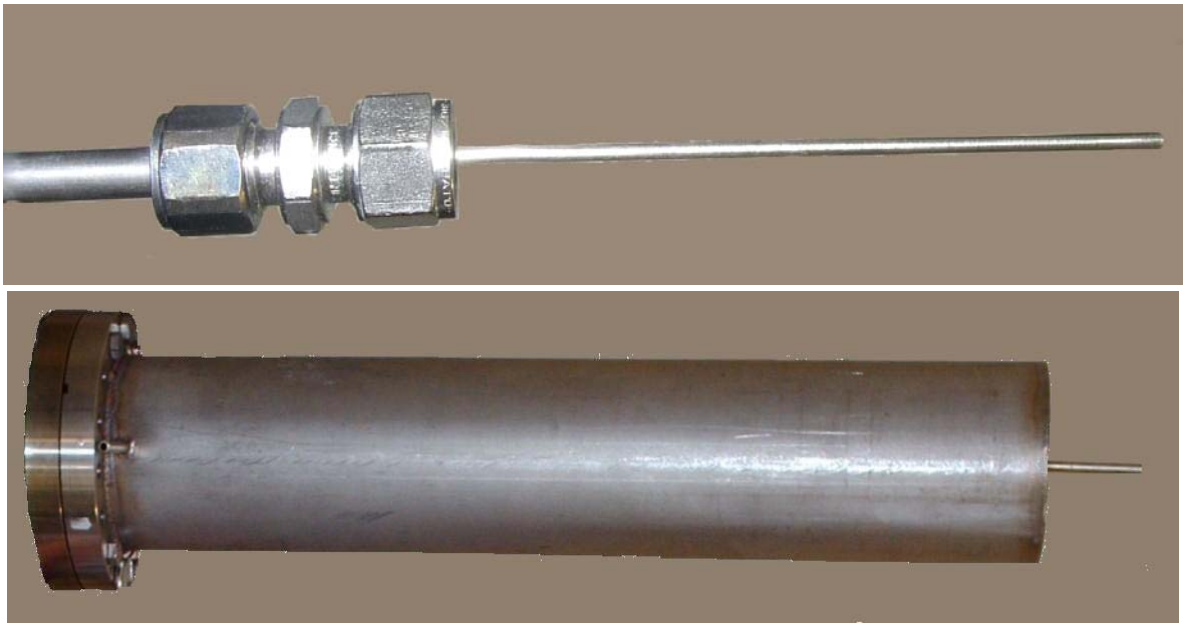

Figure 2
Top: photograph of the palladium tube attached to the stainless steel tube with a Swagelok® fitting. Bottom: photograph of the vacuum chamber

2.2 - Second design

In order to improve the calorimeter we have added a stainless steel reaction cell around the palladium tube, with a separate pumping system, so that there is no pressure rise in the vacuum chamber when deuterium diffuses through the palladium tube. Therefore heat is transferred from the reaction cell to the walls of the vacuum chamber by radiation only, independently of the amount of deuterium gas in the reaction cell. Figure 3 shows the new design. Figure 4 shows the palladium tube surrounded by the heater and a first radiation screen, as well as the reaction cell attached to the flange of the vacuum chamber

Also to improve stability versus room temperature we have added a water jacket around the whole chamber where water flows at the same temperature as in the cooling system.

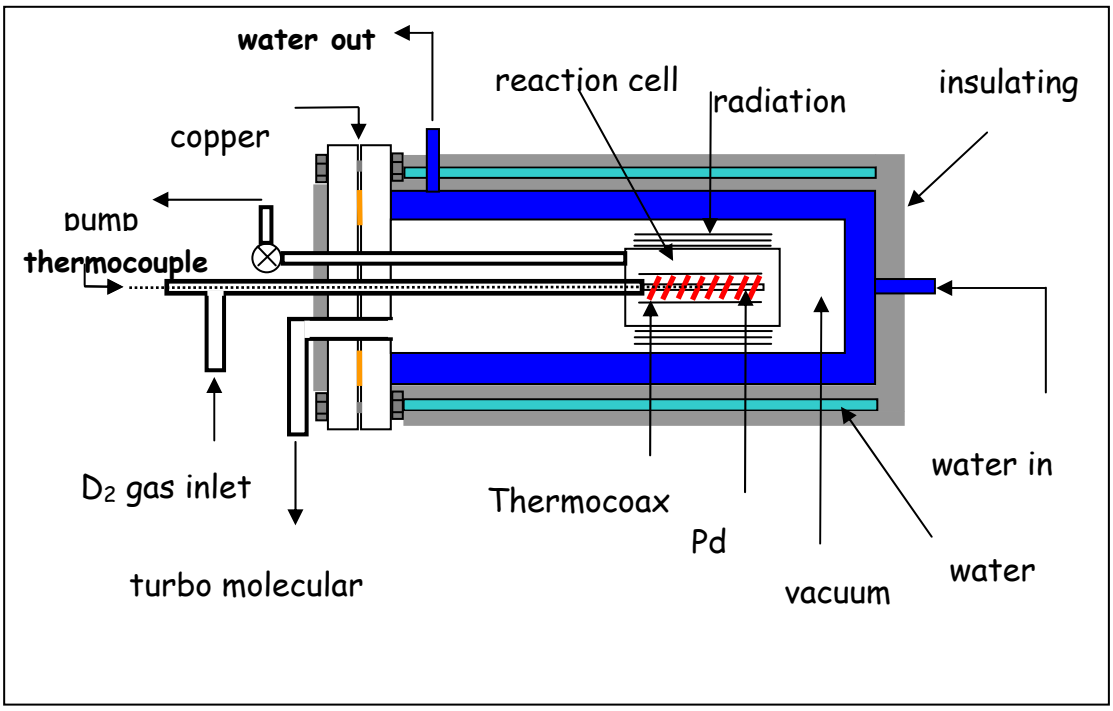

Figure 3. *Schematic of the second design where a reaction chamber as been added as well as a constant temperature water jacket*

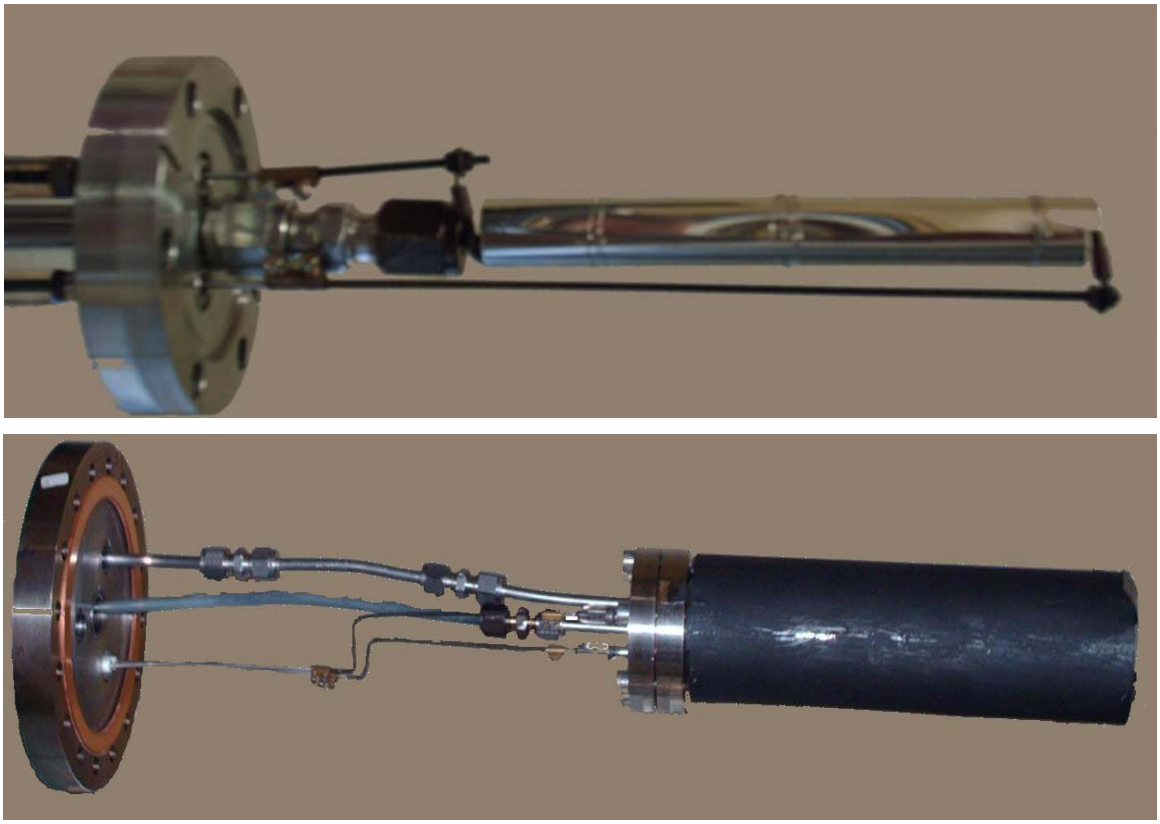

Figure 4. *Top view: palladium tube surrounded by the heater and a first radiation screen. Bottom view: the reaction cell attached to the flange of the vacuum chamber*

2.3 – Calibration

Input power is measured accurately since the heater is driven by a DC power supply. Output power is measured via the temperature difference given by two thermistors, one at the inlet, and the other one at the outlet with a precision of +/- 0.01 K. De-ionized water mass flow rate is measured with accuracy better than 1%. As mentioned above, most heat is recovered by the water flow, and therefore taken into account in determining Pout. However some heat is lost through the large flange of the vacuum chamber which is not cooled by the water flow. In order to have an accurate value of the losses we have performed a blank run without the palladium tube. We replaced it with an open stainless tube. Our calibration shows that a correction of 5 to 2 % of the input power must be added to the output power to take into account the heat loss. This value varies with input power: the larger the input power the less correction is needed in percentage.

However in order to avoid having to perform this correction, it is even better to compare the output powers without deuterium and with deuterium. Therefore no correction is needed; we simply compare the two situations.

3 – Experimental results

So far, we have realized 23 experiments. The first 11 ones were with the first design and the following 12 with the second design. We have used mostly closed palladium tubes from Goodfellow, 10 cm long, 2 mm outer diameter and 200 μm thick walls. As we had a limited number of such tubes, we had to use open ended tubes from Goodfellow that were brazed at one end. We also tried a Pd-Ag tube from Goodfellow, and in a couple of cases a stainless steel tubes filled with palladium powder, with a palladium carbon catalyst given by Case (6), and by beads similar to those of CETI (7). Our initial goal was to fill the palladium tube with palladium nano powder as Arata (2). However it turned out that the method they used Yamaura et al. (8), i.e. arc melting of a palladium zirconium alloy, then spin melting in order to produce an amorphous alloy followed by oxidation at low temperature was not available in our laboratory. Therefore we could not follow our initial goal of reproducing Arata's (2) work in its integrity. Instead we focused in other directions. We tried various alternatives: deposition of various metals such as gold, titanium or zirconium on the external surface of the tube, and letting deuterium gas diffuse out at various temperatures. We filled the palladium tube with palladium powder from Goodfellow without success. We tried to reproduce Case experiment using a palladium catalyst on carbon without success either.

For our last experiment with the first experimental design, run 11 we oxidized the palladium tube in air at 500°C for two hours, and filled it with palladium powder from Goodfellow. We did not observe any excess heat using our usual methodology: that is introduction of deuterium in the palladium tube at pressures up to 9 atmospheres, and simultaneously pumping out the vacuum chamber. For almost three weeks we tried operating at temperatures from room temperature up to 350 °C without success. At this point under three occasions as indicated on figure 5 we stopped pumping out the vacuum chamber and let deuterium pressure rise. This is when excess heat appeared as shown on figure 5.

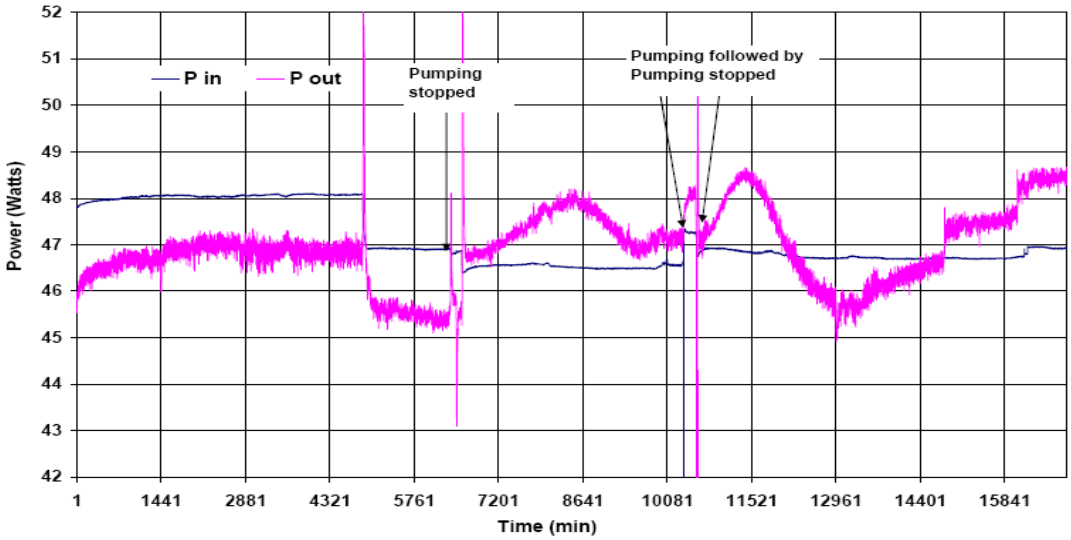

Figure 5. *Powers in and out during the final phase of the experiment showing an uncorrected excess heat of 1.7 Watts*

Before stopping pumping, Pout was about 1.2 Watt less than Pin. Therefore the actual excess heat observed should be increased by 1.2 Watt in order to obtain the correct excess heat. When pumping was stopped we observed every time an increase of Pout followed by a decrease but Pout remained above Pin.

The immediate Pout increase appearing when the vacuum chamber valve is closed is due to the fact that heat accumulated on the palladium tube and on the heating device is evacuated by radiation only when the vacuum chamber is under vacuum. However when deuterium fills the vacuum chamber there is also conduction and convection that evacuate heat. Interestingly the last part of the experiment shows an increase of Pout after rise and fall that lasted three days. When the experiment was stopped the excess heat was 1.8 Watt without correction and 3.0 Watts when corrected for the losses in the calorimeter as explained above.

Temperature at the base of the palladium tube was 85°C before excess heat developed and gradually rose to 87 °C when excess heat appeared. This is a good indication that the effect is genuine.

Figure 6 shows SEM photographs of the original tube (left) and after oxidation (right).

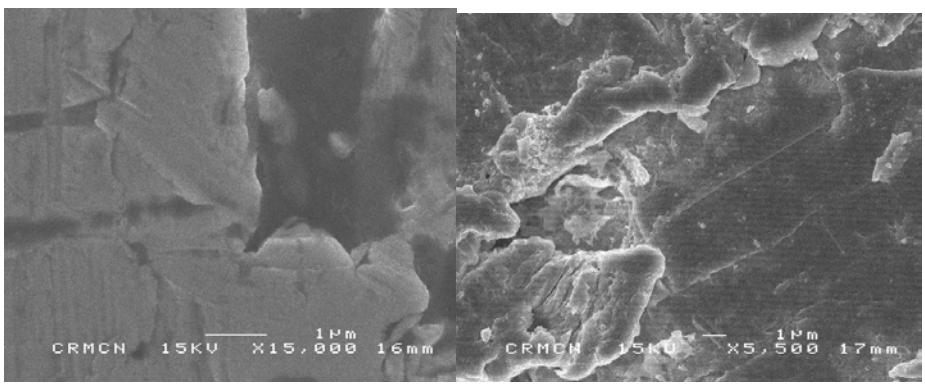

Figure 6. *SEM images of the virgin palladium tube (left), after oxidation in air for two hours at 500°C (right).*

After the successful run 11, SEM images of the tube show interesting features (figure 7). It seems that some areas of the metal have melted and recristalysed. Palladium melts at 1553°C, and the highest temperature reached by the tube was 350 °C! X-ray fluorescence shows the presence of palladium only. No trace of other metal is visible. This is not surprising since X-ray fluorescence analyses a depth of one micrometer, whereas the amount of transmuted materials if any would be probably much less.

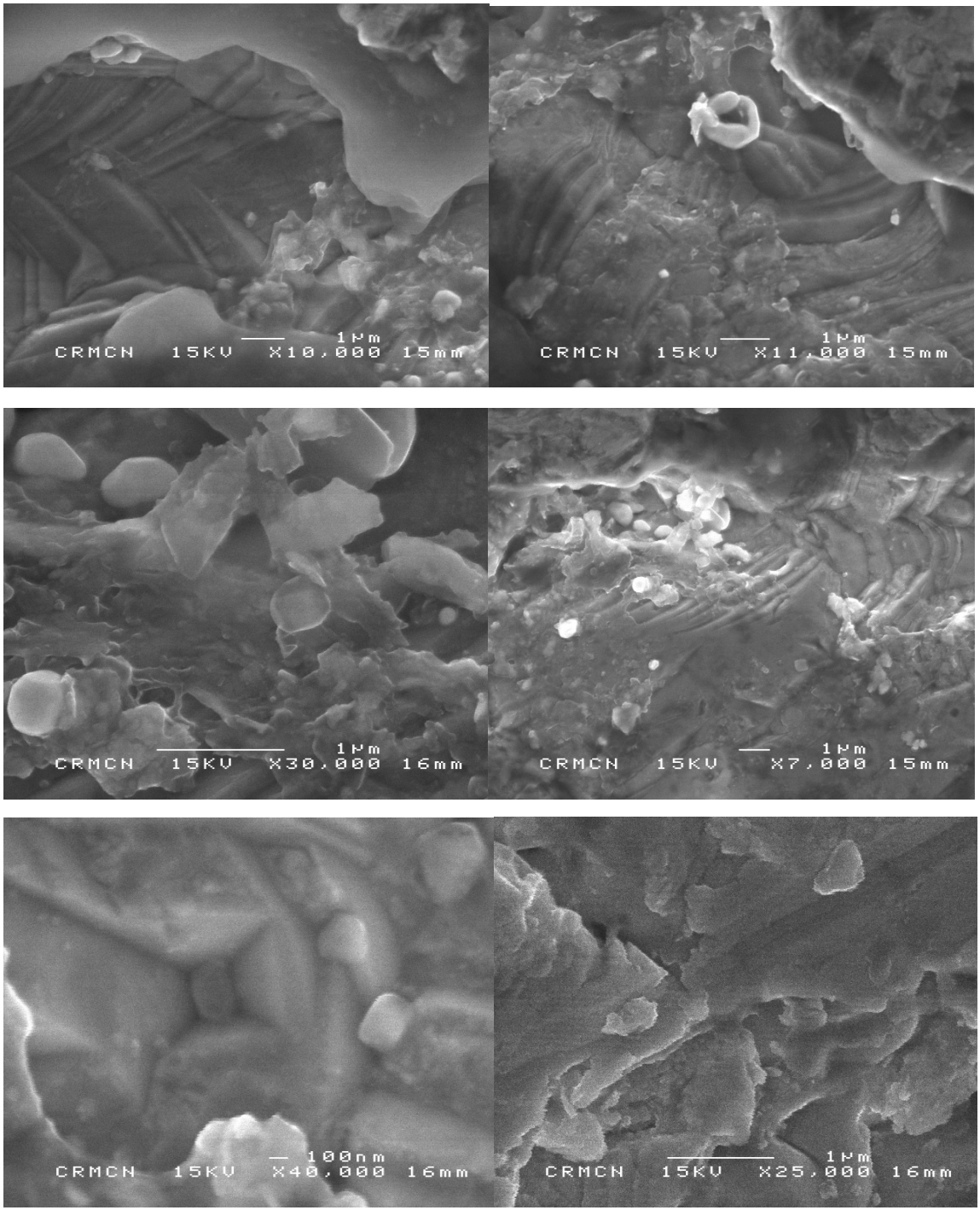

Figure 7. *SEM images of the palladium tube run 11 that produced excess heat*

In order to compare SEM images of run 11 that produced excess heat, it is interesting to compare them to those of a similar experiment that did not produce excess heat. Figure 8 shows SEM images of a palladium tube from run 20. The main difference between run 11 and 20 is the fact that the tube of run 11 was heated in air for two hours whereas the tube of run 20 was not. We do not observe the melted zone visible on figure 7.

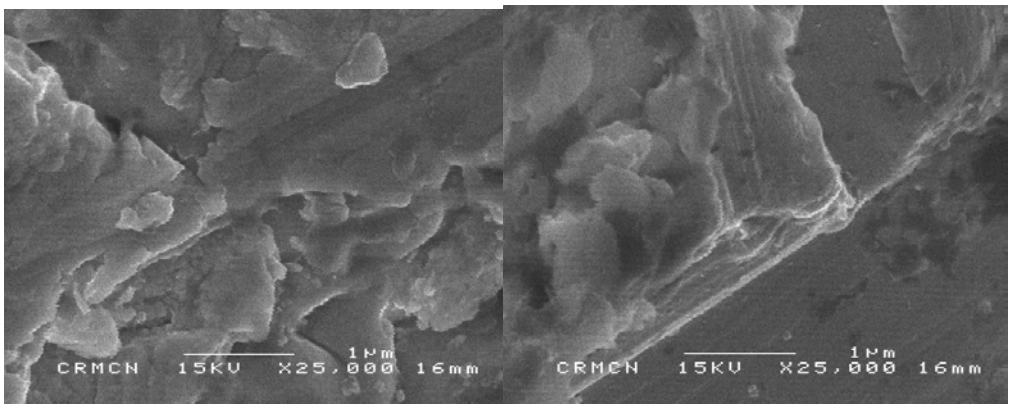

Figure 8. *SEM images of the palladium tube of run 20 that did not produce excess heat.*

4. Discussion

We have shown that diffusion of deuterium through palladium produces excess heat. The best result was obtained when the tube was oxidized in air prior to starting the experiment, and filled with palladium powder. We measured an excess heat of 3 Watts with an input power of 47 Watts, i.e. a yield of 6% that lasted three days. However, it seems that the powder did not play a role in this experiment. In the future, experiments similar to run 11 will be performed without the palladium powder in the tube to verify this assumption.

It seems that in order to get excess heat we need the following conditions:

a) A flux of deuterium through the walls of the palladium tube.
b) The palladium tube should be oxidized by heating in air at 500°C.
c) The outer surface of the tube should be in a deuterium gas environment.

Our understanding of the mechanism that can explain our experimental results is as follows: deuterium molecules dissociate at the inner surface of the tube. Inside the palladium deuterium atoms ionize and D+ ions move towards the outer surface of the tube due to the pressure difference between the inside and the outside of the tube. When a D+ reaches the outer surface two options are possible:

a) In the first scenario, a D+ recombine with an electron to produced an adsorbed D atom at the surface of the metal, then this D atom meets another D and as soon as a D_2 molecule forms, it leaves the surface.

b) In the second case, lot more rare, a D+ ion would encounter an adsorbed D and would react with it to produce a Helium-4 atom. This is why the reaction is dependant on D+ flux through the palladium, and D coverage of the outer surface. The greater the flux, the more chances a D+ would interact with an adsorbed D. The reason why the palladium should be oxidized is probably due to the fact that either oxidation modifies the surface metallurgy, or oxygen atoms bring extra electrons that play a screening role.

An interesting question is how D+ can react with D. Our understanding is that electrons are not confined to a Bohr type orbit. Instead there is a non null probability that an electron orbiting a deuteron gets sometimes very close to the nucleus. Therefore for a short period of time the D atom is analogous to a shrinked atom. The incoming D+ can therefore get very close to the nucleus of the adsorbed atom. By tunneling a non null probability of reaction exists between the two deuterium nuclei. This reaction is happening at low speed, and it is very likely that the two nuclei will configure themselves to react and produce maximum energy i.e. form a He-4 nucleus. Occasionally the other reactions producing neutrons and tritium might also happen. It is also possible that neutrons interact with the host metal and produces transmutations.

More work is necessary to confirm both our experimental results and also our model. We need to produce more excess heat in order to verify the formation of He-4. Our experimental set up is ready for such a work.

5. Conclusion

We have developed a mass flow calorimeter that allows us to perform experiments in gas phase with deuterium or hydrogen. We have shown that with a palladium tube oxidized in air at 500°C, filled with palladium powder we could observe an excess heat of 3 Watts when deuterium gas flows through the walls of the palladium tube. We have developed a simple model that explains our experimental results.

Acknowledgments

We would like to acknowledge Gilles Arthaud who built our experimental set up, Jacque Kurdjian, Michel Buxerolles and Jean-Louis Rechatain for giving us the palladium tubes.

References:

1. M. Fleischmann., S. Pons, Electroanal. Chem. 261, **1989**, p 301.
2. Y. Arata, and Y. C.Zhang, Proc. ICCF12, Yokohama, edited by A. Takahashi, Y. Iwamura, and K. Ota, World Scientific **2006** p44-54
3. Y. Arata, and Y. C. Zhang, Jpn. J. Appl. Phys. Part 2 38 (7A), L774, **1999**.
4. X. Z. Li, B. Liu, N. Cai, Q. Wei, J. Tian, and D.X.Cao, in Tenth International Conference on Cold Fusion, editors Hagelstein, P. L. and Chubb, S. R. World Scientific Publishing Co., Cambridge, MA, **2003**, p. 113.
5. G. C. Fralick, A. J. Decker, and J. W. Blue, NASA Technical Memorandum 102430, **1989**
6. L. C. Case, The Seventh International Conference on Cold Fusion, Jaeger, F. ENECO, Inc., Salt Lake City, UT, Vancouver, Canada, **1998**, pp. 48.

7. J.A. Patterson, US Patent #5,494,559, **1996**, System for electrolysis.J.A. Patterson, US Patent # 5,318,675, **1994**, Method for electrolysis of water to form metal hydride.G. Lonchampt, J. P.Biberian, L. Bonnetain, and J. Delepine, The Seventh International Conference on Cold Fusion, Jaeger, F. ENECO, Inc., Salt Lake City, UT, Vancouver, Canada, **1998**, pp. 202.
8. S. Yamaura, K. Sasamori, H. Kimura, A. Inoue, Y.C. Zhang and Y. Arata, J. Mater. Res. 17, **2002**, 1929

HIGH TEMPERATURE DEUTERIUM ABSORPTION IN PALLADIUM NANO-PARTICLES.

Francesco Celani, A. Spallone, E. Righi, G. Trenta, V. Andreassi, A. Marmigi, P. Quercia, G. Cappuccio, D. Hampai.
INFN-LNF Via E. Fermi 40, 00044 Frascati, Rome, Italy
E-mail: francesco.celani@lnf.infn.it
P. Marini, V. Di Stefano, M. Nakamura, F. Todarello, E. Purchi.
EURESYS, Via Lero 30, 00129 Rome, Italy
A. Mancini
ORIM SpA, Via Concordia 65, 62100 Piediripa, Macerata, Italy.
U. Mastromatteo
STMicroelectronics SpA, Via Tolomeo 1, 20010 Cornaredo, Milan, Italy
F. Falcioni, M. Marchesini, P. Di Biagio.
CSM SpA, Via di Castel Romano 100, 00129 Rome, Italy
P.G. Sona
Via S. Carlo 12, 20090 Segrate, Milan, Italy
F. Fontana, L. Gamberale, D. Garbelli.
*Pirelli Labs SpA, Viale Sarca 222, 20126 Milan, Italy***.**

Abstract

On the basis of the Yoshiaki Arata's *"sauna bath reactor"*, a simplified reactor (one chamber, without the second internal hollow Pd chamber were the material to be studied is filled) has been built, capable of operating at high pressures (100 bar) and at temperatures from -196 up to 350°C. With this instrument various Pd containing materials were tested: Pd black, HSA Pd black, Pd on activated carbon, Pd (from nitrate) on colloidal silica, Pd in porous γ Al_2O_3, Pd-Sr nitrate in porous γ Al_2O_3. The D/Pd ratios have been measured in all the materials. Evidence of excess heat was found with some of the tested materials.

The one chamber reactor was improved later by adding a second, reference chamber, which is similar to the working chamber, as a sort of *differential calorimeter*. Such a device is capable to highlight (and measure), in real time, the occurrence of excess heat in Pd powders or Pd containing materials put in the crucible of the measurement chamber of the instrument. With respect to the reference chamber, whose crucible is filled with inert material, the excess heat, due to the Deuterium absorption, makes the temperature of the working chamber to rise. Both the chambers are supplied with the same power input. A sample of Pd black_HSA (4.8 g) showed (at 290°C) a clear excess temperature of 13.5°C equivalent to an excess heat of up to 520milliwatts.

The direct relationship between the excess heat and the D_2 content in the Pd powder has been demonstrated: in fact, when a partial degassing of the Pd powder occurred, a subsequent decrease of the excess heat also occurred.

The anomalous excess heat, due to the close interaction, at nanometric scale, of Deuterium with Pd, seems to be clearly detected by proper experimental set-up and operating conditions.

The amount of energy detected is larger of any chemical reaction known.

1) Introduction

In Condensed Matter Nuclear Science experiments it has been recently shown that *nano-structures* of specific elements (in particular Palladium) are the key materials for the generation of anomalous effects (both of chemical and/or nuclear origin).
In an experimental, and theoretical too, paper (Ref.1), Professor and Academician Yoshiaki Arata, one of the main experimentalists active in such a specific field, showed (and explained) that extremely large quantities of Hydrogen (H) or Deuterium (D) can be absorbed into nano-sized materials, even at mild H_2 - D_2 pressures (e.g. 10bar).

The main authors and the distinctive features of their experimental approaches, using nanostructures, are listed below:

1.1) Prof. Yoshiaki **Arata;** Osaka University-Japan; (Ref. 2);
Technology: metallurgical production of nano-particles;
since 1992; Pd_black: (mainly of commercial origin) particle size: 50-1000nm;
since 2002; $[ZrO_2]_{65}$-Pd_{35}: home made, intimate mixture (Pd size:10-15nm,);

1.2) Dr. Yasuhiro **Iwamura;** Mitsubishi Heavy Industries, Yokohama-Japan; (Ref. 3,)
Technology: thin layers (10-100nm) of Pd, CaO, Sr, Cs;
since 2000; mainly micro and sub-micro electronics methods (sputtering, ion beam deposition);
The nano-sized materials (layer by layer) are deposited on a tick layer of Pd (100μm), capable to stand heavy mechanical stress (temperature up to 80^{o}C, pressure drop up to 3bar).

1.3) Dr. Francesco **Celani** and co-workers (National Institute of Nuclear Physics, Frascati-Italy); (Ref. 4).
Technology: electrolytic methods;

Fractal like surfaces (”roughness” 20-2000nm) were produced on thin (Φ=50μm) and long (100cm) Pd wires.
Behaviour and properties of the fractal like surfaces were explained since 2005 (Ref. 5).

2) Sauna bath reactor, energy source, ashes

On July 2005 Prof. Yoshiaki **Arata** introduced the “***Sauna-bath reactor”*** (Ref. 2).
The experimental set-up and the obtained results were disclosed, for the first time, during the ICCF12 Conference, held at Yokohama (Japan) on November 24-December 2, 2005.

Since 1992, (Ref. 6, and reference therein), he was able to obtain, by electrochemical loading, extremely high $D_2 - H_2$ pressures in the hollow cavity (eventually filled with some materials) of a special thick Pd cathode (the so-called Double Structure Cathode). He noted that, when Pd micro or (better) nano particles were put inside the cavity, a surprisingly high loading ratios (D/Pd –H/Pd >1) could be obtained, even at an internal $D_2 – H_2$ pressures of few bars. In case of Deuterium loading, an anomalous heath generation was also observed.

In order to reduce the strong input power required for the electrolytic current (which could hinder the excess heat), he developed the "*sauna bath reactor"*.

In the sauna bath reactor D_2, flowing trough the walls of a Pd tube, enters the internal part of the tube (the "cavity"), maintained at few hundred degrees °C, without applying external energy (like electrolysis): even few bars of D_2 external pressure (the tube is completely surrounded by a sealed SS vessel) are enough to ensure a fast diffusion into the cavity. Moreover, the D_2 gas passed trough the Pd tube is extremely pure and at the inner surface of tube is in the atomic form (D_0), easy to be absorbed by any kind of Pd (or Pd alloys) micro or nano particles located in the cavity.

The input power necessary to ensure the required temperature (100-200°C) of the system, according to our experience with a similar apparatus (total volume: 30-50 cc), is of the order of 2-6W and depends on such main experimental factors, as following:

a) intrinsic geometrical aspects of reactor;
b) thermal conduction losses due to connection tubes;
c) thermal conduction losses due the thermometer put inside the powders;
d) heat losses due to both convective motions (mass transport) and high thermal conductivity (about 0.15 W/K*m at NTP) of pressurised D_2,
*e) performances of the thermal insulation (W/K*m) material adopted.*

Further advantages of the sauna bath approach are:

a) no consumption of expensive electrolytes (like D_2O). In principle, only D_2 gas has to be filled at the beginning of the experiment and small amounts of D_2, proportional to the excess energy produced, are required for refilling.
   * It is note worthy that Arata, in dedicated experiments with Pd_black at High Surface Area (HSA) or Pd-ZrO_2 nano-particles, both loaded under pressurised D_2, was able to detect quite large amounts of ^4He and even, well measurable, amounts of the extremely rare ^3He. In fact, at the end of the experiment, it was possible to extract, by under vacuum diffusion, all the Hydrogen isotopes (H_2, D_2, T_2) present in the cavity: ^3He and ^4He, which cannot diffuse trough the Pd walls, remained in the cavity. By connecting the cavity with a high resolution Quadrupole Mass Spectrometer, Helium isotopes can be analysed without the heavy interference of large amounts of D_2.
b) Explosive recombination of D_2 with O_2 is avoided (e. g. reaction $2D_2+O_2 \rightarrow 2D_2O$, specially when sheets of Pt_black catalyser are used at the top of, tightly closed, electrolytic cells);
c) It is possible to detect even modest excess heat: the input power necessary for the warm-up of the studied material up to the "trigger temperature", can be kept fairly low by using high quality materials for the thermal insulation.

2.1) The problem of reactions for excess energy.

We recall that exist several theoretical models that try to explain the observed production of excess heat, and related ashes, by Deuterium-Pd systems.

To enter further in this argument, still now open, we recommend reading the comprehensive paper of Prof. Akito Takashi (Osaka University) presented at this Conference (Ref. 7).

3) Frascati-INFN activity in the powder nano-particles technology.

The experimental activity started on July 2006.

3a) Taking into consideration the advantages of the Arata's reactor, we decided to build up a simplified version (i.e. without the inner Pd tube) of the sauna bath reactor (all parts in AISI 304 and 316 SS), capable to operate at high pressures (100bar) and at high temperature (320^{o}C).

The apparatus consists of two extruded SS tubes (V_1 and V_2 chambers) with external-internal diameters of 12-10mm. Only one chamber, the V2, is filled with material to be studied and can undergo thermal cycles. It was called the One Chamber Reactor (OCR).

The Pd micro or nano particles were put inside a small (SS) crucible, located in the reaction chamber V_2. Starting from the external surface of the SS tube in V_2, a cascade of fibre-glass insulation wool sheets provides for thermal insulation. The bottom of reaction chamber V_2 (where the SS crucible is located) was further screened by means of several layers of thin Al foils (thickness 15μ m), as thermal radiation reflectors, and kapton.

The whole set up was put inside a glass Dewar, surrounded by a plastic insulating foam.

The V_1 chamber, maintained at room temperature, serves as D_2 storage; proper valves can interconnect the two chambers. The V_2 chamber, containing the crucible filled with the powders to be studied, can be heated by a DC power supply. The volume of each chamber is 35cc. Further details of experimental set-up are the following:

d) The joule heater used in the reactor chamber V_2 is made of a Constantan wire, a Cu-Ni alloy whose electrical resistance remains almost constant in the temperature range of 20-400^{o}C, coiled around the SS tube;
e) The heater is fed by a constant voltage stabilised power supply. The value of voltages (four contacts measurement method) and the currents flowing in the Cu-Ni resistor are digitalised (by a high resolution, 6.5 digits, ADC) and acquired/stored by the on-line computer (acquisition system Lab-View type): calculation of input power.
f) The usual acquisition time of all the parameters of the experiment (5 temperatures, 2 pressures, 2 or 4 voltages, 1 current) is 10 seconds.
g) Pipes connectors, valves, etc. are of Swagelock standard.

* For simplicity, the anomalous thermal effects, at this stage of experimentation, have been detected by the *isoperibolic methods*.

* The anomalous thermal effects could be evaluated by comparing the equilibrium temperatures (at a given and constant power input) of the reaction chamber (V_2) when filled

either with D_2 or with an inert gas, at the same pressure. ^{4}He was used as inert gas: its thermal conductivity (0.142W/K*m at NTP) is quite similar to that of D_2.

Both the chambers (volume 35cc) were equipped with very sensitive and accurate electronic pressure gauges, in order to evaluate the D/Pd ratio from the corresponding pressure drop.

3b) Tested materials; D/Pd ratio; evidences of thermal anomalous effects.

3b.1a) "Standard" Pd black (Aldrich); 2g; measured (by SEM) few particles with Φ=300-1000nm, most larger (several micron); the powder, at the beginning of the experiments, was previously baked at: 140°C, 12h, under vacuum (rotative pump equipped with a liquid nitrogen trap; pressure 10^{-3}mbar).

All the tested materials have been treated at T_max: 220°C; P_max: 25 bar.

Results:

* D/Pd=0.85 at 8 bar was achieved;
* Very weak thermal effects were detected.

3b.1b) Pd black "High Surface Area" (Engelhard→Aldrich); 2g; measured (by SEM) several particles with Φ=50-300nm; baked at 140°C, 12h, 10^{-3}mbar; T_max: 220°C; P_max: 25 bar.

Results:

* D/Pd=0.90-0.95 (at 8bar);
* Weak thermal effects, little better in respect to the "standard" Pd black were detected; heavy sintering problems appeared after D_2 absorption and repeated cycles from high to room temperatures.

3b.2) Pd on activated Carbon; Pd=5% weight; 5g; Φ=50-100nm; baking up to 190°C, 12h,

10^{-3}mbar; T_max: 220°C; P_max: 25bar. Very old material (prepared over 20 years ago).

Results:

* D/Pd=0.9-1;
* Weak thermal effects and difficulties to eliminate water and/or other gas previously absorbed by carbon.
* The D/Pd ratio close to 1 can be due to some D_2 physioabsorption in the activated carbon.

3b.3) $Pd(NO_3)_2$ in HNO_3 (10% weight) mixed with porous (nanometric size 4-5nm) colloidal silica (Pd=20% weight; SiO_2 80%); 5g; T_max 300°C; P_max: 25bar.

Results:

* D/Pd=1-1.2 at 10 bar;

* Not stable anomalous thermal effects have been detected; excess heath seems to depend, very strongly, on the Pd-silica preparation procedures. The material is promising but very large systematic work is needed.

* The D/Pd ratio larger than 1 can be explained as due to the *spillover effect*

3b.4a) γ Al_2O_3 (Φ of holes=5.8nm, Aldrich) mixed with $Pd(NO_3)_2$ in HNO_3 (10% weight). γ Al_2O_3 80% Pd 20%; total weight 5g; T_max 300°C; P_max: 75bar;

Results:

*D/Pd=1.4-2.0 at 10bar;

* Non-stable, anomalous thermal effects were detected; sintering problems appeared after high-low-high cycling temperatures.

3b.4b) γ Al_2O_3 83.3% (Φ of holes=5.8nm, Aldrich) mixed with $Pd(NO_3)_2$ 13.3% + $Sr(NO_3)_2$ 3.3%

total weight 5g; Tmax 320°C; Pmax: 75bar;

Results:

* D/Pd =2--5.

* The very large D/Pd ratio can be explained only by the *spillover effect.*

** Strong indications of excess heat, but not enough stable for long time.*

Reduced sintering problem with respect to 3b.4a), but still present.

4) Operative procedure (as at April 2007) for the preparation of the γ Al_2O_3-Pd-Sr mixtures

4.1) Total weight of, as received, γ Al_2O_3=20g

4.2) Drying.

The γ Al_2O_3 (Aldrich, Φ of holes=5.8nm) was put in a quartz crucible inside a quartz tube of a programmable oven (e.g. Barnstead Thermolyne, mod. 21100). The features were:

* Temperature ramp-up (Tr: =0.3°C/min);
* Dwell time (Tdw, at maximum temperature, 600m);
* Temperature maximum, T_max (T=25→130°C);
* Atmosphere: vacuum ($5*10^{-3}$-$1*10^{-2}$mbar) by rotary pump with LN_2 trap
* Cooling spontaneous.

4.3) Wetting and Mixing:

* 10.000g (from the original 20g) of dried γ Al_2O_3.

* Home made solutions of $Pd(NO_3)_2$ in 10% weight HNO_3 (Pd content = 0.2g/cc) and a $Sr(NO_3)_2$ solution (in H_2O) with Sr content 0.2 g/cc were prepared.

* 8cc of the Pd solution were mixed with 2cc of $Sr(NO_3)_2$ solution: *mother solution*.

* 3cc (over 10 total) of Pd-Sr *mother solution* were drop-by-drop poured on 10g of the γ Al_2O_3 powder, in a glass beaker, under a continuous mixing by a glass stick. Such a procedure is usually known as *incipient wetting impregnation*. With respect to the "standard" incipient wetting procedure, we reduced the amount of liquids from about 5 to 3 cc.

4.4) Drying *(water and HNO_3 elimination)*.

The wet material (HNO_3, H_2O) was heated in the quartz tube furnace. Vacuum is made by a high quality water pump (P_{limit}=32mbar; usually operated at 100mbar) because of corrosion problems due to the presence of HNO_3 vapours. Connection tubes in PTFE.

Furnace operating conditions: Tr=0.3°C/m; Tdw=600m; T=25→130°C; spontaneous cooling under vacuum.

4.5) 3cc of the mother solution were, drop by drop, poured again on the mixture, according to the previously described incipient wetting impregnation. Drying operations as mentioned above.

4.6) All the described operations were repeated, by dropping each time 2cc of mother solution, until the 10cc are finished.

4.7) Calcination

The powder, in the quartz crucible, was heated in the quartz tube furnace.

Operating conditions: Tr=1°C/m, Tdw=1050m; Tmax=450°C (for short time up to 500°C).

Atmosphere (vacuum):

* Tdw=0-250m; water pump (i.e. total time of water pumping, from the beginning of calcination step), is about 680m.

After 200m of Tdw, fresh air, for about 10m, was allowed to enter the quartz tube, by continuously pumping out at about 800mbar. Then, the pressure was reduced to 100mbar in static conditions: when the temperature is increased from 450°C (Tr=5°C/m) up to 500°C for short time, observe if some red colour gases (due to decomposition of Pd nitrate) are still visible. If not, reduce again the temperature to 450°C; otherwise, remain at 500°C until, after repeated "washing" operations, all the red gasses disappeared.

* Tdw=250-550m→2 stages membrane pump (PTFE type, 20mbar);
* Tdw=550-1050m→rotary pump with LN2 trap ($5*10^{-3}$-10^{-2}mbar).

4.8) Check the weight.

The weight should be about 12.8g; in fact:

Al_2O_3: 10.00g;
PdO: (Pd=1.6g+ O=0.24g) = 1.84g;
$Sr(NO_3)_2$: (Sr=0.4g+$(NO_3)_2$=0.56g)= 0.96g.

5) Deuterium loading in V_2.

5.1) PdO reduction.

D_2 gas was allowed to enter the reactor (maintained at 140°C), at low pressure (1bar) and at a very slow flux in order to avoid excessive self-heating (and, as consequence, sintering of Pd nano-particles).

PdO is reduced to metallic Pd according to the reaction: $PdO+D_2=Pd+D_2O$

In order to eliminate the D_2O formed in the reaction chamber, several cycles are performed of D_2 intake and subsequent vacuum purging by rotary pump.

Final drying, of possible residual water, by vacuum pumping (12h) at 250°C (rotary pump and LN2 trap, at about $5*10^{-3}$mbar).

5.2) Pd loading by Deuterium.

Pd loading is performed at room temperature. The D_2 absorption (D/Pd ratio) can be evaluated by the pressure variation in the D_2 storage chamber (V1); an accuracy within 2-5% can be achieved, with electronic Gauge pressure sensors (from GEMS Company) having a sensitivity of 0.25% of Full Scale.

In order to maximize the accuracy of D/Pd ratio, 2 sensors, the first one with FS=100bar and the second one with FS 25bar (with proper valve) were used.

The Pd loading procedure is explained step by step hereinafter:

* Make vacuum on chambers V1 and V2.

* Close the connection between V1 and V2 and fill with D_2 gas the chamber V1 (usually 25bar);

* A 0.5 cc volume chamber, located in between V1 and V2 chambers, (see Fig. 1) allows for a very slow passage of D_2 into the reaction chamber.

* Wait for thermal equilibrium in V2 (the temperature should increase because of the D_2 absorption by the Pd powder (exothermic). Measure the equilibrium temperature of V2.

* If necessary, refill (as many times as necessary) the V1 chamber with D2 gas at high pressure (usually 100bar) and load again V2 up to the pressure stated (recently up to 60-70 bar).

5.3) D/Pd measurement.

The abbreviation used are as following:

P_1= Absolute Pressure of chamber V1 (before connection with V2);

V_1= Volume of Chamber V1;

T_1= Temperature of Chamber V1 (before connection with V2);

P_{1F}= Absolute Pressure of Chamber V1 (after connection with V1);

V_2= Volume of Chamber V1;

T_2= Temperature of Chamber V2 (after connection with V1);

R= molar constant of gas

* The initial moles n_1 of D_2 gas, in V_1, are:

$$n_1=(P_1*V_1)/(R*T_1) \quad (1)$$

* The final moles N_{2F} of D_2 gas, after absorption by Pd powders, are:

$$n_2 = [P_{1F}*(V_1+V_2)]/[R*(T_1+T_2)/2] \quad (2)$$

* The moles (ΔM) of D_2 gas absorbed are:

$$\Delta M = n_2 - n_1 \quad (3)$$

* If M_{Pd} are the moles of Pd used, the D/Pd ratio is:

$$D/Pd = 2\Delta M/M_{Pd} \quad (4)$$

6) Evaluation of the thermal anomalies.

When the Pd loading process is completed, the temperature of the V_2 chambers is made to increase.

The heater power (watt) is step like controlled:

0→3w→0→4w→0→6w→0→8w→0→12w→0.

Anomalous heat generation is evaluated by measuring the equilibrium temperature of the V_2 chamber against the equilibrium temperature measured in previous calibration runs, when the Pd powder was kept under inert gas atmosphere (usually ^4He).

The dissipated power in the V_2 chamber normally increases by increasing the gas pressure in the chambers. That is because D_2 (or ^4He) works as an exchange gas from the hot area (close to the heater), to the coldest one (at room temperature). This effect is presented in Tab. 1.

Timer s	**TV_2 °C**	**TH_2 °C**	**Troom °C**	**Pressure bar**	**TV2 - Troom °C**	**TH_2 - T_room °C**	**$TV_2 - TH_2$ ° C**	**Note**
166000	234	257.8	21.9	62.6	212.1	235.9	-23.8	D_2, material partially active
241700	254.6	274.8	20.6	18.7	234	254.2	-20.2	"
331500	253.4	273.8	21.6	5.8	231.8	252.2	-20.4	"
332300	253.4	274.1	21.9	1.16	231.5	252.2	-20.7	"
414300	235.8	275.4	21.8	0	214	253.6	-39.6	Vacuum
420900	251.3	274.4	22.3	1	229.0	252.1	-23.1	Air

***Tab.1**. File 11apr07. One Chamber Reactor (OCR). Relationship between the temperature inside the crucible (TV2) and pressure applied. For completeness are reported also the temperatures of Joule heater and room.*

In Tab. 1 (experiment started on 11Apr07) the temperature dependence (versus pressure) of the reactor chamber is shown (input power 6.04W), when the γ Al_2O_3-Pd-$Sr(NO_3)_2$ powder was only "partially active". It was used a high quality Dewar (WKG, Germany) that, unlikely, can't be used at effective Dewar wall temperature larger than 200°C.

The pressure effect is significant and can't be neglected, in particular if small amounts of excess heat are to be detected. It is therefore necessary to perform calibration runs not only at different input powers but also at different pressures both with D_2 and ^{4}He.

By considering the fact that the thermal conductivity of H_2 (similar to D_2) varies, at 500K, of only +1.8% starting from 1bar up to 100bar (i.e. from 0.2661 to 0.2711 W/m*K), we have to argue that the large value (+6.4%) of thermal leaks due to pressure variation (up to 64bar) is due, mainly, to convective motion of gas. As a consequence, some work has to be done, in the near future, to our experimental set-up in order to reduce such large detrimental effect.

Regarding the data shown in Tab. 1, it should be noted that (timer 323300) the TV_2 – Troom is 231.5°C; by replacing the D_2 atmosphere with air, at the same pressure (1 bar), the TV_2 – Troom dropped to 229.0°C. According to our previous experience, the variation of temperature when D_2 (1 bar) or ^{4}He is replaced by air (1 bar) should be practically negligible. The registered difference of 2.5°C is supposed to be due to some residual activity of the Pd powder even at very low pressure of D_2.

6.1. Differential calorimeter.

It is well known that, in CMNS experiments, the eventual generation of excess heat is seen with scepticism and the experimental data are often strongly questioned. We realised that because of the troublesome and delicate operations necessary for the calibration of our reactor and because of the pressure effect, our experimental results could be often criticised and sometime even refused. Accordingly, in order to prevent as much as possible any criticisms and objections, we decided to modify our reactor in such a way as to eliminate both the need of the calibration runs and the hardly controlled pressure effect.

At the end of May 2007, the chamber V_1 was equipped with the Constantan Joule heater, the insulation layers and the glass Dewar, so to match as much as possible to the reaction chamber V_2.

The resistance value of the Constantan wire in the chamber V_1 (previously used in the OCR configuration as "storage chamber") was made the same that in V_2; the two resistances are connected *in series* so as to be crossed by the same current (i.e. both the chambers were supplied with the same input power).

In this way a sort of *differential calorimeter* was assembled (Fig. 1), capable to detect, in real time, any anomalous heath generation between the active material (in V_2) and the inert one (in V_1) under the same conditions of temperature and D_2 pressure.

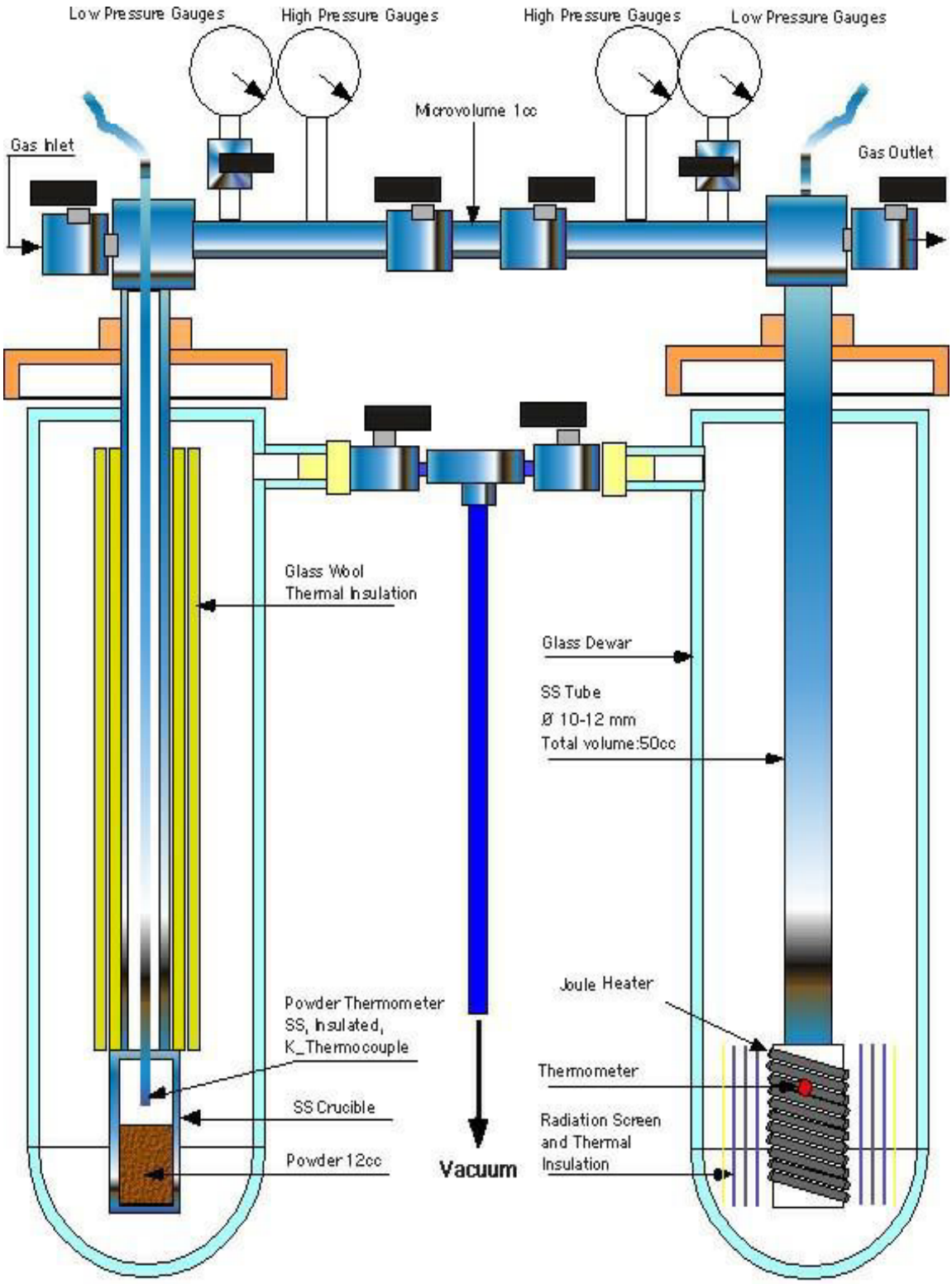

Fig.1. *Schematic of differential calorimeter.*

In preliminary runs with inert material we observed that, at constant input power, when the equilibrium temperature has been reached, the difference of temperature between the two chambers was very small (< 1°C). In these conditions the amount of the excess heat, eventually generated in V_2, could be easily estimated conservatively (i.e. supposing that the dissipations do not increase at the increasing of the temperature), through a simple proportion, as following:

* $W_{H=}$ constant input power at the heaters (watt)
* T_1= equilibrium temperature in V_1 (°C)
* T_2= equilibrium temperature in V_2 (°C)
* δ w=excess heat (watt)

As a consequence:

$$W_H/T_1 = (W_H + \delta w)/T_2 \quad (5)$$

$$\delta w = W_H*(T_2-T_1)/T_1 \quad (6)$$

Moreover, if the electric input power (by the Joule heater) to the two chambers isn't exactly the same, the equivalent temperatures differences can be corrected using chamber V1 as reference for calculations.

6.1) Pressure effects.

In the differential calorimeter the pressure effect is negligible only when the two chambers are at the same pressure (i.e. the connection valve is on). In some cases (connection valve off) it could be very interesting to examine what is happening in the V_2 chamber (i.e. a possible degassing of the Pd powder and, consequently, a sudden increase of pressure in V_2).

In order to achieve a complete knowledge of the pressure effect an experimental campaign was performed with the new differential calorimeter.

The crucible in V_1 was filled with (previously vacuum dried) pure γ Al_2O_3 (5.5g); the atmosphere was always D_2 gas. In all the experiments the input power was maintained constant (12 watt).

The results are summarised in Tab. 2.

TV_1 (°C)	TH_1 (°C)	Troom (°C)	Pressure (bar)	TV_1-Troom (°C)	TH_1-Troom (°C)	TV_1-TH_1 (°C)
281.3	276.8	25.0	74.4	256.3	251.8	+4.5
287.7	282.0	26.2	63.3	261.5	255.8	+5.7
295.9	288.3	25.6	46.88	270.3	262.7	+7.6
300.5	291.6	23.1	30.85	277.4	268.5	+8.9
305.6	295.9	24	20.43	281.6	271.9	+9.7
305.1	295.1	24.6	11.71	280.5	270.8	+10.0
305.8	296	25.9	6.8	279.9	270.1	+9.8
279.6	295.6	24.2	0	255.4	271.4	-16.0

Tab.2*. File14giu07. Differential calorimeter. Temperature-pressure dependence.*
New tick-wall Dewar (2.2mm), not silvered: it can withstand temperatures up to 350°C.
New SS crucible (volume 12cc) with thick wall (2mm). Chamber V1 volume=50cc.
Material: dried γ Alumina. Gas: Deuterium. Power: 12W.
TV_1 is the temperature measured inside the crucible filled with the γAlumina powder.
TH_1 is the temperature of the Joule heater, measured outside the SS chamber, and inside the Dewar.

* The best heat transfer efficiency is at about 20bar (TV_2 - Troom=281.6°C). By reducing the pressure (from 20.43 to 6.8bar) small variation of temperature is observed ($\Delta T/\Delta P$= +0.12°C/bar); the decrease of temperature tends to be more and more important as far as the pressure exceeds 20bar (20.4→74.4bar; $\Delta T/\Delta P$= -0.47°C/bar).

As expected, the worst condition of the heath transfer efficiency is in the vacuum condition (255.4°C).

The results are qualitatively similar to the previous OCR.

7) Results

In this paper are shown the results obtained with the differential calorimeter in a complex and long (over one month) experiment.

According to our previous results with the OCR, we tested, at first, a sample of HSA (High Surface Area) Pd_black powder, by Engelhard→Aldrich (cod. 520810-5g): it gave indications of some excess temperatures even at low D_2 pressures (<25bar). Same batch of production.

Apparent density: 4.8g/9cc=0.53g/cc

The amount of material was 4.8g (0.2g was kept as a reference).

The powder (put into the V_2 crucible) was previously degassed-baked (15h in vacuum by a rotative pump equipped with LN_2 trap at 110°C; in the previous experiments with OCR the temperature was 140°C and time 12h).

After cooling to room temperature, D_2 gas was fed in micro-steps so as to avoid that the powder temperature should exceed 55°C. The temperature measurement was made using a K type thermocouple, SS covered, with a diameter of 3mm and put inside the powders. The tip of the thermometer is at a distance of 2cm from the bottom of the crucible.

The measured D/Pd ratio, at 8.7bar and 35.5°C, was >0.92. Such value increases to >0.96 when the effects of water content and of other impurities in the Pd are taken into account.

The D_2 pressure was increased up to 64bar at 30°C.

In order to detect any eventual degassing of the Pd powder the connecting valve between the two chambers was off.

* The variation of pressure (P_2–P_1) is shown (in Fig. 2, 3, 4, 5) by the *bright-blue* line.

* The temperature gain ($\Delta T_{2\text{-}1}$ in the following) between the working and the reference chambers is in *orange*.

* The *green* line shows the temperature gain $\Delta T_{2\text{-}1}p$ corrected for the variation of pressure (P_2–P_1), according to the data presented in Tab. 2 (effect of pressure). Such effect is macroscopic only for pressure larger than 20bar and has a negative slope (about -0.47°C/bar).

* The absolute pressure (in V_2) is in *dark-blue*.

* The temperature of the V_2 chamber is in *red*.

** In order to see the results of the long time lasting experiment with enough resolution, it was divided in 4 Figures (2, 3, 4, 5), and each Fig. has some peculiarities, as shortly resumed:

* Fig. 2. File 19giu07. D_2. Starting of the experiment and several cycles 0→12→0W.

* Fig. 3. File 07lug07. D_2 →Vacuum→^{4}He. Under D_2, increased the power 12→14→16W: detected D_2 degassing and reduction of excess temperature. With ^{4}He the excess temperature went to 0°C.

* Fig. 4. File 13lug07. Several tests, at variable power, with ^{4}He (p=5.8bar@RT).

* Fig. 5. File 19lug07. Loading D_2 from LN2: no improvements of results. Larger degassing and related reduction of excess temperatures in respect to Fig. 2 and 3. Pressure reduced 80→30→18bar: the degassing increases and excess temperature vanish.

End of the experiment.

7.1) Fig. 2.

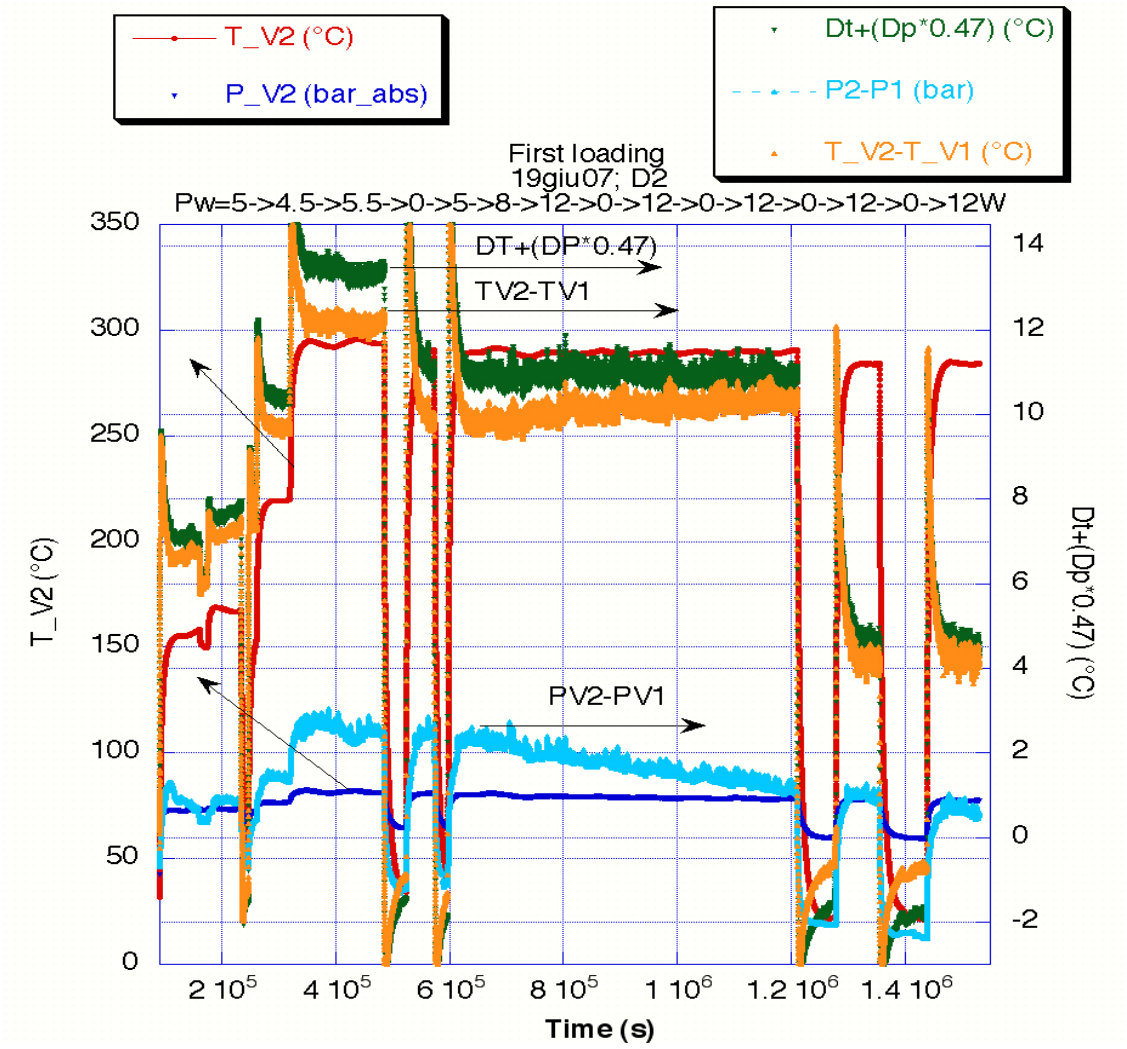

Fig. 2. *File 19giu07. Results with differential calorimeter. First loading and warming up.*

At the beginning of the experiment the heaters were supplied with 5→8→12 watts of input power. The temperature gain $\Delta Tp_{1\text{-}2}$ in V_2 increased (7→10.5→13.5°C). The excess heat, accordingly, was 220→380→520mW.

At $5*10^5$ seconds the input power was switched off and then applied again. The temperature gain $\Delta Tp_{1\text{-}2}$ in V_2 dropped from 13.5°C to 11°C (green lines).

At about $1.2*10^6$ seconds the input power was again switched off for a longer time: the temperature gain $\Delta Tp_{1\text{-}2}$ in V_2 (4.5°C) dropped down dramatically.

Switching off the power, and subsequent cooling, seems absolutely to be avoided.

It can be seen that the D_2 pressure in V_2 (blue line) slowly decreases, because of a small leak.

The data shown were corrected for such (small) effect.

7.2) Correlation between excess power and operating temperature.

The almost direct correlation between the Pd powder temperature and the excess heat generation could be explained as follows.

Taking into consideration the well known Pd-D phase diagram, it appears that, by increasing the temperature, also increases, almost in a proportional way, the amount of β phase to the detriment of an equivalent amount of α + β phase. It seems therefore that a correlation would exist between the percentage of the β phase actually present in the Pd black and the amount of the generated excess heat.

7.3) Fig. 3

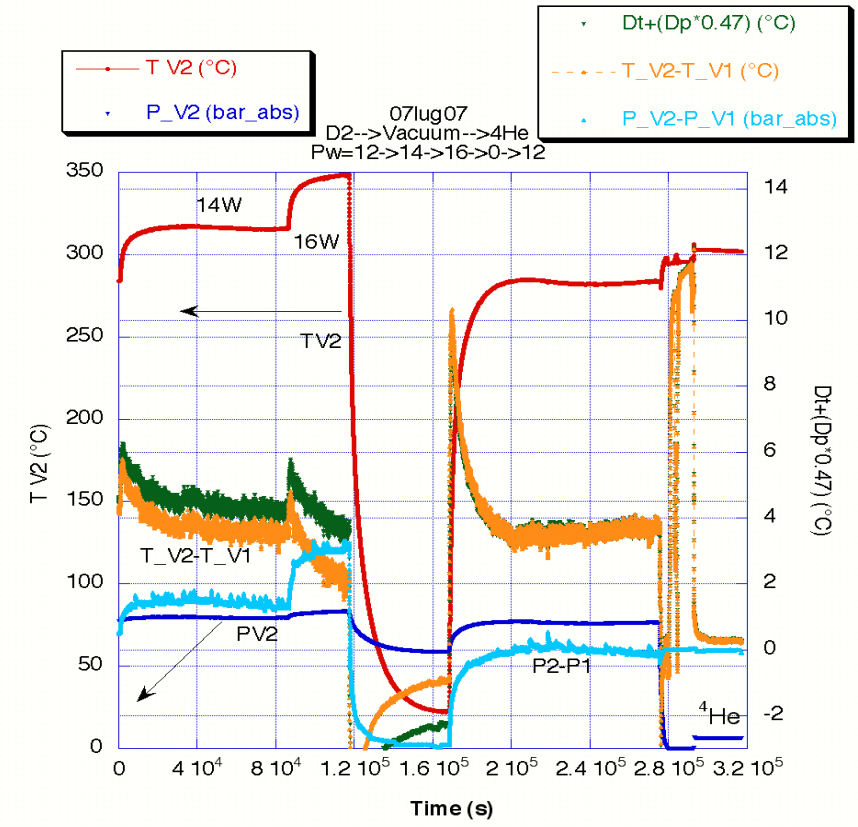

Fig. 3. *File 07lug07. Results increasing the cell temperature up to 320 and 350°C. Later, time 275000s, made vacuum and added ^{4}He. The excess temperature vanished.*

In Fig. 3 the input power was increased (12→14→16 watt). Descending slops of excess temperatures. The $\Delta Tp_{1\text{-}2}$ tends to decrease; at 16 watt of input power, abruptly, the V_2 pressure raises up (large D_2 degassing) and the $\Delta Tp_{1\text{-}2}$ drops down.

This fact is of a paramount importance; in fact, (see the Fig.2) by increasing the powder temperature, the ΔTp_{1-2} also increases. In correspondence of the powder degassing *vice versa,* the ΔTp_{1-2} decreases. The relationship between ΔTp_{1-2} and the D/Pd ratio appears to be very clear.

After a prolonged switching off, the input power was turned on (12W); the ΔT ($\cong 4°C$) showed an ascending trend. At this point, in order to ascertain that the differential calorimeter was working well (i.e. that the observed ΔTp_{1-2} was simply due to an accidental offset occurred along the time to the calorimeter), the "active" D_2 atmosphere was replaced, after vacuum degassing, by the inert ^4He in both the chambers (connecting valve on).

Null gain of temperature was expected and null (<1°C) was found:
the previous excess temperature results, shown in Fig. 2, have been validated.

7.4) Fig. 4

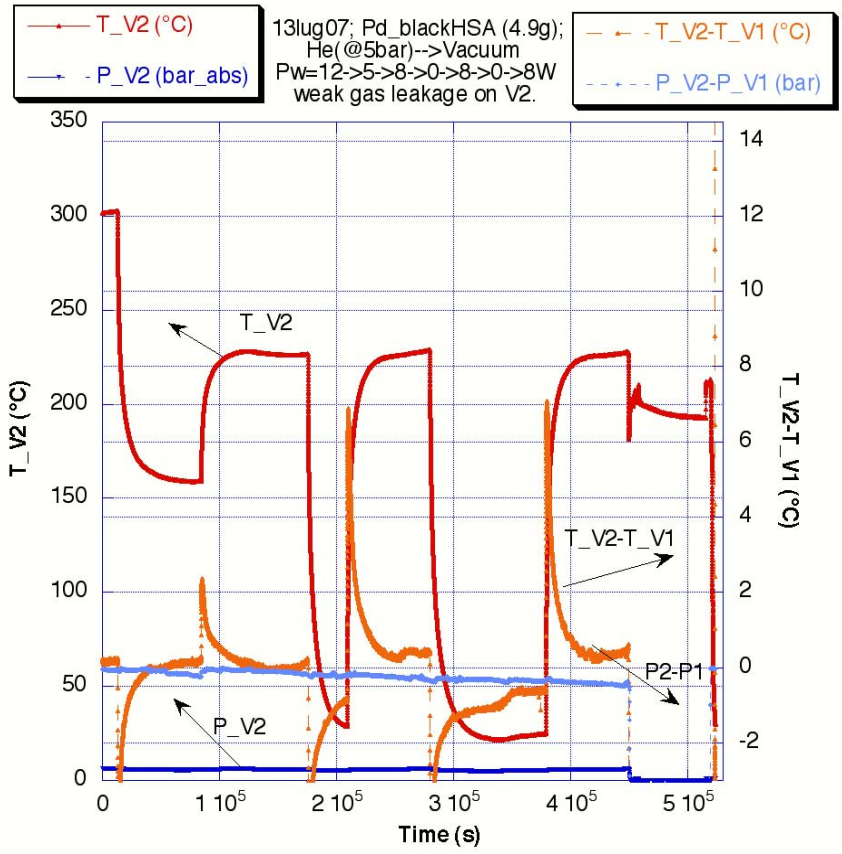

Fig.4. *File 13lug07. Experiments with ^4He at variable powers (12, 5, 8W).*

Never excess temperature was found with ^4He. The green line, that accounts of pressure effects, because very similar to orange one, was omitted for clarity.

7.5) Fig.5

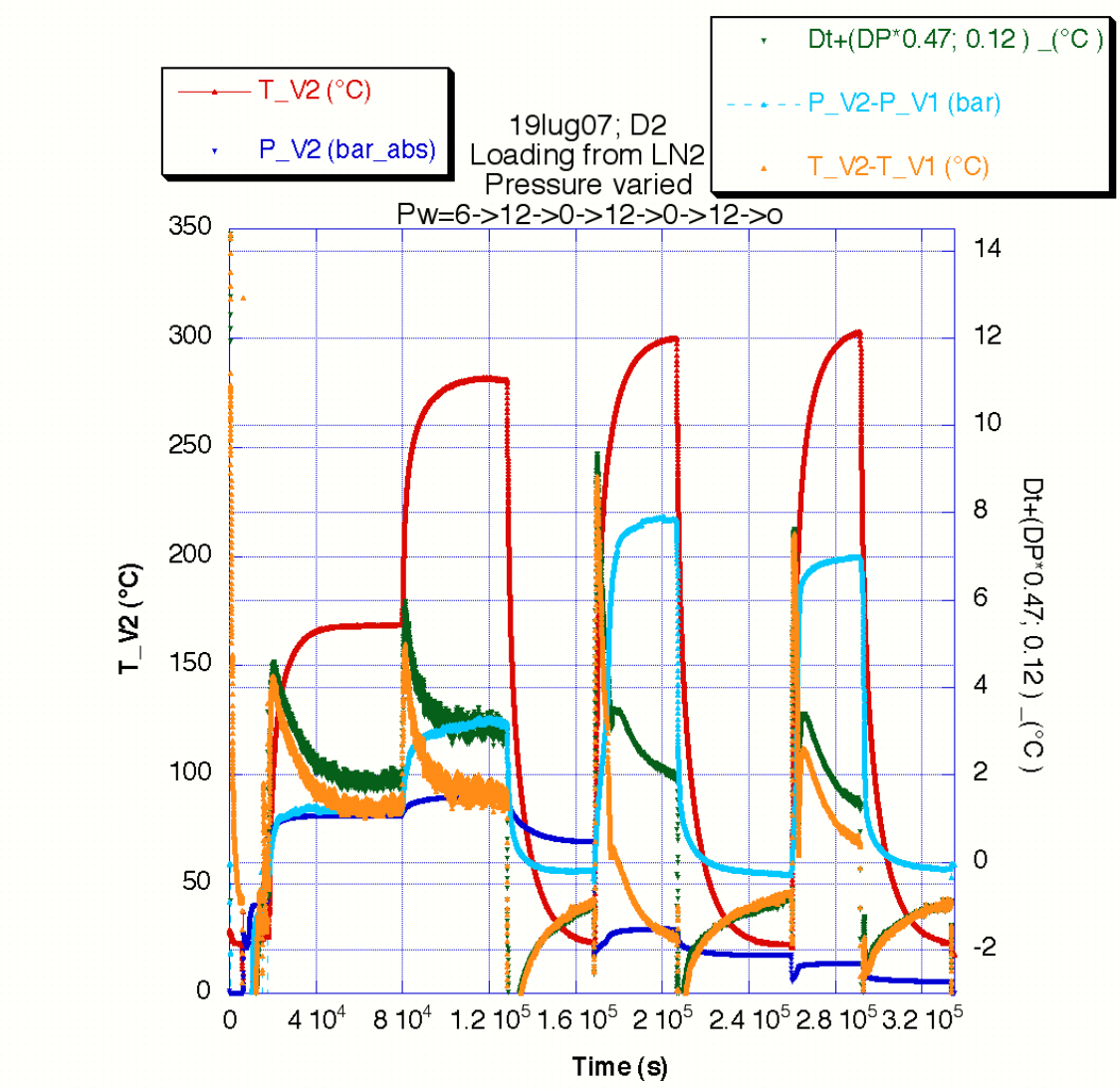

Fig. 5. *File 19lug07. Experiment with loading D_2 from LN2. The pressure was decreased, at time 165000, from 70 to 18bar; at time 255000 the pressure was decreased from 18 to 6bar.*

The loading from LN2 didn't have any practical effect. There is some excess temperature that decreases when the pressure was reduced and the deloading was large. Can be interesting to study the LN2 effect using virgin material, not damaged one as in this specific experiment.

* It is important to remark that, at the end of the experiment, the visual aspect of the Pd black powder in the crucible was consistently modified, having passed from the original dark black colour to a silver like one.

In Fig. 6 is shown, by SEM micro-photography, the typical aspect of Pd_black after the experiment. We recall that the PD_black HSA we used, according to the specifications of the

Company that sell it, has dimensions (for 10% of the volume of material) < 5.8μm. We measured particles even in the range of 100nm in the virgin material.

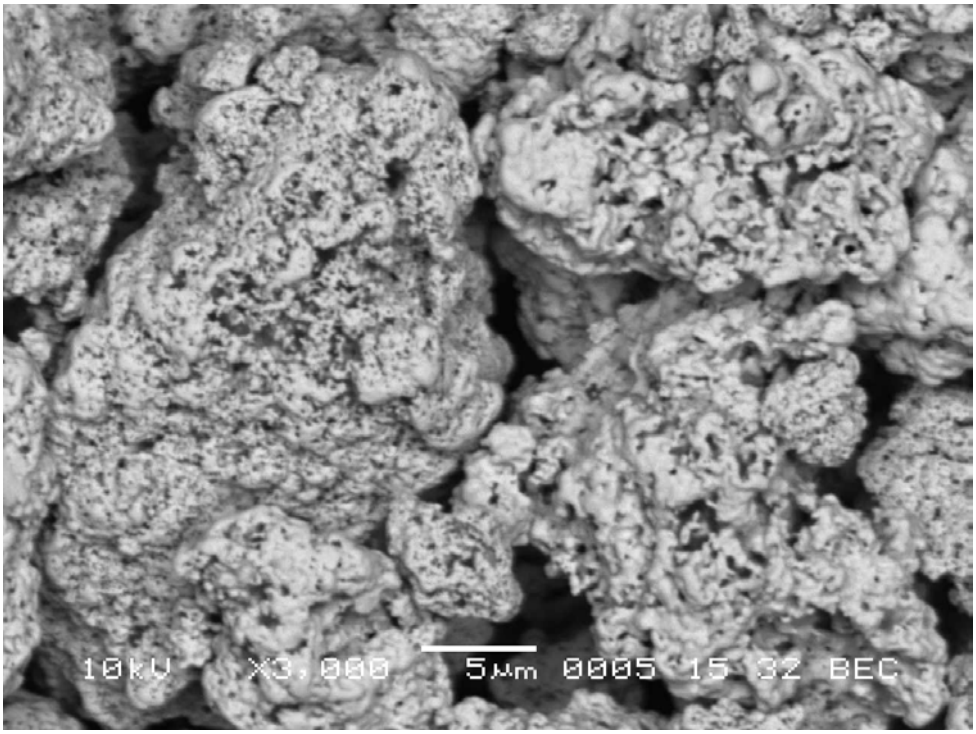

Fig. 6. *SEM photograph of Pd_black_HSA at the end of the experiment.*

It is evident that a sintering process of the Pd grains occurred along the time. The observed degassing of the Pd powder, and the consequent, sudden, drop down of the temperature gain, allows to suppose that the "activity" (i.e. the ability to produce excess heat) of the Pd nano-particles could be associated with their ability (with respect to the bulk) to prevent, up to a relatively high temperatures, the D_2 degassing.

8) Conclusions.

It has been definitely demonstrated that micro and, in particular, nano particles of Pd can absorb Deuterium gas up to D/Pd ratios >1 at pressure of about 60bar.

The new developed differential calorimeter seems to be the ideal instrument for highlighting and evaluating the excess heat produced in the working chamber. It has been shown, by operating with a High Surface Area Pd black (D/Pd ratio>0.96 at 35°C and 8.7bar,) that the excess heat increases with the Pd temperature. This fact was interrelated with the increase of the percentage of the β phase occurring when the Pd temperature increases. The anomalous heat generation seems to be associated to the ability of the Pd nano-particles to prevent the D_2 degassing even at high temperatures. It has been demonstrated that, when a degassing occurs, a strictly correlated decreasing of the excess heat also occurs.

The amount of total energy produced was so large (about 500kJ) that the origin of excess energy can't be of chemical origin, taking into consideration the amount of Pd used (4.8g, i.e. 45mM). The amount of energy produced by use is about 10 times larger of most energetic chemical reaction known.

* The results with Pd-black_HSA are in qualitative agreement with the results reported in Ref. 2.

The temperature gain, larger in our experiments at the beginning, can be explained because one or more of the following reasons:

a) Larger amounts of Pd_black-HSA
b) Different batch of production of Pd_black-HSA;
c) More mild degassing-baking temperatures;
d) Higher D_2 pressure;
e) Some unknown effect of due to the SS crucible.

* During ICCF13 we heard of other experimental results, qualitatively similar, were obtained by other two groups: one in France (Prof. J.P. Biberian, Univ. of Marseilles, Ref. 8) and the other in Russian (Prof. V.A. Kirkinskii, Russian Academy of Sciences, Novosibirsk, Ref. 9).

They obtained, with Pd black, in some specific experimental conditions, clear evidence of anomalous excess heat.

Prof. Kirkinskii and Collaborators got excess heat also with a γ Al_2O_3-Pd compound, home made in their Institute.

Prof. Biberian got large amounts of excess power (about 5W, to be reconfirmed) at 80°C using small amount of material (100mg of Pd_black produced by Goodfellow, diameter of 80-180nm) filled inside a Pd tube (oxidised in air at 500°C). D_2 gas, pressurised at 9bar, was allowed to flux from the internal of the Pd tube to the external (buffer chamber) kept under high vacuum by pumping out.

* It is worthy to note that, although gas loading of nano-materials allowed to obtain very good results from the point of view of reproducibility of the effects, from the other side, at least in our experiments, the amount of excess energy was quite low in comparison with the amount of material used (at the best, about 110mW/g). In previous experiments, using thin and long Pd wires by electrolytic methods, sometimes (but with poor reproducibility), we got some watt of excess power using only 20mg of Pd.

We think that the *flux* of Deuterium inside Palladium as to be induced: such flux was very large, at list in our experiments using thin wires, when electro-migration was applied to the wire. Something similar has to be done to the nano-materials. The experimental set-up of Prof. Biberian is a nice step to such direction.

9) Acknowledgements

* We are indebted with Prof Yoshiaki Arata (Osaka University-Japan) because give us precious suggestions in order to start our new experiments with Pd_black_HSA.

* We would like to thank, deeply, Prof. Cinzia Cristiani, (Chemical Department "Giulio Natta", Politecnico of Milan-Italy), because give us very useful suggestions about the preparation of γ Alumina materials filled with Palladium soluble salts.

References

1. Arata Y. The formation of "solid deuterium" solidified inside crystal lattice and intense solid-state nuclear fusion ("Cold Fusion"). Il Nuovo Saggiatore, Volume 20, N. 5-6, p. 66-71, 2004.
2. Arata Y., Zhang Y.-C. Development of "DS-Reactor" as the practical reactor of "Cold Fusion" based on the "DS-Cell" with "DS-Cathode" . Proc. ICCF12. Yokohama 27 Nov.-2 Dec. 2005; p. 44-54; World Scientific, ISBN 981-256-901-4
3. Iwamura Y. et al. Observation of surface distribution of products by X-ray fluorescence spectrometry during D_2 gas permeation through Pd complexes. Proc. ICCF12. Yokohama 27 Nov.-2 Dec. 2005; p. 178-187; World Scientific, ISBN 981-256-901-4
4. Celani F. et al. New procedures to make active, fractal like surfaces, on thin Pd wires. Proc. ICCF12. Yokohama 27 Nov.-2 Dec. 2005; p. 377-391; World Scientific, ISBN 981-256-901-4
5. Celani F. et al. Further studies, about new elements production, by electrolysis of cathodic Pd thin-long wires, in alcohol-water solutions (H,D) and Th-Hg salts. New procedures to produce Pd nano-structures. Proc. of 6th Meeting of Japan CF Research Society. Tokyo, April-27-28, 2005.Also at: http://wwwcf.elc.iwate-u.ac.jp/jcf/
6. Arata Y., Zhang Y.-C. Development of compact nuclear fusion reactor using solid pycnodeuterium as nuclear fuel. Proc. ICCF10. Cambridge, 24-29 August 2003; p. 139-157; World Scientific, ISBN 981-256-564-7.
7. Takahashi A., Yabuuchi N. Deuterons-to-Helium-4 channels. ICCF13, June 25-July1, 2007. Sochi. To be published by World Scientific (2007).
8. Biberian J.P., Armanet N. Excess heat production during D2 diffusion through Palladium. ICCF13, June 25-July1, 2007. Sochi. To be published by World Scientific (2007).
9. Kirkinskii V.A. Khmelnikov A.I. Set up for measuring of energy balance at interaction of metals and hydrogen isotopes gas at high temperatures and pressures. ICCF13, June 25-July1, 2007. Sochi. To be published by World Scientific (2007).

EXCESS HEAT REPRODUCIBILITY AND EVIDENCE OF ANOMALOUS ELEMENTS AFTER ELECTROLYSIS IN Pd|D_2O+H_2SO_4 ELECTROLYTIC CELLS

W.-S. Zhang [1,2] and J. Dash [1]

[1]*Low Energy Nuclear Laboratory (LENL), Portland State University*
Portland, OR 97207-0751, U.S.A., dashj@pdx.edu
[2]*Institute of Chemistry, Chinese Academy of Sciences*
P.O. Box 2709, Beijing 100080, China

Abstract

Electrolyte temperature is a key factor in excess heat production using Pd|D_2O+H_2SO_4 electrolytic cells. Best results are obtained when the electrolyte temperature is close to the boiling point. Stable excess heat is generated by events on or near the Pd cathode surface. In addition to the stable excess heat, heat bursts are sometimes observed. These occurred most frequently in experiments using 2 mm diameter tubes for the cathodes. Excess heat measured by isoperibolic calorimetry is directly verified by Seebeck envelope calorimetry. Experiments with D_2SO_4 replacing H_2SO_4 in heavy water electrolyte showed that there was no affect on excess heat production. After electrolysis, localized concentrations of silver were found on Pd cathode surfaces. Three characteristic surface features, (1) craters with rims containing electroplated Pt; (2) cracks in the sample; and (3) palladium regions around the cathode edges are preferred locations for the occurrence of silver.

I. Introduction

Anomalous excess thermal power in Pd|D_2O+H_2SO_4 electrolytic cells has been observed by isoperibolic calorimetry [1– 3]. From 2004 to 2005, the excess power was verified by Seebeck Envelope Calorimetry (SEC) [4]. Then, no excess heat was observed in SEC experiments during an eight-month period. Eventually, we found that there is a key parameter for excess heat reproducibility in isoperibolic calorimetry which had not been satisfied in SEC. From then on, we were able to obtain excess heat output from 12 consecutive samples using SEC. We will discuss this and other related issues in detail below.

Another previous discovery of our group is the presence of silver on the palladium surface after electrolysis in heavy water [1– 6]. In this paper we will present overwhelming evidence of silver production on samples. This evidence was obtained by intensive microanalysis studies.

The experimental set-up of the electrolytic cell, power and temperature measurements, and microanalysis have been reported before [4]. We will not discuss them here, except for some recent modifications.

II. Calorimetric results

During SEC experiments, we measured three characteristic temperatures, i.e. $T_{electrolyte}$, $T_{catalyst}$ and T_{top}, where $T_{electrolyte}$ is the temperature of electrolyte, which is measured by two K-type thermocouples attached to the bottom of the cell; $T_{catalyst}$ is the temperature of catalyst, which is measured by three K-type thermocouples attached on the outside of the cell at the level of the catalyst; T_{top} is the temperature on the outside of the cell top, which is measured by one K-type thermocouple attached at the center of cell cap. Another point is that all excess power results reported here do not include mass loss corrections, as before [4]. This will result in null excess power for some experiments due to the loss of the heat of recombination of H_2O and D_2O resulting from the escape of H_2, D_2, and O_2 gases.

Firstly, we demonstrate the effects of the temperature difference between the SEC wall and the electrolyte, from the initial value to the steady state value of electrolyte, on excess heat production. One example is shown in Figure 1. The cell of Exp. No. 050925 was placed in a large glass beaker (ϕ 7.2 $\times$ 11 cm^2) to prevent leakage of electrolyte; the cell of Exp. No. 051205 was placed into a cardboard box to decrease the rate of heat flow from the cell, thus raising the cell temperature. The cardboard box size is 11.5 $\times$ 11.5 $\times$ 17 cm^3, with wall thickness of 3 mm. It has a Styrofoam insert 5 cm thick with one hole (ϕ 5.7 $\times$ 4.1 cm^2) in its center to accommodate the electrolysis cell. We found that, along with the greatly increased temperature gradient in the latter experiment, excess heat was produced. There was no excess heat in experiment 050925, which ran at a lower temperature, with a much lower temperature gradient.

In Exp. No. 051205 and other similar experiments, a cardboard box was always used to increase the electrolyte temperature. In order to exclude the possibility that the signal of excess power is only the effect of the heat insulation layer around the cell, we calibrated the SEC using the cardboard box with the calibration resistor inside, as in the electrolysis experiments. A resulting calibration constant is 177.04 $\pm$ 0.09 W/V, which is within the average value 176.85 $\pm$ 0.25 W/V obtained without cardboard box around that time, as shown in Table. I. This shows that excess power is not caused by the system configuration. We repeated this calibration method several times. The device constants obtained were all consistent with that obtained without the cardboard box. Because the cardboard box increases the calibration time, we rarely calibrate the SEC using this method.

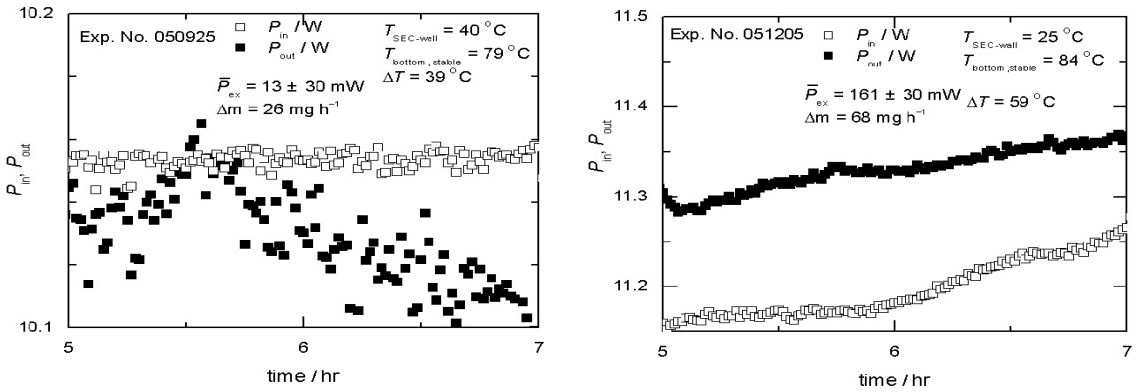

Fig. 1. *An example of the effect of electrolyte temperature increment on excess heat production. The cathode in both experiments is sample Pd-E, whose parameters are shown in Table III. The applied current is 3 A, and the current density is 0.24 A* cm^{-2}.

Table I. Device constants of SEC at wall temperature 25 ° C during 2006

Date	Input power / W	Device constant / W V^{-1}
Apr 5	9.335 ± 0.005	176.64 ± 0.14
Apr 7*	11.073 ± 0.003	177.04 ± 0.09
May 17	11.118 ± 0.003	176.63 ± 0.13
June 4	11.103 ± 0.002	177.09 ± 0.11

* For this calibration, the resistor was in the cardboard box. For the other three calibrations, the resistor without cardboard box was used.

Another series of excess power data on background and foreground temperatures for sample Pd-A besides that reported before [4] is shown in Table II, there is also an optimal background temperature for excess heat production as reported before [4]. All of these results indicate that both the temperature under steady-state in electrolysis and the background (or initial) temperature have important effects on excess heat. These two factors have different tendency on excess heat. High working temperature and low background temperature are important conditions for excess heat production. The cell with sample Pd-A was put in a large glass beaker only to prevent leakage of electrolyte onto the floor of the SEC; however, the low concentration of H_2SO_4 (5wt.% is one-fourth that the used ordinarily) in Table I of Ref. [4] and high current in Table II here ensure the high temperature of electrolyte, and hence excess power was observed. This suggests that every method which increases electrolyte temperature will be favorable for excess heat production. But this does not mean that lowering the SEC wall temperature and installing good heat insulation around the cell will increase excess power. We have conducted experiments at T_{wall} = 15 ° C and let the steady-state electrolyte temperature be close to that at T_{wall} = 25 ° C, by packing more Styrofoam around the cell with sample Pd-H; however, excess power did not change significantly. There are other unknown parameters controlling the excess power.

Table II. Excess power dependence on the initial and steady-state values of electrolyte temperatures.

Exp. No.	$T_{SEC\text{-}wall}$ / ° C	$T_{electrolyte}$ / ° C	ΔT / ° C	P_{ex}/mW	Δm/ mg h^{-1}
050105	20	79	59	271 ± 16	11
050108	25	81	56	238 ± 15	11
050110	35	88	53	492 ± 15	64
050111	40	90	50	349 ± 15	80

Note: The cathode is sample Pd-A, its size is 0.4 × 25 × 25 mm^3, surface area is 7.1 cm^2 and its weight is 1.34 g. The applied current is 3.6 A, and the current density is 0.5 A cm^{-2}.

After finding this key factor of excess heat production, we tested previously electrolyzed samples Pd-B to Pd-D, from which it had previously been difficult to produce excess heat [4]. We found that this method was successful, as expected, as shown in Table III.

Table III. Summary of excess power for various samples from Sep 2005 to Oct 2006.

Pd No.	size/mm^3	*mass*/g	*Area*/cm^2	Exp. No.	$P_{ex,max}$/mW*	Δm/mg h^{-1}	$P_{ex,burst,\ max}$/mW**	C_{Ti}/g l^{-1}
B	$0.25 \times 10 \times 61$	2.0390	14.6	060803	178 ± 14	73	Null	0
C	$0.4 \times 25 \times 25$	3.4687	12.5	060112-060211	147 ± 37	83	197	0
D	$0.05 \times 11 \times 31$	0.1628	7.1	051221-060104	151 ± 17	31	null	0
E	$0.25 \times 25 \times 25$	1.8982	12.5	050925-060711	759 ± 33***	228	623	33
F1 F2	$0.3 \times 9.4 \times 24.5$ $0.3 \times 9.4 \times 23$	0.7764 0.7346	4.7 4.4	051006-051109	461 ± 20	200	null	27
G	$0.35 \times 9 \times 41$	1.3875	7.6	060215-060223	97 ± 12	99	null	23
H	See Table IV			060309-060602	129 ± 14	47	355	8
I	$\phi 0.67 \times \phi 1.67 \times 80$	1.3064	1.6	060613-060701	356 ± 11	160	1130	0
J	$0.23 \times 7.7 \times 25$	0.6080	4.9	060817	149 ± 17	191	543	0
K	$0.23 \times 11 \times 23$	1.3875	7.6	060821	339 ± 15	276	851	0
L	$0.25 \times 10 \times 27$	0.6703	5.4	060823	174 ± 12	433	null	0
M	$0.27 \times 11 \times 26$	0.7918	5.7	060825-061010	306 ± 49	506	1144	0

* $P_{ex,max}$ is the maximum stable (usually > 1 hour) excess power during electrolyses for the sample.

** $P_{ex,burst,max}$ is the maximum burst of excess power for the sample.

*** The excess heat measured by SEC is 20.54 ± 0.90 kJ at this time.

Table IV. Summary of excess power obtained for sample Pd-H with varying thickness. The current density was about 0.6 A cm^{-2} for every experiment. As received thickness was 0.5 mm. Thickness was reduced by cold rolling.

Sample size/ mm^3	Exp. No.	P_{ex}/mW	Δm/ mg h^{-1}
0.34× 8.2× 31	060315	68 ± 16	39
0.20× 16× 16	060406	129 ± 14	47
0.15× 16× 16	060418	107 ± 15	40
0.10× 15× 17	060420	65 ± 39	39
0.03× 16× 16	060601	122 ± 9	108

From September 2005 to October 2006, we have conducted electrochemical calorimetric measurements of Pd|D_2O+H_2SO_4 with 12 Pd samples and these samples all gave excess heat using the method described above; the results are summarized in Table III.

In these samples, Pd-F consists of two pieces which are almost the same size; these were placed in two cells connected in series. Sample Pd-H was cold rolled after each run of electrolysis; the thickness changed from the original value, 0.5 mm to 0.03 mm as illustrated in Table IV. It was found that excess power does not depend strongly on the sample thickness. This may mean that excess heat is a surface effect rather than a volume effect as suggested previously [7].

Sample Pd-I is a palladium tube. About 30 mm on one end was exposed to electrolyte during electrolysis while the upper part was covered with PTFE heat-shrinkable tubing. The anode is a concentric cylinder made of Pt foil with total area of 48 cm^2. This cathode gave maximum stable excess power of 356 ± 11 mW at input power of 9.863 W during electrolysis for 7 hours and 10 minutes in Exp. No. 060620. After electrolysis for 56 hours in this run, the cell began producing heat bursts as shown in Fig. 2. The maximum heat burst is 1.1 W. The full-width at half-maximum of the heat bursts ranges from 12 minutes at its first occurrence at about 56 hours to 3.3 minutes at 110 hrs; the period of the heat bursts ranges from 3.3 hours to a few minutes. Besides Pd-I, other samples also gave heat bursts as shown in Table III. It seems that the largest heat bursts occur for thick samples. This conclusion is consistent with the results of heat-after-death experiments [8,9] and with an experiment in which an explosion occurred [10].

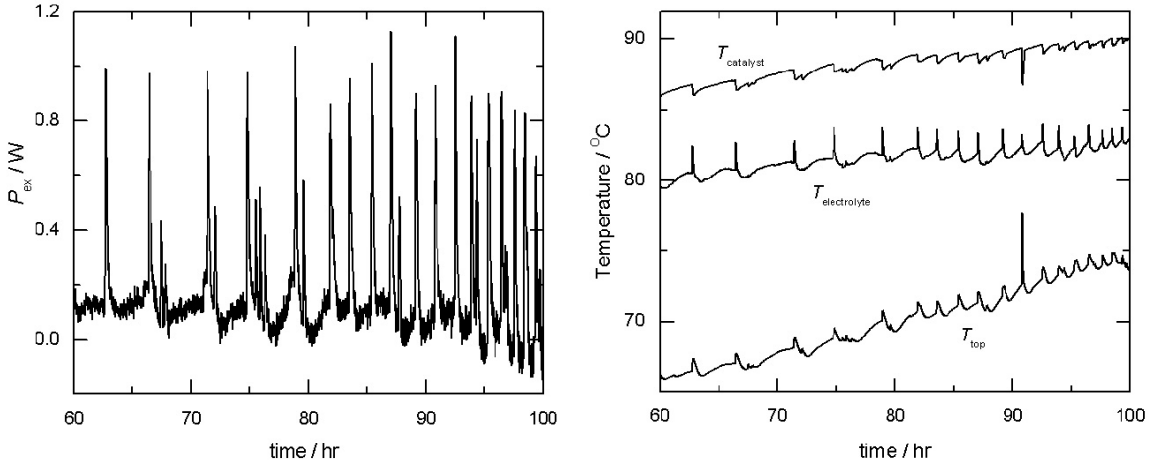

***Fig. 2**. Heat bursts and corresponding temperatures during electrolysis of sample Pd-I, a Pd tube, in Exp. No. 060620.*

Table V. Dependence of excess power on run number.

Pd No	Run 1			Run 2[1]			Notes
	Exp. No.	P_{ex}/mW	Δm /mg h^{-1}	Exp. No.	P_{ex}/mW	Δm /mg h^{-1}	
A	050101	33 ± 13	269	050103	198 ± 16	15	See note 2
C	060209	0	253	060211	108 ± 29	48	See note 3
E	051127	0	207	051129	215 ± 56	231	See note 4
F1	051012	371 ± 60	384	051015	461 ± 20	200	See note 5
F2	051021	247 ± 87	200	051024	386 ± 38	225	See note 6
H	060404	50 ± 7	58	060406	129 ± 14	47	See note 7
H	060412	81 ± 21	32	060413	119 ± 11	62	See note 8

Notes: [1] Experimental conditions of Run 2 are same as those of Run 1.
[2] Dormant for 30 days before 050101.
[3] Reverse current for 1 hour before electrolysis in 060209.
[4] Dormant for 50 days before 051127.
[5] New sample.
[6] Reverse current for 1 hour before electrolysis in 051021.
[7] Reverse current for 1 hour before electrolysis in 060404.
[8] Reverse current for 1 hour before electrolysis in 060412.

A question of the excess heat in Pd|H_2SO_4+D_2O is the role of protium ions. In order to study this, we prepared heavy water electrolyte containing D_2SO_4 instead of H_2SO_4. The D_2SO_4 is 99.5+ at.% pure (Aldrich Chemical Company). The ratio by volume of D_2O:D_2SO_4 is 6.6:1, which is close to that of H_2SO_4 in D_2O (volume ratio of D_2O:H_2SO_4 is 6.7:1). Six runs with samples Pd-D and Pd-E from Dec. 12, 2005 to Jan. 4, 2006 gave maximum excess power of 115 ± 20 mW for Pd-D and 124 ± 54 mW for Pd-E, which are not greater than those obtained with D_2O + H_2SO_4 electrolyte. These results indicate the protium ion does not reduce the excess heat production. Currently, we use 99 at.% purity D_2O, not 99.9 at.% purityD_2O which we used previously; there has been no detectable difference in excess heat production.

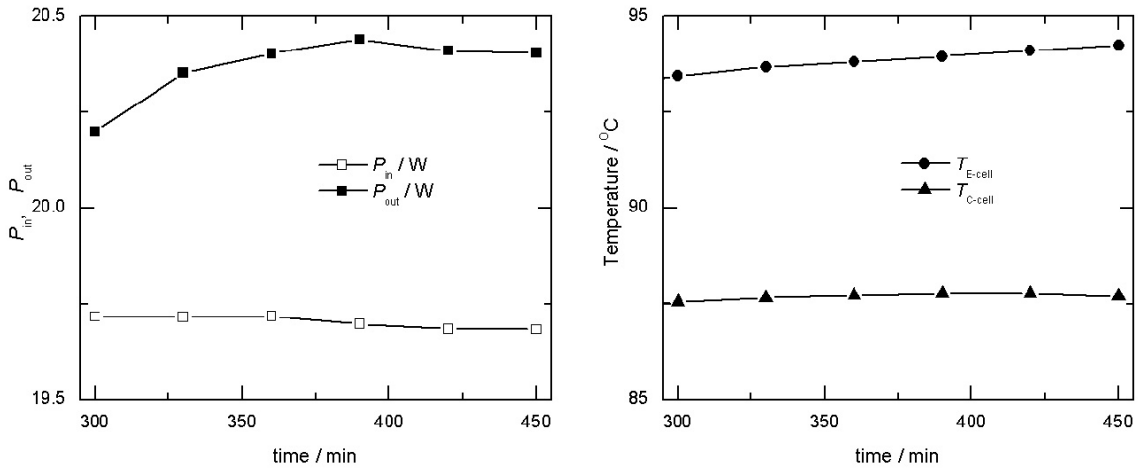

Fig. 3. *Comparison between SEC and isoperibolic calorimetry (Exp. No. 050928). The graph on the left gives results obtained with the SEC. The average excess power is 759 ± 33 mW (without including mass loss) to 1,481 ± 35 mW (including mass losses of D_2O and H_2O, 0.62 and 1.09 g, respectively). The right graph shows average temperatures from eight thermocouples attached on the outside of both the Pd|D_2O and the Pt|H_2O cells. The input power of both cells is 9.60 ± 0.03 W, the applied current is 3 A for 7 hours and 30 minutes, the air temperature in SEC is 37 °C and the excess power of the E-cell is* 783^{+716}_{-339} *mW. The error of isoperibolic calorimetry mainly comes from the uncertainty of the proportion of D_2 (H_2), O_2, and D_2O (H_2O) vapor which escape due to poor recombination by the catalyst and a flexible seal between the cell body and its top. Increased pressure in the cell increases the rate of escape of gases from the cell. The rate of mass loss from a cell, shown in the data tables above, is a measure of the rate of escape of the gases.*

In our experiments with H_2SO_4, the electrolyte was used for multiple runs. Only heavy water (about 20 grams needed after 3 A × 8 hrs electrolysis) was added to the old electrolyte to restore it to the original volume. Because of this, the H^+ concentration decreases with time in every run and from run to run. This means that our cell is a deuterium self-concentrated system and the isotopic purity of D_2O has negligible effect on excess heat production.

Another question is the validity of excess power measured by isoperibolic calorimetry which we reported previously [1– 3]. Here we report the results of isoperibolic calorimetry and SEC obtained with the same electrolytic system. As described before [1– 3], we used two cells with the same dimensions, one containing Pd|D_2O+H_2SO_4 and another containing Pt|H_2O+H_2SO_4. The concentration of H_2SO_4 in each cell is adjusted to ensure that the voltages and hence the input powers of these two cells are close to each other at the same current. These two cells are placed in a cardboard box (14 × 17 × 17.5 cm^3, 4 mm wall thickness) inside the SEC. Temperatures, current, voltages and the SEC signal are recorded with a data acquisition system. The results are shown in Fig. 3. We find that these two methods give the same excess power, within the precision of the measurements. This suggests that excess power results reported before [1– 3] are likely to be accurate.

III. Scanning electron microscope and energy dispersive spectrometer characterization

III. 1. Silver

Before and after electrolysis, we characterized the surface morphology and elemental composition of Pd cathodes by scanning electron microscopy (SEM) and energy dispersive

spectrometry (EDS). Most of samples show anomalous new element production [1– 4]. We will report results of one sample, Pd-H, whose parameters are shown in Table IV. The photo of sample Pd-H after electrolysis for 186 hours is shown in Fig. 4, the electrode bends towards the anode during long time electrolysis as observed previously [4]. The fractures on the right edge of the convex side in Fig. 4(a) (or left edge of concave side in Fig. 4(b)) were formed during cold rolling, before electrolysis. The numbered white labels are areas studied by SEM and EDS.

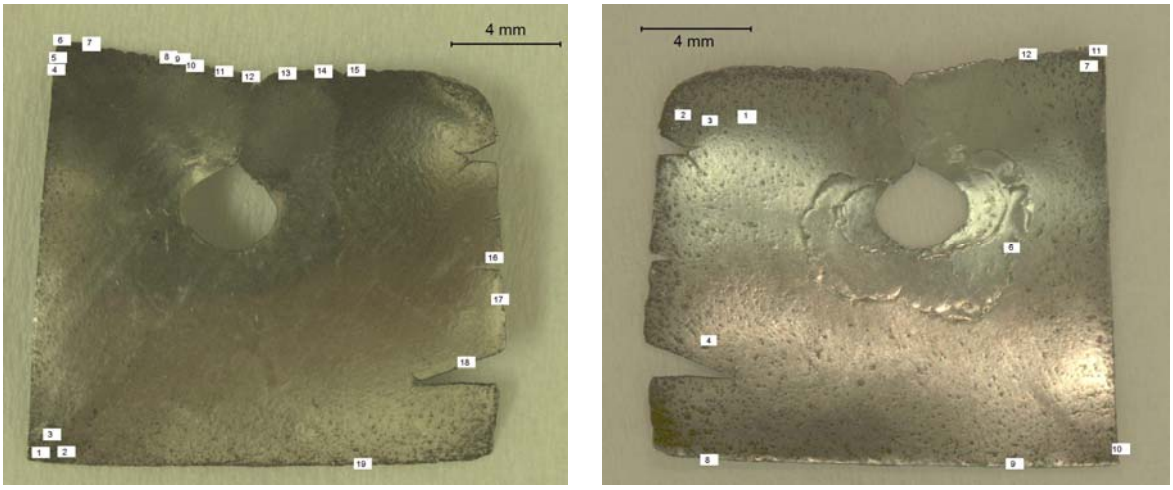

Fig. 4*. Photos of Pd cathode H after electrolysis for 186 hours. (a) (left) The convex side, which faced away from the anode; (b) (right) the concave side, which faced the anode. The hole is used to connect the cathode lead wire as described in Ref. [4]. The white rectangles indicate the positions from which X-ray spectra were taken.*

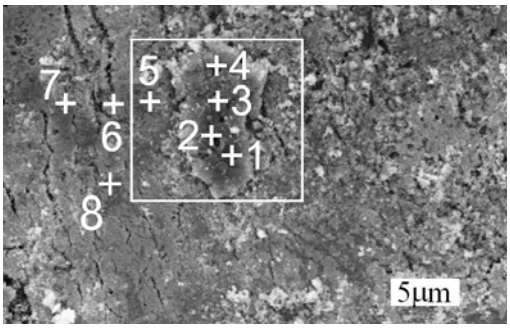

Fig. 5. *SEM picture of region #16 in Fig. 4(a). SEM No. WS060505Pd-H-CV-i16-2kX.*

Table VI. Relative atomic percent concentrations of silver at spots in Fig. 5.

Spot #	area*	1	2	3	4
Ag/(Pd+Ag)	55.3 ± 0.5	98.1 ± 1.9	92.8 ± 0.2	96.5 ± 0.2	80.9 ± 0.3
Spot #	5	6	7	8	
Ag/(Pd+Ag)	6.0 ± 1.0	4.3 ± 1.5	3.4 ± 1.0	0	

* area = the square area with white case in Fig. 5.

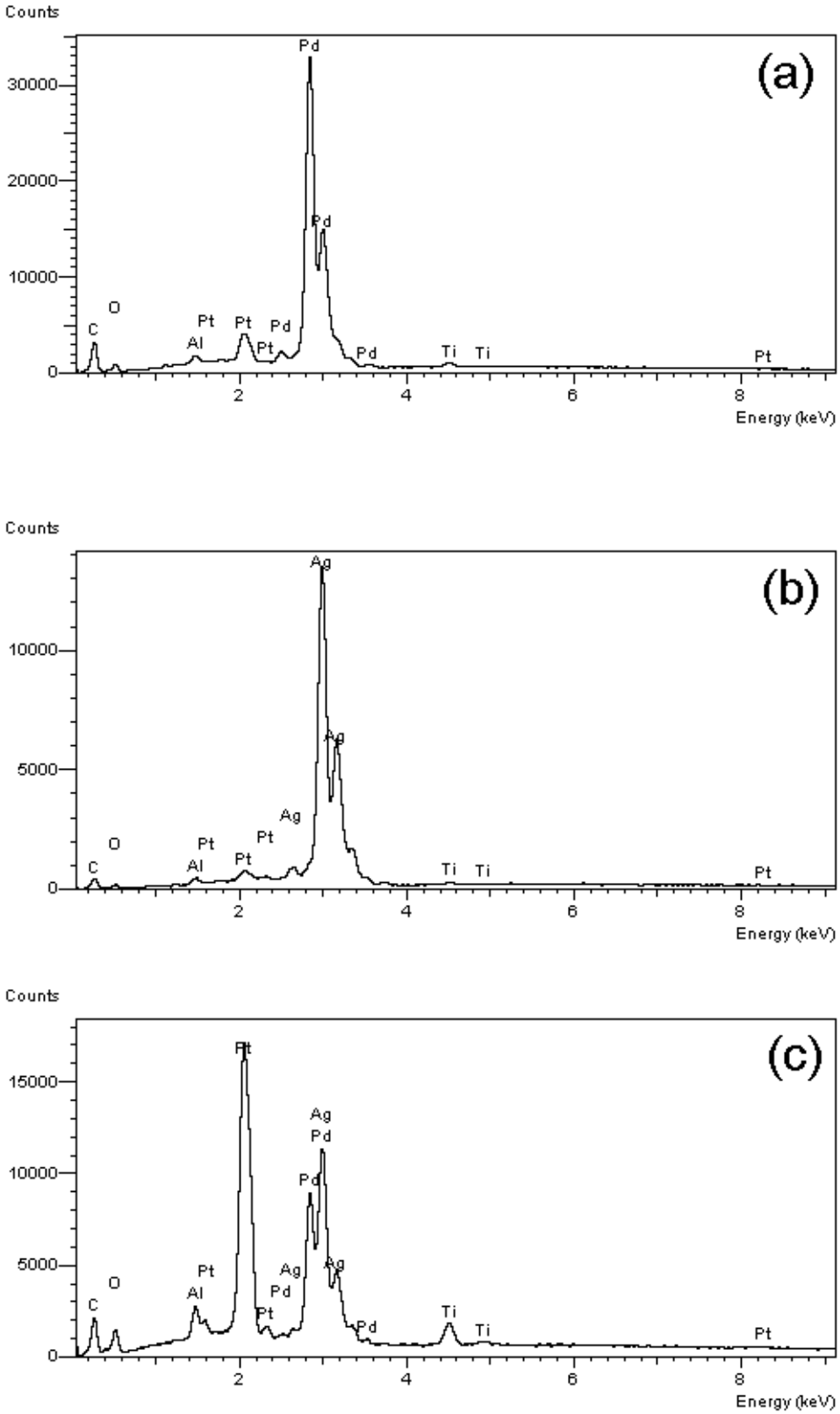

Fig. 6. *Characteristic X-ray spectra of spot #8 (a), spot #1 (b) and square area (c) shown in Fig. 5.*

Fig. 5 shows an SEM picture of region #16 in Fig. 4(a). Three characteristic X-ray spectra from this region are shown in Fig. 6. Fig 6(a) is from spot #8 in Fig. 5. The most prominent peaks in the spectrum are from Pd, the bulk metal. Other elements are from the electrolytic system: Pt is from the anode, which is slowly dissolved and deposited on the cathode; C most likely comes from back-streaming of hydrocarbons from the diffusion pump oil; Al and O are from the alumina recombination catalyst; and Ti is from the electrolyte. Ti was dissolved in the electrolyte before the experiments [3– 5].

Fig. 6(b) is from spot #1, the most prominent element here is silver; other elements are the same as those in Fig. 6(a), except for the absence of Pd. Besides spot #1, other spots in the central black region of the foot-shaped feature in Fig. 5 are almost pure silver. We obtained the EDS spectrum in Fig. 6(c) from the central region in Fig. 5. Because the characteristic Lα X-ray of Ag is at 2.98 keV, it overlaps with Pd Lβ at 2.99 keV. The expected intensity ratio of Pd Lβ /Pd Lα is 0.42, whereas the ratio of these two peaks in Fig. 6(c) exceeds 1.0. As in our previous reports [2– 5], we attribute the increase in this ratio to the presence of silver. The results of analysis of the EDS spectra are summarized in Table VI. The silver concentration is presented as a relative quantity for the convenience of comparison. Localized concentrations of silver were also detected along cracks in the microstructure shown in Fig. 5. Because of their irregular nature, these cracks probably formed during electrolysis rather than during cold rolling. These cracks also have localized concentrations of silver.

Another example is shown in Fig. 7 and Table VII.

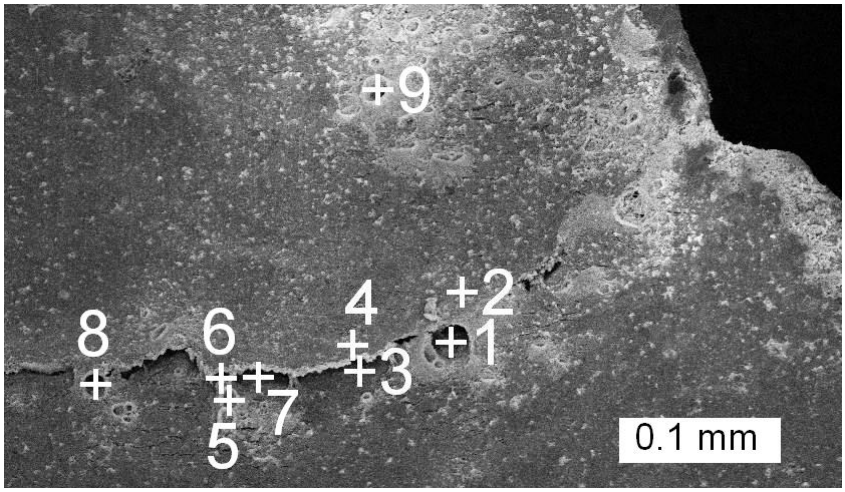

***Fig.** 7, SEM picture of region # 12 in Fig. 4(a). SEM No. WS060504Pd-H-CV-i12-150X.*

Table VII. Relative atomic percent concentrations of silver at spots in Fig. 7.

The other 5 spots which were tested have no silver.

Spot #	1	3	5	6	7
Ag/(Pd+Ag)	15.1 ± 2.6	9.4 ± 2.9	16.4 ± 6.0	11.6 ± 1.9	9.8 ± 2.2

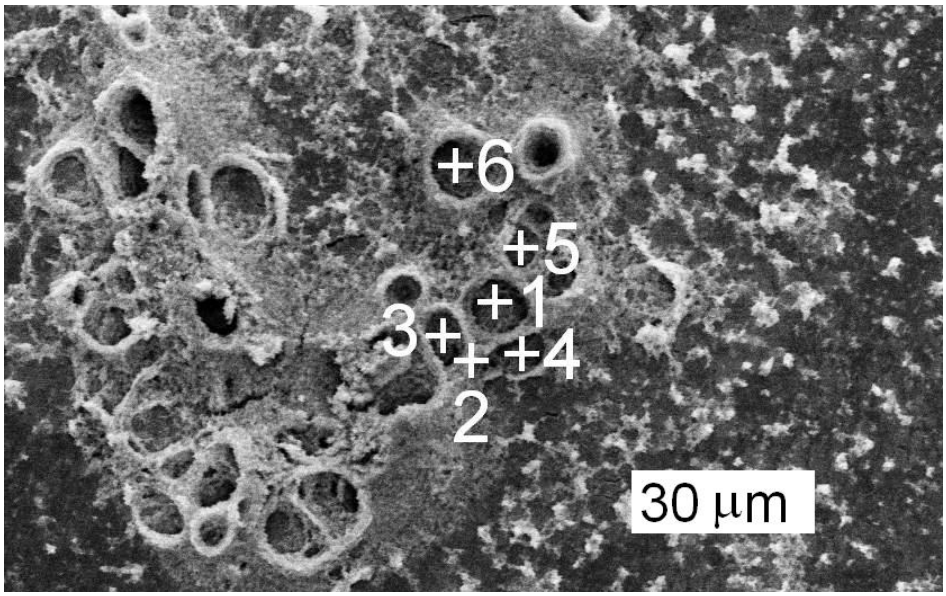

Fig. 8. *SEM picture of region # 3 in Fig. 4(a). SEM No. WS060501Pd-H-CV-i3-500X.*

Table VIII. Relative atomic percent concentrations of silver at spots shown in Fig. 8 under different acceleration voltages and at different times in 2006.

Time	Voltage/kV	spot 1	spot 4	spot 6
Apr 28 16:00-17:15	20	18.5 ± 3.7	9.2 ± 2.5	9.0 ± 3.9
Apr 28 17:45-18:15	20	18.1 ± 2.7	7.4 ± 1.7	15.0 ± 3.5
Apr 28 17:50-18:05	30	16.6 ± 2.5	8.3 ± 1.3	10.0 ± 1.8
May 1 10:20-10:45	20	15.2 ± 2.8	6.7 ± 1.4	12.4 ± 3.0
May 1 10:50-11:15	30	17.0 ± 2.3	8.2 ± 1.2	9.8 ± 1.7

The most common finding is that silver occurs in craters, such as those shown in Fig. 8. These craters with rims almost certainly formed during electrolysis. Pt deposition was concentrated on these protruding rims. We measured the silver concentration with different accelerating voltages and at different times. The results in Table VIII show that there are no obvious changes in silver concentration due to either the increase in accelerating voltage or to the passage of time.

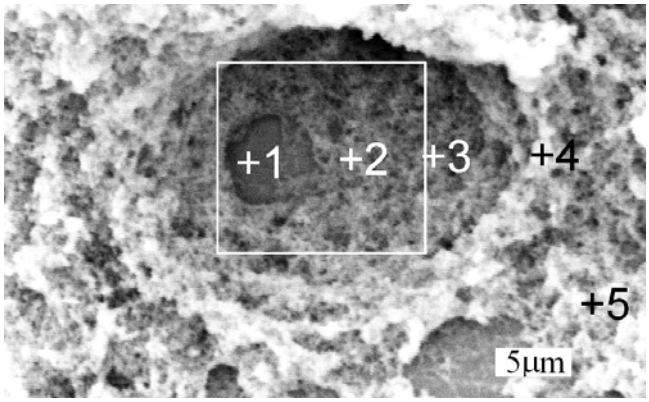

***Fig. 9**. SEM picture of crater at another time. SEM No. WS060607Pd-H-CC-i2-2kX.*

Table IX. Relative atomic percent concentrations of silver in areas and spots shown in Fig. 9.

Spot #	wa*	area**	1	2	3	4	5
Ag/(Pd+Ag)	1.2 ± 0.5	5.6 ± 0.4	6.8 ± 0.4	5.6 ± 0.3	6.3 ± 0.4	3.6 ± 0.6	1.2 ± 0.5

* wa = whole area in Fig. 9.
** area = the square area with white case in Fig. 9.

We have studied the crater shown in Fig. 9 in detail as listed in Table IX. This crater is also located on an edge on the concave side of the same sample. From these results it is concluded that the silver concentration varies by about a factor of 5 from the lowest in spot 5 to the highest in spot 1.

The silver concentration in all 19 regions in Fig. 4(a) is summarized in Table X. Concentrations labeled P were obtained with the electron beam fixed in one spot on the cathode, and A designates concentrations obtained with the electron beam scanning a known area of the cathode. The silver production on the concave side in Fig. 4(b) is summarized in Table XI.

Table X. Summary of relative Ag concentration at regions on the convex side of the Pd cathode (facing away from the anode) shown in Fig. 4(a).

Region #	1	2	3	4	5	6	7	8	9	10
Maximum Ag/Pd	0	7.7	18.5	99.1	97.9	80.4	0	11.1	9.2	8.4
Mode		P	P	A	A	P		P	P	P
Region #	11	12	13	14	15	16	17	18	19	
Maximum Ag/Pd	7.0	16.4	5.1	7.2	40.3	98.1	31.7	68.4	26.6	
Mode	P	P	P	P	P	A	P	P	A	

Table XI. Summary of relative Ag concentration at regions on the concave side of the Pd cathode (facing the anode) shown in Fig. 4(b).

Region #	1	2	3	4	6	7	8	9	10	11	12
Maximum Ag/Pd	0	5.7	0	0	5.1	5.2	8.4	17.1	12.1	13.2	95.8
Mode		P			P	P	P	P	P	A	A

Besides the H sample Pd cathode, silver was also detected on other samples, as reported before [4].

Some conclusions can be reached concerning the location of silver on the cathode after electrolysis: (1) Silver occurs preferentially around the sample edges rather than in the central area, as observed before [1– 6]; (2) silver is found more frequently on the back (convex) side of the Pd cathode than on the side facing the anode (concave side). Of course, there is another possibility: the silver on the concave side was covered by a Pt deposition layer, which is thicker than that on the convex side.

III.2. Nickel

Another anomalous element is nickel, which was detected in regions # 2 and #3 in Fig. 4(b). The SEM picture, X-ray spectrum of spot #1, and EDS measurement results from region #2 are shown in Figs. 10 and 11, and Table XII, respectively, where Ni/(Pd+Ni+Ag) from different spots ranges from 0.9 to 2.1 at.%. The average value for the whole area is Ni/(Pd+Ni) = 1.3 at.%. Region #3 in Fig. 4(b) also contains nickel, Ni/(Pd+Ni) = 1.1 to 1.9 at.% , in various spots. The nickel is concentrated in the upper left corner on concave side of the Pd-H sample. For example, Ni is not present in any of the spectra in Fig. 6. We also have observed Ni, on the order of 1 at.% or less, in other samples.

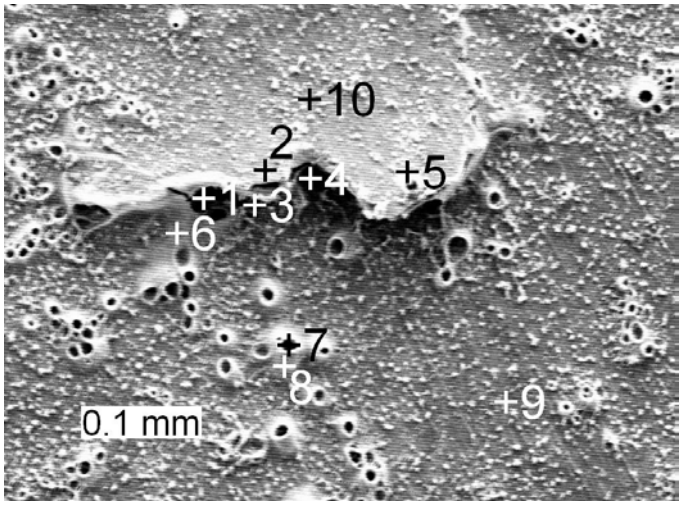

Fig. 10. *SEM picture of region #2 in Fig. 4(b). SEM No. WS060424Pd-H-CC-i2-150X*

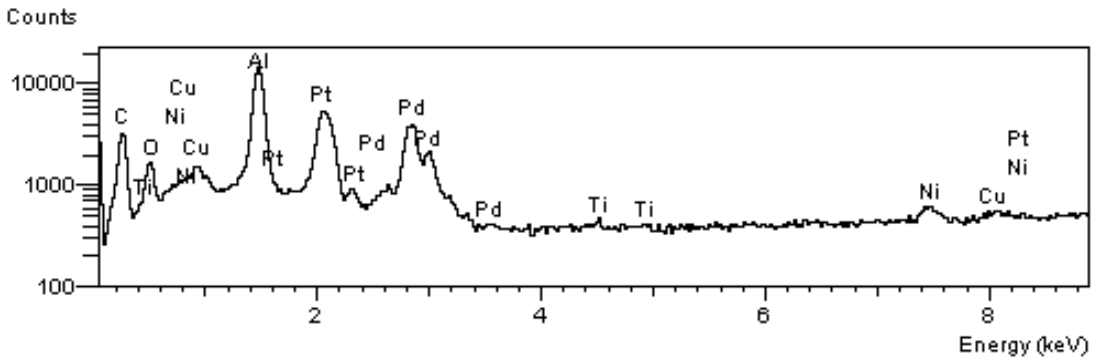

Fig. 11. Characteristic X-ray spectrum of spot #1 in Fig. 10. EDS No. WS060424Pd-H-CC-i2-150X-s1.

Table XII. Summary of relative Ag and Ni atomic percent concentration at regions shown in Fig. 10.

Spot #	Ag/(Pd+Ni+Ag)	Ni/(Pd+Ni+Ag)
wa*	0	1.3 ± 0.2
1	0	2.1 ± 0.1
2	5.7 ± 1.9	2.1 ± 0.2
3	0	1.1 ± 0.1
4	0	1.3 ± 0.1
5	0	1.5 ± 0.1
6	0	0.9 ± 0.1
7	3.3 ± 1.1	1.7 ± 0.1
8	0	1.2 ± 0.1
9	0	1.4 ± 0.1
10	0	1.9 ± 0.1

* wa = whole area in Fig. 10

What is the origin of this nickel? Ni was listed as “not detected” in the chemical analysis provided by the vendor of the Pd foil. It is very unlikely to have resulted from the cold rolling process or from electrodeposition because it is highly localized near one corner of the cathode. If it is the result of either contamination from the rolling mill or from electroplating it should not be highly localized on only one corner of the cathode. It could not have resulted from SEM systems because the stainless steel components of the SEM chamber also contain Fe and Cr. Fe and/or Cr are not present in any of the spectra. The SEM does not have components made of pure Ni. Therefore, the origin of the Ni is not known.

IV. Discussion

Since the discovery of excess heat in 1989 [11], the reproducibility has been a difficult problem [7]. Our results suggest a reason why Fleischmann and Pons and other groups observed excess heat using Dewar-type electrolytic cells and isoperibolic calorimetry [8,11– 13], but some groups using mass-flow calorimetry, had difficulty detecting excess heat, or the reproducibility was very poor. The reason is that the latter method involves a low temperature, semi-isothermal measurement. The temperature difference between the electrolytic cell and the water flowing during electrolysis is very small. Therefore, this system has to be stimulated by various methods, e.g., high input power, laser irradiation etc. [7] Even then, the reproducibility is still low because the cell temperature is not high enough.

Our experiments using small diameter Pd tubes as cathodes produced many more heat bursts than flat Pd foil cathodes. Further study using Pd tube cathodes is warranted.

Using an EDS attached to a SEM; we again have found localized concentrations of silver on the surfaces of Pd cathodes after electrolysis. On a few of the cathodes, we also found localized concentrations of nickel. Further study, such as the determination of isotopic ratios before and after electrolysis, is needed to aid in understanding the origin of the Ag and Ni.

Acknowledgement
This research was supported by a grant from the New York Community Trust.

References

1. Ambadkar A. and Dash J., Electrolysis of D_2O with a palladium cathode compared with electrolysis of H_2O with a platinum electrode: procedure and experimental details, see: http://www.newenergytimes.com/Library/2003DashJ-ColdFusionRecipe.pdf
2. Dash J. and Ambadkar A., Proc. ICCF11, Marseille, France, Oct 31 to Nov 5, 2004, P. 477.
3. Wang Q. and Dash J., Proc. ICCF12, Yokohama, Japan, Nov 27 to Dec 5, 2005, P. 140.
4. Zhang W.-S. Dash J. and Wang Q., Proc. ICCF12, Yokohama, Japan, Nov 27 to Dec 5, 2005, P. 86.
5. Dash J., Noble G. and Diman D., Trans. Fusion Tech., 1994, V.26, No.4T, P.299.
6. Miguet S. and Dash J., J. New Energy, 1996, V.1, P.23.
7. Storms E., Infinite Energy, 1998, V.4, No.21, P.16.
8. Pons S. and Fleischmann M., Trans. Fusion. Tech., 1994, V.26, No.4T, P.87.
9. Rothwell J., Cold Fusion and the Future, 2004, lenr-canr.org. P.13.
10. Zhang X.-W., Zhang W.-S. and Wang D.-L. *et al*., Proc. ICCF3, Nagoya, Japan, Oct 21 to 25, 1992, P.381.
11. Fleischmann M., Pons S. and Hawkins M., J. Electroanal. Chem., 1989, V.261, P.301; errata 1989, V.263, P.187.
12. Szpak S., Mosier-Boss P.A., Miles M.H. and Fleischmann M., Thermochim. Acta, 2004, V.410, P.101.
13. Miles M. Proc. ICCF10, Cambridge, MI, USA, Aug 24 to 29, 2003, P.23.

HEAT MEASUREMENTS AND SURFACE STUDIES OF PD WIRES AFTER BEING EXPOSED TO A H2 GAS-LOADING SYSTEM IRRADIATED WITH A YAG FREQUENCY DOUBLING LASER

J.Tian[1,2], L H Jin[1], B J Shen[1], Q S Wang[2], J Dash[2]

[1] Changchun University of Science and Technology, Changchun, Jilin 130022 China
[2] Portland State University, Portland, OR 97201 USA
tianjian@cust.edu.cn, dashj@pdx.edu

Abstract

This study involved excess heat triggering attempts with a YAG frequency doubling laser (λ=532nm) used to irradiate palladium hydrides with different gas-loading ratios. The results showed that experiments using laser stimulation produced no significant excess heat evidence. However, on the surface of Pd sample there were some new elements including Ag and Cd. These were found in localized sites by SEM and EDS analysis.

Key words: H/Pd system gas-loading, YAG frequency doubling laser, excess heat triggering

1. Introduction

Laser stimulation is a potentially useful method in excess heat research. In 2003, D.Letts and D.Cravens[1] reported a method for generating highly reproducible and appreciable excess heat from deuterated palladium electrodes in heavy water electrolysis. Then V. Violante[2] and K. Sinha[3] modified and repeated the Letts experiment in 2005 and 2006. A gas-loading system can reach a relatively high temperature with the same amount of energy than in the electrolysis system due to the lower heat capacity of gases. Hydrogen has often been thought of as a control in cold fusion experiments. It is not generally accepted that the H/Pd system can produce any abnormal phenomenon. But does the hydrogen always behave like that? What would happen when ambient conditions are changed? This report concerns the use of a YAG laser with frequency doubling. Its wavelength is 532 nm. It was used to irradiate a series of palladium hydrides with different loading ratios (x =[H]/[Pd]= 0, 0.2, 0.3, 0.4, 0.8) . After laser stimulation, all of the samples including the original Pd were studied with scanning electron microscope (SEM) for surface topography and for elemental analysis with an energy dispersive spectrometer (EDS). Dash et al [4,5] found excess heat and new elements on the surface of a Pd cathode after heavy water electrolysis. But we are not aware of any such laser triggering experiment in a H/Pd gas-loading system.

2. Experimental

2.1 Apparatus and materials

Figure 1 shows the schematic of the experimental system. In which the reaction vessel is a glass flask with the dimension ofφ=6cm and h=26cm, with capacity roughly 750 cm^3. Palladium wire (99.98%Pd) was obtained from the 621 Institute of Aero-astronaut Ministry of China. Its size wasφ0.01×50 cm and volume about $4\times10^{-3}cm^3$.

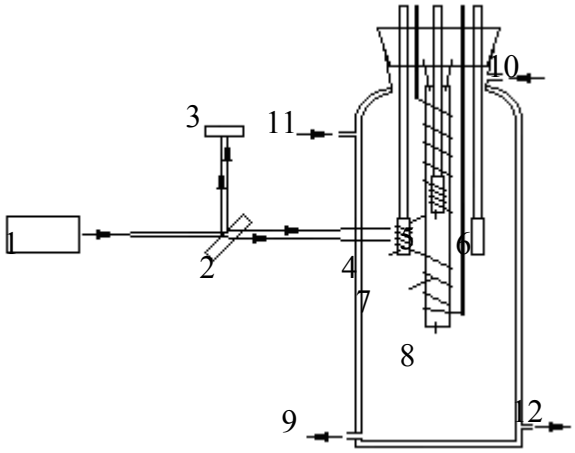

Figure 1 *The schematic of our H/Pd gas-loading and laser triggering system. In which: 1-YAG laser, 2-3/7 reflection mirror, 3-laser power meter, 4, 5, 6-Pt100 thermometer, 7- Pd wire, 8-ceramic tube frame, 9-connection to the vacuum system, 10-connection to a super-pure hydrogen gas generator, 11, 12- inlet and outlet connections to the water circulation system*

Before the experiment the Pd wire was immersed in acetone and ethanol respectively for 20 minutes, and then cleaned by distilled water to get rid of impurities on the surface. Afterwards the wire was wound on a ceramic tube frame. Three Pt100 resistance thermometers were put inside the flask. One of them was for reading the temperature of the Pd wire that was irradiated by YAG laser. Another one represented the temperature of the Pd sample that was not irradiated by the laser. The third Pt100 thermometer was for recording the gas temperature inside the flask. The function of three-seventh reflection mirror was for monitoring the change of laser power. The reaction chamber was evacuated using a mechanical pump (Chengdu Southlight 2X2-4B) and a molecular turbine (Asslar PFEIFFER D-35614). The pressure of the chamber was read by a vacuum gauge (PFEIFFER TPG-262). The hydrogen gas was generated by a super-pure hydrogen generator made by Beijing Huayuan Gas Company. The purity of the H_2 was about 99.999% after a long working time. The loading ratio was determined by the resistance of the Pd wire (four-line method to measure the voltage and the current between the Pd wire, then calculate the resistance). From the correlation between the R/R_0 and x=[H]/[Pd], we can obtain the loading ratio of the Pd wire. The DC power supply for heating the Pd wire was model WYJ-302B made by Apple Electronic Apparatus Limited Company, Shanghai, China. A data acquisition system (Keithley 2700) made in the USA was used for reading the voltage and current in the Pd circuit. Four Pt100 resistance thermometers, including the thermometer that recorded the room temperature, were monitored. Laser wavelength (λ) was 1064nm, after frequency doubling, it became 532nm, which could pass through the glass-made flask. The laser has four types of pulse frequency (1, 5, 10, $15s^{-1}$) and four kinds of working voltages (750, 800, 850, 900V). Its maximum power was 2.0W.

An important feature of this gas-loading apparatus is its water circulation system. It can keep the temperature in reaction chamber from fluctuating due to changes in ambient temperature. So the temperature of the water circulation system should be set higher than room temperature. Here 35±0.5℃ was chosen.

In order to characterize surface topography and microchemical composition, the Pd wires were taken out of the experimental chamber and examined with a SEM and an EDS after hydrogen gas-loading into Pd, and laser irradiation. The SEM model was ISI-SS40 equipped with an EDS, OXFORD model 5565.The area of the detector window was 10mm^2. Its resolution was 138 eV. The detector was coupled with ISIS software (the name of the specific program was SEMQuant) that estimated the elemental composition of a spot or area on the sample based on the X-ray spectrum. The more X-ray counts that were acquired, the more accurate that the X-ray analysis turned out to be. The accelerating voltage was set at 20 kV for all characterizations.

2.2 Experimental methods and results

2.2.1 Laser stimulation of pure palladium wire to determine background

In order to determine whether an abnormal phenomenon does exist in this system, the normal behavior should be confirmed in advance. That is, the background stimulation effect for the pure Pd wire (x=0) has to be tested before the experiment. Firstly, the system was pumped to a lower vacuum level (~2.0Pa). Then a series of laser beam powers and frequencies were applied on a section of Pd wire (about 9mm in length) for one hour. The temperature of the wire read by a Pt 100 thermometer was increasing gradually and then it reached steady state. Then the laser was turned off, and the heating coefficient (k) was calculated by the following formula: $k = \Delta T / \Delta P$ (℃/W) , where ΔT is the steady state temperature difference before and after the laser was turned on; ΔP refers to a change in laser power. But here it is the input laser power. In the laser working model of 900 V and pulse frequency of 15 s^{-1}, the heating coefficient in this system is 117±10℃/W.

2.2.2 Laser Stimulation of Pd hydride formation with different loading ratios

A laser beam was turned on and off repeatedly on the same spot of the same Pd wire for the same period (1 hour), but the loading ratio of the wire was different each time. The loading ratios of 0.2, 0.3, 0.4 and 0.8 of hydrogen in palladium were taken into account. As a typical result, the corresponding change of palladium temperature with different loading ratio when the laser irradiated the Pd sample are shown as in Figure 2.

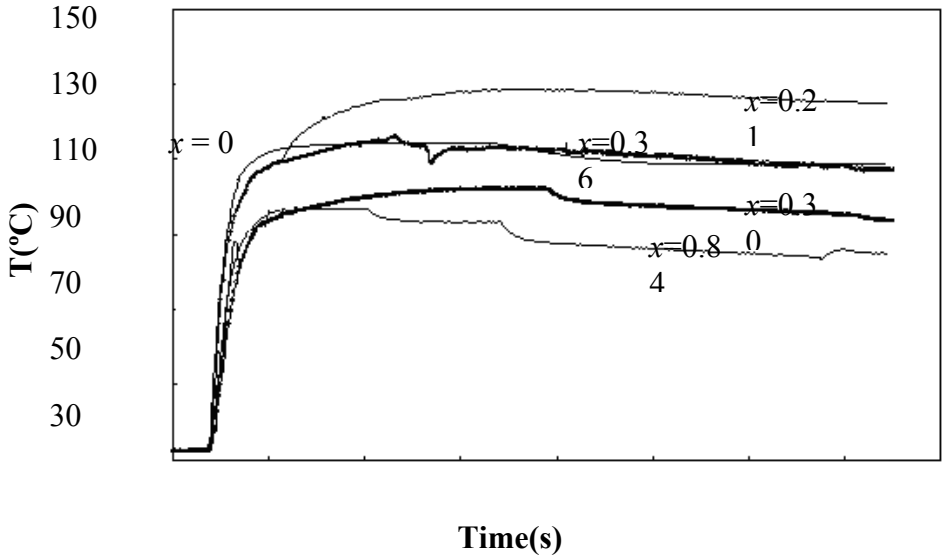

Figure 2 *Temperature of a Pd wire with various loading ratio after irradiation with a YAG laser (Power = 0.70W, V = 900 V, Pulse Frequency = 15s^{-1}). There is no significant excess thermal power in this data*

2.2.3 Topography and surface composition of Pd wire after gas-loading and laser irritating
The Pd wires were examined by SEM and EDS after hydrogen gas-loading, along with an as received Pd wire which served as a control. The samples were not cleaned before each examination. New surface topographical features with concentrations of unexpected elements, for example Ag and Cd, appeared after gas-loading. The Pd wire topography and microchemical composition before and after H gas-loading are given in Figures 3□4 and 5.

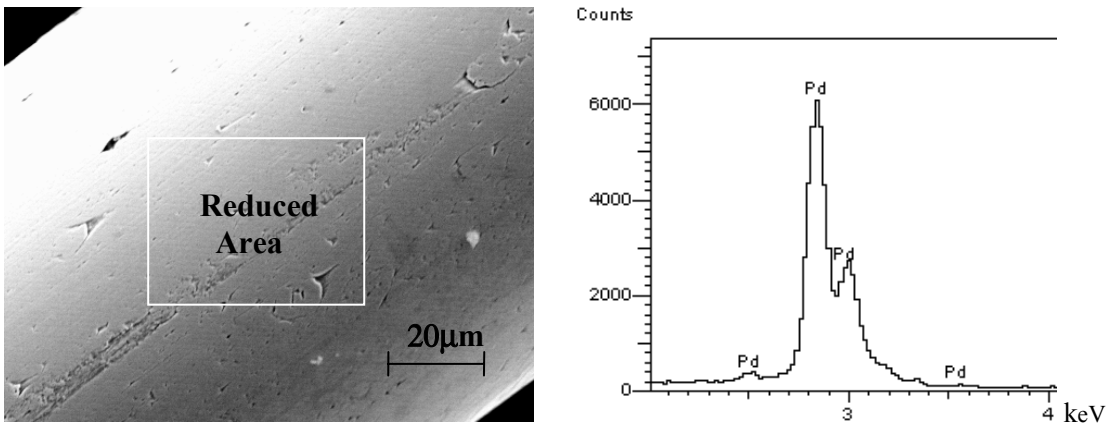

(a) (b)

(a) An image of the surface of an as received palladium wire
(b) The spectrum from the reduced area in the image of palladium wire. The pits in the reduced area contained impurities such as Si, but there was no Ag or Cd..

Figure 3 *The image and spectrum of Pd original sample before H_2 gas-loading*

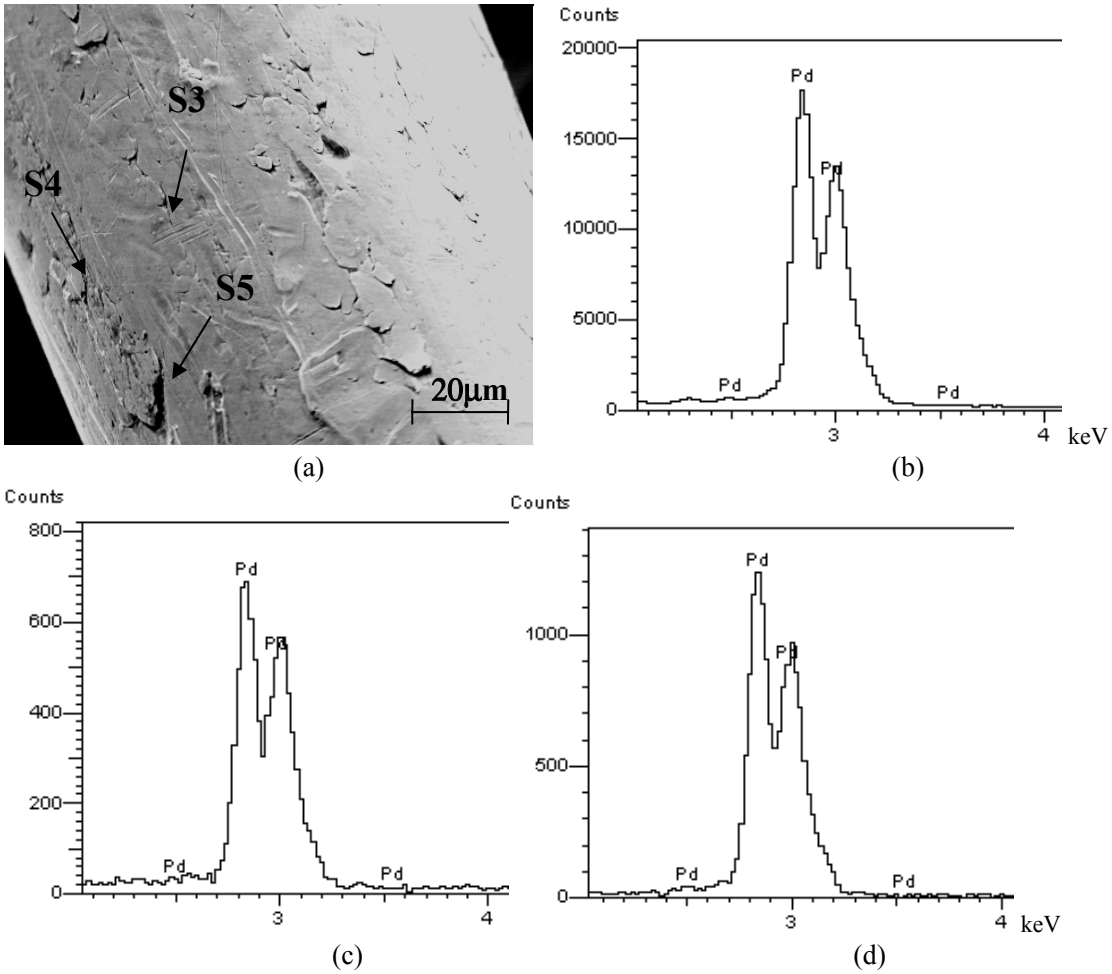

(a) The image of the surface of Pd sample after H_2 gas-loading
(b) The spectrum of spot 3 in above image
(c) The spectrum of spot 4 in above image;
(d) The spectrum of spot 5 in above image.

Figure 4 *The image and spectrums of surface of Pd sample after H_2 gas-loading 10 times*

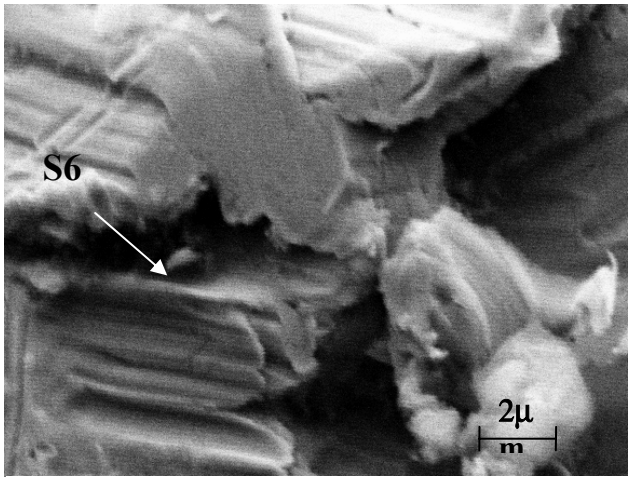

(a)

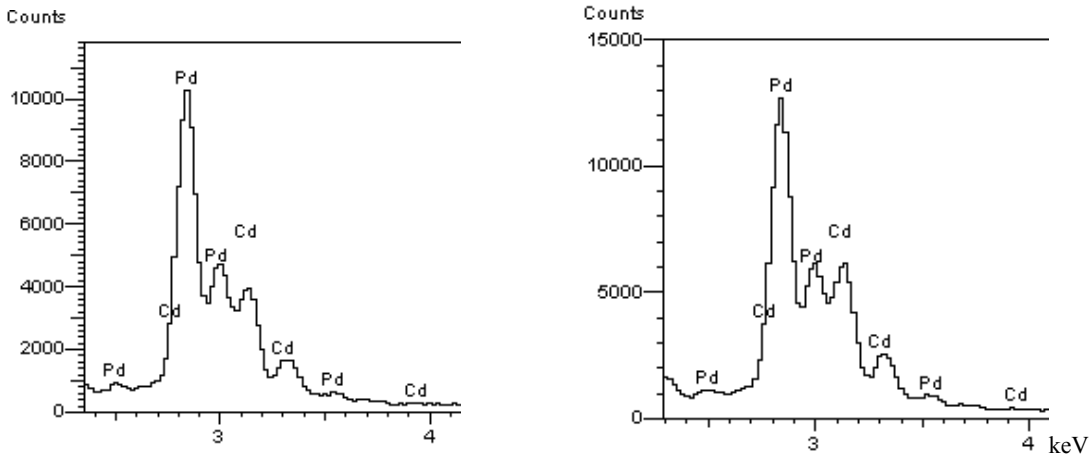

(a) An image of the surface of a Pd wire after H_2 gas-loading more than 20 times
(b) The spectrum of s6 in above image taken on Mar 23, 2007
(c) The spectrum of s6 in above image taken on Mar 26, 2007

Figure 5 *An image and spectrums of surface of Pd sample after H_2 gas-loading*

3 Analysis and discussion

3.1 Variation of excess heat with the loading ratio of Pd hydride and pulse frequency of a laser

From Figure 2 we can see that when the loading ratios were between 0.2 and 0.4, the Pd wire sometimes showed an exothermic behavior when it was irradiated with a YAG laser. In 60 experiments 13 of them produced exothermic behavior and their loading radios were located within this range. When the ratio was more than 0.8, the system had no exothermic behavior. It can be concluded that in this Pd/H system, a relatively low loading ratio can produced exothermic behavior. But in these 13 cases there were 10 times experiments which showed excess heat in the higher pulse frequencies of the laser. The explanation for this phenomenon is not clear at present.

3.2 Rough estimation for excess heat in the experiment

When the laser beam passed through the glass wall, there was a spot on the surface of Pd sample. The volume of Pd being irradiated was only about one fifth (9mm)of the whole wire. The number of Pd atoms is about 1.0×10^{20}. If they all combined with hydrogen atoms to form palladium hydride they would release heat of formation of about 6.4 joule, which corresponds to about 6.4×10^{-20} for each PdH. When the loading ratio is 0.3, as in our experiment for example, there should be 3.0×10^{19} hydrogen atoms dissolved in the bulk of palladium lattice, that is to say they would release 1.9 joule when these hydrogen atoms combined with Pd. But we measured 232.4±0.3 joules heat released from the experiment that had the most significant exothermic behavior, which corresponds with 7.73×10^{-18} joule per atom Pd. Obviously the heat we get in experiment is about 130 times more than that released in the formation of a PdH_x (x=0.3).

However, the of temperature of the Pd wire varied greatly (more than ±10℃) at high temperature (T > 100℃) duo to the instability of the laser power output. Also some H_2 was released from the Pd bulk when it was being irradiated. Because of the large uncertainty in the measurements, we will not make claims of excess heat in this paper.

Surface topographical and composition change before / after the Pd was gas-loaded with H

Surface topography change

In Figure 3(a) and Figure 4(a) (same magnification) the surface feature of Pd sample was obviously different before and after it had absorbed some certain amount of hydrogen gas. The surface became coarser than before gas-loading. There were some holes and cracks formed when the hydrogen was absorbed into the palladium lattice. This made hydrogen loading into palladium easier afterwards. That is to say, it would take less time (at least one fourth) that taken in the first time.

Surface microchemical composition change

The original Pd wire was checked by SEM and EDS before gas-loading. Eight spots were chosen for the test. All of the results showed that there nearly was 100% Pd in the sample. (see Fig.3(b)). After loading H into Pd, silver appeared in localized places like dark pits and dark cracks. The highest composition of Ag was as high as 12.79% (Fig.4 (a)s4, (b)). When the sample experienced gas-loading for longer time, for example more than 20 times, cadmium appeared in the place where Ag was usually found before. Furthermore, the concentration of Cd became higher as the time increased. The data showed that the concentration increased from 10.48% (Fig.5 (b)) during the time it was checked at beginning to 12.62% (Fig.5(c)) three days after. The detailed results could be referred in Table 1.

Table 1 The concentration of new elements on the Pd surface after H gas-loading

New element	*Element Content(%)*	*Sigma (%)*	*Atomic Ratio*	
			Ag/Pd	*Cd/Pd*
Ag	5.12	0.14	0.23	-
Ag	8.20	0.91	0.29	-
Ag	12.79	1.04	0.26	-
Cd	10.48	0.27	-	0.31
Cd	12.62	0.24	-	0.41

4. Conclusions

The following are possible conclusions which can be drawn from the experiments above:

4.1 A high loading ratio may not be a necessary condition for excess heat production. There may be an optimum ratio for each specific experimental condition.

4.2 The results of SEM and EDS reveal new elements on the palladium surface, such as silver, cadmium. These elements are clustered in localized, microscopic surface features such as cracks or pits. These elements were not found on the wires before loading.

References

1. D. Letts and D.Cravens, Laser Stimulation of Deuterated Palladium: Past and Present. Infinite Energy, 50 (2003) p10
2. V.Violante, , M.Bertolotti, E.Castagna, I.Dardik, M.McKubre, S.Moretti, S.Lesin, C.Sarto, F.Tanzella, T.Zilov. Progress in Excess Power Production by Laser Triggering, Proc. of 12th Int. Conf. on Cond. Matt. Nuc. Sc. (ICCF-12), Yokohama, Japan, Nov. 27 - Dec. 2, 2005. p55
3. K. P. Sinha and A. Meulenberg, Laser stimulation of low-energy nuclear reactions in deuterated palladium. Current Science, Vol. 91, No. 7, Oct.10, 2006. p907
4. Dash, J. and A. Ambadkar. Co-Deposition of Palladium with Hydrogen Isotopes. The Proceedings of 11th International Conference on Condensed Matter Nuclear Science. 2004. Marseille, France. p477
5. C. Cano, Comparison of Heat Output and Microchemical Changes of Palladium Cathodes under Electrolysis in Acidified Light and Heavy Water. Master of Science Thesis, Portland State University, 2002. p148

EXCESS HEAT POWER REGISTRATION IN HIGH VOLTAGE ELECTROLYSIS AND DISCHARGE SYSTEMS

A. B. Karabut

FSUE "LUCH" 24 Zheleznodorozhnaya St, Podolsk, Moscow Region, 142100, Russia.
Tel. (095) 5508129; Fax (095) 5508129; ***E-mail*** *7850.g23@g23.relcom.ru*

The Excess Heat power was registered in experiments with high-current Glow Discharge and High-Voltage Electrolysis (up to 1000 V). The experiments showed that the maximum Excess Heat power values of 5 –15 W for Glow Discharge and 180-280 W for High-Voltage Electrolysis, and Efficiency up to 160% for Glow Discharge, and 800% for High-Voltage Electrolysis, respectively, were registered at the anode/cathode voltage ranging 1000-1300 V

The X-rays were recorded during the Glow Discharge operation and after the Glow Discharge current switch off. Presumably the observed X-ray emission proceeds as a result of relaxation of excited energetic levels in the cathode solid medium. These excited levels are formed during the exposure of the cathode sample solid surface to the effect of the ions flux produced by plasma or electrolyte medium.

Hypothetical diagram (phenomenological model) Low Energy Nuclear Reaction realization in cathode solid medium of electric discharge systems for energy triggering (from 10 - 100 eV and up to 3000 eV) are discussed.

1.Introduction

The previous experiments showed what The Excess Heat value on the cathode of electric discharge systems depended of the discharge voltage value (ions flux energy). For the greater part the electric discharge systems experiments (typical electrolysis, electric discharge electrolysis) realize for low voltage (10 - 100 V). The HighVoltage was used in High current Glow Discharge experiments [1]. G.Kazyonov. These results permit to estimate the values of Excess Heat and

2.Excess Heat Registration in High Voltage Electrolysis Experiments

The Pd cathode emission spectrum shows that the most intensive radiation comes from Pd excited level ranging 1.2 – 1.5 keV. The highest Excess Heat values in high-current Glow Discharge were registered at 1100 - 1300 V Glow Discharge voltage (the energy of plasma deuterium ions bombarding the cathode surface). These results are in good agreement with Excess Heat measurements obtained in experiments with high-voltage electrolysis at cathode-anode voltage up to 1000 V. There were two sets of high-voltage electrolysis experiments with different types of electrolytic cells.

The first set of experiments involved an electrolytic cell designed as a heat capacity calorimeter. The cell designed as a water-cooled flow calorimeter was used in the second set of experiments.

2.1. Experiments with High Voltage Electrolysis Device as a Heat Capacity Calorimeter

The high-voltage electrolysis device consisted of a quartz tube with an additional circuit for a working fluid (Fig.1). The anode and cathode units were placed inside the tube. To circulate the working fluid a mixer was installed inside the circuit. The quartz tube was also provided with a thermocouple.

Four sets of experiments were carried out at the following HVE operating parameters:

1) Electrolysis in light water (H_2O) with a Pd cathode.
2) Electrolysis in light water (H_2O) with a Cu cathode.
3) Electrolysis in heavy water (D_2O) with a Pd cathode (not pre-treated Pd).
4) Electrolysis in heavy water (D_2O) with a Pd cathode (pre-treated Pd cathode by saturation in heavy water for a month).

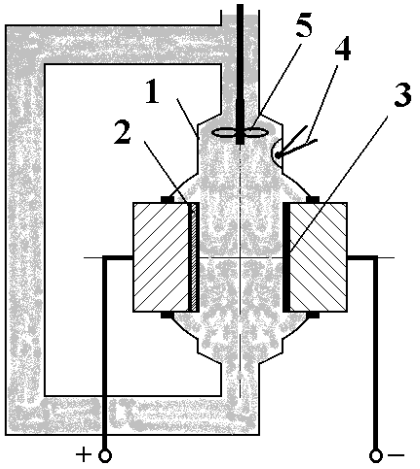

Fig.1 *. The outline of High Voltage Electrolysis device (heat capacity calorimeter): 1 – the quartz tube and the circuit with the working liquid (H_2O or D_2O), 2 – the anode, 3 – the mixer, 4 – the cathode, 5 –the thermocouples of the working liquid.*

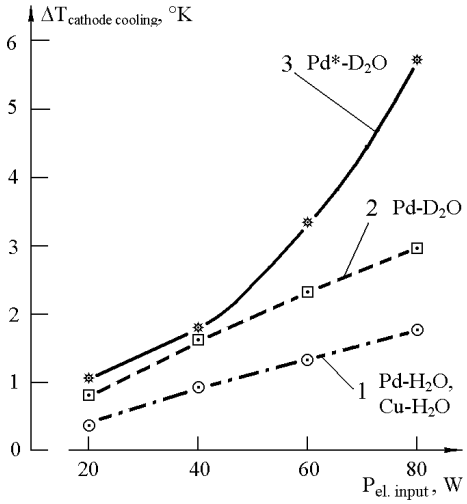

Fig.2. *Dependence of the water heat up value t (in the circuit with the working liquid, H_2O or D_2O) upon the input electric power. 1 – represents electrolysis in light water (H_2O) with the Pd and Cu cathode;*
2 – stands for electrolysis in heavy water (D_2O) with a Pd cathode (not pre-treated); 3 shows electrolysis in heavy water (D_2O) with a Pd cathode (pre-treated Pd).

The experimental procedure used was the following: In all the experiments the electric power input into the cell was constantly maintained at the same level for all types of cathodes and working liquids. During electrolysis the working liquid was kept heated. The time and temperature parameters of the working liquid were repeatedly recorded during the experiment. The electrolysis was stopped when the electrolyte temperature ran up to 80 ° C. Four different tests involving particular discreet electric power values of 20 W; 40 W; 60 W

and 80 W were carried out for each experimental system (specific cathode material and particular kind of electrolyte). The electrolyte temperature/time gradient (the electrolyte heating rate) was determined on the basis of experimentally established correlation between the electrolyte temperature versus time for each system and the cathode material versus kind of electrolyte and the electric power discreet value for a given experiment.

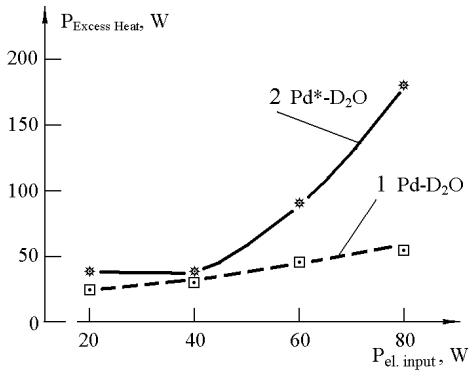

***Fig.3**. Excess Heat power value as a function of the input electric power. 1 – represents electrolysis in heavy water (D_2O) with a Pd cathode (not pre-treated Pd); 2 – shows electrolysis in heavy water (D_2O) with a Pd cathode (pre-treated Pd).*

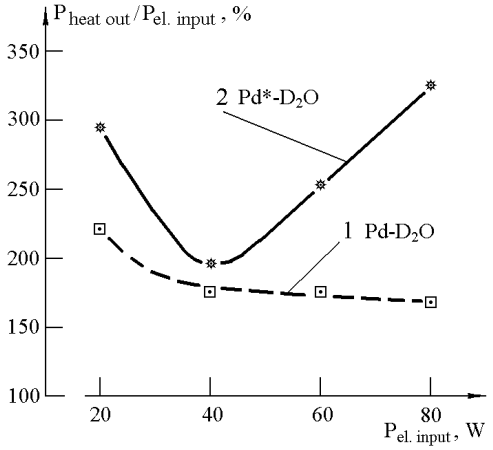

***Fig.4.** Dependence of Heat Efficiency value of the input electric power.*
1 – electrolysis in D_2O with a Pd cathode (not pre-treated Pd);
2 – represents electrolysis in heavy water (D_2O) with a Pd cathode (pre-treated Pd).

The data shows that in case of two systems: heavy water (D_2O) with Pd cathode and heavy water (D_2O) with Pd cathode (pre-treated Pd cathode by saturation in heavy water for a month) the electrolyte heating rate was several times higher than the temperature/time gradient for other systems: light water (H_2O) with Pd cathode and light water (H_2O) with Cu cathode (Fig.2). Presumably, this difference (exceeding) of temperature gradient for heavy water (D_2O) with Pd cathode is accounted for by the production of Excess Heat power in the cell.

The following procedure was used to evaluate Excess Heat power and Heat Efficiency: the change in thermal energy of electrolytic cell ($\mathbf{\Delta Q_{heat}}$) relative to time ($\mathbf{\Delta\tau}$) occurs due to (results from) the input electric power ($\mathbf{P_{el}}$) and the Excess Heat power ($\mathbf{P_{EH}}$) produced in the cell.

$$\frac{\Delta Q_{heat}}{\Delta\tau} = m \cdot c_p \frac{\Delta T}{\Delta\tau} = P_{el} + P_{EH} \qquad (1)$$

Here **m** stands for the effective mass of the cell-calorimeter; **Cp** represents the efficiency coefficient of the calorimeter mass heat capacity; **ΔT** shows the electrolyte temperature change relative to time $\Delta\tau$.

Let us denote the time/temperature gradient for each cathode/ electrolyte system as a coefficient "K". Then: $K_{Pd\text{-}H20} = (\Delta T/\Delta\tau)_{Pd\text{-}H20}$; $K_{Pd\text{-}D20} = (\Delta T/\Delta\tau)_{Pd\text{-}D20}$.

Assuming that no Excess Heat power is produced in using light water (H_2O) with Pd cathode system we arrive at $P_{EH} = 0$.

The change in electrolytic cell thermal energy for heavy water (D_2O) with Pd cathode system may be represented as:

$$K_{Pd-D2O} = m \cdot c_p \frac{\Delta T}{\Delta \tau} = P_{el} + P_{EH} \qquad (2)$$

The change in electrolytic cell thermal energy for light water (H_2O) with Pd cathode system may be termed as:

$$K_{Pd-H2O} = m \cdot c_p \frac{\Delta T}{\Delta \tau} = P_{el} \qquad (3)$$

The Excess Heat power value is equal to:

$$P_{EH} = P_{el} \cdot \left(\frac{K_{Pd-D2O}}{K_{Pd-H2O}} - 1\right) \qquad (4)$$

Thermal Efficiency (correlation of the thermal power produced in the system to the input electric power) is determined by the expression:

$$\eta = \frac{K_{Pd-D2O}}{K_{Pd-H2O}} \cdot 100\% \qquad (5)$$

In experiments with the Cu cathode in light water the results obtained are similar to those recorded with the Pd cathode in light water. Considerable increase in Excess Heat power and Heat Efficiency is recorded for Pd cathode pre-treated by saturation in D_2. Excess Heat power and Heat Efficiency values are lower in experiments with cell-calorimeter without thermal insulation (from the environment) (Fig.3, Fig.4).

2.2.Experiments with High Voltage Electrolysis Device as a Flow Calorimeter

The high-voltage electrolysis device (as a water-cooled flow calorimeter), consisted of a quartz tube with an additional circuit for a working fluid (Fig.5). The anode and cathode units were placed inside the tube. To circulate the working fluid a mixer was installed inside the circuit. One side of the flat cathode was washed by the working liquid, while the other side of it was cooled by the water flowing in a cooling tube. Thermocouples connected differentially were placed inside the water-cooling passage to take the difference in the cooling water temperature input and output. The cooling water consumption on the cathode was the same in all the experiments. High-voltage power supply (up to 5 kV at current values up to 100 mA) with a series-connected limiting resistor was used to feed the high-voltage electrolysis device.

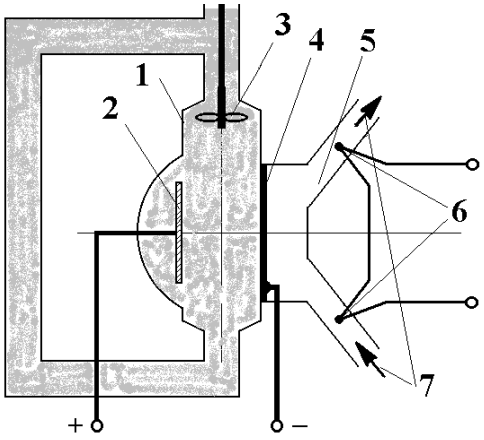

Fig.5. *The outline of High Voltage Electrolysis device (flow calorimeter): 1 – the quartz tube and the circuit with the working liquid (H_2O or D_2O), 2 – the anode, 3 – the mixer, 4 – the cathode, 5 – the cathode water cooling passage, 6 – the input and output thermocouples of the cathode water cooling passage.*

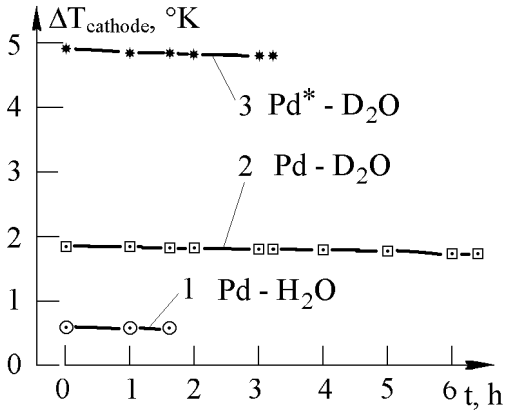

Fig.6. *Dependence of the water heat up value t (in the cathode cooling system) upon the experimental time.*
1 – represents electrolysis in light water (H_2O) with a Pd cathode;
2 – stands for electrolysis in heavy water (D_2O) with a Pd cathode (not pre-treated); 3 shows electrolysis in heavy water (D_2O) with a Pd cathode (pre-treated Pd).

The experiments were carried out using light and heavy water as a working liquid. By various techniques the voltage in the working liquid between the cathode and the anode was brought up to 800-1000 V. The electrolysis was effected without an electric discharge operating between the cathode and the anode. The water temperature inside the cooling passage was additionally controlled by mercuric thermometers.
Three sets of experiments were carried out at the following High Voltage Electrolysis operating parameters:
1) Electrolysis in light water (H_2O) with a Pd cathode.
2) Electrolysis in heavy water (D_2O) with a Pd cathode.
3) Electrolysis in heavy water (D_2O) with a Pd cathode (pre-treated Pd cathode by saturation in heavy water for a month).

The procedure of the Pd cathode pre-treatment was the following. First electrolysis was carried out with a Pd cathode in D_2O, then the Pd cathode was left for a month immersed into D_2O. The electrolysis with thus pre-treated Pd cathode was carried out alongside with measurements of electric power, and the water temperature in the cathode cooling passage. In all four cases the cathode was cooled by the tap water. The water consumption in the cathode cooling passage was the same in all the experiments. The electric power of electrolysis used in experiments with the pre-treated Pd cathode was approximately by 2 – 2.5 times less. The relative value of the output power was determined by the difference between the input and output water temperature in the cathode water cooling passage.

The following coefficient (k) of relative heat output was used:

$$k = \frac{\Delta t_{D2O} \cdot W_{el.H2O}}{\Delta t_{H2O} \cdot W_{el.D2O}} \qquad (6)$$

Here $t = (t_{out} \quad t_{in})$ represents water heat up in the cathode water cooling passage; $W_{el.}$ stands for the electric power input into the electrolytic cell in the experiments with heavy and light water, respectively.

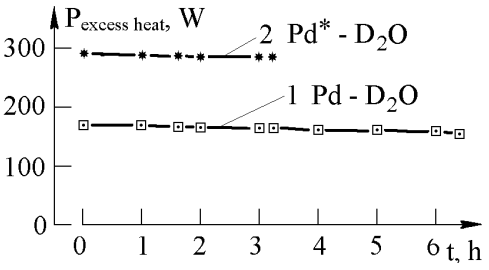

Fig.7. *Excess Heat power value as a function of experimental time. 1 – represents electrolysis in heavy water (D_2O) with a Pd cathode (not pre-treated Pd); 2 – shows electrolysis in heavy water (D_2O) with a Pd cathode (pre-treated Pd).*

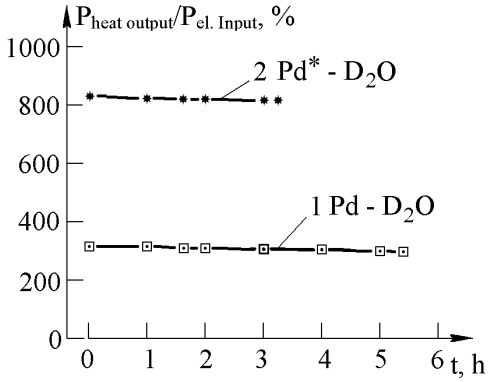

Fig.8. *Dependence of Heat Efficiency value upon the experimental time.*
1 – shows electrolysis in heavy water (D_2O) with a Pd cathode (not pre-treated Pd); 2 – represents electrolysis in heavy water (D_2O) with a Pd cathode (pre-treated Pd).

The above experimental results may be represented in terms of Excess Heat power and Efficiency values. The term Heat Efficiency implies correlation between the heat power output into the cathode water cooling system and the electric power input into the electrolytic cell during electrolysis. It may be assumed that the electric power input into the electrolytic cell, and the heat power produced in the cell are carried away by the water of the cathode cooling system. Then the Excess Heat power produced in the electrolytic cell will be determined by the following expression:

$$P_{E.H.} = P_{el.} \cdot (k \quad 1) \qquad (7)$$

And the Heat Efficiency will be equal to

$$\text{Efficiency} = k \cdot 100\%$$

Thus adapted experimental data is presented on the graphs (Fig.7 – Fig.8).

3. Excess Heat Registration in Glow Discharge Experiments

Measurements of Excess Heat power were carried out in experiments with high-current Glow. The Excess Heat registration were carried out using the glow discharge device. The pulse-periodic electric power supply was used. The big values of Excess Heat power (5 –15 W) and Efficiency (160%) were observed in conditions when the Glow Discharge operational voltage ranged 1000 - 1300 V (Fig.9, 10).

The Glow Discharge voltage area (D_2 ions energy) correspond X-ray emission energy from Pd cathode (Fig.10).

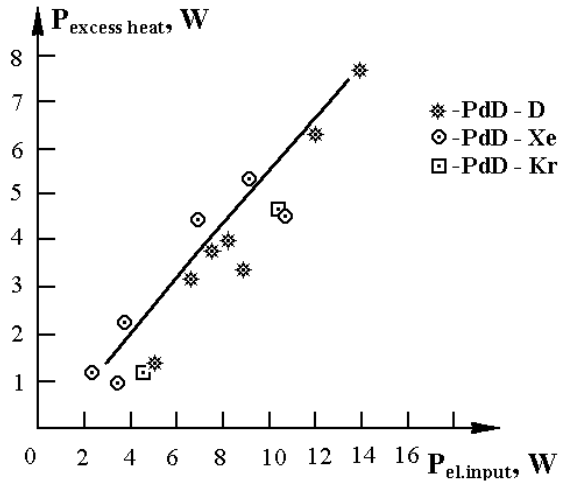

Fig.9*-. a-Excess Heat Power in relation to the input electric power.*

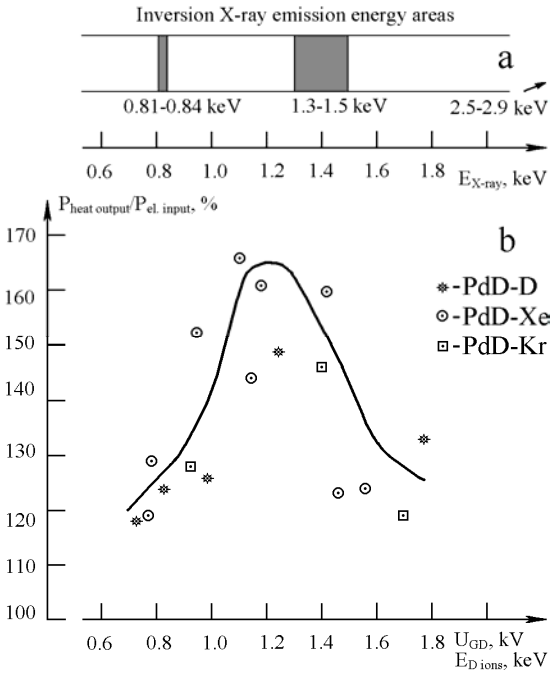

***Fig.10**. a-X-ray emission energy by the curved mica crystal X-ray spectrometer. b-Dependence of the output heat power and the input electric power ratio of the Glow Discharge voltage (deuterium ions energy) . Deuterium pre-charged Pd cathode samples in D_2, Xe and Kr discharges.*

4. X-ray energy registration

The registration of X-ray emission energy was performed using Al_2O_3-based TLD (Thermo-Luminescent Detectors) with the different thickness absorb Be foil, photomultipliers scintillating detectors with the absorb Be foil and by the X-ray spectra were recorded using the curved mica crystal X-ray spectrometer positioned on an X-ray film. The experimentally determined value of the X-ray energy increased from 1.5 to 2.0 keV when the thickness of the Be shield increased from 15 m to 30.0 m. The X-ray energy values obtained with the help of photomultiplie scintillator detectors and 15 m and 30 m- thick beryllium foils amounted to $E_{X\text{-}ray} \approx 1.0 – 2.0$ keV. The spectrum was registered both as bands of the continuum with energies ranging 0.6 - 10.0 keV and as spots resulting from the emission of series of high-density mono-energetic X-ray beams (with energies up to 0.6 - 10.0 keV) characterized by small angular divergence, which showed good agreement with the TLD and photomultiplier scintillating detectors data (Table 1).
(Table 1).
The spectrum band (ranging in energy 1.3 – 1.6 keV) was defined for Pd cathode samples in D_2 and Kr Glow Discharge (during its operation, and after, the discharge current switch off) . This result is in good agreement with the maximum value of Excess Heat power at 1000 - 1300 V Glow Discharge voltage (Fig.5.).

Table 1. X-ray energy was registered different metods.

Method of X-ray emission energy measurement	Thermo-Luminescent Detectors with Be foils screen	Photomultiplier scintillating detectors with Be foils screen	Curved mica X-ray spectrometer
X-ray energy during the Glow Discharge Operation in Pd – D	1.3 – 1.8 keV	2.0 keV	1.7 – 1.8 keV 1.3 – 1.6 keV

5. Discussion

The results of experimentation allow to draw up the following basic conclusions:

The energy and temporal characteristics of the X-ray emission from the cathode ranging 0.5 – 10.0 keV has been recorded in experiments with high-current Glow Discharge. The said X-ray emission is characterized by the following peculiarities:

1) X-rays are observed as separate X-ray bursts (up to $5 \cdot 10^5$ bursts a second and up to 10^6 X-ray quanta in a burst);
2) The emission of X-rays occurs during the Glow Discharge operation, and, after the Glow Discharge current switch off (up to 100 ms and more).
3) The X-ray emission is observed during the Glow Discharge operation in D_2,H_2 and in inert gases such as Ar, Kr and Xe.
4) The X-ray emission spectra include bands and spots within 0.5 – 10.0 keV energy range.
5)The emission spectrum consists of energetic bands specific for the cathode material used. The energy of spectral bands shows a considerable difference from M, L transition energies of electronic shells of a given cathode material.
6) Spectral bands with energies exceeding several times the energy of ions bombarding the cathode surface are registered.
7) The X-ray emission temporal characteristics (the number of X-ray bursts, the number of X-ray quanta in a burst, the time interval between the bursts) are specific for each cathode material used in experiments.

These experimental results show that the said X-ray emission is not a deceleration X-ray formed in cathode bombardment by plasma discharge ions. Presumably, some excited energetic levels are formed in the cathode solid when its surface is exposed to bombardment by the ions flux generated in plasma or electrolyte medium. The X-ray emission occurs as a result of de-excitation of these energetic levels. And as the energy of the said levels does not correlate with the energy of L,M transitions the physical nature of these phenomena remains unclear and requires additional investigation.

It may be assumed that the availability of 0.5 – 10.0 keV excited energetic levels in the cathode solid medium triggers LERN resulting in production of Excess Heat energy and nuclear ash in the volume of solid-state cathode medium..

8)The Excess Heat Power up to 10 –15 W and efficiency up to 150 % was recorded for the preliminary deuterium-charged Pd cathode samples in Xe and Kr Glow Discharges.
9)The Excess Heat Power up to 200 –280 W and efficiency up to 800 % was recorded for the preliminary deuterium-charged Pd cathode samples in High Voltage Electrolysis.
10)The Excess Heat Power maximum values were recorded at the Glow Discharge and High Voltage Electrolysis operational voltage ranging 900 – 1300 V.

11) The production of ^{4}He and impurity nuclides registered into the cathode in experiments with higt-current Glow Discharge [3].
12)The production of impurity nuclides occurs in the volume of the solid-state cathode medium.
13)The impurity nuclides are produced with changed natural isotopic impurity ratio (up to several tens of times) (Ca, Ti, Fe, Ni, Ge and others) [3].
14) Some basic isotopic impurities (with high natural abundance) not being observed. The absence of the following isotopes: ^{58}Ni, ^{70}Ge, ^{73}Ge, ^{74}Ge, ^{113}Cd, ^{116}Cd was registered. The production of some isotopes ^{13}C, ^{57}Fe, ^{48}Ti in large qualities is typical for these processes [3].
15) The emission of high-energy heavy ions was not recorded in the experiment. This allows to assume, that the nuclear reactions energy was not released as a kinetic energy of the formed impurity nuclides. The impurity nuclides may be assumed to form as nuclear isomers (the nuclei being in the excited state). The Experimental results show that the relaxation of these excited nuclear levels through the gamma- radiation channel was strongly suppressed.

The obtained experimental results allows to consider the possible energy processes in the cathode material solid. The following processes may lead to initiation of Low Energy Nuclear Reactions:

- Deuterium ions acceleration in the Glow Discharge near-cathode area to energies from several hundred eV up to a few thousand eV.
- Non-resilient processes of deuterium ions collision with the crystal lattice ions (Pd^{4+} ions for Palladium). These processes cross-section related to non-adiabatic transition is determined according to Massey criterion ξ. For ΔE = 0.7-1.5 keV (the near-cathode discharge conditions) the Massey criterion $\approx$ 1 and the non-resilient processes cross-section for optic polar phonons formation becomes close to gaso-kinetic one. Under these conditions the electron frame is displaced relative to nucleus and a dipole or optic polar phonon is formed. The initial optic polar phonons frequency is ω_{op}. At energies W=1keV $\omega_{op} = 0.95 \times 10^{19}$ sec^{-1} which is higher than the plasma frequency $\omega_p = (1.3\text{-}2.5) \times 10^{16}$ sec, plasmones are not produced and there is no compensation for the arising spatial division of charges.
- At big concentration of initial optic phonons (high charge current density) non-linear unharmonic processes start playing their essential part. Presumably, processes of the 3-rd and the 4-th order begin.

$$h\omega_{1\,in} + h\omega_{2\,in} \rightarrow h\omega_3 \quad \text{and} \quad \omega_1 < \omega_3 > \omega_2$$
$$h\omega_{1\,in} + h\omega_{2\,in} + h\omega_{3\,in} \rightarrow h\omega_4 \quad \text{and} \quad \omega_1 < \omega_4 > \omega_2, \ \omega_4 > \omega_3$$

These expressions mean that two ($h\omega_{1\,in}$, $h\omega_{2\,in}$) or three primary phonons are combined and formed into one $h\omega_3$ or $h\omega_4$. In this way out of a bog number of primary phohons with energies of 0.7 - 1.5 keV a small number of high energy phonons (up to tens and hundreds keV) is formed. The primary phonons energy spectrum is displaced in the direction of bigger values.

Presumably, some long-lived excited levels with energies up to several keV are formed in the cathode solid by the primary and secondary optic phonons energy. The excited energy levels for Pd are 0.8 – 0.84 keV, 1.3 – 1.5 keV, 2.5 – 2.9 keV.

- The non-equillibrium excited energy states with the population density of n_{exit} [cm^{-3}] and a characteristic temperature of $T_{exit} \approx 1.0 - 3.0$ keV, and more, were formed the conditions for the Low Energy Nuclear Reaction realization.

To determine the specific physical mechanism for these reactions requires some additional research. One possible type of reaction for forming the impurity nuclides can be long-range (resonant) nuclear reactions.
The following types of nuclear reactions of transmutation resulting in formation of stable nuclides are possible:

1) $Pd + mD \rightarrow [\ PdmD]\ *$
2) $[PdmD]\ * \rightarrow D^* + {}^4He + Heat$
3) $[\ PdmD]\ * \rightarrow A^* + B^* \rightarrow A + B + Heat$
4) $[PdmD]\ * \rightarrow C + Heat$

Where[PdmD] * is a short-lived intermediate compound nucleus; m-1,2,3 ...; A*, B* denote nuclear isomers of nuclides with masses less than that of Pd; A,B are stable nuclides; C stands for a nuclide with a mass more than that of Pd. At first a composite compound-nucleus in excited state is formed. Then one of the three possible modes is realized:
1) the compound nucleus may lose its excitation and form a exited Pd nucleus and ^4He.
2)the compound nucleus may split into two nuclei fragments with masses less than that of Pd. In so doing the two nuclei should be in excited isomer state (experiments show that the nuclear reactions energy is not produced in the form of nuclear fragments kinetic energy).
3) the compound nucleus may lose its excitation and form a stable nucleus of a heavier than Pd element.
All this process stages present on the diagram (Fig.11).

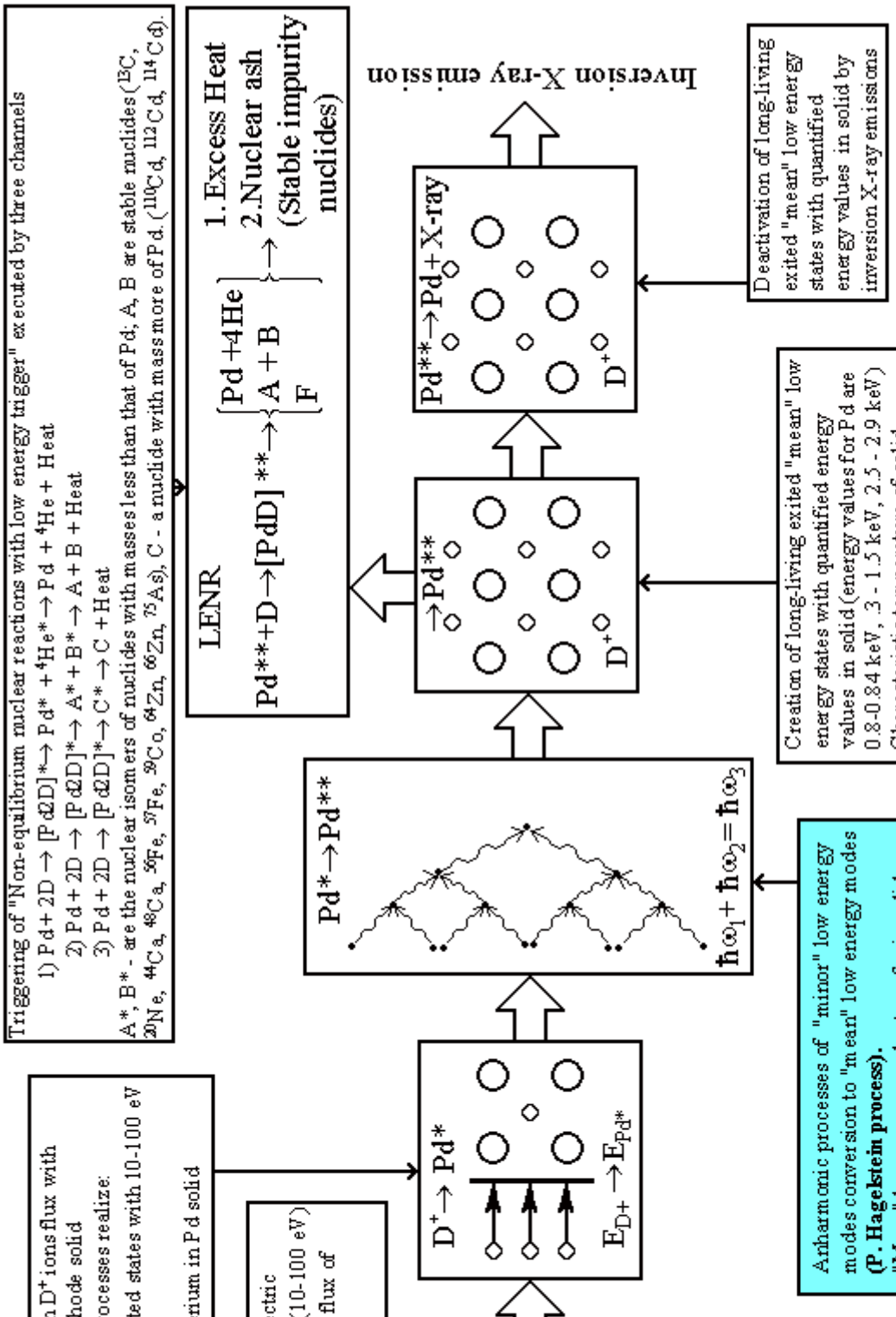

Fig.11. Hypothetical diagram (phenomenological model) Low Energy Nuclear Reaction realization in cathode solid medium of electric discharge systems for low energy triggering.

6. Conclusions

The results obtained the Glow Discharge Device producing Excess Heat power up to 5 W/cm^2 with Efficiency up to 150 % and the High Voltage Electrolysis device producing Excess Heat power up to 280 W with Efficiency up to 800 %) allow the development of a demonstration source of heat power. The development of new nuclear engineering is possible based on non-equilibrium nuclear transmutation reactions in the solid-state medium. This type of engineering may be termed as "The third way" in nuclear power-engineering as compared to that which is based on uranium nuclear fission, and thermonuclear synthesis.

References

1. Karabut A.B., Kucherov Ya.R., Savvatimova I.B.. Nuclear Product Ratio for Glow Discharge in Deuterium. Physics Letters A. 1992. V. 170. p.265,.
2. Karabut A.B.. Heat Energy Production Method. Patent #2240612, 20 November, 2004, Russian Federation.
3. Karabut A.B.. Research into low energy nuclear reactions in cathode sample solid with production of excess heat, stable and radioactive impurity nuclides. Proceedings of the 12th International Conference on Cold Fusion. December 2 – 7, 2006. Japan.
4. Karabut A.B.. Study of energetic and temporal characteristics of x-ray emission from solid-state cathode medium of high-current glow discharge. Proceedings of the 12th International Conference on Cold Fusion, December 2 – 7, 2006, Japan.
5. Kazennov G.F., Yeremyev A.V., Nikitenko A.A. et al. Experiments of anomalous output heat registration by electrolysis in heavy water. Proceedings of the 10-th Russian Conference on Cold Nuclear Transmutation of Chemical Elements and Ball Lightning, Dagomys, city of Sochi, September 29 – October 6, 2002, Russia, pp. 41 – 49.
6. Velikodnyj V.J., Yeremeyev A.V. Kazennov A.J. et al, Experiments of anomalous output heat registration by high voltage electrolysis heavy water (method detail). Proceedings of the 12-th Russian Conference on Cold Nuclear Transmutation of Chemical Elements and Ball Lightning, Dagomys, city of Sochi, September 19 –26, 2004, Russia, pp. 98 – 108.

DEVELOPMENT OF MULTI-PURPOSE INSTALLATIONS FOR ENERGY GENERATION BY WAY OF COLD NUCLEAR SYNTHESIS

A.I.Koldamasov, N.J.Bakumtsev

Nuclear Society of Russia
Intellectual International Foundation «Revision of Natural Sciences»
International Academy of scientific Discoveries and Inventions
Molodezhnaya str., 9-25, Volgodonsk, Rostov region, 347382, Russia, tel. +7(86392) 49483;
bakumtsev@vdonsk.ru

Abstract

This work gives with a brief review of processes of cold nuclear fusion on the basis of water with mixture of heavy deuterium water. The data are obtained on the real author's research installation.

The nuclear fusion is activated in "Koldamasov's cell" by cavitations and external electromagnetic field. Cavitations cause the generation of water drops (mist spray) with radius R_d and perimeter of drops ~ 6 λ_{el} . The radius is proportional to the wave length of electromagnetic radiation $R_d \sim \lambda_{el}$. The local self-interference results increase the local electromagnetic radiation energy density by many orders of magnitude and that is higher than the energy necessary for nuclear fusion ($W \gg 6{,}8 \cdot 10^8$ kilojoule/cm^3).

The high energy density causes intense optical pressure and appearance of blast waves and (or) of cumulative effects, self-synchronization of waves and resonance and processes of self-sustaining reaction. Ultrahigh optical pressure appears in the fusion zone, bringing together nuclei in the field of nuclear reaction.

The power intensity of nuclear fusion reaches $W \gg 6{,}8 \cdot 10^8$ kilojoule/cm^3 and optical pressure $P_{opt.pressure} = W \cdot 10^4$ kgs/cm^2 . The nucleus fusion follows the atoms micro explosions of nana drops with energy generation. The invention is protected by patents of the Russian Federation which refer to the reactors of cold nuclear fusion of multi – purpose modifications including those for generating hydrogen.

The design and manufacturing parameters and ways of their improvements for energy generation have been found. The data for calculations and other design basis data for development of pilot multi – purpose energy generation equipment have been obtained.

Introduction

Cold nuclear fusion hardly carves its way in the minds of academic science, therefore it would not be out of place to start statement of the article from the nuts and bolts of nuclear physics and chemistry.

The atoms nuclei consist of protons and neutrons, united together by nuclear forces. Nuclear forces are so strong, that electrostatic repulsion between the positively charged

protons which obey to the Coulomb's law, cannot overcome them and a nucleus exists as a single whole particle.

Nuclear forces act at very small distances, at an order of 10^{-11} 10^{-13} cm, and electrostatic forces show their worth both at small and large distances [1].

The energy which should be spent for fission of the nucleus into component parts (for protons and neutrons) is called bonding energy. This bond is broken down when nuclei are fused or destructed. A definite part of the energy in these processes released into environment. When nuclei are fused the energy released is three-orders larger than the energy released at nuclear fission reactions, and considerable increase of kinetic speed of reaction products ^{3}He, ^{3}T^1, ^{4}He occur. Thus, at fusion of hydrogen isotope nuclei –deuterium (a), consisting of proton (p) and neutron (n), and tritium (t), consisting of proton and two neutron under terrestrial conditions is emitted in the form of kinetic energy of final products [2]:

$$\begin{aligned} a + a &\rightarrow {}^3\text{He} + n + 3{,}3\ \text{MeV}, \\ a + a &\rightarrow {}^3\text{T}^1 + p + 4{,}0\ \text{MeV}, \\ a + t &\rightarrow {}^4\text{He} + n + 17{,}6\ \text{MeV} \end{aligned}$$

For comparison, the standard combustion reaction on which mainly the power engineering of the Earth civilization is based, emits $C + O_2 \rightarrow CO_2 + 4{,}2$ eV, that is million times less.

By this reason the nuclear fusion reactions are attractive. At fusion of deuterium nuclei available in a liter of heavy water the energy released is equal to the energy of combustion of a million liters of benzene, and without emission of hydrogen dioxide and toxic impurities, that takes place at benzene combustion. Neutrons, emitted at fusion, are liable to β-decay with a half-life period of 12,8 min.: $n \rightarrow p + e^- + \nu^-$, products of which are proton, electron and neutrino. In a free form a neutron exists for not more than 10^3 s.

When nuclear fusion reactions are taken under control they become environment friendly. Deuterium, as an active fusion component, is contained in ordinary light natural water, that is why the deuterium reserves on the Erath are considered huge, even with account of its insignificant contents (about 0,03%) in the Earth water, and the market price of deuterium amounts to approx. U.S.D. 400.00 per liter.

The problems of nuclear fusion were subjects of active discussions at annual international scientific symposia "Reconstruction of natural science", arranged since 1990. The author took part in them and informed the scientific public the very first investigation and research analysis of nuclear fusion issues.

Nuclear fusion

The concept of the controlled nuclear fusion exists since the 50's of the XX-th century, it seized a strong hold on the minds of nuclear engineering specialists after the first successful uncontrolled explosion of thermonuclear hydrogen bomb in 1953 and right away a thermonuclear research for peaceful purposes was initiated by I. Kurchatov [3].

In fact, the above nuclear reactions have just been obtained in the course of research at experimental installations, but controlled and stable fusion has not been achieved till now. It can be explained by the fact that in order to make a fusion it is necessary, as stated above, to bring nuclei together at a distance of about 10^{-11} 10^{-13} cm to overcome the Coulomb barrier, i.e. repulsion of positively charged nuclei from each other. A method of nuclei approach to a distance necessary for realization of fusion reactions, has been searched for, mainly, providing

conditions of high speed of hydrogen nuclei and its isotopes, in particular, due to high temperature, corresponding to the temperature, verified at the hydrogen bomb explosion (atomic bomb, developing a temperature of up to 10^8 °K, initiating an explosive reaction of thermonuclear fuel, for instance, deuterium + lithium), which uniquely corresponds to the nuclear fusion temperature.

High temperature was provided by the energy released at the chain decay of uranium nuclei, its value for nuclei acceleration and approach to a distance of 10^{-11} cm can be assessed from the Coulomb law for interaction of deuterium nuclei: $W \approx e \cdot e / z \approx e^2 / z$, where

e is proton charge, $e = 4{,}8 \cdot 10^{-10}$ CGSE units;

z is the distance to which the nuclei must be brought together, $z = 10^{-10}$ cm;

W is nuclei interaction energy, $W \approx 10$ KeV.

Using digital value of the Boltzmann constant

$K = 1{,}4 \cdot 10^{-16}$ erg /K ($K = 1{,}380662(44) \cdot 10^{-23}$ J/K –for 1980), evaluation of the nuclear fusion temperature amounts to $T \approx 10^8$ °K, this hundred million degrees is the minimum, which is in a number of cases requires $3 \cdot 10^8$ °K. Such temperature has not been obtained yet, it is not controllable because of plasma instability, which quickly cools the fusion zone. Hot plasma instability is the main difficulty in fusion realization, even at temperature reduction by 5-10 times, owing to the plasma density reduction to a value of $n \approx 3 \cdot 10^{14}$ particle $\cdot$ **s**/cm^3, even at specific technological improvements, such as theta-pinch effect (fast compression by magnetic field), ultra-speed heating in the pulse mode, prevention of plasma spread by spherical laser compression (inertial nuclear fusion), though realization of nuclear fusion has been planned yet in 1980 [4].

Meanwhile, the actual realization of the controlled nuclear fusion (CNF) from the beginning of the research seem possible in more than 100 years, though academician E. Velikhov's group has been already awarded with the "Global Energy" prize [5] for the RHPR international research project which is supposed to be implemented by 2030. Difficulties with the CNF gave rise to a search of other methods of nuclear transformations by synthesis with the help of transmutation.

Nuclei transmutation

The most urgent transmutation became for decontamination of middle and high activity radionuclids incidentally obtained at fission of heavy nuclei $_{92}$U, $_{91}$Pa, $_{90}$Th and others in nuclear reactors, which does not require CNF temperatures, that is related to safe burning of small actinides (Np, Am, Cm) [6], existence of which defines a long-term (for hundred thousand years) danger of even long-term warehousing of radioactive materials. A manufacturing technology of neutron illumination of nuclear reactors with fast neutrons, obtained with the help of special accelerators, working in the power mode [7] for long-living actinoids formed in the cores of ^{241}Am, ^{243}Am reactors. Such approach is rather complicated owing to necessity to create a whole sub-industry for manufacture of special high-activity targets, special accelerators and NPP complication, complication of already loaded fuel cycle of NFC of NPP.

Processes in the researches of A. Sytin, I. Chernov, S. Tsvetkov, and many others, and in experiments of Fabrikant-Rabzi and B. Bolotov [8,9,10,11,12] can be considered more ecologically compatible, these authors have drawn attention to availability of "cold fusion" in nuclei transmutation.

Typical for transmutation is recoil and absorption of one proton with formation of a neighboring element, as per Mendeleev's Table, or substances. The process can be initiated by different mechanism, with participation of neutrons, or without them, with obligatory participation of electrons, and as per Bolotov, also with participation of photons, that can be seen from performed reactions:

$$^{11}B + {}^{1}H \rightarrow {}^{12}C$$
$$^{137}Cs \rightarrow {}^{130}Xe$$
$$h_{p} \rightarrow Al_2O_3 \rightarrow 5\,Ne \rightarrow Sn^{50}$$
$$h_{p} \rightarrow Cl^{17} \rightarrow S^{16} + e$$
$$h_{p} \rightarrow Hg^{80} \rightarrow Au^{79} \quad e$$

Change of composition of isotropic mixtures of elements in the human body (^{40}K), obviously related to nuclear transformations at normal temperature, was first noticed in 1923 by P. Lazarev and V. Vernadsky. In the 70–90's the transmutation processes in living systems were studied by L. Kervran and V. Kaznacheev [13,14], the latter studied $^{12}C/^{13}C$ isotope relationship of people with regard to health and weight of labor.

In Russia in the recent years processes of biological nuclear transmutation have been studied at Moscow State University named after M. Lomonosov and have been reflected in the works of Vysotsky-Kornilova [15], and it is promoted by cooperation with the author for research of cold fusion conditions in "Koldamasov cell". Transmutation in research of Vysotsky-Kornilova is observed in growing biological cultures, in the process of their vital activity, in spite of the fact that living organisms cannot have high temperatures or micro-accelerating mechanisms, plasma waves and similar events related to the process of low temperature nuclear fusion.

Low temperature nuclear fusion

The nature is not limited so much as to synthesize hat it needs, other mechanisms of nuclear fusion without overcoming of the so called Coulomb barrier exist, as we have shown above, only at thermonuclear temperatures. Constant energy exchange and interaction as per -mesonic mechanism take place in atomic nuclei:

$$p^{+} \rightleftarrows n \cdot {}^{-}; \quad n^{-+} \rightleftarrows p^{+} \cdot {}^{-};$$
$$p\,(n) \rightleftarrows n\,(p) \cdot {}^{0}$$

Proton (p) and neutron (n) are considered here as two states of one particle (nucleon), in this case neutron [– +] potentially contains proton [+] and electron [–], and interaction exchange between nucleons also takes place in deuterium nucleus; neutron can become proton, and proton having obtained a part of mass from neutron, and electron, can become neutron (Figures 1 and 2); constant overcharging and exchange of ^{0} –mesons take place in the nucleus.

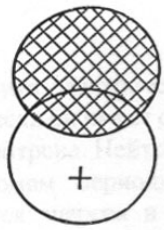

Figure 1

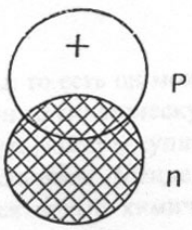

Figure 2

As a matter of fact we have to understand elementary electrical interactions in which the background of nuclear interactions is revealed, for example with an electroscope - a demonstration instrument for detection and measurement of electric charges. If two plates of the electroscope (Э) are charged with like charges with the help of external positively charged solid (ebonite), the plates will part (Figure 3), and if the third plate is charged with external negatively charged solid (glass), the plates will come together (Figure 4).

Thus, it should be clearly understood that a system of three drawn together charges, cluster of [+ – +] or [– + –] form is a neutral system!, not reacting on external coulomb charges. As a system of three plates of the electroscope becomes electrically neutral, in the same way a neutral cluster is formed in the nucleus, the cluster obtains immunity to coulomb interactions, which exists only for a moment, but this moment is enough for formation of a small-size (10^{-11} cm) neutral system in subnuclear interaction with participation of π-mesons ($^{-}$, $^{+}$), neutrons within a life time of π-mesons $2{,}6 \cdot 10^{-8}$ s; the system being similar to neutrons [16], of a neutral cluster,

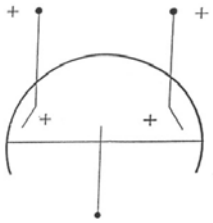

Figure 3

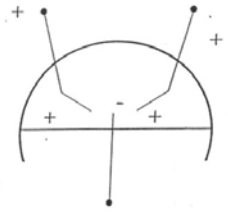

Figure 4

capable of free penetration inside the electron shells of atoms, of approach to their nuclei, bypassing the Coulomb barrier, that provides conditions of nuclear fusion and nuclei transmutation, at full ionization of nuclei.

Figure 5 shows a neutralized system (cluster) of three charges, [+ – +], of different structural clusterization at the nuclear and subnuclear levels, for instance:

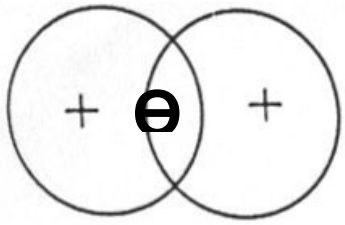

Figure 5

- deuterium nucleus as a cluster [+ – +], i.e. [(proton+) (– neutron+)], nucleus-proton of which and proton of neutron are neutralized by electron, included in neutron;

-mesoatom as a cluster [+ – +],], i.e.{proton [+] $^{-}$-meson proton [+]}, two nuclei of which –proton with $^{-}$-meson form a neutral cluster.

Figure 5 – system [– + –] can be shown also as electrically neutral:

- tritium nucleus as a cluster [+ – + – +], i.e. {[+] neutron [–] (proton [+] [–]neutron [+]}, two neutron of which shield the nucleus by their electrons.

Thus, there exists a large range of combination and structuring of different nuclear electrically neutral clusters for low temperature fusion, these clusters are not afraid of the Coulomb barrier; but for the neutral nucleus to come into nuclear interaction with formation of a new chemical element one should understand what conditions are optimal for structuring with subsequent fusion in picosecond time range, on an actual model, which was mentioned at the Russian conference on cold fusion and nuclei transmutation in 1995 [17].

The fusion practicability does not obligatorily mean a structure of two nucleons, cluster conformation of neutral nuclear structure is diverse, collective, crystal-like structured, determined, self-organized, possesses properties of a non-linear dissipative system and requires not so much the knowledge of nature to a nicety as initial creation of conditions for proton-neutron transformations and fusion, further on the nuclear nature switches on its own resource mechanism fusion mechanism and if fusion does not start, it means that the required conditions have not been provided.

Nuclear fusion is actually intensified by external magnetic field, this is an effective condition. Under the impact of an electromagnetic wave created at the inlet of the initial deuterium water in the so-called "Koldamasov's cell" (Photo 1), which is named so by the version of D. Baranov (SRC "Kristal", Moscow) [18]

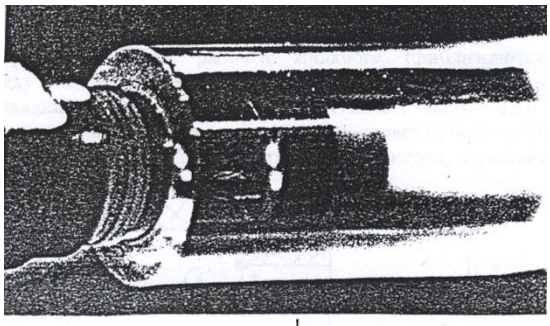

Photo 1

cavitation arises in water that results in formation of mist spray in the form of a cloud of millions of the smallest nanodrops. The drop radius R_d , with a perimeter of $6\ \lambda_{el}$, is proportional by value to the length λ_{el} of wave of electromagnetic radiation $R_к \quad \lambda_{el}$. Thanks to self-interference the local density of energy of electromagnetic radiation can reach a huge value, by many orders exceeding the energy, required for nuclear fusion ($W \gg 6{,}8 \cdot 10^8$ KJ /cm^3). Rather high energy density provides powerful light pressure of about $P_{\text{light press.}} = W_э \cdot 10^4$ kgf /cm^2, appearance of shock waves as per V. Filimonov [19], or cumulative effects as per F. Vysikailo [20], superimposition of external electromagnetic field results in self-wave and resonance synchronization and self-sustained process, even without interference in the fusion process control. The mentioned super-light pressure brings nuclei together to a distance of action of nuclear forces, when fusion is naturally inevitable. Illustration of wave processes is given below (Figures 6 and 7), which show a cyclic path of the electromagnetic wave through drops, self-interference and light pressure energy being increased with each pass, till they reach power intensity of nuclear fusion $W \gg 6{,}8\ 10^8$ KJ /cm^3 and light pressure $P_{\text{light press.}} = W \cdot 10^4$ kgf /cm^2, after that nuclei fusion takes place accompanied by microatomic explosion of the nanodrop with energy release.

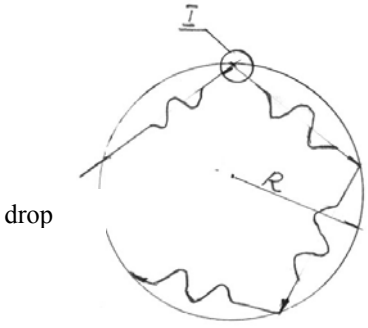

Figure 6

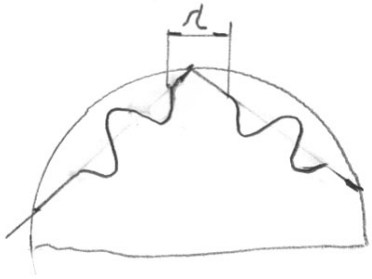

Figure 7

Many researches in Russia and abroad take part in experimental check of the author's developments [21], one should keep in mind that some nuances in researches must be thoroughly observed relative to the "fusion conditions", even time of the day, illumination, electromagnetic parameters, pressure, speed, wave aspects are important. The mentioned selective factors shall be observed in order to obtain a steady fusion, but it would be tactless to personify in this article the researchers who first obtained a result, and then unsuccessfully tried to reproduce the results, optimization of the low temperature nuclear fusion occurs in the course of live scientific contacts and discussions. It should be understood that each nanodrop of water and water solutions is a nanoreactor of nuclear fusion, where self-wave processes take place. Such disposition, by the author's opinion, of fusion processes in animate nature and abiocoen, which happen permanently, without breaks, forming various chemical compounds with energy release. Based on the stated theoretical prerequisites a nuclear reactor has been designed and tested which enables generation of energy of nuclear fusion reactions, it is shown above in Photo 1.

The reactor is steady in operation and is subject to control. 20 units of useful power are released for each unit of supplied power, the energy can be obtained both in the form of heat and in the form of electricity, of direct or alternating current, omitting a vapour-water cycle; Russian patents have been received for the nuclear fusion reactor [22, 23].

The following events happen when he reactor is in operation: if when dielectric liquid, for example water with specific electric resistance of 10^{11} Ohm · m leaks through the hole in the plate made from dielectric plastic material with the same specific electric resistance, a flow pulsation is excited, a positive electric charge of large density will appear on the inlet edge of the hole, its potential relative to the Earth will reach more than 500 kW and a bright glow will appear at the inlet of the reaction chamber. The operating liquid is supplied with the help of a gear pump with a pressure of 5-7 MPa, channel length: 25-30 mm, hole diameter: 1-2 mm.

The flow pulsation frequency is regulated by changing the number of revolutions of the electric motor; when resonance frequency of the hole is reached, the cavitation intensity increases many times. Under the impact of this cavitation the plate material emits electrons from the inlet edge, the electrons are carried away by the flow. The largest density of the positive charge (Figure 8) is achieved at the very inlet edge. The water transforms to plasma state of a toroidal form, with a density of 10^{4} J /cm^{3} and a temperature of 10000 °K, toroidal (circular) charge of which has isotropic similar density through the whole section of the plasma volume.

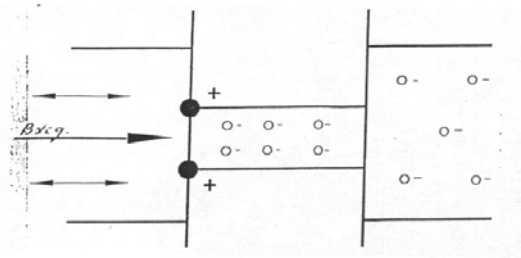

Figure 8

Deuteration of initial light water with a minor addition of heavy water, with specific electric resistance of 10^{11} Ohm · m, initiates a nuclear fusion reaction in the charge affected reaction zone. Electrodynamic and rhythmic-dynamic background of this process requires additional verification. Deuterium atoms with the operating liquid flow approach the circular positive charge of large density and under its impact lose electrons from orbits, full ionization of atoms and denudation of deuterium nuclei take place.

Electric ionization energy of atoms is not great, it amounts to 13,6 eV, that is why at a rather large distance to the hole, electrons leave their orbits of atoms and rush to the stronger electric charge of the hole edge of the reactor inlet channel (Figure 9).

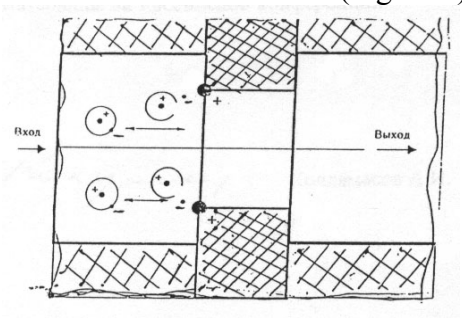

Figure 9

Atoms of deuterium having lost their electrons cease to be neutral; positively charged deuterium nuclei, being surrounded by a stronger field of positive charge of the reactor channel are drawn to the center of the channel hole, peculiar high-speed focusing of nuclear plasma occurs in the axial central section of the channel similar to a pinch-effect, and final separation of charges takes place, density of plasma nuclear filament increases several times, powerful light pressure comes into action, all this intensifies collision processes and interaction of deuterium nuclei (Figure 10), that results in nuclei fusion.

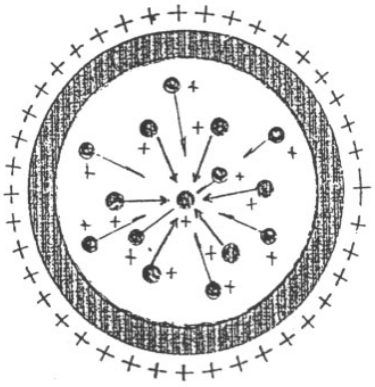

Figure 10

Frequency of acts of deuterium atoms collision depends on concentration of heavy water in the reaction mixture of initial light water and influences power intensity of the low

temperature nuclear fusion process. Mixture used for experiments and for pilot nuclear fusion reactor test is “heavy water : light water” in volume/mass relationship 1:100. The time of continuous reactor operation and of the nuclear fusion process is about 100 hours, which is sufficient for confirmation of complete reproduction of fusion at the change of day time, natural factors and technological modes. It also helped to find the ways for improving design and technological parameters of the nuclear fusion reactor for energy generation, that is protected by the Russian patent [24].

Investigation of radiation activity in compact cavitation installations of D. Baranov and other authors [25] is of great importance for revealing factors of instability and selection of optimal conditions for low temperature fusion.

Due to strategic splash of interest to hydrogen energy in the world, one of the last author’s developments together with his colleagues is a device for hydrogen production [26] as universal application of the nuclear fusion reactor. The device for hydrogen production (Figure 11) contains a body 1, made from dielectric material resistant to cavitation emission, heat impact, for example from ceramics or sapphire with an insert 2 installed in it, the insert is also made from dielectric material, for example asbestos cement or fluoroplastic, susceptible to cavitation emission, and has one or several holes 3, representing cylindrical channels with a length of 25-30 mm and a diameter of 1-2 mm. At least 2 magnets 4 are installed on the body 1, they can be constant or inductive. Flows are received by nozzles 5, 6 and 7 located behind magnets 4, nozzles 5 and 6 being electrically isolated from each other. Nozzles 5 and 6 bear the ionized flows of negative and positive potential, accordingly, and nozzle 7 bears the neutral flow. Control electrode 8 is installed behind nozzle 5 of body 1, and control electrode 9 is installed behind nozzle 6 of body 1. Collimators 10 and 11 are installed to bring the ionized flows into stable state. Contactors 12 and 13 are installed on the flow path behind control electrodes 8 and 9, accordingly, they provide earthing of the ionized flows. Collimators 10 and 11 are earthed with the help of contactors 14.

The device operates as follows: a flow of dielectric liquid – a mixture of “light water” and “heavy water” is supplied into the body 1 on insert 2. When the mixture flows through holes 3 with the flow pulsation frequency, approximately equal to the natural frequency of pulsation of hole 3, powerful resonance fluctuations of the mixture flow arise. Cavitation occurs at the inlet of hole 3 with cavitation emission accompanying it. Technological parameters of the mode: pressure: 5-7 MP; flow pulsation frequency: about 1 Hz; specific electric resistance of light and heavy water mixture: not less 10^{11} Ohm· m. The device has been manufactured and tested, total operating time of this device and others mentioned in this article is four days.

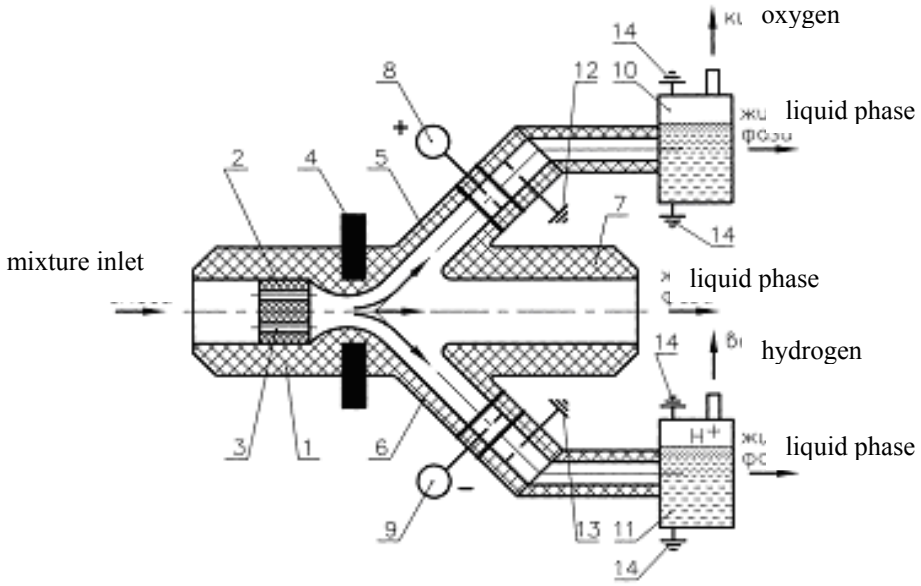

Figure 11

Summary

Based on theoretical justification, experimental investigation and trial tests of the working installation of the low temperature nuclear fusion the author obtained reliable results of actually performed fusion and required design and engineering grounds for creation of reference commercial energy generating device of multi-purpose application.

Literature:

1. F. Knoibyul, Manual for physics repetition M.: "Energoizdat", 1981
2. G. Voronov, Storm of thermonuclear fortress M.: Chief editorship of physical and mathematical literature, 1985
3. P. Astashenkov, Deed of academician Kurchatov M.: "Znanye" publishing house, 1979
4. K. Mukhin, Experimental nuclear physicsa M.: "Atomizdat", 1974
5. Thermonuclear energy – energy of the future /M.: RIA "Novosti", "ROSENERGOATOM" magazine No. 7, June 2006
6. A. Shmelev, G. Kulikov, V. Apse, V. Glebov (MIFI), D. Tsurikov (IAE) //St. Petersburg, Nuclear Society International, Third Annual Scientific Conference (Moscow, Russia, 14-18 September), 1992
7. V. Subbotin, The twenty-first centuryis a century of nuclear energy engineering – Dubna: NRI, Physics of elementary particles and atomic nucleus, v. 29, iss. 2, 1988
8. A. Sytin, N. Bakumtsev, Conception of neutronless nuclear fusion in potential field– //Volgodonsk: materials for symposium "Reconsruction of natural sciences", Volgodonsk, Russia, 13-15 April, 1990.
9. N. Nikitenkov, I. Chernov, N. Markova, Investigation of element transmutation, stimulated by low temperature nuclear fusion in niobium and in stainless steel – // M.: MSTC of venture non-traditional technologies, Materials for conference on cold nuclear fusion, Abrau-Dyurso -Novorossiysk, 28 September – 2 October, 1993.
10. G. Rabzi, A. Fabrikant, Experimental investigation of nuclear transmutation at electrolysis of H_2O by electric field of high strength – // Minsk: MP "SIEM" publishing house,

international symposium “Cold nuclear fusion and new energy sources”, scientific-technical collection, Minsk, Belarus, 24-26 May, 1994.
11. S. Tsvetkov, Possibility of using cold nuclear fusion for nuclear waste transmutation – // M.: RAN, Tr. 9 Russian conference “Cold transmutation of chemical elements nuclei and ball lightning”, Dagomys, Sochi, 30 September - 7 October, 2001.
12. B. Bolotov, Comparative data for photo- and beta-atomic fusion, in the book of B. Bolotov, “Human health in unhealthy world” – Kiev – St. Petersburg: “Piter” publishing house, 2005, page 420, left.
13. Kervran L., Prenves en biologie de transmutation a faible energie –Pris: Malon, 1975, 210p.
14. V. Kaznacheev, A. Rzhavin, L. Mikhailova, Institute of general human pathalogy RAMN, To the problem of nuclear bioenergetics of living substance –// Minsk: MI “SIEM” publishing house, international symposium “Cold nuclear fusion and new energy sources”, scientific-technical collection, Minsk, Belarus, 24-26 May, 1994.
15. V. Vysotsky, A. Kornilova, Nuclear fusion and transmutation of isotopes in biological systems –M.: “Mir” publishing house, 2003.
16. Physics of microworld, small encyclopedia, edited by D. Shirkov – M.: “Sovetskaya Encyclopedia” publishing house, 1980, p. 250
17. A. Koldamasov, Nuclear fusion in the electric charge field, – // M.: RAN, Tr. 3 Russian conference “Cold fusion and transmutation of nuclei”, Dagomys, Sochi, 1995.
18. A. Andreev, D. Baranov, A. Molodov, A. Pokrovsky, N. Sukovatin (MRTI RAN, SRC “Kristal”), Experimental installation on the base of Koldamasov’s cell – // M.: RAN, Tr. 8 Russian conference “Cold transmutation of chemical elements nuclei”, Dagomys, Sochi, 4-11 October, 2000.
19. V. Filonenko, Verification of model of synergetic activation of cold nuclear fusion – // M.: MSTC of venture non-traditional technologies, Materials for Russian conference on cold nuclear fusion, Abrau-Dyurso - Novorossiysk, 28 September – 2 October, 1993.
20. F. Vysikailo, Cumulative-dissipative structures and their crystalline systems in gas discharge plasma – // M.: RAN, Tr. 10 Russian conference “Cold transmutation of chemical elements nuclei and ball lightning”, Dagomys, Sochi, 29 September - 6 October, 2002.
21. A. Andreev, D. Baranov, A. Molodov, A. Pokrovsky, N. Sukovatin (MRTI RAN, SRC “Kristal”), Experimental installation on the base of Koldamasov’s cell – // M.: RAN, Tr. 8 Russian conference “Cold transmutation of chemical elements nuclei”, Dagomys, Sochi, 4-11 October, 2000.
22. A. Koldamasov, Nuclear reactor, Patent of VC VNIIAM RU No. 2152083, priority of 15.10.1998 – // M.: FIPS, 2000.
23. A. Koldamasov, Nuclear reactor, Patent of VC VNIIAM RU No. 2172526, priority of 27.07.1999 – // M.: FIPS, 2001.
24. A. Koldamasov, Energy generating device, Patent RU No. 2224308, priority of 12.03.2002 – // M.: FIPS, 2004.
25. D. Baranov, D. Gavritenkov, Investigation of radiation activity in compact catitation installations (SRC “Kristal”) – // M.: RAN, Tr. Russian conference “Cold transmutation of chemical elements nuclei and ball lightning”, Dagomys, Sochi, 1-8 October, 2006.
26. A. Koldamasov, S. Kravets, A. Kornilova, Method of hydrogen production and device for its realization, Patent of VC VNIIAM RU No. 2258028, priority of 22.01.2004 – // M.: FIPS, 2005.

EVIDENCE FOR CONDENSED MATTER ENHANCED NUCLEAR REACTIONS IN METALS WITH A HIGH HYDROGEN SOLUBILITY

Andrei G. Lipson[1,3], Alexei Roussetski[2], George H. Miley[3]

[1]Institute of Physical Chemistry and Electrochemistry, Russian Academy of Sciences, Moscow 119991, Russia
[2]Lebedev Physics Institute of RAS, Moscow 119991, Russia
[3]University of Illinois at Urbana-Champaign, Urbana, IL 61801, USA

1. Abstract

In this paper we present and discuss "conventional" nuclear signatures of non-equilibrium processes in deuterated metals that in our opinion could only serve as an evidence of nuclear energy release in atomic lattice, particularly CMNS. These effects include, but may not be limited by:
a. DD-reaction enhancement during low energy deuteron bombardment of metallic targets (accelerator and glow discharge experiments).
b. Low intensity emissions of DD-reaction nuclear species: 3 MeV protons, 1 MeV tritons, 2.45 MeV neutrons (in Pd-D cannot be explained by fractoemission).
c. Energetic alpha emission ($E_\alpha \geq 8$ MeV). These alphas cannot be emitted by natural radionuclides or from cosmic background.
d. Soft X-ray emission ($E_x \leq 1.5$ keV) in experiments with pulsed Glow discharge with Ti, Pd and other metal cathodes as well as during D-desorption from Pd/PdO:D_x .

2. Introduction

Under the term LENR or CMNS (in more broad sense) we understand specific nuclear processes at very low kinetic energy of projectile nuclei (say, $kT < E_{lab} < 1$ keV) that are enhanced by strictly non-equilibrium condensed matter/crystalline lattice environment. These peculiarities make LENR (and nuclear cross-sections) drastically distinctive from the nuclear reactions taking place in vacuum/plasma collision. In more broad sense the LENR/CMNS effects are also include nuclear, electrochemical, material science (condensed matter physics) and other aspects and can be considered as an interdisciplinary research area.
So far typical LENR experiments on excess heat generation do not show signatures of nuclear effects giving a low credit with respect to nuclear origin of these processes. Very often, the magnitude of specific heat in excess heat generation experiments is considered as a main evidence of the nuclear processes in electrolysis experiments. However, even keV/Pd-atom range of specific energy of Excess heat would be not enough to convince physicist in a nuclear origin of the effect observed. The same is referenced to He-4 and tritium accumulation as well as to so-called transmutations. Only changes (e.g., appearance of additional elements and isotopic shifts) in stable isotope are observed. Because these species are detected in atomic form they cannot be considered as a direct consequence of LENR.

Furthermore, if the He-4 detected was really from a giant enhancement of d(d,)^{4}He channel of DD-reaction (the rate is ~ 10^{11} s^{-1} to generate ~ 1 W of thermal power), why no sign of intensive (at least 10^4/s rate) of d(d,p)t and d(d,n)^{3}He channels (even suggesting their suppression by factor 10^7 compared to "main" He-4 channel) would be seen ? The absence of intensive X-rays also makes this issue highly controversial. Thus, the results allowing to extract unambiguous proofs for condensed nuclear science (CMNS) nuclear origin, that are enable to convince majority of physicists in reality of CMNS should be primarily considered at this point.

In our opinion, at present, the following effects observed by at least several researchers, independently must be only considered as real nuclear signatures of CMNS:

- DD-reaction enhancement during low energy deuteron bombardment of metallic targets (accelerators and glow discharge experiments)
- Low intensity emissions of DD-reaction nuclear particles: 3 MeV protons, 1 MeV tritons, 2.45 MeV neutrons
- Energetic alpha emission ($E_\alpha \geq 8.0$ MeV). These alphas cannot be emitted by natural radionuclides/cosmic background.
- Soft X-ray ($E_x \leq 1.5$ keV) emission in experiments with pulsed Glow Discharge and during D-desorption from Pd/PdO:D_x .

The listed items have been detected systematically in independent experiments by many researchers. Which is why, the nuclear/X-ray emission results mentioned here indicate the ways to convince physical society in nuclear origin of CMNS effects, including of higher level such as excess heat and transmutation production. Below we are going to consider some details of these listed experiments.

3. Enhancement of DD-reaction in metal targets

Recent accelerator experiments at $(E_{pr})_{lab} \leq$ 5.0 keV (Ref. 3-7, 11-16) show enhanced electron screening effects at the deuteron/electron densities encountered in a majority of deuterated metallic targets. These measurements show a significant increase ("enhancement") in the reaction rate (i.e. increased astrophysical factor S) at lower energies.

F. Raiola et al. (Refs. 6, 7, 11), systematically measured the low energy (down to E_{lab}= 5 keV) yields of D(d,p)T reactions and corresponding screening potentials for deuterated targets using about 30 different elements over the Periodic table, including both metals and some non-metal elements. A majority of the targets resulted in a "large" screening potential U_e > 100 eV, excluding, mainly, metals of group 4 (Ti, Zr, Hf) and group 11 (Cu, Ag, Au). The accelerator they used had a weak deuteron beam current, ranging from 1-54 μA. Therefore, reactions could only be measured at a relatively high energy (E_{lab} > 5.0 keV) before the signal/background ration became too small for accurate results.

J. Kasagi et al. (Refs. 14-15), operating with a higher current (D^+ beam current ranging 60-400 μA), recently measured D(d,p)T yields in several metal and metal oxide targets down to E_d = 2.5 keV. They found that the screening potential value U_e is strongly affected by the diffusivity of D in metals. Metals possessing a low D diffusivity and a high activation energy of D diffusion, Ti and Au, had lower screening potentials of 65 ± 15 eV and 70 ± 10 eV, respectively. These screening potentials are only two times above that for D_2 gaseous targets. However, for Pd and PdO targets having a high diffusivity, screening factors of U_e = 310 and 600 eV, were found, respectively[4].

Analyzing enhancement data, A. Lipson has found [9,10] that Screening potential U_e in any metal target (Me) of periodic system can be satisfactorily described by a logarithmic

function of the bombarding deuteron flux F (F = J ~ y=Me/D). This conclusion is well illustrated by F. Raiola et al data obtained during deuteron bombardment of more than 60 elements of periodic table (at the target-beam conditions T_0=290K, J_0=0.03mA/cm2, E_d≥5keV) and plotted in Fig. 1

So far, studies using accelerators have deal with relatively low beam currents ($J_d \leq$ 400 μ A) allowing deuteron energies down to $E_d \geq$ 2.5 keV before the background noise overwhelms the signal . For comparison as indicated in Table I, the GD current densities can be about 3 orders of magnitude allowing much lower energy measurements.

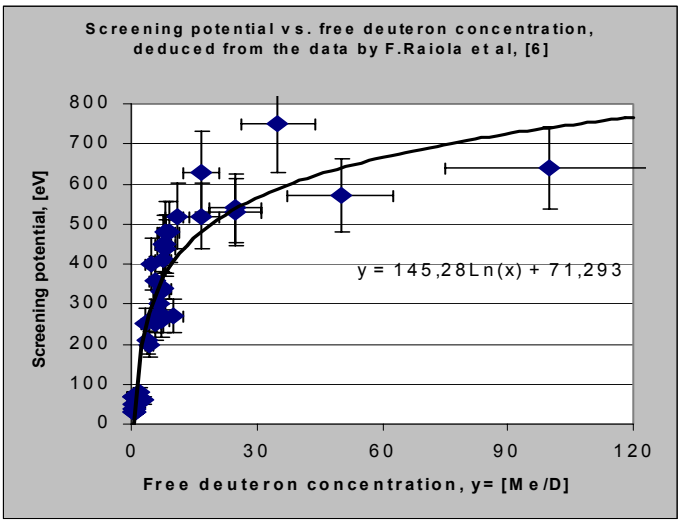

Figure 1 *Screening potential vs. free deuteron concentration in the target (y = Me/D) for 42 elements of periodic table. Each point on the graph characterizes a specific metal and to be consistent with increase in y = Me/D as follows: Hf, Y, Lu, Sc, Gd, Tm, Ti, Ce, Yb, Sm, Zr, Er, Pr, Eu, Ho, La, Ge, C, W, Sr, Ir, Ba, Ru, Au, Ag, Re, Ni, Nb, Ta, Zn, Bi, Mo, Mn, Mg, Cu, Rh, Fe, Pt, V, Pb, Pd, In, Tl*

Table I. Comparison of High Current, Low Energy D Accelerator and Pulsed GD

Parameter	*High Current Accelerator	**Pulsed Glow Discharge
I, range	10-400 μA	100-600 mA
E_d(lab), keV, range	100.0- 2.0	2.5- 0.40
W_{max}, [W]	2.0	200.0
P, mm Hg	$5*10^{-7}$, vacuum	2.0-10.0, D_2
T,K, target	100-350	200-2000
D^+ energy spread	± 1.0%	± 10.0%

*The accelerator uses a Duoplasmatron (E_d = 50 keV) ion source
**Power supply is a periodic current pulse generator. with 1ms width and on-to off ratio of 0.10 -0.30 (Ref.2)

The disadvantage of a larger energy spread in the GD case is outweighed by the higher current and lower voltage capability.
Recently, high-current glow discharge measurement showed strong enhancement of DD-yield – about 9 orders of magnitude at E_d =1 keV in Ti target (A. Lipson et al., JETP, **100**, 1175 (2005).
In order to illustrate this giant enhancement effect we show some details of glow discharge experiment.
Initial studies of the enhancement of the D-D reaction rate in solids under D bombardment have been done using a GD especially designed for this need. The detection of charged particles from the DD-reaction and also detecting of X-rays emitted from the surface was carried out in-situ in a GD vacuum chamber during discharge operation at different voltages and currents. A diagram of the glow discharge apparatus with appropriate detectors is shown in Fig. 1.
Due to the electrical noise during pulsing, a key to successful use of this technique is employment of CR-39 track detectors for charged particle measurement (x-ray measurement also under solid state TLD detectors). With proper calibration these detectors provide a sensitive measure of the particle energy. Protons were used in the present DD case since they are easier to detect with the method than the alpha. Since the proton fluxes in this low energy range are extremely low, the foils are left position for hours while the device is pulsed (as much as ten hours in present work). This provides a time integration of the signal which is essential for accounts. Fortunately the GD apparatus can operate very stably for the long periods required[2]

The distance between the moving Mo anode and the removable cathode-target (thickness h = 0.01 cm, area S = 0.64 cm^2) was varied over 4.0- 5.0 mm. The current and voltage repetitive pulses had a square - shaped pulse, duration $\Delta\tau \approx$ 200-400 μs, pulse repetition frequency of 5 kHz and a short arise time (less than 1.0 μs). The pulse parameters are continuously monitored during the discharge operation by a two channel 100 MHz memory-type oscilloscope. A stable glow discharge was achieved at P = 2.0 - 9.0 mm Hg without pulsations or instabilities within a time resolution of ~ 10 ns.

Entire CR-39 technique for 3.0 MeV proton detection in glow discharge, including CR-39 filtering, calibration and etching is described in details in Ref. [2]. In brief, both proton calibration with VanDeGraaf accelerator and estimates, using Al foil filters show that 2.7-3 MeV protons at etching conditions used produce tracks with diameter of 5.2 μm.

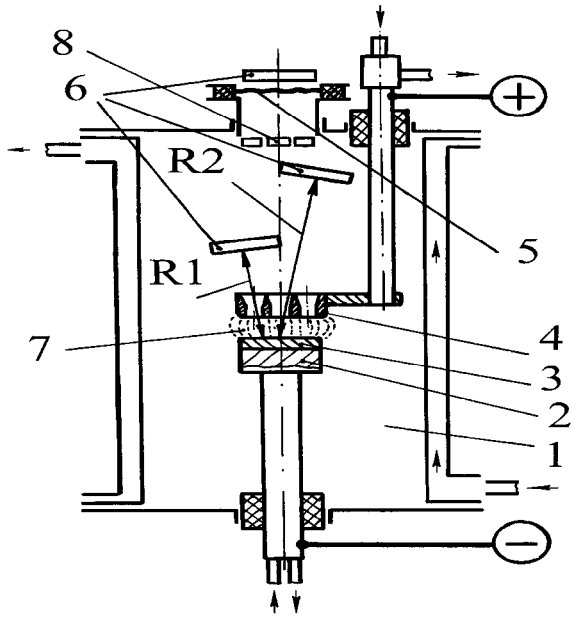

Figure. 2 *Schematic diagram of glow discharge set up: 1-vacuum chamber; 2-cathode support, 3 – cathode, 4- Mo anode with holes; 5-15 μm thick Be-foil; 6-CR-39 detectors (upper is the Background CR-39); 7-discharge zone supply; 8-scintillator/X-ray detector.*

For illustration a typical distributions of charged particle tracks vs. their diameters for deuterium GD for two different voltages U=2175 V and U = 805 V at the same current I = 250 mA is presented in Fig.2. The position of DD-3.0 MeV proton tracks at track diameter d = 5.2 μm is in good agreement with calibration data and previous measurement at U=1.25 kV..

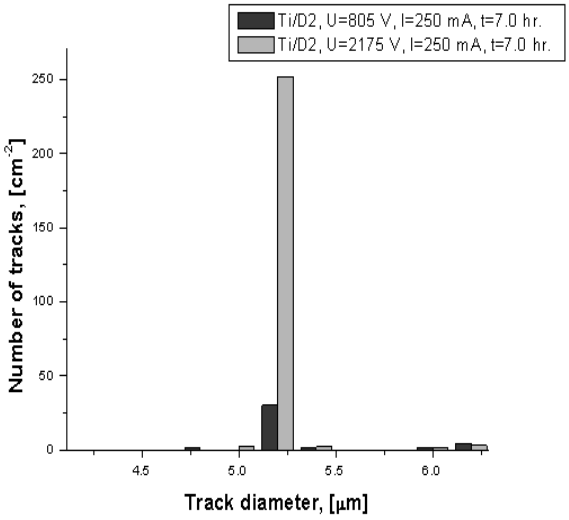

Figure. 3 *3.0 MeV proton yield detected by 11 μm Al covered CR-39 detectors in deuterium GD at the same current and two different accelerating voltages: U_1 = 805 V and U_2 = 2175 V.*

Initial experiments were carried out from 0.8-2.45 kV with currents covering 240-450 mA using a Ti cathode as the target. The duration of each experiment was about 7.0 hrs Measurements with CR-39 track detectors covered with Al-foils showed a statistically

significant number of 3.0-MeV proton tracks in this range of V-I. Net CR-39 results on 5.2 μm track rate where obtained by subtracting of Background result (obtained with special CR-39 detector attached to the cathode space of glow discharge chamber (Fig. 1, position 6, upper CR-39) from the Foreground counts obtained during glow discharge operation. Moreover, the reference experiments performed with H_2 glow discharge, instead of D2 showed no counts in the track diameter range of interest corresponding to 3 MeV DD-protons

As reference values for the extreme case of a thick target, proton yields for a "thick" cathode bombarded with deuterons having energy E_d, were calculated from[13]:

$$Y_t(E_d) = \int_0^{E_d} N_D(x)\sigma_{lab}(E)(dE/dx)^{-1}\,dE \qquad (1)$$

Here $N_D(x)$, $\sigma_{lab}(E)$ and dE/dx are the density of deuterons in the Ti-cathode, the reaction cross section and the stopping power of deuterons in Ti, respectively. The Bosch and Halle (B&H) formulation was used to for the "sequence" cross section of higher energies with an extrapolation to lower energies [1].The stopping power of deuterons in the Ti-target is assumed to be proportional to the projectile velocity at low deuteron energies [14-15]

The yields of 3.0-MeV protons obtained at different deuteron energies ranging from 0.8-2.45 keV were normalized to those at maximal voltage U=2.45 kV, taking into account the power of discharge or effective temperature at the target surface that both affect the change of effective deuteron concentration in the Ti ($N_D(x)$). This correction is needed to take into account the change in deuterium concentration in the Ti-target surface. The correction coefficient k is given as [2]:

$$k(W,T) = \exp[-\frac{\varepsilon_d \Delta T}{k_B T_m T_0}(W_m / W_x)],$$

where ε_d = 0.04 eV is the activation energy of deuteron escape from the Ti surface during bombardment; T_m = 1941 K is the Ti melting point, T_0 = 290 K is the initial target temperature, $\Delta T = T_m - T_0$, W_m = 906.5 W - is a max amplitude power at $E_d = eU_m$ = 2.45 keV and I_m = 370 mA; W_x - is a current amplitude power corresponding to any other (lower) voltage and current in GD with Ti-target. The value of ε_d is determined from accelerator data [14] using an Arrhenius plot of 3.0 MeV proton yields for Ti-target at 180-195 K, E_d=10.0 keV.

For comparative purposes, an enhancement factor, f(E) , defined as the ratio of the actual yield to the bare cross section prediction, is given as [13]

$$f(E) = Y_p(E)/Y_b(E) = \exp[\pi\eta(E)U_e/E] \qquad (2)$$

Here $Y_p(E)$ – is the experimental yield of DD-protons in GD, $Y_b(E)$ – is the bare cross section yield at the same energy determined by the B&H approximation; $2\pi\eta = 31.29Z^2(\mu/E)^{1/2}$ is the Sommerfeld parameter (here Z – is the charge number of deuteron in the case of D+ projectile and target, μ - is the reduced mass and E-is the center of mass deuteron energy), respectively. Thus f(E) is directly related to the screening effect on the reaction rate.
The is illustrated in Fig 3 where data from accelerator experiments [9](curve 1) and the GD experiments with a Ti-target/cathode (curve 2) are shown.

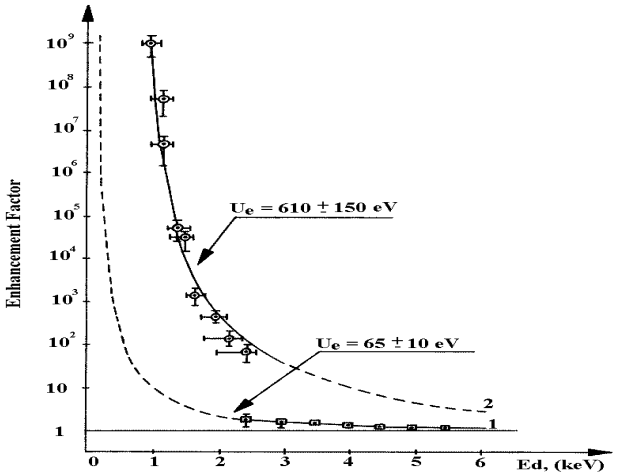

Figure. 4 *DD-reaction enhancement factor calculated with formula (2) for the Ti target during deuteron bombardment with accelerator[14] (curve 1) and the GD[2] (curve 2). The solid parts of the curves corresponded to the deuteron energy ranges where DD-reaction yield was measured experimentally while dashed represents expected .*

In accelerator measurements with the Ti-target at $2.5 < E_d < 10.0$ keV, the deduced screening potential is $U_e = 65 \pm 10$ eV (Ref.4). However for the GD experiment at high current, the screening potential is as large as $U_s = 620 \pm 140$ eV. This striking result illustrates how important the higher deuteron/electron densities in the target (due to the higher currents in the GD) can be.

In light of these results, the high current GD is seen to be a valuable technique for simulation of the plasma edge effects at the metal surface in a fusion system. . Experiments performed with candidate first wall and divertor should provide essential information on DD and DT reaction enhancement and emission of accompanying X-ray quanta. Simultaneously, more research is needed to study the effects that may result for the large helium buildup and x-ray radiation catalyzed corrosion near their surface layers.

Entire data obtained in accelerator and GD experiments give a serious background to CMNS effects at low deuteron energies, convincing that LENR at energies ~ kT still exist and remain non-negligible.

4. Low intensity emissions of nuclear species from DD-reaction

The low intensity emissions of nuclear species from DD-reaction in deuterated condensed matter have been observed by many researchers in various types of experiments. During last 18 years using different nuclear detectors the signatures of d(d,p)t and D(d,n)3He reaction were detected in these experiments. Below we list only few types of experiments in which neutron emission has been detected.

-Fracture of deuterated dielectrics, LiD, D_2O-ice (fractoemission): V.A. Kluyev, A.G. Lipson et al, Sov. Tech. Phys. Lett., 1986 (In ~ 10-20 n/impact), M. Srinivasan et al, Phys. Lett. A (1997).

-Electrolysis of Pd and Ti in D2O: S.E. Jones et al, Nature 1989, A. Takahashi et al, 1989, T. Bressani et al, 1991, etc.

-Acoustic cavitation in D2O with Ti horn: A.G. Lipson et al, Sov. Tech. Phys. Lett., 1990. (In ~ 0.5 n/s).

-Ferroelectric phase transition through Curie point (Tc – 220 K) in DKDP single crystal, A.G. Lipson et al, JETP, 1993 (I_n ~ 20 n/transition).
-Superconducting phase transition (Tc = 92 K) in deuterated HTSC ceramic YBa2Cu3O7-x , A.G. Lipson et al, Tech. Phys., 1995 (In ~ 20-30 n/transition).
-Exothermic deuterium desorption from Pd/PdO:Dx heterostructure, A.G. Lipson et al, Sov.Tech. Phys. Lett., 1992 (BF3), Fusion Tech., 2000 (NE-213).

Below we briefly illustrate typical neutron emission measurement during exothermic deuterium desorption from Au/Pd/PdO:Dx heterostructure peformed in Hokkaido University by Russian-Japan collaboration in 1997-1998 with high efficiency NE-213 scintillator detector system.

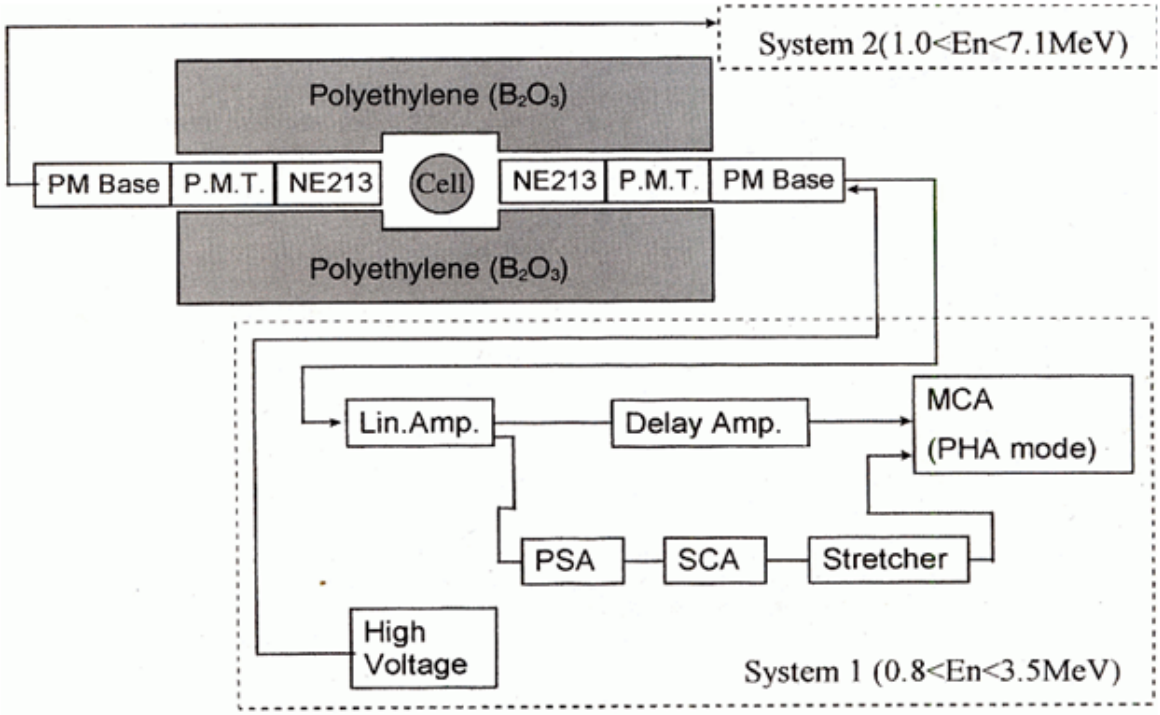

Figure 5 *Neutron detection from Au/Pd/PdO:Dx sample (in the cell) with pair of NE-213 low Background/20m underground facility, Hokkaido University (A. Lipson et al . Fusion Tech, 38, 2000), total efficiency with respect to 2.45 MeV neutrons* $\Sigma\varepsilon_n$*(2.45 MeV) = 10 %*

During detailed Foreground and Background measurements and then Background subtracting (total duration $\tau \sim 3x10^6$ s) the following proton recoil spectra have been obtained for each of the couple of NE-213 detectors (Fig.6). As seen from Fig.6 the peak for both detectors is observed near position of 2.5 MeV. However, in contrast to conventional DD-neutron spectra, statistically significant counts are detected up to E + 4.5 MeV energy (low gain system). In fig. 7 more detailed data presented for neutron counts in the range of 2-3 MeV. This data confirm emission of 2.45 MeV neutrons during deuterium desorption from Au/Pd/PdO:Dx heterostructure samples.

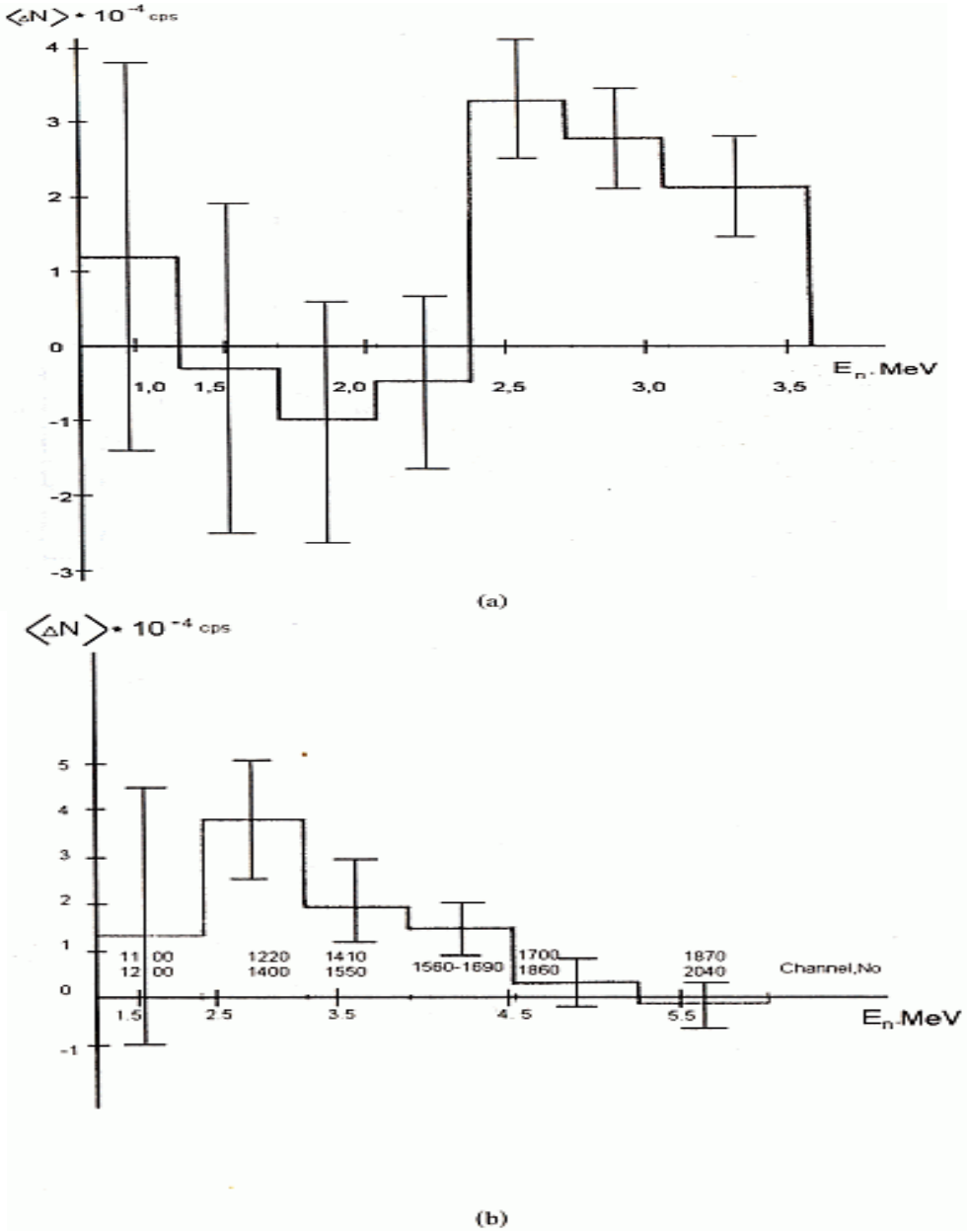

Figure 6. *Energy distributions of neutron counts from NE-213 detectors (the Background subtracted): high gain system 1 (a), low gain system 2 (b)*

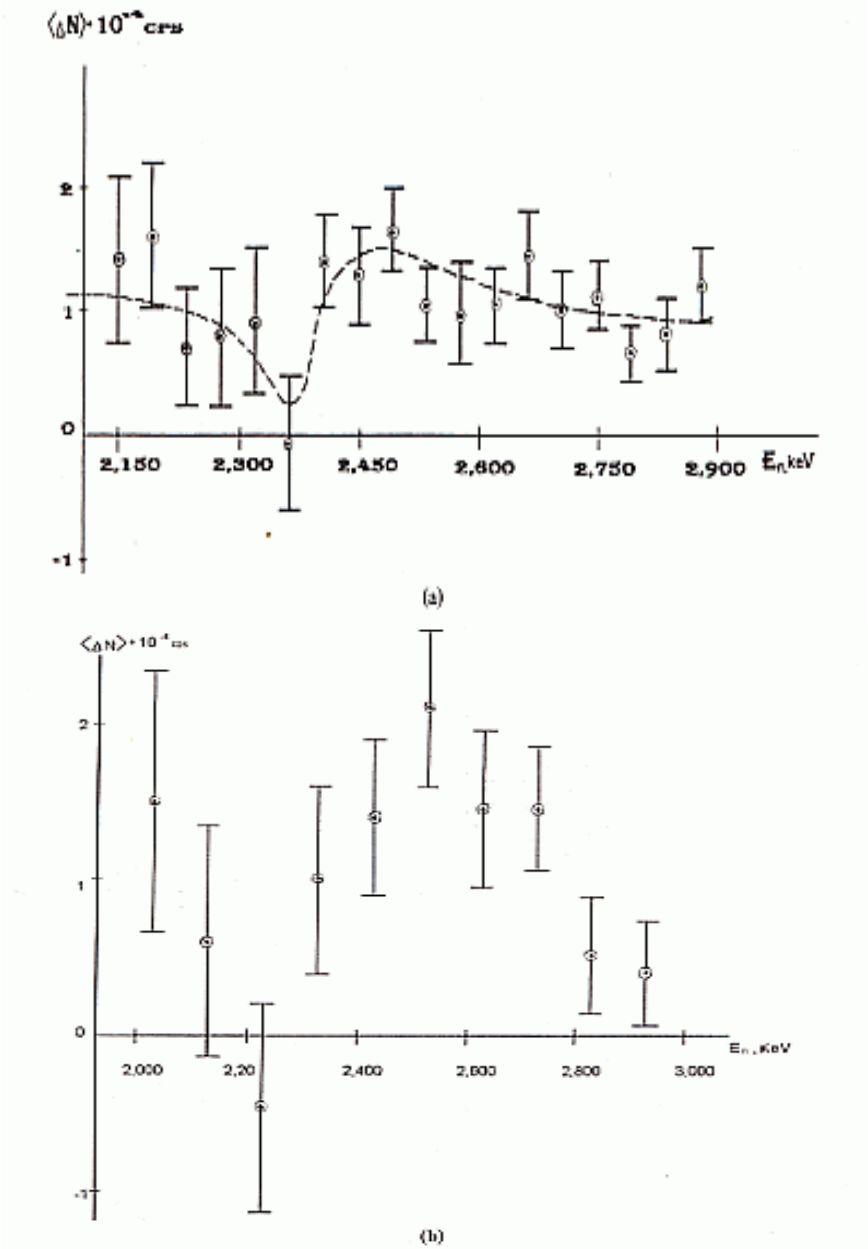

Figure 7. *Neutron spectra of Au/Pd/PdO:Dx sample (with background subtracting) in the 2-3 MeV range derived from high gain (a) and low gain (b) NE-213 detectors:*

Thus, it was found that 2.45 MeV neutron emission rate in 4π -steradian is $I_n = (1.8 \pm 0.19)x10^{-2}$ n/s .

In other types of experiments on search for nuclear signature of CMNS at $E_d \sim kT$ the emissions of charged particles from d(d,p)t reaction have been detected. Below we list only few such examples:

- p-t coincidence measurements at thermal deuterium desorption from TiDx system (S.E. Jones et al, ICCF-10).
- Random 3 MeV proton emission in Pd/PdO:Dx during exothermic deuterium desorption measured with surface Si barrier detectors (A.G. Lipson et al, Fusion Tech., 2000).
- Reproducible 3 MeV proton and energetic alpha (E > 10 MeV emissions in controllable D-desorption from Pd/PdO:Dx with CR-39 (Lipson et al, ICCF10-12)

The phenomenon of random spontaneous 3 MeV proton emission in Pd/PdO:Dx heterostructure during exothermic D-desorption in vacuum at room temperature is illustrated in Figs. 8, 9

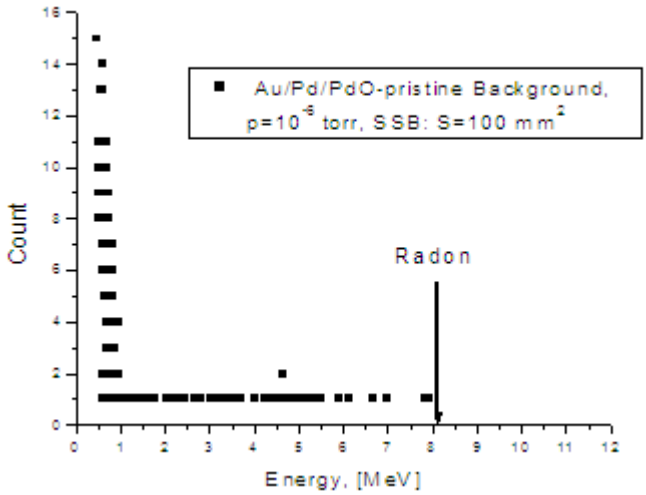

Figure 8 *Typical charged particle background in vacuum (t=8 days in a row). Au/Pd/PdO pristine sample is in front of the SSB-1 (d=15 mm)*

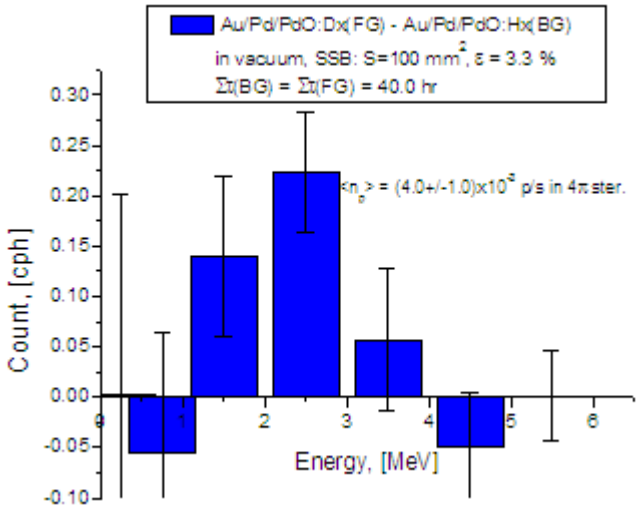

Figure 9. *Typical weak spontaneous DD-proton emission from Au/Pd/PdO:Dx (after electrolytic D-loading) in vacuum with Au/Pd/PdO:Hx Background subtracting.*

As seen from the Figs 8 and 9 the excess counts above the Background are appeared in the energy range of 1.5-3.0 MeV. These counts correspond to 3.0 MeV protons from DD-reaction originated at the Pd-PdO interface and at depth of several microns beneath the surface. Notice that the mean count rate of 3 MeV protons is found to be $<n_p> = 4x10^{-3}$ p/s. This count rate is only 5 times less than that of 2.45 MeV neutron emission rate from the similar samples due to proton losses in the sample during their escape.

Thus, we show that statistically significant low intensity emissions of DD-reaction products are observed in CMNS experiments These emissions are found to be and in a good correlation.

5. Energetic alpha emission

In 1998 we found that metal targets with a high hydrogen/deuterium solubility (Pd and Ti) being underwent either by electrolysis, glow discharge deuteron-bombardment or powerful pulsed laser irradiation demonstrate energetic charged particles emissions (ECPE), including alphas ($9.0 < E\alpha < 15.0$ MeV) and protons/deuterons ($E_p(E_d) \sim 1.7(2.8$ MeV)) [3]. Based on similarities between energy spectra of charged particles emitted in D/H Pd and Ti loading processes (Electrolysis, GD) with those emitted in the laser irradiation of TiH(Dx) targets we have speculated that the ECPE from the Pd and Ti targets is determined by focusing of the energy applied during H-loading to the cathode in some specific lattice sites near surface (possibly the sites of a high internal strain) containing light nuclei (including He^4).On the other hand, the coherent energy transfer from DD-reaction sites in metal deuterides accordingly to P. Hagelstein [4] would suggest the emission of alphas and protons in the same energy range as they were observed in our experiments.
As an example in Fig. 10 below we depicted the results of first convincing experiment on energetic alpha- particle emission. This experiment has been performed in Tohoku University using Au/Pd/PdO:Dx heterostructure electrochemically loaded with deuterium in after-electrolysis mode. The dE-E Si surface barrier detector pair (with almost zero Background) has been served as a charged particle detector. The two-dimensional spectrum obtained during total 550 hr of exposure with 20 individual samples unambiguously confirms occurrence of energetic alpha emission (with energies from 10 and up to 14 MeV) in the Pd/PdO heterstructure after deuterium loading.

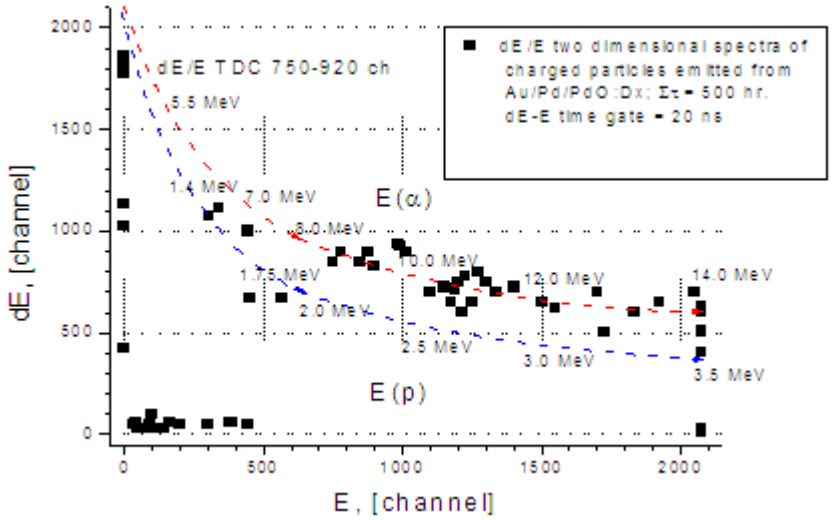

Figure 10: *dE/E (SSB: dE=20mm, E=100 mm) 2-dimensional spectra of charged particles from Au/Pd/PdO:Dx (after electrolysis). The energetic alpha emission rate was found to be $<N\alpha> = (6.4\pm1.2)x10^{-4}$ [s^{-1}] in 4π- steradian.*

Further detailed studies with track CR-39 detectors have shown that energetic alpha emission is observed also during in-situ electrolysis runs as well as during glow discharge deuteron bombardment and picoseond laser striking of the Pd and Ti targets loaded with deuterium or hydrogen. As an example below we consider in details some reproducible results observed during CR-39 detectors exposure with Pd/PdO:Dx heterostructure in after-electrolysis (exothermic D-desorption) mode.
The samples of Pd/PdO were synthesized by thermal growing of thin oxide layer (PdO_y) of 20 nm thick on top of 110 μm thick annealed cold worked Pd foils (area 2.3x1.1 cm^2) using an

oxygen-propane torch. The electrochemical loading of Pd/PdO cathodes by x=D/Pd = 0.7 has been carried out with low current density (j ~ 20 mA/cm2) electrolysis in 1M-LiOD/D_2O solution using a special cell with divided cathode and anodic spaces. Immediately after achieving an x=0.7 loading ratio, the electrolysis is interrupted. The Pd/PdO:D_x sample with attached CR-39 or thermal luminescent (TLD) detectors is placed under mechanical loading (m=150 g) for one hour at T =20 ° C. During this time the Pd/PdO:D_x sample showed signs of heating up to 7.0 ° C caused by exothermic deuterium desorption. About 90% of initial deuterium content was found to be desorbed through Pd-PdO interface during t = 1.0 hr. In control experiments a similar Pd/PdO sample electrochemically loaded with hydrogen in 1-M NaOH/H2O electrolyte and exposed to CR-39 detectors has been employed. In blank/background experiments, unloaded Pd/PdO heterostructure samples were used with CR-39.Both open and filtered CR-39 track detectors have been applied in our experiments in order to estimate type and energy distributions of emitted particles.
Pd/PdO:D_x runs with CR-39 detectors showed a highly reproducible yield of 3 MeV protons from DD-reaction accompanied by energetic alpha emission in the range of 11-16 MeV. These emissions are not detected in the blank experiments with unloaded Pd/PdO heterostructure. Integral charged particle spectra obtained with open CR-39 detectors (without filter) during 12 runs with duration ~ 1 hour (corresponded to effective time of D-desorption (Fig.1) for reference (Background) Pd/PdO and Foreground Pd/PdO:Dx samples, respectively are shown in Fig. 3.

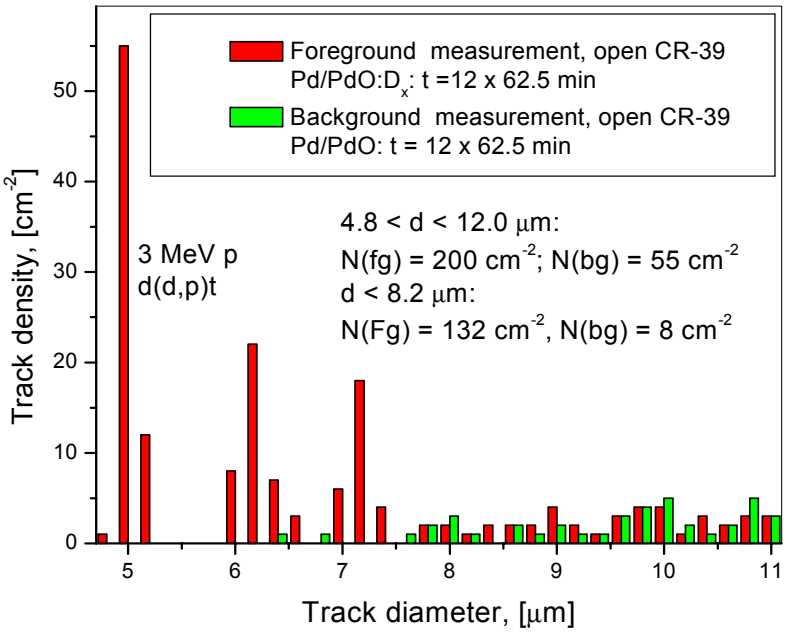

***Figure 11**: Foreground and Background counts from Pd/PdO:Dx and Pd/PdO, respectively: open CR-39 detector. Pay attention to high Foreground /Background ratio, especially below d = 8 μm.*

As seen, Background spectrum contains no tracks around 5 μm in diameter and only 8 tracks with diameter d < 8.2 μm. At d > 8.0 μm the Background spectrum contains usual alpha counts from radionuclides of radon and toron series presenting in the ambient atmosphere. In contrast, the Foreground spectrum showed three peak areas at d < 8.2 μm with total number of counts N=132, while at larger track diameters the number of counts is quite

comparable with Background. Accordingly to our earlier data and accelerator calibration of CR-39 with proton and alpha beams [3,4] the maximum near d = 5 μm belongs to 3 MeV protons; the group of counts near d=6.2 μm can be ascribed to lower energy protons/deuterons (E_p/E_d ~ 1.7/2.8 MeV) and counts around d = 7.2 μm were associated with high energy alphas in the range of 11-16 MeV.
In order to confirm our assumption concerning presence of 3 MeV protons as DD-reaction signature we compared open CR-39 spectra for Pd/PdO:Dx and Pd/PdO:Hx samples (Fig.4).

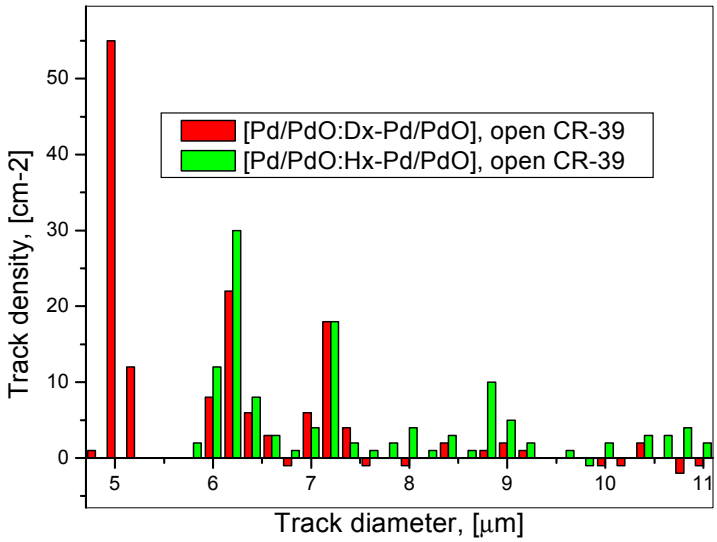

***Figure 12**: Comparison of Pd/PdO:Dx and Pd/PdO:Hx track distribution (with Background Pd/PdO counts subtraction): Main difference is the ~ 5 μm peak in Pd/PdO:Dx. No such peak in Pd/PdO:Hx.*

As seen for Fig. 12 the spectra of Pd/PdO:Dx and Pd/PdO:Hx look similar with only one exclusion: there are no counts at d < 6 μm have been found for Pd/PdO:Hx heterostructure. Thus, the group of counts associated with 5 μm peak belongs only to deuterated Pd/PdO sample. This peculiarity confirms our assumption concerning emission of 3 Mev protons (DD-reaction signature) in Pd/PdO:Dx heterostructure. On the other hand, the groups of counts around 6.2 and 7.2 μm are appeared in both Pd/PdO:Dx and Pd/PdO:Hx samples . This fact does not contradict to our earlier data showing presence of energetic alpha and proton/deuteron emissions independently on hydrogen or deuterium loading in Pd/PdO.
In order to present further proofs of proton and alpha emissions in Pd/PdO:Dx and Pd/PdO:Hx samples we performed special runs with CR-39 detectors filtered with 11 and 44 μm Al foils and 25 μm Cu foil. In Fig. 13 the Background Pd/PdO and Foreground Pd/PdO:Dx charged particle spectra obtained with CR-39 detector filtered with 44 μm Al is presented.

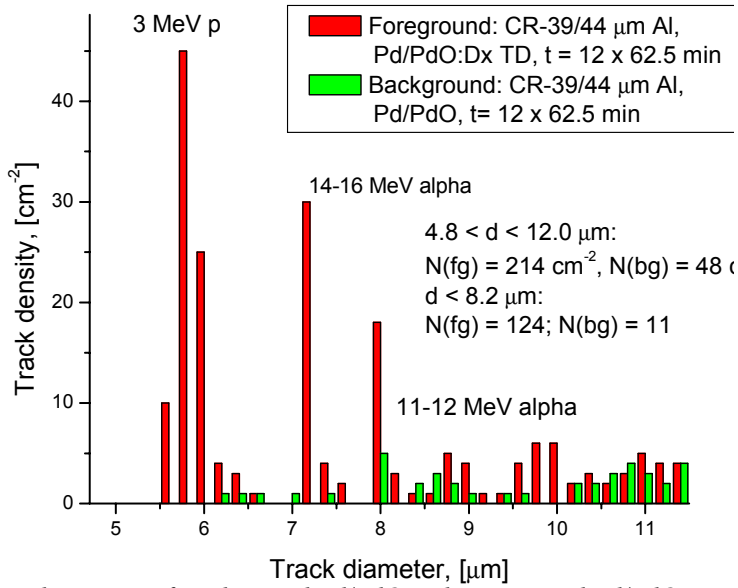

***Figure 13**: CR-39 charged particle spectra of Background Pd/PdO and Foreground Pd/PdO:Dx samples with 44 μm Al filter. Compared to open CR-39: shift of DD-proton track band from 5 to 5.6-6.2 μm diameters; splitting of alpha track band from 7.2 to 7.3–8 μm diameters. Note large Fg/Bg ratio at d < 8 μm.*

The other example of charged particle filtering with 25 μm Cu foil for both Pd/PdO:Dx and Pd/PdO:Hx samples is shown in Fig.14:

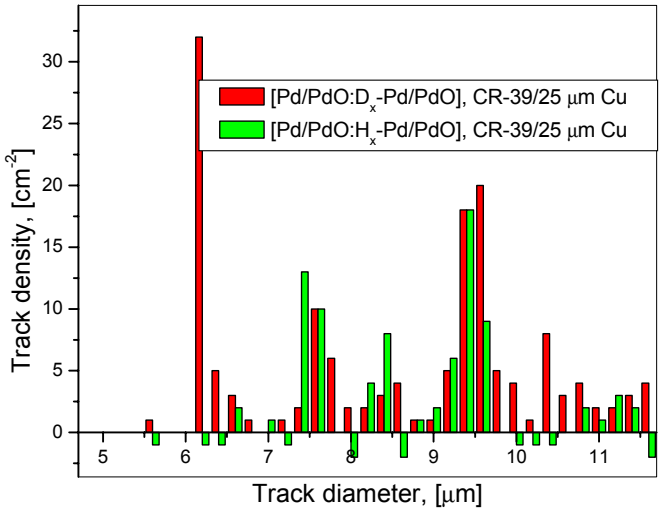

***Figure 14**: Charged particle spectra for Pd/PdO:Dx and Pd/PdO:Hx filtered with 25 μm Cu (with background subtraction). Alpha particle spectra of both H and D-loaded samples look similar.*

As seen from Fig.14 the 3.0 MeV proton band in Pd/PdO:Dx shifts further compared to the run with 44 μm Al filter to diameter ranging d = 6.2-6.6 μm. This shift is expected accordingly to stopping range of 3.0 MeV protons in copper. Notice that no counts were detected in this range for Pd/PdO:Hx sample. The shifts and amplitudes of alpha particle spectra for both H and D-loaded Pd/PdO samples look similar and indicate presence of the

same groups of alphas with energies 11-12 MeV (9.2-9.8 μm band) and 14-16 MeV(7.4-7.6 μm band) as were detected in experiment with 44 μm Al filter.
The summary energy spectrum, based on the measurements with open and filtered CR-39 detectors of energetic alphas in the range of track diameters 7.0-7.8 micron is shown in Fig.15

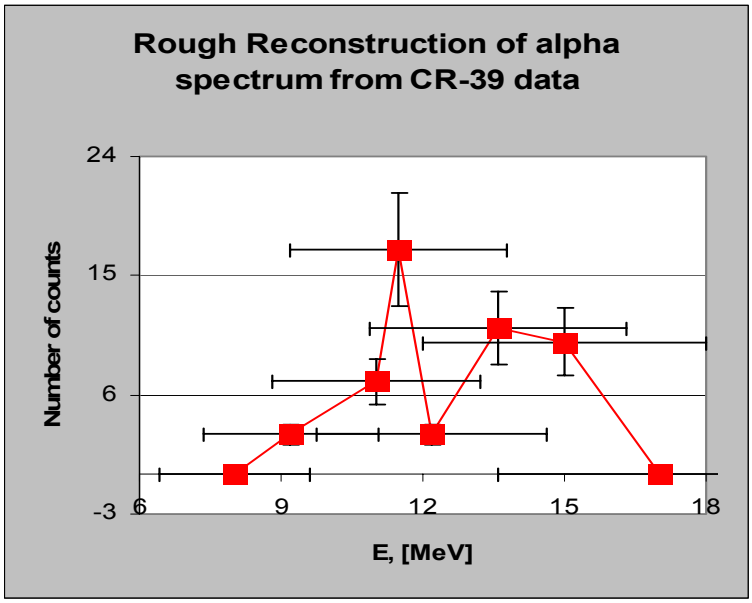

Figure 15. *Reconstructed Energetic alpha spectra for Pd/PdO:Dx samples, based on accelerator alpha calibration and stopping ranges of alphas in Al and Cu filters.*

The results of measurements with Pd/PdO:D(H)x samples are following:

- Using critical angles for 11-16 MeV alphas c = 42 ° we obtain the yield of energetic alpha particles in Pd/PdO:Dx during exothermic D-desorption Y = (5.5±0.9)x10-3 /s in 4 ster.
- Pd/PdO:Hx samples during H-desorption demonstrate 11-16 MeV spectra that are very similar to that of Pd/PdO:Dx. The yield of alphas at H-desorption is also similar to D-desorption case.
- Reproducibilty of both DD-reaction and energetic alpha emissions during D-desorption is close to 100%.

These results are found to be fully conivincable and confirm existence of energetic alpha emission from the surface of metals with a large hydrogen(deuterium) solubility.

6. Soft X-ray emission from the Pd and Ti cathodes

X- ray emission in CMNS experiments is one of the top priority issues that could convince physical society in reality of nuclear effects in metal-deuterium systems. So far, the search for X-ray emission in CMNS effects has been focused on evidence for Pd Kαβ - characteristic X-rays (Ex ~ 21 keV). These efforts were unsuccessful, though. Later, softer X-rays with energy E_x < 10 keV have been detected in electrolysis runs using semiconductor X-ray detectors by A. Takahashi et al, (ICCF-8 Proc., 2000) and by V. Violante et al, (Proc. ICCF-10, 2003). Due to difficulties to detect X-rays with semiconductor X-ray detectors in electrolysis we suggested to use Thermal Luminescent Dosimeters (TLD) with sets of filters for X-ray detection both during in situ electrolysis and in thermal D-desorption (after-electrolysis) mode (A. Lipson et al, ICCF-10, 2003). Simultaneously A. Karabut has proposed

to use TLD with set of Be-filters in order to estimate energy of X-ray spectra emitted by metal cathodes in glow discharge experiments (ICCF-8, 2000). Later A. Karabut first utilized soft X-ray spectrometer with bent LiF crystal for spectral measurements of X-rays in glow discharge (ICCF-12, 2005).

As an examples of soft X-ray detection below we show some spectacular results obtained during X-ray measurements from the Ti/Pd cathode in glow discharge and from Pd/PdO:Dx heterostructure in the D-desorption mode.

The schematic representation of A. Karabut's GD set up for X-ray measurement are shown in Fig. 16

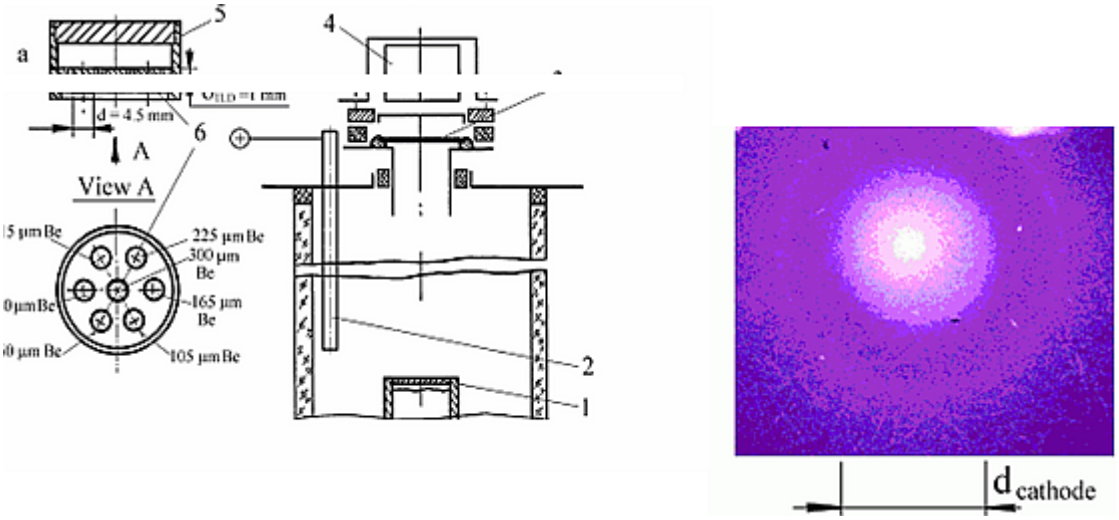

Figure 16. *Schematic representation of an "open cathode" (2) experiment. The TLD are inserted into cassette (6). X-ray image of this Ti-cathode using the pin-hole camera (4) (right photo). The objective of 0.3 mm diameter is narrowed by use of a 15μm Be shield in front of the camera. (The image is a positive imprint)*

The X-ray energy estimate with 7 TLD (filtered with Be of different thickness) are shown in Fig. 17. According to TLD measurement, the mean energy of X-ray quanta, emitted from the Ti cathode is <Ex> = 1.35 keV.

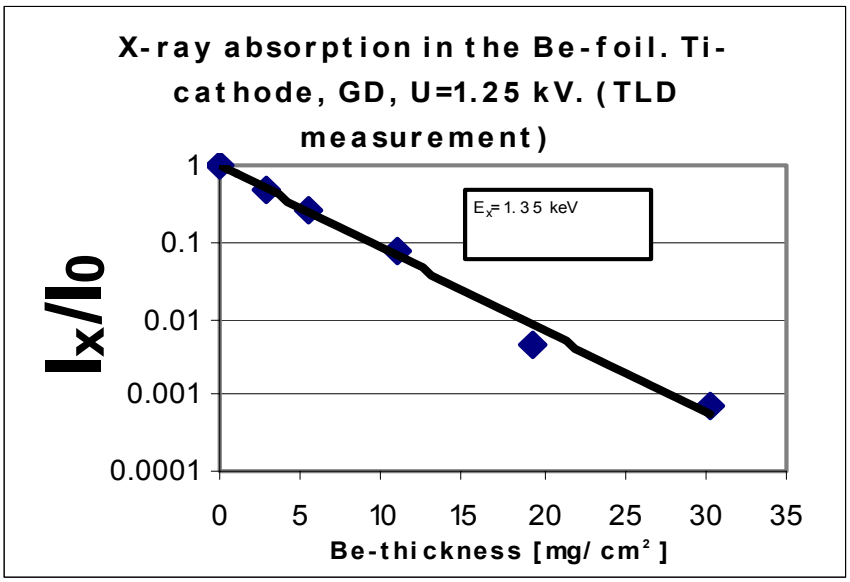

Figure 17. *X-ray energy measurement in Ti/D2 Pulsed Karabut's type glow discharge (A. Lipson et al, JETP, 2005).*

Correlation between the GD current pulses and X-ray emission is shown in Fig. 18.

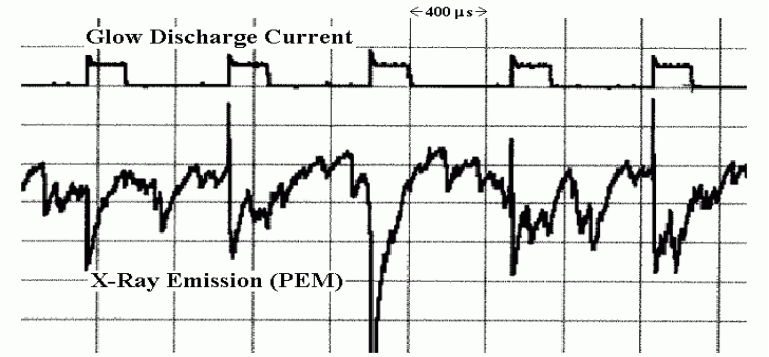

Figure 18. *Correlation between X-ray emission and current pulses in Karabut's GD.*

Finally, the yield of X-ray vs. effective discharge power is depicted in Fig.19.

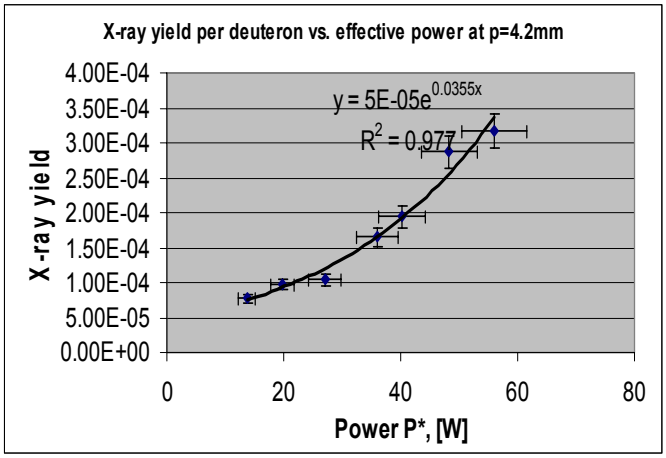

Figure 19. *X-ray yield from Ti-cathode vs. Effective power P*=UIQ; The yield is described by a formula:* $I_x = I_0 \exp[(\varepsilon/kT_m)P^*_x/P^*_0]$.

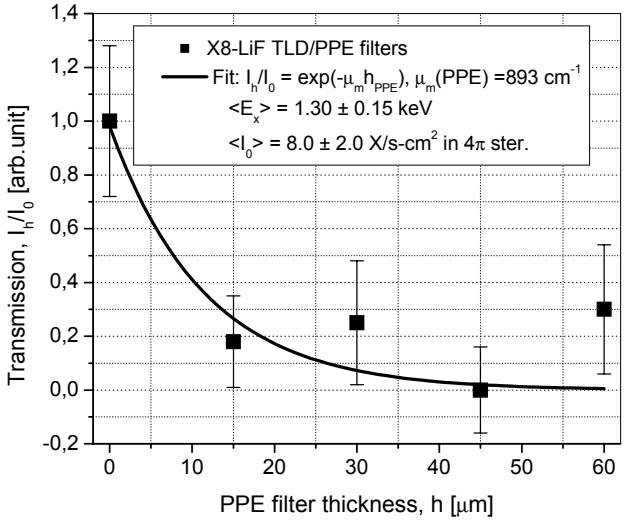

Figure 20: *Transmission of polypropylene filters (*$\alpha = I_h/I_0$*, where* I_h *–is the X-ray dose in TLD filtered with PPE of h μm thick and* I_0 *– is the X-ray dose in an open TLD at h=0) versus thickness of PPE filter.*

Another example of reproducible X-ray emissions during exothermic D-desorption from Pd/PdO:Dx cathodes (after electrolysis) is shown below. It was found that nuclear emissions from the surface of Pd/PdO:Dx heterostructure cathode are accompanied by soft X-ray emission. The X-ray TLD measurements (5 pairs of X8 LiF TLD with various filter thickness) performed with Pd/PdO:Dx sample showed non-negligible X-ray dose in Foreground TLD chips (attached to the Pd/PdO:Dx sample) compared with Background detectors.

In Fig. 20 the transmission of PP filters (that covers TLD pair) with respect to detected X-ray quanta is given as a function of PP filter thickness:

X-ray transmission dependence vs. PP filter thickness allows to reconstruct initial energy of X-ray quanta emitted from the surface of Pd/PdO:Dx cathode during exothermic D-desorption (Fig. 9). The fit of transmission curve showed mass-absorption coefficient $\mu(PPE) = 893$ cm^{-1}, corresponding to mean energy of X-ray quanta $\langle E_x \rangle = 1.30 \pm 0.15$ keV.

The open TLD showed dose $D = 12 \pm 2$ mrad = 120 μGy with Background subtracted ($D(Fg) = 21.0 \pm 1.0$ mrad, $D(Bg) = 9.0 \pm 1.0$ mrad) . In SI system the equation connecting the dose D_x [Gy] absorbed by LiF TLD with area $s = 0.04$ cm^2 and mean flux $\langle \ _x \rangle$ would be written as follows [8]:

$$\langle \Phi_x \rangle = 2D_x\rho(LiF)/1.6\times10^{-13}\ [J/MeV]\times E_x\times \mu_m\times (s/1cm^2)\tau \cong (8 \pm 2)\ X\text{-quanta/cm}^2\text{-s},$$

where (LiF) – is the density of LiF, $E_x = 1.3$ keV is the X-ray quanta energy and $= 7 \times 10^5$ s – is the total time of TLD exposure with Pd/PdO:Dx sample; $\mu_m(1.3\ keV) = 7\times10^5$ cm^2/g – is the LiF mass-absorption coefficient for 1.3 keV quanta obtained by extrapolation of known data in the range of 4-10 keV to lower energies [8].

Note that estimated dose obtained from the charged particle absorption by LiF TLD (i.e., emitted from the surface of Pd/PdO:Dx) would be less than 1 mrad (below detection limit).

Entire results showed that Exothermic D-desorption is that obvious link between DD-screening, soft X-ray emission and high energy alpha generation from the surface of Pd/PdO:Dx. Note that the energy of X-ray quanta emitted from Pd/PdO:Dx is in good agreement with that reported by Karabut in glow discharge runs. This suggests similar mechanism caused by D-desorption from the cathode.

7. Conclusions

In present Review it is shown that four most important features of CMNS exist unambiguously:

- DD-reaction enhancement during low energy deuteron bombardment of metallic targets (accelerators and glow discharge experiments)
- Low intensity emissions of DD-reaction nuclear particles: 3 MeV protons, 1 MeV tritons, 2.45 MeV neutrons
- Energetic alpha emission ($E_\alpha \geq 8.0$ MeV). These alphas cannot be emitted by natural radionuclides/cosmic background.
- Soft X-ray ($E_x \leq 1.5$ keV) emission in experiments with pulsed Glow Discharge and during D-desorption from Pd/PdO:D_x .
- Observed nuclear effects in metals cannot be explained by fracto-fusion because the electric field inside the cracks would be too low. Phonon energy of D-desorption focusing or/and concentration in some specific lattice sites near surface (the sites of a high internal strain ?)

- DD-reaction, energetic alphas and X-ray emissions suggest anomalous energy release via "active" lattice sites of non-equilibrium metal deuterides, indicating at least intra-atomic electric field release ($E \sim 10^{10}$ V/cm)

In conclusion, taking into account above results we also show the ways how to convince physicists in a nuclear origin of Excess Heat effect. To this aim the following experiments are required:

- Complete experiment with simultaneous detection of excess heat, atomic 4He, 3T, charged particles (DD-products +energetic alphas) and neutron emissions, as well as soft X-rays ($E_x \leq 2.0$ keV), not characteristic K_α of Pd)
- Search for correlations between excess heat events and emissions of atomic, nuclear species and X-rays
- Special electrolytic cells and appropriate state-of- the-art calorimetric and nuclear detection equipment.
- To use novel (nanostructured/nanolayered) samples as the cathodes (Pd-SWCNT-Pd, Pd-Re-Pd and PdO-Pd-PdO) with enhanced charged particle yield.

References

1. H.S. Bosch and G.M. Halle, "Improved Formulas for Fusion Cross-sections and Thermal Reactivities", *Nucl. Fusion*, 32, 611(1992).
2. A.G. Lipson, A.S. Roussetski, A.B. Karabut and G.H. Miley, "DD Reaction Enhancement and X-ray Generation in a High-current Pulsed Glow Discharge in Deuterium with Titanium Cathode at 0.8–2.45 kV", *JETP*, 100, 1175 (2005).
3. M. Junker, A. D'alessandro, S. Zavatarelli et al., "Cross Section of ^{3}He(^{3}He,2*p*)^{4}He Measured at Solar Energies", *Phys. Rev.*, C 57, 2700 (1998).
4. M. Aliotta, F. Raiola, G. Gyurky et al., "Electron Screening Effect in the Reactions ^{3}He(d,p)^{4}He and d(^{3}He,p)^{4}He*", *Nucl. Phys.*, A690, 790 (2001).
5. K. Czerski, A. Hulke, A. Biller et al., "Enhancement of the Electron Screening Effect for D+D Fusion Reactions in Metallic Environments", *Europhys. Lett.*, 54, 449 (2001).
6. F. Raiola, P. Migliardi, G. Gyurky et al., "Enhanced Electron Screening in d (d, p)t for Deuterated Ta*", *Eur. Phys. J.*, A13, 377 (2002).
7. F. Raiola, P. Migliardi, L. Gang et al., "Electron Screening in d(d,p)t for Deuterated Metals and the Periodic Table", *Phys. Lett.,* B547, 193 (2002).
8. D. Reiter, "Edge Plasma Physics Overview", *Trans. Fusion Tech.*, 33, 249 (1998).
9. A.G. Lipson et al, "Enhancement of First wall damage in ITER type TOKAMAK due to LENR effects", Proc. Of 12th International Conference on Condensed Matter Nuclear Science, 2005, Yokohama, Japan, to be published.
10. A.G. Lipson, "Edge plasma effects in ITER-type TOKAMAK caused by an enhancement of DD/DT reaction in metals at high current-low energy deuteron bombardment ", Proc. 7-th International Workshop on Anomalies in metal-deuterium systems Asti, Italy, 2006, PPT presentation
11. V. Violante, A. Torre, G. Silvaggi and G.H. Miley, "Three-dimensional Analysis of the Lattice Confinement Effect on Ion Dynamics in Condensed Matter and Lattice Effect on the d-d Nuclear Reaction Channel", *Fusion Tech.*, 39, 266(2001).
12. U. Greife, F. Gorris, M. Junker et al., *Z. Phys.*, A465, 150 (1995).
13. F. Raiola, et al. (LUNA collaboration), "Electron Screening in d(d,p)t for Deuterated Metals" , *Nucl. Physics*, A719, 61C (2003).

14. H. Yuki, J. Kasagi , A. G. Lipson et al, "Anomalous Enhancement of DD Reaction in Pd and Au/Pd/PdO Heterostructure Targets under Low-Energy Deuteron Bombardment", *JETP Lett.*, 68, 785 (1998).
15. J. Kasagi, H. Yuki, T. Baba et al, "Strongly Enhanced DD Fusion Reaction in Metals Observed for keV D^+ Bombardment", *J. Phys. Soc. Jpn*., v71, 2881 (2002).
16. K. Eder, D. Semard, P. Bauer et al., "Absence of a "Threshold Effect" in the Energy Loss of Slow Protons Traversing Large-Band-Gap Insulators", *Phys. Rev. Lett.*, 79, 4112 (1997).
17. S.P. Moller, A. Csete, T. Ichioka et al., "Antiproton Stopping at Low Energies: Confirmation of Velocity-Proportional Stopping Power", *Phys. Rev. Lett.,* 88, 193201 (2002).
18. G. H. Miley., A. G. Lipson., R. Smith, et al.,"Evidence for intense soft X-ray emission from a hydride target undergoing intense deuteron bombardment.". *Transactions of the American Nuclear Society*, Winter Meeting 889-890 (2005).

REPLICATION OF ENERGETICS HEAT AND TRITIUM PRODUCTION

M. McKubre* michael.mckubre@sri.com and F. Tanzella*,
V. Violante, C. Sibilia***, T. Zilov**** and I. Dardik*****

**SRI International. Menlo Park, California, USA.*
***ENEA, Frascati, Italy, ***University of Rome, Italy,*
***** Energetics Technologies Inc., Omer, Israel,*
****** Energetics LLC., New Jersey, USA.*

Abstract

Difficulty in replicating the experiments of others has led to a criticism of an apparent irreproducibility that has severely handicapped the development and emergence of the field of Condensed Matter Nuclear Science (CMNS). Probably the most important experimental program in the CMNS and potentially any other emerging energy field is that undertaken by Energetics Technologies and presented at each of the past ICCF conferences with reports of factors of 10 or more power and energy gain in both D_2 gas phase and D_2O electrolytic experiments [1, 2, 3].

In the past year SRI has succeeded in reproducing the major results of excess power and tritium production in D_2O electrolytic experiments. Similar replication has also been accomplished at ENEA (Frascati) with support from the University of Rome. These results will be reported seperately. There can be very little doubt that there is a heat production in the D/Pd system on the scale of 100's or 1000's of eV per palladium or absorbed deuterium atom, that there is an associated but not quantitatively correlated nuclear product (in this case tritium), and that the effect is reproducible under defined conditions. Detailed results will be reported.

References

1. Dardik, I., *et al*, «Intensification of low energy nuclear reactions using superwave excitation», Proc. ICCF10 Cambridge, MA, (2003), pp. 61.
2. Dardik, I., *et al*, « Excess heat in electrolysis experiments at Energetics Technologies », Proc. ICCF11 Marseilles, France, (2004), pp. 84.
3. Dardik, I., *et al*, « Progress in electrolysis experiments at Energetics Technologies », Proc. ICCF12 Yokohama, Japan, (2005).

THE FLEISCHMANN-PONS EFFECT

M. C. H. McKubre

Energy Research Laboratory
SRI International, Menlo Park, CA, 94025, USA.
Michael.McKubre@SRI.com

Introduction:

The public announcement on March 23rd 1989 by Professors Fleischmann and Pons of the discovery of nuclear-level heat effects in palladium deuteride came as a surprise to most. The extent and degree of surprise has been greatly overstated by those who were not researching actively at that time. Essentially everybody who heard the news and had the means to do so, diverted their attention to theoretical and practical considerations of replicability. Professors of chemistry and physics entered their laboratories, in some cases for the first time in decades with serious intent. Their near universal purpose was to be among the first few to reproduce, in some cases real, in some cases hypothetical or mistaken aspects of the "Fleischmann-Pons" effect.

The dilemma all were confronted with immediately was; what to reproduce? What conditions were necessary and sufficient to produce the heat effect? It was clear that it was not going to be easy. The history of palladium deuteride research, while nowhere near as rich as that of palladium hydride studies, was nevertheless sufficiently well established to be certain that anomalous effects were either subtle or not present under ordinary conditions. If the needed (and as yet unstated) conditions were extraordinary, then few if any groups could approach the technical competence of the Fleischmann-Pons team, or the experience of Martin Fleischmann who had studied the Pd-D system electrochemically since 1948.

In this light the failures that resulted might have been predicted. The purpose of this paper is to address the question: how might this failure of process have been avoided? Is there a logical thought process that might have guided research to improve our probability of arriving more directly at a satisfactory conclusion? In an attempt to answer this question and present some possible benefit to future science we propose retrospectively, one possible set of questions that might have been asked in 1989 as a process to be followed to a logical conclusion. In a future publication we will examine the disorderly answering of these questions to evaluate what we might have acheived in an ordered process and to evaluate the present state of the field.

Questions unanswered in 1989:

The following series of question might have been posed in early 1989, solely on the basis of public pronouncement and preliminary data release from Fleischmann and Pons:

1. **Q1** *Is there unexplained heat?*
    - *a.* Is there anything that needs an explanation?
        - *i.* Could the heat measured be the product of chemical reactions or energy storage effects?
        - *ii.* Is the heat truly of nuclear scale?
        - *iii.* By what factor do chemical and nuclear energy scales differ?
    - *b.* What are the calorimetric uncertainties?
        - *i.* Are the heat effects observed statistically significant?
        - *ii.* Could the result reported be an effect of systematic error?
        - *iii.* Can the heat be measured in a calorimeter of different operating principle?
    - *c.* Is the heat effect transportable to another laboratory?

2. **Q2** *Is the heat output sensibly correlated with inputs?*
    - a. Is there an initiation effect?
        - i. Is there a time before which no heat effect can be observed?
        - ii. If so, what might cause this delay?
        - iii. (How) can it be avoided?
    - b. What makes the heat intensity increase or decrease?
        - i. Is the deuterium concentration important?
        - ii. What is the effect of increasing or decreasing the deuterium loading?
        - iii. Is this a threshold effect?
        - iv. (How) can the D:Pd atomic ratio be known?
        - v. Can this be measured *in situ*?
        - vi. What are the roles of temperature and pressure?
        - vii. (How) does the presence of protons in the electrolyte or Pd lattice play a role?
    - c. Is heat production a surface or bulk effect?

i. Does heat scale with cathode volume?
ii. Does heat scale with cathode surface area?
iii. Does heat scale with surface cathode roughness?
iv. Is the heat effect a property of the D-Pd system?

d. Is electrochemistry necessary for the effect?
   i. Does the effect behave systematically in response to changing current density – what is the role of electrochemical kinetics?
   ii. What are the roles of electrochemical thermodynamics and deuterium chemical potential?
   iii. Is the role of electrochemistry confined to loading deuterium into the palladium lattice?
   iv. Can the effect be produced in palladium loaded by other means?
e. Is electrochemistry sufficient for the effect?
   i. Is the role of electrochemistry confined to loading deuterium into the palladium lattice?
   ii. What is the role of electrolyte and surface impurities?
   iii. Is there a triggering effect associated with current?
   iv. Can other means be used to trigger the effect?
f. What is the role of palladium?
   i. Is the important (unique?) characteristic of palladium the hydrogen (deuterium) solubility, mobility, permeability or something else?
   ii. Is crystal size or metallurgical micro-structure important?
   iii. Can other metals (elements or alloys) be used?
   iv. Can cathodes be used to produce the heat effect in shapes other than wires (or cubes)?

3. **Q3** *Are nuclear processes associated with the effect?*
   a. An argument was made that the measured heat energy being larger by orders of magnitude than known mechanical or chemical energy implies a nuclear source.
      i. Is this argument plausible?
      ii. Is it compelling?

iii. What other primary energy sources are known or might be imagined that could produce similar effects?

b. Are we really thinking about fusion: d-p, d-d, d-Li, *etc*.?

i. What is the relevance of high energy or plasma pairwise fusion effects to putative solid-state nuclear reactions?

ii. Can concerns about conservation of energy and momentum be addressed using many-body or wave overlap concepts?

iii. What is the effect of changing hydrogen and/or lithium isotope distributions in the experiment?

c. What are the numbers (and detection limits) on all pertinent prompt energetic radiation and emissions from heat producing and non heat producing experiments?

i. X-ray?

ii. Gamma-ray?

iii. Neutron?

iv. Charged particle: beta, proton, alpha, *etc*.?

d. Is there any evidence of tritium released promptly or post-test in the electrolyte or cathode from heat producing and non heat producing experiments?

e. Is there any change of palladium isotope distributions post-test from heat producing and non heat producing experiments?

f. Is there any evidence of palladium lattice or impurity gamma or beta activation post-test from heat producing and non heat producing experiments?

g. Should we expect the primary quantitative products or heat producing reactions to be at fixed branching ratio or in any way correlated with secondary nuclear reaction products[1]?

h. What, if any, understanding can we take from the absence of neutrons at

---

[1] It was apparently Fleischmann's early view, expressed in the following quote [2], that neutron and possibly other prompt emission should be corellated with heat production. *„Surprisngly, much of the research effort has been directed at a search for neutrons… without first attempting to verify the production of excess enthalpy. Predictabbly, the search for neutrons without excess enthalpy has been a fruitless one"*.

unhealthy (and therefore unmistakable) radiation levels[2]

4. **Q4** *Is nuclear ash correlated with the excess heat?*
    a. In the absence of intense radiation what options remain for potential nuclear ash that are aneutronic in their creation and non-radioactive?
        i. Helium [^{3}He and ^{4}He]?
        ii. Other light elements [Li Be, B, C]?
        iii. Higher Z isotope shifts [Pd and impurities]?
    b. What quantities of these products are expected from the measured heat energies?
        i. What is the postulated reactant and reaction?
        ii. In which phases are the products expected to be found [bulk metal, near surface, electrolyte, gas]?
        iii. What are the background concentrations of potential products?
    c. What means are available and suitable to search for these product isotopes?
        i. Mass spectroscopy?
        ii. Neutron activation analysis?
        iii. Other?

    d. What are the potential problems?
        i. Sensitivity?
        ii. Background?
        iii. Isotope specificity?
        iv. Interferences?
        v. Matrix effects?
        vi. Range of specificity?

5. **Q5** *Are their other nuclear effects?*

---

[2] Heavy emphasis and associated weight of opinion placed on the absence of a putative nuclear product (neutrons) that obviously could not be quantitatively associated with the effect under study (heat) appears to support our expressed opinion that with logical planning, weighting and sequencing of experiments we might have avoided some of the emotional, political and scientific missteps made in investigating the Fleischmann-Pons effect.

A claimed breadth of nuclear processes is characteristic of the effect diversely addressed as: the Fleischmann-Pons effect; cold fusion; low energy or chemically activated nuclear reactions; condensed matter nuclear reactions. Imprinted indelibly into our individual and collective consciousness, the name "cold fusion" in fact appears to have originated with Jones and Rafelski [1-3]. These authors invoked the phrase "cold nuclear fusion" to describe muon catalyzed pairwise d-d fusion[3] and later argued in 1989 that this effect was responsible for low level neutron generation in condensed matter reactions[4]. Although the evidence for heat effects in palladium deuteride was clear at that time [5] and ultimately determined to be sound [6], direct evidence of commensurate fusion product creation was slow in coming [7 and see reviews 6, 8,9]. To this date no evidence has been accumulated of reactant consumption in d-d heat production, and the measured product distributions, $^{4}He >> {}^{3}H >> n°$, cannot be associated plausibly with two body fusion effects.

Despite the current absence of a full d + d = ^{4}He mass balance and the skewed product distribution that supports Schwinger's observation that "the circumstances of cold fusion are not those of hot fusion", we will in this review assert the position that the primary process of the Fleischmann-Pons effect is cold fusion, although certainly not muonic or pairwise[4]. The original claim was of nuclear level heat production, and this product is of primary engineering significance. Both are significant motivations although obviously significantly more work is needed to study and define the parameter space of excess heat production, and to determine it's practical utility.

Clues nevertheless are present in the secondary and tertiary nuclear effects that may guide us to identify what nuclear processes are and are not occurring in our condensed matter nuclear experiments. At this point the clues are numerous but difficult to interpret. Claims have been advanced for essentially every "conventional" nuclear product as well as some distinctly exotic products or intermediates. In Table 11 of his excellent review, [9] Storms summarizes the method and products of over 50 experiments in which heat is not a sole or primary product. In evaluating this evidence critically two questions are paramount in guiding future theory that must account quantitatively not only for the primary but also secondary and tertiary nuclear product formation:

---

[3] Other reactions are possible, including p-d and d-t. The idea of muon catalyzed fusion itself is due to Sakharov and Frank and was first observed experimentally by Alvarez in 1957.

[4] That is to say as the primary process deuterium is consumed to produce ^{4}He in a many body reaction mediated by a lattice with the resultant heat energy coupled to the lattice.

a. Under what conditions were the experiments performed?
   i. Host material?
   ii. Pressure, temperature, loading?
   iii. Impurity and defect distributions?
   iv. Stimulus and perturbation dynamics?

b. What are the nuclear (and other) products in all channels?
   i. Quantity?
   ii. Energy?
   iii. Time evolution?
   iv. Sensitivity, accuracy and reliability of measurement?

6. **Q6** *What is the nuclear process?*

Given adequate and accurate answers to all questions **4 a-d** and **5 a** and **b**, theorists will be in a position to make definite and quantitatively predictive statements in answer to this question. We have not reached this point. Theory and theorists continue to provide excellent support and guidance but the questions of the moment still are largely experimental. Our assertions that in the "primary process deuterium is consumed to produce ^{4}He in a many body reaction mediated by a lattice with the resultant heat energy coupled to the lattice" should be treated as an hypothesis undergoing test. In addition to posing questions for experimental test, the demands of theory will be to answer the following crucial uncertainties:

a. What are parametric effects in intensive and extensive scaling?
b. What are the hazards and limitations?

7. **Q7** *What is the future*?

This is a tremendous list of questions, still incomplete and growing with hindsight. We do not suggest that any individual or single research group did or should have addressed a majority of items before beginning experimentation. It is almost certain, however, that all of these questions were anticipated and more, in the collective talent and wisdom of the worldwide effort in early 1989. By elaborating detailed answers developed retrospectively to a few critical questions we intend to suggest that, if this wisdom been collected and used to anticipate the problems, then much more rapid progress could have been made to resolve the underlying question: what is the Fleischmann-Pons effect?

In our view, critical to converting a rational and sufficient set of questions to be

answered, into a practical and efficient work plan, is the recognition that the plan is sequential. It is a process that must be followed step-by-step with satisfactory conclusion or near completion of each step before venturing to the next. Focusing just on the large enumerated questions[5] [**Q1** – **Q6**] for example, there is little point in an intense, time-consuming and expensive phenomenological study to answer question **Q2,** unless and until it is clear that the effect is real and not of mundane origin. Similarly, an examination of theoretical options that is well bounded, cannot take place efficiently until we know that the heat effect is real [**Q2**], is nuclear [**Q3**], is quantitatively and temporally correlated with product ash [**Q4**], and has associated secondary, tertiary and missing branches [**Q5**][6].

This last point might surprise or appall theorists who have been perhaps the greatest contributors in discussions and publications on the Fleischmann-Pons effect. As will be discussed later, however, we are not even now at the point of bounding all nuclear effects even in the best studied sub-system, the electrochemical palladium deuterium system, to permit efficient transition from **Q5** to **Q6** and hence to attempt rational assessment of **Q7**. For independent verification of this conclusion we need look no further than the plethora of conflicting models presently proposed to explain the effect as it is, or as it is hypothesized[7].

In deference to the the ardor, enthusiasm and impatience of the people who have brought the field to the point it is today it is tempting, at this point to attempt and answer to **Q7** and thus ignore the advice and primary conclusions of this work that:

1. The process outlined is sequential, and
2. Each step is entered into with maximum effect only as the previous one is concluding.

Exhibiting unusual discipline we will not succumb to this temptation except to say that the future is likely to be very bright. Even at this early stage of development it is clear that Fleischmann and Pons have pointed us to a way to command the power of the nucleus, without the need to resort to gigantic, elite and expensive machines. Will this fact become an important part of the answer to man's growing energy dilemma? So far in this process

---

[5] In some cases the sub-questions and sub-sub-questions can be addressed and answered in parallel; in some cases they are coupled or dependent. Where possible we have nevertheless attempted to preserve a logical order sequenced with time.

[6] That is not to say that theory and experiment cannot continue to support each other on the pathway from Q1 to Q7. Many of the concerns in Q#, for example, require a theoretical answer.

[7] The existence of these models was and is necessary to counter mischievous and irrational assertions of critics that the Fleischmann-Pons heat effect violates known laws of physics. Again, until we know what nuclear physical effects are and are not present this negative assertion is even more premature than the speculative models proposed to account for various of the effects observed.

nothing has been identified to make us suspect that the answer to this final question will be no.

References:

1. S.E. Jones, *et al*, "Observation of Unexpected Density Effects in Muon-Catalyzed d-t Fusion," **Physical Review Letters** 56: 588-591 (1986).
2. S.E. Jones, "Muon-Catalysed Fusion Revisited," **Nature** 321: 127-133 (1986).
3. J. Rafelski and S.E. Jones, "Cold Nuclear Fusion," **Scientific American**, 257: 84-89 (1987).
4. S.E. Jones, E.P. Palmer, J.B. Czirr, D.L. Decker, G.L. Jensen, J.M. Thorne, and S.F. Taylor & J. Rafelski, "Observation of Cold Nuclear Fusion in Condensed Matter," **Nature** 338: 737-740 (April 1989).
5. M. Fleischmann and S. Pons, **J. Electroanal. Chem., 261**, 301 (1989).
6. C. G. Beaudette, “Excess Heat”, **Oak Grove Press**, (2002).
7. M. H. Miles, R. A. Hollins, B. F. Bush, J. J. Lagowski and R. E. Miles, ”Correlation of excess power and helium production during D2 O and H2 O electrolysis using palladium cathodes”, **J. Electroanal. Chem**. 346, 99 (1993).
8. P. L. Hagelstein, M. C. H. McKubre *et al*, **Proceedings ICCF-11**, 23 (2004.
9. E. Storms, “The Science of Low Energy Nuclear Reaction”, **World Scientific Press**, (2007).

BURSTS OF COUNT RATE OF BETA-RADIOACTIVE SOURCES DURING LONG-TERM MEASUREMENTS

A.G. Parkhomov

Institute for Time Problem Researches, Lomonosov Moscow State University
alexparh@mail.ru

When scanning the celestial sphere by a reflecting telescope with radioactive sources of ^{60}Co or ^{40}K at the focus, bursts in the count rate were registered. There were registered as single bursts with duration of about 1 second and an increase in the count rate up to three orders of magnitude so more prolonged (up to several hours) events that consisted of short bursts of various amplitude distributed in time in some complicated manner. The conformity of observable effects to the predicted developments of very low energy neutrino space flows is marked. The received results show a capability of substantial growth of speed of beta-radioactive decay.

Introduction

The radioactive decay refers to the highly stable and predictable processes. According to present views, there occurs an exponential drop in the number of particles radiated in a unit of time with fluctuations corresponding to the Poisson distribution. The detection of the smallest deviation of such behavior points to the existence of unknown actions or not yet studied properties of space and time. The importance of these researches is obvious. It is clear that they require a combination of high accuracy with carefulness of conclusions.

To investigate anomalies in the course of some processes, an experimental setup was build up that was characterized by the completeness and long duration of measurements great number of simultaneously investigated processes (information was read from 20 channels), thermostatting of the majority of detectors and power sources as well as the possibility of long-standing uninterrupted registration of signals in combination with high accuracy in determining time points of events [1, 11]. Besides the alpha- and beta- radioactivity, rhythms and fluctuations of various processes (low-frequency noise in semiconductor devices, generation of oscillations by instruments with quartz resonators) together with the analysis of the course of temperature and radiation background were investigated.

The experimental setup

The signals coming from each detector to the input of recording computer were pulses the spacing of which depended on the value of measured parameter (amplitude of noise, frequency of generation, count rate of the detector of particles, temperature, etc). The computer registered only the number of channel and time point of coming of the next pulse. The pulse repetition frequency was not large (approximately one pulse per minute); therefore information was recorded extremely compactly which was very important during the long-term multi-channel registration. The information stored in the computer was automatically (or on command of an operator) discharged to a floppy disc several times per day, which allowed to transmit information to another computer without disturbing the process of continual registration. The value of the measured parameter was restored when processing the results according to the known dependence of the said parameter on the duration of pulse spacing in each channel.

The registration of extremely small variations of the radioactive decay count rate or the frequency of generators with quartz generators requires the most accurate measurement of time. The exactness of computer's clock is insufficient for pursuance of good measurements. To improve them, the quartz resonator of the computer's clock was temperature-controlled.

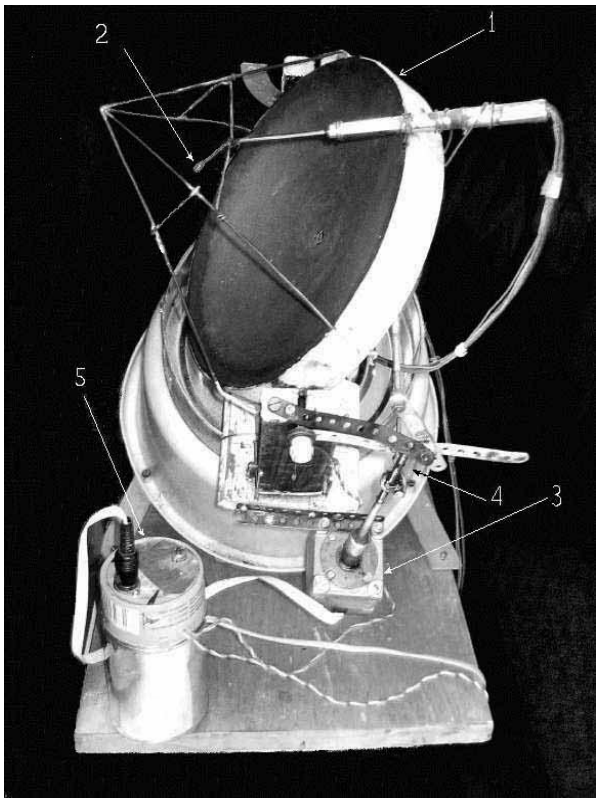

Fig. 1. *The telescope for observation of bursts.*
1 - Steel mirror with parabolic surface,
2 - G-M counter with mounted ^{60}Co-source
3 - motor operating in step-by-step mode
4 - mechanism of rotation around the axis of declinations
5 - control unit for the motor

Besides, the radio signals of exact time were applied every hour to one of inputs of the computer. This allowed, when processing the results, to introduce corrections reducing the errors in determination of absolute time down to 0.05 seconds. To minimize temperature influences, the most of detectors together with their power sources were placed in a constant-temperature cabinet or have an individual

thermostat. Additionally, the temperature near the setup and in the cabinet-thermostat was recorded to monitor possible thermal influences.

The bursts of radioactivity were detected with the aid of a reflecting telescope at the focus of which a beta-radioactive source connected with a G-M counter was positioned. The photograph of the telescope is shown in **Fig.1**. The reflecting mirror of steel with the parabolic surface 22 *cm* in diameter has the focal length of 10 cm. The beta-radioactive source is placed at the focus of the mirror and connected with a miniature G-M counter with the sensitive volume 2 *mm* in diameter and 6 mm in length.

As the beta sources were applied:

- Foil by the size 2x4 мм^2 by thickness of 0,1 mm, containing radioactive ^{60}Co;
- Or ball of diameter 3 mm from K_2CO_3. The natural mixture of isotopes of a potassium contains 0, 12 % radioactive ^{40}K.

The telescope has two reciprocally perpendicular axes of rotation, one of them is parallel to the Earth′ s axis and allows changes in the direction of the telescope along the celestial equator (hour angle), and another axis makes possible to vary the deflection from that (declination). The declination can follow a predetermined program.

The pulses from the G-M counter arrived to a frequency divider, the sequence of pulses time points from divider were recorded into the PC′ s memory. The count rate was determined as the ratio of the count-down k of the divider (that is, the number of particles counted over the pulse spacing) to the length of this interval as measured by the computer′ s clock [1]. Such a method of continual measurement of count rate offers an advantage over the traditional one (counting the number of pulses over a fixes time) not only in the absence of missing of pulses and simplicity of realization but in the automatic enhancement in speed of measuring with an increase of count rate of pulses. This was of primary importance for the study in consideration. An ordinary count rate was in the mid-2004 about of 5 *pulses per second* (at the background counting 0.01 *pulses per second*), which corresponded, if using the divider with k = 256, the recording of information by the computer with intervals about 1 *minute*. Sometimes the count rate increased up to several thousand *pulses per second* within the span of ~1 *second*. Then the time for collecting 256 pulses (i.e. e. interval between events of recording) shortened down to some ten′ s fractions of a second, which allowed not only recording the fact of a burst but to follow its dynamics, too.

Basic results

Analysis of results obtained over the five-year period of investigations is presented in the paper [1]. The considerable duration of practically uninterrupted observations made it possible to reveal rhythms of periods up to a year as well as to investigate the thin structure of more short rhythms. When measuring the rate of beta-sources ^{60}Co and ^{90}Sr-^{90}Y, rhythmical variations with amplitudes of 0.3 % from the average value with the period of a year, 0.02 % with the period of a month, and 0.005 % with the daily period. Stable rhythmical changes in the decay rate for the α-source ^{239}Pu were not detected (the upper limit was equal to 0.01 % from the average). Rhythmical variations in count rate of β -sources were also detected by Yu. A. Baurov with the coworkers [2].

The investigations on the setup with a beta-source at the focus of the parabolic mirror were started in spring of 1999. The processing of averaged results revealed an exponential fall in the count rate that is in a good accordance with the known 5.27-year half-life period of ^{60}Co. The long duration of measurements made it possible to establish that this monotone fall was superimposed by rhythmical changes in the count rate with the period of one year and amplitude of 0.3% from the average count rate [1]. Besides, rather considerable bursts of count rate with duration from some seconds to several hours were sometimes recorded, too. We managed to detect such bursts only due to long duration of almost uninterrupted observations because the summary duration of recorded bursts were no more than 1/1000 of setup operation time.

In the first stage of investigations, the telescope was oriented in a nearly eastward direction at a fixed inclination to the horizon. When rotating together with the Earth, the telescope "scanned" a strip of the celestial sphere around 1° of width. The astronomic coordinates of the place on the celestial sphere to that the telescope was directed at the moment (declination and right ascension) were determined accurate to ~1° with the aid of astronomic tables from the solar image motion observations. In **Fig.2** is shown the change in count rate for one of the bursts. The recordings of some other bursts are given in the paper [1].

The **Table 1** gives information on the bursts recorded from June, 1999, till January, 2002 (date, Moscow summer time of starts and ends of anomalous parts, time of the minimum distance t_{min} between the direction of the telescope and the Sun, declination of the scanning line δ (in degrees), and the ratio K of the maximum count rate in the anomalous part to the average count rate before and after the anomaly.

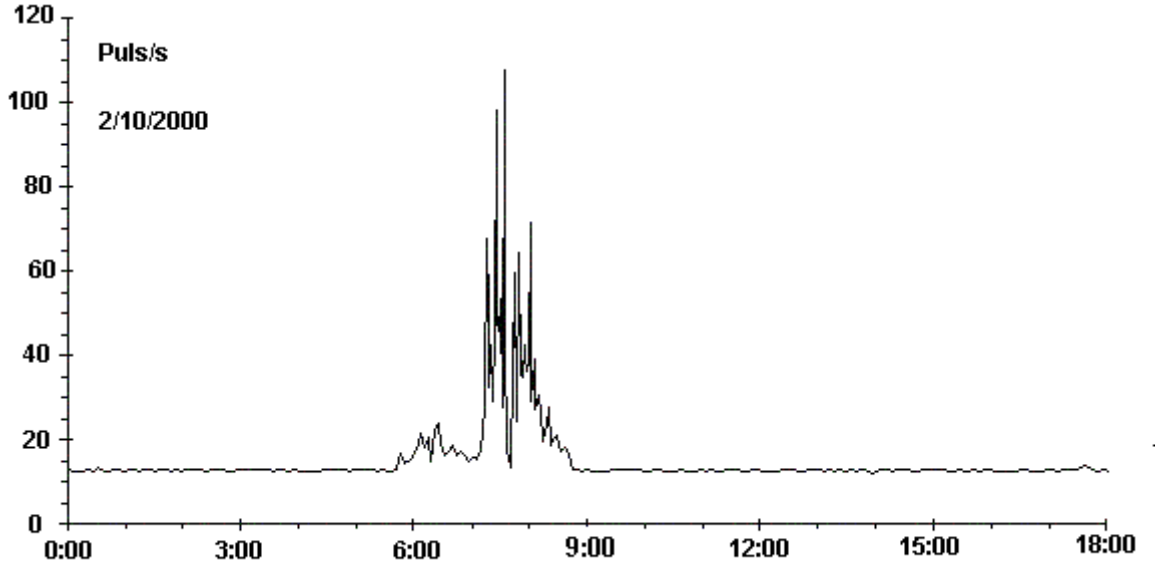

Fig.2. *Example of registration of the count rate of ^{60}Co source located at the focus of reflecting telescope. Declination of scanning line is 12°. The most near approach to the Sun is 14° at 8:50.*

Table 1.

Date	Start	End	*min*	δ	*K*
13.06.1999	8:40	12:10	8:45	23	2,66
13.06.1999	13:40	15:30	8:45	23	1,27
14.06.1999	8:32	8:44	8:45	23	1,22
19.08.1999	11:34	11:47	8:45	23	1,19
21.01.2000	17:56	20:55	8:45	16	1,40
04.02.2000	14:11	14:23	8:45	16	1,62
10.07.2000	19:30	19:58	8:50	21	1,32
07.08.2000	20:40	21:24	8:50	21	1,25
05.09.2000	5:09	5:14	8:50	21	5,63
06.09.2000	8:16	8:45	8:50	21	2,22
07.09.2000	7:55	8:21	8:50	21	1,22
14.09.2000	6:06	6:48	8:50	12	1,59
02.10.2000	5:40	8:40	8:50	12	8,73
02.10.2000	21:40	22:20	8:50	12	96
03.10.2000	0:00	5:50	8:50	12	159
26.03.2001	9:04	9:07	8:50	12	3,53
28.03.2001	20:33	21:27	8:50	12	1,40
29.03.2001	9:35	9:45	8:50	12	3,87
30.03.2001	8:20	12:20	8:50	12	3,70
31.03.2001	8:12	8:17	8:50	12	1,20
03.04.2001	10:12	10:43	8:50	12	1,38
30.06.2001	16:17	16:34	8:50	12	1,09
20.07.2001	4:09	4:16	10:25	17	1,12
24.09.2001	11:49	12:36	10:25	14	1,08
24.09.2001	19:14	23:17	9:25	8	1,14
25.09.2001	15:30	16:20	9:25	8	1,38
12.12.2001	4:38	5:40	9:25	8	1,30

In the time indicated, the average count rate changed from 15.8 to 10.5 *pulses per second.* The count rate was determined by the time of accumulation of 4096 pulses. The Table 1 contains the bursts with an increase of the count rate of more than 8% (an excess above the average more than 5 standard deviations). From April, 2002 to March, 2004 additional 22 such bursts were recorded.

The effectiveness of observations was sharply enhanced when going from one-dimensional scanning to two-dimensional one [11]. For this purpose, an oscillating motion perpendicular to the line of scanning associated with the daily rotation of the Earth, was given to the telescope (amplitude up to 40°, “right” motion =

5-10 *minutes*, "reverse" motion = 30-60 *seconds*, start and end times of the reverse motion were recorded by the computer). Examples of the images obtained are shown in Fig.3. It is seen that the positions of bursts is different for neighboring days.

Within 65 days of experiments from April, 2004 till April, 2005, 310 bursts exceeding the average count rate by more than 5 standard deviations, were registered (average count rate about of 5 *pulses per second* was determined from the time of accumulation of 256 pulses).

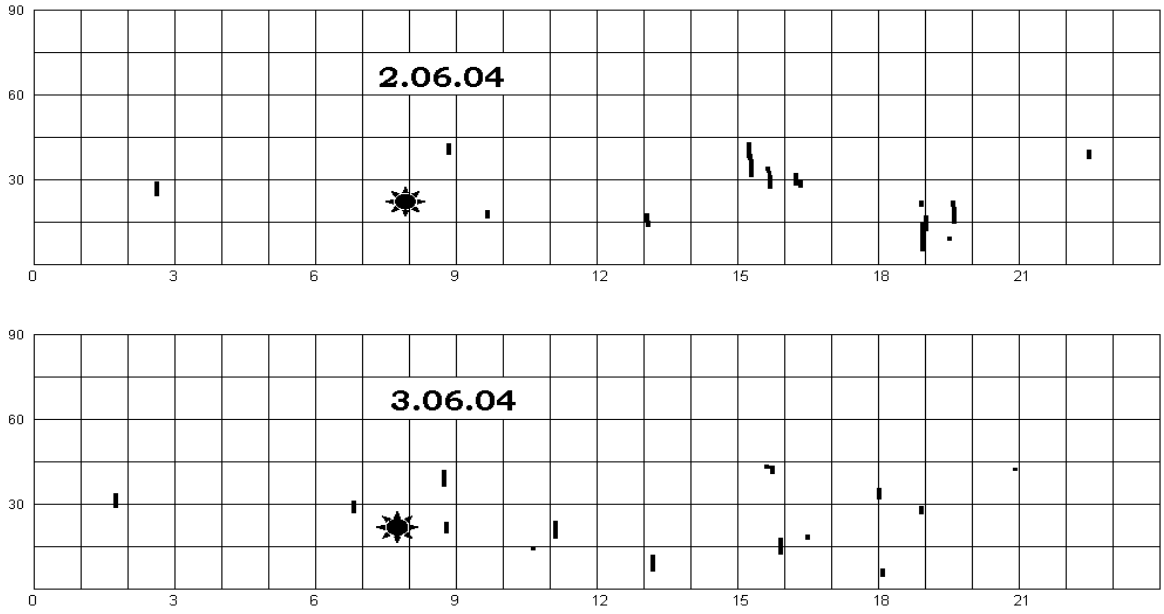

Fig. 3. *The bursts in the count rate of ^{60}Co source during two-dimensional scanning the celestial sphere, June 2-3, 2004. Horizontal axis is Moscow summer time, vertical axis is declination in degrees. The range of swinging 4 - 44 degrees, time of forward motion 320 s, time of reverse motion 32 s. Image of the Sun in the focus of telescope at 7:56, the declination 23°. The location of the Sun is asterisked. Bursts are shown with the count rate exceeding the average one by more than 5 standard deviations.*

Fig. 4 shows the distribution of the bursts over the celestial sphere relative to immobile stars (above) and relative to the immobile Sun (below). The data of four-month` observations were generalized. On the upper image there are seen condensations of bursts in areas of celestial sphere with right ascensions α being equal to approximately 4, 12, and 16 hours that correspond to the constellations Taurus, Canes Venatici, and Serpents. In the regions of α = 2-3 *hours* and α = 14-15 *hours* (near the constellations Pisces and Bootes), no bursts at all were recorded. On the lower image, a condensation of bursts is seen near the telescope′ s direction to the Sun up to the angular distance about of 10° as well as the absence of recorded bursts within the span between 2 and 5 hours (30°-75°) before the approach of telescope′ s orientation to the Sun.

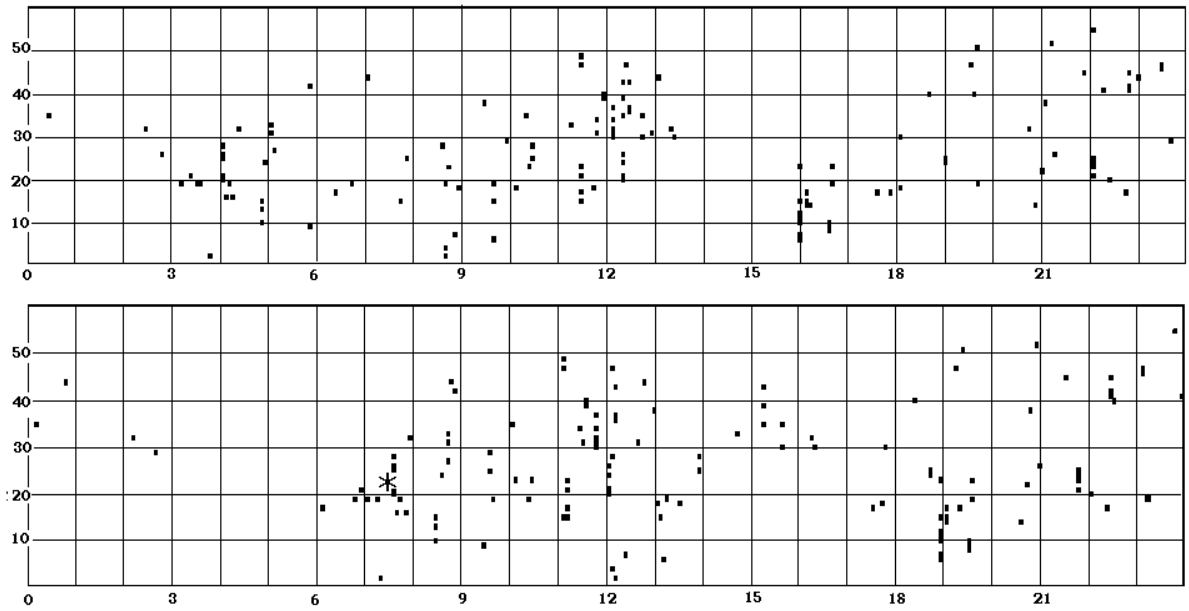

***Fig.4**. Distribution of bursts of the count rate of ^{60}Co source over the celestial sphere. Generalization of scanning results from May till August 2004. Above data are in the equatorial coordinate system, below data – relative to the immobile Sun (asterisked). The vertical axis is declination in degrees, the horizontal scale represents above the right ascension, and below the Moscow summer time. One hour corresponds to 15 degrees. Noted are the places of bursts with exceeding by more than 5 standard deviations above the average count rate.*

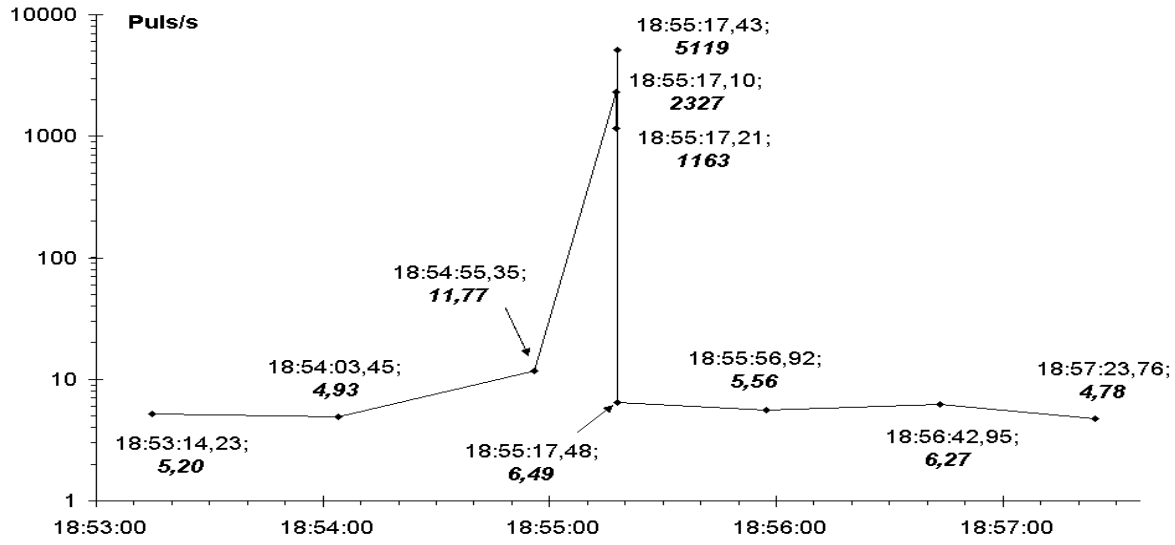

***Fig. 5**. The burst of the count rate of ^{60}Co source recorded the 3-d of June 2004 at the declination of 26°. There are indicated the count rate and time (accurate within hundredth parts of second).*

Fig. 5 shows the count rate during one of short single bursts. The general duration of the burst was about of 20 *seconds*, and the interval with the highest count rate (more than 1000 *pulses per second*) lasted lesser than a *second.*

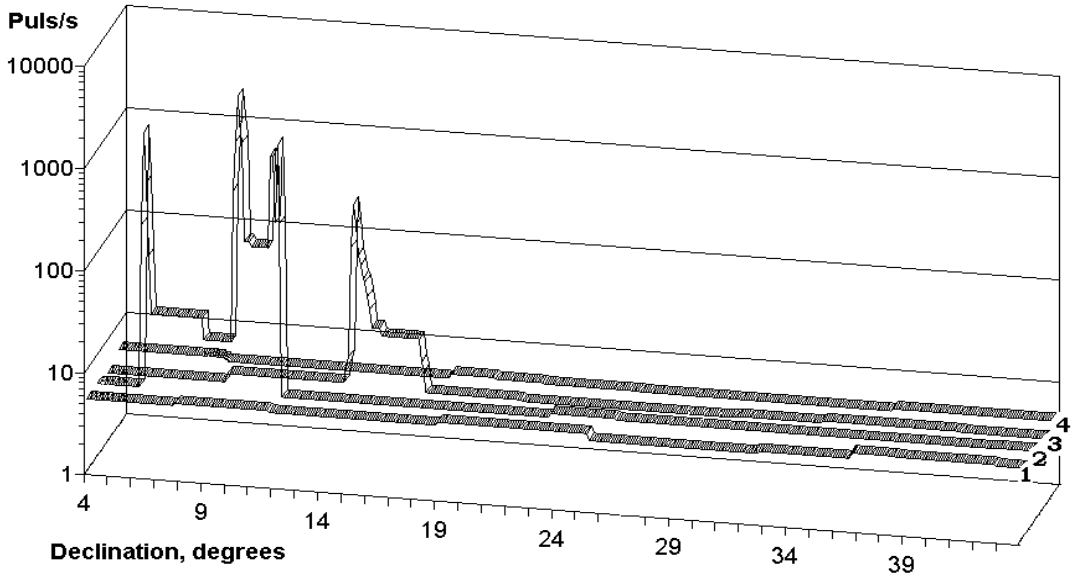

Fig. 6. *The burst of the count rate of ^{60}Co source recorded the 2-d of June 2004. Four sequential scans in the neighborhood of 19:00.*

Fig. 6 represents a dynamics of count rate changes when recording a burst appeared close to 19:00 2/06/2004 during two consecutive scans displaced in time by 6 *minutes* which corresponded to a shift of 1.5° in right ascension. The presence of a burst in two consecutive scans testifies that the area of the celestial sphere associated with the indicated event, has an angular dimension of several degrees and "life time" more than 6 *minutes*. The scanning after a day did not found any burst in this place (see f**ig. 3**)

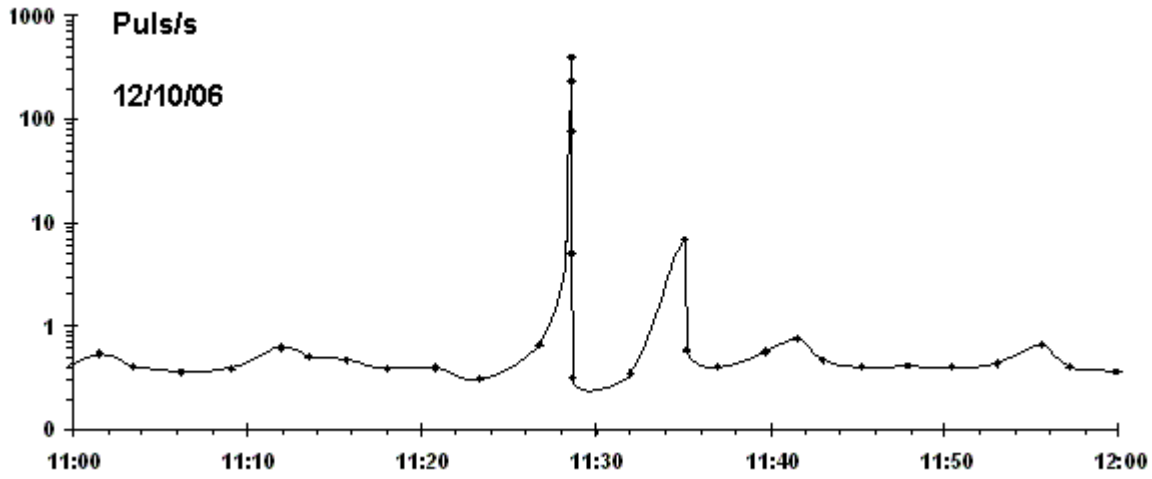

Fig. 7*. Example of registration of the count rate of ^{40}K source located at the focus of reflecting telescope.*

The application as beta source ^{40}K in a natural mixture of isotopes is connected to measurement of low speed of the account compared to a background. However and in this case authentic bursts are registered. For 4 months of observations there were 34 bursts exceeding mean speed of the account more than twice. One from them is shown in a **fig. 7**.

The information accumulated leads to the following conclusions.

1. The probability of recording a burst depends on the orientation of the telescope. In some intervals the number of registered events riches 0.1 *per square degree*, whereas in other parts of the celestial sphere of more than 1000 *square degrees* there is no event.

2. The number of bursts per day and their connection with the orientation of the telescope are not reproduced unambiguously, though in the following days bursts in the nearest regions of the celestial sphere are sometimes observed.

3. The time dynamics of bursts is very variable. The simplest type is single bursts with duration of some *seconds* at a rather common increase in count rate by more than three orders of magnitude. More long events (with duration up to several hours) consist of short bursts of different amplitude and are distributed in time in an intricate manner.

4. With the availability of ten-tenths cloud, no statistically reliable bursts are recorded.

5. Placement of the telescope beyond a window glass as well as the shielding by aluminum foil, do not noticeably influence experimental results.

Discussion of results

Foremost a question arises of whether or not the effects observed were connected with the action of ordinary factors of the type of electromagnetic interferences, instabilities in power supply or noise and defects in electronics. This question may be answered negatively with a high degree of confidence since:

1. There were no bursts when the G-M counter used in the setup, operated outside the telescope during several months (as with a radioactive source so without it).

2. Together with the signals coming from the setup in consideration, that same computer registered signals from another counter (with the beta-source ^{90}Sr-^{90}Y) also located outside the telescope and fed from the same source of power [1]. The reference counter detected no bursts.

3. Burst was observed in two consecutive scans (see, for example, f**ig. 6**). It is improbable that interferences or instabilities in the instrumentation were so exactly synchronized with the orientation of the telescope.

4. It is doubtful that the absence of interferences could be connected with the availability of cloud.

The second question is whether the effects observed were associated with the variation of radioactivity or with some processes in the G -M counter. The experiments with a counter without radioactive source that was placed at the focus of the telescope give grounds to a conclusion about the influence just of the change of radioactivity. In experiments without radioactive source, bursts in count rate were recorded too, but no more than up to 10 *pulses per second* at a background value of about 0.01 *pulses per second* [6-8]. As that background was due to the radioactivity of the substance from which the counter was made, the effect observed was probably also connected with the influence on the radioactivity.

Eloquent evidences that there were registered precisely the bursts of radioactivity were obtained when using for detecting bursts two counters of different type fed from different power sources (**fig.8**).

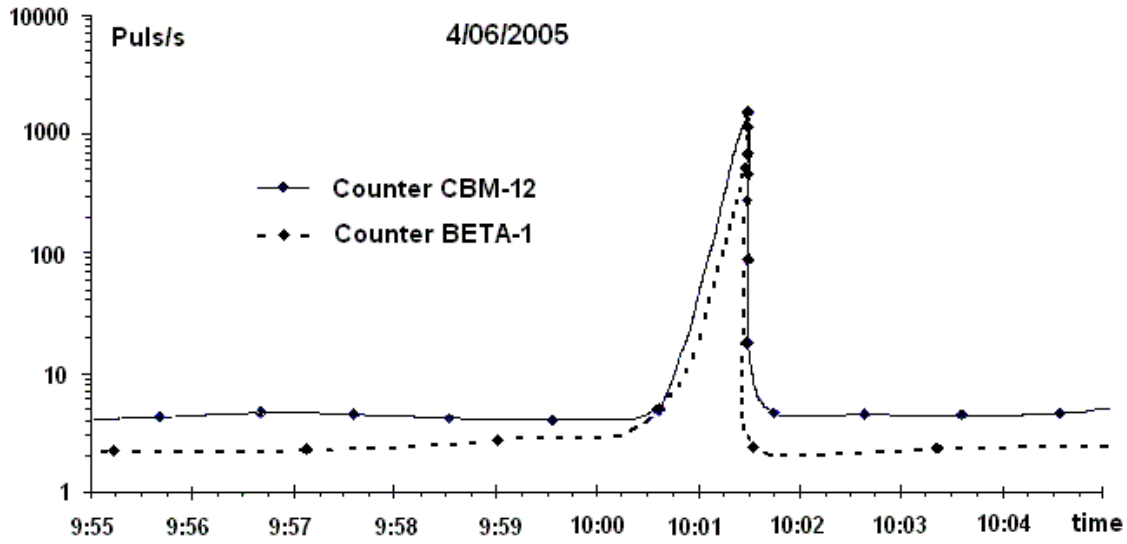

Fig. 8. *The simultaneous registration of count rate of ^{60}Co source by two G-M counters. The cylindrical counter CBM-12 is positioned adjacent to a source being at the focus of the telescope. The end-window counter BETA-1 is at the distance of 1.5 cm from the source.*

About a nature of the registered agent

The combination of data obtained allows an assumption that the appearance of bursts is connected with the presence of a focusing mirror that concentrates flows of some agent coming out of space. That agent should have the following properties:

1. Ability for influencing the beta-radioactivity;

2. Capability to specula reflection from smooth surfaces.

The information, received during experiments, allows to make and other conclusions about properties of the agent:

3. Strong variability in time and on directions;

4. Irregularity of probability distribution of bursts registration on celestial sphere;

5. Inability to pass through clouds;

6. Ability to pass through glass and aluminium.

I shall notice that the properties 2-6 of the registered agent are similar to that observed at astronomical researches N.A. Kozyrev and his followers using a reflecting telescope with the resistor, placed in focus, as the detector [3-5]. It gives the basis for the assumption of identity of the agents, obtained in ours and Kozyrev's experiments.

Set of all listed properties has one from components of a dark matter – very low energy neutrino, having mass distinct from zero. These properties were predicted 15 years back in [6-9] and have found confirmation as a result of long-term purposeful experiments.

The substance making a dark matter can not be fixed. It is in motion, similarly to stars, cosmic dust and gas. Speed of motion of objects in a gravitational field of a Galaxy is some hundreds km/c. The flows of substance driven with such speed, are rather effectively subjected to a focusing in gravitational fields of planets, stars, black holes, therefore there are local short-term bursts of fluencies. The smooth rhythmic density changes of a flow are connected to orbital motions.

On the first sight, the presence of effects connected with very low energy neutrino, perceived by the simple installations, seems impossible. This judgment proceeds from a simple extrapolation of properties of these particles which are known from nuclear physics experiments. But the extrapolation more than on 10 orders on a power scale is wrongful: it that most what to judge properties of liquid helium, investigating alpha-particles. In the field of very low energy neutrino interacts with substance completely differently than at high energy, being reflected, refracting and dissipating similarly to light, but practically being not absorbed [6,7]. The absorption is possible only at interaction with beta-radioactive nucleuses as a result of return beta-decay. The clouds consisting of set refracting drops are effective disseminations and destroy monodirectional flows.

I shall notice, that the assumption of influence on tritium beta-decays of space flows of very low energy neutrino - sole offered explanation of strange results received at measurement of neutrino mass (negativity of a square of mass, strong fluctuations, semi-annual rhythm) [10].

References

1. Parkhomov A.G., Maklyaev E.F. Investigation of Rhythms and Fluctuations during Long-term Measurements of Radioactivity, Frequency of Quartz Resonators, Noise in Semiconductors, Temperature, and Atmospheric Pressure. Fizicheskaya Mysl Rossii. 2004. No.1. P. 1-12 (in Russian) http://www.chronos.msu.ru/RREPORTS/parkhomov_ritmy/parkhomov_ritmy.htm
2. Baurov Yu. A., Konradov A. A., Kushniruk V. F., et al. Experimental Investigations of changes in β-decay rate of ^{60}Co and ^{137}Cs. Modern Physycs Letters A. 2001. No. 16(32). P. 2089-2101.
3. Akimov A. E., Kovalchuk G. U., Pugach A. F., et al. Preliminary Results of Astronomical Observations by the N. A. Kozyrev's Procedure. Preprint of GAO-92-5P, 1992. Kiev. P.16 (in Russian).
4. Lavrentyev M. M., Yeganova I. A., Lutset M. K., et al. About Distance Influence of Stars on Resistor. Doklady AN SSSR. 1990. No. 314(2). P. 355-368 (in Russian).
5. Kozyrev N. A. Selected Works. Leningrad University Publishing House. 1991. 448 p. (in Russian). http://www.timashev.ru/Kozyrev.
6. Parkhomov A. G. Dark Matter: Role in Cosmo-Terrestrial Interactions and Perspectives of Usages. Soznaniye I Fizicheskaya Realnostj. 1998. No. 3(6). P.24-35 (in Russian). http://www.chronos.msu.ru/Public/parkhomov_skrytaya.html
7. Parkhomov A. G. Astronomical Observations by the N. A. Kozyrev's Procedure and the Problem of Instantaneous Transmission of Signal. Fizicheskaya Mysl Rossii. 2000. No.1. P.18-25 (in Russian). http://www.chronos.msu.ru/Public/parkhomov_astronomicheskiye.html.
8. Parkhomov A. G, an Unusual Cosmic Radiation. Detection, Hypotheses, Testing Experiments. Moscow: MNTTs VENT, 1995, 51 p. (in Russian).
9. Parkhomov A. G. Distribution and Motion of Dark Matter. Moscow: MNTTs VENT, 1993, 76 p. (in Russian). http://www.chronos.msu.ru/RREPORTS/parkhomov_raspredelenie.pdf
10. Lobashev V.M., Aseev V.N., Belesev A.I. DIRECT SEARCH FOR THE MASS OF NEUTRINO AND ANOMALY IN THE TRITIUM BETA-SPECTRU. Physics Letters B 460. 1999. P.227-235.
11. Parkhomov A.G. Bursts of Count Rate of Beta-Radioactive Sources during Long-Term Measurements. International Journal of Pure and Applied Physics. 2005. V. 1. No.2. P. 119-128. http://www.ripublication.com/ijpap/1001.pdf

THE ANALYSES OF TEST DATA OF CAVITATION HEAT-GENERATOR OF «TMK-25» TYPE

A.V. Pinaev

Lavrentyev Institute of Hydrodynamics SB RAS, Novosibirsk, avpin@ngs.ru

Introduction

Within last decades about tens hydrodynamic heat generators are created and patented, in which the water is heated up with the help of cavitation technique [1-4]. In a series of the patents [1,3] the factor of transformation of an energy or potency of heat generator $C_E > 1$ is marked. Under C_E of heat generator the ratio of useful thermal energy or potency accordingly to the expended electric power or potency is understood. The presence $C_E > 1$ at release of an additional energy from a working medium (water) during a cavitation does not contradict a conservation law of an energy and specifies an incompleteness of our knowledge about happening processes.

In the present work the experimental test data on heat generator TMK-25 are analysed and the effect of release of an additional energy is established at a cavitation. The similar researches are of interest in connection with inevitable necessity of use of ecologically pure, renewed sources of an energy in the future.

The test of heat generator consist of two stages: heat of water in a tank by a volume 860 liters and self-cooling of a tank up to reference temperature. The drive for cavitation technique was served by two electric motors with a passport potency of 22 KW, $\cos\varphi = 0,89$, efficiency $\eta =$ 0,905 and frequency of rotation 2940 rev/min. By work of heat generator the potency, consumed by electric motors, was approximately twice less their passport potency. Cavitation technique [4] represented the cylindrical volume with two flat rigidly by fixed disks (stator) and two counterrotation disks (curls), which rotated with frequency 4200 rev/min.

The dynamic filing of temperature on an input (entrance) (t_{in}) and exit (t_{out}) of cavitator, charge of water through cavitator G, filing of temperature in a tank at three levels on a height, removal of the observations of the electric meter was carried out through everyone by 5 mines. During all time of heat (t_1 = 2 h. 20 mines) the residual of temperatures $\Delta t_{dyn} = t_{out} - t_{in} =$ $4 \div 6,5\ ^{\circ}C$. The transmitter for measure of temperature on an input of cavitator, was located on the pipeline on a distance 1,8 m from cavitator. The transmitter for a measurement of temperature on the output pipeline of cavitator was removed on a distance 4 m from cavitator. On this distance the temperature of water was stabilized [5-7], that allowed to exclude an error in the definition t_{out}.

The second stage (cooling of a tank) last t_2 = 21 h. 15 mines at the closed from above tank. Directly ahead of the beginning of cooling of a tank temperature at the top of a tank was about 95 $^{\circ}C$, final – about 38 $^{\circ}C$. Temperature in a room for this time has decreased with 20 up to 16 $^{\circ}C$.

Accumulated at heat a thermal energy in water $Q_{1f} = C_f m_f \Delta t_0 =$ 49020 Kcal, the energy for heat of a steel tank and cavitator cases by a common mass m_s = 460 kgs, make $Q_{2s} = C_s m_s \Delta t_0 =$ 2884 Kcal. Useful heat contained in heated up water and the steel elements of installation $Q_{12} = Q_{1f} + Q_{2s}$ = 51904 Kcal.

Then, magnitude of factor of transformation of and energy:

- For the user, without the account of efficiency of electric motors, at the electric power, expended on the counter, W_Σ = 62,2 kwh = 53482 Kcal, $C_{E1} = Q_{12}/W_\Sigma = 0,97$.
- Is exacter, in view of efficiency of electric motors, $C_{E2} = Q_{12}/W_\Sigma\,\eta = 1,072$.
- Is even more exact, taking into account the energy for heat of water and installation, environment ΔQ_{13} = 5658 Kcal and on evaporation of water (4,4 liter) ΔQ_{vap} = 2460 Kcal, $C_E = \left(Q_{12} + \Delta Q_{13} + \Delta Q_{vap}\right)/W_0$ = 1,24 = 124%.

The deriving C_E = 1,24 means, that, most probably, in the given installation the additional energy from a working medium - water - is selected. Recognizing that in the researched thermal machine 50 % ≤ efficiency < 100 %, we shall estimate magnitude additionally selected of heat in cavitator ΔQ^+: $\Delta Q_1^+ = W_0/2 + (Q_0 - W_0)$ □ 35820 ≥ $\Delta Q^+ > \Delta Q_2^+ = Q_0 - W_0$ □ 11620 Kcal. Let's accept average magnitude $\langle \Delta Q^+ \rangle = \left(\Delta Q_1^+ + \Delta Q_2^+\right)/2$ □ 23720 Kcal, then specific heat release, designed for all mass of water, $q_f = \langle \Delta Q^+ \rangle / m_f$ = 27,6 Kcal/kgs.

From obtained experimental data the dynamic $C_{E\,dyn}$ is calculated for any time interval (τ = 300 sec) $C_{E\,dyn} = GC_f \rho\, \Delta t_{dyn} / (\Delta W/\tau)$, where $\rho = 10^3$ kg/m^3, C_f = 1 Kcal/kgs· K. Average magnitude $\langle C_{E\,dyn} \rangle$ = 1,2. The magnitude $\langle C_{E\,dyn} \rangle$ coincides with a good exactitude with integrated C_E = 1,24. The summarized average error of the definition of integrated and dynamic factors of transformation did not exceed 7-8%.

The account of heat loses on a convection and radiation on a technique [8] is carried out. It is shown, that with a good degree of an exactitude, the warm, accumulated by tank at heat of the steel case and water (Q_{13} = 51528 Kcal = 59,93 KW-H), coincides with a heat given up tank at cooling up to same reference temperature (56,8 KW-H).

The unusual character of processes accompanying work of installation is remarked also. On going out from cavitator the pipeline made of a gummed hose, the deviation of an arrow(pointer) of a magnetic compass from normal direction from 30° up to 180° was observed. Along the pipeline near to cavitator the rotation of an arrow of a compass was observed. The anomalous behaviour of a magnetic arrow was observed also in different points about a wall of a tank on his height.

Possible mechanisms of release of an additional energy in a system.

1. During a cavitation the formation of associative clusters $(H_2O)_n$ happens and simultaneously the heat is released, where $n > 6$ [5,10,12]. The mechanism of formation of an additional energy is known at the expense of a release of an energy of multiple hydrogen connections (energy of one hydrogen connection ~ 0,1 eV). The warming up of bubbles grows out transformations of an energy of normal oscillations of hydrogen connections in associative $(H_2O)_n$. At such mechanism of heat the temperature in bubbles can achieve millions degrees [10].

From positions of a thermodynamics a limiting relation of thermal capacities of water in its different condition (liquid and rigid phases) $C_f/C_s = 2$. The formation of associative

clusters in water orders a structure of water, doing it by "ice-like", and reduces a thermal capacity. But such partially ordered "ice-like" condition is unstablis and is accompanied by an inverse endo-thermic transition in an initial condition. I.e. the heat in the beginning is selected, and then partially is swallowed.

2. In [1] the formation of additional heat in cavitation system directly correlate to nuclear reactions, in a proof that the appropriate measurements are done and the graphs of magnification of intensity $\gamma + \beta$ and neutron radiations in an association from time are reduced. The similar mechanism is considered in [16,17].

3. The hypothesis about a possibility of a course of nuclear reactions is known at low temperatures (CNS) with participation dy-neutron [6,14]. Dy-neutron, or the double neutron is formed in an outcome of short-term capture driven of electron by the atomic nucleus of a deuterium (as at known to K-capture): $^2\mathrm{D} + \mathrm{e}^-$. There is a reaction satisfying to known conservation laws and which are flowing past with the large velocity $\left({}^2\mathrm{D} + \mathrm{e}^- \right) + \mathrm{P} \rightarrow {}^3\mathrm{T} + \nu + 5{,}98$ MeV. In this reaction the electron immediately participates in a nuclear reaction, which yields are the atomic nucleus of tritium and neutrino. And it is remarked in [18], that in responses CNS the exit of tritium is on 8 order more exit of ^{3}He and neutrons. At a raise of temperature, when already practically there are no atoms of a deuterium and the plasma almost all is ionized, the reactions with formation of tritium is not observed. Besides Dy-neutron can enter at low temperatures in a reaction with the atomic nucleus not only hydrogen, but also other elements. In our case the reactions of dy-neutron with the nucleus of iron and carbon which is included in structure of steel are possible [14]. Two last reactions with the greater probability can flow past close near contradictory rotated rotors of cavitator, as in this area the cavitation happens. Apparently, due to these reaction the hardening of curls and stators happens the darkness of a surface, and they further are not exposed to corrosion.

4. At force heat or electrolysis of water the expansion on ions H^+ and OH^- on a reaction $H_2O = H^+ + OH^-$ happens which approximately twice energetically is more favourably, than reaction of water decomposition on H_2 and O_2 [15]. Then at capture by ions of hydrogen of electrons from walls of a grounded tank and association of two atoms of hydrogen in a molecule of hydrogen $H + H = H_2$ the release of an energy 436 KJ/mole of hydrogen happens, that approximately twice it is more, than at combustion of hydrogen [19]. Other part of ions of hydrogen incorporates to oxygen: $4H^+ + O_2 = 2H_2O^+$ (the ion H_2O^+ further seizes electron from walls of a tank and turns to a molecule of water) with release of an energy exceeding expenditure of an energy on a reaction of a dissociation. These reactions, as a matter of fact, are reactions of combustion of water and explain a raise of caloric value of water-coal or water-mazut suspensions in fire-chambers on 10-20 % [20,21].

Conclusions:

Heat generator TMK-25 is highly effective heating installation, as in view of heat, accumulated by a tank, energy loses and expenditures of the electric power at a stage of heat of water integrated $C_E = 1{,}24$. The magnitude of average dynamic factor of transformation of an energy of installation at a stage of heat $\langle C \rangle = 1{,}2$, that with a good exactitude coincides E_{dyn} with integrated $C_E = 1{,}24$.

The results of measurements in whole show, that the cavitation-heating equipment is a system of an open type, in which, most probably, the energy from a working medium – water - acts. Recognizing that in the researched thermal machine real 50 % < efficiency < 100 %, magnitude of selected additional heat $35820 \geq \Delta Q^+ > 11620$ Kcal.

As a substantiation of a last conclusion the possible mechanisms of release of an additional energy in an outcome mechanical activation of liquid are reduced. Apparently, basic mechanisms of an energy release are low-temperature nuclear synthesis without an exit of neutrons and combustion of water.

References

1. Kladov A.F. A mode of deriving of an energy. The patent RU 2054604 C1 from 20.02.1996.
2. Kladov A.F. A ultrasonic catalyst. The patent RU 2085273 C1 from 27.07.1997.
3. Petrakov A.D. A mode of deriving of an energy and resonance pump – generator. The patent RU 2142604 C1 from 26.01.1998.
4. Kochkin S.S., Atamanov V.V. Cavitation-rotational heat generator. The patent RU 2269075 C1 from 05.07.2004. Is published 27.01.2006 Bul. № 3.
5. Fominsky L.P., Shevchenko T.G. etc. Illusory heat superunit hydrodynamic heat generator // Anomalous physical appearances in a power engineering and prospect of creation of untraditional radiants of an energy. Сб. The reports of a scientific and technical conference (June 15-16, 2005, Kharkov, Ukraine). - Kharkov: OOO «Infobank», 2005. -with. 308-317.
6. Potapov Y.S., Fominsky L.P. A rotational power engineering and cold nuclear synthesis from positions of the theory of driving. Kishinev-Cherkassuy: «oko-plus», 2000. -387 with.
7. Furmakov E.F. Whether hydrodynamic heat generators can work superefficiently? // In «Problems of a research installed » S.-Pb. 2004.
8. Kutateladze S.S., Borishansky V.M. A manual on a heat transfer. - M. -L.: 1959. -414 with.
9. Enokhovich A.S. A brief manual on Physics.- M.: A higher school, 1976. -288 with.
10. Lipson A.G., Kuznezhov V.A. About the mechanism of concentration and transformation of an energy of a sound field in water at mono-bubbles sono-luminosity // J. Ph. Chemistry. -2002.-V. 76, № 1. - with. 116-122.
11. Lipson A.G., Lyakhov B.F. etc. Generation of yields of nuclear synthesis at the combined action of a cavitation and electrolysis on a surface titanium in deuterium electrolytes // J. Tech. Ph. -1993. -V. 63, № 7 - with. 187-196.
12. Lipson A.G., Kuznezhov V.A. Shaping associatives of water in field of forces at the presence of inorganic impurity // J. Phys. Chemistry. -1996. -V. 70, № 9. - with. 1718-1722.
13. Margulis M.A. Sono-luminosity // Uspekhi Phys. Sciences. -2000. -V. 170, № 3. - with. 263-287.
14. Fominsky L.P. Quasi-neutral deuteron - key to cold nuclear synthesis // Anomalous physical appearances in a power engineering and prospect of creation of untraditional radiants of an energy. /The reports of a scientific and technical conference (June 15-16, 2005, Kharkov, Ukraine). - Kharkov: OOO «Infobank», 2005. - with. 294-301.
15. Fominsky L.P. How the water burns//ib. 302-307.
16. Nigmatulin R.I., Gubaydulin A.A., Beregova O.Sh. A method superforce of resonance compression bubble liquid by moderate acyclic action // The Reports of RAS. -2000. -V. 374, № 4. - with. 489-492.
17. Talayarkhan R.P., West C.D. et al. Evidence for Nuclear Emissions During Acoustic Cavitation // Science. -8 marh 2002. -V. 295 -P. 1868-1873.
18. Zharev V.A. Low-temperature nuclear synthesis // Uspekhi Phys. Sciences. -1990. –V. 160, № 11. -with. 1-53.
19. Glinka N.L. Common chemistry. -L.: Chemistry, 1988.
20. Nezametdinov A.B., Gorlovsky S.I. Suspension for burning. patents USSR № 1273386, MPK C10 L1/32. 1986. Bul. № 44.
21. Volikov A.N. Burning water-mazut suspension. -L.: Nedra, 1990. -160 with.

DECAY IN TUNGSTEN IRRADIATED BY LOW ENERGY DEUTERIUM IONS

Irina Savvatimova*, Gennady Savvatimov*, Alla Kornilova**

Federal State Unitary Enterprise Research Institute "Luch" E-ail:U10492@dialup.podolsk.ru"*
*Moscow State University***

The analysis of tungsten and tantalum foils before, during and after deuterium discharge with the gamma/x-ray - spectrometry method is submitted. The light isotopes in tungsten decay in more elements after deuterium discharge is observed. The comparison of thermoionization mass-spectrometry and x-ray/gamma emission data allowed to suppose that the peaks observed in gamma spectra belong to the following isotopes: $^{169}Yb_{70}$; $^{171m}Yb_{70}$; $^{172}Hf_{72}$; $^{178}Yb_{70}$; $^{180}Yb_{70}$; $^{180m}Hf_{72}$; $^{170}Hf_{72}$. Correlation of TIMS and Gamma spectrometry data leads to the assumption that the appearance of light isotopes in the tungsten was as a result (effect) of the process stimulation (initiation) by low energy deuterium discharge.

1. Introduction

The weak gamma – emission, short time neutron bursts, Neutron and gamma spectra are measured. It was published in the previous papers earlier [1-2]. Neutrons with energy up to 17 MeV are detected. Neutron groups (2.45 MeV and 14 MeV) intensity ratio shows anomalous type of nuclear reaction [1-2].

The blackening of the x-ray films being in contact with Pd, Ti and Ag foils after an irradiation by deuterium discharge were found [3-6]. The blackening of x-ray films being inside and outside of the discharge chamber with stainless steel wall was observed [6]. In accordance with the radiography, the radioactive isotopes corresponding of different energy were observed on Pd cathode after deuterium discharge: high-energy and low-energy components [3].

The Uranium radioactivity changing after deuterium and hydrogen discharge was found [7-9]. The increasing of alpha emission into four times for deuterium discharge after 500 hours both sides (irradiated and unirradiated) was observed. The increasing of beta and gamma emission was less than the alpha emission. The comparison of the intensity of energy

peaks in gamma spectra allow to see the changing of ratio energy peaks of thorium and uranium [10].

Results of appearance of more light isotopes in tungsten and tantalum foils after exposure in deuterium discharge using x-ray and gamma ray spectroscopy are presented in this article.

2. Methods

2.1. Experimental Method

Deuterium discharge was used as experimental method. The experimental setup is shown on Figure 1.

The x-ray/gamma ray CdTe XR 100T detector (Amptec) for energy peaks estimation of x-ray/gamma emission of W and Ta before, during and after irradiation in deuterium discharge was applicable. X- ray/gamma intensity for the different deuterium discharge parameters was analyzed in counts per second (cps).Gamma spectra during deuterium discharge were obtained through double quartz tube. The average intensity of x-ray and gamma ray was estimated as the total counts, divided into time of spectrum recording.

Fig.1. *The gas discharge setup with CdTe detector location.*

Location of CdTe detector (1) is shown on Fig. 1.

2.2. Analytical Method.

X- ray/Gamma spectrometry was used as Analytical Method.

The distance between Be window of detector and W foil during deuterium discharge is about ~ 50 mm (6mm is the thickness of double quartz tube + 3 mm layer of cooling flow water + 40 mm Deuterium gas pressure ~ 5Torr).

Tungsten foil was located in contact with Beryllium window on the distance ~1mm during gamma/x-ray spectrometry after deuterium discharge exposure

Analyzed foils had the diameter ~20mm and ion's irradiated zone.

2.2. Characterization of CdTe detector for the x-ray and gamma ray spectrometry

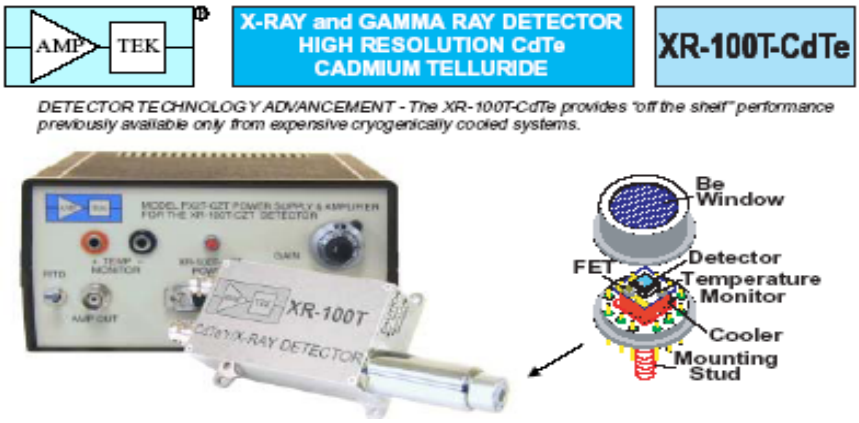

Figure 2a. *X-ray and gamma ray detector CdTe XR 100T detector (Amptec)*

CdTe detectors (Amptek XR100) includes shaping amplifier using the DP4 digital pulse processing technology, integrated multichannel analyze, power supplies, USB interface to personal computer, with software to support instrument control, data acquisition, and analysis (Fig.2a). **The XR-100T-CdTe is capable of detecting energies from a few keV to several hundreds of keV.**

This system has the thermoelectric cooler with feedback

The Amptek PX4 is an interface between Armtek's XR100 series of X-ray and γ-ray detectors and a personal computer with data acquisition, control, and analysis software. The PX4 includes three major components: a shaping amplifier, based on a state of the high performance, low power DP4 digital pulse processor, a multichannel analyzer, and power supplies.

The pulse processing and MCA function of the PX4 are based on Armtek's DP4 digital pulse processor. The PX4 offers several performance advantages over traditional analog systems, including higher energy resolution, reduced ballistic deficit, higher throughput, better pile-up rejection, enhanced stability, and the ability to adjust shaping time parameters over a wide range to optimize performance. The PX4 includes a USB interface.

The PX4 is a component in the complete signal processing chain of a nuclear instrumentation system. It replaces many different components in a traditional instrumentation system: the shaping amplifier, the multichannel analyzer, logic devices, high voltage power supplies, and several auxiliary components.

The PX4 digitizes the preamplifier output, applies real-time digital processing to the signal, detects the peak amplitude (digitally), and bins this value in its histogramming memory, generating an energy spectrum.

The MultiChannel Analyzer (MCA) gives the number of events with the corresponding peak value.

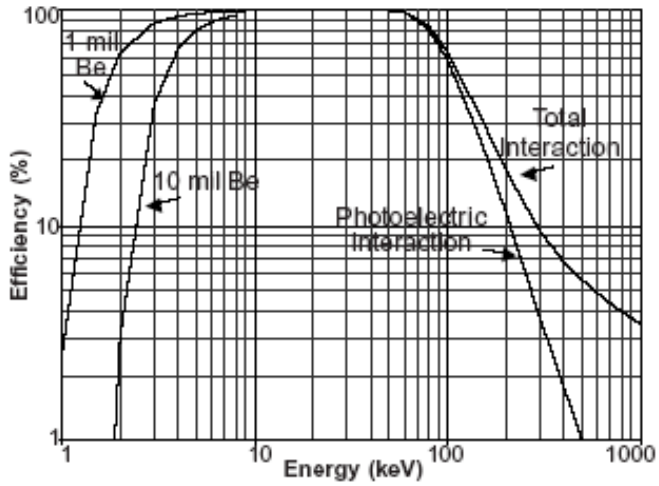

FIGURE 2. 1 mm Thick CdTe Detection Efficiency

Figure 2b *Efficiency of The thick of Be CdTe detector window was 250 microns.*

CdTe detector with 1 mm thick has 100% efficiency from 8 keV to 60 keV (Fig.2b)

These fluctuations are observed as rise time variations of the voltage step at the output of the charge sensitive preamplifier. As a result, the acquired spectra suffer from increase

background counts and degraded energy resolution. To reduce these effects a Rise Time Discrimination (RTD) circuit has been developed for the PX2T amplifier.

Cooling the FET reduces its leakage current and increases the transconductance, which in turn reduce the electronic noise of the system.

Model ***XR-100T-CdTe*** is a new high performance X-Ray and Gamma Ray Detector, Preamplifier, and Cooler system using 3 x 3 x 1 mm3 Cadmium Telluride (CdTe) diode detector mounted on a thermoelectric cooler**.** Also, on the cooler are mounted the input FET and feedback components to the Amptek A250 charge sensitive preamp. The internal components are kept at approximately -30°C, and can be monitored by a temperature sensitive integrated circuit. The hermetic TO-8 package of the detector has a light tight, vacuum tight 10 mil (250 □m) Beryllium window

The calibration CdTe detector of soft radiation (diameter 9mm and thickness 1 mm) was made. The efficiency of CdTe detector is shown below on Figure 3 and Table 1. Estimation of efficiency was made with Monte-Carlo calculation for isotropic source for case of the foils in contact with Beryllium window of CdTe detector. The efficiency of CdTe detector of soft radiation is shown on the Figure(Fig.2b) and Table 1. The CdTe detector diameter was 9mm and thickness was 1 mm.

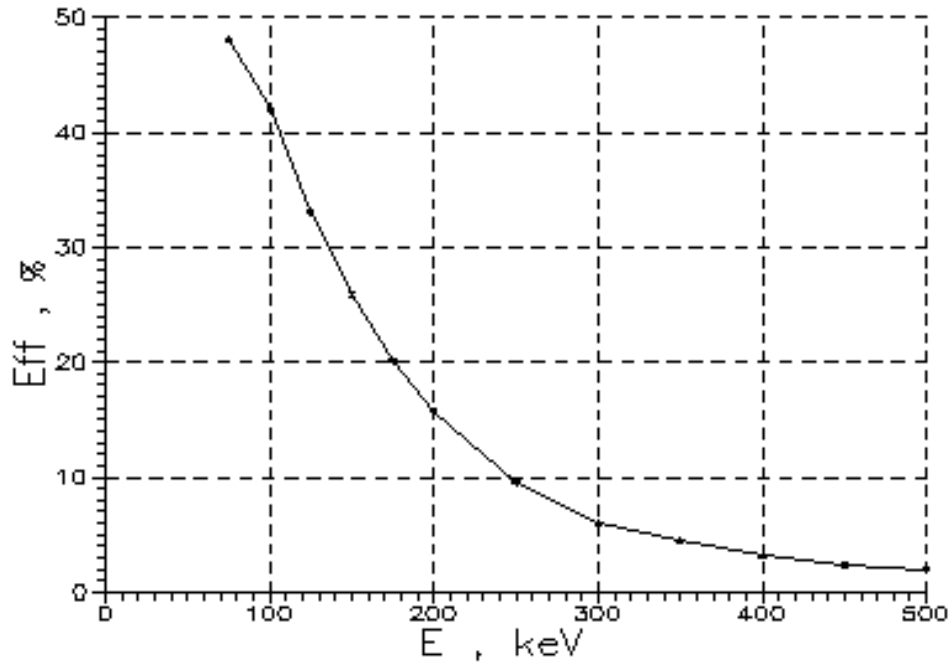

Figure 3. *The efficiency of CdTe detector for case of the foils in contact with Beryllium window of CdTe detector*

Table 1

The cdte detector efficiency for case of the foils in contact with beryllium window of detector

E keV	**75**	**100**	**125**	**150**	**175**	**200**	**250**	**300**	**350**	**400**	**450**	**500**
Eff %	**48.1**	**42.0**	**33.12**	**25.87**	**20.1**	**15.8**	**9.55**	**6.0**	**4.43**	**3.2**	**2.34**	**2.0**

2.3. Estimation of Gamma/ X-ray intensity.

Estimation of Gamma/ X-ray intensity as the value of energy peaks were fulfilled in counts per second (CPS).

3. Experimental results.

Gamma emission before, during and after of Deuterium Discharge (DGD) experiments with refractory metals (W, Ta) was measured.

5 series of the gamma emission measurements using gamma/x ray CdTe XR 100T detector were carry out: 1- during DGD experiments outside of double quartz walls; 2 - after DGD experiments outside of double quartz walls; 3 - W foils after DGD experiments placed near Be window (~1mm) of gamma/x ray CdTe detector; 4 - W foils before experiments and 5 - background.

Reproducibility of gamma/x ray spectra for closed conditions (for short time intervals) in these spectra was shown. Compare of energy peaks in gamma spectra of tungsten and tantalum after GDG showed the repeatability of energy peaks in spectra of different exposed foils during and after GDG experiments. Series of the main isotopes peaks were compared by two different methods (Gamma spectrometry and mass spectrometry).

Intensity of gamma emission for the different foils depended of exposure dose, current density and other experimental parameters

Main energy peaks of more intensive isotopes in different experiments were reproduced and identified using gamma/x ray energy spectra with CdTe detector.

It was shown, that Gamma/x-ray emission after stopping of experiment still takes place.

X-ray and Gamma-ray spectra for W and Ta during and after irradiation in the deuterium discharge using Gamma/X ray CdTe detector is presented on the Figures 4-6.

The X-ray/gamma spectra of tungsten (#1820) for the different conditions during and after deuterium glow discharge

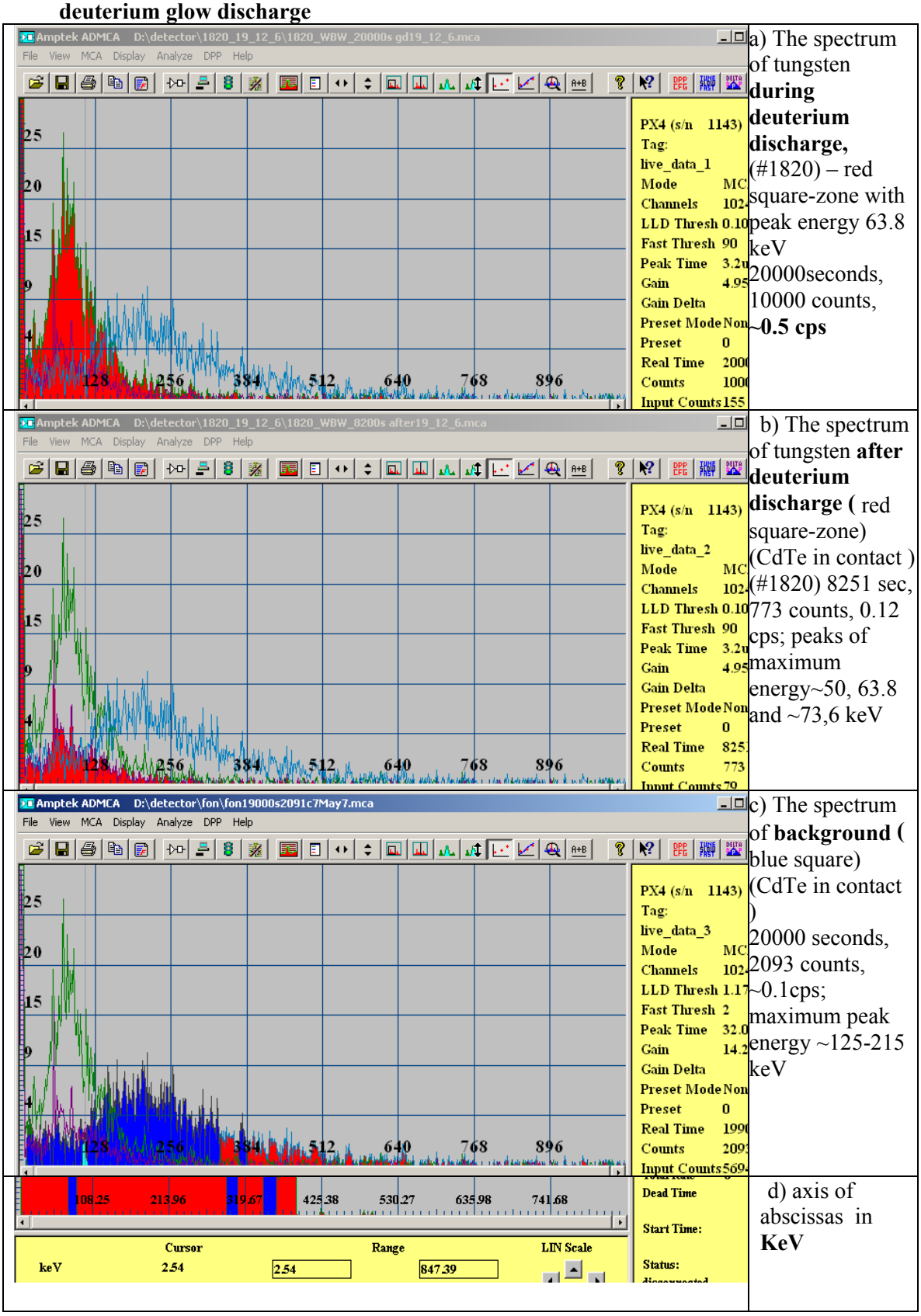

a) The spectrum of tungsten **during deuterium discharge,** (#1820) – red square-zone with peak energy 63.8 keV 20000seconds, 10000 counts, **~0.5 cps**

b) The spectrum of tungsten **after deuterium discharge (** red square-zone) (CdTe in contact) (#1820) 8251 sec, 773 counts, 0.12 cps; peaks of maximum energy~50, 63.8 and ~73,6 keV

c) The spectrum of **background (** blue square) (CdTe in contact) 20000 seconds, 2093 counts, ~0.1cps; maximum peak energy ~125-215 keV

d) axis of abscissas in **KeV**

Figure 4. *The spectrum of x-ray gamma emission during deuterium discharge*

X-ray and gamma emission of w during the deuterium glow discharge (#1817)

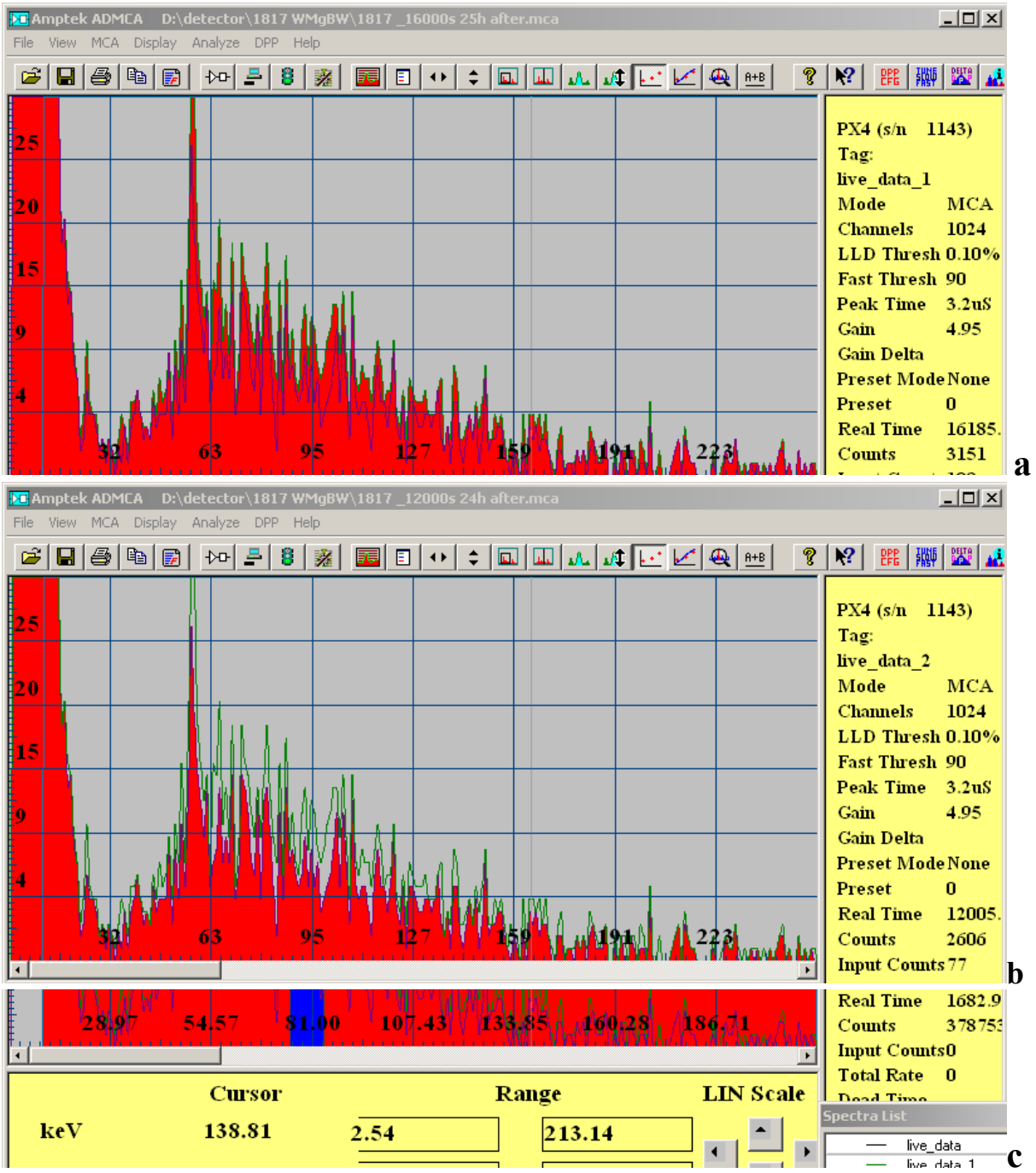

Figure 5. *Gamma spectra of tungsten after glow discharge.*

Figure 5 includes the x-ray/gamma ray spectra of W foil (1817) after deuterium discharge (a and b) and c – The energy in keV is on the abscissa axis, where: a. After Glow Discharge 16000sec; rate ~0.195 CPS; b. After Glow Discharge12000sec; rate ~0.217 CPS.

Figure 5 (a and b) is the illustration of reproducibility of the main energy peaks for the different time intervals (12000seconds and 16000 seconds). The peaks energy and their

intensity had a good reproducible. Main energy peaks of more intensive isotopes in different experiments were reproduced and identified using gamma/x ray CdTe detector.

The examples of W foil spectra during of Deuterium discharge.

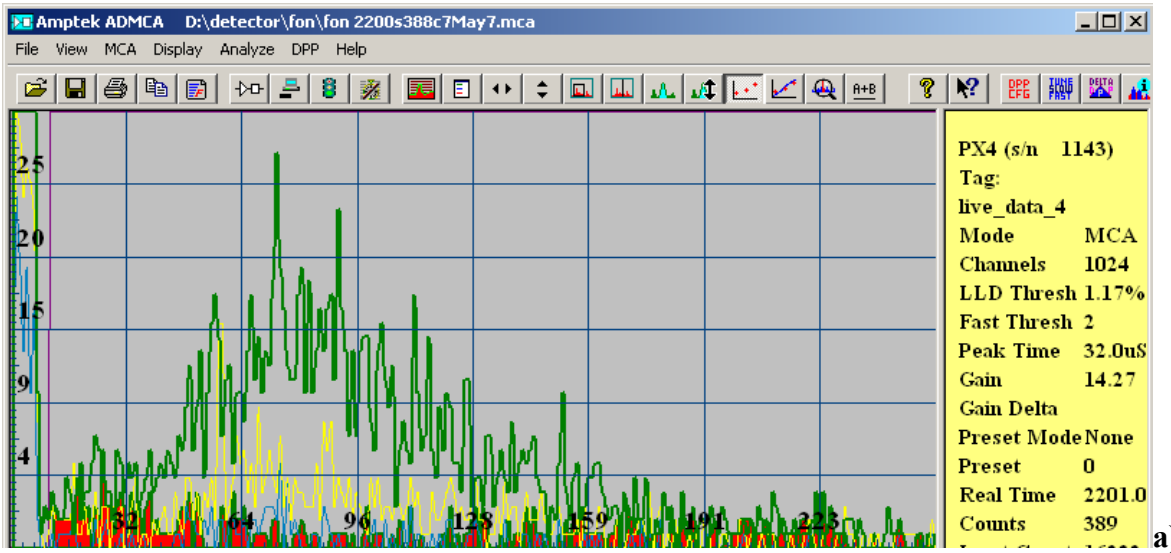

a)

Figure 6 a. *Time recording =2200 sec., counts = 389, intensity = 0.17cps (background's intensity = 0.09± 0.05 cps)*

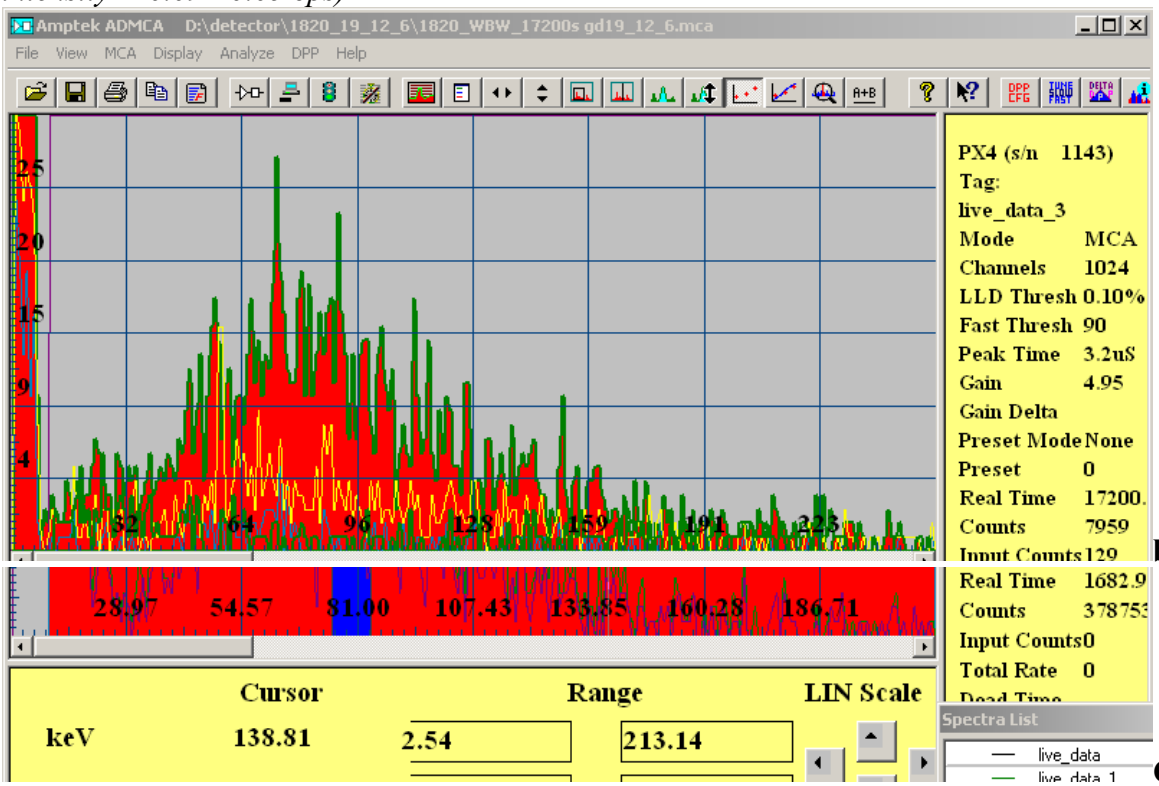

b)

c

Figure 6b. *Time recording =17200 sec., counts = 7959, average intensity = 0.46cps*

Peak time is 4.77(7) h in intensity (Table 4) and the peak intensity is 3.5 cps for ~ 5.5 hours of experimental time. It is the time with high intensity on Fig. 7.

Gamma/ X-ray intensity of emission for the different specimens was analyzed.

The intensity of Gamma emission depended on experimental time, dose, current and other parameters.

Gamma/x-ray emission after stopping of experiment still takes place.

3. Correlation of TIMS and Gamma spectrometry data

3.1. Comparison of main isotopes was observed using two different methods (mass spectrometry and Gamma spectrometry).

Isotopes of more light elements during and after exposure in deuterium discharge were selected using the block of energy peaks for each isotope and mass spectrometry data.

The definition of isotopes according to energy peaks in gamma/x-ray spectra and comparison with isotope mass peaks intensity in mass-spectra were fulfilled.

Table 2

Peaks energy from tungsten and tantalum after deuterium glow discharge in the gamma spectra using x - ray /gamma cdte detector (for the first group of isotopes)

W	W	W	Ta	Isotope	Eγ keV	Half-life	Decay mode	I γ(%)	Mass
1817	1820	1818	1824						
kev, after									
	20,7	20,7	20,7±1	$^{169}Yb_{70}$	20,75	32d	ε	0,19	169
42±1	43	42	42,18	$^{169}Yb_{70}$	42,76	32d	ε	0,25	169
50±1	51,2	50,44	51	$^{169}Yb_{70}$	51,1	32d	ε	0,018	169
63±1	63	62,83	63,5±0,5	$^{169}Yb_{70}$	63,12	32d	ε	44,2	169
19±1	19,89	19,06	19.1	^{171m}Yb	19,39	5,25ms	IT	14,8	171
22,5±1	23,19	23,19	23.2	$^{172}Hf_{72}$	23.4	1,87 y	ε		172
24±1	24	24,02	24,84	$^{172}Hf_{72}$	23,93	1,87 y	ε	20,3	172
60±1	60,5	60,35	60,5±0,5	$^{172}Hf_{72}$	60,65	1.87 y	ε	1,1	172
67±1	63	62,35	67.5	$^{172}Hf_{72}$	67,3	1,87 y	ε	5,3	172
91±1	91±1	91,74	91	$^{172}Hf_{72}$	91,3	1,87 y	ε	0,11	172
115±1	114	114,03	114,03	$^{172}Hf_{72}$	114,06	1,87 y	ε	2,6	172
115±1		115	115.6	$^{172}Hf_{72}$	116,1	1,87 y	ε	0,034	172
119±1	119	118,99	119,8	$^{172}Hf_{72}$	119	1,87 y	ε		172
129,03	129	127,25	127.5	$^{172}Hf_{72}$	127,9	1,87 y	ε	1,46	172
42±1	43	42	42,18	$^{178}Yb_{70}$	42,4	74m	β-	6,7	178
13±1	14,1	14,1	13,3	$^{180}Yb_{70}$	13,9	2,4m	β-		180
57±1	58,7	57,05	57,88	$^{180m}Hf_{72}$	57.555	5.5h	IT	48.0	180m

*Nine peaks correspond to $^{172}Hf_{72}$.

* The isotope with IT 99.7%, β -0.3% and T1/2=5.47 h was suggested as $^{180m}Hf_{72}$.

Table 3
Peaks energy from tungsten and tantalum after deuterium glow discharge in the gamma spectra using x - ray /gamma cdte detector (for the second group of isotopes)

W 1817	W 1820	W 1818	Ta 1824	Isotope	Isotope's Eγ , keV	Half-life	Decay mode	I γ (%)	Mass, TIMS
Kev, contact*									
1	2	3	4	5	6	7	8	9	10
45± 1	45,10	44,46	46,46	$^{170}Hf_{72}$	44,52	16,01 h	$\varepsilon + \beta^+$	0,32	170
55,4	55,5	55,4	55,4	$^{170}Hf_{72}$	55,2	16,01 h	$\varepsilon + \beta^+$	1.1	170
99,9	99,0	100,8	100,8	$^{170}Hf_{72}$	99,93	16,01h	$\varepsilon + \beta^+$	2	170
113,2	113,3	113,2	113,2	$^{170}Hf_{72}$	113,9	16,01h	$\varepsilon + \beta^+$	0.18	170
115,6	115,0	115,7	115.6	$^{170}Hf_{72}$	115,5	16,01h	$\varepsilon + \beta^+$	0,2	170
133,0	132,0	132,2	132,7	$^{170}Hf_{72}$	132,2	16,01h	$\varepsilon + \beta^+$	0,044	170
138,81	138,5	138,0	138,8	$^{170}Hf_{72}$	139,2	16,01h	$\varepsilon + \beta^+$	0,018	170

- These gamma energy peaks were observed for the different W and Ta foils. It means – the same isotopes are created for the different conditions at deuterium discharge and after experiment stopping.
- Contact* - it means that foil after exposure was located in contact with detector's Be window.
- Seven peaks correspond to $^{170}Hf_{72}$.

The comparison of these data allows the supposing that the gamma spectra peaks observed belong to the following isotopes: $^{169}Yb_{70}$; $^{171m}Yb_{70}$; $^{172}Hf_{72}$; $^{178}Yb_{70}$; $^{180}Yb_{70}$; $^{180m}Hf_{72}$; $^{170}Hf_{72}$.

The same isotopes are created for the different conditions after deuterium discharge

Correlation of TIMS and Gamma spectrometry data leads to the assumption that the heavy isotopes decay under low energy impact

Main isotopes Hf and Yb in different experiments with W and Ta foils for various time intervals were observed.

3.1. Estimation of Gamma/ X-ray emission intensity (value of energy peaks) and mass spectrometry data were fulfilled in CPS.

Gamma Emission From W During of Deuterium Glow Discharge

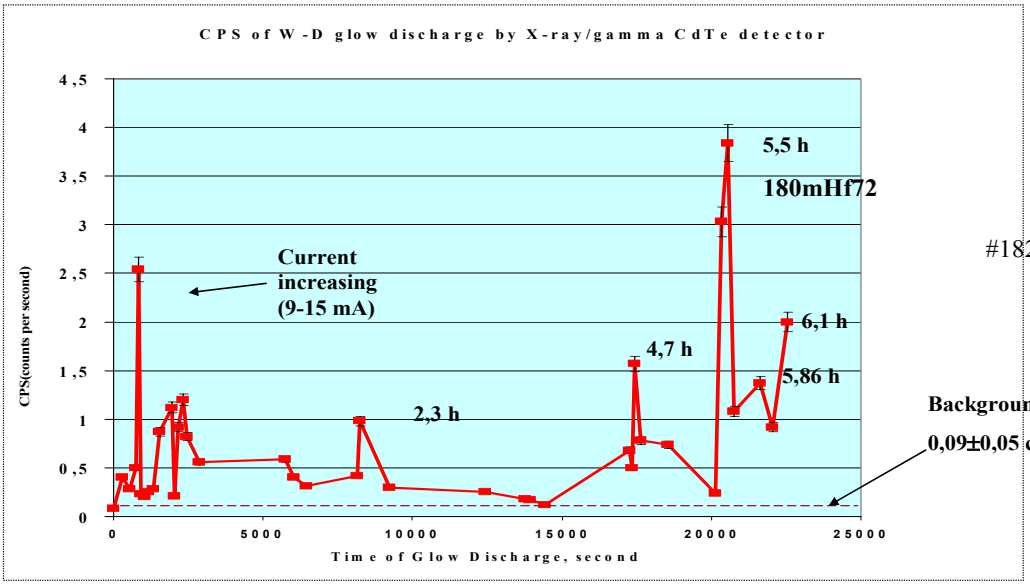

Figure 7. *The intensity of emission in CPS vs. experimental time during Deuterium discharge.*

The intensity of emission was 3.5 cps after ~ 5.5 hours experiment. Average intensity is 0.5 cps (five times more of background). Background = 0.09±0.005 cps.

Table 4

The intensity peaks vs. peak time in gamma spectrometry measurement

1817 Cps	Peak Time after	1818 Cps	Peak Time after	1819 Cps	Time Peak after	1820 Cps	Peak Time after	1820 Cps	Peak Time During
1*	2*	3*	4*	5*	6*	7*	8*	9**	10**
8	24.5m	0,16	13m			0.48	14.3 m	2.54	14.7 m
1,28	28m	0,44	28m	0.91	~30m	0.37	27.6 m		27.6m
		0,5	35m	0.96	34.16			1.12	35m
31,4	43m			1.57	40			1.20	44.6
		0.21	51.7m	0.82	52m			0.56	50m
0,52	1.05 h			1.0	1.25				1.66h
						0.32	2 h		2.29h
								0.68	4.8h
								1.57	5.25h
								8.13	5.7
		0.24	21.55h					1.08	6.1
		0,7	46,13h					1,37	6,3 h

•

- *Column 1-8 – the measurements were made in contact of foil after exposure with Be window of detector.
- ** Column 9-10 - the measurements were made in contact Be window of detector with quartz tube. It means that CdTe detector was on the ~50 mm distance from discharge zone during Deuterium Discharge.
- All measurements of CPS in the empty cells are $\leq 0.07 \pm 0.02$ cps.
- Background was 0.09 ± 0.006 cps for the most measurements.
- The using of hand recording of counts and time in seconds was done. It means the intensity in cps and peak time could not measure very exactly.

Defect of mass, spin and parity were included for the next formula:

$$^{182}_{74}W + ^{2}_{1}D \rightarrow ^{178}_{72}Hf + ^{4}_{2}He + ^{1}_{1}p + ^{1}_{0}n + \sim 1MeV$$

-48 (0+) +13(1+) = -52(0+) +2,45(0+) +7,3 (1/2+) + 8,07(1/2+) + ~1 MeV

Conclusion

1. X-ray/gamma emission is going *during* deuterium discharge experiments under 1000 ± 200 Voltage and *after stopping* of these experiments from the foils irradiated by deuterium ions.
2. The *same isotopes* are defined for the different conditions experiments during and after deuterium discharge.
3. The several x-ray and gamma of peaks and radiation intensity (cps) have been chosen for each prospective isotope $^{169}Yb_{70}$; $^{171m}Yb_{70}$; $^{172}Hf_{72}$; $^{178}Yb_{70}$; $^{180}Yb_{70}$; $^{180m}Hf_{72}$; $^{170}Hf_{72}$.
4. The *comparison of thermoionization mass-spectrometry and x-ray/gamma* emission data allowed to suppose, that the peaks observed in gamma spectra belong to the following isotopes: $^{169}Yb_{70}$; $^{171m}Yb_{70}$; $^{172}Hf_{72}$; $^{178}Yb_{70}$; $^{180}Yb_{70}$; $^{180m}Hf_{72}$; $^{170}Hf_{72}$.
5. Correlation of TIMS and Gamma spectrometry data leads to the assumption that *the appearance of light isotopes in the tungsten and tantalum was as a result (effect) of the stimulation (initiation)* by low energy deuterium discharge.

Aknowledjments

The authors thanks Dr. Starostin for the estimation of CdTe detector efficiency.

Reference

1. Karabut A.B., Kucherov Ya.R., Savvatimova I.B. "Nuclear product ratio for glow discharge in deuterium". **Physics Letters** A, 170, 265-272 (1992).
2. A.B. Karabut, Ya.R. Kucherov, I.B. Savvatimova, The Investigation Of Deuterium Nuclei Fusion At Glow Discharge Cathode " **Fusion Technology** Vol.20 Dec.1991 (P.924-928)
3. Savvatimova I.B., Kucherov Ya., Karabut A.B., "Cathode Material Change after Deuterium Glow Discharge Experiments", "**Transaction of Fusion Technology**"(ICCF4, Dec. 1993); v.26, number 4T (1994), pp. 389-394.
4. Savvatimova I. Transmutation in cathode materials exposed at glow discharge by low energy ions. Nuclear phenomena or ion irradiation result? Proceeding, ICCF-7, 1998, 342-350.
5. Savvatimova I.B, Karabut A.B. Nuclear Reaction Products Registration on the Cathode after Deuterium Glow Discharge. Surface, V. 1, Moscow: RAN, 1996, p.63-75.
6. Savvatimova I.B Reproducibility of experimental in glow discharge and process accompanying deuterium ions bombardment. ICCF8, Italian Physical Society, Bologna, Italy, 2000, P.277
7. J. Dash, I. Savvatimova, S. Frantz, E. Weis and H. Kozima, "Effects of Glow Discharge with Hydrogen Isotope Plasmas on Radioactivity" Proc. ICENES 2002, p. 122 (2002) 2003.
8. J.Dash, I.Savvatimova, S.Frantz Proc.11th Int. Conf. on Emerging Nuclear Energy Systems. Univ New Mexico, Albuqueque, NM, pp.122-127 (2002);
9. J.Dash, I Savvatimova Effects of Glow Discharge with Hydrogen Isotope Plasmas on Radioactivity of Uranium, Proc. Of American Nuclear Society Conf., San Diego, 6 June, 2003.
10. I.Savvatimova, J.Dash, S.Frantz The changing of radioactivity of uranium after irradiation in the Hydrogen plasma of glow discharge, Proc.10th Russian. Conf. on Cold Nuclear Transmutation of Chemical Elements and Ball Lighting. Dagomys, Sochy, Russia, pp.64-74 (2002) 2003.

CALORIMETRY IN Pt/K_2CO_3/Pd LIGHT WATER ELECTROLYSIS SYSTEM

J.Tian*,, L H Jin[1]*, B J Shen*, C Y Wang*, J W Guo***

** Changchun University of Science and Technology, NEL*
*** Portland State University, Department of Physics*
tianjian@cust.edu.cn, jtian@pdx.edu

Followed the experiments of Pt/K_2CO_3(Na_2CO_3)/Ni light water electrolysis by Noninski [1] and Tian [2], some calorimetry of Pt/K_2CO_3/Pd in light water electrolysis was carried out. A similar Pt/Na_2CO_3/Pt light water cell in series was used as a control. When some certain electric currents were passed through the circuit the temperatures in both experimental (E) and reference (C) cells changed. It can be seen that there was an obvious difference in temperature property by comparing the change of heating coefficient ($k = \Delta T / P$) respectively.

When the input current was 0.071A the power in the E and C cells were 0.21W and 0.27W respectively, i.e. more energy was used in the C cell. But the temperature in both cells were reversed. The temperature in the E cell was about 5° higher than that in the C cell. When the system reached steady state after 10 hours' electrolysis, the average heating coefficient in the E cell (k_{Na2CO3}) was 13.88°/W and the coefficient in the C-cell (k_{K2CO3}) was10.89°/WThe difference of heating coefficient between two cells was nearly 3/°W. During 11 hours' electrolysis the input energy to the E cell was 7.56×10^3J. But the output energy that was measured was up to 1.0×10^4J. The total "excess heat" was roughly about 3×10^3J. There was no "excess heat" in the C cell.

Another interesting phenomenon was found in the experiment. When the electrolysis was carried out for about 100 seconds, the temperature in the E cell was obviously increased by 0.6°And this higher temperature in the E cell was kept for about 10 minutes. When the time of electrolysis reached 747 seconds, the temperature dropped back approximately 0.3°.In this duration the "anomalous excess heat" was about 26.7J. But the temperature in the C cell did not have any obvious change in the meantime. There was also no temperature increase when the electrolyte of K_2CO_3 was changed to Na_2CO_3 in the E cell.

References

1. Noninski V. Excess heat during the electrolysis of a light water solution of K_2CO_3 with a nickel cathode. Fusion Technology. 1992. V.21. P.163-167
2. Tian J. et al. "Excess Heat" during the electrolyzing in Pt/K_2CO_3/Ni light water system. Proceedings of ICCF-11. Oct. 31– Nov. 5, 2004. Marseilles, France. P.103-106

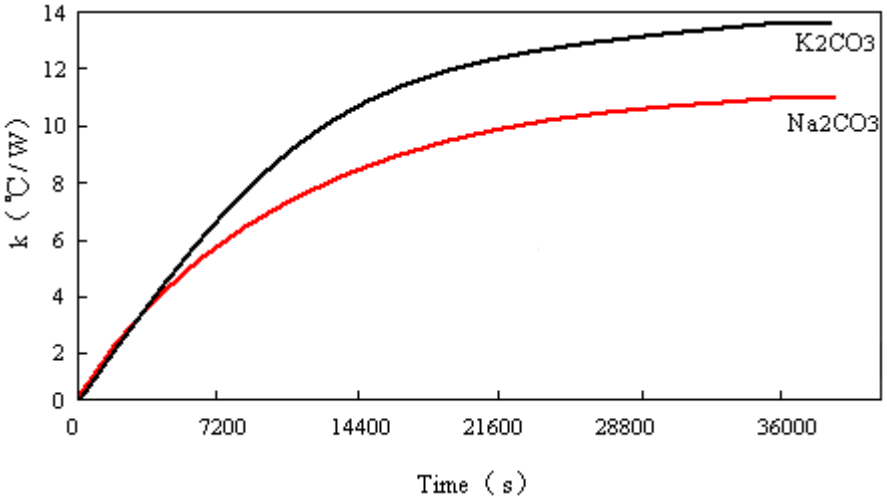
14
12
10
8
6
4
2
0
k（℃/W）
0
7200
14400
21600
28800
36000
Time（s）
K2CO3
Na2CO3

EXCESS HEAT WHILE SATURATION OF TITANIUM BY DEUTERIUM AND AIR MIXTURE.

S.A. Tsvetkov

Kurchatov st. 4-13, Zarechny, Sverlovsk region, 624250, Russia
tflower@uraltc.ru tel.:+7 34377 39656

According to previously received data, while saturation of titanium with deuterium and air mixture, temperature rising of 45° C was registered for the titanium deuteride sample in comparison with a similar sample saturated with pure deuterium. The calculation of excess heat based on the data is given. The results are compared with the data on heat for uranium division and heat nuclear fusion.

CALORIMETRIC RESULTS OF ENEA COOPERATIVE EXPERIMENTS

V. Violante* violante@frascati.enea.it , F. Sarto*, E.Castagna*
C. Sibilia, M.Bertolotti**, R. Li Voti**, G.Leahu****
M. McKubre*, F. Tanzella***,**
K.Grabowski, G.Hubler**, D. Knies****,**
T. Zilov***, and I. Dardik******

**ENEA- Fusione, Tecnologie e Presidio Nucleari, Centro Ricerche Frascati,*
00044 Frascati, Rome, Italy, CP 65
***Dip. Energetica Univ. La Sapienza Rome, Italy*
****SRI International. Menlo Park, California, USA.*
***** Naval Research Laboratory Washington DC, USA*
****** Energetics Technologies Inc., Omer, Israel,*
******* Energetics LLC., New Jersey, USA.*

Abstract

The main research work in ENEA (Italian Agency for Energy New Technologies and Environment) in the field of Condensed Matter Nuclear Science was oriented towards material science in order to increase both the magnitude and reproducibility of excess of power production.

The work was performed within a cooperative framework involving University of Rome La Sapienza, SRI, Energetics and also NRL that has been established specifically for fundamental research in the field of material science. Such a research strategy was conceived to gain a significant control of the phenomenon in order to create appropriate conditions to operate diagnostics both for seeking nuclear products and related signals and to define the physics of the process.

The excess of heat reproducibility increased up to more than 60% and the gain, in some occasions, was larger that 100%.

Material processes developed at ENEA have been successfully used also in the other Institutions involved in the cooperation both in loading and in calorimetric experiments.

The amplitude of the signals giving a very high signal/noise ratio, the gains in energy, the level of transferred reproducibility and their correlation with the status of the material, are well above noise and error bar criteria. Detailed experimental results will be reported.

Introduction

Excess of power production during electrochemical deuterium loading in palladium was discovered by M. Fleishmann and S. Pons in 1989 [1]. The reproducibility of the effect was suddenly discovered to be very low. Some years late (1992) McKubre (SRI) [2] and Kunimazu (IMRA Japan) [3] discovered that the excess of power production was a threshold effect occurring only (but not always) when the average deuterium concentration into the palladium lattice exceeded the atomic fraction value D/Pd = 0.9. Such a discovery moved the research activity towards the aspects of material science concerning the mechanisms controlling the hydrogen isotopes mass transfer into metal lattices.

The dissolution of hydrogen isotopes into a metal lattice is not only a problem of thermodynamic equilibrium between the hydrogen inside the lattice and the hydrogen in the external phase (gas or liquid) but is also a problem of not equilibrium because of the occurrence of a transport process. The two aspects of the phenomenon are correlated since the equilibrium concentration of the solute is achieved when the chemical potentials of the hydrogen in both phases are equal and since the transport process inside the metal lattice is driven by the gradient of the chemical potential.

The migration of interstitials in a metal under an applied external bending is well known as Gorsky effect [4]. The deformation field produces the defects migration toward the expanded areas. Lewis and co-workers [5,6,7] showed that internal stresses are generated during insertion and diffusion of interstitial hydrogen and that the resulting strain production represents an opposing force to the flux produced by the concentration gradient.

In the following is studied the effect of the stress as limiting factor in achieving the deuterium loading threshold in palladium to have excess of power production.

Research activity at ENEA, in the field of Condensed Matter Nuclear Science, has been oriented to material science in order to increase the reproducibility of excess of power production during loading of palladium with deuterium. Metallurgy and status of the interface have been studied to realize a proper material conceived for increasing the control of the excess of power production.

The flow calorimetric system was also carried out on the basis of a 3D transient finite element modelling of the apparatus.

Field of stress limiting the hydrogen isotopes solubility in palladium

The fields of force, like the stress field, modifying the free energy of the system, modify the chemical potential of the hydrogen in solid solution in a metal lattice.

The hydrogen isotopes dissolving into a metal (i.e. palladium) occupies interstitial positions and expands the lattice. This process generates a stress field when remarkable concentration differences (strong gradients or coexistence of different phases) are created.

The situation is quite similar to the stress produced by a temperature gradient.

Therefore the loading process may be inhibited by a stress gradient, for instance behind the external surface, where the effect is traceable to the effect of a strong temperature gradient. Thus, in the zone at high concentration, compressed by the zone at low concentration, the chemical potential of the solute increases and the loading can be inhibited.

The equation describing the diffusive transport controlled both by the concentration gradient and by the stress field is [8]:

$$\frac{\partial \bar{c}}{\partial \tau} = \frac{\partial^2 \bar{c}}{\partial \bar{x}^2} - (1-\eta) b \frac{\bar{V}E}{RT} \left(\frac{\partial \bar{c}}{\partial \bar{x}} \right)^2 - (1-\eta) b \frac{\bar{V}E}{RT} \bar{c} \frac{\partial^2 \bar{c}}{\partial \bar{x}^2} \qquad (1)$$

where $\bar{c} = c/c_0$ is the dimensionless concentration (c_0 is the metal atoms concentration), $\bar{x} = x/L$ where L is the characteristic length of the system (typically the thickness or the radius), $\tau = L^2/D$, with $D = Mc(\partial\mu/\partial c)$, where M is the mobility and μ the chemical potential., b=0.044, E the Young's module, $\bar{V}$ the molar volume and where we introduced η as a parameter giving the percentage of stress that is released by plastic deformation or by dislocation slipping; it is clear that when the release of the stress is complete the transport equation reduces to the Fick's one.

Equation (1) describes the interstitial diffusion of hydrogen into a metal (e.g. palladium) under a stress field. The effect of stress at steady state translates on a different concentration profile, then a different loading that depends on the properties of the material such as the Young module.

The transport equation (1), including the calculation of the relaxed stress on the basis of the mechanical properties of the material (σ_r), is solved with the boundary conditions:

$\bar{c}=1 \;\; \bar{x}=0$ and $\partial\bar{c}/\partial\bar{x}=0 \quad \bar{x}=L/2$.

Calculations have been done by using indicative values of the Young module. Fig. 1 shows the equilibrium concentration profile, from the external side up to the symmetry plane, for a palladium foil with Young's Module value of 1.0 x 10^{11} Pa (these value is chosen in order to magnify the effect). It is clear that the loading reduces with respect to the Fick's equilibrium profile.

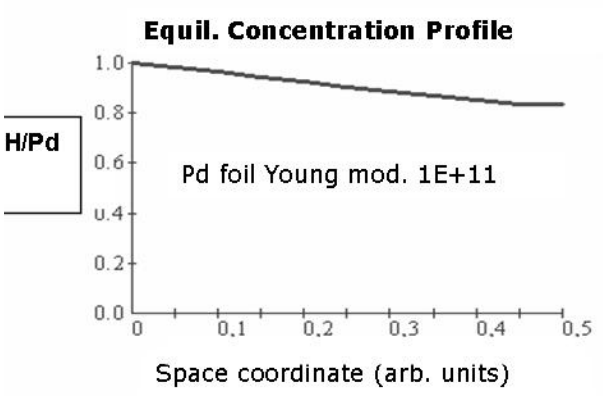

Fig.1- *Equilibrium H concentration profile within a Pd foil (Young module = 1E+11Pa).*

Grain boundary/grain diffusion

Before concluding this section concerning the impact of the metallurgy on the hydrogen isotopes dissolution into the metal lattice we analyze the effect of the grain boundary on the diffusion process during the loading. The grain boundary/grain system is schematically shown in Fig. 4.

A mass balance, by neglecting the fields of forces, leads to the following system of partial differential equations describing the diffusive process [9]:

$$\frac{\partial C_b}{\partial t} = D_b \frac{\partial^2 C_b}{\partial y^2} + \frac{2D_g}{\delta}\left(\frac{\partial C_g}{\partial x}\right)_{x=\delta/2} \tag{2}$$

$$\frac{\partial C}{\partial t} = D_g \nabla^2 C_g \tag{3}$$

to be solved with the following initial and boundary conditions:

$$y=0,\ t=0\ C=C_0;\ \ y>0,\ t=0\ C=0;\ \ x=0,\ C_g=C_b \qquad (4)$$

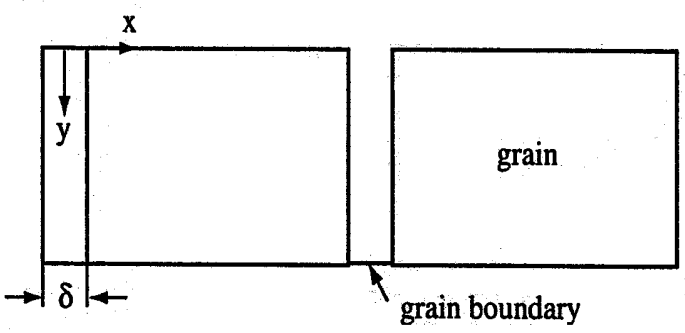

Fig. 2- *Schematic classic representation for grain/grain boundary system*

D is the diffusion coefficient, δ the grain boundary size, C the solute concentration. The subscripts *g* and *b* point to the grain and to the grain boundary respectively. The solution, in closed form, of the system of equations (2-3), with the conditions (4) is:

$$C_g(x,y,t) = C_0 \exp\left[\frac{-y\sqrt{2}}{(\pi D_g t)^{1/2}(\delta D_b / D_g)^{1/2}}\right]\left[1 - erf\left(\frac{x}{2\sqrt{D_g t}}\right)\right] \qquad (5)$$

It may be easily verified that the larger are the diffusion coefficient in the grain boundary and the size of the grain boundary the lower the concentration gradient (then the stress field into the grain).

The previous modeling approach shows that the stress field may act differently moving grain by grain. Such a mechanism may be responsible of the low reproducibility of high loading of deuterium into the palladium lattice.

Materials

The model allows us to seek for a material able to minimize the stress field by minimizing the concentration gradients. An homogeneous loading should produce such an effect. Some treatments, based on cold rolling and annealing steps allowed to optimize metallurgical structure of the materials in order to increase the H(D) loading. The rough material was

palladium foil 1 mm thick able to reach a loading ratio of about 0.75 - 0.8 (hydrogen atomic ratio). The treatment has been done in two steps:

1) Cold rolling of the row material leading Pd foil 50 μm thick.
2) Annealing at temperatures around 900 °C for a time that may exceed one hr.

Figure 3 shows the effect of the treatment (i.e. of the metallurgical structure on the H (D) loading).

H/Pd=0.97 has been obtained in the sample cold worked and annealed.

On the basis of the mechanisms considered above a possible interpretation of such a results is that in the last considered sample the concentration profiles are maintained relatively flat because of the reduced size of the grains and because of a proper boundary grain diffusion. Loading tests have shown a satisfactory reproducibility.

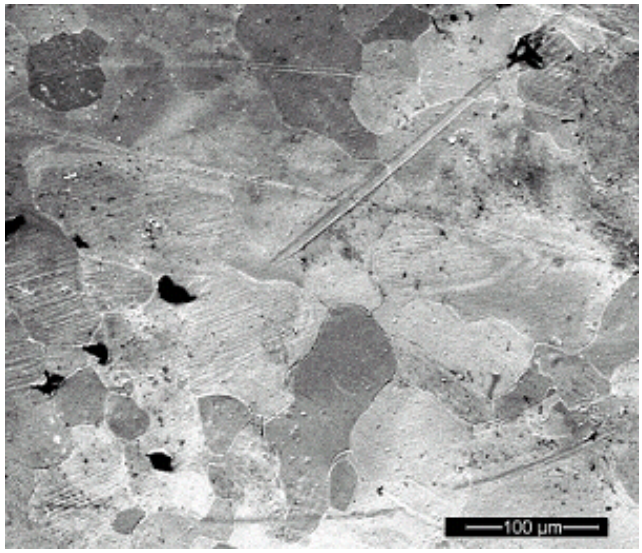

Fig. 3*- Pd cold worked and annealed.*

Calorimetric system

The calorimetric experimental activity is based on flow calorimeters equipped with electrochemical cells, where pre-treated palladium cathodes have been electrochemically loaded by using LiOD 0.1 M electrolyte. Laser irradiation was applied during the electrolysis in some experiment.

The calorimetric cells have been designed to have the required sensitivity and measurement accuracy by using a three dimensional, time dependent, finite element modelling.

Two helium tight cells (He leakage < 2E-10 mbar l/s) are used, the first one is working into a cooled water jacket, the other has the coolant pipe (steel covered by a thin teflon layer) passing into the electrolyte. The second cell is also equipped with two windows for the laser irradiation.

The two cells have a volume of the electrolyte of 30 and 60 ml respectively.

The calorimetric electrochemical cell is embedded into an insulator and operated into a thermostatic box (Memmert ± 0.05 ° C). The coolant, coming from a thermostatic bath (Haake ± 0.05 ° C), is passing through an high precision mass flow meter and controller (Bronkhorst, 0.3-0.1 cc/s) and the input and output temperatures of the coolant, passing into the calorimeter are measured by two PT-100 thermometers read by a Lake Shore instrument (model 218). Electrolyte temperature is also measured in the same way. A scheme of the system is shown in Fig. 4.

The closed electrochemical cell is equipped with a recombiner and with an MKS pressure gauge. Cell power supply is an AMEL galvanostat, modulated, during the HI-LO current mode by an HP33120 wave function generator. Galvanostatic operation allows to have a scalar product between current and voltage (this is the input power for a closed cell under DC current). Current and voltage are measured by means of two HP34401A 6.5 digit multimeters. Typically the cells operate with voltage and current ranging between 2.5 and 12 V and 5-500 mA. Reading of the box, bath, room temperatures and reading of the cell pressure is performed with an HP34970A. The data acquisition system is realized with a LabView program and GPIB connections.

Output power is measured by means of the mass flow rate and coolant temperatures, R/Ro measurement is done by means of an HP- 4284 (four wires measurement).

Several experiments have been done by using light water (LiOH 0.1 M electrolyte) obtaining a calorimeter efficiency of 97.5% (output=0.975 input, because of the heat losses).

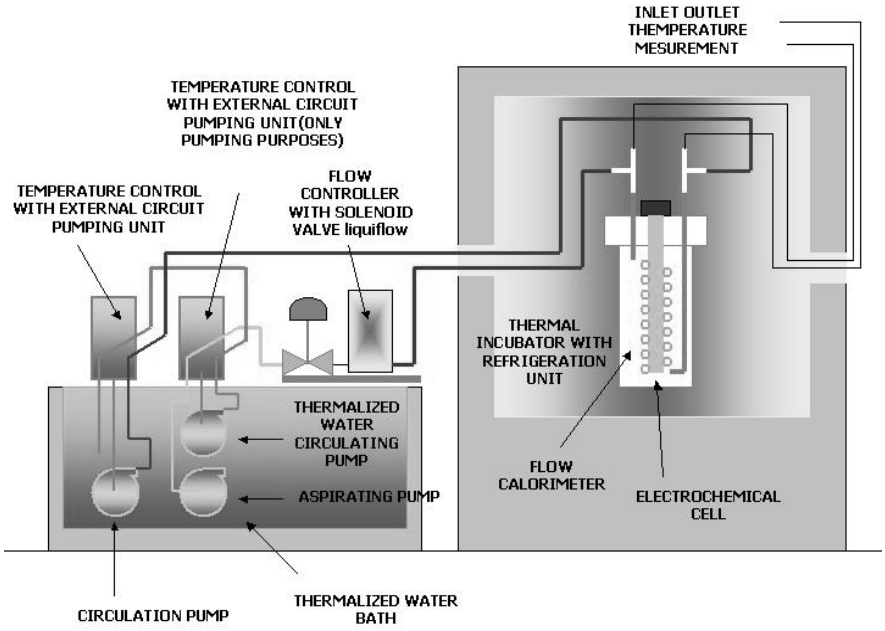

Fig.4- *Flow calorimeter system.*

The cathode is a Pd foil (20 x 10 mm x 50 microns) between two platinum foils (symmetric 45 x 15 mm), the anode-cathode distance is 6 mm.

Figure 5 and Fig. 6 show the temperature field in the cells under typical operating conditions.

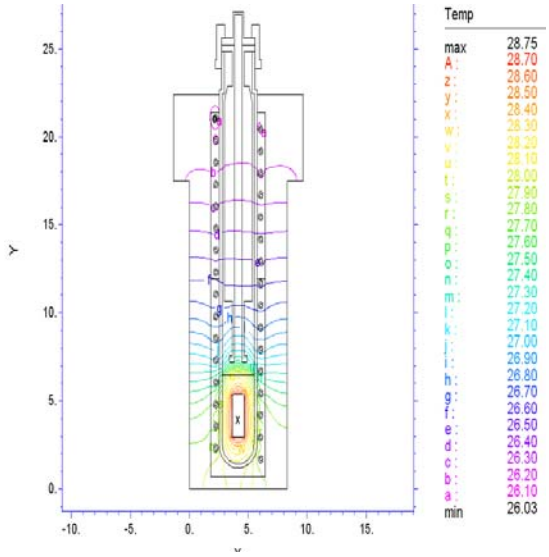

Fig.5-*Calculated 2-D temperature distribution in the electrochemical cell*

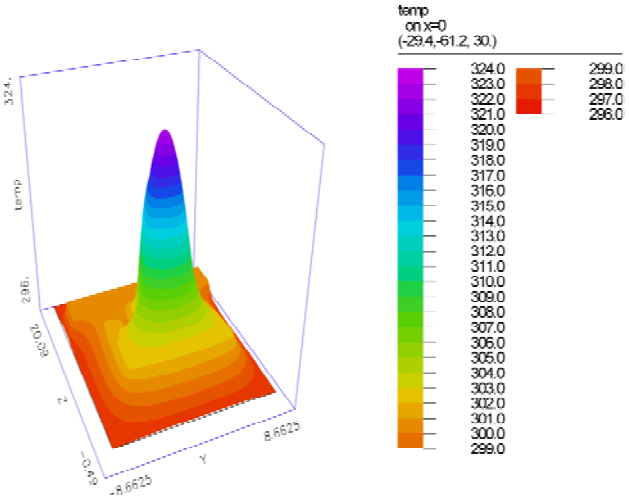

Fig.6-*Calculated 3-D Temperature distribution in the electrochemical cell*

Experimental activity

Several running with light water have been done both to estimate the efficiency of the calorimeters and to study if anomalous thermal behaviour was occurring loading palladium with hydrogen.

No excess of power production has been observed by using H_2O despites a very high loading (H/Pd=0.97) was always achieved.

The sensitivity of the calorimeter was estimated to be 50 mW ± 20 mW.

During the first experimental campaign some excess of heat have been observed giving rise to an energy gain.

Similar evidences, during the same period, have been observed with laser triggering. The small statistics done with laser triggered experiments seems to be indicative of a stabilizing effect on the excess of power production.

This experimental campaign showed a very high reproducibility in loading above the threshold, close to 100%, and significant reproducibility in the occurrence of the excess of heat that was around 25-30%. It was clear that the loading above the threshold, in the average value estimated to be around D/Pd = 0.9, was a necessary condition to obtain the production of excess of power.

Starting from such an observation a further work was developed to enhance the reproducibility of the excess. The strategy was always oriented in the field of material science but was extended to a wide spectrum of aspects. Metallurgy was integrated with the status of the material at the surface, with the processes at the interface and with the electrochemical experimental conditions and this work was jointly performed by ENEA, SRI, NRL, University of Rome and Energetics.

Even if this extended material science approach is still in progress an improvement at experimental level was obtained leading an increasing of the reproducibility (in ENEA, SRI and Energetics) up to 70-75%.

Some of the experimental results obtained at ENEA will be described in the following.

Sample L14 showed a good loading up to D/Pd = 0.95 and was etched with nitric acid for 60 sec and with 100% acqua regia for 60 sec before the electrolysis. During the experiment the current and voltage ranged between 10 - 15 mA and 2.4 – 3.5 V respectively.

The maximum was achieved at very low current (13 mA on 6 cm^2 of cathodic surface).

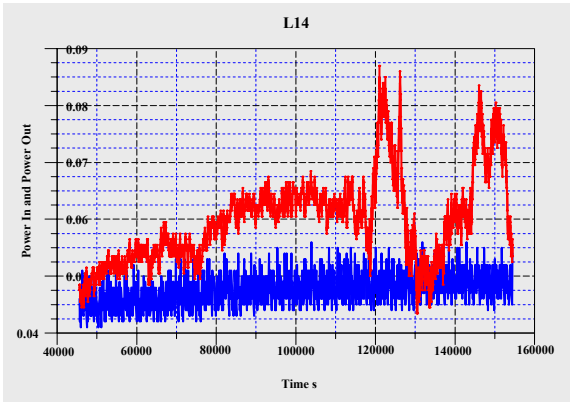

***Fig.** 7-Excess of power (sample L14)*

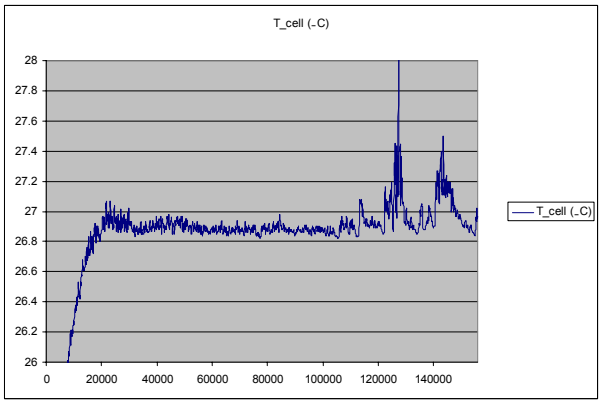

***Fig. 8-** Electrolyte temperature (sample L14)*

Excess of power occurred as shown in Fig. 7, where the measure uncertainty is taken into account. Both heat bursts are very well correlated with the electrolyte temperature, as may be seen from Figure 9. Temperature of the electrolyte was monitored with a PT100 thermometer as well as the inlet and outlet coolant temperature. Notice that the electrolyte temperature was read with a different temperature reader, so that bad functioning of the temperature reader may be excluded. The amplitude of the excess achieved 80% of the input in the peak.

A larger excess was obtained with sample L17, the evolution of the input and output power is shown in Fig. 9. The second burst is long enough to have the calorimeter more or less at the

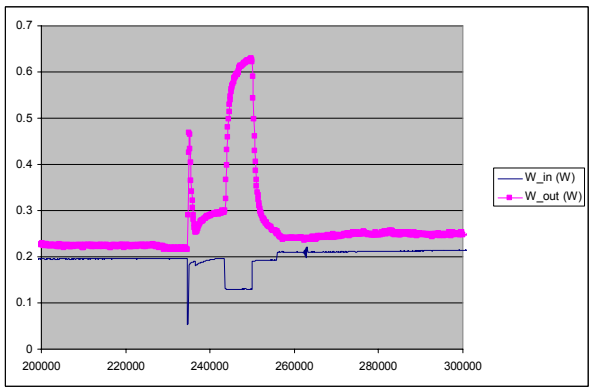

***Fig.9-** Input and output (upper curve) power evolution in the experiment L17.*

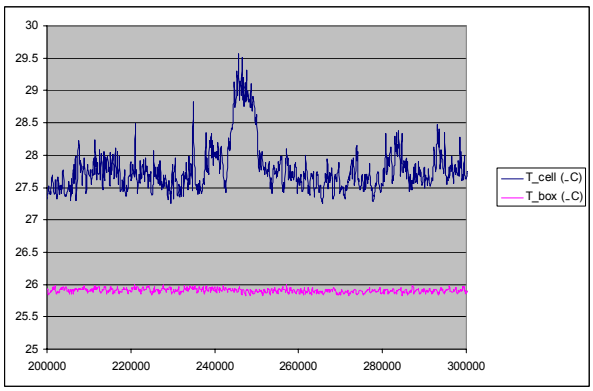

***Fig.10-** Electrolyte temperature evolution: temperature increasing is very well correlated with the excess of power.*

steady state. We can see in Fig. 9 that during the excess of power the input power reduces, this effect is due to the power supply operating mode (galvanostat) because the strong excess of power, up to 620 mW, produced a temperature increasing of the electrolyte that was

responsible of a reduction of the electrolyte resistivity (showed in Fig.10) and probably also of the over voltage, so that a less voltage was required to maintain the set point current. The consequence was the reduction of the input power during the burst. In conclusion we had 620 mW of output with an input of 125 mW so that the output gain was 500%. The specimen L17 was etched like L14 and the voltage and current ranges were: 10- 65 mA and 2.6 – 4.5 V.

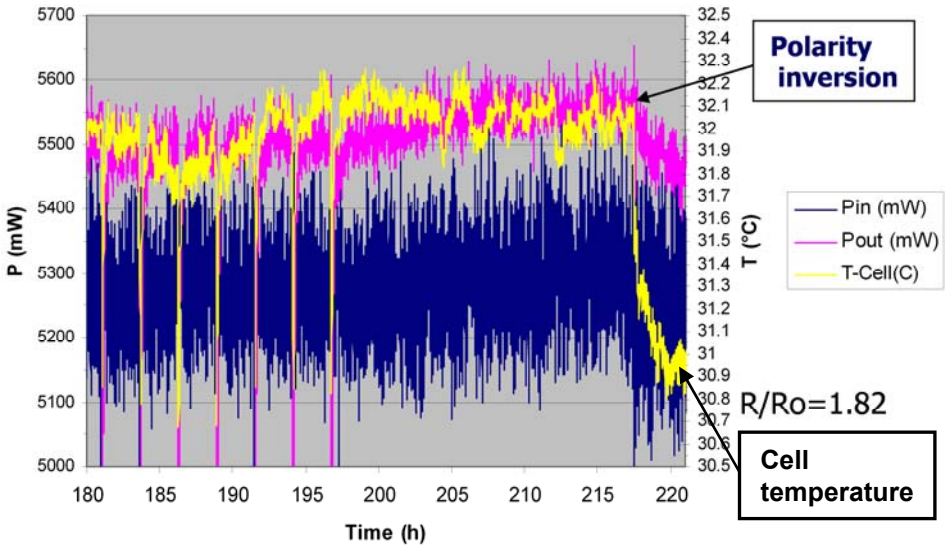

Fig.11- *Temperature and Output Power decreasing after changing electric polarity, Pin=constant*

A very stable effect seems to be obtained with L35 sample, under laser irradiation. An excess ranging between 200 and 250 mW, well above the measurement uncertainty was observed during laser (632 nm) irradiation .

Figure 11 shows the cell temperature and output power decreasing due to electric current polarity switching during sample L35 electrolysis. The two consistent effects, produced by the deloading of the cathode due to the current inversion, are a further proof of the presence of an excess of heat.

Conclusions

Research activity at ENEA, in the field of Condensed Matter Nuclear Science, has been oriented to material science in order to increase the reproducibility of excess of power production during loading of palladium with deuterium.

A finite elements model has been developed to simulate the calorimeters thermal response; such a simulation allowed to obtain real efficiency of 97.5%. The sensitivity of the calorimeter was estimated to be 50 mW ± 20 mW.

Palladium metallurgy and surface structure have been optimized to improve system reactivity, in accordance with theory relating material status with hydrogen loading.

Even if the extended material science approach is still in progress an improvement at experimental level was obtained leading an increasing of the reproducibility (in ENEA, SRI and Energetics) at the level of 70-75%.

Some of the observed excesses of power are presented. Sample L14 showed a good loading up to D/Pd = 0.95, the amplitude of the excess achieved is 80% of the input in the peak.

The larger excess, giving a gain of 500%, was obtained with sample L17.

As happens with L35 sample, it seems that laser triggering acts as a stabilizer of the phenomenon, i.e. rising low excesses heat which are quite stable in time. The low excesses level could be ascribed to the small spot size of laser beam.

References

1. M.Fleishmann, S.Pons. Electrochemically Induced Nuclear Fusion of Deuterium. J. Electroanal. Chem. 1989. V. 261. P. 301
2. M. C. H. McKubre, S. Crouch-Baker, A. M. Riley, S. I. Smedly, F. L. Tanzella. Excess Power Observation in Electrochemical Studies of the D/Pd System; the Influence of Loading. Proc. Third Int. Conf on Cold Fusion, Nagoya (Japan) October 20-25. 1992. P.5
3. K. Kunimatsu, N. Hasegawa, A. Kubota, N. Imai, M. Ishikawa, H. Akita and Y. Tsuchida. Deuterium Loading Ratio and Excess Heat Generation during Electrolysis of Heavy Water by a Palladium Cathode in a Closed Cell Using a Partially Immersed Fuel Cell Anode. Proc. Third Int. Conf on Cold Fusion, Nagoya (Japan) October 20-25. 1992. P.31
4. H. Wipf. J. Less-Common Met. 1976. V. 49. No 291
5. F.A. Lewis, J. P. Magennis, S.G. McKee and P. J. M. Ssebuwufu. Hydrogen chemical potentials and diffusion coefficients in hydrogen diffusion membranes. Nature (London). 1983. V. 306. P. 673-675
6. F. A. Lewis, B. Baranowski and K. Kandasamy. J. Less Common Met. 1987. V. 134. L27
7. F. A. Lewis, X. Tong, K. Kandasamy, R. V. Bucur, and Y. Sakamoto. Electrochem. Acta. 1993. V. 218. No. 57.
8. A. De Ninno, A. La Barbera, V. Violante. Consequences of Lattice Expansive Strain Gradients on Hydrogen Loading in Palladium. Phys. Rev. B. 1997. V. 56. No. 5. P. 2417-2420.
9. J.D. Fast. Gases in Metals. The Gresham Press. 1976. P. 148.
10. P.G. Shewmon. Diffusion in Solids. Mc Graw Hill. 1967. P.166

LARGE CHANGE IN ISOTOPIC RATIO OF LI WITH ANOMALOUS ^{6}LIH FORMATION BY LIGHT WATER ELECTROLYSIS

H. Yamada and S. Nagao

Department of Electrical and Electronic Engineering, Iwate University, Ueda 4-3-5, Morioka, 020-8551 Japan
yamadahi@iwate-u.ac.jp

We performed DC electrolysis of Li contained H_2O solution for 2 weeks using Pt foil anode and Ni film cathode. The electrolyte cell is made of polytetrafluoroethylene with volume of 500ml. In order to investigate the change in the composition of elements on Ni surface electrode, we prepared the control Ni film sample. The control Ni film was immersed into a part of the solution for the same period of 2 weeks without electrolysis.

After the electrolysis, the surfaces of Ni cathode and the control sample were analyzed by time-of-flight secondary ion mass spectroscopy (TOF-SIMS) (ULVAC-PHI: TFS-2100). The primary ion in TOF-SIMS was Ga^{+} and measured area was 40×40 micron square. Three randomly selected areas on the Ni film surface were analyzed.

The isotopic ratio of Li for the control sample fairly agrees with that of natural one. Almost no count of ^{6}LiH also ^{7}LiH was detected for the control sample. To the contrary, an enormous count of ^{6}Li was detected for the Ni electrode after electrolysis, which increased the natural isotopic ratio ^{6}Li/^{7}Li from ~0.08 to the anomalous values of 0.51-1.61. The count peak of ^{7}Li was clearly separated from that of ^{6}LiH in the figure of spectrum. In other words, no overlapping between these counts was observed. Of particular interest is that almost no count for ^{7}LiH was detected, even though an enormous count of ^{6}LiH was detected. This would imply that the molecule ^{6}LiH was formed during the electrolysis.

If these phenomena were caused by a cold nuclear transmutation, the following is one of plausible processes. Element ^{7}Li was transmuted into ^{6}Li, accompanied by simultaneous emissions of proton and electron. The proton would collide with another proton in surrounding molecules H_2O and might immediately take the low energy state. Next, a part of such low energy protons could be captured by their MOTHERs ^{6}Li to form molecules ^{6}LiH.

REPORT ON ELECTROLYSIS EXPERIMENTS AT ENERGETICS TECHNOLOGIES

I. Dardik, T. Zilov, H. Branover, A. El-Boher, E. Greenspan, B. Khachaturov, V. Krakov, S. Lesin, A.Shapiro and M. Tsirlin

Energetics Technologies
P.O.Box 3026
Omer Industrial Park
Omer, Israel
E-mail: *lesin@energetics.il.co*

Abstract

Several different types of cathodes and modes of operation were experimented with in the electrolytic cells in an attempt to increase the reproducibility of excess heat generation and to increase the coefficient of performance. All these experiments used Dardik's modified SuperWaves to drive the electrolysis. The highest reproducibility is obtained with ultra-sound excitation. Also promising are Pd/SWCNT/Pd targets made of a sandwich of palladium and Single Wall Carbon Nanotubes, as well as Pd foils that underwent etching by glow-discharge of deuterium ions.

Significant amount of excess heat was generated and very large coefficient-of-performance was obtained in several experiments. The largest excess power obtained was nearly 20 watts corresponding to a coefficient-of-performance of approximately 2500%. The total excess energy generated is 3.5 MJ amounting to specific excess energy of ~15.3 KeV per Pd atom. This is at least three orders of magnitude larger than the energy that can be generated by chemical reactions or that can be stored in the form of mechanical energy. The corresponding average specific power is 48 W per gram Pd. For comparison, the average specific power in commercial nuclear fission reactors is between 20 to 50 W per gram uranium.

1. Introduction

Energetics Technologies (ET) was established in 2001 to investigate possibilities for generating energy from Cold Fusion, also referred to as Low Energy Nuclear Reactions (LENR) or Condensed Matter Nuclear Science (CMNS), using a new approach of wave excitation. The new approach involves use of so-called "waves-waving-waves" or SuperWaves for driving the processes that generate LENR [1, 2]. The idea of SuperWaves for enhancing the probability of LENR was first proposed by Dr. Irving I. Dardik based on his vision of nature described in [3]. The SuperWaves used in ET electrolysis experiments are briefly described in Section 2.

The primary objective of the ET electrolysis experiments is to improve the reproducibility of excess heat generation. An additional objective is an amplification of the power and energy gains obtained in these experiments. Several experimental approaches are pursued in an attempt of achieving these objectives: Optimization of the Super Waves and development of new types of targets for the cathode or target preparation and pretreatment procedures, including:

- Modification of cathode surface by special annealing-etching procedures jointly developed with ENEA (Frascati) and the University of Rome
- Modification of cathode surface by SuperWaves glow discharge etching
- Development of multi-layers cathodes
- Development of cathodes that include single-wall carbon nanotubes (SWCNT)
- Use of ultrasonic wave driven cavitation for in-situ cleaning of the cathode surface, generation of dislocations and assistance in loading.

Experimental results in each of these research areas are reported along with results from metallurgical and the X-ray analysis of the cathodes.

Following a description of the above approaches along with a statistical summary of the results of the electrolytic experiments done so far in the different approaches described above (Sec. 3), a description of each of the approaches along with illustrations are provided in Sec. 4 through 9. A summary of results obtained in a number of the most successful excess heat generating experiments is given in Sec. 10. A description of the electrolysis cell developed and used by Energetics Technologies can be found in References 1 and 2.

Successful replications of Energetics Technologies heat production experiments were accomplished at SRI and at ENEA (Frascati). Results of the SRI and ENEA experiments will be presented separately.

2. SuperWaves

The idea of SuperWaves for enhancing the probability of LENR was first proposed by Dr. Irving I. Dardik based on his vision of nature described in [3]. The waves waving waves are a special modulation of several waves of different frequency and amplitude.

Figure 1 illustrates the principles of formation of the SuperWaves being used for the ET electrolytic cell experiments. The figure shows a total of four levels of modulation – a fundamental mode, $F_0(t)$, on top of which two higher frequency modes – $F_1(t)$ and $F_2(t)$, are superimposed. The amplitude, A_i, and frequency, ω_i, of each of the super-imposed waves are adjustable. An illustration of a series of wave packets actually used in the ET electrolysis experiments is given in Figure 2. The figure gives a computer screen display of the time dependent current used to drive the electrolysis. This modulated current is generated by a special computer program developed by ET for Lab VIEW.

$$F_0(t) = A_0 \sin^2(\omega_0 t)$$

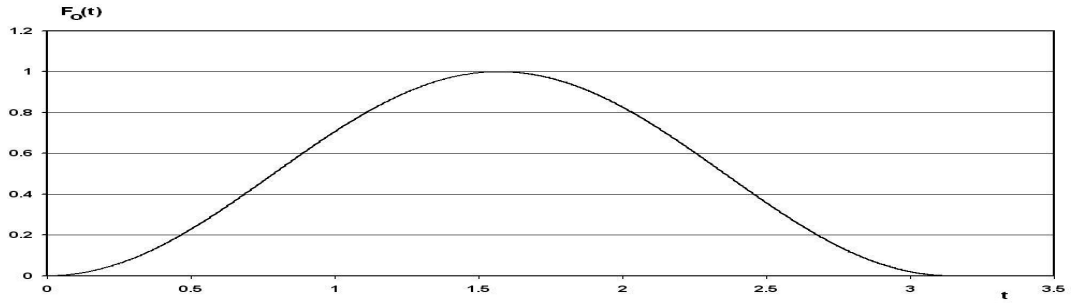

$$F_1(t) = A_0 \sin^2(\omega_0 t)(1 + A_1 \sin^2(\omega_1 t))$$

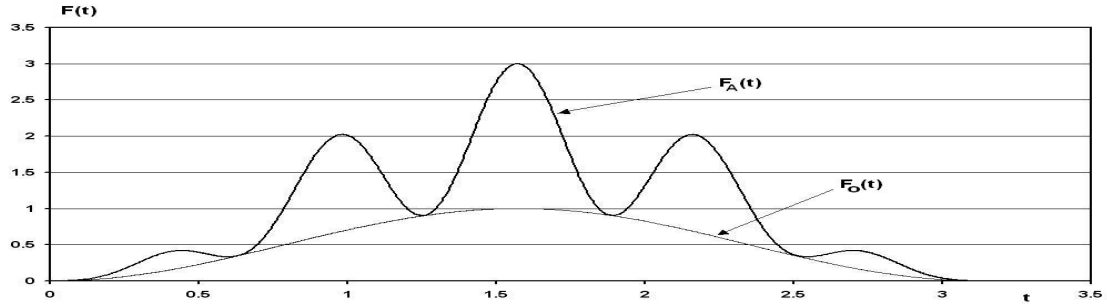

$$F_2(t) = A_0 \sin^2(\omega_0 t)[1 + A_1 \sin^2(\omega_1 t)(1 + A_2 \sin^2(\omega_2 t))]$$

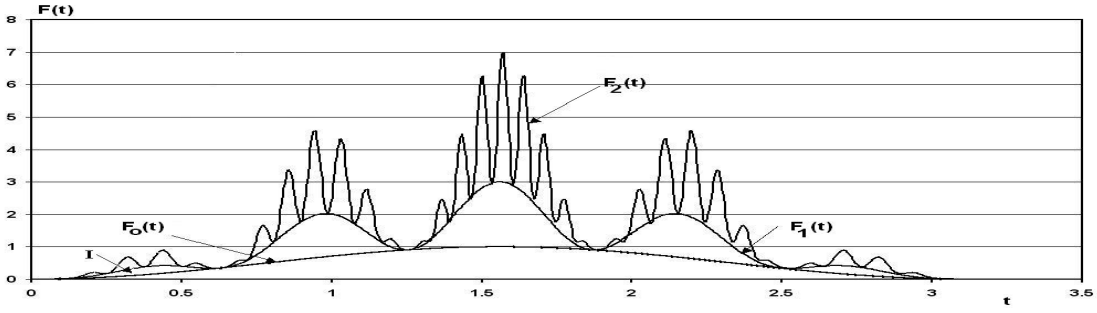

$$F_3(t) = A_0 \sin^2(\omega_0 t)[1 + A_1 \sin^2(\omega_1 t)(1 + A_2 \sin^2(\omega_2 t)(1 + A_3 \sin^2(\omega_3 t)))]$$

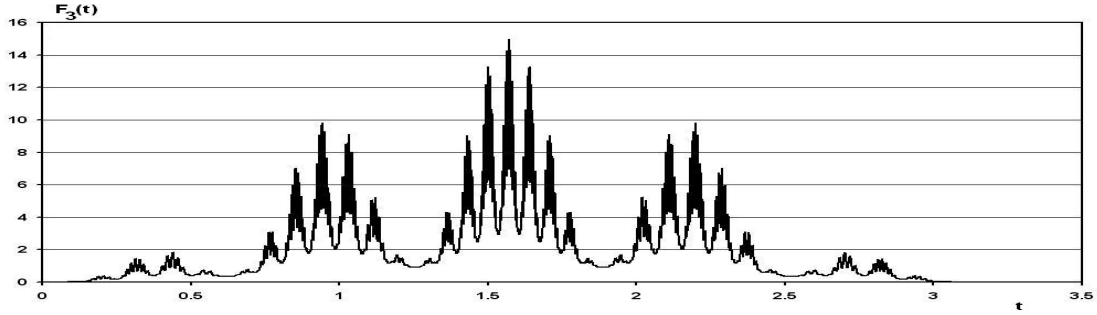

Fig. 1 *Principles of SuperWaves formation*

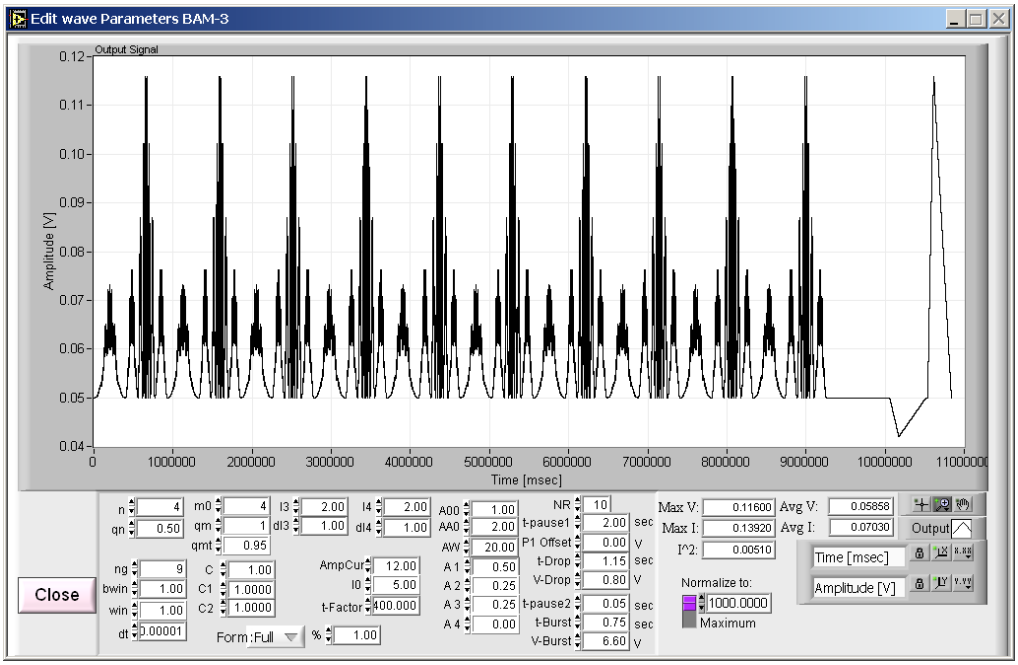

Figure 2 *A typical sequence of SuperWaves packets used for ET electrolysis experiments*

3. Type of Cathodes Used and Statistical Summary of Results Obtained

The following types of cathodes were experimented with:

- Palladium foils pre-treated by Dr. Vittorio Violante et al. of ENEA [4]
- Palladium foils pre-treated by Dr. Vittorio Violante et al. of ENEA that underwent a special optical screening by Prof. Concita Cibilia et al. of the University of Rome
- Commercially supplied Palladium foils or Pd foils pre-treated at Energetics, that underwent etching at ET using a glow discharge cell specially designed for this function
- Foils made of commercially supplied palladium-nickel alloy
- Targets made of commercially supplied 50 μm thick palladium foil on top of which where deposited or fabricated thin layers of either PdO or other metal, such as Ni or Re. These multilayer cathodes were fabricated by Dr. Andrei Lipson et al.[8]
- Targets made of commercially supplied 50 μm thick palladium foil on top of which where deposited a thin layer of Single Wall Carbon Nano-tubes (SWCNT) that are coated by a thin layer of Pd on top. These Pd-SWCNT-Pd sandwich targets were fabricated by Dr. Andrei Lipson et al.[1]

All the above targets were used as cathodes in the ET electrolysis cells and were driven by SuperWaves. A relatively new set of experiments used electrolytic cells that were modified to incorporate ultra-sonic transducers that can generate cavitation in the electrolyte in the vicinity of the Pd cathode. The cathodes used in the ultra-sonic (US) driven cells are palladium foils prepared by ET.
A large fraction of the experiments used 50 μm thick palladium (Pd) foils for the cathode. Prior to its use the Pd cathode is annealed at 870°C in vacuum for 1h. Then it is etched in

[8] From the A.N. Frumkin Institute of Physical Chemistry and Electrochemistry of the Russian Academy of Science.

Nitric Acid 65-67% for 1 min and in Aqua Regia 1:1 water solution for 1 min. Following etching it is rinsed in D_2O four times, in ethanol 95% twice, and in ethanol "absolute" once. The final step before mounting into the cell is drying in vacuum at ambient temperature for 24 hours.

Table 1 gives a summary of the electrolytic cell experiments performed so far at ET, arranged by the cathode type. The right-most column gives the percent of the cathodes that gave 5% or more excess heat; it is a measure of the reproducibility of EH generation. The following sections provide illustrations of results obtained with different types of cathodes. As will be illustrated in Section 8, significant excess heat was obtained in several experiments using most of the type of targets defined in Table 1.

Table 1 Number of Electrolysis Experiments by Category and Fraction that Gave Excess Heat

Number of experiments by category	№ of exp.	EH giving experiments	
		№ of exp.	% of exp.
50 microns Pd foil - regular*	98	16	16
50 microns Pd foil* - optically tested**	20	3	15
Glow discharge etching	21	10	50
PdNi alloy	16	3	19
Multilayer*** Pd/Me(MeO)/Pd [Me ≡ Metal]	25	6	24
Single Wall Carbon Nano Tubes Pd composite***	59	11	19
Total	253	49	19
US excited electrolysis	25	14	56

* Foils prepared by Dr. V. Violante et al
** Foils tested by Prof. C. Cibilia et al
*** Targets prepared by Dr. A. Lipson et al.

4. ENEA prepared Pd foil cathodes

Significant amount of excess heat was generated by two of the foils: foil # 56 and foil # 64. The description of these experiments was presented in References 1 and 2. The impressive amount of excess power and excess energy obtained in these experiments are summarized in Section 10. An attempt was made to create cathode surface similar to that of foil #64:

- embed "black spots" on the surface using special rolling procedure
- anneal under similar condition
- find the right etching procedure
- specify the surface properties by an optical method

Unfortunately, no statistically significant improvement in performance has been found. Table 2 gives the number of experiments performed at ET with these targets and the percentage of the experiments that gave excess heat. When EH was measured, the power gain was relatively low – n the order of 10-15% of the input power, P_{in}.

Table 2 Statistics of Electrolysis Experiments Done with Pd Targets Prepared by ENEA

Type of target	Number of experiments	No. of experiments giving EH	% of experiments that gave EH
50 microns Pd foil – regular	98	16	16
50 μ Pd foil – optically screened	20	3	15

5. Glow-discharge etched Pd cathodes

A series of experiments were performed using for the cathode 50 μm thick Pd foils that underwent glow-discharge (GD) etching at ET. Several types of gases were tried for the discharge, as indicated in Table 3 that summarizes the electrolysis experiments carried-out. Etching with Argon caused strong mechanical defects on the surface; 3 out of 4 foils etched with Ar had totally destroyed surface. On the other hand, etching with deuterium did not destroy the surface and did not develop cracks in the foils. In addition, one of the deuterium etched foils[9] gave the largest excess heat of the etched foils – approximately 14 Watts corresponding to a COP of 75%. As a result, deuterium was chosen as the preferred gas for GD etching.

Table 3.Summary of the ET Electrolysis Experiments Using GD-Etched Pd Targets

Glow discharge gas	No. of significant experiments	Giving EH		COP	R_o/R
		No.	%		
Initial Series					
Argon	1	1	100%	10-20%	Peak
Helium -Deuterium	5	2	40%	20%	1.93-1.32
Deuterium	5	1	20%	25-75%	1.87-1.26
Helium	2	1	50%	10%	1.88-1.62
Total	**13**	5	38%		
Recent Series					
Deuterium	8	5	62.5%	10-25%	1.95-1.22

Under the action of the deuterium plasma glow discharge, the initial Pd surface undergoes significant changes, as illustrated in Figure 3. These changes are due to the processes of Pd atoms sputtering by the deuterium plasma with their partial condensation and a subsequent growth of Pd crystals under the conditions of high super-saturation. As a result of a competitive growth, palladium crystals of pyramidal shape are grown, with their faces formed by {111} planes. Thus, the GD etching results in the formation of a highly developed surface.

Relatively high reproducibility of over 60% was obtained in the most recent series of experiments that used deuterium ions for the etching (Table 3). Some of the cathodes reached very high loading.

[9] Experiment # 141 described below

Figure 4 illustrates excess heat generating experiment using for the cathode a Pd foil that was etched using deuterium discharge – experiment #141. The EH generation lasted for approximately 90 hours giving a maximum excess heat of approximately 14 watts and a total of excess energy generation of approximately 2.4 MJ as compared with a total net energy investment of approximately 3.6 MJ; that is a total excess energy of about 66%.

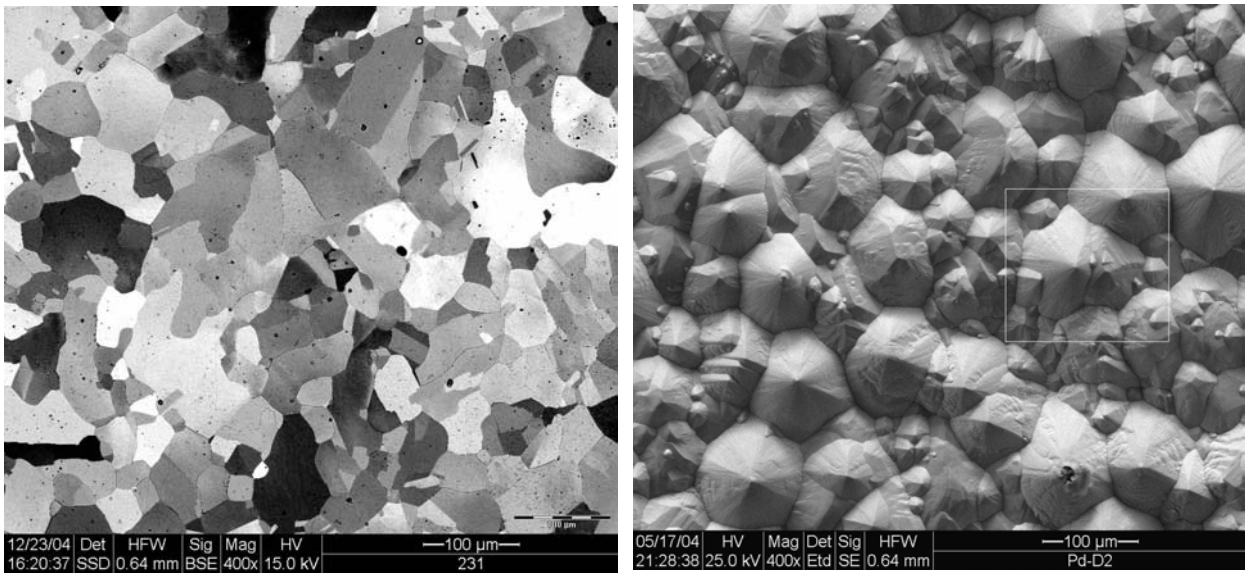

a b

Fig. 3 *Surface of Pd foil before (a) and after (b) undergoing glow-discharge etching with deuterium ions*

Fig. 4 *Excess heat (P_x) excess energy (E_x) generated in Pd foil that underwent glow-discharge etching with deuterium ions; experiment # 141. COP=66%*

6. Pd-Ni cathodes

A commercial alloy of palladium with 5 weight % nickel was investigated. Although the phase diagrams of Pd-D and Pd-Ni-D are similar – in particular, both systems are characterized by the presence of spinodal decomposition below the critical point, the addition of Ni affects both the mechanical properties of palladium and the processes of deuterium (hydrogen) absorption and desorption. This effect is due to the possibility of a local decomposition of Pd-Ni solid solution and to the substantial difference – of about 3 orders of magnitude, between deuterium diffusion rates in unalloyed Pd and Ni. These factors can lead to development of micro-heterogeneity in the alloy in the course of electrolysis.

Figure 5 compares the surface of the PdNi alloy before and after the electrolysis. This specific foil gave 14KJ of "heat after death". After its etching in aqua-regia, pore clusters become evident on the surface of the alloy (Fig. 5 left). Their appearance can be caused by non-equilibrium state of the alloy in the initial state or/and by preferential etching of nickel-rich regions. Better understanding of this phenomenon calls for additional studies.

Black spots on the surface of samples after electrolysis (Fig. 5 right) are the products of pyrolysis of lubricant used in the course of the alloy rolling. (Naturally, there are similar spots on the initial surface of the alloy). This Figure also shows a complicated sub grain structure of the alloy formed in the process of electrolysis. This structure can be due to the mentioned micro-heterogeneity of the alloy.

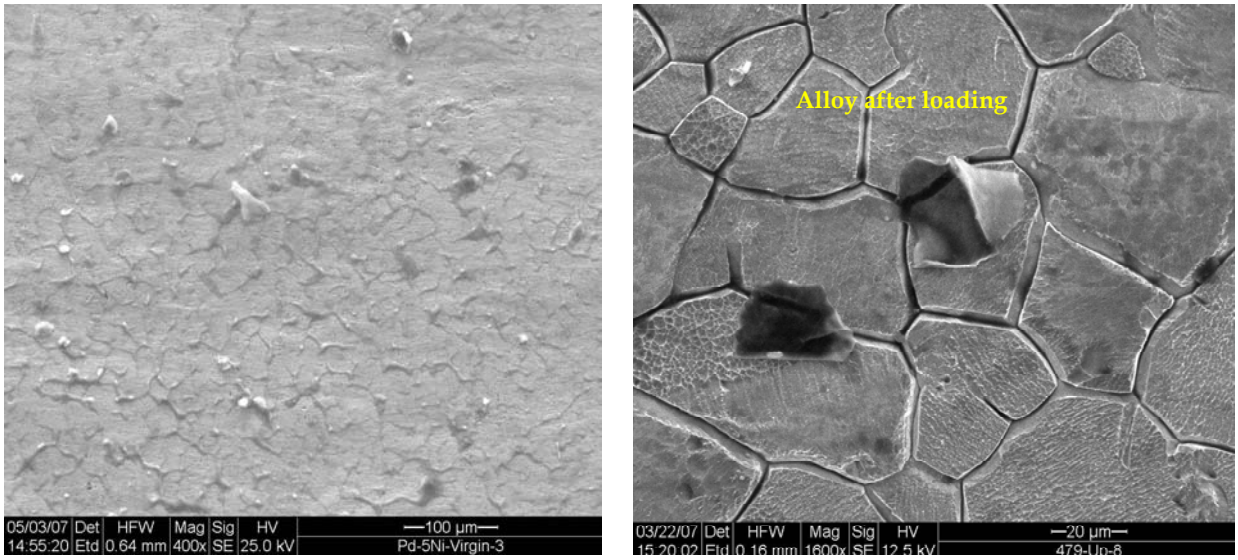

Fig. 5 *Surface of Pd-Ni alloy cathode before (left) and after (right) electrolysis; Experiment # 479*

Fig.6 shows excess heat generated from Pd-Ni alloy foil. Maximal COP is higher than 100%.
A characteristic feature of the experiments with Pd-Ni alloy cathodes is a very high loading, as evidenced by the low resistance ratio (R/R_o) illustrated in Figure 7 (top). Despite of the high loading, this experiment (#477) did not generate excess heat as shown at the bottom plot of Figure 6. The equality of P_{out} (red line) to the net input power, P_{inet} (black line), on average, is, in a way, an evidence of the adequate calibration of our calorimeter.

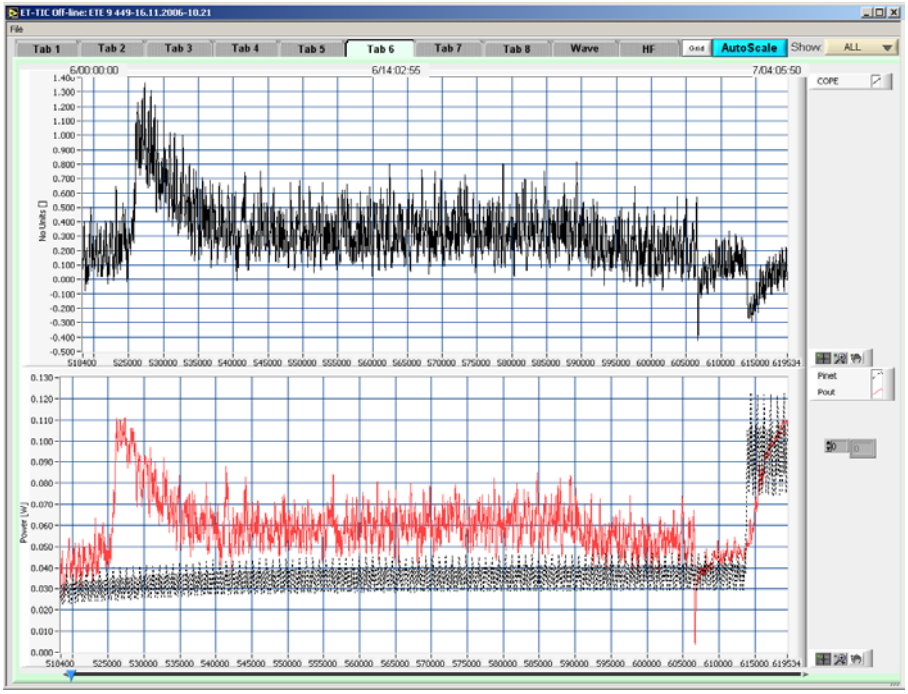

Fig.6 *Excess Heat generated in Pd-Ni alloy foil, experiment #449*

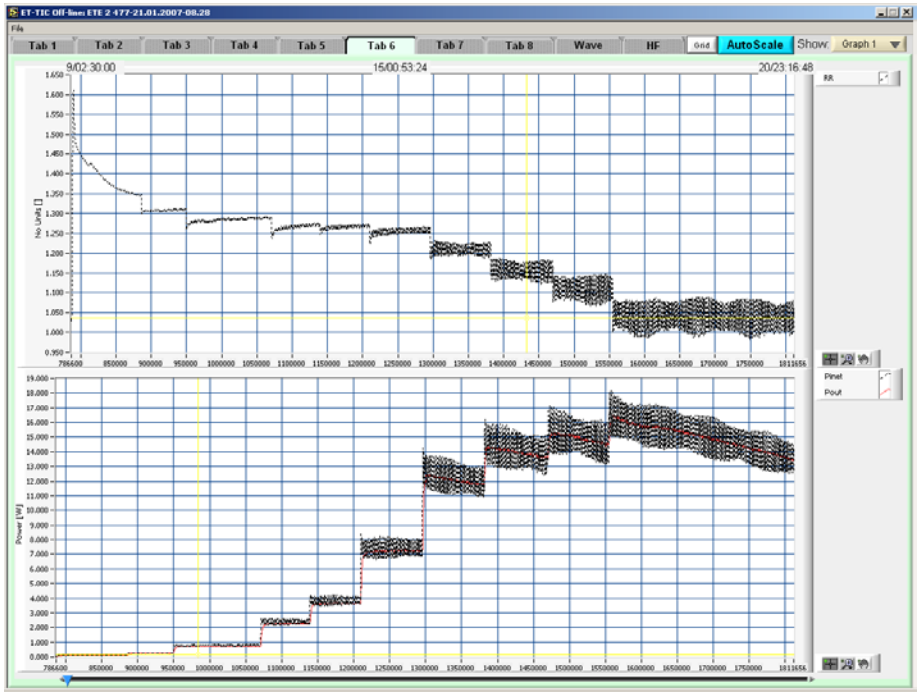

Fig. 7 *Resistance ratio (top) and input/output power (bottom) evolution with time in electrolysis; experiment #477 using a Pd-Ni alloy cathode.*

Another unique feature of this Pd-Ni foil was found to be its relatively slow rate of deuterium deloading after the termination of the electrolysis. This is illustrated in Figure 8 that pertains to experiment # 449. This experiment gave excess heat. The development of micro-heterogeneity in the Pd-5Ni alloy foil before and during the electrolysis is accompanied by the formation of defects such as dislocations and dislocation walls .These formations provide deep deuterium traps that may be responsible for the relatively low rate of deuterium desorption from the alloy in air that is seen in Figure 8. The data shown in this figure is obtained by X-ray diffraction method. The relative contents of α and β phases was evaluated by the measured ratios of the intensities of (220) and (311) X-ray peaks. As shown in Figure 8, even after a 5-month exposure, the share of β -phase remains significant.

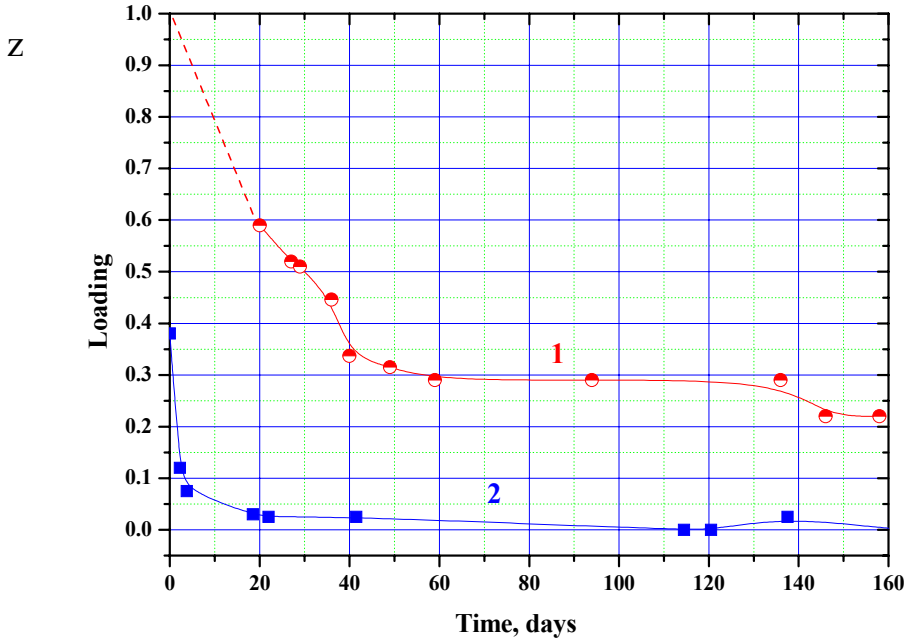

Fig. 8 *Estimated D/Pd atom ratio as a function of time after shut down of the electrolysis experiment: 1-Pd-5Ni alloy (Exp. #449), 2-Pd.*

7. Multilayer cathodes

Three types of multilayer cathodes were experimented with, all using a 50 μm thick Pd foil for the substrate. The substrate was coated with 5 to 7 layers of PdOx, Ni or Re alternating with 6-8 layers of Pd. The outer layer is always Pd. These multilayer cathodes are expected to feature higher deuterium diffusivity than plain Pd cathodes of comparable dimensions. Figure 9 is an illustration of the surface of a multi-layer Pd-Re cathode prior to electrolysis. Despite the fact that palladium and rhenium layers were applied successively, the multi-layer target does not consist of clearly distinguishable alternating layers of different materials. This is due to a specific structure of electrolytically deposited Pd layer (see Fig. 9c). Of 24 targets experimented with, 6 gave EH.

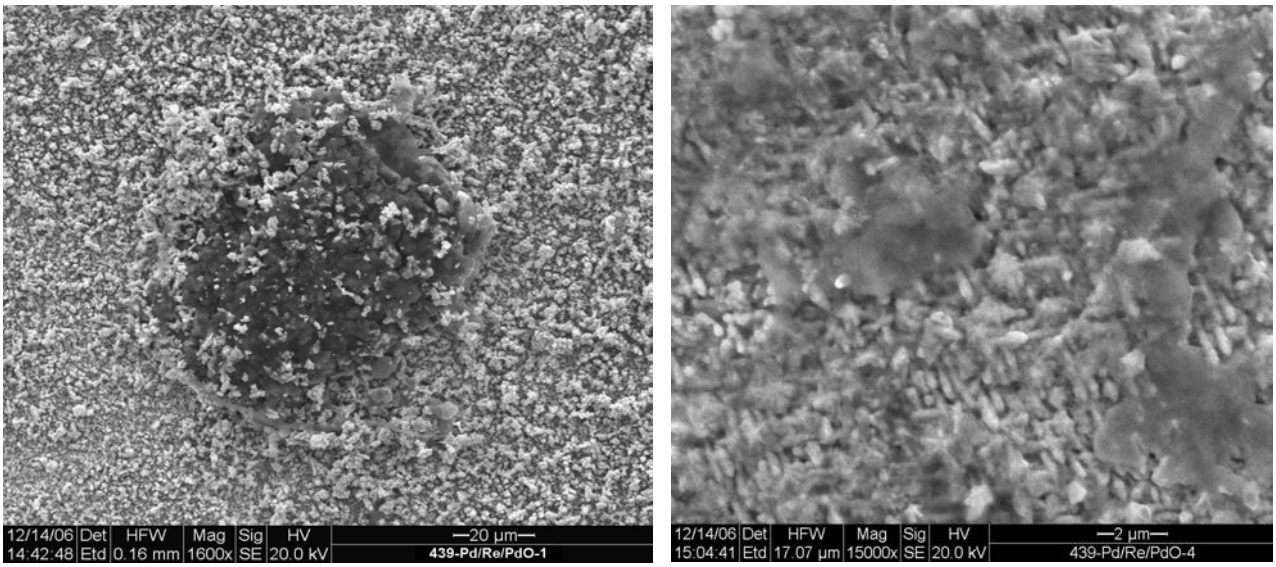

Fig. 9 *Surface of multi-layer Pd-Re foil. Black shaded area in (a) is enriched in Re; (d) shows EDS spectrum of this Re spot area; (d) typical structure of top Pd layer deposited by electrolytic method. This target was used in electrolysis experiment # 375*

Figure 10 shows the excess energy generated by the multi-layer Pd-Re cathode shown in Figure 9 – experiment # 375. While the excess energy generated is relatively small (~0.85 MJ), the excess power got to approximately 2.5 W. At this power level the electrolysis was stopped, the cathode was extracted from the cell and a CR-39 track detector was attached to the cathode surface for 71 hours starting approximately 10 minutes after turning off the electrolysis current. Figure 11 shows the resulting reading of this CR-39 detector after

subtraction of the background, as analyzed by Dr. Andrei Lipson and Alexei Rusetskiy. Tracks of ~3 MeV protons and of 11 to 16 MeV alpha particles are clearly observed; they support ET measurement of excess heat although no correlation between the two types of measurement was attempted.

Fig. 10 *Excess energy (top) and net input power (P_{inet}) and output power (P_{out}) in electrolysis experiment # 375 using Pd-Re multilayer cathode*

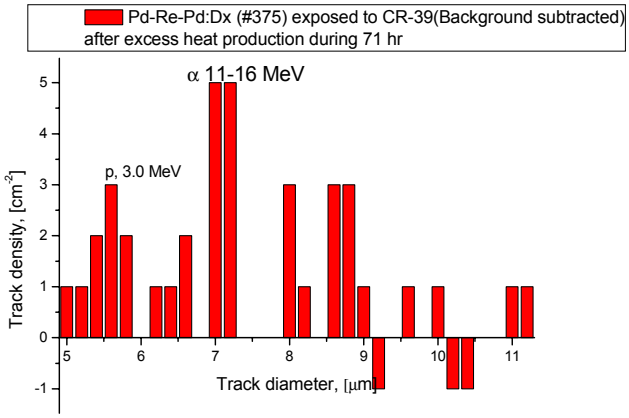

Fig. 11 *Excess energy (top) and net input power (P_{inet}) and output power (P_{out}) in electrolysis experiment # 375 using Pd-Re multilayer cathode.*

8. Pd-SWCNT-Pd cathodes

The targets containing Singe Wall Carbon Nano Tubes (SWCNT) consisted of 50 μm thick Pd foil that was coated with 3 layers – 0.5 to 0.8 μm of electrochemically deposited Pd, several mg of SWCNT followed by a 0.5 to 1.0 μm of electrochemically deposited Pd coating. These Pd-SWCNT-Pd sandwich type targets were produced by Dr. Andrei Lipson et

al. of the A.N. Frumkin Institute of Physical Chemistry and Electrochemistry of the Russian Academy of Science. Figure 12 gives a view of the outer surface of the Pd outer coating (left) and of the SWCNT layer below this coating (right).
Six series of experiments were conducted so far using SWCNT; they differ in the type and source of the SWCNT and in the manufacturing process of the Pd-SWCNT-Pd sandwich. Table 3 gives selected specifications of the six batches of Pd-SWCNT-Pd sandwich targets and the reproducibility of excess-heat generation. It is seen that the first batch of Pd-SWCNT-Pd targets gave a high reproducibility of 75%. Unfortunately, as we tried to improve the Pd-SWCNT-Pd targets their performance degraded. This performance degradation may be due to the fact that the SWCNT we purchased for the third and following batches were of different specifications than the SWCNT used for the first two batches; they were manufactured by a different company using different processes and have different impurities.

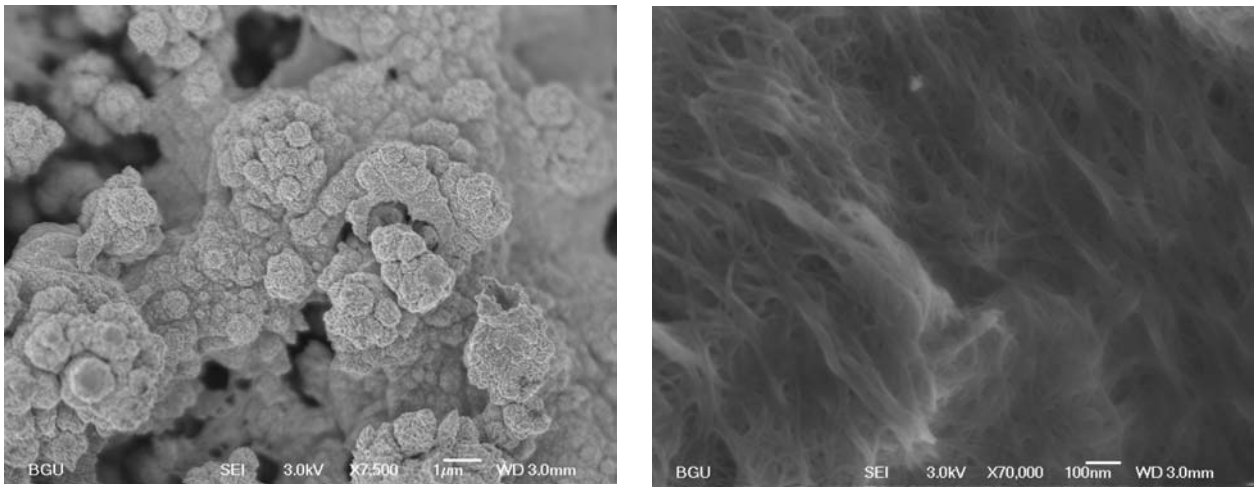

Fig. 12 *A view of the outer surface of the Pd outer coating (left) and of the SWCNT layer below this coating (right).*

Table 4 Summary of ET Experiments Performed Using 1 to 2.5 mg SWCNT Containing Cathodes

Series #	**1**	**2**	**3**	**4**	**6**
SWCNT manufacturer	CNI (old)	CNI (old)	Helix	Alfa Aesar	CNI (new)
Purity, %	95	95	90	>96	95
Diameter, nm	1.1-1.2	1.1-1.2	1.1-1.2	1.1-1.2	1.1-1.2
Length, μm	1-2	1-2	0.5-40	10-20	1-2
Amount, mg					
Adhesion	bad	good	very bad	excellent	excellent
No. of experiments	4	11	13	16(tested 12)	16(tested 8)
EH giving experiments	3	4	3	0	0
% giving EH	75	36	23	0	0

Figure 13 illustrates an excess-heat generating experiment using a Pd-SWCNT-Pd sandwich cathode from Series # 1 (Table 4). Although the absolute value of excess heat generated was small, its value appears to be insensitive to the input power as illustrated on the right hand

side of Figure 12; P_{out} was fluctuating around 200 mW while P_{inet} dropped from around 140 mW to around 40 mW. The corresponding maximum COP was approximately 200%. When P_{inet} was suddenly increased, at around 1,200,000 seconds into the experiment, the excess heat disappeared, giving credibility to the interpretation of the excess-heat prior to the power ramp as real excess-heat.

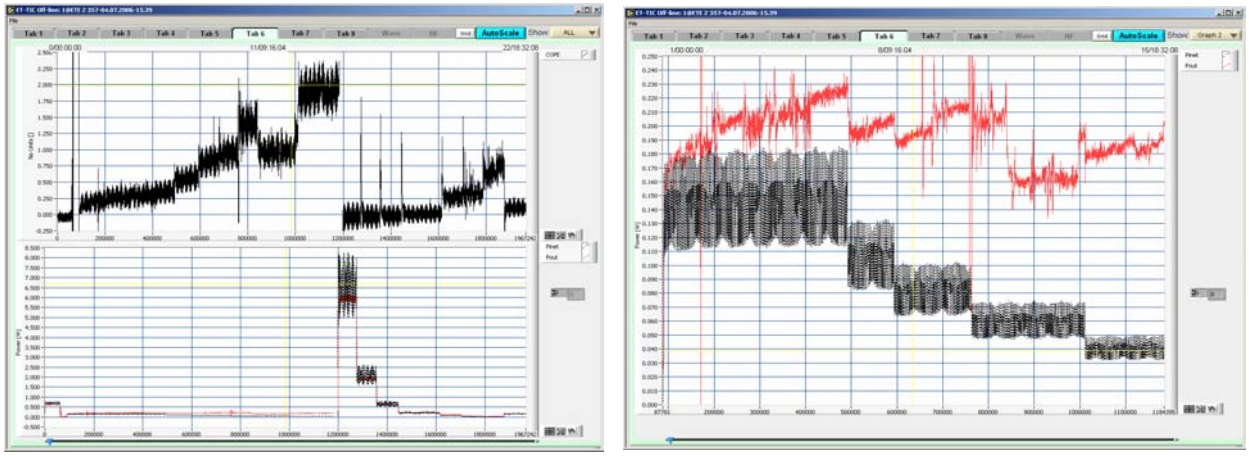

Fig. 13 *Performance of electrolysis experiment # 357 using Pd-SWCNT-Pd multilayer cathode. (a) P_{out} and net input power (P_{inet}) – left bottom and in expanded scale on right (b) COP (left top)*

9. Ultra-sonic driven Pd cathodes

Since its early days Energetics Technologies planned to conduct experiments that combine ultra-sonic (US) excitation with electrolysis [1]. Since then the design of the electrolysis cell having US excitation have undergone a number of conceptual variations. The first concept was to use a spherical cell in which the US waves would be greatly focused. This concept has not been realized due to technical difficulties.

The next design concept involved use of cylindrical electrolysis cell, a photograph of which is shown in Figure 14, immersed in a water jacket that is surrounded by a cylindrical piezo ceramic ultrasound transducer. The cathode used in this (and all other) US excited electrolytic cells is a palladium foil, 60 x 3.0-3.5 x 0.03-0.035 mm in dimension, that was made at ET by rolling a 0.5-1.0 mm thick Pd wire. The anode is a helical platinum wire wound around the cathode over a perforated layer of Teflon (See Figure 14). This setup had no calorimeter and was exposed to the laboratory temperature. The power deposited in the cell by the US generator and by the electrolysis current, as well as the excess heat, if present, was removed from the system by circulating cooled water through the jacket at a constant flow rate. This setup did not provide for accurate means to measure the output power, and therefore the excess heat. However, the difference between the electrolyte temperature and the cooling water jacket temperature was found insensitive to the US power and can be used to determine whether or not there was excess heat and to get a rough estimate of the amount of EH. This setup is referred to as Setup A.

Setup A has evolved into Setup B in which a flow calorimeter system has been incorporated within the water jacket in between the electrolysis cell and the US transducer. A schematic view of the layout of Setup B system is given in Figure 15. Setup B system was also exposed

to the laboratory temperature, making the power output quantification too sensitive to fluctuations in the ambient temperature.

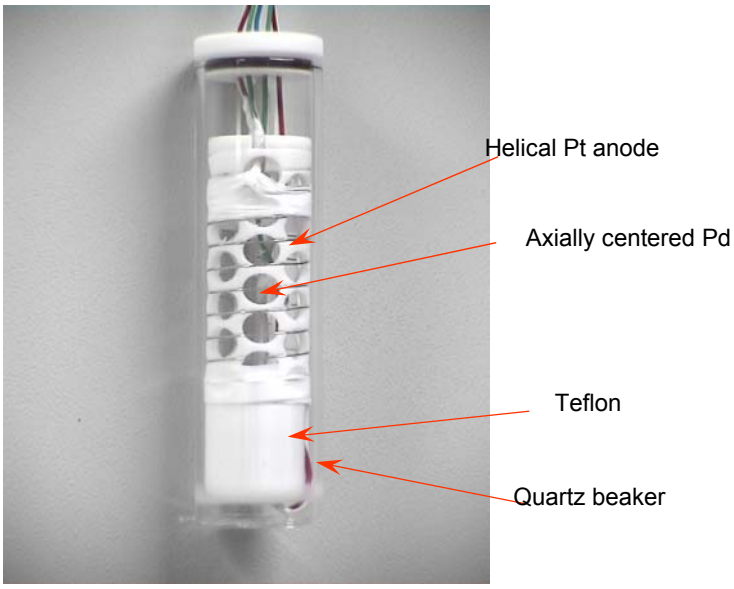

Fig. 14 *Photograph of the early version of the ET electrolytic cell used in the system with the ultrasonic-generator excitation*

The most recent design of electrolytic cell with US excitation features both a flow calorimeter and an incubator that maintains the experimental setup in tightly regulated outer temperature. This incubator with the system enclosed is shown in Fig. 16. The US transducer is of a different design – rather than being cylindrical, as in Setups A and B, it consists of four tubular transducers located at 90 degrees from each other, as seen in Figs. 16 and 17. As a result of this geometrical arrangement, the design of the anodes was modified as shown in Figure 40 (compare with Fig. 14). The resulting setup is referred to as Setup C. Analysis of uncertainties in the calorimetry of Setup C concluded that the uncertainty in P_{ex} determination is approximately 80 mW.

The maximum power level that the US transducer can operate at is in the range 10-40W for Setups A and B and 100W for Setup C. The frequency of the acoustic waves used in the experiments is 20KHz for setups A and C and 40 KHz for setup B.

Table 5 summarizes the electrolysis experiments performed using the US excitation, and gives statistics on the fraction of these experiments that gave excess-heat. The reproducibility is quite high; in particular in the more recent experiments (performed during 2007). Figures 19 through 21 give selected results from two of the electrolysis experiments performed with US excitation. The mode of operation of these experiments was application of US excitation for periods of 24 hours at a time while the electrolysis current was applied continuously.

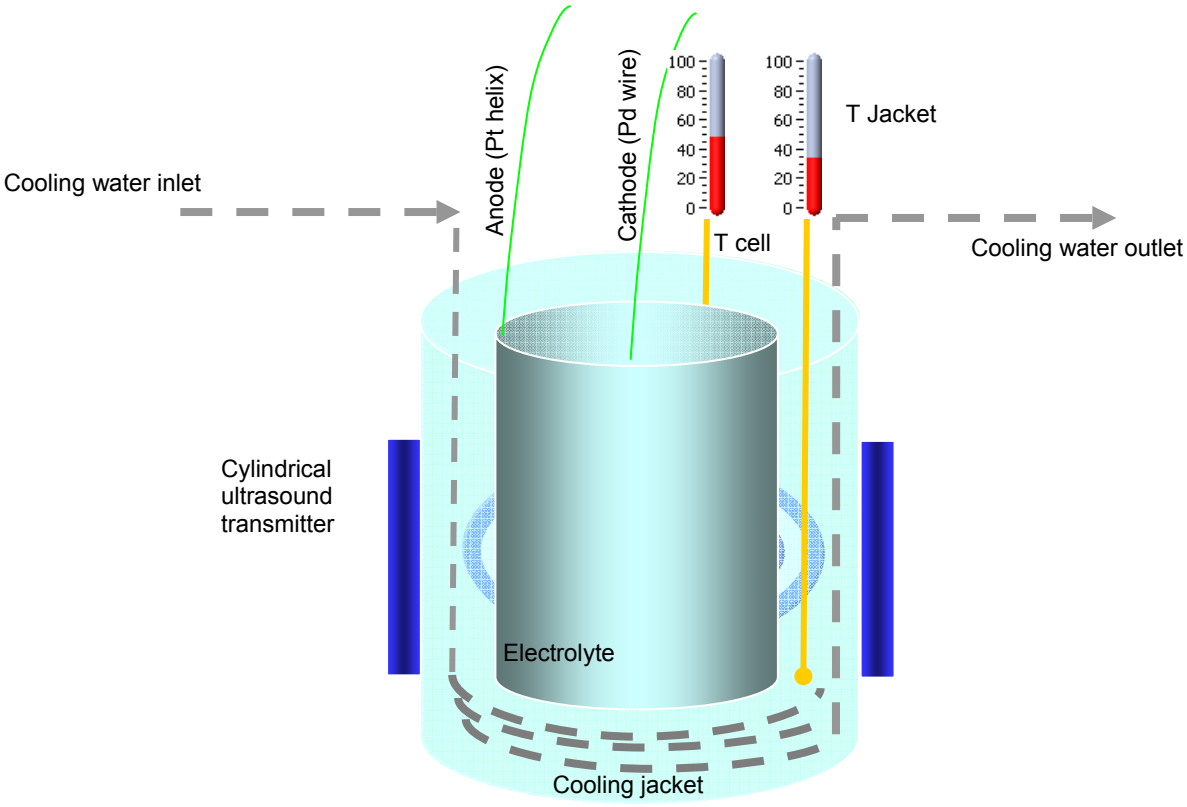

Fig. 15 *Schematics of the ET Setup B electrolytic cell system with ultrasonic-generator excitation*

Fig. 16 *Photograph of the most recent version of the ET electrolytic cell system assembly with ultrasonic-generator excitation. The system is installed inside a constant temperature incubator.*

Fig. 17 *Photograph of the hardware of the flow calorimeter of the latest version of the ET electrolytic cell used in the system with the ultrasonic-generator excitation*

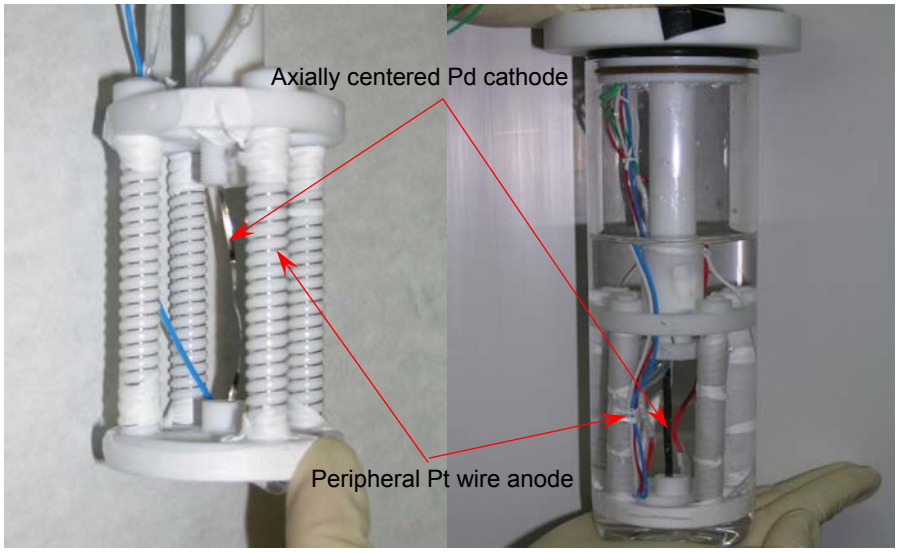

Fig. 18 *Photograph of the latest version of the ET electrolytic cell used in the system with the ultrasonic-generator excitation*

Table 5 Summary of ET Electrolysis Experiments Performed Using Ultra-Sound Excitation

Setup type	Year	Calorimeter	Thermo-stated	# of experiments	# giving EH	% giving EH
A	2006	no	no	6	4	67
B	2006	yes	no	13	6	46
	2007	yes	no	2	2	100
C	2006	yes	yes	2	0	0
	2007	yes	yes	2	2	100
Total				25	14	56

Figure 19 shows that excess heat started in experiment # ETUS3-5 approximately 5 days after initiation of the experiment. The vertical pink spikes in the figure are heating effects due to the application of the US generator and are ignored in the excess-heat analysis. In between approximately the 20^{th} and 30^{th} day of the experiment the EH level was in the vicinity of 0.2 watts while the net input energy was approximately 1 W. Around the 31^{th} day the electrolysis was turned off but and EH was kept on. In fact, the EH was increasing in time after application of the US excitation up to approximately 0.7 W. This "heat-after-death" lasted for approximately 7 days, at which time the electrolysis current was turned on again. At approximately 56 days, after ramping P_{in} up and down in stepwise manner, P_{in} was turned off again but P_{out} kept on for several days at a level of approximately 0.6 watts before it started dropping in value. At about 60 days into the experiment the Pd cathode was replaced by a Pt cathode following which P_{out} became zero. This proves that our calorimeter was well calibrated so that the excess heat measured following the turning off of the electrolysis current at about the 56^{th} day is, indeed, heat-after-death.

Figure 20 shows the evolution of the resistance ratio, R/R_o, of the cathode of experiment # ETUS3-5. The step function like increase in the R/R_o is a result of the turning on of the US generator that causes deuterium deloading possibly due to the cathode temperature increase. The general trend is a decline in the R/R_o ratio with an increase in the electrolysis current (or P_{in}.). R/R_o deeps at around 45 days when P_{in} is at its maximum.

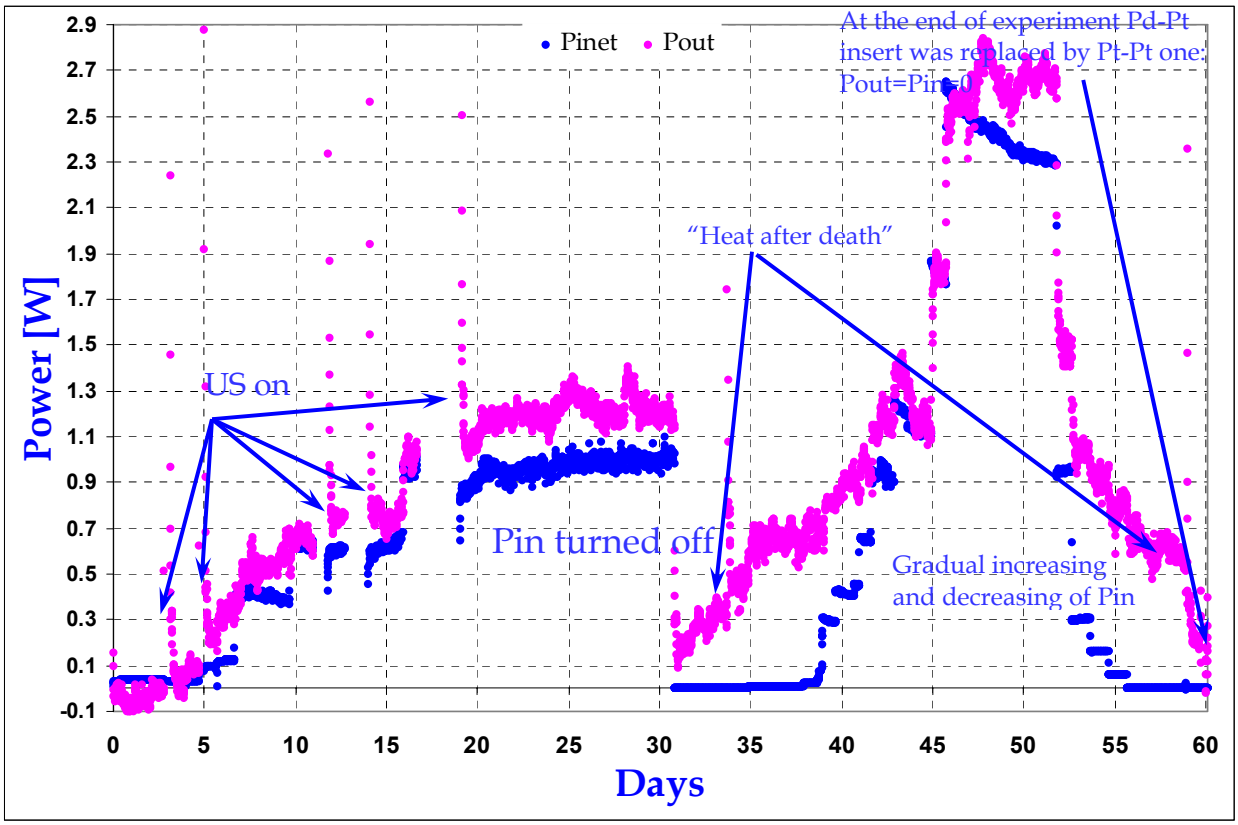

Fig. 19 *Net input power (P_{inet} – in blue) and output power (P_{out} – in violet) in ultrasonically excited electrolysis experiment # ETUS3-5 using Setup C*

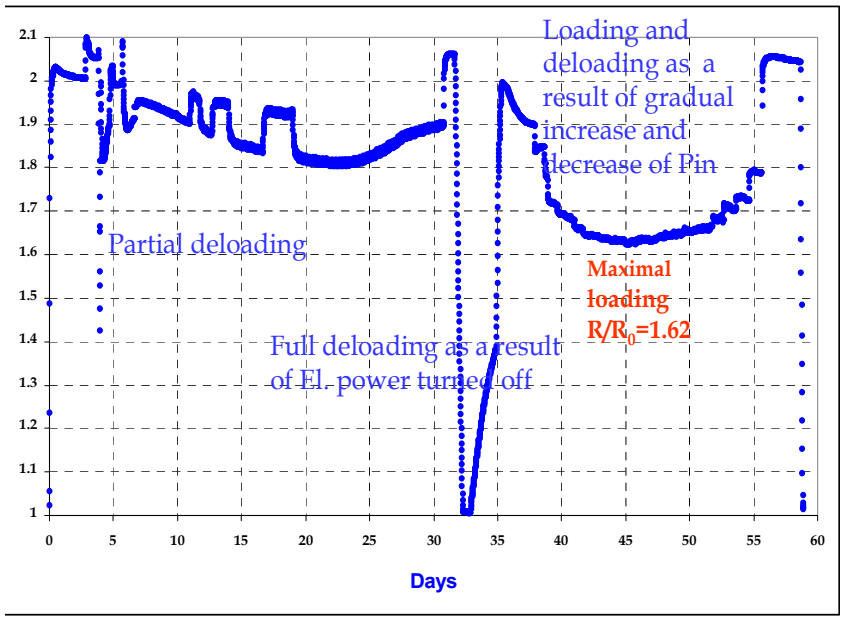

Fig. 20 *Resistance ratio in the ultrasonically excited electrolysis experiment # ETUS3-5 using Setup C*

Figure 21 displays the evolution of P_{inet} and P_{out} in electrolysis experiment # ETUS3-6. The US generators were turned on 4 times for 24 hours while the electrolysis power was always

on at a low P_{in} level of less than 0.2 W. After the first session of US excitation the output power gradually dropped to zero. After the second session of US excitation P_{out} dropped to zero and then started increasing. After the 3rd session of US excitation P_{out} dropped to zero at which time the 4th session of US excitation was applied (it would have been preferable to wait longer before applying the 4th session) P_{in} dropped to zero and then increased up to approximately 1 W and then gradually declined. At about 2,400,000 seconds into the experiment P_{in} was turned off following which P_{out} dropped to zero. Applying P_{in} again did not succeed reviving the excess heat generation. These last two steps again provide a strong evidence that the EH recorded earlier in this experiment is real and not a result of miscalibration. Note that the session of EH generation following the 4th session of US excitation lasted for approximately two weeks and the maximum COP exceeded 500%.

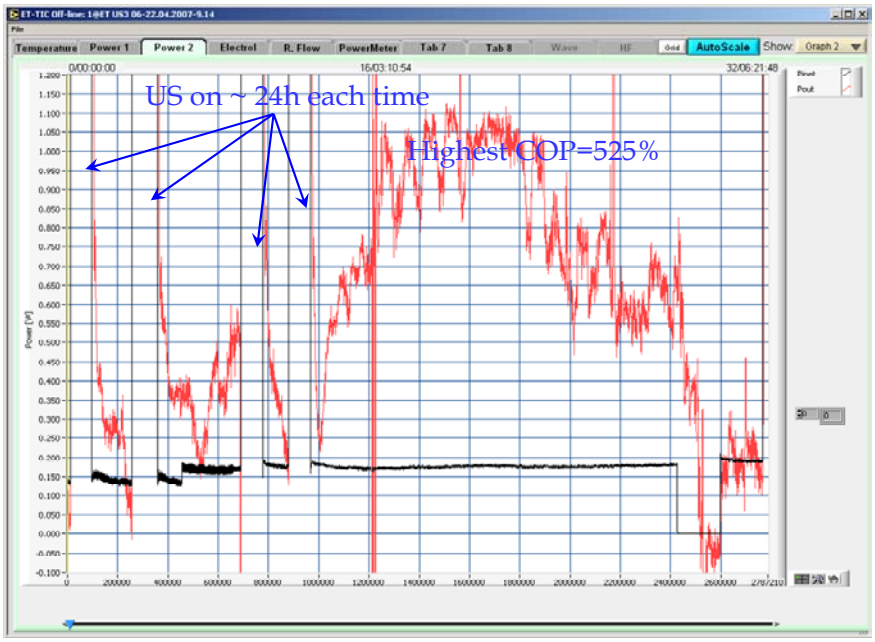

Fig. 21 *Net input power (P_{inet} – in black) and output power (P_{out} – in red) in ultrasonically excited electrolysis experiment # ETUS3-6 using Setup C*

Figure 22 compares the surface of the Pd cathode after electrolysis experiment # ETUS3-6 (a) with the surface of the cathode of electrolysis experiment # 64 (b) that was not excited by US waves. The morphology of the two cathodes is highly different. The cavitation introduces considerable changes in the structure of the Pd surface; instead of a structure consisting of slip bands formed in the course of plastic deformation of palladium due to deuterium absorption and resulting lattice expansion (Fig. 22b), cavitation effect leads to the formation of a cellular structure (Fig. 22a). Evidently, such a structure contains a high concentration of defects – potential deuterium traps. This causes low deuterium desorption rate from such samples in the air.

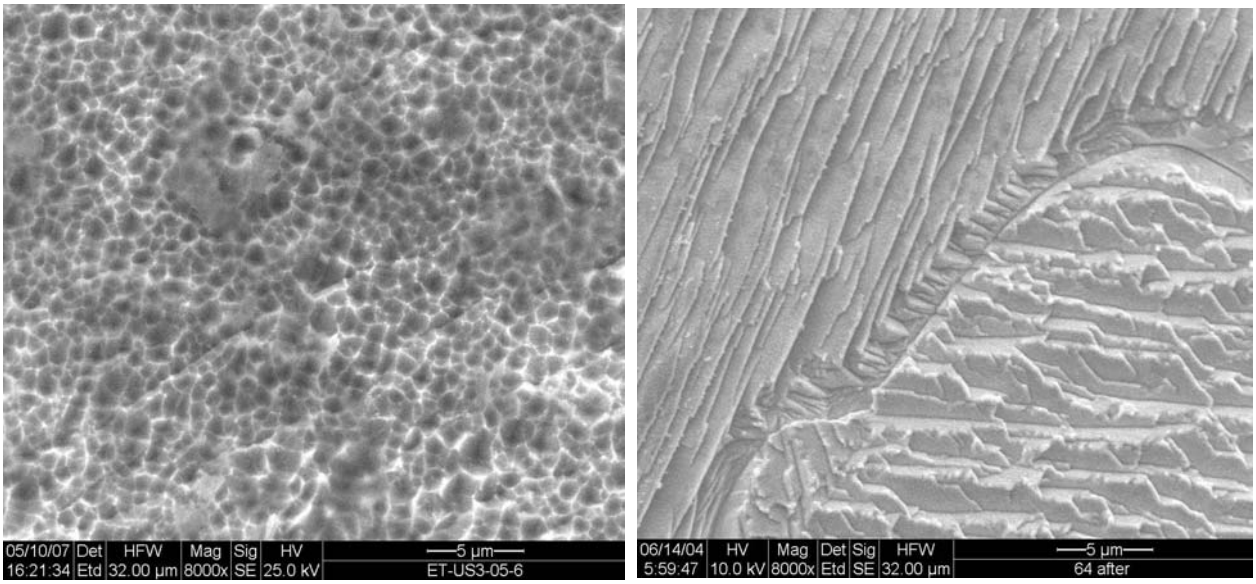

a b

Fig. 22 *Comparison of (a) ETUS3-6 and (b) ETE-64 (no US) surface after experiment – both gave EH. Secondary electron microscope image magnification of x8000*

10. Summary of the most energetic excess heat experiments

Table 6 summarizes selected performance characteristics of the eight electrolysis experiments that so far generated the largest amount of excess power, P_x, or excess energy, E_x. The "specific excess heat" given in watts per gram of palladium that was exposed to the electrolyte is a measure of the utilization effectiveness of the palladium. The maximum specific EH obtained so far – nearly 70 W/g of Pd, is even higher than the typical specific heat in commercial fission reactors – 20 to 50 Watts per gram of uranium. The "specific excess energy" expressed in kilo-electron-volt generated per palladium atom or per deuterium atom in the cathode (the ratio of D to Pd atoms in the cathode is nearly 1) is an indicator of whether or not the EH could be chemical or mechanical (stored energy) in nature. The maximum specific EE obtained in ET electrolysis experiment is over 20 KeV per Pd or D atom. This is to be compared with heat of desorption of D from the Pd lattice of approximately 0.3 eV per D atom; heat of D oxidation of approximately 1.5 eV per D atom; and heat of evaporation of Pd (an upper bound on the possible stored energy in the Pd lattice) of ~ 31 eV per Pd atom. All of these are three to four orders of magnitude smaller than the specific EE. This provides a strong, yet not conclusive indication that the EE generated in the ET experiments reported above is, indeed, of nuclear origin.

Table 6 Selected Characteristics of the Eight ET Electrolysis Experiments that Generated Largest Amount of Excess Power or Excess Energy

Experiment #	56	64a	64b	141	357	US1-15	US3-05	US3-06
Cathode	ENEA	ENEA	ENEA	GD	SWCNT	US	US	US
E_x, MJ	3.1	1.1	3.5	2.4	0.11	0.19	1.1	1.32
P_x, W	3	19	11	14	0.18	0.25	0.8	0.9
Max COP, %	80	2500	1500	75	200	600	3000	525
Duration of EH, h	300	17	80	90	310	280	960	445
Specific* EH, W/g Pd	11	71	48	29	0.5	3.5	6	15
Specific* EE, KeV/Pd	13.5	4.8	15.7	10.9	0.6	3.9	22.8	27.4

* pertaining to effective part of cathode

11. Conclusions

Several different types of cathodes and modes of operation were experimented with in the electrolytic cells in an attempt to increase the reproducibility of excess heat generation and to increase the coefficient of performance. All these experiments used Dardik's modified SuperWaves to drive the electrolysis.

The highest reproducibility is obtained with ultra-sound excitation. However, the total energy invested in driving the US generators is large – it is larger than the excess energy generated. It is necessary to optimize the application of the US excitation of the cold fusion process by, among other things, reducing the duration of each session and, possibly, increasing the time between the turnings on of the US generators. The mechanisms through which US excitation help the EH generation need be thoroughly investigated.

The first series of Pd/SWCNT/Pd sandwich targets had high reproducibility. An investigation of the ingredients required for the manufacturing of successful Pd/SWCNT/Pd targets is underway. Also promising are Pd foils that underwent etching using glow-discharge with deuterium. Pd-Ni alloy features very high loading and exceptionally slow deloading of deuterium indicating presence of deep traps. Additional experiments with Pd-Ni cathodes are desirable.

Significant "Heat-after-death" was obtained in one of the ultrasonically excited electrolytic experiments and in addition there was an indication that "heat-after-death" could also be obtained in the experiment with one of the Pd/SWCNT/Pd targets. "Heat-after-death" was obtained from a sister Pd/SWCNT/Pd target from the same production batch that was experimented with at SRI in an attempt to replicate the ET results [5]. It is suggested that SuperWaves exposure could create a long-term effect (memory) in the cathode in the form of spontaneous lattice oscillations that result in the heat release.

Significant amount of excess heat was generated and very large coefficient-of-performance was obtained in several experiments. The most successful of these experiments, done using foil #64 that was prepared by Dr. Vittorio Violante et al. of ENEA in Frascati, Italy. It generated excess heat a couple of times: (1) Approximately 5 hours into the first loading of deuterium into the Pd cathode – giving an average power gain of ~2500% during 17 hours.

The average current density was 7 mA/cm^2. (2) The same foil was deloaded after the excess heat generation stopped for no apparent reason and than loaded again. After 16 hours of loading excess heat was generated again at an average level of ~1500% for 80 hours. The average current density was 8.4 mA/cm^2. At the end of the two experiments the tritium concentration in the electrolyte is estimated to be ~750% of its pre-experiment level. The total amount of excess energy generated is approximately 1.1 MJ and 3.5 MJ in, respectively, the first and second experiments. This amount of excess energy corresponds to, respectively, ~4.8 KeV or ~15.3 KeV per Pd atom. These are at least three orders of magnitude larger than the energy than can be generated by chemical reactions or that can be stored in the form of mechanical energy. The corresponding average specific power is 71 or 48 W per gram Pd. For comparison, the average specific power in commercial nuclear fission reactors is between 20 to 50 W per gram uranium.

Nuclear reaction-products were not detected, with sufficient certainty, on and near the surface of the targets that generated excess heat. However, no helium measurement has been attempted. Likewise, no on-line measurement of nuclear reaction products has been attempted, as yet. Nevertheless, tracks of protons and alpha particles were detected on a CR-39 track detector that was attached to a multi-layer Pd/Re target that was removed from the electrolytic cell in which it gave excess heat while the electrolysis was on. In-situ measurement of charged particles and neutrons will soon be attempted. Measurement, by our collaborators, of the amount of helium accumulated in a closed cell during the electrolysis experiment is planned as well.

Acknowledgment

This work was fully funded by Mr. Sidney Kimmel.

References

[1] I. Dardik, H. Branover, A. El-Boher, D. Gazit, E. Golbreich, E. Greenspan, A. Kapusta, B. Khachaturov, V. Krakov, S. Lesin, B. Michailovitch, G. Shani And T. Zilov, “Intensification of Low Energy Nuclear Reactions Using SuperWaves Excitation,” Proc. of the Tenth International Conference on Cold Fusion ICCF-10, Cambridge, MA, August 2003.

[2] I. Dardik, T. Zilov, H. Branover, A. El-Boher, E. Greenspan, B. Khachaturov, V. Krakov, S. Lesin and M. Tsirlin, “Excess Heat in Electrolysis Experiments at Energetics Technologies,” Presented at the 11th International Conference on Cold Fusion, ICCF-11, Marseilles, France, November, 1 - 6, 2004.

[3] I. Dardik, “SuperWaves Reality,” Proc. of the Tenth International Conference on Cold Fusion ICCF-10, Cambridge, MA, August 2003.

[4] L. Bettinali, D. Lecci, A. Pizzuto and V. Violante, “Procedimento metallurgico per aumentare la capacita di assorbimento dell’idrogeno da parte di alcuni metalli come il palladio, il nichel e loro leghr,” Italian Patent Application, September 15, 2004.

[5] M. C. H. McKubre, F. L. Tanzella, I. Dardik, A. El Boher, T. Zilov, E. Greenspan, C. Sibilia and V. Violante, "Replication of Condensed Matter Heat Production". To be published in the American Chemical Society Low Energy Nuclear Reactions Sourcebook.

PRECISION MEASUREMENT OF EXCESS ENERGY IN ELECTROLYTIC SYSTEM Pd/D/H_2SO_4 AND INVERSE-POWER DISTRIBUTION OF ENERGY PULSES VS. EXCESS ENERGY

H. Kozima[1,2], W.-S. Zhang[2,3], and J. Dash[2]

[1] *Cold Fusion Research Laboratory, 597-16 Yatsu, Aoi, Shizuoka 421-1202, Japan*
E-mail: hjrfq930@ybb.ne.jp
[2] *Low Energy Nuclear Laboratory, Portland State University, Portland, OR 97207-0751, U.S.A.,*
[3] *Institute of Chemistry, Chinese Academy of Sciences, P.O. Box 2709, Beijing 100080, China*

Abstract

Excess energy was measured with a Seebeck envelope calorimeter in an electrolytic system containing a 2 mm diameter Pd tube cathode. After about 50 hours of electrolysis, many power pulses (P_{ex} < ~0.5 W) and bursts (P_{ex} > ~0.5 W) of excess power P_{ex} were observed. The distribution of the number of power pulses $N(P_{ex})$ with definite excess power P_{ex} plotted on a logarithmic scale is expressed as a straight line with a gradient ~ – 2 for P_{ex} < ~0.5 W showing the typical behavior of the 1/*f* noise. The distribution for P_{ex} > ~0.5 W deviates from this regularity. These characteristic behaviors are discussed in relation to complexity in the mechanism of the excess energy generation in the experimental system.

1. Introduction

There are several problems in the cold fusion phenomenon (CFP) which make it difficult for scientists to accept. The most important problem is the irreproducibility of experimental results. There are many examples, especially in nuclear physics, where events are governed by probabilistic law; decay of a radioactive nuclide and collision of a particle with a group of other particles are the most common examples. Therefore, we have to be satisfied with statistical or qualitative reproducibility in such processes occurring in the CFP.

A second problem might be the mental threshold necessary to accept the idea that some kinds of nuclear reactions occur in solids differently from those in free space. At the center of this problem, there is the idea that the probabilities of nuclear fusions (especially *d-d* fusion) in solids become many orders (several tens of orders) of magnitude higher than in vacuum. This point might be at the core of the controversy between proponents and skeptical scientists since the report of the CFP in 1989 [1].

There are some hundreds of positive CFP experimental data sets obtained during the past 18 years, ranging from emission of particles, including neutrons, protons, tritons, and alpha particles, beta and gamma rays, to the generation of almost all light and heavy nuclei in the

periodic table. Each element generated is accompanied by excess energy. These data sets are very complicated in their nature, as we see above from the list of products. The systems producing them are also complicated in their materials and methods.

To find a key to reconcile these complicated experimental data sets within the framework of modern physics, we have investigated the CFP phenomenologically at first [2] and then quantum mechanically, based on clues obtained from the data sets [3, 4].

The second point discussed above has a secret in itself. If nuclear reactions occur only between charged particles, it is apparent that such nuclear reactions could not be much different in vacuum than in solids due to the shortness of the nuclear force range of about 1 fm (= 10^{-15} m) compared with lattice constants of solids of about 1 Å (=10^{-10} m) as discussed in our paper and book [3, 4]. But the secret is a role of the neutron. In the experimental data sets, there are several showing important roles of neutrons. If experiments were performed in environments where no thermal neutrons exist, the CFP did not occur [5]. If experiments were done with artificial thermal neutron sources, the CFP were intensified [6].

Thus, it is natural to assume that thermal neutrons play some role in catalyzing the CFP. The model (TNCF model) including the so-called trapped neutrons in materials has been successfully applied to many experimental data sets with only one parameter to consistently explain observed results. Natural extension of this model should be a quantum mechanical verification of the premises used in the model as preliminary results have shown in recent reports [3, 4].

The first point discussed above has a somewhat different nature. There is no question that a many-body system gives values of observables (physical properties) as averages over many constituent particles, in general. This is not appropriate for an observable which is measured individually not as an average. A nuclear reaction in solids is such a case where we measure reaction products individually; e.g. emission of neutrons (or other particles) is an example and excess energy pulses are another, if time resolution is fine enough to discriminate among different pulses. Then, the distribution of pulses against the strength of them will obey an inverse-power law, as many phenomena in many-body complex systems such as earthquakes [7], undersea ocean currents [8] and intensities of light from some astronomical sources [8].

Thus, it is possible to confirm the complexity of the CFP by checking the intensity distribution of excess energy pulses and their natural irreproducibility. Fortunately, there are a few systematic data sets of excess energy generation. Extensive experimental data by McKubre et al. [9] were roughly analyzed and the results showed inverse proportionality. [4]

In this paper, we analyze experiments obtained in the Low Energy Nuclear Laboratory (LENL), Portland State University using a Seebeck envelope calorimeter (SEC), and we show that the excess energy pulses obey the inverse power law. Also, that there appears a peculiar behavior in high energy pulses (bursts), suggesting the existence of a positive feed-back mechanism. These results will be discussed in relation to complexity.

2. Experimental

We used a closed cell (Fig.1), similar to that used before [10, 11] except that the height is less in order to fit into the Seebeck envelope calorimeter SEC. The electrolytic cell is a Pyrex cylinder (capacity is about 280 ml, ϕ_{in} = 50.7 mm and ϕ_{out} = 57.0 mm, wall thickness = 3.2 mm, h = 142 mm). A PTFE female top cap has ϕ_{out} = 65 mm and ϕ_{in} = 57 mm; it has two 1mm diameter holes for the electrode lead wires. A PTFE plate (ϕ 50 mm) with many 0.8 mm holes, which also has two 1 mm diameter holes for the electrode lead wires, is used for suspending recombination catalyst above the electrode. A PTFE rod fastened to the perforated plate and the top cap serves to suspend the catalyst a fixed distance above the electrolyte.

A gasket made of ethylene propylene (resistant to sulfuric acid) is used to seal the top cap against the top edge of the Pyrex cylinder.

The Pd cathode is a 80 mm long palladium tube, ϕ_{out} = 1.67 mm, ϕ_{in} = 0.67 mm, The upper 50 mm of the Pd cathode is sealed against the Pt lead wire with heat-shrunk PTFE tubing. The platinum anode is a U-shaped foil 37.5 × 23.8 × 0.12 mm^3. The Pt anode lead wire is crimped to the anode foil. The anode lead wire is also encased in heat-shrunk PTFE tubing.

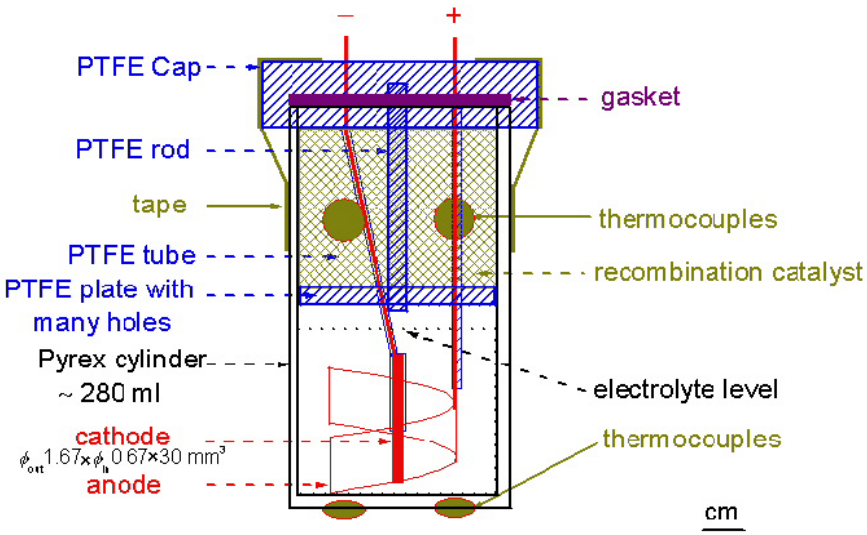

Fig. 1. *Cell with Pd tube cathode and Pt foil anode which was used for electrolysis.*

The electrolyte is heavy water (99.9 at.%, Aldrich catalog #347167) mixed with 96.4% H_2SO_4 (J.T. Baker, Lot # K10030) in the volume ratio of 6.7:1.

3. Experimental results and discussion

The size of the Pd tube cathode is the same as that used by Zhang et al. [12]: dimensions are 0.67ϕ × 1.67ϕ × 80 mm^3, but only the lower 30mm of the Pd tube was exposed to electrolyte.

Using this value we obtain following numerical data about the Pd cathode; Surface area S = 3 × π (0.067 + 0.167) cm^2 = 2.21 cm^2, Effective volume V_{eff} (assuming a thickness of 1 micrometer at the surface);

$V_{eff} = 10^{-4}$ S = 2.21 ×10^{-4} cm^3.

According to the TNCF model [4] (assuming only the CF version of the $n + d$ reaction) and thermalization of the liberated energy in the sample,

$n + d = t$ (6.98 keV) + Q (6.25 MeV). (1)

The number of reactions N in time τ is given as follows [2 – 4]:

$N = 0.35\, n_n v_n n_d V \sigma_{nd} \tau$ (2)

where $0.35 n_n v_n$ is the flow density of the trapped thermal neutrons per unit area and time, n_d is the density of deuterons, σ_{nd} = 5.5 × 10^{-28} cm^2 is the cross section of the reaction (1) for a thermal neutron..

The number of reactions N is related to the number of reactions N_Q producing excess energy Q (in MeV) defined by a relation

$N_Q = Q$ (MeV)/5 (MeV),

if we assume the energy liberated in a nuclear reaction is on average 5 MeV (actually, the energy is 6.25 MeV if we assume only the reaction (1)).

Putting

$n_d = 6.88 \times 10^{22}$ cm^{-3}
for the sample composition PdD, and the neutron velocity
$v_n = 2.2 \times 10^5$ cm/s
for the thermal neutron in (2), we can calculate the parameter n_n, density of trapped neutrons, in the TNCF model using the observed excess energy Q in a time τ. The value n_n is given as follows if we assume $N = N_Q$:

$$n_n = (\alpha_w /5)(1/0.35 v_n n_d V_{eff} \sigma_{nd} \tau),$$

where a parameter α_w is defined for convenience in the following discussion as

$$\alpha_w = Q /\tau,$$

which gives the excess thermal power in watts. The parameter α_w in watt (W) is also expressed by α in MeV/s as

$$\alpha_w = 6.24 \times 10^{12}\ \alpha \text{ (MeV/s)}.$$

Using numerical values given above and also $\tau = 1$ (s) in the above relation, we obtain the final result

$$n_n = 7.2 \times 10^{15}\ \alpha_w \text{ (cm}^{-3}\text{)}. \qquad (3)$$

3,1 Experimental data;

Case 1. Active period with excess power pulses in the LENL data.

In the experimental data sets obtained in LENL, there are active periods with many excess power pulses generating excess power of about $\alpha_w = 0.1 – 0.2$ W. In these periods, we take $\alpha_w = 0.1$ W for analysis, for simplicity.

Then, we obtain the density of the trapped neutrons from formula (3);

$$n_n = 7.2 \times 10^{14} \text{ (cm}^{-3}\text{)}. \qquad (4)$$

Case 2. Bursts in the LENL data.

In the experimental data sets obtained in LENL, there are excess
Power pulses and bursts (rather large pulses than 0.5 W) up to 2 watts. Some of these bursts are shown in Figs. 2 and 3.

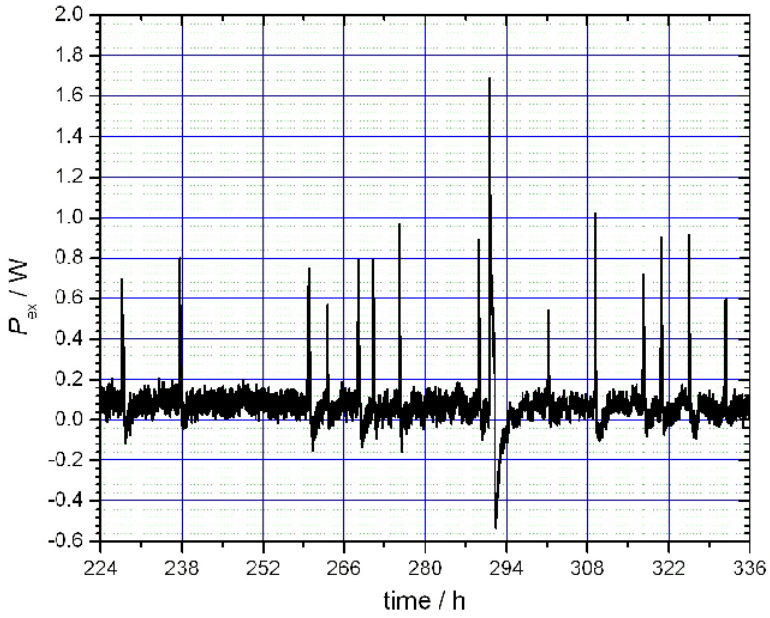

Fig. 2. *Excess power pulses and bursts during a 112 hour period of an experiment (061026) which lasted 14 days as a whole.*

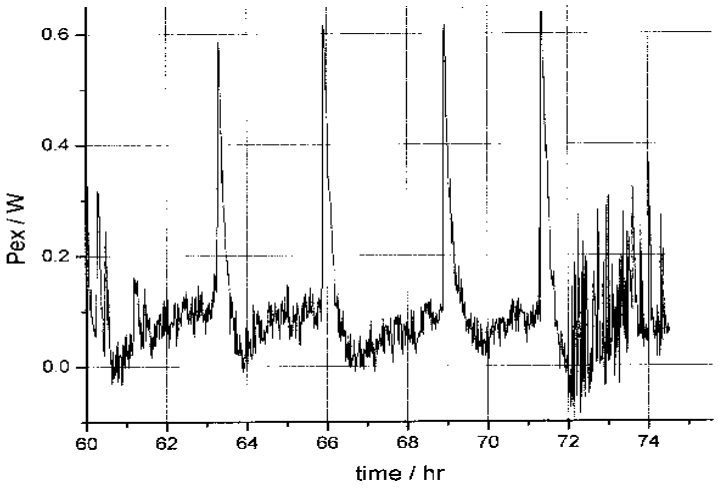

Fig. 3. *Excess power pulses during a 14 hour period of an experiment (070108) which lasted 12 days as a whole.*

During most of the experiment the excess power was about 0.1±0.1 W. Most of the large bursts were less than 1 W, but there was one burst which reached 2 W. Following each large burst, the SEC recorded negative power. It is possible that recombination power was lost due to increase in gas pressure in the cell when the power burst occurred. The o-ring seal at the top of the cell is not rigid. Therefore, an increase in gas pressure inside the cell could cause an increase in the rate of escape of recombination gases, thus reducing the temperature in the space occupied by the recombination catalyst.

For the cases of bursts (0.5 W $\leq P_{ex} \leq$ 2 W), we take α_w = 2 W for analysis, for simplicity. Then, the density of the trapped neutrons (3) for the bursts is given as

$$n_n = 7.2 \times 10^{16} \text{ (cm}^{-3}\text{)}. \quad (5)$$

Case 3. Experiment of Zhang et al. [12]

In this experiment with an explosion as explained in their paper [12], we can assume the excess power of

$$P_{ex} = 1.9 \times 10^5 \text{ W}.$$

This means that the parameter α_w defined above is given as $\alpha_w = 1.9 \times 10^5$ W and we obtain the value of the parameter (3) for the explosion as

$$n_n = 1.4 \times 10^{20} \text{ (cm}^{-3}\text{)}. \quad (6)$$

3.2 Discussion

In our analyses obtained until 1998 and published as a book [2, 4], we determined the parameter n_n for more than 60 experimental data sets giving values between $10^8 - 10^{13}$ cm^{-3};

$$n_n = 10^8 - 10^{13} \text{ cm}^{-3}. \quad (7)$$

It is interesting to compare the value of the parameter n_n given in the relation (7) with the values (4) – (6) determined in the above Cases. The experimental data given in the Case 1 have the parameter (4) in the range given in (7). On the other hand, the parameters (5) and (6) of the Cases 2 and 3 are the largest values of n_n, exceeding the range expressed in the relation (7).

These large values of the parameter n_n in Cases 2 and 3 show, of course, the large value of the excess energy in a reduced form, making it easy to compare the intensities of the

reactions. Then, we have to discriminate the latter cases (Cases 2 and 3) from such "normal" events in the CFP as the Case 1 giving the value n_n in the relation (7).
This characteristic feature of Case 2 (and Case 3) is also shown by plotting a N_P vs. P_{ex} diagram, where N_P is the frequency of a definite excess power evolution P_{ex} such as given in Fig. 2.13 of [4] for the data by McKubre et al. [9].

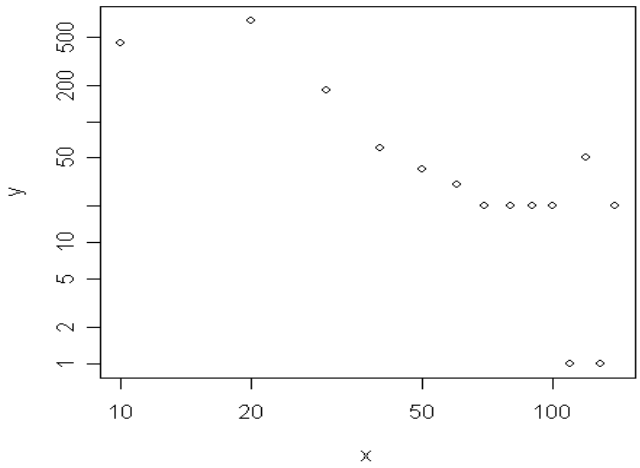

Fig. 4. *Distribution of the frequency N_P (= y) producing excess power P_{ex} (= x). To depict log-log curve, values of N_P and P_{ex} were arbitrarily multiplied by 10^n. (x = 100 in this figure corresponds to P_{ex} = 1 W)*

The corresponding figure in the case of the data sets obtained in LENL (including Cases 1 and 2) is depicted in Fig. 4. Data points were counted from excess power peaks (about 250 pulses and bursts) in such diagrams as Figs. 2 and 3 in the following time periods in three runs; 1) time period 86.8 – 88.4 hours of run #060620, 2) time period 3 – 12 hours of run #061007, 3) time period 22 – 90 hours of run #070108.

Figure 4 shows following facts (x = 100 correspond to P_{ex} = 1 W in this figure):

Region A, x = 20 – 60.

The data points in the range from x = 20 to 60 are considered to be on a straight line with a gradient ≈ – 2.

This value of the gradient ≈ – 2 is compared with the value ≈ – 1 [4] obtained for the data by McKubre et al. [9]. These values for two data sets may depend on characteristics of the cathodes used in the experiments, if we consider the Gutenberg-Richter law of earthquakes, discussed above. In the case of the earthquakes, it is said that the exponent (≈ –1.7) of the inverse-power law depends on location, and it fluctuates with time [7].

Region B, x > 60.

The data points in the range x > 60 deviate from the straight line. Some points are very low and some very high above the extrapolated straight line from Region A.

The data in region A is similar to the data depicted in the Fig. 2.13 [4] for the data obtained by McKubre et al. [9], but it has a different gradient. On the contrary, the data in region B has a different characteristic and should be analyzed with different factors from those used in the case of the data in region A.

One possible explanation for the difference in characteristics of the data in region B and those in region A is in the behavior of complex systems with nonlinear interaction resulting in self-organization and chaos. We may imagine the following processes 1) – 3).

1) If the temperature of the experimental system is lower than a critical temperature T_c (from the experiment, we may take it higher than 60 degC; $T_c \geq 60$ degC), there are no cold fusion reactions.

2) Increasing the temperature higher than T_c ($T_c < 90$ degC as confirmed by experiments), the cold fusion reactions start to occur and produce excess energy inducing more reactions as we see in the occurrence of many pulses.

This means that the critical temperature T_c in this case is in between 60 and 90 degC (60 degC $\leqq T_c \leqq 90$ degC).

3) We may assume that higher temperature is more favorable for the CFP if other conditions are the same. Then, when the temperature of the sample increases due to CF reactions generating more excess energy than dissipating energy from the system and the shape of the tubular cathode is favorable of the positive feedback of the CFP, there may occur a positive feedback which increases the temperature of the system, thus inducing more CF reactions.

This positive feedback results in the excess energy bursts as seen in region B. When the cycle of the positive feedback last long, there may appear negative feedbacks due to changes of other parameters (e.g. decrease of D/Pd ratio, change of lattice structure, changes in surface composition, etc.) to over -compensate the positive feedback and reduce the sample temperature.

The explosions observed by Zhang et al. [12] and also by Biberian [13], both of whom used tubular Pd cathodes, might be the extreme examples of this positive feed-back when the negative feedback did not work well to prevent the explosions. The other explosions experienced by Fleischmann et al. [1] and Mizuno et al. [14] may be explained by similar processes.

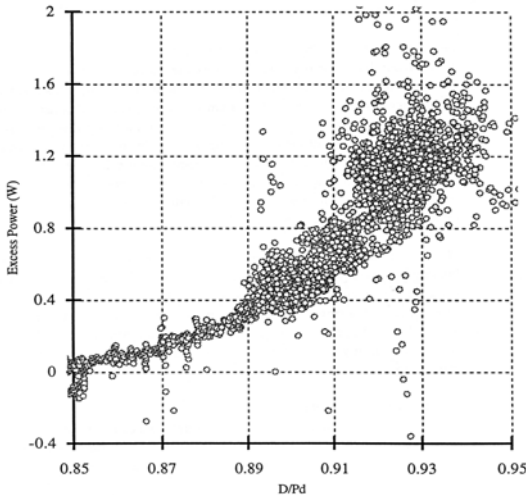

Fig. 5. *Variation of excess power with loading ratio D/Pd obtained by McKubre et al. [9].*

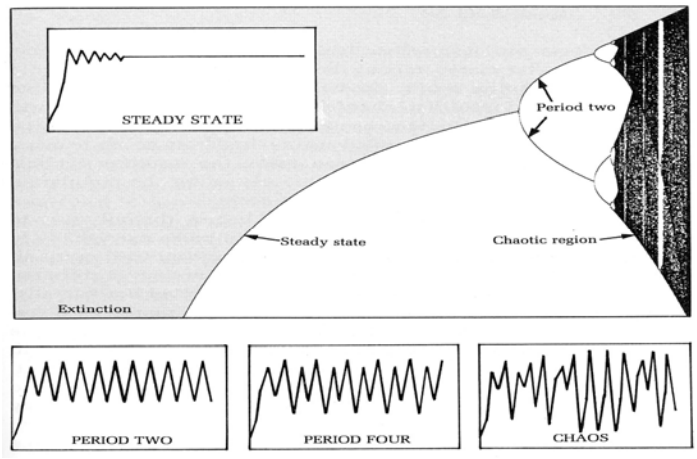

Fig. 6. *Bifurcation diagram to show period-doubling and chaos (From "Chaos" by J. Gleick [15]. p.71). The main figure depicts x_∞ (ordinate, x_n at $n = \infty$) vs. the parameter λ(abscissa) of the logistic difference equation, i.e. l.d.e., $x_{n+1} = \lambda x_n(1 - x_n)$ $(0 < x_0 < 1)$. The inserted figures, a) Steady state, b) Period two, c) period four, and d) chaos, depict variations of x_n with increase of suffix n (temporal variation if n increases with time) for four values of λ; a) $1 < \lambda < 3$, b) $3 < \lambda < 3.4$, c) $\lambda \simeq 3.7$, d) $4 < \lambda$. The region a), b) and d) correspond to "Steady state", "Period two" and "Chaotic region" in the main figure, respectively.*

A similar figure was obtained by McKubre et al. [9] for the dependence of P_{ex} on D/Pd ratio as reproduced in Fig. 5.

Figure 6 shows the classic graph (Fig. 7) of the evolution of the final equilibrium states of the logistic difference equation (l.d.e.), well-known in the field of complexity [15].

We see a bifurcation in Fig. 4 similar to that of the state into "Period two" in Fig. 6 of l.d.e.

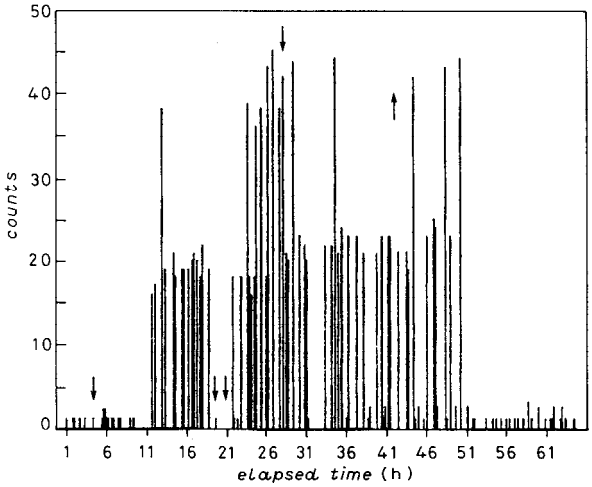

Fig. 7. *Diagram showing the time evolution of the neutron emission counts (ordinate) during the first run (7-10 April, 1989) by De Ninno et al. [16]. The values indicated are integral counts over periods of 10 minutes.*

Temporal evolution of the excess power generation depicted in Figs. 2 and 3 also shows the time dependence of excess power similar to those of l.d.e. depicted in the inserted figures "Chaos" and "Period four" in Fig. 6.

The dispersion of experimental data points in Fig. 5 obtained by McKubre et al. [9] may be the manifestation of chaos appeared in l.d.e. shown in the rightmost part of Fig. 6.

It is possible to add another example of the bifurcation-like behavior in the temporal evolution of the CFP in the neutron emission as shown in Fig. 7 [16]. In this figure, the number of neutron counts is plotted on the ordinate as integral values over periods of 10 minutes. This does not necessarily reproduce faithfully the microscopic processes occurring in the sample. The figure shows, however, similar characteristics to those appearing in the data of excess power production obtained in LENL such as the bifurcation and the positive feedback of the CFP shown in Figs. 2 and 3.

It is noticed in the experiment by De Ninno et al. [16] that parameters (T, η = D/Ti ratio, etc.) were varied by cycling change of temperature between 77 K and the room temperature.

At present, we have only an analogy between the data sets of the CFP and the complexity depicted by the l.d.e. Though we have shown only three experimental data sets by Dash et al., McKubre et al. [9] and De Ninno et al. [16], there are many data sets in the CFP showing characteristics common in complexity.

4. Conclusion

Almost all CF systems satisfy the sufficient conditions for the occurrence of complexity which is common in any nonintegrable system with Poincaré resonances (both in classical and quantum mechanics), according to the definition by I. Prigogine [17]. That is, they are open, non-equilibrium (far– from- equilibrium), many body systems with non-linear interactions between components.

In addition to this general nature of CF systems, we have many experimental data sets in the CFP that show characteristics of many-body systems and complexity. The most outstanding examples of them are the two laws we have found before, that show many-body effects of the CFP;

(1) **The first law**; The Inverse-Power Law of $N(P_{ex})$ vs. P_{ex} Relation, where $N(P_{ex})$ is the number of events producing excess power P_{ex} ([4] §2.12 and Fig. 1) and

(2) **The second law**; The Stability Effect in the Yield of Product Elements by nuclear transmutation ([4] §2.11).

The third law described in this paper shows the chaotic nature of the CFP, i.e.

(3) **The third law**; The Bifurcation and Chaos of the Cold Fusion Phenomenon in the occurrences of excess energy (Figs. 2, 3, 4 and 5) and neutron emission (Fig. 7).

The last law shown in this paper by comparison with the l.d.e. may be legitimated by a discovery by Feigenbaum that “there are certain universal laws governing the transition from regular to chaotic behavior, roughly speaking, completely different systems can go chaotic in the same way [18].

Another characteristic we could notice from Fig. 4, depicted by data analysis from the point of view of the inverse-power law, is the appearance of positive feedback in reactions participating in the CFP. This point of view gives us a consistent perspective that makes it possible to understand such various heterogeneous data sets in this field as null results, e.g. [5], small and large pulses of excess power (e.g. Figs. 2 and 3) and neutron emission (e.g. [18]), and explosions [1, 12 – 14].

From the specification of CF systems sufficient to expect characteristics of the stochastic processes and complexity to occur in them and the three laws (or regularities) found in the CFP as described above, we understand that the CFP is a phenomenon governed by probabilistic laws and complexity. Therefore, investigation of the CFP should be performed

realizing its nature of the open, non-equilibrium system composed of many components combined together with nonlinear interactions. Many controversies surrounding the CFP can be resolved by our realization of its nature. New developments may be expected if we establish the science of the cold fusion phenomenon.

We have to realize also that our knowledge in natural science is not complete. There remain unexplored research fields in physics such as halo nuclei with medium mass numbers and also wavefunctions of occluded protons/deuterons in fcc/hcp transition metals. These properties of exotic nuclei and protons/deuterons wavefunctions may be closely related to the occurrence of the CFP, as we have explored a few steps already as reported in [3, 4].

Acknowledgment

This work is supported by a grant from the New York Community Trust.

References

1. M. Fleischmann, S. Pons and M. Hawkins, "Electrochemically induced Nuclear Fusion of Deuterium," *J. Electroanal. Chem*., **261**, 301 – 308 (1989).
2. H. Kozima, *Discovery of the Cold Fusion Phenomenon*, Ohtake Shuppan, Tokyo, 1998. ISBN: 4-87186-044-2.
3. H. Kozima, "Quantum Physics of Cold Fusion Phenomenon," in *Developments in Quantum Physics*, eds. K. Krasnoholovets and F. Columbus, Nova Science Publishers, Inc. 2004. ISBN: 1-59454-003-9. And also H. Kozima, *Rep. Fac. Science, Shizuoka Univ.* **39**, 21 – 90 (2005).
4. H. Kozima, *The Science of the Cold Fusion Phenomenon*, Elsevier Science, London, 2006. ISBN-10: 0-08-045110-1
5 For instance, S.E. Jones, D.E. Jones, D.S. Shelton and S.F. Taylor, "Search for Neutron, Gamma and X-Ray Emission form Pd./LiOD Electrolytic Cells: A Null Results," *Trans. Fusion Technol*. **26**, 143 (1994).
6. For instance, B. Stella, M. Corradi, F. Ferrarotto, V. Milone, F. Celani and A. Spallone, "Evidence for Stimulated Emission of Neutrons in Deuterated Palladium," *Proc. ICCF3*, p. 437 (1993)
7. For instance, L. Anton, "Simple equation for earthquake distribution" *Phys. Rev*. **E59**, 7213 – 7215 (1999). And also B. Gutenberg and C.F. Richter, *Ann. Geophys*. (C.N.R.S.) **9**, 1 (1956).
8. W.H. Press, "Flicker Noises in Astronomy and Elsewhere," *Comments Astrophys*. **7**, 103 – 119 (1978)
9. M.C.H. McKubre, S. Crouch-Baker, Riley, S.I. Smedley and F.L. Tanzella, "Excess Power Observed in Electrochemical Studies of the D/Pd System," *Proc. ICCF3* , pp. 5 – 19 (1993).
10. W.-S. Zhang, J. Dash and Q. Wang, "Seebeck Envelop Calorimetry with a Pd/D_2O + H_2SO_4 Electrolytic Cell," *Proc. ICCF12,* pp. 86 – 96 (2006).
11. W.-S. Zhang and J. Dash, Excess Heat Reproducibility and Evidence of Anomalous Elements after Electrolysis in Pd/ Pd/D_2O + H_2SO_4 Electrolytic Cell" *Proc. ICCF13* (to be published)
12. X. Zhang, W-S. Zhang, D. Wang, S. Chen, Y. Fu, D. Fan and W. Chen, "On the Explosion in a Deuterium/Palladium Electrolytic System, "*Proc. ICCF3,* p. 381 (1992).
13. J.-P. Biberian, "Explosion during an electrolysis experiment in an open cell mass flow calorimeter," presented at *6th International Workshop on Anomalities in Hydrogen/Deuterium loaded Metals*, Siena, Italy, May 13-15 2005.

14. T. Mizuno and Toriyabe, “Anomalous energy generation during conventional electrolysis” *Proceedings of ICCF12*, pp. 65 – 74, (2006)
15. J. Gleick, *Chaos*, Penguin books, ISBN 0-14-00.9250-1
16. A. De Ninno, A. Frattolillo, G. Lollobattista, G. Martinio, M. Martone, M. Mori, S. Podda and F. Scaramuzzi, ”Evidence of Emission of Neutrons from a Titanium-Deuterium System,” *Europhys. Lett*. **9**, 221 (1989)
17. I. Prigogine, *The End of Certainty***,** The Free Press, New York, 1996. ISBN 0-684-83705-6
18. S.H. Strogatz, *Nonlinear Dynamics and Chaos*, p. 3, Westview Press, 1994. ISBN-10; 0-7382-0453-6.

Innovative Engineering and Projects (IP)

A FLOW CALORIMETER FOR GLOW DISCHARGE EXPERIMENTS

R. F. Cantwell, S.S. Booth, M.L. McConnell

Coolescence, LLC
2450 Central Ave Suite F, Boulder, CO 80301 USA
rick@coolescence.com

Coolescence, LLC has developed a flow calorimeter, for the purpose of detecting excess heat in glow discharge cold fusion experiments. Accurate calorimetry is an essential tool for the detection, quantification, and verification of excess heat. The calorimeter functions by pumping temperature controlled fluid at a set rate though a jacket on an experimental chamber, measuring the temperature of the incoming and exiting fluid, and utilizing the temperature change to calculate power. The entire apparatus is housed in a small temperature controlled enclosure. The calorimeter design incorporates refinements such as, fluid temperature polishing, dual temperature probe redundancy, a LabView™ control system, and a custom built form fitting calorimeter block. This calorimeter is an advancement over previous Coolescence designs, with a 95% power capture efficiency, a sensitivity of +/- 10 mw or 1% of input power, and has been tested for power inputs up to 10 W.

Details of calorimeter construction and performance are discussed.

PURPOSEFUL SYNTHESIS OF CHEMICAL ELEMENTS AND ECOLOGICALLY PURE MOBILE SOURCES OF ENERGY

V.A. Krivitsky [*] **and F.A. Gareev** [**]

[*] *Dubna University, Dubna, Russia*
[**] *Joint Institute for Nuclear Research, Dubna, Russia,*
gareev@thsun1.jinr.ru

It is well known, that the natural geo-transmutation of chemical elements occurs in the atmosphere and earth in the regions of a strong change in geo-, bio-, acoustic-, and electromagnetic fields.

The mineral row materials contain the same accompanying chemical combinations which are independent of mineral deposit. This means that the formation of chemical elements occurs in the same physical and chemical conditions. These conditions were simulated on the fundamental cooperative resonance synchronization principle. The experimental facility was constructed on the basis of our model which provided with the calculated final chemical elements. These experimental results indicate new possibilities for, simulating, inducing and controlling nuclear reactions by low energy external fields. The borrowing from the geo-transmutation mechanisms of chemical elements creates the fundamental directions in low energy nuclear reaction researches for construction of new ecologically pure mobile sources of energy independent of oil, gas and coal, new substances, and technologies.

Geochemistry and petrology are exactly those science disciplines which have accumulated a valuable material on agent evolution in the Earth history. Nevertheless, so far this wealth has not been embraced by a common, comprehensive evolutionary idea which could solve and give answers to a number of questions raised by geochemistry and petrography before geology and science in general.

The marked above physical theories fast established in scientific practice allow us to argue that to solve the majority of accumulated problems and contradictions in the junction of modern knowledge of geochemistry, petrology, mineralogy and ore-formation processes we

should speak not about complex atom structure and its place in material structures and symmetries but about its complex **behaviour** and **condition** considering atom of chemical element AS A PROCESS. In other words, it is necessary to persistently and consistently change over to consideration of alterations (redistribution) in its own dynamic system – mass-energy – in history of chemical evolution of the Earth.

The named physical postulates, on one hand, are extensive geochemical material on dispersion, isomorphism and paragenesis of chemical elements, and, on the other hand, show that in history of geochemical Earth evolution there is a symmetric nuclei division. We suggest to calling the phenomenon of symmetric division a nuclear dissociation (cold dissociation).

Taking isomorphism as a complex value of chemical elements' affinity rate, on basis of over five hundreds evidences of their isomorphic relations in minerals and formations there has been built a diagram (Figure 1).

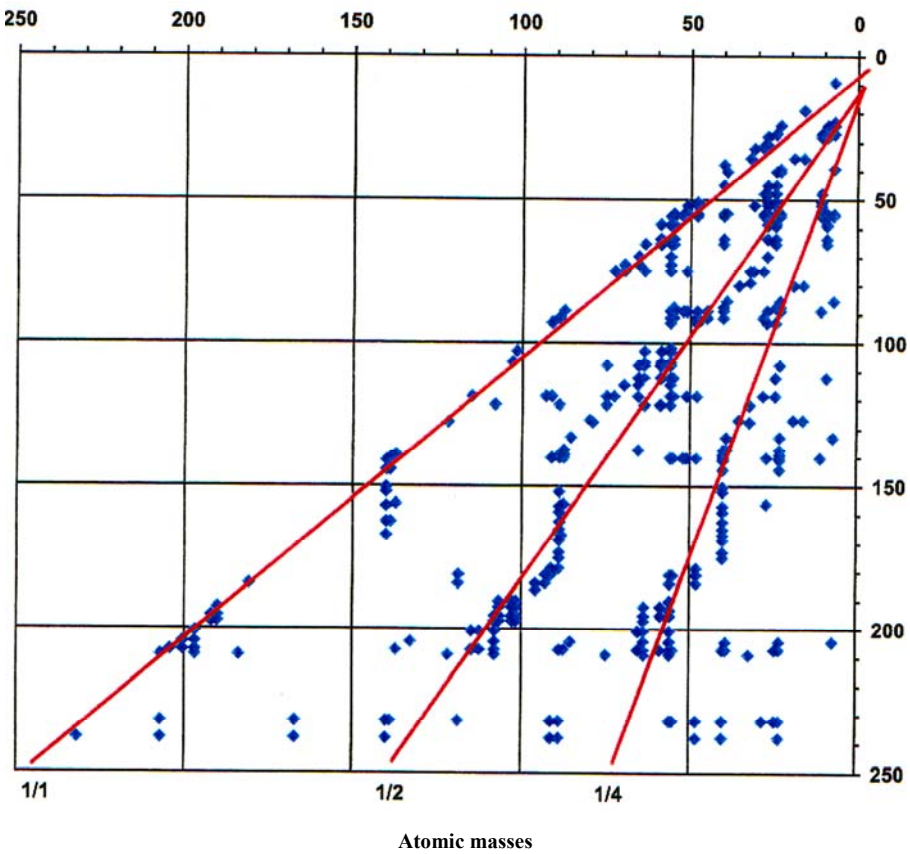

Figure 1. *Isomorphic ratio of elements according to their atom masses. The replace atomic masses are on abscises, the replaced atomic masses are on ordinate. The ratios of atomic masses 1/1, ½ and 1/4 disposed along lines 1/1, ½ and ¼.*

It reflects the general tendency of the process of nuclear dissociation in conditions of crust, from uranium to hydrogen.

The processes of nuclear dissociation preferably develop by the way of correlation of atomic masses and atomic charges of isomorphically replacing each other elements with the ratio $\frac{1}{2^n}$; where $n = 0..4$.

In what conditions can we expect the process of nuclear dissociation? The geophysical and geochemical data show that the basic state of substance in the Earth's subsoil, in which there is a possibility of evolution, is, first of all, protomagma and magma solutions-melts forming plums-upwellings and gas-liquid fluid-dynamic systems separating from them. It has been found that plum-upwelling systems are generated on the border of the Earth core and the lower mantle. As it has been shown before [2] in such conditions chemical agent in great depth lose its periodicity and chemical elements no longer comply with Mendeleyev law and plutonic substance itself is presented as naked nuclei and free electrons with a quite high free-running frequency and a high speed of rotation around their own axes. Let us call these dynamic systems **protonucleus**.

So, which general physical laws in nature can control and be responsible for such an express, almost multiple division of protonuclei and nuclei of chemical elements? The said multiplicity of division is determined by two important mutually complementary regularities.

The first regularity. Multiple division of protonuclei complies with the universal principle of resonance synchronisation and self-organisation of micro- and macrosystems suggested by F.A. Gareev [1].

Let us consider decomposition of two resonances r and R through the following binary channels: $r \to a + b$, $R \to A + B$ presuming that $a = A$ and $b = B$. Then energies of the particles $A(a)$ and $B(b)$ will be determined with the following equations:

$$E_A = \frac{m_R c^2}{2} + \Delta E_{AB},\ E_B = \frac{m_R c^2}{2} - \Delta E_{AB},\ E_a = \frac{m_r c^2}{2} + E_{ab},\ E_b = \frac{m_r c^2}{2} - \Delta E_{ab}, \qquad (1)$$

$$\Delta E_{AB} = \frac{\left(m_A^2 - m_B^2\right)c^2}{2m_R}, \quad \Delta E_{ab} = \frac{\left(m_a^2 - m_b^2\right)c^2}{2m_r}. \qquad (2)$$

The empirical research on distribution of masses of chemical elements in isomorphic compositions have shown that atom nuclei and protonuclei are natural resonances which very often decompose through the same binary channel where the difference of energies of

decomposed particles from half of rest mass of considered protonuclei resonances is in inverse proportion to mass of corresponding resonance.

The second regularity. Multiple binary division of atom nuclei and protonuclei can be explained using the law of rotating free bodies: mass centres of all free rotating bodies formed by decomposition of primary protonucleus body have the same lineal speed:

$$V_c = R_{ci}\frac{2\pi}{t_i} = R_{ci}\omega_i = const\,, \qquad (3)$$

where R_{ci} – rotation radius of protonucleus i; ω_i – angle rotation speed of protonucleus i; t_i – its rotation time.

Note two conclusions resulting from the given correlation:

The first : mass of nucleus m limited by rotation radius Rci makes half of mass of the primary protonucleus mi. In other words, in rotation radius protonuclei mass is divided exactly in two; analytically this can be expressed as:

$$m_{ci} = \frac{1}{2}m_i\,, \qquad (4)$$

where m – mass limited by rotation radius R.

The second: in absence of density gradient rotation radius is determined by the following ratio:

$$R_{ci} = \frac{R_i}{\sqrt[3]{2}}\,. \qquad (5)$$

The given ratio suggests invariability of volume occupied by protonucleus before and after its division.

Assuming that atom nuclei and protonuclei in plum-upwellings, fluid-dynamic systems have high frequencies of rotation and vibration, the division action itself starts at the moment of resonance influence on atom nuclei and protonuclei from outside.

Negotiation of potential barrier (or nucleus division barrier) develops afterwards as a process of resonance tunnel transpiration through the barrier which is well-known in quantum mechanics. In result a separated group of nucleons forms a new atom nucleus making an isomorphic pair of elements with the initial (mother) protonucleus (see Table 1).

The most studied isomorphic pairs of elements as an example of multiple binary division of protonuclei.

Table 1

1.	**Pt**	R=2,240 → R_c=1,778	**9.**	**Fe**	R=1,476 → R_c=1,171
	Rh	R=1,810		**Al**	R=1,158
2.	**Re**	R=2,208 → R_c=1,758	**10.**	**Fe**	R=1,476 → R_c=1,171
	Mo	R=1,768		**Mg**	R=1,118
3.	**Ta**	R=2,184 → R_c=1,734	**11.**	**Ti**	R=1,402 →R_c=1,113
	Nb	R=1,749		**Si**	R=1,174
4.	**Hf**	R=2,174 → R_c=1,762	**12.**	**Ti**	R=1,402 - R_c=1,113
	Zr	R=1,743		**Mg**	R=1,118
5.	**Lu**	R=2,160 → R_c=1,714	**13.**	**Ca**	R=1,321 → R_c=1,049
	Y	R=1,724		**Mg**	R=1,118
6.	**Cd**	R=1,864 → R_c=1,479	**14.**	**Ca**	R=1,321 → R_c=1,049
	Zn	R=1,556		**Na**	R=1,098
7.	**Nb**	R=1,749 → R_c=1,388	**15.**	**K**	R=1,311 → R_c=1,040
	Ti	R=1,402		**Na**	R=1,098
8.	**Rb**	R=1,701 → R_c=1,350			
	K	R=1,311			

Physical basis of the empiric conclusion about multiplicity of protonuclei division is the universal principle of resonance synchronization and self-organization of micro- and macro-systems. It suggests that elementary particles, atom nuclei, atoms in crystals and organic compositions have quasicrystal homologous structures based on the same fundamental

physical laws, and their corresponding frequencies, speeds, impulses and movement energies are quantized, comparable and, consequently, synchronized.

As a result of synchronization and self-organization of protonuclei in magma sources and fluid-dynamic systems an infinite number of protonuclei and chemical elements, which can be considered as sets, enter the lithosphere and the Earth crust. Generally, such sets occur in nonlinear dynamic systems and, first of all, in discrete dynamic systems. Such sets are dynamic fractals.

We can assume that as a result of nuclear dissociation processes in the lithosphere and the Earth crust occur and develop symmetry structures representing two simplest types of fractals. The first fractals are dendrites, i.e. when some set is partied into groups of two elements having similarity with binary system of calculation. The second ones are the Cantor set or Cantor dust.

The fractal features of the Cantor dust have a great meaning in geochemical nature of the Earth as many fractals have the similar features of set. Presenting chemical elements as the Cantor dust formed in result of nuclear dissociation of protonuclei we are, finally, close to solution of the primary problem of geochemistry – the problem of dispersion of chemical elements in the lithosphere and the Earth crust.

The found number of correlations allows us to conclude that protonuclei and atom nuclei of chemical elements are microsystems built under the mathematical principle of sequential distribution of series of numbers of significant values.

Consequently, the basis of origin of every chemical element is its **antecedent** protonucleus or atom nucleus performing its function. This allows to conclude that the major number of chemical elements is **generated** (occur) not simultaneously but sequentially in course of nuclear dissociation (cold dissociation) of protonuclei and atom nuclei in geochemical evolution of the Earth and the Solar system.

Altogether there has been determined seven such sequences. In general they coincide with the periodic sequence of Mendeleyev's table but located in reverse order emphasising the character of nuclear dissociation process. The specified sequence of element formation can be presented using a self-similar fractal such as the Cantor dust.

A convincing example of reality of nuclear dissociation processes in the Earth crust is presence of binary system of chemical elements in minerals of ore substance. The elements forming pairs have quite close atom masses owing to the fact that they are generated from one protonucleus or atom nuclei, as it was shown above, in result of division of its mass into two

approximately even parts. The occurred this way chemical elements in conditions of further mineral forming form independent ore minerals or comprise more complex minerals. This situation is much more often seen in nature as these pairs of elements represent one of the branches of nuclear dissociation of massive protonucleus. Here are some most often met pairs of elements and minerals.

$Be-Li$ – beryl-lepidalite; $Fe-Mn$ – granites; $Fe-Ni$ – pentlandite; $Fe-Cu$ – chalcopyrite; $Fe-Zn$ – pyrite, blende; $Cd-Ag$ – blende, argentite; $Ag-In$ – argentite, fade ores; $In-Sn$ – blende; $Sb-Te$ – fade ores; $Au-Tl$; $Pb-Tl$ – galenite; $Ga-Ge$ – feldspars and many other pairs of elements.

Some of the specified pairs of elements can be observed in pentlandite and chalcopyrite presented in form of fractal-dendrite occurred in result of nuclear dissociation of massive protonucleus (Figure 2).

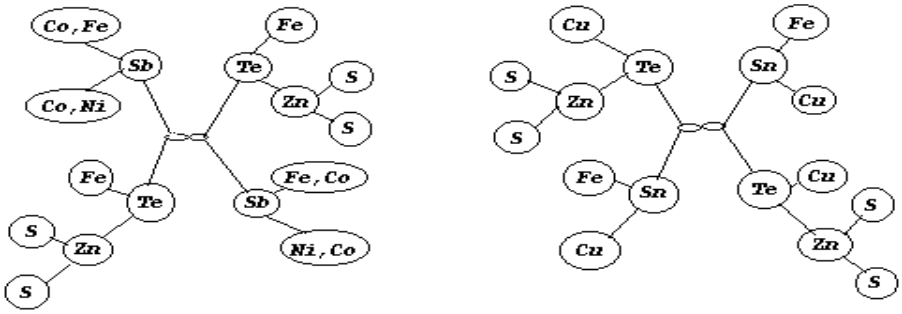

Figure 2. *Fractal-dendrites: pentlandite and chalcopyrite.*

Experimental method. Figure 2 presents a block scheme of the unit used in the experiments in which metal smelts are influenced by pulse current in magnetic field. The impulse generator was designed and assembled specifically for the experiment based on reversibly switched on dynistors generating microsecond impulses of high amperage currents [5].

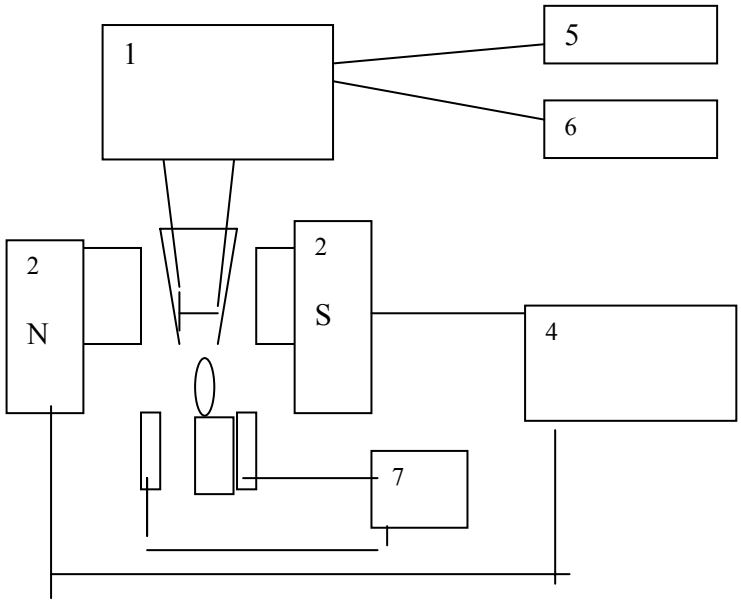

Figure 3. *Block scheme of the experimental unit for metal smelts impulse influencing. The unit consists of the following basic elements: 1. impulse generator; 2. constant magnet; 3. processing chamber; 4. electromagnet power source; 5. oscillograph; 6. frequency indicator; 7. neutrons and gamma-ray emission sensors; 8. gas burner (propane-air).*

General characteristics of the unit. $U = 1000V = const$, I change from 0 to $7500A$ depending on Rm, sinusoid damped oscillation $T_{\min} = 25$ microseconds of the first impulse in damped oscillation, frequency of damped impulses from 1 to 400 Hz.

Experiment process. The tested metals were placed into alundum capsule mounted between the poles of constant electromagnet with magnetic field intensity of 1.2 *tesla*. Metal button consisting of lead HCA, copper OSC and Na_2O_2 HCA in ratio $8:1:1$, total weight $270g$, was heated up with gas burner to $1100^{\circ}C$ during 30 minutes. Then, without cutting off the burner, the smelt was entered by two tungsten electrodes energized with direct current from the impulse generator. Duration of impulse influence was from 60 to 180 sec. Altogether, there were performed 21 tests using impulse influencing the smelt with current.

In course of the tests there was found out that depending on time of influencing the smelt two morphologic kinds of metal are separated after its hardening. The first: there were no visible structural alterations during 60 seconds of influencing the smelt. The second: visible phase transitions and liquation process occurred when the smelt was influenced from 100 to 180 seconds. There were two clear phases. The first – light one when the hardened smelt turns into a microcrystalline discrete mass which then easily disseminates into separate

fine crystals with size $0.1-1.0\,mm$. As the further chemical and structural analysis showed, the most significant lead cold dissociation processes are observed in this very phase. The second phase – heavy, malleable one which is similar to a substance condition after a short time influencing with impulse current. The two phases volume ratio is $1:25$.

Chemical analysis of the two received samples was carried out using three methods. X-ray dispersive microanalysis using the system AN-10000 (England) with scanning microscope JCM-35CF was performed in the analytical center FGUP VNIITS. X-ray spectrum analysis using x-ray spectrometer PW – 2400 was performed in IGEM RAN by I.A.Roschina. Phase analysis using x-ray spectrum microanalyzer CAMEBAX MICROBEAM was performed by V.G.Senin in GEOCHI RAN. The results of the chemical analyses are shown in Table 2.

Table 2. ***Results of x-ray dispersive and x-ray spectrum analyses.***

Test N	Time, condition of influence	Pb	Sb	Sn	Ag	Pd	Mo	Cu	Total
1	60 sec.	74,70	9,30	3,45	0,15	0,70	0,55	11,10	100,0
2	60 sec.	94,00	0,20	0,90	0,10	1,20	0,50	3,10	100,0
3	60 sec.	87,10	2,80	0,70	-,10	0,90	1,50	6,90	100,0
4	60 sec.	89,95	1,70	1,55	0,10	0,70	1,25	4,70	100,0
5	60 sec. In magnetic field	80,90	7,14	1,10	0,27	0,60	1,00	8,94	100,0
6	60 sec. Increased frequency in m.f.	85,00	0,80	0,90	0,20	1,10	1,90	10,20	100,1
7	100 sec. In m.f.	29,00	11,20	0,20	0,10	0,10	0,70	58,40	99,90
8	120 sec. In m.f.	45,69	24,92	3,66	0,00	0,00	0,00	25,73	100,0
9 main phase	120 sec. In m.f.	64,90	16,28	3,37	0,05	0,00	0,00	15,46	100,0
10 light phase	120 sec. In m.f.	9,47	35,71	5,28	0,10	0,00	0,00	49,54	100,0
11	180 sec. In m.f.	7,14	29,89	5,41	0,05	0,005	0,005	56,47	98,96

As we can see from Table 2, the performed smelts tests with different duration of impulse current influence show a pronounced rising tendency in intensity of nuclear dissociation of lead atomic nuclei. Besides, it is necessary to note that there is an almost direct dependence between the contents of copper and antimony in the received samples. This is characteristic of both various times of influence and the two different phases.

Appealing to the earlier suggested scheme of geochemical chain of element formation [7], it is clearly seen that the received results prove the principle of dichotomy in element formation as a result of nuclear dissociation, that is a consecutive, almost multiple division of the whole into two parts then another division of each part into two almost equal parts and so on. In case of nuclear dissociation of lead atomic nucleus this division can be schematically presented as follows:

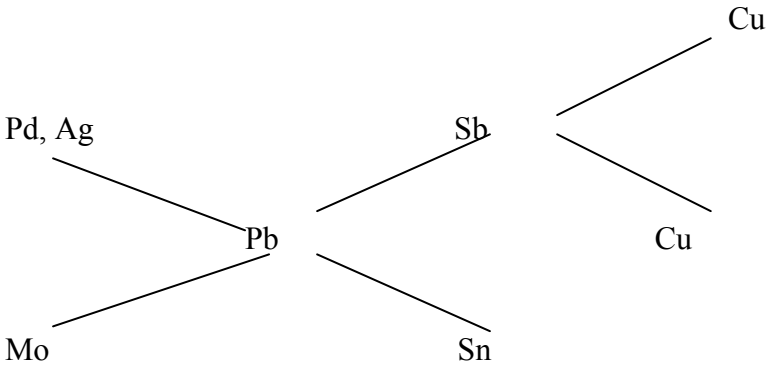

There is one more important fact that must be noted. The showed reaction of nuclear dissociation of lead atomic nucleus has analogies in geochemical processes both in the terrestrial crust and on the lunar surface.

An analog of the suggested reaction in the terrestrial crust is cuprostebit (Cu_2Sb) found in the south of Greenland. Found later in the South Ural cuprostebit is met in coalescence with stistait (Pb, Sn, Sb) – a natural combination of a triple system $Sn - Sb - Pb$ presented by native stannum, antimony and lead [8].

As another analog of the cold transmutation reaction it is possible to name the results received by O.A. Bogatikov et al in examination of lunar regolit delivered by AS “Luna-16” and “Luna-24”. They managed to detect and diagnose micron particles of hard smelt of copper, zinc, gold and silver, as well as aggregates of native molybdenum which had never been observed in nature before [5, 6].

Conclusion

It is well known [7] that the natural geo-transmutation of chemical elements occurs in the atmosphere and earth in the regions of a strong change in geo-, bio-, acoustic-, and electromagnetic fields.

The mineral row materials contain the same accompanying chemical combinations which are independent of mineral deposit [7]. This means that the formation of chemical elements occurs in the same physical and chemical conditions. These conditions were simulated on the fundamental cooperative resonance synchronization principle [1]. The experimental facility was constructed on the basis of our model which provided with the calculated final chemical elements. These experimental results indicate new possibilities for, simulating, inducing and controlling nuclear reactions by low energy external fields. The borrowing from the geo-transmutation mechanisms of chemical elements creates the fundamental directions in low energy nuclear reaction researches for construction of new ecologically pure mobile sources of energy independent of oil, gas and coal, new substances, and technologies.

References

1. F.A. Gareev. Universality of Huygense synchronisation principle and harmony in the nature. Symposium. Selected works of the second Siberian Conference on mathematical problems of space and time physics of complex systems (PST-98) – Searching for mathematical regularities of creation. Novosibirsk. Institute of mathematics, 1999, pp. 92-110; F.A. Gareev, I.E. Zhidkova. Quantization of differences between atomic and nuclear rest masses and selforganization of atoms and nuclei. E-print http://arxiv.org/pdf/nucl-th/0610002 30 September 2006.
2. R.M. Kronover. Fractals and chaos in dynamic systems. Basic theory. Moscow. Postmarket, 2000, p. 352. Picture 7.
3. H. Takayasu. Fractals in physics. Moscow, Mir, 1988, p.249.
4. E.Feder. Fractals. Moscow, Mir, 1991, p.276.
5. O.A. Bogatikov, A.I. Gorshkov, A.V. Mohov et al. The first finding of native molybdenum, silver sulphide and hard solution of iron and stannum in the lunar soil. Geohimiya, 2001, №6, pp. 665-670.
6. O.A. Bogatikov, A.I. Gorshkov, A.V. Mohov et al. Fine Au. Hard solution of Cu-Zn-Au-Ag and native Mo in regolit from AS “Luna” DAN, 2002. V.386, №3, pp. 368-371.
7. V.A. Krivitskiy. Transmutation of chemical elements in evolution of the Earth: from hypothesis to realty and experiment. M. MPGU press, 2003, p.204.
8. M.I. Novgorodova. Native metals in hydrothermal ores. M. Nauka, 1983, p.287.

INSPECTION METHOD TO CHECK QUALITY OF NUCLEAR TRANSMUTATION MEDIA

B.U.Rodionov[1], M.S.Godin[2], I.B. Savvatimova[3]

1- Moscow Eng & Phys Inst (State University),
2- Institute for High Temperatures of RAS,
3- Federal State Unitary Association Scientific Research Institute "Lutch" , Podolsk, Russia

The instability of work of "alchemical reactors", which have been researched in various laboratories all over the world, can be connected with absence of quality surveillance of the working media, in which occur (or which causes) nuclear transmutations.

For such control it is offered to use registration of currents on strings of a hypothetical dark matter. It is supposed, that the strings of this matter – "fluxes", with a diameter of 60 femtometers (1fm = 1fermi = 1 f = 10^{-13} cm), could penetrate any substance. Low energy nuclear reactions are possible at presence of these fluxes. A current is being measured by its magnetic influence on the specially developed flux ammeter - fammeter.

Modern Alchemy

From ancient times alchemy is searching methods of energy and new nuclei generations by special matter – "philosopher's stone". Now the ancient Chemistry or arabic al-kimiya is modern Egypt and the "philosopher's stone" is a dineutrons, tachions, ersions or fluxes.

We suppose firstly, that instability of "alchemical" nuclear transmutations and "alchemical" reactors, which have been researched in various laboratories all over the world, can be connected with absence of quality surveillance of the working media, in which occur (or which causes) nuclear transmutations.

We suppose, secondly, that this working media is invisible astrophysical dark matter and this dark matter has been placed on the Earth everywhere.

We suppose thirdly, that this active dark matter is thread-like. Its threads – filaments or ***fluxes****, which diameter is some femtometers - penetrate any substance (see fig.1), and low*

energy nuclear reaction are possible at presence of this fluxes in ordinary atomic-molecular matter – in gases, liquids or in solids. As filaments have diameter about diameter of atomic nucleus (few femtometers), they will easily pass through any dense substance of usual nuclear-molecular structure.

Vortical World. As is known, in basis of vectors u_1 , u_2 , u_3 any real vector $x = \xi_1 u_1 + \xi_2 u_2 + \xi_3 u_3$ can be presented by matrix $H = \xi_1 S_1 + \xi_2 S_2 + \xi_3 S_3$, where S_1 , S_2 и S_3 – Pauli matrixes of ***spin*****.** Each rotation vector can completely similarly represented by a matrix of rotation, which is expressed through ***quaternions***. The mentioned above conformity x and H is ***isomorphism*****.** It means, that in mathematical three-dimensional space the usual vectors are connected to rotations.

Vector, forming linear space**,** in our model is the vector of intensity of a ***magnetic field H*** [1,2]. As known, this vector is directly connected to rotation of elementary electrical charges. As such charges we consider electrons and quarks, forming two coaxial solenoids (fig.2). External solenoid carrying electron currents, internal solenoid carrying u- and d – quark (anti quark) currents. The quark solenoid is the central part of a cylindrical whirlwind atom – its cylindrical nucleus.

Cylindrical atoms. It is natural, that the quark solenoid radius can not essentially exceed confinement radius, which approximately corresponds to proton radius (about 1.5 f = 1.5×10^{-15} m). The charge of an electronic whirlwind compensates a charge of the central quark whirlwind. These coaxial solenoids can be considered as ***cylindrical atom***. Such cylindrical atom can be infinitely long.

Elementary particles. The cylindrical atom can also form the closed lines - loop, thoroid. The toroidal atom may be much less usual spherical atoms - almost so small, as compound elementary particles (as proton or neutron). Invisible any long cylindrical atoms we name *"**fluxes**",* because magnetic fluxes are stabilizing them.

It is possible, that such virtual cylindrical atoms create invisible environment of our Universe – its ***physical vacuum*****.**

"Vortical ether" models from long vortical strings put forward since XVIII of century (I. Bernoulli, 1736). In modern work from properties vortical ether the Maxwell equations obtained, hence, vortical ether are deduced has Lorentz invariance and does not contradict the *theory of a relativity.*

Flux Model and Theory

On B.Rodionov's model [1] such filaments – ***fluxes*** - can be cylindrical atoms (fig.2). The nucleus of such cylindrical atom can represent a quark - gluon filament stabilized by quantum of a magnetic flow, and an electronic shell - an electronic Bose-liquid with properties of super fluidity and superconductivity.

Quantum of a magnetic flux

The Rodionov's theorem. The charged particle goes in a constant homogeneous magnetic field on a circle (spiral) covering an integer of quanta of a magnetic flux.

The proof. The particle with speed v will move to a field H under action of Lorentz force $evH/c = \beta eH$, counterbalanced entrifugal force $\gamma mv^2/r = P\beta/r$. Here e is electrical charge of a particle, γ is a Lorentz factor $(1 - \beta^2)^{-1/2}$, $\beta = (v/c)$, c is speed of light, r is radius of a circle, on which goes a particle with mass m and with its momentum $P = \gamma\beta mc^2$. From equality $\beta eH = P\beta/r$ we can write

$$H = (P/re). \qquad (1)$$

All expressios are given in absolute (Gauss) system of units and they are correct at any speeds of a particle.

On known H and r we shall find a magnetic flux Φ inside a circle, on which the particle goes: $\Phi = H \pi r^2$. Let's substitute in this formula expression (1) for H, we have

$$\Phi = (P \pi r /e). \qquad (2)$$

The module of the angular momentum of a rotating particle is

$$(Pr /c) = Lh, \qquad (3)$$

where L = 0,1,2, … its orbital quantum number, h is Planck constant.
P founded from (3) we substitute in (2) and we see quantum of magnetic flux Φ_o in

$$\Phi = L(\pi ch /e) = L \Phi_o,$$

as was to be shown.

The value, found by us, of quantum of a magnetic flux $\Phi_o = \pi ch /e$ – the fundamental physical constant. Nowadays it is known as quantum of a magnetic flux $\Phi_o = 2.07 \times 10^{-7}$ Mx = 2.07×10^{-15} Wb. Quanta of a magnetic flux is mathematical analog of Faraday magnetic field lines.

Where we see the quantum magnetic fluxes

The quanta of a magnetic flux show themselves in the various physical phenomena observable experimentally. Let's mention two fundamental phenomena marked per last years by the Nobel Prizes – Abrikosov's whirlwinds and fractional quantum Hall effect (R.B.Laughlin, H. Störmer and D.Tsui, Nobel Prizes 1998).

In supercondactors of the second type around quanta of a magnetic flux the electronic whirlwinds are formed. This whirlwinds known as Abrikosov's whirlwinds. Each Abrikosov's whirlwind «pierces» a superconductor along a direction of an external magnetic field and concludes inside itself just quantum of a magnetic flux. Inside a microscopic electronic whirlwind the superconductivity is lost.

On a magnetic flux quanta the carriers of a charge in experiments on fractional quantum Hall effect are formed. It is important to note, that the charges of such carriers equal to quark charges. The minimal charge, as well as at d – quark is (1/3) e.

We have assumed the existence of Abrikosov's whirlwinds analogues, but not in superconductors. The quarks and electrons whirlwinds can its existance in physical vacuum.

Flux Properties

Intensity of a magnetic field H inside the long solenoid (in absolute system of units) is given by $H = (4\pi j/c)$, in which j is current on unit of the solenoid length. For our case of rotating particles $j = e\eta v/2\pi r$, in which e is the charge of a particle, rotating on a circle radius r with speed v, η is a number of rotating charges on unit of the solenoid length. Just as we did(made) it above, we shall find a magnetic flow already in section of our solenoid of radius r and we shall equate to his(its) quantum of a magnetic flow. From here, taking into account, that radius of the solenoid we determine from (1), we shall receive

$$r = Lch/2\beta\eta\, e^2 \qquad (4).$$

Rotated quarks will be kept insite quark whirlwind by gluon forces, which are the most powerful forces in a nature. As quarks on confinement radius are relativistic especially, it is possible to consider that $\beta = 1$ in (4), then we have

$$r = (Lch/\, 2e^2\eta). \qquad (5)$$

Number of rotating charges on unit of length of the solenoid we shall define (determine) on known density ρ of valence quarks in nucleon.

If nucleon is a sphere with radius r_N and with three valence quarks, we have quark density on unit of nucleon volume about $3/(4\pi r_N^3/3)$ whence

$$\eta \approx \pi r^2 3/(4\pi r_N^3/3). \quad (6)$$

Having substituted the found η in (5), we write

$$r \approx 0.6\, r_N (Lch/e^2)^{1/3}. \quad (7)$$

For e, equal to a electron charge, and L = 1 we have $r \approx 3\, r_N \approx 5$ f = 5×10^{-15} m, that exceeds confinement radius a little.

Actually it is necessary to take into account, that η can be much higher, and quark solenoid radius may be appreciablly below it received by us.

Since Pauli's principle demands identical statuses for every fermion of flux, all quarks should be united in «Cooper pairs» of bosons and inside quark whirlwind rotate this «quark bosons gas» with the double electrical charge of particles.

Quark bosons density can considerably exceed nucleon quark density, as the Pauli principle does not prevent identical statuses of bosons.

The weak dependence of a quark whirlwind radius from charge of rotated particles (as a root cubic) allows to consider that the radius (7) is realistic enough. On radius (7) of a flux cylindrical nucleus at once we shall find intensity of a magnetic field (magnetic induction) $H = \Phi_o/\pi r^2 \approx 3 \times 10^{17}$ Gs = 3×10^{13} T, density of energy on unit of flux length $H^2/8\pi$ and mass of unit of flux length $(\pi r^2 H^2/8\pi c^2) \approx 1$ ng/m.

Received «magnetic» mass of flux length unit approximately corresponds to mass of nucleons densely placed on the same length $(1.6 \times 10^{-24}\text{g} / 3 \times 10^{15}\text{m}) \approx 0.5$ ng/m.

The bottom border of radius of the electronic flux shell we also can search on (7), as electrons are united in “Cooper’s pairs” by its powerful magnetic attraction. Thus, the bottom border of electronic radius of flux approximately coincides with quark whirlwind radius and in electronic whirlwind rotate relativistic bosons with double electron charge.

The top border of electronic whirlwind radius we have estimated from a condition of equality of centrifugal force of electron and Coulomb’s force of electron attraction to a quark cylindrical nucleus. It is a cylindrical and relativistic variant of “Bohr atom” account. From

here rating of the top border of radius of the electronic shell r_e is 6 L r approximately. At L =1 we have r_e ~ 30 f.

Characteristics of fluxes are given in the table

Quark solenoid diameter~10 f	Mass per meter ~ 1 ng / m
Electron shell diameter ~ 60 f	Gap energy ~ 5 GeV
Flux length – unlimited	Gap force ~ 10 ton
Magnetic induction ~ 3.10^{13} T	Electric charge ~ 0.5 C / km
Field stored energy ~ 30 kJ/m	Electron binding energy ~ 5 MeV

Nuclear Reactions

Earlier nuclear reactions on the fluxes (see fig.3) have been discussed in [1-3]. Fluxes create around itself the interconnected collectives of atoms and molecules - quantum ensembles [3]. In quantum ensembles because of direct interaction of its particles even nuclear processes are possible. Nuclear activity of flux thread matter forms explains, on our opinion, stars and planets nuclear compositions, they energy and radiation. In any bodies with flux threads to be possible cold nuclear transmutation.

Nuclear reactions have not place without nuclei localization on fluxes. Conditions for nuclei localization on fluxes follow from de Broglie wavelength $\lambda = h/p = d_f/2$, in which h is Planck constant, p is momentum of nucleus, $(d_f/2)$ is radius of flux ($3 \cdot 10^{-12}$ *cm).*

Thus, localization speed v for nucleus with mass number A and its kinetic energy T are

$$v \approx (2 \cdot 10^3 / A) \text{ km / s}$$

$$T \approx (20 / A) \text{ keV}$$

Flux observations

Zn-Ga Spread Leap for Earth's Crust Elements

For speed of Earth's revolution 30 km/s all nuclides with mass number A > 66 may have been captured and transformed by fluxes. Thus, probably, we have Zinc-Gallium spread leap (mass spread, %):

$_{28}$Ni (0.02) $_{29}$Cu (0.01) $_{30}$Zn (0.02) - farther elements spread fall on tens or hundreds times usually! - $_{31}$Ga (10^{-4}), $_{32}$Ge ($4 \cdot 10^{-4}$), $_{33}$As ($5 \cdot 10^{-4}$), …

Some such nuclear processes are periodical. They can be connected, for example, with the Earth rotation around its axis, with the Moon rotation around the Earth or with rotation of system the Earth - Moon around the Sun.

Various very complex chemical and biological processes are possible althow [3]. The interest to known "astrological" results of the professor Simon E. Shnoll [4], showing about certain cosmophysical factors influence on radioactive decay, strengthens the researches of the professor Nikolaj G.Goleminov, which not only has confirmed with the help of the improved technique basic results of Shnoll's group, but also in addition has established influence of the Moon phases on a terrestrial radio-activity [5]. Space non homogeneous of threads and flux electromagnetic and nuclear activity are explained Shnoll-Goleminov nuclear effects.

Andrei Olkhovatov has got collection of the descriptions of geophysical meteors - strange luminescences in an atmosphere and local explosions creating on the Earth "lunar" craters improbable from the point of view of traditional science. Nuclear activity of "fluxes" explains Olkhovatov's "meteors"[6].

Liquid Bubble Accelerator?

Now there is a numerous world community of the scientists engaged in problems " cold nuclear transmutation " - of mysterious set of nuclear transformations. The number of the publications about observable not clear nuclear transformations steadily grows. Whether it is possible to explain this phenomenon, not resorting to accusation of the experimenters of carelessness or, it is worse than that, in falsification of results of their measurements?

If powerful influences on dielectrics occur due to transmutations, it is possible to explain them by formation of microscopic cracks or bubbles (cavities) in liquids. In cavities then there is ions and electrons acceleration of up to energy, sufficient for overcoming of Coulomb barrier, interfering to course of ordinary nuclear reactions. At bubble expansion in liquid, placed in an electrical field, on walls of a bubble the charges of an opposite signs Q were formed. Then because of electrical capacity reduction in expansion process of a bubble along a vector of external electrical field intensity from the initial size d up to final D the increase of a difference of potentials between opposite walls of a bubble U = Q/C about D/d is possible. At d ~ 10^{-8} cm (characteristic interatomic distance) and D ~ 10^{-4} cm (the size of

a cavity) D/d value is received ~ 10^4. At usual energy of break of molecules about 1 eV and appropriate initial value of a difference of bubble walls potentials about 1volt we can receive in process of expansion of a bubble a difference of potentials between its walls U about 10 kV. Further we can receive multiplication of potential U at the electrical discharges between charged walls of the next (neighbouring) bubbles. So, on a chain from N of the consistently located bubbles the difference of potentials can achieve value about NU. Hence, at N ~100 in a chain of bubbles there can be voltage about megavolt, sufficient for overcoming by the sped up ion of a barrier of this or that nuclear reaction.

It is possible, that the described mechanism of ions acceleration in extending vacuum microcavities (in cracks) will explain results of some experiments on " cold nuclear transmutation ". Probably, the mechanism of particles acceleration, offered by us, plays an essential role in an atmosphere (in cloudy drops) and at oceans. But it obviously can not explain available results of experiments on transmutations in the gas discharge, Shnoll-Goleminov nuclear astrology and Olchovatov's geophysical meteors. In opinion of the author of the given paper all discussed above experimental results can be interpreted as displays of strings (threads) of a hypothetical matter – "fluxes". However detailed explanation of the available unusual phenomena on the basis of properties of a unusual matter is premature - at first it is necessary to find it in direct experiments.

The fluxes search in dielectric liquids

The structure of a liquid is dynamical and can quickly adapt to varied external influences.

If fluxes penetrate all bodies and their influence on these bodies varies in time, for example, because of change of flux density by Earth or Moon rotation, how we already discussed above, fluxes can cause in liquids located not far apart, various synchronous changes of their properties. Probably, today such changes are perceived by the researchers as casual fluctuations. For the first time on abnormal - not casual - character of viscosity fluctuations of biological liquids (blood) have paid attention biophysics. For past half-centuries, first of all, due to works of group of the professor Shnoll, the laws in various «casual» chemical and physical processes - even such, as radioactive disintegration are found. However absence of a rational physical explanation of such laws till now does not allow many researchers to engage in this problem.

For researchers of the various characteristics of liquids we can to put series of experiences for detection of non casual character of this characteristics fluctuations. For this purpose it is desirable to carry out measurements of same physical parameter of a liquid on two, and it is better - on the large number of independent identical devices. These measuring devices it is desirable to have got on various distances from each other. If the devices measure the vector characteristics - such, as polarization of a light beam or ion drift velocity in a liquid, it is desirable these measuring devices to place under different corners to an axis of the Earth rotation. All subjects declared on the given conference are interesting to such of correlation measurements:properties of charge carriers, electrical conduction, space charge effect, pre-breakdown and breakdown phenomena, interaction of radiation with liquids, optical properties, biophysics phenomena and so on. Intermolecular emptinesses (Frenkel's holes) can be transformed in liquids into thread-like vacuum channels. The movement of electrons of ionization in liquids with such channels may depend on the orientation of the channels inside (produced by ions) and outside electric fields, as well as from the length and tightness of the vacuum channels. Thus the dark matter is changing the liquid structure and its radiation properties constantly even if dark matter itself does not ionize and not excite the liquid. Such production of correlation experiences on driven or rotating platforms and on the companions of the Earth is interesting.

Fibrous World

All matter, which we know, has string like form already externally or has string internal structure. All biological tissues are alike - internal structure of cell penetrated by thready channels. Their membrane also «are weaved» from string like fibers. There are many forms of string or cotton wool like inorganic crystals (most known is asbestos). Other solids consist of the densely stacked ordered fibres, which is seen even by a unaided eye. Three-dimensional lattice of crystalline solids atoms (molecules) located on almost ideal direct lines. After evaporation of various materials (by electrical discharge or laser) in gas the condensed atoms (molecule) usually form fibres.

On space photos of the Earth the hurricanes are similar to huge spirals of fibrous chains of clouds. The spiral galaxies like terrestrial hurricanes, only instead of drops of water a fibre of galaxy spirals consist of stars. The Universe like cotton wool consist of galaxies chains. Thus, all substance like global cotton wool. It allow to assume, that all forms of a matter, seen by us, are structured by invisible strings, on which atoms, molecule, micro- and

macroparticles, stars and galaxies «thread» as beads in a necklace. Such invisible strings connecting all substance of the Universe, may be fluxes.

At liquid hardening process, caused by electromagnetic interaction, molecules can be placed on the threads of the dark matter and so can shape three-dimensional lattice of crystals. As all substance of the Universe is in relative movement, we notice, that reorganization of all structures by fluxes is a permanent process.

The biology facts, difficultly giving in to an explanation, have been submitted by Vladimir L. Voejkov [7]. For example, surprising properties mitogenetical radiation open by the professor Gurvich more half-century back till now are not explained Gurvich had searched a strange light, energy and information transit through solids and liquids in biology (Gurvich rays). A kind of mysterious magnetic fields peculiarity of Earth are "magnetic non potentiality" and Nikolai Kulanin's magnetogeomorphology effect [8].

Cosmic Linear Dark Matter Possible Displays

In a normal (latent) status fluxes are invisible. May be, flux threads penetrate through ordinary atomic matter including a solid bodies and associate with all celestial and the ground objects. Distance between flux threads 10^5 km is enough for Universe hidden mass explanation. On stars and planets flux thread density may be very high. If distance between threads is about normal atomic diameter the flux wadding can put in solid and liquid bodies strongly and to carry they away (in this case flux dark matter density is exceeded 100 kg/cm^3). May be, electromagnetic pinch-effect in normal atomic matter with dens flax wadding can black hole form.

Superconductivity of flux threads forms the Universe electromagnetic properties. Wave guides by flux thread can be responsible for super bright optical or radio celestial objects existence, visual non homogeneous Universe.

We think, that dense thread (string) dark matter is displayed themselves on Earth at earthquakes, hurricanes, tornadoes probably.We think, that dense thread (string) dark matter is displayed themselves on Earth at earthquakes, hurricanes, tornadoes and tides probably.

Registration of vertical currents on their magnetic effect

For more than a hundred year the problem of the so called vertical currents has been existing, the vertical currents flow along the terrestrial radius and through the bowls and the Earth's atmosphere. The geophysicists consider the vertical currents in relation to the necessity to explain the regional spatial changes in the horizontal constituent of a geomagnetic field (inclination). The first maps of vertical current distribution, which were calculated by A.W. Rücker, for the British Isles (1891[8]), have resulted in a paradoxical big magnitude for the density of these hypothetical currents – up to 2 A/km^2 in the north of Scotland. This magnitude is approximately close to the average density of telluric currents (around 2 A/km^2), but surpasses the maximum possible density of ion current on earth level in billion times - around 2 μA/km^2.

With the increase in the accuracy of magnetic measurements and the decrease in the distance between the measuring stations up to few meters, it was established that the magnitude of the vertical currents at some places on Earth can be even bigger. By the geomagnetic measurements on a small scale areas N.V. Kulanin has established, that the density of vertical currents can reach unbelievable values – of order 100 A/m^2. On a more or less contrast relief their value usually varies from 10 μA/m^2 up to 10 mA/m^2 (from 10 A/km^2 up to 10 kA/km^2 [8]). Such experimental results are accepted by the geophysicists with a deal of skepticism since a physical model is absent, which would explain the existence non-ionic atmosphere currents (with a density higher than 2 μA/km^2).

Fammeter

For the direct measurement current's value in any environment or surroundings, we have tested a sensor – fammeter (flux ammeter) – which consist of sensor of external current and the attached to it shielded power cable with line or autonomous power supply [10]. The sensor fammeter represents a hollow steel tore with a height of 30 mm and outer diameter of 150 mm and inner diameter of 80 mm. Through the tore the measured current i or a special calibration current to set up the sensor I passes through. The steel shell acts like magnetic and electromagnetic shield of the sensor. Inside this shield are placed two enclosed circular similar magnetic conductors' cores 1 and 2 made of amorphous iron with a rectangular hysteresis loop ((fig. 4). The magnetic conductor circles are placed in alignment, with a circle diameter d, they cover a cross section area of $s = \pi d^2/4 \approx 10^{-2}$ m^2, through which the current i is measured.

For this circular core, three windings of copper wire exist: w_1 – to create a weak permanent magnetic flux inside the circle, w_2 – for the purpose of creating instant impulsive magnetic flux, which temporarily sets each circle into saturation state (fig. 4), and the measuring inductor w_3 . In the absence of a direct current (i or I on fig.4) through the surface, which is covered by each circle, both cores are magnetized by the impulsive current of the similar hysteresis looping. A constant current in the windings of w_2 magnetizes the core and sets it into a state corresponding to the point a on the upward part of the hysteresis loop. A rectangular current impulse in the windings of w_3 with a repeating period of T (approximately 2 ms) magnetizes the cores and sets into a state corresponding to point b on the saturation section of the hysteresis loops. At the same time on the measurement windings of w_3 (from here on, this symbol refers to number of rings in the measuring inductor) two similar voltage impulses are formed u_1 and u_2. Since the measurement windings have been set up with an opposite current flow, and the resulting voltage on the output of the sensor corresponds to the value $u = u_1 - u_2$ which is approximately zero. When there is an i current passing through circular cores, the direction related to the i additional constituent of the intensity of magnetic field $\delta H = i / \pi d$ does coincide with one of the circular cores, while the other opposite to the direction of the initial intensity vector of the magnetic field H (dotted line on fig.4). The cores are magnetized – one of them from the state of point a_1, and the other from the state of point a_2, to the state of point b by a different private cycles of hysteresis loops. the area under the curve that is showing the dependency of voltage impulse to the time on the outlet of the sensor is equal to

$$(B_1 - B_2)\, sw_3 = \mu\mu_0 j sw_3 d/2,$$

where $(B_1 - B_2)$ – represents the differences in magnetic induction between the points a_1 and a_2 (fig. 4), μ - is the relative magnetic permeability on the upward part of the hysteresis loop, μ_0 – magnetic permeability of the vacuum, j – the density of the measured current. The relatively high value of the amorphous iron magnetic permeability on this upward part ($\geq 10^6$) ensures the necessary sensitivity of the fammeter sensor. The signal coming from the outlet of the sensor is manipulated by the electronic block (which has been already mentioned in the description of this fammeter) is fixed by micro ammeter with a point indicator. Naturally, the change in direction of the current i changes the sign of the voltage on the outlet of the sensor.

Measurements

The described fammeter [10] has confidently determined signals that correspond to a value of $j \geq 1$ mA/m^2. Smaller currents were determined as the average value of the micro ammeter of the fammeter electronic block at consecutive measurements. While experimenting with the fammeter, it was observed that the resulting readings did vary in time, and in average would correspond to the density of the measured currents j of values approximate to 1 mA/m^2. For this particular reason, the further readings were made in series of no less than six couples of measurements. In order to get rid of the effect of geomagnetic field, that penetrates through the shield and the influences external effects on the shield a differential measurement method was used. For this reason we repeated each reading in the series twice – for two symmetrical orientations of the sensor near the vertical line, each time corresponding to the maximum module of the currently measured signal. The differences of each pair signals were fixed. This measuring method allowed to further improve the accuracy of the measurement by an order, up to 0,2 mA/m^2.

Results

The measurements that were taken along many days showed distinct current density correlations with the constant effect of the astro- and geophysical phenomenon, such as the change in the Earth positioning in relation to the Sun [10].

The sunrise is fixed by the fammeter with accuracy up to a minute (this is the required time for making a pair of measurements) in accordance to the exact minimum of current density in a series of six pair's consecutive measurements. For example, the series that was held at the 7th of march 2006 between 07:02 and 07:07 (Moscow mean time) the average current density was –0,8 mA/m^2 (the minus sign indicates that in this case the direction of the positive charges' movement is toward the center of the Earth). At the minute of the sunrise (at 07:06) the density of the current in an stepwise manner decreased to a value of -2,2 mA/m^2. On the next day the 8th of march 2006, we had a corresponded set of statistical values in the duration of time starting at 07:01 till 07:06, the average current density was -0,1 mA/m^2, and at the minute of sunrise there was an increase in the value up to -2,0 mA/m^2. The frequent repetition of this effect is due to the fact that we are registering a previously unknown phenomenon that is connected to the sunrise and not to the noises of the sensor. At the same time, there are days with predominantly positive or negative, and days with varying in

directions vertical currents. In which the average positive current increases towards the night and is minimal during night time, and the negative current is of minimal value during the day [10].

Conclusion

1. Flux theory is *ordinary* academic physics with unusual conclusions
2. The flux model of environment (active dark matter) can explain the many natural and artificial facts, which have now primitive or nonscientific explanations.
3. The flux model of environment and flux model of cold nuclear activity can explain the time-place instability phenomena in nature and in laboratories. It is supposed, that fluctuation of various parameters of liquids researching it is possible to find out geo- and astrophysical flux fields.
4. We hope, that further elaboration of the electric currents measurements on the flux in near cosmos, on Earth and around "alchemical" equipment apart will make clear reasons of its – fluxes and equipment - function.
5. Such researches will allow not only to receive the fundamental information on a new kind of a matter and about its interaction with substances, but also to develop of a different sort useful geophysical liquids detectors. They can be used, for example, for a prediction of artifishial and natural phenomena, which is harmful for people.

References

1. B.Rodionov Thready (Linear) Dark Matter Possible Displays. Gravitation & Cosmology, v.8, Supplement, 2002. Pp.214-215, see also on p.209 On the Way to New Physics
2. B.Rodionov, "Multyparticle Nuclear Reactions" in Problems of Cold Nuclear Transmutation of Chemical Elements and Ball Lightning, Proceedings of the11-th Russian Conference, Dagomys-Sochi,2003. Moscow, 2004, pp.189-19 (Russian).
3. B.Rodionov, I.Savvatimova "Unusual Structures on the Material Surfaces Irradiated by Low-Energy Ions" in Condensed matter nuclear science, Proc. of the 12-th Int. Conf. On Cold Fusion. Ed. Akito Takahashi, Ken-Ichiro ota Yosuhiro Iwamura, World Sc.Publ. Co.Pte Ltd. New Jersey-London-Singapore-Bejing-Shanghai-Hong Kong – Taipei-Chennai, 2006, pp 421-429S.

4. E.Shnoll, E.V.Pozharski, T.A.Zenchenko, V.A.Kolombet, I.M.Zvereva and A.A.Konradov “Fine Structure of Distributions in Measurements of Different Processes as Affected by Geophysical and Cosmophysical Factors,”Phys. Chem.Earth (A), vol.24,no.8, pp.711-714, 1999.
5. N.G.Goleminov,”Possible Nuclear Activity of Dark Matter” Gravitation & Cosmology, v.8, Supplement, 2002. Pp.219-220
6. A.Olkhovatov and B.Rodionov “Tunguska Shine”, “Basic Knowledge Laboratory”, 1999, p. 196-240, Russian.
7. L.V.Belousov, V.L.Voejkov and S.A.Popp Gurvich Mitogenetical Rays. Nature, № 3, 1997, p. 64-80, Russian
8. Nicolas V.Kulanin. New Aspects of the Magnetogeomorphological Effect. Gravitation & Cosmology. V. 8. Supplement, 2002. Moscow. P. 225-226.
9. Rücker A.V. Recent Researches on Terrestrial Magnetism. Nature, 1897. V.57, No 1468. P.160-163.
10. B.U.Rodionov, M.V.Nemtzov and A.I.Zaitzev ‘Registration of Electrical Current in Physical Vacuum”. Proc. Asia-Pacific Conf. On Environmental Electromagnetics – GEEM’2006, vol.2 of 2, Aug.1-4,2006 Dalian, China, pp.648-651; see also Proceedings Second International Symposium on Unconventional Plasmas, ISUP-06, 14-16 August 2006, Eindhoven, The Netherlands. Editors D.K. Callebaut, G. C. Dijkhuis & H. Kikuchi

ILLUSTRATION

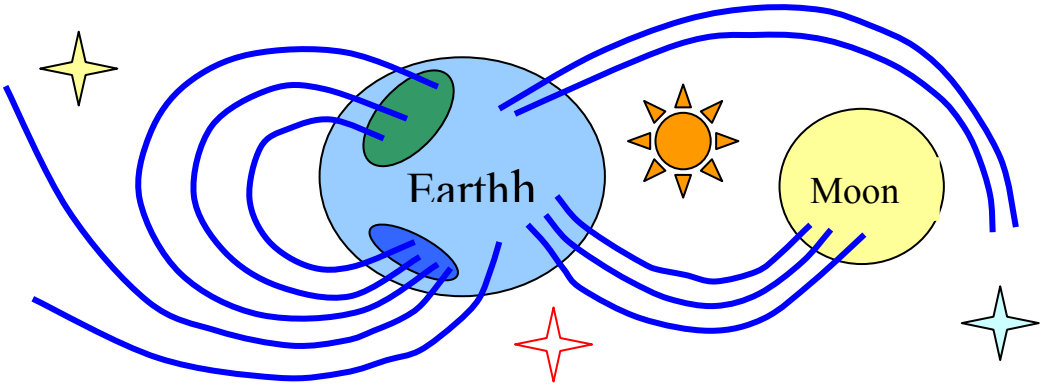

Fig.1

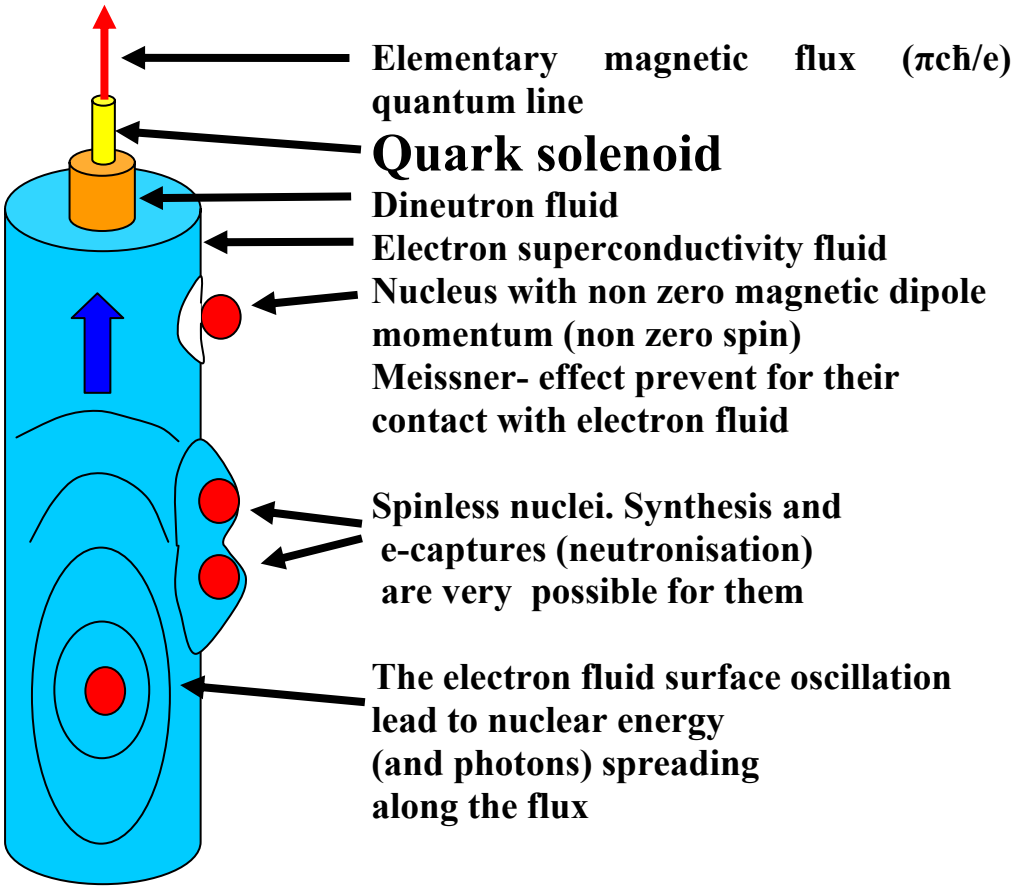

Fig.2. Flux structure

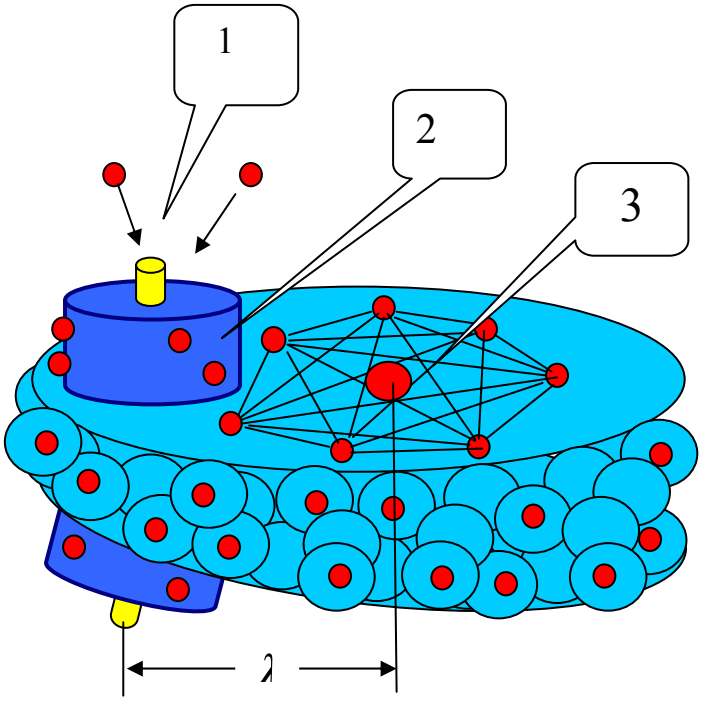

Fig.3. Nuclear Reactions:

1. On the flux end that is the magnetic pole with Dirac's magnetic charge
2. On the flux electronic shell that is a very good screen for electric charges of nuclei and place for electron captures
3. On the quantum molecular ensemble, which fluxes formed

Registration Circuit

Two similar magnetic conductors' cores

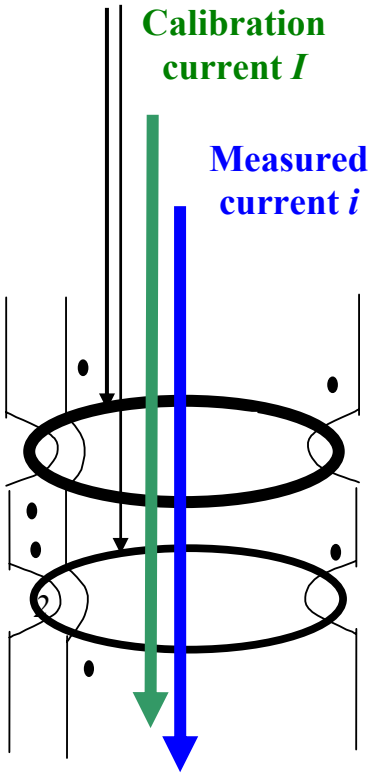

w_1 w_2 - *Coiles* - w_3

Signal Formation
Prof. M.V.Nemtzov's Idea

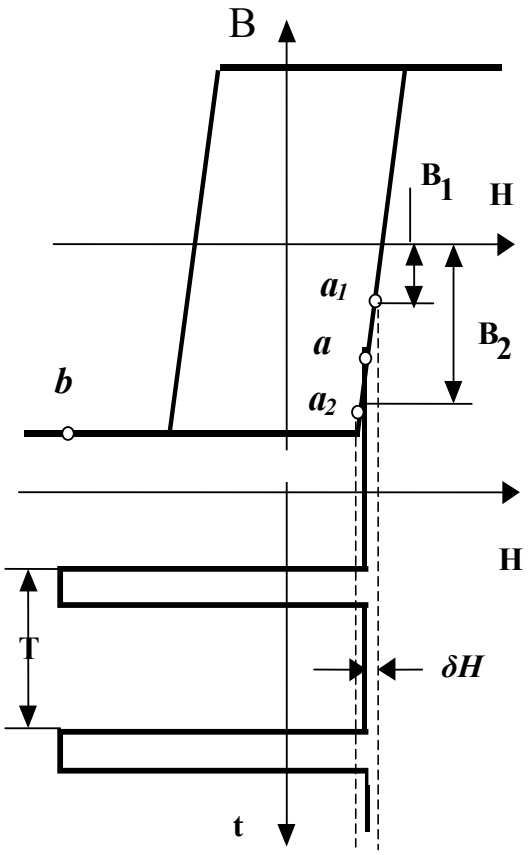

Fig.4 Fammeter

w_1 – to create a weak permanent magnetic flux inside the circle, w_2 – for the purpose of creating instant impulsive magnetic flux, which temporarily sets each circle into saturation state (signal formation picture), and w_3 - the measuring inductor.

COLD FUSION HEATERS

Talbot A. Chubb

Greenwich Corp., 5023 N. 38th St., Arlington VA 22207, USA, tchubb@aol.com

Abstract

One successful approach towards development of cold fusion heaters makes use of interfaces between ionic crystal solids and nanometal palladium as sites for promoting radiationless dd fusion. Iwamura et al. (1998) used deuterium permeation through plates of Pd metal containing layers of CaO separated by layers of sputtered Pd and achieved Watt level excess heat in electrolysis-driven permeation studies. Arata and Zhang (2002) used a powdered composite of ZrO_2 and nanoPd inside an electrolysis-pressurized Pd bottle cathode and achieved 10 W of excess heat for 3 weeks. Arata and Zhang (2007) (ICCF12) used the same ZrO_2, nanoPd composite in a gas-pressurized Pd bottle in a demonstration of excess heat at elevated temperature. It is argued that their ICCF12 fusion heat was about 0.6 W, which compares with an external heater power of 1.7 W. If this fusion power could be increased by a factor of 3, the heater could be disconnected after reaching operating temperature. Studies and discussion by Yamaura et al. on the ZrO_2, nanoPd composites support a view that substantial deuterium is stored in the interface region between ZrO_2 and nanoPd. It is argued that epitaxial deuterium on ZrO_2 crystals interfaced with nanoPd is in the form of quasiparticles that have the lattice geometry needed for 2-dimensional Ion Band State fusion. Past studies show that increasing the deuterium chemical potential and fluxing lead to higher fusion rates.

Introduction

This paper focuses on 3 subjects: further analysis of Arata and Zhang's (A-Z's) ICCF12 gas-loading fusion study using ZrO_2, nanoPd powder and its implications regarding autonomous cold fusion heaters[1], a modeling of Yamaura et al.'s comments on the ZrO_2-nanometal interface environment[2], and argument that high deuterium chemical potential and fluxing flow should continue to be used in pursuit of practical cold fusion heaters.

The A-Z Excess Heat Studies, Background

Since 1994 A-Z have carried out a highly successful program studying the production of cold fusion heat in nanometal Pd, mostly in the form of Pd-black.[3] Their program has utilized electrolysis of heavy water electrolyte to deposit D atoms onto the cylindrical surface of a Pd-metal bottle with stainless steel (ss) ends. Their bottles, called "DS-cathodes", were filled

with Pd-black. The powder was thoroughly evacuated, but presumably not reduced, before being sealed within the bottle and exposed to D_2 gas. During their tests, electrolysis deposited D atoms onto the surface of the bottle's Pd cylinder. Deuterium then diffused through the cylinder and onto the surface of Pd black, rapidly spreading over the assembly of contacting Pd grains. The catalytic name for such surface deuterium is "Spillover Deuterium". The gradual pressure build-up of intergranular D_2 gas within a DS-cathode has been shown to exceed 800 atm. Post-run analysis of gases desorbed from Pd-black that had produced heat showed substantial adsorbed water[4] and clearly detectable ^{4}He gas[5]. The desorbed ^{4}He was less than that commensurate with excess heat at 24 MeV per ^{4}He atom detected, probably because of leakage through the surface-stressed bottle subsequent to heat generation.[6] Post-run desorbed ^{3}He has also been detected, some of which is known to have been produced by decay of ^{3}H.[7]

In 2002 A-Z reported on a study in which the Pd-black in the bottle cathode was replaced by a powdered composite of ZrO_2 and nanoPd.[8] This study was the first to use a nanometal other than Pd-black. Yamaura et al. published a description of the manufacturing method by which the composite was produced. Yamaura et al. have characterized the powder by its absorption and desorption of hydrogen during pressure change studies, its crystal structure as deduced from x-ray Bragg diffraction and electron scattering, and by images showing Pd embedded in a ZrO_2 crystal matrix. In the A-Z (2002) electrolysis study, the powder produced a continuous 10-W of excess heat for 3-weeks, at which point the run was terminated.

Calculation of Fusion Heat Power in A-Z's ICCF12 Gas Loading Study

In ICCF12 A-Z reported on a study in which ZrO_2, nanoPd composite was used in a gas loading experiment at elevated temperature.[1] No electrolysis was employed. A-Z replaced the electrolysis cell used in their DS-cathode studies with a gas containment vessel called an "outer stainless vessel", or "ss-vessel". The interior Pd bottle that had been used as a Pd cathode in the electrolysis studies was renamed the "inner Pd-vessel" in the gas loading studies. The outer ss-vessel was embedded in an insulated heater coil, which was used to raise the temperature of the assembly before adding gas to the test system. In their 2002 fusion study, they filled the inner cylinder with powdered composite, pumped it down with a 10^{-7} Torr vaccum for 2 days, and sealed it off under vacuum.[8]

The gas loading fusion tests were performed in a 2 step operation, as shown in Figure 1. The first step was a warm-up period during which the assembly was heated and temperature stabilized at a desired operating temperature. During the warm-up period the coaxial volume between inner and outer cylindrical vessels was kept under vacuum. To shorten the warm-up period A-Z turned on the heater coil at an initial power of about 21W, as shown in their Figure 8. As the temperature T_{ss} of the ss outer vessel rose, they reduced the heater power so as to gradually approach a stabilization temperature of Tss = ~140 ^{o}C. Stabilization at 141 ^{o}C required a steady input power of 1.71 W, as shown in A-Z's Figure 8, and as reproduced in the left plot of this paper's Figure 1. The second step initiated cold fusion energy production. A-Z flowed D_2 gas into the coaxial volume between inner and outer vessels until the pressure reaching about 80 atmosphere. Gas diffused through the Pd wall of the inner vessel, and was absorbed by the ZrO_2, nanoPd composite, releasing transient chemical reaction heat. During

the rise in gas pressure in the inner cylinder, the temperature of both inner and outer vessels gradually rose, with the inner vessel temperature rising above that of the outer vessel. T_{ss} stabilized at ~183 ^{o}C. Throughout this period the heater power was kept at 1.71 W. The rise of T_{ss} was 42 ^{o}C. This temperature rise can be used to calculate the fusion heat being generated inside the inner vessel, under the assumption that fusion power from the inner vessel and heater coil power produce equal increases in T_{ss} per Watt. If the heat flow path from the ss vessel to the room temperature environment is from the ends to the ss-vessel, which includes the D_2 supply tube, the assumption should be valid. The calculated fusion heat is 0.61 W. Details are shown in Figure 1. The fusion power was more than one third of the heater power that maintained T_{ss} at 141 ^{o}C. This means that if one could increase heat production by a factor of 3, one could turn off the heater and maintain a temperature of 183 ^{o}C with zero input energy. A heater that continues to stay hot with no external power would be a convincing demonstration of cold fusion heat.

It is not clear whether one should expect the fusion rate in deuterided ZrO_2, nanoPd composite at 80 atm to increase or decreases with increasing temperature between 141 ^{o}C and 183 ^{o}C. It seems possible that the fusion rate at 141 ^{o}C is a factor of 2.9 higher than at 183 ^{o}C. If so, A-Z could have turned off their heater power once the composite had absorbed its equilibrium fraction of deuterium. They would then have demonstrated autonomous cold fusion heater operation.

ZrO_2, nanoPd Composite as a dd-fusion Host

Fabrication of ZrO_2, nanoPd composite appears to be an important step forward in development of cold fusion heaters. The material is produced using a documented protocol. It stores deuterium at a D/metal ratio about 3 times that achievable in bulk Pd metal. It seems to establish conditions promoting dd fusion using reversible equilibrium chemistry. The heat producing deuteride seems to survive heat generation for week-long periods without noticeable degradation.

Fabrication and characterization of ZrO_2, Pd composite is described in a paper by Yamaura *et al.* titled "Hydrogen absorption of nanoscale Pd particles embedded in ZrO_2 matrix prepared from Zr-Pd amorphous alloys".[2] The ZrO_2, nanoPd composite was prepared by oxidizing ribbons of rapidly solidified amorphous Zr_{65} Pd_{35} atom % alloy. X-ray diffraction showed that the ZrO_2 was present in a mixed structure of monoclinic and cubic phases. No other distinct phase was seen. The absence of Pd x-ray diffraction peaks was presumed to be due to extremely small particle sizes of the Pd phase. Electron diffraction spectra of selected areas showed fcc Pd (111), Pd (200), etc. reflections. Transmission electron micrograph images gave an estimated nanoPd volume of about 20%. The images showed a spherical morphology and an averaged Pd particle size of about 10 nm, with the Pd particles isolated from each other. The main feature emphasized was the remarkable ability of the material to absorb hydrogen gas. Ordinary Pd metal is famous for its ability to absorb hydrogen, but the nanoPd material absorbs about 3 times more hydrogen per Pd metal atom. In bulk Pd metal the H/Pd ratio x in equilibrium with H_2 gas at 100 atmosphere near room temperature is about x = 0.82. The ZrO_2, nanoPd showed a ratio x = ~ 2.9. A separate study using ZrO_2, nanoAu composite showed that essentially none of the absorbed hydrogen is stored in the ZrO_2 crystalline component. So, where does the hydrogen go? Some of it enters the Pd metal lattice, just as

occurs with bulk Pd. In hydrided bulk Pd, H ions occupy octahedral sites in the fcc lattice. Yamaura *et al.* suggest that much of the H in the nanocomposite may go into a "tremendously large interface area in the composite" between nanoPd and ZrO_2 crystal. Deuterium-saturated interface regions[9] are candidate hosts for dd-fusion reactions in accord with Ion Band State Theory[10].

In building on the Yamaura *et al.* work, I quote their 2002 suggestion, "In addition to the dispersion state of Pd particles in the nanocomposite, the ultrafine particle size of about 10 nm in an isolated state allows us to presume that the tremendously large area of interface of the nanoscale Pd powders has rather loose atomic configurations with higher volume fractions of vacancies which are favorable for the absorption of hydrogen. In Fig. 5, it is conceivable that a large amount of hydrogen can be trapped at the interface between Pd particles and ZrO_2 matrix, while the plateau stage becomes narrower as previously reported.[5-8]" The Yamaura *et al.* references 5-8 refer to publications between 1988 and 1999. "Zuettel *et al.* reported that hydrogen absorption of solitary Pd clusters decreased with a decrease of cluster size. Pundt *et al.* studied hydrogen absorption of composite material consisting of isolated Pd clusters dispersed in a polymer matrix and reported that hydrogen solubility increased and the miscibility gap became narrower as compared with those of the bulk Pd metal. Eastman *et al.* showed that the hydrogen solubility of nanocrystalline and coarse-grained Pd metals increased with decreasing grain size and the miscibility gap of Pd nanocrystals was smaller than that of Pd bulk." The hydrogen absorption/desorption data reported by Yamaura *et al.*[2] is in essential agreement with that reported by Arata and Zhang. Arata and Zhang[8] measured the H_2 absorption/desorption properties of a test sample of ZrO_2, nanoPd composite before running a cold fusion test. They then used over-voltage electrolysis to load a run sample with deuterium, and obtained 3 weeks of excess heat at a 10 W level, as shown in their Fig. 4.

When hydrogen is added slowly to a test sample of bulk Pd in the form of metal filings, the equilibrium H/Pd ratio x increases with pressure. When the gas pressure is reduced, x decreases. The P vs. x curve during absorption is higher than during desorption, demonstrating hysteresis. Hysteresis causes energy loss when Pd is used for cyclic storage of hydrogen. The hysteresis is primarily due to the fact that the hydrogen is stored in self-trapping sites. When an H^+ ion enters an octahedral site in Pd's fcc lattice, the adjacent Pd atoms move apart to provide volume for the electron charge needed to neutralize the ion. The elastic strain energy expended in self-trapping is not fully recovered during desorption. Similar hysteresis is observed when hydrogen is stored in and removed from ZrO_2, nanoPd composite at subatmospheric pressure. But at H_2 pressures > 1 atmosphere, Yamaura *et al.*'s measurements show little or no hysteresis in the cyclic storage process.[2] Absence of hysteresis in the higher pressure regime suggests storage of H^+ in non-self-trapping sites. (I write H^+ instead of H because metal physics treats the neutralizing "electron" as part of the metal and not part of an atom.) Self-trapping breaks periodic symmetry, which violates conditions required for cold fusion as predicted by Ion Band State Theory.[10] A requirement for periodic order means that some deuterium must partially fill an array of non-self-trapping potential wells for dd-cold fusion to occur.[11]

The Nuclear Active Environment

In deuterided ZrO_2, nanoPd composite there are two types of location where cold fusion could be occurring. Both are arrays of unit cells containing non-self-trapping sites which can become partially filled with deuterium. One type of unit cell array provides a communicating network of shallow potential wells, with wells located at the two tetrahedral sites and the single octahedral site of the Pd fcc unit cell. An unoccupied octahedral site has too deep a potential well to meet the shallow well requirement. To function as a shallow potential well, the octahedral site must already contain a D^+ ion. It can then provide accommodation for additional deuterium within its peripheral volume. Referring to bulk Pd, McKubre and Tanzella state in *Proc. ICCF12*, "Present theory and results focus new attention on the very high loading region as x approaches or even exceeds unity, where double occupation of octahedral sites, tetrahedral site occupancy, new phase formation or new electrical states, may be relevant to the underlying physical process of excess heat and nuclear production".[12]

The other candidate array is a ZrO_2, nanoPd interface. Deuterium in the interface can be modeled as a form of crystalline liquid metal plasmoid (LMP)[13]. The ionic solid ZrO_2 is stabilized by its highly negative Gibbs free energy. It imposes a periodic electrostatic field on the adjacent volume. This periodic E-field serves as a lattice template that imposes lattice order on adhering Pd metal atoms. This problem has recently been modeled for Pd metal cluster configurations in contact with MgO.[14] Energies were calculated for exact epitaxial mapping of Pd atoms onto the MgO(001) pattern. If an epitaxial layer of interface deuterium between ZrO_2 and Pd metal clusters lowers system energy and helps stabilized epitaxial Pd atoms, the interfacial deuterons would reside in non-self-trapping sites because of the stability of the ionic crystal. In contrast, the spaces between the non-epitaxial Pd atoms would serve as potential wells accommodating dissolved interstial deuterium in self-trapping sites. This structure fits the description given by Yamaura *et al.* when they "presume that the tremendously large area of interface of the nanoscale Pd powders has rather loose atomic configurations with higher volume fractions of vacancies which are favorable for the absorption of hydrogen".[2] Yamaura's rather loose atomic configuration of interface Pd atoms would configure itself so as to minimize system energy by allowing a near epitaxial Pd layer to exactly match onto the periodic electrostatic field imposed by the ZrO_2. In the crystalline LMP picture wavelike epitaxial deuteron quasiparticles have superfluid behavior like the atoms in well studied atom Bose condensates in optical lattices.[15,16] Lab experiments and energy-minimizing calculations are needed to further define the crystalline LMP picture.

The crystalline LMP model is an extension of an ionic solid, Pd-metal interface picture[9] proposed to explain the transmutation observations by Iwamura *et al.*.[17] The Iwamura transmutations seem to be exothermic alpha-addition nuclear reactions. The overall process is explainable as a four-step process in which the first step is a dd fusion to ^4He. The final step is the 2-alpha addition reaction that changes ^{133}Cs into ^{141}Pr.[9] The Iwamura *et al.* process is a gas-driven permeation process. It uses a permeation reactor plate containing 5 CaO layers separated by 5 layers of sputtered Pd. Control studies show that reactor plates without the CaO layers do not support the transmutation process. Interfaces between ionic solid CaO and loosely organized Pd seem to fit the same crystalline LMP picture described above.

High Deuterium Chemical Potential and Fluxing

A-Z's 2002 study using over-potential electrolysis onto a DS-cathode produced about 20 times the fusion power per gram Pd as achieved in their 2007 gas loading study. Iwamura *et al.* published work in 1998 which used overpotential electrolysis to drive deuterium permeation through permeation plates containing CaO, sputtered-Pd interfaces. They reported 5 runs showing Watt-level excess heat.[18] This fusion power is maybe 100 times larger than the heat power produced in their subsequent transmutation runs. It is therefore argued that it is important to included elevated deuterium chemical potential and deuterium fluxing in the pursuit of near-term practical cold fusion heaters. It may also be important to include and modify the solid electrolyte methods pioneered by Biberean.[19] A closed loop process in which D_2 gas is converted into surface deuterium so as to load a metal and/or to drive a deuterium flow at high deuterium chemical potential greatly reduces the parasitic power loss and impurity problems associated with heavy water electrolysis.

References and Comments

1. Y. Arata and Y-C Zhang, "Development of 'DS-Reactor' as the practical reactor of 'cold fusion' based on 'DS-cell' with 'DS cathode', *Proc. ICCF12*, 44 (2006).
2. S. Yamaura, K Sasamori, H. Kimura, A. Inoue, Y-C Zhang, and Y. Arata, "Hydrogen absorption of nanoscale Pd particles embedded in ZrO_2 matrix prepared from Zr-Pd amorphous alloys" J. Mater. Res. **17**, 1329 (2002).
3. Y. Arata and Y-C Zhang, "A New Energy *caused* by '*Spillover Deuterium*'", *Proc. Japan Acad.* **70B**, 106 (1994).
4. W.B. Clarke, B.M. Oliver, M. McKubre, F.L. Tanzella, and P. Tripodi, "Search for ^{3}He and ^{4}He in Arata-style Cathodes II. Evidence for Tritium Production", *Fus. Sci. and Technolog.* **40**, 152, (2001).
5. Y. Arata and Y-C Zhang, "Anomalous Production of gaseous ^{4}He at the inside of 'DS-Cathode' during D_2O-Electrolysis", *Proc. Japan Acad.* **75B**, 28 (1999).
6. T.A. Chubb, "Modeling the ^{3}He Concentration in a Clarke *et al.* Gas Sample from an Arata-Style Cathode", *Proc. ICCF9*, 67 (2002).
7. P.L. Hagelstein, M.C.H. McKubre, D.J. Nagel, T.A. Chubb and R.J. Hekman, "New Physical Effects in Metal Deuterides, *Proc. ICCF11*, 23 (2002). See pp. 51-52.
8. Y. Arata and Y-C Zhang, "Formation of condensed metallic deuterium lattice and nuclear fusion", *Proc. Japan Acad.* **78B**, 57 (2002).
9. T.A. Chubb, "II. Inhibited Diffusion Driven Surface Transmutations", *Proc. ICCF11*, 678 (2006).
10. T.A. Chubb and S.R. Chubb, "Cold Fusion as an Interaction between Ion Band States", *Fusion Technol.* **20** , 93 (1991).
11. T.A. Chubb, "LENR: Superfluids, Self-trapping and Non-self-trapping States", *Proc. ICCF10*, 767 (2006).
12. M.C.H. McKubre and F.L. Tanzella, "Using H/Pd and D/Pd Loading: Method and Significance", *Proc. ICCF12*, 392 (2006).
13. LMP is a term used by Robert Bass in his modeling of ball lightning.
14. G. Barcaro, A. Fortunelli, G. Rossi, F. Nita, and R. Ferrando, "Epitaxy, Truncations, and Overhangs, in Palladium Nanoclusters Adsorbed on MgO(001)", *Phys. Rev. Lett.* **98**, 156101 (2007).

15. D. Jaksch, C. Bruder, J. I. Cirac, C. W. Gardiner, and P. Zoller, "Cold Bosonic Atoms in Optical Lattices", *Phys. Rev. Lett*. **81**, 3108 (1998).
16. M. Greiner, O. Mandel, T. Esslinger, T. W. Hansch, and I. Bloch, "Quantum phase transition from a superfluid to a Mott insulator in a gas of ultracold atoms", *Nature* **413**, 39 (2002).
17. Y. Iwamura. M. Sakano, and T. Itoh, "Elemental Analysis of Pd Complexes: Effects of D_2 Gas Permeation", *Jpn. J. Appl. Phys.* **41**, 4642 (2002).
18. Y. Iwamura , T. Itoh, N. Gotoh, M. Sakano, I. Toyoda, and H. Sakano, "Detection of Anomalous Elements, X-Ray and Excess Heat Induced by Continuous Diffusion of Deuterium Through Multi-Layer Cathode (Pd/CaO/Pd)", *Proc. ICCF7*, 167 (1998).
19. J-P Biberian, and G. Lonchampt, "Deuterium Gas Loading of Palladium Using a Solid State Electrolyte", *Proc. ICCF9*, 17 (2002).

Quantifying Excess Heat, in Arata and Zhang ICCF12

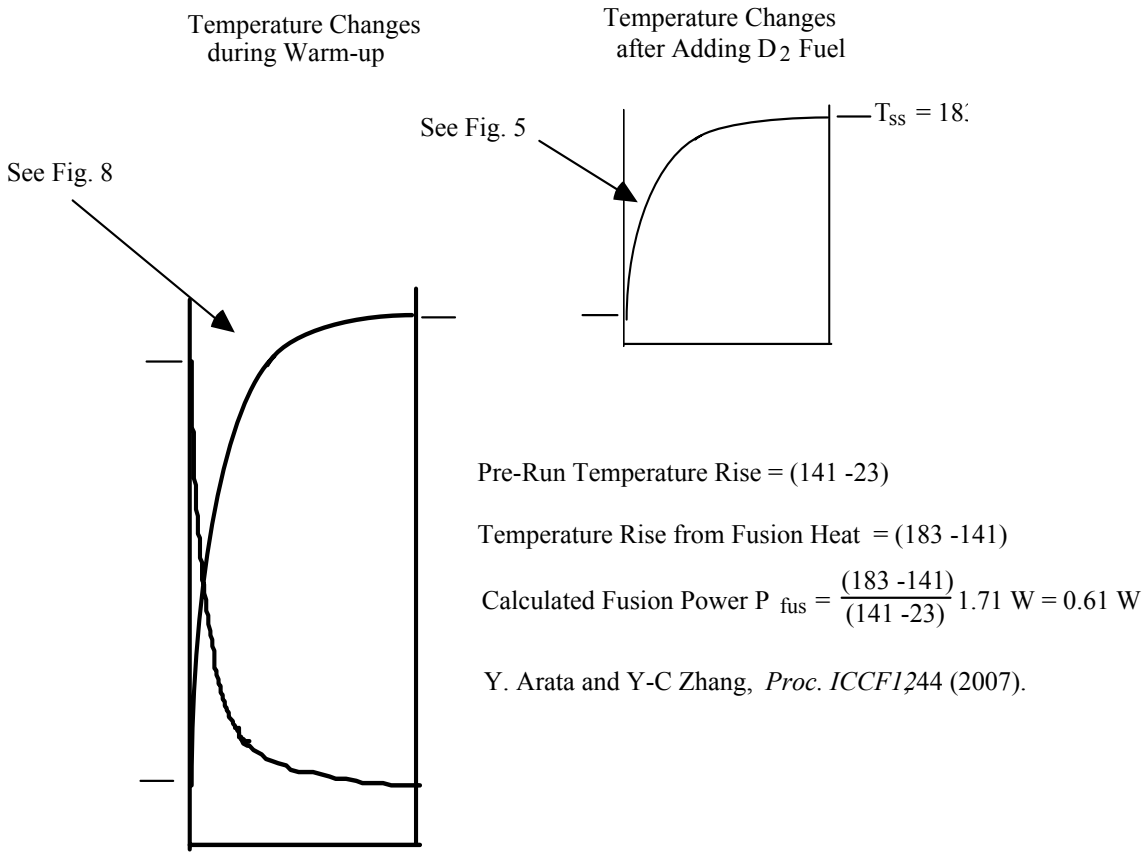

Figure 1. *Temperature and heater power history used in calculation of cold fusion power produced by gas loading of ZrO_2, nanoPd composite. Lower left plot taken from A-Z ICCF12 paper, Figure 8. Upper right plot taken from Figure 5. Calculation of power assumes fusion power and heater power affect temperature of outer ss vessel equally.*

CHEMICAL TRANSFORMATIONS ON A BASIS OF ELECTRICAL DISCHARGE

G.V. Tarasenko,

Aktau, Kazakhstan.

Many investigations show electrical discharges in the Earth's crust, as in thunderstorm clouds. Linear lightings generate spherical formations. Spherical concretions represent an example of discharge activity in the earth's crust. Experimental works on realization of electric discharges in conditions close to natural have been carried out on a basis of geological - geophysical investigations of the Earth planet and spherical concretions (Tarasenko G.V. 1993-2007). Different components of bed-fluids and rocks were located in reactor vessel. Reactor vessel was placed in electric engine stator, designed for 30 kW, with delivered voltage 20-30 V, the current was raised up 35 A. At the same time electrical discharges were realized in the reactor vessel using a capacity battery with total capacity of 16 μF at 6 kV. The vessel was heated up to 70^0C during this process. Smooth development of arc discharge took place at the spherical discharger. Pressure was raised up to 300 atm at energy put to the reactor vessel. After reassembling of the reactor vessel and fluids discharge one could find spherical asphalt – rosin residuals. Their formations we connect with cold nuclear synthesis taking place due electric discharges and leading to separation of fluids and coalescence of solid minerals.

These experiments confirm formation of spherical concretions, coal, polymetals, etc. from products of mud vulcanizm and bed-fluids generated in the mantle and the lithosphere. For obtaining of a new energy source it is necessary to separate a mechanism at which there will be available all devices for copying of the Earth planet processes.

CYCLONIC – CAVITATIONAL GENERATOR

*** M.D. Berkova, *V.Y. Velikodny, *V.G. Grishin, *V.V. Popov, **A.A Bykov**

**Institute of applied mechanics RAS, Moscow, Russia*
***Moscow Institute of Physics and Technology (MIPT), Dolgoprudny, Russia*
E-mail: *Vvelikodny@mail.ru*

For some years in the Laboratory of physical and chemical hydroaerodynamics IAM RAS together with a number of Institutes researches of cavitational tteatment of water in the vortical generator were carried out. We received high transformation coefficient of electric energy in thermal - $k \geq 10-13$.

This high result is caused by realization of a resonance in cavitational device. Realization of resonance became possible owing to a feedback: cavitational device - spectrum analyzer. It opens opportunities of significant economy of the electric power (if the pump unit is set in motion by electricity), economy of gas or carbon fuel (if the pump unit works on these kinds of fuel).

Introduction.

The fact is known, that at cavitations in water, wetting by water of a surface of a firm body a quantity of energy that leads to heating is allocated. In the given work theoretical consideration of the given effects from the point of view of cluster structures of water and experimental research of quantity of emited energy have been made.

Hypothesis I. Processes of cluster destruction.

Molecules and atoms of any firm or liquid substance form the ordered structures named clusters. The kind of structure is defined by a minimum of energy of communication of elements in it. It's possible to single out some coordination spheres concerning some atom or a molecule, in first of which, the nearest neighbours enter into and in the second – those that are further and current is further. The liquid differs from firm bodies that energy of interaction with the second coordination sphere is less than energy of thermal movement and so small clusters are formed which almost freely move relatively each other. In firm bodies

energy of interaction of particle with the third coordination sphere is less than thermal energy and therefore the body keeps the form.

Molecules of water possess enough greater dipole moment equal 1,85 Debve in rarefied vapor. In liquid this moment is notably more, as experiments show. From the principle of minimum of energy the near order for dipole moments is represented on Fig. 1. In total a particle interacts with twelve nearest particles.

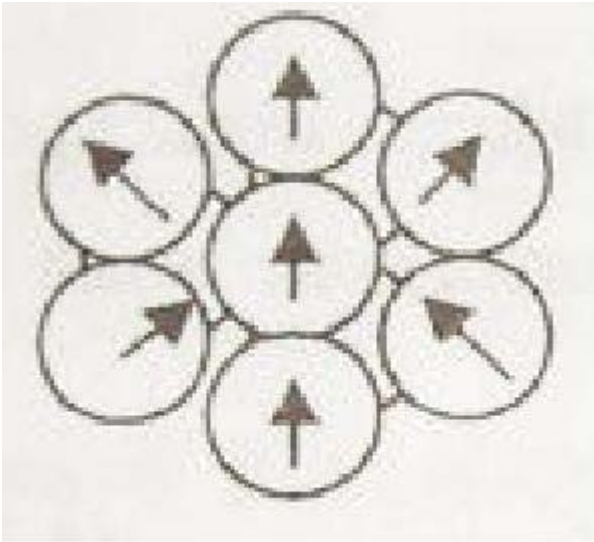

Fig. 1

Energy of interaction share divides on energy of covalent interactions and a dipole-dipole energy. Covalent interaction can be calculated by methods of multipartial interaction. Energy of interaction of is calculated with the formula:

$$E_{\partial un} = \frac{1}{2}\left[\frac{4p^2}{4\pi\varepsilon_0 r^3} + \frac{8\cos^2 60^0 p^2}{4\pi\varepsilon_0 r^3} + \frac{8\cos^2 30^0 p^2}{3\cdot 4\pi\varepsilon_0 r^3}\right]$$

Where p – dipole moment of water molecule.

While rising of temperature electric dipoles make torsion oscillations. Only two degrees of freedom result in weakening of interaction between dipoles. The probability of excitation of torsion oscillations is defined by integral of a kind:

$$P_i = \int_{E_{\partial un}}^{\infty} C\exp(-\frac{e}{kT})de$$

It is necessary to subtract energy KkT/2, where k - Boltzman constant, K-quantity of the nearest neighbours. Then we receive, that energy of interaction is equal:

$$E_{св} = KE_{ков} + E_{\partial un} - KP_i kT/2$$

On surfaces of water energy of communication decreases for the value caused by absence of three molecules in cluster from the direction of surface. From here it is possible to receive coefficient of surface tension as the attitude of change of cluster energy to the sectional area of the cluster.

$$\sigma = \frac{3E_{ков} + 2(\frac{2\cos^2 30^0 p}{3 \cdot 4\pi\varepsilon_0 r^3} - P_3 kT)}{R^2}$$

The share of molecules which forms clusters are calculated under the formula:

$$P_i = \int_0^{E_{св}} C \exp(-\frac{e}{kT}) de$$

Where C- normalization factor.

Let's consider the results of theoretical calculations of energy of cluster communication and coefficient of surface tension:

Dependence of binding energy (eV) and coefficient of surface tension (joule/m^2) from temperature (K).

Пара-метры	Температура, К										
	273	277	298	300	310	320	330	340	350	360	373
$E_{св}$	0,48	0,48	0,47	0,47	0,46	0,45	0,45	0,44	0,43	0,43	0,42
$E_{эксп}$	0,47	0,47	0,46	0,45	0,45	0,45	0,45	0,44	0,43	0,43	0,42
$\sigma_{теор}$	.081	.080	.077	.076	.074	.072	.070	.067	.065	.062	.058
$\sigma_{эксп}$	.076	.076	.073	.071	.070	.069	.067	.064	.062	.061	.059

Fig.2

Experimental and calculated value very well coincide.

Thus, energy liberation in micro bubble medium is explained by big total area of water surface in bubbles and the emitted energy can be estimated as product of coefficient of surface tension on the area of a surface.

The order of carrying out of experiment and experimental installation.

From the aforesaid it is visible, that for continuous energy liberation the continuous creation of the new areas of water surface is required. For this purpose cavitator approaches. It is swirler (helix of Archimedean) and nozzle which disperses water and strongly reduces pressure Fig. 3. Thus the gas soluted in water forms the big number of bubbles. And at working temperatures 50-70^{0}C in a zone of underpressure there is an intensive boiling and are formed vapor micro bubbles. It is clear, that the area of water surface in this case can be very big. On Fig. 3 position of tube (the stream to radiator) can be adjusted by the metric screw.

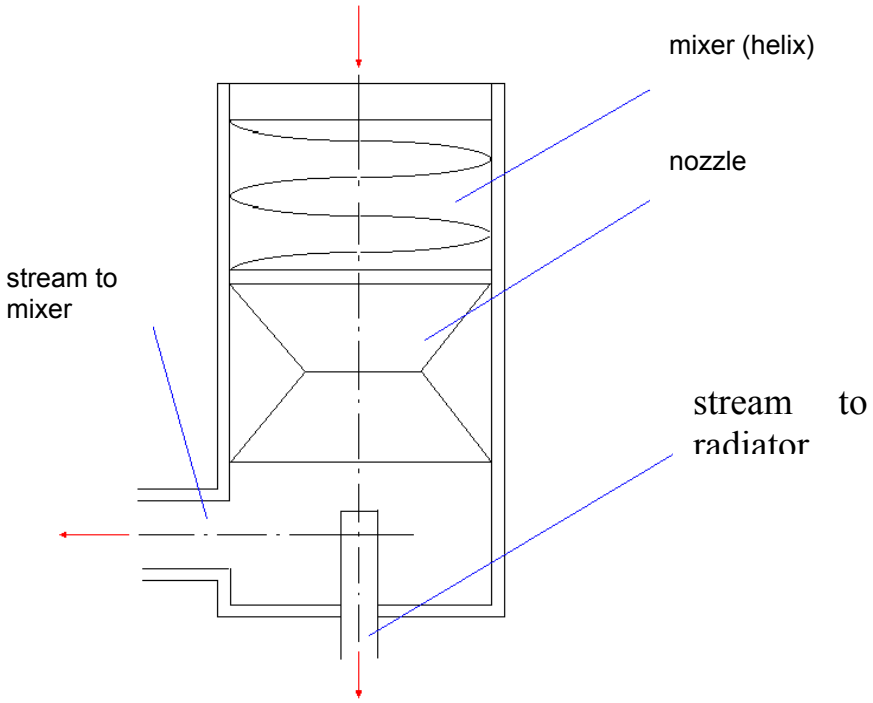

Fig. 3

Further it is required to define the emitted energy. It probably to make when the system to be in balance, so all received energy is picked out in environment. In this case it is required to know temperature drop on a tube and the charge of water. The emitted energy is equal:

$$P = CQ\Delta T$$

where C – water heat capacity, Q - charge and ΔT - temperature drop.

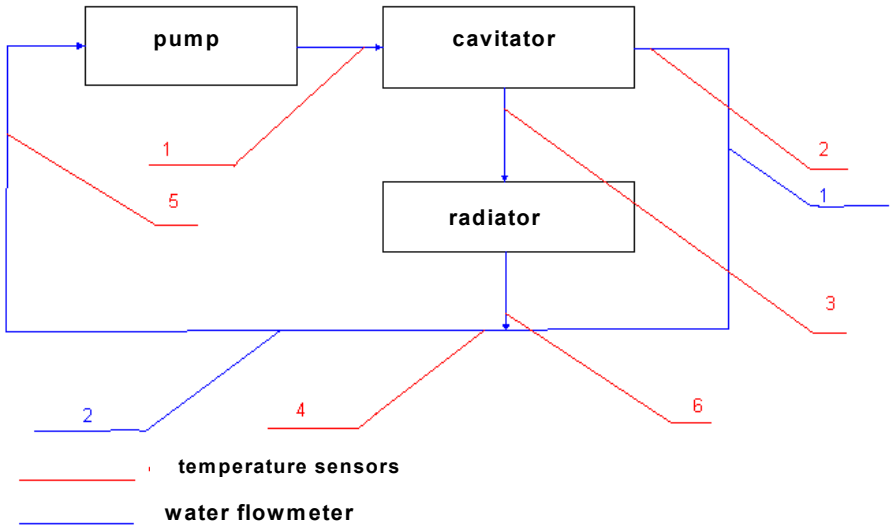

Fig. 4

On fig. 4 the diagram of installation is represented. By arrows the direction of water current is shown. In the beginning the pump lifts pressure up to 20 atmospheres. Passing through the cavitator, pressure falls up to 0,7 atmospheres and micro bubble medium is formed. Then water passes through radiator. Intensity of cooling of radiator can vary.

The experiment consists in waiting a stationary condition and to define capacity of thermal losses. They will be equal to capacity of the pump work with liquid and capacity of thermal emission in bubble medium. On a Photo 1 appearance the general view of the thermal pump is presented.

Photo. 1

Experimental results and their analysis

On installation a number of experiments have been made. Dependence of a thermal emission depending on temperature is received and it is certain, that the thermal emission keeps to constants within four hours. It is shown on Fig. 5, Fig. 6 and Fig.7.

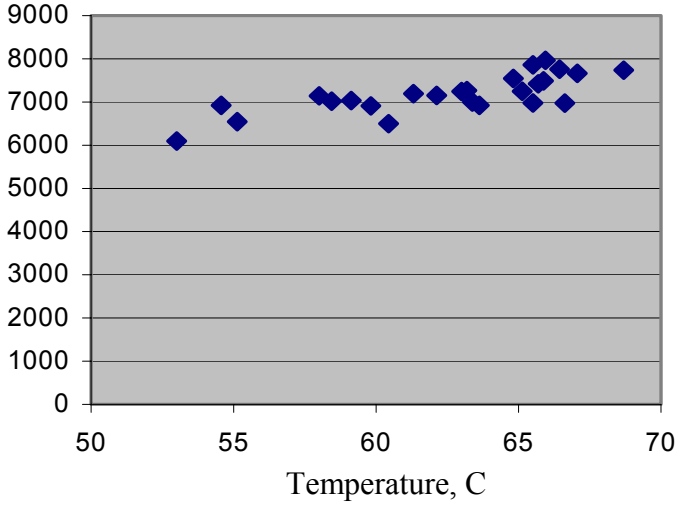

Fig.5. *Dependence of capacity of thermal losses (W) from temperature (^{0}C)*

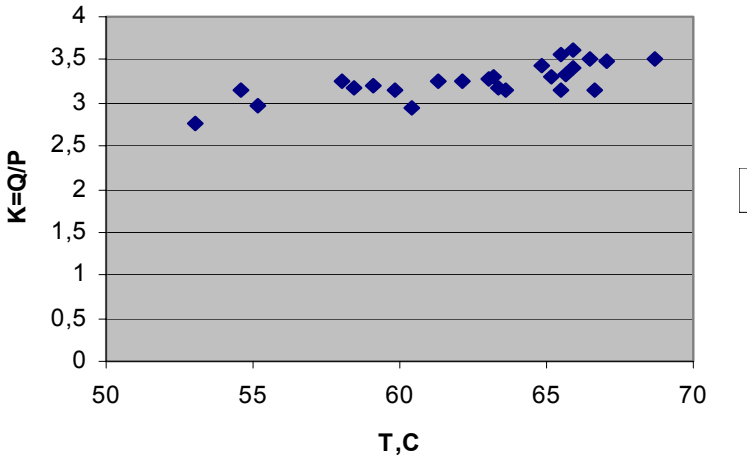

Fig. 6. *Dependence of the attitude of capacity of thermal losses to capacity of the pump from temperature (^{0}C)*

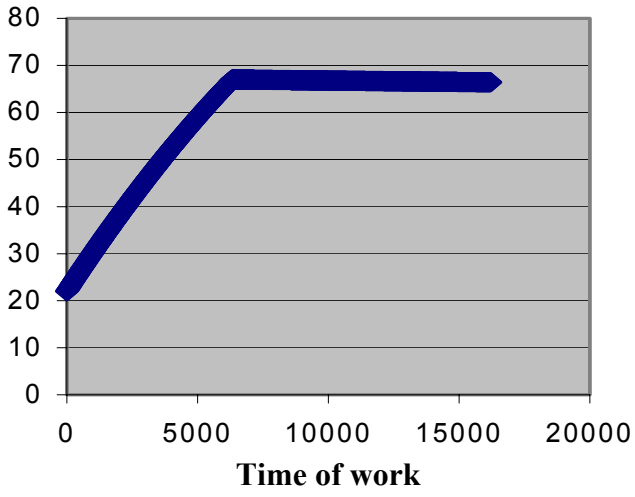

Fig. 7 *. Dependence of the temperature from the time of work.*

As one can see from the diagram, capacity of thermal emission can exceed capacity of the pump in 3,5 times. It occurs due to energy of internal constraints. What ones it is finally not known? Experiment by definition of time during which the effect can be supported has been made. On Fig.7 it is shown, that it occurs more than four hours and the thermal emission does not vary.

In installation 10 liters of water are used. It is possible to define, how many energy is reserved in this volume in clusters at temperature 340 K:

$$E = E_{св} \frac{VN_a P_{св}}{13\mu}$$

where μ - molar mass of water, N_a - Avogadro constant, V - volume in liters.

Here the litre of water weighs one kg is used. $P_{св}$ - probability of that a particle is connected with cluster. 13 in denominator because there are 13 molecules of water in cluster. Under the formula it is received:

$E=1,8x10^6$ joules

Capacity of the engine is equal 2.2 kW, i.e. capacity of internal sources is equal about 5 kW. Having divided the energy of water clusters on the given capacity, we receive, that installation should work only 6 minutes. In experiment the operating time is 4 hours, that is clusters' destruction is not the basic energy source in the thermal pump.

In the subsequent experiments the working part of installation (see Fig.3) has been modernized. The critical section of nozzle has been increased twice. Pressure in precombustion chamber has decreased owing to reduction of losses up to 15 atm. Experiment was spent on 19.01.2007. The "record" excess of received thermal energy above spent electric energy has been received. In a point of a maximum k=13,4. This phenomenal result opens an opportunity, at operating mode of work of " the thermal machine " on an optimum mode, to refuse from taking away of electric energy from a network. The perspective scheme of such installation is presented on Fig. 8.

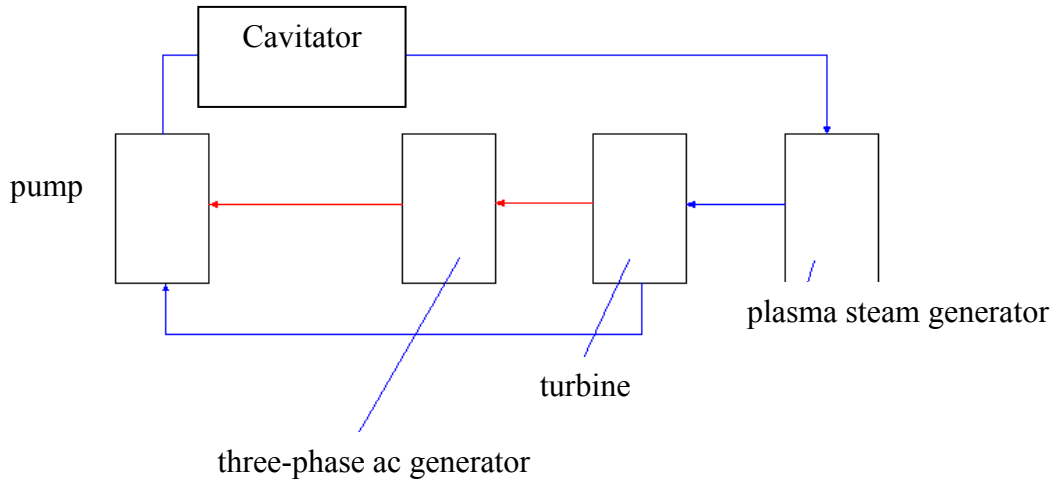

Fig. 8

Dependence of capacity of thermal losses from temperature

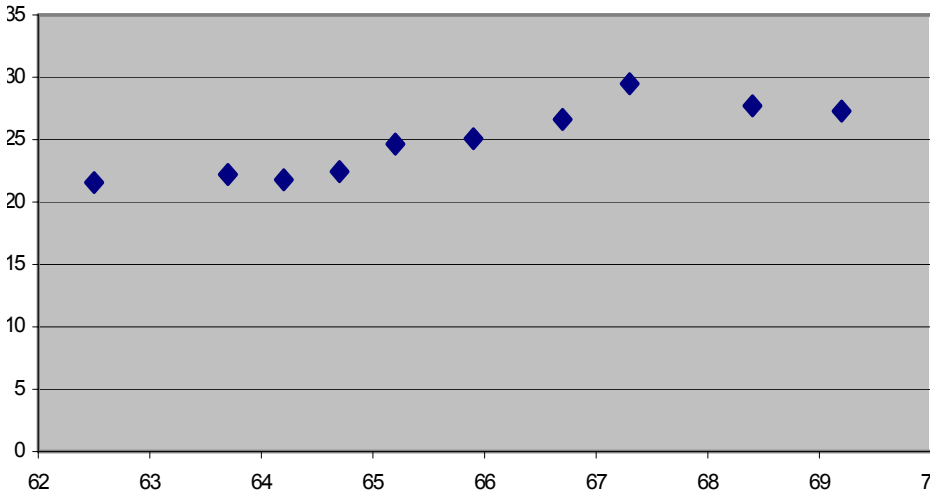

Fig. 9

In figure 9 the total output of thermal energy is presented at capacity of electric motor W=2,2 of kW.

In the last experiment, except heat sensors, installation has been equipped by two acoustic sensors. The typical spectrum of acoustic radiation is presented on Fig.10.

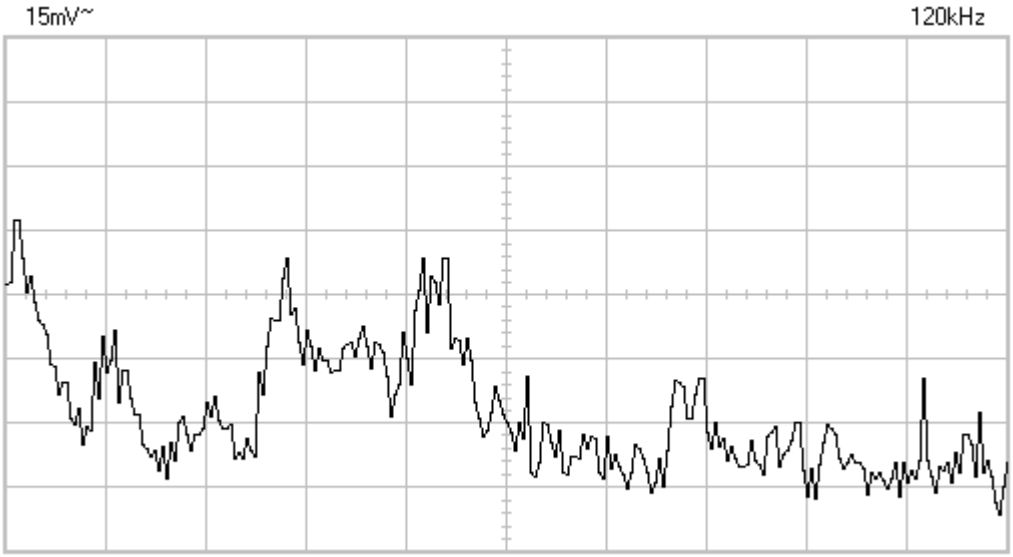

Fig. 10

From spectral characteristics it is visible, that the significant share of energy of acoustic fluctuations is concentrated in a range 35 - 50 kilohertz. Subsequently we had been made the whole series of experiments with a new nozzle configuration. Results is on Fig. 11.

Dependence of the attitude of capacity of thermal losses to capacity of the engine

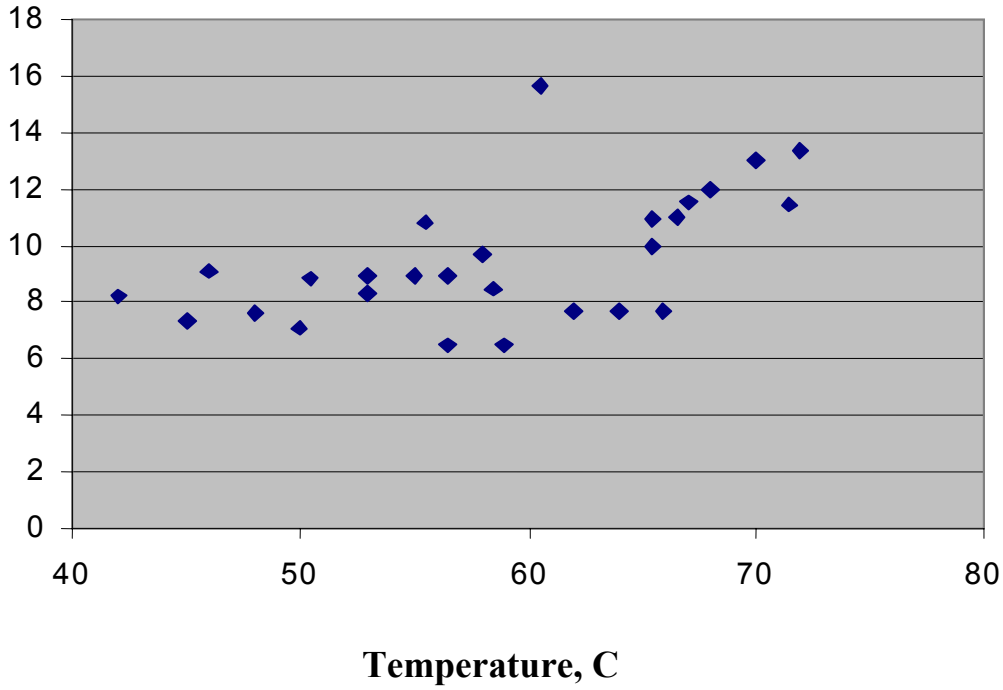

Fig. 11

Conclusions:

1. Installation for research of transformation of internal energy of water in thermal, in various modes of operation is created;
2. Stable results on transformation of electric energy in thermal with factor k=3 are reached;
3. The perspective installation diagram is developed;
4. 19.02.2007 the "record" factor of transformation of electric energy in thermal was been received.
5. The cluster hypothesis requires serious updating;
6. Other hypotheses are possible (for example, see Yu.A.Baurova's book).

References:

1. V.Yu.Velikodny, V.G.Grishin. Experimental research of vortical heaters work with a remote contour // Cold Nuclear Transmutation of Chemical Elements and Ball Lightning. Moscow, 2003. P. 27- 32.
2. V.Yu.Velikodny, V.G.Grishin. Experimental research of work of vortical heaters //Cold Nuclear Transmutation. Moscow, 2002. P. 99-105.
3. Yu.A.Baurov. Structure of physical space and new way of reception of energy. M.: Krechet, 1998. 240 p.

PLASMA TECHNOLOGIES IN ECOLOGICAL PROBLEMS

M.D.Berkova, *A.A.Bykov, V.Yu.Velikodny, V.P.Vorotilin, V.G.Grishin, *Yu.V.Dobrynetc, O.V.Krychenko, L.K Nikitenko, V.V Popov, E.N Rychagov, **B.N.Tolkunov

Institute of Applied Mechanics RAS, Moscow, Russia
** Moscow Institute of Physics and Technology (MIPT), Dolgoprudny, Russia*
*** Scientific Association for High Temperatures RAS, Moscow, Russia*
E-mail: ***Vvelikodny@mail.ru***

At the Laboratory of physical and chemical hydroaerodynamics IAM RAS together with a number of Institutes of the Russian Academy of Science, branch Institutes, educational Institutes within the limits of a problem of cold nuclear transmutation of chemical elements researches of anode electric discharge are carried out. During these researches the direction which already can be used widely in national economy has come to light. It has appeared that volumetric diffusion discharge in porous electrolyte as a type of anode discharge ideally approaches for biologically and chemically strongly polluted waters treatment. The high surface area in bubble medium where on water-air border the discharge is taking place allows making deep water treatment with the minimal power expenses even at presence steady microorganisms and chemical reagents which deactivation by other methods is problematic.

Introduction.

Using the term “Ballast Waters” (BW) we mean: some volume of the drawn water for increase of the tanker draft after it’s unloading in port for navigability restoration (a liquid ballast).

The water ballast is necessary for safe and effective exploiting of a modern craft, but at the same time it can represent serious threat to ecology, to economy and health. Entering of undesirable kinds in new ecosystems is recognized by the International Community by one of threats to the World Ocean.

Results of researches show, that in time, sufficient for transition of a sea craft from one Europe region to another, for example, from Baltic Sea to North Sea (3-4 days), all plankton community without any essential changes are transferred in water ballast. In coast-to-coast flights (10-14 days) the number of organisms in water ballast decreases, but some kinds of them are kept and are quite capable for vital activity. Substantial growth of the navy tonnage

and reduction of transportations time have broken existence of biogeographical barriers and the danger of alien kinds moving in a new habitat has increased tenfold. Cases of catastrophic "ballast" invasions, caused heavy ecological and economic consequences have become more frequent.

The glaring example is changes in Black Sea ecosystem which have occurred after predatory Mnemiopsis Leydyi moving in with craft water ballast from north-west coastal areas of Atlantic Ocean. Being a very prolific organism having a wide food spectrum, the new alien was the ideal object for colonization of Black Sea. For the first time having appeared in Black sea in 1982, in 1989 it gave enormous flash of number and biomass reached billion tons. As a result biomass fodder plankton has sharply decreased. Its qualitative structure has considerably decreased. Becoming the food competitor, and also the consumer of caviar and fish larvas (such as khamsa, jack mackerels, sprats), Mnemiopsis damaged to their stocks. As a result catch of these kinds have considerably decreased, that annually causes the significant damage to economy.

For prevention, reduction and liquidation of such carry of harmful water and pathogenic organisms by an establishment and realization of rules of the control of ship ballast waters and deposits and management the International convention on the control of ship ballast waters and deposits and management by them is directed [1].

At the present time the set of methods of water treatment from mechanical impurity and microorganisms is developed. The main from them are:

- mechanical filtration;
- a hydrocyclonic filtration;
- ozonization;
- hydrocavitation processing;
- acoustic processing;
- ultra-violet processing;
- passing of electric current;
- biochemical additives;
- x-ray processing;
- shock waves.

In the given section the new method and the equipment for water treatment from the biological impurity; based on plasma ignition in the water-air microporous medium is considered. Patent search and the accessible literatures review have shown that the given

method is new and has no analogues. Results of experiments on water treatment from seaweed and microorganisms on model set are presented. Results of these experiments show, that the plasma method of treatment sterilizes water up to acceptable level.

In the present work an application of the method of microporous liquids disinfection on a surface of phase section gas-liquid (a bubble surface) by volumetric-diffusion discharge is considered. In microporous medium this surface is developed enough.

Therefore processing by heat, radiation, acoustics, shock waves, ozone (in case of water air bubbling), chlorine (for salty water) and electric current simultaneously the great enough volume of biological or chemical polluted liquid is exposed. This explains the high bactericidal effect in comparison with other methods.

Let's note conclusive benefits of the given method and the devices, consisting in that all energy injected in the discharge goes on destruction of microflora and destruction of chemical pollution of organic and inorganic character.

The bactericidal effect of installation is provided by means of the biophysical processes complex initiated at the plasma discharge in liquid culture of microorganisms. The plasma discharge is characterized by the following disinfectant components:

- thermal component (plasma temperature up to 5000 degrees (the narrow section zone gas-liquid), temperature of the processed liquid with culture of microorganisms up to 44°C;
- shock wave, acoustic a component;
- electromagnetic component;
- ultra-violet radiation;
- ozonization, chlorination.

Therefore, the following bactericidal mechanisms are possible:

1) Thermo inactivation of microorganisms (1), protein of lipoproteid complex of biomembranes denaturation, coagulation of hyaloplasm proteins, coming after the damages of a cellular surface (3) breaking at the temperature from above 38°C which appeared from the contact of a cell with the discharge.

2) Macromolecular biopolymers destruction (2) in vivo, provoked by pulse change of pressure, a hypostasis and the degeneration of cells, a fragmentation of colonies.

3) Bacteriostatic action, bioliquids destruction due to anomalies (7) in interaction of electric forces and forces of surface tension of vesicular hydrophobic lipoproteid structures

providing morphological characteristics procariotic microorganisms of (6) as consequence, deformation of microorganisms, abnormalities of membranes semipenetration.

4) Radiomimetic influence UV (4) consisting in formation of peroxides, destruction peptide bonds of protein by ultra-violet radiation of a range 280-200 nanometers, causing also destruction (8) of nucleotide consecution in microorganisms' genome, mutations.

5) Photo effect on polymer-immobilized (5) of biomembranes metalloenzyme, initiating inhibition of catalytic metabolic processes.

6) Ozonization gives the same radiomimetic results as transformation consequent of oxygen to its allotropic form (ozone) ionizing radiation or UV can be.

Experiment.

At the present time on the basis of application of principles of biologically polluted microporous liquids disinfection by volumetric-diffusion plasma discharge disinfectant reactors of different volume and productivity are designed. The laboratory biological reactor of "small" productivity Q <0,3 m^3 per hour and the "great pilot installation" Q <25 m^3 per hour of biologically and chemically polluted water (including different salinity) have been created. On the "small biological reactor " the wide spectrum of researches has been led.

1. Volt-ampere characteristics of the discharge at various salinity of processable water have been got.
2. Forcing characteristics have been registered.
3. Researches of influence of the discharge on rather large organisms (krill) and seaweed have been carried out.
4. Researches of influence of the discharge on various bacteria culture have been carried out.
5. Tests have shown high efficiency at processing biologically polluted water.

The basic scheme of installation "small biological reactor" located in faculty " Physical mechanics MIPT " is presented on fig. 1.

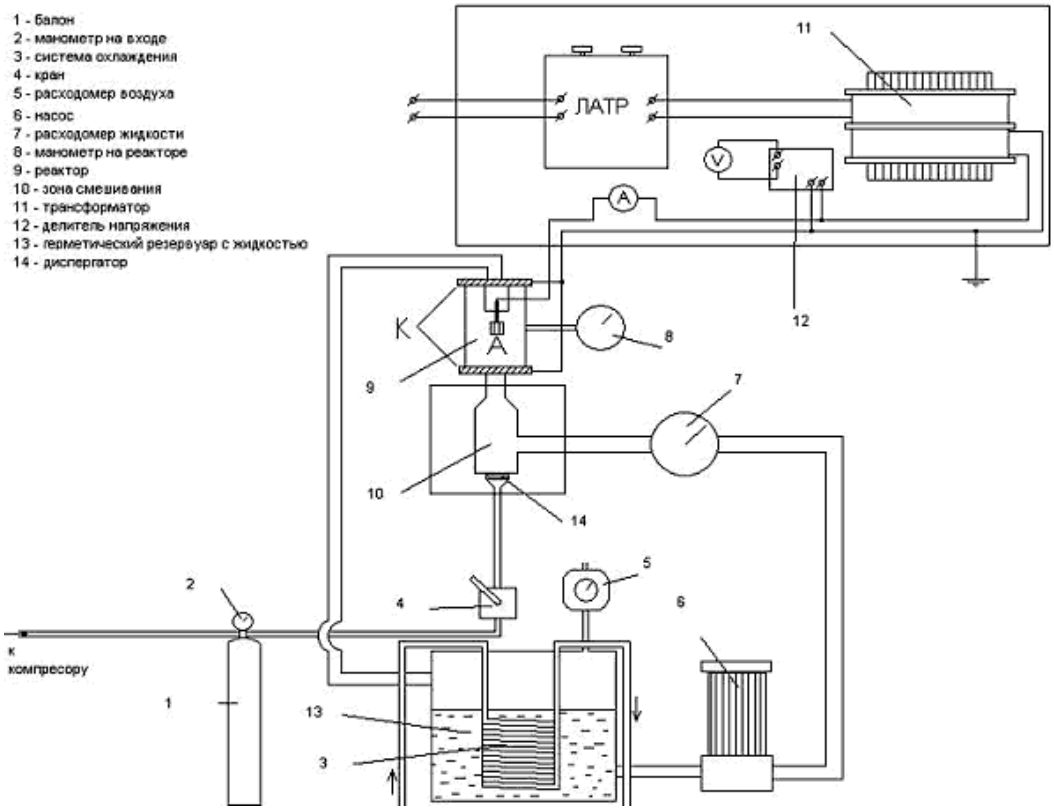

Fig.1

Work of the reactor in different modes is presented in Figures 2,3.

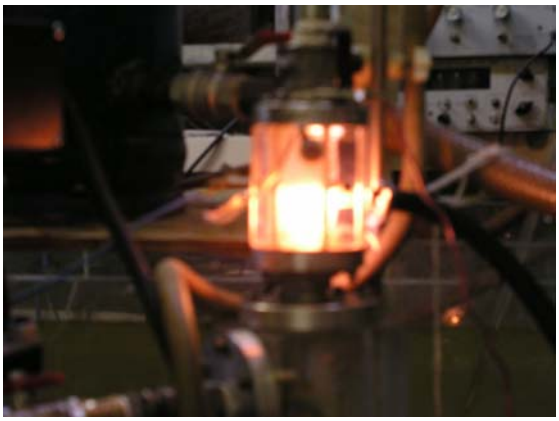

Fig.2

Fig.3

The data received on "small laboratory reactor" are considered. Volt-ampere characteristics of the discharge at various salinity of biologically polluted water have been got, dependence of defeat of bacteria and larger microorganisms and seaweed from time of processing and from the energy has been investigated at deactivation of volume 30 liters.

Volt-ampere characteristics of plasma volumetric-diffusion discharge installation in the microporous liquid depending on salinity of water.

Air charge =0.644 liter/sec;
volume of the water tank = 33 liters;

water charge =0,08 liter/sec;

air pressure =8 atm;

There are two tests without the salt.

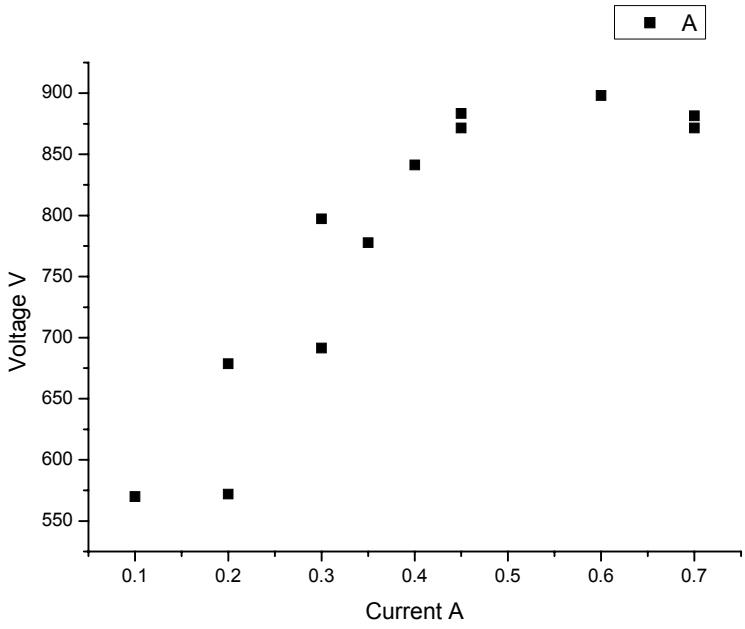

Fig. 4

Salinity of water is equal 20 pro mil;

air pressure =8.8 atm;

water charge =0,03 liter/sec.

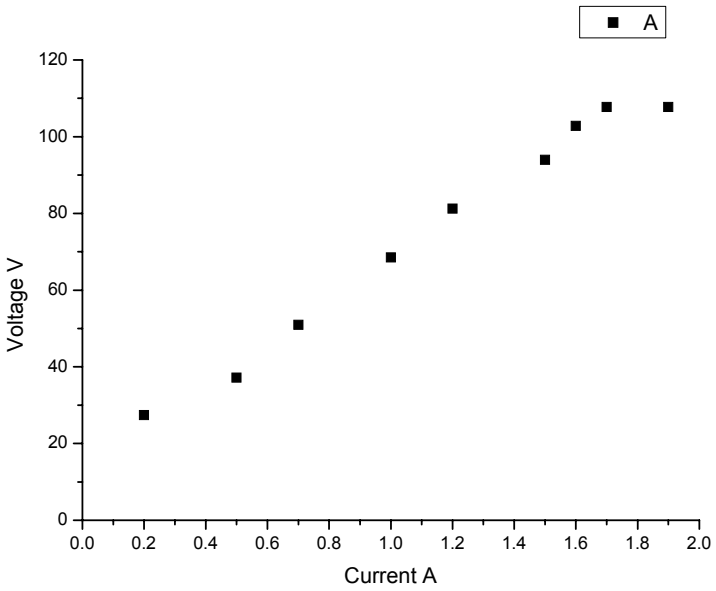

Fig.5

At ignition of the discharge volt-ampere characteristic reaches saturation. At increase of water salinity the voltage monotonously decreases and the current increases at a threshold of ignition of the discharge. At processing concerning large microorganisms the direct scheme was used - on input of the reactor micro seaweed and microorganisms were fed and on output tests were selected. On fig. 6 organisms and seaweed in an initial condition are presented. On fig. 7 microorganisms and seaweed are after processing by the discharge.

Fig. 6

Fig.7

The same way influence of the electric discharge on a number of microorganisms culture was investigated. We used Bifidobacterium bifidum (1 culture) and Lactobacillus acidophilus (culture EP 317/402).

We shall consider the bactericidal effect received on Lactobacillus sp.

The contrasted microphoto (MIKROS-400).	Explanation
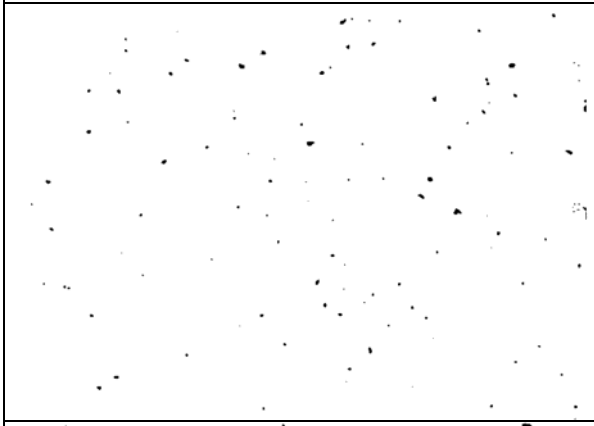	9:37 a.m. Control test (before experiment). Quantity of bacteria in sight - nearby 100. A biomass alive.
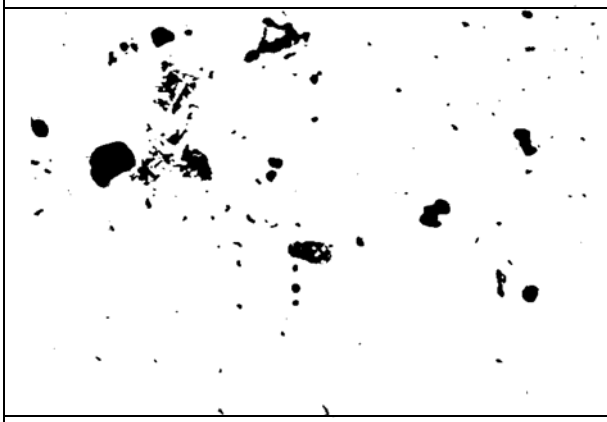	9:42 a.m. Current 1.7 A, voltage up to 470 V. Quantity of alive bacteria in sight nearby 30. The rest - in the form of coagulates.
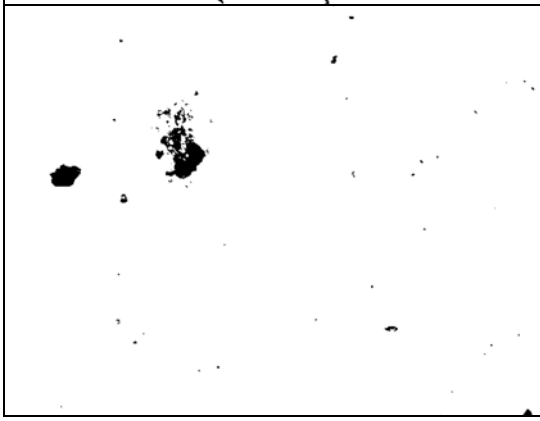	9:47 a.m. Current 1.6 A, voltage 440-450 V. Quantity of alive bacteria in sight nearby 10. The rare whole coagulate precipitate.

From the statistical point of view, the graph of distribution of bacteria quantity from time can be approximated by the certain kinds of statistical distribution, namely: logarithmic, geometrical and exponential.

Dependence of quantity of bacteria on an operating time of the installation

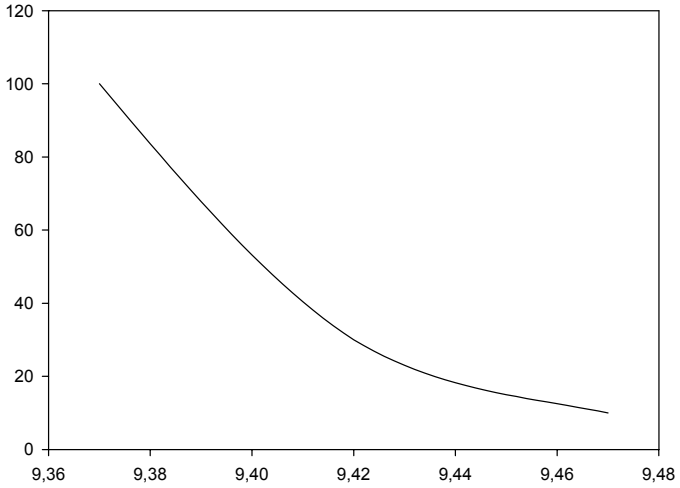

Meaning the fact that a question is in exact parameters (time and quantity of microorganisms), it is logical to recognize, that distribution has a real basis in the form of the biophysical-biochemical processes leading finally to the maximal disinfection of a microporous liquid. The most active, from the theoretical positions, disinfectant factor is coagulation under influence of shock waves and thermal effect.

On the basis of results that were received on the "small laboratory installation" the "great pilot semi-industrial installation" has been developed. The principle scheme of installation is presented on Fig.8.

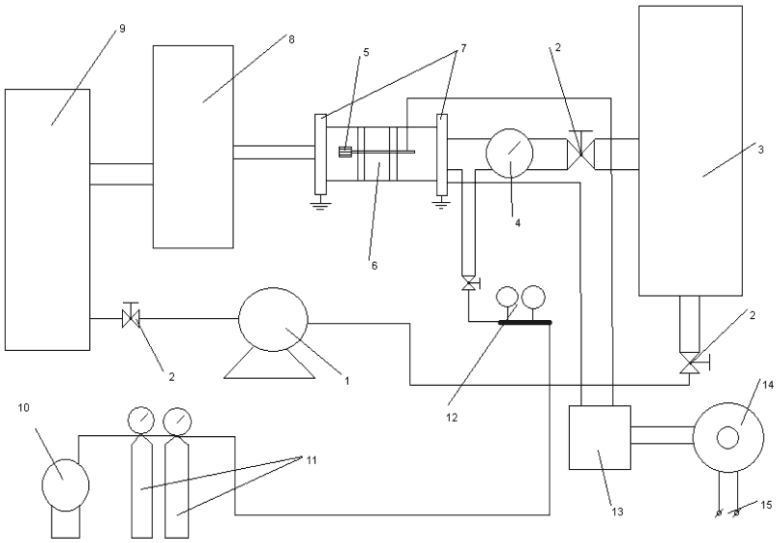

1 – pump, 2 - stop-cock, 3 – receiver for water, 4 - flowmeter , 5 – anode, 6 – catode, 7 – bioreactor, 8 – receiver for gas- dispersion mixture, 9 - gas separator, 10 – compressor, 11 – receivers, 12 – gas flowmeter, 13 – transformer, 14 – latr, 15 - ac source.

Fig. 8

General view of working part of "bioreactor" with porous liquid and in operating mode of the discharge is presented on Fig. 9 and Fig.10.

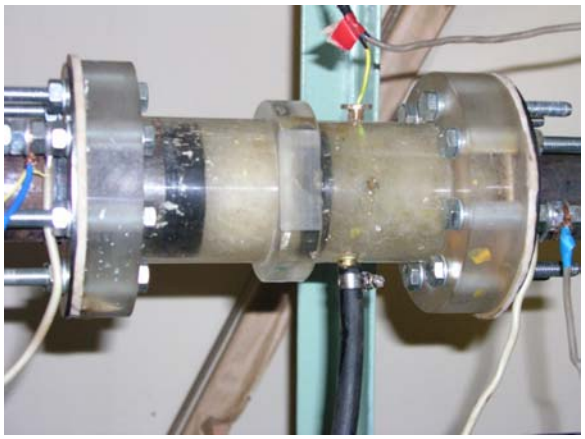

Fig.9

Fig.10

A typical volt-ampere characteristic of "bioreactor" is presented on Fig.11.

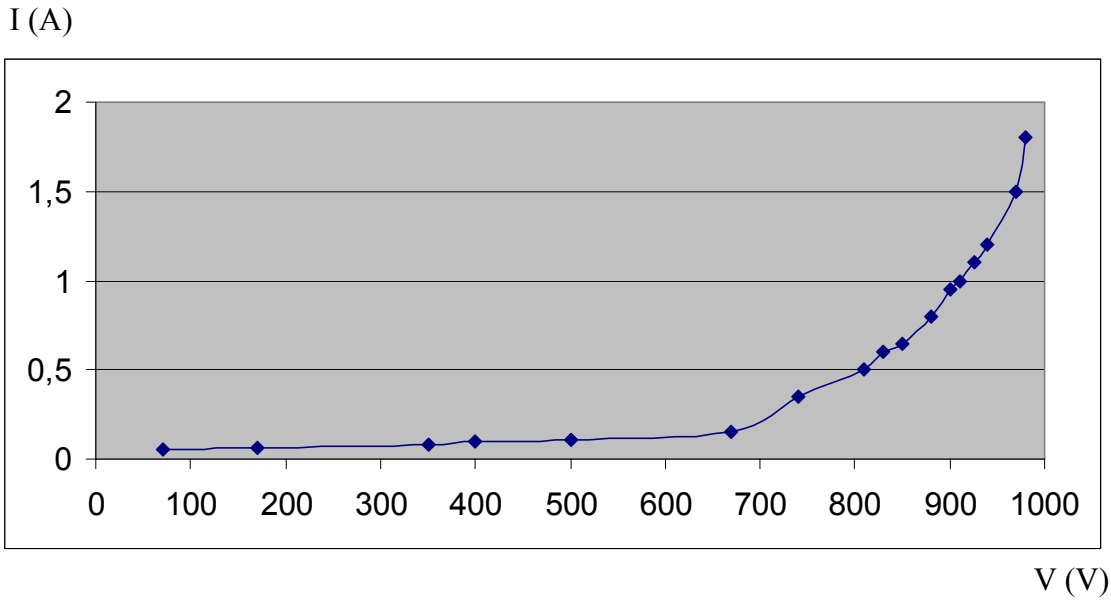

Fig.11

The charge of gas Qg = 0.996 m^3/hour; Q_{liq}=16.22 m^3/hour; volumetric gas content φ=5%.

Charge of electric power W=0,2-0,6 kw-hour on M^3 of the polluted water depending on stability of microorganisms or chemical substances.

Conclusions:

1. Devices for plasma treatment of ballast water and sewage have been developed.
2. High efficiency of a plasma method at processing of biologically polluted waters has been shown.
3. Volt-ampere characteristics of "biological" reactors have been got. High power efficiency of the "big" biological reactor is shown.

References:

1. International Convention for the Control and Management of Ships' Ballast Water and Sediments. SPb., 2004.
2. V.Ya.Munblit, V.L.Talrose, V.I.Trofimov. Thermoinactivation of microorganisms. Moscow, 1985.
3. K.Simonesku, K.Oprea. Mechanochemistry of high-molecular substances. Moscow, 1970.
4. A.Policard, M.Bessis. Elements de pathologie cellulaire. Paris 1968.
5. Z.M.Bacq, P.Alexander. Fundamentals of radiobiology. Oxford-London-New York-Paris 1961.
6. O.V.Michailov. Gelatin- immobilize metalcomplexes. Moscow, 2004.
7. Yu.S.Chentsov. General cytology. Moscow, 1995.
8. V.N.Shabalin, S.N.Shatohina. Morphology of man's biological liquids. Moscow, 2001.
9. N.V.Luchnik. Biophysics of cytogenetic and genetic code. Leningrad, 1968.
10. F.M.Gaisin, E.E.Son. Beginning and development of the volumetric discharge between firm and liquid electrodes. //Chemistry of plasma, Vol.16. M., 1990, p. 120-156.
11. V.Yu.Velikodny, V.G.Grishin. Plasmadynamic generation of hydrogen in natural water. // Proc. 11-th Rus. Conf. On Cold Nuclear Transmutation and Ball Lightning. Dagomys, Sochi, 28 Sep – 5 Oct 2003, M., 2004, p. 25-36.
12. M.Henze, P.Harremoes, J. la Cour Jansen, E.Arvin. Spildevandsrensining biologisk og kemisk. Lingbi, 1995.

ADVANCED PROJECTS OF ENERGY GENERATING UNITS

I.V.Goryachev, I.N.Goryacheva

Russian Research Center "Kurchatov Institute"

I.

After the 9th International Conference on Condensed Matter Nuclear Science in Beijing, China,in 2002 we in Russia came to a conclusion that it was time to start engineering to develop and design energy generating devices based on new physics. By that moment there were registered several inventions which could be implemented as the initial basis for solving this problem. Those inventions stipulated different approaches towards the likely solutions of the key problem to prove the practical importance of the new direction in generating environmentally clean energy.

One of the direction in searching for a likely solution of the problem was connected with implementation of so called **Koldomasov Reactor** (Patents RU 2 152 083, 2 224 308) which represented a hydraulic closed system filled with purified water circulating under high pressure and creating plasmoid inside a cavitation cell. The inventor stipulated that inside flowing ionized water in such a cell can be created conditions for deuterium nuclei fusion.

Other researchers tried to use transformer oil instead of highly purified water. Their interpretation of the excess heat registered in such installations based on the discovery of Russian academician R.Avramenko who disclosed the effect of generating excess energy in circuits containing a plasmoid element.
Several versions of Koldomasov device were designed and tested. One of the installation of that kind was created at Kurchatov Institute and intended for investigating the processes of generating excess thermal and/or electrical energy generated in the result of deuterium nuclei fusion inside flowing ionized water. The schematic of that installation and the photograph are presented below. The installation incorporated apparatus to produce highly purified water. It also stipulated a possibility to add up to 1% of heavy water to the circulating flow. The parameters of that set up are shown in the Table.

Another group of researchers lead by Dr.Godin experimented with analogous installation using transformer oil. Several pictures demonstrate some details of their experiments.

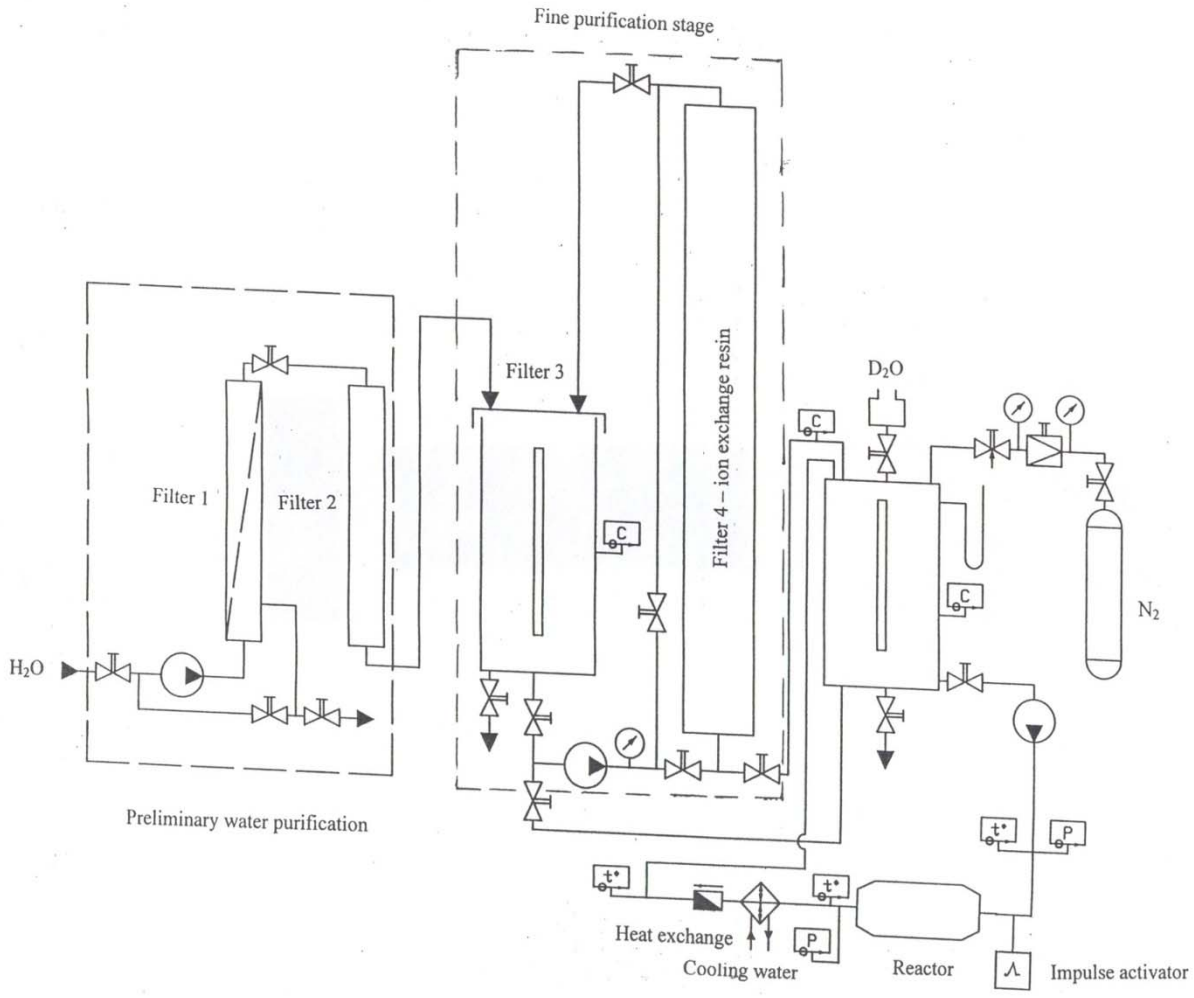

Schematic of a Koldomasov type installation designed at Russian Research Center "Kurchatov institute"

Kurchatov's installation

Technical parameters of Kurchatov's Installation

Parameters	Units	Value
Consumption of initial water	l/h	200
Capacity of the preliminary purification stage	l/h	50
Specific resistance of water after first stage	MOhm·cm	1.0
Power consumed by first stage of purification	kW	1.0
Water consumption in the fine purification stage	m3/h	1.6
Specific resistance of finally purified water	MOhm·cm	Up to 1000
Amount of heavy water added	%%	1 – 3
Power consumed by the stage of fine purification	kW	0.4
Water flow rate in the reactor circuit	l/h	730
Water pressure in the reactor circuit	MPa	6.0
Frequency of impulse activator	kHz	≈1.0
Initial water temperature in the circuit	0C	20 – 25
Water temperature after reactor	^{0}C	60 – 80
Power consumed in the circuit	kW	3.0
Level of excess heat generated	kW	Up to 60

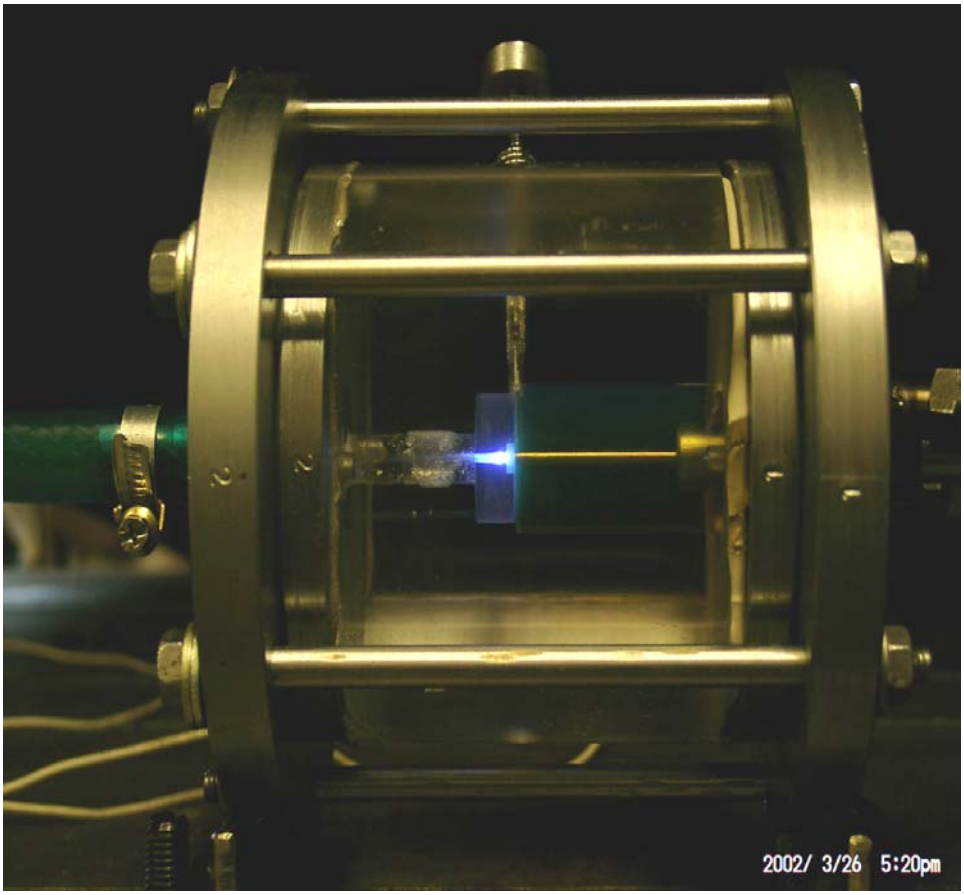

Plasmoid generated at the exit from conical nozzle
with brass throttle insertion

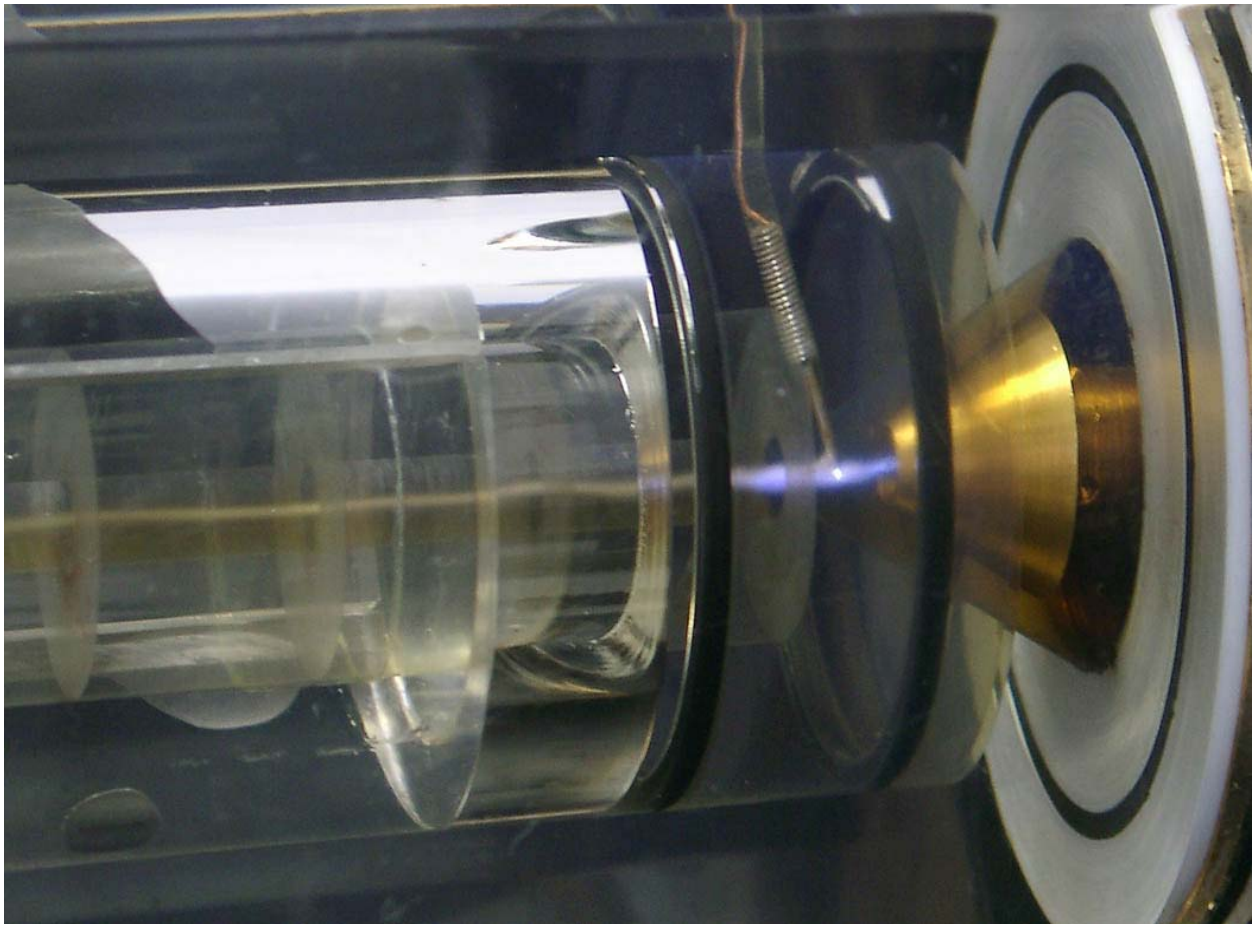

Taking energy from plasmoid by means of needle-shaped electrode

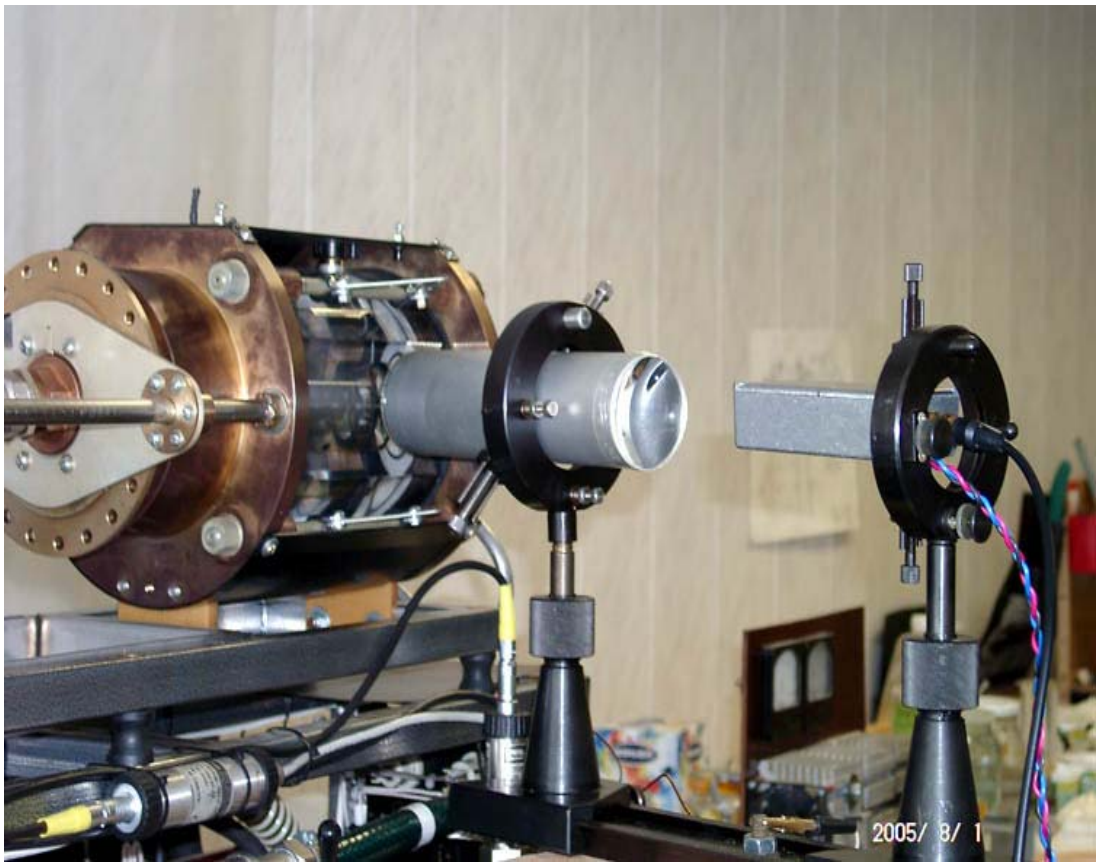

Cavitation cell with optical detector set-up

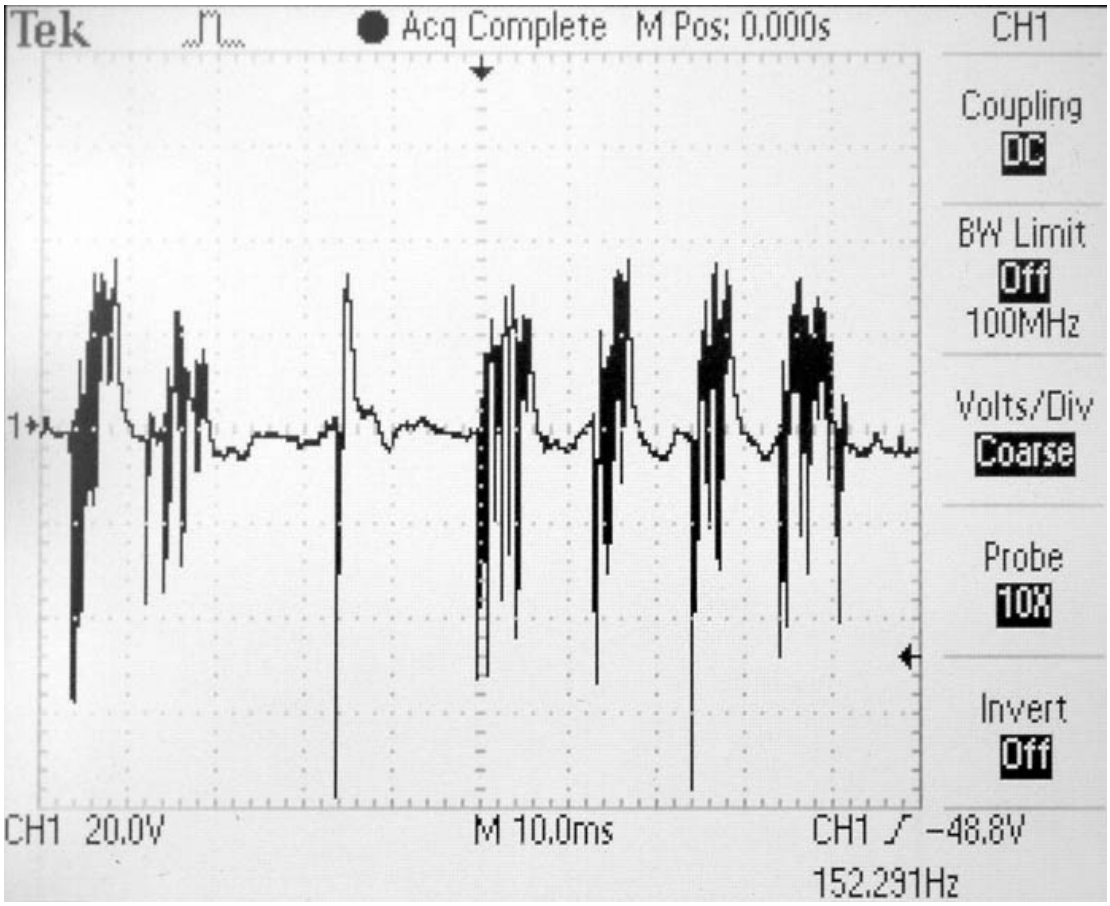

Typical voltage oscillations on the electrode

II.

Another version of a brand new source of electricity was developed by inventor named Oleg Gritskevitch in mid seventies based on the article by A.Koldomasov titled "Ball lightning in liquid" published in 1972 in the "Technique of youth" journal. Nowadays this direction of new energy engineering is presented by two patents of **Hydromagnetic Gritskevich Dynamo** (Patents RU 2 174 735, RU 2 183 899)

About the inventor: Oleg Gritskevich was born in 1936. He was educated as electrical engineer and worked at the Far East Branch of the Academy of Sciences of the USSR. He was graded Doctor of Sciences, Member of Russian Academy of Natural Sciences , Member of Russian Physical Society. He had more than 70 inventions mostly in high technologies but used to hide "know-how" when registering his patents. Unfortunately he often failed to realize his inventions though many of them were recognized to be quite feasible and effective.

About his nvention: The first two models were constructed and tested at the Pacific Research Institute in Vladivostok. In 1991 he got an offer from the Armenian Academy of Sciences to construct and implement his Dynamo in Armenia. The third version of his machine was constructed in Armenia in late 1992 and worked till January 1997 when it was destroyed during the Armenian-Azerbaijan war. Also some of his associates died.
The inventor presented report about his generator in 1999 in Salt-Lake city (USA) at the Conference on "New Energy". During four months after the Conference he negotiated with a likely strategic investor but they failed to arrange joint venture and the inventor returned back to Russia. In mid 2000 the inventor was invited to reproduce the Armenian version of the Dynamo at one of the Defense enterprise near Moscow. But there appeared difficulties with funding the work and it was stopped. Later in 2001 they undertook one more attempt to realize the project abroad in cooperation with Canadian company "DG Capital Canada" in Toronto but because of the difficulties with moving to Canada it was also interrupted. Soon after that the inventor dies and his son moved to Estonia where in 2002 he registered joint company "Sintos Systems". So far there is no any information if he continued further attempts to realized the projects or not.

About the Armenian Generator: The model created in Armenia had the mass of about 900 kg (including the water contained inside) and the diameter of about 200 cm. The case of the generator was made of firm optical polystyrene. The inside surface of the thoroidal case was plated with 1μ thick layer of monocrystalline $BaTiO_3$. Ultrapure water with specific resistance of 18 MOhm·cm was used to fill up the case of the generator. Two batteries of capacitors of 10 Farads each were used to start up the process. The energy of the start-up discharge amounted to 20 kJ at 100 kV voltage and 0.05A current. The start-up period lasted from 3 to 5 minutes. The initial impulse electro-hydrolic shock pressure reached about 200 bars. After initial starting water circulation inside the case and getting the $BaTiO_3$ crystals polarized an electric battery of 14.4W power created turbulent water flowing inside the case. 32 electrodes made of palladium (totally 2 kg of Pd was used) provided ionization of water by high voltage discharges.
The average output power of the Generator was 1.5MW DC. Sometimes the output power reached 2.5MW and was limited just by the temperature of the cooling water (it was preferred to be not higher than 550C). Once the power was up to 8.8 MW during 1 minute unless the water boiled.

In the result of those tests it was estimated that creation of this kind electrical generators with power of up to 1000 MW was quite feasible. The estimated cost of manufacturing such Generator is $500/kW (as compared to $5000/kW for NPP or $4000/kW for wind generators. The initial cost of electricity can be approximately 0.1 c/kW-h without consuming any fuel from outside source and without polluting the environment.

Gritskevich's Patent RU2174735

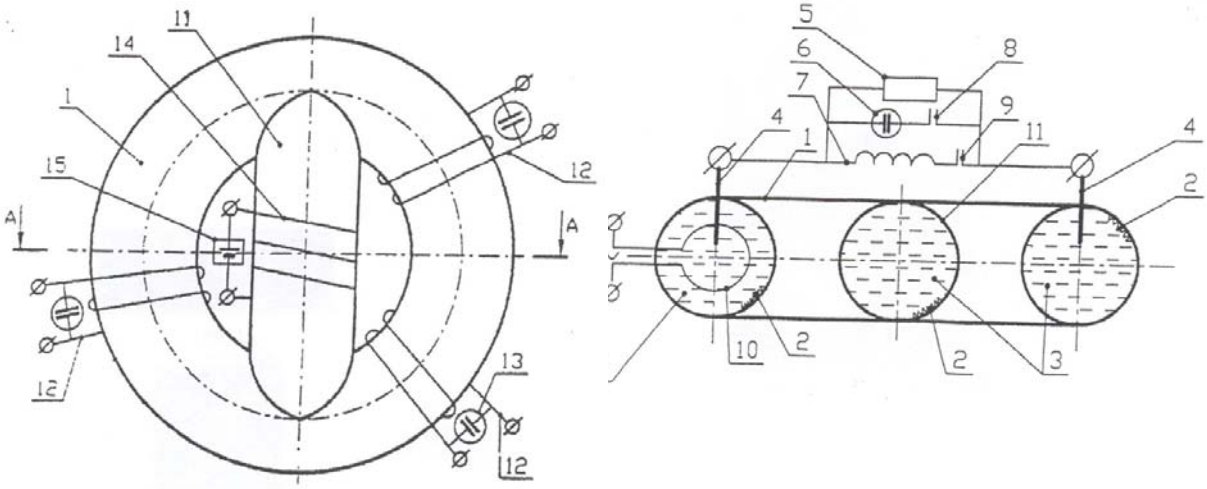

1. Dielectric tank.
2. Segnetoelectric coating ($BaTiO_3$).
3. Polar liquid (Mix of 5-10% D_2O and SuperQ H_2O)
4. Electrodes for ionizing.
5. Controlled charger.
6. Molecular energy storage (accumulator).
7. Inductive energy storage.
8. Controlled switcher.
9. Controlled switcher.
10. Exciting coils.
11. Stabilization chamber.
12. Power coil with loading.
13. Molecular energy storage (accumulator).
14. Coil of the stabilization chamber.
15. DC power supply.

There is a group of scientists in Moscow that works in cooperation with "Kurchatov Institute" trying to reproduce the Generator. But the work goes slowly because of lack of funding.

Assembling a Gritskevich type thoroidal generator at a laboratory

III.

One of most promising direction of works aimed at creation of sophisticated power generating facilities is developing installations based on implementation the phenomena of low energy transmutation of nuclei.

The phenomenon of nuclear transmutation was observed by many researchers under various conditions, in particular: at glow discharge in palladium and other rare earth metals, at electronic melting zirconium in a vacuum furnace, at ultrasonic processing saline water, at electrical explosions of metal foils in dielectric liquids, under influence of pulsed current onto lead in magnetic field.

Dr. Kuznetsov's group concentrated on developing technologies based on generating excess energy in the result of transmuting atoms of oxygen in water under the impact of specially organized electromagnetic radiation: H216O —> 18O + 2ν + 11.6 MeV (10-12J). The neutrinos emitted carry away half of the energy yield. The rest of the yield energy heat the water media of the reaction.

Transmutation of water is a complicated physical process comprising several phases. First of all, special device generates electromagnetic radiation with specially organized space-time structure. The electromagnetic radiation then is transformed into "transmutation radiation" (TM-radiation) by means of phase invertors. TM-radiation influences the molecules of water and produces a physical process of transition H216O into H218O. The diagram hereinafter gives theoretical interpretation of the transmutation process:

Under the influence of specially frequency-amplitude fitted TM-radiation a molecule of H216O is being restructured: electrons of the hydrogen atoms take the positions of electron orbitals of the 16O atom and the protons (hydrogen nuclei) move to the 16O nucleus. The two electrons are captured by the protons. In the result of capturing the electrons (reverse β-process) two neutrons and two neutrinos appear. The neutrinos freely escape from the atom while the neutrons get into the 16O nucleus thus forming a nucleus of 18O isotope. Characteristic time of the process is equal to 10-23 s. Since the acting TM-radiation is tuned to the resonance parameters of H216O the generated 18O atoms do not undergo further transmutation. The atoms 18O then remain stable. No any ionizing radiation is emitted. The energy of 10-12J per transmutation of one molecule of H216O is absorbed by the volume of water and heats it up.

In order to generate 100 kW of thermal energy 1017 transitions per second should happen. It means that consumption of water will amount to $3 \cdot 10\text{-}6$ g of water, so the daily (24 hour operation) consumption of water will not exceed 0.3 g.

Based on this physics several versions of energy generating devices can be designed and constructed. Their likely characteristics are presented below.

Diagram of Transmutation of Molecule of Water H_2O in Atom of Oxygen O^{18}

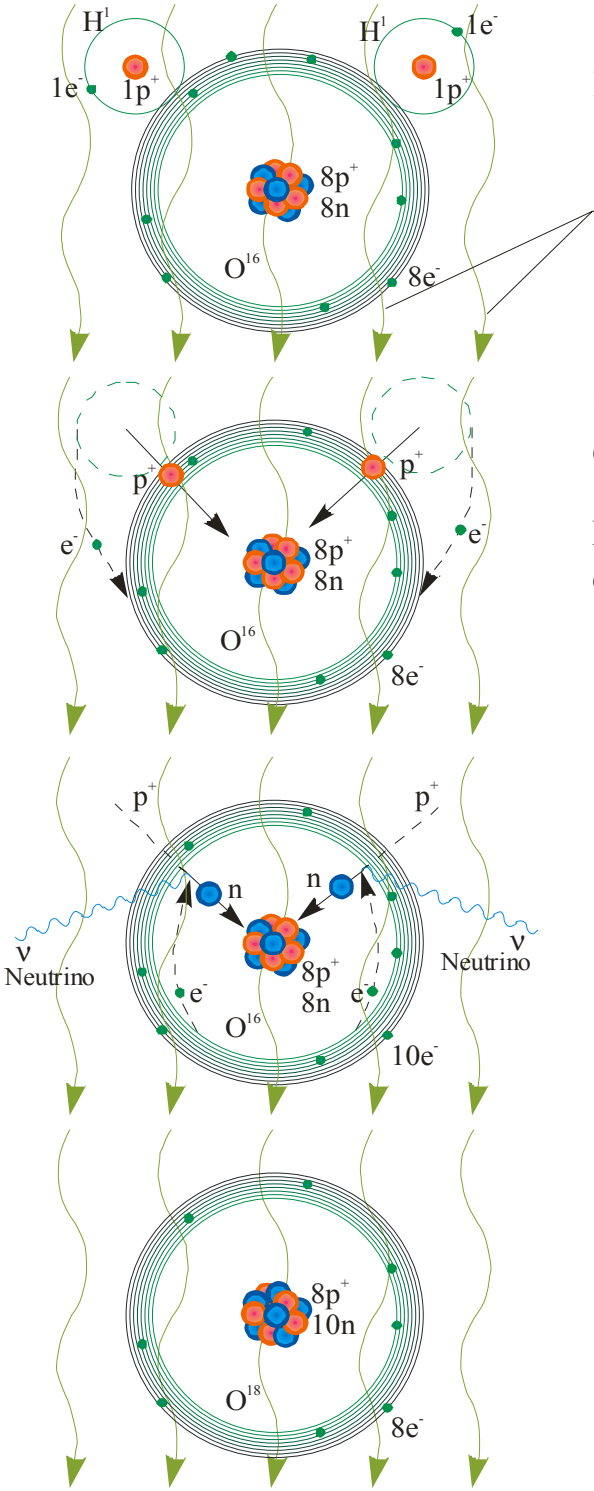

Initial molecule of water H_2O^{16}

TM-radiation

Structural readjustment of elecrton-nuclear structure of H_2O^{16}

Resonance frequency of H_2O^{16} coincides to TM-radiation frequency

Transition of atom-nuclear structure of H_2O^{16} to O^{18}

Resonance frequency of H_2O^{16} coincides to TM-radiation frequency

Final state of atom of O^{18}

Resonance frequency of O^{18} does not coincide to TM-radiation frequency

TECHNICAL PARAMETERS OF ENUMM.

Overall dimensions of ENUMM	∅400 × 937 mm
Weight, without water	~150 kg
Output thermal power	100 kW
Power of AC master generator	1 kW
Generator power supply	220 V, 50 Hz
Water consumption	300 mg /day
Period of continuous operation	1-2 years

TECHNICAL PARAMETERS OF ENUMMF

Overall dimensions of ENUMMF	∅680 × 799 mm
Weight, without water	~320 kg
Power of AC master generator	5.2 kW
Generator power supply	220 V, 50 Hz
Water consumption	300 mg /day
Period of continuous operation	1-2 years

TECHNICAL PARAMETERS OF TM-12

Overall dimensions of TM	∅3598 × 5000 mm
Weight, without water	~16 t
Output thermal power	25 MW
Power of AC master generator	62 kW
Generator power supply	220 V, 50 Hz
Mass of water	8.4 t
Water consumption	64.8 g/day
Period of continuous operation	1-2 years
Temperature of water steam produced	300-320 ^{0}C
Pressure	14-20 atm

TM-Electrical Power Station

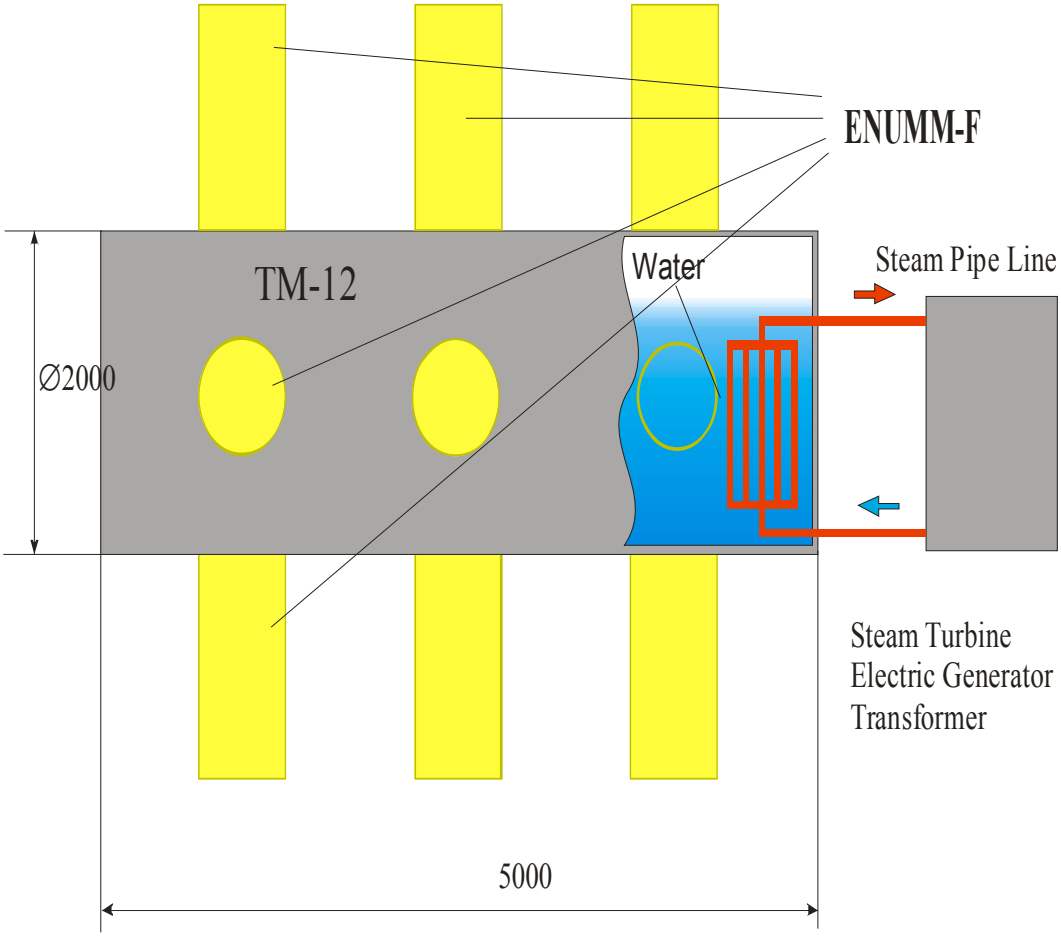

Low Power Energetic Unit

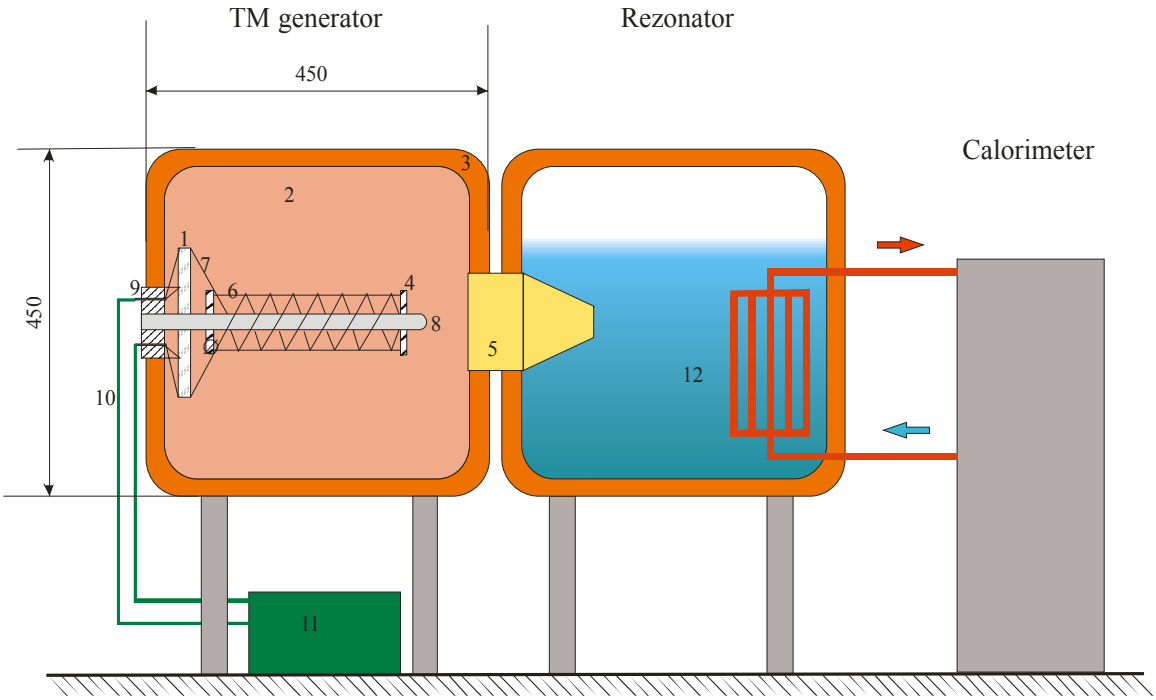

1. Reflector (Cu, Ag)
2. Gas volume
3. Vacuum jacket
4. Insulators
5. Optical adapter (quartz)
6. Quartz thread
7. Electrode thread
8. Central electrode
9. Ceramic insulator
10. Conductors
11. Electric pulse generator
12. Heat-exchanger

Block diagram of ENUMM installation

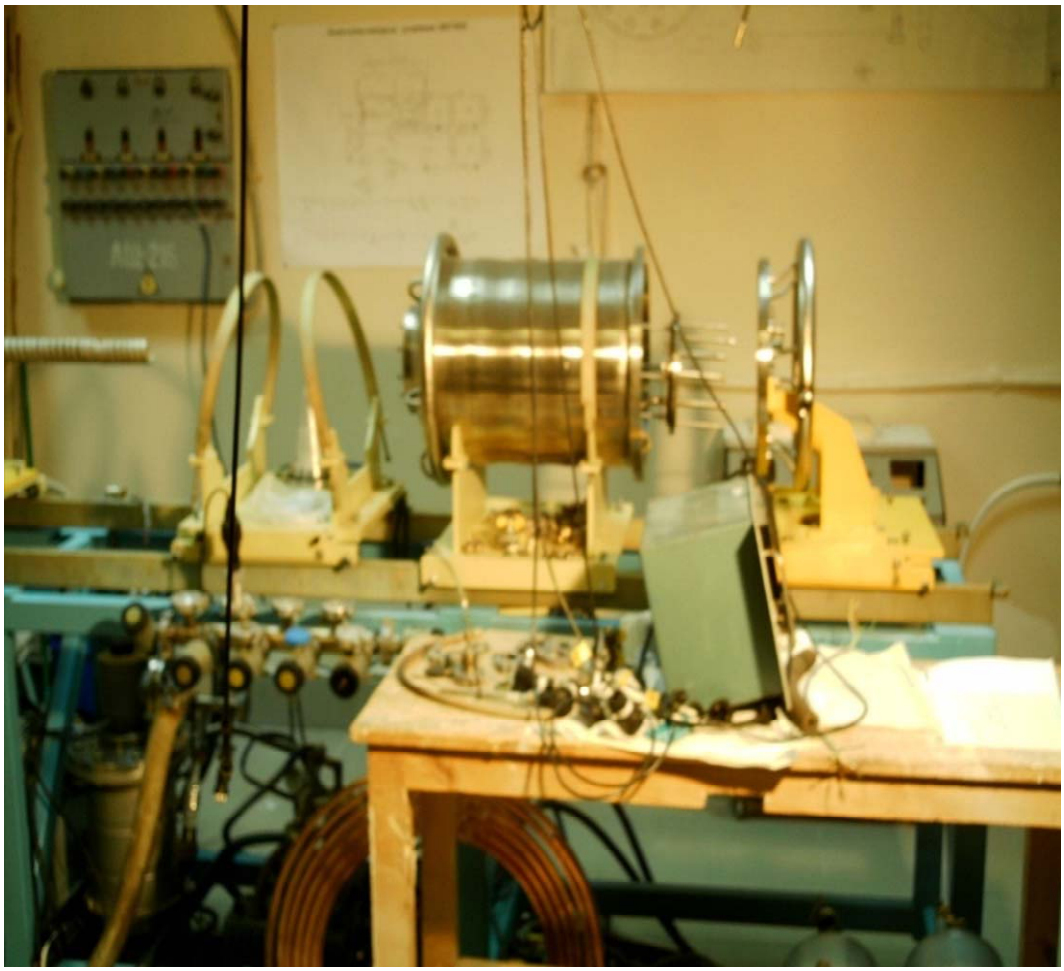

Assembling a prototype of ENUMM unit

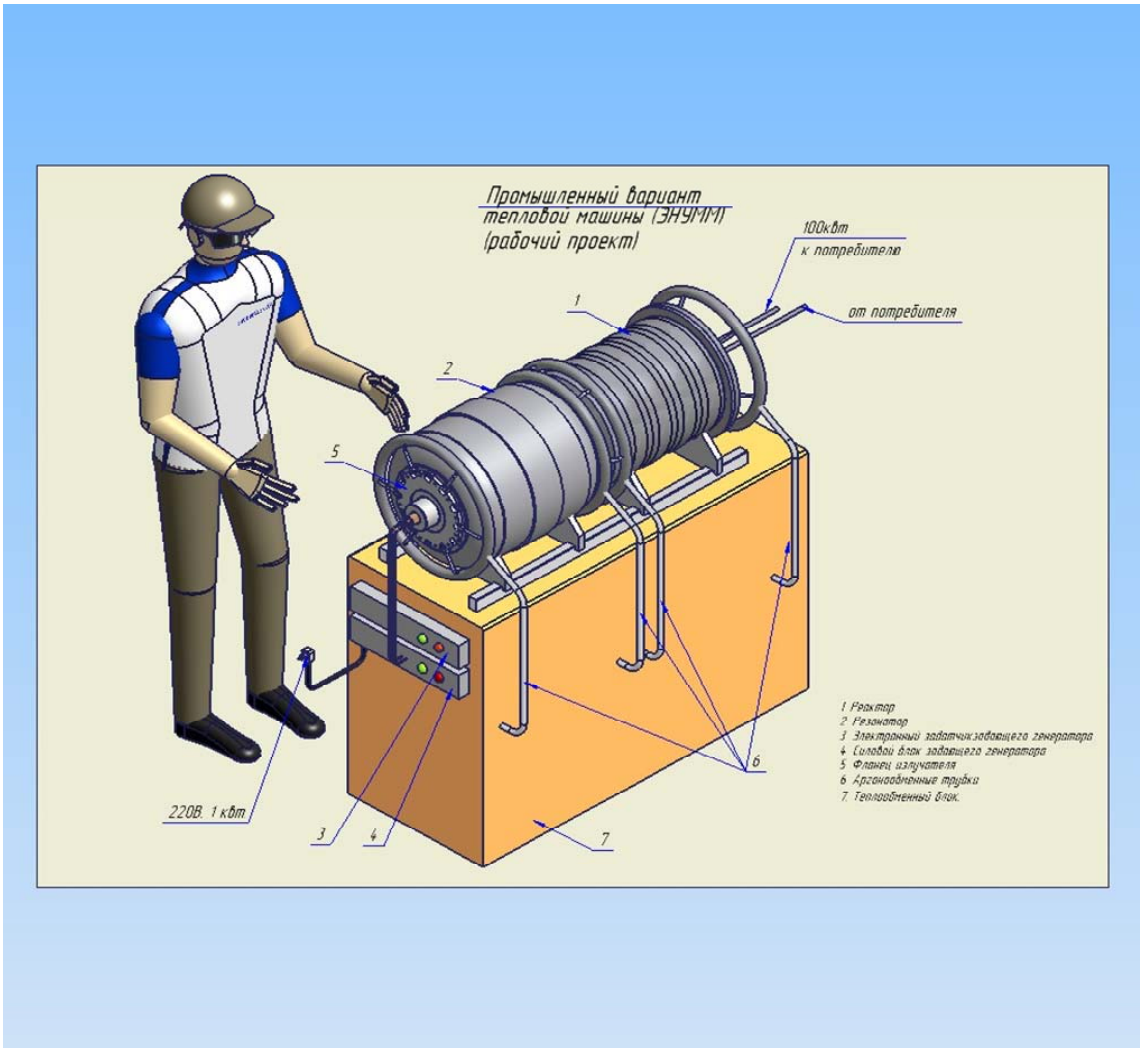

Computer simulation of ENUMM generator

Materials and Conditions (MC)

SURFACE PLASMONS EXCITATION ON METAL AND METAL HYDRIDE SURFACES

E.Castagna(*), V. Violante(**) , C.Sibilia(*), F. Sarto(**)

(*) La Sapienza University, Via Scarpa, 14 00100 (Roma) Italy
(**) ENEA Frascati Research Center V.le E. Fermi 45 00044 Frascati (RM) Italy

Abstract

Surface plasmons (polaritons) are quantum of plasma oscillations created by the collective oscillation of electrons on a solid surface.

As a surface phenomenon, SP excitations is strictly dependent from the physical and morphological properties of interface between metal and non-metal media: while bulk plasmons frequency ω_p is a constant typical of the considered material, the SP one, ω_{sp}, is also a function of boundary conditions, i.e. non-metal dielectric constant and metal surface roughness**.** The latter condition is quite interesting if using a laser beam incident on metal surface to excite SP. To obtain SP excitation in this way one has to fulfill the matching condition between laser wave vector and SP ones real component; such an excitation is theoretically not allowed on a smooth interface, because both energy and momentum conservation could not be respected. Moreover, electric field has to belong to the incidence plane, i.e. the wave has to be polarized in the p mode: if the electric field is perpendicular to incidence plane, and thus parallel to the interface (s-type polarization), it would assume the same value in the two mediums, without giving rise to the charge displacement needed to excite surface plasmons. Using a prism coupler placed on the surface, a minimum of the reflectance in the laser beam intensity, for an incidence angle larger than the total reflection one, indicates a resonant condition for plasmons creation. An interfacial corrugation could act as a diffraction lattice, increasing incident radiation wave vector, thus satisfying the requested matching condition.

INTERPLAY BTWEEN DEUTERON AND HOST ATOMS IN METAL DEDUCED FROM LOW-ENERGY BEAM EXPERIMENTS

H. Yonemura, Y. Ishikawa and J. Kasagi

Laboratory of Nuclear Science, Tohoku University, Sendai, Japan
kasagi@lns.tohoku.ac.jp

Abstract

In order to investigate the interplay between deuteron and host atoms in metal, yield ratios of protons to tritons in the D(d,p)t reaction in various metals have been measured for $10 < E_d < 20$ keV with a Si detector placed at 148^o. The observed yield ratios are much smaller than the simple kinematical values, and, systematically decrease as Z number of metal increases. Monte Carlo simulations, which include an electronic energy loss process together with nuclear energy loss and scattering of deuteron on host atoms, have been carried out. It is found that, in order to reduce the ratio, a strongly screened potential which gives more isotropic angular distributions for the deuteron scattering on host atoms in metal is required. We discuss the screening energy of the D+D reactions in metal, also.

1. Introduction

It was found from deuteron beam experiments that screening potential for the DD reaction in metal shows very large values up to 300 eV [1-3]: this causes enhanced reaction rates at energies far below the Coulomb barrier. However, the origin of the large screening is not understood well, yet. In addition, the reaction products observed in cold fusion experiments suggested the change of reaction mechanism from the normal DD reaction to the unknown collective or cooperative DD reaction.

In order to see any change of reaction mechanism in beam experiments, we have continued measurements of nuclear reactions induced by deuterons with various conditions of host metals. Recently, the following measurement has been carried out: Yield ratio of protons to tritons in the D(d,p)t reaction in various metals.

The measurement has provided important information on the effective interaction between deuteron and atom in metal environment. In the present work, we show the results and discuss on the interplay between deuterons and the surrounding environments, especially on effective deuteron-atom interactions in various metals.

2. Yield ratio of protons to tritons in the D+D→p+t reaction in metal

Since the screening energy for the DD reaction in metals is much larger than the energy scale of the atomic systems, one might expect the effects on the kinematical quantities. We have

tested the possibility to see such an effect in yield ratios of protons to tritons in the D+D→p+t reaction detected with a single detector. The measured ratio is equal to the ratio of the solid angle ratio of protons to tritons which depends only on the bombarding energy as well as the detection angle, as shown as follows;

$$R = \frac{Y_p}{Y_t} = \frac{\left(dN_p/d\Omega_{lab}\right)}{\left(dN_t/d\Omega_{l\,ab}\right)} = \frac{\left(d\sigma/d\Omega_{cm}\right)_p}{\left(d\sigma/d\Omega_{cm}\right)_t}\frac{\left(d\Omega_{cm}/d\Omega_{lab}\right)_p}{\left(d\Omega_{cm}/d\Omega_{lab}\right)_t} = \frac{\left(d\Omega_{cm}/d\Omega_{lab}\right)_p}{\left(d\Omega_{cm}/d\Omega_{lab}\right)_t}. \quad (4)$$

Here, $(d\sigma/d\Omega_{cm(lab)})_{p(t)}$ is the differential cross section at the detected angle in the center-of-mass (laboratory) system for the proton (triton). Thus, the yield ratios of protons to tritons are easily predicted from the reaction kinematics, and any deviation from the kinematical calculation requires the change of the kinematics of the two-body colliding system.

Yield ratios of protons to tritons for the D+D → p+t reaction in metal have been measured with deuteron beams obtained from a low-energy ion beam generator at the Laboratory of Nuclear Science of Tohoku University. Protons and tritons were detected with a Si detector placed at 145 degrees with respect to the beam direction. The measurements performed for bombarding energies from 10 to 20 keV by 1 keV steps. Thin foils of various metals, ranging from Be (Z = 4) to Au (Z = 79), were bombarded as the host for the DD reaction. In order to obtain statistically significant results, both protons (and also tritons) were accumulated at least 1.6×10^5 counts at each bombarding energy for each foil.

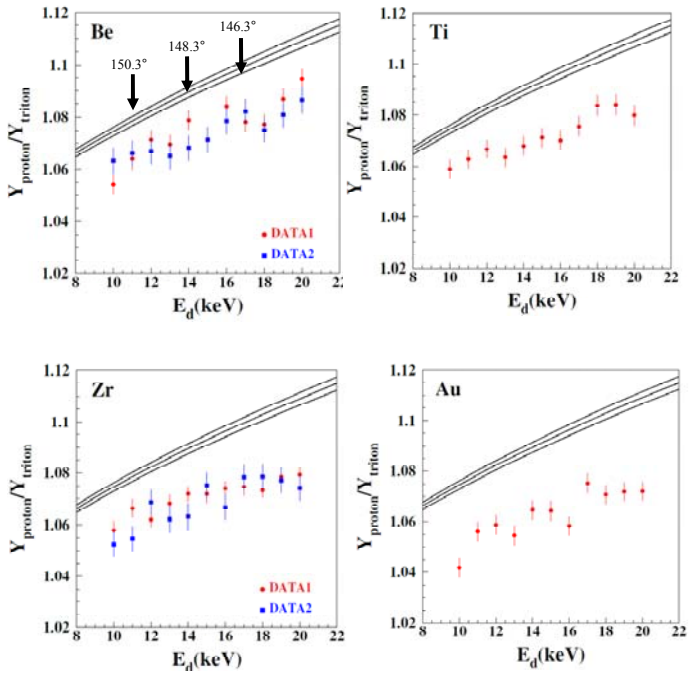

Fig. 1. *p/t yield ratio in the D(d,p)t reactions in Be, Ti, Zr and Au as a function of the incident deuteron energy. Solid lines show simple kinematical calculations for* θ_d *=148.3*^{o} *+/- 2.0*^{o}.

In Fig. 1, we show the p/t yield ratios measured for Be, Ti, Zr and Au compared with simple kinematical calculations which are shown with solid lines corresponding to detection angle (θ_d) of 148.3^o +/- 2.0^o. Although the kinematical calculations explain the trend of the p/t yield ratios, they always overestimate. The deviation becomes larger as the atomic number (Z) of host metal increases. In order to show the deviations more clearly, the mean value of the p/t ratios for each host metal is plotted as a function of Z in Fig. 2, where the averaged p/t ratios

are plotted with solid circles. The value calculated with a simple two-body kinematics for θ_d = 148.3^o is also shown with a solid line which is independent of Z. The experimental p/t values are about 2% smaller than the simple prediction and become smaller for larger Z. A dotted line in Fig. 2 corresponds to the two-body kinematics for θ_d =125^o. This indicates that the direction of an incident deuteron, which finally interacts with a target deuteron in metal and emits proton or triton, is changed due to the multiple scattering with host metal atoms.

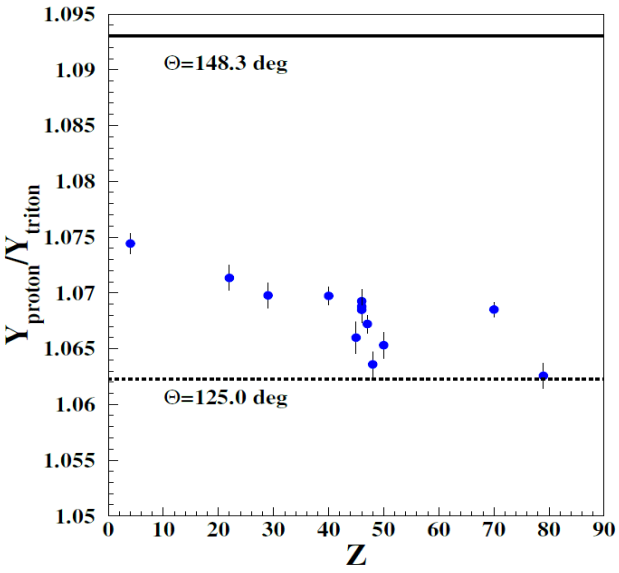

Fig. 2. *Values of p/t yield ratios versus Z of host atom. Closed circles are averaged over for deuteron bombarding energy between 10 and 20 keV. A solid line corresponds to the kinematical calculation for θ_d=148.3^o and a dashed line for θ_d=125^o.*

3. Multiple scattering and angular distribution of deuteron on host atom

In the metal foil, an incident deuteron scatters on host atoms during energy loss process and finally reacts with the target deuteron. Thus the kinematical conditions mostly differ from the two-body collision. We have carried out Monte Carlo simulations for the D+D reactions in metal and the experimental data are compared with the simulations.

We have modified the TRIM code [4]: latest data from SRIM [4] are employed for the electric energy loss and Ziegler's Universal potential is employed as a standard effective interaction: The Universal potential between deuteron and host atom determines scattering probability and angular distribution of scattered deuterons. The D+D reactions are assumed to occur in each step with a weight factor of σ(Ed) at that moment. The effect of the finite size of the incident beam and the detector are included in the simulation.

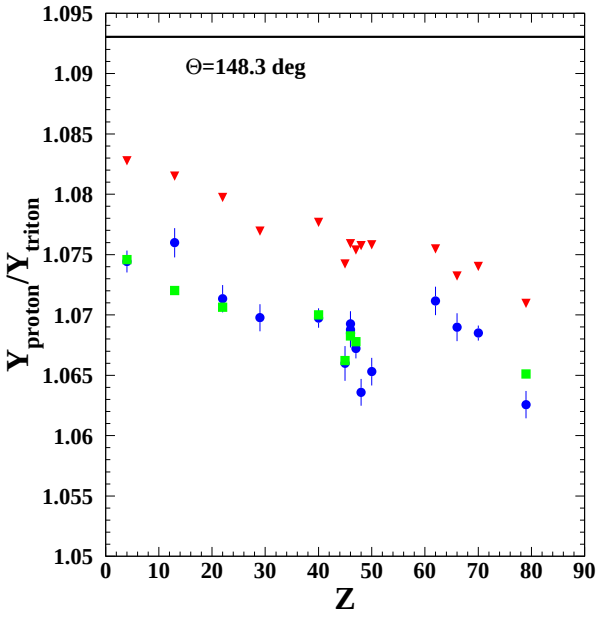

Fig. 3. *Averaged p/t ratios compared with calculations. Solid circles are experimental p/t ratios, triangles are results of the calculation with the universal potential, and squares are those with stronger screening.*

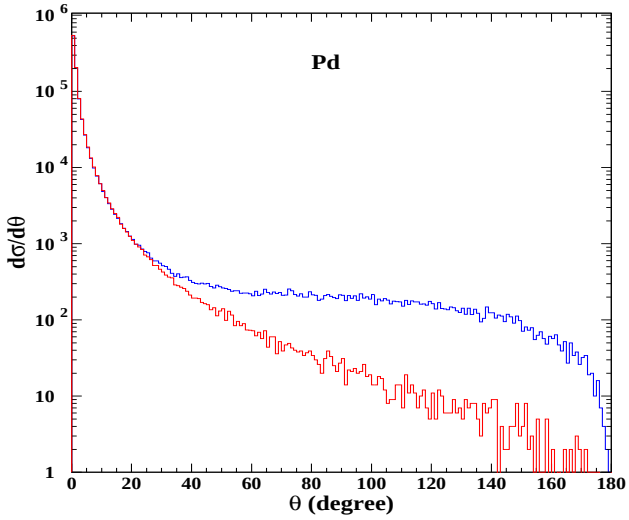

Fig. 4. *Angular distributions used in the calculation for deuteron scattering on host atoms. The lower one corresponds to the universal potential, while the upper additional isotropic part added.*

In Fig. 3 we compare the averaged p/t ratios (solid circles) with the calculated results (triangles). As shown, the scattering of deuteron on host atom changes p/t yield very much: it lowered the ratios about 1 to 2% and reproduces the trend of Z dependence. However, the data are still smaller than the calculations. We infer that the probability of backward scattering plays an important role. In order to reduce the ratio, larger probability of backward scattering is required. The squares correspond to the simulations in which isotropic angular

distribution is artificially added to the standard (Ziegler's Universal potential) calculations. Absolute values of the yield ratios together with the Z dependence are explained very well by the modification of the angular distribution. In Fig. 4, we show the angular distributions ($d\sigma/d\theta$) of the deuteron-Pd scattering in Pd metal for Ed = 15 keV, which are employed in the simulation. The angular distribution calculated with the Universal potential which is used in the standard TRIM code is monotonically decreasing with the increase of the scattering angle. On the other hand, the angular distribution which reproduces the p/t yield ratio shows enhanced backward scattering.

4. Discussion on screening potential between deuteron and atom in metal

In metal environment, the conduction electrons play an important role to reduce the Coulomb repulsive potential between a deuteron and a host nucleus. In a naïve picture, the screened electrostatic potential of the nucleus with atomic number Z existing in the sea of conduction electrons is given by the Thomas-Fermi model: $\phi_s(r) = Ze/r \exp(-r/R_s)$; R_s is called a screening length, $R_s = (6\pi e^2 n_e/E_F)^{-1/2}$, n_e is the number density of electrons and E_F is the Fermi energy of the electrons. On the other hand, the universal potential deduced by Ziegler is expressed as,

$$\varphi(\frac{r}{a}) = 0.18\exp(-3.2\frac{r}{a}) + 0.51\exp(-0.94\frac{r}{a}) + 0.28\exp(-0.40\frac{r}{a}) + 0.028\exp(-0.20\frac{r}{a}).$$

Here, a is defined as $a = 0.8854a_0/(Z_1^{0.23} + Z_2^{0.23})$, where a_0 is Bohr radius and Z_1 and Z_2 are the atomic number of the projectile and the target.

The screening predicted by the universal potential is slightly stronger than that from the Thomas-Fermi model. For a Pd-D system, for example, Rs = 0.16 A is given by the Thomas-Fermi model, while Rs = 0.12 A is deduced from the universal potential. However, the universal potential alone cannot explain the p/t yield ratio and the more isotropic angular distribution is required for the scattering of deuteron on Pd, as discussed above. This means that the effective potential between the deuteron and the Pd atom gives much shorter screening length. In order to reproduce the angular distribution in Fig. 4, Rs 0.02 A is deduced; this is about 1/6 of the screening length predicted by the universal potential. Thus, much stronger screening mechanism might exist for deuteron-nucleus collision in the metal environment. It should be noticed that the stronger screening is required to explain the existence of an enhanced backward scattering of the nucleus-deuteron collisions in metal.

It might be expected that a similar enhanced mechanism can occur, also, for the D+D reaction in metal. For the D+D reaction, the universal potential gives Rs = 0.20 A, which correspond to the screening energy Us = 73 eV (again, slightly larger than the Thomas-Fermi screening, 50 eV). Thus, Rs = 0.03 A or Us = 440 eV is expected for the D+D reaction in Pd from a very simple consideration; the value of this large screening is close to the one obtained in the cross section measurements for the D+D reaction in Pd and in PdO.

5. Summary

We have measured the p/t yield ratio in the D+D reaction in metal with a single detector for the deuteron bombarding energy between 10 and 20 keV. The ratio is equal to the ratio of the solid angle ratio of protons to tritons, and depends only on the emitting angle with respect to the deuteron direction as well as the collision energy. A deviation of the ratio from a simple kinematical calculation was examined in detail by including the multiple scattering effects.

It was found out that averaged values of the p/t ratio for E_d between 10 and 20 keV are much smaller than the simple kinematical values, and, systematically decrease as Z number of metal increases. Monte Carlo simulations, which include an electronic energy loss process together with nuclear energy loss and scattering processes have been carried out. The standard calculation is the one which employs the Ziegler's universal potential between a deuteron and a host metal atom. Although the standard calculation reduces the ratio significantly and reproduces the trend of the experimental data, the observed deviations cannot be fully explained. In order to reduce the ratio, a strongly screened potential which gives more isotropic angular distributions for the deuteron scattering on host atoms in metal is required. The screening length for the Pd-D system deduced from the angular distribution gives 0.02 A, which is much shorter than expected from the universal potential between deuteron and Pd. Although an origin of such an enhanced mechanism of the screening is unknown, a screening potential of about 400 eV can be expected for the D+D reaction in Pd when similar enhancement is applied to the D+D reaction. Further investigations serve to fundamental understanding and to develop many applications.

This work is partially supported by the Grant-in-Aid for Scientific Research (No. 16340062 and 19340051) by JSPS.

References

1. H. Yuki et al., JETP Lett. 68 (1998) 823 ; J. Kasagi et al., J. Phys. Soc. Jpn, 71 (2002) 2881.
2. K. Czerski et al., Eur. Phys. Lett. 54 (2001) 449.
3. F. Raiola et al., Phys. Lett. B547 (2002) 193.
4. J.F. Ziegler and J.P. Biersack, code SRIM and TRIM, http//www.srim.org

NOVEL HIGHLY D-LOADED/HIGH D-DIFFUSIVITY NANOSTRUCTURED MATERIALS ON THE PD SUBSTRATE AS A POTENTIAL MEDIA TO ENHANCE LOW ENERGY NUCLEAR REACTIONS

A.G. Lipson[1], A.S Roussetski[2], B.F. Lyakhov[1], E.I. Saunin[1], D.M. Sakov[1], A.Yu.Tsivadze[1]

[1]Institute of Physical Chemistry and Electrochemistry, Russian Academy of Sciences, Moscow 119991, Russia
[2]P.N. Lebedev Physics Institute, Russian Academy of Sciences, Moscow 119991, Russia

1. Abstract

In order to enhance LENR effects in Pd-D system, two novel highly D- loaded/ high D-diffusivity materials containing multilayer structures deposited on top of Pd substrate have been explored. The first composite material synthesized in our Laboratory is representing a high capacity hydrogen storage media consisting of Single Wall carbon nanotube (SWCNT) layer encapsulated by thin Pd films electrodeposited on top of Pd foil (Pd-SWCNT composite). The second cathode material is a multilayer Pd-Re-Pd-Re structure electrodeposited on top of 50 micron Pd foil (Pd-Re multilayer). Results on nuclear emissions from Pd-SWCNT and Pd-Re multilayer cathodes during D-desorption showed that these novel materials are enable to enhance the LENR effects in deuterated solids and could be used as new type of cathodes allowing to trigger and enhance fusion reactions (compared to pristine Pd) during electrolysis.

2. Introduction

After more than 18 years studies of CMNS effects many issues concerning their nuclear nature are still at the table. So far typical LENR experiments on excess heat generation do not show signatures of nuclear effects giving a low credit with respect to nuclear origin of these processes. Very often, the magnitude of specific heat in excess heat generation experiments is considered as a main evidence of the nuclear processes in electrolysis experiments. However, even keV/Pd-atom range of specific energy of Excess heat would be not enough to convince physicist in a nuclear origin of the effect observed. Earlier we have already shown that Pd/PdO heterostructures loaded with deuterium generate DD-reaction products (3 MeV protons) as well as energetic alpha particles (10-16 MeV). This proof of nuclear origin of LENR was, however, concerned to exothermic deuterium desorption, taking place in an afterelectrolysis period. The ultimate goal of current research is to show *in-situ* statistically significant nuclear signatures during deuterium loading of nanostructured Pd compounds in one electrolysis run. On one side, it is hard to provide charged particle detection in-situ due to presence of the electrolyte, failure of the detector contact with the Pd foil cathode and possible mechanical damage of track detector's surface (in case of too tight detector

attachment). On another side, the issue of the Pd-based cathode material selection must be crucial to trigger nuclear processes caused by deuterium impingement in it. Pristine Pd cathodes (even with a special treatment, such as annealing and etching) do not show measurable nuclear emissions during and after D-loading.
To enhance CNMS effects in electrochemical processes, we now propose to switch to the novel Pd based nanostructured materials (as the cathodes), allowing a large deuterium loading and/or high D – diffusivity at the surface resulting in a large DD-screening, drastic changes in phonon spectra as well as high quantum entanglement of deuteron pairs. To this goal, two novel highly D- loaded/ high D-diffusivity materials containing multilayer structures deposited on top of Pd substrate have been explored.

3. **Experimental: Pd-SWCNT properties**

In order to enhance LENR processes at the surface we synthesized a composite material representing a high capacity hydrogen storage media consisting of Single Walled Carbon Nanotube (SWCNT) layers encapsulated by thin Pd films electrodeposited on top of Pd foil (Pd-SWCNT composite) (Fig.1). The SWCNT, etched in concentrated nitric acid can be easy loaded with hydrogen by electrolysis of the Pd-SWCNT cathode and reproducibly show high capacity value (8-12 wt. % of H_2) or loading ratio H/C ~1.5.
Palladium metals possess a unique property to dissociate molecular hydrogen into an atomic form while simultaneously exhibiting high H-diffusivity of a quantum character. Thus, if SWCNT's could be embedded into a Pd–matrix, the result would be an atomic hydrogen/proton flux tunneling into the nanotubes during the H-loading. Based on the assumption that significant hydrogen flux can permeate through the Pd coating into the SWCNTs openings, hydrogen could be effectively loaded into the nanotubes.
Here we explored a new synergetic approach based upon combining the unique Pd properties high H-flux diffusivity) with that of SWCNT (high potential capacity) with respect to hydrogen. Three types of SWCNTs with the same diameter (1.3 nm), but various lengths, and purity were evaluated: (1) HiPco^{TM} Bucky^{TM} tubes, lot #79, manufactured by Carbon Technologies Inc., (length range 0.5-1.5 μm, purity 95%); (2) SWCNT 7782-42-5, Helix Material Solutions, Inc., (length range 2-20μm, purity 90%); (3) SWCNT Alfa-Aeser (length range 15-40 μm, purity 95%). The 50- μm thick cold- rolled Pd foils (Johnson and Mathew, 99.95 %), with an area of S =1.5-2.0 cm^2 were used as the substrate for SWCNT deposition. To clear the nanotube openings from steric obstacles, the SWCNTs were etched in concentrated nitric acid, for 3 h at T=300 K. The procedure for the Pd foil preparation is described in [11]. A thin Pd layer of ~ 0.6 μm thick was electroplated onto the Pd foil (Pd′ layer) on both sides from the $PdCl_2$ electrolyte [12]. The gel of the SWCNT was extracted from the water suspension with pH = 6.5, and applied by dipping the top of the Pd′/Pd/Pd′ sample. To encapsulate the SWCNT in the Pd matrix, an additional thin layer of Pd was electroplated on the SWCNTs, coating both sides. The synthesized Pd′/SWCNT/Pd′/Pd/Pd′/SWCNT/Pd′ composite foil was subjected to a final annealing in a high vacuum at t = 500 °C for 2 h. Similar reference foils of Pd′/Pd/Pd′ type (with electroplated Pd, but no SWCNTs) were used for comparative analysis of the hydrogen content in the SWCNT. The Pd substrates of reference samples were cut from the same Pd sheets that served for preparation of composite samples with SWCNT (1),(2) and (3), respectively. Other types of reference samples were synthesized similarly to the Pd′/SWCNT/Pd′/Pd/Pd′/SWCNT/Pd′ samples, but using only the original SWCNTs (1*) that were not etched in HNO_3 .

The interface SEM images of the Pd′/SWCNT/Pd′/Pd/Pd′/SWCNT/Pd′ samples are presented in Fig. 1 At a higher resolution (×120000, Fig. 1(b)) the internal interface between the SWCNT filaments (image in the center) and the electrodeposited Pd coating (site at the edges in gray) are clear and distinctive.

Both the Pd′/SWCNT/Pd′/Pd/Pd′/SWCNT/Pd′ (composite) and the Pd′/Pd/Pd′ (reference) samples were electrochemically loaded with hydrogen in a special cell with a platinum anode, containing 1 M NaOH solution [11]. The electrolysis was preformed at a fixed temperature in a galavanostatic mode at a constant current, with densities ranging from 3 to 30 mA/cm^2 for a period of 0.5 to 4.0 h. The total electric charge density that passed through the cathode was kept constant at Q=45 C/cm^2. Immediately after the electrolysis procedure, the samples were transferred into a Dewar glass containing liquid nitrogen to prevent spontaneous hydrogen desorption at ambient temperature. Next, the Dewar glass with the sample was connected to the input of the vacuum desorption apparatus where the samples were rapidly heated to 673 K. The absolute hydrogen concentration in the samples was determined by an isothermic vacuum desorption technique at T = 673 K with a residual gas pressure of 2.0×10^{-6} torr.

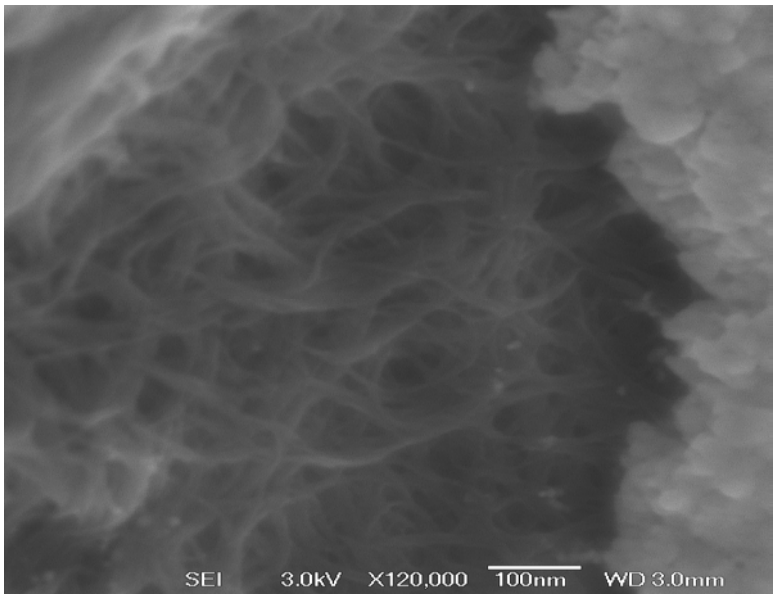

Figure 1. *SEM image of the Pd-SWCNT interface after 1 min -etching in nitric acid: magnification at x 120000*

All samples tested, showed detectable amounts of desorbed hydrogen (Table I). The volume of released hydrogen from the Pd′/SWCNT/Pd′/Pd/Pd′/SWCNT/Pd′ composite cathodes with the etched SWCNT (1), (2), (3) – (Table I, lines 2,4,6) exhibited approximately 20% to 25 % excess hydrogen, compared to the reference samples of Pd′/Pd/Pd′ without the SWCNT (Table I, lines 1,3,5,7). Compared to the reference samples (lines 1,3,5,7) however, there was no excess H_2 in the composite sample with non-etched SWCNT (1*) (Table I, line 8), thus indicating an absence of SWCNT loading.

Table I

Volumetric hydrogen concentration in the Pd′/SWCNT/Pd′/Pd/Pd′/SWCNT/Pd composite and the Pd′/Pd/Pd′ reference samples loaded by electrolysis at a constant temperature, T=290 K. The electrolysis charge transferred through the cathode is Q = 45 C/cm^2.

#	Sample type	Mass [g]	Desorbed H_2 Volume, [cm^3]	<x>=[H]/[Pd]	C_H, [% wt.]
1	Pd′/Pd/Pd′	0.208	14.61±0.21	0.68±0.01	-
2	Pd′/SWCNT/Pd′/Pd/Pd′/SWCNT/Pd′-(1), M(SWCNT)=2.8 mg	0.207	18.40±0.32	0.86±0.03	12.0±1.4
3	Pd′/Pd/Pd′	0.142	9.83±0.12	0.66±0.01	-
4	Pd′/SWCNT/Pd′/Pd/Pd′/SWCNT/Pd′-(2), M(SWCNT)=2.2 mg	0.146	11.80±0.20	0.79±0.02	8.0±1.0
5	Pd′/Pd/Pd′	0.140	9.80±0.13	0.66±0.01	-
6	Pd′/SWCNT/Pd′/Pd/Pd′/SWCNT/Pd′-(3), M(SWCNT)=1.8 mg,	0.141	11.39±0.23	0.78±0.02	7.8±1.2
7	Pd′/Pd/Pd′	0.145	10.13±0.24	0.66±0.02	-
8	Pd′/SWCNT/Pd′/Pd/Pd′/SWCNT/Pd′-(1*), M(SWCNT)=1.8 mg	0.148	10.04±0.20	0.65±0.02	0

The samples of Pd′/SWCNT/Pd′/Pd/Pd′/SWCNT/Pd′ - (1), (2) and (3) are synthesized with the SWCNT of types (1), (2) and (3), respectively. The sample of Pd′/SWCNT/Pd′/Pd/Pd′/SWCNT/Pd′-(1*) is prepared with non-etched SWCNT of type (1). $<x> = [H]/[Pd] = [2N_L V] /(mN_A/M_A)$, where N_L – is the Loschmidt number; V – is the desorbed H_2 volume; N_A – is the Avogadro number, M_A –is the atomic weight of Pd; m- is the Pd mass. C_H is the SWCNT hydrogen capacity.

The repeatability of the hydrogen loading in the Pd′/SWCNT/Pd′/Pd/Pd′/SWCNT/Pd′ sample with SWCNT (1) is shown in Fig 2. During the five loading-deloading cycles, the effective loading ratio x= [H]/[Pd] in this sample had only minor fluctuations, which were comparable with the systematic error of volumetric hydrogen measurements, resulting in $<x_{eff}> = 0.86 \pm 0.03$, while the reference Pd′/Pd/Pd′ sample (Fig.2, curve 1) exhibited a constant value of $<x> = 0.68\pm0.01$. Note that the magnitude of the H/Pd ratio of $x\leq0.7$ is normally characterized as the highest Pd loading (PdH_x β-phase) that can be achieved electrochemically at a relatively low current density (j < 100 mA/cm^2) in an alkaline solution [15,16]. At the same time, the effective [H]/[Pd] loading ratio for composite samples with etched SWCNTs (1,2,3) (Table I) is well above the characteristic value of x = 0.7. Thus, etched SWCNTs encapsulated by layers of Pd electroplated onto a Pd substrate provide additional hydrogen storage capacity.

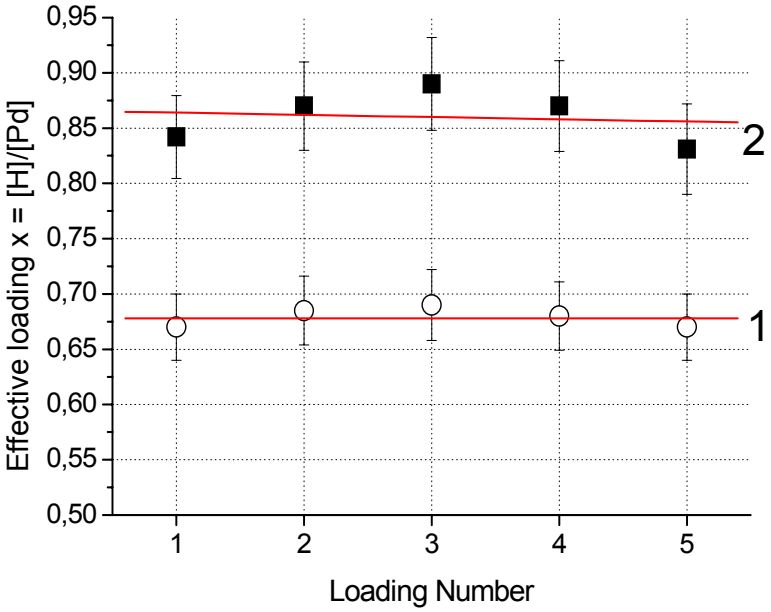

Figure 2. Hydrogen loading reproducibility for the Pd′/SWCNT/Pd′/Pd/Pd′/SWCNT/Pd′ with SWCNT- (1), (curve 2) and for the reference sample of Pd′/Pd/Pd′ (curve 1): 5 consecutive loading-deloading cycles. The loading: electrolysis at j=5.0 mA/cm^2 for 2.5 h. The deloading: vacuum heating at T=673 K.

The kinetics of H_2 escape from the SWCNT (1) at a constant temperature T=290 K are shown in (Fig. 3). The reference sample (curve1), demonstrates only a small reduction in loading x= H/Pd in the first 15 min (from 0.67 to 0.64). In contrast, the Pd′/SWCNT/Pd′/Pd/Pd′/SWCNT/Pd′ composite sample (curve 2), shows an exponential decay of effective loading, reaching x = H/Pd ~ 0.64 at t ≥ 60 min. Thus, the net H-loading contribution of the SWCNT remains above zero for at least 1 h (curve 3), after terminating loading. The short-time hydrogen desorption constant of SWCNTs (1) at room temperature suggests a low binding energy of hydrogen inside the SWCNT. This conclusion is also supported by measurements of effective hydrogen loading in both the composite and reference samples versus loading temperature in the range of 289-323 K.

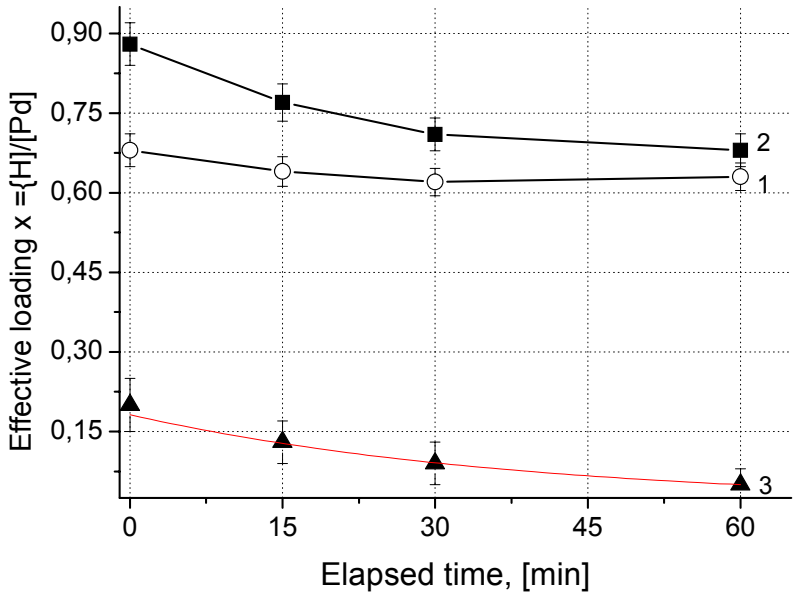

Figure 3. Effective hydrogen loading in the Pd′/SWCNT/Pd′/Pd/Pd′/SWCNT/Pd′ sample with SWCNT-(1) vs. time elapsed after completing the electrolysis at T=290 K (curve 2); the same for the reference sample of Pd′/Pd/Pd′ (curve 1); net loading in the SWCNT with the reference loading subtracted (curve 3).

The H-loading into the Pd′/Pd/Pd′ sample at temperatures above 290 K (Fig. 4) does not appear to be activation-dependent (curve1) because the β-phase in PdH_x cannot thermally decompose below T ~400 K [17]. On the contrary, in the case of the composite cathode (Fig.4, curve 2) a clear activation dependence (expressed as a reduction of effective loading vs. T) is observed. At T>315 K, the loading in both the Pd′/SWCNT/Pd′/Pd/Pd′/SWCNT/Pd′ and the Pd′/Pd/Pd′ samples becomes the same as a result of full SWCNT deloading. The experimental dependence of the effective hydrogen loading in the Pd′/SWCNT/Pd′/Pd/Pd′/SWCNT/Pd′ sample (Fig.4, curve 2) vs. temperature T can be satisfactorily fitted with a Boltzman sigmoidal function: $x(T) = a(b-a)\{1+\exp[(T-T_0)/c]\}^{-1}$, where a, b and c – are the numerical constants, and T_0 = 303.65 K, indicating the stability of hydrogen in the composite cathode at T≤ 273 K**.** The Arrhenius plot of the effective loading x(T) for the Pd′/SWCNT/Pd′/Pd/Pd′/SWCNT/Pd′ cathode is shown in the inset of (Fig.4.). The linear fit is consistent with the activation energy of the hydrogen absorption/desorption $\varepsilon_H = 0.14 \pm 0.02$ eV/H_2-molecule, which supports the existence of the hydrogen physisorption in the SWCNT [7-9].

The results obtained on activation energies of hydrogen in Pd-SWCNT–Pd nanostructured composite allow us to build up an energy diagram of hydrogen transport at the interface between the Pd matrix and nanotubes.

In summary, we found that electrochemically loaded SWCNTs encapsulated by thin Pd coatings onto a Pd foil provides a reproducible high gravimetric capacity (8-12 % wt.) with respect to hydrogen, well exceeding the 6 % wt. minimal requirement for practical application. We also demonstrated that hydrogen absorption occurs mainly within the inner space of the SWCNT and depends on the SWCNT length and purity. The activation energy of the hydrogen desorption from the SWCNT in this composite material was 0.14 eV/H_2-molecule, thus indicating relatively weak hydrogen binding in the nanotubes. These peculiarities of D-loading and binding in SWCNT suggest a high energy concentration over

D-loaded nanotubes resulting in both large electron screening of deuterons and phonon focusing inside the SWCNT encapsulated by Pd.

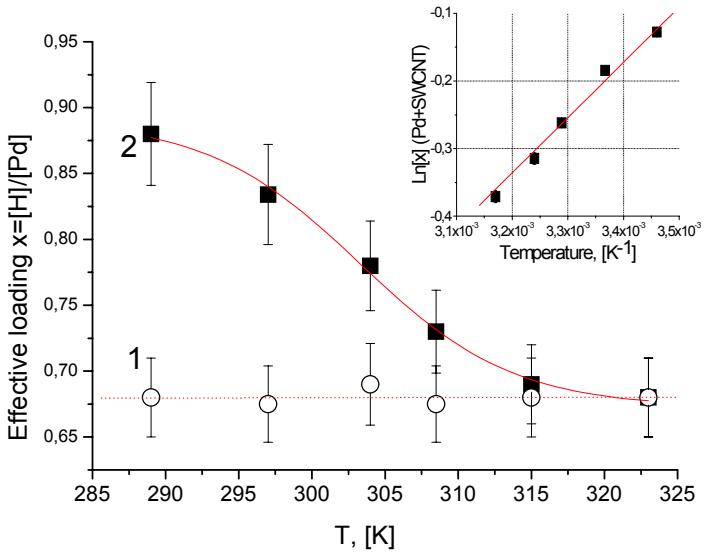

Figure4. Effective hydrogen loading in the Pd′/Pd/Pd′ (curve 1) and in the Pd′/SWCNT/Pd′/Pd/Pd′/SWCNT/Pd′ with SWCNT (1) (curve 2) samples vs the loading temperature. Samples were loaded at j=5.0 mA/cm^2 for 2.5 h.
Inset shows Arrhenius plot for the curve 2 data in the coordinates (1/T, Ln[x]). The linear fit is consistent with the activation energy of hydrogen absorption ε_H = 0.14 ± 0.02 eV/H_2-molecule.

4. Experimental: Nuclear Measurements

4.1. In-situ electrolysis

In order to confirm last conclusions on profitable properties of advanced Pd-SWCNT nanostructured composite material, in terms of LENR enhancement, we have performed cgarfed particles measurements in Pd-SWCNT – Deuterium system using CR-39 track detector technique. To this goal following series of experiments have been carried out:

- Charged particle detection: CR-39 (Landauer inc) with set of metal foil filters (Al 33 μm , Cu 25 μm thick) in order to estimate type and energy of emitted particles.
- Two types of experiment:

(a) in-situ electrolysis with Pd-SWCNT and Pd cathodes, separately both during 122 hr in 0.3 M LiOD/D2O electrolyte at j = 30 mA/cm2.
(b) Exothermic D-desorption from the cathodes after the short electrolysis (terminated as soon as loading reach x=D/Pd= 0.7).Time of exposure t = 10 x 3600 s, (t chosen accordingly maximal D-desorption rate).

To perform CR-39 measurements during in-situ electrolysis a special detector/cathode holder has been designed and manufactured. This holder allowed us to provide a full contact of CR_39 detector with the cathodes surface and simultaneously to prevent a damage of the CR-39 surface from the mechanical stress induced by D-loading into the cathode. A special

rubber filler has been inserted into the movable box of sample holder in order to soften deformation of the cathode sample.

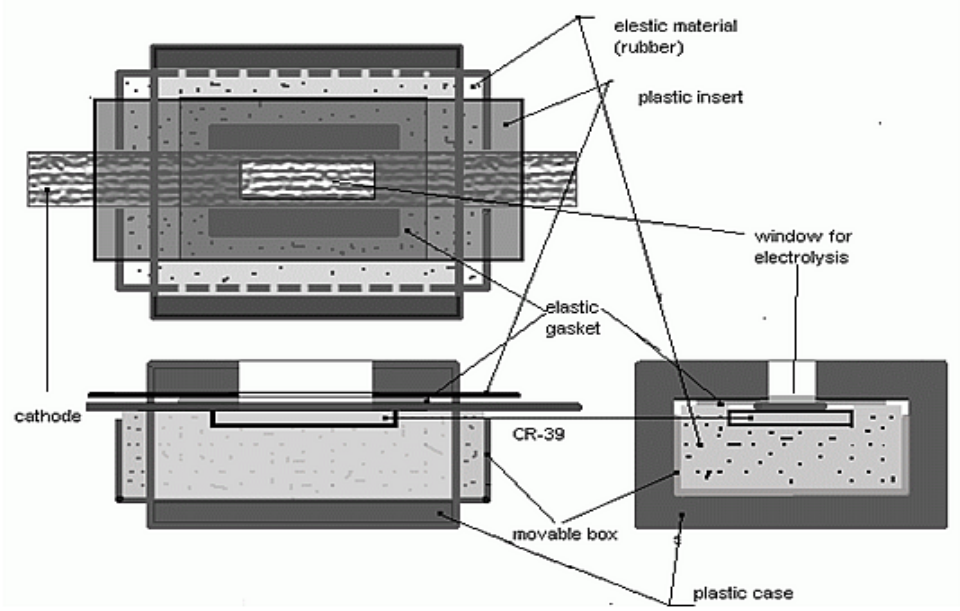

Figure 5. Design of the CR-39/cathode holder assembly for in-situ charged particle measurement during electrolysis experiment.

The CR-39 spectra (track number vs. track diameter) obtained during in-situ electrolysis measurements with the pristine Pd cathode (a) and with the nanostructured Pd-SWCNT-Pd cathode (b) are presented in Fig.6

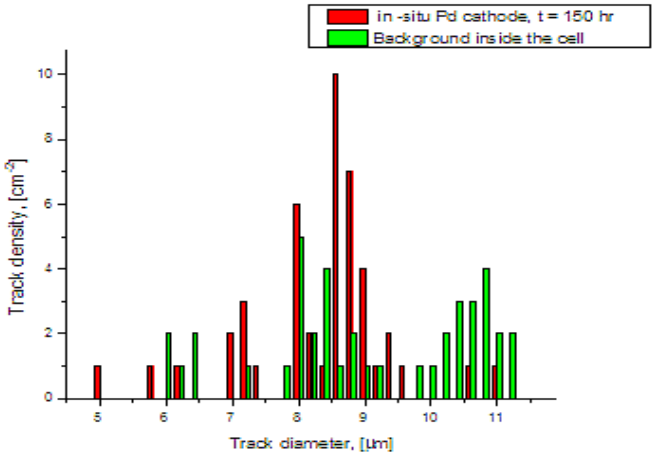

Figure 6a: In-situ electrolysis spectrum of CR-39 track detector attached to the pristine Pd cathode (red), the Background measurement result (CR-39 detector immersed in the electrolyte) is shown in green color.

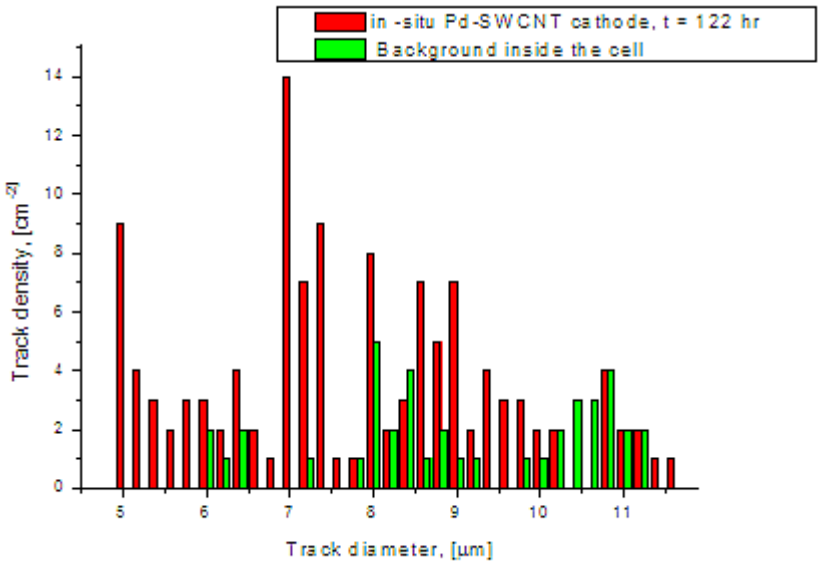

***Figure 6b**:* In-situ electrolysis spectrum of CR-39 track detector attached to the Pd-SWCNT-Pd cathode (red), the Background measurement result (CR-39 detector immersed in the electrolyte) is shown in green color.

The results of Background subtraction for both pristine Pd cathode and Pd-SWCNT nanostructured composite sample are shown in Fig. 7 (a,b) As seen from the figures, reflecting the net charged particle spectra, the character of track density vs. track diameter for pristine Pd and Pd-SWCNT cathodes is found to be completely different. There are no statistically significant tracks was found for pristine Pd cathode at track diameters ranging below 8 µm. At the same time, after subtracting of the Background there are two peaks well seen in the Pd-SWCNT CR-39 spectrum. According to calibrations and our earlier results the peak in the range of 5-5.6 µm track diameter corresponds to 3.0 MeV protons from DD-reaction occurred near the surface of the Pd-SWCNT cathode during electrolysis. Simultaneously, the peak in the range of 7.0-7.8 µm track diameters can be identified as a signature of energetic alpha-particles with energies ranging from 11 to 16 MeV, approximately.

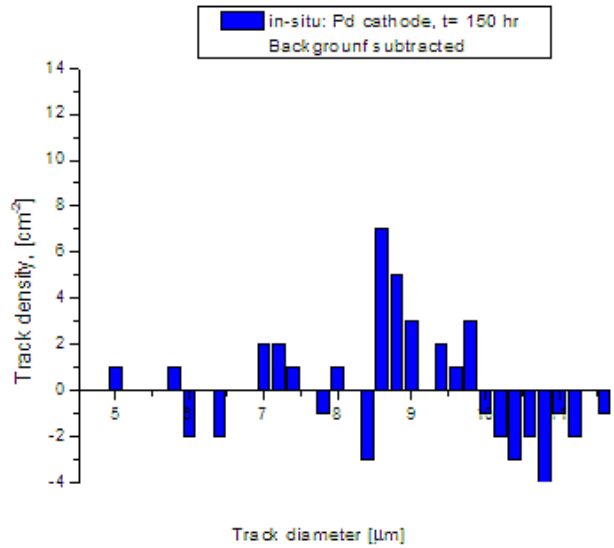

Figure 7a Net track density of CR-39 detector exposed with the pristine Pd cathode

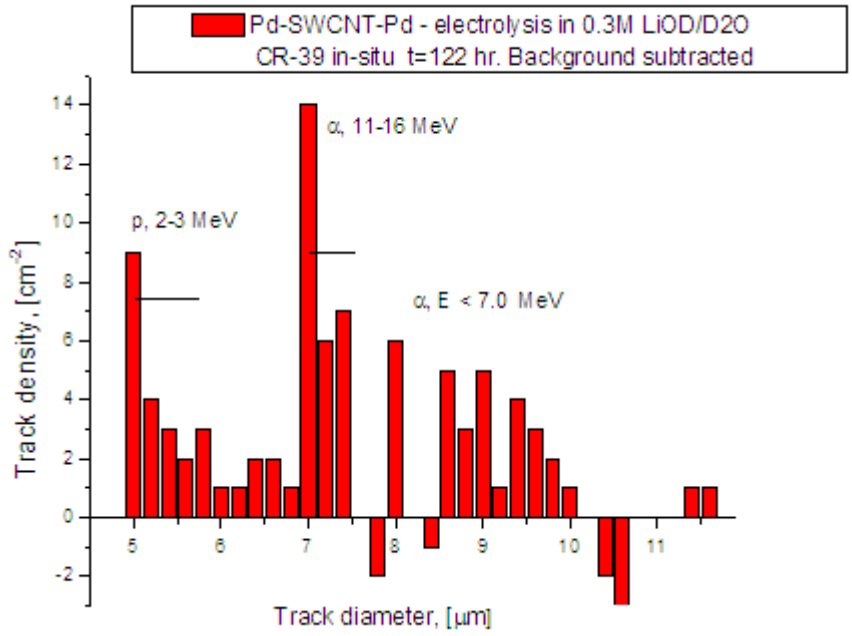

Figure 7b Net track density of CR-39 detector exposed with the Pd-SWCNT- Pd nanostructured cathode.

The average rate of nuclear emissions from Pd-SWCNT cathode during 122 hr of electrolysis is found to be statistically significant and constitutes taking into account detection efficiency []:

$\langle N_p \rangle = (5.24 \pm 1.09) \times 10^{-4}$ p/s-cm^2 for 3.0 MeV DD-protons and $\langle N_\alpha \rangle = (1.04 \pm 0.15) \times 10^{-3}$ α/s-cm^2 for energetic alphas, respectively.

For comparative purpose in Fig. 8 one can see the net contribution of the SWCNT (D/C = 1.5) in the charged particle emissions when the Pd cathode CR-39 result is subtracted from that of the Pd/SWCNT/Pd one.

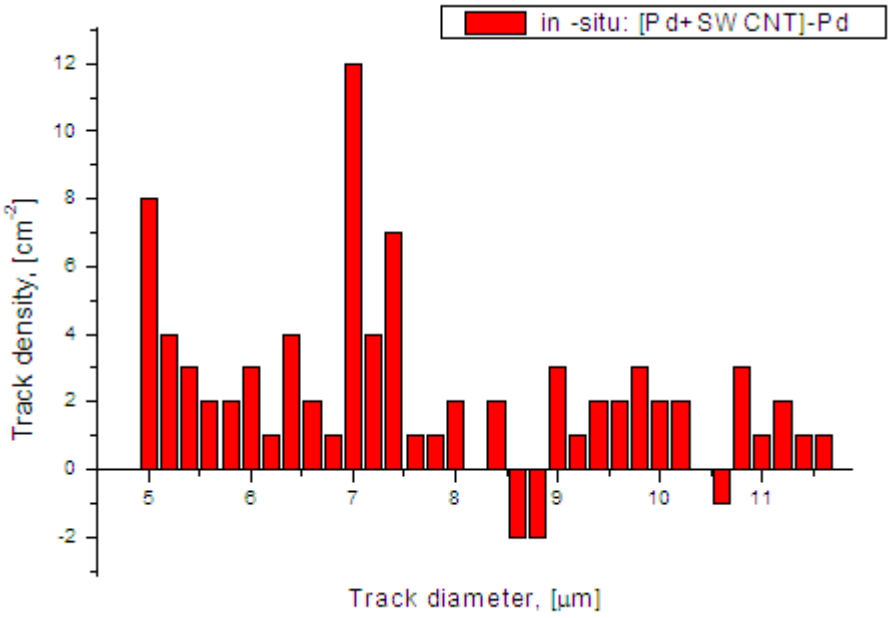

Figure 8. Net SWCNT (D/C = 1.5) contribution in charged particle emissions in-situ: the Pd cathode CR-39 result is subtracted from that of the Pd/SWCNT/Pd

It is well seen (compare Fig.8 and 7b) that almost all contribution of charged particle tracks during in-situ electrolysis is caused by presence of SWCNT in the Pd-SWCNT-Pd composite cathode.

4.2. D-desorption after electrolysis

Charged particle emissions during after electrolysis period have been studied with Pd-SWCNT-Pd and Pd-Re-Pd multilayer structures (50 μm Pd base coated with 6 Pd-Re layers of 0.5 μm each). To this goal 10 electrolysis –D-desorption cycles were performed with each sample. The duration of electrolysis has been chosen by this way in order to provide mean loading ratio of the sample x = D/Pd = 0.7. The D-desorption run with exposure of the samples to CR-39 detectors has been carried out at t = 20 C during 1.0 hr. Thus, in total, the time of Foreground CR-39 detector exposure for each individual sample was t = 10x3600 = 36000 s. To provide particle identification and their energy estimate the sets of 25 μm Cu and 33 μm Al filters were also used.
The results of after electrolysis measurements with Pd-SWCNT-Pd sample are shown in Fig.9 The inset from the right shows net charged particle emission with the Background subtracting. As seen from the Fig.9, a two band charged particle track structure is observed in Pd-SWCNT sample after electrolysis. The similar charged particle structure has been found with this samples during in-situ electrolysis with the open CR-39 detector. The numerical results on charged particle emission averaged over 10 hr of the exposure are the following:
$<N_p>$ = =(1.7±0.7) x10^{-3} p/s-cm^2 for 3.0 MeV DD-protons and $<N_\alpha>$ = (2.8±0.9)x10^{-3} α/s-cm^2 for energetic alphas, respectively.
These results in absolute value are a bit higher than that in in-situ measurements, but less statistically significant. In order to be sure that real proton and alphas were observed during sample exposure to the open CR-39 we have performed also additional measurements with the CR-39 detectors filtered with metallic foils. The data obtained during Pd-SWCNT-Pd sample exposure with the those CR-39 detectors is shown in Fig. 10 a,b. These data show that at least alpha particles are identified quite correct.

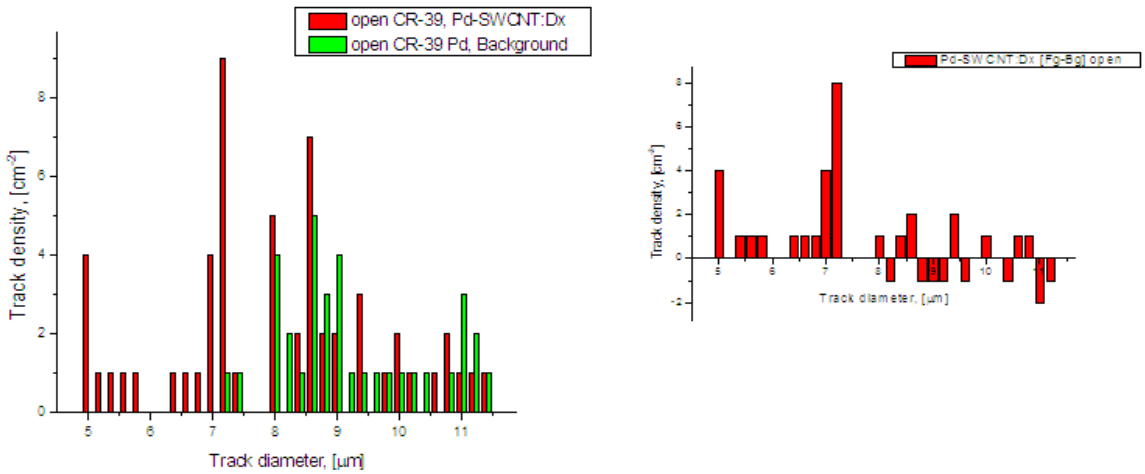

Figure 9. Pd/SWCNT/Pd after electrolysis: t = 10 x 3600 s, open CR-39 data. The red inset from the right shows net charged particle emission with the Background subtracting.

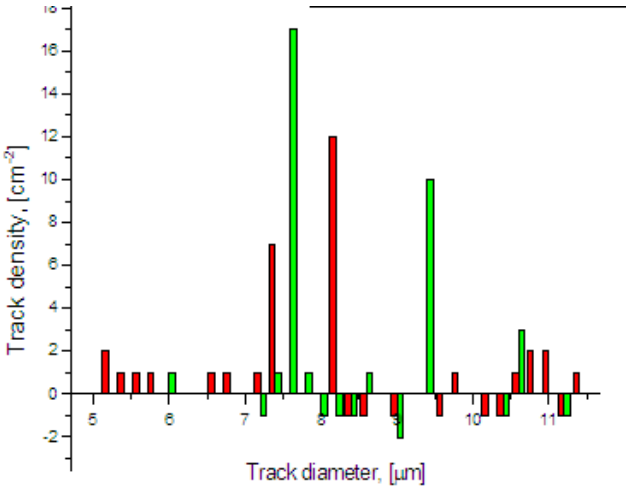

Figure10a. The charged particles emissions (with the background subtracting) from Pd-SWCNT-Pd cathode after electrolysis : CR-39 + 33 µm Al filter – red; CR-39 + 25 µm Cu filter-green

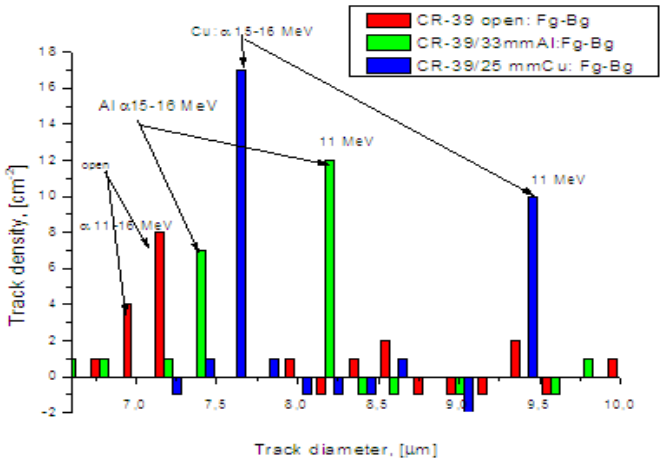

Figure 10b. Alpha particle identification (Foreground-Background data) with open and filtered CR-39 detectors. The energies of alphas are in good agreement with the accelerator calibration and their stopping ranges in Al and Cu foils.

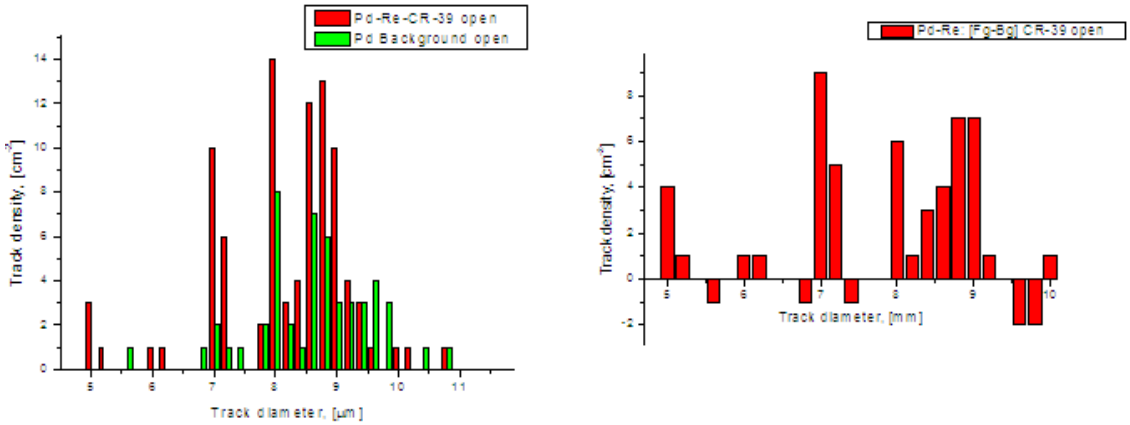

Figure 11. The charged particle emissions from Pd-Re-Pd:Dx sample after electrolysis with the open CR-39 detector. The right inset shows net effect with the Background subtracted.

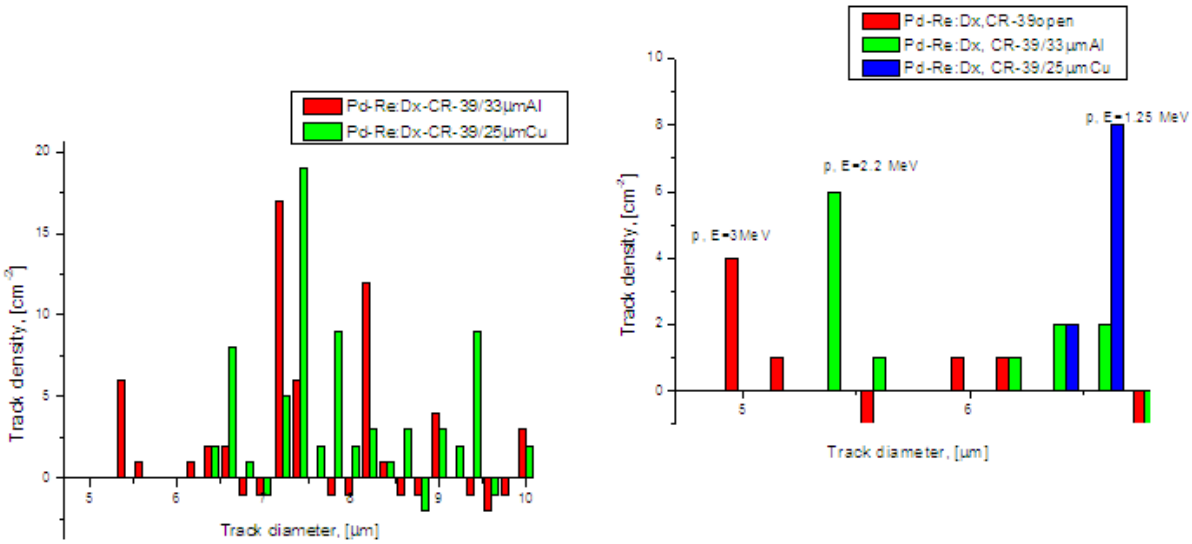

Figure 12. Pd/Re/Pd:Dx after electrolysis: t = 10 x 3600 s, 33μm Al and 25μm Cu filtered CR-39 data. Right graph shows 3 MeV proton identification

The CR-39 measurements performed with the Pd-Re-Pd multilayer structure after electrolysis showed the results similar to that obtained with the Pd-SWCNT-Pd cathode. The data on charged particle emission is shown in Fig. 11 and 12.

Due to similarity of the results obtained for Pd-SWCNT and Pd-Re cathodes in aftoelectrolysis runs we assume that the same energetic alpha particles have been emitted during these runs with both samples in the D-thermal desorption mode. The summary of energetic alpha spectra representing the sum of the Pd/Re:Dx+Pd/SWCNT:Dx runs with the filtered CR-39 detectors after reconstruction of the energy spectra (according to our alpha calibration curves obtained with the accelerator []) is shown in Fig. 13. As seen, within the standard deviation the spectrum obtained with the 33 μm Al filter is quite similar to that for 25 μm Cu. Both spectra contain low energy (10-12 MeV) and high energy (14-16 MeV) components.

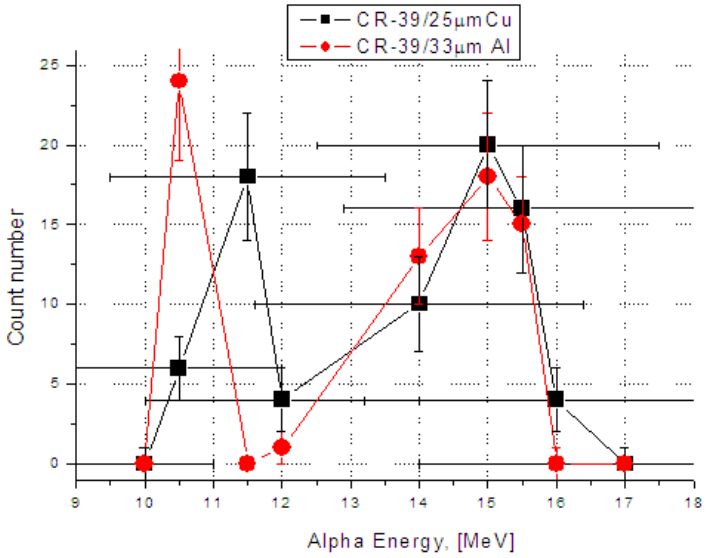

Figure 13. Reconstruction of alpha spectra for the CR-39 detectors with 25μm Cu and 33 μm Al filters for the sum of the Pd/Re:Dx+Pd/SWCNT:Dx runs (Background subtracted).

5. Conclusions

- First in-situ CR-39 measurements showed that the Pd/SWCNT/Pd cathode during electrolysis generates both 3.0 MeV (DD) protons and high energy alphas in contrast to the pristine Pd cathode showing a null result. The Pd/SWCNT/Pd cathode in-situ gives a statistically significant result just in one 5- days electrolysis run.
- The results (in particular, the absence of electrolyte penetration and CR-39 surface damage as well as coincidence of track diameters with those obtained in dry experiments) also show that a new sample/detector- holder assembly tested in the electrolysis runs provides a suitable technique for charged particle detection during in-situ electrolysis experiments.
- The charged particle emission results obtained with the Pd/SWCNT/Pd:Dx cathode after its D-loading (in exothermic D-desorption mode) show lower significance, especially for DD-reaction products (3 MeV protons). The results for the Pd/Re/Pd:Dx sample are similar to that obtained with the Pd/SWCNT/Pd cathode.
- Both the samples, however, show a reproducible energetic alpha emission with the two peak (11 and 15 MeV) spectra, which similar to that for the Pd/PdO:D(H) system, but differ from the alpha spectra generated by TiDx (only one peak at $E\alpha \sim 14$ MeV).
- Entire results show that nanostructured composite materials deposited onto the Pd foil substrate and providing high D-loading/high D-diffusivity allow to enhance CMNS effects compared to the pristine Pd cathode during both in-situ electrolysis and exothermic D-desorption measurements.
- The charged particles detected during in-situ and after electrolysis experiments show both DD-reaction and energetic alpha particle signatures. This indicates the same origin of the CMNS effects occurred during and after electrochemical loading of the cathodes.
- The CMNS effects could be further enhanced with increase in D/C ratio (> 1.5) in SWCNTs encapsulated by thin Pd layers onto a Pd substrate.

LUMINESCENCE OF MICRO-BUBBLES FROM LIQUIDS

Kuzmin R., Serov P.

Physical Faculty of Moscow State University by the name of M. Lomonosov.
E-mail: Kuzmin_Runar@mail.ru, Serovpoul@mail.ru

The report presents the results of experimental studies and theoretical analysis of luminous bubbles from boiling liquid (water), diluted with luminous additives. Exit of micro-bubbles across the border section (between gas phase and liquid phase) exceeds liquid vapor layer several times. Normal micro-bubbles emitting through the border section between gas and liquid phase shows on the collective impact of micro-bubbles (the analogue to Mossbauer's effect). A comparison of luminous bubbles and their explosion afterwards with the ball passing formations (laboratory lightning ball) was given.

The time of super-accumulative processes in the gas phase influence on the spatial change of micro-bubbles. As illustrations of macro-quantization (under the limits of Ghaizenberg's ratio of uncertainties), the results of experiments with evaporating liquid, liquid flowing from wettable holes, the formation of gas bubbles in the liquid are given. In the latter case, the liquid can be described as similar to quark-gluon vacuum, when bubbles' "non-emitting" from the "hadronic" liquids requires more energy. All results presented in the phenomenological theory framework of graduated energy transfer.

Nuclear Transmutation (NT)

SURFACE STUDIES AFTER LOADING METALS WITH HYDROGEN AND/OR DEUTERIUM

J. Dash and D.S. Silver

Low Energy Nuclear Laboratory
Portland State University
Portland, Oregon
dashj@pdx.edu

Abstract

Surface studies of 40 μm thick Pd foils after electrolysis in D_2O / H_2SO_4 electrolyte for six minutes found inversions in isotopic ratios. Anomalous isotopic ratios were also found on the surface of a 350 μm thick Pd foil after electrolysis in the same electrolyte for 74 hours.

Introduction

Our 1994 publication [1] presented evidence of localized, microscopic surface concentrations of gold and silver on palladium cathodes which had been electrolyzed in an electrolyte containing either H_2SO_4 and D_2O or H_2SO_4 and H_2O. The unique capabilities of a scanning electron microscope (SEM) equipped with an energy dispersive spectrometer (EDS) made it possible to locate concentrations of these elements on a microscopic scale. Our experiments included the detection of excess heat. We suggested that the excess heat and unexpected elements could be explained by the energy released during transmutation of platinum to gold and palladium to silver in the presence of thermal neutrons.

A previous study by another group also reported elemental anomalies on the surface of palladium after electrochemical loading of deuterium [2]. A near surface enrichment of rhenium and silver was detected by x-ray photoelectron microscopy (XPS). These elements are present as impurities in the starting palladium at levels (50 ppm Rh and 100 ppm Ag), well below the XPS detection limit. It is not clear why nickel, which is present before electrolysis as an impurity at the 200-300 ppm level, was not similarly enriched to a concentration which could be detected by XPS. This report does not include a bulk analysis of a Pd cathode after electrolysis. The authors concluded that surface segregation of Rh and Ag impurities is most likely due to the forcing current and time during long-term electrolysis.

In another study by the same group [3], time-of-flight-secondary ion mass spectroscopy (TOF-SIMS) measurements of the Pd blank (no electrolysis) and Pd electrolyzed in H_2O gave the natural abundances of the stable Pd isotopes. However, two samples electrolyzed in D_2O

had more than 20% increases in Pd 106 intensities and decreases in Pd 105 intensities. These researchers suggested the possibility that Pd 105 obtained a neutron and became Pd 106. Although this SIMS research seemed promising, it was not mentioned in a later publication from this group [2]. Apparently, this research was terminated.

In 1994 we also published a report on the changes in surface topography and microcomposition of a palladium cathode caused by electrolysis in acidified light water [4]. A thin palladium cathode became bent and torn during electrolysis in acidified light water. Localized changes in composition, including the possibility of the formation of silver by neutron absorption, were reported.

Results of our SIMS study of Pd foils before and after electrolysis were presented in 1996 [5]. We found that there was an isotopic inversion on the surface of a Pd foil cathode which had been electrolyzed in acidified heavy water. In the spectrum from the control (unelectrolyzed Pd foil), the signal from Pd 106 (natural abundance 27.33 at.%) was slightly greater than the signal from Pd 108 (natural abundance 26.46 at.%). However, a SIMS spectrum from an electrolyzed Pd foil had a more intense signal from Pd 108 than from Pd 106. The difference between these two abundances decreases with increasing sputtering time. After sputtering for 50 minutes to a depth of about 0.3 μm, these two isotopes have the same abundance.
The same report included data on excess thermal power (0.3 W maximum) which was observed from electrolysis of acidified heavy water with a Pd foil cathode, compared with an identical cell containing a Pt cathode. After about 70 hours of electrolysis and a dormant period of 75 days, the cells were again electrolyzed. In 5 consecutive experiments totaling 20 hours over a period of 2 weeks the cell with the Pt cathode produced as much as 0.3 W excess thermal power compared with the cell containing a Pd cathode.

In 1997 we published the results of electrolysis experiments with titanium cathodes [6]. One experiment produced about 1 W excess thermal power compared with a control. Geiger-Mueller counters used to monitor radiation emitted by the cells showed no significant difference compared to background. LiF chips sealed in plastic and placed inside the cells before electrolysis also showed no significant difference compared to background. The Ti cathodes was examined before and after electrolysis, using SEM and EDS. A new microscopic feature on a cathode after electrolysis contained appreciable vanadium, one atomic number higher than titanium, just as silver is one atomic number higher than palladium and gold is one atomic number higher than platinum.

In the same publication [6], we presented evidence of microscopic, time-dependent changes in fibers on the surface of a Pd cathode which had been electrolyzed about 6 months earlier. Distinct changes in the morphology of one of the fibers occurred in two days during storage at room temperature and atmospheric pressure. An EDS spectrum of a new, oval-shaped feature showed that it contained an appreciable amount of silver. A spectrum from the same spot one month later suggested that silver was changing to cadmium, which is one atomic number greater than silver. This is further evidence which supports the possibility of transmutation.

Experimental methods

Palladium (AESAR stock # 11514) was cold rolled from 500 to 40 μm thickness. Each cathode was prepared from a piece of this foil 2 cm long and 0.8 cm wide which was spot welded to a Pt lead wire. The anodes were prepared in the same way, using Pt foil spot welded to a Pt lead wire.

The electrolyte contained 20 ml D_2O and 3.5 ml H_2SO_4 in one cell. A second cell contained 20 ml deionized H_2O and 3.5 ml H_2SO_4.. The heavy water and light water cells were connected in series (Fig. 1).

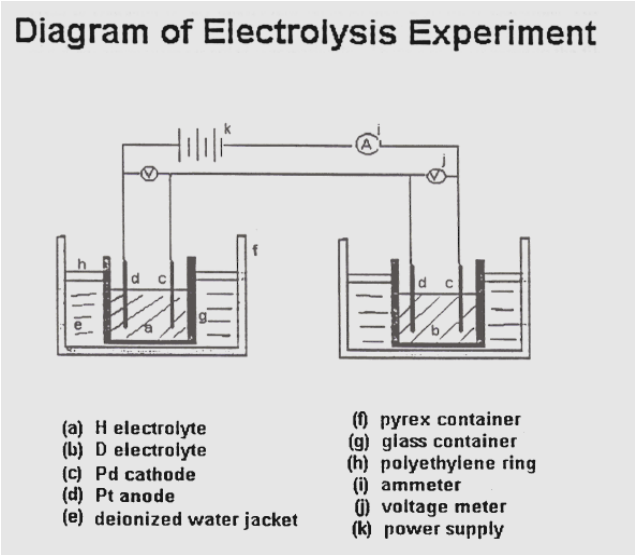

Fig.. 1. *The heavy water and light water cells are connected in series. Each cell has a Pd cathode and a Pt anode. All heavy water cathodes bent toward their anode 45 to 90 degrees, but the light water cathodes bent toward their anode only slightly.*

In one experiment the time of electrolysis was 6 minutes at a current density of about 0.25 A per cm^2. After microscopy of the electrodes was completed, SIMS analysis was performed on a control (no electrolysis) Pd foil from the same cold rolled strip, and on the Pd cathodes from the light water and heavy water cells.

The instrument used for these analyses was a PHI II SIMS, Model 3500, linked to a General Balzer 16 mm rod quadrupole mass spectrometer. Each sample was bombarded with a 3 KV Cs ion beam which scanned an area of about 1.4 mm x 1mm. Pd was sputtered from the cathode at the rate of about 0.1 nm per second. By sputtering for long times, it was possible to obtain the relative abundances of the isotopes versus depth.

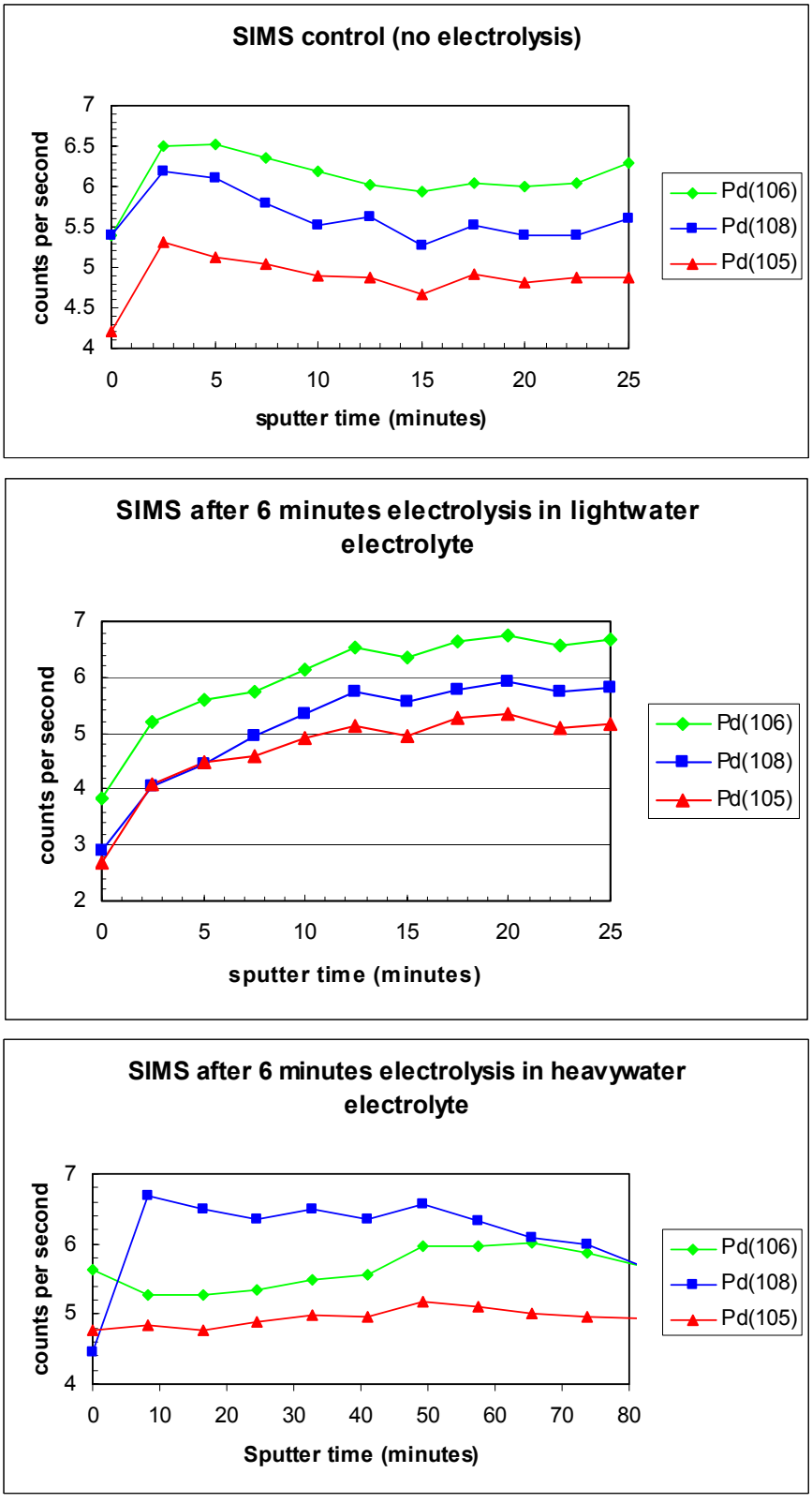

Fig. 2. *Depth profiles for the most abundant Pd isotopes : top – control (no electrolysis) , center – after H_2O electrolysis; bottom – after D_2O electrolysis.*

Results and discussion

The uppermost graph in Fig. 2 gives the signal intensities for the three most abundant Pd isotopes as a function of sputtering time for the control (no electrolysis) foil. As expected, Pd 106 gives the highest signal intensity (counts per second CPS), Pd 108 is next, and Pd 105 gives the lowest signal intensity. There is no significant change in signal intensity with increasing sputter time, i.e. with increasing depth into the sample. This is similar to the three other depth profiles taken from other locations on the unelectrolyzed control foil.

The SIMS results for the Pd foil which was electrolyzed for 6 minutes in H_2O electrolyte are given in the center graph, Fig. 2. After sputtering for 5 minutes, the relative intensities are in proportion to their natural isotopic abundances, i.e., 27.3% for Pd 106, 26.5% for Pd 108, and 22.3% for Pd 105. After 12 minutes of sputtering, the signal intensities are almost constant for all three isotopes until sputtering was stopped after 25 minutes. Four other regions on the same sample gave very similar depth profiles.

SIMS profiles were taken from nine different regions of the Pd foil which was electrolyzed in D_2O electrolyte. The bottom graph, Fig 2, shows a typical profile. After sputtering for about 10 minutes, there is clearly an inversion in signal intensity : Pd 108 now has greater signal intensity than Pd 106, whereas the opposite is expected, based on natural abundances. All nine of the depth profiles from this foil show this inversion. This suggests the possibility that Pd 106 absorbs a neutron, and becomes Pd 107 which beta decays to produce Ag 107, a stable isotope. Another possibility is that 106 PdD forms during electrolysis. This would appear in the SIMS spectrum as mass 108, thus increasing
the Pd 108 signal and diminishing the Pd 106 signal.
The bottom graph in Fig. 2 shows that the difference in signal intensities of Pd 106 and Pd 108 diminishes with increasing sputtering time. After 65 minutes, corresponding to a depth of about 0.4 μm, the signals from these two isotopes are identical. It appears that the process which caused the changes in signal intensities is confined to the outermost layers of the cathode surface. This is not surprising because the time of electrolysis was

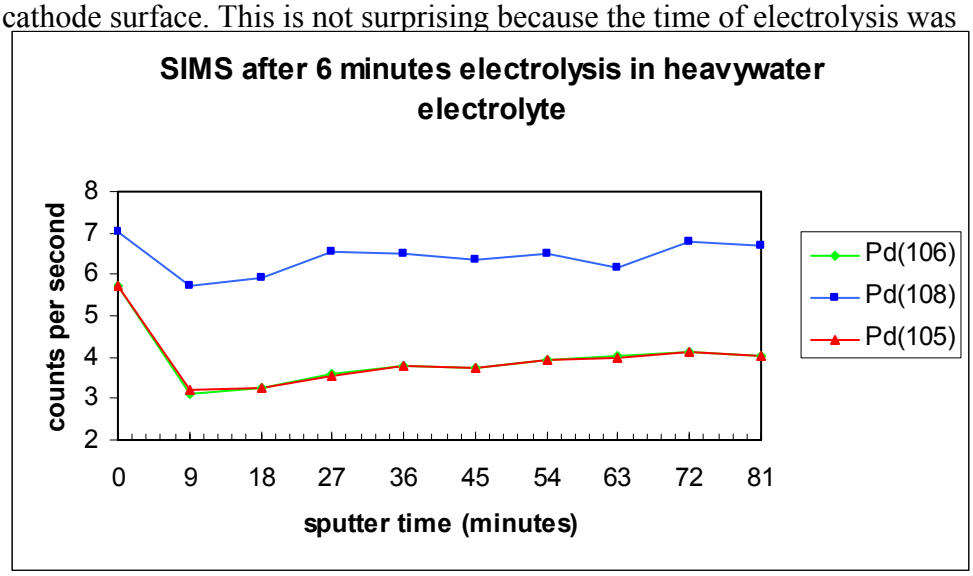

Fig. 3. *SIMS depth profile from a different area of the same Pd cathode.*
only 6 minutes, which would be insufficient for uniform hydride or deuteride formation.

Fig. 3 shows a SIMS depth profile from a different area of the same Pd cathode after electrolysis for 6 minutes in D_2O electrolyte. The signal from Pd 106 is far less than expected. It coincides with the signal from Pd 105 which has a natural abundance 5 at.% less than Pd 105. The signal from Pd 108 is consistently greater than that from Pd 105 and Pd 106 throughout the 81 minute sputtering time. There is no tendency for merger of the Pd 106 and Pd 108 signals, such as that shown in the bottom graph, Fig. 2.

SIMS profiles for 8 of the 9 analyzed areas of the heavy water electrolyzed Pd cathode show that there is also an inversion in the abundance of Pd 104 (11.14 at.% natural abundance) and Pd 110 (11.72 at.% natural abundance). Data for the control and for the light water and heavy water electrolyzed Pd cathodes are given in Fig. 4. The signal from Pd 110 is greater than the signal from Pd 104 throughout 25 minutes of sputtering, both for the control (upper graph) and for the 6 minute H2O electrolyzed Pd cathode (center graph). The lower graph gives data for the Pd cathode after electrolysis for 6 minutes in D_2O electrolyte. It shows that the signal from Pd 110 is only about half the intensity of the signal for this isotope in the upper 2 graphs, whereas the signal from Pd 104 for this cathode is only slightly less than that in the upper 2 graphs. The inversion is almost constant throughout the 81 minute sputtering time. Its cause may have may have a similar explanation to those suggested above for the 106/108 inversion.

In another experiment, Pd from the same stock was cold rolled from 0.5 to 0.35 mm thickness. A cathode 25 x 23 x 0.35 mm^3 was prepared from this. Electrolyte was prepared containing 6.7 g D_2O : 1 g H_2SO_4 and about 0.02 g Ti per ml of solution. Electrolysis was performed for about 6 hours per day for 8 days. Excess power compared to a control cell was observed for every run. It ranged from 0.5 to 2.6 W. The average was 1.8 W.

During electrolysis the Pd cathode bent toward the Pt anode to form a concave surface facing the anode. After electrolysis both the concave and convex surfaces were analyzed blind by National Renewable Energy Laboratory (NREL) scientists. The analyses included SIMS, SEM, and Auger Electron Spectroscopy (AES). SEM and AES data are given in Figs. 5 and 6 and Tables 1 and 2.

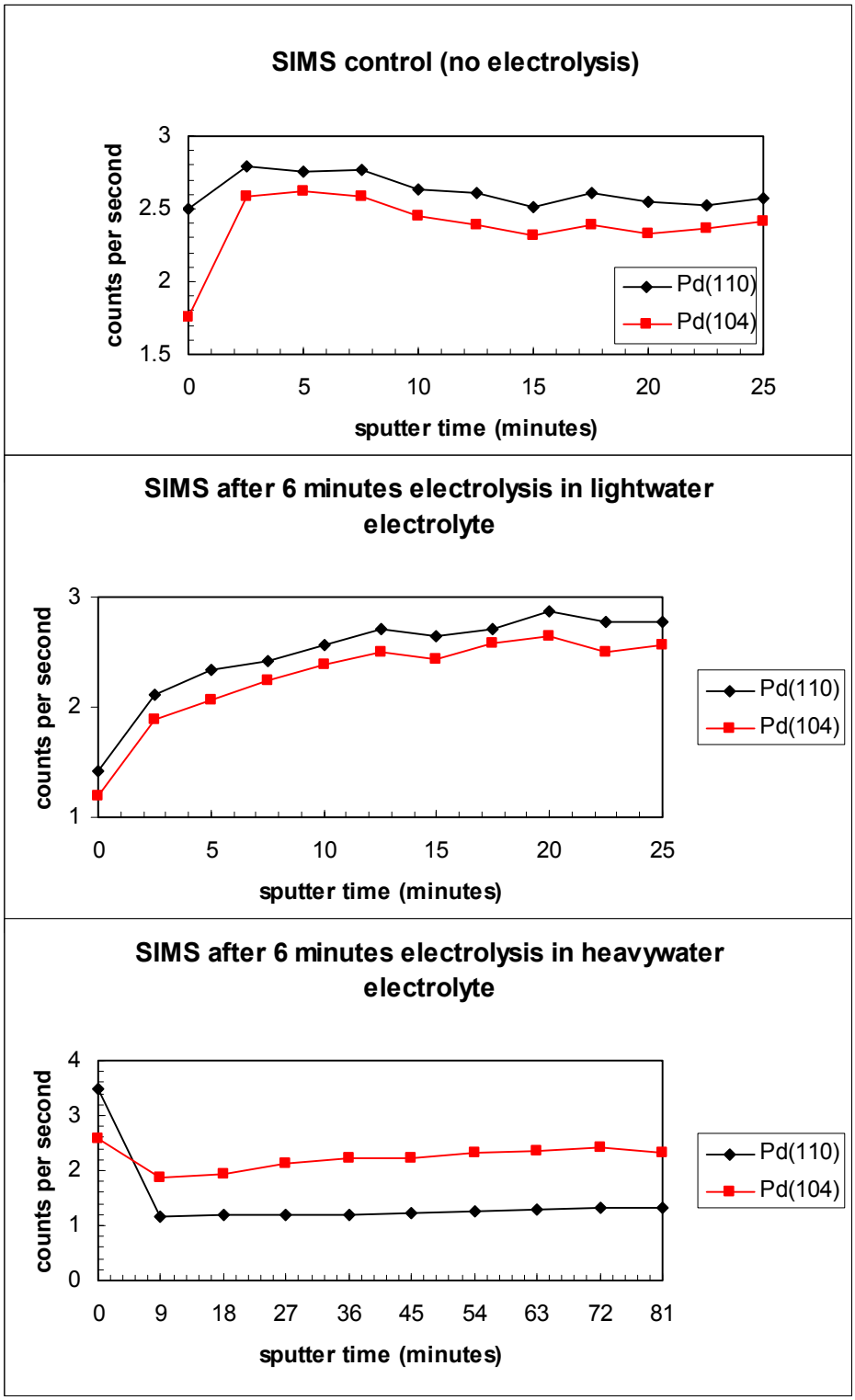

Fig. 4. *SIMS depth profiles for Pd 104 and Pd 110.*

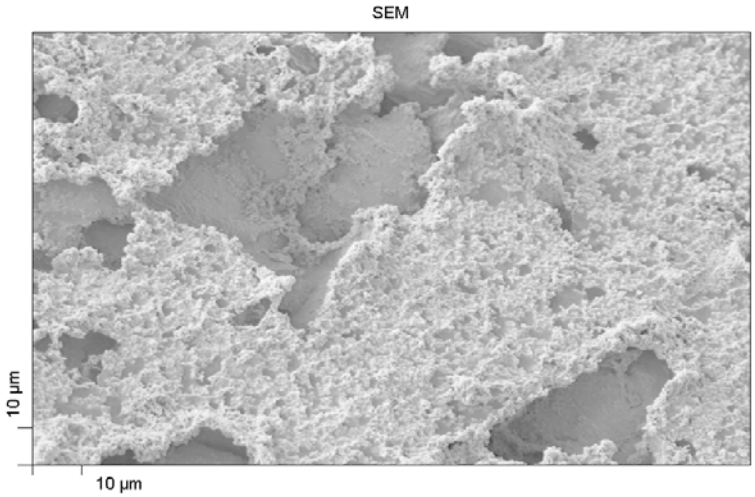

Fig. 5. *SEM photo of the concave side of the Pd cathode.*

AES analyses were taken from the two large dark gray areas and from the light gray area.

Dark gray	C	O	S	N	Pd	Pt
As-received	48.5	21.6	2.3	12.4	12.0	3.1
20 sec sputter	45.9	14.6	3.3	13.1	21.2	1.9

Light gray	C	O	S	N	Pd	Pt
As-received	54.2	17.4	1.9	10.3	6.4	9.9
20 sec sputter			2.6		79.0	18.4

Dark gray	C	O	S	N	Pd	Pt
As-received	54.3	16.9	2.9	12.6	10.3	3.0
20 sec sputter	45.5	14.8	4.0	13.9	15.5	6.3

Table 1. AES analyses (at.%) of dark gray and light gray areas in Fig. 5. The dark gray areas have large concentrations of C, O, and N before and after sputtering. These elements were also found on the light gray area as received, but not after sputtering.

Data for the convex side of the Pd cathode after electrolysis are given in Fig. 6 and Table 2.

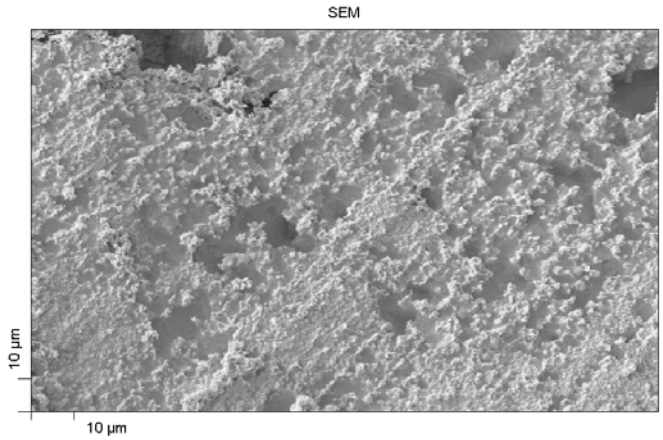

Fig. 6. *SEM photo of the convex side of the Pd cathode after electrolysis.*

Dark gray	Cl	O	S	N	Pd	Pt
As-received	2.4	13.9	2.2	11.3	68.0	2.1
20 sec sputter	1.1	9.8	3.3	9.8	73.5	2.6

Light gray	Cl	O	S	N	Pd	Pt
As-received	3.0	9.8	1.1	8.3	75.0	2.8
20 sec sputter	0.7		0.6		94.5	4.2

Table 2. AES analyses (at.%) of the convex side of the Pd cathode after electrolysis. Carbon was not detected on this side of the cathode. After sputtering, oxygen and nitrogen were not detected. Chlorine was detected on both light and dark gray areas.

Figs. 5 and 6 show that both sides of the Pd cathode contain a mixture of smooth, dark gray areas in a matrix of mottled, light gray areas. As received, the outermost layers of the concave side of the Pd cathode contain about 50 at.% C, but C was not detected on the convex side. It is difficult to accept that this difference could be caused by contamination. The main difference between the two sides is that the concave side had higher current density during electrolysis. If C was deposited on the concave side, it should have also been deposited on the convex side, but to a lesser extent.

The origin of the Cl on the convex side only is also puzzling. Again, contamination or deposition during electrolysis is expected to affect both sides.

The SIMS data on the same Pd cathode after electrolysis does not contain any inversions of isotopic abundance such as those in Figs. 2 – 4, but there are significant differences compared with the control, a pure (99.999 %) Pd foil which had not been electrolyzed. For example, there are no changes in isotopic abundance in the depth profiles for the control. Fig. 8 shows the count rate for masses 107 and 109 for the convex side of the electrolyzed Pd foil. The average count rate is about 50% greater for mass 107 than for mass 109,

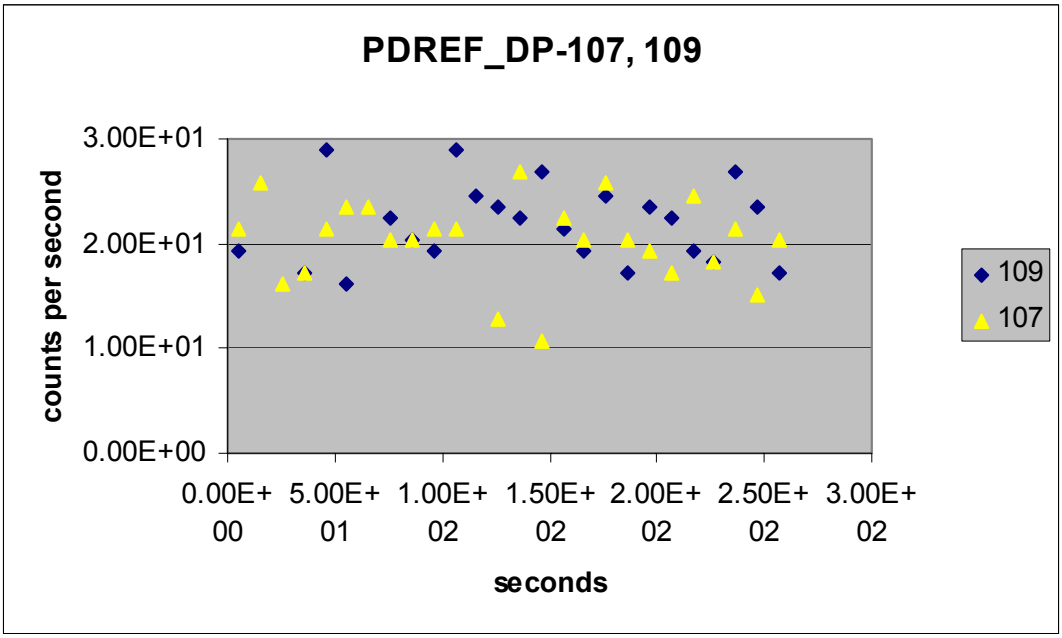

Fig. 7. *Counts per second for the control Pd foil from masses 107 and 109. The count rate does not change with increasing depth into the foil. The average counts per second is about 22 for both masses.*

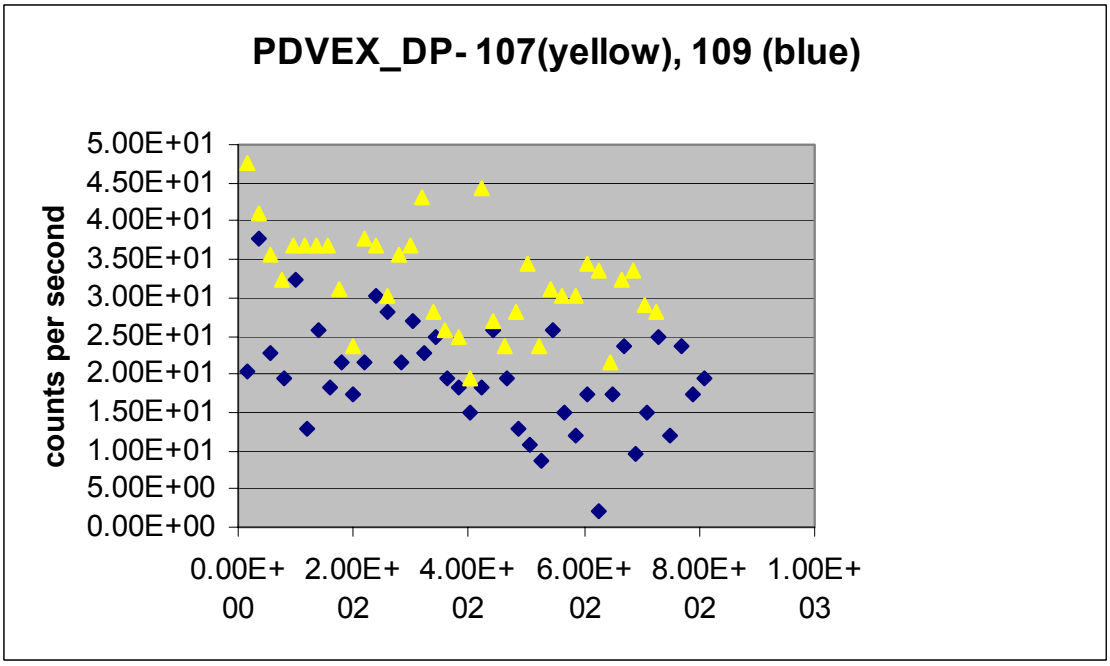

Fig. 8. Counts per second versus sputtering time (seconds) for the convex side of the electrolyzed Pd foil, which faced away from the anode during electrolysis. Compared with the control, there is less overlap of the data for mass 107 (yellow) with the data for mass 109 (blue). The average counts per second is about 30 for mass 107 and 20 for mass 109.

The SIMS depth profiles for masses 107 and 109 from the concave side of the electrolyzed Pd cathode are shown in Fig. 9. Here, it is apparent that the count rates for both 107 and 109 decrease with increasing sputtering time, and the count rate for 107 is

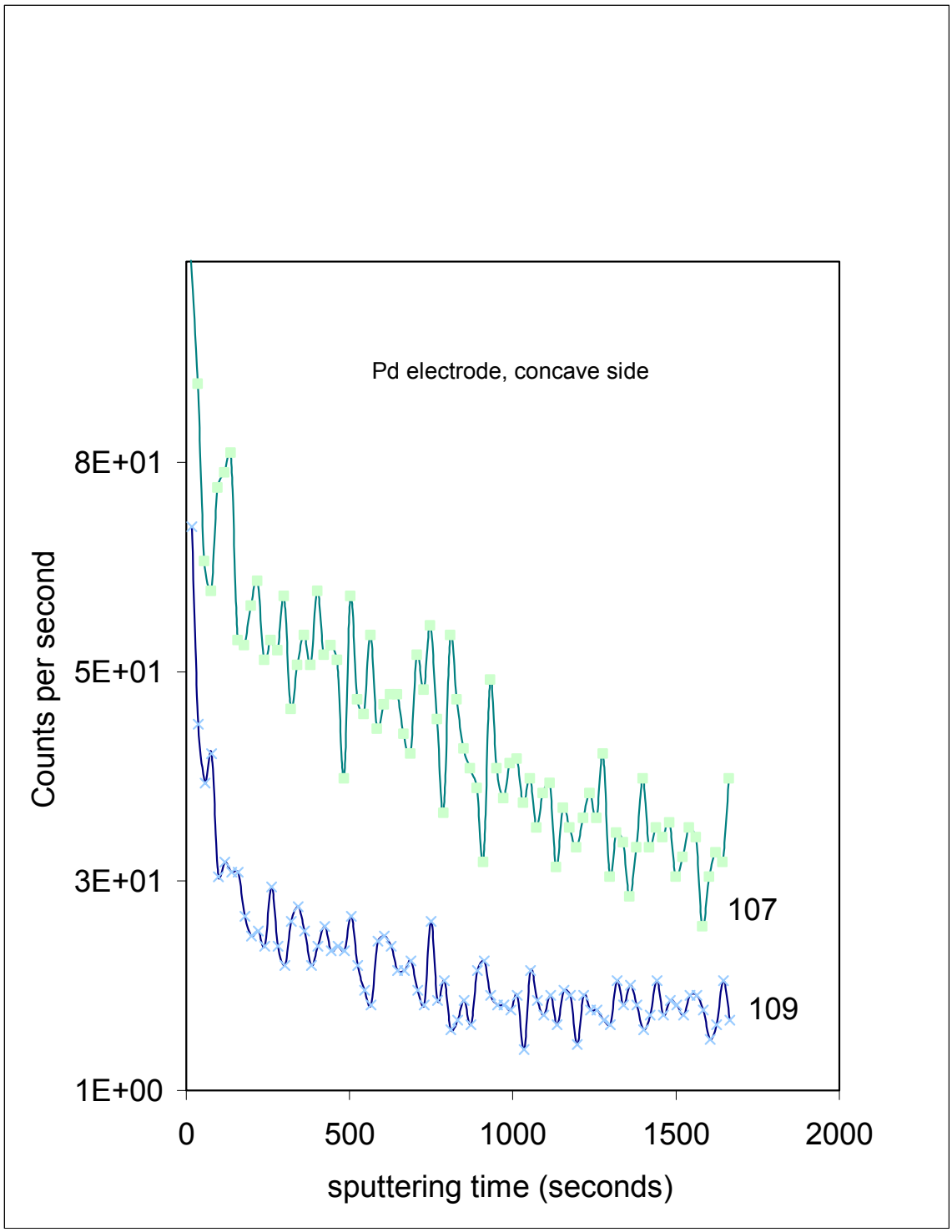

Fig. 9. *Depth profile of the signals from masses107 and 109 for the Pd cathode after electrolysis (concave side).*

about double that of 109 throughout 1700 seconds of sputtering. There is no overlap of the count rates from these two masses. At the start of sputtering the signal from mass 107 is about 90 cps, and this falls to about 35 cps at the end of sputtering.The signal from mass 109 falls from about 75 cps to about 15 cps during the same time period.

Masses 107 and 109 are stable isotopes of Ag, so transmutation by absorption of thermal neutrons is one possible explanation for the presence of these isotopes. Another possibility is that PdH and PdD are formed. Then, 105 PdD would appear at 107.This could be an explanation for the ratio 107/109 ~ 2 in Fig. 8, whereas the expected ratio is ~ 1.1 for Ag. However, if 105 PdD is present, then 108 PdH should also be present. This would appear at mass 109 in the SIMS spectrum, and the 109 signal would be enhanced. Fig. 8 shows that there is enhancement of the 109 signal for several hundred seconds sputtering time compared with the 109 signal from the control in Fig. 7. Because there is no change in abundance with depth into the control Pd foil and because the 107/109 ratio is as expected, it seems likely that the signals from these two isotopes are due to Ag impurity which is uniformly distributed throughout the control Pd foil.

Fig. 10 gives another example of changes in isotopic abundance on the concave surface of the 0.35 mm thick Pd cathode with increase in sputtering time. At the surface, the ratio of the isotopic abundance of 105 Pd to that of 104 Pd is about six, whereas the natural abundance ratio for these two isotopes is about two. After rising initially, the abundances of these two isotopes fall and converge, so that the abundance ratio is about 2.5

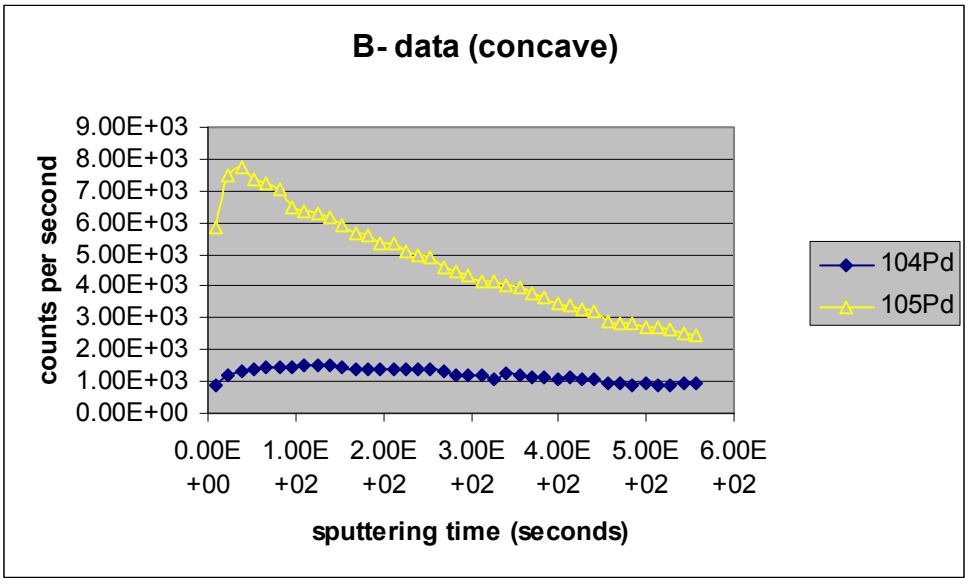

Fig. 10. Variation of isotopic abundance on the concave side of a 0.35 mm thick Pd cathode with increase in sputtering time. The rate of sputtering is about 0.8 nm per second, so the data in this figure represents isotopic abundance to a depth of about 0.4 μm.
after sputtering for about 550 seconds. On the convex side, the isotopic abundance of 104 and 105 Pd changes with increasing sputtering time, but the ratio 105 Pd / 104 Pd is close to the natural abundance.

Summary and Conclusions

SIMS spectra from 40 μm thick Pd foil cathodes after electrolysis in H_2O/H_2SO_4 electrolyte for 6 minutes show no significant changes in isotopic abundance compared with the control which was not electrolyzed. However, Pd foil cathodes electrolyzed in D_2O/H_2SO_4 electrolyte had inversions in which the Pd 108 signal exceeded the Pd 106 signal and the Pd 104 signal exceeded the Pd 110 signal. These inversions may have been caused by the formation of PdD and PdH. For example, 106 PdD would appear at 108, thus increasing the abundance of Pd 108. Also, 102 PdD would appear at 104, thus increasing the abundance of Pd 104. Another possibility is that transmutation to Ag occurred. This would require the presence of thermal neutrons [7].

A much thicker Pd foil (350 μm thick) electrolyzed for 74 hours in D_2O/H_2SO_4 electrolyte did not show inversions of isotopic abundance, but it did show significant differences in the SIMS spectra compared with the control. The occurrence of weak signals of almost the same intensity from the control at masses 107 and 109 suggests that Ag is present as an impurity in the control. The SIMS spectrum from the concave side of the electrolyzed Pd foil has about twice the intensity of the signal at mass 107 compared with mass109. Based on natural abundance, the ratio of the signals should be 107/109 ~ 1.1, instead of the observed 2. Any attempt to explain these results should include the effects of PdH and PdD which are formed during electrolysis. PdH would appear in the SIMS spectrum at 107 and 109, but their ratio should be ~ 1, not the observed 2. Another possibility is that transmutation to Ag occurred. Ag was detected by EDS in localized concentrations on both sides of this Pd cathode after electrolysis. Large concentrations of C on the concave side were detected by EDS studies, in agreement with the AES results. EDS also detected C on the convex side of the Pd cathode, but at much lower concentrations. This suggests that the C content is related to the current density during electrolysis. The high C content is on the concave surface which faced the Pt foil anode and therefore had much higher current density than the convex surface, which faced away from the anode. The changes in the SIMS spectra are also much greater on the concave side. Fig. 9 shows one example. There are others, too numerous to present in this report.

Since 1989, there have been many other reports of anomalous elements resulting from the interaction of metals with hydrogen isotopes [8-14]. The results reported here add to that growing body of evidence.

Acknowledgement

We are grateful for the financial support received during the past decade from the U.S. Army Research Office, the Drexler Foundation, and the New York Community Trust. We are also grateful to Dr. Sally Asher and associates at NREL who performed the SEM, AES, and SIMS analyses on the 0.35 mm thick Pd cathode.

References

1. J. Dash, G. Noble, and D. Diman, Trans.of Fusion Technology **26,** 299(1994).
2. D.R. Rolison and W.E. O'Grady, Anal. Chem. **63**, 1697(1991).

3. D.R. Rolison, W.E. O'Grady, R.J. Doyle, Jr, and P.P. Trzaskoma, Proc. ICCF**1**, 272(1990).
4. J. Dash, G. Noble, and D. Diman, Cold Fusion Source Book, p.172, H. Fox, editor, Fusion Information Center, P.O. Box 58639, Salt Lake City, Utah 84158.
5. J. Dash, Proc. ICCF**6,** 477(1996).
6. J. Dash, R. Kopecek, and S. Miguet, Proc. 32nd Intersociety Energy Conversion Engineering Conf. **2**, 1350(1997).
7. H. Kozima, The Science of the Cold Fusion Phenomenon, Elsevier, San Diego(2006).
8. R. Notoya, Fusion Technology **24**, 202(1993).
9. F. G. Will, K. Cedzynska, Trans. of Fusion Technology **26**, 209(1994).
10. R. Bush and R. Eagleton, ibid, 344.
11. I. Savvatimova, Y.R. Kucherov, and A.B. Karabut, ibid, 389.
12. G.H. Miley, G. Narne, M.J. Williams, J.A. Patterson, J. Nix, D. Cravens, and H. Hora, ICCF**6**, 629(1996).
13. D. Chicea, Condensed Matter Nuclear Science, P.L. Hagelstein and S.R. Chubb, editors,World Scientific Publishing Co., NJ, 2006, p.475.
14. N. Nikitenov, D.Y. Kolokolov, I.P. Chernov, and Y.I. Tyurin, Vacuum, in press.

TRANSMUTATION REACTIONS INDUCED BY D_2 GAS PERMEATION THROUGH PD COMPLEXES (Pd/CaO/Pd)

Y. Iwamura *(yasuhiro_iwamura@mhi.co.jp)* [1], T. Itoh[1], N.Yamazak[1], S.Kuribayashi[1], Y.Terada[2], T.Ishikawa[3], A.Kishida[3], K.Fukutani[4],D.Sekiba[4], M.Wilde[4], S.Ogura[4], H.Yamashita[4], M.Matsumoto[4], T.Okano[4], H.Matsuzaki[4], H.Yonemura[5], J.Kasagi[5], T.Nebiki[6], T.Narusawa[6]

[1]Advanced Technology Research Center, Mitsubishi Heavy Industries, Ltd.,
[2]Japan Synchrotron Radiation Research Institute (JASRI), [3]SPring-8/RIKEN, [4]Univ. of Tokyo,
[5]Tohoku Univ., [6]Kochi Univ. of Technology, JAPAN

We have been studying on low energy nuclear transmutation reactions induced by D2 gas permeation through Pd multilayer complexes. Transmutation reactions of Cs into Pr, Ba into Sm and Sr into Mo were observed. Especially, transmutation of Cs into Pr has been confirmed by "in-situ" measurement using x-ray fluorescence spectrometry (XRF) at SPring-8. Up to now, we reported that transmutation reactions seem to occur at localized spot near surface within 100nm under our experimental conditions.

In this conference, we present recent progress of our research; measurement of depth profile of hydrogen for a Pd complex during permeation using a resonance nuclear reaction $^{1}H(^{15}N,\alpha\gamma)^{12}C$. The resonance width is so narrow that we expect depth resolution under 10nm. Identification for an unidentified peak that appears during transmutation experiments of Cs into Pr at SPring-8 by changing x-ray excitation energy will be also presented.

INVESTIGATION OF MEMORY PHENOMENA IN WATER AND STUDY OF ISOTOPES TRANSMUTATION IN GROWING BIOLOGICAL SYSTEMS CONTAINING ACTIVATED WATER

Vladimir I.Vysotskii*, Alla A.Kornilova, Alexandr B.Tashyrev*****

**Kiev National Shevchenko University, Kiev, Ukraine*
***Moscow State University, Moscow, Russia*
****Institute of Microbiology and Virology , Kiev, Ukraine*

Introduction

The objectives of conducted investigations were to study the possibility and conditions of optimization of low-energy transmutation of different isotopes in growing microbiological cultures. The history of this optimization problem is connected with the several observed anomalies in our previous examinations of the effect of isotope transmutation in different living systems.

During 1995-2006 we have conducted several series of experiments related to isotope transmutation in growing microbiological cultures with controlled conditions of growth in water-containing nutrient mediums [1]. In these experiments, we have used both heavy and light water. These experiments were based on several nuclear reactions

$Mn^{55}+d^{2}=Fe^{57}$,

$Na^{23}+P^{31}=Fe^{54}$

that are adapted to metabolic processes in any biological systems.

The result of these reactions is the formation of rare stable isotopes of Fe, concentrations of which in natural iron are very low and equals 2.2 - 5.8%. Iron is the integral and important part of the majority of live organisms (see, e.g. [1]). Importantly, for most biological objects, the “regular” isotope Fe^{56} and the rare Mossbauer isotopes Fe^{54} and Fe^{57} are identical nuclei.

The effectiveness of nuclear transmutation in each of these experiments differed by several times or orders at variation of conditions of growth and kinds of cultures!

On Fig. 1 the results of Mossbauer spectroscopy investigation of microbiological cultures grown in heavy-hydrous (D_2O) sugar-salt nutrient medium deficient in *Fe* but additionally containing Mn^{55} isotope [1] are presented.

Experiments were conducted using several bacterial cultures (e.g., *Bacillus subtilis, Escherichia coli*) as well as the yeast culture *Saccharomyces cerevisiae*.

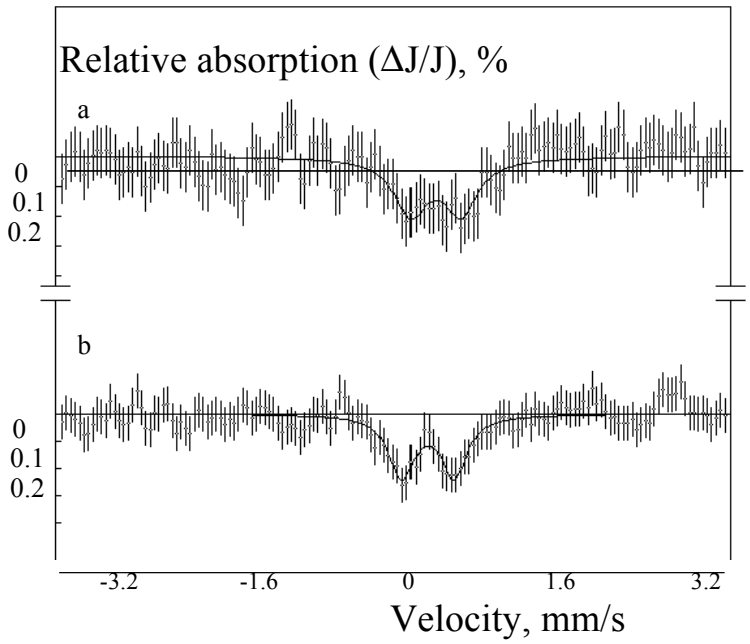

Fig.1. Mossbauer spectra of grown cultures in different identical flasks. Culture *Saccharomyces cerevisiae T-8* grown in D_2O with the presence of Mn^{55} isotope.

The effectiveness of isotope transmutation in these experiments in the case of the reaction $Mn^{55}+d^2=Fe^5$ was equal

$$\lambda_{DMn} \approx N(Fe^{57})/N(D^2 + Mn^{55})\Delta t \approx 10^{-8}$$

(synthesized Fe^{57} nuclei per s and per pair of D^2 and Mn^{55} nuclei).

On Fig. 2 presented the results of Mossbauer spectroscopy investigation of different biological object - *MCT* compound [2].

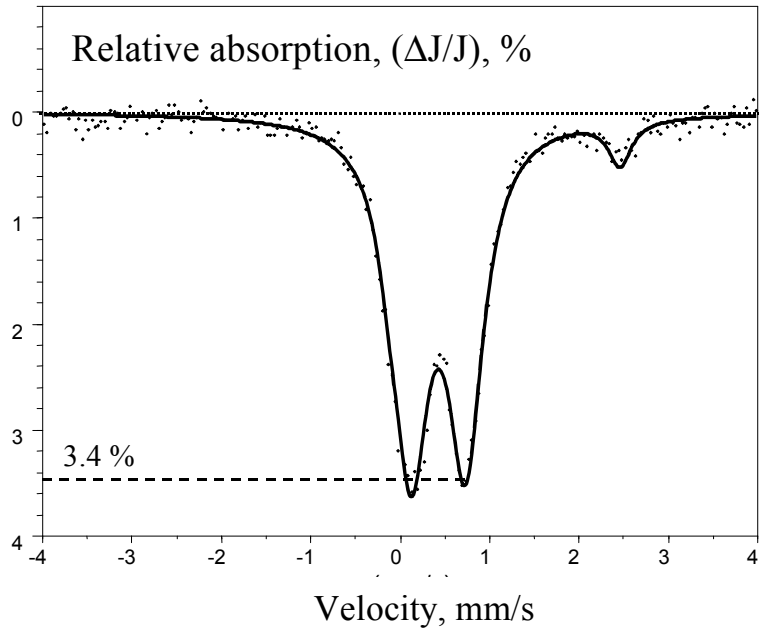

Fig.2. Mossbauer specter of microbiological *MCT* grown in the volume with presence of D_2O and Mn^{55} isotope (experiments on transmutation): $\Delta J_{max}/J \approx 3.4$ % is the magnitude of Mossbauer resonance.

The base of used *MCT* compound is microbe syntrophin associations of thousands different microorganisms [2] that are in the state of full natural symbiosis.

In this case the effectiveness of isotope transmutation was equal:

$\lambda_{DMn} \approx N(Fe^{57})/N(Mn^{55})\Delta t \approx (0.5...1).10^{-6}$

(synthesized Fe^{57} nuclei per *s* and per single Mn^{55} nucleus).

Very large difference in effectiveness of the same nuclear reaction in these different experiments is inexplicable.

In several cases we have observed abrupt change of the effectiveness of the same nuclear reaction with the presence of the same cultures in flasks that were situated in different places of the same laboratory or in different times in the same place! From the other hand the temperature of growing cultures in nutrient medium in all cases was approximately the same.

It was mystery!

We suppose that these anomalies are connected with random influence on water (on water-containing nutrient mediums) of weak low-frequency electromagnetic background in

different places of the same laboratory or in different times in the same place in the laboratory. The origin of these fields could be bound with influence of different outside laboratory equipment, which dies not concern these experiments.

In the process of vital activity of any biological object, the most important chemical compound is water.

It is well known that water:

- is a base of the intracellular liquid,
- forms the transport paths for the transfer of vitally necessary chemical elements,
- forms the necessary state of these elements in the form of atomic and molecular ions,
- play the main role at cell division and DNA replication;
- is the most universal solvent.

The spatial structure of water agrees ideally with the secondary structure of a DNA macromolecule, by guaranteeing the maximally stable existence of the double helix formed of complementary pairs of nucleotides.

This list is far from being complete and can be continued.

At the same time, water is one of the most mysterious chemical compounds. Anomalous properties of water became long ago a classical example of the manifestations of characteristics of nontrivial systems.

Up to now, there are no adequate answers to the questions about:

- spatial structure of water on molecular and supermolecular levels;
- existence of numerous paradoxes of water memory and the nature of water memory;
- duration of water memory and possibility of its control.

We performed a cycle of complex studies of activated water and water memory, by using the activator of water, which was earlier studied by us [3] and allowed us to obtain a number of results in the whole spectrum of physical, biological and nuclear applications.

1. Physical-molecular properties and the problem of memory of activated water

Water was activated by the action of nonionizing Molecular Resonance Effect Technology (MRET) [3]. Investigated activator of water is the stationary source of low-frequency resonant electromagnetic field with composite space structure and very weak amplitude. The device includes the working body consisting of a polymeric matrix formed by oriented

threads of a linear polymer with the alloying admixtures of various chemical elements and compounds. The polymer itself, according to the patent (see [3] for details), has the properties of both ferroelectric and piezoelectric. This polymer is surrounded by the system of mutually perpendicular pairs of oriented constant magnets positioned in turn, the field intensity of each magnet being 4000 *Oe*. Periodic optical pulses (frequency is about 7-8 Hz) acting on the oriented polymeric system. The motion of the electric charges and the magnetic moments of atoms in the strong circular field of the constant magnets generates a variable low-intense electromagnetic field (about 1 *Oe*) with complicated spatial structure. This field oscillates with the frequency of the repetition of optical exciting pulses and includes both the electric and magnetic components.

The generated electromagnetic field acts on water positioned near the open end of the polymeric activator and changes its structure, which is reflected in the long-term change of the properties of water.

It was discovered in our detailed physical experiments that under the action of this irradiation there are very essential modifications of the basic physical-molecular and biophysical properties of distilled water.

1.1. **Anomalous electrodynamic characteristics of activated water**

In this section, we consider the main electrodynamic characteristics of activated water.

In the process of studies, we determined the electrodynamic properties of activated water as functions of three basic parameters:

- the water activation duration,
- the water storage duration after the activation,
- the temperature of activated water storage.

The influence of some of these parameters was investigated comprehensively (for example, the influence of the storage duration and the storage temperature after the activation).

In Fig. 3a the results of the base studies of the electrodynamic characteristics of initial nonactivated distillated water completely analogous to water which was then subjected to the procedure of activation are presented. The studies were carried out at a temperature of 20^0 C.

It follows from these results that the initial distillated water has a low value of conductivity, $\sigma \approx 3.10^{-5}$ S/cm^2, and the dielectric permittivity close to the "standard" one,

$\varepsilon'(\omega) \approx 90$, at the frequency of alternating electric current in the range $\omega \geq 10^3$-10^7 Hz. This value of the dielectric permittivity well agrees with the Debye mechanism of orientational polarizability of independent molecules of water. The maximum value of the dielectric loss tangent $(tg\delta)_{max} \approx 120$ and corresponds to a frequency of 1522 Hz.

With decrease in the frequency to $\omega < 10^2$ Hz, a sharp decrease of the conductivity and a very sharp monotonous increase of the dielectric permittivity were registered. In the studied region of superlow frequencies (at $\omega \leq 10^{-1}$ Hz), the effective dielectric permittivity reaches a very great value $\varepsilon'(\omega) \approx 10^8$.

In Fig. 3b and Fig.3c we present the specific features of the electrodynamic characteristics of water activated for 30 min and stored up to the time moment of the measurement at a temperature of 20^0 C and 40^0 C. It is seen that these samples of water preserves some general regularities (a sharp decrease of the dielectric permittivity and the conductivity on the activation of water and their gradual recovery in the process of storage) and, at the same time, reveals the significant differences such as a significantly faster relaxation of the parameters with increase of the storage duration. In particular, for 5 h of the storage, the maximum value of the dielectric permittivity and the conductivity grew by 200% (see Fig 3b).

One of the most important problems is the determination of the duration of "the memory of water" on the basis of the performed experiments.

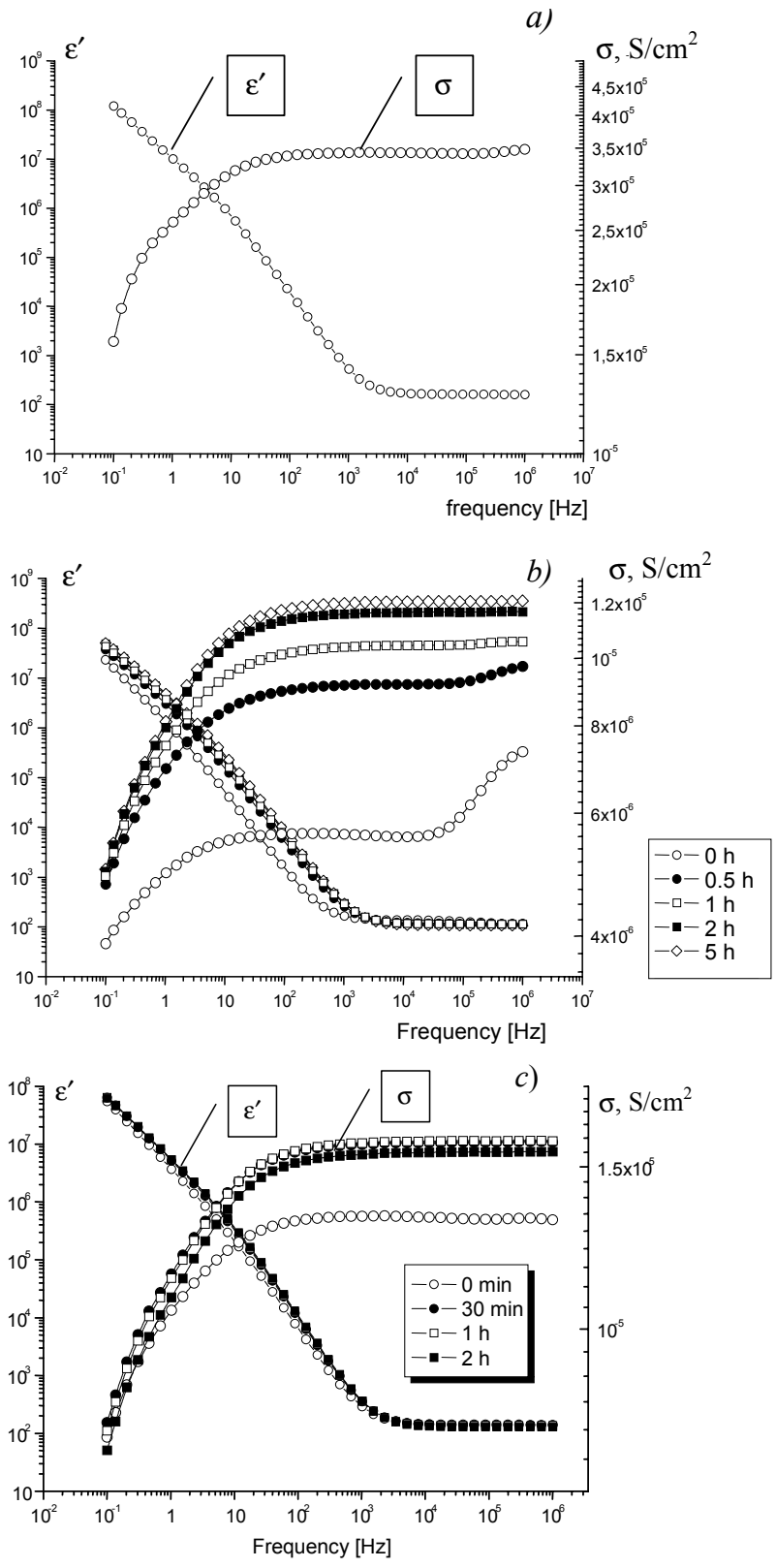

Fig. 3. Dielectric permittivity ε′ and conductivity σ of a water versus the frequency: *a*) initial nonactivated distilled water at 20^0 C; *b)* the same distilled water activated for 30 min and stored at a temperature of 20^0C; *c)* the same water activated for 30 min and stored at a temperature of 40^0C.

In Fig. 4, we present the dependence of the relaxation change of $\varepsilon'(\omega,t)$ on the storage duration of activated water after the activation.

These results correspond to the frequency ω = 10 Hz and are obtained on the direct processing of the above-discussed spectra obtained for water stored for the different time intervals at different temperatures after the activation. Water was activated for 30 min.

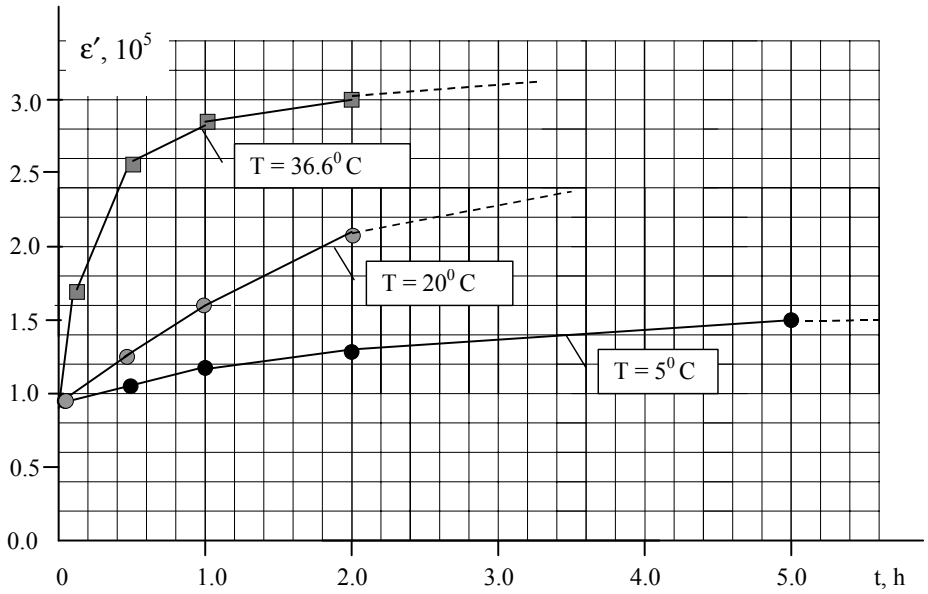

Fig. 4. Relaxation of the dielectric permittivity of activated water $\varepsilon'(\omega)$ at the frequency f = 10 Hz ($\omega = 2\pi f \approx 62$ sec^{-1}) versus the storage duration after the activation. Three curves correspond to three temperatures of the storage of water (T =5^{0}C, 20^{0}C, and 36.6^{0}C).

It is seen that, at very great storage duration, the anomalous electrodynamics properties of activated water gradually disappear. The duration of preservation of these properties depends very significantly on the storage temperature.

By extrapolating the obtained dependences of the relaxation change of the parameters of water $\varepsilon'(\omega)$ and $\sigma(\omega)$ by the exponential law

$$\varepsilon'(\omega,t) \approx \varepsilon'(\omega,\infty) + \Delta\varepsilon'(\omega)[1-\exp(-t/T_W)],$$

$$\sigma(\omega,t) \approx \sigma(\omega,\infty) + \Delta\sigma(\omega)[1-\exp(-t/T_W)],$$

we can estimate the duration of relaxation T_W.

It is seen from Fig.4 that the duration of relaxation T_W of the mentioned electrodynamic characteristics of activated water becomes very great (at least 5-7 days) at a comparatively low temperature (at 5^0 C). With increase of the temperature of the storage, this duration

rapidly decreases. The duration of relaxation is 10-15 h at a temperature of 20^0 C and is equal to at most 4-6 h at a temperature of 40^0 C close to the temperature of a human body. These results qualitatively agree with the calculations of water memory performed in our works [3,4].

1.2. Anomalous viscosity characteristics of activated water

Viscosity is one of the most important characteristics of water. The particular meaning of the viscosity of water in any physical and biophysical systems is related to the transport functions of water and to the dependence of the motion and the evolution of macromolecules, ions, cells, viruses, and other microobjects on the properties of water, in which they are placed in alive organisms.

In our experiments, the viscosity of water was measured with the help of a rheometer. The studies were executed on the basis of a measuring cell. It consisted of two immovable coaxial cylinders 1 and 2. In the region between them, there is a rotor (a rotating coaxial cylinder 3 coaxial with cylinders 1 and 2). Water under study is placed in the free region between the surfaces of immovable cylinders 1 and 2 and the rotor. With the help of this system of coaxial cylinders, we performed the measurements at low shear stresses.

To study the influence of the activation of water on its viscosity, we executed several series of measurements of the dynamical viscosity η as a function of the applied stress τ with different fractions of water (the initial nonactivated distillated water and an analogous water activated for different time intervals) at two temperatures (20^0C and 36.6^0C).

In Fig. 5 we present the results of studies of the viscosity coefficient for initial distillated nonactivated water and for the samples of water which were obtained for the duration of activation of 15, 30, 45, and 60 min and were at a temperature of 36.6^0C in the process of measurement. With regard for the fact that the anomalous properties of activated water relax rapidly with increase of the temperature, the measurements were carried out at once after the activation of water.

It was discovered that at very low velocity of motion of investigated activated water (tension less than 0.01 Pa) viscosity of water, activated during 60 min, decrease by 80-100 times at 20^0 C in relation to the same but nonactivated water. Minimal viscosity at such temperature will be for water activated during 30 min. In this case viscosity decrease by 300 times! It is seen from the obtained data that an increase of the water activation duration leads

to a very significant decrease of the viscosity coefficient in the region of small mechanical stresses at this temperature (relative to the initial nonactivated water).

It is necessary to note that the absolute values of the viscosities of nonactivated and activated water samples in the region of small mechanical stresses increase significantly with the temperature.

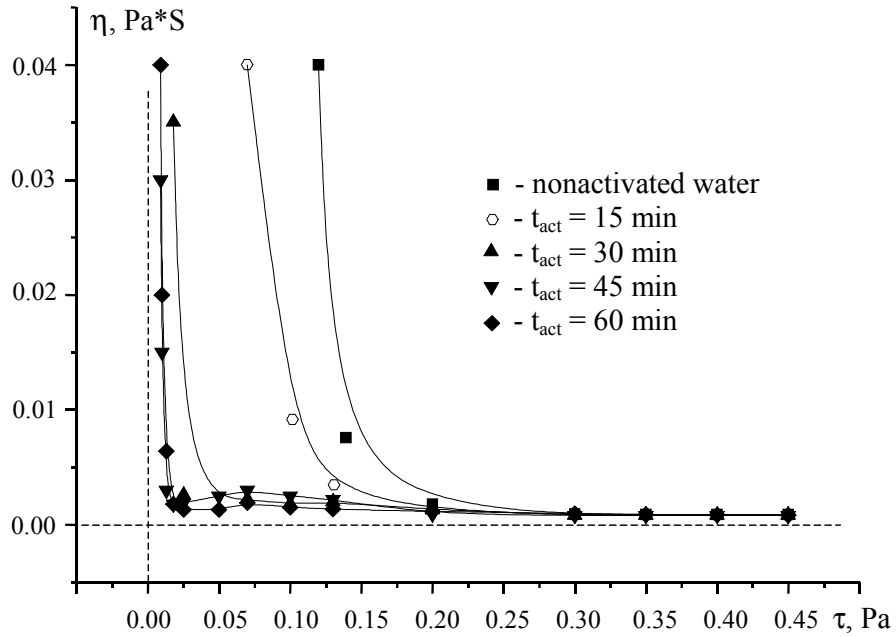

Fig. 5. Viscosity η of nonactivated water and four fractions of activated water in the region of small shear stresses τ at a temperature of 36.6^0C.

It was discovered that duration of internal storage of these abnormal characteristics of activated water equals several days or weeks at low temperature (close to 0^0 C). The problem and concrete mechanism of long time memory of activated water were studied earlier in [1,2].

The change in the dispersive electrodynamic properties of water can render a very strong influence (by means of a modification of the electrostatic forces between separated charges and forces of the van der Waals type defining the interaction of the systems of neutral atoms and molecules) on the long-range interaction of such basis elements of alive systems as cells, viruses, biological macromolecules, enzymes, etc.

Viscosity, surface tension, and other mechanical properties of water which play a very important role in the processes of vital activity turn out to be directly related to the electrodynamic characteristics of water.

It is seen from Fig. 5 that a change (increase) of the duration of activation in the limits of 1 h leads to a monotonous displacement of the curve of the viscosity coefficient as a function

of the applied mechanical stress to the side of less viscosities. The position of the minimum of the viscosity coefficient is also shifted with increase of the duration of activation from $\tau \approx 0.1$ Pa for the duration of activation of 30 min to $\tau \approx 0.05$-0.02 Pa for the duration of activation of 45-60 min. Very important is the circumstance that the viscosity of activated water in the region of very small shear stresses at the vitally important temperature 36.6^0C, like the case of a lower temperature of 20^0 C, is by several orders less than that of ordinary (nonactivated) water.

1.3. Influence of the activation of water on pH

It is well known that a value of the hydrogen index pH of the intracellular and intercellular water-salt medium is one of the essential factors of the influence on the course of biochemical processes and the development of alive organisms. With the purpose to study the influence of the activation of water on pH, we studied the dependence of pH on the duration of activation of water (water was activated for 15, 30, 45, and 60 min), on the temperature (at 4°C and 20°C), and the duration of storage of this water after the completion of the activation.

In experiments, we use water obtained on the distillation directly prior to the studies. Then the 100-ml samples of activated water were stored in standard graduated flasks of 250 ml in volume closed by rubber plugs. The first 3.5 h after the activation, all samples including the control ones were at room temperature (20°C). Then, according to the conditions of the experiment, a half of flasks was placed into a cooler and was stored there at 4°C, and the other half remained at 20°C. The control samples with analogous, but nonactivated water were present in both versions.

Each measurement of water activated for a definite time interval was repeated three times. Then we determined the mean value. The final error of measurements in each series was at most $\Delta(\text{pH}) \approx 0.1$.

The detailed studies of all the samples of water obtained for the different durations of activation were performed with a short time interval (in each 30 min) for the first 3.5 h after the completion of its activation at a temperature of water 20°C. The subsequent measurements were performed regularly for 16 days with an interval of 1-2 days for different fractions of water stored at temperatures of 4°C and 20°C. The samples of water taken from a cooler, where they were stored at a temperature of 4°C, were placed prior to the measurement

in a thermostat, where their temperature was rapidly increased to 20°C. Then we measured the hydrogen index. The results of measurements are presented in Figs. 6 and 7.

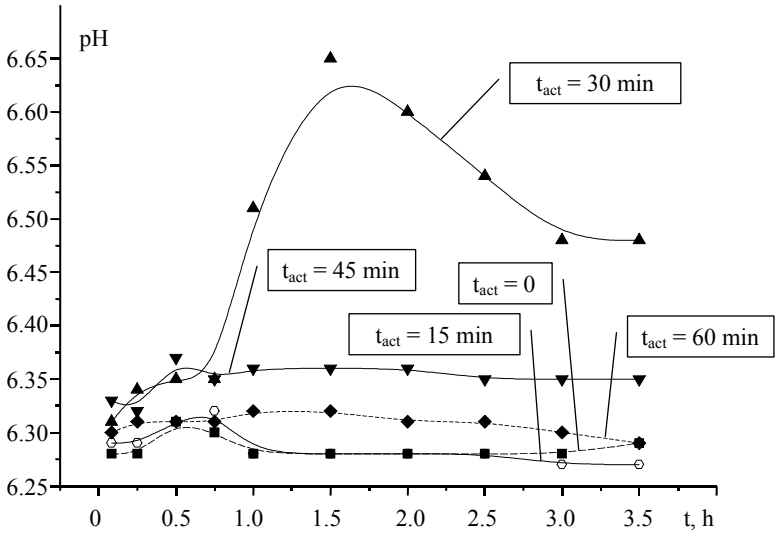

Fig. 6. Hydrogen index pH of different fractions of activated water versus the duration of its storage at a temperature of 20^0C in the first hours after the activation.

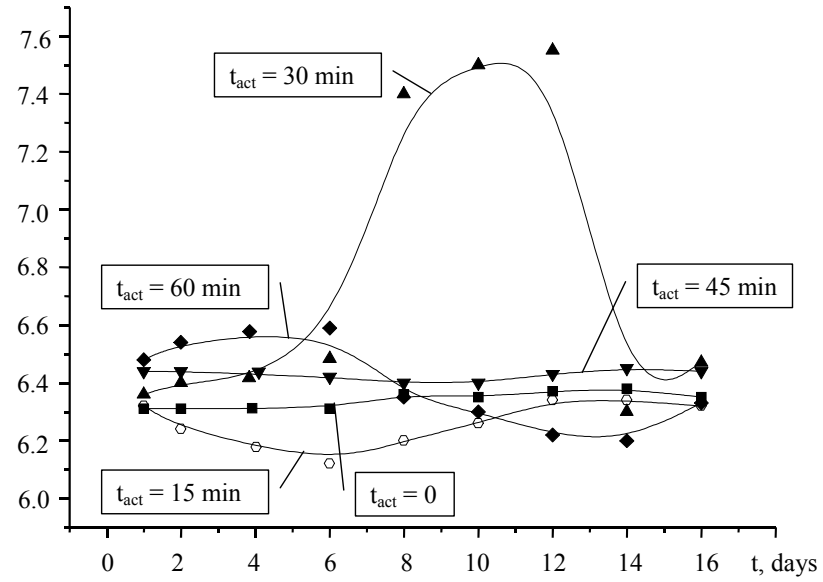

Fig. 7. Influence of the water activation duration on pH depending of the time of its storage at a temperature of 20°C.

In addition, the separate measurements were carried out by using the samples of nonactivated water and activated water stored after the activation at a temperature of 4°C for 120 days.

It was established that a quite insignificant alkalization of water occurred during the direct action of non-ionizing activator on water. In particular, when the hydrogen index for the initial distillated nonactivated water $(pH)_0$ = 6.28, a value of pH at once after the completion of the activation for 15, 30, 45, and 60 min was equal to $(pH)_{15}$ = 6.29,

$(pH)_{30}$ = 6.31, $(pH)_{45}$ = 6.33, $(pH)_{60}$ = 6.30. The further studies showed that the process of alkalization of activated water became gradually more intense for the first 1.5 – 2 h of its storage after the activation. These data are presented in Fig. 6.

The effect of the increase in pH is especially clearly manifested for water activated for 30 min. In this case, a value of pH increased from pH=6.31 to pH=6.65 during 1.5 h after the completion of the activation and then decreased gradually for 2 h down to pH=6.45. A small increase of pH was also observed for water activated for 45 min. For the rest fractions of activated water, the changes for the first hours of the storage were insignificant.

The study of the samples of activated water and control one at a longer time interval of the storage at two temperatures (4°C and 20°C) showed that the anomaly in the behavior of pH observed directly after the activation of water during 30 min was not unitary. In the process of storage, we registered the additional spontaneous increase of pH to a value exceeding the first maximum. The greatest changes in pH were discovered in the same fraction of water in 9-11 days of the storage at various temperatures. In particular, in 9 days of the storage, a value of pH grew to pH =7.4-7.5 [as compared with pH= 6.30-6.36 in control samples of nonactivated water which were stored at the same temperatures 4°C and 20°C. A half-width of this maximum (the duration of its existence) corresponded to $\Delta t \approx 4$ days at a water storage temperature of 4°C and $\Delta t \approx 6$ days при 20°C. Thereafter, there occurred a spontaneous decrease of pH which "returned" to its initial value, pH ≈ 6.3-6.4, only in 14 days. This maximum was observed on all samples of water stored and measured separately which correspond to the duration of activation of 30 min and the storage temperatures of 4°C and 20°C. There are the weighty reasons suppose that similar oscillations can exist also for a greater duration of the storage of water.

We note that the fluctuations of pH for control (nonactivated) water stored under the same conditions were practically invariable (with regard for the errors of measurements).

It is worth noting the essential fact that the displacement of pH to the alkaline side was fixed also at a long-term (for 120 days) storage of the samples of activated and control water. All these samples were obtained at the same time on the basis of identical distillated water.

In conclusion, we note that the presence of great ordered spontaneous changes in pH for the great duration of storage of water activated in a certain manner testifies directly to the existence of the "memory" of water. The presence of such great ordered changes in the properties of activated water is related, most likely, to certain phase transitions. Very curious is the fact that the time moment of the realization of these phase transitions, as well as the

amplitude of changes in pH, does not depend (or weakly depends) on the temperature of the storage of activated water and is approximately equal to 10-11 days. At the same time, the half-width of the region of this spontaneous change depends rather sharply on the temperature.

2. Investigation of inhibition biological activity of activated water

The examination of influence of activated water on growth of strain *Escherichia coli* microbiological cultures on nutrient medium meat broth with 1.5% agar was carried out.

The study of the cultural-physiological parameters of culture *Escherichia coli* during its growth on the activated and nonactivated agarized medium was made with the purpose to determine the effect of the activation on the survivability of cells, the growth rate of colonies on the base of survived cells, and the shape and the size of grown cells. Cultivation of colonies was produced at 20^0 C in aerobic conditions on the surface of agar during 32 hours.

The cultural-morphological properties of culture *Escherichia coli* (the size, shape, and color of colonies and cells) are the important criteria of the effect of activated water on microorganisms. The change of the mentioned parameters evidences for influence of the activation on the cell division processes, the synthesis of the structural components of cells, pigments, the “programming” of the formation of a stereometry of colonies, etc.

Initial view of Petri dishes with different variants of activated medium at the beginning of experiments and the general view in 7 hours after beginning of experiments are presented in Fig.8. The general view of the dishes with different fractions of activated nutrient medium in 29 hours after beginning of experiments is shown in Fig .9. It was observed for the first time that at low initial concentration of cells of investigated culture *Escherichia coli* in nutrient medium water activated during 0.5 hour and 1 hour have suppressed culture growth in $N_C/N_{0.5} = 27$ and $N_C/N_{1.0} = 303$ times. At the increasing of water activation time, inhibition of conditionally pathohenic strain growth is more effective. In this case, activated water leads to inhibition of *Escherichia coli* i.e. decreasing of rate of growth.

The strong influence of activated water on the process of cloning of microorganisms, their division, the size of microorganisms' colony and the form of cell-like division has been discovered. It was observed during direct microscopy investigation that one of the reasons of abnormal growth is connected with suppressed division of cells in activated nutrient medium.

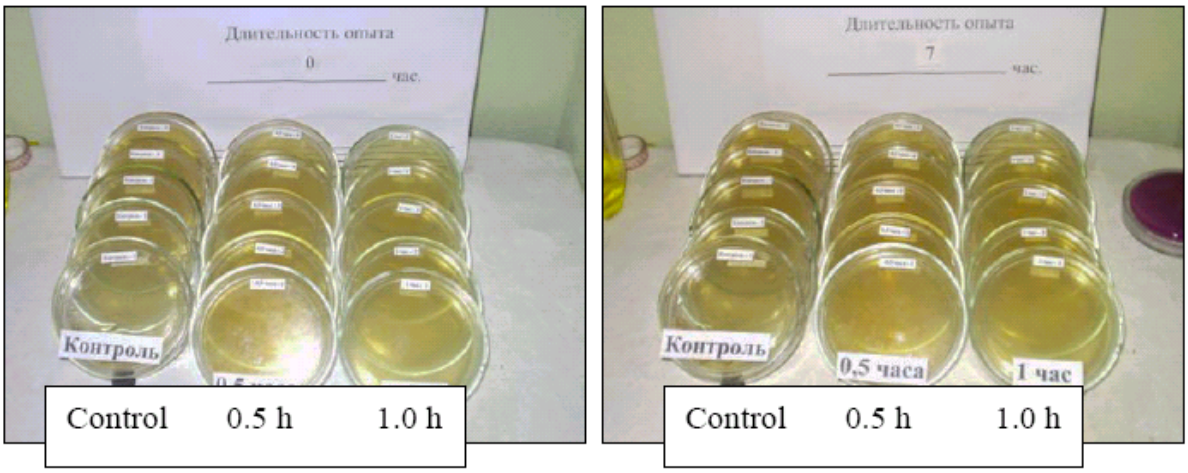

Fig. 8. General view of Petri dishes at the beginning of experiments (left) and in 7 hours after beginning of experiments (right). Identical very small amount of *Escherichia coli* cells was inoculated on a surface of three fractions of activated nutrient medium (t_{act}=0.5 h, t_{act}= 1.0 h and control). Colonies of microorganisms are absent in all dishes.

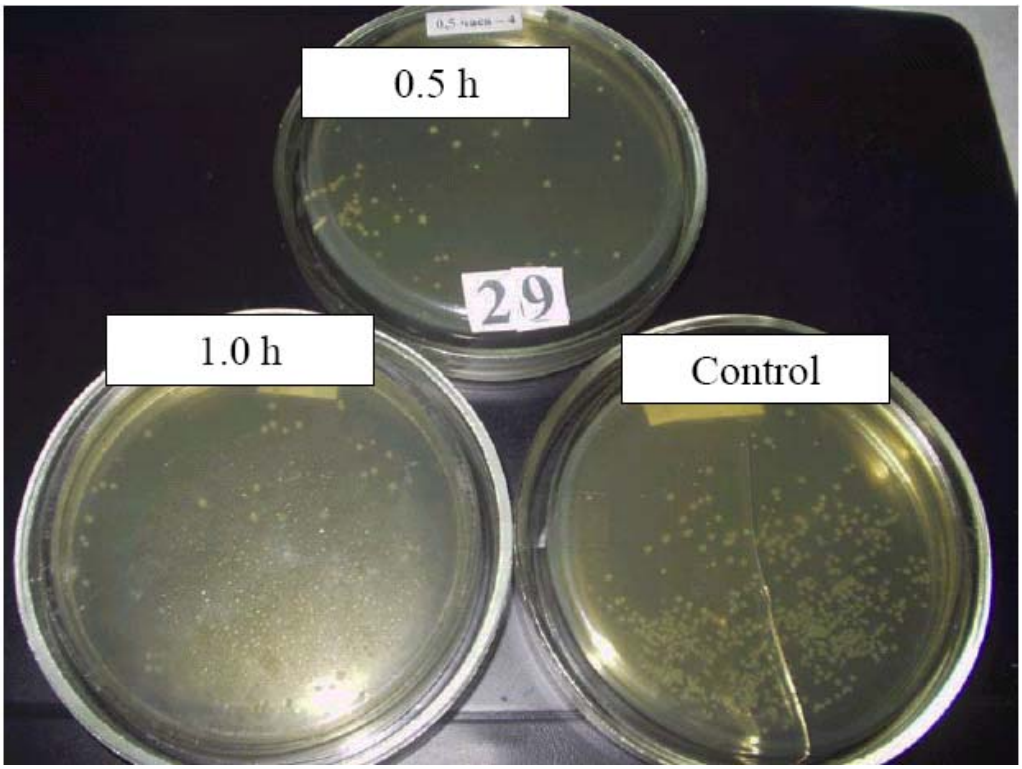

Fig. 9. View of the most representative Petri dishes with grown colonies of *Escherichia coli K-12* in 29 hours after beginning of experiments.
a) Control. Number of cells is $N_C = 1.7.10^8$ cells/ml. Averaged diameter of grown colonies is d = 1.2 mm; b) t_{act} = 0.5 h. Number of cells is $N_{0.5} = 6.4.10^6$ cells/ml; c) t_{act} = 1.0 h. Number of cells is $N_{1.0} = 5.6.10^5$ cells/ml.

The anomaly of the cell division is manifested in this case through the creation in the colonies of *Escherichia coli* culture of the so-called “squibs” which are “blown” cells, whose division is violated but the growth is preserved. In the case of activated media we have observed many of cells, which after completion of growth are not parted after division and the linear line-ups consisting from 2-3 sequentially or more of paired cells form.

In Fig. 10 we present the photos of fragments of the system of cells that were grown on the surfaces of the nonactivated and activated agarized nutrient media. These fragments correspond to Fig. 9.

As seen from the fragment shown in Fig. 10, the main part of cells on the surface of the nonactivated medium corresponds to the shape “standard” for culture *Escherichia coli* (like elongate linear sticks), and the number of anomalous (nonseparated) cells is few. The estimations given above show that the concentration of anomalous cells is at most 4%, which is within the statistic fluctuations.

The basically different pattern of the morphology of cells is observed for the culture grown on the activated medium. As follows from the magnified fragment of the surface of such nutrient medium shown in Fig. 10, the anomalous cells become the dominating component of the process of division of cells. Their relative concentration exceeds that of normal cells by a factor of 2.7. It is worth to note that, in this case, not only nonseparated linear chains containing 2-3 cells are formed. We observe also the great number of nonseparated branched chains of cells with a complicated branched structure that contains many (up to 10-20) nonseparated cells in some cases. With regard for the fact that the cell division process in such anomalous systems is to be suppressed severely, one of the natural reasons for the formation of these superstructures is, apparently, the mutual joining of individual linear nonseparated fragments. It is seen that, although the cell division process occurs most likely in accordance with the natural laws, the division rate of cells is sharply decreased on the last stage of their growth. It seems almost evident that just the change of the properties of activated water plays the key role on this last stage.

This is conditioned by the fact that just the energetic characteristics of the cell division process, which leads to the increase of both the surface and the total surface energy of dividing cells, are directly connected with the influence of the “external” (with respect to cells) water which is the base of the nutrient medium on their surface energy. The results of bactericidal (bacteriostatic) action of activated water on culture *Escherichia coli* growth are shown on Fig. 11.

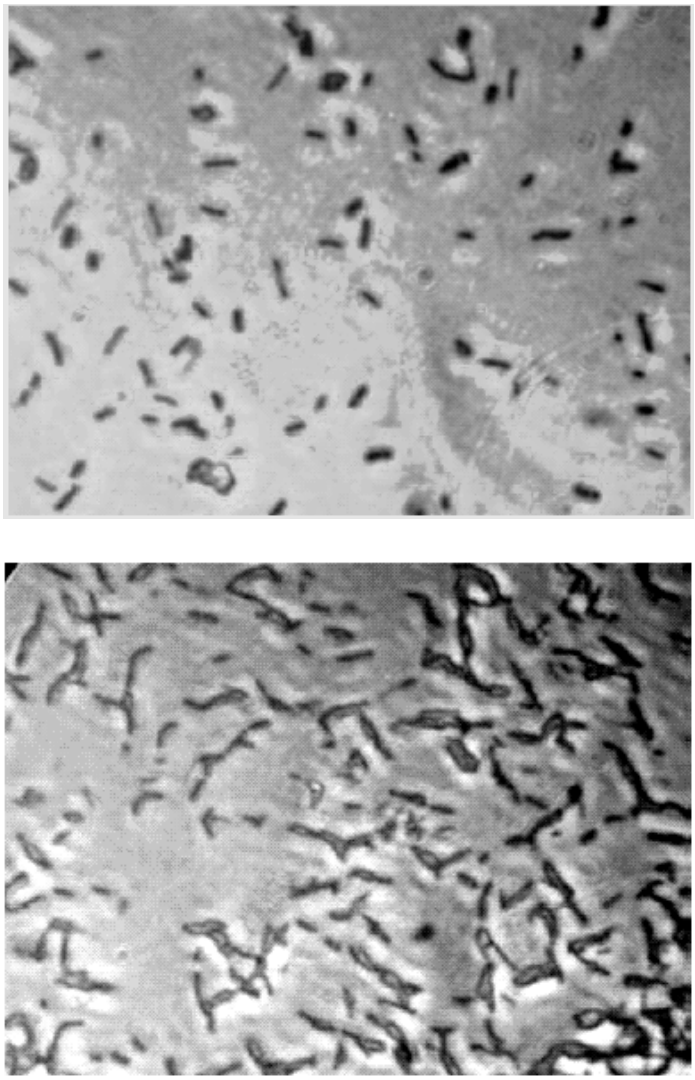

Fig. 10. Microscopic photos of cells of *Escherichia coli* grown on nonactivated medium (upper photo) and on the same but activated medium with t_{act} = 1 hour (lower photo).

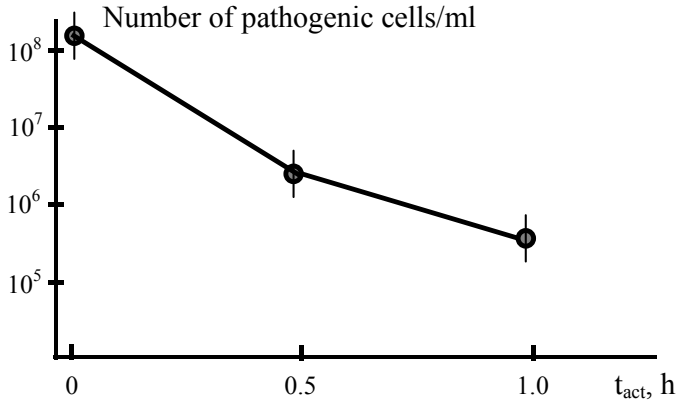

Fig. 11. Bactericidal (bacteriostatic) action of different fraction of activated water on culture *Escherichia coli* growing under aerobic conditions

The biophysical reasons of strong action of activated medium on the process of cloning and growth of pathogenic microorganisms are connected with:

- abnormal physical properties (viscosity, conductivity and permittivity) of activated water (activated medium);
- influence of such water (medium) during process of cells division on the balance of forces in the area of a cell walls;
- abnormal dynamics of the process of cells division in a volume of activated medium.

Activated water renders the bactericidal (or bacteriostatic) action on culture *Escherichia coli* growing under aerobic conditions. It is necessary to expect a similar influence under the action on other pathogenic cultures (for example, activated water should suppress the development of conditionally pathogenic bacteria *Citrobacter,* etc.).

2. Transmutation of intermediate mass isotopes in growing biological cultures in activated water

Our experiments on nuclear transmutation of intermediate mass isotopes in activated water were based on the expected

$Na^{23}+P^{31}=Fe^{54}$

reaction in growing culture in sugar-salt nutrient medium deficient in Fe but containing controlled quantity of Na^{23} and P^{31} isotopes. The reaction results in generation of the rare Fe^{54} isotope, concentration η=5,8% of which in the natural iron (mainly Fe^{56} with natural concentration η=91,7%) is very low. The research was carried out on the basis of the same bacterial culture *Escherichia coli***.** The composition of the nutrient medium is presented in Table 1.

Table 1. The composition of the nutrient medium.

Components	Concentration in the medium (%)	Admixture of Fe (no more) relative (%)
Sucrose	2	10^{-4}
$MgSO_4$	0,05	2.10^{-4}
$CaCO_3$	0,2	$1,5.10^{-4}$
KCl	0,05	3.10^{-4}
$NaNO_3$	0,5	2.10^{-4}
K_2HPO_4 (in transmutation experiments)	0,2	5.10^{-4}
Pure distilled water (activated or nonactivated H_2O)	100 (100 ml)	10^{-7}

All initial dry ingredients of the sugar-salt nutrient medium were investigated on SIMS mass-spectrometer. The same investigation was held with a part of the bacterial culture inoculum.

The cultures were grown in the thermostat at the optimal temperature 30^0 C during 48 hours. After completing each series, the obtained biological substance was separated using a centrifuge, cleaned in the distilled water and dried. The results of SIMS-analyses of cultures that were grown during experiments on isotope transmutation in regular and activated water are presented in Fig. 12.

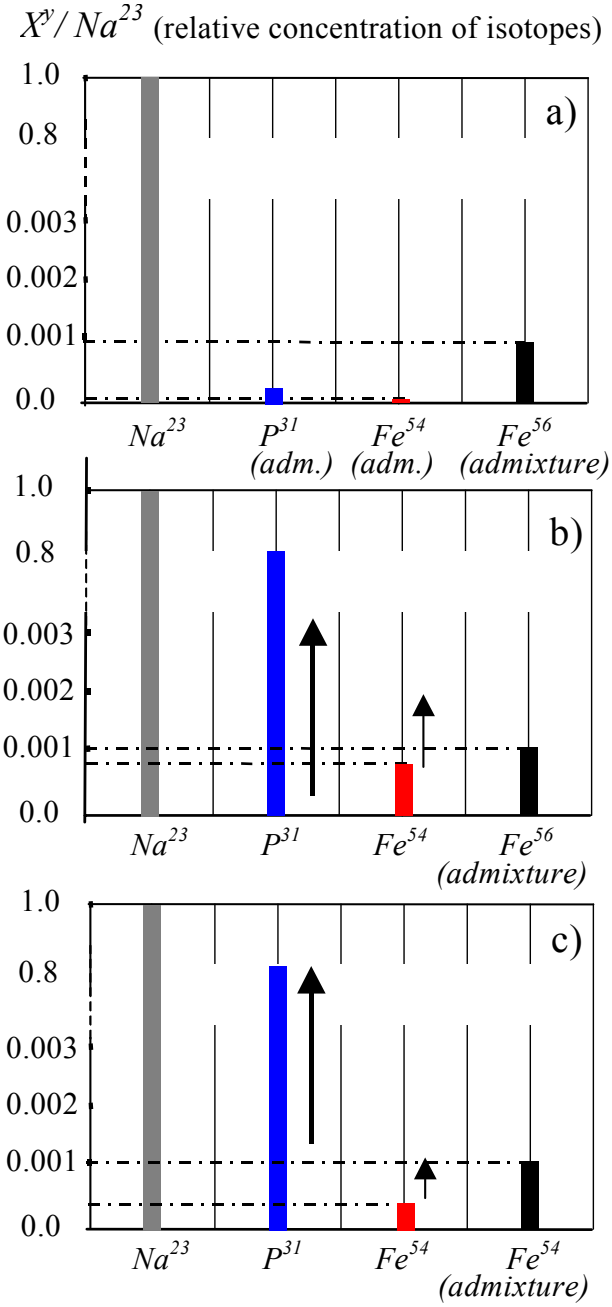

Fig.12. Mass-spectrum of culture *Escherichia coli* (dried biological substances) that was grown in sugar-salt nutrient medium with presence of Na^{23} ($NaNO_3$ salt) and P^{31} (K_2HPO_4 salt) in activated and nonactivated water (H_2O).

a) Control case - presence of Na^{23} (salt $NaNO_3$) and nonactivated water (P^{31} isotope was absent); $\eta(Fe^{54})/\eta(Fe^{56}) \approx 0{,}05$.

b) Experiment at transmutation conditions - presence of Na^{23} ($NaNO_3$ salt), P^{31} (K_2HPO_4 salt) and nonactivated water; $\eta(Fe^{54})/\eta(Fe^{56}) \approx 0{,}8$; Effectiveness of isotope transmutation is: $\lambda \approx N(Fe^{54})/N(P^{31}+Na^{23})\Delta t \approx 10^{-9}$ (synthesized Fe^{54} nuclei per s and per pair of P^{31} and Na^{23} nuclei).

c) Experiment at transmutation conditions - presence of Na^{23} ($NaNO_3$ salt), P^{31} (K_2HPO_4 salt) and activated water (t_{act} = 30 min); $\eta(Fe^{54})/\eta(Fe^{56}) \approx 0{,}4$; Effectiveness of isotope transmutation is: $\lambda \approx 0.5.10^{-9}$ (synthesized Fe^{54} nuclei per s and per pair of P^{31} and Na^{23} nuclei).

Conclusions.

The performed detailed studies have shown that activated water has a number of special or anomalous properties relative to similar, but nonactivated water.

It is worth to note the following essential features of activated water:

- It is characterized by a very great change (the reduction by 5 and more times) of the dielectric permittivity and the conductivity in the field of low and very low frequencies;
- A very significant reduction of both the viscosity and the coefficient of friction (the reduction by 10-100 times and more) is registered in the regions of small pressures acting on this water and of small speeds of its movement;
- The temporal nonmonotone behavior of the hydrogen index pH is revealed, and this change can be characterized by sharp maxima or minima for a certain type of activated water which are manifested in many days after the completion of the activation of water and have the form corresponding to phase transitions;
- Anomalous properties of activated water are preserved during a large time interval which can last many hours and days.
- Duration of preservation of the anomalous properties of activated water depends strongly on its temperature (it increases as the temperature drops and decreases as the temperature grows).
- It was observed for the first time that at low initial concentration of cells of investigated culture *Escherichia coli* in nutrient medium activated water have suppressed culture growth in 3 - 100 times!
- At the increasing of water activation time, inhibition of microbiological systems growth is more effective. In activated water the effect of anomalous division of grown cells takes place. In the control experiment, i.e. on the culture growth on the nonactivated agarized medium, the number of anomalous cells (4%) does not exceed the usual stochastic deviation.
- The presence of weak low-frequency magnetic fields in laboratory and environment leads to activation of water and to strong influences on the process of nuclear transmutation in growing biological systems (the effects of weakening and inhibition take place).

These properties can be used for the explanation of some effects of the anomalous influence of such water on biological objects and on phenomena at electrolysis and cold fusion in heavy water.

References

1. Vysotskii V.I, Kornilova A.A. Nuclear Fusion and transmutation of isotopes in biological systems, Moscow, MIR Publishing House, 2003
2. Vysotskii V. I., Kornilova A. A., Tashirev A.B. Kornilova J. Experimental observation and combined investigation of high-performance fusion of iron-region isotopes in optimal growing microbiological associations. Proceedings of ICCF12, Japan, 2005. P. 206-213
3. Vysotskii V.I., Smirnov I.V., Kornilova A.A. Introduction to the Biophysics of Activated Water, Universal Publishiers, Roca Raton, Florida, USA, 2005.
4. Vysotskii V.I., Kornilova A.A. Physical foundation of long-time water memory. Moscow University Physics Bulletin, 2004. V.59, No.3. p. 58-63.

RESONANT TUNNELING IN GLOW DISCHARGE EXPERIMENTS

David Y. Chung* and James Lindesay**

Dept. of Physics, Howard University, Washington, DC
** dchung@howard.edu , ** jlindesay@howard.edu*

Abstract

Some earlier work using resonant tunneling (RT) in the description of the nuclear transmutation (NT) phenomenon in electrolysis has been documented in the past [4]. Here we will concentrate on glow discharge experiments where excess heat and NT have been observed by many authors [1, 2, and 3]. Chicea [5] pointed out the screening effect in electron clusters and found that the apparent fusion rate can be greatly increased in discharge experiments. Here we make use of the screening potential due to the plasma layer in glow discharge experiments to investigate the possible RT effects at low energies.

We have numerically solved the Schrödinger equation in a simple model with a charged particle in a screened Coulomb potential with a double layer. We assume that nuclear forces dominate on nuclear size scales, thereby cutting off the Coulomb repulsion. The results for the probability of tunneling through the barrier were very interesting. At certain energies of the incoming particles, there are very sharp resonances which enhances the probability several order of magnitude higher than with non-resonant tunneling. The possibility of resonant enhancement occurs because of the screening of the Coulomb potential due to the plasma layer. This may provide a possible explanation for the fusion reactions which may occur near the surface of the electrodes. And as a result, NT and excess heat can be produced as observed by many experimenters. Detail calculations and results will be presented in this paper

1. Introduction

There have been many interesting glow discharge (GD) experiments performed in the past [1, 2, 3]. Not only has the production of excess heat been observed, but
there is also some evidence of nuclear transmutation (NT). The production of new elements which have different isotopic abundance from what naturally occurs is convincing evidence of that a nuclear reaction has occurred. However, on the theoretical side, it is still very difficult to explain the details of the results GD experiments where several different elements have been produced at the electrode and in the solution.

In this paper, we have developed a simple model to calculate the tunneling probability of a proton through the Coulomb barrier of the electrode material. This probability can be enhanced from screening by the existence of the plasma layer just outside of the electrode in the GD experiment.

Recently there have been a few papers relating nuclear reactions with the resonance tunneling (RT) [4]. However, these papers have not addressed GD experiments directly.

The concept of Chicea [5] in describing the electron screening effect due to clusters is of particular importance. In a serious of papers, he examined the increase of the probability density due to the electron cluster, thereby increasing the chance of fusion in the nuclei by orders of magnitude. However no direct comparison with the experiments was done.

In this paper we used a model potential which is relevant to the metal surface of an electrode (in our case, a graphite rod) at different voltages in a GD experiment. We model the expected barriers due to the existence of the double layer and plasma layer to calculate the solutions of the Schrödinger equation (see Figure 1). We calculate the relative probability of a proton to tunnel through these barriers to the surface of the electrode nuclei.

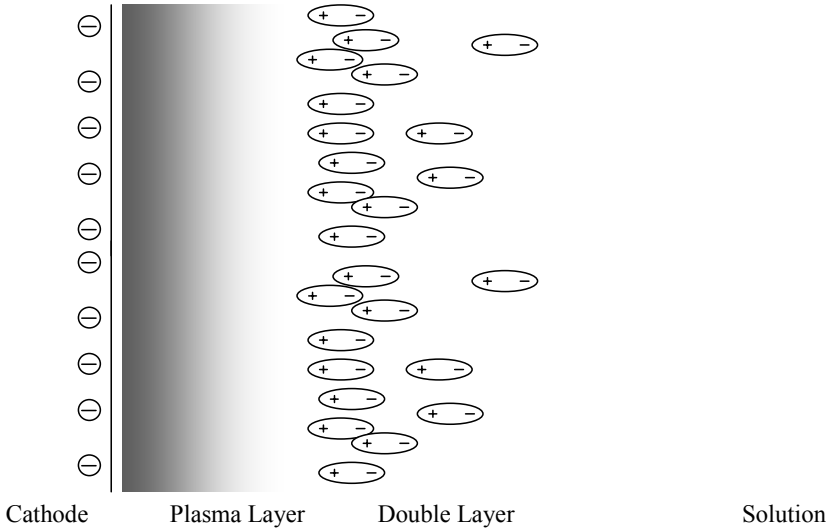

Figure 1 Cathode, plasma layer and double layer

It is of interest that there were sharp peaks in the probability vs. energy plot at low energies (few eV) for the parameters used. We believe this resonance enhancement is partially responsible for the nuclear transmutations in the GD experiments so far performed. Furthermore, the RT enhancement due to the condensed matter environment can also pave the way to study other similar experiments such as using multiple layers in Peterson's cell [6] and transmutation experiments of Iwamura [7] and the series of experiments of Kasagi [8,9].

2. Model calculations of the resonant tunneling in gd experiments

The one dimensional Schrödinger equation for proton

$$-\frac{d^2}{dx^2}\psi(x)+Z\frac{2m_p e^2}{\hbar^2}\frac{e^{-x/\lambda}}{x}\psi(x)=\frac{2m_p}{\hbar^2}\psi(x)$$

where Mp is the mass of the proton, will be solved using λ as the screening length due to the plasma layer just outside of the electrode in the experiment with atomic number Z and atomic mass number A. The model potential is shown in Figure 2, where U_d and d are the potential height and width of the electric double layer, and U_n and r_o are the nuclear potential and the

size of the proton. The nucleus is assumed to have a size of $A^{1/3}r_o$. The screened Coulomb potential barrier is assumed to extend to the nuclear surface. The distance d_p is the plasma layer thickness. In this simple model, many parameters are chosen to have values within an order of magnitude of expected values. Once the wave function ψ is solved, one can then calculate the relative probability P(x) for a given input proton energy U.

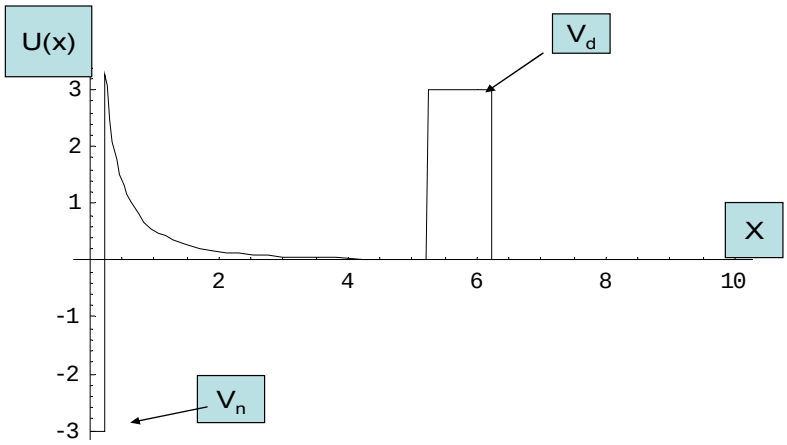

Figure 2 Model potential for plasma and double layers

The numerical solution of the equation is difficult due to the scale of the Coulomb potential near the nuclear surface. Computationally, this problem is handled by using values for the nucleon size r_o that give stable results, then extrapolating these results to the phenomenological value $r_o \approx 2x10^{-5}$ Angstroms. The calculations were carried out using a program developed in Mathematica©. The details of the calculations will be described and published in a different paper. The results of the calculations are discussed in the next section.

3. **Result of calculations**

We will summarize our results as follows:

The relative probability P(x) of a proton tunneling through the barriers is shown in Fig. 3. We define this relative probability as the ratio of the square of the wave function at the nuclear surface to the maximum amplitude squared in the region external to the double layer. One can see that for the parameters used there are several very sharp resonant peaks at relatively low energies (2-12 eV), and the resonances sharpen with decreasing resonant energy. In addition, the peaks become much sharper as the nuclear size (parameterized using r_o) decreases. We are able to calculate the width at half maximum Γ for resonant energy E_r. The sharpness of the peaks is due in part of the rapid rise of Coulomb potential near the nuclear surface, i.e. as $r \rightarrow 10^{-5}$ A.

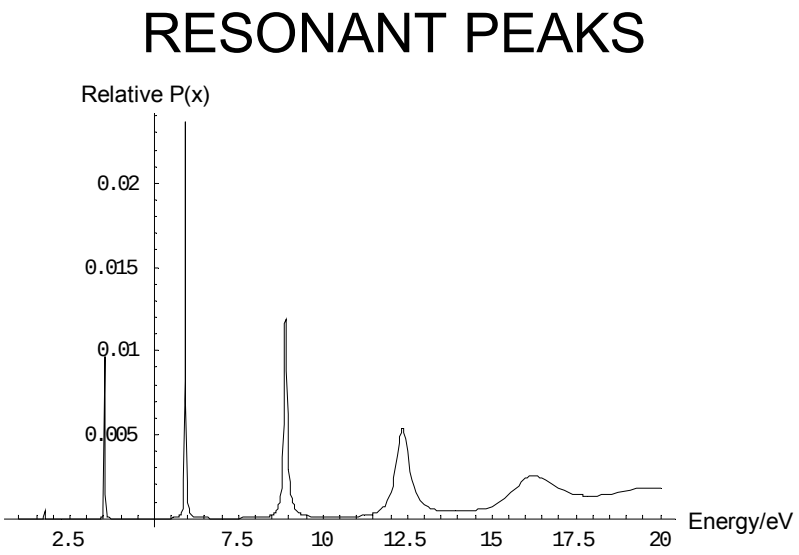

Figure 3 Resonant peaks

Fig. 4 demonstrates the variation of the resonant behavior as the nucleon size r_o varies.

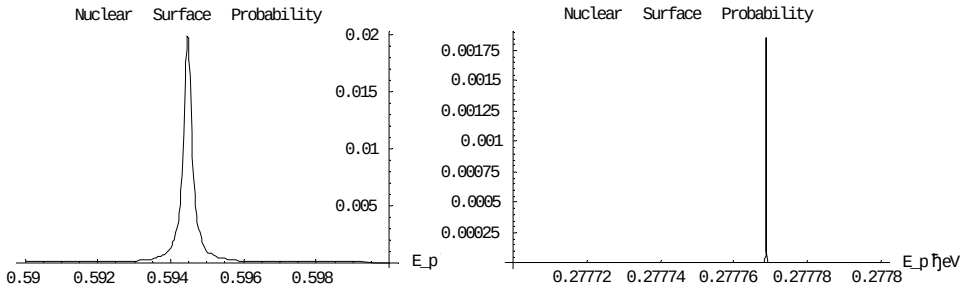

r_o=0.01 r_o=0.002

Figure 4 P(x) as a function of energy and nucleon scale r_o

Fig. 5 demonstrates the enhancement of a wave function at resonance. One notices that the size of the wave function inside the plasma layer is very large in comparison to the size outside of the double layer (ie incoming wave from right).

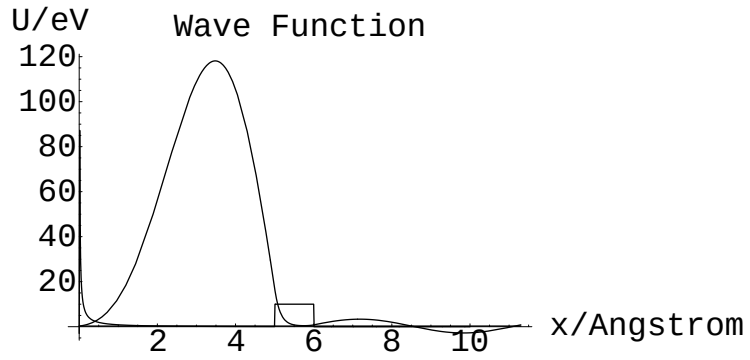

Figure 5 Resonant enhancement of wave function

As previously mentioned, in our calculations, it is numerically difficult to calculate the precise resonant energies and widths for nuclear size near 10^{-5} A due to the sharpness of the peaks and roundoff errors. Therefore we can calculate point by point as r_o is reduced and extrapolate to physical values for r_o. Similarly, we can do the same for the relative probability P(x). The results are given in Fig. 6.

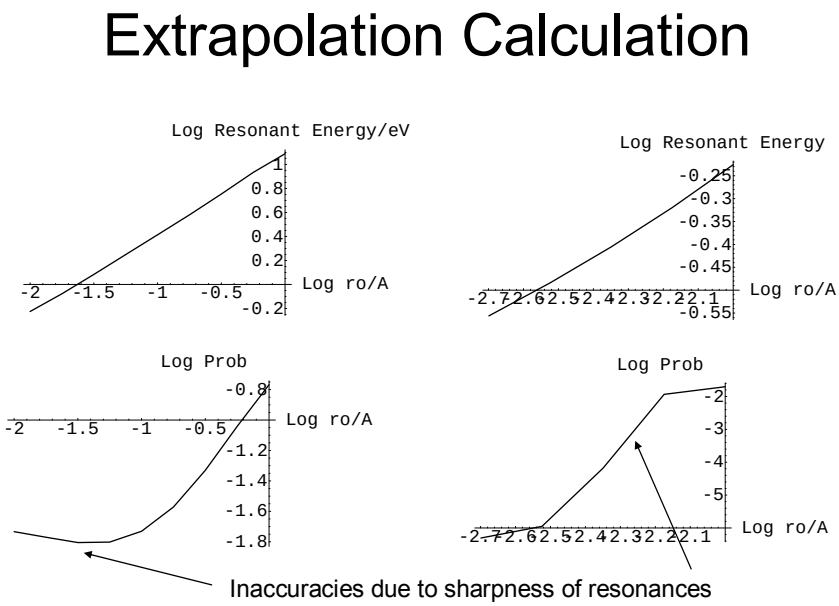

Figure 6 Numerical results for varying nuclear size

In a real experimental situation, thermal effects have to be considered, that is the Boltzmann factor will decrease the actual number of protons involved in the tunneling process at the resonant peak somewhat. This 'suppression factor' $f \approx \Gamma/k_B T$, can be estimated for a given temperature. For room temperature, T= 300 deg. K, f is of the order of 10^{-19}. This number then needs to be multiplied by P(x) from the extrapolation in Fig.6 to estimate the relative number of thermal protons expected to reach the nuclear surface. We expect the number of protons involved in tunneling per unit time to be of the order of Avogadro's number 10^{23}. We are continuing our efforts to estimate stable values for the expected resonant enhancements for physical nuclear scales.

4. Discussions and conclusion

With our model potential, we have solved the Schrödinger equation and found that there is a high relative probability P(x) for a proton to tunnel though the double and plasma layers to get very close to the nuclear surface thereby produce fusion reactions at very low energies (a few eV).
The enhancement of the P(x) is mainly due to two factors: 1. the existence of a double layer and 2. The screening effect due to the existence of the plasma layer near the surface of the electrode that makes the Coulomb barrier "tighter" to tunnel through. These factors create a 'quantum well' which can increase the probability of tunneling by many order of magnitude at resonance.

In a GD experiment, both of these conditions exist. Therefore it can be concluded that there is enhanced probability that a proton can tunnel through the nuclear Coulomb barrier of the cathode electrode and produce fusion reaction at relatively low energies (low applied voltages), such as found in many experiments in GD [1, 2, 3]. However, due to the crude model and also many of the actual experimental parameters are rather unknown at the present time. It is still not possible to predict what NT products will be produced at what voltages. But future experiments can be designed to test this model.

Furthermore, other related experiments, such as Iwamura's TN [7] on the surface of a complex structure of Pd/CaO/Pd. A 'multiple quantum well' structure similar to those in semiconductors can be assumed and a model calculations can be carried out to predict the tunneling probability of deuteron to create fusion reaction on the surface at resonance. Similar calculations can also be done with the multiple layers of Miley's experiments [6]. The enhancement of nuclear yield in the many experiments of Kasagi [8, 9] could also be estimated with the present model. In general, the condensed matter environment as host materials can give the enhancement for the low energy nuclear reactions to take place. Luo et al [11] have also discussed the screening effect in the solid state environment in PdH system. The knowledge and richness of many calculations in the semiconductor devices (such as tunnel diode and resonant tunnel diode) can be used as general guidance in the LENR.

References

1. Mizuno, T, Ohmori, T and Akimoto, T. Generation of Heat and Products during Plasma Electrolysis, 10th ICCF, 2003. Mizuno, T, Chung, D.Y., Senftle, F, and Aoki, Y. Same title as above, 11th ICCF, (2004).
2. Warner, J. and Dash, J., Electrolysis of D2O with Titanium cathodes: Enhancement of excess heat and further evidence of possible transmutation, ICCF-9, pp.118-119 (2002).
3. Cirillo, D. and Iorio, V., Transmutation of metal at low energy in a confined plasma in water, ICCF-11, (2004).
4. Li, X. Z. et al, Sub-barrier fusion and selective resonant tunneling, Phys. Rev. C, vol.61, p.024610, (2000).
5. Chicea, D., About deuterium nuclear reaction rate in condensed matter, ICCF-7 (2000).
6. Miley, G. and Patterson, J.A., Nuclear transmutation in thin-film coatings undergoing electrolysis, J. New Energy, Vol. 1, pp.11-15, (1996).
7. Iwamura,Y., Sakano, M., Sakai, S. and Kuribayashi, S, Low energy transmutation correlation between Deuterium flux and nuclear products, in condensed matter induced by D2 gas permeation through Pd complexes: ICCF-10, p.68 (2003).
8. Kasagi, J., Hideyuki Y. ,Taiji, B., Takashi, N., Tsutomu, O. and Lipson, A.G., et al, Strongly enhanced DD fusion reaction in metals observed for keV D+ bombardment, J. of Phys. Soc. of Japan, vol. 71, pp.2881-2885 (2002).
9. Manasreh, O. 'Simiconductor Heterojunctions And Nanostructures' McGraw-Hill, NY. (2005).
10. Luo, N., Sherstha, P.J., Miley, G.H. and Violante, V., Enhancement of nuclear reactions due to screening effects of core electrons, ICCF 10, (2003).

CREATION OF MORE LIGHT ELEMENTS IN TUNGSTEN IRRADIATED BY LOW-ENERGY DEUTERIUM IONS.

Irina Savvatimova

Federal State Unitary Enterprise Research Institute "Luch"
E-mail:U10492@dialup.podolsk.ru

The analysis of tungsten and tantalum foils after deuterium discharge with the thermoionization mass-spectrometry method is submitted. Tungsten isotopes decay in more light elements after deuterium discharge is observed. More high intensity of the light isotopes with mass numbers 169, 170, 171, 178, 180 after deuterium discharge exposure was found. The increasing of the peak magnitudes in mass spectra for these isotopes with the masses lighter, than W isotopes by a factor 5 - 400 was observed. This increase was from 5-50 cps into 100-20000 cps for this group of isotopes.

1. Introduction

The changing chemical and isotope structure of palladium and titanium was published in the previous papers earlier [1 - 5]. The weak gamma – emission, short time neutron bursts [6 - 7], change of surface structure and of an elemental and isotopic composition of Pd cathode were observed. The increasing of impurities in Pd amounted into 0.5-5 % (100-10000 times), which were not detected in an original material.

The blackening of the x-ray films being in contact with Pd, Ti and Ag foils after an irradiation by deuterium discharge were found [3, 7 and 8]. The blackening of x-ray films being inside and outside of the discharge chamber with stainless steel wall was observed [3, 9]. In accordance with the radiography analysis results the presence of the radioactive isotopes with various energy of emission on Pd cathode after deuterium discharge had shown: high-energy and low-energy components [3]. Observed effects were explained by fusion-fission reaction on the cathode (An interaction of a palladium lattice with deuterium and by the subsequent decay on more light elements). The majority of the found elements after deuterium discharge were observed mainly in local zones (hot points) [1, 2, 3, and 8].

Groups of elements such as Sc, Ti, V; Ag, Cd, In; P, Cl, Br, Ge, As, Kr, Sr, Y, Ru, Xe were found out in Pd after an irradiation by ions of all types (D, H, Ar, Ar + Xe), but within various content. The relation of integral sum of all impurity elements in Pd foils after irradiation by D, H, and Ar ions was estimated as ratio 10: (2-3):1, accordingly[9].

The considerable changes of the isotope ratio 10B/11B; 12C/13C; 60Ni/61Ni/62; 40Ca/44Ca and 90Zr/91Zr were observed and were published in paper / 6/. Change of the isotope ratio in Ag 109/107 from ratio 1/1 in initial Pd up to3/1 and 9/1 was found out in papers [5, 9].

The Uranium radioactivity changing after deuterium and hydrogen discharge was found [10, 11].

The creation of more light isotopes in tungsten and tantalum after exposure in deuterium discharge was shown with thermoionization mass spectrometry. These results are presented in this article. The possible reactions for explanations are suggested.

Two series of experiments were fulfilled: First set–"right away"- W foil was analyzed with thermoionization mass-spectrometer (TIMS) - every 15 minutes after experiments in deuterium discharge. Second set - W foils were analyzed with TIMS ~ after 3, 4, 5 months.

The increasing of the peak magnitudes for separate isotopes with masses more light than W isotopes by factor 5 – 400 was observed.

2. Methods

2.1. Experimental Method

Deuterium discharge was used as experimental method. The experimental setup is shown on Figure 1 and Figure 2.

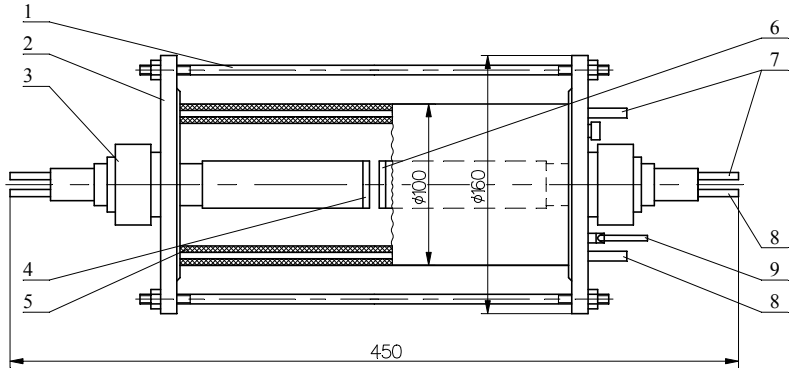

Fig.1. *Glow Discharge Apparatus. 1- ties, 2 - flange, 3 - input of power, 4 – anode, 5 – double quartz tube, 6 – cathode, 7, 8 - input and output of the cooling water (anode, cathode and space between double quartz tube), 9 – thermocouple input.*

***Fig.2**. Glow Discharge Installation*

Glow Discharge Installation was made with using of double quartz tubes with cooling water between these quartz tubes.

The sequence of operations before discharge experiments was following. Vacuum degassing was fulfilled into 10^{-3} Torr. Deuterium loading was carried out to 3-10 Torr.

Molybdenum was used as Anode. W foil was placed on Cathode. W foil had ~ 100 microns thickness and ~20 mm diameter. Anode and Cathode were cooled by flow water.

2.2. Analytical Method.

Thermoionization mass-spectrometry was used as analytical method. Estimation of isotopes (ions) intensity in mass spectra under thermoionization mass-spectrometry (TIMS) is done in counts per second (CPS).

Characterization of tims analyzes

The analysis was performed using «Finnigan» MAT-262 and "Triton" mass spectrometers in range of mass 166-206. Temperature of foils analyzed was ~ 1800ºC. The analyzed tungsten strip had the width ~ 1 mm, the length ~ 20 mm and the thickness ~ 100 microns. The strip was cut off from the central part of W foil, irradiated by Deuterons**.** Analyzing zone included the unirradiated part of W foil as well, which led to reduction of more light isotopes contribution**.** The spectra of minimal intensity (CPS) were removed from the table of TIMS

data**.** The data regarding to mass numbers 185 and 187 corresponding to Rhenium (Re) isotopes were removed from the table data as well, due to Re usage for TIMS device as a cathode. The cathode had two W foils layers. Side of foil irradiated with deuterium ions was analyzed.

TIMS calibration on Re was the example of precise definition of isotope mass.

The Figure 3 illustrates the TIMS spectra calibration using Re cathode. Example of precise definition of isotope mass is the left spectrum. 186.95 mass is Re187 estimated very exactly. Peaks of ^{185}Re and of ^{187}Re isotopes are presented on the right spectrum.

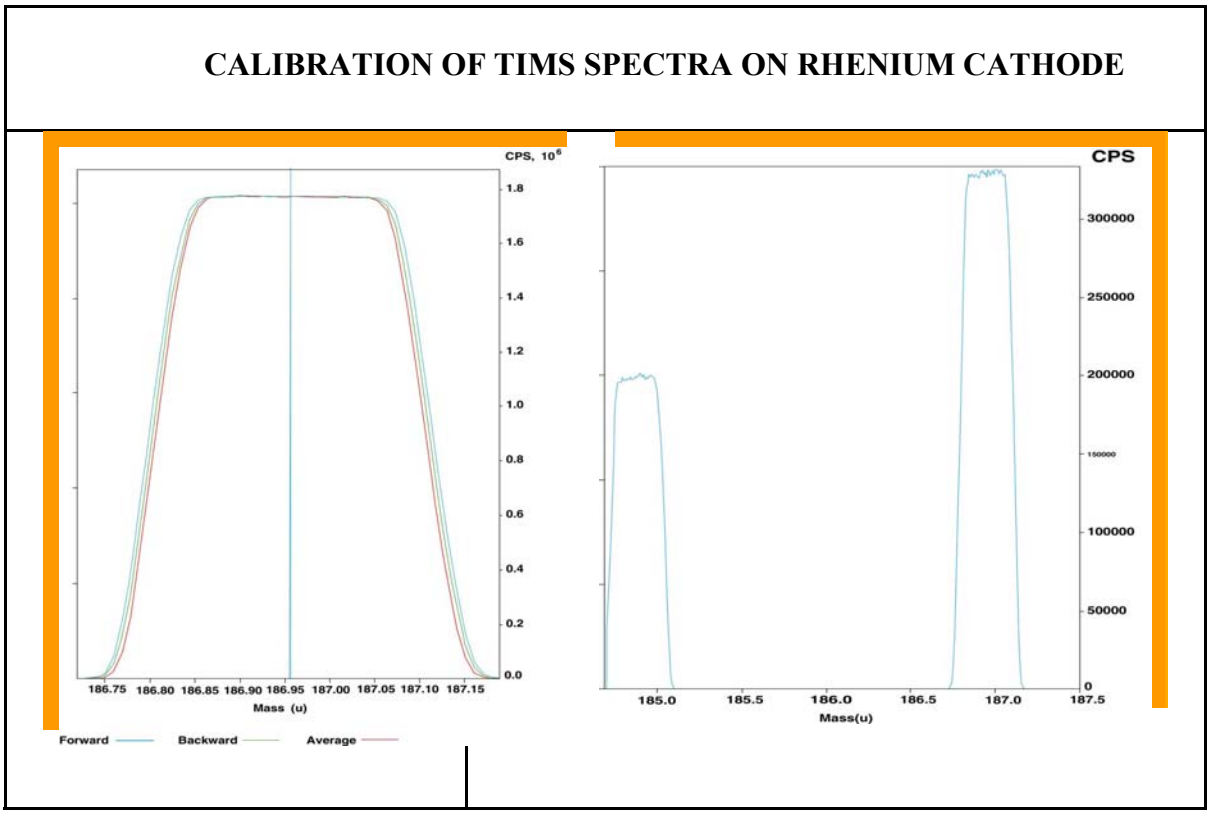

Figure 3. *Calibration of TIMS spectra on isotopes of Rhenium.*

TIMS spectra measurements have the good reproducibility after small time interval. The significant difference in isotopes intensity was observed for the different conditions of experiments: especially, dose of exposure and time interval after experiment stopping. The confirmation of spectra reproducibility is presented on the Figure 4.

REPRODUCIBILITY OF SPECTRA WITH TIMS METHOD

14.05.07 13:01 **1600 cps Mass 170**	**14.05.07 13:04** **1600 cps Mass 170**
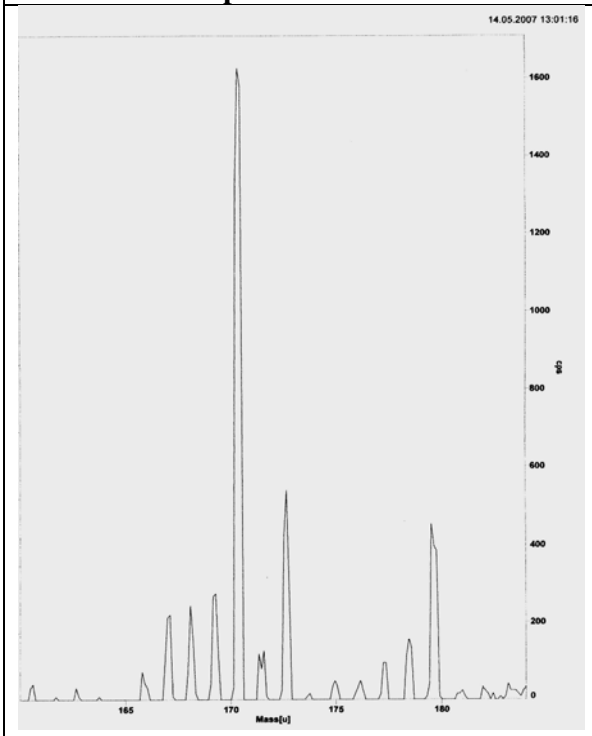	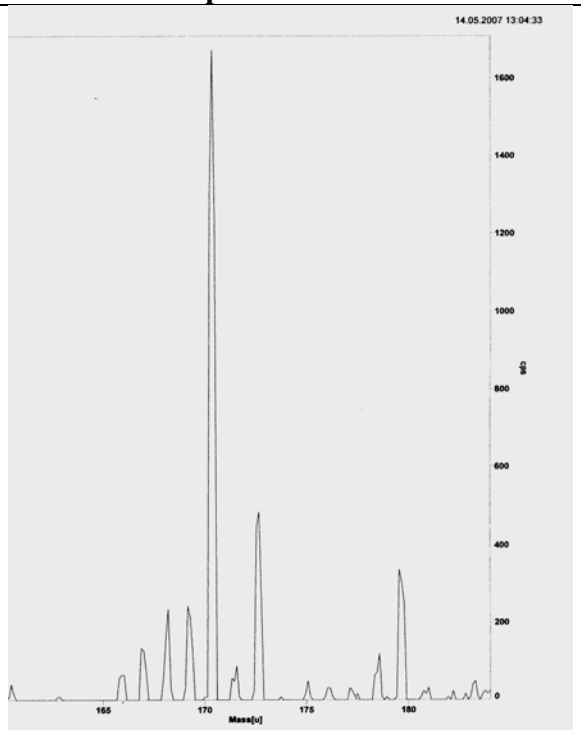

Figure 4. *TIMS spectra of the same W foil with time interval between analyses is about 3 minutes.*

Time Interval between the Right and Left Spectra was about ~ 3 minutes. It is possible to estimate that the intensity of main isotopes is closed for the both spectra. The main isotopes and their intensity are corresponding to each other.

3. Experiments

Two series analyses of W and Ta after Deuterium Glow Discharge experiments were carrying out with Thermoionization mass-spectrometry (TIMS). First set–"right away"- foil was analyzed every 15 minutes after experiment immediately («Finnigan» MAT -262 TIMS). Second set - foils were analyzed ~ 3-5 months after experiments with "Triton" thermoionization mass-spectrometry. Compare data of initial tungsten mass spectra and tungsten mass spectra after deuterium bombardment presented in the tables l and 2. Main isotopes changes in different experiments with W and Ta foils for various time intervals were

investigated in detail for mass range 166-210. The increasing of the separate isotopes with masses lighter than tungsten isotopes masses by factor 5 – 400 was observed. Temperature of analyze was ~ 1800oC.

Mass spectrum of initial W in the 170 -182 mass range (CPS) is presented on Fig.5.

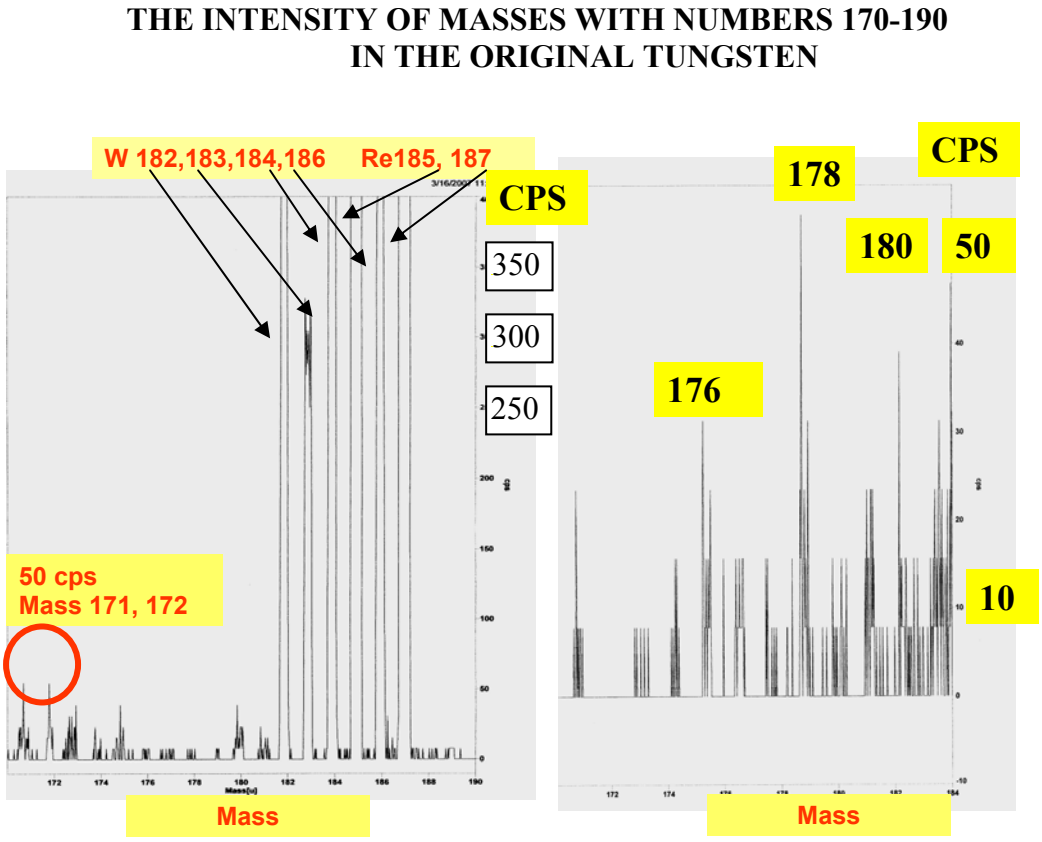

Figure 5. *Mass spectra of initial W in the 170-182 mass range (CPS).*

As it can be seen, the intensity of isotopes in initial W with mass numbers 170-180 was 10-50 cps.

Mass spectra of W (1820-23.04.07) after Deuterium discharge for 170-182 mass range for the same foil with two minutes interval shown on Fig.6.

MASS SPECTRA OF TUNGSTEN (1820-23.04.07) AFTER DEUTERIUM DISCHARGE FOR THE SAME FOIL.

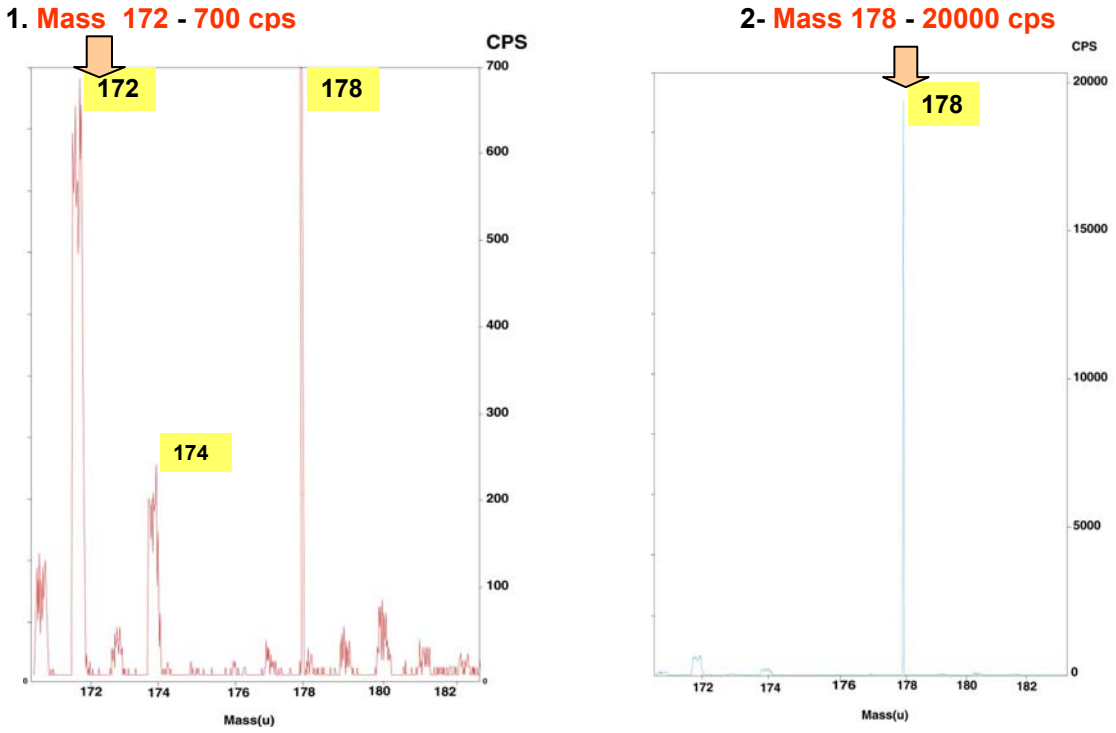

Figure 6. *Mass spectra of W #1820 through ~ 4 months after Deuterium discharge stopping.*

Mass 172 is equal ~ 700 cps on the left spectrum and mass 178 is equal ~ 20000 cps on the right spectrum (Figure 6). These isotopes intensity were 10 - 50 cps before experiments. The increasing of 172 and 178 masses intensity of the same tungsten foil from 12 to 400 times, accordantly.

Next results are the increasing of more light isotopes intensity in Tantalum spectra (Fig 7).

THE CREATION of MORE LIGHT ISOTOPES in Ta.

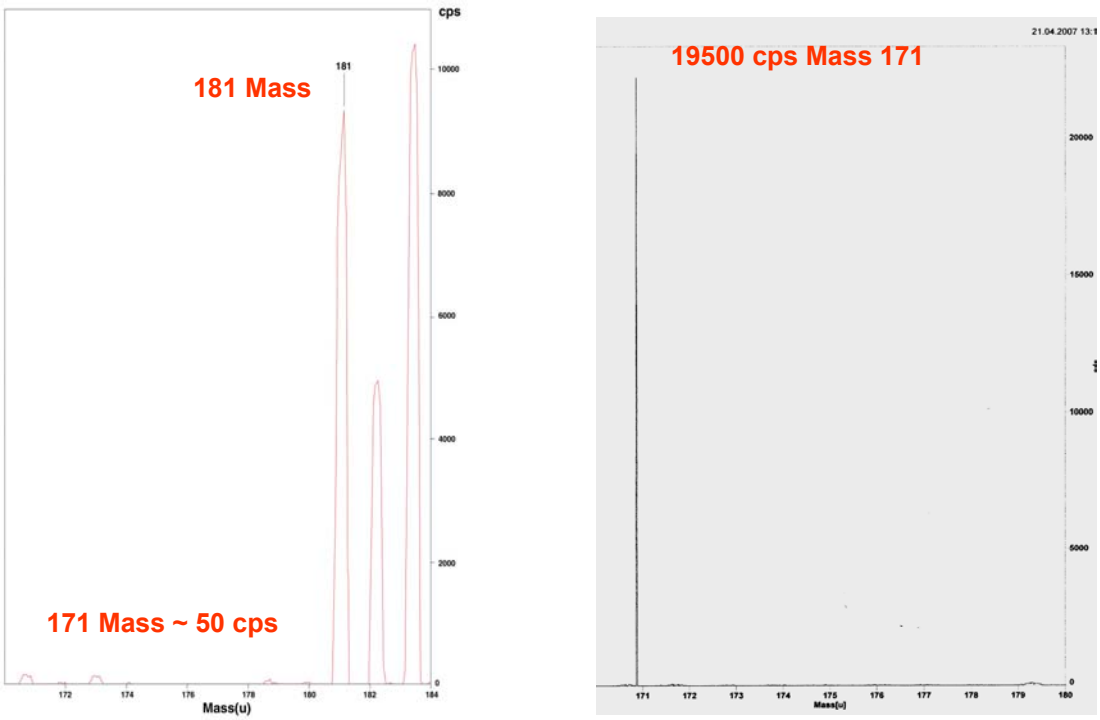

Figure 7. *Ta before (left) and after (right) the Deuterium Discharge.*

Ta before (left) and after (right) the Deuterium Discharge were compare.
Intensity of 171 mass was ~ 50 cps before experiment. Intensity of 171 mass after experiment became 19500 cps. The increasing of mass 171 intensity is ~ into 390 times.

Mass 9 in Ta before (left) and after (right) of the Deuterium Discharge was grown from 50 to 20000 cps or into 500 (Fig.15).

4. Results

Data of two series of experiments were getting. First set-"right away"- W foil was analyzed with thermoionization mass-spectrometer (TIMS) - every 15 minutes after experiments in deuterium discharge. Second set - W foils were analyzed with TIMS ~ through 3, 4 and 5 months after experiments.

The data of intensity of separate isotopes in the tungsten foils after both set of analyses were included in the table 1 and 2.

The experimental results of the first set presented in table 1.

Table 1.

INTENSITY OF THE MORE LIGHT ISOTOPES IN TUNGSTEN FOILS, IRRADIATED BY DEUTERIUM AND ANALYZED WITH TERMO - IONIZATION MASS-SPECTROMETRY METHOD (COUNTS PER SECOND - CPS)* Set 1**

Time* Mass	84*	101*	137*	1062*	1073*	1133*	1150*	**Origin W
168			40	30	60	2000	30	10 ±10
170			40	55	50	1600	100	5 ±5
171			60	95	100	100	70	5 ±5
172			70	100	100	200	100	0
173			80	75	70	300	100	15 ±15
174			30	55	60	200	100	5 ±5
175			40	55	70	40	85	5 ±5
176			40	55	40	95	75	5 ±5
177			40	55	40	10	100	10 ±10
180		70	10	45	100	20	30	25 ±5
181		100	10	30	40	50		5 ±5
189	70		20	30	10		50	5 ±5
193	60		20	30	10		0	5 ±5
194	70		40	65	0		10	10 ±10

*First line shows the time in minutes after experiment.

**Last column is intensity of isotopes in the initial W.

***Set 1- The first analysis was carried out through 45 minutes after experiment. Farther the every analysis was fulfilled through 15 minutes during ~3 hours and then after ~10 hours analysis was made through 15 minutes during few hours also.

Data of the Table 1 - First set of the experiments with tungsten demonstrate that decay of the heavier isotopes into the more light ones goes on after stopping of the experiment. The increasing is from ~20 into 200 times for the separate isotopes.

The investigation of tungsten foils irradiated in deuterium discharge with different dose after 3, 4 and 5 months of the experiment stopping included in the table 2.

Table 2

INTENSITY OF THE MORE LIGHT ISOTOPES IN TUNGSTEN FOILS, IRRADIATED BY DEUTERIUM AND ANALYZED BY TERMO- IONIZATION MASS - SPECTROMETRY METHOD (COUNTS PER SECOND -CPS)* Set 2**

# exper	#1817				#1820					#1821	Original
Date Mass	16.3.7 *	16.3.7 *	19.3.7 *	20.3.07 *	21.4.7 **	21.4.7 **	23.4.7 **	14.5.7 ***	14.05.07 ***	20.3.7 ***	****
1	2	3	4	5	**6**	**7**	8	9	**10**	11	12
168		0			**235**	**200**	75		**130**		30±10
169		25			**475**	**500**	85		**243**		30±10
170		70			**600**	**600**			**243**		30±10
171	40	70	40	45	**950**	**950**	150	140	**1670**	25	35±10
172	80	80	55	55	**5000**	**6000**	700	15	40	65	20±10
173	**400**	**400**	**300**	**300**	**200**	**200**	50	40	**488**	**200**	25±10
174	45	50	25	30	**1600**	**1615**	230	8	0	46	15±10
175	125	170	75	80	15		15	35	300	70	20±5
176*	8	8	8	8	30		15	50	0		20±5
177	8	8	8	0	30		40	130	35		8±1
178	15	8	0	8	50		**19500**	20	30		8±1
179	0	8	0	8	70		60	**220**	**100**		30±10
180	25	15	8	0			80	**480**	**320**		20±5
181			0	120			40	**1000**			30±5

Columns 2-5, 11 – results of analysis after 3 months after experiments.

Columns 6-8 – results of analysis after 4 months after experiments.

Columns 9-10 – results of analysis after 5 months after experiments.

Columns 9****- average CPS of isotopes in the original spectra for 3-5 analyzed tungsten foils during of all months.

5. Discussion

Assuming, that mass 176 corresponds to $^{176m}Yb_{70,}$ whose half-life is - 11.4 sec (IT) that may prove the possible cause why the isotope's intensity has not been detected.

Result on mass-spectrometry data includes:

•Characterization of refractory metal (W, Ta) during and after Deuterium Discharge confirmed that heavy isotopes decay occurs with thermoionization mass spectrometry results.

•The group of more light mass isotopes 169, 170, 171, 178, 180 with higher intensity was finding using thermoionization mass spectrometry after deuterium discharge soon after experiment and after 3, 4 and 5 mouths after deuterium discharge finished.

•**I**sotopes with more light masses (comparing to W isotopes masses) have been creating for at least 3-5 months after the exposure to the Deuterium Discharge. The observed increasing of the separate more light isotopes was into 5 - 400 times (from 5-50 cps into 100-20000 cps).

•Tungsten and tantalum isotopes decay in more light elements after exposure in deuterium discharge with of thermoionization mass spectrometers were shown.

It is necessary to note, that the mass number 8 and 9 number mass were found after tungsten exposure in the deuterium discharge. These masses (8 and 9) were not observed always.

Experiment with Tantalum was carried out for more understanding and explanation of the possible mechanism of the process. It was made, because the tantalum has only one stable isotope with mass 181. As can see in Figure 7 and 8, the increasing only one isotope with mass number 171 (less of the main stable isotope) was found. It is significant only one light isotope with mass number 9 was observed for tantalum experiment.

Mass 9 in Ta before (left) and after (right) of the Deuterium Discharge

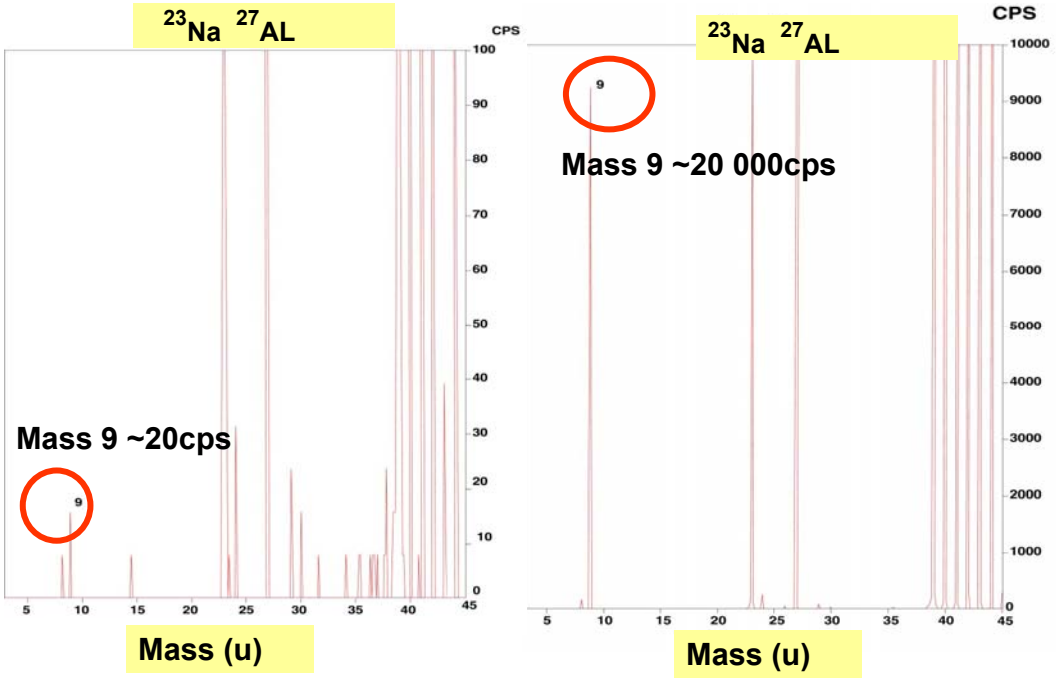

Figure 8. *The significant grown of 9 mass in Ta spectra observing after Deuterium Discharge.*

Mass 9 in Ta before (left) and after (right) of the Deuterium Discharge was grown from 50 to 20000 cps or into 400.

This observing effect allows to suggest the possibility of the following reactions:

$$_1D^2 + {}_{74}W^{186} \rightarrow {}_{72}Hf^{178} + {}_3Li^{10*}$$
(1+)(+13 MeV) + (0+)(-45.7 MeV)→ (0+)(-52.4 MeV) + (2+)(+20.9 MeV) +1.2 MeV [Δ1+]

$$_3Li^{10*} \rightarrow n + {}_3Li^{9*}$$
(1-, 2-) (1.2MeV) (+33.05 MeV) → (1/2+)(+7.3 MeV) + (3/2-)(+24.95 MeV) +2 MeV [Δ 1-]

$$_3Li^{9*} \rightarrow \underline{^{178ms:\ \beta^-}} \rightarrow {}_4Be^9 + 13.61MeV$$
(3/2-)(+24.95) →(3/2-)(+11.34)+ 13.61MeV ;

This is only one variant of the probable reaction. But the alternate could be better for the reflection of this complex process. So polyneutron theory of transmutation, suggested by John Fisher [13], can be applicable. It is necessary to pay more attention to the electro-magnetic excitation for stimulation of this process. It was noted early [9] and Peter Hagelstein published in his paper [14]. The cluster decay and the neutrino and dineutrons participation in this process can take a place also [15] .

It is require more scrutinizing and of problem study. However the getting of new applications and new detail knowledge are need of some bankroll. Nevertheless it is impossible without the special financial supporting. It is the vicious circle which we have in our favourable direction of research.

Conclusion:

1. The isotopes with masses 169, 170, 171, 178, 180, 181 (less than W and Ta isotopes) after deuterium Glow Discharge were found in W and Ta initial matters by TIMS.

2. The isotopic changes continue to occur at least 3 - 5 months after Glow Discharge exposure. The observed increase of the separate isotopes with masses less Tungsten and Tantalum isotopes were by a factor 5 – 1000 times.

3. The comparison of mass spectra with gamma spectra allows to suppose the exist of next isotopes : $^{169}_{70}Yb$; $^{170}_{72}Hf$; $^{171m}_{70}Yb$; $^{172}_{72}Hf$; $^{178}_{70}Yb$; $^{180}_{70}Yb$; $^{180m}_{72}Hf$ [16]

4. The ligth masses with numbers 8 and 9 were found also.

Reference

1. Savvatimova and D.Gavritenkov, Results of analysis of Ti foil after glow discharge, Proceedings of the ICCF11 (2004), p. 438-458.
2. Savvatimova and D.Gavritenkov, Influence of the glow discharge parameters on the structure and isotope composition of cathode materials, in Proceedings of the ICCF12 (2005), p. 231-252
3. Savvatimova I.B., Kucherov Ya., Karabut A.B., "Cathode Material Change after Deuterium Glow Discharge Experiments", "**Transaction of Fusion Technology**"(ICCF4, Dec. 1993); v.26, number 4T (1994), pp. 389-394.
4. Savvatimova I. Transmutation in cathode materials exposed at glow discharge by low energy ions. Nuclear phenomena or ion irradiation result? Proceeding, ICCF-7, 1998, 342-350.
5. Savvatimova I.B, Karabut A.B. Nuclear Reaction Products Registration on the Cathode after Deuterium Glow Discharge. Surface, V. 1, Moscow: RAN, 1996, p.63-75.
6. Karabut A.B., Kucherov Ya.R., Savvatimova I.B. "Nuclear product ratio for glow discharge in deuterium". **Physics Letters** A, 170, 265-272 (1992).
7. Karabut A.B., Kucherov Ya.R., Savvatimova I.B., The Investigation Of Deuterium Nuclei Fusion At Glow Discharge Cathode " **Fusion Technology** Vol.20 Dec.1991 (P.924-928)
8. Savvatimova I.B Reproducibility of experimental in glow discharge and process accompanying deuterium ions bombardment. ICCF8, Italian Physical Society, Bologna, Italy, 2000, P.277
9. .Savvatimova I.B, Senchukov A.D.., Chernov I.P.., Transmutation Phenomena in the Palladium Cathode after Ions Irradiation at the Glow Discharge. Proceedings, The 6th Int. Conf. on Cold Fusion. Proc. Oct. 13-18, 1996- Japan, 1996, p.575-579.
10. Dash J., Savvatimova I.,. Frantz S, Weis E. and Kozima H., "Effects of Glow Discharge with Hydrogen Isotope Plasmas on Radioactivity" Proc. ICENES 2002, p. 122 (2002) 20
11. Dash J., Savvatimova I., Frantz S., Proc.11th Int. Conf. on Emerging Nuclear Energy Systems. Univ New Mexico, Albuquerque, NM, pp.122-127 (2002);
12. .Dash J, Savvatimova I, Effects of Glow Discharge with Hydrogen Isotope Plasmas on Radioactivity of Uranium, Proc. Of American Nuclear Society Conf., San Diego, 6 June, 2003.
13. Fisher J., Polyneutron theory of transmutation. Proceedings of the 12 International Conference on Cold Fusion ICCF12 (Yokohama, Japan, 2005), p. 516-520.
14. Hagelstein P., Proceedings of the 6th International Conference on Cold Fusion ICCF6. Oct. 13-18, 1996- Japan, 1996
15. .Muromtzev V, Platonov V. and Savvatimova I, Neutrino-dineutron reactions, Proceedings of the 12 International Conference on Cold Fusion ICCF12 (Yokohama, Japan, 2005), p. 571-576.
16. Savvatimova I., Savvatimov G., Kornilova A., Decay in tungsten irradiated by low energy deuterium ions, This Proc.13th Int. Conf.ICCF13, Sochy, Russia, 2007.

XPS STUDY ON SURFACE LAYER ELEMENTS OF Pd/CaO MULTILAYER COMPLEX WITH AND WITHOUT DEUTERIUM PERMEATION

Tatsumi Hioki, Naoko Takahashi, and Tomoyoshi Motohiro

Frontier Research Center, Toyota Central Research & Development Laboratories, Inc., Nagakute, Aichi 480-1192, Japan, ***E-mail: hioki@mosk.tytlabs.co.jp***

Abstract

X-ray photoelectron spectroscopy (XPS) was used to examine the surface layer elements of Pd/CaO multi-layer complex with and without D2 permeation treatment, in order to reproduce the results reported by Iwamura et al. The structure of the multi-layer was the same as that reported by Iwamura et al; Sr or Cs/Pd(40nm)/CaO(2nm)/Pd(18nm)/ CaO(2nm)/Pd(18nm)/ CaO(2nm)/Pd(18nm)/CaO(2nm)/PdO(18nm)/CaO(2nm)/Pd(25 or 50μm). Sr or Cs was electrochemically deposited on the multi-layer complexes. D2 permeation treatment was conducted at 343K for a period of 13-16days. For samples deposited with Sr, a comparison of XPS spectra with and without D2 permeation treatment indicated that with D2 permeation treatment, Sr3p decreased slightly and the peak corresponding to Mo3d and/or S2s increased. The existence of S was confirmed from S2p peaks for all the samples studied and the peak corresponding to Mo3d and/or S2s was mainly attributed to S2s. Therefore it is necessary to exclude the contamination of S to examine the conversion of Sr to Mo by using XPS. For samples deposited with Cs, an XPS peak suggesting Pr4d was observed for a sample treated with D2 permeation, while the peak was not observed for a sample without D2 permeation treatment. The intensity of the possible Pr4d peak was fairly small compared to that of Cs3d peak and the rate of conversion from Cs to Pr was much smaller than the values reported by Iwamura et al. In order to further examine whether the observed Pr is caused by a chemical process including chemical contamination, or is generated by nuclear transmutation, it is required to find a condition to improve the conversion rate.

1. Introduction

Nuclear transmutation in flowing deuterium gas system with CaO/Pd multiplayer structure has firstly been reported by Iwamura et al.[1] They have suggested that Sr and Cs converts to Mo and Pr, respectively, by using x-ray photoelectron spectroscopy (XPS) and secondary ion mass spectroscopy. The isotopic ratio for the converted Mo was clearly different from the natural one, suggesting the phenomenon being caused by a nuclear process. By using similar method, they have further found[2] that Ba converts to Sm. These phenomena of nuclear

transmutation have been indicated to occur only in the surface layer of less than about 10nm.[3] By using micro-beam X-ray florescence spectroscopy, the distribution of the transmutation sites in the lateral direction has been revealed to be non-uniform.[4]

A few experiments have been reported to confirm the nuclear transmutation observed by Iwamura et al.. Higashiyama et al.[5] have used fast- neutron activation analysis and have confirmed the existence of Pr in a sample after D2 permeation treatment. Kitamura et al.[6] have used a single CaO/Pd layer structure and have reported that most of the Sr atoms deposited at the interface of the layered structure (i.e. CaO/Sr/Pd) change to Mo after D2 gas permeation, though the direction of the gas flow is reversed from that of Iwamura et al.. Celani et al.[7] have reported that the elemental conversions, Sr to Mo and Cs to Pr, are also observed in electrochemical systems.

A serious question for these experimental results is whether the observed elements is generated as a result of nuclear reaction, or is caused by chemical processes or by chemical contaminations. Replication experiments by many other groups will be useful to clarify the nature of the phenomenon. In this paper, we will report preliminary results of a replication experiment performed in our laboratory.

2. Experimental

2.1 Sample preparation

Pd foils 25μm or 50μm thick (99.97%; Nilaco Co. Ltd)) were used as substrates. They were cleaned ultrasonically with acetone. The Pd foil was sputter- deposited with CaO 2nm thick and then with Pd 18nm thick. The procedure was repeated 5 times, followed by a deposition of Pd 40nm thick. On top of the layered structure, Sr or Cs was deposited by using the electrochemical method in the same manner as reported by Iwamura et al..[1] Heavy water solutions of 0.4mM Sr(NO3)2 (99%; Koujundo Chemical Laboratory Co., Ltd) and 0.1mM CsNO3 (99.99%; Koujundo Chemical Laboratory Co., Ltd) were used to deposit Sr and Cs, respectively. The deposition time was about 10s with a current of about 1mA. The overall structure of the samples prepared was Sr or Cs/Pd(40nm)/CaO(2nm)/ Pd(18nm)/CaO(2nm)/Pd(18nm)/CaO(2nm)/Pd(18nm)/ CaO(2nm)/ Pd(18nm)/CaO(2nm)/ Pd (25μm or 50μm), which was the same as that reported by Iwamura et al..[1]

2.2 D2 gas permeation

In Fig.1, the method of D2 gas permeation is shown schematically. The D2 gas permeation treatment was performed at 343K, following Iwamura et al..[1] The upstream

chamber connected to a reservoir (0.60L) was first evacuated by a rotary pump with a fore-line trap with zeolite and then filled with D2 gas up to a pressure of 0.25MPa. Since the down stream chamber was evacuated with a turbo molecular pump, the D2 gas started to flow through the sample. The sample was mounted so that the multi-layer side faced the upstream chamber.

2.3 XPS measurements

Two XPS instruments were used to analyze the surface layer elements of the samples. One is PHI- 5500MC (ULVAC-PHI, INC.) equipped with a Al(Kα) X-ray source generated from a twin target (Al and Mg). Another one is Quantera SXM (ULVAC-PHI, INC.) with a

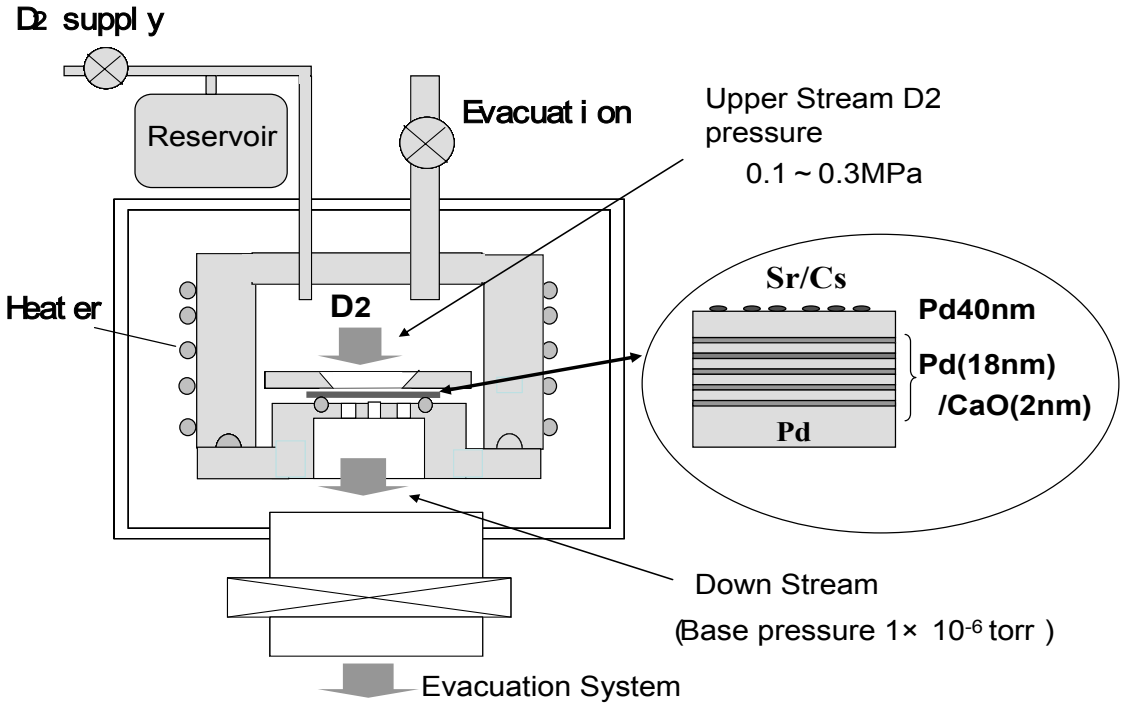

Figure 1 *Schematic of D2 permeation system.*

monochromated Al(Kα) X-ray source. The sample deposited with Sr was mainly analyzed with the twin target instrument, while XPS spectra for samples deposited with Cs were taken with monochromatic Al(Kα). When we used the twin target instrument for a sample deposited with Cs, it was found that a ghost peak appeared at a binding energy of 957eV, which was close to the binding energy for Pr3d3/2 (952eV for metallic Pr). It was revealed that the ghost

peak was Cs3d5/2 peak exited by a contaminated Mg(Kα) X-ray. The intensity of the ghost peak was significant when the deposited amount of Cs was comparatively large.

3. Results and Discussion

3.1 D2 permeation

Figure 2 shows the upstream pressure as a function of time for a sample deposited with Sr (Pd substrate: 25μ□). The upstream pressure decreases with time, because the D2 gas in the upstream chamber including the reservoir flows to the downstream chamber. When the

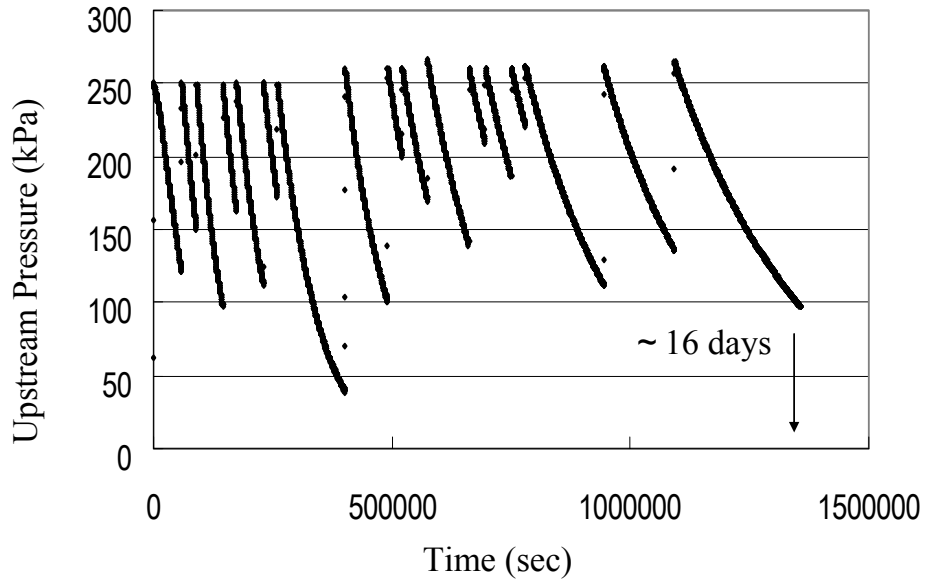

Figure 2 *Upper stream pressure as a function of time recorded for a Sr-deposited sample.*

upstream pressure decreased to about 0.1MPa, the upstream chamber was refilled with D2 gas up to the initial pressure. The procedure was repeated for a period of about 16 days. The slope of the curves in Fig.2 indicates the speed of the D2 gas flow. The speed was initially about 1.1SCCM (Standard Cubic Centimeter per Minute) at 0.25MPa, but with an increase of time it decreased gradually and reached a value of 0.3SCCM after 16 days. The average D2 flow rate was 0.5SCCM, which was lower than the highest value reported by Iwamura et al. by about 6 times, if we assumed that the sample area for D2 flow was nearly the same (□18mm in diameter).

Figure 3 shows a photograph of the samples after D2 gas permeation treatments. When a Pd substrate 25μm thick was used, the sample deformed heavily, while the deformation was small for a sample 50μm thick. The deformation is caused by the large volume expansion

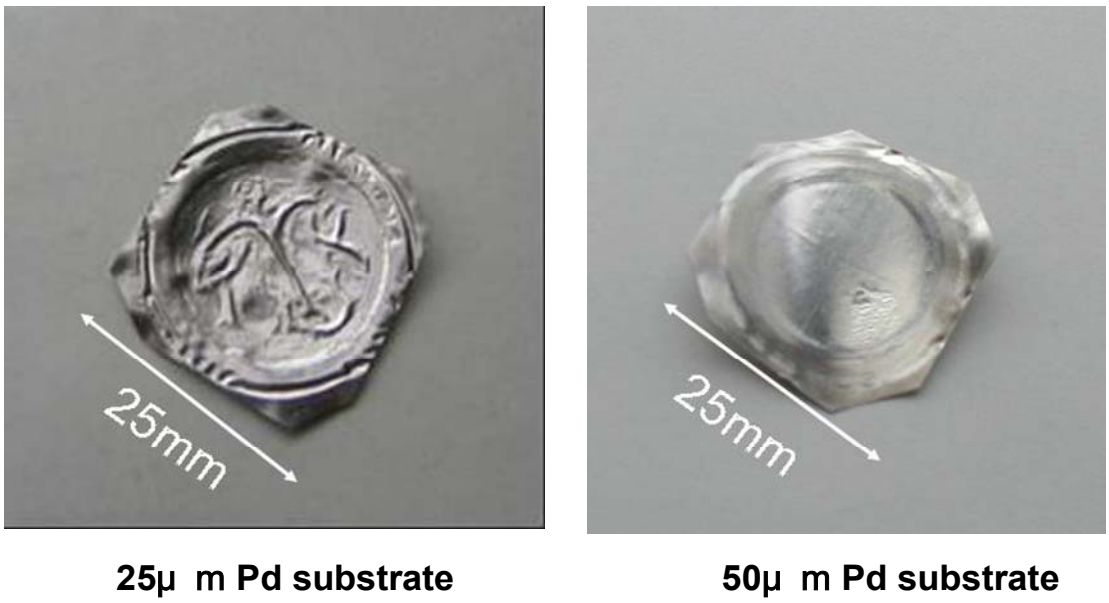

Figure 3 *View of samples after D2 permeation treatment.*

(□20□) of Pd accompanied with absorption of deuterium, while the expansion is constrained at the O-ring seal for vacuum.

3.2 XPS analyses

3.2.1 Sr- deposited samples

Two samples of Sr-deposited multi-layer complex 25μm thick were prepared. One sample was treated with D2 permeation for a period of 16 days as shown in Fig.2. The other sample was used as a reference for XPS analysis.

Figure 4 compares wide scan spectra for the samples with and without D2 permeation treatment. Peaks that are comparatively large are C1s, O (KLL Auger), Si2p (and Si2s), N1s and those from Pd. It is seen that with D2 permeation treatment, C and N decreases and both Si and O increase. The reason for these changes is not clear at present. The increase in Si and O may be caused by adsorption of Si- or O- containing molecules during the D2 permeation treatment. The molecules may come from the vacuum pump system used. The decrease in C and N may be caused by chemical reducing reactions of adsorbed C- or N-containing

molecules with deuterium as a reducing agent. As a result of reducing reaction, C and N may be removed as a volatile or gaseous fragment. Although the sample temperature during the D2 permeation treatment is comparatively low , Pd may work as a catalyst to enhance the reducing reaction.

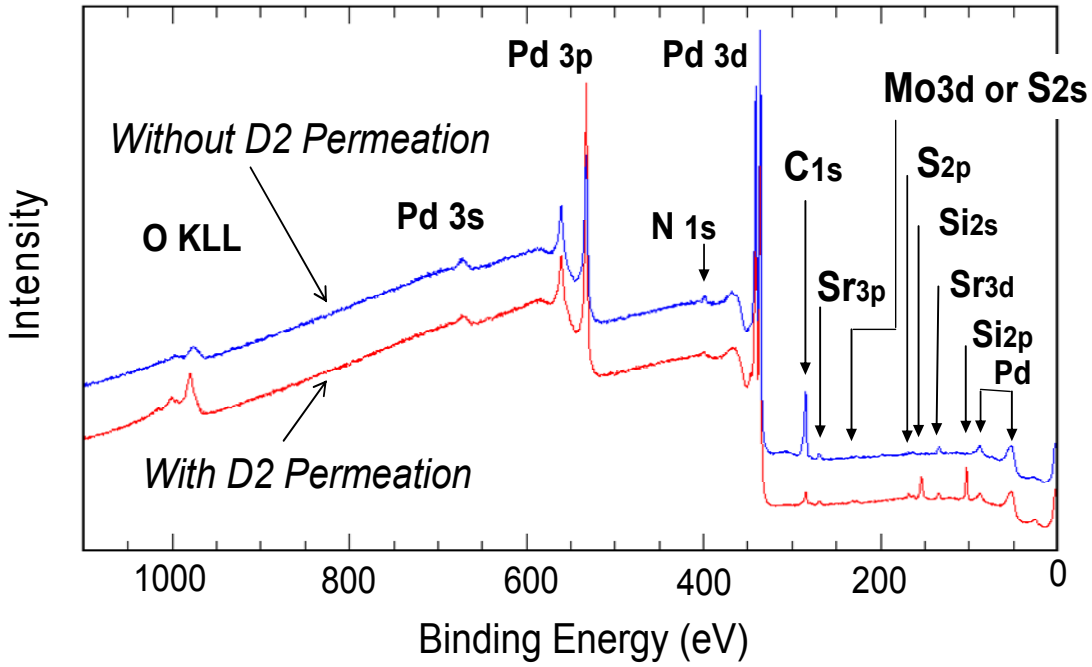

Figure 4 *Wide scan spectra for Sr-deposited samples with and without D2 permeation treatment.*

In order to examine the changes for Sr and Mo, narrow scan spectra were taken for Sr3p (□270eV) and Mo3d (□228eV). The data are shown in Fig.5. The narrow scan spectra were taken by using the signal averaging technique with hundreds of repeated scans in order to improve the signal to noise ratio. In Fig.5, it seems that Mo increases a little in accordance with a little decrease in Sr. This may indicate a conversion of Sr to Mo. However, it is noted that a peak around 228eV (Mo3d5/2) is already seen in the sample without D2 permeation treatment. The peak is mostly attributed to S2s, which has nearly the same binding energy with that of Mo3d5/2. The existence of S in the samples is confirmed by examining the

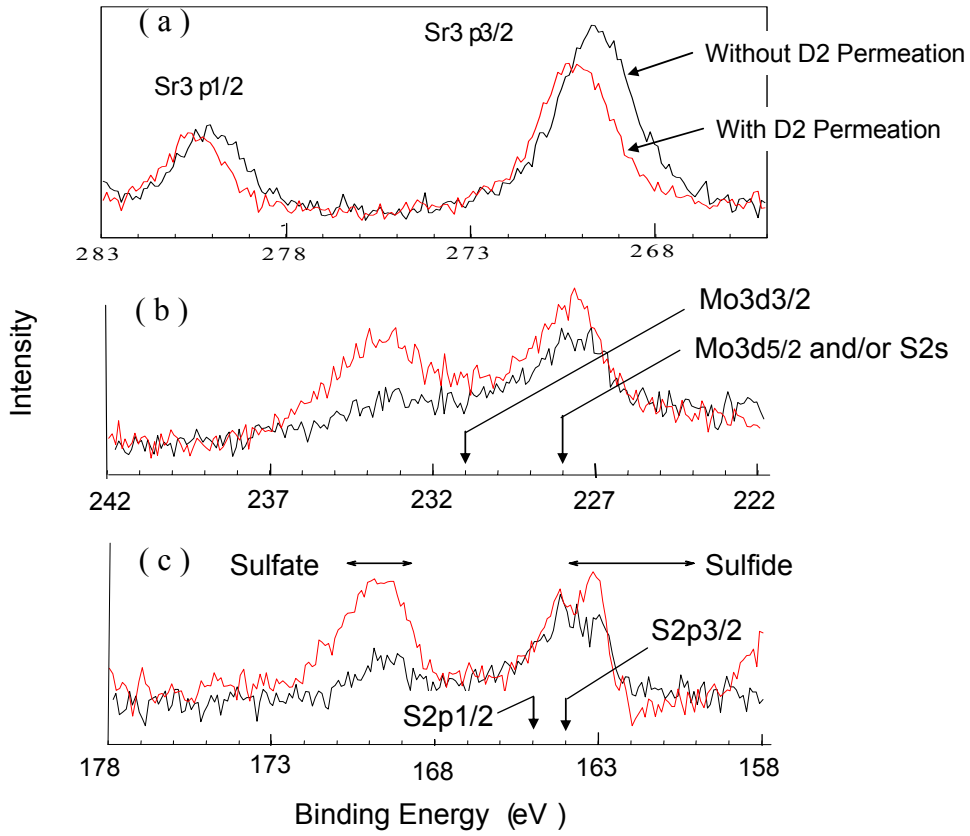

Figure 5 *Narrow scan spectra for Sr-deposited samples with and without D2 permeation treatment. (a) Spectra around Sr3p. (b) Spectra around Mo3d; the binding energy of Mo3d5/2 (228eV) agrees with that of S2s.*[8] *(c) Spectra around S2p.*

ıts

in the present samples. The spectra around S2p are also shown in Fig.5. The peak at □164eV is attributed to sulfides, probably to metal sulfides like PdS and the peak at □169.5eV to sulfates like organic ones. The separation of these two peaks is 5.5eV and this value agrees well with the separation of the two peaks around Mo3d and /or S2s (5.5eV) . Therefore, the peak around 228eV is mostly due to S. Even if a small amount of Mo is present, it is difficult to evaluate the quantity separately from that of S. In order to examine the conversion of Sr to Mo by using XPS, it is required to prepare samples which are not contaminated with S.

3.2.2 Cs- deposited samples

Figure 6 and 7 shows spectra around Pr3d and Pr4d for Cs-deposited samples with and without D2 permeation. For this case the substrate Pd was 50μm thick, but the D2 flow rate

was almost the same as for the case of Sr-deposited sample 25μm thick. The D2 permeation treatment was conducted for a period of 13 days at 343K.

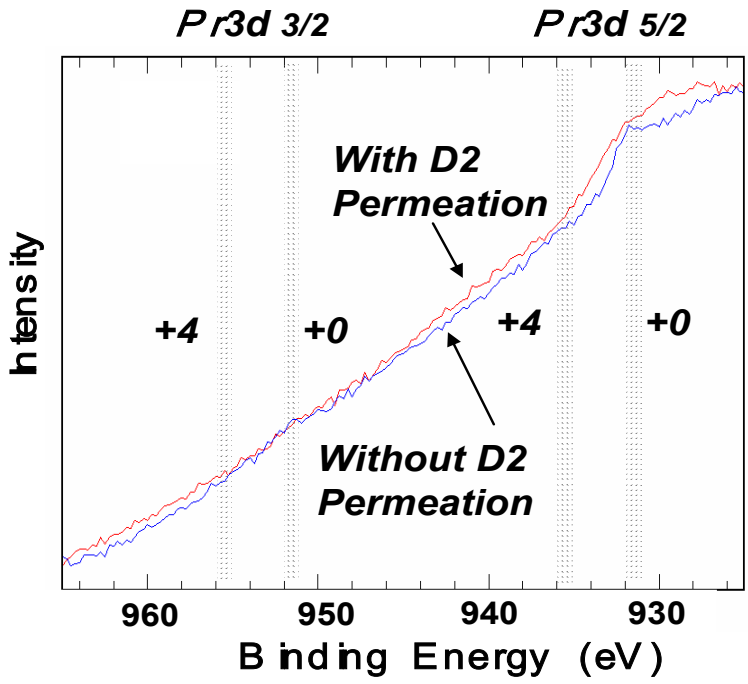

Figure 6 *Narrow scan spectra around Pr3d for Cs-deposited samples with and without D2 permeation treatment. The binding energies of Pr3d5/2 are 931.8eV for metallic Pr (valence number: 0) and 935.5eV for PrO2 (valence number: +4).*[8] *Similarly, the binding energies for Pr3d3/2 are shown.*

As seen in Fig.6, for the spectra around Pr3d, no noticeable change is observed between the samples with and without D2 permeation. However, in Fig.7, a peak is observed at 115eV, which agrees with the binding energy of Pr4d5/2 (115eV). [8] The peak is partly overlapped with a broad peak at around 120eV. The broad peak is attributed to a satellite peak of Si.

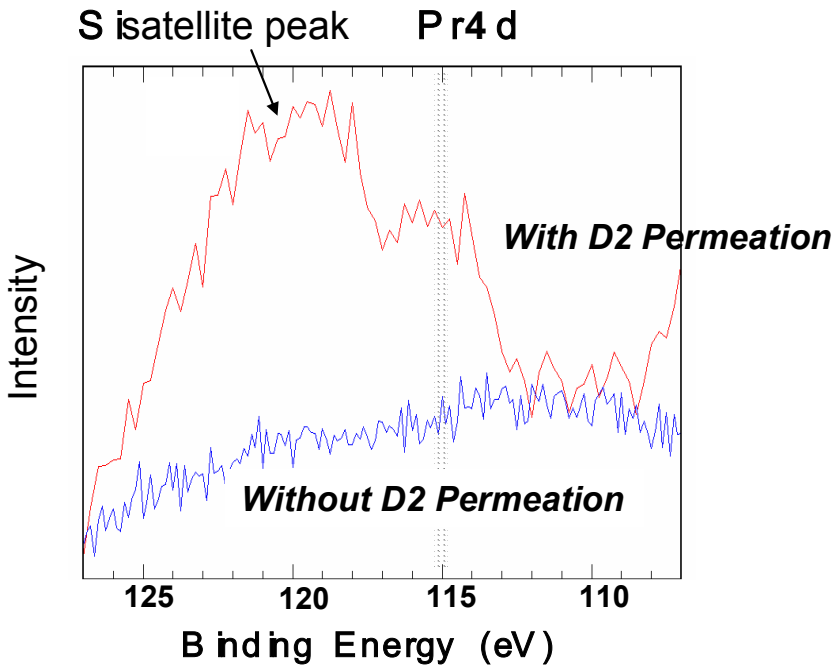

Figure 7 *Narrow scan spectra around Pr4d for Cs-deposited samples with and without D2 permeation treatment.*

Because the peak at 115eV is not observed for the sample without D2 permeation treatment, this peak seems to indicate an emergence of Pr in the sample after D2 permeation treatment. In order to further examine if there is any XPS, Auger, or satellite peaks at around 115eV, spectra are taken for SiO2, Mg, and a powder sample of CsNO3. The results are shown in Fig.8. There are satellite peaks at 121eV for Cs, at 120eV for Si, and at 112eV for Mg. However, all of these peaks do not fall on 115eV. Therefore, it is probable that the peak at 115eV in Fig.7 indicates the existence of Pr in the sample after D2 permeation treatment. Because Pr3d is the largest XPS peak of Pr, a Pr3d peak should be observed. However, as shown in Fig.6, no noticeable peak was observed. The reasons for this are; (1) there are a large Cs Auger peak close to Pr3d5/2 and Pr3d peaks fall on a steep envelope of the Cs Auger peak (see Fig.6), i.e. small Pr3d peaks are embedded in the large background, (2) the fact that the binding energy for Pr4d (115eV) is much smaller than that of Pr3d (932eV) means the

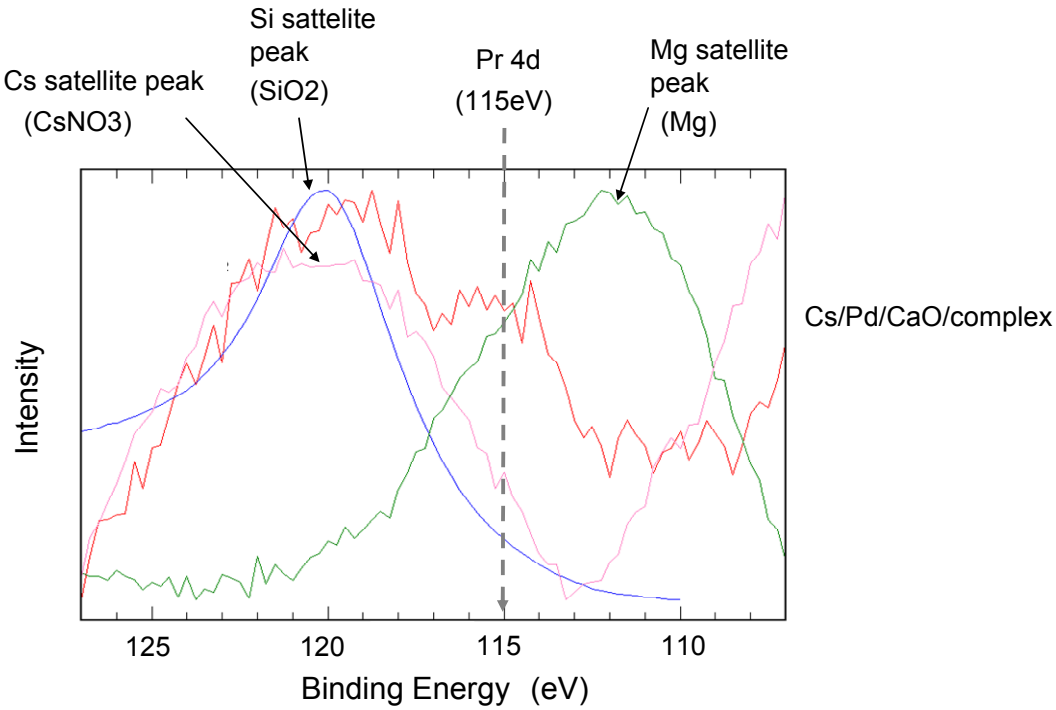

Figure8 *Spectra around the binding energy of 115eV for samples SiO2, Mg and CsNO3. The spectrum for Cs-deposited multi-layer sample after D2 permeation is also shown.*

background level is generally much smaller for Pr4d, which is advantageous to enhance signal to noise ratio by using the signal averaging technique combined with many-times-scanning. Observing Pr4d rather than Pr3d may be effective especially when Cs Auger peak is large or the deposited amount of Cs is significant.

The intensity of the probable Pr4d peak was very small compared to the intensity of Cs3d5/2. The ratio η □ (Pr atoms)/[(Pr atoms + Cs atoms)] was at most a few %. Therefore, η was much smaller than the value reported by Iwamura et al. According to them, η can take a value as large as 80%, especially when the flow rate of D2 gas is high[3]. In order to improve η, it is expected to enhance the speed of D2 flow.

4. Summary

A replication experiment was performed in order to reproduce the results reported by Iwamura group. XPS spectra were compared for the Sr- or Cs-deposited multi-layer complexes with and without D2 permeation treatments.

Sr to Mo conversion

(1) Owing to S contamination, it was impossible to derive a definite conclusion on the conversion of Sr to Mo.

(2) For examining the conversion of Sr to Mo by using XPS analysis, preparing S-free sample is important and contamination of S from experimental environments should be excluded.

Cs to Pr conversion

(3) An XPS peak suggesting Pr4d was observed for a sample with D2 permeation treatment, while the peak was not observed for a sample without D2 permeation.

(4) Observing Pr4d peak rather than Pr3d peak may be useful for examining the conversion of Cs to Pr by XPS analysis, especially when the deposited amount of Cs is significant.

Acknowledgments

The authors would like to thank Prof. J. Kasagi, Dr. Y. Iwamura, and Prof. A. Kitamura for valuable discussions. Thanks are also due to A. Itoh for preparing multi-layer structure by ion sputtering.

References

1. Y. Iwamura, M. Sakano, and T. Itoh, *Jpn. J. Appl. Phys.* 41, 4642(2002).
2. Y. Iwamura, T.Itoh, M.Sakano, S.Kuribayashi, Y.Terada, T.Ishikwa, and J.Kasagi, *Proc. ICCF11*, Marseilles, France, Oct.31-Nov.5(2004), World Scientific, Singapore, pp.339-350.
3. Y. Iwamura, T.Itoh, M.Sakano, and S.Kuribayashi, *Proc. ICCF10*, Cambridge, USA, 24-29 August (2003), World Scientific, Singapore, pp.435-446.
4. Y. Iwamura, T. Itoh, M. Sakano, N. Yamazaki, S. Kuribayashi, Y.Terada, and T.Ishikawa, *Proc. ICCF12*, Yokohama, Japan, 27 Nov.-2 Dec (2005) pp.178-187.
5. T. Higashiyama et al., *Proc. ICCF10*, Cambridge, USA, 24-29 August (2003), World Scientific, Singapore.
6. A. Kitamura, R. Nishio, H.Iwai, R.Satoh, A.Taniike, and Y.Furuyama, *Proc. ICCF12*, Yokohama, Japan, 27 Nov.-2 Dec (2005) pp.272-277.
7 .F. Celani et al., *Proc. ICCF10*, Cambridge, USA, 24-29 August (2003), World Scientific, Singapore.
8. J.F.Moulder et al., *Handbook of X-ray Photoelectron Spectroscopy*, Perkin-Elmer Corporation, 1992.

Social, Political and Philosophical Issues (SP)

FROM COLD FUSION TO LOW ENERGY NUCLEAR REACTIONS: 2007 REVIEW

Steven B. Krivit

New Energy Times, 369-B Third Street, #556 San Rafael, CA 94901 USA
steven1@newenergytimes.com

Introduction

This paper presents an overview of the field of low energy nuclear reactions (LENR), a branch of condensed matter nuclear science. It explains some of the various terminology that has been used to describe this field since it debuted as "cold fusion" in 1989.

The paper also reviews some of the most interesting news and developments regarding low energy nuclear reaction experiments and theory, and some of the trends that have affected the field over the last 18 years. It concludes with a list of resources and information for scientists, journalists and decision makers.

Overview of Low Energy Nuclear Reactions

Condensed matter nuclear science studies nuclear effects in or on condensed matter, including low energy nuclear reactions, an entirely new branch of science that gained widespread attention beginning in 1989 with the announcement of a previously unrecognized source of energy by Martin Fleischmann and Stanley Pons that came to be known as "cold fusion."

Two groups of LENR research are recognized. The first includes a set of reactions like those observed by Fleischmann and Pons that use palladium and deuterium and yield excess heat and helium-4.

The other group of reactions is a wide assortment of nuclear transmutation reactions that may occur with either hydrogen or deuterium. Anomalous nuclear effects and products are reported that involve light as well as heavy elements.[1]

Understanding the Nature of the Reactions

The worldwide LENR research effort includes 200 researchers in 13 nations. Over the last 18 years, 12 international conferences have been held, as well as 7 regional conferences in Italy, 14 in Russia and 7 in Japan.

The significant questions that face this field of research are:

a) Are LENRs a genuine nuclear reaction?
b) If so, is there a release of excess energy? and
c) Are transmutations possible?

If the answers to these questions turn out to be positive, the next questions will be:

d) Is the energy release cost-effective? and
e) Are the transmutations useful?

Many methods have been claimed to produce either anomalous power and/or nuclear products.[2]

Dominant products claimed for the D/Pd reaction are heat and helium-4. Several researchers claim to have measured close correlations of the two.[3-6]

Other products and effects that are claimed are tritium evolution,[7,8] X-rays,[9,10] neutron emissions,[11,12] gamma rays,[13] craters in cathodes,[14] charged particles,[15] hot spots on cathodes,[16] and heavy element transmutation.[17,18]

Excess heat has been difficult to repeat and reproduce and thus remains a difficult claim to confirm. Some interesting excess heat claims are presented.[19]

Despite the fact that repeatability and reproducibility are still challenging, the required parameters for achieving the excess heat effect are well understood. First, a high atomic loading ratio of D into Pd is required. In most conditions, 0.90 is the minimum threshold required to produce an excess heat effect. Second, a high electrical current density in the cathode is needed, 250 mA/cm2 under most conditions. The third requirement is for some kind of dynamic trigger to impose a deuterium flux in, on or around the cathode. The challenge that researchers face is how to achieve these conditions.

Some of The Most Interesting Research Developments

Work by Andrei Lipson (RAS), Alexei Roussetskii (Lebedev Physical Institute), George Miley (UIUC) E.I. Saunin (RAS) and Stanislaw Szpak, Pamela Boss and Frank Gordon (SPAWAR Systems Center San Diego) with investigations of charged particles is reviewed.[21, 15]

The theory proposed by Allan Widom and Lewis Larsen will be briefly reviewed.[20] The theory may be able to explain what have been described as the three miracles of "cold fusion": the lack of strong neutron emissions; the mystery of how the Coulomb barrier is penetrated; and the lack of strong emission of gamma or x-rays.

Resources

The paper will introduce resources for further exploring the field of low energy nuclear reactions. These include:
The New Energy Times Resource Index, http://newenergytimes.com/start
New Energy Times Magazine, http://newenergytimes.com/news

The LENR online library, http://lenr.org
International Society for Condensed Matter Nuclear Science, http://iscmns.org

Acknowledgements

The author acknowledges the sponsors of New Energy Institute Inc. for their generous support.

References

1. Nagel, D. (2006). Low Energy Nuclear Reactions: Status and Navy Contributions. *Proceedings of the 2006 Naval S&T Partnership Conference*, Washington, D.C.
2. Storms, E. (2001). Cold Fusion: An Objective Assessment. *http://newenergytimes.com/Library/StormsE-2001-ObjectiveAssessment.pdf*.
3. Miles, M. (2003). Correlation of Excess Enthalpy and Helium-4 Production: A Review. *Proceedings of the Tenth International Conference on Cold Fusion,* Cambridge, Mass.
4. Arata, Y. (2004). The Formation of "Solid Deuterium" Solidified Inside Crystal Lattice and Intense Solid-State Nuclear Fusion ("Cold Fusion"). *Il Nuovo Saggiatore*, Vol. 20, No.5-6, p. 66.
5. Bush, Benjamin F., et al. (1991). Helium Production during the Electrolysis of D2O in Cold Fusion Experiments. *J. Electroanal. Chem.*, 304, p. 271
6. Gozzi, D., et al. (1998). X-ray, Heat Excess and 4He in the D:Pd System. *Journal of Electroanalytical Chemistry*, 452.
7. McKubre et al. (2003). Review of Experimental Measurements Involving DD Reactions. *Proceedings of the Tenth International Conference on Cold Fusion*, Cambridge, Mass.
8. Storms, Edmund, and Talcott, Carol, (1990). Electrolytic Tritium Production. *Fusion Technology*, Vol. 17, p. 680.
9. Karabut, A.B. (2002). X-Ray Emission in the High-Current Glow Discharge Experiments. *Proceedings of the 9th International Conference on Cold Fusion, Condensed Matter Nuclear Science*, Tsinghua Univ., Beijing, China.
10. Szpak, S., Mosier-Boss, P.A. and Smith, J.J. (1996). On the Behavior of the Cathodically Polarized Pd/D System: Search for Emanating Radiation. *Physics Letters A*, Vol. 210, p. 382.
11. Mizuno, T., et al. (2001). Neutron Evolution from a Palladium Electrode by Alternate Absorption Treatment of Deuterium and Hydrogen. *Japanese Journal of Applied Physics*, 40, p. L989.
12. Lipson, A.G., and D.M. Sakov. (1994). Increase in the Intensity of the External Neutron Flux in the Irradiation of a KD2PO4 Crystal at the Point of the Ferroelectric Transition. *Tech. Phys. Lett.*, 20, p. 954.
13. Mizuno, T., et al. (1977). Anomalous Gamma Peak Evolution from SrCe Solid State Electrolyte Charged in D2 Gas. *Int. J. Hydrogen Energy*, 22, p. 23.
14. Szpak, S., et al. (2005). The Effect of an External Electric Field on Surface Morphology of Co-deposited Pd/D Films. *Journal of Electroanalytical Chemistry*, Vol. 580, p. 284-290.
15. Szpak, S., Mosier-Boss, P.A. and Gordon, F.E. (2006). Experimental Evidence for LENR in a Polarized Pd/D Lattice. *Proceedings of the 2006 Naval S&T Partnership Conference*, Washington, D.C.
16. Mosier-Boss, P.A., and S. Szpak. (1999). The Pd/(N)H System: Transport Processes and Development of Thermal Instabilities. *Il Nuovo Cimento, Soc. Ital. Fis. A*, Vol.112, p. 577.

17. Iwamura, Y., et al. (2002). Elemental Analysis of Pd Complexes: Effects of D2 Gas Permeation. *Japanese Journal of Applied Physics*, Vol. 41 p. 4642–4650.
18. Higashiyama, T., et al. (2003). Replication of MHI Transmutation Experiment by D2 Gas Permeation through Pd Complex. *Proceedings of the Tenth International Conference on Cold Fusion*, Cambridge, Mass.
19. El Boher et al. (2004). Excess Heat In Electrolysis Experiments At Energetics Technologies. *Proceedings of 11th International Conference on Cold Fusion*, Marseilles, France.
20. Widom, A., and Larsen, L. (2006). Ultra Low Momentum Neutron Catalyzed Nuclear Reactions on Metallic Hydride Surfaces. *European Physical Journal C - Particles and Fields*, Vol. 46(1), p.107.
21. Lipson, A.G., et al., "Phenomenon of an Energetic Charged Particle Emission From Hydrogen/Deuterium Loaded Metals." Proceedings of Tenth International Conference on Cold Fusion, Cambridge, MA, (2003)

FROM COLD FUSION TOWARDS NUCLEAR TRANSMUTATION – PPROBABLE ALTERNATIVE FOR NUCLEAR POWER ENGINEERING (GLANCE FROM RUSSIA)

Igor Goryachev, Yu.Bazhutov

1.Short historical review

On 23 of March 1989 at the University of Utah (USA) there was held a press-briefing were it was announced about the outstanding discovery that immediately agitated the scientific community all around the world. The highly experienced electrochemists Martin Fleischmann and Stanley Pons had discovered a phenomenon which according to their interpretation was actually nuclear fusion that could be run using pretty simple laboratory equipment and actually at the normal temperature [1]. They also stated that the energy yield was approximately three times as much compared the energy consumed and the process was not accompanied by any kind of dangerous irradiation. Almost the same results were observed by another group of American physicists headed by professor Steven Jones [2].

Immediately after that announcement the scientists at more than 200 laboratories in 25 countries rushed to replicate those experiments. At once leaders appeared: by the end of the Summer 1989 at three Indian National laboratories about 20 groups of scientists were engaged in the researching the phenomenon of cold nuclear fusion being funded by the Indian Government; In Japan from the very beginning more than 100 scientists from 15 universities were involved in the research and soon after that around 90 scientific groups were carrying out the investigations under full funding from the part of the Ministry of International Trade and Industry; a group for developing the problems of cold nuclear fusion was established at the National Institute of nuclear Fusion; in China the works on cold fusion got massive state support from the very beginning. In the Summer 1992 Japanese scientists declared that there were no more skeptics in Japan about the reality of cold nuclear fusion. By that time the total amount of annual state funding the problem by the powerful Ministry of International Trade and Industry exceeded 100 mln. dollars.

In the Soviet Union long before Fleischmann and Ponse's announcement there existed interest to such an unusual and contradictory phenomenon as "cold nuclear fusion". The first theoretical prediction and evaluation of a possibility to realize fusion of Deuterium nuclei under high pressure were made in some works of academician Ya.Zeldovich in early 60's. The thermonuclear boom after that had delayed for longer than 20 years the feasibility research for new sources of energy. In early 80's there were published theoretical works on a possibility of Deuterium fusion in solids (v.Vysotski, R.Kuzmin). A number of researchers under the leadership of academician B.V.Deryagin at the Institute of Physical Chemistry of the Soviet Academy of Sciences experimentally observed phenomena of appearing nuclear products (neutrons) while mechanically destroying solids containing Deuterium (D_2O or

LiD). Their experimental results were partly published in scientific journals, nevertheless they were not considered to be phenomena principally unknown to science and were not presented as fore-telling about new scientific direction though those results contradicted to the adopted theoretical views.

Following the discovery by Fleischmann and Pons about 50 scientific groups at many research institutes of the Soviet Union also began working to verify the newly discovered phenomenon. At the All-Union Conference on the problems of cold fusion which was held in March 1991 in the Joint Institute of Nuclear Research (town of Dubna, Moscow region) about 100 papers were presented.

Against that background it became clear that there was negligible support of such research in the USA. At the initial period all the results of the works made by American researchers submitted for publication were handed over for reviewing to the experts in controlled thermonuclear fusion at the universities of Princeton, Harvard, Yale and California and regularly got negative notes. Partly the reason related to the obligations of the US Ministry of Energy to provide funding the works on controlled thermonuclear fusion carried on at those universities. Discovery of cold nuclear fusion was interpreted by the scientists of those universities as a threat to their research, so they voluntarily or not tried to discredit the new idea. Their efforts resulted in issuing a pretty pretentious report by the Cold Fusion Section of the Consulting Committee on Experimental Research of the US DOE. Thus, the President Bush Administration turned out to be completely disinfected about the works in this field. By that time the total expenses on developing controlled thermonuclear fusion exceeded 20 billion dollars while the highest result achieved turned out to be the yield of energy not more than 12% of the energy consumed. At the same time it is worth to stress out that by mid 90's the American scientists achieved 400% excess of out let energy as compared to the energy consumed to initiate and support the operation of the devices based on the newly discovered phenomenon; to do that they spent just 25 mln. dollars. Though for the time being those results could not made be fully reproducible. It caused inevitable strong resistance to the new direction which threatened with loss of funding. Despite the main results in cold fusion were obtained at the leading National Laboratories of the USA funded by the US DOE (Los Alamos, Oak Ridge, Brookhaven, NRL, Massachusetts Institute of Technology, a number of leading Universities) the influence of the thermonuclear lobby had resulted in cutting down state funding the works on cold nuclear fusion. In the result the US Nation Institute of Cold Fusion which was organized under the auspices from the Utah Governor and support by the Regent Board of the University of Utah in late Summer 1989 was closed in the Summer of 1991.

2. Current status

Nevertheless, the problems of cold fusion continued to be developed by the scientists of more than 30 countries, the most active works were carried on in Japan, Italy, Russia, China, India and mostly by individual scientists and private companies in the USA as well. In Russia against a background of initial failures of some scientific groups which undertook rash attempts to reproduce the effects announced by Fleischmann and Pons there happened first decrease in interest towards the supposed new direction in physics especially from the part of official science that resulted in shortening the number of research groups involved. But after that gradually the number of such groups achieved about 30 and since then stays stable at that

level. Those groups unite more than 20 PhD's and 10 DSc (Doctors of sciences which is the higher scholar grade in Russia). Despite full absence of state funding Russian scientists continued persistent investigations in new field of science. Several groups managed to get some pretty small financial support from foreign investors? In particular, from American, Japanese , and Korean investors. Several groups got support from Russian investors and industrial enterprises in Russia interested in the likely perspectives of developing new technical products with great possibilities of their commercial use.

Thanks to the efforts of a large group of enthusiastic scientists all over the world (300-350 persons) the research works in cold fusion continued though the pioneers Fleischmann and Pons had to leave the USA in December 1990 to continue their research in Niece (France) under financial support from the Japanese "TECHNOVA" company.

During the period of time after the discovery by Fleischmann and Pons more than 3000 scientific books and articles were published throughout the world by scientists from more than 200 laboratories in 30 countries describing the results of experimental and theoretical works in the field of cold fusion. At the same period of time the patent agencies of many countries issued about 200 patents on the inventions related to implementation of cold fusion phenomenon.

Unfortunately, in Russia after 1991 there is no practical possibility to publish the results of cold fusion research in scientific journals. The only printed edition for Russian cold fusion scientific community became the Collections of the Proceedings of Russian annual conferences on cold nuclear transmutation which are published actually by the community itself though the Editorial Board consists of highly qualified specialists in this branch of science.

Professional meetings of scientists from various countries were annually held as "International Conferences on Cold Fusion" (ICCF). According to the opinion of many scientists the turning-point in scientific recognition of Cold Fusion Phenomenon became the Second ICCF-2 in Como (Italy) which was held in the Summer 1992. The Conference which was chaired by the leading Italian scientist Juliano Preparata had clarified the main factors that determined (as it was understood at that moment) displaying the phenomenon, in particular: availability of Palladium-Deuterium system of Palladium saturated with Deuterium up to higher than 85%. The reactions in such system were surely accompanied with generation of He^4.

In the USA researchers Bush and Eagleton at the Polytechnical University of California achieved the yield of heat on their installation with density of (per 1 cm^3 of electrode volume) almost 30 times as much as compared to the heat generating rods of modern nuclear reactors. The Italian scientists from Frascati Research center (Rome) had proved that the density of energy generated in Palladium-Deuterium system can amount up to 600 kW/cm^3 while theoretical limit being of the order of 1000 kW/cm^3. It opened wide perspectives of implementing new phenomenon in energy production. It became quite evident that the newly discovered phenomenon is a reality.

Further investigations did not disproved that conclusion but quite the contrary widened the boundaries of possible manifestation of the phenomenon. By 2000 it became evident that though the high degree of saturating Palladium with Deuterium was a necessary condition but

far from being sufficient for generating excess heat. Moreover, Palladium itself lost the importance of its exclusiveness as the media where the reactions of fusing nuclei of deuterium became possible. In particular, the results of the experiments with Nickel-Hydrogen (protium or with little additives of deuterium) systems definitely evidenced about that. In addition, in the experiments on the methods of initiating the reactions of cold fusion which were carried out not only with electrolysis but also using different ways of introducing hydrogen into solids (from a gas phase, under the influence of glow discharge, while blasting wires, etc.) there appeared evidences of transmutation effects, i.e. converting nuclei of various chemical elements into different ones. It was determined that to initiate the reactions of fusion it was not only the grade of saturating the condensed media with Deuterium (Hydrogen) but also the rate (speed) of saturating it.

In Russia beginning with the Autumn 1993 we keep holding annual National conferences on the problems of cold fusion (after 1994 those conferences are titled "Russian Conferences on Cold Transmutation of Nuclei of Chemical Elements" and beginning 2002 Conference this title was added with "… and Ball Lightning"). These Conferences are regularly attended by 30-40 Russian Scientists and by the scientists from the Republics of the former Soviet Union (Ukraine, Belorussia, Moldova) and from abroad. During last 13 years more than 300 papers were presented at the Conferences on the results of experimental and theoretical investigations by scientists of more than 30 research groups working in different cities of Russian Federation. Also more than 40 scientists from USA, Japan, France, Italy, Germany, Portugal, Austria, Great Britain, Israel, China, and Korea attended the conferences. Some of them demonstrated high interest in the details of investigations carried on by Russian scientists and took advantage of possibilities to visit Russian laboratories in person. The Proceedings of every Conference are published in the Collections of scientific papers which are distributed both by the Russian National Book Chamber within Russia and by the Cold Fusion Community itself among Russian and Foreign scientific communities and are available for consideration and critics. Also Russian scientists had published during the same period pf time several decades of scientific articles in foreign journals and registered 12 patents on the original innovative inventions. Several more patent applications are now being pended.

Regarding organizational matters it can be mentioned that in Russia in 1991 there was established a Council on the problems of Cold Fusion headed by academician A.Baraboshkin. After 1995 the activities of Russian cold fusion community was coordinated by the Interdisciplinary Coordinating Committee on Cold Fusion under the leadership of the Vice-president of the Russian Academy of Sciences academician O.Nefedov. In 2004 it was reorganized into Coordinating Council affiliated with the Russian Physical Society, academician A.Rukhadze being its chairman.

Russian scientists gained authority and international recognition for their activities in the field of cold fusion and nuclear transmutation. More than 20 Russian scientists took part in the international conferences on cold fusion and presented totally more than 100 papers which the third largest number after scientists of the USA and Japan. At the last two International Conferences – ICCF-10 in November 2003 in the USA and ICCF-11 in November 2004 in France the number of Russian presentations turned out to be the second largest after the USA.

Three representative of Russia are incorporated into the list of the International Coordinating Committee on the problems of cold fusion. A number of Russian scientists were nominated and awarder the title of "Scientist of the Year" based on the results of the appropriate analysis of the status of research in the field that was carried out by the American Information Center on Cold Fusion. Several Russian scientists were invited to carry on their research works in some scientific laboratories of the USA, Japan, Italy, Korea, and Israel. At the ICCF-11 the International Coordinating Committee on the Problems of Cold Fusion adopted Russia as the host country to hold ICCF-13 in 2007.

Lately among the international cold fusion community there appeared proposals to abandon the term "cold nuclear fusion" as being not quite adequate with the essence of the phenomenon; instead they proposed to introduce another one, namely "Condensed Matter Nuclear Science".

Meanwhile the situation with funding research works in the field of cold fusion did not become better and in many cases even shortened. It became clear that such a situation was caused not only by budget limitations but also by lack of trust from the part of academic science. At the same time the interdependence between those factors became evident: on the one hand, it is difficult to gain trust in absence of funding and, on the other hand, it is difficult to get funding in absence of trust.

Nevertheless, by the beginning of the XXI century the results of many year scientific activities of scientists all over the world and getting scientific community acquainted with those results began yield fruit. Confidence and interest towards the investigations in cold nuclear fusion began increasing. Some objective factors facilitated that process, namely:

- Multiple reproduction by scientists of different laboratories of the effects accompanying the phenomenon being investigated, as well as determination of their connection with affecting factors. Appearance of great amount of publications in serious scientific journals with correct evaluation of all possible errors have inevitably resulted in forming stable opinion about their scientific reality.
- Appearance of multiple evidences of transmutation effects which could not help attracting interest of scientific community.
- Development of theoretical models and approaches towards explanation of the phenomena related with a possibility of direct experimental verification of trustworthiness of the theoretical issues.

Based on those reasons the pessimism existing among scientific community regarding a possibility of obtaining appreciable state support for the research activities in this field began changing for cautious optimism. These hopes the scientific community related to the appearing actual possibility to demonstrate real technologies of generating not only low grade thermal energy ($100 – 110^0$C), but also heat of sufficiently high temperature ($250 – 350^0$C), as well as Tritium in commercially valuable quantities and also a possibility of implementing the effects of transmutation to produce useful isotopes or remediation of harmful radioactive nuclides.

In spite of all those factors the chances to preserve the new scientific direction as the one having favourable perspective were estimated as 50:50, though among the scientific community there had established a firm belief that the phenomenon of low energy nuclear

reactions in condensed matter was a reality and that the effects observed could not be simply neglected, and that the mankind would definitely come across some time early or later.
The new turning-point appeared in 2002 in connection with holding the 9-th International Conference on Cold Fusion in China. At his Conference a number of leading scientists expressed their opinions that it could be China that would become the country that would be capable to take advantage of the great possibilities related to wide practical implementation of the new physical phenomenon. The reason for such conclusion was not only the real successes of the Chinese scientists involved but also the high practical efficiency of their efforts thanks to the wide state support of their research which in addition was combined with active participation of private business in developing and implementation of the technologies based on the phenomenon of cold nuclear fusion. One of the most striking example of this kind was the "Great Wall Titanium Gold" Company that financed the works and took direct part with its technical means and production capabilities in the research of the scientists of the Department of Physics of the Beijing Singhua University. The scientists in other countries who for the time being can not account on the support from the part of their governments should only search for any other possibilities of funding their works and looking for investments.

Potentially this direction of research may be financed by the industry, private investors, government and/or funds of various kind. The industry and private investors are interested first of all in obtaining patents, markets and incomes, preferably in the nearest years. Taking into account the real current capabilities of the technologies based on the phenomenon under consideration those conditions are difficult to gain. The governments as a rule are sensitive towards public opinion and the opinion of the scientific establishment and do not demonstrate their readiness to invest into risky projects. The Funds also want to know what and how soon the appropriate applied technologies can appear and how much those technologies can be useful for social needs. Such perspectives are not yet sufficiently clear.

Thus, no one of the supposed source of funding provides assurance in the possibility of its realization. The solution may probably come with appearance of political figures and private investors who would be able to realize the highly promising potential capabilities of the new physics. In their turn the scientists themselves should facilitate this process to come true first of all by distributing trustworthy and convincing information about the results of their research and the likely application projects related.

The appropriate stimulation could be given as it often happened before the change in relation towards the problem in the USA (which in its turn is being influenced by the situation in China). And some indications of such change began appear of late.

Till now the main source of funding cold fusion research in the USA was the SRI-International (Stanford Research Institute) in California and the Naval research Laboratory in Washington DC, which invest totally 5 mln. dollars per year.

In late 2003 a group of American scientists made an official proposal to the US Ministry of Energy to reconsider the position of the Ministry regarding the problem of cold nuclear fusion. In August 2004 at the Department of science of the Ministry there took place hearing on the problem with participation of scientific experts from the USA, Italy and Russia. One of those attending experts professor David Nagel from George Washington University addressed the leaderships of the Ministry of Energy, National Foundation of Science and

other agencies financing scientific research with an appeal to meet the needs of the new scientific direction and provide financial support for the projects based on it.
Though the official declaration of the Ministry of Energy adopted in the result of that hearing does not stipulate issuing a Federal program on Cold Fusion it recommends the related agencies to make decisions on funding the appropriate research in the field of low energy nuclear reactions based on the analysis of the reality of the specific projects. Simultaneously the experts attracted attention to the necessity of concentrating efforts of the researchers on determination of the features of the deuterized metals using the most sophisticated equipment and methods.

At the 11th International Conference on Cold Fusion that was held in France in November 2004 an active support to the research in this new field of contemporary physics was expressed by the famous British scientist a Noble Prize Winner Brian Josephson.

The next stage in developing research on the problems of the phenomena connected with possibilities of realization of low energy nuclear reactions in condensed matter was the 12th International conference ICCF-12, which was held in November-December 2005 г. in Japan. By the time of having this Conference held there began its interaction activities the "International Society for Condensed Matter Nuclear Science" (ISCMNS), which was founded in 2004 and first exhibited itself at the ICCF-11 in France. Through the activities of that Society stable exchange of information between the scientists of different member-countries is being carried on which undoubtedly facilitates to elaborate objective evaluation of the significance and trust worthiness of the results of experimental and theoretical investigations obtained by scientists. At present more than 20 Russian scientists are the members of the Society.

At the Japanese Conference which was held under the sponsorship support from the part of ISCMNS and the Japanese Cold Fusion Research society the idea which got special support was the opinion that among other directions of research on the problems of cold fusion the most promising works with a view to practical applicability were those in the field of low energy transmutation of chemical elements intended first of all for remediation of radioactive waste. This idea was repeatedly spoken before at many Russian conferences beginning the 1st Russian conference on Cold Nuclear Fusion in 1993 [4-6].

With reference to that it is worth noting that the title of Russian National annual Conference on the topic of this new field of physics beginning 1994 was changed for "Russian Conference on Cold Transmutation of Chemical Elements" thus anticipating the development of world wide scientific conception in physics.

The International Coordinating Committee on Cold Fusion Problems that was held while the ICCF-12 Conference chose Russia as the host country for next International Conference on Cold Fusion – ICCF-13 in 2007. This decision may be considered as recognition of the merits of Russian scientists working in this field the physics of XXI century by the international scientific community.

No doubt the newly discovered phenomenon has wide perspectives of implementation in many directions of practical activities. The future will certainly come true! It is just very important not to be late by the time of its appearance. Russia do have scientific potential to be

at least among the first three prize winners if not the first one. This possibility should not be missed!

3. Perspectives

Now let's consider what perspectives of developing break-through technologies does the physics of low energy nuclear transmutation open if the appropriate concentration of man power and finance has been provided at this strategically important direction?

Before answering this question it would be in place to explain shortly modern understanding the even phenomenon of low energy transmutation of nuclei of chemical elements as it is seen by Russian scientists at the moment.

The history of physics of subatomic matter began with experiments by Becquerel, Roentgen, and Rutherford at the boundary of 19^{th} and 20^{th} centuries. The energy yield in those experiments was small but it turned out to be quite sufficient for physicists to realize that they came across new laws ruling the world of elementary particles which make up the surrounding world. While time was passing by it became necessary to implement accelerators of elementary particles with ever increasing energy to extend our knowledge. Implementation of the accelerators made it possible to find out major laws of the world of elementary particles. The latest really outstanding discovery in modern physics were the results of the experiments fulfilled using the CERN accelerating facility in Geneva in 1983 that proved the existence of weak electrical interactions combining weak nuclear and electromagnetic interactions. But it turned out the last outstanding discovery of the 20^{th} century. While assuming the high importance of the achievements of quantum mechanics, quantum electrodynamics, nuclear physics and physics of elementary particles the 20^{th} century failed to solve the fundamental problems which those scientific theories were supposed to explain, in particular:

- What is the mass of matter and what kind of physical mechanism does generate it?
- Why the inertial and gravitational masses are equal?
- What is the electrical charge? Is it just the feature of matter or can be attributed to any other phenomenon?
- What are the de-Broigle waves of matter?
- Why the speed of light is the highest possible speed?
- Why the Pauli Principle is being followed?
- What is the reason for realization of all the motions according to the principle of the least action?
- What is the energy?
- Why the laws of conservation of energy, impulse and angular moment are followed to in all cases?
- What is the spin of particles? According to Quantum Mechanics a dot particle should not obtain spin.
- What is the time and how it is connected with matter?..

In late 80's of the 20^{th} century it became clear that the fundamental scientific research in pretty wide field of scientific directions faced crisis. There was no and is not available definitely any scientific approach towards solving the problems mentioned above. The reason for the contemporary natural science being helpless is that the modern theories of matter

exhausted their predicting potentials contained in them initially. As any kind of crisis the crisis of modern natural science is determined by two factors:

1. High cost of the accelerating facilities and the equipment related. For example, the LHC accelerator in Geneva with detectors costs 7 bln. USD. It prevents majority of scientists to carry on investigations at the front boundaries of natural science as it is understood by scientists today.
2. Absence of radically new discoveries which could possibly change the qualitative level of modern technologies. Because of that the governments of the leading countries have lost confidence towards up-to-date science and do not desire to fund research as they did it after the World War II. As an example of such attitude it can be mentioned blocking by the US Congress of construction of the accelerating facility SSC in Texas that would cost 12 bln. USD.

At present the most urgent problems arose before the worldwide community which are crucially decisive for the future of mankind, in particular:

1. Searching for effective alternative sources of energy.
2. Cleaning the environment from radioactive and chemical contamination.
3. Providing proper health care for the population and some other.

The level of contemporary science does not allow to solve those problems in cardinal way. Under the pressure of the above mentioned problems many scientists began thinking about new directions of investigation that would make it possible to find new sources of energy using relatively chip technologies and cardinally new basis. One of such directions turned out to become the discovery of Fleischmann and Pons who announced about their observation of the reaction of fusing light nuclei in laboratory conditions. Their experiments differed from classical works with "hot" plasma in that according to their opinion the nuclear reaction of fusion ran at normal room temperature. To achieve that effect they saturated a sample of Palladium with atoms of Hydrogen isotopes. On having the sample saturated with the appropriate amount of "dissolved" Hydrogen in Palladium the neutron detectors located around the set-up registered yield of neutrons at the level exceeding the background which in their opinion proved the existence of nuclear reaction of fusion. Since the reaction was run at the room temperature it was named "cold" – Cold Fusion. This experiment initiated high interest not only of physicists but also among the worldwide community. So, it evidently demonstrated the existence of high interest towards searching for alternative sources of energy. At all nuclear research centers all over the world there were undertaken attempts to reproduce the experiment. Unfortunately disappointedly most of them failed to reproduce the effect. As a rule the detectors used in those experiments either did not registered anything or they displayed some vague flashes which were not synchronized with the process of saturating Palladium with Hydrogen and all of those flashes turned out to be at the level close to the background. In other words there were recurrence in the experiments on Cold Fusion. In compliance with the laws of science the experiment is considered successful if under some fixed conditions the physical effect is repeated not depending of the specific laboratory carrying it on or the composition of the research group involved. Since then the experience on Cold Fusion turned into a synonym of pseudo-science or scientific mystification in the eyes of physicists and public.

The history looks quite different with regard to another physical phenomenon, namely "low energy transmutation of nuclei of chemical elements" (LENT). From early 90's last century several groups of scientists observed on their experimental installations an unusual

phenomenon of converting some chemical elements into different ones and appearance of radiation of previously unknown nature (let's name it "transmutation radiation", or TM-radiation). In those experiments either both phenomena were observed simultaneously or were not observed at all.

The heart of the phenomenon consists in the fact that in condensed matter under the relatively energetically weak (relative to the energies typical for nuclear interactions) impact on liquid and solid media some initial chemical elements are converted into other ones. This effect becomes apparent in various processes. Let's focus on the most bright of them which were described in Russian publications:

a) In glow discharge experiments with Palladium and other metal cathodes [7-11];

b) In experiments with electron melting ingots of Zirconium in vacuum furnace [12];

c) At cavitation process in water and salt water solutions [13];

d) In experiments with electrical blasting metal foils in liquid dielectric media [14,15];

e) Under electric discharges in water-mineral media [16,17];

f) When impacting molten lead with powerful electric current in strong magnetic field [18];

g) In growing biological cultures [19,20]

and in some other cases.

In all those experiments in line with the effect of appearance new elements which were not available in the initial material before initiating the mentioned processes in the products of transmutation there was observed the change in relation of chemical isotopes. The products of transmutation in those experiments are stable isotopes. Also there was not registered any radioactive radiation in such experiments. Moreover, there are statements about converting of radioactive isotopes into stable ones. One more important peculiarity of NTM processes is that in case of possibility to fulfill the appropriate measurements some excess heat energy was registered as well. The process of transmutation is also accompanied with TM-radiation, which results in appearance tracks on photo emulsions and thin sections of metals, those tracks being quite different from those caused by classic nuclear radiation. Though that TM-radiation is ionizing radiation it is obviously not dangerous for human health. Moreover, the experimental data do apparently indicate that TM-radiation is beneficial for the health of human beings.

Around those experiments there had formed a situation which was characterized by practically complete absence of any explanation of the nature of the phenomenon observed. Actually, though the phenomenon of cold nuclear fusion was not experimentally reliably confirmed but a huge amount of publications appeared containing various theoretical explanations for the mechanism of the reaction.

Contrary to that as for the problem of NTM-low energy transmutation of nuclei of chemical elements is concerned the phenomenon has been registered for sure but there were few theoretical works published which described at least approximately the reasons of NTM exhibition. In Russia one of the first and the most developed theoretical model of NTM is the so called Erzion Model of Catalytic Transmutation of Nuclei [21,22]. This model explains the results of a number experiments in this field [23-26] and makes it possible to propose setting-up new experiments as well as supposes a possibility of utter remediation of radioactive waste by means of converting radioactive isotopes into stable ones [27-30, 3-5].

Another work in this field was an article by a group of scientists from Dubna, published in the Proceedings of the Louis de Broglie in France [15], that turned out to be the first one to

present computer simulation of the NTM process. The calculations fulfilled by the authors were in compliance with experiments.

What is the difference between Cold Fusion and NTM regarding the laws of physics? This is not a simple question. Nevertheless it is possible to discuss what Fleischmann and Pons expected from this phenomenon.

According to the laws of nuclear physics the process of fusing light nuclei – thermonuclear fusion is energetically advantage process. In order to have an event of nuclear fusion happen the nuclei should come close together to the distance where nuclear forces of attraction become stronger than the electrical forces of repulsion because the nuclei are positively charged and hence they are repulsed. Using scientific terminology the nuclei should overcome the Coulomb barrier. For the reaction mentioned above the coulomb barrier is equal to ~ MeV, which corresponds to the plasma temperature of tens of millions of degrees. This is the key problem of the whole direction of thermonuclear energy: they need to warm up plasma to as high temperature as possible and to retain the plasma of hot hydrogen atoms as long as possible so that they while colliding could get fused thus initiating thermonuclear reaction. So far they failed to achieve that effect. Meanwhile tens of billions of dollars have already been invested into thermonuclear research.

In theoretical models of Cold Fusion type it is supposed that on the accelerating potentials of a Palladium ingot or in associated quantum processes of the lattice it becomes possible to make Hydrogen nuclei come so close to one another that the process of fusion may begin. And that is it! There is just witty implementation of the known laws of the physics of solid state and quantum mechanics. By the way, actually we are sceptic regarding the models like Cold Fusion! The reason is that if it even became possible to provide stable process of nuclear fusion at the room temperature it would not evidently mean that the Palladium matrix with hydrogen solved in it could be preserved. The fact is that if the experimental installation really generated excess nuclear energy in commercially viable amount the flux of accompanying neutrons would turn out to be so high that it would immediately destroy the Palladium ingot and the equipment nearby. So, our attitude towards the mechanism of Cold Fusion as a source of energy is negative. In our opinion, this process will never come true.!

Things are quite different regarding NTM. The scientific groups that are now engaged in studying NTM have chanced to come across the phenomenon of transmutation of chemical elements. Long after that they kept trying to get rid of the effect because it contradicted to the known laws! Nevertheless, step-by-step the details of new physics became evident.

First of all it should be recognized that so far the specific laws of physics which control the reactions of cold nuclear transmutation are not known at full scale. According to the existing suppositions the phenomenon of NTM goes on as follows:

When impacting a dense media with specially formed electromagnetic radiation the Erzions (more correctly they should be called Enions i.e. barion analogs of mezon Erzions), which are weakly bound (~10 eV) with the nuclei of the atoms, are released from being captured and begin to rotate with high frequency the nuclear chains of catalytic transmutation, such which nucleon composition corresponds to the final product atoms. The process can go with transition of heavy atoms into light ones and vice verse. These processes can not be called either fusion or fission of nuclei because as a rule they do not result in appearance of

excited radioactive nuclei and hence in irradiating of ionizing radiation. NTM is not accompanied by nuclear radiation and the final nuclei are not radioactive ones! Modern physics did not come across such phenomenon! Nevertheless, though being a kind of paradox one the NTM always follows definite laws. The quantum mechanics can not explain that phenomenon. It turned out however, that the newly developed "Theory of weak interactions" does not allow to explain the process of NTM [15]. It is impossible to give a detailed description of the process within the frames of a single article. But it can be stated that in NTM there displayed the unknown before physical laws that are probably more fundamental than the laws of the physics of XX century.

The developed knowledge of new physics can even now to become the basics for designing new technologies which potentially are able to change the whole picture of human civilization. The following technologies relate to the particular ones:

1. Producing chip and environmentally clean electric and thermal energy without generating harmful residuals;
2. Utter remediation of radioactive waste by means of converting radioactive isotopes into stable ones;
3. Neutralization of hazardous industrial waste and toxic substances by converting them into inert materials;
4. Production of precious and rare metals, such as silver, gold, platinum metals, rare earth metals out of less expensive elements;
5. Generating brand new materials and alloys which are specific both for constituting elements and structure;
6. Implementation of TM-radiation for both industrial and medical needs.

At present a number of projects are offered which are based on using the phenomenon of low energy transmutation of the nucleai of chemical elements. The following projects may be mentioned among those ones in particular:

1. Electric and heat power supply installations of various power using water as fuel.
2. Electric power supply installations of up to 100 kW and higher based on transmutation of oxygen nuclei.
3. Electric and heat generating facilities of high power based on transmutation of Zirconium nuclei.
4. Facility for production of new elements and isotopes out of cheap accessible metals.
5. Installation for remediation of radioactive waste by converting radioactive isotopes into stable ones.
6. Installation for destruction of toxic and war gases.
7. Methods of implementing TM-radiation for medical purposes.

Taking into account the above said it can be stated that the newly discovered physical phenomenon – Cold transmutation of Nuclei of Chemical Elements (Condensed Matter Nuclear Science) is actually a powerful reserve for developing breakthrough technologies which deserves to pay close attention at and be actively supported.

Additional information about the status of research and developments in the field of cold nuclear transmutation can be obtained from a number of publications and web sites [31-34].

References

1. Fleischmann M., Pons S. Hawkins M. // Journal Electroanal.Chem., 1989, **261**, 301-308.
2. Jones S.E., Palmer E.P., Griss J.B. et al. // Nature, 1989, **338**, 737.
3. Arzhannikov A.V., Kezerashvili G.Ya., Krugljakov E.P. "About Russian conferences on cold fusion and nuclear transmutation" . Achievements of Physical Sciences. 1999, № 6, v. 169.
4. Bazhutov Yu.N., Koretski V.P., Kuznetsov A.B. "Burning out radioactive isotopes and generating some stable isotopes within the erzion model", Proceedings of RCCF-1, M., 1994, p.44-47.
5. Bazhutov Yu.N., Koretski V.P., Kordjukevich V.O., Sakharov E.M. "Setting uo experiment on burning out radioactive waste within the erzion model", Proceedings of RCCF&NT-2, M., 1995, p.169-174.
6. Bazhutov Yu.N., Koretski V.P., "Possibility of processing radioactive waste within the erzion model", Proceedings of RCCF&NT-3, M., 1996, p.277-280.
7. Karabut A.B., Kucherov Ya.R., Savvatimova I.B. Phys. Letters A, 170 (1992), pp.265-272.
8. Savvatimova I.B., Karabut A.B., "Surface", 1, M. RAS., 1996, p.63-75.
9. Savvatimova I.B., Karabut A.B., "Surface", 1, M. RAS., 1996, p.76-81.
10. Karabut A.B. Proceedings of the 7th Russian Conference on Cold Nuclear Transmutetion (RCCNT-7), M., 2000, p.27-35.
11. Karabut A.B. Proceedings RCCNT-9, M., 2002, p.86-98.
12. Solin M.I. Physical idea of Russia,№1, p.43-58.
13. KladovA.Cavitation destruction of matter. http://roslo.narod.ru/rao/raol.htm
14. Urutskoev L.I., Liksonov V.I., Tsinoev V.G. "Applied physics", 2000, №4, p.83-100.
15. Urutskoev L.I., Liksonov V.I., Tsinoev V.G.. Annales de la Fondation Louis de Broglie, vol.27, #4, 2002, pp. 701-726.
16. Kuznetsov V. D., Mishinsky G. V., Penkov F. M., Arbuzov V.I., Zhemenik V.I. «Low Energy Transmutation of Atomic Nuclei of Chemical Elements». Journal Annales de la Fondation Louis de Broglie, vol.28, №2, 2003. http://FondationLouisdeBroglie.org
17. Zelenski V.F., Polyashenko R.F. "Generating isotope $_{73}Ta^{183}$ in the process of pulse electrolysis of solution $LiOH+D_2O$ in a cell with Palladium cathode and Tungsten anode", Proceedings of RCCNT-9, M., 2002, p.46-54.
18. Balakirev V.F., Krymski V.V., Bolotov B.V. et al. "Interconverting of chemical elements", Ed. V.F.Balakirev, Ekaterinburg, Urals Branch of RAS, 2003, p.28-48.
19. Krivitski V.A. "Geoinformatics", 2003, №1, p.42-500. Transmutation of chemical elements and Evolution of the Earth, M., 2001, Moscow Pedagogical State University, 2003.
20. Vysotskii V.I., Korniliva A.A., Samoylenko I.I., Zykov G.A. Proceedings of RCCNT-8, M., 2001, p.163-169.
21. Vysotskii V.I., Korniliva A.A. Nuclear fusion and transmutation of isotopes in biological systems, M., MIR PH, 2003.
22. Bazhutov Yu.N., Vereshkov G.M. "New stable adorns in cosmic rays, theoretical interpretation and possible role in catalisis of cold nuclear fusion". Preprint **1**, CNIIMash, 1990, p.1-56.
23. Bazhutov Yu.N., Vereshkov G.M. ,Kuksa V.I. "About a possibility of exsisting new stable adorns – hypothetical catalysts of cold nuclear transmutation", Proc. RCCNT-3, Moscow, 1996, p.157-201.
24. Bazhutov Yu.N., Kuznetsov A.B., "Interpretation of experiments on transmutation within the Erzion model", Proc. RCCNT-1, M., 1994, p.40-43.

25. Bazhutov Yu.N., Kuznetsov A.B., “Interpretation of new set of experiments on transmutation within the Erzion model”, Proc. RCCNT-2, M., 1995, p.25-29.
26.Bazhutov Yu.N. “Erzion model of catalyst nuclear transmutation and interpretation of ball-lightning and other abnormal geophysical phenomenon based on that model”, Proc. RCCNT-3, Moscow, 1996, p.202-210.
27.Bazhutov.Yu.N. “Analysis of the results of experiments by Urutskoev’s group within the frames of erzion catalysis”, Proc. RCCNT-9, Moscow, 2002, p.141-145.
28.Bazhutov Yu.N. “Possible consequences of the fact of reality of erzions existing within the frames of erzion model of cold nuclear transmutation”, Proc. RCCNT-7, Moscow, 2000, p.191-197.
29.Bazhutov Yu.N. “Erzion structure of magnetic «fluxes» and possible consequences of their existence in the Nature”, Proc.RCCNT-10, Moscow, 2003, p.12-18.
30.Bazhutov Yu.N., Pletnikov E.V. “Searching in organic scintillator chains of catalytic erzion-nuclear reactions initiated by slowing erzions of space origination”, Proc. RCCNT&BL-12, Moscow, 2005, p.49-54.
31.Bazhutov Yu.N.”Possible generation of neutron flashes within the frames of erzion model and registration of them”, Proc. RCCNT&BL-13, Moscow, 2005, p.31.
32.http://cosmos.izmiran.ru/CNT&BL
33.http://www.iscmns.org
34.http://www.lenr-canr.org
35.http://www.newenergytimes.com

4. PREPARATA MEDAL LECTURE - A TRIBUTE TO GIULIANO PREPARATA, A TRUE PIONEER IN COLD FUSION THEORY

George H. Miley

Dept. of Nuclear, Plasma and Radiological Engineering
University of Illinois, Urbana, IL 61801 USA
ghmiley@uiuc.edu

Anyone who attended an ICCF meeting before 2000 remembers the brilliant and fiery theoretical physicist, Giuliano Preparata. He provided new insight into the deep mysteries of cold fusion, and greatly enlivened the meetings with his lively debates. My own discussions with him usually concerned thin film electrolysis. I recall encountering him after one of his ICCF talks and questioning one of his conclusions. Giuliano snapped back – "George, you haven't read chapter 8 of my book!! Read it before you talk to me again!" I responded that I had read it but still didn't understand!! Giuliano took pity on me and just laughed (As others knowing him will recognize, this was a "mild" interaction compared to usual). His book, *QED Coherence in Matter*, is a gem; it provides a view into Giuliano's unique approach to coherence of matter and cold fusion (the "famous" chapter 8). It is not easy reading, so, I subsequently put his book in my briefcase and pulled it out whenever I found time on a trip. Indeed, I still had it with me when I sadly learned of his untimely passing. I pulled the book out and stared at the cover, then moved to the dedication page where Giuliano credits his father for teaching him the meaning of "honour and honesty". His father must have been proud since Giuliano learned the lesson well. The community lost a leading light that day.

Giuliano was born in Padova, Italy in 1942. After receiving his Ph.D. in 1964, he became emersed in strong interaction physics theory. In 1967, he joined Princeton University and after several positions, ended up in 1970 as Assoc. Professor at NYU. From 1980 until his death, he was the Chair Person of High Energy Nuclear Physics at Milan University. In the early days of cold fusion, Giuliano joined the activities of the National Cold Fusion Institute in Salt Lake City. This experience peaked his interest in the physics of this exciting new field. His later cold fusion research was done at Milan University and in collaboration with the ENEA Fascati Laboratory where he played a key role in both theory and interpretation of cold fusion experiments.

This lecture includes recollections of Giuliano's participation in ICCF meetings. In addition, the relation of his coherence theory to other more recent theories will be discussed.

Theoretical Models and Results Interpretation (TM)

RESONANCE TRANSFER OF NEUTRON FROM DEUTERON – MECHANISM OF LOW ENERGY NUCLEUS REACTIONS IN METALS.

D.D. Afonichev

Institute for Metals Superplasticity Problems, RAS, st. Khalturina 39, Ufa, 450001, Russia
afon@imsp.da.ru

The first information on cold hydrogen nuclear fusion was provided in 1926 in the publication by German chemists F.Paneth and K.Peters [1] who detected the formation of helium from palladium powder saturated by hydrogen. In 1989 researchers M.Fleischmann and S.Pons published a paper devoted to cold nuclear fusion at electrochemical saturation of palladium cathode in deuterium water solutions which aroused a novel interest to cold deuterium nuclear fusion. However, because of the absence of a theoretical model of the mechanism of cold nuclear occurrence the existence of such reactions has not been proved reliably yet.

For developing a possible mechanism of cold nuclear fusion occurrence we first of all used our own experimental data. The experiments dealing with measurement of products of nuclear fusion at deformation of deuterium saturated titanium alloy samples revealed the accumulation of tritium in some samples [3]. Reasoning from that we proposed that **D+D** interaction should occur via tritium channel [4]. We did not make measurement of ^{4}**He**. However, after publication of the announcement on attaining of high concentration of this isotope ($C_{^{4}He} = 10^{14}$-10^{18}) [5] we decided to apply the proposed mechanism to interaction **D+T** which results in generation of ^{4}**He** [6]. Our views on possible transmutation of elements under conditions of cold nuclear fusions became less skeptical. We assume that the elements detected in papers devoted to cold nuclear fusion [7-9] cannot be all initiated from such a phenomenon and many of them are formed due to ascending diffusion as noted earlier [10,11]. The absence of ionizing radiations revealed in studies on transmutation allows assuming an operation of a special mechanism of such cold nuclear fusion reactions.

In reactions with hydrogen dissolved in metal for intrusion into the nucleus of another element protium ($\mathbf{p}^{+}$) should overpass the Coulomb barrier of such nucleus charge and only a high rate of proton can provide such conditions. In particular, for light nuclei such a rate should be $E_{\mathbf{p}} \sim n\times100$ kev and for heavy nuclei it should be $E_{\mathbf{p}} \sim n\times1$ Mev [12]. The participation of nucleuses with a charge larger than (+1) in such low energy reactions is all the more less probable since the Coulomb barrier essentially increases in this case.

In terms of the fact mentioned above, we assume that cold nuclear fusion can be explained only by the interaction of deuteron with other nuclei. In all experiments described in papers devoted to cold nuclear fusion the interaction between deuterons and nuclei of other elements (D, T et al) was considered in metallic matrix. Only due to unique properties of deuteron nucleus the neutron can transfer to other nuclei and even to ones being heavier than D and T. As a result, new nucleuses are formed. For nucleus having a mass of 3 and more the

bond energy of neutron in a nucleus is higher than in deuteron and the neutron can hardly exit these nuclei under conditions of cold nuclear fusion.

The originality of deuteron displays in friability of its nucleus being due to low bond energy between particles in the nucleus. The low bond energy of nucleons in deuteron can be explained by the fact that particles spend much of their time in the area not subjected to the action of nuclear forces [13]. The nucleons in deuteron are in the triplet state $^3\mathbf{S}_1$ (orbital moment **L**=0), but the presence of the quadrupole moment testifies that state $^3\mathbf{D}_1$ (**L**=2) is added which volume fraction $\mathbf{p}_D$, is about 6% ($\mathbf{p}_D \approx 6$ %) [12]. Contrary to the basic state the distance between proton and neutron in the nucleus in state $^3\mathbf{D}_1$ is increased. The penetration of the neutron from a deuteron nucleus to another nucleus is easy since it does not have to overcome any Coulomb barrier. That is why the presence of the long term vicinity of the deuteron and another nucleus (**D** and $^{\mathbf{m}}\mathbf{A}$, where **D** - deuteron, and $^{\mathbf{m}}\mathbf{A}$ – nucleus of another element (**M>3**)) provides conditions for transfer of the neutron from **D** to $^{\mathbf{m}}\mathbf{A}$ that results in formation of **p** and $^{\mathbf{m+1}}\mathbf{A}$.

Let us consider in detail the occurrence of such a process in solid body (state).

The interaction of pairs of ions (**D**+**D**) and (**D**+**T**), occurring via resonance transfer of the neutron from one deuteron to another, results in formation of proton ($^1\mathbf{p}$) and tritium nucleus ($^3\mathbf{T}$) [4]:

$$^2\mathbf{D} + {}^2\mathbf{D} = {}^3\mathbf{T} + {}^1\mathbf{p} \qquad \textbf{(1)}$$

or from the deuteron to tritium results in formation of $^1\mathbf{p}$ and helium nucleus ($^4\mathbf{He}$) [6]:

$$^2\mathbf{D} + {}^3\mathbf{T} = {}^4\mathbf{H} + {}^1\mathbf{p} \rightarrow {}^4\mathbf{He} + {}^1\mathbf{p} + \mathbf{e}^- \qquad \textbf{(2)}$$

Note that already in 1990 Dr.J. Schwinger in his presentation on the First Annual Conference on Cold Fusion made a conclusion that the root-mean-square shift of the bi-nuclear deuteron system ($\mathbf{D_2}$) from the equilibrium state by 25% increases the rate of tritium formation by a factor of 10^7 [14]. However, at that time this fact did not attract due attention.

Let us consider the operation of this mechanism as applied to the transmutation of heavy elements. Note that the conditions of fusion occurrence identified in [4, 6] should remain in force. In particular, firstly, it occurs only in a fine layer near the sample surface and, secondly, the state of the system should be non-equilibrium to provide the motive force of the process.

It has been noted [4] that in the ideal crystal lattice of metallic matrix deuterons move one by one. As for quasi-ion $^2\mathbf{D_2}^+$ and ion ($\mathbf{DA}^+$) they can be generated only in defects of crystal structure. Moreover, they can move only along long range defects and for occurrence of fusion the size of defects in cross section should be optimal. When their size is small the movement of ions is retarded and in the case of their large size the action of crystal lattice on the moving system becomes weaker. As $\mathbf{DA}^+$ moves along the defect with an optimal size, vibrations are initiated in the ion and at definite resonance frequency the neutron from the deuteron starts to undergo the effect of nuclear forces from nucleus $^{\mathbf{m}}\mathbf{A}$. As a result, new nucleus $^{\mathbf{m+1}}\mathbf{A}$ are formed:

$$^2\mathbf{D} + {}^{\mathbf{m}}\mathbf{A} = {}^1\mathbf{p} + {}^{\mathbf{m+1}}\mathbf{A} \qquad \textbf{(3)}.$$

The mass of $^{\mathbf{m}}\mathbf{A}$ is larger than $^2\mathbf{D}$, especially for heavy elements and the rate of movement of ion $\mathbf{DA}^+$ is less than that of $^2\mathbf{D_2}^+$. Since the concentration of deuterons in metal is always higher than that of impurities and the rate of diffusion of **D** is higher than **A**, then while moving along the defect of crystal lattice the ^{m+1}A comes into successive contact with other deuterons and the heavy nucleus absorbs several neutrons:

$$^2\mathbf{D} + {}^{\mathbf{m+1}}\mathbf{A} = {}^1\mathbf{p} + {}^{\mathbf{m+2}}\mathbf{A} \qquad \textbf{(4)}$$

and so on.

Such a mechanism of nuclear fusion is possible due to exciting vibrations in the system $\mathbf{DA}^+$ when it moves in the variable field of the crystal lattice. However, in each

definite case the probability of nuclear fusion depends on a number of factors, namely, a constant of $\mathbf{DA}^+$ stability, a structure of metal surface layer, an energy and a structure of initial and generating nuclei as well as other parameters.

If we consider the energy of reaction (3) for interaction of the deuteron and isotope $^{137}\mathbf{Ba}$ [9] which was used by Ya. Iwamura [9]) using the data on mass defects from [15] we obtain that this reaction results in the excess of fusion energy ΔE=6,4 Mev. This energy is distributed between products of nuclear fusion but since the difference between their masses is much essential almost all this energy is taken by proton. Unlike the dissolved hydrogen, as mentioned above, the high energetic proton can react with surrounding nuclei itself leading to further nuclear fusion.

Theoretically reactions (3, 4) and parallel reactions with high energetic protons are possible. However, only multiple experiments can confirm their occurrence.

Reasoning from the mechanism of occurrence of low energetic reactions due to transfer of neutron from deuteron to another nucleus from exciting vibrations of the system of these nuclei when it moves along defects of crystal structure in the variable field of the crystal lattice one can explain the fact of non-reproductivity of experiments on cold nuclear fusion. It is well known that due to dissolution of hydrogen isotopes the constant of metal crystal lattice increases that initiates a growth of internal stresses [16]. These stresses are responsible for deformation of the metallic matrix and formation of crystal structure defects (dislocations, vacancies, etc.). Defects interact with interstitial impurities, in particular, dissolved hydrogen isotopes as in our case. So at dissolution of deuterium deuterons being in metal undergo a process of self-organization and in some cases one can even success in detecting products of cold nuclear fusion and thermal effects.

The paper [3] on deformation of titanium alloy samples with deuterium has shown that high-frequency electromagnetic radiation within the radio wave range and tritium concentration excess can be obtained only for samples with gross coarse-grained structure, at the concentration of deuterium CD = 11-13 at. % and the temperature $T=710^0$ C. Surely, each concrete experiment requires specified structure of the metal to be used but for obtaining the reproducible results the structure should be pre-processed.

Reference

1. F. Pannet, K. Peters Ber. Dtsch. Chemisch. Ges., 1926, Bd. 11, Abt. B.S. pp. 2039-2048.
2. Fleischmann M., Pons S. J.Electroanal, 1989,v.261,p.301.
3. Afonichev D.D., Murzinova M.A. Indicator of the process of cold fusion., Int. J. Hydrogen Energy. 2003, V 28, No 9 pp. 1005-1010.
4. D.D. Afonichev, Mechanism of cold fusion via tritium channel, Int. J. Hydrogen Energy 2006, V 31, No 4, pp 551-553.
5. G. Russ, Reproducible Solid-State Nuclear Fusion: Experimental Evidence, Theoretical Notions, and Possibilities for Commercial Development., Theory of Condensed Matter Group Special Seminar, Cambridge, October 21st., 2005.
6. D.D. Afonichev, Mechanism of ^{4}He Formation Under Low Energy Nucleus Reactions in Solid State. European Physical Journal (In press.)
7. A.B. Karabut, Ya.R. Kucherov and I.B. Savvatimova, *Phys. Lett.* 1992, *A* **170**, 265.
8. R. Kopecek and J. Dash, *J. New Ener*. 1996, **1**, 46.
9. Y. Iwamura, T. Itoh, M. Sakano, et al., Nuclear transmutation induced by deuterium permeation through the Pd complexes detected by surface and bulk analysis methods., ICCF-11, Marseilles, 2004.

10. D.R.Rolison, W.E. O'Grady, R.J. Doyle, Jr., and P.P. Trzaskoma Anomalies in the Surface Analysis of Deuterated Palladium, the First Annual Conference on Cold Fusion. 1990.
11. D. D. Afonichev, Ascending Diffusion or Transmutation, ICCF10, Boston, 2003.
12. Physical Encyclopaedia, //Ed. Prohorov A.M., M., Sovetskaya encyclopedia, 1983, p. 915.
13. G.E. Brown, A.D. Jackson, The Nucleon- Nucleon Interaction, North-Holland Publishing Company, Amsterdam·Oxford, American Elsevier Publishing Company, Inc. – New York, 1976.
14. J. Schwinger Nuclear Energy in an Atomic Lattice, the First Annual Conference on Cold Fusion. 1990.
15. G. Audi, A.H. Wapstra, Nuclear Physics A595, 1995, pp. 409-480.
16. U. Zwicker, Titan und Titanlegierungen, Shringer-Verlag, Berlin-Heidenberg-New York, 1974.

CONDENSED MATTER NUCLEAR EFFECTS UNDER PLATONIC SYMMETRY *

Akito Takahashi†

Osaka University, professor emeritus, Osaka, 565-0804 Japan
High Scientific Research Laboratory, Tsu, Mie, 514-0033 Japan

Norio Yabuuchi*

High Scientific Research Laboratory
Tsu, Mie, 514-0033 Japan

Transient Bose-type condensations of deuteron cluster in near surface lattice or on surface trapping points are modeled as TSC (Tetrahedral Symmetric Condensate) or OSC (Octahedral Symmetric Condensate) with bosonized pseudo-particle states of symmetrically arranged electrons alternatively to symmetrically arranged deuterons, which cause very enhanced 4d or 6d multi-body fusion reactions to produce ^{4}He main products. Multi-particle arrangements by Platonic Symmetry can play intrinsic roles there in four steps: 1) molecular state arrangement, 2) Coulomb barrier penetration and 3) strong interaction at initial state, and 4) final state break-up. Philosophical background of Platonic Symmetry (PS) is first mentioned. Substantiated models for the 4 steps are shown with some numerical results. The molecular dynamics treatment of TSC motion by Langevin equation is briefly introduced.

1 Introduction

1.1. Cluster Fusion Model

We have developed cluster deuteron fusion model as a possible underlying mechanism of condensed matter nuclear effects[1-9]. The formation of transient Bose condensate e.g. TSC (Tetrahedral Symmetric Condensate) of alternative deuteron-electron arrangement of 4 deuterons and 4 'electron-balls' under Platonic polyhedral symmetry is the key idea[7]. Quantification with mathematical formulas was elaborated based on EQPET (Electronic Quasi-Particle Expansion Theory)[1-7] which supposed the *bosonization* of electrons in the TSC cluster. Hence two aspects are of essential philosophical concepts; the *Platonic symmetry* for achieving system-charge-neutrality and local energy minimum state in condensed matter and the *electrons bosonization*.
TSC can realize much closer inter-nuclear d-d distance, equivalently much larger quantum mechanical tunneling probability through Coulomb barrier (screened adiabatic Coulomb potential) and predominantly strong multi-body (especially 4D) fusion reaction of strong Platonic nuclear interaction, which leads to clean He ash and mass-8-charge-4 shifted cold transmutation of host or added metal nucleus (or M + 4p/TSC reactions).

* This paper is submittal to Proceedings of ICCF13.

1.2. The Idea of Platonic Polyhedral Arrangement

The idea of Platonic polyhedral arrangement for the state of substance in nature was seen already in philosophies of Greek scholars Plato and Aristotle. The idea was transferred to modern philosophy in physics, as Werner Heisenberg discussed in his book *Physics and Philosophy*[10]. Especially, in Chapter 9 of the book, he argued on the concept of "form".
What makes matter to be real existence is "form". Heisenberg postulated a force that forms elementary particles, borrowing from Platonic and Aristotelian philosophy to name this force a "form"; form theory is developed in his *Physics and Philosophy: The Revolution in Modern Science*. Carl Friedrich von Weizsäcker[18] similarly applied the concept of 'forms' to molecules, atoms, and elementary particles. The Platonic symmetry (polyhedral arrangement) can thus be regarded as a seed of ordering process (or self-organization) in molecules, proteins, and bio-medical systems also. Norio Yabuuchi[11, 17] discussed about the "form" with Platonic arrangement in physics. For example, bookcase is made of woods. Woods are matter (or material). "Form" makes woods to be a bookcase[18]. For other example in our case, TSC (tetrahedral symmetric condensate) is made of 4 deuterons (or protons) and 4 electrons. Deuterons (or protons) and electrons are matter (materials), and "form" makes 4 deuterons (or protons) and 4 electrons to be a TSC. The Platonic symmetry plays an intrinsic role in the "form" of TSC.
When theorizing about condensate deuterium fusion reaction, employing a hierarchical model that posits transition to structures having Platonic symmetry (regular polyhedra) enables theoretical development by the same analogy. Strong nuclear interaction in the case of a regular-tetrahedral condensate, and a model of transition between Platonic-structure arrangements are able to be discussed[8]. The hierarchy stands from microscopic nuclear strong interaction to rather macroscopic many particle interactions in condensed matter and moreover to very large molecules as DNA. We discuss some of these hierarchical strata in the following.

2. Platonic Symmetry in Molecules and Lattices

Examples are seen in molecules like, SiO_2 compounds, yellow phosphor crystal, methane (CH_4), diamond, ice, and so on. Four hydrogen atoms of methane take four vertexes of regular tetrahedron and surrounding the central carbon atom at the center-of-mass. H_2O molecules combine to make tetrahedral arrangement when ice is forming. Alum is of octahedral crystal. Feature of polyhedral arrangements is shown in Fig.1, for regular tetrahedron and regular octahedron.

Other examples are seen in lattice-atom arrangements, like PdDx. This is similar to the NaCl crystal lattice. Deuteron (or proton) occupies octahedral site in Pd-lattice. Four neighboring deuterons in PdD lattice make a tetrahedral arrangement with the center-of-mass point at the central tetrahedral site. When one Pd-atom point becomes vacant, 6 neighboring deuterons make an octahedral arrangement (See **Fig.2**).

***Fig.1**: Feature of Platonic symmetrical arrangement*

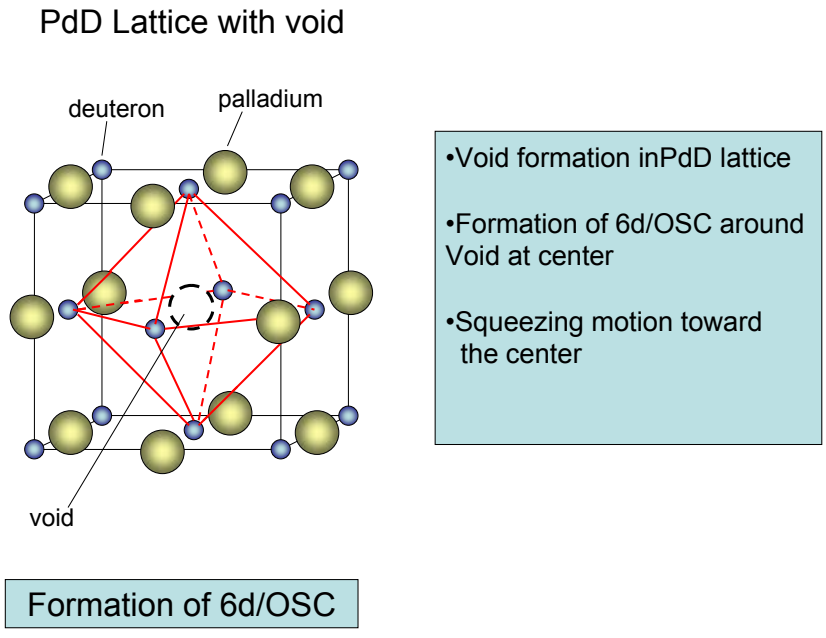

***Fig.2:** PdD lattice and formation of octahedral arrangement for 6 deuterons at neighboring octahedral sites around central defect-point (void)*

3. Bosonization of Fermions by Platonic Symmetry

3.1 Cooper pair e*(2,2) by electron pair in dynamic motion in condensed matter

The formation of transient Cooper pair e*(2, 2) of two electrons in condensed matter containing deuterons may play a fundamental role in the condensed matter nuclear effects. Formation of dde*(2, 2) state (transient Bose condensation; TBC) by beam-target reaction was theorized[5)] to estimate the screening energy (360 eV) for d-d Coulombic interaction of beam-target experiments, to result in good agreements with experimental values (310-320 eV) for PdDx target with incident deuteron beam by Kasagi[12)] and Huke[13)] experiments. The 3D fusion experiment by Takahashi et al[14)] suggested that the life time of dde*(2,2) state to be on the order of 0.1 ms, according to Takahashi's fusion rate model[5)]. We regard that the *bosonization* of electron-pair is one of necessary conditions for realizing Platonic symmetrical arrangements in many deuteron systems (D-cluster) in condensed matter.

3.2 Quadruplet e*(4,4) state by tetrahedral arrangement of 4 electrons in 4d/TSC configuration

We have extended the EQPET/TSC models[1-9)] for theorizing deuteron-cluster (D-cluster) fusion processes in palladium-deuterium systems. The dynamic formation of TSC (Tetrahedral Symmetric Condensate) is assumed for three cases a), b) and c) as;

a) One is the TSC formation in regular PdD lattice in D-flow from O-site to T-site by D-lattice-phonon excitation. b) The second model is the TSC formation by the collision-combination process of trapped D_2 molecule, being lost freedom of rotation, and incoming D_2 molecule on surface of metal-D systems. c) The third idea is the random formation of TSC by combination of two bosonized molecules of dde*(2,2) in the near surface of Fermi-level gap of PdDx and CaO(or other); generation of Cooper pair near on Fermi surface may play key role in this case (our paper to Proc. JCF7). The case a) is the formation of TSC by four independent Ds under the Platonic symmetry of constraint in surrounding lattice conditions. The case b) is the formation of TSC by two D_2 molecules under constraint on surface conditions. The case c) is the formation of condensed (smaller size) D_2 molecule by bosonized electrons, e*(2,2), then to form TSC by combination of two condensed D_2 molecules. Condensation (squeezing motion) of TSC starts after the TSC(t=0) formations for the cases a) and b), while the further condensation occurs after the combination of two condensed molecules in the case c).

The feature of TSC is illustrated as the orthogonal coupling of two regular tetrahedrons of four deuterons and four electrons as shown in **Fig.3**.

We have used a semi-classical model for TSC dynamic squeezing motion[1-9)] as illustrated in **Fig.4**. Here we assumed that the Platonic symmetrical condition is kept in linear Newtonian motion for all particles. To keep the Platonic arrangement in dynamic motion, strong central condensation force is required. A primitive semi-classical analysis on the TSC condensation force was made previously[15)]. Once the initial condition for TSC (t=0) state is formed under constraints of condensed matter, strong condensation force works on squeezing motion of TSC which finally gets into the TSC-minimum state with about 10 fm diameter as charge-neutral very small entity. At the TSC-minimum state, short range (few fm) strong interaction works to make simultaneous 4D cluster fusion. Then the intermediate compound nucleus ^{8}Be* by 4D fusion breaks up to two α-particles.

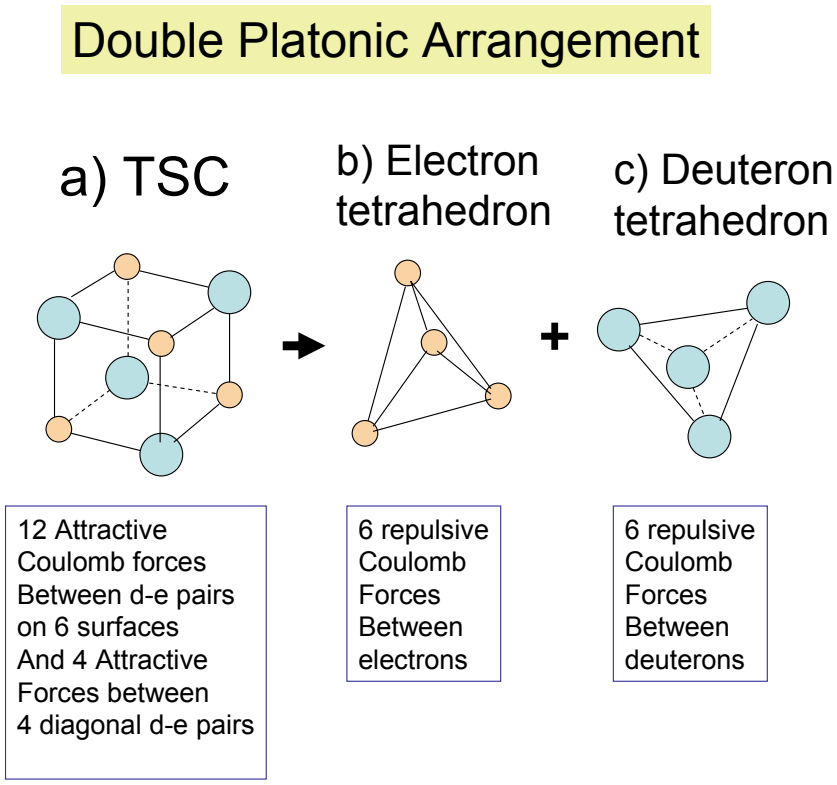

Fig.3: *Tetrahedral Symmetric Condensate (TSC), 4 electrons make quadruplet e*(4,4) state*

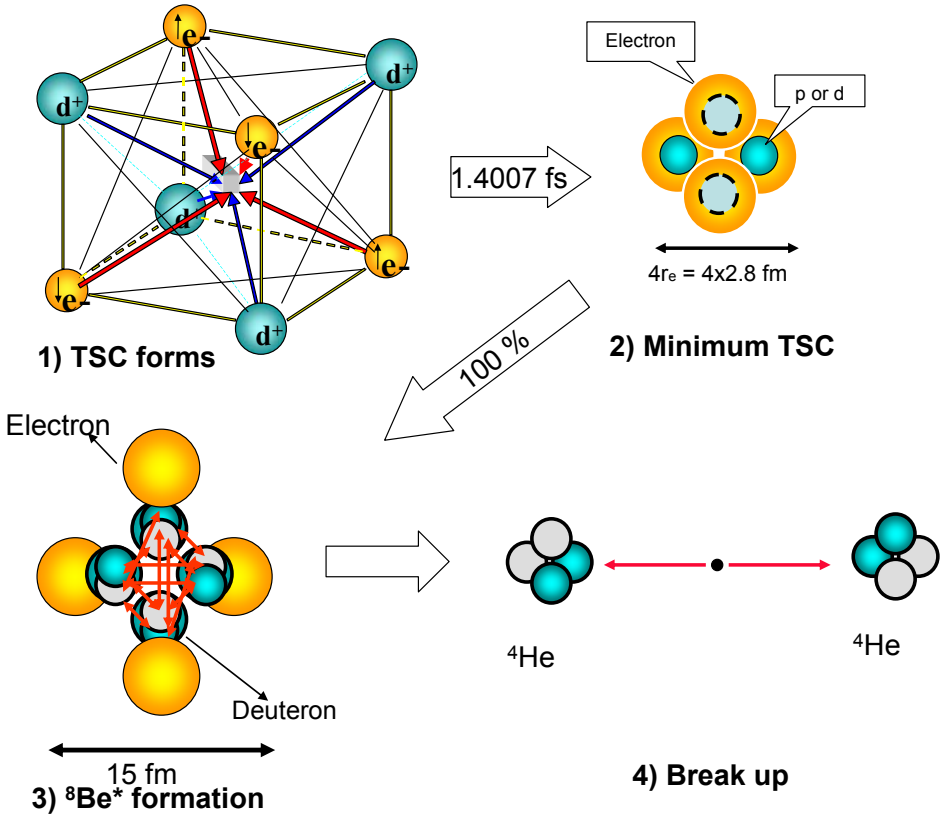

Fig.4*: Illustration of 4D/TSC squeezing motion and 4D cluster fusion*

4. Molecular Dynamics of TSC Motion by Langevin Equation

4.1 Langevin Equation and simple cases

More exact treatment of TSC squeezing motion under the "averaged" Platonic symmetry of 8 particles (4 deuterons plus 4 electrons) can be investigated using the following Langevin equation (non-linear stochastic differential equation).

$$m_d \frac{d^2 R_{de}(t)}{dt^2} = -\frac{8.38}{R_{de}{}^2} - \varsigma \frac{dR_{de}(t)}{dt} + f(t) \qquad (1)$$

Here $R_{de}(t)$ is the distance between deuteron and nearest center of "electron ball" of TSC. The inter-nuclear distance between two deuterons is given as $R_{dd} = \sqrt{2} R_{de}$. And m_d is the deuteron mass. The first term of right hand side of Eq.(1) is the condensation force (average Coulombic attraction) of TSC given in Reference-15. The second term of right side is the friction term which reflects in the balancing force of TSC system by diluted spread of quantum mechanical electron clouds around 4 centers of "electron balls". The friction term is very large due to the Pauli repulsion (fermion nature) of electrons, unless the *bosonization* of electrons is realized. Therefore, the *bosonization of electrons* is essential to the TSC squeezing motion. The third term of right side is the random fluctuation term.

To solve the Langevin equation by developing appropriate physics models for the second and third terms (friction and random fluctuation terms) is of our future study.

When the condensation force is adiabatically approximated with constant acceleration ($F = -m_d \alpha$) by the adiabatically bosonized dde* approximation (EQPET)[6] and we assume the zero friction, the expected value of deuteron-electron position is given as,

$$\langle R_{de}(t) \rangle = R_0 - v_0 t - \frac{1}{2} \alpha t^2 \qquad (2)$$

, because the ensemble averaging of f(t) is zero, i.e., $\langle f(t) \rangle = 0$ and where

$$\alpha = \frac{8.38}{m_d (R_{de*(m,Z)})^2} \qquad (3)$$

with $R_{de*(2,2)} = 13.2 pm$ and $R_{de*(4,4)} = 3.3 pm$ for adiabatic time intervals[6].in the time-dependent EQPET analysis. The initial velocity at t=0 is v_0.

This is the simplest approximation we used previously[15, 6] (where the third term of Eq.(2) was further neglected). For e*(2,2), using the $E=mc^2$ relation, we obtain $\alpha = 2.3x10^3$ (pm/(fs)^2). Using Eq.(2) with this condition, TSC gets to the TSC-min (about 10 fm diameter) in 0.1 fs, which is much shorter time than about 60 fs we estimated previously[6].

To treat the squeezing motion in more rigorous way, we need to solve the Langevin equation Eq.(1) by defining the balancing force and random fluctuation. Evaluation of expected value $\langle R_{de}(t) \rangle$ and variance $\langle R_{de}{}^2(t) \rangle - \langle R_{de}(t) \rangle^2$ will give the first order averaged information on the TSC squeezing motion. When the variance is not large in the adiabatic approximation with

the bosonized-electrons states, we will have a solution in a form of expected value Eq.(2) plus perturbation term q(t) as,

$$\langle R_{de}(t)\rangle = R_0 - v_0 t - \frac{1}{2}\alpha t^2 + q(t) \tag{4}$$

By substituting,

$$R_{de}(t) = R_0 - r(t) \tag{5}$$

The Langevin equation is converted to the equation for velocity, $v(t) = \frac{dr(t)}{dt}$, as;

$$\frac{dv(t)}{dt} = \frac{8.38}{m_d (R_0 - r(t))^2} - \frac{\varsigma v(t)}{m_d} - \frac{f(t)}{m_d} \tag{6}$$

Taking ensemble average of Eq.(6), we obtain, using $\langle f(t)\rangle = 0$,

$$\frac{d\langle v(t)\rangle}{dt} = \frac{8.38}{m_d}\left\langle \frac{1}{(R_0 - r(t))^2} \right\rangle - \frac{\varsigma}{m_d}\langle v(t)\rangle \tag{7}$$

We need to solve this non-linear equation by evaluating the effect of friction term and to evaluate variance by the quantum mechanical random fluctuation term f(t).
As the first order approximation by using the adiabatic bosonized model (EQPET)[6], assuming constant acceleration, we obtain the following approximate solution,

$$\langle v(t)\rangle = \frac{m_d \alpha}{\varsigma}[1 - \exp(-\frac{\varsigma}{m_d} t)] \tag{8}$$

For the case of small friction, $\frac{\varsigma}{m_d} t << 1$, we get $\langle v(t)\rangle = \alpha t$ as linear Newtonian motion.

If the friction is large, velocity approaches to constant, $\langle v(\infty)\rangle = \frac{m_d \alpha}{\varsigma}$, which is analogous to the case we used constant velocity for the time-dependent EQPET analysis of TSC[6]. This is also analogous to the falling motion of rain drop in air.
The ensemble average $\langle G\rangle_{ensemble}$ can be regarded as the quantum mechanical average $\langle \Psi | G | \Psi \rangle$, the expectation value, for an observable G, to be related to the quantum mechanical treatment, by defining f(t) by using the Gaussian wave function.

4.2 Models of TSC Molecular Dynamics Motion

The friction of outer-spread electron clouds from 4 centers of electron-balls can be regarded smaller than the balancing forces of D_2 molecule potential $V_s(1,1)$ and EQPET molecules dde* potentials $V_s(2,2)$ and $V_s(4,4)$, which are given in our previous papers[1-7].

The balancing forces (positive, namely repulsive) of these molecular state potentials are given by,

$$F_{balance} = -\frac{\partial V_s(m,Z)}{\partial R_{dd}} \tag{9}$$

[***Model A***]: If we replace the friction term with the balancing force Eq.(8), the Langevin equation becomes,

$$m_d \frac{d^2 R_{de}(t)}{dt^2} = -\frac{8.38}{R_{de}{}^2} - \frac{\partial V_s(m,Z)}{\partial R_{de}} + f(t) \tag{10}$$

where $R_{dd} = \sqrt{2} R_{de}$. Here we modeled TSC as an orthogonal coupling of two D_2-type molecules, and condensing force is given per one D_2-type condensed molecule of TSC.
Numerical values were calculated for the first term (TSC condensation force) and the second term (balancing force by molecular potential) of right side of Eq.(10), as graph is given in **Fig.5**.
We see that central condensation force is always much greater than balancing forces, so that TSC can condense until the TSC-minimum state is reached. Since the friction term of TSC motion will be smaller than these balancing forces, we can conclude that the complete central condensation motion of TSC is realistic.

[***Model B***] Moreover, for estimating the maximum possible friction, we need to consider that forces to 6 d-d edges of deuteron tetrahedron are balanced with total TSC condensation Coulombic force plus balancing forces of 6 dede (D_2 molecule-like) faces of TSC cube. In this case, the Langevin equation for a TSC molecular dynamics becomes,

$$6m_d \frac{d^2 R_{dd}}{dt^2} = -\frac{8.38\sqrt{2}}{R_{dd}{}^2} - 6\frac{\partial V_s(R_{dd};m,Z)}{\partial R_{dd}} + f(t) \tag{11}$$

Here left side term is given as $6(m_d \frac{d^2(R_{dd}/2)}{dt^2} + m_d \frac{d^2(R_{dd}/2)}{dt^2})$ for 6 faces with dede-type molecular-like d-d pairs condensing to the mid point of d-d distance, respectively. In this case, sum of the second and third terms of right side may become positive for small Rdd. Therefore, deceleration (slowing down) of TSC condensation will happen in the range of small Rdd before reaching at TSC-minimum state. We need more precise numerical analysis for this case, since it is interesting if the deceleration in the last stage will make “soft landing” (with small velocity) to TSC-minimum state, which would then have elongated life time.

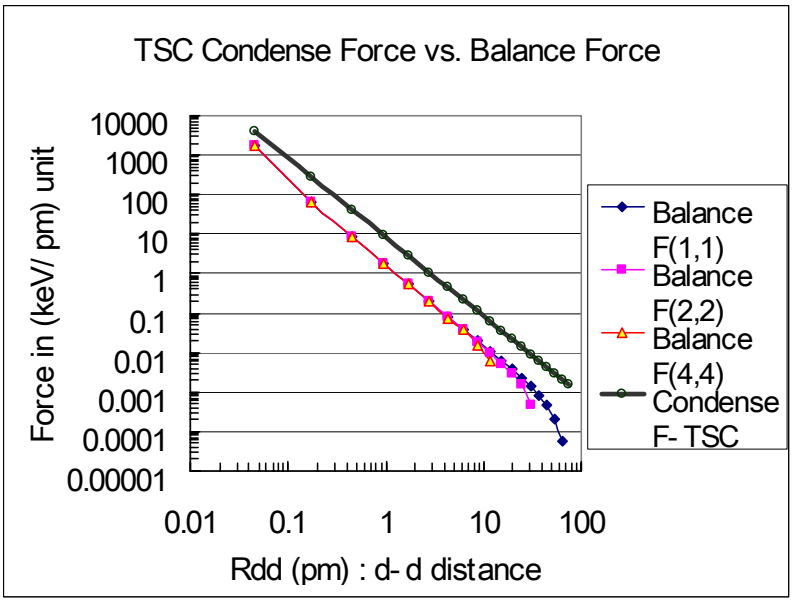

(Condense F-TSC) = $-8.38/R_{dd}^2$; negative values

(Balance F)= $-dV_s/dR$; positive values

Fig.5: *Coulombic condensation force (Condense F-TSC) and balancing force of molecular binding (Balance F) for TSC condensation motion. Central condensation force is always greater than balancing forces to realize TSC condensation into TSC-minimum state.*

[***Step 1***]: If f(t) = 0, Equations (10) and (11) which are nonlinear with complicated functions of R_{dd} can be solved numerically using the coupled time-step method[19] for velocity and R_{dd} with given initial velocity v_0 and position R(0); this is our future work to carry out so as to know expected values of final velocity and size of TSC-minimum. Formulas of Verlet's method[19] for programming a computer code (TSC Langevin Step1) are:

$$G(r,t) = \frac{1.975}{m_d[R(0)-r(t)]^2} + \frac{1}{m_d}\frac{\partial V_s(R_{dd};m,Z)}{\partial R_{dd}} \tag{12}$$

$$R_{dd}(t) = R(0) - r(t) \tag{13}$$

$$\frac{d^2r(t)}{dt^2} = G(r,t) \tag{14}$$

$$r(t+\Delta t) = r(t) + v(t)\Delta(t) + \frac{1}{2}G(r,t)(\Delta t)^2 \tag{15}$$

$$v(t+\Delta t) = v(t) + \frac{\Delta t}{2}[G(r,t+\Delta t) + G(r,t)] \tag{16}$$

We will be able to show numerical results in detail in the forthcoming reports. A preliminary result is shown in **Fig.6** using dde*(2,2) potential and plotted in reversed time scale.

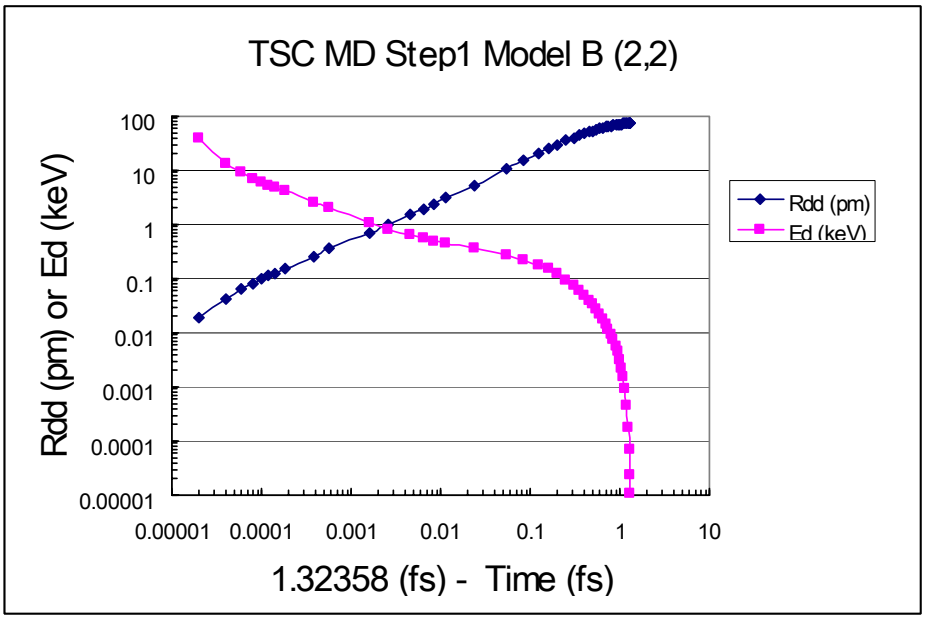

Fig.6: *Molecular dynamics calculation of TSC condensation motion by Model-B; Rapid acceleration happened within $2x10^{-20}$ s (0.00002 fs) for R_{dd} < 50 fm (0.05 pm) to reach final deuteron relative kinetic energy E_d=39 keV at R_{dd}=19 fm, in this case, finishing condensation in 1.32358 fs. Deuteron with relative deuteron kinetic energy of 39keV at R_{dd}=19 fm is confined with adiabatic trapping potential of TSC system Coulomb energy -11.85/0.019+6xV_s(2,2) = -177.6 keV.*

Table-1: Barrier Factors for d-d pair of 4d/TSC under condensation, as a function of d-d distance R_{dd}

Rdd=Rgs (pm)	P2d ; 2D Barrier Factor	P4d; 4D Barrier Factor
0.0206 (TSC-min)	4.44E-2	1.98E-3
0.0412	1.06E-2	1.12E-4
0.103	1.43E-3	2.05E-6
0.206	3.35E-5	1.12E-9
0.412	9.40E-7	2.16E-13
0.805 (μdd)	1.00E-9	1.00E-18
1.03	9.69E-11	9.40E-21
2.06	6.89E-15	4.75E-29
4.12	9.38E-21	8.79E-41
10.3	2.16E-32	4.67E-64
21.8 (dde*(2,2)	1.30E-46	1.69E-92
74.1 (D2 molecule)	1.00E-85	1.00E-170

We need further to model the random quantum mechanical fluctuation term f(t) to analyze variances of TSC motion by the Langevin equations. Source of quantum mechanical random fluctuation force can be formulated as fluctuation (distortion from Platonic symmetry) of main TSC condensation force by the fluctuation of d-d distance with approximated Gaussian

squared wave function for deuteron at randomly generated position. We need to develop a computer simulation code (Step-2).
Barrier factors of d-d pair for fusion rate estimation under TSC condensation are given in **Table-1** as a function of Rdd, which were calculated by HWEQPET code in Step-2 and the detail will be reported elsewhere. Using these barrier factors to fusion rate formula of Fermi's 1st golden rule[7],

$$\lambda_{nd} = \frac{2}{\hbar}\langle W \rangle P_{nd}(r_0) = 3.04\times 10^{21} P_{nd}(r_0)\langle W \rangle \qquad (17)$$

, we obtained fusion rates for assumed steady molecules as given in **Table-2**. By molecular dynamics calculation given in Fig.6, TSC-min state exists within about $\Delta t=2x10^{-20}$ s, within which 4D/TSC decays with $\exp(-\lambda 4dx\Delta t)=\exp(-7.4)=0.0006$; namely 4D fusion happens almost 100% by the end of condensation. *Therefore 4D fusion rate (1/s) in condensed matter becomes equal to TSC production rate (1/s).* This is very much large 4D fusion rate per 4D/TSC, while 2D fusion rate is very small as 3.2E-27 (1/s) per dde*(2,2) by Cooper pair molecule generation.

Table-2: Fusion rates of assumed steady molecules, compared with muonic(μ)-dd values

Molecule	Rdd=Rgs (pm)	Pnd(r_0) ;Barrier-Factor	<W> (MeV)	λ2d (f/s)	λ4d (f/s)
D_2	74.1	1.0E-85	0.008	2.4E-66	
dde*(2,2)	21.8	1.3E-46	0.008	3.2E-27	
μdd	0.805	1.0E-9	0.008	2.4E+10	
4D/TSC-min	0.021	1.9E-3	62		3.7E+20

Due to the limitation of space here, the detail of ***Step2*** formulas and calculations will be given[20] in the forthcoming CMNS Workshop at Catania, October 2007. Brief summary is as follows; Gaussian wave functions for d-d pairs and their ground state energies are first obtained by variational method, for D_2 and EQPET molecules. Then same sigma-value (0.3 $R_{dd}(t)$ was obtained) is used for time-dependent Gaussian wave functions of d-d pairs of TSC system to calculate the ensemble-averaged <f(t)> for changes of Coulomb energy and force of distorted TSC system from the ideal Platonic symmetry. The form of <f(t)> becomes C/R_{dd}^2 type deceleration force as positive bias to main condensation force, to be about 15 % bias. Molecular dynamics calculation by the Verlet time-step method was then done to obtain mean relative final-stage d-d kinetic energy 13.68 keV with -130.4 keV deep trapping TSC potential at R_{dd}-minimum = 25 fm and time-to-TSC-minimum =1.4007 fs. Mean kinetic energy of electron of a "dede" EQPET molecule of TSC system was estimated as 57.6 keV at R_{dd} =25 fm. These time-dependent potential can be also approximated by $V_s(R_{dd};m,2)$ potentials with the empirical relation of $m=4.36x10^4/R_{dd}$, (R_{dd} in fm unit) and 2D and 4D fusion rates were calculated using these $V_s(R_{dd};m,2)$ potentials. Here e*(m,2) is heavy mass Cooper pair with m from 2 to 2000.

5. Platonic Symmetry in D-Cluster Fusion (Strong Interaction)

5.1 Average feature of nucleons

No constantly neutron or proton state in nucleus exists. Strong interaction (sticking force by π^+ and π^- exchange; Yukawa-Wigner force) alternatively change nucleon state <nuc> from neutron state <n> to proton state <p> - or reversed – state very fast.

Average feature of nucleon <nuc> is therefore,

$$\langle nuc \rangle = \frac{N\langle n \rangle + Z\langle p \rangle}{A} \tag{18}$$

Here N is the total number of neutron state and Z is the total number of proton state in a nucleus. If N=Z, we have ideal exchange (if neglecting Coulomb repulsion between <p> states),

$$\langle nuc \rangle_{N=Z} = \frac{\langle n \rangle + \langle p \rangle}{2} \tag{19}$$

This is a kind of "Bosonized State of nucleon", since apparent total spin = 0.

^{4}He nucleus can be regarded as orthogonal coupling (quadruplet of nucleons) of two bosonized pairs to form regular tetrahedron of 4 <nuc>s, namely Platonic symmetry arrangement for alpha-cluster.

The above image is the feature of individual nucleon in mass number A nucleus, and reflects how the Yukawa-Wigner force works in confining nucleons in a nucleus.

5.2 2D fusion break-up channels and PS arrangements

The intermediate compound nucleus ^{4}He*(Ex = 23.8MeV) has three out-going channels with [n]/[t]/[^{4}He] = 0.5/0.5/10^{-7} branching ratios[16]. The highly excited state of ^{4}He*(23.8MeV) seems not keeping the tetrahedral arrangement (α-cluster of 4 nucleons). The feature of the excited state and break-ups to [n]- and [t]-emission channels is illustrated in **Fig.7**.

The excited state ^{4}He* (23.8MeV) is regarded there as "broken" α-cluster of 4 nucleons, which has a dangling proton-branch or neutron-branch. There happens scission of dangling branch to break up to [p]- or [n]-emission channel with same weight.

5.3 4D fusion break-up by Platonic Symmetry

In the case of ^{8}Be* by 4D cluster fusion, there happens the rearrangement of Platonic configuration from the "cubic"-state to the tandem collective state of two α-cluster of 4 nucleons, ^{8}Be cluster is highly unstable. The feature is illustrated in **Fig.8**.

Similarly, in the case of 6D/OSC (Octahedral Symmetric Condensate), the intermediate compound nucleus ^{12}C* by 6D cluster fusion breaks up with alpha-clusters into three α-clusters of 4 nucleons.

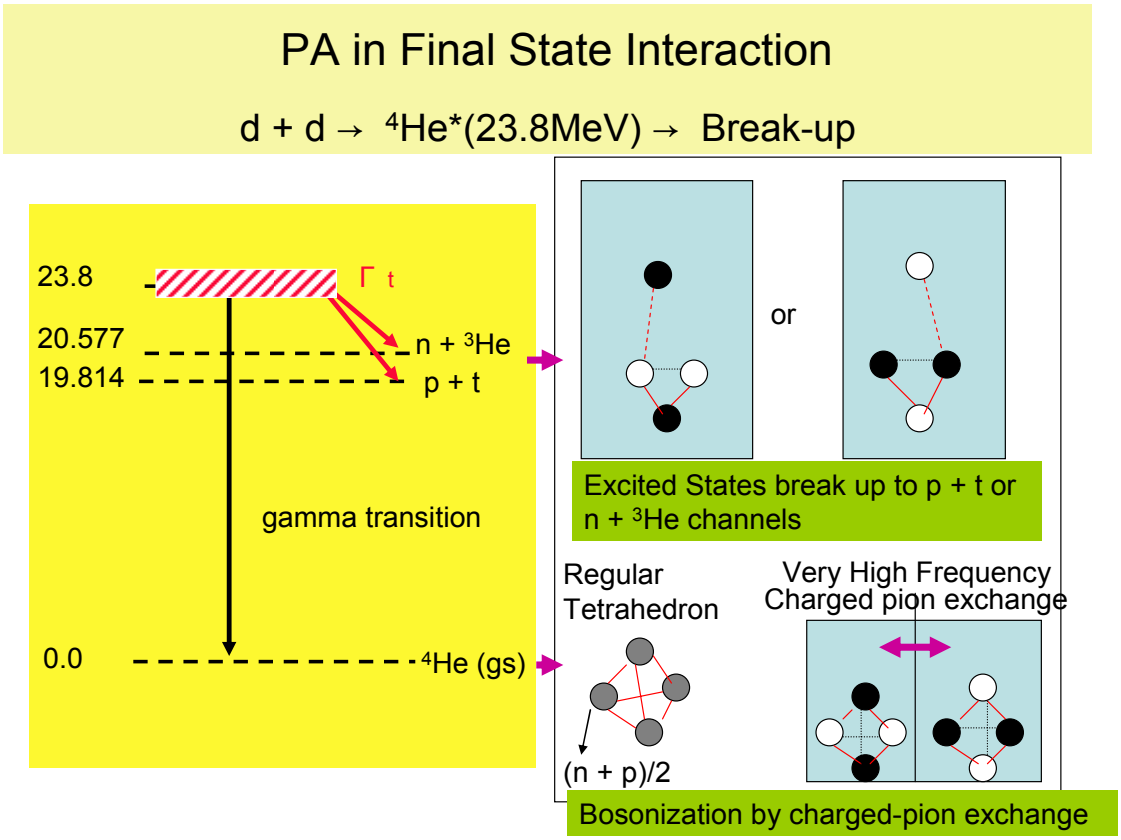

Fig.7: *Distortion of Platonic Arrangement (PA) in the final state interaction of d+d fusion*

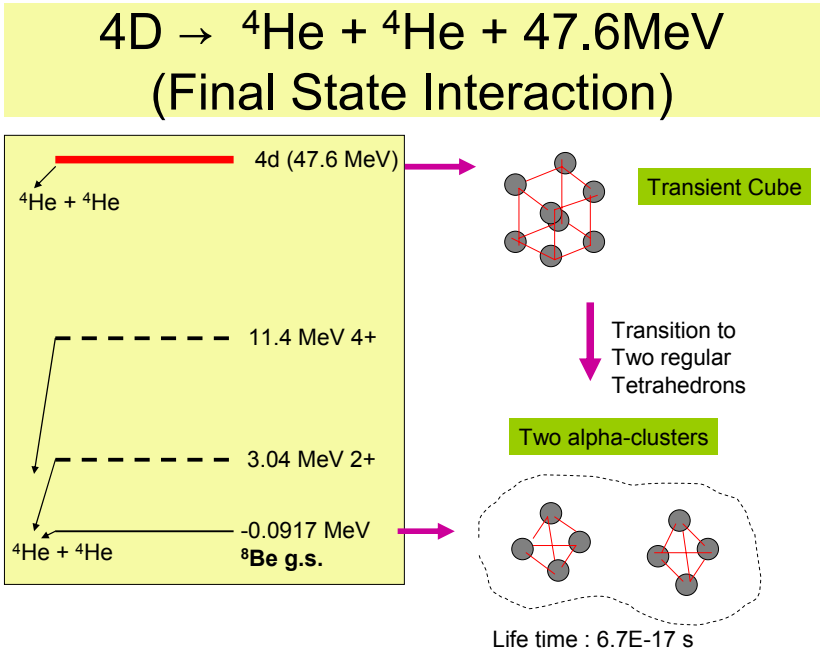

Fig.8*: Rearrangement of Platonic configuration from "cube" to tandem α-cluster, for* $^{8}Be^{*}$ *by 4D cluster fusion (right hand side) and decay channels (left)*

6. Conclusions

1. The Platonic symmetrical arrangement (PA) appears in many-body systems as molecules, and lattices to realize the energy-minimum state of system.
2. PA appears in condensed matter nuclear effects for multi-body Coulombic interactions and nuclear strong interactions.
3. TSC (tetrahedral symmetric condensate) and OSC (octahedral symmetric condensate) are examples for actual states of PA in condensed matter nuclear effects.
4. Dynamic PA is of key for deuteron-cluster fusion in condensed matter.
5. Bosonization of electrons plays a key role for the "form" of TSC (tetrahedral symmetric condensate) and OSC (octahedral symmetric condensate).
6. The philosophical concept "form" is of background "idea", originally categorized by Plato and extended by Heisenberg and Weizsaecker, and is useful for physics of condensed matter nuclear effects.
7. Molecular dynamics of TSC motion by Langevin equations is briefly introduced. It was numerically shown that TSC can condense into the TSC-minimum state (about 10fm size charge-neutral entity) by strong condensation force under Platonic symmetry which is almost always greater than quantum mechanical balancing forces of D_2 molecule and EQPET molecule states.

References

1) A. Takahashi: Mechanism of deuteron cluster fusion by EQPET model, *Condensed Matter Nuclear Science,* Proc. ICCF10, pp.809-818, World Scientific Publ. Co., 2006 (ISBN-891-256-564-7)
2) A. Takahashi: ^{3}He/^{4}He production ratios by tetrahedral symmetric condensation, *Condensed Matter Nuclear Science,* Proc. ICCF11, pp.730-742, World Scientific Publ. Co., 2006 (ISBN-981-256-640-6)
3) A. Takahashi: Deuteron cluster fusion and related nuclear reactions in metal-deuterium/hydrogen systems, *Recent Res. Devel. Physics*, 6(2005)pp.1-28, ISBN: 81-7895-171-1
4) A. Takahashi: Deuteron cluster fusion and ash, Proc. ASTI5 Meeting, see http://www.iscmns.org/ ,Asti, Italy, 2004, to be published in *J. Condensed Matter Nuclear Science*, Vol.1, No.1 (2007)
5) A. Takahashi: A theoretical summary of condensed matter nuclear effects, Proc. Siena2005 Workshop, to be published in *J. Condensed Matter Nuclear Science*, Vol.1, No.1 (2007); see also A. Takahashi: Brief Theoretical Summary of Condensed Matter Nuclear Effects, Acta Physica et Chemica, Debrecen, Hungary, Vol.38-39, (2005)341-356
6) A. Takahashi: Time-dependent EQPET analysis of TSC, *Condensed Matter Nuclear Science*, Proc. ICCF12, Yokohama 2005, World Scientific Publ. Co., pp.454-461 (2006) ISBN=981-256-901-4
7) A. Takahashi and N. Yabuuchi: Fusion rates for bosonized condensates, Asti2006 Workshop on Anomalies in Hydrogen/Deuterium Loaded Metals, September 2006, see http://www.iscmns.org/ ASTI, to be published in *J. Condensed Matter Nuclear Science*, Vol.1, No.1 (2007)
8) N. Yabuuchi and A. Takahashi: Proc. JCF7, Kagoshima Japan, April 2006, to be published in http://wwwcf.elc.iwate-u.ac.jp/jcf/
9) A. Takahashi and N. Yabuuchi: Comments on role of CaO layer in Iwamura transmutation, ibid.
10) Werner Heisenberg: *Physics and Philosophy*, Harper & Row, New York, 1958

11) Norio Yabuuchi: *Meta Physics Founded on Atomic Physics*, Toshi-Kogyo Co., 1977
12) J. Kasagi, et al.: *J. Phys. Soc. Jpn*, 71 (2002) 2881-2885
13) A. Huke: PhD Thesis, Technical University of Berlin, 2004
14) A. Takahashi, et al: *Phys. Lett. A*, 255 (1999) 89
15) A. Takahashi, N. Yabuuchi: On Condensation Force of TSC, Proc. Asti06 Workshop, see http://www.iscmns.org/asti06/program.htm , to be published in *J. Condensed Matter Nuclear Science*, Vol.1, No.1 (2007)
16) A. Takahashi, N. Yabuuchi: Deuterons-to-He-4 Channels, this ICCF13 meeting
17) N. Yabuuchi and A. Takahashi: Form of Nuclear Fusion in Solid Crystals, this ICCF13 Meeting
18) C. F. Weizsaecker: *Die Einheit der Natur*, Carl Hanser Verlag, 1971
19) L. Verlet: *Phys. Rev.*, 159 (1967) 98; see also Akira Ueda: *Computer Simulation*, *atomic motion in macroscopic systems,* Chap.2 (in Japanese), Asakura Publ., Tokyo (1996)
20) A. Takahashi, N. Yabuuchi: Study on 4D/TSC condensation motion by non-linear Langevin Equation, submitted to Proc. New Energy Technologies, American Chemical Society, March, 2007, USA (to be published from Oxford Univ. Press)

DEUTERONS-TO-HELIUM-4 CHANNELS*

Akito Takahashi†

Osaka University, professor emeritus, Osaka Japan
High Scientific Research Laboratory, Tsu, Mie, Japan

Norio Yabuuchi

High Scientific Research Laboratory, Tsu, Mie, Japan

Comments and discussions are summarized on possible ^{4}He production channels for two-body and multi-body deuteron-related fusion reactions.
The reason why ^{4}He production channel by two-body d+d fusion can not be major branch is discussed in the view that the idea of reversed kinetic process (namely negative kinetic energy) is hardly realized to go to lower ^{4}He excited state than threshold excited states for n and p emission channels.
Then, the participation of third interaction into d-d strong interaction is generally discussed for going out to ^{4}He production channels. As forces of the third interaction, gravity, weak-interaction, electro-magnetic interaction and strong interaction are briefly compared. Cluster deuteron fusion processes under Platonic symmetrical constraint in condensed matter are lastly discussed. 4D fusion by TSC (Tetrahedral Symmetric Condensate) and its outgoing channels, mainly going out to 2 ^{4}He-particles emission, is briefly discussed.

1. Introduction

Major criteria of theoretically modeling the process of "radiation-less excess heat with ^{4}He ash" as condensed matter nuclear effects (CMNE) are:

A) How can the mutual Coulombic repulsion between deuterons be overcome, so as to reach at significant level of deuteron-related fusion rates?
B) How can ^{4}He generation channel be predominant?
C) How can hard radiations be suppressed?
D) What kinds of environments in/on condensed matter are incubating CMNE?

Many researchers[1-11)] have been concentrated in the criteria A) and D), although controversial efforts were done for the criteria B) and C). This paper focuses on B).

"The major ash of helium-4 by two-body deuteron fusion reaction can not be expected." This comment is very true, as far as we concern about emitted particles in final state

* This work is supported by High Scientific Research Laboratory.

interactions by fusion reactions which are commonly data-based. This means that we need to *invent* some new nuclear process in condensed matter for explaining helium-4 production in correlation with excess heat[1,2]. The authors think that the direct coupling of excited nucleus in final state with lattice (e.g., metal-deuteride system) to transfer nuclear excited energy directly to lattice (vibration) is impossibly difficult as one of authors discussed in Appendix of our Siena05 paper1[1)] and our keynote paper to ICCF12[2)] (see http://www.iscmns.org/iccf12/).

In our 4D cluster fusion model by TSC formation (Criterion D) and condensation which would realize the super-screening condition for Coulombic repulsion (Criterion A), two 23.8MeV alpha-particles are produced in 180 degree opposite directions by the final state interaction of ^{8}Be* (excited state) break-up[1,2)](Criterion B). With known knowledge of ionization and X-ray producing cross sections of 23.8 MeV alpha-particle in e.g. PdDx, production of about 22 keV Pd K-X-rays should be with very small rate and main radiation would be bremsstrahlung X-rays in the region less than about 4 keV by slowing down of convey-electrons of alpha-particle. Components by L- and M-X-rays (in less than 5 keV region) may appear with visible weights (peaks). Production of secondary neutrons by D(α,n) process by 23.8 MeV alpha-particle is also with very small rate, since cross sections are small. Most kinetic energy of 23.8 MeV alpha-particle will be lost by ionization and knock-on with atoms of PdDx (effectively with Pd atoms), associating with soft X-rays by convey electrons, to deposit finally the released nuclear energy as lattice vibration (phonon) energy of PdDx. Therefore, the detection of Soft X-rays is of key issue. However, due to strong attenuation of soft X-rays in the PdDx layer and cell materials, observation from outside will be difficult (Criterion C).

Thus "apparently radiation-less" fusion reaction may be explained by our Cluster Fusion model.

Of course, other challenging models have been proposed by Hagelstein[3)], Li[4)], Chubb-Chubb[5)], Swartz[6)] , Preparata[11)] and others. So, it is worthwhile to summarize here in this paper about comments and discussions on possible helium-4 (^{4}He) production channels by deuteron-based fusion reactions, to make further progress in investigations on this key problem.

2. Summary of two-body d-d fusion

To get to certain lower excited state (probably to be referred to assumed levels as 20.21 MeV by Swartz[6)] or Schwinger-Preparata P-wave state[11)] as shown in Fig.1) of ^{4}He*, we may have in principle various ways. See **Fig.1** for ^{4}He level charts and related reactions. One simple way is excitation by incident gamma-rays with energy more than 20.21 MeV, which may have resonance photon absorption at Eg =20.21 MeV with some narrow energy width (maybe on the order of several tens meV). One of other ways is usage of the p + t reaction with (20.21-19.814) = 0.396 MeV relative kinetic (beam) energy. Conventional d + d reaction can not go there since ^{4}He* excited energy with zero relative kinetic energy is 23.8MeV. So, Swartz[6)] is assuming to take this 3.6 MeV difference – (23.8 minus 20.21) - by his hypothetical Phuson interaction, for which we are discussing below about its feasibility. Anyway his assumed 20.21MeV state of 'special d-d fusion' should reach at there through d+d strong interaction, and therefore we need to consider the competition race among n-, p- and gamma-emission channels with own partial energy widths, because we have to start or compete with the <d-d> admixture state by d + d to ^{4}He*(E_x=23.8MeV) or some by-passed routes if invented. So, anyway we need to treat the competition among particle emission break-ups and gamma (or electromagnetic) transitions. To treat photon channel only is

therefore misleading. We stress that the p + t break-up channel, [t] channel is dominant due to large partial energy width, defeating the gamma-ray emission transition [γ] channel, for the 20.21 MeV state of ^{4}He if this were attained in d-d interaction in condensed matter at all (We are however very pessimistic to this possibility).

We can not change branching ratios after the (virtual) intermediate compound state ^{4}He*(E_x = 23.8MeV + E_k) with very short life (on the order of 10^{-22} s), since no force-exchange bosons can transfer energy (or any information) from the intermediate compound nucleus to surrounding nuclei, atoms and lattices which are locating in distances larger than 0.1 nm. We need traveling time of force-exchange boson (photon for electro-magnetic interaction) more than 3×10^{-19} s which is very much larger than the life time of ^{4}He* (E_x = 23.8MeV +E_k). The branching ratios, [n]/[t]/[γ] of d-d fusion should keep therefore almost constant values, 0.5/0.5/10-7 for E_k = 0.025eV to about 100 keV. (See **Fig.2** for illustrating the feature of branching). Here E_k is the relative kinetic energy of d-d interaction.

To change out-going channels, namely branching ratios, we need the participation of *Third Interaction* into the d-d strong interaction process during the initial sate interaction stage (see Fig.3). The third interaction should be effective enough quantitatively to change the virtual intermediate excited state of ^{4}He*(E_x), or other deuteron-related compound nuclei states.

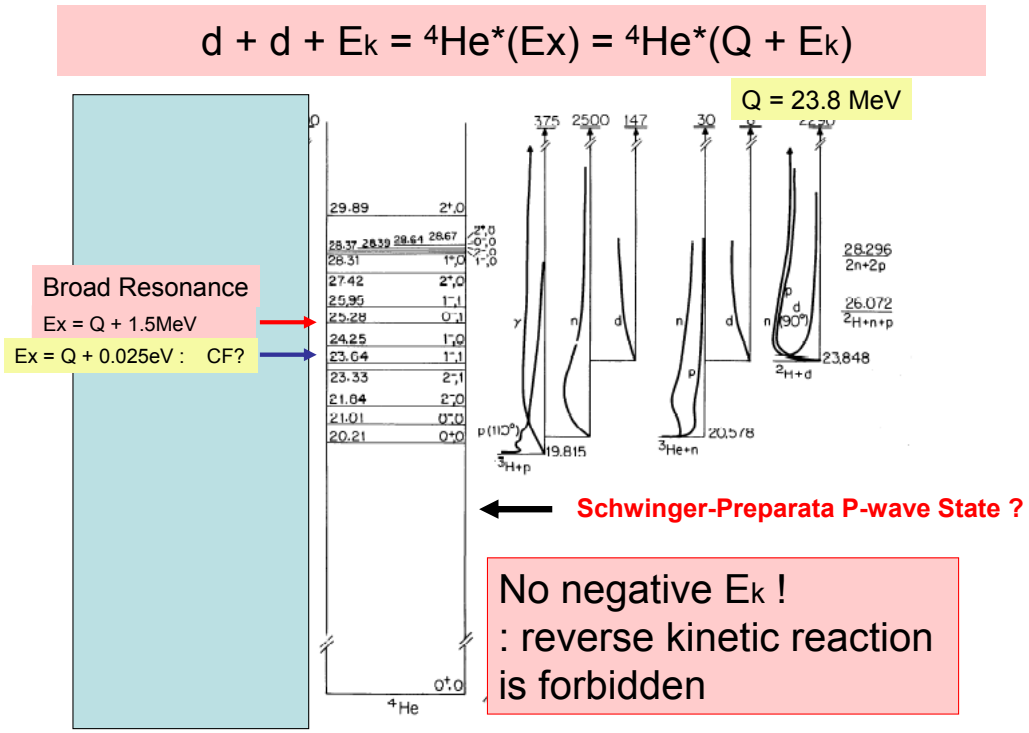

***Fig. 1**: Nuclear level chart of ^{4}He with relating reactions and assumed Schwinger-Preparata state; Here Q is the Q-value of d-d reaction to be 23.8 MeV, and E_k is the relative kinetic energy of d-d interaction.*

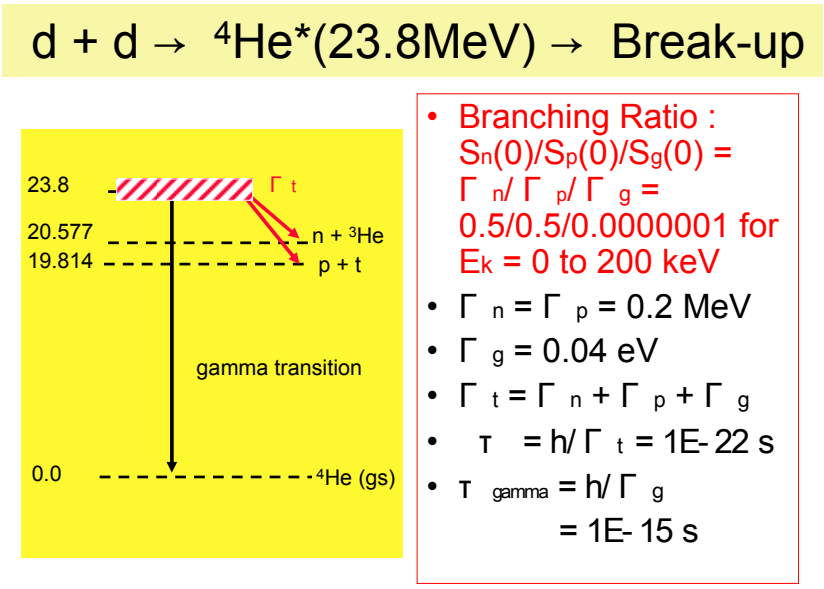

Fig.2: *Out-going channels of d+d reaction and branching ratios*

3. Possibility of Third Interaction Participating in d-d Reaction

We may understand the idea that some third interaction getting in the d-d strong interaction may change the excited state with spin parity of ^{4}He* as intermediate compound state. This *should happen in the initial state interaction* for d-d reactions under some environment (namely condensed matter), due to 10^{-22} s very short life of ^{4}He*. In principle, possibilities exist for the field-couplings with 1) additional strong nuclear force interaction, 2) additional weak-nuclear force interaction, 3) additional electromagnetic interaction and 4) gravity (graviton) interaction.

Our cluster fusion model[1,2] treats the possibility 1). The model by M. Swartz[6], as well as Hagelstein[3], Chubb[5], Preparata[11] and others, treats (we think) the possibility 3), as lattice-phonon is in the category of electro-magnetic interaction. We mean, they should quantitatively show that the coupling with their special phonons (Phuson by Swartz, for instance) or QED photons with d-d strong interaction is large enough to change the state of intermediate compound nucleus and thus change the final state density distribution out of ^{4}He*.

We think, the intrinsic problem there is how much the third interaction can change the relative transition matrix (T matrix, square of which is proportional to transition rate or cross section[2]). (See **Fig.3**.) In our crude estimation, electro-magnetic interaction can change the intermediate compound state with maximum weight of 1E-4 (just on the order) compared with the d-d strong interaction as usual charged pion exchange; see **Table-1**. In our opinion, only the additional interaction by strong nuclear force seems able to change out-going paths of break-ups of deuteron-related fusion process significantly. Other three interactions seem too weak to change the final state interaction practically with visible weight. However, we keep our mind open if somebody finds (or has found) the way to overcome this intrinsic difficulties for electro-magnetic interactions[3-6].

Table-1: Comparison of relative strength of field coupling

Force Field	Coupling Coefficient	Relative Strength
Strong Interaction	f^2/hc	1.0
Electro-Magnetic Interaction	e^2/hc	$7.3x10^{-3}$
Weak Interaction	$(ghc)^2(mc/h)^4$	$5.0x10^{-14}$
Gravity	GM^2/hc	$2.0x10^{-39}$

Note: Sdd = $1.1x10^2$ keVb (strong interaction), Spp = $1x10^{-22}$ keVb (weak interaction), and Cross-Section $\propto$ (T-matrix)^2

A figure for the ^{4}He* final state interaction is given in **Fig.2** (please see it). The first threshold state of ^{4}He* break-up locates at 19.814 MeV, which corresponds to the threshold of p + t break-up. The second threshold state of ^{4}He* break-up locates at 20.577 MeV, which corresponds to the threshold of n + ^{3}He break-up. To refer authorized level scheme, please see original data of nuclear chart in Fig.1 (referred at; http://www.tunl.duke.edu/nucldata/)

Therefore, if ^{4}He* can be excited to "unknown" energy level below 19.814 MeV as assumed by Schwinger-Preparata[11] and Swartz[6], we would have preferred decay to ^{4}He at ground state via electro-magnetic transition. Here, energy width of that "unknown" excited sate should be very much thin (about 4E-8 eV due to Heisenberg uncertainty; one needs to theorize how this very thin width is attained) to have several ns life time, as we imagine. Unfortunately, such a level has never been observed in nuclear physics experiments up to now. So, we understand we should invent it by some way consistently with known nuclear physics knowledge. Even if there may occur the sub-19.8MeV state in the initial state interaction between the d-d strong interaction and the phonon (or QED) mediated interaction, the nuclear excited energy of ^{4}He*(Ex = 19.8 MeV or less) should be emitted by single photon quantum or less-probably few photon quanta of nuclear electromagnetic transition. To realize small photon quanta (less than 40 eV that is atom displacement energy in Pd metal lattice, for example) and so many (more than $4.95x10^5$) QED photons[11] to transfer the nuclear excited energy to lattice phonons, we need direct coupling between the strong force of d-d interaction and the QED electro-magnetic force field of so many photon-phonon coupling states. No quantitative studies have been done.

We also mean that if ^{4}He* excited energy is larger than 19.814 MeV we should have dominant break ups to two particle emission channels (p + t and n + ^{3}He), since energy widths are, in nuclear physics knowledge (we discuss below), on the order of 0.1-0.5 MeV for particle (p, t, n, ^{3}He) emission channels with resonances at that two levels. As given in **Fig. 2** of this paper, branching ratios are defined by ratios of partial energy width over total energy width. By adopting experimental branching ratios, i.e., 0.5/0.5/0.0000001 for n-, p-, and gamma-emission channels, the gamma-width should be on the order of 1E-2 eV for the transition to the ^{4}He ground state. The gamma-transition time (life time) is given to be about 1E-15 s (1 fs; which is typical transition time for nuclear excited state to decay with electromagnetic wave - photon - emission for prompt decay channels).

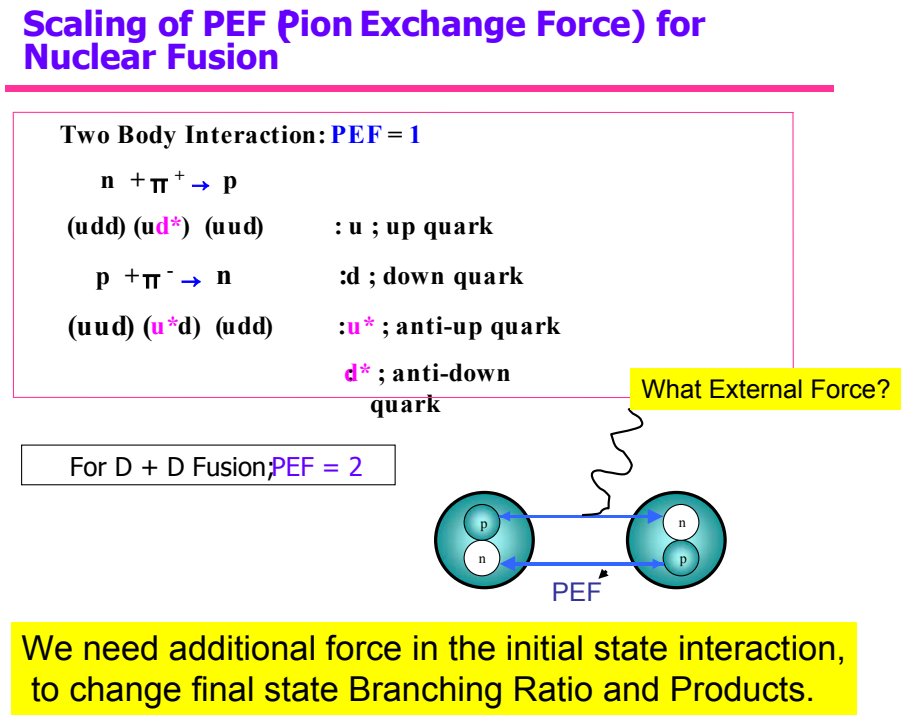

***Fig. 3**: Modeling of strong interaction (Yukawa model) and third interaction*

In our understanding, estimation of energy width for nuclear reaction is usually done by fitting with some theory, for instance the R-matrix theory[7)], to measured energy-dependent cross section curves which has resonance state (for known fusion reactions) at identified E-value by experiment. The d-d fusion has resonance at about 1.5 MeV, cross sections around which have been given experimentally quite accurately. To fit the R-matrix parameters to these d-d cross sections, we get energy width to be on the order of 0.4 MeV for ^{4}He*. Consequently, life time of ^{4}He* is calculated as $\hbar/\Gamma$, here Γ is the energy width for the excited state. The life time is calculated to be on the order of 1E-22 s (10^{-22} s).

In our understanding, R-matrix theory contains several undefined parameters which we have to get by only fitting to experimental data. So, this is empirical way of "theory". Partial energy widths for n + ^{3}He (20.577 MeV state) and p + t (19.814 MeV state) are estimated to be on the order of 0.2 MeV, by 0.5/0.5 branching ratio of d-d fusion. So, these two threshold states seem to slightly overlap within the tail of Heisenberg uncertainty (at two-sigma deviation). For example analysis of DT cross sections by R-matrix, you see the paper[7)].

We should study and consider how the third interaction (see Fig.3), for examples, by Phuson[6)] and coherent QED photons-exchange[11)] with the d-d strong field can change the intermediate compound ^{4}He* state, enough quantitatively, and what has taken more than about 3.8 MeV missing energy (difference between 23.8 MeV as ^{4}He* in usually known process by mass-defect and 20 MeV of Swartz's assumed process, for example), within its special life time, on which we will have a lot of discussions for proposed "unknown" excited state of ^{4}He*.

Usually, ns order life times are seen for isomeric states of special nuclei-isotopes (all heavier nuclei as Swartz referred for Moessbauer effect[6)]) for electro-magnetic transitions, but such isomeric states are not seen for light nuclei (especially deuteron has no excited states).

If ns order life time for special ^{4}He* state with "new" Very Thin Total Energy Width would be proved theoretically[4)], it must be great invention and we will be able to utilize this state for other nuclear physics/chemistry works. Unfortunately nuclear physics studies in the past have not found such a state and given no excited states below 19.8 MeV.

As far as we understand on R-matrix calculations, S(0)-values at E_k (relative deuteron energy in CM system of d + d interaction) =0 should be the same for Cold Fusion and we can rely on this to use for quantitative estimation of CMNS/CF fusion rates. This is due to the fact that fusion nuclear reactions take place at very near surface of sticking sphere of charged-pion exchange[8)] (see also our Asti5 paper and our ppt slide for ICCF12 Sunday Tutorial Class; http://www.iscmns.org/iccf12/TakahashiRates.pdf), namely on r=R0=about 5fm surface. In our understanding on minimum approaching distance (classical turning point of deuteron motion, namely b-parameter[1,2)]) by classical Newtonian motion in Shielded Coulomb Potentials, ever modeled and given numerically, could not be less than 50 fm, which is still very far from the very short range of fusion-sticking force (namely about 5 fm), so that we have to take into account factor about 10^{-4} at best for QM-penetration probability through the shielded Coulomb potential. In our understanding therefore, Born-Oppenheimer approximation (adiabatic treatments for many steps of wave function calculation; see Fig.4) can hold for the theorization of CMNS. Strong interaction is so short ranged force and becomes quite independent of electromagnetic interactions including QED photons or phonons like Phuson.

To treat quantitatively the direct coupling between the d-d strong interaction and the electromagnetic Phuson (phonon) or QED photons with so many (more than 10^5) coupled channels is really needed, as well as Hagelstein[3)] has been trying so, for the model to verify. The evaluation of life-time of <d-d> admixture in the coupled interaction is the key, if there exists much longer (more than 3(nm)x($3x10^{-18}$ (s/nm))x10^5 (Pd atoms) $\fallingdotseq$ 1 ps (10^{-12} s)) than the strong interaction time (less than about 10^{-21} s). The close pair <d-d> should exist out of strong interaction range to avoid rapid break up, but the d-d distance should be close enough (about 1pm according to our HWEQPET estimation[12)]) to have large d-d fusion rate comparable to observed heat level. The barrier of the problem is so high.

4. Deuteron-Cluster Fusion

In our 4d/TSC or 4p/TSC models[2,8,9,10)], Coulomb barrier shielding is conceived to attain automatically by strong condensation motion to the central focal point keeping averaged charge neutrality of the system (focal point is T-site in one of our model for PdDx lattice dynamics). Barrier penetration probability calculation for 2d pair or 4d cluster can be approximated by the EQPET formalism in average. And empirical treatment was applied for multi-body strong interaction between many deuterons under the Platonic symmetry. See **Fig.4**, for the treating process with three steps by Born-Oppenheimer Approximation.

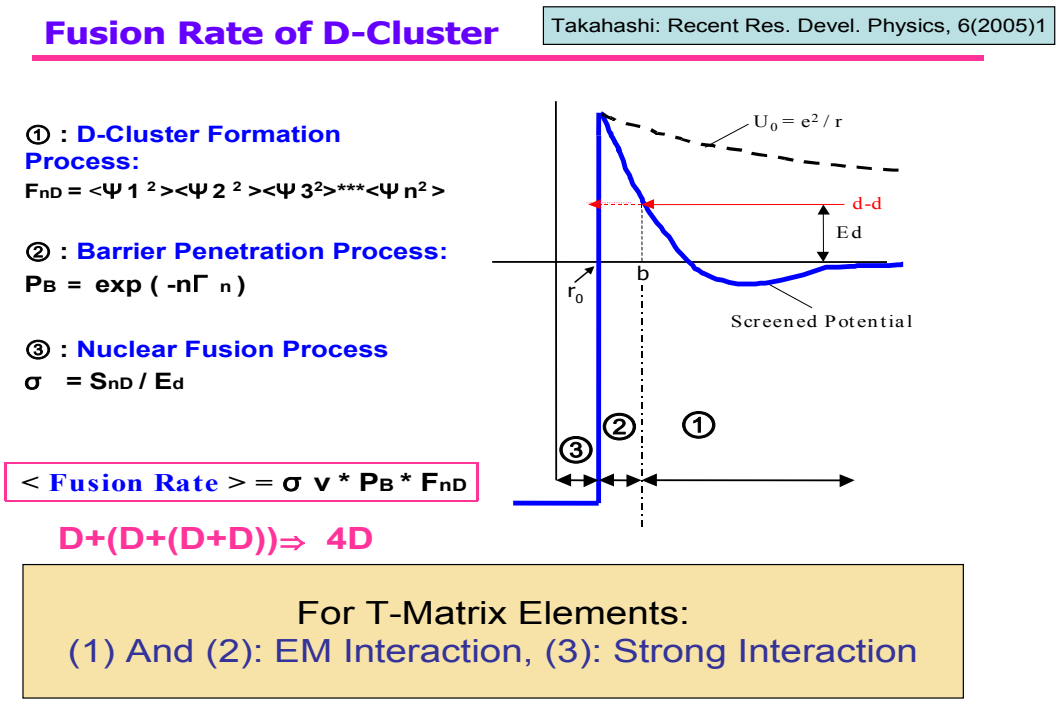

Fig. 4: *Treatment of D-cluster fusion by Born-Oppenheimer Approximation*

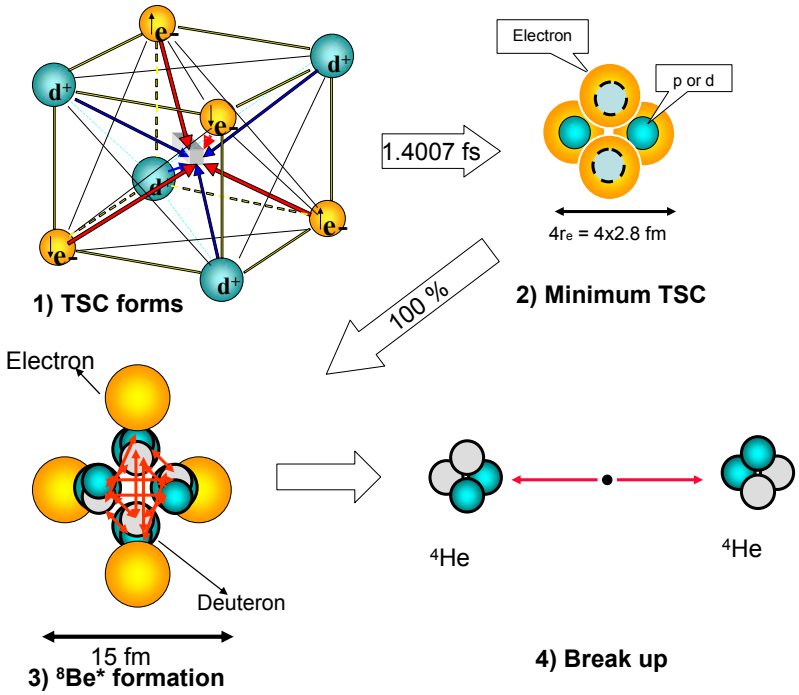

Fig. 5: *Illustration of dynamic condensation motion and 4D fusion by TSC; TSC gets to TSC-minimum state in 1.4007 fs, and 4D fusion takes place with 100% microscopic yield per TSC*[12].

When TSC gets to TSC-minimum-state, we can also use STTBA formulas (see our paper to Siena05[2)]) to calculate barrier penetration probability. You see examples of more general numerical estimation in Ref-9.

Basic philosophical idea is of transient squeezing motion of 4D (or 4H) clusters under the constraint of Platonic polyhedral symmetry, which also requires spin arrangement for associating 4 electrons to make "bosonized state". However, the bosonized state (quadruplet, e*(4,4)) is automatically formed when TSC configuration is formed in ordering process in/on condensed matter[8,9,10)].

To initiate TSC formation, three models are speculated (modeled with assumption). One is the TSC formation in regular PdD lattice in D-flow from O-site to T-site by D-lattice-phonon excitation. The second model is the TSC formation by the collision-combination process of trapped D_2 molecule, being lost freedom of rotation, and incoming D_2 molecule on surface of metal-D systems. The third idea is the random formation of TSC by combination of two bosonized molecules of dde*(2,2) in the near surface of Fermi-level gap of PdDx and CaO(or other); generation of Cooper pair near on Fermi surface may play key role in this case (our paper to Proc. JCF7).

For the cluster fusion of 4D to ^{8}Be* (then breaking up to two ^{4}He particles), we can reason why gamma-rays and hard X-rays are not visible, neither neutrons, as written in *Introduction*.

To theoretically clarify the TSC squeezing motion based on time-dependent QM models[10)], we need further studies. One trial of semi-classical approach was presented at ASTI06 Workshop[9)], which shows that strong condensation force under constraint may happen once TSC (t=0) state is formed. A molecular dynamics study of TSC condensation motion is also done based on a Langevin equation as reported in our separate paper to this ICCF13 meeting[12)]. *A 4D/TSC finishes condensation in 1.4007 fs, and 4D fusion takes place with 100% probability to produce two ^{4}He nuclei + 47.6 MeV per TSC generation. Therefore, twice of TSC generation rate (tsc/s/cc) becomes ^{4}He generation rate (^{4}He/s/cc).* A rate of 10^{11} 4D-fusion/s corresponds to the order of 1 watt power level.

An illustration of simple image of TSC condensation and 4D fusion[12)] is copied in **Fig**.5.

5. Concluding Remarks

1) The lowest excited energy of ^{4}He*, intermediate compound nucleus, by two-body d+d fusion reaction is 23.8 MeV. Lower excited energy than 23.8 MeV is forbidden by kinematics. As a result, [n]/[t]/[^{4}He] branching ratio becomes almost constant values as $0.5/0.5/10^{-7}$ for Ek = 0eV to 100keV (relative kinetic energy of reaction).

2)If there happens the ^{4}He* (Ex) state with Ex < 19.8 MeV, the final product becomes ^{4}He with ground state, after electromagnetic transition. To realize this process by d + d reaction, there should exist the third coupling field which must take more than the 4 MeV difference energy (23.8 – 19.8) of the d-d system in the initial sate interaction.

3)The many-body interaction process between the d+d pairing and the third field of photon-phonon coupling in the lattice of condensed matter may be considered. Due to the very short range force of d+d strong interaction and its very short life time of virtual intermediate compound state, no processes have ever been proved to remove the 4 MeV gap energy. Moreover, the field coupling constant of electro-magnetic interaction looks too weak, on the order of 10^{-2} of that for the strong interaction, to drastically change the state of d + d strong interaction for fusion. Quantitative studies on transition probabilities will be needed.

4) Deuteron-cluster fusion, i.e. 4D fusion, may produce ^{4}He final product as major ash of reaction. To realize the conditions of 4D fusion, the microscopic ordering/constraint process

for the dynamic Platonic symmetry should be satisfied. The EQPET/TSC model is one of theoretical models, although we need further investigations to establish[12)].

References

1. A. Takahashi: A Theoretical Summary of Condensed Matter Nuclear Effects, Proc. Siena2005 Workshop, see http://www.iscmns.org/siena05/Siena05Takahashi1.doc , to be published in *J. Condensed Matter Nuclear Science*, Vol.1, No.1 (2007)
2. A. Takahashi: Progress in Condensed Matter Nuclear Science, Proc. ICCF12, World Scientific Publ. Co., pp. 1-25 (2006)
3. P. Hagelstein: Models for Anomalies in Condensed Matter Deuterides, Proc. ICCF12, World Scientific Publ. Co., pp.441-453 (2006)
4. X. Z. Li, *Laser and Particle Beams*, 22(4) (2004).
5. S. Chubb: Framework for understanding LENR processes, using conventional condensed matter physics, Proc. ICCF11, pp.646-664, World Scientific Publ., (2006)
6. M. Swartz: "Phusons in Nuclear Reactions in Solids", *Fusion Technology*, 31, 228-236 (1997)
7. G. M. Hale, T. L. Tally (LANL): *Trans. Fusion Technology*, 26 (1994) 442-450
8. A. Takahashi, N. Yabuuchi; Fusion Rates of Bosonized Condensates, Proc. Asti06 Workshop, see http://www.iscmns.org/asti06/program.htm , to be published in *J. Condensed Matter Nuclear Science*, Vol.1, No.1 (2007)
9. A. Takahashi, N. Yabuuchi; On Condensation Force of TSC, ibid.
10. A. Takahashi: Time-dependent EQPET analysis of TSC, Proc. ICCF12, pp. , World Scientific Publ. Co., pp.454-461 (2006)
11. G. Preparata: *Trans. Fusion Technology*, 26 (1994) 397-407
12. A. Takahashi, N. Yabuuchi; Condensed Matter Nuclear Effects under Platonic Symmtery, Proc. ICCF13 (This meeting)

EFFECTIVE ELECTRICAL CHARGE IN DISORDERED SEMICONDUCTORS

D. Alexandrov

Department of Electrical Engineering, Lakehead University, Canada
dimiter.alexandrov@lakeheadu.ca

Introduction

The author's research progress in the field of disordered semiconductors related to InN is connected with discovering of energy pockets for the electrons in the structures of these alloys [1, 2]. In this paper it is found that if electrons are located in the structures of these semiconductors their electrical charge changes, which can be less or greater than the electron charge in the vacuum, i.e. the electron obtains effective electrical charge. Possibilities, that the deuterium cationic atoms to have similar behavior in solids, are discussed.

Results

The LCAO energy sub-bands CB1 (it is the minimum of the conduction band) and VB1 (it is the maximum of the valence band), which are parts of a corresponding LCAO electron band structure, are calculated for the following semiconductors: $In_xGa_{1-x}N$, $In_xAl_{1-x}N$, InN:O and non-stoichiometric InN:In. They are provided in Fig.1 for InN:O. Energy pockets for electrons in CB1 (sectors 5 and 2 in Fig.1 with states Γ^5_{c1} and Γ^2_{c1} respectively) are identified.

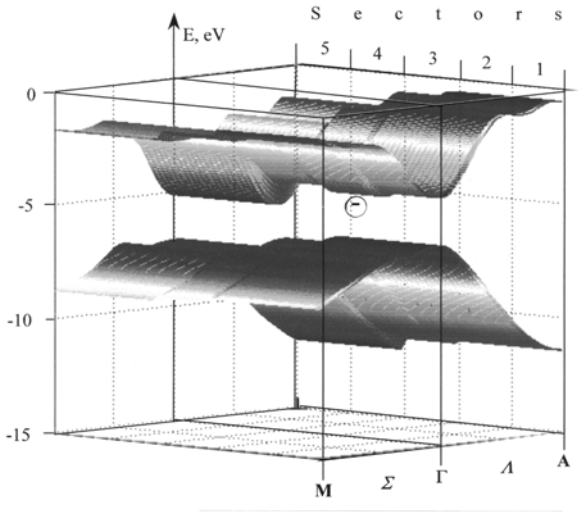

Fig.1

It is found that if electron is in solid having variable energy band gap across the crystal its electrical charge changes – it can be greater or less than $1.6*10^{-19}$C. Even the effective electron charge can approach zero value. These results come on the basis of model, which has been developed by the author, considering a break of electron charge symmetry in solids of this type.It is discussed this model can be used for determination of the effective charge of a deuterium cationic atom if its charge symmetry is broken due to interaction with ions of solids.

[1] D. Alexandrov, S. Butcher, T. Tansley, Phys. Stat. Sol. (a), **203** (1)**,** 25 (2006).

[2] D. Alexandrov, Journal of Crystal Growth, **246**, 325 (2002).

POSSIBLE GENERATION OF NEUTRONS BIRSTS IN FRAMEWORK OF ERZION MODEL & THEIR POSSIBLE REGISTRATION

Yu.N. Bazhutov

Institute of Terrestrial Magnetism, Ionosphere and Radiowave Propagation (RAS), 142092, Troitsk, Moscow region, Russia, bazhutov@izmiran.ru;

In framework of Erzion model charged Cosmic Ray Erzion, stopping in special substance, begins to create Erzion nuclear catalysis chains with generation of neutrons bursts during ~ 1-1000 mks. It is proposed to use 2 methods for such neutrons bursts registration: as with registration of thermal neutrons in gas counters, so with fast neutrons registration in large (>m^3) plastic scintillator. It is expected that such thermal neutron bursts in real Neutron Monitors must be appeared every day. Such events from fast neutrons can be observed every day also on the Spectrometric Scintillation Super-Telescope (SSTIS) creating in IZMIRAN for cosmic rays monitoring.

At Cosmic Rays studying in the field of Air Showers on the Tian-Shan FIAN Cosmic Ray Station Neutron Monitor the very long neutron impulses bursts (~ ms) of large intensity had been discovered [1]. These neutrons bursts (see Fig.1) couldn't find usual orthodox interpretation. So author proposes Erzion interpretation of this phenomenon based on Erzion model [2-4]. Erzion model is consequence of mirror chiral symmetry which proposes the existence of stable massive U* - antiquark (Mc^2~200 GeV, Q = -2/3). This antiquark together with usual d-quark composes massive stable negative charged meson named as negative Erzion ($Э^-$= {U*,d}), which captured by proton creates stable neutral 5-quark bag ($Э_N$= {U*,u,u,d,d}), named as Enion, alone stable Erzion baryon. In according with this mirror model, created by G. Vereshkov, the stable neutral Erzion ($Э^0$= {U*,u}) must exist, which captured by neutron creates the same Enion. Enion due to his special peculiarity, caused by his special quantum numbers, has strong repulsive forces. But due to his dipole electric moment thermolized Enion can attract nuclear & create connected state with rather small bounded energy from E_b~1,5eV for proton up to E_b~60eV for Pb^{208}. The main condition for creation of such stable long-lived state is absence of exothermic exchange reactions with such nuclear. Such nuclei were named as Donor nuclei (H^1, He^4,C^{12},O^{16},Ni^{64},…). In nuclear exchange reactions Erzions ($Э^-$,$Э^0$) must convert into Enions ($Э_N$) or Erzions with another charge ($Э^0$,$Э^-$) and inversely. Such way there are exist only 6 different Erzion nuclear exchange reactions on any nuclear with 6 their special reaction energies (negative for endothermic reaction & positive for exothermic reaction) on each nuclear. Such way in almost any matter we have very small concentration (C($Э_N$)~10^{-15} per nuclear) of captured Enions. When this Enions became free they can react with nuclei by means of exchange exothermic Erzion nuclear reactions with very large cross sections (σ~Mbn). Such way the frequency of such reactions is equal to GHz in best conditions. At usual temperatures only exothermic

reactions can run. There are few such reactions among stable isotopes of all chemical elements.

In the usual matter consisted from stable isotopes of light chemical elements only following Erzion nuclear catalytic reactions can run [5]:

$^{1}H\ (Э^{-}, Э^{0})\ ^{0}n + 1{,}65$ MeV	(100 %)	(1)
$^{2}H\ (Э^{-}, Э_{N})\ ^{0}n + 5{,}6$ MeV	(0,016 %)	(2)
$^{2}H\ (Э_{N}, Э^{0})\ ^{3}H + 0{,}1$ MeV	(0,016 %)	(3)
$^{2}H\ (Э^{0}, Э_{N})\ ^{1}H + 3{,}9$ MeV	(0,016 %)	(4)
$Li^{6}\ (Э_{N}, Э^{0})\ ^{7}Li + 1{,}1$ MeV	(7,5 %)	(5)
$Li^{6}\ (Э^{0}, Э_{N})\ ^{5}Li + 0{,}5$ MeV	(7,5 %)	(6)
$^{5}Li \rightarrow {}^{4}He + {}^{1}H + 1{,}7$ MeV		
$Li^{6}\ (Э^{-}, Э_{N})\ ^{5}He + 3{,}2$ MeV	(7,5 %)	(7)
$^{5}He \rightarrow {}^{4}He + {}^{0}n + 1{,}36$ MeV		
$^{7}Li\ (Э_{N}, Э^{-})\ ^{8}Be + 9{,}5$ MeV	(92,5 %)	(8)
$^{8}Be \rightarrow 2 \cdot {}^{4}He + 4{,}8$ MeV		
$^{13}C\ (Э_{N}, Э^{0})\ ^{14}C + 2{,}0$ MeV	(1,1 %)	(9)
$^{13}C\ (Э^{0}, Э_{N})\ ^{12}C + 1{,}2$ MeV	(1,1 %)	(10)
$^{14}C\ (Э_{N}, Э^{-})\ ^{15}N + 2{,}4$ MeV	(---)	(11)
$^{14}N\ (Э^{-}, Э^{0})\ ^{14}C + 2{,}3$ MeV	(99,6 %)	(12)
$^{14}N\ (Э^{-}, Э_{N})\ ^{13}C + 0{,}25$ MeV	(99,6 %)	(13)
$^{14}N\ (Э_{N}, Э^{0})\ ^{15}N + 4{,}7$ MeV	(99,6 %)	(14)
$^{15}N\ (Э_{N}, Э^{-})\ ^{16}O + 4{,}3$ MeV	(0,37 %)	(15)
$^{17}O\ (Э_{N}, Э^{0})\ ^{18}O + 1{,}9$ MeV	(0,038 %)	(16)
$^{17}O\ (Э^{0}, Э_{N})\ ^{16}O + 2{,}0$ MeV	(0,038 %)	(17)
$^{18}O\ (Э_{N}, Э^{-})\ ^{19}F + 0{,}2$ MeV	(0,2 %)	(18)
$^{19}F\ (Э_{N}, Э^{0})\ ^{20}F + 0{,}45$ MeV	(100%)	(19)
$^{19}F\ (Э_{N}, Э^{-})\ ^{20}Ne + 5{,}05$ MeV	(100 %)	(20)
$^{23}Na\ (Э_{N}, Э^{0})\ ^{24}Na + 0{,}8$ MeV	(100 %)	(21)
$^{23}Na\ (Э_{N}, Э^{-})\ ^{24}Mg + 3{,}9$ MeV	(100 %)	(22)
$^{27}Al\ (Э_{N}, Э^{0})\ ^{28}Al + 1{,}6$ MeV	(100 %)	(23)
$^{27}Al\ (Э_{N}, Э^{-})\ ^{28}Si + 3{,}8$ MeV	(100 %)	(24)

In the case of FIAN experiment inside of the Air Shower cores from the rather high energy of origin hadron ($\sim 10^{17}$eV) it is possible the birth of large number of Erzions or Enions (~100). Each of them stopping in organic matter of the Neutron Monitor, surrounding neutrons counters & consisting from such chemical elements as H, C, N, O, begins to create such catalysis Erzion-nuclear reactions chains (reactions (3,4), (9,10) & (16,17)) with the frequency of ~ (10-100) MHz during the time of ~ (10-1000) mks. In the chains end they will be captured by donor isotopes or go away from the matter. During catalysis Erzion-nuclear chains in the reactions (1, 2 & 7) through the conversion of $Э_N$ to $Э^-$ in the reactions (15,18,20,22,24) the neutrons will be borned with the frequency of ~ (10-100) кHz. May be exactly they were registered in the FIAN experiment [1].

If during cosmic ray registration where alone cosmic Erzions run with small intensity ($J_Э \sim 10^{-7}$см$^{-2}$s^{-1}) [2-4], one can use special materials (H, Li, F, Na, Al…), instead of organic matter, where nuclei of C^{12} & O^{16} atoms break off Erzion nuclear reaction chain, capturing Enions into bound states. In this case we can observe long (10-1000 mks) neutrons pulses

burst (see fig.1). Such special materials may be very high pure salt of LiF or pure Al metal with the addition of ~ 10 % of Li. It is expected in this special material of 4000kg mass the neutron pulses bursts must be appeared every day ($(M \cdot T) \sim 3000\ kg \cdot day$).

Such neutrons bursts may be registered in the standard large Neutron Monitors if one change Pb breeder around gas neutron counters (with He^3 or BF_3) by our special material. One can use the fast neutron registration method. For this purposes one can use already existed large detectors from plastic or liquid scintillator by registering in them rejected protons from scattering of fast neutrons, if one can add the layers of special materials of large mass. By the way soon such large new installation (STISS) for studding of cosmic ray muons & Erzion searching will begin to start in IZMIRAN (Moscow) [6]. In fig.2 one can see this installation with plastic scintillator mass of M~800kg (1 - plastic scintillator of 1m*1m*0,1m size, 2 - light isolating case, 3 - Photomultipliers). Such neutrons pulses bursts must be registered in this installation almost every day, if between 2 detector layers the special material layer of (Al/Li~1%) (M ~3000 kg, $\rho h \sim 65 g/cm^2$) must be placed.

In conclusion I want thank my colleagues A.P.Koshelev, E.V.Pletnikov & V.G.Yanke for interest & fruitful discussions of this problem.

References

1. Antonova V.P., Chubenko A.P., Kryukov S.V. et al. J. Phys. G: Nucl. Part. Phys., V. 28, P.251, (2002).
2. Bazhutov Yu.N., Vereshkov G.M. " New Stable Hadrons in Cosmic Rays, their theoretical interpretation & Possible Role in Catalysis of Cold Nuclear Fusion". Preprint N 1, CSRIMash (1990).
3. Bazhutov Yu.N., Vereshkov G.M., Kuksa V.I. “On Possibility of New Stable Hadrons Existence – Hypothetic Catalysts of Cold Nuclear Transmutation”. Proceeding of the 3-d Russian Conference on Cold Fusion & Nuclear Transmutation, Moscow, 157 (1996).
4. Bazhutov Yu.N., Vereshkov G.M. Proceedings ICCF-4, Hawaii, 4, 8-1 (1993).
5. Bazhutov Yu.N., Kuznetsov A.B., Pletnikov E.V. "Spectroscopy of Erzion Catalytic Nuclear Transmutation". Preprint № 1 SRC PhTP «Erzion», CSRIMash, 1-172, (1993).
6. Bazhutov Yu.N., Bazhutova S.Yu., Kartyshov V.G., Nekrasov V.V., Pletnikov E.V. «Scintillation Spectrometer Super-Telescope IZMIRAN for Muons Monitoring & Erzions Search in Cosmic Rays». Proceeding of the 11-th Russian Conference on Cold Nuclear Transmutation of Chemical Elements & Ball Lightning, Moscow, 12-17 (2004).

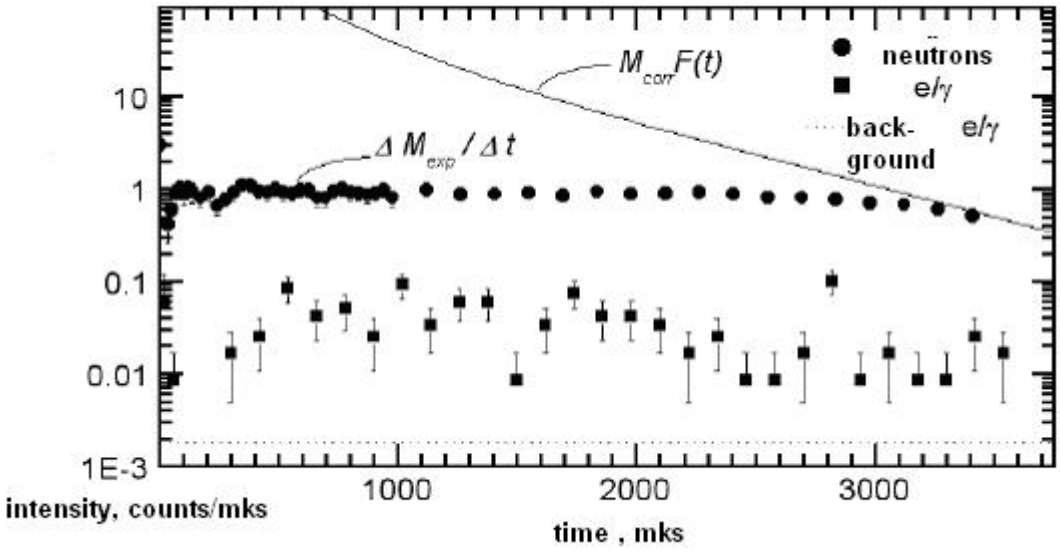

Fig.1 *Neutrons time distribution inside of neutrons bursts & accompany electron-photon component in Air Showers with parameters:* $N_e=2\cdot10^7$, $s=0.78$, $R\sim10$м

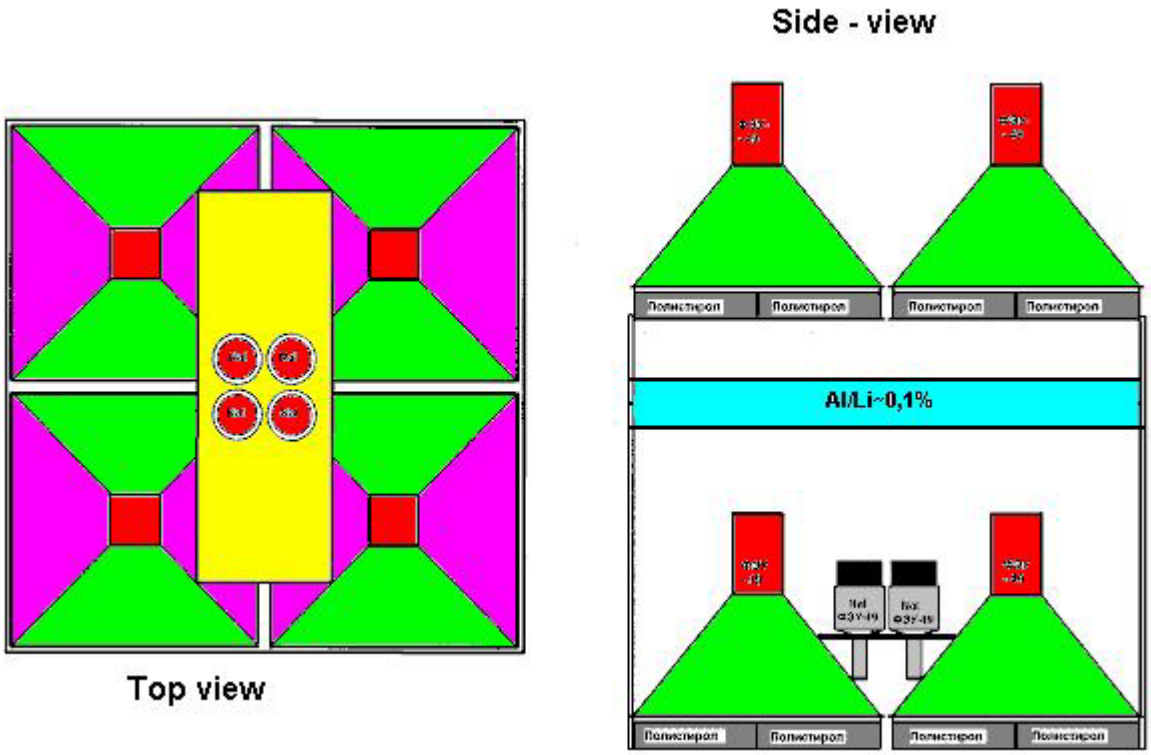

Fig.2. *Spectrometric Scintillation Super-Telescope (SSTIS) Scheme*

ESSENCE of ERZION MODEL

Yu.N. Bazhutov

Institute of Terrestrial Magnetism, Ionosphere and Radiowave Propagation (RAS), 142092, Troitsk, Moscow region, Russia, bazhutov@izmiran.ru ;

It is described the essence of Erzion Model, it's appearance from Cosmic Rays in 1982 & it's development to explain the main features of Cold Fusion Experiments.

Erzion Model can give principle explanation for many problems in Astrophysics and Geophysics, such as: 1) Dark matter in Universe; 2) Solar neutrino problem; 3) Jupiter energetic disbalance; 4) Tritium & He^3 abundance in volcano products; 5) Ball-lightning & forest fire nature and some else.

Some applied problems can be decided in framework of Erzion Model, such as: 1) to create the new energy-capacious, ecology-pure with rather simple technology nuclear energetics; 2) principle & radical utilization of radioactive wastes; 3) cheap production of some chemical elements & isotopes (gold for example).

Erzion Model can explain many experiments in Cold Fusion & can predict many new experiments for it's testing.

Erzion Model History in Cosmic Rays & Cold Fusion

The hypothesis of the new stable massive hadrons existence in Cosmic Rays has been appeared in 1981 to explain abnormal energy spectrum of vertical component of Cosmic Rays Muons [1]. Many characteristics of this hadron (named later as Erzion) such as: mass, charge, lifetime, intensity & spectrum, nuclear interaction modes & paths – were predicted phenomenologically. From this year the direct Erzions search had started [2-4].

Moreover Erzion existence could explain also some other abnormal experimental results in Cosmic Rays such as:

1. Long length hadron cascades;
2. Delayed particles in Air Showers;
3. High energy neutral particles flux from local space sources;
4. Large across momentums in high energy cascades and etc.

But it was great present for author that Erzion existence in nature could explain on principle the new Fleishmann & Pons Phenomena of Cold Fusion [5,6] by Erzion Catalysis Mechanism [7].

For strong theoretical interpretation of such exotic particles existence in nature in 1990 the Mirror model $U(1)xSU_l(2)xSU_r(2)xSU(3)$ had been proposed by Vereshkov G.M. [8-10]. This model without any contradiction with all world totality of experimental results in high energy & cosmic ray physics could explain main part of abnormal experimental results in orthodox physics & main unusual features in Cold Fusion such as:

1. Suppression of the neutron to tritium yield (10^3 – 10^{11} times);
2. Reducing of tritium to energy yield (~ 10^3 times);
3. Unstationary condition of CF reactions running;
4. Great yield fluctuation (up to 10^5 times);
5. New isotopes & element production & etc.

The essence of Erzion model

In framework of this Mirror model the new massive & stable Mirror antiquark (U*) must exist with very small concentration as a relict component relatively to usual quarks (C_{U*} / $C_{u,d}$ ~ 10^{-15}). This antiquark can be hadronized together with our usual (u) or (d) quarks into new meson pair: neutral Erzion – $Э^0$={U*,u}, or negative charged Erzion $Э^-$={U*,d}. The features of quark numbers of this antiquark U* are going to the unusual feature of repulsion forces of strong interaction of Erzions. Such way this mesons couldn't be captured by all nuclear besides only nucleons forming 5-quark bag, stable singlet state, named as Enion ($Э_N$={U*,u,u,d,d}). As you can see from fig.1, this particle can dissociate or to charged pair ($Э_N$= $Э^-$ + p – ΔE1), or to neutral pair ($Э^0$ + n – ΔE2).

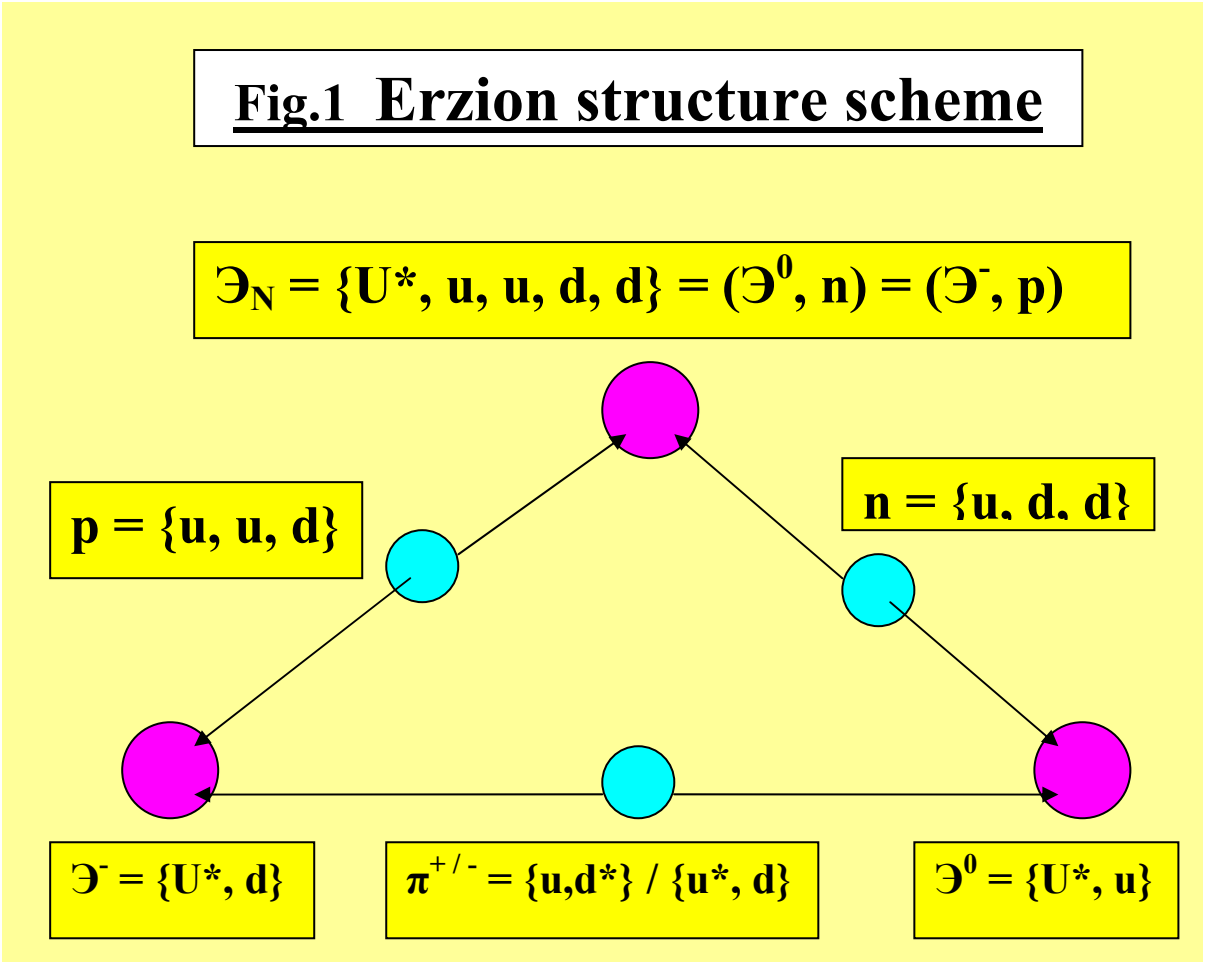

Such way in nuclear exchange reactions these Erzions & Enions can be changed each to another with changing number of nucleons in nuclear. On the every nuclear only 6 nuclear exchange reactions can run by Erzion catalysis mechanism:

1. $(A,Z) + Э_N = Э^0 + (A+1, Z) + \Delta E_1$;
2. $(A,Z) + Э_N = Э^- + (A+1, Z+1) + \Delta E_2$;
3. $(A,Z) + Э^0 = Э_N + (A-1, Z) + \Delta E_3$;
4. $(A,Z) + Э^0 = Э^- + (A, Z+1) + \Delta E_4$;
5. $(A,Z) + Э^- = Э_N + (A-1, Z-1) + \Delta E_5$;
6. $(A,Z) + Э^- = Э^0 + (A, Z-1) + \Delta E_6$;

In this Erzion Catalysis model we have only 2 free energy parameters (ΔE1 & ΔE2), which we can choose for proper Cold Fusion reactions. So in framework of Erzion Catalysis model we can know all energy reactions for all nuclear Erzion reactions & can predict what reactions (exothermic) can be running.

Enion due to his special peculiarity, caused by his special quantum numbers, has strong repulsive forces. But due to his dipole electric moment thermolized Enion can attract nuclear & create connected state with rather small bounded energy from E_b~1,5eV for proton up to E_b~60eV for Pb^{208}. The main condition for creation of such stable long-lived state is absence of exothermic exchange reactions with such nuclear. Such nuclei were named as Donor nuclei (H^1, He^4,C^{12},O^{16},Ni^{64},…). In nuclear exchange reactions Erzions ($Э^-$,$Э^0$) must convert into Enions ($Э_N$) or Erzions with another charge ($Э^0$,$Э^-$) and inversely. Such way there are exist only 6 different Erzion nuclear exchange reactions on any nuclear (see above - 1.,2.,3.,4.,5.,6.) with 6 their special reaction energies (ΔE_1, ΔE_2, ΔE_3, ΔE_4, ΔE_5, ΔE_6 - negative for endothermic reaction & positive for exothermic reaction) on each nuclear. Such way in almost any matter we have very small concentration ($C(Э_N)$~10^{-15} per nuclear) of captured Enions. When this Enions became free they can react with nuclei by means of exchange exothermic Erzion nuclear reactions with very large cross sections (σ~Mbn). Such way the frequency of such reactions chain is equal to GHz at best conditions.

At usual temperatures only exothermic reactions can run. There are few such reactions among stable isotopes of all chemical elements. In the usual matter consisted from stable isotopes of light chemical elements only following Erzion nuclear catalytic reactions can run [11]:

$^1H\ (Э^-, Э^0)\ ^0n + 1{,}65$ MeV	(100 %)	(1)
$^2H\ (Э^-, Э_N)\ ^0n + 5{,}6$ MeV	(0,016 %)	(2)
$^2H\ (Э_N, Э^0)\ ^3H + 0{,}1$ MeV	(0,016 %)	(3)
$^2H\ (Э^0, Э_N)\ ^1H + 3{,}9$ MeV	(0,016 %)	(4)
$Li^6\ (Э_N, Э^0)\ ^7Li + 1{,}1$ MeV	(7,5 %)	(5)
$Li^6\ (Э^0, Э_N)\ ^5Li + 0{,}5$ MeV	(7,5 %)	(6)
$^5Li \rightarrow\ ^4He + ^1H + 1{,}7$ MeV		
$Li^6\ (Э^-, Э_N)\ ^5He + 3{,}2$ MeV	(7,5 %)	(7)
$^5He \rightarrow\ ^4He + ^0n + 1{,}36$ MeV		
$^7Li\ (Э_N, Э^-)\ ^8Be + 9{,}5$ MeV	(92,5 %)	(8)
$^8Be \rightarrow\ 2 \cdot ^4He + 4{,}8$ MeV		
$^{13}C\ (Э_N, Э^0)\ ^{14}C + 2{,}0$ MeV	(1,1 %)	(9)
$^{13}C\ (Э^0, Э_N)\ ^{12}C + 1{,}2$ MeV	(1,1 %)	(10)
$^{14}C\ (Э_N, Э^-)\ ^{15}N + 2{,}4$ MeV	(---)	(11)
$^{14}N\ (Э^-, Э^0)\ ^{14}C + 2{,}3$ MeV	(99,6 %)	(12)
$^{14}N\ (Э^-, Э_N)\ ^{13}C + 0{,}25$ MeV	(99,6 %)	(13)

^{14}N ($Э_N$, $Э^0$) ^{15}N + 4,7 MeV	(99,6 %)	(14)
^{15}N ($Э_N$, $Э^-$) ^{16}O + 4,3 MeV	(0,37 %)	(15)
^{17}O ($Э_N$, $Э^0$) ^{18}O + 1,9 MeV	(0,038 %)	(16)
^{17}O ($Э^0$, $Э_N$) ^{16}O + 2,0 MeV	(0,038 %)	(17)
^{18}O ($Э_N$, $Э^-$) ^{19}F + 0,2 MeV	(0,2 %)	(18)
^{19}F ($Э_N$, $Э^0$) ^{20}F + 0,45 MeV	(100%)	(19)
^{19}F ($Э_N$, $Э^-$) ^{20}Ne + 5,05 MeV	(100 %)	(20)
^{23}Na ($Э_N$, $Э^0$) ^{24}Na + 0,8 MeV	(100 %)	(21)
^{23}Na ($Э_N$, $Э^-$) ^{24}Mg + 3,9 MeV	(100 %)	(22)
^{27}Al ($Э_N$, $Э^0$) ^{28}Al + 1,6 MeV	(100 %)	(23)
^{27}Al ($Э_N$, $Э^-$) ^{28}Si + 3,8 MeV	(100 %)	(24)

As you can see, the rarest reactions are with neutral Erzion - $Э^0$. There are only 11 stable isotopes reacting with this Erzion, named as Converters. So if you want have the reserved Erzion nuclear reaction chains you must have in your reactor system besides Donor isotopes such Converter isotopes. The best among them is Deuterium [12]. For generating neutrons you must have Hydrogen or Lithium elements in your CF reactor.

All our CF experiments [13-17] (only some last from them) fulfilled in accordance with Erzion model predictions & every time they confirmed it and had success.

Erzion Model in Astrophysics, Geophysics & Practice

Erzion Model can give principle explanation for many problems in Astrophysics and Geophysics [10,18,19], such as:

1) Dark matter in Universe;
2) Solar neutrino problem;
3) Jupiter energetic disbalance;
4) Tritium & He^3 abundance in Volcano products;
5) Ball-lightning & Forest Inflame nature and some else.

Some applied problems can be decided in framework of Erzion Model [10,19], such as:

1) Creating the new energy-capacious, ecology-pure with rather simple technology nuclear energetics;
2) Principle & radical utilization of radioactive wastes;
3) Cheap production of some chemical elements & isotopes (gold for example).

Conclusion

I want thank everybody who helped me last 20 years in work on developing of such very interest & fruitful problem of Erzion Catalytic Model & hope that it will reach success.

References

1. Bazhutov Yu.N., Khrenov B.A., [Khristiansen G.B.] “About One Opportunity of Second Shower Spectrum Interpretation Observed at Small Depth Underground”, Izvestiya AN USSR, ser. Phys., 1982, v.46, 9, p.2425-2427.

2. Bazhutov Yu.N., “A Search for the Decay of Hypothetical Penetrating Particles”, Proc. 18-th Int. Cosmic Ray Conference, Bangalore, 1983, He-2, 2-18, p.24-26.
3. Abramov A.V., Bazhutov Yu.N., Khrenov B.A. et al. “Search for Massive Charged Elementary Particles” Proc. All-Union Cosmic Ray Conference, Alma-Ata 1989, v.1, p.101-102.
4. Bazhutov Yu.N., Vereshkov G.M. “Search for New Stable Hadrons in Cosmic Rays”, Preprint No.2, Central Research Institute of Machine Building, 1990.
5. Fleischmann M., Pons S., Hawkins M., Journal Electroanalytic Chemistry, 1989, v261, p.301.
6. Jones S.E., Palmer E.P., Criss J.B. et al., Nature, 1989, v338, p.737.
7. Bazhutov Yu.N., Vereshkov G.M., Kuzmin R.N. & Frolov A.M. “Interpretation of Cold Fusion by Erzion Catalysis”, Proc. “Plasma Physics and some questions of General Physics”, CSRIMash, Kaliningrad, Moscow region, 1990, p.67-79.
8. Bazhutov Yu.N., Vereshkov G.M. «New Stable Hadrons in Cosmic Rays, their Theoretical Interpretation & Possible Role in Catalysis of Cold Nuclear Fusion». Preprint No.1, Central Research Institute of Machine Building, 1990.
9. Bazhutov Yu.N., Vereshkov G.M. “A Model of Cold Nuclear Transmutation by the Erzion Catalysis”, Proceedings of ICCF-4, Hawaii, 1993, v.4, 8-1.
10. Bazhutov Yu.N., Vereshkov G.M., Kuksa V.I. «On a Possibility of Existing New Stable Hadrons-Hypothetical Catalyst of Cold Nuclear Transmutation». Proceeding of 3-d Russian Conf. On Cold Fusion & Nuclear Transmutation, Dagomys-1995, Moscow, 1996, p.157.
11. Bazhutov Yu.N., [Kuznetsov A.B.], Pletnikov E.V. "Spectroscopy of Erzion Catalytic Nuclear Transmutation". Preprint № 1 SRC PhTP «Erzion», CSRIMash, 1993, p.1-172.
12. Bazhutov Yu.N. “Influence of Spin & Parity Preservation Lows on Erzion Model Predictions in Cold Fusion Experiments”, Proceedings of ICCF-7, Vancouver, 1998, p.437-440.
13. Bazhutov Yu.N., Koretsky V.P., [Kuznetsov A.B.] et al. “Tritium, Neutron & Radiocarbon Registration with the Yusmar Hydrofacility Running”, Proceedings of ICCF-6, Japan, 1996, v.1, p.387-391.
14. Bazhutov Yu.N., Koretsky V.P. “Neutron Generation at Ultrasonic Cavitation of some Liquids”, Proceedings of ICCF-7, Vancouver, 1998, p.427-436.
15. Bazhutov Yu.N., Bazhutova S.Yu., Dyad’kin A.P., et al. “Calorimetric & Neutron Diagnostics of Liquids during Laser Irradiation”, Proceedings of ICCF-11, Marseilles, 2004, p.374-378.
16. Bazhutov Yu.N., Grishin V.G., [Nosov V.N.] “Electrolysis with Gas Discharge at Anode”, Proceeding of 10-th Russian Conference on Cold Nuclear Transmutation, Dagomys-2002, Moscow, 2003, p.19-26.
17. Bazhutov Yu.N., Grishin V.G., [Eremeev A.V.], Velikodny V.Yu. et al. “Nuclear Diagnostic of Cold Nuclear Transmutation at Electrolysis with Anode Gas Discharge in Water Solutions”, Proceeding of 13-th Russian Conference on Cold Nuclear Transmutation, Dagomys-2005, Moscow, 2006, p.71-83.
18. Bazhutov Yu.N. “Erzion Construction of Magnetic” Rodionov” Fluxes & Possible Consequences of their Existence in Nature”, Proceeding of 10-th Russian Conference on Cold Nuclear Transmutation, Dagomys-2002, Moscow, 2003, p.12-18.
19. Bazhutov Yu.N. “Erzion Discovery in Cosmic Rays and its Possible Great Role in Nature in Framework of Erzion Model in Cold Nuclear Transmutation”, Proceedings of ICCF-8, Lerici (La Spezia), 2000, p.269-275.

PROGRESS ON PHONON EXCHANGE MODELS FOR EXCESS HEAT IN METAL DEUTERIDES

Peter L. Hagelstein and Irfan U. Chaudary

Research Laboratory of Electronics,
Massachusetts Institute of Technology,
Cambridge, MA 02139 ,USA
E-mail: plh@mit.edu

Abstract

Excess heat in the Fleischmann-Pons experiment without commensurate energetic particles implies a violation of local energy and momentum conservation. Models based on excitation transfer can produce a violation of local energy and momentum conservation under conditions where total energy and momentum are conserved. We present idealized spin-boson models that illustrate the excitation transfer mechanism. Spin-boson models also exhibit anomalous energy exchange, in which a large quantum is converted into many small quanta. We consider a model in which excitation transfer is followed by anomalous energy exchange, and we find an analytic solution for the coherent dynamics. The associated rates for the spin-boson models are too slow to be relevant to experiment. Spin-boson models augmented with oscillator loss show dramatically increased excitation transfer and anomalous energy exchange rates due to the elimination of destructive interference. The resulting rates can be comparable with experiment for reasonable assumptions about populations, matrix elements, and screening factors.

1. Introduction

The principal theoretical problem encountered in connection with the excess heat effect in the Fleischmann-Pons experiment [1] is the absence of energetic particles commensurate with the thermal energy produced. One foundation of nuclear physics is the conservation of local energy and momentum in scattering, decay, and reaction processes (a foundation which dates back to the time of Rutherford [2,3]). If local energy and momentum are conserved in an exothermic reaction, then the reaction energy must be expressed through energetic particles. In the Fleischmann-Pons experiment, an excess of energy is claimed, yet no experiment reported since 1989 has given any indication of energetic particles in amounts that would correspond to the energy produced.

Consequently, whatever physical process is responsible for the excess heat effect must violate local energy and momentum conservation if nuclear [4]. In 1989 the argument was made [1] that the energy produced was far too great to be of chemical or solid state origin, and hence must be nuclear through a process of elimination. No other kind of energy source was capable

in principle of the available energy density implied by the total energy release. Over the years a number of observations of ^{4}He production have been reported, and in some cases where the total amount of ^{4}He produced is correlated with the total excess energy measured. The reaction *Q*-value deduced from these experiments is near 24 MeV, which corresponds to the mass difference between two deuterons and ^{4}He (see [5] and references therein).

These considerations provide some guidance as to what kind of new physical process should be sought in the development of a theoretical model. For example, the experimental results seem to provide support for reactions in which two deuterons interact in some new kind of way, such that ^{4}He is made as a result. However, the absence of energetic particle production in association with the energy produced places severe constraints on what kinds of models may be relevant. For example, in previous years much energy was put into searches for anomalous screening effects, which might allow two deuterons to tunnel together more rapidly. Deuteron-deuteron fusion experiments at low beam energy have shown that very large anomalous screening effects are present in the case of a metal deuteride environment [6-8]. Nevertheless, such models do not address what is most important, which is the absence of energetic products. Anomalous screening by itself would lead to the production of energetic conventional deuteron-deuteron fusion products if strong enough; whereas experiments appear to show ^{4}He (in the absence of 24 MeV gammas) with no commensurate energetic particles of any kind.

2. Excitation transfer

In response to this discussion, our attention should then focus on new physical processes in which local energy and momentum conservation is violated. Of course, minor violations of local energy and momentum conservation occur in the case of gamma absorption and emission is a solid, in which a small amount of momentum and energy is exchanged with the lattice in non-Mossbauer transitions. There is no possibility in our view of a new kind of process in which a large MeV-level quantum is exchanged with the lattice directly to produce a large number of low energy quanta.

The only real possibility for a violation of local energy and momentum conservation that remains is then through an excitation transfer process. We are not aware of any discussion of excitation transfer processes for excited states or reacting nuclei at a distance in the nuclear physics literature. However, excitation transfer is well known in biophysics [9,10]. In this case, atoms or molecules, which are distant, can exchange excitation through Coulomb coupling. Coupling between the two systems results in excitation transfer as a quantum coherent process, so that the interaction must be sufficiently strong to produce a transfer prior to decoherence of the entangled system. Unfortunately, Coulomb coupling falls off rapidly with distance, so that excitation transfer in atomic and molecular systems is limited to a short characteristic distance (the Forster length). There is no possibility of significant nuclear excitation transfer mediated through Coulomb coupling since the associated Forster length is very small.

2.1 Generalization of excitation transfer

If we adopt a more generalized view of excitation transfer, we might view excitation transfer as involving an off-resonant coupling between two equivalent two-level systems and extended

common modes. For example, it is possible to analyze Coulomb coupling between dipoles mathematically in a picture in which each two-level system couples to common longitudinal photon modes. Since longitudinal photons have zero energy, the interaction is strongly off-resonant, and intermediate states are produced with energies very different than the initial state energy. Destructive interference between the contributions of the different longitudinal photon modes then produces the spatial dependence associated with Coulomb coupling.
Viewed this way, it is a relatively small step to a generalization of the effect where other modes are substituted in place of the longitudinal photon modes. For example, coupling to vibrational modes instead of longitudinal photon modes would produce a modified excitation transfer mechanism, with a different spatial dependence. The possibility of indirect coupling between two-level systems has been discussed in the literature [11]. Discussion of phonon-mediated indirect coupling has appeared in the solid state literature recently [12]. To extend such a model to the nuclear case requires phonon exchange in association with a nuclear transition. Aside from our interest in this problem, this seems not to have been explored in the literature previously outside of recoil effects associated with neutron capture and gamma transitions.

3. Idealized excitation transfer model

We can illustrate excitation transfer with the aid of an idealized model. Consider a pair of two-level systems that are coupled to a common oscillator, as described by the Hamiltonian

$$\hat{H} = \Delta E_1 \frac{\hat{s}_z^{(1)}}{\hbar} + \Delta E_2 \frac{\hat{s}_z^{(2)}}{\hbar} + \hbar\omega_0 \hat{a}^\dagger \hat{a} + V_1\left(\hat{a}^\dagger + \hat{a}\right)\frac{2\hat{s}_x^{(1)}}{\hbar} + V_2\left(\hat{a}^\dagger + \hat{a}\right)\frac{2\hat{s}_x^{(2)}}{\hbar} \quad (1)$$

Here, the components of the spin operator $\hat{s}^{(j)}$ for the two-level system *j* allow us to describe two individual two-level systems interacting with an oscillator (which is described by creation and annihilation operators $\hat{a}^\dagger$ and $\hat{a}$). Coupling between the two-level systems and the oscillator is assumed to be proportional to the coupling coefficients V_1 and V_2. We are interested in this problem in the limit in which the oscillator is highly excited, and where the oscillator energy $\hbar\omega_0$ is much less than the transition energies ΔE_1 and ΔE_2. This model is a reduced version of the one discussed in [13] and in [14].

3.1 Energy levels and resonance condition

In this model, coupling between each two-level system and oscillator leads to an increase in the two-level transition energy, while the two-level systems have little impact on the oscillator. Energy levels are given approximately by

$$E_{n,m_1m_2} = \Delta E_1\left(g_1\right)m_1 + \Delta E_2\left(g_2\right)m_2 + \hbar\omega_0 n \quad (2)$$

where the dimensionless coupling strengths g_1 and g_2 are given by

$$g_1 = \frac{V_1\sqrt{n}}{\Delta E_1} \qquad g_2 = \frac{V_2\sqrt{n}}{\Delta E_1}$$

The dressed transition energies are given approximately by [15]

$$\Delta E_j(g) = \frac{\Delta E_j}{\pi}\int_{-\sqrt{\varepsilon}}^{\sqrt{\varepsilon}}\sqrt{\frac{1+8g^2y^2/n}{\varepsilon-y^2}}dy \tag{3}$$

with $\varepsilon = 2n+1$.

Excitation transfer may occur when two of these levels are degenerate. For example, when

$$\Delta E_2(g_2) - \Delta E_1(g_1) \;=\; \delta n\hbar\omega_0 \tag{4}$$

the dressed energy of the second two-level system matches the dressed energy of the first two-level system plus δn oscillator quanta. If δn is even, then the system can oscillate between two states in which excitation has been transferred from one system to the other (with some energy exchange with the oscillator).

3.2 Dynamics

On resonance, the system undergoes coherent Rabi oscillations between the two states, with dynamics given by

$$p(t) = \cos^2\frac{|V|t}{\hbar} \tag{5}$$

where *p(t)* is the occupation probability of an initial state, with *V* the associated coupling matrix element. In an analytic WKB approximation this coupling matrix element is given approximately by

$$V = \frac{2\hbar\omega_0 g_1 g_2}{\pi n}\int_{-\sqrt{\varepsilon}}^{\sqrt{\varepsilon}}\frac{1}{\sqrt{\varepsilon-y^2}}\frac{\cos\Delta\phi(y)}{\left[1+8\left(\frac{V_1 y}{\Delta E_1}\right)^2\right]\left[1+8\left(\frac{V_2 y}{\Delta E_2}\right)^2\right]}dy \tag{6}$$

where

$$\Delta\phi(y) = \frac{\Delta E_1}{\hbar\omega_0}\int_0^y\sqrt{\frac{1+8V_1^2(y')^2/\Delta E_1^2}{\varepsilon-(y')^2}}dy' - \frac{\Delta E_2}{\hbar\omega_0}\int_0^y\sqrt{\frac{1+8V_2^2(y')^2/\Delta E_2^2}{\varepsilon-(y')^2}}dy' \tag{7}$$

Results are illustrated for a specific example in Figure 1.

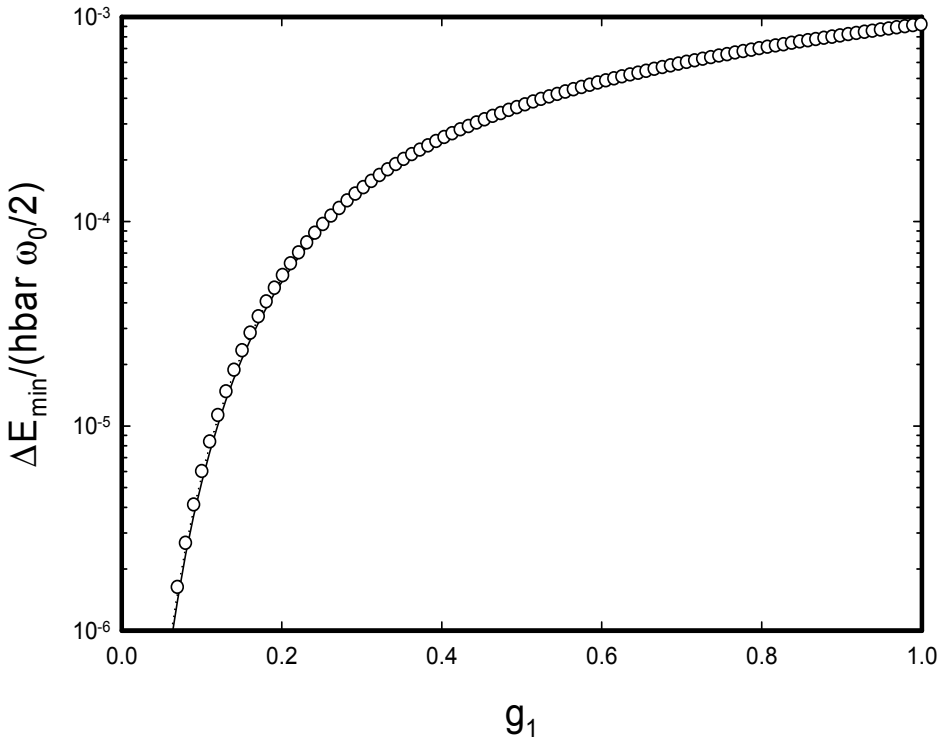

Figure 1: *Level splittings* $\Delta E_{\min} = 2|V|$ *at the anticrossings for excitation transfer for* $\Delta E_1 = 53\hbar\omega_0$ *and* $\Delta E_2 = 51\hbar\omega_0$ *with* $\delta n = -2$ *and* $n_0 = 1000$. *Results are presented for direct calculations with* $\hat{H}$ *as given by Equation (1) at individual resonances – open circles; results from the WKB approximation – solid line. This calculation is discussed in [4].*

3.3 Discussion

We draw attention to a number of features concerning this model and result. This model is the simplest possible that is capable of supporting an excitation transfer effect due to indirect coupling, and from the results we see that the effect is indeed present. We find that for significant excitation transfer to occur within the model, the resonance condition must be satisfied precisely, and the transfer rate observed is slow. We have found a rotation [13,15] which divides up the problem into an adiabatic piece, which is responsible for most of the level shift, and a dynamical piece, which is responsible for dynamical coupling between near resonant states. This allows us to treat excitation transfer coupling using a first-order matrix element even when multi-quantum transitions are involved.

We conclude that excitation transfer through off-resonant indirect coupling can arise in simple models involving coupling between two-level systems and an oscillator. Although the model is highly idealized, we have in mind applying the ideas in the case where the excited state of the first two-level system is a molecular D_2 at a site in a metal deuteride, and where the ground state is ^{4}He located at the same site. The oscillator in this model stands in for a highly excited phonon mode that is common to both sites. The second two-level system represents the ground state and an excited state of a receiver nucleus. The excitation transfer process

illustrated by the idealized model here is intended to shed some light on how excitation might be transferred from the D_2 upper state to another nucleus, leaving behind a ^{4}He nucleus. Such a mechanism would violate local energy and momentum conservation in the $D_2/^4$He system, although overall energy and momentum conservation within the coupled oscillator and two-site nuclear system would be maintained. We note that in this kind of transfer process, the excitation energy is not transferred to the oscillator (in contrast to the assertions made by the reviewers at the 2004 DoE review). Unfortunately, the excitation transfer rates associated with this idealized model are much too slow to be relevant to excess heat production, so we will need to modify the model in some way to strengthen the effect.

4. Anomalous energy exchange

Were we to succeed in transferring the excitation from the $D_2/^4$He system to produce excitation in a nucleus at another site, it would be reasonable to expect that this excited nucleus might decay, resulting in energetic charged particles as a consequence of local energy and momentum conservation. If so, then the system would proceed to express the reaction energy from the first site as energetic decay products from the second site, in contrast to observations. We might propose that another coherent excitation transfer process occurs prior to such an incoherent decay process, as we have in our previous ICCF conference proceedings papers. However, in such a proposal we still would not have faced up to the basic problem: we need to find a mechanism to dump the energy that does not involve decay via energetic particles. In our previous ICCF papers, we proposed that sequential excitation transfers from one site to another could eventually transfer energy to the oscillator, as long as a small amount of energy exchange occurred in association with each transfer process.

To shed light on this, we have studied idealized models for this effect, which we will term ``anomalous energy exchange." As it turns out, the simplest version of the problem is one that is well studied in the literature, in the context of the Bloch-Siegert resonances [16] associated with the Rabi Hamiltonian [17] and spin-boson Hamiltonian [18]. In both models, one finds dynamical transitions directly between states in which one unit of two-level system excitation is exchanged for a large number of oscillator quanta. What is interesting in these models relative to our previous discussion is that excitation transfers from site to other sites are not required in order for the effect to occur. Only a single two-level system interacting with an oscillator is required.

5. Idealized model for anomalous energy exchange

The simplest model that exhibits the effect is the basic spin-boson model, given here by

$$\hat{H} = \Delta E \frac{\hat{s}_z}{\hbar} + \hbar\omega_0 \hat{a}^\dagger \hat{a} + V\left(\hat{a}^\dagger + \hat{a}\right)\frac{2\hat{s}_x}{\hbar} \tag{8}$$

Once again we are interested in the model when the oscillator energy $\hbar\omega_0$ is much less than the two-level system energy ΔE. The energy levels are given approximately by

$$E_{m,n} = \Delta E\left(g\right)m + \hbar\omega_0 n \tag{9}$$

A resonance occurs when the dressed transition energy $\Delta E(g)$ is matched to an odd number of oscillator quanta

$$\Delta E(g) = \Delta n \hbar \omega_0 \tag{10}$$

When this occurs, the system can undergo coherent Rabi oscillations between states in which a two-level system quantum is exchanged for many oscillator quanta.

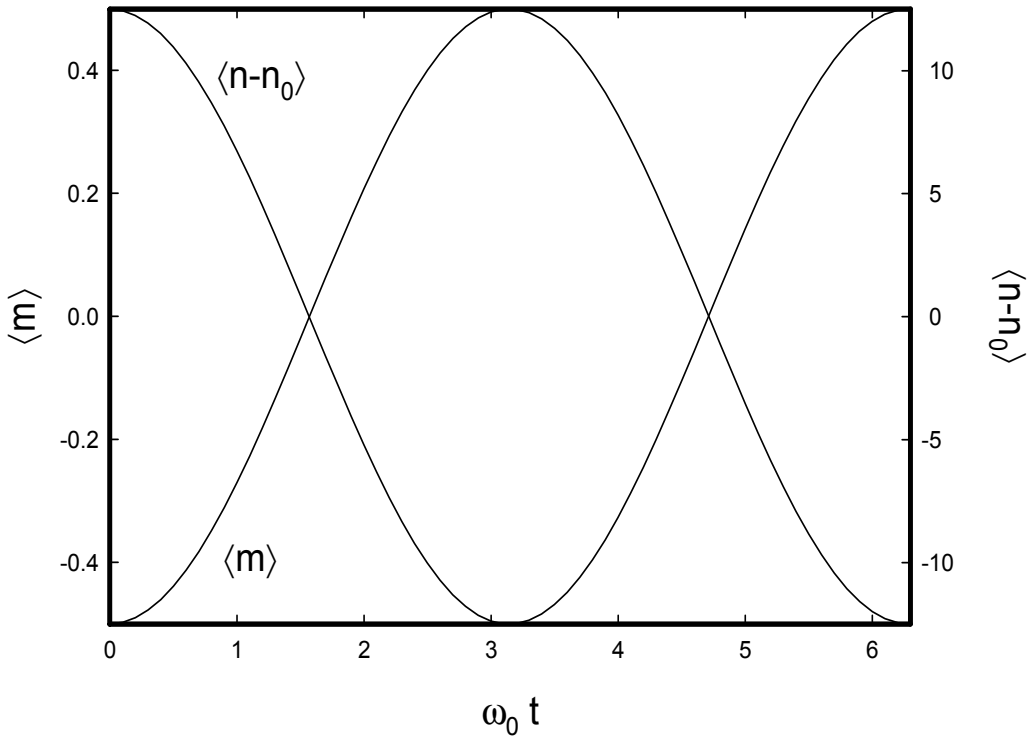

Figure 2. *Expectation values* $\langle m \rangle$ *and* $\langle n - n_0 \rangle$ *for an example in which the dressed two-level system energy* $\Delta E(g)$ *is matched to 25* $\hbar\omega_0$. *Here,* $\omega_0 = |U|/2\hbar$.

5.1 Dynamics

At resonance, the dynamics can be oscillatory with a probability for the system initialized in one of the resonant states given by

$$p(t) = \cos^2 \frac{|U|t}{\hbar} \tag{11}$$

where U is the associated coupling matrix element. This corresponds to the situation illustrated in Figure 2.

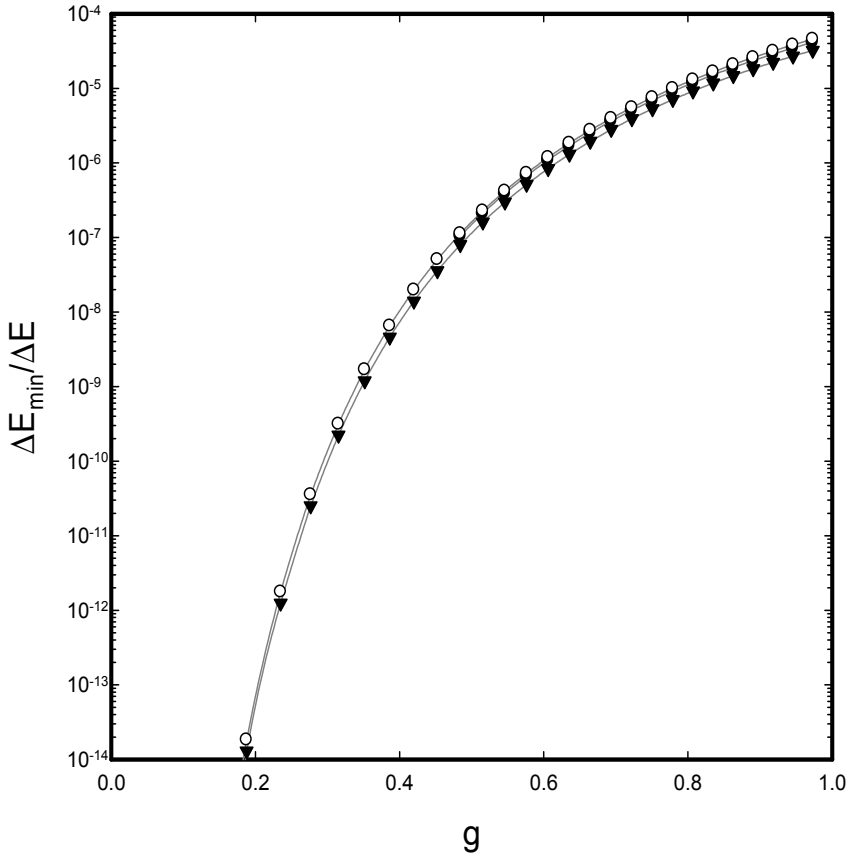

Figure 3. *Energy separation* $E_{\min} = 2|U|$ *at resonance as a function of the dimensionless coupling strength g for the case* $\Delta E = 31\hbar\omega_0$ *for* $n = 10^8$. *Exact results from solution of* $\hat{H}$ *problem – solid circles; WKB approximation - open circles; analytic result - solid triangles. The WKB result lies nearly on top of the exact result. The rightmost resonance is for* $\Delta E(g) = 85\hbar\omega_0$.

We have found that this coupling matrix can be approximated using an analytic WKB approximation as

$$U = i\frac{\hbar\omega_0}{\pi}\int_{-\sqrt{\varepsilon}}^{\sqrt{\varepsilon}} \frac{\cos\left\{\dfrac{\Delta E}{\hbar\omega_0}\displaystyle\int_0^y \sqrt{\dfrac{1+8V^2\left(y'\right)^2/\Delta E^2}{\varepsilon-\left(y'\right)^2}}\,dy'\right\}}{1+8\left(\dfrac{Vy}{\Delta E}\right)}\,dy \tag{12}$$

where $\varepsilon = 2n+1$. This result is an analytic large *n* WKB approximation to the results discussed in [19]. In Figure 3 we show the level splitting at resonance from a direct calculation of the spin-boson Hamiltonian [Equation (8)], from a WKB approximation of the result discussed in [19], and from the analytic large *n* WKB approximation given here.

5.2 Discussion

The basic spin-boson model exhibits an anomalous energy exchange something like what we need for describing excess heat in the Fleischmann-Pons experiment. To see the effect in the spin-boson model, a precise resonance must be present. In the rotated version of the problem, the multi-quantum transition can be described using a first-order coupling with a complicated matrix element, as discussed in [19]. This allows us to think of transitions where many quanta are exchanged in terms similar to that involving single quantum exchange.

The anomalous energy exchange effect itself in this model is relatively weak, requiring moderate to strong coupling, and producing a coherent rate that becomes slower the more quanta are exchanged. Although this kind of anomalous coupling qualitatively similar to what we need to convert an MeV quantum into a large number of low energy quanta, such models are simply not strong enough to lead to relevant conversion rates for the excess heat problem. Once again, we need to enhance the effect in order to develop models relevant to excess heat production.

6. Excitation transfer followed by anomalous energy exchange

In the discussion above, we see that very simple spin-boson models exhibit excitation transfer effects as well as anomalous energy coupling. Both are required to account for energy production without commensurate energetic particle emission in the Fleischmann-Pons experiment. The question arises then whether it is possible to develop a spin-boson type model which illustrates excitation transfer from one two-level system to another, followed by anomalous energy exchange between the second two-level system and the oscillator. Recognizing that the simple spin-boson models are too weak to account quantitatively for the excess heat effect, it is nevertheless interesting to develop such a model in the simpler system as we can obtain analytic solutions which can shed light on the mechanism under consideration.

6.1 Idealized model

Once again we consider a pair of two-level systems coupled to a common oscillator, using the same Hamiltonian as considered above:

$$\hat{H} = \Delta E_1 \frac{\hat{s}_z^{(1)}}{\hbar} + \Delta E_2 \frac{\hat{s}_z^{(2)}}{\hbar} + \hbar\omega_0 \hat{a}^\dagger \hat{a} + V_1\left(\hat{a}^\dagger + \hat{a}\right)\frac{2\hat{s}_x^{(1)}}{\hbar} + V_2\left(\hat{a}^\dagger + \hat{a}\right)\frac{2\hat{s}_x^{(2)}}{\hbar}$$

It is possible to select three states in the rotated version of the problem that are degenerate in the absence of the coupling responsible for excitation transfer and in the absence of coupling responsible for anomalous energy exchange [4]. The energy levels in this case are given approximately by

$$E_{n,m_1m_2} = \Delta E_1\left(g_1\right)m_1 + \Delta E_2\left(g_2\right)m_2 + \hbar\omega_0 n$$

6.2 Resonance conditions

We consider three states with energy eigenvalues in the rotated frame given by

$$E_1 = \frac{\Delta E_1(g_1)}{2} - \frac{\Delta E_2(g_2)}{2} + \hbar\omega_0(n_0 + \delta n)$$
$$E_2 = \frac{\Delta E_1(g_1)}{2} - \frac{\Delta E_2(g_2)}{2} + \hbar\omega_0 n_0$$
$$E_3 = \frac{\Delta E_1(g_1)}{2} - \frac{\Delta E_2(g_2)}{2} + \hbar\omega_0(n_0 + \Delta n) \tag{13}$$

A transition between the first state and the second state is an excitation transfer step in which the first two-level system is lowered and the second raised. This process is resonant when

$$\Delta E_2(g_2) = \Delta E_1(g_1) + \delta n\hbar\omega_0$$

A transition between the second state and the third state is an anomalous energy exchange step in which the second two-level excitation is exchanged for a large number of oscillator quanta. This process is resonant when

$$\Delta E_2(g_2) = \Delta n\hbar\omega_0$$

6.3 Dynamics

The system dynamics when both transitions are near resonance can be described using a three-state model of the form

$$\psi(t) = c_1(t)\phi_1 + c_2(t)\phi_2 + c_3(t)\phi_3 \tag{14}$$

where the $c_j(t)$ are expansion coefficients, and where the ϕ_j are the basis states in the rotate frame that correspond to the three dressed energies given above. The dynamics are described by

$$i\hbar\frac{d}{dt}\begin{pmatrix} c_1(t) \\ c_2(t) \\ c_3(t) \end{pmatrix} = \begin{pmatrix} E_1 & V_{12} & 0 \\ V_{21} & E_2 & V_{23} \\ 0 & V_{32} & E_3 \end{pmatrix}\begin{pmatrix} c_1(t) \\ c_2(t) \\ c_3(t) \end{pmatrix} \tag{15}$$

where the V_{jk} are matrix elements similar to those discussed in the previous sections.

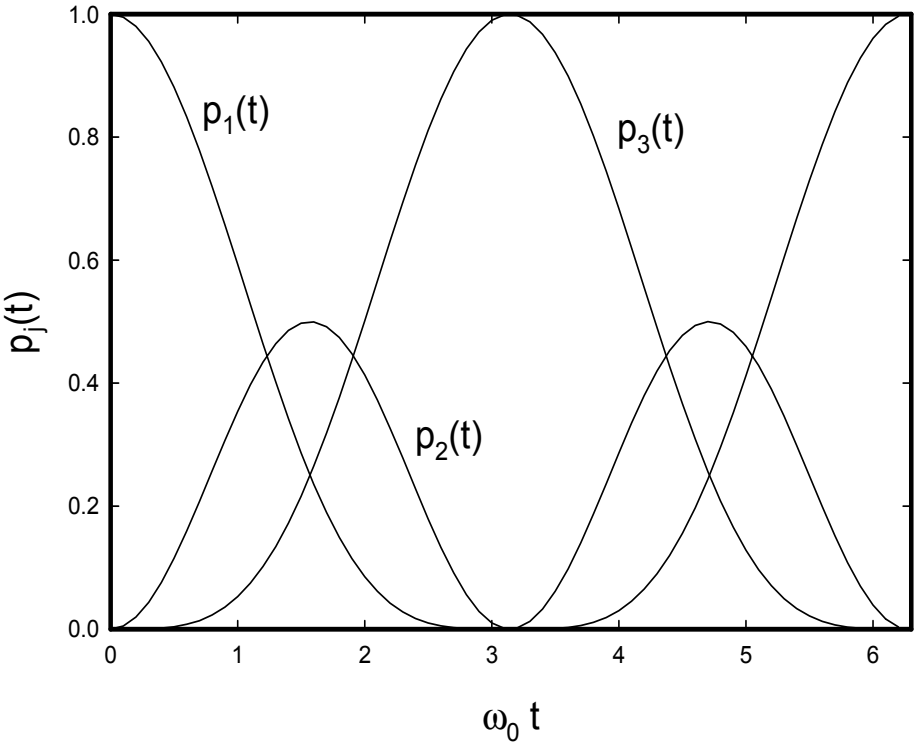

Figure 4. *Probabilities for excitation transfer followed by energy exchange under conditions where all states are degenerate in the absence of coupling, and when the coupling strengths are matched. In the first state (with probability p_1), only the first two-level system is excited; in the second (with probability p_2), only the second two-level system is excited; and in the third (with probability p_3), neither two-level system is excited. The frequency ω_0 in this case is $\sqrt{2}V/\hbar$.*

In general, the three-state dynamics are very complicated, and we would spend much effort seeking to explain the significance. Perhaps more interesting to us in regard to this discussion is the special case in which the levels are degenerate and the coupling matrix elements equal in magnitude. In this special case, the resulting probabilities are given by

$$p_1(t) = \left[\frac{1+\cos\left(\sqrt{2}|V|t/\hbar\right)}{2}\right]^2$$

$$p_2(t) = \left[\frac{\sin\left(\sqrt{2}|V|t/\hbar\right)}{\sqrt{2}}\right]^2$$

$$p_3(t) = \left[\frac{1-\cos\left(\sqrt{2}|V|t/\hbar\right)}{2}\right]^2 \qquad (16)$$

where

$$\left|V_{12}\right| = \left|V_{32}\right| = \left|V_{23}\right| = \left|V_{32}\right| = \left|V\right|$$

Results are illustrated in Figure 4 for this special case illustrating the analytic solutions. In this model, the system first undergoes an excitation transfer step, and then an energy exchange step. The associated dynamics are coherent throughout, and the system continues cycling back and forth between the three states periodically. This is discussed further in [4], in which model parameters are given for a specific case that was found to work this way.

6.2 Discussion

We have succeeded in developing idealized models based on spin-boson type Hamiltonians which exhibit coherent excitation transfer and anomalous energy exchange effects, similar to what is required for a description of the excess heat effect. In this model, the molecular D_2 state at a vacancy site inside the metal deuteride is represented by the upper state of the first two-level system, and the product ^{4}He state at the same site is represented by the lower state. In this idealized model energy conversion itself occurs through the interaction of only a single receiver-side nucleus (as represented by the second two-level system) interacting with the oscillator. There are no site-to-site excitation transfers in this simplified model, yet efficient energy exchange occurs.

7. Loss

We have discussed previously that the augmentation of the idealized spin-boson models leads to a dramatic increase in the excitation transfer and anomalous energy exchange rates (for example, see [4]). The increase is sufficiently large that the resulting rates appear to be relevant to excess heat production.

7.1 Idealized model including loss and Dicke effects

The simplest model which includes these effects, along with Dicke enhancement effects, is given formally by the following Hamiltonian

$$\hat{H} = \Delta E_1 \frac{\hat{S}_z^{(1)}}{\hbar} + \Delta E_2 \frac{\hat{S}_z^{(2)}}{\hbar} + \hbar\omega_0 \hat{a}^\dagger \hat{a} - i\frac{\hbar}{2}\hat{\Gamma}(E) + V_1\left(\hat{a}^\dagger + \hat{a}\right)\frac{2\hat{S}_x^{(1)}}{\hbar} + V_2\left(\hat{a}^\dagger + \hat{a}\right)\frac{2\hat{S}_x^{(1)}}{\hbar} \quad (17)$$

Here, we consider matched sets of two-level systems (implemented through the many-pseudospin operators $\hat{S}_j$, whereas we used single pseudospin operators $\hat{s}_j$ above) for the donor (D_2/^{4}He) two-level systems and receiver two-level systems. On the one hand, such a model includes new effects associated with sequential excitation transfer and anomalous energy exchange steps, which is of interest in addressing the production of macroscopic amounts of energy. On the other hand, this kind of model also describes cooperative effects between reactions at different sites, under the simplifying assumption that states and interactions at each site are equivalent.

7.2 Implementation of loss

Included also in this model is a loss term $-i\hbar\hat{\Gamma}(E)/2$ that is intended to capture energetic decays associated with the oscillator (this is discussed more fully in [13]). It is reasonable to assume that the excited states of the two-level systems will have decay channels available. For example, the two deuterons can fuse to make energetic t+p and n+^{3}He. One would expect decay channels to be accessible in excited states of receiver nuclei as well. However, neither of these processes impacts the excitation transfer and anomalous energy exchange rates, other than to damp both processes due to loss of excitation. It can be shown directly that the incoherent decay channels associated with the D_2/^{4}He two-level system are not competitive with the coherent process under discussion, since the associated decay rates are unchanged from the situation in the absence of the coherent process (and are therefore very small). The situation on the receiver side is less clear at present, since much less is known from experiment about which nuclei and states are involved.

However, a different loss mechanism can have an enormous impact on the excitation transfer and anomalous energy exchange rates. If there occur strong loss channels for the oscillator in the vicinity of the two-level system transition energy, then the dynamics are altered fundamentally. An example of such a process might be a lattice-induced disintegration process, in which a constituent nucleus of the lattice fissions due in the course of transfer or exchange processes. The reason that the rates are impacted is because the rates for both processes are significantly reduced over the available coupling strength due to the interaction terms present in the Hamiltonian due to destructive interference effects. Oscillator loss channels can remove this interference, leading to a dramatic acceleration in both rates.

7.3 Interference effects in excitation transfer

The impact of loss on the destructive interference can be seen most readily in the case of excitation transfer in the weak coupling regime. In the case of excitation transfer between two individual two-level systems, six states contribute at lowest order in perturbation theory. There are initial and final states (states 1 and 6), in which the excitation of the two-level systems is switched, but where the oscillator excitation will be assumed unchanged. Then there are four off-resonant intermediate states in which both two-level systems are unexcited (states 2 and 3), or both excited (states 4 and 5), with oscillator excitation increased or decreased by one. If the intermediate states are eliminated, then the effective coupling between the initial and final states is [4]

$$V_{16}(E) = V_1 V_2 \left[\frac{n}{E - H_2 + i\hbar\Gamma/2} + \frac{n+1}{E - H_3 + i\hbar\Gamma/2} + \frac{n}{e - H_4} + \frac{n+1}{E - H_5} \right] \quad (18)$$

Since states 2 and 3 have energies much less than the available energy E, oscillator decay channels are accessible, which is reflected here by the appearance of loss terms associated with their contributions. Since states 4 and 5 have energies much greater than the available energy E, the oscillator decay channels are not accessible.

In the absence of loss ($\Gamma = 0$), strong interference occurs between the contributions from the different off-resonant states. In this case, the effective interaction reduces to

$$V_{16}(E) \to \frac{V_1 V_2 \hbar\omega_0}{\left[\Delta E(g)\right]^2 - (\hbar\omega_0)^2} \quad \text{(no loss)} \tag{19}$$

This model can reproduce the excitation transfer results in the $\delta n = 0$ limit described earlier. On the other hand, if the loss is very strong, then the interference is removed. In the limit of infinite loss, the effective interaction becomes

$$V_{16}(E) \to \frac{2V_1 V_2 \Delta E(g) n}{\left[\Delta E(g)\right]^2 - (\hbar\omega_0)^2} \quad \text{(infinite loss)} \tag{20}$$

The effective interaction increases between these two limits by a factor of

$$\frac{\Delta E(g)}{\hbar\omega_0} n$$

This is an enormous effect. We see that the augmentation of the model with loss dramatically impacts the rate of excitation transfer.

7.4 Strong coupling limit

In [13] we examined the strong coupling limit of the lossy model, and developed estimates for dynamical rates. In light of the discussion above, it is perhaps not surprising that the maximum possible rates are closely associated with the interaction terms in the model.

For example, on the receiver side the maximum rate for phonon exchange is

$$\left[\frac{dn}{dt}\right]_{\max} = \frac{V_2\sqrt{n}}{\hbar}\left(2\sqrt{S_2^2 - M_2^2}\right) \tag{21}$$

where S_2 and M_2 are receiver-side Dicke numbers. In essence, if there were only a single two-level system on the receiver side, this maximum anomalous energy transfer rate corresponds to the exchange of an oscillator quantum in association with each individual transition. If there are many receiver-side ground state nuclei, and only a few excited state receiver-side nuclei, then the rate will be proportional to the square root factor in the expression, which will evaluate roughly to the square root of the product of ground state and excited state nuclei of the receiver nuclei.

In the case of excitation transfer, the maximum rate depends on the coupling on both the donor side and the receiver side. However, since the donor side (D_2/^{4}He) involves a hindered matrix element (since the Coulomb interaction produces a dramatic reduction in the overlap between the molecular D_2 state and the ^{4}He state), it seems reasonable to examine the limit in which this part of the process is rate limiting. In this case, the maximum excitation transfer rate is

$$\left[\frac{d\left(M_1 - M_2\right)}{dt}\right]_{\max} = \frac{V_1\sqrt{n}}{\hbar}\left(4\sqrt{S_1^2 - M_1^2}\right) \tag{22}$$

In essence, the model indicates that when loss is present, excitation transfer can proceed at the fastest rate that coherent transitions can occur. It is this rate which can be sufficiently fast to be relevant to excess heat production in the Fleischmann-Pons experiment.

8. Coupling matrix element

The evaluation and use of this model depends on the strength of the coupling between nuclei and phonons. We have recently developed a formalism with which detailed calculation can be made [20]. In that reference, we speculated that the coupling between molecular D_2 states and the ^{4}He ground state could take place indirectly through n+^{3}He channels. However, more recently we have found a direct coupling that will be dominant. A detailed calculation of this matrix element is in process, and will be reported on in the future. Nevertheless, some features have become apparent already in the process.

8.1 Compressional phonon mode interactions

It is clear that coupling occurs in the case of compressional phonon modes. Transverse phonon modes will participate only weakly if at all. This may be connected with observations by the ENEA Frascati group [21] that excess heat bursts resulting from laser stimulation occurs for TM polarization (which drive compressional surface plasmon modes [22]), and not for TE polarization. It may also be consistent with recent laser beating experiments reported by Letts et al [23], in which a response was observed at beat frequencies in the THz range within the optical phonon band, once again where TM polarization is required. At issue is the question of which modes are participating. Optical phonon modes would be advantageous for anomalous energy exchange since the frequency is greater; whereas excitation transfer could involve lower energy modes (there being no obvious requirement that both processes need be mediated by a single mode).

It seems clear also that the coupling will be strongest in the case of molecular D_2 S=2 (nuclear spin) states. This may have a connection with some experiments (such as [23]) in which the presence of a magnetic field seems to influence the effect.

8.2 Estimate and screening effects

Nevertheless, it is possible to estimate the interaction matrix element crudely based on elementary considerations. For example, the deuterons must tunnel through the Coulomb barrier to interact, so we expect a Gamow factor. Similarly, there is a significant volume change between localization of the deuterons in molecular D_2 and localization at the nuclear scale. Keeping these factors in mind, we would expect the matrix element to be on the order of

$$V_1\sqrt{n} \to M_{fi} \approx \sqrt{\frac{v_{nuc}}{v_{mol}}}e^{-G_u} \tag{23}$$

Here, M_{fi} is the matrix element for a strong-force mediated transition between a molecular D_2 state and ^{4}He state involving phonon exchange; v_{nuc} is a characteristic nuclear volume and v_{mol} is the volume associated with the relative coordinate between the two-deuterons in the molecular D_2 state; G is the Gamow factor associated with tunneling through the Coulomb barrier; the parameter u is the residual interaction strength which is expected to be of order 1 MeV.

In the case of molecular D_2 in vacuum, this matrix element produces reaction rates at the femtowatt level or less for reasonable assumptions about the number of D_2 molecules that participate. Based on the beam experiments of [6-8] we know that screening is important in metal deuterides. In [13] we estimated that a screening energy of about 115 eV would be required to obtain agreement between this model and excess power in the Fleischmann-Pons experiment, assuming that the molecular D_2 species were constrained to be in the outer part of the cathode at sites with single host atom vacancies.

9. Conclusions

Any explanation of excess heat in the Fleischmann-Pons experiment must confront the absence of energetic particles commensurate with excess energy production. The implication is that whatever process is responsible for excess heat violates local energy and momentum conservation. The experimental observation of ^{4}He as an ash with a reaction Q-value of 24 MeV points toward reaction mechanisms involving deuteron-deuteron interactions that result in ^{4}He. Based on these considerations, we have proposed and studied reaction mechanisms in which excitation transfer stabilizes ^{4}He at the initial reaction site (violating local energy and momentum conservation), with the large energy quantum of the reaction converted to lower energy quanta through anomalous energy exchange.

We have examined idealized spin-boson models to illustrate the off-resonant excitation transfer and anomalous energy exchange effects. The simplest possible models that could possibly exhibit such effects show them clearly, as we have presented here. It is possible to develop spin-boson type models in which excitation transfer is followed by matched anomalous energy exchange, in which we can solve analytically for the associated coherent dynamics. These models make clear that the required mechanisms exist and can be studied independently or together at our leisure. The associated dynamics in these examples is coherent, and we are able to treat excitation transfer and anomalous energy exchange through moderately complicated first-order matrix elements in a rotated version of the problem.

Although we learn much from the idealized models, they are simply not strong enough to account for the excess heat effect, since the associated dynamical rates are too slow. The reason that the rates are slow is that destructive interference occurs in both cases. Models that include oscillator loss at the two-level transition energy have greatly enhanced rates of both excitation transfer and anomalous energy exchange due to the elimination of this destructive interference. Such models are capable of predicting reaction rates in the range of observations based on crude estimates for the coupling matrix element, given significant screening (but screening which is modest in comparison to low energy deuteron-deuteron fusion experiments at low energy).

References

1. M. Fleischmann, S. Pons and M. Hawkins, *J. Electroanal Chem*., **201**, p.301 (1989); Errata, **263** p. 187 (1990). See also M. Fleischmann, S. Pons, M.W. Anderson, L.J. Li and M. Hawkins, *J. Electroanal. Chem*., **287**, p. 293 (1990).
2. C. G. Darwin, *Phil. Mag*. **27** 499 (1914).
3. P. M. S. Blackett, *Proc. Royal Soc. London* **A107** 349 (1925).
4. P. L. Hagelstein and I. U. Chaudhary, to appear in an ACS topical volume on low energy nuclear reactions, edited by J. Marwan and S. Krivit, in press.
5. P.L. Hagelstein, M.C.H. McKubre, D.J. Nagel, T.A. Chubb, and R.J. Hekman, *Condensed Matter Nuclear Science, Proceedings of the 11th International Conference on Cold Fusion*, Marseilles, France, Nov. 2004, ed. J.P. Biberian, World Scientific, p. 23 (2006).
6. F. Raiola, L. Gang, C. Bonomo, G. Gyurky, M. Aliotta, H. W. Becker, R. Bonetti, C. Broggini, P. Corvisiero, A. D'Onofrio, Z. Fulop, G. Gervino, L. Gianella, M. Junker, P. Prati, V. Roca, C. Rolfs, M. Romano, E. Somorjai, F. Streider, F. Terrasi, G. Fiorentini, K. Langanke, and J. Winter, *Eur. Phys. J. A* **19** 283 (2004).
7. C. Rolfs, *Prog. Theoretical Phys. Suppl*. **154** 373 (2004).
8. F. Raiola, B. Buchard, Z. Fulop, G. Gyurky, S. Zeng, J. Cruz, A. Di Leva, B. Limata, M. Fonseca, H. Luis, M. Aliotta, H. W. Becker, C. Broggini, A. D'Onofrio, L. Gianlanella, G. Imbriani, A. P. Jesus, M. Junker, J. P. Ribereiro, V. Roca, C. Rolfs, M. Romano, E. Somorjai, F. Streider, and F. Terrasi, *J. Phys. G: Nucl. Phys*. **31** 1141 (2005).
9. Th. Forster, *Discuss. Faraday Soc*. **27** 7 (1959).
10. *Resonance Energy Transfer*, edited by D. L. Andrews and A. A. Demidov, John Wiley and sons, New York (1999).
11. G. Juzeliunas and D. L. Andrews, *Phys. Rev. B* **50** 13371 (1994).
12. T. Vorrath and T. Brandes, *Phys. Rev. B* **68** 035309 (2003).
13. P. L. Hagelstein and I. U. Chaudhary, ArXiV:cond-mat/0612306.
14. P. L. Hagelstein and I. U. Chaudhary, *Current Trends in International Fusion Research – Proceedings of the Seventh Symposium*. Edited by Emilio Panarella and Roger Raman. NRC Research Press, National Research Council of Canada, Ottowa, (2007).
15. P. L. Hagelstein and I. U. Chaudhary, ArXiV:0709.1958.
16. F. Bloch and A. Siegert *Phys. Rev*. **57** 522 (1940).
17. J. Shirley *Phys. Rev*. **138**, B979 (1965).
18. Cohen-Tannoudji C, Dupont-Roc J, and Fabre C, *J. Phys. B* **6** L214 (1973).
19. P. L. Hagelstein and I. U. Chaudhary, ArXiV:0709.1961.
20. I.U. Chaudhary and P. L. Hagelstein, ArXiV:cond-mat/0606585.
21. M. Apicella, E. Castagna, L. Capobianco, L. D'Aulerio, G. Mazzitelli, F. Sarto, A. Rosada, E. Santoro, V. Violante, M. McKubre, F. Tanzella, C. Sibilia *Proceedings of the 12th International Conference on Cold Fusion*, edited by A. Takahashi, K.-I. Ota, and Y. Iwamura, page 117 (2005).
22. E. Castagna, C. Sibilia, S. Paoloni, V. Violante, and F. Sarto, *Proceedings of the 12th International Conference on Cold Fusion*, edited by A. Takahashi, K.-I. Ota, and Y. Iwamura, page 156 (2005).
23. D. Letts, D. Cravens, and P. L. Hagelstein, to appear in an ACS topical volume on low energy nuclear reactions, edited by J. Marwan and S. Krivit, in press.

ROLES OF APPROXIMATE SYMMETRY AND FINITE SIZE IN THE QUANTUM ELECTRODYNAMICS (QED) OF DEUTERON (D)-D FUSION IN PDD

Scott R. Chubb

Research Systems Inc., 9822 Pebble Weigh Ct., Burke, VA

Abstract

Basic ideas about how resonant electromagnetic interactions (EMI's) can take place in finite solids are reviewed. These ideas not only provide a basis for conventional, electron energy band theory (which explains charge and heat transport in solids), but they also explain how through finite size effects, when deuterons (d's) occupy energy band states in PdD, it is possible to create many of the kinds of effects envisioned by Giuliano Preparata. In particular, the boundary of a lattice is never known, prior to some form of measurement. Giuliano Preparata implicitly recognized this fact and suggested boundary effects could be quite important. In fact, a known phenomenon, initially identified by Felix Bloch, commonly referred to as a "Bloch Oscillation," does approach the kind of very low frequency, plasma oscillation, suggested by Giuliano Preparata. When the additional possibility of an ordered lattice being allowed to accelerate is included, a form of Galilean invariance with respect to rigid translations can take place, provided collisions are stifled. The semi-classical limit, of the resulting dynamics, leads to an intuitive picture that is strikingly similar to the one suggested by Giuliano Preparata. One important difference is that the underlying limit, in which collisions are stifled, provides a new way for tunneling to take place, through a variant of "Zener tunneling" (involving ions, as opposed to electrons). The theory predicts that the orientation of the external fields in the SPAWAR protocol[1,2] has direct bearing on the emission of high-energy particles and that nano-scale particles, of a particular size, provide an optimal environment for initiating Low Energy Nuclear Reactions (LENR) in PdD.

Introduction

In Cold Fusion (CF), a variant of the helium-4 (α particle) producing fusion reaction (which rarely occurs in conventional fusion) appears to be dominant. Most nuclear physicists assume the conventional form of this reaction occurs infrequently because it creates considerably more energy than the other fusion reactions and that the most frequent reactions minimize the amount of energy that is released. This assumption is wrong. It does not include subtleties involving electromagnetic interaction (EMI). It does apply when deuterons (d's) have high velocity, initially, and collide at a point, provided they are not "prepared" through EMI, in a particular way. Far from the reaction, for the $d+d \rightarrow \alpha + \gamma$ reaction to take place, particular selection rules apply, involving total d-d spin and angular momentum. In a solid, richer forms of time-dependent EMI can take place through non-linear coupling between photons, electrons, their spins, and other charged particles. Further complicating the problem is the fact

that the γ ray that one would expect to be present in the normal helium-4 (α-particle) producing reaction can appear and disappear through adsorption and emission by electrons in the associated environment, that can (and must, in most situations) result in "parametric down-conversion" (PDC) processes[3], even in relatively small crystals.

Through PDC processes, the γ ray associated with the conventional $d+d\rightarrow \alpha + \gamma$ reaction, in principle, can be converted into many different optical, infra-red, microwave, or lower frequency forms of radiation, coherently or incoherently, and that the "α" particle (henceforth referred to as helium-4, when it has lower energy<1000 eV, but as an "α" particle when its energy is greater than this) can be "emitted" with negligibly small energy. Nothing, in the relevant physics of EMI forbids this kind of thing. It can happen when very non-linear forms of "impedance matching" take place. The High-Energy community physicists, who have been viewed as being experts on nuclear effects and have judged and pre-judged whether or not the kinds of effects associated with CF can take place, have not considered this possibility. For this reason, they simply are not "experts" of the relevant physics. In particular, charge need not be conserved locally when it is impossible to measure either the charge or current. When this occurs, a form of broken gauge symmetry can take place (resulting from finite size effects), in which portions of the "lattice" can appear to not conserve charge, in a particular region of space, when many charged particles move in lock-step, a limit that is contrary to the situation in which charge is assumed to be conserved locally, and changes in EMI in response to changes in the charge, are assumed to preserve gauge symmetry, locally[4].

At the boundaries of solids, these kinds of effects can occur in situations in which the associated momentum and energy can grow with increasing time. In particularly unusual situations, associated with PdD_x , as $x\rightarrow 1$, fluctuations in charge (of deuterons and electrons into and away from the lattice for values of x immediately above and below the value x=1) can cause this kind of effect to occur because the net electron-deuteron charge that is allowed to enter the lattice, locally, can increase (when x is above the value x=1) and decrease (when x is below the value x=1), as a consequence of the strongly anti-bonding behavior of the electrons, and the associated electron, energy band states (near the Fermi energy) in PdD. As a result, in a finite metallic PdD lattice, a form of "preparation" can take place, involving, effectively, a form of dissociation between the nucleus of each D from its electron. This can occur, provided the fluctuations in charge into and away from the lattice are sufficiently small, over a sufficiently long period of time. This can result in possible forms of nuclear reaction.

This kind of effect can alter possible forms of nuclear fusion in PdD because : 1. Since deuterium atoms (D's) do not have core electrons, their nuclei (d's) intrinsically have the potential to interact through EMI's involving each other and the host electrons without being required to move rapidly in order for the separation between deuterons to be reduced (which is not the case in situations involving atoms that have more than one electron); 2. It is known that EMI effects are required in the one form of nuclear fusion reaction, associated with the $d+d\rightarrow \alpha + \gamma$, that seems to be important in CF related phenomena; and 3. $d + d \rightarrow$helium-4 + 23.8 MeV reactions (in a host material) are allowed to occur, provided momentum is allowed to change sufficiently rapidly (even in a quasi-discontinuous manner, for example, through wave function cusps [5]).

An important point is that even classically, when a particle has mass m, velocity $\vec{v}$, charge q, and momentum $\vec{p}$, the relationship between these variables is $m\vec{v} = \vec{p} - \frac{e}{c}\vec{A}$, as opposed to the situation associated with a static, time-independent Coulomb potential situation, where $m\vec{v} = \vec{p}$. (Here, $\vec{A}$, which is a non-local function, is the vector potential[4]; as an operator, in

2^{nd} quantized form, it is defined to create or destroy a photon.) In particular, in the more general situation associated with the last two d+d reactions, non-local effects are required. In any nano-scale PdD "crystal," as opposed to a static, electrostatic, "Coulomb" barrier, being involved in d+d→helium-4 (or α-particle) reactions, for example, a more sophisticated, time-dependent, quantum electro-dynamic, "QED," barrier is probably involved. Giuliano Preparata [6,7] recognized this possibility and that the barrier that prevents fusion in free space should be very different in solids, but superficially, it appeared that he relied on an over-simplified model, in which interactions with charged matter were treated semi-classically, through a modified form of free particle interaction.

In fact, in a more realistic theory [8-10], based on a generalization of the conventional semi-classical model of (electron [11], and ion [5,12]) energy band theory, the simplest approximation of the most relevant picture, in the semi-classical limit, shares many of the intuitive features of the plasma picture suggested by Giuliano Preparata. Important differences exist. Giuliano Preparata assumed well-defined boundaries exist in a solid, so that the lattice could be treated as being stationary with respect to its external environment. In a real solid, it is never possible to determine precisely where the lattice begins and ends, where its boundaries are located, and whether or not it is in motion. The generalized energy band picture that applies to finite lattices is considerably richer because it includes quantum mechanical effects that are implied by these facts.

This paper is organized in the following way. In the next section, details about known results associated with the importance of electromagnetic interactions (EMI's), that are not widely appreciated and have been neglected, by nuclear physicists, in the conventional d+d→α +γ reaction are discussed. As opposed to the sudden impact situation (in which details about the EMI are important only at the location where two d's collide, at a point), as in the Coulomb Barrier approximation, a different situation can occur in resonant EMI, involving an adiabatic process, in which, for example, momentum can be imparted repetitively in such a way that constructive interference occurs between incoming and outgoing matter (deuteron-d) waves. As a consequence of symmetry-related effects, in these resonant EMI's, these kinds of changes in momentum can occur at many locations and in ways that can significantly reinforce the associated effects. An important, resonant effect can take place, in which small amounts of momentum are imparted, repetitively, to an ordered lattice, rigidly. This can, over time, lead to large, non-local changes in momentum. (A useful analogy, concerning how momentum can increase through these kinds of processes involves how the momentum of a tether ball can increase, with time, when a child repetitively hits the tether ball just as its momentum is approaching a minimum.)

In the third and fourth sections, a new, important result is identified, associated with this form of coupling: A particular limit in which Bragg scattering and the resonant coupling of a many-d/many-electron energy band system can systematically become coupled, based on a common theorem, known from solid state physics, but not widely recognized in situations involving EMI-- that single photons and particles, in the limit of perfect resonance (which occurs when energy and momentum are conserved, relative to the center of mass, of the solid), can obey a form of Bloch Symmetry, defined by Bloch's theorem, as it applies in the single particle Schroedinger equation, that is used to describe electrons in periodically ordered solids.

In the fourth (final) section, the semi-classical equations are used to describe the limit in which these resonant effects can lead to d+d LENR reactions in solids, in triggering x-ray emission in smaller crystals, and the emission of high energy particles. The analysis suggests the orientation of static, external, magnetic and/or electric fields, used in experiments, involving the SPAWAR protocol[1,2], can cause the emission of high-energy particles.

Importance of the QED (as Opposed to the Coulomb) barrier in d+d→α+γ

In the conventional picture of nuclear fusion, a static Coulomb barrier is used to explain how same-charged, d's can have appreciable overlap. This limit makes good sense when the initial and final particles have high velocity, and the relevant quantum mechanics does not require that details about the time dependence of the EMI be included, when the d's are far apart.

In this conventional picture, d's at nuclear distances interact entirely through the strong force, the distinction between protons (p's) and neutrons (n's), at the point of nuclear contact, effectively (except through differences in kinetic energy, associated with changes in mass that do not relate to time-dependent EMI effects), is inconsequential, and the normal, intuitive picture that nuclear physicists have applies: The most frequent reactions occur when the amount of nuclear energy that is released is minimized. For this reason, the common intuition is that the least common reaction ($d+d\rightarrow\alpha+\gamma$) occurs infrequently because the energy release (23.8 MeV) is considerably (7 to 8 times) larger than it is in the remaining reactions. In fact, this picture is not right. Important details about time-dependent, EMI effects are responsible for the fact that the $d+d\rightarrow\alpha+\gamma$ reaction occurs rarely (a fact that was not appreciated even by Schwinger[13] and Preparata[6]) have been ignored.

In particular, although $d+d\rightarrow\alpha+\gamma$ rarely occurs, the reverse reaction (the photo-dissociation process: $\gamma+\alpha\rightarrow d+d$) has been studied in detail. It is known, implicitly, as a consequence, as opposed to a static Coulomb Barrier being required (which is widely believed to inhibit nuclear fusion), and the common, intuitive idea that the large energy release that is involved is responsible for the reaction occurring infrequently, an alternative model applies: Selection rules exist and a well-defined, time-dependent EMI transition is involved in the photo-dissociation process. From a detailed comparison between measurements of d-d photo-dissociation cross-section and theoretical studies (based on the Resonant Group Method[14]), the analysis shows quite conclusively that the reaction can be explained, in terms of a well-characterized (quadrupolar) transition, in which the total spin of the final state d's vanishes. The analysis also shows that it is necessary to include the effects of EMI (including implicit rules associated with the fact that the d's must obey Bose Einstein statistics with respect to EMI) on length and time-scales that are far from the location of the photo-dissociation process. Because in QED, the rate of any transition is proportional to the absolute square of the associated transition matrix element, by construction, the theory requires that a transition rate forward in time be equal to the comparable rate for a transition backward in time. This means that the selection rules that apply in the photo-dissociation process, $\gamma+\alpha\rightarrow d+d$, also apply in the $d+d\rightarrow\alpha+\gamma$ reaction. As a consequence, the common intuition, that this reaction does not occur frequently because of the large energy release, is wrong. Elsewhere[15], motivating arguments are presented that imply that the arguments associated with the fact that EMI plays an important role in $d+d\rightarrow\alpha+\gamma$, in free space, also suggest that EMI plays a key role in $d+d\rightarrow{}^4He+23.8MeV$ in solids.

Single Particle Resonant Processes in Solids

Bloch[16] pointed out that for an infinitely-repeating periodic lattice, each energy band eigenvalue ε is also a periodic function with respect to displacements by reciprocal lattice vectors $\vec{G}$[17],

$$\varepsilon(\vec{k}) = \varepsilon(\vec{k} + \vec{G}). \qquad (3)$$

Eq.3 implies forms of degeneracy that have physical consequences that are known to be important at low temperature. However, this degeneracy has been treated in an approximate fashion. Intuitively, one would think that finite size effects must affect this relationship. In fact, this is true. In order to quantify potential deficiencies, associated with this, it is both useful and necessary to examine how conventional textbooks deal with the "apparent" ambiguities and redundancies associated with Eq.3. In particular, the language and "rigor" (or language and lack of "rigor") are associated with the idea that each electron is a "quasi-particle." In the initial picture, each electron is assumed to behave as a wave that is represented using a quasi-particle wave function $\psi_{\varepsilon(\vec{k})}(\vec{r})$, which is assumed to be an eigenstate of a single particle Hamiltonian, has an energy eigenvalue, $\varepsilon(\vec{k})$, and both $\psi_{\varepsilon(\vec{k})}(\vec{r})$ and $\varepsilon(\vec{k})$ are derived from a single particle Schroedinger equation, of the form,

$$\frac{-\hbar^2}{2m}\nabla^2\psi_{\varepsilon(\vec{k})}(\vec{r}) + V(\vec{r})\psi_{\varepsilon(\vec{k})}(\vec{r}) = \varepsilon(\vec{k})\psi_{\varepsilon(\vec{k})}(\vec{r}). \qquad (4)$$

Here, $V(\vec{r}) = V(\vec{r} + \vec{R}_n)$ is a periodic function with respect to spatial displacements defined by discrete Bravais lattice vectors, $\vec{R}_n$. Each of these vectors is constructed from a linear combination of integer (n_α) multiples of primitive vectors $\vec{b}_\alpha$,

$$\vec{R}_n = \sum_{\alpha=1,3} n_\alpha \vec{b}_\alpha \quad ; -N_\alpha \le n_\alpha \le N_\alpha - 1 \,, \qquad (5)$$

and N_α is (traditionally) assumed to be a large number. In particular, when Born-von Karman boundary conditions[20] are imposed, $\psi_{\varepsilon(\vec{k})}(\vec{r})$ is required to be a periodic function with respect to translations $\vec{L}_\alpha = 2N_\alpha \vec{b}_\alpha$

$$\psi_{\varepsilon(\vec{k})}(\vec{r}) = \psi_{\varepsilon(\vec{k})}(\vec{r} + \vec{L}). \qquad (6)$$

Also, since it is assumed that V is periodic with respect to translations, defined by $\vec{R}_n$, $\psi_{\varepsilon(\vec{k})}(\vec{r})$ can be required to be an eigenstate of the translation operator $T(\vec{R}_n)$ associated with the same form of translation; i.e.,

$$T(\vec{R}_n)\psi_{\varepsilon(\vec{k})}(\vec{r}) = \psi_{\varepsilon(\vec{k})}(\vec{r} + \vec{R}_n) = \lambda(\vec{R}_n)\psi_{\varepsilon(\vec{k})}(\vec{r}), \qquad (7)$$

where $\lambda(\vec{R}_n)$ is the eigenvalue associated with the translation. Because repetitively translating the coordinate $\vec{r}$ by $\vec{b}_\alpha$ involves applying the translation operator $T(\vec{b}_\alpha)$ repetitively to $\psi_{\varepsilon(\vec{k})}(\vec{r})$, repetitive multiplications of $\psi_{\varepsilon(\vec{k})}(\vec{r})$ by $T(\vec{b}_\alpha)$ result in repetitive additions of $\vec{b}_\alpha$ to $\vec{r}$. This implies that Eq. 7 can be re-written, in terms of the eigenvalues $\lambda(\vec{R}_n)$ (with R_n defined by Eq. 5), using

$$T(\vec{R}_n)\psi_{\varepsilon(\vec{k})}(\vec{r}) = \psi_{\varepsilon(\vec{k})}(\vec{r} + \vec{R}_n) = \lambda(\vec{b}_1)^{n_1}\lambda(\vec{b}_2)^{n_2}\lambda(\vec{b}_3)^{n_3}\psi_{\varepsilon(\vec{k})}(\vec{r}). \qquad (8)$$

To determine $\lambda(\vec{b}_\alpha)$, the right hand side of Eq. 8 is evaluated in the limit that $\vec{R}_n \Rightarrow \vec{L}_\alpha = 2N_\alpha \vec{b}_\alpha$ and the result is substituted into Eq. 6. Then, it follows that $\lambda(\vec{b}_\alpha)^{2N_\alpha} = 1$. This last expression, in principle, has an infinite number of solutions, defined by the requirement that $2N_\alpha \ln(\lambda(\vec{b}_\alpha)) = 2\pi i m_\alpha$, where. in principle, m_α could be any arbitrary integer, and

$$\lambda(\vec{b}_\alpha) = e^{\frac{\pi i m_\alpha}{N_\alpha}}. \qquad (9)$$

In fact, in a real situation, involving a finite crystal lattice, possible values for m_α only occur that are consistent with the system being in its ground state (GS) or its lowest lying excited states (which in the absence of outside interactions are degenerate with the GS), provided, $-N_\alpha \le m_\alpha \le N_\alpha - 1$, or $-N_\alpha + 1 \le m_\alpha \le N_\alpha$.

Eqs. 8 and 9 are the basis of the single particle form of Bloch's theorem. In particular, after Eq. 9 is substituted into Eq. 8, it follows that

$$\psi_{\varepsilon(\vec{k})}(\vec{r}+\vec{R}_n) = e^{i\pi \sum_{\alpha=1,3} \frac{(n_\alpha m_\alpha)}{N_\alpha}} \psi_{\varepsilon(\vec{k})}(\vec{r}) = e^{i\vec{k}_m \bullet \vec{R}_n} \psi_{\varepsilon(\vec{k})}(\vec{r}), \qquad (10)$$

where

$$\vec{k}_m = \sum_{\alpha=1,3} \frac{m_\alpha \vec{g}_\alpha}{2N_\alpha}, \qquad (11)$$

and the three reciprocal lattice primitive vectors $\vec{g}_\alpha$ are constructed using,

$$\vec{g}_\alpha \bullet \vec{b}_{\alpha'} = 2\pi\delta_\alpha^{\alpha'}.$$

(Here, $\delta_\alpha^{\alpha'}$ is the Kroneker delta symbol, which is defined to equal unity when $\alpha = \alpha'$ and to vanish when $\alpha \ne \alpha'$.)

As alluded to above, although technically the value of m_α can be any arbitrary integer, in the true many-body system, in order for the GS of the system to have minimal overlap with external perturbations, the analysis, outlined here[8-10] requires that $-N_\alpha \le m_\alpha \le N_\alpha - 1$ (or $-N_\alpha + 1 \le m_\alpha \le N_\alpha$) when the Bravais Lattice vector space indices are also restricted to the values, $-N_\alpha \le n_\alpha \le N_\alpha - 1$ (or $-N_\alpha + 1 \le n_\alpha \le N_\alpha$). This result is required in order for the forward and inverse transformations of the discrete Fourier transformation to be defined.

To minimize overlap with the GS, it also is necessary to de-numerate possible states, near to, and including, the GS in finite lattices, provided the lowest energy states of the system preserve a restricted form of translational symmetry[9,10,18,19]. The symmetry occurs as a result of Galilean invariance with respect to rigid translations that can take place during any scattering process that can be viewed as coherently displacing the lattice, by transferring all of the momentum that is imparted during the process directly to the center of mass of the lattice, while preserving periodic order within the lattice. This can take place when rigid displacements occur, in which the center of mass of any sub-lattice, within the lattice, is translated by a Bravais Lattice vector, while the separation between each pair of potentially interacting particles is held fixed. As a result of this kind of symmetry, it is possible to identify potential states that are mutually orthogonal to each other but are degenerate in the limit in which the lattice does not interact with the external environment. Each of these states is defined by one of the values of m_α in Eq. 11.

This symmetry is also responsible for the (implicit) degeneracy that exists associated with the propagation either of photons (Eq. 2) or quasi-particles (Eq.3), in the single particle situation. In particular, the frequency (energy) of the associated photon (particle) does not change in Eq.2 (Eq. 3) within the context of Bragg Scattering (energy band theory) when a reciprocal lattice vector $\vec{G}$ is added to the wave-vector $\vec{k}$. In an infinitely-repeating, stationary lattice, the associated degeneracy is unrestricted and not unique. It occurs when $N_\alpha \le |m_\alpha|$; in particular, this condition holds when $m_\alpha = j_\alpha 2N_\alpha + m_\alpha'$, and $-N_\alpha \le m_\alpha' \le N_\alpha - 1$, in Eq.11. In this situation,

$$\vec{k}_m = \sum_{\alpha=1,3} \frac{m_\alpha \vec{g}_\alpha}{2N_\alpha} = \sum_{\alpha=1,3} j_\alpha \vec{g}_\alpha + \vec{k}_{m'} = \vec{G}_j + \vec{k}_{m'}, \qquad (12)$$

where the reciprocal lattice vector $\vec{G}_j$ is defined as a linear combination of integer (j_α) multiples of the reciprocal lattice primitive vectors, g_α,

$$\vec{G}_j = \sum_{\alpha=1,3} j_\alpha \vec{g}_\alpha , \qquad (13)$$

and $\vec{k}_{m'} = \sum_{\alpha=1,3} \frac{m'_m \vec{g}_\alpha}{2N_\alpha}$ is a wave-vector that is consistent with the constraint (which has been conventionally stated as the requirement that the wave-vector $\vec{k}_{m'}$ have a restricted magnitude and direction) that requires it to be in the First Brillouin Zone--which is equivalent to requiring that $-N_\alpha \le m'_\alpha \le N_\alpha - 1$.

In most modern textbooks, Eq.2 is derived by demonstrating that it is equivalent to Eq. 1, based on wave-vectors and Reciprocal Lattice Vectors, defined by the boundary conditions, associated with Eqs. 5-11. The possibility that Eqs.5-11 also might apply to photons is new. When this possibility applies, intuitive ideas, suggested by Giuliano Preparata, about "trapped photons" can provide a basis for understanding how forms of oscillation, and resonance, can take place that can induce the kind of plasma picture that he suggested.

Bloch actually identified Eq. 3, in the context of Eqs. 4-11, using a more general formalism (involving multiple scattering theory[21,22], which actually is related to Eq. 2) that is very different from how his theory is presented in most modern textbooks. Bloch identified that Eqs. 3-5 could be related to the more general problem, associated with a "well-defined" form of scattering, in which, as opposed to solving an imprecise eigenvalue problem, involving approximate boundary conditions, the associated solutions can be derived from an asymptotic limit involving single particles scattering off an array of scattering centers, in which the lifetime of the resulting state becomes infinitely long[15].

Such a state involves a situation in which energy and momentum are rigorously conserved in a particular region of space, as a result of a "perfect" form of matching condition, in which the net flux of particles into the region vanishes. This form of matching provides a useful way to define perfect resonance. The associated state can be viewed as arising from a situation in which, effectively, "no scattering" occurs, within the region. Modern textbooks suggest the associated problem can be expressed through forms of a related eigenvalue problem involving "quasi-particles" and energy minimization. Although this is a convenient way to present the material, the manner in which it is presented is imprecise.

In the (multiple-scattering) situation, considered by Bloch, charge is not required to be conserved locally in the dynamic form that most high energy physicists assume to be true, in which the time evolution of the density ρ and flux of charged particles, $\rho\vec{v}$, are related through the equality, $\frac{\partial \rho}{\partial t} = -\nabla \bullet (\rho \vec{v})$. In the context of multiple-scattering, charge is conserved, but not locally. At the boundaries of the lattice, relative to the zero of energy (V_o) of the solid, for each value of $\vec{k}$, oscillatory solutions, $\varepsilon(\vec{k}) - V_o > 0$, and static or exponentially decaying solutions, $\varepsilon(\vec{k}) - V_o \le 0$, are required to match wave functions that do require that charge be conserved locally.

This can occur (in an operative sense) by using the kinds of semi-classical pictures suggested by Bloch, that are consistent with multiple scattering theory, involving single particle forms of scattering, in which, "discontinuous" changes in logarithmic derivative of the single particle wave function are allowed to take place, at the boundaries. Within the context of the semi-classical physics that formed the basis of Bloch's theory, these forms of discontinuities are allowed to occur by allowing for forms of negative kinetic energy, through imaginary forms of wave-vector $\vec{k}$ and momentum (defined by $\vec{p} = \hbar\vec{k}$). A potentially

important point, in this context, is that when these negative forms of kinetic energy are allowed, a generalization of "tunneling" associated with the conventional (Gamow-Teller) picture can occur, in which, as opposed to a situation in which the tunneling is assumed to involve two particles, at a specific location, a more general form of "tunneling" can take place, involving quasi-particles (in Bloch's and, later, Zener's pictures) at a microscopically large but macroscopically small number of locations, involving a large number of particles.

In a more precise argument, the complete many-body, physical picture actually does reduce to this limit when it is required that, as opposed to the approximate picture, involving "quasi-particles", an alternative picture applies, involving an extreme limit in which vanishing-ly small levels of interaction are allowed to take place. In particular, in the limit of vanishing-ly small interaction, at any particular location (associated with rigidly moving the lattice), implicit forms of degeneracy, associated with forms of EMI that are not included in the conventional pictures suggested by Bloch can come into play. Within this context, Bloch's ideas about using these kinds of semi-classical arguments can be replaced by more refined, microscopically defined, forms of interaction[8-10], that do not alter the limiting boundary effects, and equations suggested by Bloch.

These forms of interaction involve the simplest forms of degeneracy associated with Eqs.2 and 3. In particular, these forms of degeneracy can involve changes in the spins of the charged particles that are involved. Both forms of degeneracy are associated with non-local forms of coupling associated with the vector potential $\vec{A}$ and the implicitly important point that for situations involving non-neutral regions of space, the momentum of a particle or a collection of particles is not simply related to the product of the mass of the particle or collection of particles with the associated velocity of the particle or collection of particles. In particular, when the charge of a particle (or collection of particles) is q and its mass is M, its momentum $\vec{p}$, obeys the relationship $M\vec{v} = \vec{p} - q/c\vec{A}$. An important point is that in the limit in which nearly perfectly elastic forms of resonance are allowed to take place, the semi-classical picture and the more precise picture, based on a more specific, microscopic theory of the relevant EMI both apply.

Bloch suggested that a semi-classical picture, involving wave-packet propagation, could be useful for understanding how the "quasi-particle" eigenstates he postulated, heuristically, could be used to describe charge transport. Within this context, he used a semi-classical wave packet picture to develop an approximate form of EMI, based on the Lorentz force law. Here, he replaced the physical velocity of each charge with a form of "group velocity", $\vec{v}_G(\vec{k})$, defined by

$$\vec{v}_G(\vec{k}) = \frac{1}{\hbar}\nabla_{\vec{k}}\varepsilon(\vec{k}) \ . \qquad (15)$$

He also suggested that beginning from this approximate picture, the propagation of charge (through quasi-particle, wave-packets), could be explained by replacing the physical charge, with the quasi-particle charge, and the physical velocity with the "quasi-particle group velocity", $\vec{v}_G(\vec{k})$, and by allowing the momentum $\vec{p} = \hbar\vec{k}$ to evolve using a form of Lorentz force law, in which, $\vec{p}$ propagates in time, as if it is replaced by $\hbar\vec{k}$, based on the assumption that the physical velocity $\vec{v}$, is replaced with $\vec{v}_G(\vec{k})$. As a consequence, he identified an effective electromagnetic force F_{em}, which he related to time rate of change of an effective momentum p(t):

$$\frac{dp(t)}{dt} = \frac{\hbar dk(t)}{dt} = F_{em} = q\vec{E} + \frac{qv_G(k(t))}{c} \times \vec{B}, \qquad (16)$$

where $\vec{E}$ and $\vec{B}$, respectively, are the applied electric and magnetic fields, and $v_G(k(t))$ satisfies Eq. 15.

Bloch pointed out that when the same kind of wave-packet propagation picture is used, in the limit involving a constant, time-independent, constant electric field $\vec{E}$ (which means $\vec{B}$ vanishes), a form of resonance could take place, in which in the presence of $\vec{E}$, the momentum distribution of the wave packet would oscillate when a resonant condition takes place, that he reasoned would occur when the product of the applied, constant, electrical force $q\vec{E}$ with an interval of time t_n, equals $\hbar\vec{G}_n$. The associated form of resonance is referred to as a Bloch Oscillation.

In the limit in which perfect, or nearly perfect forms of resonance occur, approximate forms of Bloch oscillations can occur in which momentum, associated with scattering events can take place, and the lattice, as a whole, moves coherently. Quantum mechanics actually requires that this kind of effect take place, provided the imparted momentum is sufficient and occurs for a sufficiently long time. In principle, eigenstates can be identified through asymptotically vanishing forms of scattering from multiple-scattering theory. This idea applies universally in situations involving elastic processes (i.e., when energy is conserved), in finite solids through a generalization associated with situations involving many particles[8,10,18,19].

Resonant EMI's Involving Many Photons and Many Charged Particles in Low Energy Nuclear Reactions (LENR) in PdD

In the generalization of the multiple scattering formalism[8-10], many particles are included and solutions to the wave equation are replaced with a general form of interaction, involving arbitrarily perturbing a configuration that is close to being in its GS. Within this context, Bloch's theorem can also be generalized. As opposed to requiring that Born-von Karman boundary conditions apply, the only restriction associated with the theory is that no net flux, of particles into a particular volume of space take place, either for describing the GS or the lowest lying excited states.

Because it is never possible to determine, in the absence of any form of interaction, if a "lattice" is in motion or at rest, its zero of velocity (or momentum) is not known. As a consequence, the effect of its relative motion and possible acceleration, or "its gauge" (i.e., the gradient of the phase of the many-body wave function, in situations in which many particles can share a common phase, through preferred forms of coherent motion) is not known, in general. Although in most situations, the associated many-body physics is extremely complicated, how the GS and lowest lying excited states evolve, in a number of the heuristically derived results related to applying the semi-classical theory of transport, based on Eqs. 2-16, also is applicable to the complete many-body situation, where the same equations are used to determine the zeroes of energy and momentum. In this more general situation, all of the relevant QED effects are also included[8-10].

Within the context of the generalization of multiple-scattering theory, photons (as a consequence of Eqs. 1 and 2) can be required to obey Bloch's theorem, as they would in situations involving non-interaction, in a particular region of space (where a fixed gauge can be assumed) provided at the boundaries of the region, appropriate wave function matching conditions, involving solutions to the Helmholtz equation, that are consistent with Maxwell's equations, and the requirement that photons behave as they do asymptotically far from the solid, are imposed. These "conditions" require that the wave propagation of emitting "photons," in conventional situations, would not appear to be exponentially growing or decreasing, as a function of time, and that the transmissions preserve gauge symmetry.

By assumption when an appropriate solution for the GS and lowest-lying excited states occurs, no interactions are assumed to take place, no net flux of particles occurs, associated with any solution, involving the particles, into regions where the wave equations apply, either for the photons or the charged particles. Because the region associated with where this form of "non-interaction" can take place can be infinitesimally small, the single particle problem, involving either photons or electrons, can be related to more general problems; where and how electrons or photons propagate in this region can: 1. Be treated as being entirely elastic (a situation associated with identifying the eigenstates of the GS), or 2.) Involve partially elastic solutions (which introduce forms of dissipation at the boundaries of the region); 3. Occur with different forms of scattering, when periodic order either is present or approximately present; 4.) Involve approximate forms of boundary conditions (previously assumed to require large dimension—for example the boundary conditions that apply when the Born-von Karman boundary conditions are used) that may be assumed but need not be required; and 5.) Involve resonant forms of reaction, in which small amounts of momentum can be imparted to the center of mass of all of the charged particles associated with possible interactions, from an external force, periodically, that can be stored and amplified, with time, resulting in Low Energy Nuclear Reactions (LENR).

A novel result is that Bragg Scattering of light also potentially can couple to electrons and deuterons, in unexpected, but similar ways (through Bloch's theorem), but because of our inability to distinguish dissipation effects, involving, poorly defined resonance, from potentially more dominant forms of resonance, a number of important, unifying ideas, associated with the resonance problem (considered by Bloch) and how it has been presented, have been ignored. Very important points are: 1. In the true many-body physics situation, the origin of the approximate single particle picture that has been quoted in text books, being related to what Bloch proposed, has not been appropriately expressed; 2. The possible consequences of this relate to a very foreign limit, in the context of conventional thinking associated with nuclear physics—the limit associated with an effective form of coupling in which momentum can be stored as a result of elastic forms of scattering in which the "lattice" effectively can acquire higher velocity, quantum mechanically, in response to an externally applied, static field, with low velocity, and *without any tangible forms of collision*; 3. How through resonant effects, coupled to a limit involving negligible perturbation, over sufficiently long periods of time, it can be possible to induce coherent forms of momentum transfer, involving many particles, being released, preferentially, in particular ways.

In this context, particular forms of resonant phenomena[15] can be described at a basic level, through approximate forms of attenuation (losses) when possible, quasi-elastic reflections can occur gradually, over a sufficient period of time. The underlying, asymptotic boundary conditions, which are quite foreign to situations involving thermonuclear fusion, are quite attainable, in nano-crystalline structures.

The generalized form of Bloch's theorem[9,10] applies for each kind of charged particle, asymptotically, for arbitrary many-body interactions, provided overlap between the GS and lowest-lying excited states is minimized. A new and novel result is that a many photon wave function also obeys the same generalized form of Bloch's theorem[10] in interior (bulk) regions (where rigid translations are allowed to take place). This requires the photons share a specific, common gauge, which, we may define by the requirement that as the lattice moves rigidly, each charged particle coordinate remain fixed relative to its center-of-mass and to the center-of-mass (R_{cm}) of all of the charged particles in the lattice. The generalization of Bloch's theorem to situations involving many particles has a complicated mathematical relationship[9,10]. In the most coherent situation (which is associated with the Zener tunneling limit[18,19]), discussed below, all of the d's that can occupy an ion band state can

occupy the same state, since d's are bosons and they obey Bose-Einstein statistics. For this reason, in its lowest energy configuration, the many-body wave function Φ_d of the ion band state d's can be written in a considerably simpler form than is presented elsewhere [18,19]:

$$\Phi_d = \exp(iN_d \bullet \vec{k}_m \bullet \vec{R}^d_{cm})\Psi_d, \qquad (17)$$

where $\vec{R}^d_{cm}$ is the center of mass of all of the deuterons in the lattice, Ψ_d is the complete many-body deuteron wave function, relative to a reference frame that is stationary with respect to the center-of-mass of the lattice,

$$\vec{k}_m = \sum_{\alpha=1,3} \frac{m_\alpha \vec{g}_\alpha}{2N_\alpha}, \qquad -N_\alpha \le m_\alpha \le N_\alpha - 1,$$

is one of the wave-vectors in the first Brillouin zone, and N_d, is the number of deuterons that occupy ion band states within the lattice.

In finite crystalline structures, in the limit involving the lowest energy excitations of the GS and lowest-lying excited states, the only allowable perturbations occur through rigid translations in which the integers n_α and m_α that are used, respectively to define the Bravais Lattice Vectors and Reciprocal Lattice Vectors, are required to have the same range of possible values (between $-N_\alpha$ and $N_\alpha - 1$ or $-N_\alpha + 1$ and N_α, relative to a reference frame that is stationary with respect to the center of mass of the lattice). This requirement insures that both the discrete Fourier transformation of quantities related to the Bravais Lattice, and the inverse transformation are unique. It also minimizes the overlap between any of the lowest-lying states.

The lowest energy configurations permit this when the motion is perfectly rigid, provided the lattice is sufficiently large but also sufficiently small. Within this context, when this can take place, in a situation involving either minimizing the available energy, or through a carefully configured environment, involving a dynamical form of interaction (for example, in appropriately engineered nano-scale crystals), EMI resonant effects that can create higher energy nuclear particles can occur when externally applied, static electromagnetic fields (electrical or magnetic, or both) are applied. Richer forms of coupling are also possible, associated with applying alternating electrical and magnetic fields. The associated forms of coupling involve, in the simplest approximation, a generalization of the ideas suggested by Giuliano Preparata.

As opposed to the picture, involving "plasmas" in solids that Giuliano Preparata suggested, there is a picture, first identified by Bloch, that was further developed by Zener, associated with a situation in which collisions by charged particles are stifled (in a situation involving electrons). In this picture, oscillations of the lowest energy "quasi-particles" are envisioned to take place, in a lattice, possessing a fixed orientation. The associated oscillations, as mentioned in the last section, are referred to as "Bloch Oscillations." Zener suggested that if these oscillations are real, at a certain point, tunneling, based on an approximate picture, associated with single particle quantum mechanics would have to take place. This phenomenon (which was observed, indirectly, 15 years ago[23]) can explain a new effect[18], not envisioned by Preparata, in which (in the PdD situations) momentum can be stored, through rigid displacements of the charge of the electrons and ions that occupy or potentially can occupy energy band states.

The picture, associated with Bloch Oscillations, in a finite lattice can be generalized, and the idea that the tunneling concept might apply (which Zener[24] suggested, by assumption) can also be generalized[9,18,19]. For Bloch Oscillations to lead to Zener tunneling, a natural form of resonance has to take place in which as a function of time t, when the applied force $q\vec{E}$ is sufficiently weak (so that collisions within the solid actually are stifled) an equality $q\vec{E}t = \hbar\vec{G}$ ($\vec{G}$=reciprocal lattice vector) can occur, any number of times, in which momentum

is transferred elastically to the center of mass of the lattice. In most situations, involving electrons, this form of interaction is stifled by collisions. But, for understanding the lowest energy and momentum situation, involving ions (d's) the effect can be quite real in PdD. The reason is that asymptotically, fluctuations involving small changes in the loading parameter x in PdD_{1+x} can induce the kinds of small perturbations in the external forcing that can lead to the kinds of resonant effects associated with Zener tunneling, involving ions, d's, as opposed to electrons.

Zener suggested, in the context of Bloch's imprecise model, a unifying theme that can provide a way to overcome doubts that most nuclear physicists have about how "tunneling might occur" in a way that they possibly would agree with through an alternative effect, in which a lattice conceivably could allow tunneling to take place, coherently. Unfortunately, because of subtleties involved in how this might take place, most nuclear physicists would not appreciate what Zener suggested. He suggested that each time $q\vec{E}t = \hbar\vec{G}$, a "beating phenomenon" could take place, in which momentum (not energy) could be transferred to all of the charged energy band state "quasi-particles" (electrons, in the case he considered) and that this momentum could "be stored" and "amplified" appropriately.

In earlier papers, I pointed out that the insulator model that Zener was referring to could apply to fully-loaded $PdD_{1\pm\delta}$, as δ becomes vanishing-ly small, and that, as opposed to a situation potentially involving electrons, it could involve d's. Within this context, because d's are bosons, forms of coherence can take place in which the d's effectively behave as a Bose Einstein condensate, similar to the kind of Bose Einstein condensates that can form when neutral alkali atoms are optically cooled and interact with an optical lattice[9,23]. When this takes place, the resonant effects can involve a macroscopically small but microscopically large number of nuclei that are effectively tuned to a form of resonant condition that with time can induce non-local forms of coupling that can result in d+d→helium-4 forms of reaction. An important point involves the role of EMI and resonant EMI in making this possible. The failure of conventional nuclear physicists to recognize this has undermined meaningful dialogue about this subject.

By requiring that the associated dynamics occur in the reference frame that is stationary with respect to the relative motion of the center of mass, it follows that when the semi-classical equations associated with Eq. 16 are valid, as a function of time, in order for the most coherent forms of reaction to take place, the center of mass of the lattice accelerates in such a way that its acceleration does not occur too rapidly or too slowly. Bounds for not accelerating too rapidly or too slowly are responsible for the limits that were estimated previously[18,19]. These bounds imply that crystal size is important and plays a role in how "tunneling" can take place as rapidly as possible in order for nuclear reaction to take place. Other effects can be important. Whether or not avoiding collisions, that could disrupt the associated process, is potentially valuable is an open question. These earlier estimates, of relevant forms of transport, have suggested that optimal sizes for potentially reactive crystals should have characteristic dimensions of ~ 30-50 nm.

In the rest frame of the laboratory, when the solid is exposed to an outside, external electric field (as in conventional LENR), in the alternative rest frame, in which the center of mass is stationary but accelerates, relative to the laboratory rest frame, the external electric field that is applied in the laboratory rest frame, will be different than the electric field in the center-of-mass rest frame, and a magnetic field will also be created. The presence of these different fields can result in new forms of interaction that can lead to new effects.

A concrete example that illustrates the origin of the resulting effects involves estimating the power P that is transferred to a charge, in the rest frame of the ordered solid, and how P changes as a function of time. In particular, in the rest frame of the location that is stationary

with respect to the center of mass, P is defined by the dot product of the local force F_{em} and velocity v; i.e. when $P=\vec{F}_{em}\bullet\vec{v}$, and, to insure that, as a function of time, minimal coupling to outside processes take place, instantaneously, P is required to be constant. Then, coupling can take place between the electric and magnetic fields that can result in forms of dissipation that can impede electromagnetic propagation from taking place. In particular, in the limit in which P from possible reactions is constant, for each state, possessing wave-vector $\vec{k}$, involving mass M, the associated power is $\frac{\hbar\vec{k}\bullet F_{em}}{M}$. In the "rest frame" that is stationary with respect to the center-of-mass, $\hbar\frac{d\vec{k}}{dt}=0$. This means that,

$$\frac{dP}{dt}=\frac{q\hbar}{M}\frac{d\vec{k}\bullet F_{em}}{dt}=\frac{q\hbar}{M}\frac{\vec{k}\bullet\partial(\vec{E}+\nabla_k\varepsilon(k)/c\times\vec{B})}{\partial t}=0, \qquad (17)$$

where q is the charge, and M is the mass of the particle that interacts with the electromagnetic field. Eq. 17 implies

$$-q\frac{\partial\vec{k}\bullet\vec{E}}{\partial t}=q\bullet\vec{k}\bullet(\frac{\nabla_{\vec{k}}\varepsilon(\vec{k})}{c}\times\frac{\partial\vec{B}}{\partial t})=-q\bullet\vec{k}\bullet(\nabla_{\vec{k}}\varepsilon(\vec{k})\times(\nabla\times\vec{E}))\ . \qquad (18)$$

In the co-deposition experiments, we may assume that the dominant applied field is vertically oriented, approximately, relative to the samples, and approximately constant. If $\vec{A}$ is real at the boundary of the lattice, it's imaginary component vanishes. This condition can be imposed by assigning a particular gauge condition and/or by requiring that the "boundary" of the lattice be defined to take place at a location $\vec{r}_{boundary}$ where $\vec{k}\bullet\vec{r}_{boundary}=\pi n$, where n is an integer. When the electric field in Eq. 18 is uniformly constant, both sides of Eq. 18 vanish, identically, but if the lattice is allowed to move, in principle, the lowest energy (Bloch state) photon fields will emit radiation whenever $\vec{k}\bullet\vec{r}_{boundary}=\pi n$. If an applied field $\vec{E}'$, perpendicular to the initial field is introduced, the requirement that $\vec{A}$ be real at the boundary of the lattice leads to a different situation. In particular, in the idealized limit that $\vec{E}'$ varies in the vertical direction and is pointed in the x direction, Eq. 18 implies

$$\frac{\partial\vec{k}\bullet\vec{E}'}{\partial t}=\frac{\partial k_x E_x'}{\partial t}=-\nabla_{k_z}\varepsilon(\vec{k})\frac{\partial k_x E_x'}{\partial z}. \qquad (19)$$

Eq.19 is a wave equation. Its solution is an arbitrary, differentiable function P(t):

$$P=k_x E_x'=P(t+\frac{z}{\nabla_{k_z}\varepsilon}). \qquad (20)$$

When $\nabla_{k_z}\varepsilon(\vec{k})$ becomes vanishing-ly small or large, the solution to Eq. 20 either becomes time independent or spatially uniform. In either case, the fields can be expected to become localized. This form of localization of the electromagnetic fields is strikingly similar to the kind of effect that Giuliano Preparata referred to as "trapped photons". When this kind of effect can take place, provided sufficient momentum is available, as opposed to the forms of X-ray emission that would be expected when $\vec{k}\bullet\vec{r}_{boundary}=\pi n$, because the momentum is required to be localized at the boundaries of the lattice, it is plausible that high energy particles would be released. This argument suggests that details about the orientation of the applied fields, in the SPAWAR protocol experiments, might be important.

References

[1] Steven B. Krivit, " Extraordinary Courage: Report on Some LENR Presentations at the 2007 American Physical Society Meeting."
http://www.newenergytimes.com/news/2007/2007KrivitS-Extraordinary Courage.pdf.
[2]S. Szpak, P.A. Mosier-Boss, F.E. Gordon, Naturwissenschaften 94, 511–514 (2007).
[3] D. N. Klyshko, Photons and Nonlinear Optics. *(*Gordon and Breach Science Publishers, New York, 1988).
[4] Chubb, S.R. and T.A. Chubb. Proc ICCF9, 57 (2003).
http://www.lenr-canr.org/acrobat/ChubbSRrelationsh.pdf.
[5] S.R. Chubb and T.A. Chubb, Fusion Technol. **24**, 403 (1993).
[6]G. Preparata,, Proc ICCF1, 91 (1990).
[7]Giuliano Preparata, QED Coherence in Matter. (World Scientific, New Jersey, 1995), Chap. 8, pp 153-178.
[8] S.R. Chubb and T.A. Chubb, Proc. ICCF8, 385 (2000).
http://www.lenr-canr.org/acrobat/ChubbSRtheoretica.pdf
[9] S.R. Chubb, "Role of Broken Gauge Symmetry in Transport Phenomena Involving Neutral and Charged Particles in Finite Lattice," Proc Roy Soc, submitted (2006).
http://arxiv.org/abs/cond-mat/0512363v1
[10] S.R. Chubb, Proc ICCF10, 735 (2005).
[11]Neil W. Ashcroft and N. David Mermin, Solid State Physics. (Saunders College Publishing, Fort Worth, 1976), Chap 12, 213-242.
[12] T.A. Chubb, T.A. and S.R. Chubb, Fus Tech, **20**, 93 (1991).
[13] J. Schwinger, Proc ICCF1, 130 (1990).
http://www.lenr-canr.org/acrobat/SchwingerJnuclearene.pdf
[14] D.R. Thompson, Nucl Phys **A154**, 442 (1970).
[15]S.R. Chubb, "Resonant Electromagnetic Interaction (EMI) in Low Energy Nuclear Reactions (LENR)," submitted to special Proceedings of American Chemical Society Symposium (Eds. J. Marwan and S.B. Krivit), (2007).
[16] Neil W. Ashcroft and N. David Mermin, Solid State Physics. (Saunders College Publishing, Fort Worth, 1976),, Chap. 5, pp. 86-94.
[17] ibid, Chap. 8, p. 141
[18] S.R. Chubb, Proc ICCF11, 646 (2006).
[19] S.R. Chubb, Proc. ICCF12, 430 (2006).
[20] Neil W. Ashcroft and N. David Mermin, Solid State Physics. (Saunders College Publishing, Fort Worth, 1976), Chap. 8, p.135.
[21] Michael Melich, private communication.
[22] Antonios Gonis and William H. Butler, Multiple Scattering in Solids. (Springer-Verlag, New York, 2000), 282 pp.
[23] J. Feldmann, K. Leo, J. Shah, D.A.B. Miller, D.A.B., J.E. Cunningham, T. Meier, G. von Plessen, G., A. Schulze, P. Thomas, and S. Schmitt-Rink, Phys. Rev. B **46**, 7252 (1992).
[24] C. Zener, *Proc. R. Soc.* A **145,** 523-529 (1934).
[25]O. Morsch, J.H. Muller, M. Cristiani, D. Ciampini, and E. Arimondo, Phys. Rev. Lett. **87**, 1040402/1-4.

THE INTERACTIONS OF ERZIONS WITH NATURAL ISOTOPES

William Collis
mr.collis@physics.org

Abstract

In the early 1990s, Hagelstein proposed that neutrons could be transferred between natural isotopes producing energy and explaining transmutation of heavy nuclei. The beauty of this idea was that there is no Coulomb barrier for neutral particles. Alas, the nuclear energy barrier, typically 8 MeV, is sufficient to suppress the rate of neutron hopping to immeasurably small values, and the idea was duly abandoned.

However it may be that other Exotic Neutral Particles (ENP) could catalyse neutron transfer without insuperable energy barriers. Independently John Fisher proposed a model involving poly-neutrons and Yuri Bazhutov proposed another based on Erzions. Both classes of particles are, of course hypothetical, but share numerous common features. In particular, the rates of reaction are expected to be very high permitting a tiny number of ENPs to create substantial heat and transmutation products.

The purpose of this paper is to examine whether the Erzion model is able to explain CMNS phenomena. To do so, we use ENSAP, a PC based software tool to enumerate **all** possible interactions of the hypothetical Erzions with natural isotopes. In some cases, beta radioactive products may be expected, and experiments should be designed to look for them.

In addition, beta radio-activity may be predicted but not observed. To preserve the Erzion model, it may be necessary to change masses of the particles.

Reaction Rates

An initial objection to all ENP theories is that ENPs have not been directly detected and identified. This may be because there may be very few of them. If so, it is necessary to demonstrate that nuclear reaction rates are exceptionally high to explain measurable “excess heat”. Further we need to demonstrate that the catalytic ENP is reasonably well confined to prevent sustained power. For example, neutrons have typical capture cross sections measured in mb and their mean free path can be of the order of cm. In contrast, ENPs may have cross sections 6 orders of magnitude larger and mean free paths measured in microns. They may be good candidates to explain hot spots and localized melting in metal electrodes.

The origin of this potent nuclear reactivity is primarily due to:

a) No Coulomb barrier to approach a target nucleus (like neutrons).
b) Usually no Coulomb barrier for the separation of products (unlike most neutron induced transmutations).
c) No slow electro-magnetic interactions (gamma emission).
d) Conservation of spin and parity.

This is illustrated by 2 neutron induced transmutations:

$$1n + 3He \rightarrow 1H + 3H + 0.764 \text{ MeV} \quad (1)$$
$$1n + 6Li \rightarrow 3H + 4He + 4.783 \text{ MeV} \quad (2)$$

In both cases products are charged, but nevertheless all the criteria above (a,d) are met and in fact the cross sections are 5000 and 1000 barns.

Introduction to Erzions

Erzions are conjectured to be a class of hadrons containing a heavy anti-quark {U*}1. Only 3 are of interest to CMNS namely:

Table. Nuclear Properties of Erzions

Erzion	Delta (MeV)	Quarks	Spin/Parity	
$Э^-$	+0.7900	{U*d}	0-	Beta Radio-active
$Э^o$	-1.8200	{U*u}	0-	Stable
$Э_N$	+0.0000	{U*uudd}	1/2-	Stable

Because the heavy anti-quark {U*} is never destroyed, Erzion Number is conserved which simplifies analysis of possible reactions. In all reactions, one form of Erzion is converted into another. This means that we only need to know the relative masses not the absolute masses to calculate reaction energies. In the above table I have set the Delta of E_N to zero.
In order to explain tritium production in deuterated metals without the simultaneous production of 14.1 MeV neutrons Bazhutov [1] postulates that tritons must be produced at very low energy – insufficient to react further with other deuterons.

$$Э_N + 2H \rightarrow Э^o + 3H + 0.006 \text{ MeV}$$

This fixes the mass of the $Э^o$. Because the $Э^-$ is massive and charged it is strongly attracted to positively charged nuclei where it may react or may simply decay. Its precise mass has not been determined.

Analyzing Erzion Interactions with natural stable isotopes

Given the nuclear properties outlined above it is possible to exhaustively search for all exothermic interactions of Erzions with naturally occurring stable isotopes. We can then compare those reactions with observations (or lack thereof!) in Cold Fusion experiments. To do this we used an enhanced version of ENSAP software which runs on a PC5. Throughout this paper we use the masses assigned to the 3 Erzions by Bazhutov [1], but these may require revision as discussed in the conclusion of this paper.

Table 1. $Э_N$ interactions with natural stable isotopes
(Spin and parity conserved)

$Э_N$ + 2H (0.02%) -> $Э^o$ + 3H (beta-) + 0.006 MeV
$Э_N$ + 3He (0.00%) -> $Э^o$ + 4He (100.%) + 14.326 MeV
$Э_N$ + 19F (100.%) -> $Э^-$ + 20Ne (90.5%) + 4.764 MeV
$Э_N$ + 26Mg (11.0%) -> $Э^o$ + 27Mg (beta-) + 0.192 MeV
$Э_N$ + 27Al (100.%) -> $Э^o$ + 28Al (beta-) + 1.474 MeV
$Э_N$ + 28Si (92.3%) -> $Э^o$ + 29Si (4.68%) + 2.222 MeV
$Э_N$ + 29Si (4.68%) -> $Э^o$ + 30Si (3.09%) + 4.358 MeV
$Э_N$ + 31P (100.%) -> $Э^-$ + 32S (95.0%) + 0.785 MeV
$Э_N$ + 31P (100.%) -> $Э^o$ + 32P (beta-) + 1.684 MeV
$Э_N$ + 35Cl (75.8%) -> $Э^o$ + 36Cl (beta-) + 2.328 MeV
$Э_N$ + 40K (0.01%) -> $Э^-$ + 41Ca (Э.C.) + 0.812 MeV
$Э_N$ + 75As (100.%) -> $Э^o$ + 76As (beta-) + 1.077 MeV
$Э_N$ + 85Rb (72.2%) -> $Э^o$ + 86Rb (beta-) + 2.400 MeV
$Э_N$ + 110Cd (12.5%) -> $Э^o$ + 111Cd (12.8%) + 0.727 MeV
$Э_N$ + 111Cd (12.8%) -> $Э^o$ + 112Cd (24.1%) + 3.144 MeV
$Э_N$ + 112Cd (24.1%) -> $Э^o$ + 113Cd (12.2%) + 0.289 MeV
$Э_N$ + 113Cd (12.2%) -> $Э^o$ + 114Cd (28.7%) + 2.791 MeV
$Э_N$ + 112Sn (0.97%) -> $Э^o$ + 113Sn (beta+) + 1.491 MeV
$Э_N$ + 114Sn (0.66%) -> $Э^o$ + 115Sn (0.34%) + 1.295 MeV
$Э_N$ + 115Sn (0.34%) -> $Э^o$ + 116Sn (14.5%) + 3.312 MeV
$Э_N$ + 116Sn (14.5%) -> $Э^o$ + 117Sn (7.68%) + 0.693 MeV
$Э_N$ + 117Sn (7.68%) -> $Э^o$ + 118Sn (24.2%) + 3.075 MeV
$Э_N$ + 118Sn (24.2%) -> $Э^o$ + 119Sn (8.59%) + 0.234 MeV
$Э_N$ + 119Sn (8.59%) -> $Э^o$ + 120Sn (32.6%) + 2.856 MeV
$Э_N$ + 120Te (0.09%) -> $Э^o$ + 121Te (beta+) + 0.975 MeV
$Э_N$ + 122Te (2.55%) -> $Э^o$ + 123Te (0.89%) + 0.678 MeV
$Э_N$ + 123Te (0.89%) -> $Э^o$ + 124Te (4.74%) + 3.174 MeV
$Э_N$ + 124Te (4.74%) -> $Э^o$ + 125Te (7.07%) + 0.325 MeV
$Э_N$ + 125Te (7.07%) -> $Э^o$ + 126Te (18.8%) + 2.862 MeV
$Э_N$ + 124Xe (0.10%) -> $Э^o$ + 125Xe (beta+) + 1.352 MeV
$Э_N$ + 126Xe (0.09%) -> $Э^o$ + 127Xe (Э.C.) + 0.972 MeV
$Э_N$ + 128Xe (1.91%) -> $Э^o$ + 129Xe (26.4%) + 0.656 MeV
$Э_N$ + 129Xe (26.4%) -> $Э^o$ + 130Xe (4.07%) + 3.004 MeV
$Э_N$ + 133Cs (100%) -> $Э^o$ + 134Cs (beta-) + 0.640 MeV
$Э_N$ + 130Ba (0.11%) -> $Э^o$ + 131Ba (beta+) + 1.242 MeV
$Э_N$ + 132Ba (0.10%) -> $Э^o$ + 133Ba (Э.C.) + 0.938 MeV

Table 2. $Э^{o}$ interactions with natural stable isotopes

Key: PV=Parity Violation. [n] = failure to conserve spin

$Э^{o}$ + 2H (0.02%) -> $Э_{N}$ + 1H (100%) + 4.027 MeV[0]
$Э^{o}$ + 6Li (7.59%) -> $Э_{N}$ + 5Li(p) + 0.586 MeV[0] PV
$Э^{o}$ + 9Be (100.%) -> $Э_{N}$ + 8Be(alpha) + 4.586 MeV[1] PV
$Э^{o}$ + 13C (1.11%) -> $Э_{N}$ + 12C (98.9%) + 1.305 MeV[0] PV
$Э^{o}$ + 17O (0.04%) -> $Э_{N}$ + 16O (99.8%) + 2.108 MeV[2]
$Э^{o}$ + 143Nd(12.2%) -> $Э_{N}$ + 142Nd(27.2%) + 0.128 MeV[3] PV
$Э^{o}$ + 145Nd(8.30%) -> $Э_{N}$ + 144Nd(23.8%) + 0.495 MeV[3] PV
$Э^{o}$ + 149Sm(13.8%) -> $Э_{N}$ + 148Sm(11.2%) + 0.380 MeV[3] PV
$Э^{o}$ + 179Hf(13.6%) -> $Э_{N}$ + 178Hf(27.3%) + 0.152 MeV[4]
$Э^{o}$ + 183W (14.3%) -> $Э_{N}$ + 182W (26.5%) + 0.059 MeV[0] PV
$Э^{o}$ + 189Os(16.2%) -> $Э_{N}$ + 188Os(13.3%) + 0.334 MeV[1] PV
$Э^{o}$ + 195Pt(33.8%) -> $Э_{N}$ + 194Pt(33.0%) + 0.147 MeV[0] PV
$Э^{o}$ + 201Hg(13.2%) -> $Э_{N}$ + 200Hg(23.1%) + 0.021 MeV[1] PV

Table 3. $Э^{-}$ interactions with light natural isotopes (A < 35)

$Э^{-}$ + 1H (100.%) -> $Э^{o}$ + 1n (beta-) + 1.828 MeV[0]
$Э^{-}$ + 2H (0.02%) -> $Э_{N}$ + 1n (beta-) + 5.854 MeV[0]
$Э^{-}$ + 3He(0.00%) -> $Э^{o}$ + 3H (beta-) + 2.591 MeV[0]
$Э^{-}$ + 3He(0.00%) -> $Э_{N}$ + 2H (0.02%) + 2.586 MeV[0]
$Э^{-}$ + 6Li(7.59%) -> $Э_{N}$ + 5He(n) + 3.486 MeV[0] PV
$Э^{-}$ + 10B (19.8%) -> $Э^{o}$ + 10Be(beta-) + 2.054 MeV[3]
$Э^{-}$ + 10B (19.8%) -> $Э_{N}$ + 9Be(100.%) + 1.493 MeV[1] PV
$Э^{-}$ + 14N (99.7%) -> $Э^{o}$ + 14C (beta-) + 2.454 MeV[1]
$Э^{-}$ + 14N (99.7%) -> $Э_{N}$ + 13C (1.11%) + 0.528 MeV[0] PV
$Э^{-}$ + 19F (100.%) -> $Э_{N}$ + 18O (0.20%) + 0.085 MeV[0]
$Э^{-}$ + 31P (100.%) -> $Э^{o}$+ 31Si(beta-) + 1.118 MeV[1]
$Э^{-}$ + 31P (100.%) -> $Э_{N}$ + 30Si(3.09%) + 0.782 MeV[0]
$Э^{-}$ + 32S (95.0%) -> $Э^{o}$ + 32P (beta-) + 0.899 MeV[1]
$Э^{-}$ + 33S (0.75%) -> $Э^{o}$ + 33P (beta-) + 2.361 MeV[1]
$Э^{-}$ + 35Cl(75.8%) -> $Э^{o}$ + 35S (beta-) + 2.443 MeV[0]

Discussion: Erzions and Cold Fusion

Table 2 shows all interactions of $Э^o$ with natural isotopes. Fast protons are predicted to be a product of deuterium and 4He from 6Li. Other reactions are possible but because no gammas and no beta radio-active products are formed, these may be difficult to detect. These "predictions" concur remarkably well with observation.

In all cases in Table 2, $Э^o$ is simply accepts a neutron from a donor nucleus to become $Э_N$. Table 1 shows how $Э_N$ may further react (to save space only reactions which perfectly conserve spin and parity are shown). Some of the products are beta radioactive (see Table 4), but such radio-activity could escape detection because:
a) The precursor isotope is absent.
b) Failure to monitor gamma emission.
c) The beta decay does not produce gammas or only gammas of low intensity.
d) The half life may be long.
e) Gamma emission may be masked by "natural" radio-activity (e.g. 87Rb)

Table 4. Properties of some predicted radio-active products.

27Mg	9.458 min	0.84376 MeV (71.8%)
28Al	2.24 min	No gammas
32P	14.262 days	No gammas
36Cl	301,000 years	0.511 MeV (<0.03%)
86Rb	18.642 days	540 MeV (1.55%)
134Cs	2.06 years	many

It is not very clear from Table 1, what acceptor isotope is converting $Э_N$ back into $Э^o$. Ideally we might like to see titanium or palladium performing this in order to explain why these deuterated metals can generate excess heat. Unfortunately, such reactions may be inhibited by spin and parity considerations.

Table 5. Regeneration of $Э^o$ in metal deuterium systems

46Ti (8.25%) + $Э_N$ -> $Э^o$ + 47Ti (7.44%) +2.626 MeV[2] PV
47Ti (7.44%) + $Э_N$ -> $Э^o$ + 48Ti (73.7%) +5.375 MeV[2] PV
48Ti (73.7%) + $Э_N$ -> $Э^o$ + 49Ti (5.41%) +1.891 MeV[3] PV
49Ti (5.41%) + $Э_N$ -> $Э^o$ + 50Ti (5.18%) +4.688 MeV[3] PV
50Ti (5.18%) + $Э_N$ -> $Э^o$ + 51Ti (beta-) +0.121 MeV[1] PV
102Pd (1.02%) + $Э_N$ -> $Э^o$ + 103Pd (Э.C.) +1.373 MeV[2]
104Pd (11.1%) + $Э_N$ -> $Э^o$ + 105Pd (22.3%) +0.843 MeV[2]
105Pd (22.3%) + $Э_N$ -> $Э^o$ + 106Pd (27.3%) +3.311 MeV[2]
106Pd (27.3%) + $Э_N$ -> $Э^o$ + 107Pd (beta-) +0.287 MeV[2]

Neutron Generation in Hydrogen and Deuterium systems

As already mentioned, the $Э^-$ unlike the neutral Erzions, interacts quite strongly with condensed matter, particularly heavy nuclei, forming exotic atoms. In such an immobilized state it will usually remain inert until it beta decays. We can regard systems that generate $Э^-$ to be "poisoned" – negligible heat is produced because most Erzions are immobilized although nuclear decay continues. In isotopic hydrogen gas, there are few competing heavy nuclei and such exotic atoms could result in nuclear reactions generating neutrons:

$Э^- + 1H \rightarrow Э^o + 1n + 1.828$ MeV
$Э^- + 2H \rightarrow Э_N + 1n + 5.854$ MeV

We are not aware of any other explanation for neutron generation in light hydrogen systems6. $Э^-$ may also be able to catalyze fusion in the same way that negative muons can do so. However its mass / half-life would need to be much lower than a muon's in order to account for the low fusion rates observed.

Conclusion

There are many similarities between Erzion and poly-neutron theory3. Both theories explain excess heat and transmutation by shuttling neutrons between nuclei. However whereas a poly-neutrons can grow indefinitely on a "fuel" such as deuterium, Erzions are obliged to find an acceptor nucleus. This may be an impurity in the system and consequently, may not be very reproducible.

The question arises how to test and distinguish the theories. We have already seen that Erzion theory predicts radio-active activation of magnesium with a short half life and hard gamma emission from 27Mg. Poly-neutron theory in contrast predicts 28Mg production (half-life 21 hours).

Erzion theory predicts copious 4He production in pure beryllium as well as generation of 10Be. Although 10Be is beta radio-active, its decay produces no gammas.
$Э^o + 9Be\ (100\%) \rightarrow Э_N + 8Be\ (alpha) + 4.586$ MeV[1] PV
$Э_N + 9Be\ (100\%) \rightarrow Э^o + 10Be\ (beta\text{-}) + 0.561$ MeV[1] PV

Although gammas may possibly be suppressed as Table 4 shows, energetic beta decay will produce bremstrahlung (J Dufour, personal communication) radiation due to the passage of energetic electrons through condensed matter. As these are not observed, some correction is required.

One of the most remarkable features of Erzion theory is the elegance with which radio-activity is suppressed without invoking any new physics. Firstly, little radioactivity is produced by $Э^o$ interactions, simply because they are not very energetic. In contrast $Э_N$ interactions are energetic and one would expect that neutron transfer to induce beta-radioactivity in many products as Table 1 shows. However any beta radioactivity will involve the transformation of a neutron into a proton. So if it is more energetically favorable, the $Э_N$ may transfer a proton instead generating a product which is much more likely to be stable (plus $Э^-$). In order for this to work systematically of course it will be necessary to adjust the masses (and perhaps other parameters) of the Erzions and this will be the work of a future paper.

In this way we have suppressed radio-activity in one product, only to generate radioactive Э⁻! Consequently a reduction in Э⁻ mass is probably required to make any resulting bremstrahlung undetectable.

Outstanding concerns regarding the Erzion Model include:

.How is it possible that the conjectured heavy quark does not decay?
.As conceived by Bazhutov, Erzions can only transmute isotopes by 1 amu at a time. Consequently, Iwamura's results cannot be explained. It may be necessary to extend the family of Erzions, following John Fisher's model, by allowing multiple neutrons, e.g. {Uuuudddd}

References

1. Bazhutov Yuri N.; "Influence of Spin and Parity Preservation Laws on Erzion Model Predictions in Cold Fusion Experiments", in The Seventh International Conference on Cold Fusion. 1998, pp 437-440. Vancouver, Canada: ENECO, Inc., Salt Lake City, UT.
2. Hagelstein P L, Kaushik S.; "Neutron Transfer Reactions", Proc. ICCF4, Vol 1, 10-21. 1993.
3. Fisher J C, "Poly-neutrons as agents for Cold Fusion reactions", Fusion Technology Vol 22, p 511, Dec 1992.
4. Collis W; "Nuclear Reactions of Cold Fusion - A systematic Study", Proc ICCF5, Monte Carlo.
5. Collis W; "ENSAP Software Tool to Analyze Nuclear Reactions" in The Seventh International Conference on Cold Fusion. 1998. Vancouver, Canada: ENECO, Inc., Salt Lake City, UT. (Demo version at www.iscmns.org/software/ENSAP/ensap.htm)
6. E. Campari, S. Focardi, V. Gabbani, V. Montalbano, F. Piantelli, S. Veronesi, "Overview On H-Ni Systems: Old Experiments And New Setup", presented at 5th Asti Workshop on Anomalies in Hydrogen / Deuterium Loaded Metals, 2004, www.iscmns.org/meetings/asti/papers/Piantelli.doc

USE OF A QUANTUM MECHANICAL TUNNELING MODEL TO EXPLAIN THE GLOW DISCHARGE CHARACTERISTIC I-V CURVE

David y. Chung*, Thomas K.T. Hsieh and Frank Senftle***

**DEPARTMENT OF PHYSICS, HOWARD UNIVERSITY,*
WASHINGTON, D.C. 20059, USA
*** Science Department, Hudson County Community*
College, Jersey City, N.J., 07306, USA
e-mail address: dchung@howard.edu

Abstract

The glow discharge (GD) observed during the ordinary electrolysis of an aqueous solution has been known for several years. The essential results can be described in detail by the characteristic I-V curve into specific regions. The excess heat and abnormal hydrogen production and associated nuclear transmutation (NT) have been reported by many papers [1-3].

In this paper, a quantum mechanical tunneling model will be described to explain the glow discharge experiments. Using an model similar to the semiconductor tunnel diode, one can construct a phenomenological theory to explain many aspects of the glow discharge experiments. A model calculation using transfer matrix method to solve the relevant Schrödinger equation for a single barrier tunneling problem has been done. (Double barrier problems have also been tried). The calculated results can be used to compare with our experimental results. The general agreement of the characteristic I-V curve with that of tunnel diode and other features gave us confidence of the theoretical tunneling model. The resonant phenomena with two barriers gives a very large probability of electronic tunneling near the resonant energy which may be used to explain some of the recent experiments in which nuclear transmutation appeared to have been observed [4].

1. Introduction

Much experimental work has been done over the past 60 years by Kellogg [5], Hinckley [6-8], Sengupta [9], and others in order to explain glow discharge electrolysis. The current explanation, while adequate, is not completely satisfactory. For Instance, the shape of the current-voltage (I-V) curve for GD is strikingly similar to the I-V curve for a tunnel diode. Why? Can we learn more about GD by examining the tunnel diode? In this paper we attempt to show the reason for the common characteristics between the tunnel diode and GD, when there is a single potential barrier. When more than one potential barrier is present we show that the probability of tunneling is enhanced, and, thus greatly increases the chance of nuclear

reaction taking place near or at the electrode surface. It is pertinent to first discuss briefly the operational mechanism of the tunnel diode and GD in an electrolytic cell.

2. **The Tunnel Diode**

The tunnel diode derives its special characteristics from the fact that its **p** an **n** regions are heavily doped with specific impurities. Similar to a normal pn junction, the doped pn junction presents a barrier to the free flow of electrons. However, the high concentration of impurities in the **p** and **n** regions causes the depletion layer between these regions to become so narrow that electrons and holes can tunnel through the potential barrier with relative ease (quantum mechanical tunneling). Assuming forward bias operation, and as the voltage increases, the electron states in the conduction band in the **n** region will increasingly become better aligned with hole states in the valence band in the **p** region. As a result, the current across the junction will increase (A to B in Figure 1). When the voltage reaches a certain value (point B), misalignment between the conduction and valence band begins to take place. At the same time the resistance increases while the current drops with increasing voltage. This negative differential resistance (NDR) is a specific characteristic of a tunnel diode. As the voltage is further increased, the tunneling current becomes increasingly less significant, and near a second critical voltage (near point D), the **pn** junction takes on normal diode action, i.e. the current increases with voltage. It seems apparent that any current – carrying device in which the resistance is essentially constant with increasing <u>low</u> voltage, but which increases with voltage at <u>higher</u> voltages, will have a characteristic I-V curve similar to that in Figure 1.

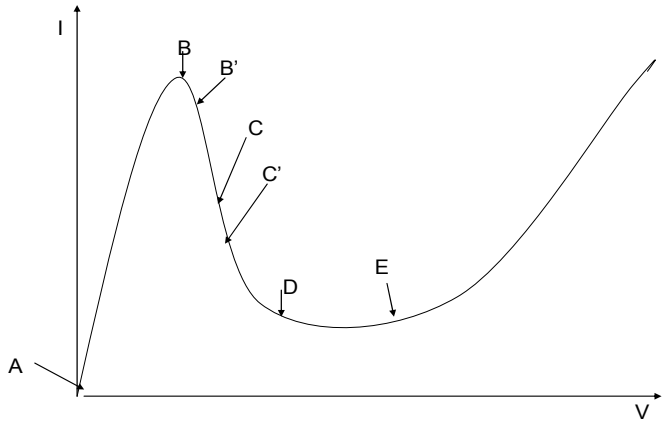

Typical I-V characteristic curve for a tunnel diode and glow discharge

3. **The Electrolytic Cell and Glow Discharge Electrolysis**

Brockeris and Reddy [10] have pointed out several properties of an electrode in an electrolytic solution which are analogous to semiconductors. For a very small potential across the electrodes, the polarized water molecules and ions in the electrolyte line up opposite to their counter charges on the electrode surface. The sheath of charges formed is called the electric double layer. Similar to a pn junction, the electric double layer presents a potential barrier to the free flow of electrons to the solution and vice versa. As the voltage increases from A to B (Figure 1) the potential barrier (region between the electrode and the electrolyte) will remain about the same. As the resistance from A to B is essentially constant, the electrons gain energy with increasing voltage, and the current will increase similar to a normal pn junction.

When the voltage is increased to point B, the current becomes high enough to produce significant Joule heating of the electrode. The vapor bubbles formed by the heating become major and erratic impedance to the current flow. At a slightly higher voltage, small pockets of vapor form which enhance the resistance and the current starts to drop. When these pockets coalesce to form a sheath on the electrode surface, the area of the electrode surface in contact with the liquid is restricted. As a consequence, violent gas bubbles form, but then stop suddenly as the voltage increases to about point B' (Figure 1), where the vapor sheath coverage is complete. If the voltage is increased further, the temperature increases and the vapor sheath gradually reverts to a hot gas starting at about the point C. At some voltage between points C and D arcing between the electrode and solution starts and gradually increases at higher voltages. The increased arcing gradually converts the hot gas sheath into a plasma, and the electrode becomes white hot (at about point D). The transformation of gas to a plasma gradually decreases the resistance due to the increased conductivity of the plasma. Near point D and beyond the current begins to increase again as the potential is now high enough for the electrons to go over the potential barrier.

From the above description of GD, one can assume that the tunnel diode and the electrolyte cell both respond similar to a normal pn junction between A and B (Figure 1). Between points B and D the tunnel diode and GD electrolyte both exhibit NDR characteristics for different reasons. In the tunnel diode the NDR is due to the electronic properties of the diode junction. In the electrolytic cell the resistance (potential barrier) increases step-wise throughout the range B to D. From points B to B' the potential barrier is due the formation of a vapor sheath on the electrode surface. This sheath gradually converts to a hot gas sheath (B' to C'), and finally into a plasma (C' to D and beyond). Thus, the characteristics of the total

potential barrier changes somewhat from B to D. Many of the parameters needed to make a meaningful calculation are unknown. Never-the-less it is possible to estimate the approximate numerical values so that a meaningful interpretation can be made.

4. **Calculation of the I-V Curve for Glow Discharge Electrolysis**

The common property of the tunnel diode and GD is a region of negative differential resistance, and thus one should be able to use a similar expression for the current in a tunnel diode (with the proper parameters for GD) to calculate an I-V curve similar to that in Figure 1. We start with the Schrödinger equation which describes the path of an electron through a single potential barrier.

$$\frac{d^2\Psi(x)}{dx^2} - \frac{2m}{\hbar^2}[U(x) - E(x)]\Psi(x) = 0 \qquad (1)$$

Where Ψ(x) is the wave function of the electron with energy E(x) going through the barrier, U(x) is the barrier height, m is the electron mass, x is the distance from the electrode surface to any point in the solution, and ħ is Planck's constant. Figure 2 shows a typical potential

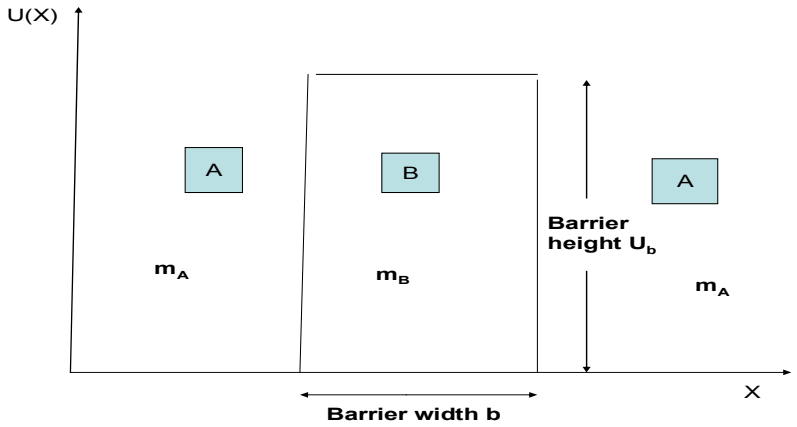

Figure 2. *The potential model for a single barrier with width b.*

barrier which can be used with equation (1) to show the effects of the various layers encountered in GD. The methods of solving the equation with the proper boundary conditions and using transfer matrix are well documented in the quantum mechanical text books [11, 12]. Therefore we will only describe the convention and the notations used in our calculations.

One can write the general solutions to the one-dimensional Schrödinger wave equation in all three regions of the barrier encountered in the electrolytic cell as:

$$\Psi(x)=\begin{cases} C_1^+ e^{ik_1 x}+C_1^- e^{-ik_1 x}, & x<0 \\ C_2^+ Ai[\rho(x)]+C_2^- Bi[\rho(x)], & 0<x<b \\ C_3^+ e^{ik_3 x}+C_3^- e^{-ik_3 x}, & x>b \end{cases}$$

Where Ai and Bi are Airy functions and

$$k_1=\frac{\sqrt{2m_A E_e+eV_A}}{\hbar},$$

$$k_3=\frac{\sqrt{2m_A(E_e+eV_A)}}{\hbar},$$

$$\rho(x)=\frac{x}{\lambda_0}+\beta_0,$$

$$\lambda_0=\left(-\frac{b\hbar^{1/2}}{2m_B eV}\right)^{1/3}$$

$$\beta_0=\frac{b}{eV\lambda_0}(E-U)$$

And $C_1^+, C_1^-, C_2^+, C_2^-, C_3^+$, and C_3^- are arbitrary constants, and m_A, m_B are the effective masses in regions A and B respectively.

Using matrix notation:

$$\begin{bmatrix} C_1^+ \\ C_1^- \end{bmatrix}=\begin{bmatrix} M_{total}^{11} & M_{total}^{12} \\ M_{total}^{21} & M_{total}^{22} \end{bmatrix}\begin{bmatrix} C_3^+ \\ 0 \end{bmatrix}$$

Thus, the transmission coefficient T can be written as:

$$T=\frac{\upsilon_3\Psi_t^*\Psi_t}{\upsilon_1\Psi_i^*\Psi_i}=\frac{k_3}{k_1}\left|\frac{C_3^+}{C_1^+}\right|^2=\frac{k_3}{k_1}\left|\frac{1}{M_{total}^{11}}\right|^2 \qquad (3)$$

where $\upsilon_i=\frac{\hbar k_i}{m}$, $\Psi^*(x)$ is the complex conjugate of $\Psi(x)$. The current density $J=\frac{I}{area}$ can then be evaluated from

$$J=\frac{1}{2\pi^2}\int_0^\infty dke\upsilon T(E)\int_0^\infty f(E)n^+(E)kdk. \qquad (4)$$

$f(E)$ is the Fermi-Dirac distribution function and $n^+(E)$ can be estimated using Boltzmann distribution function for a given temperature. With estimated values for the various

parameters we can then calculate the numerical probability coefficient T, and the I-V characteristic curve by a computer program (Mathematica).

It is worth mentioning that if one makes a calculation of a double barrier, the shape of the I-V curve is qualitatively the same (with slightly shifted in energy) as that of a single barrier. Thus the I-V curves of both single and double barriers in electrolytic cell are similar because the parameters in the integration (equation 4) are qualitatively similar.

Discussion of Results

1. Several wave functions for a model using two potential barriers are shown in Fig. 3. The barrier height, the width, and the distance between the barriers are all estimated values. The effective mass of the electrons in different parts of the barriers are also estimated to be close to those in solids. Here the wave functions decay exponentially within the barriers. However, they will be enhanced greatly at resonance energy, E_r. In Figure 3, the probability of an electron tunneling through the barriers is shown in the right side of Fig. 3 as a function of incoming energy (related to the biased voltage).

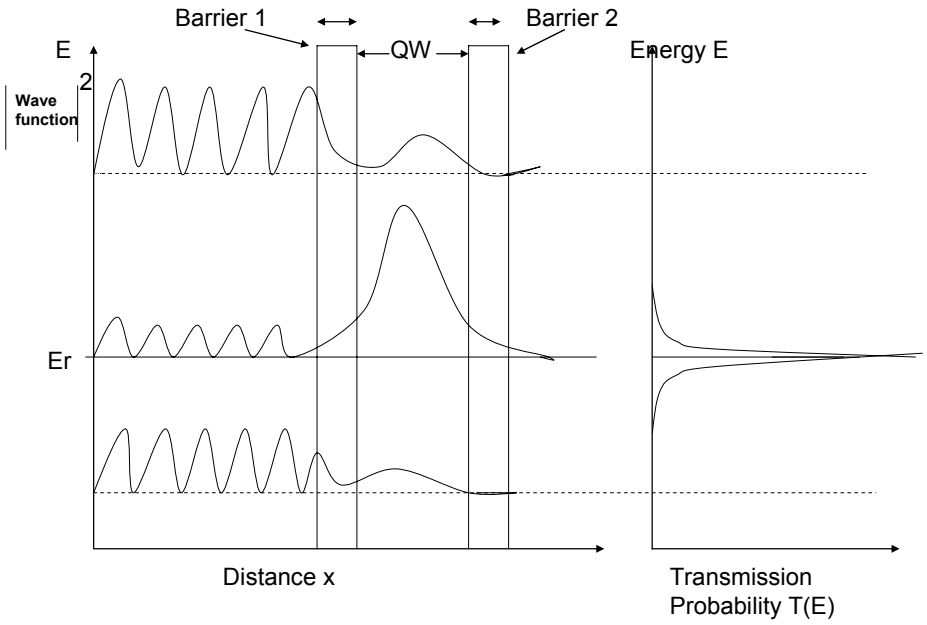

Figure 3. Resonance effect: the wave function reaches its maximum if the tunneling electrons is equal to the level in quantum well (QW).

2. One notices that the probability is relatively high at the resonant energy, E_r. In the cases of more then one resonant energy, e.g. two E_r's as shown in Fig. 4. There is a high probability that the electrons can tunnel into the nuclei of the electrode material so that fusion may take place. As a result, new elements may be produced at relative low energy. Figure 4 shows the calculated tunneling probability as a function of energy. Two resonant peaks are displaced. It is noted that the probabilities are very close to one at resonances.

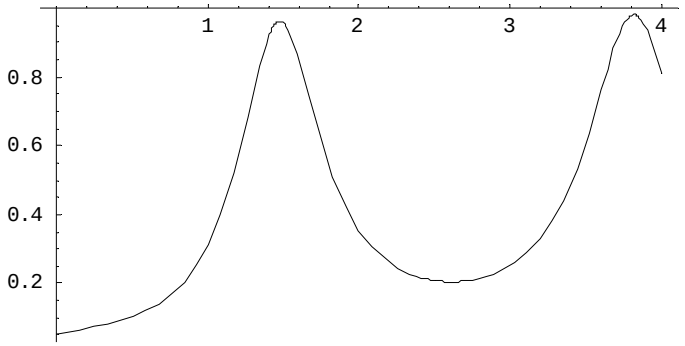

Fig.4. *Calculated tunneling probability as a function of energy (in arbitrary units). Two resonant peaks are displaced. One noticed that the probabilities are very close to one at resonances*

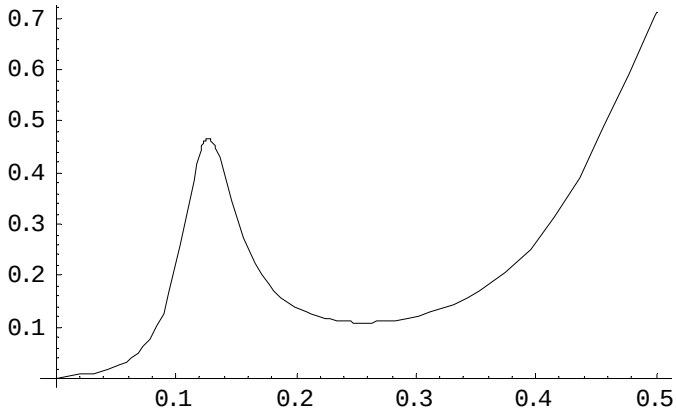

Fig. 5. *Typical results of the calculated I-V curve (in arbitrary units).*

3. The characteristic I-V curve was also calculated and shown in Fig. 5. As one would expect, it is very similar to that of a TD (Figure 1). However, the reasons are very different as we have discussed in earlier section. The most important part we learn from the RTD is that for two or more barriers there is an enhancement of the probabilities of electron tunneling at resonant energies.

Conclusions

1. We have found many similarities between the semiconductor diode, resonant tunnel diode and the glow discharge in electrolyte. Similar characteristic I-V curves are obtained and discussed in terms of tunneling of the electrons through potential barriers.
2. We have calculated an approximate I-V curve, and can describe the GD experiment at each point in terms of tunneling. The discussion of the NDR for the GD experiment is very similar to a semiconductor. NDR associated with PdH experiment is also discussed in the paper by Luo et al [13].
3. We can also calculate the enhancement of the probability of tunneling of charged particles due to resonance effect (double and plasma layers) and screening in the Coulomb potential. This is given in a separate paper at this conference.
4. It should be noted that our model calculations are very crude approximation to the real experiment. Many of the parameters used in the calculations are not known at the present time. However, many interesting qualitative results were produced. We can learn a great deal from the sophisticated calculations in 'quantum well' devices in semiconductors [11]. Future work should be focused on measurement of the experimental parameters, so that better and quantitative comparison can be made with the theoretical model calculations. Also from the qualitative results, some suggestions and predictions can be made to related experiments [4]. We believe that we are heading in the right direction for better understanding of LENR by using the knowledge and experience in condensed matter semiconductor physics.

References

1. Mizuno, T, Ohmori, T and Akimoto, T. Generation of Heat and Products during Plasma Electrolysis, 10th ICCF, 2003. Mizuno, T, Chung, D.Y., Senftle, F, and Aoki, Y., Same title as above, 11th ICCF, 2004.
2. Warner, J. and Dash, J., Electrolysis of D2O with Titanium cathodes: Enhancement of excess heat and further evidence of possible transmutation, ICCF-9, pp.118-119 2002.
3. Cirillo, D. and Iorio, V., Transmutation of metal at low energy in a confined plasma in water, ICCF-11, 2004.
4. Iwamura,Y., Sakano, M., Sakai, S. and Kuribayashi, S, Low.Energy transmutation correlation between Deuterium flux and Nuclear products, in condensed matter induced by D2 gasPermeation through Pd complexes: ICCF-10, p.68, 2003.
5. Kellogg, H., 1950, Anode Effect in Aqueous Electrolysis, J. Elect. Chem. Soc., 97, 132-142.

6. Davis, R., and Hickling, A., 1952, Glow Discharge Electrolysis. Part I. The Anodic Formation of Hydrogen Peroxide in Inert Electrolytics, J. Chem. Soc., pgs 3595-3602.
7. Hickling, A., and Linacre, 1954, Glow-Discharge Electrolysis. Part II the Anodic Oxidation of Ferrous Sulphate, J. Chem. Soc, pg 751.
8. Hickling, A., 1971, Electrochemical Processes in Glow Discharge at the Gas-Solution Interface, in Modern Aspects of Electrochemistry, eds J. O'M Bockris and B.E. Conway, Vol 6, pgs- 329-373, Butterworth, London.
9. Sengupta, S., Singh, R., and Srivastava, 1998, A Study of the Origin of Nonfaradic Behaviour of Anodic Contact Glow Discharge Electrolysis. J. Electrochem. Soc., 145, 2209-2213.
10. Bockris, J. O'. M. and Reddy, A. K., 1997, in Modern Electrochemistry, Rosetta ed., Plenums Press, New York, N.Y., USA.
11. Ch. 4, tunneling through potential barriers, 'SIMICONDUCTOR HETEROJUNCTIONS AND NANOSTRUCTURES' by Omar Manasreh, McGraw-Hill, NY. 2005
12. 12 Ch. 8. 'INTRODUCTORY APPLIED QUANTUM AND STATISTICAL MECHANICS' by P.L. Hagelstein, S.D. Senturia and T.P. Orlando, Wiley-Interscience, NY. 2005.
13. 13. Luo, N., Sherstha, P.J., Miley, G.H. and Violante, V., Enhancement of nuclear reactions due to screening effects of core electrons, ICCF 10, 2003.

FUNDAMENTAL INTERACTIONS AND THEIR RELATIVE CONTRIBUTION TO THE NUCLEAR REACTIONS AT LOW ENERGIES.

N.V. Samsonenko

PFU of Russia, Moscow

The influence of the fundamental interactions (strong, week, electromagnetic and gravitational) on the low energy processes in condensed media is analyzed. It is shown that the gravitational interaction on the distances of atomic or nuclear order is negligibly small and can be ignored, but the electromagnetic interaction, under certain definite conditions can lead to the considerable increase of the probabilities of different reactions (including nuclear) and generate exotic bounded states, yet experimentally unobserved at present ("neutrino atoms", dineutrons, dineutrinos, "magnetic" hydrogen etc.). The existence of such states (including virtual) can explain the observable exotic phenomena of nuclear transmutation of elements in condensed media.

References

1. N.V.Samsonenko, D.V.Tahti, F.Ndahayo. On the Barut-Vigier model of the hydrogen atom. Phys. Lett. A220 (1996) 297-301.
2. N.V.Samsonenko, D.V.Tahti, F.Ndahayo. Reply to the comment on "On the Barut-Vigier model of the hydrogen atom". Phys. Lett. A229 (1997) 133-134.
3. N.V.Samsonenko, A.F.Gay, D.V.Tahti, F.Ndahayo. On electromagnetic structure of nuclear forces using deuteron as an example. Materials of the 6th Russian conference on CNF- Sochi, 1966. (in Russian).

ON THE POSSIBILITY OF THE DINEUTRON EXISTENCE AND THE DIFFICULTIES OF IT'S EXPERIMENTAL DETECTION

N.V. Samsonenko, S.L.Doubkov

PFU of Russia, Moscow

In the frames of nonrelativistic quantum mechanics with due regard for spin-spin and spin-orbital interactions the possibility of the bounded states (real and virtual) with negative (common nuclei), positive (resonances) and zero energies is investigated. The case with zero energy due to the limited lifetime (instability) despite of good localization should most likely be considered as resonances.

It is shown that proceeding from the general principles of quantum theory (ordinary Schrödinger equation with traditional insertion of electromagnetic interaction by extension of derivatives and inclusion of Pauli term is used) the Hamiltonian without free parameters which under certain condition permits the existence of exact solutions for bounded states of two neutrons (dineutron) can be obtained. The dineutron properties, the difficulties of it's detection and the effects of its existence on traditional nuclear physics including nuclear transmutation of elements at low energies are analyzed.

THEORY OF COLD NUCLEAR TRANSMUTATION[1]

Mikio Fukuhara

Institute for Materials Research, Tohoku University
fukuhara@imr.tohoku.ac.jp

Abstract

The cold transmutation observed on the surfaces of Sr- or Cs-doped Pd/(CaO+ Pd)Pd complexes is interpreted to be a result of virtual ${}^{8}_{4}\mathrm{X}$ particle addition by the confinement of four interstitial solute deuterons jumping from four tetragonal sites to octahedral sites along [111] directions in a Pd/CaO lattice and electrostatic attraction due to the charge transfer in the chains of atoms; *i.e.*, an alternating tetrahedral-octahedral site arrays with the aid of the electron-phonon charge-density wave coupling and electropionic attraction effects due to the capture of excited electrons from Pd and Ca by vacuum pumping:

$${}^{88}_{38}\mathrm{Sr} + 4\,{}^{2}_{1}\mathrm{D} + 8\,\mathrm{e}^{*} \rightarrow {}^{96}_{42}\mathrm{Mo}$$

$${}^{133}_{55}\mathrm{Cs} + 4\,{}^{2}_{1}\mathrm{D} + 8\,\mathrm{e}^{*} \rightarrow {}^{141}_{59}\mathrm{Pr}$$

$${}^{137}_{56}\mathrm{Ba} + 6\,{}^{2}_{1}\mathrm{D} + 12\,\mathrm{e}^{*} \rightarrow {}^{149}_{62}\mathrm{Sm}$$

$${}^{138}_{56}\mathrm{Ba} + 6\,{}^{2}_{1}\mathrm{D} + 12\,\mathrm{e}^{*} \rightarrow {}^{150}_{62}\mathrm{Sm}.$$

The deuterons are a source of supply for reparation for mass balance in the transmutation. The roles of CaO are dissolution of Sr and Cs and the creation of a good route for deuteron rushing by aid of vacuum pumping.
* E-mail address: fukuhara@imr.tohoku.ac.jp

1. Introduction

Recently, Iwamura and coworkers [2,3] have reported that nuclear transmutations are observed on the surfaces of Pd/(CaO+Pd)Pd (hereafter referred to as Pd/ CaO) complexes, which consist of a thin Pd layer, alternating CaO and Pd layers, and bulk Pd, after subjecting the Pd complexes to D_2 gas permeation. When Cs, Sr, and Ba were added on the surfaces of the Pd complexes, Pr, Mo, and Sm emerged on the surfaces whereas the amount of Cs, Sr, and Ba decreased after the Pd complexes were subjected to D_2 gas penetration at 343 K and 1 atom for about one and two weeks. It was also noted that the increases in mass number are 8 and

12, and those in atomic number are 4 and 6 for the former and latter transmutations, respectively. This indicates the occurrence of cold (low-energy) nuclear transmutations from Cs to Pr, from Sr to Mo, and from Ba to Sm:

$$^{88}_{38}\mathrm{Sr} \rightarrow {}^{96}_{42}\mathrm{Mo} \qquad (1)$$

$$^{133}_{55}\mathrm{Cs} \rightarrow {}^{141}_{59}\mathrm{Pr} \qquad (2)$$

$$^{137}_{56}\mathrm{Ba} \rightarrow {}^{149}_{62}\mathrm{Sm} \qquad (3)$$

$$^{138}_{56}\mathrm{Ba} \rightarrow {}^{150}_{62}\mathrm{Sm}. \qquad (4)$$

Following the works of Iwamura and coworkers [2,3], Celani *et al*. [4] Kitamura *et al*.[5] and Yamada *et al*. [6] have confirmed the same results in different laboratories with different analytical methods. However, nobody has resolved any reasons for the transmutations yet. Furthermore, the role of Ca in the transmutations remains unknown.

Our interest lies in studying the dynamic interaction among deuterons in the Pd/ CaO lattice, assuming that the deuterons jump from the tetragonal sites to the octahedral sites to formation of a transient particle using the dynamics of an electron-phonon- coupled charged density wave (CDW) system. In this paper, a new interaction model is proposed on the basis of the collective resonance (excitation) of electrons and the resulting photon emissions from Pd and Ca atoms. The central problem of this work is to explain how the deuterons react with each other when there exists a potential barrier so high that it should not be possible for the deuterons to draw sufficiently near to interact. For experimental confirmation, the question is raised as to whether the compressive forces exerted by the metal structure could lead to such a confinement of deuteron pairs at the necessary close proximity. [7,8] In addition, the compensation of mass balance in transmutations is an open question.

We have investigated the physical roles of electrons and electron neutrinos for electromagnetic and weak atomic interactions and have reported that the electrons and neutrinos in a nucleus enhance the fusion reaction as well as the catalytic effect of neutral pions. [9] A cold transmutation being similar to the cold fusion is currently a hot topic in low-energy cold fusion science, although few works have been reported on this subject. [2-5,9-12]

2. Dynamic Interaction between He Nuclei and Formation of $^{8}_{4}X$

We first focus our discussion on eqs. (1) and (2) for a transmutation mechanism. From the reactions (1) and (2), we note the common point that the increases in mass number and atomic number are 8 and 4, respectively. Although increase in atomic number for eqs. (1) and (2) can be attained by two time- double β decay of Sr and Ca elements [9], it is impossible to get the increase in mass number. It is actually encouraging to consider a virtual $^{8}_{4}X$ particle for the processes. This is a transient particle that does not exist in nature. To elucidate both transmutation reactions, eqs. (1) and (2), we must consider the possible formation of the $^{8}_{4}X$ particle. In this case, it is necessary that the D, Pd and Ca elements are involved in the transmutations. If the $^{8}_{4}X$ particle exists, we can consider the following processes.

$$^{88}_{38}Sr + {}^{8}_{4}X = {}^{96}_{42}Mo \qquad (5)$$

$$^{133}_{55}Cs + {}^{8}_{4}X = {}^{141}_{59}Pr \qquad (6)$$

The $^{8}_{4}X$ is a four-*np* state whose isospin wave function is antisymmetric, where *n* and *p* are the neutron and proton, respectively. The first-order internuclear force among protons and neutrons in the $^{8}_{4}X$ nucleus must be mediated by eight charged pions, $\pi^{\pm}$, and eight neutral pions, π^{0}. On the other hand, the helium $^{4}_{2}He$ particle is composed of two protons and two

neutrons. These four nucleons must be combined by the attractive mediation of two charged and two neutral pions. Thus, the ${}^{8}_{4}\mathrm{X}$ can be formed by two helium nuclei,

$$ {}^{4}_{2}\mathrm{He} + {}^{4}_{2}\mathrm{He} = {}^{8}_{4}\mathrm{X}. \qquad (7) $$

We have already reported a neutral-pion-catalyzed fusion based on the collective resonance (excitation) effect of electrons derived from Pd. [13)]

$$ {}^{2}_{1}\mathrm{D} + {}^{2}_{1}\mathrm{D} + 2\,\pi^{0} = {}^{4}_{2}\mathrm{He}. \qquad (8) $$

From eqs. (5) and (6), we can obtain the following equation,

$$ 4\,{}^{2}_{1}\mathrm{D} + 4\,\pi^{0} = {}^{8}_{4}\mathrm{X}. \qquad (9) $$

If eq. (7) can occur from D_2 gas passing through the Pd/CaO complexes, we can replace the above-mentioned transmutations, eqs. (5) and (6), by

$$ {}^{88}_{38}\mathrm{Sr} + 4\,{}^{2}_{1}\mathrm{D} + 4\,\pi^{0} = {}^{96}_{42}\mathrm{Mo} \qquad (10) $$

$$ {}^{133}_{55}\mathrm{Cs} + 4\,{}^{2}_{1}\mathrm{D} + 4\,\pi^{0} = {}^{141}_{59}\mathrm{Pr}. \qquad (11) $$

Here, pions are responsible for all low-energy nuclear interactions; [14)] the pions within the nucleus allow the nucleonic species to bind together and transmute with each other.[10)] On the basis of isospin symmetry rule, a neutral pion is produced by the emission of excited electrons e* derived from palladium atoms: [15)]

$$ e^{-} \rightarrow e^{*}, \gamma, \qquad (12) $$

$$ \gamma + \gamma = \pi^{o}. \qquad (13) $$

On the other hand, an electron reacts with a deuteron to form a neutral pion and an electron neutrino: [16, 17)]

$$ e^{-} + {}^{2}\mathrm{D} \rightarrow $$

$$ \pi^{o} + \nu + \gamma. \qquad (14) $$

Kenny [16] has termed eq. (12) as the "electropionic reaction". Fukuhara[13] has also reported the following formula for the formation of helium:

$$^{2}D + ^{2}D + 4\,e^{*} = ^{4}He. \qquad (15)$$

From eqs. (10)-(13) and (15), we obtain

$$^{88}_{38}Sr + 4\,^{2}_{1}D + 8\,e^{*} \rightarrow ^{96}_{42}Mo \qquad (16)$$

$$^{133}_{55}Cs + 4\,^{2}_{1}D + 8\,e^{*} \rightarrow ^{141}_{59}Pr \qquad (17)$$

with the aid of the electropionic attraction due to the capture of the excited electrons and deuterons. In eqs. (16) and (17), D is a source of supply for reparation for mass balance in a nuclear transmutation. Since eqs. (16) and (17) are nonequilibrium (irreversible) equations, they do not obey the rules of parity and momentum balance. On the other hand, in the irreversible endothermic reaction proposed by Glansdorff and Prigogine [18], a marked enhancement is expected on the basis of the thermal factor of $\exp(-\Delta G/kT)$, where ΔG is the change in Gibbs energy for the entire system.

3. Roles of Pd, Ca and D for Transmutation

In the previous section, with a view to promoting transmutation process, the virtual $^{8}_{4}X$ particle, formed by two helium nuclei, was proposed. Notwithstanding such a necessary condition, it is further necessary to get reasonable reasons. Next, we consider a sufficient condition for a dynamic reaction.

In previous papers,[19,20] the reason why nitrogen exists so abundantly in the Earth's atmosphere has been interpreted as a result of the endothermic nuclear transmutation of carbon and oxygen atom pairs in a carbonate (Ca,D) CO_3 lattice of mantle,

$$^{12}C + ^{16}O + ^{2}D \rightarrow 2\,^{14}N + 2\,^{4}He, \qquad (18)$$

through the nuclear attraction effect due to the deuteron catalysis of nitrogen formation, based on double β decay during the Archean era. In this case, the configuration and cross section of the D-inserted compound (Ca,D) CO_3 resemble those of the Pd/CaO complexes in this study. Hence, by analogy, we can image the atomic configuration of D-inserted Pd- and CaO-coupled lattices with faced-centered cubic (fcc) structures (Fig. 1). Furthermore, we have reported the electron and the neutrino in a nucleus enhance the fusion reaction[9] as well as the catalytic effect of neutral pions for formation of nitrogen in Eartth[19].

Since deuterium can be inserted in to the tetrahedral sites of the Pd and CaO lattices, the atoms

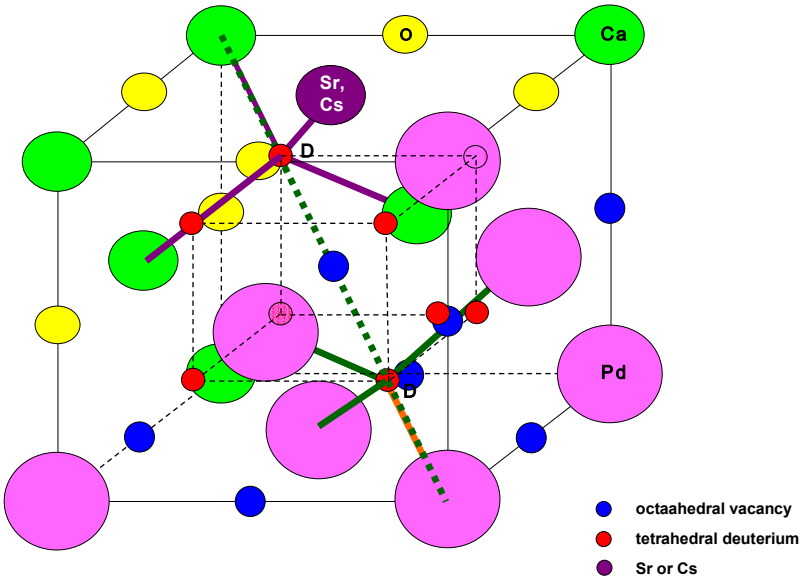

Fig.1 Sr-or Cs (small purple solid)-doped Pd/CaO complex crystal with tetrahedral D sites (small red solid) and octahedral vacancy sites (small blue solid) in Pd (large pink solid)/ Ca(middle light green solid)O(middle yellow solid) fcc lattice. The bold dot line indicates a chain (Ca-tetrahedral-site D- octahedral-site vacancy- tetrahedral-site D-Pd) along a <111> direction.

along four [111] directions are lined up in chains as follows: Ca-tetrahedral-site D-octahedral-site vacancy-tetrahedral-site D-Pd. The interstitial deuterons in PdDx and CaO are immersed in a sea of conduction electrons derived from the palladium and calcium atoms. Since the oxide CaO of Ca has an fcc lattice similar to that of Pd, it is suitable for the permutation of D_2 gases. Indeed, the bond lengths of Ca-D in CaO and Pd-D in Pd $D_{0.63}$ are 0.2080 and 0.1755 nm,[21] respectively, with a mismatch within ±16 %. Thus the useage of the CaO layer

promotes deuteron rushing by help of vacuum pumping. The actual passing route of deuterons is along four <111> directions in Fig. 1.

Next, we consider the cause of the local transition of deuterons in views of chemical potential effects in the Pd/ CaO complexes. Here, we note that coherency stress arises in the fluctuations of defects when atomic defects in crystals expand or contract the crystal lattice[22] because the elastic interaction between the defects is mediated by the strain fields of the defects. The coherency stress and long-ranged elastic interaction are characteristic of a solid state with the defects. Indeed, the potential minimum for a hydrogen atom located at the tetrahedral interstice of a base-centered-cubic (bcc) β-$VH_{0.5}$ crystal is markedly displaced toward the crystal position of the octahedral interstice when the c axis, more precisely the [112] direction c-axis, is uniformly elongated by an external force at a constant volume. [23] Because the atomic configuration of the {001} plane of bcc-β-$VH_{0.5}$ surrounded by four tetrahedral interstitials is similar to that of the {110} plane of the fcc PdD crystal, the coherency stresses along the [111] directions of substochiometric PdDx could arise in the fluctuations of the defects. Hence, by analogy, we infer that the forced vacuum pumping in the fcc Pd/CaO complex [2,3] causes coherency stress and the resulting large slope of chemical potentials for the deuterons, leading to deuteron rushing along the [111] directions. Thus, the local transition of the tetragonal deuterons by vacuum pumping would aid the transition. This is a necessary condition for the dynamic interaction of interest.

4. Possible Collective Resonance and Three-Dimensional CDW

As an interaction mode for the Pd-Ca-D system, we note that the breathing-mode displacement (Fig. 2) of the oxygen atoms in the perovskite solid solution $BaPb_{1-x}Bi_xO_3$

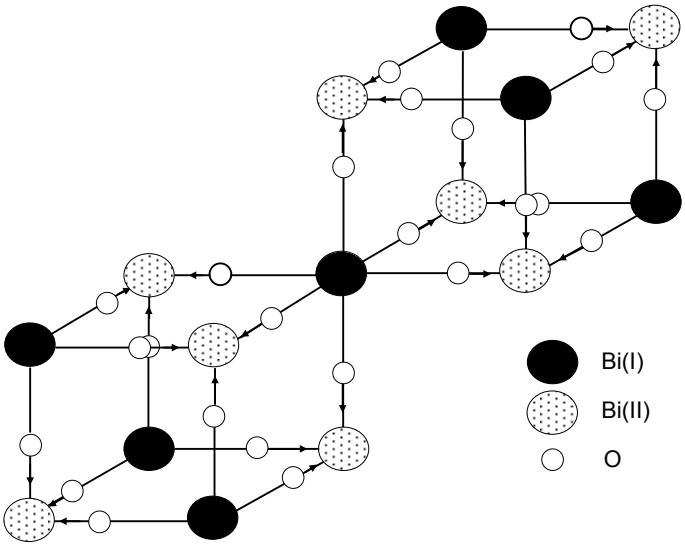

Fig.2 Breathing mode distortions of O atoms that form alternating arrays of inequivalent Bi(I)-Bi(II) sites.[19)]

causes the alternating expansion and contraction of the oxygen octahedral around the nonequilivalent Bi(I) and Bi(II) atoms [24)] and leads to a complete charge disproportion [charge-density wave (CDW) instability] state, *i.e.*, an alternating Bi^{3+}-Bi^{5+} array. [25)] In this case, the Fermi surface nests perfectly and the situation is favorable for the formation of a CDW. The CDW doubles the unit cell and creates a gap near the Fermi level. Because the deuteron atoms exist as itinerant deuterons in the Pd/CaO complex lattice, we expect a similar situation to occur for the Pd/CaO complexes.

As described in the previous section, the interstitial deuterons in the Pd and CaO lattices are surrounded tetrahedrally by four Pd atoms and four Ca atoms in a sea of conduction electrons. The CDWs are formed mostly in such materials, in which the atoms are lined up in chains (*i.e.*, an alternating tetrahedral $D^{+\delta}$-$Pd^{10-\delta}$ and $D^{+\delta}$-$Ca^{10-\delta}$ array [26)]), the following breathing-mode-like displacement of the deuterons occurs along the [111] directions.

The longitudinal deformation $\xi(z)$ of the phase $\phi(z)$ of the $2k_F$ CDW along the chain directions induces the charge redistribution $\xi u(z)$ with the wavelength $2\pi/\xi q$ and long-ranged

Coulomb forces, giving an optical frequency ($\omega^2 \neq 0$) at a longitudinal phason, which is a type of collective mode, *i.e.*, an exciting state:

$$u(z) = \sqrt{\frac{2}{\omega_{2k_F}}} \frac{\Delta}{g} \cos(2 k_F z + \phi(z)) \qquad (19)$$

$$\xi u(z) = \frac{1}{\pi} \frac{\partial \varphi}{\partial z} \qquad (20)$$

where g is the electron-phonon coupling constant, k_F the wave vector of the Fermi level, ω_{2k_F} the phonon energy for the lattice of the wavenumber $2k_F$, and 2Δ energy gap at the Fermi level. Thus, the tetrahedral-site deuterons are positively charged, and the octahedral-site vacancy is oppositely negatively induced. [27)]

When the further enrichment of deuterium leads to octahedral site occupancy by vacuum pumping, the positively charged tetrahedral-site deuterons plunge into the negatively charged octahedral-site vacancy owing to the electrostatic force in addition to the Coulomb force (A-type in Fig. 3). This leads to the confinement of deuteron pairs or the formation of deuteron clusters stuck with electrons at the necessary close proximity. Furthermore, when four tetrahedral-site deuterons simultaneously rush into the octahedral site along the [111] directions, the ${}^{8}_{4}\mathrm{X}$ nucleus would be formed as the fusion product, *i.e.*, the activated state product. Since the product is the transient particle of a shape isomer in the nucleus, it fuses with ${}^{88}_{38}\mathrm{Sr}$ or ${}^{133}_{55}\mathrm{Cs}$ occupying the Ca sites in the CaO lattice (Fig.1) in a moment, leading to the transmutation of interest. Another role of CaO is the dissolution of Sr and Cs. The jumping location of these interstitial solute deuterons

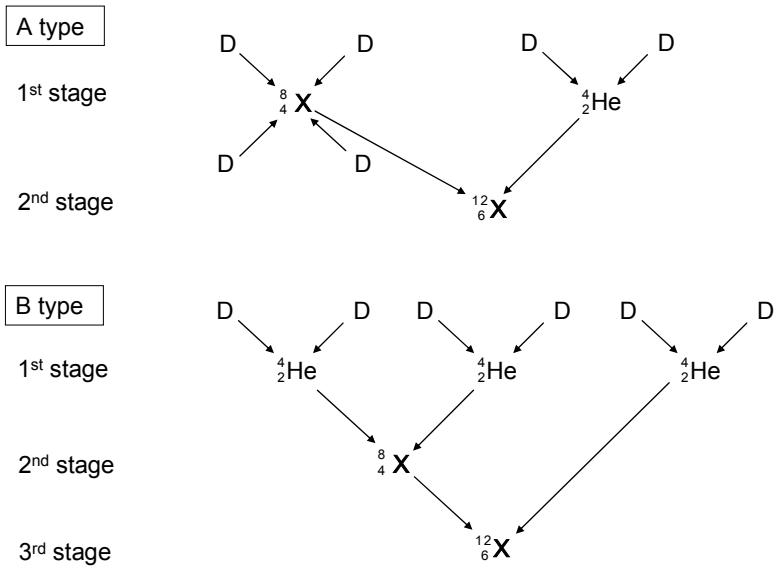

Fig.3 Transient transmutations (A- and B-types) of deuterons along [111] directions in Pd/CaO lattice.

is necessary for the transmutation. Because the CDW wavelength changes with the number of electrons, many electrons make the wavelength smaller, *i.e.*, the confinement stronger. It is known that the total oscillator strength in the collective resonance is approximately equal to the total number of oscillating electrons; [28] it is ~10 for the 4*d* resonance in Pd and ~10 for the 3*s*, 3*p,* and 4*s* electrons in Ca. The collective effect is strong only at energies above the first ionization threshold. The peak of the collective resonance is approximately at a frequency at which the atomic dielectric function $\varepsilon\ (k,\omega)$ with nonzero ω is zero. [29] Thus, the considerable confinement of two deuteron pairs could be attained by electrostatic attraction due to the collective resonance of many electrons.

On the other hand, the electron emission occurs when the collective motion of the excited state ceases, as described in eq. (12). It has reported that the emission of charged particles and the acceleration of the electrical charge enhance nuclear reactions, such as a fractofusion.[30, 31] In such a case, the excited electrons are generated by the rapid fracture and/or sliding of Pd crystals. The rapid permutation of the deuterons by vacuum pumping

would occur the excited electrons, as well as the effects of rapid fracture and crystal sliding. Furthermore, as can be observed from eqs. (10) and (11), the electron emission induces the physical catalysis of neutral pions for the transmutation of interest. [13)]

5. Dynamic Interaction between He Nuclei and the Formation of $^{12}_{6}X$

Lastly, we consider the other type's transmutations in eqs. (3) and (4). If the transmutations for eqs. (3) and (4) can be formed by another virtual $^{12}_{6}X$ particle, we can obtain the following formulae, as well as the above-mentioned procedure:

$$^{137}_{56}Ba + 6\,^{2}_{1}D + 6\,\pi^{0} \rightarrow {}^{149}_{62}Sm \qquad (21)$$

$$^{138}_{56}Ba + 6\,^{2}_{1}D + 6\,\pi^{0} \rightarrow {}^{150}_{62}Sm \qquad (22)$$

$$^{137}_{56}Ba + 6\,^{2}_{1}D + 12\,e^{*} \rightarrow {}^{149}_{62}Sm \qquad (23)$$

$$^{138}_{56}Ba + 6\,^{2}_{1}D + 12\,e^{*} \rightarrow {}^{150}_{62}Sm. \qquad (24)$$

Thus, we can image the reaction processes along [111] directions in a large slope of deuteron potentials by vacuum pumping. This is a scheme of type B in Fig. 3.

6. Conclusions

The nuclear transmutation $^{88}_{38}Sr \rightarrow {}^{96}_{42}Mo$, $^{133}_{55}Cs \rightarrow {}^{141}_{59}Pr$, $^{137}_{56}Ba \rightarrow {}^{149}_{62}Sm$ and $^{138}_{56}Ba \rightarrow {}^{150}_{62}Sm$ in the Pd/CaO complexes reported by Iwamura and coworker was interpreted as a result of the virtual $^{8}_{4}X$ particle and $^{12}_{6}X$ additions due to the confinement of four deuterons at necessary close proximity. The necessary condition for the transmutation is the jumping location transition of four interstitial solute deuterons from tetrahedral sites to octahedral sites along [111] directions, which arises from the large slope of deuteron chemical potentials. A

sufficient condition can be attained by electrostatic attraction among the deuterons due to the charge transfer in the chains of atoms (*i.e.*, an alternating tetrahedral-octahedral site array) with the aid of the electron-phonon CDW coupling based on the collective resonance of many oscillating electrons derived from Pd and Ca:

$$^{88}_{38}\mathrm{Sr} + 4\,^{2}_{1}\mathrm{D} + 8\,\mathrm{e}^{*} \rightarrow {}^{96}_{42}\mathrm{Mo}$$

$$^{133}_{55}\mathrm{Cs} + 4\,^{2}_{1}\mathrm{D} + 8\,\mathrm{e}^{*} \rightarrow {}^{141}_{59}\mathrm{Pr}.$$

The deuterons are a source of supply for reparation for mass balance in the transmutation. In the irreversible endothermic reaction, the marked enhancement is expected. The roles of CaO are the dissolution of Sr and Cs in Pd/CaO lattice, and the creation of a good route for deuteron rushing. In the case of the transmutations of $^{149}_{62}\mathrm{Sm}$ and $^{150}_{62}\mathrm{Sm}$, the following reactions can be proposed:

$$^{137}_{56}\mathrm{Ba} + 6\,^{2}_{1}\mathrm{D} + 12\,\mathrm{e}^{*} \rightarrow {}^{149}_{62}\mathrm{Sm}$$

$$^{138}_{56}\mathrm{Ba} + 6\,^{2}_{1}\mathrm{D} + 12\,\mathrm{e}^{*} \rightarrow {}^{150}_{62}\mathrm{Sm}.$$

References

1) M.Fukuhara, Jpn. J. Appl. Phys. **46, 5A** (2007) 3035.
2) Y. Iwamura, M. Sakano, and T. Itoh, Jpn. J. Appl. Phys. **41** (2002) 4642.
3) Y. Iwamura, T. Itoh, M. Sakano, N. Yamazaki, S. Kuribayashi, Y. Terada, T. Ishikawa, and J. Kasagi: *Condensed Matter Nuclear Science*, J. P. Biberian, Ed. (World Scientific Publishing, Singapore, 2004), pp. 339-358.
4) F.Celani, A.Spallone, P.Marini, V. di Strefano, M.Nakamura, A.Mancini, G.G'Agostaro, E.Right, G.Trenta, P.Quercia, C.Catena, V.Andreassi, F.Fontana, D.Garbelli, L.Gamberale, D.Azzarone,E.Celia, F.Falcioni, M.Marchsini and E.Novaro, Proc.4th Meeting of Jpn CF Res.Soc., Iwate University, Japan, pp.17-21.
5) A. Kitamura, R. Nishio, H. Iwai, R. Satoh, A. Taniike, and Y. Furuyama, *Condensed*

Matter Nuclear Science, A. Takahashi, K. Ota, and Y. Iwamura Eds. (World Scientific Publishing, Singapore, 2006), pp.272-277.

6) H.Yamada, S.Narita, S.Taniguchi, T.Ushirozawa, S.Kurihara, M.Higashizawa, H.Sawada and M.Itagaki, Proc.7th Meet. Japan Cold Fusion Research Society, Tokyo, 2006, p. 28.
7) M. Gai, S. L. Rugari, R. H. France, B. J. Lund, Z. Zhao, A. J. Davenport, H. S. Isaacs, and K. G. Lynn, Nature **340** (1989) 29.
8) D. E. Williams, D. J. S. Findlay, D. H. Craston, M. R. Sené, M. Bailey, S. Croft, B. W. Hooton, C. P. Jones, A. R. J. Kucernak, J. A. Mason, and R. I. Taylor, Nature **340** (1989) 375.
9) M.Fukuhara, Proc.6th Meet. Japan Cold Fusion Research Society, Tokyo, 2005, pp. 53-57.
10) S. E Jones, E. P. Palmer, J. B. Czirr, D. L. Decker, J. M, Thorne, S. F. Taylor, and J. Rafelsli, Nature **338** (1989) 737.
11) T. Mizuno, T. Ohmori and M. Enyo, Electrochem. **64** (1996) 1160.
12) F. Celani, A. Spallone, E. Righi, G. Trenta, C. Catena, G. D'agostraro, P. Quercia, V. Andreassi, P. Marini, V. Distefano, M. Nakamura, A. Mancini, P. G. Sona, F. Fontana, L. Gamberale, D. Garbelli, E. Celia, F. Falcioni, M. Marchesini, E. Novaro, and U. Mastromatteo: *Condensed Matter Nuclear Science*, J. P. Biberian, Ed. (World Scientific Publishing, Singapore, 2004), pp. 108-127.
13) M. Fukuhara, Fusion Sci.Tech. **43** (2003) 128.
14) D. F. Measday, and G. A. Miller, Annu. Rev. Nucl. Part. Phys. **29** (1979)121.
15) R. P. Feymann: *The Theory of Fundamental Processes*, (Benjamin/Cummings Publishing, London 1961) p.37.
16) J. P. Kenny, Fusion Technol. **19** (1991) 547.
17) M. Fukuhara, Fusion Technol. **34** (1998) 151.
18) P. Glansdorff and I. Prigogine, *Thermodynamic Theory of Structure, Stability and Fluctuations* (Wiley-Interscience, London, 1971).
19) M. Fukuhara, Nuovo Cimento **27** (2004) 99.
20) M.Fukuhara, Proc.7th Meet. Japan Cold Fusion Research Society, Kagoshima, 2006, pp. 71-73.
21) J. M.Rowe, J. J. Rush and H. G. Smith, H. G. Smith, M. Mostoller, and H. E. Flotow, Phys.Rev.Lett. **33** (1974) 1207.

22) S. Uchida, K. Kitazawa and S. Tanaka, Phase Transitions **8** (1987) 95.

23) H. Wipf, J. Volkl and G. Alefeld, Z.Phys.B, **76** (1989) 353.

24) H. Sugimoto, J. Phys. Soc. Jpn. **59** (1984) 2529.

25) L. F. Mattheiss and D. R. Hamman, Phys.Rev., **B28** (1983) 427.

26) S. Brown and G. Grüner, Sci.Am. **4** (1994) 28.

27) R. A. Swalin: *Thermodynamics of Solids* (John Wiley & Sons, New York, 1962) p. 275.

28) G. Mukhopdhyay and S. Lundqvist, J.Phys.,B, **12** (1979) 121297.

29) M. Fukuhara, Phys.Status Solidi B, **175** (1993) 421.

30) P. R. Price, Nature **343** (1990) 542.

31) J. T. Dickinson, L. C. Jensen, S. C. Langford, R. R. Ryan, and E. Garcia, J.Mater. Res. **5** (1990) 109.

NEW DISCOVERY: QUANTIZATION OF ATOMIC AND NUCLEAR REST MASSES AND SELF-ORGANIZATION OF ATOMS AND NUCLEI

F.A. Gareev [*], G.F. Gareeva [*] and I.E. Zhidkova [**]

[*] *Joint Institute for Nuclear Research ,BLTP, Dubna, Russia,*
gareev@thsun1.jinr.ru
[**] *University Dubna, mathematics department, Dubna, Russia*

Introduction

The review of possible stimulation mechanisms of LENR (low energy nuclear reaction) is presented in [1, 2, 3]. We have concluded that transmutation of nuclei at low energies and excess heat are possible in the framework of the known fundamental physical laws, the universal cooperative resonance synchronization principle [1], and different enhancement mechanisms of reaction processes [2]. The superlow energy of external fields, the excitation and ionization of atoms may play the role of a trigger for LENR. Superlow energy of external fields may stimulate LENR [3]. We give strong arguments that the cooperative resonance synchronization mechanisms are responsible for explanation of how the electron volt world can influence the nuclear mega electron volt world.

Nuclear physicists are absolutely sure that this cannot happen. Almost all nuclear experiments were carried out in conditions when colliding particles interacted with the nuclear targets which represented a gas or a solid body. The nuclei of the target are in the neutral atoms surrounded by orbital electrons. All existing experimental data under such conditions teach us that nuclear low energy transmutations are NOT OBSEDVED due to the Coulomb barrier.

LENR with transmutation of nuclei occurs in different conditions and different processes but these processes have common properties: interacting nuclei are in the ionized atoms or completely without electrons (bare nuclei). Therefore, LENR with bare nuclei and nuclei in ionized atoms demonstrated drastically different properties in comparison with nuclei in neutral atoms [2].

- LENRs take places in open systems in which all frequencies and phases are coordinated according to the universal cooperative resonance synchronization principle. Poor reproducibility of experimental results and extreme difficulties of their interpretation in the framework of the modern standard theoretical physics are the main reasons for the persistent non recognition of cold fusion and transmutation phenomena.

Recent progress in both directions is remarkable in spite of being rejected by physical society and this phenomenon is a key point for further success in the corresponding fundamental and applied research. The results of this research field can provide new ecologically pure sources of energy, substances, and technologies.

The possibilities of inducing and controlling nuclear reactions at low temperatures and pressures by using different low-energy fields and various physical and chemical processes were discussed in [2, 3]. The aim of this paper is to present the results of phenomenological quantization of atomic and nuclear masses and their differences which can bring new possibilities for inducing and controlling nuclear reactions by atomic processes and new interpretation of self-organizations of the hierarchical systems in the Universe.

HOW DO THE ATOMS and NUCLEI HAVE THEIR PERPETUAL MOTIONS?

Hydrogen Atom in Classical Mechanics

Is it possible to understand some properties of a hydrogen atom from classical mechanics? The Hamiltonian for a hydrogen atom is

$$H = \frac{m_p \vec{v}_p^{\,2}}{2} + \frac{m_e \vec{v}_e^{\,2}}{2} - \frac{e^2}{\left|\vec{r}_p - \vec{r}_e\right|}. \tag{1}$$

All notations are standard. The definition of the center of mass is

$$m_p \vec{r}_p + m_e \vec{r}_e = 0, \tag{2}$$

and the relative distance between electron and proton is

$$\vec{r} = \vec{r}_p - \vec{r}_e. \tag{3}$$

Equations (1) – (3) lead to the results:

$$\vec{r}_p = \frac{m_e}{m_p + m_e}\vec{r}, \quad \vec{r}_e = -\frac{m_p}{m_p + m_e}\vec{r}, \tag{4}$$

$$H = \frac{\mu \vec{v}^2}{2} - \frac{e^2}{r}, \tag{5}$$

where

$$\mu = \frac{m_p m_e}{m_p + m_e}. \tag{6}$$

The Hamiltonian (5) coincides with the Hamiltonian for the fictitious material point with reduced mass μ moving in the external field $-e^2/r$. If we known the trajectory of this fictitious particle $\vec{r} = \vec{r}(t)$ then we can reconstruct the trajectories of electron and proton using equations (4):

$$\vec{r_p}(t) = \frac{m_e}{m_p + m_e} * \vec{r}\,(\mathrm{t}), \quad \vec{r_e}(t) = -\frac{m_p}{m_p + m_e}\vec{r}(t). \tag{7}$$

It is evident from (7) that the proton and electron move in the opposite directions synchronously.

SO THE MOTIONS OF PROTON, ELECTRON and THEIR RELATIVE MOTION OCCUR WITH EQUAL FREQUENCY

$$\omega_p = \omega_e = \omega_\mu. \tag{8}$$

We can get from (7) that

$$\vec{P_p} = \vec{P}, \quad \vec{P_e} = -\vec{P}, \tag{9}$$

where $\vec{P_i} = m_i \vec{v_i}$. All three impulses are equal to each other in absolute value, which means the equality of

$$\lambda_D(p) = \lambda_D(e) = \lambda_D(\mu) = h/P. \tag{10}$$

- *Therefore, the motions of proton and electron and their relative motion in the hydrogen atom occur with the same FREQUENCY, IMPULSE (linear momentum) and the de Broglie WAVELENGTH. All motions are synchronized and self-sustained. Therefore, the whole system -hydrogen atom is nondecomposable into independent motions of proton and electron.*

We have proved [4] that the same conclusion should be correct for all nuclei and atoms.

Quantization of Nuclear and Atomic Rest Masses

Almost all quant mechanical models describe excited states of nuclei, atoms, molecules, condensed matter,... neglecting the structure of the ground state of the investigated systems. Therefore, we have very restricted information about the properties of nuclei, atoms,... in their GROUND STATES. Note that the mutual influence of the nucleon and electron spins (the superfine splitting), the Mossbauer effect,… are well-known. The processes going in the surrounding matter of nuclei change the nuclear moments and interactions of nucleons in nuclei.

- *We proved that the motions of proton and electron in the hydrogen atom in the ground state occur with the same frequency; therefore, their motions are synchronized. The cooperation in motion of nucleons in nuclei and electrons in atoms in their ground states is still an open problem. We formulate a very simple and audacious working hypothesis: the nuclear and the corresponding atomic processes must be considered as a unified entirely determined whole process. The nucleons in nuclei and the electrons in atoms form open nondecomposable whole systems in which all frequencies and phases of nucleons and electrons are coordinated according to the universal cooperative resonance synchronization principle.*

This hypothesis can be proved at least partly by investigation of the difference between nuclear and atomic rest masses. We performed this analysis for the first time (details in [4]).

The rest mass differences of atoms in the β-decay (single and double) and electron capture (single and double) processes, α-decay, the differences between nuclear and atomic rest masses are quantized by formula [4] (in $\frac{MeV}{c^2}$)

$$\Delta M = 0.0076293945 \cdot \frac{n_1}{n_2}, \quad n_1 = 1,2,3,\ldots, n_2 = 1,2,4,8\,. \tag{11}$$

The accuracy of this formula (SEVEN SIGNIFICANT NUMBERS) could be increased if we take into account in our calculations all masses of atoms and nuclei (3177) with TEN SIGNIFICANT numbers

$$M = 0.0076293945312 \cdot \frac{n_1}{n_2}, \quad n_1 = 1,2,3,\ldots, n_2 = 1,2,4,8\,. \tag{12}$$

Note that this quantization rule is justified for atoms and nuclei with different A, N and Z, and the nuclei and atoms represent coherent synchronized systems - a complex of coupled oscillators (resonators). It means that nucleons in nuclei and electrons in atoms contain all necessary information about the structure of other nuclei and atoms. This information is used and reproduced by simple rational relations, according to the fundamental conservation law of energy. Remember that the following relations exist:

$$E = Mc^2 = h\nu, \tag{13}$$

where E is energy, h is the Planck constant, and ν is frequency. Schrodinger wrote that an interaction between microscopical physical objects is controlled by specific resonance laws. According to these laws, any interaction in a microscopic hierarchic wave system a exhibits resonance character

$$\sum_{j=1}^{N} q_{ij} \nu_j = 0, \tag{14}$$

where i=1,2,3,... is a number of linear independent relations, q_{ij} is the matrix consisting of only integer numbers. Note that the binary relations from (14) can be rewritten in the following way:

$$\nu_i = \frac{n_j}{n_i} \nu_j, \;\; n_i(n_j) = \pm 1, \pm 2, \pm 3, ..., \tag{15}$$

In the classical case the resonance occurs only when the frequency of the external field is close to the proper frequency of the system. The commonly accepted point of view is that the integer numbers in resonance conditions (15) must be small numbers. In the case of the argumental pendulum D.B. Douboshenski and Ya.A. Duboshinsky [5] stable oscillations are maintained by an efficient coupling between subsystems whose frequencies can differ by two or more orders of magnitude. We come to the conclusion that the integer numbers n_i and n_j can be any numbers:

$$1 - 10^9 \;\; .$$

We originated the universal cooperative resonance synchronization principle and this principle is the consequence of the conservation law of energy.

The cooperative resonance synchronized processes occur in the whole system: cooperative processes including all nucleons and electrons in atoms, in condensed matter and in surrounds when the resonance conditions (15) fulfilled fall subsystems and the whole

system. In this case, the threshold energy Q can be drastically decreased by internal energy of the whole system or even more – for example, the electron capture by proton in nuclei can be accompanied by emission of internal binding energy (which is forbidden for the case of the electron capture by free protons) – main source of excess heat phenomenon in LENR. A half-life of neutron in nuclei changes dramatically and depends on the isotopes.

As a final result, the nucleons in nuclei and electrons in atoms have commensurable frequencies and the differences between those frequencies are responsible for creation of beating modes. The phase velocity of standing beating waves can be extremely high; therefore, the nucleons in nuclei and electrons in atoms should get information from each other almost immediately (instantaneously) using phase velocity. Remember that the beating (modulated) modes are responsible for radio and TV-casting.

The universal cooperative resonance synchronization principle is responsible for the very unity of the nuclei and atoms. The quantization atomic and nuclear masses (12) with the same quanta of mass confirmed our working hypothesis: atoms and nuclei are open systems in which all motions are self-coordinated.

Conclusion

Note that the quantization rule (11, 12) is justified for atoms and nuclei with different A, N and Z, and the nuclei and atoms represent coherent synchronized systems – a complex of coupled oscillators (resonators). It means that nucleons in nuclei and electrons in atoms contain all necessary information about the structure of other nuclei and atoms. This information is used and reproduced by simple rational relations, according to the fundamental conservation law of energy-momentum. We originated the universal cooperative resonance synchronization principle and this principle is the consequence of the conservation law of energy-momentum. As a final result, the nucleons in nuclei and electrons in atoms have commensurable frequencies and the differences between those frequencies are responsible for creation of beating modes. The phase velocity of standing beating waves can be extremely high; therefore, all objects of the Universe should get information from each other almost immediately (instantaneously) using phase velocity [1, 3]. Remember that the beating (modulated) modes are responsible for radio and TV-casting.

Therefore, we came to understand the Mach principle. There are different interpretations of the Mach principle. The Mach principle can be viewed as an entire universe being altered by the changes in a single particle and vice versa.

- *The universal cooperative resonance synchronization principle is responsible for the very unity of the Universe.*

We have shown only a very small part of our calculations by formula (11, 12) and the corresponding comparison with experimental data for atomic and nuclear rest mass differences. This formula produces a surprisingly high accuracy description of the existing experimental data. Our non complete tentative analysis has shown that the quantization of rest mass differences demonstrated very interesting periodical properties in the whole Mendeleev periodic table. We hope that it is possible to create an analog of the Mendeleev periodic table describing atomic and nuclear properties of the atomic and nuclear systems simultaneously.

We have proved [1, 2] the homology of atom, molecule (in living molecules too including DNA) and crystal structures. So inter atomic distances in molecules, crystals and solid-state matter can be written in the following way:

$$d = \frac{n_1}{n_2}\lambda_e, \tag{16}$$

where λ_e=0.3324918 nm is the de Broglie electron wavelength in a hydrogen atom in the ground state ($\lambda_e = \lambda_p$ in a hydrogen atom in the ground state) and $n_1\ (n_2) = 1, 2, 3, \ldots$.

In 1953 Schwartz [6] proposed considering the nuclear and the corresponding atomic transitions as a unified process. This process contains the beta-decay which represents the transition of nucleon from state to state with emission of electron and antineutrino, and simultaneously the transition of atomic shell from the initial state to the final one. A complete and strict solution of this problem is still needed.

We did the first step to consider the nuclear and atomic rest masses as unified processes (coupled resonators) which led us to establish the corresponding phenomenological quantization formula (11), and can bring new possibilities for inducing and controlling nuclear reactions by atomic processes and new interpretation of self-organization of the hierarchial systems in the Universe including the living cells.

LENR can be stimulated and controlled by the superlow energy external fields. If frequencies of an external field are commensurable with frequencies of nucleon and electron motions, then we should have a resonance enhancement of LENR. Anomalies of LENR in

condensed matter (in plasma) and many anomalies in different branches in science and technologies (for example, homoeopathy, influence of music in nature, rhythms, nanostructures…) should be results of cooperative resonance synchronization frequencies of subsystems with open system frequencies, with surrounding and external field frequencies. In these cases threshold energy can be drastically decreased by internal energy of the whole system – the systems are going to change their structures if more stable systems result. Therefore, we have now real possibilities to stimulate and control many anomalous phenomena including LOW ENERGY NUCLEAR REACTIONS even SUPER-CONDUCTIVITY [1].

We have in principle found a possible way to ACHIVE SUPER-CONDUCTIVITY AT ROOM TEMPERATURE [1].

References

1. Gareev, F.A. In: FPB-98, Novosibirsk, June 1998, p.92; Gareev, F.A.; G.F. Gareeva In: Novosibirsk, July 2000, p.161; Gareev, F.A.; Zhidkova, I.E.; Ratis, Yu.L. Preprint JINR P4-2004-68, Dubna, 2004 (in russian).

2. Gareev, F.A.; Zhidkova, I.E.; Ratis, Yu.L. In Proc. of ICCF11, Marseille: France: 31 October – 5 November, 2004, p.459; Gareev, F.A; Zhidkova, I.E. E-print arXiv nucl-th/0505021 v1 8 May 2005; E-print arXiv nucl-th/0511092 v1 30 November 2005; E-print arXiv nucl-th/0601015 v1 5 January 2006.

3. Gareev, F.A; Zhidkova, I.E. In Proc. of ICCF12, November 27 – December 2, 2005, Yokohama, Japan, in http://www.iscmns.org/iccf12/program.htm.

4. Gareev, F.A.; Zhidkova, I.E. E-print arXiv nucl-th/0610002 30 Sep 2006.

5. Doubochinski, D.B.; Duboshinsky, Ya.B. Dokladee Akademii Nauk SSSR, 204, N5, 1065 (1972).

6. Schwartz, H.M. J. Chem. Phys. 21, p.45, 1953.

CALCULATION OF TUNNELING PROBABILITY FOR THE STRONGLY SCREENED COULOMB BARRIER, AND CHECK-UP OF PROBABILITY OF WKB APPROACH

A.I. Goncharov*, V.A. Kirkinskii, V.V. Samovolik***

**Altai State University, department of Physics and Technology, gonch@theory.asu.ru*
***Institute of Geology and Mineralogy, Siberian Branch of the Russian Academy of Sciences, kirkinsk@uiggm.nsc.ru*

Transmission probability through Coulomb barrier for collisions of thermal deuterons in presence of strong screening was calculated by means of exact decision of Schrödinger equation. It was shown that probability calculated by the WKB method is strongly overestimated.

In a number of models of cold nuclear fusion (for example, for reaction d+d→^{4}He+γ +Q), the strong screening of Coulomb repulsion by the negatively charged particles (electrons, muons and hypothetic stable heavy particles) was assumed.

For calculation of influence of this screening, the shifted Coulomb potential is often used:

$$V(r) = \begin{cases} \dfrac{e^2}{r} - \dfrac{e^2}{r_s}, & r_n \le r \le r_s, \\ 0, & r < r_n \ \ or \ \ r > r_s. \end{cases} \qquad (1)$$

Here r is distance between of deuterons; $r_n \approx 10^{-13}$ cm – range of action of nuclear forces; $r_s = 10^{-11} - 10^{-10}$ cm – screening radius. We note once more that we consider the case of very strong screening, when $r_s \quad r_B$ or, in other words, screening energy $E_s = e^2/r_s$ is great: $E_s \approx 10^3 - 10^4$ eV, and so the potential barrier is highly narrow.

Formula for fusion rate contains transmission probability through barrier D. This value is often calculated by the WKB method, which is based on quasiclassical approach. In this approach factor D is [1]

$$D_{WKB} \approx \exp\left\{ -\frac{2}{\hbar} \int_{r_n}^{r_0} \sqrt{2\mu(V-E)}\, dr \right\}, \qquad (2)$$

where μ is reduced mass of pair of deuterons, E – overall kinetic energy of deuterons in center-of-mass system (collision energy); here we assume $E=2E_d$, where E_d is kinetic energy of deuteron; r_0 is turning point of classical trajectory.

One of the necessary conditions applicability a formula (2) is that de Broglie wavelength λ of particle must be a small value in contrast with barrier width:

$$\lambda << r_0 - r_n. \qquad (3)$$

Wavelength of thermal deuterons $E_d \approx 0.025$ eV is much greater than barrier width:

$\lambda \approx 10^{-8}$ cm $\quad r_0 - r_n \approx 2.5 \cdot 10^{-11}$ cm, i.e., condition (3) of applicability of formula (2) is fail.

The aim of our paper consists in exact calculation of transmission probability D and in making a comparison with D_{WKB}. We will consider only s-collisions because mainly such collisions yield fusion reactions.

Method of calculation D will be founded on analytical decision of Schrödinger equation

$$\frac{\hbar^2}{2\mu}\Delta\Psi(r) + [E - V(r)]\Psi(r) = 0.$$

At first let us find solutions in the regions of radius r where $V(r)$ is continuous and smooth function.

In the regions where $V=0$, solutions are

$$\Psi_1(r) = C_1 \frac{e^{\frac{i}{\hbar}pr}}{r} + \frac{e^{-\frac{i}{\hbar}pr}}{r}, \quad \text{if } r \geq r_s; \qquad (4)$$

$$\Psi_3(r) = C_3 \frac{e^{-\frac{i}{\hbar}pr}}{r}, \quad \text{if } r \leq r_n. \qquad (5)$$

Here C_1, C_3 are constants; p is momentum of particle. Solution (4) is a sum of incident and reflected waves, and solution (5) is transmitted wave.

$$\Psi_2(r) = e^{-iqr}[C_2^m M(\alpha,\gamma,2iqr) + C_2^u U(\alpha,\gamma,2iqr)], \qquad (6)$$

Solution of Schrödinger equation in the region $r_n \leq r \leq r_s$ is given by

where $q = [2\mu(E+e^2/r_s)]^{1/2}/\nabla$; M, U – Kummer functions [2] with parameters

$\alpha = 1 - i\mu e^2/(\nabla^2 q)$, $\quad \gamma = 2$.

Transmission probability equal to

$$D = |C_3|^2. \qquad (7)$$

Factor C_3 is to be found when finding the unified wave function in the region $0 \le r < \infty$; for that it is necessary to lace functions (4), (5), (6) and their first derivatives at the boundaries of regions, i.e. at the points r_s and r_n:

$$\begin{cases} \Psi_1(r_s) = \Psi_2(r_s), \\ \Psi_1'(r_s) = \Psi_2'(r_s), \\ \Psi_2(r_n) = \Psi_3(r_n), \\ \Psi_2'(r_n) = \Psi_3'(r_n). \end{cases}$$

These conditions present itself system of linear algebraic equations with respect to C_1, C_3, C^m_2, C^u_2.

Calculations were conducted under following numerical value of parameters:

- screening radius $r_s = 2.5 \cdot 10^{-11}$ cm (corresponds to Bohr radius of mesoatom);
- reduced mass of particle (pair of deuterons) $\mu = 0.167 \cdot 10^{-23}$ g;
- kinetic energy of particle $E = 2E_d \ge 0.05$ eV;
- range of action of nuclear forces $r_n = 10^{-13}$ cm.

Results of calculations are provided in Table 1.

Table 1. Transmission probabilities through barrier (1)

E_d, eV	D	D_{WKB}	D_{WKB}/D
0.025	$0.113 \cdot 10^{-9}$	$0.607 \cdot 10^{-5}$	53494.
0.05	$0.227 \cdot 10^{-9}$	$0.607 \cdot 10^{-5}$	26748.
0.1	$0.454 \cdot 10^{-9}$	$0.607 \cdot 10^{-5}$	13375.
0.25	$0.113 \cdot 10^{-8}$	$0.607 \cdot 10^{-5}$	5351.
2.5	$0.114 \cdot 10^{-7}$	$0.610 \cdot 10^{-5}$	537.
25.	$0.115 \cdot 10^{-6}$	$0.642 \cdot 10^{-5}$	55.6
250.	$0.135 \cdot 10^{-5}$	$0.103 \cdot 10^{-4}$	7.7
2500.	$0.628 \cdot 10^{-4}$	$0.201 \cdot 10^{-3}$	3.2

According to this table, *at rapprochement of low energy deuterons, transmission probability through barrier (1), calculated by formula (2), is overestimated by a factor of $10^4 - 10^5$. In as much as once overestimated fusion rate.*

For verification of this conclusion, we have compared D_{WKB} with exact probability D in the event of two more simple potentials with the same width (under given energy) and height, as beside shifted Coulomb potential: square barrier and bell-shaped barrier

$$V(x) = \frac{V_0}{\cosh^2 \alpha x}. \qquad (8)$$

Transmission probability for square barrier equal to [1]

$$D = \frac{4k^2\chi^2}{(\chi^2 + k^2)^2 \sinh^2 a\chi + 4\chi^2 k^2},$$

where a – barrier width, $k = (2\mu E)^{1/2}/\nabla$ - wavenumber; $\chi = [2\mu(V_0 - E)]^{1/2}/\nabla$, V_0 – barrier height. Transmission probability for barrier (8) equal to [1]

$$D = \frac{\sinh^2 \frac{\pi k}{\alpha}}{\sinh^2 \frac{\pi k}{\alpha} + \cosh^2\left(\frac{\pi}{2}\sqrt{\frac{8\mu V_0}{\hbar^2\alpha^2} - 1}\right)}, \quad \text{if } \frac{8\mu V_0}{\hbar^2\alpha^2} > 1.$$

Under given kinetic energy of particle E, height V_0 and width x_0 of this barrier, parameter α is calculated by formula

$$\alpha = \frac{1}{x_0}\operatorname{arch}\sqrt{\frac{V_0}{E}}.$$

Calculations were executed for particles with reduced mass $\mu = m_d/2$ and energy $E = 0.05$ eV. As a result following ratios of probabilities $\delta = D_{WKB}/D$ were found: $\delta = 3 \cdot 10^6$ in the event of square barrier and $\delta = 4.7 \cdot 10^4$ in the event of barrier (8). These numbers confirm the conclusion about *considerable overestimation of transmission probability, calculated by WKB method, for collision of thermal deuterons in presence of strong screening.*

This work is supported by RFBR (grant No 05-05-64930).

References

1. L.D. Landau and E.M. Lifshitz. Course of Theoretical Physics. Vol.3. Quantum Mechanics. Non-relativistic theory. – 1977.

2. M. Abramowitz and I. Stegun. Handbook of Mathematical Functions. – 1964.

ANOMALOUS NUCLEAR REACTIONS CREATED BY TORSION FIELD WITHIN ELECTROCHEMICAL SYSTEMS

Xingliu JIANG and Lijun HAN

Science School, Beihang University, Beijing 100037, China

Physicists know that we are immersed in an energy field—zero point electromagnetic energy field. The vacuum is now considered as filled with randomly fluctuating fields having the zero point energy spectrum. Anomalous heat and nuclear phenomena in electrical discharge systems including electrochemical cells with ultrafast processes within double layers could be explained by tapping the zero point energy associated with dynamic Casimir effect. Nuclear products with high concentration, unidentified tracks with highly collimated lines of low energy nuclear reactions in the electrochemical systems and glow discharge devices were recorded by CR-39 solid detectors and photo-films, and localized spots with chemical alterations were observed at our laboratory and others in world. The yields of nuclear transmutation products are related to the current distribution on the cathode surface. Transient processes in an open dynamic system always create vortex effect. A theoretical model of vortex dynamics creating torsion field proposed by Xingliu Jiang has been used for explanation of so called "cold fusion". Anomalous nuclear reactions generated by axial accelerated particles due to the torsion field are essential.

Submitted to ICCF-13

POLYNEUTRON THEORY

John C. Fisher

600 Arbol Verde, Carpinteria, CA 93013
jcfisher@fisherstone.com

Abstract

I suggest that neutron clusters of sufficient size are bound and stable against strong decay; and that they can react with ordinary nuclei by transferring neutrons to them, accepting neutrons from them, and binding with them to form composite nuclei. Implications of this enlarged scope of low energy nuclear physics include a chain reaction with nuclear fuel ^{2}H that produces energy, ^{4}He, ^{3}H, and a wide range of nuclear transmutations. Natural explanations emerge for these and other LENR nuclear phenomena for which evidence has been accumulating over the past two decades.

Polyneutron theory is based on the idea that conventional nuclear theory accounts for all LENR phenomena.

Low energy nuclear reactions require neutral particles. We are familiar with neutrons, which are responsible for ordinary nuclear reactions. Because neutrons have no electric charge they can approach any nucleus. There is no coulomb barrier. They can react with many different nuclei.

Consider fission of uranium. When a neutron meets and joins a uranium nucleus the nucleus can fission into two nuclei. These nuclei emit two or three neutrons as they settle into their ground states, so one neutron leads to two or three. Each of the two or three causes fission of another uranium nucleus and becomes two or three itself, and so on. We have a chain reaction that builds up to a level where we can get useful power.

But neutrons are not seen in the LENR phenomena that we study. We need another kind of neutral particle and it must be something to which conventional nuclear physics applies. What could it be?

One possibility is neutron clusters, or polyneutrons. These are isotopes of the neutron. Their existence enlarges the table of isotopes. If we knew the masses of polyneutrons we could calculate which polyneutron reactions would be exothermic, how much energy they would produce, and what products they would produce. Now the questions become: How can we determine if polyneutrons actually exist? How can we determine their masses?

I suggest this can be done the same way we determined that neutrons actually exist. Nobody has ever seen a neutron. The approach was to hypothesize a neutron: its mass, its spin, its magnetic moment; then to use the hypothesis to try to understand experiments; to try to deduce the properties that a neutron would need to have in order to explain the experiments; and finally to become confident that the idea of a neutron having these

properties was a good idea, and that it made sense to accept that neutrons really do exist. That's how we came to accept neutrons.

For polyneutrons the same approach applies. We hypothesize that polyneutrons exist. We use this hypothesis to try to understand experiments, to try to deduce the properties that polyneutrons must have in order to explain the experiments, and finally to become confident that the idea of polyneutrons is a good idea and that it makes sense to accept that polyneutrons really do exist. [Of course it may be that this effort will fail, and that the polyneutron idea will be proven wrong and will be discarded. We do not yet know. As yet there are too few experimental results to guide us and the estimates of polyneutron masses are not very accurate.]

But we cannot discard the polyneutron idea just because experiment shows that di-neutrons and tri-neutrons are not bound. A recent experiment at CERN suggests that four neutrons are bound. The binding strength may increase for larger numbers. We have to consider polyneutrons composed of hundreds, or even thousands, of neutrons.

Experiment can place quantitative requirements on polyneutron properties. For example, there must be a chain reaction to build up large numbers of polyneutrons, just as there is a chain reaction to build up the numbers of neutrons in ordinary reactors. Otherwise the energies from polyneutron reactions would be too small.

For neutrons we have the reaction chain neutron → fission of uranium → two or three neutrons, and so on. There is a different path for polyneutrons, beginning with polyneutron growth. A polyneutron absorbs a neutron from a deuterium nucleus, leaving a hydrogen nucleus and a larger polyneutron. (Or it absorbs two neutrons from an oxygen-18 nucleus, leaving an oxygen-16 nucleus and a larger polyneutron.) By many iterations of such incremental growth reactions a polyneutron will grow bigger and bigger. When it is large enough the reaction energy generated in the growth reaction can cause it to fission into two smaller polyneutrons. These then can grow and fission, and so on. We have a polyneutron chain reaction.

This explanation for a polyneutron chain reaction provides a constraint on polyneutron masses. Polyneutron growth is possible only when neutrons are more strongly bound to the polyneutron than to the deuterium and oxygen-18 nuclei from which they come: the masses of the products have to be smaller than the masses of the reactants. This constraint suggests how experiment can begin to assign quantitative values to polyneutron masses.

Other experiments that can further constrain the masses of polyneutrons include observations of helium, of tritium, of Miley and Iwamura transmutations, of energy from electrolysis, of energy from diffusion of deuterium through a palladium film with cadmium oxide under the surface, of an Oriani shower of 150,000 alpha particles in the vapor over an electrolyte, of smaller showers of hundreds of alphas, and of relatively isolated alphas not clearly from showers. It must be possible to assign properties to polyneutrons such that all these phenomena can be explained.

Conversely any reaction that is energetically possible for polyneutrons must be observable. We cannot have implications that are not actually expressed. Consider polyneutron decay as an example. We know that a free neutron transforms into a proton plus an electron plus an antineutrino, with a half-life of about 15 minutes. This is beta decay. We expect that the neutrons in a polyneutron can undergo beta decay, perhaps at a faster rate. In consequence we expect the following series of reactions. First a neutron in a polyneutron decays to a proton. The proton cannot escape the cluster. Its mass as a free particle is too large. It stays bound. Then another neutron beta decays. Now it is energetically favorable for an alpha particle (a helium nucleus composed of two protons and two neutrons) to be emitted. This leaves a new polyneutron with four fewer neutrons. The process repeats over and over:

beta, beta, alpha; beta, beta, alpha; … and so on until the polyneutron is fully transformed to helium.

Hence overall the decay of a polyneutron must be observed as emission of a sequence of alpha particles. If these are rapid and if decay occurs in a vapor a CR39 detector will record a shower of alpha particles. If the emissions are slower the polyneutron may move between alpha emissions and a more nearly random pattern of tracks will be produced. Fortunately for the theory both showers and random patterns have been observed. Polyneutrons pass this test.

Additional experiments are required to determine the energies of the alpha particles and thereby to pin down more closely the required masses of the polyneutrons. So far it seems possible to assign masses that are consistent with experiment. These are approximate masses because the available experiments are insufficient to constrain them more tightly. But it does seem that we are moving toward polyneutron reality. This is only a beginning, but polyneutron theory seems to have survived so far.

I want to emphasize that throughout this work ordinary nuclear theory has been applied. No new fundamental particles are required---just neutrons and protons, recognizing that some nuclei contain no protons. Success of the theory depends on its ability, with these simple assumptions, to universally provide quantification and understanding of all the LENR phenomena. If it cannot do this, or if it predicts phenomena that do not actually occur, it will be proven wrong.

ABOUT THE FEATURES OF LEPTON TERLETSKI QUADRIGA IN ELECTROMAGNETIC VACUUM

L.I.Kholodov[1)], I.V.Goryachev[2)]

1) Barmin Design Bureau of General Machinebuilding
2) Russian Research Center "Kurchatov Institute"

The worldwide physical community is becoming more and more consolidated in understanding that it would most likely have to revise many old theoretical theses in physics during the nearest 10-20 years to come since the new intellectual scientific revolution in natural sciences as a whole is approaching. This revolution was probably initiated with the idea by E.Gliner who suggested in 1965 hypothesis assuming the initial condition of the entire matter in the Universe being just vacuum though that theory was hard to take in within any "reasonable" frames of comprehension. In those years vacuum was understood as void (emptiness, "nothing"). No wonder that even such an outstanding famous theoretician in physics as Yakov Zeldovich at first was very critical regarding the Gliner's idea. But 15 years later this idea turned out to become a fundamental principle in theoretical cosmology.

Approximately at the same time another outstanding physicist Ya. Terletski suggested a supposition that every physical field with positive density of energy had a double field with negative density of energy. From that assumption it resulted that in line with appearing particles with zero average energy and zero average momentum out of vacuum there should appear both particles with positive mass (referred to as "positons") and particles with negative mass ("negatons"). Later based on his hypothesis Terletski came to a conclusion that groups of four particles ("quadrigae") consisting of a pair of positons and a pair of negatons can occur out of mere vacuum (i.e., out of "nothing").

Later in his work "Cosmological consequences of the hypothesis of occurring complexes of particles with positive and negative mass out of vacuum" published in the proceedings of the VII All-Union Conference «Modern theoretical and experimental problems of the Theory of Relativity and Gravitation» (city of Yerevan, Armenia, 1988) and in the collection «Problems of theoretical physics» (Peoples Friendship University PH, Moscow, 1990), Ya. Terletski developed his theory that stipulated a possibility of spontaneous appearing fours (quadrigae) of particles consisting of a pair of positons and a pair of negatons out of pure vacuum (i.e., out of "nothing").

Terletski's work was taken as the basis for considering a wide scope of problems of modern physics that resulted in composing a collection of articles: .

Leonid I. Kholodov, Igor V. Goryachev

NEW APPROACH TO UNDERSTANDING ORIGINATION OF MATTER AND ENERGY IN THE UNIVERSE

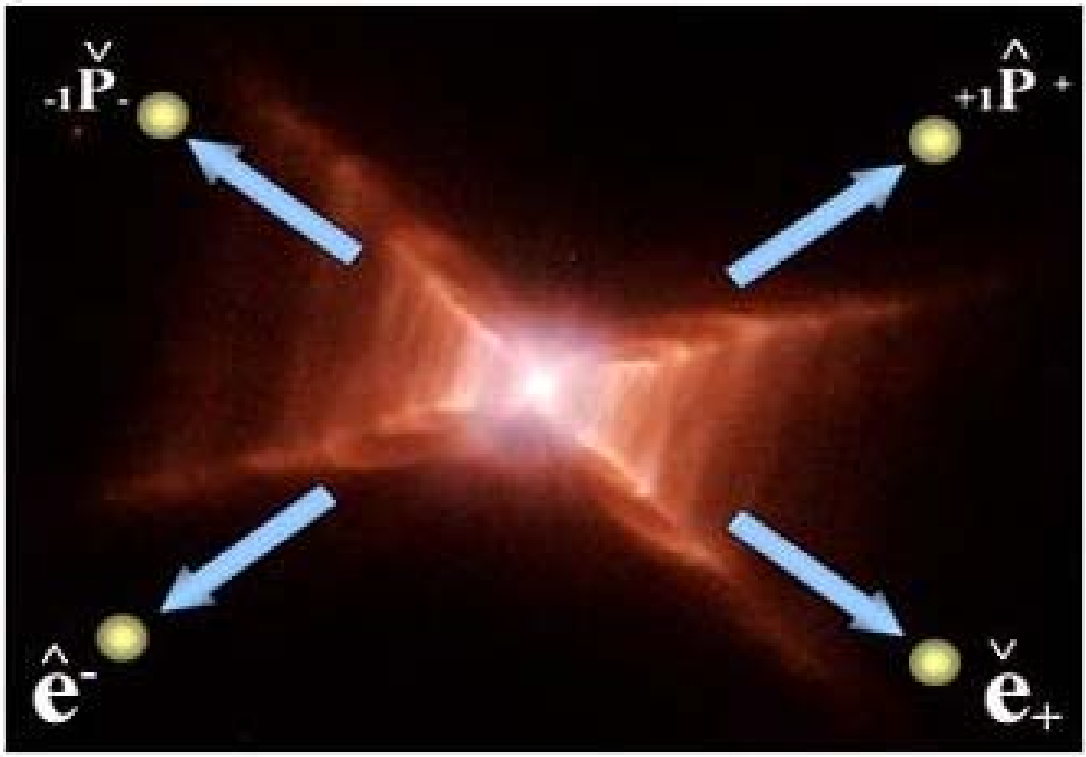

Moscow - 2007

Abstract

The paper presented hereinafter is actually a fragment from the book "New Approach to Understanding Origination of Matter and Energy in the Universe"

The features of Lepton Terletski Quadriga (LTQ) in vacuum with electro-magnetic constants ε_0 and μ_0 have been considered. The consideration is based on the assumption that ε_0 and μ_0 are correspondingly specific linear capacity and inductance of electro-magnetic structure of vacuum in the form of LTQ:

$$\varepsilon_0 = \varepsilon_{LTQ} = C/l \text{ и } \mu_0 = \mu_{LTQ} = L/l ,$$

where C and L – capacity and inductance of positon electric dipole $\hat{e}^+ - \hat{e}^- \bar{p}_{\acute{Y}} = e\bar{l}$ and of magnetic negaton dipole $\breve{e}_+ - \breve{e}_- \bar{p}_M = g\bar{l}$ LTQ.

It is shown that if the positon energy of LTQ to defined through ε_0 as $\hat{W} = \frac{e^2}{2C} = \frac{e^2}{2\varepsilon_0}\frac{1}{l}$

and to compare it with the energy of a quantum $E = \hbar\omega = h\frac{c}{\lambda}$; $h\frac{c}{\lambda} = \frac{e^2}{2\varepsilon_0}\frac{1}{l}$, then l will come up to $l = \frac{e^2}{2\varepsilon_0 hc}\lambda = 7{,}3 * 10^{-3}\lambda = \alpha\lambda$.

Then it follows that the CONSTANT OF FINE STRUCTURE is equal to the relation of the length of the positon dipole $\hat{e}^+ - \hat{e}^-$ to the quantum wave length $\alpha = l/\lambda$. Based on that it was proposed to determine that LTQ is the electromagnetic cell of vacuum with $\varepsilon_0 = \varepsilon_{LTQ}$ and $\mu_0 = \mu_{LTQ}$, that provides the equal phase speed of quanta of different frequencies: $v_\varphi = \frac{1}{\sqrt{\varepsilon_0\mu_0}} = \frac{1}{\sqrt{\varepsilon_{LTQ}\mu_{LTQ}}} = C = C_{LTQ}$, which looks like in an electric line of transferring energy without losses $v_\varphi = \frac{1}{\sqrt{C_0 L_0}}$, where C_0, L_0 - capacity and inductance per unit of the line length.

There has been considered participation of LTQ and α in forming more complicated structures of physical vacuum and demonstrated a hypothetical hierarchy of qualitatively different levels of matter states in vacuum which is characterized by the local constants $e_k = \alpha^k e$, $g_k = \alpha^k g$, $h_k = h\alpha^{2k}$ at $e^2 k/hkc = e^2/hk = \alpha$, where k=0,1,2… ∞ provided that transitions of quanta inbetween the levels are admitted according the following versions: $\omega_k = \omega_0 = \text{const}$ and $E_k = E_0 = \text{const}$. It is shown the difference between the constant C in rotating movement and $C_{Bk} = C$ in straight line movement is equal to $C_{\Pi к} = C/\alpha^k$. On the levels k=1,2…∞ the constant $C_{\Pi к}$ increases up to …∞ while the energy of quanta decreases $E_k = h_k C_k/\lambda = h\alpha^{2k} \cdot C/\alpha^k \cdot 1/\lambda = hc/\lambda\,\alpha^k$. On the first level k=1 of the "hierarchy" the energy of a quantum $E_{\gamma 1} = 511 \cdot 10^5 \cdot \alpha = 3{,}73$ keV which coincides with the Avramenko constant $W_{КВ} = e^2 mc/h = 3{,}73$ keV.

The work also contains comparison of the R.Avramenko concept of availability of the natural background of electroniv Bose-condensate in vacuum with the Y.Terletski hypothesis of

appearing out of vacuum quadrigae of particles with positive and negative masses, in particular with regard to the nature of the hidden mass in the Universe, instant transitions of interactions, nature of neutrino.

I.

In this paper the authors continued considering the role of LTQ in vacuum; the model of the LTQ being presented in Fig.1 [1].

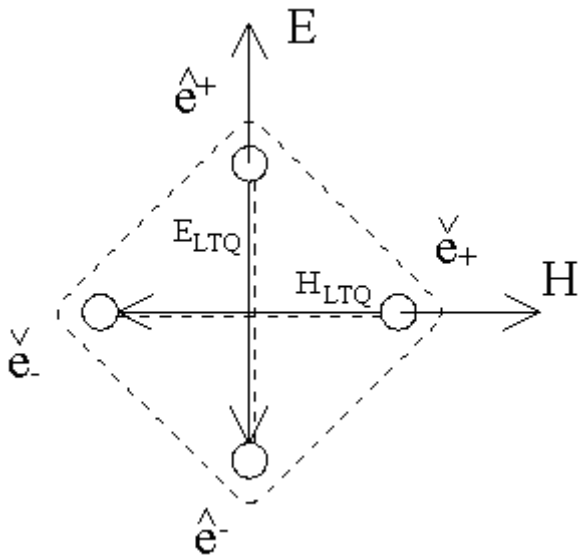

Fig.1. *LTQ in the form of virtual vacuum excitation.*

Many physicists consider vacuum as just empty space. At the same time vacuum has real electrical and magnetic characteristics without which it is hard to imagine physics as a science about the features of matter; also electrical engineering and some other fields of knowledge can hardly be imagined without those characteristics. Those characteristics are as follows:

- electrical constant $\varepsilon_0 \approx \frac{1}{4\pi 9*10^9}\frac{F}{m}$, (1)

- magnetic constant $\mu_0 \approx 4\pi*10^{-7}\frac{H}{m}$, (2)

- electrodynamic constant $\tilde{N} = \frac{1}{\sqrt{\varepsilon_0\mu_0}} \approx 3*10^8\frac{m}{s}$, (3)

- specific resistance of vacuum $Z_c = \sqrt{\frac{\mu_0}{\varepsilon_0}} = 120\pi \approx 377Om.$ (4)

Having the above indicated parameters says in favour of electromagnetic structure of vacuum. That is why we tried to find out how the LTQ can be coordinated with the electromagnetic constants $\varepsilon_0, \mu_0, C, Z_c$.

The following laws of conservation take place in LTQ:

$$\sum m = 0, \sum E = 0, \sum p = 0, \sum q_e = 0, \sum q_g = 0, \sum L = 0, \sum B = 0.$$

While $\sum E = 0$: $E^+ + E^- = 0$, $E^+ = -E^-$ (5)

It can be seen in Fig.1 that positons $\hat{e}^+ - \hat{e}^-$ make up electrical dipole $\bar{p}_{\acute{Y}} = q_e \bar{l}$ with the capacity C and the energy of field being equal to:

$$\hat{W} = \frac{CU^2}{2} = \frac{Q^2}{2C} = \frac{\varepsilon_0 E^2 V}{2}. \quad (6)$$

It can also be seen in Fig.1 that negatons $\breve{e}_+ - \breve{e}_-$ make up magnetic dipole $\bar{p}_M = q_g \bar{l}$ with inductance L and the energy of field being equal to:

$$\breve{W} = \frac{LI^2}{2} = \frac{\psi^2}{2L} = \frac{\mu_0 H^2 V}{2} \quad (7)$$

We assumed that:

- the electrical constant ε_0 is a linear specific capacity of positon dipole $\hat{e}^+ - \hat{e}^-$:

$$\varepsilon_0 = \varepsilon_{LTQ}\left[\frac{T^4 I^2}{L^3 M}\right] = \frac{C}{l}\left[\frac{T^4 I^2}{L^2 M}\frac{1}{L}\right], \quad (8)$$

- magnetic constant μ_0 is a linear specific inductance of negaton dipole $\breve{e}_+ - \breve{e}_-$:

$$\mu_0 = \mu_{LTQ}\left[\frac{LM}{T^2 I^2}\right] = \frac{L}{l}\left[\frac{L^2 M}{T^2 I^2}\frac{1}{L}\right]. \quad (9)$$

We also assumed that if $\varepsilon_0 = \varepsilon_{LTQ}$ can be used to determine positon energy $\hat{W}$ of LTQ:

$$\hat{W} = \frac{Q^2}{2C} = \frac{Q^2}{2\varepsilon_0}\frac{1`}{l}, \quad (10)$$

And compare it with the energy of quantum $E^+ = \hbar\omega = hc/\lambda$:

$$\frac{hc}{\lambda} = \frac{e^2}{2\varepsilon_0}\frac{1}{l}, \quad (11)$$

then the length of dipole $\bar{p}_{\acute{Y}} = e\bar{l}$:

$$l = \frac{e^2}{2\varepsilon_0}\frac{1}{hc}\lambda, \quad (12)$$

Turns out to be equal to:

$$l = \frac{(1{,}6*10^{-19})^2 \lambda}{2*0{,}885*10^{-11}*6{,}626*10^{-34}*3*10^8} \approx 7{,}28*10^{-3}\lambda = \alpha\lambda. \quad (13)$$

which results in:

$$\frac{l}{\lambda} = \alpha! \tag{14}$$

So, the most important fundamental scale parameter of microworld – the constant of fine structure $\alpha = 1/137$ is actually the relation of the LTQ $\bar{p}_{\acute{Y}} = e\bar{l}$ to the quantum wavelength λ with energy $\hat{W} = E^{+}$.

The LTQ negaton energy $\breve{W}$ of its magnetic dipole $\bar{p}_M = g\bar{l}$ and its length l, in our opinion, should be in modulus equal to positon ones so that the sum of all above mentioned laws of conservation is equal to zero.

As is known, in a lossles line of transmission the phase speed of electrical signals does not depend on the frequency:

$$v_\varphi = \frac{\omega}{\beta} = \frac{1}{\sqrt{C_0 L_0}}, \tag{15}$$

where C_0, L_0 - are the capacity and inductance per a unit of length, and β - factor of the phase, defining the variation of the phase per unit of length.

It means that the signals of different frequencies spread along the line of transmission with the same speed without distorsion [2].

In vacuum signals of different frequencies also spread without distortion with the same phase speed:

$$v_\varphi = \frac{1}{\sqrt{\varepsilon_0 \mu_0}} = \frac{1}{\sqrt{\varepsilon_{LTQ} \mu_{LTQ}}} = C = C_{LTQ}. \tag{16}$$

So we come to the conclusion that LTQ is actually electromagnetic vacuum cell having the characteristics analogous to a line of transmitting electrical signals without distortion which provides spreading signals (quanta) in electromagnetic vacuum with the same phase speed without losses.

II.

In a number of works [3, 4 and other] we showed that there can take place a hypothetical hierarchy of qualitatively different levels os matter status in vacuum (“Hierarchy”), which are characterized by the local constants in the forms of succession of the constant of fine structure α^k è α^{2k} (fig.2)**:**

$$e_k = \alpha^k e,\ g_k = \alpha^k g,\ \hbar_k = \hbar\alpha^{2k}, \text{ где k = 0, 1, 2…}\infty \text{ и } \frac{e_k^{\,2}}{\hbar_k c} = \frac{e^2}{\hbar c} = \alpha. \tag{17}$$

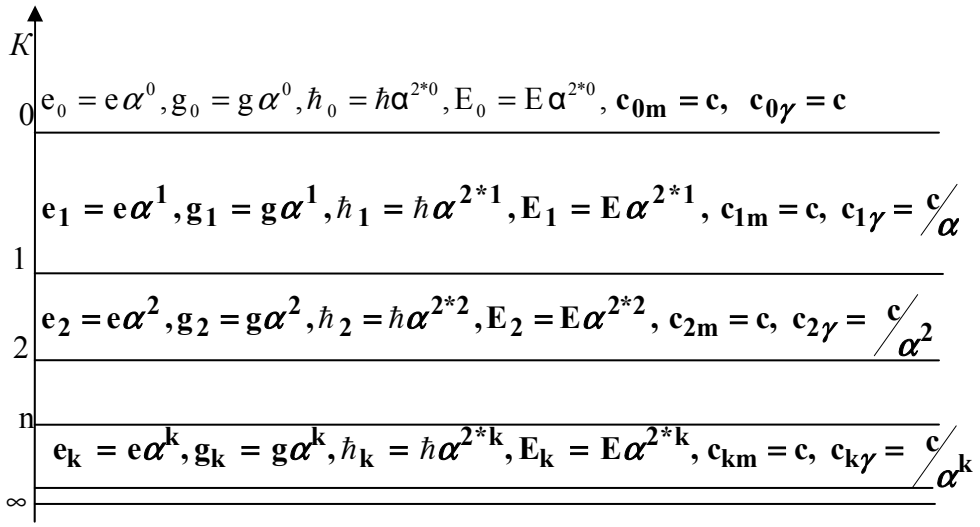

Fig.2. *Hierarchy of qualitatively different levels of matter in vacuum at* $k \to \infty: \; e_k \to 0, \; g_k \to 0, \; \hbar_k \to 0, \; E_k \to 0, \; m_k^{\pm} \to 0, \; c_{km} = \tilde{n}\, \grave{e}\, \tilde{n}_{\hat{e}\gamma} \to \infty$.

Multiplicity of qualitatively different states of matter in vacuum should be interconnected and admit transitions of quanta (particles) from one level onto another one following some laws. We have considered two versions of determinating quanta of energy and particles.

$$E = \hbar\omega = mc^2 . \tag{18}$$

From the level κ=0 onto the levels $k = 0,1,2...\infty$ and back when the constants are:

$$1.\ \omega_k = \omega_0 = const , \tag{19}$$

$$2.\ E_k = E_0 = const . \tag{20}$$

In the first version of determination the sizes of particle are constant while the mass and energy change

$$m_k = \omega_0 \frac{h_k}{c^2} = \omega_0 \hbar_0 \frac{\alpha^{2k}}{c^2} = m_0 \alpha^{2k} , \tag{21}$$

$$E_k = \hbar_k \omega_k = \hbar_k \omega_0 = \hbar_0 \alpha^{2k} \omega_0 = E_0 \alpha^{2k} . \tag{22}$$

In the second version the mass and energy of quanta are constant on all levels of "Hierarchy"

$$m_k = m_0 = const , \tag{23}$$

$$E_k = E_0 = const . \tag{24}$$

While the frequency ω_k and the constant $\hbar_k$ change as follows:

$$E_k = \hbar_k \omega_k = \hbar_0 \omega_0 = E_0 = const ,$$

hence

$$\omega_k = \omega_0 \frac{\hbar_0}{\hbar_k} = \omega_0 \frac{\hbar\alpha^{2*0}}{\hbar\alpha^{2*k}} = \omega\alpha^{-2k} . \tag{25}$$

Graphically the qualitative picture of location of the levels of hierarchy of matter state in vacuum and the versions of reflections of quanta (particles) from the level k = 0 onto the levels k = 1, 2, 3, … are shown in Fig.3.

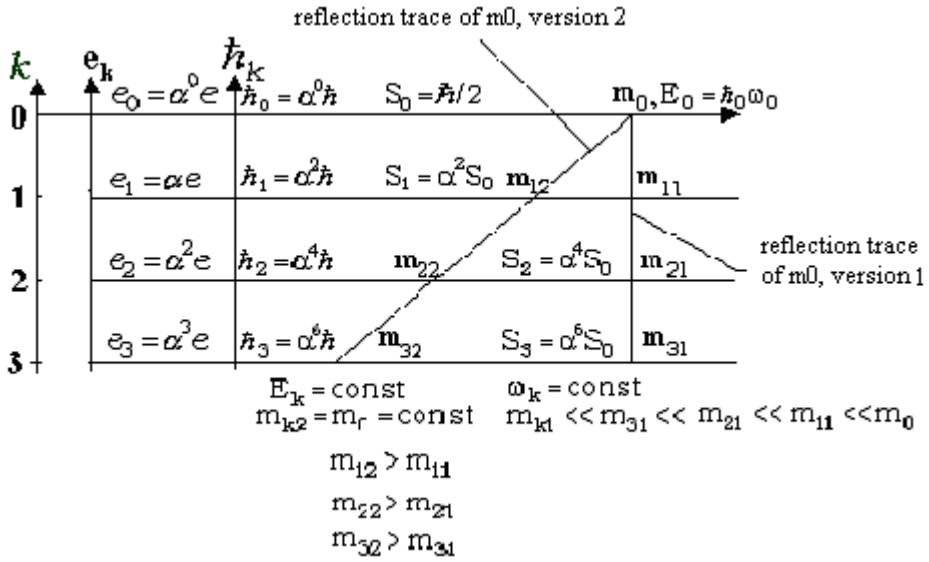

Fig.3. *Graph of reflection of quanta and particle in the "Hierarchy"*

In the "Hierarchy" there exist isotropic and similarity of the space. It is just the conception of a point is extended: it turns into "matryoshka" with infinite number of qualitatively different states of matter. Depending on how the point is considered: at $\omega = const$ or at $E = const$, qualitative change of its characteristics happens:

- at $\omega = const$ the transitions from $k = 0$ tp $k = \infty$ result in step-by-step changing energy E_k and mass m_k, associated with the point of the particle – i.e. in their changing by quantizing proportional to $\left(\alpha^k\right)^{2n}$;
- at $E = const$ the transitions from $k = 0$ to $k = \infty$ result in step-by-step quantizing of their frequency from ω_0 to $\omega_k = \infty$.

Hence, it can be concluded that each point of the space has infinite quantized energy and wave dualism.

The elementary particles e, p, n and others are located on the main level k=0 of the "Hierarchy". Their analogues e_k, p_k, n_k…and others can exist on the levels k = 1, 2…∞. For example, the so called Okhatrin leptons [3] having mass equal to:

$$m_\nu = k_c m_H = 2{,}8 * 10^{-9} * m_H, \qquad (26)$$

where m_H is the mass of the elementary particle and $k_c = \left(\alpha^2\right)^2 = 2{,}8 * 10^{-9}$ - conformity factor.

Okhatrin expressed a consideration that microleptons can be incorporated into the structure of atoms and their nuclei and also locate around the electrons.

When deriving the general formula of scaling the levels of the "Hierarchy" (17)

$$\alpha = \frac{e_k^2}{\hbar_k C} = \frac{\left(e\alpha^k\right)^2}{\hbar\alpha^{2k} C} = \frac{e}{\hbar C}.$$

The velocity of light C was admitted to be the same on all the levels k=1, 2, 3, …∞ .

Let's consider to what extent such postulate is justified under the traditional understanding of the nature of physical vacuum. On the level k=0 C is an electrodynamical constant which is a function of the electrical ε_0 and magnetic μ_0 constants of vacuum

$$C = \frac{1}{\sqrt{\varepsilon_0 \mu_0}}. \tag{27}$$

In order to determine if C is the same constant on all the levels of the hierarchy k=1, 2, 3, …∞, we would need to verify whether ε_0 and μ_0 stay unchanged on all the levels k of the hierarchy.

On the level k=0 there exist interrelation between the electric charge e and the electrical constant of vacuum ε_0. This connection is described by the formula:

$$e = N\varepsilon_0, \tag{28}$$

whence

$$N = \frac{e}{\varepsilon_0}, \qquad \frac{e}{N} = \varepsilon_0. \tag{29}$$

Let's assume that the same interrelation between electriccharge and electrical constant is affective for the whole succession of the electrical charges of the hierarchy

$$N = N = const. \tag{30}$$

Then the electrical constant ε_{ok} for each level k=1, 2, 3, …∞ will be as follows:

$$\varepsilon_{ok} = \frac{e_k}{N} = \frac{e \cdot \alpha^k}{N} = \varepsilon_o \alpha^k. \tag{31}$$

Suppose that there exists the analogous interrelation between magnetic charge and magnetic constant of vacuum

$$g = M\mu_o \tag{32}$$

$$M = \frac{g}{\mu_o}; \qquad \frac{g}{M} = \mu_o. \tag{33}$$

Whence at M=Const for each level k=1, 2, 3, …∞ we will get the constant μ_{ok}

$$\mu_{ok} = \frac{g}{M} = \frac{g\alpha^k}{M} = \mu_o \alpha^k, \tag{34}$$

The specific wave resistance of vacuum on the level k=0 is equal to:

$$Z_c = \frac{E_m}{H_m} = \sqrt{\frac{\mu_o}{\varepsilon_o}} = 377\,Ohm \tag{35}$$

The specific wave resistance of vacuum on the levels k=1, 2, 3, …∞ will come to:

$$Z_{\tilde{n}k} = \sqrt{\frac{\mu_{ik}}{\varepsilon_{ok}}} = \sqrt{\frac{\mu_i \alpha^n}{\varepsilon_o \alpha^n}} = \sqrt{\frac{\mu_o}{\varepsilon_o}} = Z_{co} = 377\,Ohm \qquad (36)$$

Since $Z_{ck} = Z_{co}$ it makes

$$\frac{E_{mk}}{H_{mk}} = \frac{E_{mo}}{H_{mo}}. \qquad (37)$$

Whence it is evident that it is impossible to determine experimentally the difference between the levels of the "Hierarchy" through the wave characteristics of electromagnetic field.

At the same time the electrodynamic constant of vacuum C turns out to be locally the same for each level *k*=1, 2, 3, …∞ that increases in line with the increase of the level number up to infinity:

$$C_k = \frac{1}{\sqrt{\varepsilon_{ok} \cdot \mu_{ok}}} = \frac{1}{\sqrt{\varepsilon_o \alpha^k \cdot \mu_o \alpha^k}} = \frac{1}{\sqrt{\varepsilon_o \mu_o} \cdot \alpha^k} = \frac{C_0}{\alpha^k} = \frac{C}{\alpha^k} \qquad (38)$$

In order to solve the contradiction between the initial postulate $C = Const$ and the resultant $C_k = \infty$ we propose to take into account the following considerations.

So far it was not common in physics to pay attention at the fact that the velocity of light C is actually implemented in two ways: as the limit velocity of rectilinear motion $C_П$ and as the limit speed of rotation C_B. In rectilinear motion a particle mass, according to the Special Theory of Relativity, depends from the velocity: $m = \frac{m_o}{\sqrt{1-\frac{v^2}{C^2}}}$ and at v → C, $m \to \infty$, but it never reaches the limit value. (39)

In internal rotation the particle mass does not change and its speed has a limited value equal to $C = C_B$. In this case C_B may be considered as a particle generating speed.

On the level k=0 $C_П = C_B$, hence we can consider just C = Const independently from the type of motion which is typical for modern physics.

Having the hierarchy available of the qualitatively different levels of matter the equality $C_П = C_B = C = Const$ will be valid only for the transitions between levels k=1, 2, …∞ of the particles with definite static mass. This limitation is not valid for the photons having no static mass. That's why the velocity of propogation of electromagnetic waves at k=1, 2, 3, …∞, also approaching infinity according formula (38).

The energy of quanta (photons) in the space of "Hierarchy" k=1, 2, 3, …∞, propogating with velocity $C_n = \frac{C}{\alpha^k}$ at ω and λ=const is determined by formula

$$E_k = \hbar_k \omega = \hbar_k \frac{C_k}{\lambda} = \hbar \alpha^{2k} \frac{C}{\alpha^k \lambda} = \hbar \frac{C}{\lambda} \alpha^k = E_0 \alpha^k \qquad (40)$$

That's why the energy of γ-quantum in the "hierarchy" k=0, 1, 2…∞ will be quantized decreasing as α^k:

k=0 $E_{\gamma 0} = E_0 \alpha^0 = 511 * 10^5 eV$

k=1 $E_{\gamma 1} = E_0 \alpha^1 = 511 * 10^5 * \alpha = 3{,}73 keV$

k=2 $E_{\gamma 2} = E_0 \alpha^2 = 511 * 10^5 * \alpha^2 = 27{,}2 eV$

k=3 $E_{\gamma 3} = E_0 \alpha^3 = 511 * 10^5 * \alpha^3 = 0{,}198 eV$

k=4 $E_{\gamma 4} = E_0 \alpha^4 = 511 * 10^5 * \alpha^4 = 1{,}45 * 10^{-3} eV$

. . . . . .

Since in the "Hierarchy" versions of reflection of quanta from the level k=0 onto the levels k=1, 2…∞ and back, then on the level k=0 there will be the following resonant magnitudes of energy corresponding to the levels k=1, 2…: 3,73keV, 27,3eV,… (Fig.4).

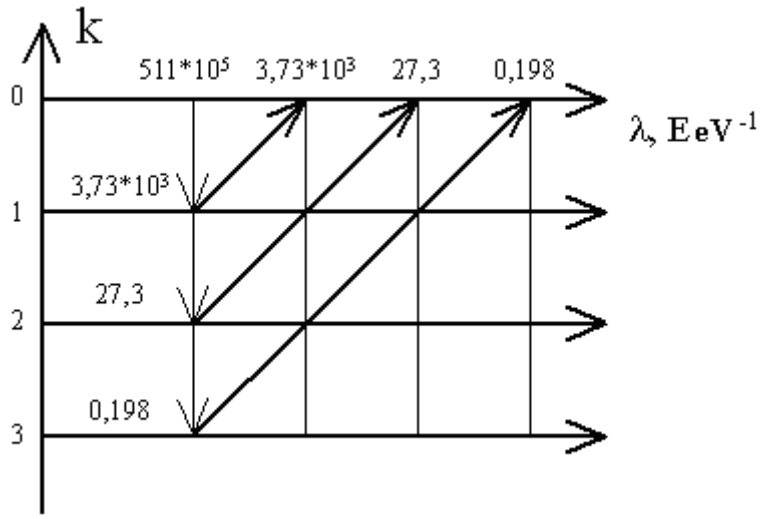

Fig.4.*Reflecting γ-quantum from the level k=0 → k=1, 2… and back k=1, 2…→ k=0.*

III.

Confirmation of such quantizing of electromagnetic vacuum on the levels k=1, 2… and a possibility of reflecting quanta onto the commonly used in physics level k=0 can be seen frpm the experiments of academician R.Avramenko and his associates. They derived a new constant

$$W_{KB} = \frac{e^2 mc}{\hbar} = 3{,}73 keV\,, \qquad (41)$$

which specify additional energy per particle (electron) in its propogation in convection current [6].

This experimental constant W_{KB} coincides in magnitude with our theoretically derived resonant quantum energy of γ-quantum in "hierarchy" on the level k=1:

$$W_{KB} = \frac{e^2 mc}{\hbar} = \frac{e^2 mc}{\hbar} * \frac{c}{c} = \frac{e^2}{\hbar c} * mc^2 = \alpha * mc^2 = \alpha * \frac{hc}{\lambda} = E_{k1}, \qquad (42)$$

Since the energy of electron and γ-quantum are the same mc^2 actually represent the potential static energy of electron and the energy of γ-quantum $\frac{hc}{\lambda}$ is the kinetic energy of the same quantum.

R.Avramenko had formulated the concept of natural background of electron Boze-condensate (BEBC). According to his concept the Universe is filled with the field of condensate of electrons with a non-zero static mass, the electrons being coupled like the Kuper pairs in superconductors.

According to Avramenko's supposition existence of BEBC justifies availability of the constant W_{KB} in vacuum and allows to answer many fundamental questions of modern astrophysics and physics such as:

1. About the nature of hidden mass in the Universe. Avramenko admits that BEBC comprises >90% of the whole mass of the Universe ;
2. Possibility of instant transition of interactions;
3. About the nature of neutrino. According to the concept neutrino as a particle simply does not exist since the impulse and the energy in β-decay is partly transferred to BEBC.

In our opinion, these Avramenko's statements need to be evaluated taking into account different models of physical vacuum. A probable model for such a case can be the stipulated model of physical vacuum that is being developed in our works. We call it "Terletski type vacuum".

Based on the laws of symmetry Ya.Terletski supposed that every physical field with positive density of energy $g^+>0$ should exist a "double" field with negative density of energy $g^-<0$. This supposition shpuld enevitably result in the phenomenon that in line with appearing particles with zero average energy and zero average momenntun out of vacuum there should appear particles with both with positive mass (positons) and with negative mass (negatons).

We take the basic Terletski hypothesis stipulating a possibility of appearing out of pure vacuum (i.e., out of nothing) fours (quadrigae) of particles consisting of a pair of positons and a pair of negatons [7]. In section I above (Fig.1) it was shown that electromagnetic vacuum is mostly based on Lepton Terletski Quadriga (LTQ), consisting of electrical dipole $\breve{e}^+ - \breve{e}^-, \bar{p} = e\bar{l}$ and magnetic dipole $\breve{e}_+ - \breve{e}_-, \bar{p} = g\bar{l}$. Fig.5 shows a "hierarchical" LTQ, in which $\breve{e}^{\pm} \to \breve{e}_k^{\pm}$ and $\breve{e}_{\pm} \to \breve{e}_{\pm k}$:

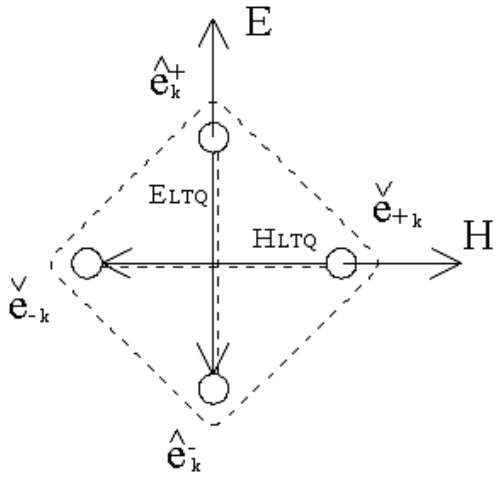

Fig.5. *LTQ in the form of virtual vacuum excitation in "Hierarchy"*

Assuming availability of BEBC the whole Universe should consist of a continuous negative electrical charge. The Kooper mechanism is introduced to overcome Coulomb repulsion of charges.

In LTQ's act Coulomb mechanism of attraction of opposite charges (with taking into account quantizung charges in "Hierarchy"), and their appearing happens with polarization under the influence of external electrical E and magnetic H fields. So, the resultant both electrical and magnetic charges of vacuum in the Universe each will be equal to zero.

In LTQ's as well as in BEBC particles are considered in the form of deBroigle wave packs with total spin equal to zero. That's why LTQ obtains the features of Boson. Simultaneously LTQ, as is shown in section I, is an electromagnetic cell of vacuum with characterisrics of a line for transition of electrical signals without losses which provides propogation of signals (quanta) in electromagnetic vacuum with the same phase velocity without losses. It means that LTQ has absolute optical transparency [2]. This feature of BEBC was not investigated in R.Avramenko's works. Under the influence of external fields and at weak interaction of particles LTQ is transformed into vector boson with spin s=1.

The mass of positon dipole LTQ $\overline{p}_e = e\overline{l}$ of the pair $\hat{e}^+ - \hat{e}^-$ is equal to double positive mass of electron as well as in BEBC. So, Terletsky type vacuum can comply with the Avramenko's supposition that the hidden positive mass of the Universe is contained in the electrons of BEBC. Additional positive mass in Terletsky type vacuum can be got at the expense of the total energy of the particles, filling vacuum in the space of the levels k=1, 2…∞ of the "Hierarchy".

Avramenko states about a possibility of instant transfering interactions of particles (quanta) based on experiments unknown to us. Such a possibility was not proved with calculations either. In Terletsky type vacuum increasing of the velocity of transferring interactions is provided by the fact that the velocity of straight linear propogation of quanta in "Hierarchy" reaches infinity with increasing the number of the level k=1, 2…∞ $C_n = \dfrac{C}{\alpha^{k\to\infty}} \to \infty$.

In our work [8] it was shown that the modern system of symmetry CPT considers physical processes only in the space of positive mass. That's why it seems as though the law of symmetry are violated for neutrino. When CPT is extended into the space of negative masses such a violation is abolished. We call such a widen CPT-symmetry a Terletsky type

symmetry T(CPT). The full picture of neutrino and antineutrino symmetry in T(CPT) is shown in Fig.6.

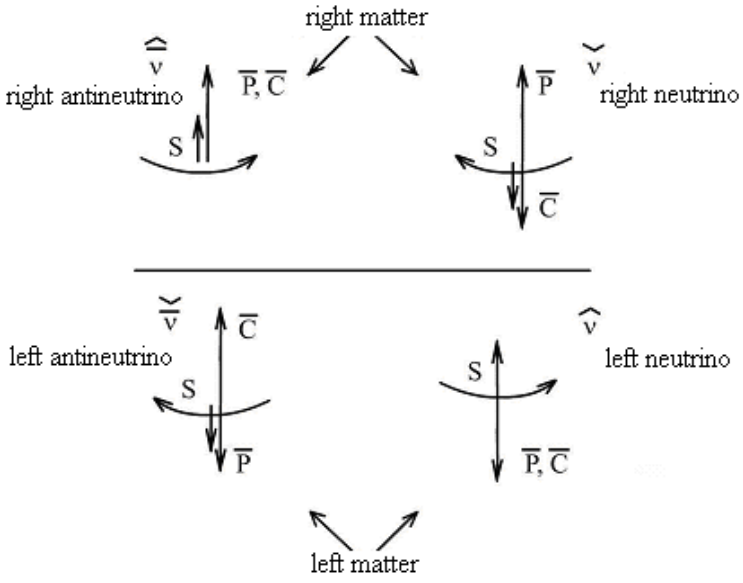

Fig.6. *T(CPT) neutrino and antineutrino*

R.Avramenko determined mostly right that the impulse and energy in β-decay are partly transferred to BEBC. But it yet does not mean that neutrino as a particle does not exist. In our works [4,9] it was shown that in β-decaying neutron does really interact with vacuum. In that process LTQ, having spin s=0, transforms into Z-boson with spin s=1, which then interacts with one of neutron d-quarks, turning it into u-quark. In the result of that interactions neutron transforms into proton and an electron and a antineutrino are irradiated into space from the decaying Z-boson (Fig.7).

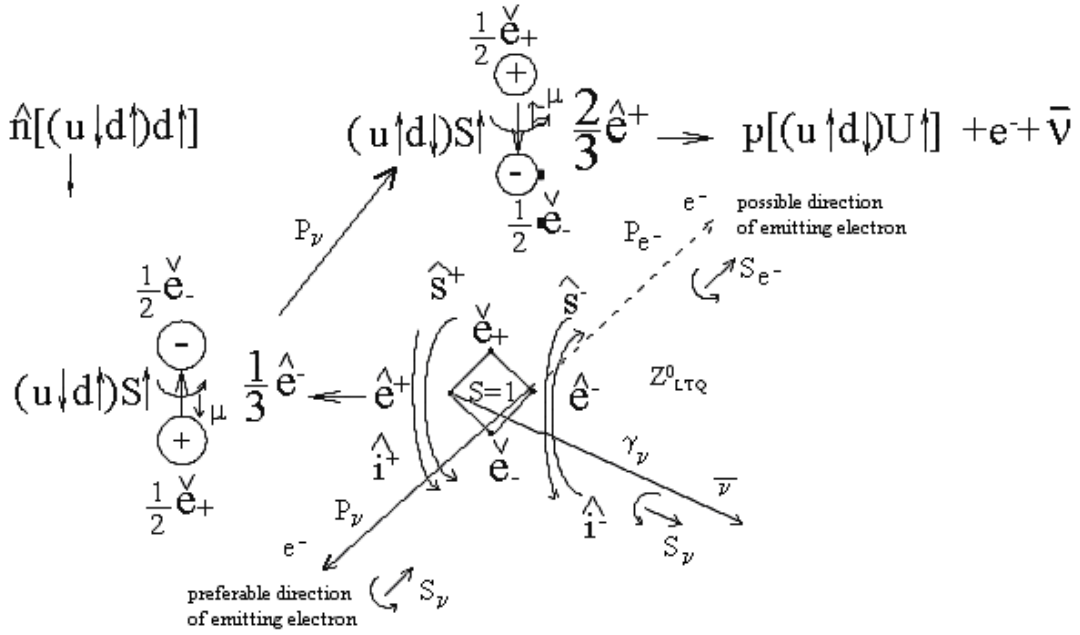

Fig.7. *LTQ model of neutron β-decaying*

Comparison of Avramenko's concept and Terletsky's hypothesis and the consequences derived from them are summarized in Table.1.

Table 1.

Features	Model of vacuum	
	R.Avramenko's model	Ya.Terletsky's model
1. Quantum addition of energy per particle (electron)	$W_{KB} = \frac{e^2 mc}{\hbar} = 3{,}73 êýÂ$	$W_{KI} = h\frac{C}{\lambda}\alpha = 3{,}73 êýÂ$
2. Hidden mass of the Universe	>90% mass of the Universe	>90% mass of the Universe
3. Total electrical charge of the Universe	∞	0
4. Possibility of instant transfer of interactions	Experimentally visible but not proved theoretically	Available since $C_{ÏÊ} = \frac{C}{\alpha^k}$, k=1,2…$\infty$
5. Quantizing charge of **e**	$e = const$	$e_k = \alpha^k e$, k=0,1,2…
6. Quantizing of Plank constant $\hbar$	$\hbar = const$	$\hbar_k = \hbar\alpha^{2k}$
7. Quantizing of electrical constant ε_0	$\varepsilon_0 = const$	$\varepsilon_k = \varepsilon_0\alpha^k$
8. Quantizing of magnetic constant μ_0	$\mu_0 = const$	$\mu_k = \mu_0\alpha^k$
9. Mechanism of transferring electromagnetic interaction	?	Provided $\lambda = \alpha \cdot l$ of a dipole
10. Mechanism of transferring weak interaction	?	Provided by means of $Z_{0\,LTQ}$
11. Availability of neutrino	Not available	Being an elementary fundamental particle

It follows from the table that the Avramenk's model of vacuum and Terletsky's one coinside in such fundamental parameters as $W_{KB} = W_{KI}$, hidden mass of the Universe, instant transfer of interactions. So, it would be reasonable to continue developing both models using experimental means.

References

1. Kholodov L.I., Goryachev I.V. About the features of Terletski Lepton Quadriga. Proceedings of 14th Russian Conference on cold nuclear transmutation and Ball lightning. –M., 2006.
2. Demirchan K.S., Neuman L.G., Korovkin N.V., Chechurin V.L. Theoretical basics of electrical engineering, v.2,3 , C-Пб, 2003.
3. Kholodov L.I. Non-traditional view on the structure of physical vacuum. –M., Russian Peoples Friendship University, 2000.

4.Kholodov L.I., Goryachev I.V., «Preliminary considerations about dynamic features of Terletsky Quadriga». Proceedings of 11-th Russian Conference on Cold Transmutation of Nuclei of Chemical elements and Ball Lightning. – M., 2004, p.210-227.
5.Okhatrin A.F. Microlepton concept of biolocation effects. "Argus" № 1. Sverdlovsk, 1991.
6.Future is opened with quantum key. Collection of academician R.Avramenko's articles. – M., "Chemistry", 2000.
7.Ya.P.Terletsky. Cosmological consequences of the hypothesis of appearing out of vacuum of complexes of particles with positive and negative mass. Proceedings of the 7th All-Union conference "Modern theoretical and experimental problems of the Theory of Relativity and Gravitation", Yerevan, Yerevan State University, 1988г., p.457.
8.Kholodov L.I., Goryachev I.V. Some considerations about the mechanism of appearing Terletsky Quadrigae out of vacuum. Proceedings of 14-th Russian Conference on Cold Transmutation of Nuclei of Chemical elements and Ball Lightning. – M., 2006.
9.Kholodov L.I., Goryachev I.V. Considerations about preserving eventy in LTQ-weak interaction. Proceedings of 14-th Russian Conference on Cold Transmutation of Nuclei of Chemical elements and Ball Lightning. – M., 2006.

ESTIMATION OF GEOFUSION PROBABILITY

V.A. Kirkinskii

Institute of Geology and Mineralogy, Siberian Branch of the Russian Academy of Sciences, Novosibirsk, 630090, prospect Acad. Koptyga, 3, Russia

kirkinsk@uiggm.nsk.ru

Abstract

Fusion reaction probability in the Earth is analyzed on the base of the suggested earlier theoretical model, computer modeling and experimentally revealed conditions favorable for the fusion reactions. It is shown that several fractions of percent of hydrogen in the Earth's core can afford the heat flow $13*10^{13}$ W from it found by geophysicists. In the oceanic rifts contact of alumosilicate melts with sea water causes its boiling and hydrothermal processes, accompanied by cavitation phenomena and red-ox reactions - factors favorable for the fusion reactions. The correlation of heat and helium flow points to a possibility of nuclear fusion. Zones of lithosphere plates subduction are another probable regions for natural fusion reactions.

Conditions for nuclear fusion in the Earth are much less suitable than in artificial systems first of all by low deuterium content in natural hydrogen (0.015%), nevertheless some processes similar to that initiated experimentally can exist in the nature. Diffusion of hydrogen atoms in native iron, cavitation in water solutions, red-ox reactions etc. are among them. We based on theoretical analysis, computer modeling and experimentally revealed conditions favorable for the fusion reactions to seek for geological situations where fusion products can probably occur.

Earth's core. It is generally taken to judge the Earth's core chemical composition from density and elastic properties determined from geophysical data and also by analogy with the composition of ferriferous meteorites. Almost all researchers are agreed now that metal iron is a bulk core component. The lower value of the core density compared to the pure iron shock

adiabatic curve is associated with the presence of lighter impurities. Different authors anticipate that nickel, silicium, sulfur, oxygen, hydrogen, carbon and other elements are impurities. The hypothesis that the iron core contains hydrogen was first made by Lynch [1] and more fully discussed by Kuhn and Rittman [2]. Such view point was maintained by other researchers. This conjecture is supported now by physicochemical experiments.

The structure of γ-iron contains up to 70 at. % of hydrogen at 7 GPa and at the temperature of several hundreds of centigrade degrees [3]. Hydrogen solubility in the iron crystalline structure should be higher at temperature and pressure corresponding to the Earth core parameters.

Hydrogen, on the other hand, is the most abundant Cosmo chemical element. During the accretion of planets it can enter the composition of the forming core as immediately from the gas phase and also during further gravitational differentiation due to the interaction with hydrogen containing minerals. Hydrogen emission into the gas phase does not occur due to the high pressure inside the planet, as it should be accompanied by a positive volume effect. Experiments demonstrate that the removal of minor hydrogen impurities (several percents) from the structure of metals fails even if gas is pumped out at high temperatures for a long time. This is accountable to the stable position of its atoms in the crystalline structure. Thus it can be stated with large level of confidence that the Earth core should contain hydrogen as interstitial impurity.

With EODD model (model of dynamic deformation of electron orbitals), elaborated earlier [4,5], we calculated probabilities of rapproachement of hydrogen ions and a rate of nuclear reaction during their diffusion along the octahedral positions of γ-iron crystal structure (which is stable at high pressures). The computer modeling was performed at the energy 0.01eV corresponded to the height of the power barrier between these positions. In 1% of 17800 numerical experiments for favorable conditions (deuterons reside in adjacent positions, they move symmetrically at small angle to each other) nuclei of hydrogen atoms draw together up to the distance of less than 0.01 nm. This is defined by a screening of charges by 3d electrons of iron atoms. In this case the rate of nuclear reaction between them caused by the probability of the under barrier passage will be 10^{-3} s^{-1} per DD pair. The coefficient of transition to random trajectories of deuterons is 10^{-10}. The rate of D+D reaction for iron deuteride at deuterium content of 0.1 at. % will be 10^{-12} s^{-1} per DD pair. For natural iron hydride it will be 10^{-20} s^{-1} per DD pair if high mobility of hydrogen atoms takes place, which occurs at the Earth's core temperature. The number of DH pairs for D+H reaction will

increase four orders of magnitude compared to DD pairs, and the reaction cross-section will decrease only two orders of magnitude in this interval of energies. Hence the reaction rate will be $10^{-18}s^{-1}$ per DH pair for 0.1 at. % hydrogen content. The conversion to the energy efficiency of nuclear reaction D+H = ^{3}He+ γ (5.5 MeV) and the Earth's core mass of $1{,}88*10^{25}$ g shows $11*10^{12}$ W average power liberated by the core. According to the recent evaluations of American geophysicists the heat flow from the Earth's core is $13*10^{12}$ W. These evaluations demonstrate that hydrogen content of tenth fractions of at. % can provide a heat flow from the Earth core calculated by geophysicists. This conclusion is of fundamental importance to understand thermal history of the Earth.

Earth's mantle. Native iron as inclusions in basalts and other rocks of mantle origin has been repeatedly described in the literature. Their formation is related to the action of the flows of hydrogen, methane and other gases, which reduce bivalent iron of aluminum silicate melts of basic composition. The results of α-iron analyses, which demonstrate significant hydrogen contents, support this fact. We have previously conducted theoretical modeling of nuclear interaction of hydrogen isotopes in the body-centered α-iron structure, where hydrogen atoms are located in tetrahedral interstices of the crystalline structure [4,6]. The calculated rate for the favorable situations (see above) is $10^{1.5}$ s^{-1} per DD pair. This is four orders of magnitude lower than in palladium deuteride, but 4.5 orders higher than in γ-iron. The recalculation for random trajectories of hydrogen ions in the crystalline structure shows that at similar temperature the rate of fusion reactions will be of the same order as for hydrogen isotopes in γ-iron, due to the lower hydrogen solubility as compared to γ-Fe [6]. These reactions followed by helium formation are likely to appear mainly in the local areas, where hydrogen flows occur. Experiments and theoretical calculations of nuclear reactions rates have not yet been performed. It may be suggested that the Lower mantle, especially D layer at the core boundary, is the most probable zone for these reactions. Favorable factors are a possibility for hydrogen to come from the core, high temperature (2000-4000^{o}C), resulting in high mobility of hydrogen atoms and an elevated quantity of free electrons due to the ionic emission.

Subduction zones of lithosphere plates. The process of downsinking of sedimentary and metamorphic rocks with water-containing minerals into the astenosphere causes their dehydration at high temperatures at a depth, explosive vapor-gas mixtures in volcanoes and geysers and cavitation processes that can involve nuclear fusion according to the experimental data. These zones extend thousands kilometers and have been acted for hundreds of millions

years, hence the geochemical role of these reactions, for helium isotopes formation particularly, may be considerable.

Rift zones. Contacts of sea water with hot alumosilicate melts in oceanic regions are going in the rift zones of lithosphere plates. These processes are followed by a sea water boiling and intensive hydrothermal processes. The correlation of heat and helium flows indirectly favors this hypothesis. Similar to the subduction zones, rift zones have enormous dimensions and are determined nearly in all geological epochs, therefore the contribution of such reaction into the planet power generation and formation of the composition of the atmosphere noble gases can be rather great.

"Hot spots". Similar processes occur during volcanic eruptions and in geysers and above the uplifts of mantle plums. For example, in the magmatic rocks of Hawaii and Iceland $^3He/^4He$ ratio is several tens times greater than in the atmosphere. In 10 samples from Kilauea volcano tritium content appeared to be an order of magnitude higher than the background content for the corresponding rocks. High $^3He/^4He$ ratios have been determined in Iceland geysers and Galapagos Islands, tritium has been also found in the latter case. Tritium occurence, which is not connected to the nuclear tests, is inconsistent with the usually accepted point of view on the abyssal origin of these geochemical anomalies, because its half-life period is only 12.4 years.

Areas and processes listed here are the most probable and wide spread for execution of nuclear fusion reaction in the nature. It is impossible to evaluate quantitatively the abundance of nuclear reactions in geological setting at this point of research. However the conducted analysis makes it possible to choose natural objects with the aim to find the products of these reactions.

This work is supported by RFBR (grant No 05-05-64930).

References

1. Lynch J. A new theory of the Earth's core. Trans. Amer. Geophys. Union. 1937. V.18. P.123-124.
2. Kuhn W., Rittmann A. Ueber den Zustand des Erdinnern und seine Entstehung aus einem homogenen Urzustand. Geol. Rundschau. 1941.B.32, P.215-256.
3. V. E. Antonov V. E., I. T. Belash, I. T. Ponyatovskii E. G. Scripta Metall. 1982. V.16**.** No 20, P.203.

4. Kirkinskii V. A., Novikov Yu. A. Theoretical modeling of cold fusion. Novosibirsk. Novosibirsk State University. 2002.105 p.
5. Kirkinskii V. A., Novikov Yu. A. Modelling of dynamic screening effects in solid state. Europhysics Letters. 2005.V.67**.** No.3. P. 362-368.
6. Kirkinskii V. A., Novikov Yu. A. Fusion reaction probability in iron hydride and the problem of nucleosynthesis in the Earth interior, in the book: Condensed Matter Nuclear Science. Proceedings of ICCF-9. May 2002. Beijing China, P.166-169, ed. by Xing Z. Li. International Convention Center at Tsinghua University. 2003. P.166-169.

PHYSICS OF THE COLD FUSION PHENOMENON

Hideo Kozima

Cold Fusion Research Laboratory
Oya 597-16, Aoi, Shizuoka, 421-1202, Japan

Abstract

The cold fusion phenomenon (CFP) is investigated quantum mechanically using a recent knowledge of nuclear and solid-state physics; neutron halo of exotic nuclei and non-localized proton/deuteron wavefunctions. Characteristics of the CFP including various nuclear events are essentially explained by the resulting inter-nuclear *n-n* interaction mediated by protons/deuterons in transition-metal hydrides and deuterides (T-MH/D). It is shown also that events in the CFP have characteristics of complexity in accordance with the complicated structures of T-MH/D where occurs the CFP, thus resolving the controversial lack of the quantitative reproducibility.

1. Introduction

Since the discovery of the cold fusion phenomenon (CFP) by Fleischmann et al. [1] in 1989, hundreds of experimental data sets have been accumulated in both transition-metal hydrides and deuterides. The data sets range widely over various events from the emissions of neutron, charged particles and gamma ray to nuclear transmutations generating almost all elements in the periodic table. Excess energy accompanies each event. We have to construct a science of these facts in the CFP, as H. Poincaré said a hundred years ago: *Science is build up of facts, as a house is built of stones; but an accumulation of facts is no more a science than a heap of stones is a house* [2].

To have a unified point of view for these diverse and complicated experimental data sets [3 – 6], we have developed a phenomenological model (TNCF model) at first and then the neutron drop model for the CFP. These works were published in papers and also in two books [3, 4] and a review paper [5]. Some quantum mechanical investigations on the bases of premises assumed in these models were also performed in recent works [3 – 5].

After publication of the recent book [4], we have further developed the idea of complexity in several phases of the CFP. Almost all CF systems satisfy the sufficient conditions for the occurrence of complexity which is common in any nonintegrable system with Poincaré resonances (both in classical and quantum) according to I. Prigogine [7]. That is, they are open, non -equilibrium (far-from-equilibrium), many body systems with non-linear interactions between active components (agents). In addition to this general nature of CF systems, we have many experimental data sets in CFP that show characteristics of complexity.

Most outstanding examples of them are the two laws we have found, i.e. (1) the inverse-power law of $N(P_{ex})$ vs. P_{ex} relation, where $N(P_{ex})$ is the number of events producing excess power P_{ex} ([4] §2.12) and (2) the stability effect in the yield of product elements by the nuclear transmutation ([4] §2.11). In addition to these two laws, we will point out here a third law, (3) the bifurcation of the CFP in occurrence of excess energy and nuclear transmutation reactions [8]. Several features of the CFP related with these laws, especially the third law, are qualitatively depicted in this paper.

The discovery of the cold fusion phenomenon (CFP) was made in an electrolytic system with Pd cathodes by Fleischmann et al. [1] in 1989. At almost the same time, Jones et al. [9] reported independently detection of 2.45 MeV neutrons in similar electrolytic systems (with Pd and Ti cathodes) to that used by Fleischmann et al.

They analyzed their experimental data sets assuming that immense (more than 10^{25} times) amplification of the probability of fusion reactions of two deuterons occurs in transition-metal deuterides (Fleischmann's or H-P's hypothesis).

Due to the experimental and theoretical barriers inherent in the system where occurs the CFP to be accepted straightforwardly, this phenomenon has been excluded from established research fields of science and has survived in obscurity for 18 years.

Experimental barriers against CFP to be accepted by scientists are lack of quantitative reproducibility, difficulty in excess energy measurement, and also in neutron detection. The most important barrier is the lack of quantitative reproducibility which is apparently expected only for simple systems. We have known many examples of this lack of quantitative reproducibility (i.e. existence of qualitative reproducibility). One of these examples is the decay of radioactive nuclide, e.g. $^{224}_{88}$Ra which decays by alpha emission with a half-life of 3.66 days. In this case, we can determine only statistically a number $N(t)$ of nuclei at a time t if we know $N(0)$.

Therefore, we should not expect the quantitative reproducibility for events in CFP where nuclear processes surely participate in.

Theoretical barriers against CFP are mainly related with the Fleischmann's hypothesis. Based on the firm knowledge established in nuclear physics by the end of 20th century, possibility of any nuclear reaction observable in room-temperature solids without any acceleration mechanism has been denied. It says that nuclear reactions between or among charged nuclei occur effectively only in a high-energy region with mutual nuclear energies of millions electron volt (MeV). In this common sense denying the CFP, however, there is a presupposition that only charged nuclei participate in CFP excluding possible participation of neutrons.

In the eighteen years after the discovery of a part of the CFP by Fleischmann et al.[1] and Jones et al. [9], there have appeared experimental data sets revealing the complicated nature of the CFP [3 – 6]. Events of the CFP have been obtained not only in deuterium systems (systems containing deuterium, D) but also in protium systems (containing hydrogen, H). It became clear that the CFP does not occur when there are no ambient neutrons and that the CFP is enhanced by an artificial thermal neutron irradiation [3 – 5]. Furthermore, there have been observed various new nuclides supposed to be generated in both deuterium and protium systems. These features have clearly shown that the Fleischmann's hypothesis is not fundamental for the CFP.

The variety of the products of the CFP demands us to have a definite point of view to investigate this phenomenon. It is possible to consider the protium and deuterium systems as independent fields with different fundamental mechanisms for their CF events. Or it is possible to explore a new nuclear physics on the CFP not explored in the orthodox nuclear physics we have at hand. A possible reconciliation of the CFP and the nuclear physics may be

attained using the neutron as an agent relying on the unexplored nature of neutrons in solids and on nuclear properties at around the neutron evaporation level that is under development at present [4, 5].

It is noticed also that there are correlations between the CFP and atomic behavior of H and D in the transition-metal hydrides and deuterides (T-MH /D): the CFP occurs only in *fcc* (and *hcp*) T-MH/D where hydrogen isotopes (H and/or D) have not localized at a specific interstice. The CFP does not occur in *bcc* T-MH/D where the H and/or D atom localizes at an interstice [4, 5].

Furthermore, the host atoms in T-MD/H where the CFP occurs have characteristic nuclides that seem to have the neutron evaporation level with wavefunctions extended out from ordinary nuclear surfaces [4, 5].

Therefore, physics of the CFP should be investigated in conjunction with nuclear physics of the host nuclides and solid state physics of hydrogen isotopes in T-MH/D.

Turning our viewpoint from microscopic to macroscopic, we notice the systems where the CFP occurs have very complicated structures. They are multi-component, inhomogeneous, non-equilibrium, open systems with components interacting nonlinearly each other under influence of mass flow of H/D, of electric field, of irradiation of ambient thermal and epi-thermal neutrons, and sometimes of irradiation of charged particles (in discharge systems).

It is well known that there occurs a phenomenon called complexity in such an open, non-equilibrium system with components interacting nonlinearly. Therefore, we have to expect to observe complexity in the systems where we have observed the CFP.

In the CFP, some features characteristic to many-particle systems have been found in the analyses of the experimental data sets [4, 5]. More direct features of the CFP corresponding to complexity was obtained by Dash et al. as reported in the paper presented at ICCF13 [8].

In Chapter 2, we give a brief survey of nuclear properties supposed to be related with CFP and of wavefunctions of H/D in *fcc*/*hcp* T-MH/D. In Chapter 3, we investigate complexity in the CFP. In Conclusion, we summarize physics of the CFP as briefly presented in this paper.

2. Nuclear and Solid-State Properties of Transition-Metal Deuterides and Hydrides (T-MH/D)

In this Chapter, we give an explanation of neutron physics in T-MH/D based on nuclear properties of exotic nuclei developed in these twenty years and solid-state physics of hydrogen isotopes in them.

2.1 Wavefunctions of Neutrons in Evaporation Levels of Exotic Nuclei

Properties of nuclides in their ground and high-energy excited states have been explored extensively in the last century applying neutrons, gamma rays and high energy particles accelerated by various machines to make charged nuclei approach each other close enough in the range of the short-range nuclear force overcoming Coulomb repulsion between them.

However, there has remained a field kept untouched by these researches until recently; the nuclei in their low excited state are alien to those in the ground states and higher excited states. Especially, investigation of the states of nuclei at their so-called neutron evaporation level had started only twenty years ago. Now, there are several review articles on this problem telling following facts [10, 11]; there exist many nuclei with the so-called neutron halo extending far out of the nuclear core that is the nucleus figured out in orthodox nuclear physics. It is recognized now the necessity to treat nuclei tenderly to know their behavior in states at or near the neutron evaporation level.

On the other hand, there appeared a new field of investigation related with the states of nuclei at their lower excited states; the cold fusion phenomenon (CFP). At first, this field was considered as a part of the orthodox nuclear physics when a part of its events was discovered and proclaimed in 1989 [1, 9]. The content of the phenomenon unexpectedly increased into huge amount with profound variety in these 18 years after its discovery. Now, we know that the CFP occurs both in protium and deuterium systems and includes such events as nuclear transmutations producing almost all nuclides from pre-existed nuclei Ti, Ni, Pd, *n*, *p*, *d*, Li, K, S, O, and so forth in CF systems, emissions of neutrons, photons, and charged particles (*p*, alpha, and so forth) accompanying excess energy.

To show some phases of the recent development in nuclear physics, we cite here a figure (Fig. 1) showing extension of neutron density outside the nuclear core and a table (Table 1) showing confirmed nuclides in the halo states [10]. The investigation of the halo states of nuclei is in an infantile state and only a few data has been obtained for small mass-number nuclides as shown in Table 1.

To know the present extent of out knowledge in this field, we summarize the nuclear properties of the neutron halo closely related to the CFP from our point of view [10, 11]:
1) "Thresholds," the transition points between bound discrete states and a continuous spectrum, give rise to many fascinating phenomena. Among the newest of them are the so-called halo states that occur in some nuclei near the limit of particle stability.

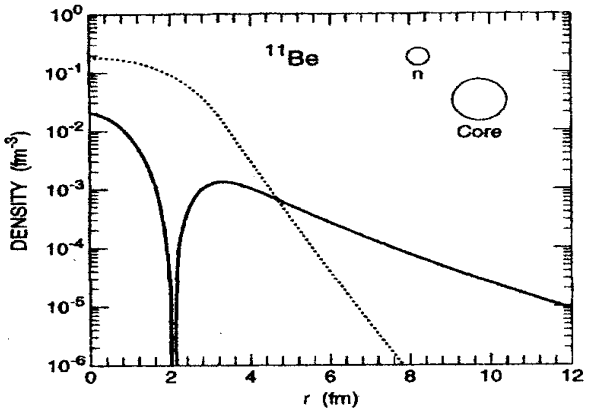

Fig. 1. *Plot of the ^{11}Be density [10]. The upper right cornet shows the simplified picture of a halo nucleus as a two-body system with an inert core and a halo neutron. Dotted line, core density as a function of radius; solid line, the density obtained in a Hartree –Fock calculation with the neutron in a $2s_{1/2}$ orbital and a single-neutron separation energy adjusted (to agree better with experiment) to 0.51 MeV. Note the very far-extended, dilute tail that is the characterizing feature of a halo [10].*

TABLE I. Halo states. For each state the excitation and separation energies and the angular momentum of the halo particle(s) are listed.

Nucleus	E_x (MeV)	$S-E^a$ (keV)	Configuration	l	K
^{11}Be	g.s.	504	$n+{}^{10}$Be	0	
^{11}Be	0.32	184	$n+{}^{10}$Be	1	
^{17}F	0.50	105	$p+{}^{16}$O	0	
^{6}He	g.s.	973	$n+n+{}^{4}$He		2
^{11}Li	g.s.	310	$n+n+{}^{9}$Li		?
^{14}Be	g.s.	1340	$n+n+{}^{12}$Be		?

[a]From Audi and Wapstra, 1993.

Table 1. (Table 1 of Reference [10].)

2) Only very loosely bound neutrons in an *s* state relative to the core provide an ideal halo.
3) Arbitrary large values of the mean-square radius could occur in nuclei, at least in principle.
4) If a neutron halo is defined as a divergent root-mean-square (r.m.s.) radius of the halo for the neutron separation energy S_n approaching zero, then a two-body (i.e. single-neutron) halo is possible only if the orbital angular momentum $l = 0, 1$.
5) The conditions for a three-body (two neutron) halo are more restrictive and the radius is at most logarithmically divergent.
6) The known cases of even-*n* halos have the Borromean property, namely that both the two-body sub-systems (A + *n*) and (*n* + *n*) are unbound.
7) Mass calculations suggest that halo states will occur symmetrically at the neutron drip line for most elements.
8) Our knowledge is restricted to five cases in total (He, Li, Be). (Cf. Table 1)
9) Halo states have unusually large nuclear and electric reaction cross sections.
10) The large size of the halo implies a narrow momentum distribution.
11) The halo neutron is in a mixed state containing its ground sate and continuum states.
12) A halo neutron has a probability distribution that extends far beyond the core.
13) ^{11}Be, an example of the neutron halo size: The wave functions for the case of a single-neutron halo correspond to calculated (with Woods – Saxon potential) r.m.s. radii of the $l = 0$, 1 states of 5.99 and 5.66 fm, respectively. For comparison, the r.m.s. radius of a normal *p*-shell nucleus is 2.5 fm.

Thus, we do not know yet exactly what kind of wavefunctions the halo neutrons have in the medium mass-number nuclides such as Ti, Ni and Pd. However our knowledge about them is scarce yet, there surely exist neutrons with extended wavefunctions in lattice nuclei in CF materials.

We have utilized this property of neutron wavefunctions expected from experimental data sets in the estimation for the possible interaction of two neutrons in different lattice nuclei mediated by interstitial protons or deuterons which we called *the super-nuclear interaction* [4, 5]. The super-nuclear interaction makes possible formation of the neutron bands at the zero-energy level in which high density neutron states (CF-matter) are formed at surface/boundary regions. This state of neutrons has been the essential factor to make possible the CFP to occur.

Therefore, it is necessary to have not only the extended neutron wavefunction but also the proton/deuteron wavefunction (cf. §2.2 below) having contact interaction with the neutron to realize the CF-matter and finally the CFP.

2.2 Wavefunctions of Protons/Deuterons in Transition-Metal Hydrides and Deuterides (T-MH/D)

It is a surprising fact that almost all cold fusion phenomenon (CFP) has been observed in *fcc* (and *hcp*) transition-metal hydrides and deuterides exclusively in metals Ti, Ni, and Pd. It is also true that there are selective combinations among the metal and hydrogen isotopes (and alkaline elements and other elements in electrolyte) such as Pd-D-Li, Ni-H-K and others.

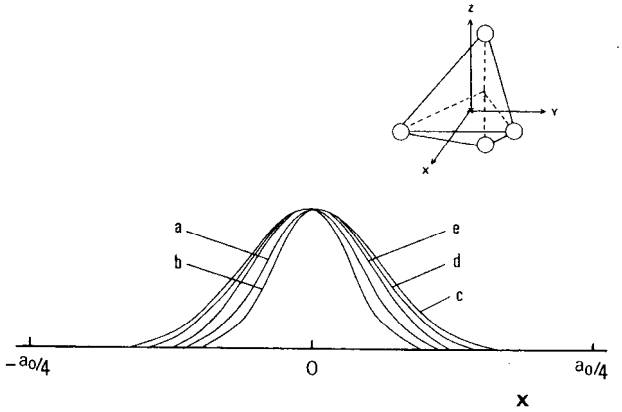

***Fig. 2**. Density profiles of H and D on T-sites in bcc metals (Nb, V, Ta) in the x-direction shown in the inset. Profiles calculated for a) a H-atom and b) a D-atom in Nb. Profiles observed by Reidinger et al. for c) $VD_{0.79}$ at 70 degC, d) $NbH_{0.82}$ at 119 degC and $NbD_{0.73}$ at 140 degC and e) $TaH_{0.20}$ at 150 degC. (Fig. 5 of H. Sugimoto and Y. Fukai, J. Phys. Soc. Japan **51** (8), pp. 2554 – 2561 (1982))*

On the other hand, the transition-metal hydrides and deuterides (T-MH/D) have been investigated for more than 100 years for their peculiar diffusion and occlusion properties of hydrogen isotopes.

Therefore, it is natural to investigate the physical properties of these transition-metal hydrides and deuterides in connection with the occurrence of the CFP. We have had speculated this problem a little in the recent papers and compiled them in a recent report [5] and a book [4].

It is interesting to know that the physical behavior of hydrogen isotopes in transition metals is divided into two classes; one in *bcc* metals (V, Nb, Ta etc.) and the other in *fcc* (and *hcp*) metals (Ti, Ni, Pd etc.). In the first class (*bcc* metals) a nucleus of hydrogen isotopes are localized in an interstitial site (interstice) and there are a few works to determine the profile of their wavefunctions as illustrated in Figs. 2 and 3. Accordingly, vibration and diffusion properties of these localized hydrogen isotopes have characteristics in accordance with the localization of the nuclei [5§2.2, 4§3.6].

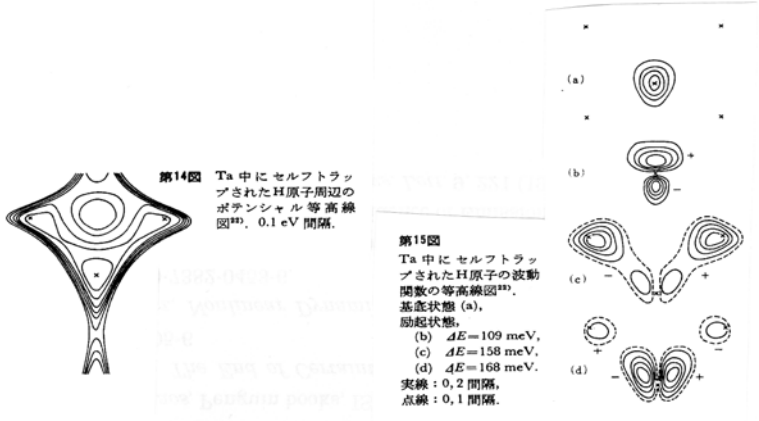

***Fig. 3.** Localization of a hydrogen atom at an interstice in a bcc transition metal Ta (after Y. Fukai, Kotai-Butsuri (in Japanese) **16**, 253 (1981)). Left; potential contour lines around a self-trapped H-atom in Ta. Right: Contour lines of H-atom wavefunction self-trapped in Ta. From top to bottom; (a) Ground state, (b) – (d) excited states with excitation energies of ΔE = 109, 158 and 168 meV, respectively. In excited states, wavefunctions extend to the nearest lattice points and interstices.*

On the other hand, in the second class (*fcc* and *hcp* metals), a nucleus of hydrogen isotopes is not localized at an interstitial site but extend to several interstices [5§2.2, 4§3.6]. And, therefore, vibration and diffusion characteristics of hydrogen isotopes are not discussed in parallel to the first class (*bcc* metals). In this class, there are no work on the wavefunctions of a proton and a deuteron in these metals suggesting difficulty to determine wavefunctions of non-localized particles (proton and deuteron).

In relation to the occurrence of the super-nuclear interaction proposed by us [4§3.7.2, 5§3], we have to estimate the wavefunction $\Phi(\boldsymbol{R}; \boldsymbol{b}_j)$ of interstitial proton (or deuteron) at around a nearest neighbor lattice nucleus. The super-nuclear interaction determines the width of the neutron band and then the neutron density at a boundary/surface region. The latter is related to the CF matter that interacts especially with adsorbed or absorbed nuclei and also with lattice nuclei at the boundary/surface region.

We have formulated this scenario in the frame of the second-order perturbation theory [4, 5]. On the same line described in these publications, we discuss here a possibility to determine the proton/deuteron wavefunction in terms of the data obtained in the CFP research.

Let us write down the proton/deuteron wavefunction $\Phi(\boldsymbol{R}; \boldsymbol{b}_j)$ at an interstice $\boldsymbol{b}_j$ (the suffix *j* specifies the interstice) as a linear combination of localized wavefunctions (Wannier functions) $W(\boldsymbol{R}; a_i)$ at nearest-neighbor lattice points $\boldsymbol{a}_i$ (the suffix *i* specifies the lattice point) around the interstice $\boldsymbol{b}_j$ as follows (neglecting the spin part);

$$\Phi(\boldsymbol{R}; \boldsymbol{b}_j) = \Sigma_i A_{ji} W(\boldsymbol{R}; \boldsymbol{a}_i). \quad (1)$$

The coefficients A_{ji} give a density of a proton/deuteron at one of the adjacent lattice points $\boldsymbol{a}_i$ of the interstice $\boldsymbol{b}_j$.

If we know $\Phi(\boldsymbol{R}; \boldsymbol{b}_j)$, the Wannier function $W(\boldsymbol{R}; \boldsymbol{a}_i)$ at the site $\boldsymbol{a}_i$ is calculated inversely from $\Phi(\boldsymbol{R}; \boldsymbol{b}_j)$ by an inverse transformation of the equation (1);

$$W(\boldsymbol{R}; \boldsymbol{a}_i) = \Sigma_j B_{ij} \Phi(\boldsymbol{R}; \boldsymbol{b}_j). \quad (2)$$

The coefficients B_{ij} is calculated by A_{ji} and vice versa. In the simplest case where the Wannier function is expressed as a 1*s*-type function that has a finite value at the origin, we can determine the wavefunction of the proton/ deuteron if we know the value A_{ji} by some means.

From the estimation of the width of the neutron valence band ([4§3.7, 5§3.2]) responsible to the experimental data of the CFP, we can determine the matrix element of the proton/deuteron – neutron interaction if we know the latter wavefunction. The neutron wavefunction in a nucleus at its halo state has been investigated intensively for light nuclei in nuclear physics. We will be able to know concrete information about neutron wavefunctions in medium mass-number nuclei like Ni and Pd in near future. Then, we might be able to calculate the proton/deuteron wavefunctions from experimental data obtained in the CFP. The resulting wavefunction will give information about the nature of the protons/deuterons related to their diffusion and vibration properties in *fcc* and *hcp* transition metals.

The interrelation between the solid-state physics of the T-MH/D and the CFP is not explored at all yet. However, as we have pointed out recently [4, 5], there are apparent correlations between them. Intentional researches of this interrelation will be fruitful for both fields which have been investigated independently hitherto as if they are isolated fields.

2.3 Possible States of Neutrons in T-MH/D and the CFP

When optimum conditions for wavefunctions of neutrons in lattice nuclei (§2.1) and of hydrogen isotopes (§2.2) were satisfied in the transition-metal hydrides/deuterides (T-MH/D), we can expect formation of neutron bands around zero and then the CF matter in surface/boundary regions of the sample [4, 5].

2.3.1 Neutron – Proton Interaction in Solids

The overlapping of the proton wavefunction $\varphi_p(\boldsymbol{R} - \boldsymbol{b}_j)$ on an interstice at $\boldsymbol{b}_j$ with a nucleon (neutron) wavefunction $\psi_n(\boldsymbol{x}, \boldsymbol{a}_i)$ on an adjacent lattice nucleus at $\boldsymbol{a}_i$ results in a proton-neutron interaction through the nuclear force. The nuclear interaction is expressed by a potential whose form is taken, for example, as the square-well type (neglecting spin-dependence and the imaginary part):

$$V_s(\boldsymbol{r} - \boldsymbol{R}) = -V^{(s)}_0, \quad (|\boldsymbol{r} - \boldsymbol{R}| < b)$$
$$= 0, \qquad (|\boldsymbol{r} - \boldsymbol{R}| > b) \qquad (3)$$

where $V^{(s)}_0 \simeq 3.5$ MeV and $b \simeq 2.2\times10^{-13}$ cm. The choice of this potential out of several possible types does not make a large difference to the result for the low energy phenomena we are considering in this paper.

This interaction pulls two neutron states in different lattice nuclei into coupling as shown below. We will call this coupling the super-nuclear interaction.

2.3.2 Super-Nuclear Interaction between Neutrons in Different Lattice Nuclei and Neutron Valence Band

If there is an interaction between a neutron in a lattice nucleus at $\boldsymbol{a}_i$ and a proton/deuteron at an interstice $\boldsymbol{b}_j$ next to the lattice point $\boldsymbol{a}_i$, there appears an interaction between two neutrons in two lattice nuclei at $\boldsymbol{a}_i$ and $\boldsymbol{a}_{i'}$ interacting with the same proton/deuteron at $\boldsymbol{b}_j$ when $\boldsymbol{a}_{i'}$ is also a neighbor of $\boldsymbol{b}_j$. The coupled neutrons in lattice nuclei reveal a dispersed energy spectrum called the energy band. We investigate this possibility below.

(a) Total Energy of *fcc* Transition-Metal Hydrides and Deuterides

In the second-order perturbation approximation taking the square well potential (3) for the nuclear interaction, the total energy $E_{k,\{p\alpha\}}$ of this system composed of occluded protons (deuterons) and a neutron in an excited level of lattice nuclei expressed as a Bloch state is written down as follows [5]:

$$E_{k,\{p\alpha\}} = E_{\{n,\,p\alpha\}} + \sum_{k',\,i,\,i',\,j} \exp[-i(\boldsymbol{k}\boldsymbol{a}_i - \boldsymbol{k}'\boldsymbol{a}_{i'})]\, v_{np}(ii'j) \qquad (4)$$

$$E_{\{n,\,p\alpha\}} = E_{\{n\}}{}^{(p)} + \sum_j \varepsilon_{pj}, \qquad (5)$$

$$v_{np}(ii'j) = \sum_{\{p'\}\neq\{p\}} P\int dE\, \rho_n(E)\, (\langle np;ij|V|n'p';ij\rangle(\langle n'p';i'j|V|np;i'j\rangle)/(E+\varepsilon_{p'p}) \qquad (6)$$

$$V(\boldsymbol{r}) = V_s(\boldsymbol{r}), \qquad (7)$$

$$\langle np;ij|V|n'p';ij\rangle = \iint d\boldsymbol{r} d\boldsymbol{R}_j$$
$$\times \psi_{\{n\}}{}^*(\boldsymbol{r} - \boldsymbol{a}_i)\varphi_p{}^*(\boldsymbol{R}_j - \boldsymbol{b}_j)\, V_s(\boldsymbol{r} - \boldsymbol{R}_j)\psi_{\{n'\}}{}^*(\boldsymbol{r} - \boldsymbol{a}_i)\, \varphi_{p'}{}^*(\boldsymbol{R}_j - \boldsymbol{b}_j), \quad (8)$$

where summations over i and i' in (4) are only over the nearest neighbor lattice points $\boldsymbol{a}_i$ and $\boldsymbol{a}_{i'}$ of an interstice $\boldsymbol{b}_j$, $\rho_n(E)$ is a density of states for neutron energy levels, and

$$\varepsilon_{p'p} \equiv \varepsilon_{p'} - \varepsilon_p,\ E \equiv E_{\{n'\}} - E_{\{n\}}.$$

Further, the summation over p' in (6) reduces to $(n_p+1)(n_p+2)$, the degeneracy of the energy ε_{np}, times summation over n_p. $E_{\{n\}}{}^{(p)}$ is an energy of a neutron in an excited state $\psi_{\{n\}}(\boldsymbol{r} - \boldsymbol{a}_i)$ in a lattice nucleus at $\boldsymbol{a}_i$ when occluded protons are in states p_α, and ε_{pj} in (5) is an energy of a proton in a state $\varphi_{pj}(\boldsymbol{R}_j - \boldsymbol{b}_j)$ at an interstice $\boldsymbol{b}_j$. We ignore the p-dependence of $E_{\{n\}}{}^{(p)}$ hereafter in this work.

Thus, the matrix elements (8) calculated for neutron states around the evaporation level and proton (deuteron) states of Bloch functions are at most 10^{20} times larger than the value calculated for a lower excited state of a neutron in nucleus and a localized state of a proton (deuteron). If this matrix element is effective, there appears an interaction between two neutrons in different lattice nuclei mediated by occluded hydrogen isotopes at interstices. This interaction is a long-range one reaching from a lattice point to another having its origin in the

internucleon strong interaction; we may call it the *super-nuclear interaction* between neutrons in different lattice nuclei, or the inter-nuclear n-n interaction mediated by protons/deuterons in T-MH/D. The super-nuclear interaction is illustratively depicted in Fig. 4.

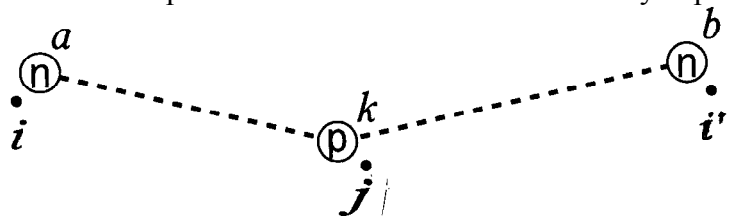

Fig. 4 *Super-nuclear interaction between two neutrons* ***a*** *and* ***b*** *in lattice nuclei* ***i*** *and* ***i'*** *mediated by a proton (or a deuteron) k at an adjacent interstitial site* ***j****.*

Finally, the effective potential $v_{np}(ii'j)$ (6) is estimated as a function of the principal value I of the integration which appeared in that equation using the result of an order of magnitude calculation

$$<np;ij|V|n'p';ij> = 3.2 \times 10^{-14}\ ,\ \text{(eV)} \qquad (9)$$

and assuming the insensitiveness of the matrix elements to the energy:

$$v_{np}(ii'j) = 1 \times 10^{-27}\, I,\ \ (\text{eV})^2 \qquad (10)$$

$$I \equiv \mathrm{P}\int dE\, \rho_n(E)/E \simeq (\rho_n(E)/\delta\varepsilon)\Delta\varepsilon.$$

We can, then, estimate the approximate value of the integral (principal value) I, taking following values $\rho_n(E) \simeq 10^3\ \text{keV}^{-1}$, $\delta\varepsilon \simeq 10^{-3}$ keV, and $\Delta\varepsilon \simeq 1$ keV on the assumption that single-particle energy-level difference is $\simeq 1$ keV and the level density increases to a value 10^3 times larger than that of single particle motion:

$$I \simeq \rho_n(\varepsilon)\Delta\varepsilon/\delta\varepsilon = 10^6\ .\ (\text{eV}^{-1}) \qquad (11)$$

Thus, an order of magnitude of $v_{np}(ii'j)$ in a crystal PdH becomes

$$v_{np}(ii'j) \simeq 1 \times 10^{-24}\ (\text{eV}). \qquad (12)$$

Including the enhancement factors α and β defined to take into several effects [4, 5], we obtain the final result:

$$v_{np}(ii'j) \simeq 1 \times 10^{-24}\, \alpha^2\beta^2\ \ (\text{eV}). \qquad (13)$$

The enhancement factor α is for the level density of neutrons in a nucleus and another enhancement factor β is for the probability amplitude of a proton (deuteron) wavefunction at a lattice nucleus with $\alpha_{max}^2 = 10^{12}$ and $\beta_{max}^2 = 10^{20}$.

(b) Neutron Valence Band in PdH

To show briefly the crystal-structure dependence of the bandwidth Δ of the neutron valence band, we will make a simplification of the super-nuclear interaction (6) between adjacent nuclei at a_i and $a_{i'}$ assuming that it depends only on the magnitude of the vector $a_l \equiv a_i - a_{i'}$.

Then, we can rewrite the total energy (4) and have the energy spectrum of the neutron Bloch waves in the *fcc* lattice (a is the side of the lattice cube);

$$\varepsilon_k = E_{\{n,p\}} - \gamma_{n,p} - 2\times 4\gamma'_{n,p}\,(\cos k_y a/4\ \cos k_z a/4 + \cos k_z a/4\ \cos k_x a/4 + \cos k_x a/4 \times \cos k_y a/4)$$
$$- 2\gamma'_{n,p}\,(\cos k_x a + \cos k_y a + \cos k_z a\,) \qquad (14)$$

$$E_{\{n,p\}} = E_{\{n\}} + \textstyle\sum_j \varepsilon_{pj}\ , \qquad (15)$$

$$-\gamma_{n,p} = v_{np}(0), \qquad (16)$$

$$-\gamma'_{n,p} = v_{np}(ii'j). \qquad (17)$$

The shifts $\gamma_{n,p}$ of energy level $E_{\{n,p\}}$ may be negative in appropriate situations. A characteristic of this energy band formation is the contributions not only from nearest neighbors ((0, $\pm a/2$, $\pm a/2$), etc.) but also from next nearest neighbors (($\pm a$, 0, 0), etc.)

Putting the value $v_{np}(ii'j) \simeq 1 \times 10^{-24}\ \alpha^2\beta^2$ in (17), we obtain the bandwidth Δ from (14) as follows:

$\Delta \simeq 2.5\times10^{-23}\alpha^2\beta^2$ (eV).

The value of the bandwidth $\Delta \simeq 2.5$ GeV for $\alpha_{max} = 10^6$ and $\beta_{max} = 10^{10}$ is obtained by the assumptions that the level density at excited levels around the evaporation energy is similarly strongly magnified by collective modes as observed by neutron resonance absorption experiments and that the excited proton states are expressed by plane waves. The first assumption has no experimental basis at present and seems too exaggerated the situation to be real. We may assume rather small value as $\alpha = 10^2$ or 10^3 instead of 10^6. Then, the bandwidth may have a value about $\Delta \simeq 1 - 10^2$ eV for $\beta = \beta_{max}$.

The assumption, on the other hand, of a plane wave for the proton (deuteron) Bloch state ($\beta_n = 10^{10}$) may overestimate the matrix elements (8) by several orders of magnitude making the bandwidth down to $\Delta \simeq 10^{-2} - 1$ eV if we take $\beta = 10^8$ - 10^9.

On the other hand, if the bandwidth Δ is less than the thermal energy $\simeq 25$ meV of ions at room temperature, the concept of the neutron band may be not realistic and the neutrons should be treated as localized at lattice nuclei. This requires $\alpha^2\beta^2 > 10^{21}$ for a realistic neutron valence band. This means that the parameters to realize the neutron valence band should be $\alpha > 10^{5.5}$ for $\beta = 10^5$ and $\beta > 10^7$ for $\alpha = 10^3$.

(c) Accumulation of Neutrons at Surface/Boundary Regions

When there is a neutron valence band in a crystal, accumulation of neutrons at surface/boundary regions occurs by coherent reflection of neutron Bloch wave at these region as shown in Fig. 5 [4].

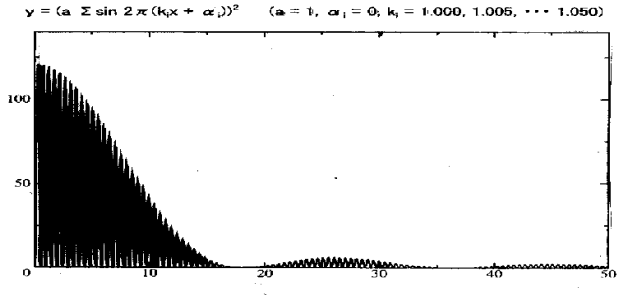

Fig. 5*. Neutron density accumulation of 11 neutrons reflected coherently at boundary.*

This scenario may be a most plausible one to explain the CFP consistently with physical properties of nuclei and hydrogen isotopes in T-MH/D.

3. Complexity in the cold fusion phenomenon (CFP)

In this Chapter, we investigate a phase of the CFP as a complexity based on the experimental data sets.

3.1 Agents and Interaction

In many-particle systems including agents (constituents responsible for appropriate effects) interacting nonlinearly each other, there occur various events composing a phenomenon called complexity as a whole. The complexity includes such events as bifurcations of a stable state to several ones by variation of a parameter in the system, chaos, fractals, self-organization (automatic appearance of new organized state) or emergence, and so forth.

In the CFP, we have used complex systems composed of host metal atoms, occluded hydrogen isotopes, unavoidably included ambient neutrons, adsorbed/absorbed active elements in surface/boundary regions during experiment, and others. Based on our insight into physics of the CFP, we can choose agents from particles composing the CF system for explanation of the CFP.

When we notice such characteristics of the CF materials as open, non-equilibrium, unstable, many-particle systems interacting nonlinearly, we understand why the CFP has only qualitative reproducibility [4, 5]. Furthermore, to overcome the theoretical barrier against the CFP pointed out in Introduction, we have to take neutrons as a member of agents in our treatment. Then, our agents for the CFP are supposed to be transition-metal nuclei with occluded hydrogen isotopes, neutrons included in CF materials (in the state discussed in §2), and minor element nuclei on/in surface/boundary regions of the samples.

3.2 Parameters – loading ratio (D/Pd, H/Ni), Temperature, Electric Field, Density Gradients

It is well known that characteristics of the complexity in a complex system depend on parameters of the system. A typical example of the feature is illustrated in Fig. 6 for the logistic difference equation (l.d.e.) with a parameter λ: $x_{n+1} = \lambda x_n(1 - x_n)$ $(0 < x_0 < 1, \lambda > 0)$. Bifurcations and finally chaos appear in the diagram of x_∞ vs. λ [12].

In contrast to the simple structure of l.d.e., CF systems are tremendously complicated; we can list up such parameters responsible to the CFP on the basis of our experience as the loading ratio η (and its gradient) of D (or H) to the host metal ($\eta \equiv$ D/Pd, H/Ni and so on), temperature T (and its gradient) of the sample, electric field applied to the sample, and so on.

It is possible to have various events in the CFP more complex than those appeared in Fig. 6 in l.d.e. One example of chaotic behavior in the CFP as a function of the parameter η = D/Pd was obtained by McKubre et al. [13] (c.f. also Fig. 6 of [8]).

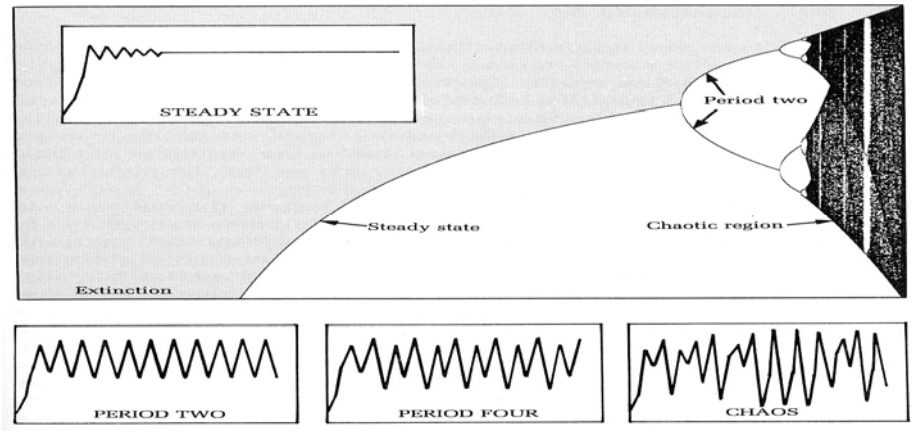

Fig. 6 *Period-doubling and Chaos (From "Chaos" by J. Gleick [12, p.71]). Four small figures inserted depict variation of x_n in terms of the increase of n for different values of λ. The main figure depicts x_∞ (x_n at $n = \infty$) vs. the parameter λ (abscissa) of the logistic difference equation (l.d.e.) $x_{n+1} = \lambda x_n(1 - x_n)$ $(0 < x_0 < 1)$.*

Another example of complexity in the CFP was illustrated in Figs. 4 and 5 in [8] from the data obtained by Dash et al. In their data sets obtained in precision experiments, we could read out bifurcation and the positive feedback behavior of the excess power generation as a function of temperature *T*. Furthermore, data of the neutron emission from TiDx by De Ninno et al. may be another example of the bifurcation in the CFP as explained in our paper [8].

Based on the conjecture about the positive feedback in the excess power generation, we can give unified explanation of explosions observed in the CFP hitherto. Examples in the following paragraphs may be explained by the positive feedback mechanism observed in the experiment as analyzed in [8] but without appropriate negative feedback to stop the explosion.

There are several reports of explosions occurred in CFP experiments. The two experiences by Zhang et al. [14] and Biberian [15] were reported in conferences and we have concrete data. In these cases, they used electrolytic system with similar cathodes of Pd pipes to the one used in [8]. Another example of the explosions in CFP experiments was reported by T. Mizuno [16]. In this case, the experimental system was also electrolytic but a tungsten plate as a cathode with light water and electrolyte K_2CO_3.

There are further more two cases of explosions which are legendary. The first of them was written in the pioneering paper by Fleischmann, et al. [1]. In the Table 1 of their paper, there are words "Warning! Ignition?" for a cubic sample of $1 \times 1 \times 1$ cm^3. Details of this explosion was not made clear due to scant data reserved after the accident in the confused situation induced by the extraordinary event.

The second of them occurred in the SRI (Stanford Research Institute) [17] resulting in fatal human damage. This case was ascribed to an explosion of mixture gas of hydrogen and oxygen. If it is the case, we can exclude this case from the explosion of CF samples due to uncontrolled positive feedback of energy production by cold fusion reactions.

4. Conclusion

We have found three laws or rules in the CFP: 1). The stability effect in production of new nuclides; the more the nuclides stable, the more often they are generated in CF materials [4]. 2) The inverse-power law for excess power productions; the number of observation $N(P)$ of an excess power P in a CF material is expressed as an inverse-power of P with an exponent – 1 to – 2, i.e. $N(P) = C/P^b$ (C: constant, $b = -1 \sim -2$) [4, 5]. 3) The bifurcation of excess power generation P as a function of a sample temperature T; the magnitude of excess power P generated in PdD_x ($x = 0.8 \sim 1.0$) samples becomes finite above a critical temperature T_0 increasing with T and experiences bifurcation to two branches of higher and lower excess power. In the higher P branch, there appears a positive feedback mechanism to increase P radically.

These laws are essential to many-particle systems with own characteristics. The first law (the stability effect) is discovered by comparison of the number of observation $N_{ob}(Z)$ of a nucleus with a proton number Z and the relative abundance $H(Z)$ of the nucleus in the universe. $H(Z)$ is a result of many-particle interactions in stars and this law suggests existence of similar interactions in CF materials at surface/boundary regions where nuclear transmutation occurs.

The second law (the inverse-power law) is frequently observed in complex systems in non-equilibrium condition. One of the well-known examples of this law is the Gutemberg-Richter's formula [4 (§2.12), 5] describing a relation between the energy E of an earthquake and its frequency $P(E)$;

$P(E) = AE^{-b}$, (A; constant).

It is told that the exponent b has been supposed to be equal to 2 at first (when it was proposed in 1942) and converged to 1.7 at present [8].

The third law (the bifurcation of the excess power production as a function of the sample temperature T) is a typical manifestation of complexity. The most simple example of this behavior is demonstrated by the logistic difference equation (l.d.e.); $x_{n+1} = \lambda x_n(1 - x_n)$ (λ; positive parameter, $0 < x_0 < 1$) [12]. If we plot x_∞ as a function of the parameter λ, the graph shows bifurcations and chaos. We have shown the bifurcation of the excess power in the CFP as a function of the sample temperature [8]. The chaotic behavior depicted in Fig. 6 suggests that the excess power production observed by McKubre et al. [13] can be interpreted as a chaos as explained in [8].

In addition to the bifurcation, we have noticed the occurrence of the positive feedback to increase excess power in PdD_x samples [8]. Fortunately, the positive feedback in the data analyzed by us [8] did not last too long and terminated at the maximum power less than about 20 W by some negative feedback mechanisms.

However, there were several reports of explosion in PdD_x [1, 14, 15] and WH_x [16] systems that may be results of the positive feedback in the production of excess energy not restrained by effective negative feedback mechanisms.

Thus, the CFP characterized by these laws in addition to such various events summarized in Table 2.1 of Reference [4] has to be treated as a complexity occurring in open, non-equilibrium, inhomogeneous, multi -component systems with nonlinear interactions between agents.

In this paper, we have given first few steps to understand fundamental properties of agents in CF materials participating in the complexity when there are optimum arrangements of host atoms and occluded hydrogen isotopes in the surface/boundary regions of T-MH/D under influence of thermal neutrons: 1) neutron wavefunctions of host lattice nuclei (Ni, Ti, Pd, - - -) might be responsible for the CFP, especially when these nuclei become exotic with a large excess number of neutrons; 2) wavefunctions of occluded protons/deuterons at interstices of *fcc*/*hcp* transition-metal hydrides /deuterides (T-MH/D) should be responsible for the CFP in these materials. Correlation between the CFP and known physical properties of T-MH/D is explained consistently by the nature of these wavefunctions; 3) the super-nuclear interactions between neutrons in adjacent lattice nuclei mediated by proton/deuteron wavefunctions in 2) explains qualitatively fundamental features of the CFP summarized in References [3 – 5] and especially in Chapter 2 of Reference [4].

We may expect that the characteristics of the CFP will be understood as a complexity including atomic and nuclear interactions in compound systems composed of exotic lattice nuclei of transition metals (Ni, Ti, Pd, - - -) occluding hydrogen isotopes (H and/or D) with high loading ratio ($\eta > 0.8$) under irradiation of ambient or artificial thermal and epithermal neutrons.

If we establish such physics of the CFP on the line outlined in this paper, we can then develop possible application of the CFP as energy sources, generation of new or rare elements, elimination of hazardous radioactive waste, and so forth.

This work is supported by a grant from the New York Community Trust.

References

1. M. Fleischmann, S. Pons and M. Hawkins, "Electrochemically induced Nuclear Fusion of Deuterium," *J. Electroanal. Chem*., **261**, 301 – 308 (1989).
2. H. Poincaré, *Science and Hypothesis*, (translated by W.J.G. in 1905) Chapter IX, p. 141, Dover, NY, 1952. Library of Congress Catalogue Card Number: 53-13673.
3. H. Kozima, *Discovery of the Cold Fusion Phenomenon*, Ohtake Shuppan, Tokyo, 1998. ISBN: 4-87186-044-2.
4. H. Kozima, *The Science of the Cold Fusion Phenomenon*, Elsevier Science, 2006. ISBN-10: 0-08-045110-1.
5. H. Kozima, "Quantum Physics of Cold Fusion Phenomenon," in *Developments in Quantum Physics*, ed. V. Krasnoholovets and F. Columbus, Nova Science, N.Y., 2004. ISBN: 1-59454-003-9. And also H. Kozima, *Rep. Fac. Science, Shizuoka Univ.* **39**, 21 – 90 (2005).
6. E. Storms, *The Science of Low Energy Nuclear Reaction*, World Scientific, Singapore, 2007. ISBN-10 981-270-620-8.
7. I. Prigogine, *The End of Certainty***,** The Free Press, New York, 1996.
8. H. Kozima, W.-S. Zhang and J. Dash, "Precision Measurement of Excess Energy in Electrolytic System Pd/D/H_2SO_4 and Inverse-power Distribution of Energy Pulses vs. Excess Energy" *Proc. ICCF13* (to be published).
9. S.E. Jones, E.P. Palmer, J.B. Czirr, D.L. Decker, G.L. Jensen, J.M. Thorne and S.E. Tayler, "Observation of Cold Nuclear Fusion in Condensed Matter," *Nature* **338**, 737 – 740 (1989)
10. K. Riisager, "Neutron Halo States" *Rev. Mod. Phys*. **68**, 1106 – 1116 (1994).
11. P.G. Hansen, "Nuclear Halo: Structure and Reactions" *Nuclear Physics*, **A588**, 1c – 10c (1995).
12. J. Gleick, *Chaos*, Penguin books, ISBN 0-14-00.9250-1
13. M.C.H. McKubre, S. Crouch-Baker, Riley, S.I. Smedley and F.L. Tanzella, "Excess Power Observed in Electrochemical Studies of the D/Pd System," *Proc. ICCF3* (Oct. 21 – 25, 1992, Nagoya, Japan) pp. 5 – 19, Universal Academy Press, Inc., Tokyo, 1993.
14. X. Zhang, W-S. Zhang, D. Wang, S. Chen, Y. Fu, D. Fan and W. Chen, "On the Explosion in a Deuterium/Palladium Electrolytic System, "*Proc. ICCF3,* pp. 381 – 384 (1992).
15. J.-P. Biberian, "Explosion during an electrolysis experiment in an open cell mass flow calorimeter," *6th International Workshop on Anomalies in Hydrogen/Deuterium loaded Metals*, Siena, Italy, May 13-15 2005.
16. T. Mizuno and Y. Toriyabe, "Anomalous energy generation during conventional electrolysis" *Proceedings of ICCF12*, pp. 65 – 74, (2006)
17. S.I. Smedley, S. Crouch-Baker, M.C.H. McKubre and F.L. Tanzella, "The January *2, 1992,* Explosion in a Deuterium/Palladium Electrolytic System at SRI International" *Proc. ICCF3,* pp. 139 – 151 (1992).

THE EXTENDED MICRO HOT FUSION SCENARIO

Rainer W. Kühne

Tuckermannstr. 35, 38118 Braunschweig, Germany
kuehne70@gmx.de

The cold fusion neutron emissions, neutron bursts, and heat bursts can be explained by the extended micro hot fusion scenario. I describe the model and present the experimental evidence.

During the years 1986 and 1989 three experimental teams independently reported to have discovered cold fusion. The experiments differed strongly from one another, both in the applied methods and the reported results. Hence, the observational results need not necessarily result from one unique physical mechanism. Let us take a brief look at these three types of cold fusion.

Type 1: Mechanically treated LiD and heavy ice samples were reported to have emitted neutron bursts which have lasted for roughly ten minutes [1, 2].

Type 2: Motivated by geophysical observations (anomalous isotope ratios [3, 4]), electrolysis of deuterided metal was performed and reported to have generated low levels of neutrons of 2.5 MeV energy [3]. These emissions appeared a few hours after the start of electrolysis and terminated several hours later [3].

Type 3: Electrolysis of deuterided metals was reported to have emitted high levels of heat appearing days after the start of electrolysis [5-7]. Signals of nuclear fusion (neutrons, gamma rays) were at least 10 orders of magnitude too small to explain the reported heat emissions [5-7].

The experiments of type 1 were motivated by positive results of fracto-emission experiments and explained by the fracto-fusion model [1, 2]. An analogous "micro hot fusion" scenario was suggested [8] for the explanation of the type 2 experiments.

The micro hot fusion scenario can be described as follows [9, 10].

When hydrogen is absorbed by metals, then it forms bubbles around impurities and lattice defects of the metal. During their growth until a diameter of several micrometers, the bubbles deform the metal lattice and create mechanical stresses. After several hours, the mechanical stresses have become strong enough to create cracks which propagate through the metal lattice. The cracks are formed preferentially between the hydride bubbles and the weaker hydrided metal. Palladium dihydride is a semi-metal. Therefore the different

electronegativities of metal and hydrogen generate positively electrically charged hydride bubble surfaces. Hence, the crack sides become electrically charged. Within the cracks of typically one micrometer width and ten to hundred micrometers length there arises an electric field strength of one hundred million volts per centimeter. Within strongly hydrided metals, electrons are bound stronger than hydrogen nuclei. Therefore the electric field within the cracks allows the hydrogen nuclei of the bubbles to accelerate until they reach energies of typically ten kilo-electron-volts.

Within the weaker hydrided metal, the hydrogen nuclei transfer their kinetic energy of several kilo-electron-volts to the metal lattice during a path of one tenth of a micrometer. This energy transfer creates hot spots within the hydrided metal with a mean temperature of typically ten thousand degrees Celsius and a pressure of ten billion Pascal. Within the hot spots, the hydrided metal is gaseous. Because of the high internal pressure, the hot spots transfer their heat energy explosively to the surrounding solid hydrided metal, where the explosions generate further cracks. When such a crack collides with the surface of a hydrided bubble, then the electrically charged bubble surface generates a strong electric field within the crack. Again, the electric field accelerates hydrogen nuclei from the bubble until they get several kilo-electron-volts of energy. Hence, a cycle reaction of the creation of cracks, electric fields, kilo-electron-volt hydrogen nuclei, hot spots, and micro-explosions is generated. This cycle reaction might result in the pulverization and even explosion of the entire metal hydride.

If the hydrogen isotope deuterium is used, then this cycle reaction is accompanied by fusion reactions. These fusion reactions occur when the kilo-electron-volt deuterons reach the other crack side and fuse with the non-accelerated deuterons of the weaker hydrided metal. This cycle reaction which includes deuteron fusion reactions is called the “extended micro hot fusion scenario”. This scenario was suggested by Roman Sioda and me [9, 11]. It is able to explain the neutron emissions reported by Jones et al. [3, 4], the neutron bursts reported by De Ninno et al. [12, 13] and Menlove et al. [14, 15], the simultaneous heat and neutron bursts reported by Gozzi et al. [16, 17], and the explosions of cold fusion cells reported by Fleischmann et al. [5].

The experimental evidence for the extended micro hot fusion scenario is presented in the table.

Table: Cold Fusion Phenomena which Can Be Explained by Extended Micro Hot Fusion

No.	Phenomenon	Explanation
1	Emission of 2.5 MeV neutrons [3, 4, 18-24]	Deuteron-deuteron fusion $d(d, n)^3He$
2	Emission of 3.0 MeV protons [25-27]	Deuteron-deuteron fusion d(d,p)t
3	Near-surface process for palladium [3, 4, 9, 28]	Crack-formation near palladium surface [29]
4	Deuterium gas emission [30, 31]	Gas desorption by crack formation [9]
5	Acoustic emissions simultaneously with neutron [32, 33] and proton bursts [34]	Relaxation of metal lattice by crack formation [35]

6	Radio emission simultaneously with proton bursts [34]	Formation of high electric fields within the cracks [35]
7	Disappearance of neutron emission several hours after the start of electrolysis [3, 4, 18, 19, 36]	Bubble growth time is between 0.1 sec and 1 day [37]; fracture time is several hours [38]
8	Emission of 10**4 ... 10**7 neutrons per cm**3 of electrode material (many experiments where neutrons have been detected)	Calculation: Refs. [37, 38]
9	Ratio of 100 emitted neutrons per Joule liberated [16, 17, 30, 39, 40]	Only 1 of 10**12 of the keV deuterons undergoes fusion reactions [11]
10	Heat emission from light hydrogen loaded cells [41]	Formation of bubbles, cracks and electric fields is independent of the hydrogen isotope used
11	Emission of keV electrons [42-46], positively charged keV ions [43, 47], X-rays [48-51], radio-waves [44] and electrification [52, 53] from various hydrided materials and neutron emission [1, 2, 54, 55] from deuterided materials minutes after mechanical treatment	Fracto-emission by formation of strong electric fields with 10**7 ... 10**8 V/cm and 10**4 ... 10**5 V [1, 2, 50, 56]
12	Many non-successful experiments [57-87]	Various possible explanations including [9, 88-90]: (a) too low sensitivity of detectors; (b) electrodes had long pre-loading times and measurements were performed only after the termination of the emissions

References

1. V. A. Klyuev et al., Sov. Tech. Phys. Lett. 12, 551 (1986).
2. B. V. Derjaguin et al., Colloid. J. USSR 48, 8 (1986).
3. S. E. Jones et al., Nature 338, 737 (1989).
4. S. E. Jones et al., J. Fusion Energy 9, 199 (1990).
5. M. Fleischmann et al., J. Electroanal. Chem. 261, 301 (1989).
6. M. Fleischmann et al., J. Electroanal. Chem. 263, 187 (1989).
7. M. Fleischmann et al., J. Electroanal. Chem. 287, 293 (1990).
8. J. S. Cohen and J. D. Davies, Nature 338, 705 (1989).

9. R. W. Kühne, Fusion Technol. 25, 198 (1994).
10. R. W. Kühne, Fusion Technol. 37, 265 (2000).
11. R. W. Kühne and R. E. Sioda, Fusion Technology 27, 187 (1995).
12. A. De Ninno et al., Nuovo Cimento A 101, 841 (1989).
13. A. De Ninno et al., Europhysics Letters 9, 221 (1989).
14. H. O. Menlove et al., J. Fusion Energy 9, 215 (1990).
15. H. O. Menlove et al., J. Fusion Energy 9, 495 (1990).
16. D. Gozzi et al., Nuovo Cim. A 103, 143 (1990).
17. D. Gozzi et al., SIF Conf. Proc. 24, 241 (1990).
18. A. Bertin et al., Nuovo Cim. A 101, 997 (1989).
19. A. Bertin et al., J. Fusion Energy 9, 209 (1990).
20. K. L. Wolf et al., J. Fusion Energy 9, 105 (1990).
21. K. L. Wolf et al., AIP Conf. Proc. 228, 341 (1991).
22. T. Bressani et al., Nuovo Cim. A 104, 1413 (1991).
23. E. Botta et al., Nuovo Cim. A 105, 1663 (1992).
24. M. Bittner et al., Fusion Technol. 23, 346 (1993).
25. R. Taniguchi et al., Jap. J. Appl. Phys. 28, L2021 (1989).
26. S. E. Jones et al., AIP Conf. Proc. 228, 397 (1991).
27. G. F. Cerofolini et al., Nuovo Cim. A 105, 741 (1992).
28. N. Wada and K. Nishizawa, Jap. J. Appl. Phys. 28, L2017 (1989).
29. P. B. Price, Nature 343, 542 (1990).
30. E. Yamaguchi and T. Nishioka, Jap. J. Appl. Phys. 29, L666 (1990).
31. Y. Arata and Y. C. Zhang, Proc. Jpn. Acad. B 66, 1 (1990).
32. P. I. Golubnichii et al., AIP Conf. Proc. 228, 151 (1991).
33 P. I. Golubnichii et al., JETP Lett. 53, 122 (1991).
34. P. I. Golubnichii et al., AIP Conf. Proc. 228, 146 (1991).
35. P. I. Golubnichii et al., Sov. Phys. Dokl. 34, 628 (1989).
36. B. Emmoth et al., SIF Conf. Proc. 24, 79 (1990).
37. S. E. Segre et al., Europhys. Lett. 11, 201 (1990).
38. V. A. Tsarev, Sov. Phys. Usp. 33, 881 (1990).
39. D. Gozzi et al., J. Fusion Energy 9, 241 (1990).
40. A. G. Lipson et al., Sov. Tech. Phys. Lett. 18, 673 (1992).
41. E. Yamaguchi and T. Nishioka, AIP Conf. Proc. 228, 354 (1991).
42. V. V. Karassev et al., Dokl. Akad. Nauk 88, 777 (1953).
43. J. Wolbrandt et al., Phys. St. Sol. A 27, 53 (1975).
44. J. T. Dickinson et al., J. Mater. Sci. 16, 2897 (1981).
45. J. Mathison et al. J. Appl. Phys. 65, 1923 (1989).
46. A. G. Lipson et al., Sov. Tech. Phys. Lett. 15, 783 (1989).
47. J. T. Dickinson et al., J. Mater. Res. 5, 109 (1990).
48. V. V. Lymar et al., IX-All Union Conf. Acoustics (Moscow, Nauka, 1977), p. 65.
49. T. M. Belyaeva et al., Sov. Tech. Phys. Lett. 10, 341 (1984).
50. V. I. Berkov et al., Sov. Phys. Dokl. 32, 381 (1987).
51. V. A. Klyuev et al., Dokl. Akad. Nauk 279, 415 (1984).
52. M. I. Kornfeld, J. Phys. D 11, 1295 (1978).
53. Yu. I. Golovin et al., Sov. Phys. Sol. St. 27, 671 (1985).
54. M. A. Yaroslavskii, Sov. Phys. Dokl. 34, 637 (1989).
55. M. A. Yaroslavskii, Sov. Phys. Dokl. 34, 648 (1989).
56. B. V. Derjaguin et al., Sov. Phys. Dokl. 19, 208 (1974).
57. M. Gai et al., Nature 340, 29 (1989).

58. E. Kashy et al., Phys. Rev. C 40, 1 (1989).
59. K. D. Schilling et al., Z. Phys. A 336, 1 (1990).
60. R. D. Armstrong et al., Electrochimica Acta 34, 1319 (1989).
61. R. D. Armstrong et al., J. Electroanal. Chem. 272, 293 (1989).
62. N. S. Lewis et al., Nature 340, 525 (1989).
63. D. E. Williams et al., Nature 342, 375 (1989).
64. M. H. Salamon et al., Nature 344, 401 (1990).
65. M. M. Broer et al., Phys. Rev. C 40, 1559 (1989).
66. M. R. Deakin et al., Phys. Rev. C 40, 1851 (1989).
67. K. E. Rehm et al., Phys. Rev. C 41, 45 (1990).
68. J. R. Southon et al., Phys. Rev. C 41, 1899 (1990).
69. J. F. Ziegler et al., Phys. Rev. Lett. 62, 2929 (1989).
70. P. B. Price et al., Phys. Rev. Lett. 63, 1926 (1989).
71. J. P. Briand et al., Phys. Lett. A 145, 187 (1990).
72. R. Aleksan et al., Phys. Lett. B 234, 389 (1990).
73. G. M. Miskelly et al., Science 246, 793 (1989).
74. D. Alber et al., Z. Phys. A 333, 319 (1989).
75. S. Blagus et al., Z. Phys. A 333, 321 (1989).
76. A. Baurichter et al., Z. Phys. B 76, 1 (1989).
77. G. Schrieder et al., Z. Phys. B 76, 141 (1989).
78. D. A. Roberts et al., Phys. Rev. C 42, 1809 (1990).
79. J. J. G. Durocher et al., Can. J. Phys. 67, 624 (1989).
80. R. Behrisch et al., Nucl. Fusion 29, 1187 (1989).
81. J. Roth et al., Nucl. Fusion 30, 441 (1990).
82. G. P. Chambers et al., Phys. Rev. B 41, 5388 (1990).
83. G. M. McCracken et al., J. Phys. D 23, 469 (1990).
84. F. Botter et al., Phys. Lett. B 232, 536 (1989).
85. V. Eberhard et al., Z. Phys. A 334, 357 (1989).
86. B. Balke et al., Phys. Rev. C 42, 30 (1990).
87. I. F. Silvera and F. Moshary, Phys. Rev. B 42, 9143 (1990).
88. R. W. Kühne, Phys. Lett. A 155, 467 (1991).
89. R. W. Kühne, Phys. Lett. A 159, 208 (1991).
90. R. W. Kühne, Magazin2000plus 232, 24 (2006) (= arxiv: physics/0604119).

GRAVIATOMS WITH LEPTONS AND MESONS

Yu. P. Laptev*, M. L. Fil'chenkov and S. V. Kopylov*****

** Bauman Moscow State Technical University,*
Department of Physics, ***yplaptev@rambler.ru***
*** Peoples' Friendship University of Russia, Moscow,*
Institute of Gravitation and Cosmology, ***fmichael@mail.ru***
**** Moscow State Open University, Department of Physics,* ***kopsv@mail.ru***

Abstract

Bound quantum systems maintaining a particle in orbit around a mini-hole, called graviatoms, are considered. The graviatoms prove to exist only under some conditions, which are satisfied for systems containing leptons and mesons. Electromagnetic and gravitational radiations of charged particles in the graviatoms are comparable with Hawking's mini-hole radiation. Bound quantum systems with the neutrino has a macroscopic size, nevertheless, the neutrino energy levels are quantized. For macro-bodies two cases are possible: Bohr's levels outside the body and Thomson's – inside it. The gravitational radiation proves to be negligibly small. Stable graviatoms with baryon constituents are impossible. The internal structure of the baryons, consisting of quarks and gluons, should be taken into account. There occurs a so-called quantum accretion of baryons onto a mini-hole. The whole problem is solvable within the framework of quantum chromodynamics and quantum electrohydrodynamics.

1. Introduction

As known, there exist bound quantum systems[1] due to electromagnetic interaction, for example atoms and molecules. Atomic nuclei and hadrons are examples of the quantum systems bound via strong interaction.

Planets, stars and galaxies are classical systems bound by gravity. Newton's gravitational force is about forty orders weaker than Coulomb's force for micro-particles. That is why gravity is usually neglected in elementary particle physics.

However, if one component of the system is assumed to be considerably massive and has a small dimension and the other is an elementary particle, then a quantum system can be formed, for example, as a result of capturing particles by mini-holes in the early Universe. Such systems are called graviatoms [1].

[1] Quantum system definition: the de Broglie wave length for a particle is about a system size

Another example of the quantum systems bound by gravity is macro-bodies capturing neutrinos having de Broglie's wave length of macroscopic value.

2. Approach

We consider Schrödinger's equation for hydrogen-like graviatoms, which describes a radial motion of a particle in the mini-hole potential, and find their energy levels. The angular wave function is the well-known eigen function of the orbital momentum operator for a hydrogen-like atom.

Schrödinger's equation for the graviatom

$$\frac{1}{r^2}\frac{d}{dr}\left(r^2\frac{dR_{pl}}{dr}\right)-\frac{l(l+1)}{r^2}R_{pl}+\frac{2m}{\hbar^2}\left(E+\frac{mc^2r_g}{2r}\right)R_{pl}=0 \qquad (1)$$

describes a radial motion of a particle with the mass m in the mini-hole potential, where $r_g=2GM/c^2$ and M are the mini-hole gravitational radius and mass respectively.

The energy spectrum is of hydrogen-like form

$$E=-\frac{G^2M^2m^3}{2\hbar^2n^2}. \qquad (2)$$

3. Graviatom existence conditions

A graviatom can exist if the following conditions are fulfilled [2, 3]:

- the geometrical condition $L>r_g+R$, where L is the characteristic size of the graviatom and R is the characteristic size of a particle;
- the stability condition given by
  (a) $\tau_{gr}<\tau_H$, where τ_{gr} is the graviatom lifetime and τ_H is the mini-hole lifetime, and
  (b) $\tau_{gr}<\tau_p$, where τ_p is the particle lifetime (for unstable particles);
- the indestructibility condition (due to tidal forces and the Hawking effect) $E_d<E_b$, where E_d is the destructive energy and E_b is the binding energy.

The charged particles satisfying these conditions are the **electron, muon, tau lepton, wino, pion** and **kaon**.

The conditions of existence the graviatoms reduce to the relation between the masses of the mini-hole and particle, with their product being approximately constant equal to the Planck mass (figure 1).

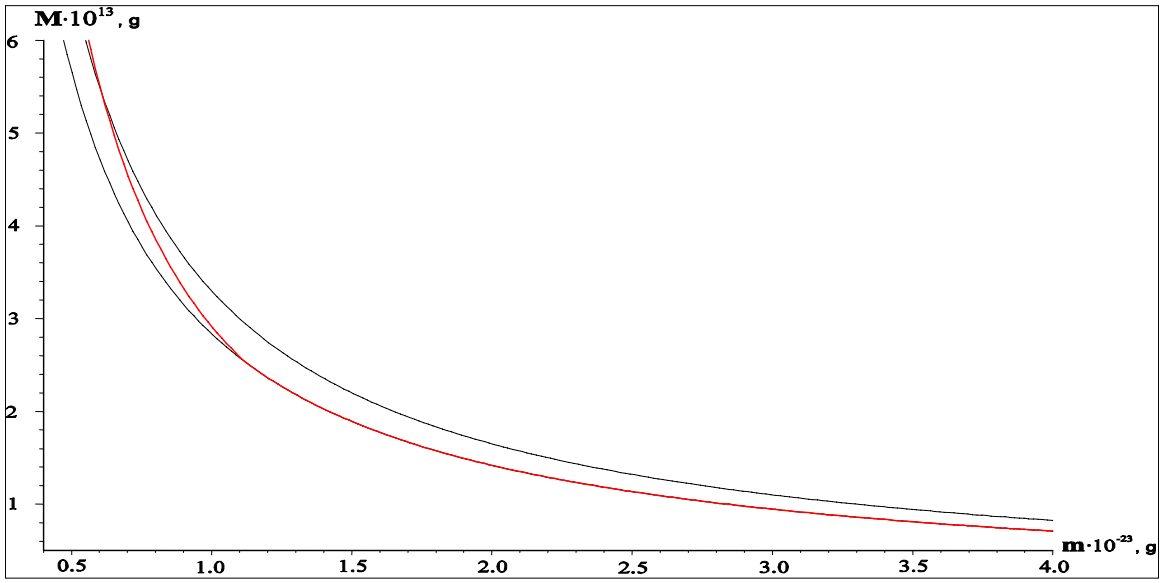

Figure 1. *The upper and lower curves indicate the range of values related to the geometrical condition (the upper one) and to Hawking effect (the lower one). The middle curve is related to the particle stability condition (*$\tau_p = 10^{-22}\,s$*).*

4. Graviatom radiation

The intensity of the electric dipole radiation of a particle with mass m and charge e in the gravitational field of a mini-hole is

$$I_{fi}^{d} = \frac{2\hbar e^2 \omega_{if}^3 f_{if}}{mc^3}, \tag{3}$$

where $\omega_{if} = (E_i - E_f)/\hbar$ is the frequency of the transition $i \to f$ and f_{if} is the oscillator strength.

The electric quadrupole radiation intensity for the transition $3d \to 1s$ is

$$I_{13}^{q} = \frac{6\hbar e^2 \omega_{31}^3}{mc^3} f_{3d\to 1s}. \tag{4}$$

The gravitational radiation intensity for the transition $3d \to 1s$ is

$$I_{13}^{g} = \frac{24\hbar GM\omega_{31}^3}{c^3} f_{3d\to 1s}. \tag{5}$$

The mini-hole creates particles near its horizon due to Hawking's effect, its power

$$P_H = \frac{\hbar c^6}{15360\pi G^2 M^2}\,. \tag{6}$$

The Hawking energy

$$E_H = \frac{b\hbar c^3}{8\pi GM}\,, \tag{7}$$

where b=2.822, following Wien's displacement law.

We evaluate the intensity of electric dipole and quadrupole radiation of a charged particle in the gravitational field of the mini-hole. The oscillator strengths are given by the well-known formulae for the hydrogen-like atoms. The gravitational radiation for transition 3d to 1s is also calculated. The graviatom radiations are compared with Hawking's effect. The formulae for Hawking's radiation power and energy are also presented.

The electric dipole, gravitational and Hawking's radiation prove to be comparable. It is possible for graviatoms involving electrons, muons and pions to have existed up to now. The gravitational fine-structure constant appears to be greater than the electromagnetic one but does not exceed the unity, so the perturbation theory remains valid.

The mini-hole masses for the graviatoms involving electrons, muons and pions exceed the value of 4.38×10^{14} g, which means that it is possible for such graviatoms to have existed up to now. The gravitational equivalent of the fine-structure constant

$$\frac{GMm}{\hbar c} = 0.608 \div 0.707\,. \tag{8}$$

Thus, the perturbation theory remains valid.

5. Systems with neutrinos

The de Broglie wave length for a neutrino [4]

$$\lambda\!\!\!^{-}_{dB} = \frac{\hbar^2}{GMm_\nu^2}\,, \tag{9}$$

where m_ν is the neutrino mass, is of macroscopic value ($10^1 \div 10^6$ cm).

Macro-bodies capture neutrinos on both Bohr's hydrogen-like levels (outside the body) and Thomson's oscillatory ones (inside the body). The oscillation frequency $\omega = (4/3\,\pi\rho G)^{1/2}$, the gravitational radiation intensity

$$I_{mb} = \frac{\hbar^{7/3}(4/3\pi\rho G)^{1/2}}{c^5 m_\nu^{5/2}}, \tag{10}$$

where ρ is the macro-body density.

Bound quantum systems with the neutrino has a macroscopic size, nevertheless, the neutrino energy levels are quantized. For macro-bodies two cases are possible: Bohr's levels outside the body and Thomson's – inside it. The gravitational radiation proves to be negligibly small.

6. Conclusion

The graviatom can contain only leptons and mesons. The observable stellar magnitude for graviatom electromagnetic radiation exceeds 23^m.

Stable graviatoms with baryon constituents are impossible. The internal structure of the baryons, consisting of quarks and gluons, should be taken into account. There occurs a so-called quantum accretion of baryons onto a mini-hole. The whole problem is solvable within the framework of quantum chromodynamics and quantum electrohydrodynamics.

Neutrinos can form quantum macro-systems.

Of interest is the fact that from the galaxy rotation curves it follows that the dark matter mass is proportional to the distance from the galaxy centre. Similarly, the total mass of neutrinos on the n-th level is proportional to their orbit radius.

The description of gravitationally bound macro-systems with neutrinos maybe helpful for solving the dark matter problem in the Universe.

References

1. Yu. Laptev, M.L. Fil'chenkov. Abstr. 41 All-Russ. Conf. on Probl. of Math., Inform., Phys. and Chem ., PFUR 2005, p. 60.
2. M.L. Fil'chenkov, Yu. P. Laptev, Grav. & Cosmol., v. 12, N.1 (2006) 65-68.
3. Yu. P. Laptev, M.L. Fil'chenkov. Astron. Astroph. Trans., v. 25, No 1. (2006) 33-42.
4. Yu. P. Laptev, S.V. Kopylov, M.L. Fil'chenkov, 43 All-Russ. Conf. on Probl. of Math., Inform., Phys. and Chem., PFUR 2007, p. 73.

SELECTIVE RESONANT TUNNELING MODEL FOR LATTICE CONFINED DEUTERONS

Xing Z. Li, Qing M. Wei, Bin Liu

Department of Physics, Tsinghua University, Beijing 100084, CHINA
lxz-dmp@tsinghua.edu.cn

Selective resonant tunneling has been successfully applied to both hot fusion and "cold fusion". It gives not only the best formula to calculate the hot fusion cross-section of d+t, d+d, and d+^{3}He in the low energy region, but also explains the puzzle of "excess heat" without strong neutron and gamma radiation for low energy nuclear reaction. In the present paper, it is shown that when deuterons are confined by crystal lattice, the Block Theorem requires:

(1) A deuterium flux is necessary to keep the quantum steady state in the lattice;

(2) The fusion reaction rate is enhanced by a factor of θ. Here θ is a big number in the order of 10^{27} (Gamow factor in the beam-target case is in the order of $(1/\theta)^2$).

(3) The Chubb-Bloch state of electrons which provide the stronger screening effect.

The density of states in energy band would be discussed along with the Chubb-Bloch state of deuterons in lattice. It may provide a mechanism of negative feedback to stabilize the steady state which is necessary for this macroscopic quantum mechanic phenomenon.

This research is supported by the Natural Science Foundation of China (#10475045), Ministry of Science and Technology (Division of Fundamental Research), and Tsinghua University (985-II, Basic Research Funds)

References

1. Xing Z. Li, Jian Tian , Ming Y. Mei and Chong X. Li, "Sub-barrier Fusion and Selective Resonant Tunneling," Phys. Rev. ,C **61**, 024610 (2000)

2. Xing Z. Li, Bin Liu, Si Chen, Qing Ming Wei, and Heinrich Hora, "Fusion cross-sections for inertial fusion energy," Laser and Particle Beam, **22**, 469 (2004)

3. Xing Z. Li, et al., "Correlation between abnormal deuterium flux and heat flow in a D/Pd system," J. Phys. D: Appl. Phys. **36,** 3095–3097, (2003)

PHOTON/PHONON-AIDED LOW-ENERGY NUCLEAR REACTIONS IN CONDENSED MATTER

A.Meulenberg[*] and K.P.Sinha[**]

[*] *Visiting Scientist - Department of Instrumentation, IISc, India* (***mules333@gmail.com***)
[**] *Department of Physics, IISc, Bangalore, India* (***kpsinha@gmail.com***)

Abstract

Models to account for the observed experimental results for low-energy nuclear reactions in palladium-deuteride systems have been extended from earlier work [1]. The crucial idea is a mechanism of improved probability for the needed penetration of the Coulomb barrier for a D-D reaction. This facilitation occurs, in condensed matter, with the formation of D^- ions at special frequency modes (e.g. via phonons) and, specifically for the laser-stimulated case, with utilization of an enhanced optical potential at a selected interface or structure. Spatial-confinement and alignment modes in various media are explored. Resonant modes, in particular, are studied as a means of raising the interaction rate and/or peak energies in a low average-energy medium. Such mechanisms, which may be coupled to work in concert to increase the probability of barrier penetration, are of greatest interest.

References

[1] Sinha, K. P. and Meulenberg, A., "On the Laser Stimulation of Low-Energy Nuclear Reactions in Deuterated Palladium," Current Science, V 91, No. 7, 10 Oct. 2006, p. 907

CLUSTER REACTIONS IN LENRS

George H. Miley[1], Andrei Lipson[1], Nie Luo[1], Heinz Hora[2], and Prajakti Joshi Shrestha[1]

[1]Department of Nuclear, Plasma and Radiological Engineering
University of Illinois, Urbana, Il 61801
[2]Dept. Theoretical Physics, University of NSW, Sydney 2052, Australia

A distinctive array of nuclear reaction products was observed previously in the "Patterson" flowing packed-bed type electrolytic cell experiments using multi-layer thin films of metals on mm-size plastic beads [1]. The swimming electron layer and a new magic number theory were proposed to explain this. More recently these theories have been expanded into a "cluster" model to explain a wider range of transmutation experiments [2]. The cluster model is consistent with certain measurements of energetic charged-particle emission during thin film electrolysis, with observations suggesting localized reactions and also with x-ray production during plasma bombardment experiments [3-6]. The cluster reaction concept and supporting experimental data will be discussed in this presentation. In addition to explaining transmutations, if understood and optimized, cluster reactions could lead to an important new power source based on LENR.

1. G.H. Miley, and J.A. Patterson, "Nuclear Transmutation in Thin-film Coatings Undergoing Electrolysis," J. New Energy, 1993, vol. 1, pp.11-15,
2. Hora, H. and G.H. Miley, "New magic numbers from low energy nuclear transmutations predict element (306)X(126) for compound reactions", Czech. J. Phys., **48**: p1111. (1996).
3. G. H. Miley and P. J. Shrestha, "Review of Transmutation Reactions in Solids", Proceedings, ICCF-10, 2005, Boston, MA.
4. G. H. Miley, Andrei Lipson, et al, "Intense non-linear soft x-ray emission from a hydride target during pulsed D bombardment**"** ICCF-12, 2005, Nagoya, Japan.
5. A. Lipson, G.H. Miley, et al., "Emergence of a High-Temperature Superconductivity in Hydrogen Cycled Pd compounds suggest localized Superstochiometric H/D Sites", ICCF-12, 2005, Nagoya, Japan.
6. J. Dash, G. Noble, and D. Diman, "Surface Morphology and Micro-composition of Palladium Cathodes after Electrolysis …and: Correlation with Excess Heat*", Trans. Fusion Tech*., 1994. **26**(4T): p. 299.

ISSUES FOR CHARGED-PARTICLE AND X-RAY EMISSION IN LENR EXPERIMENTS

George H. Miley[1], Lawrence P.G. Forsley[2], Pamela A. Mosier-Boss[3]

[1]Dept. of Nuclear, Plasma and Radiological Engr. University of Illinois, Urbana, IL 61801 USA,
[2]JWK Technologies Corporation, Suite 1000, 7617 Little River Turnpike, Annandale, VA 22003
[3]SPAWAR Systems Center San Diego, Code 2373, San Diego, CA 92152

Various researchers have reported charged particle emission from cold fusion experiments based on CR-39 tracking methods [1-3]. Low energy x-rays have also been observed by some using solid-state detectors and also TLD methods. In several cases, attempts have been made to correlate emissions with cold fusion reactions, but this remains open to interpretation. The design for these experiments differs in detail but generally involved electrolysis. The characteristics of these radiations as reported by various researchers differ greatly. Lipson et al. [1] found distinct energy groups of charged particles, identified as ~ 1-MeV protons and ~ 10-MeV alpha particles. P. Mosier Boss, et al., [2] as well as .R. Oriani and J. Fisher [3] report dense track clusters due to unidentified particles, sometimes coming for regions outside of the electrode. Soft x-ray emission has also been reported in other types of experiments. A. Karabut S.A. Kolomeychenko [4] report 1-keV coherent x-ray radiation emission during plasma bombardment experiments while Miley et al., [5] find softer diffuse emission under somewhat different discharge characteristics.

In principle, the origin of all of these emissions should be from a common reaction, but the differences seem too large to justify. Some explanations are discussed in the presentation.

1. A.G. Lipson, A.S. Roussetski, et al., "Reproducible nuclear …desorption", ICCF-12, Yokohama, Japan (2005).
2. P. A. Mosier-Boss, et al., "Thermal and Nuclear Aspects of the Pd/D2O System", ed. S. Szpak and P.A. Mosier-Boss. Vols. 1-2, SPAWAR Sys. Ctr., San Diego, U.S. Navy 2002.
3. R. A. Oriani and J.C. Fisher, "Energetic particle shower in the vapor from electrolysis", ICCF-11, Marseille, France, 2004.
4. A. B. Karabut and S.A. Kolomeychenko, "Experimental Research into …..Discharge", ICCF-10, Cambridge, MA, 2003.
5. G.H. Miley, Y. Yang, et al., "Intense Non-linear Soft X-ray ….Bombardment", ICCF-12, Yokohama, Japan, (2005).

PHENOMELOGICAL MODEL OF LOW ENERGY ELEMENT TRANSMUTATION AND ELEMENT DISTRIBUTION IN TRANSMUTATION PRODUCTS.

G.V. Mishinsky, V.D. Kuznetsov.

City of Dubna, Moscow region, Russia, ***mysh@nrmail.jinr.ru***

Introduction

During the last 15 years [1], communications about experimental evidence of abnormal physical phenomenon – low energy transmutation of atomic nuclei of chemical elements – are regularly published in the press. The essence of this phenomenon consists in the fact that chemical elements turn into other chemical elements in low excited, from the point of view of nuclear physics, condensed media.

The phenomenon of low energy element transmutation (hereafter – LEET or transmutation) was registered, for example; at the glow discharge in palladium and other metal cathodes [1-5], at electron beam melting of zirconium ingots in vacuum furnace [6], at electron explosions of metal targets [7] and electric explosions of metal foils in liquid dielectric medium [8,9], at application of pulse current to lead [10], at electric discharge in water-mineral medium [11], at ultrasound processing of water salines [12], in growing biological structures [13] and others.

In addition to the fact that *new elements appear* in all these experiments, which were absent in initial material prior to beginning of said processes, *an isotopes relation* of chemical elements distinct from natural distribution [1-7] is registered in transmutation products. As a rule, *stable isotopes* of elements are transmutation products in the majority of experiments. Moreover, a communication on transformation of radioactive isotopes into stable ones is available [7,12]. In some experiments [3-5,7,10] it was possible to register x-ray and gamma-ray radiation, radiation of charged particles as well as radioactive isotopes. At that, by estimate of authors of publications [3-5], the number of stable isotopes produced as a result of transmutation is 10^{12}-10^{13} times more than that of radioactive isotopes. Other peculiarity of LEET process is the fact *that excessive heat energy* [1,2,4,5,6,8,11,12] was registered where it was possible to do so. Some authors underline that transmutation process is accompanied by *unknown radiation*, which leaves its “strange” traces in photoemulsions, on thin sections of metals, and which, at interaction with matter, changes its structure and chemical composition [6,8,12,14,15].

1. Phenomenological model.

Let's note straight away that element transformations indicated in introduction can not be explained by modern physical ideas due to both impossibility of overcoming the Coulomb barrier by nuclei and impossibility to build observed elements at conservation of proton number [9,16,17]. To remove the last contradiction, we have to include electrons into inlet or outlet channel, thus supposing a possibility of weak interactions, at that, not breaking conservation laws of electric and lepton charge. The fact of obtaining, in transmutation reactions, many chemical elements at electron-beam and electric explosions [7-9], including heavy elements: tungsten, tantalum, lead, which are impossible to obtain in pair reactions in relatively element-light medium leads us to conclusion, that at transmutation many atoms interact simultaneously [7, 9,14]:

$$\sum_i c_i \, {}^{N_i}_{Z_i}A_i + e^- \sum_i c_i \, Z_i \rightarrow \sum_j c_j \, {}^{N_j}_{Z_j}B_j + e^- \sum_J c_J \, Z_J + l\nu(\tilde{\nu}) + Q \quad (1),$$

where ${}^{N}_{Z}A, {}^{N}_{Z}B$ - nuclides with charge Z and nucleon quantity N; nuclides ${}^{N}_{Z}B$, are as a rule stable; e^- - atomic electrons; c_i, c_j – quantity of nuclides ${}^{N_i}_{Z_i}A, {}^{N_j}_{Z_j}B_j$ in inlet and outlet channels, correspondingly; $l\nu(\tilde{\nu})$ - l -number of neutrino or antineutrino. Neutrino and antineutrino appear in reaction equations for conservation of lepton charge.

Furthermore, we must be sure that nuclear reactions (1), leading to strange elements observed in experiments are exothermic $Q \geq 0$. Preliminary conclusion on possibilities of such reactions is obtained from consideration of picture of coupling energy per nucleon in nuclei of initial matter Fig.1. Energy is released in these reactions at the expense of difference in sums of masses of atomic nuclei in inlet and outlet reaction channels. Such processes are known, this is fission of nuclei into two fragments, for example, spontaneous fission of nucleus ^{238}U, and thermonuclear fusion, when, on the contrary, a fusion reaction of two light nuclei takes place. As mentioned above, energy is released in these two processes at the expense of difference in sums of masses of initial and end atomic nuclei. The same occurs in transmutation process, but in this case one or two nuclei or a whole conglomerate of atomic nuclei can take part in the reaction. At that, both processes are realized in multi-atom transmutation reactions: fusion of many atomic nuclei (atoms) into one common formation and subsequent division of this formation into many atoms. It should be underlined that the above reaction equation (1) represents apparently just the known – nuclear part of this complicated process, but does not reflect in any way, for example, the appearance of unknown radiation in LEET reactions.

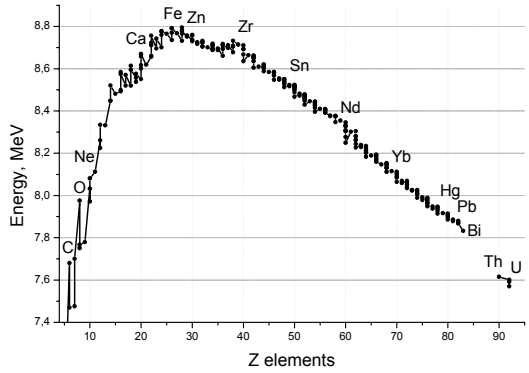

Fig.. 1 Coupling energy per nucleon in stable atomic nuclei

Surely, in calculations, not only mass of a nucleus, but also mass of l electrons should be taken into account in energy balance. Furthermore, for purity of calculations, we took into account also coupling energy of electrons in atoms. A reference book was used to analyze possible reactions [18]. The table included stable and radioactive isotopes with half-life time over 10 years or, in case of absence of stable isotopes, an isotope with maximal possible lifetime was taken. Coupling energy of atomic electrons was taken into account by the formula $E_A = 16.Z^{7/3}$ within the framework of Thomas-Fermi model [19]. For technical reasons, we took into account not more than three outlet nuclides, i.e. all reactions were considered:

$$\sum_i c_i \, {}^{N_i}_{Z_i}A_i + l e^- = {}^{N_1}_{Z_1}B_1 + {}^{N_2}_{Z_2}B_2 + l\nu_e + Q \; ; \quad \sum_i c_i \, {}^{N_i}_{Z_i}A_i + l e^- = {}^{N_1}_{Z_1}B_1 + {}^{N_2}_{Z_2}B_2 + {}^{N_3}_{Z_3}B_3 + l\nu_e + Q \; ;$$

$$\sum_i c_i \, {}^{N_i}_{Z_i}A_i = {}^{N_1}_{Z_1}B_1 + {}^{N_2}_{Z_2}B_2 + le^- + l\tilde{\nu}_e + Q \; ; \quad \sum_i c_i \, {}^{N_i}_{Z_i}A_i = {}^{N_1}_{Z_1}B_1 + {}^{N_2}_{Z_2}B_2 + {}^{N_3}_{Z_3}B_3 + le^- + l\tilde{\nu}_e + Q \; ,$$

where le^-, $l\nu_e$, $l\tilde{\nu}_e$ – l-number of electrons, neutrino and antineutrino, correspondingly. At that, conservation conditions of quantity of nucleons $\sum_i c_i N_i = N_1 + N_2$ и $\sum_i c_i N_i = N_1 + N_2 + N_3$, full charge conservation $\sum_i c_i Z_i \pm l = Z_1 + Z_2$ and $\sum_i c_i Z_i \pm l = Z_1 + Z_2 + Z_3$ and positive balance of energy $Q \geq 0$ should be met.

Thus, the calculations done show that the process of appearance of strange elements in low energy transmutation reaction does not contradict to energy conservation law and they can be obtained from initial nuclei at positive energy output [9].

2. Classification of transmutation processes

As it was already mentioned, the end state of transmutation process is a set of stable nuclides (at present, 272 stable nuclides can be counted). This final set of nuclides is different for

transmutation processes, which occur either for a short time (electron and electric explosions Fig.2c), or, when, in the process of LEET, the medium recommences continuously (electric discharge in aqueous-mineral medium Fig.2d), if compared with time-extended processes, in which the medium is not replaced by a new one (melting of zirconium - Fig.2a, ultrasound processing [USP] of salt solutions - Fig.7b). In given figures, it can be seen, that in case of electric explosion and electric discharge, the appearance of strange elements is irregular, and in case of Zr-melting and USP, transmutation products are a broad spectrum of chemical elements.

As shown in [9], a possible cause of this difference is the duration of LEET processes in these experiments. Actually, electric explosion occurs during tens of microseconds, in two other cases it occurs during tens of minutes – zirconium melting and even days – ultrasoundprocessing. And though it is not known what time the transmutation reaction takes, what time the conditions for its appearance in the medium exist, it is realistic to assume that transmutation reaction density per medium unit is much greater during Zr-melting and USP than in the case of electric explosion. Due to above it can be assumed that transmutation reactions at electric explosions occur, to significant degree, under participation of initial material only, and in cases of Zr-melting and USP, secondary elements – products of previous

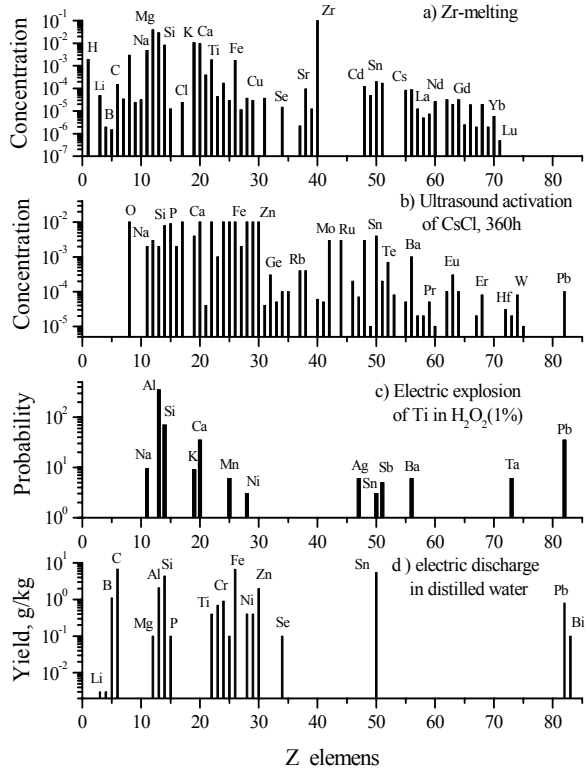

Fig.2 a) Elements distribution at Zr-melting,
b) Element composition of CsCl-solution after 360-hours of ultrasound activation;
c) Elements yield, obtained as a result of electric explosion of Ti-foil in 1% hydrogen peroxide**;**
d) Elements yield at processing in electric discharge of distilled water.

transmutations – can be involved. Obviously, the last circumstance causes an extension of element spectra, which are obtained in transmutation products.

By present moment, rather many experiments on low energy element transmutation have been carried out, so they can be classified.

- First of all, experiments on LEET can be classified according to a method applied, for example: electric discharge, melting, cavitation, etc.
- Another important feature of the process is *repetition factor* of participation of chemical elements in transmutation reactions. *Single* processes can take place in LEET reactions, when initial, primary chemical elements only participate in them. These processes are: experiments on electron explosion [7] and on electric explosion of metallic foils in liquid media [8,9], and experiments on electric discharge in water-mineral medium [11, page.28]. Experiments where *multiple* LEET processes with participation of both primary and secondary chemical elements are: for example, ultrasound processes of aqueous salt solutions [12]. Also, prolonged multiple processes are possible. Les us call them, for short, *hypermultiple* processes. Mainly secondary chemical elements participate at the end of these processes in transmutation reactions. Electron melting of zirconium ingots in vacuum furnace should be ascribed to such experiments [6].
- Other feature of the process is its energy intensity or, in other words, *energy density* of excited medium. Obviously, the number of atoms in the input channel of LEET reaction and, consequently, the element composition of transmutation products depends on this feature of the process.
- *Initial medium composition* by chemical elements obviously influences element composition of LEET products. This is true, at least, for single and multiple transmutation processes.

3. Number of atoms in input channel of transmutation reactions.

When discussing transmutation product spectrum in paper [9] for the case of zirconium melting, it was stated that a broad spectrum of elements can be obtained in two ways: either at serial accumulation first of light elements with a relative low energy coupling, and then on their basis – accumulation of heavy elements, either at once, accumulation of light and heavy elements from a large quantity of initial nucleus in input channel – parallel accumulation.

Obviously, consecutive mechanism in obtaining a broad spectrum of chemical elements in transmutation products takes place in experiments on ultrasound processing of aqueous salt

solutions [12]. As can be seen from Fig. 3b, chloride lithium solution (LiCl), after its processing during 8 hours, showed the appearance of such chemical elements as Sc, V, Cr, Zn. Those elements were missing in the solution after its processing during two hours Fig.3a. The amount of F, Mg, P, Ca, Mn, Fe also increased significantly. At the same time (8 hours), heavier chemical elements, which appeared in the solution after 24-hour treatment (Fig.3c) are missing in the solution. For last measurement time, such an element as Rubidium (Rb) has a concentration comparable to concentration of zinc, and that is why it should be present in the solution after its 8-hour activation, if we allow a consecutive and not parallel mechanism of element production (a large amount of initial nuclei in the input channel). The same can be said about cesium (Cs), which concentration exceeds the zinc concentration by more than an order. It may be concluded from this circumstance that, first, light elements starting from ^{19}F to ^{70}Zn are produced in water solution in this experiment, which are consequently a material for production of heavier chemical elements.

If we assume that at initial stage of transmutation process, when salt concentration is low, mainly water molecules participate in reactions, them we can evaluate a number of molecules participating in transmutation process and area of space occupied by them. To obtain elements from ^{19}F to ^{70}Zn, sufficient are 1(+hydrogen) – 4 molecules of water (Fig.3d), and area occupied by them is equal to $\sim 5 \cdot 10^{-8}$ cm. Thus, a number of atoms participating in transmutation process can amount, in this case to 4-12 atoms (H_2O-molecule - 3 atoms).

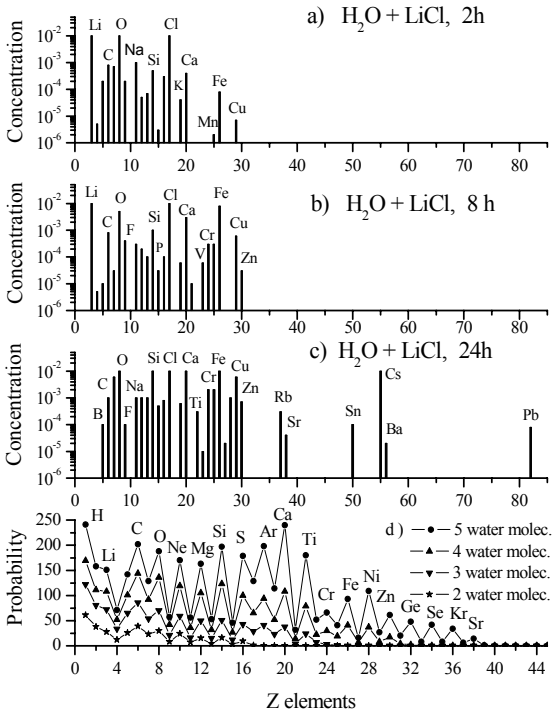

Fig.3 Element composition of LiCl-solution after a) 2-hour and b) 8-hour ultrasound activation and, c) after 24-hour ultrasound activation;
d) Calculation of element yield, when 2 to 5 molecules of water are involved in transmutation process.

However, it should be remembered that, in experiments with electric explosion [8,9] and electric discharge in distilled water [11], heavy elements – Ta, Pb, Bi (Fig.2c,d) were found in transmutation products, which, according to calculations [9], can be produced by elements of light medium only. So, the number of atoms participating in transmutation reaction can be significantly higher, i.e. 25 atoms and more, Fig.6. The changes in the number of atoms in input channel for comparable USP experiments and electric explosion-electric discharge experiments are connected to various values of energy density of excited water medium in these experiments.

So, the greater the energy density of excited medium, the greater the amount of atoms, which can be involved in the input channel of transmutation reaction.

Naturally, this concerns the extension of range of number of atoms in the input channel. The change of number of atoms in the input channel of transmutation process, in its turn, causes a change of element spectrum of products at reaction output. Experiments on electric explosion of titanium foil in glycerin -$C_3H_8O_3$ ([9] can confirm this conclusion, Tab.6, Fig.12a). A power of electric explosion, if compared with other three experiments, was increased in experiment No.660, this caused an appearance of lead and disappearance of manganese in the spectrum.

Discussing again the experiments on ultrasound processing of LiCl solution, it should be noted that such elements as titanium (Z=22) and nickel (Z=28) are present in the spectrum, after 24-hour solution treatment with same concentration as that of zinc, and are absent in 8-hour spectrum (Fig.3b,c). Thus, for some reason, these elements are also produced in consecutive way. It is obvious that other chemical elements would appear in the solution in case of continuation of transmutation process. This can be well seen on the example of ultrasound processing of CsCl solution during 360 hours (Fig.2b).

4. Element production in the process of transmutation.

The calculations executed also clearly demonstrate that if secondary elements are involved in transmutation processes, its products may contain atomic nuclei of practically all chemical elements, regardless of from which chemical element or compound those processes started. In Fig.4 shows calculation bar charts of possible end products (outlet channel) of transmutation reactions for various elements in the inlet channel. The abscissa axis shows a charge of chemical element, the ordinate axis demonstrates how many times the present element appeared at calculation in various outlet channels. Two atoms of aluminum

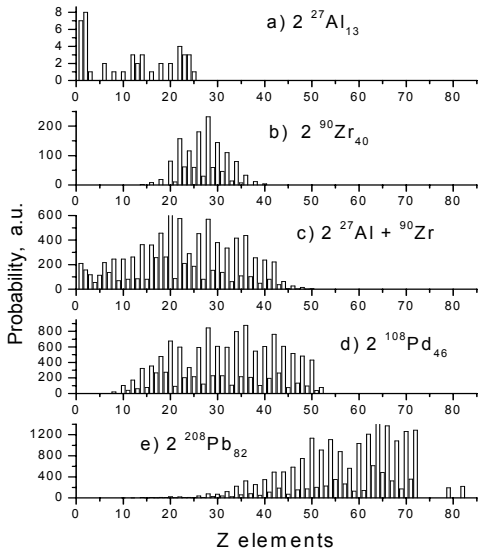

Fig.4 Calculation of possible end products of transmutation reactions for various elements in inlet channel.

$^{27}_{13}Al$ (Fig.4a) or two atoms of zirconium $^{90}_{40}Zr$ (Fig.4b), or two atoms of aluminum $^{27}_{13}Al$ and one atom of zirconium $^{90}_{40}Zr$ (Fig.4c), or two atoms of palladium $^{108}_{46}Pd$ or two atoms of lead $^{108}_{82}Pb$ (Fig.4e) are involved in outlet channel. It is appropriate to note that calculation spectrum for $^{108}_{46}Pd$ (Fig.4d) sufficiently well reflects a spectrum of elements obtained in works with glow discharge with palladium cathode ([4,Fig.1]). Two same nucleus are taken here as an example in each four cases in the inlet channel. It is clear that involvement of other elements in transmutation reaction from distributions given in Fig.4, causes an extension of spectrum of chemical elements. An increase of atoms in inlet channel causes the same, because of increased number of possible combinations in outlet channel (Fig.4c). It is completely obvious that the more elements form a medium at the beginning of transmutation process, the richer is the spectrum of chemical elements in its products.

It should be noted that at the very beginning of time-extended transmutation processes, the maximum of element spectrum obtained in outlet channel will be located not far from initial element.

Significant odd-even fluctuations of elements in the yield of possible end products also draw attention.

Transmutation process will not start within phenomenological model if primary elements are iron and nickel isotopes with a maximal known coupling energy per nucleon (^{56}Fe -8,790MeV, ^{58}Fe -8,792MeV and ^{62}Ni - 8,794MeV), in other words, if they are in a minimal energetic state. As calculations showed, however, the transmutation process can

proceed at the expense of other isotopes of Fe and Ni that have a relatively smaller coupling energy.

Thus, the model demonstrates that *multiple and hypermultiple transmutation processes inevitably cause an appearance, in its products, of atomic nuclei of practically all chemical elements from which chemical element or compound those processes started.*

Elements, which possess no stable isotopes, may be an exemption.

In addition to that, *element spectrum in LEET products can depend on energy density of exited medium, by means of a number of atoms in inlet channel.*

Evidently, phenomenological model allows to produce, as a result of LEET processes super-heavy elements (Z>100), if they are stable [7].

5. "Universal" distribution.

It is evident that if the medium has a set of elements, which turn into each other, the quantitative relations between them should be reflected by a certain distribution.

Let us consider the transmutation processes in more detail by the example of electric explosion and zirconium melting. For obviousness, Fig.5a,b gives assumed energetic schemes of these transmutation processes: electric explosion (Fig.5a) and zirconium melting (Fig.5b). The ordinate axis should show the sum of nuclides masses in energetic units, which are involved in transmutation process. But as a number of atoms involved in the inlet channel of transmutation reaction can vary, it is convenient to proceed to a scale, connected to energy per nucleon E/N. Then, a whole group of initial states can be represented in this scale (with isotope precision) as "one" state. Left column gives initial states, the right one – end states. As was said above, sets of stable elements are end states. Such sets can be infinite in number.

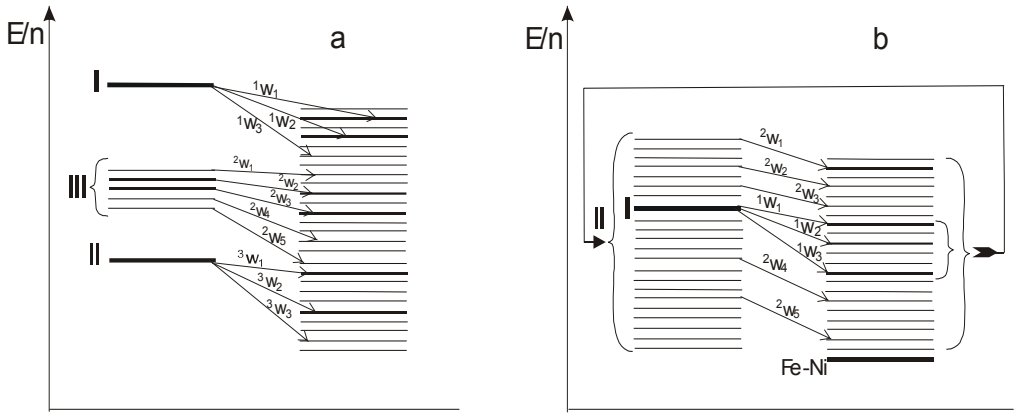

Fig.5 Assumed schemes of energetic transmutation processes for cases: Electric explosion (single transitions); b) zirconium melting (hypermultiple processes).

However conservation laws – conservation of energy, angular momentum, number of nucleons etc. in each particular transmutation act reduce this set up to countable quantity.

Three groups of initial states Fig.5a are available for case of electric explosion of metallic foil in dielectric medium. The first group (I) is represented by states, when reaction participants are atoms of dielectric medium only, second group (II) corresponds to states, when atoms of metallic foil only take part in transmutation reaction and the third group (III) includes mixed states, when simultaneously both foil atoms and dielectric medium atoms take part in the reaction. Last states represent a "group" even within the scale E/N, because the ratio of medium atoms and metal foil atoms in the inlet channel can vary. As we have assumed that transmutation at electric explosion occurs with involvement of initial material only, then transitions from initial states into end states are single. Each such transition happens with its own probability (w). It would appear reasonable that some transitions prevail. Evidently, it is for this reason that the spectrum of end elements for electric explosion is rather restricted. Probabilities of transitions obviously depend on many values: energy released during transition; angular state momentum; number of nucleon in inlet channel and number of nuclides in outlet channel; number of weak transitions; and most probably, on nuclear features of nuclides themselves. The last assumption is evident from experimental data on electric explosion and aqueous electric discharge. Really, such elements as antimony, tin and lead are practically always present in end products for these cases. Additionally, as was mentioned above, light elements from sodium to zinc prevail in transmutation processes in all experiments.

As distinct from electric explosion, at electron melting of zirconium in vacuum furnace, its natural composition is sole initial element (group I, Fig.5b) for production of all elements represented in Fig.2a. As mentioned above, the appearance of such a broad element spectrum is likely to be connected to involvement of products of previous transmutations in consecutive transmutation reactions (group II, Fig.5b).

Let us assume that medium always has conditions for transmutation processes. At initial development stage of transmutation processes, when the number of zirconium atoms prevails over the number of atoms of secondary elements, nuclide distribution of transmutation products will be evidently of non-regular character, i.e. the same as for the case of electric explosion (single transitions). Distribution of stable nuclei is understood here as nuclide distribution. Nuclide distribution can substantially change only then, when a number of zirconium atoms diminishes by that much that secondary element atoms will start to enter

transmutation reactions between each other with greater probability, then with atoms of initial matter. As mentioned above, atomic nuclei of practically all chemical elements will appear simultaneously in transmutation products. In the long run, hypermultiple transmutation processes will lead to a situation, when the number of zirconium atoms will become comparable with or less than a number of atoms of secondary elements. By that time, mutual transformation of elements into each other will lead to a certain, *quasi-equilibrium distribution*.

The distribution would be in the state of equilibrium, if transmutation reactions proceed without energy loss. It is known from statistical physics and thermodynamics that irreversible processes in closed system inevitably end in its transition into the state of equilibrium. [18]. We dared to apply the laws of statistical physics and thermodynamics to transmutation processes basing on the fact that transmutation can be represented not as energy exchange between particles, but as exchange of nucleon portions between nuclides ($E=mc^2$), though in multi-particle interaction, and all kinds of sets from a limited number of stable nuclides can be used as statistical ensemble. Transmutation processes are really irreversible, but they are executed in an open system, with mass (energy) loss for transmutation reaction itself. The lost mass is transformed into kinetic energy of nuclides, is brought away by neutrino and unknown radiation. It is clear that calculated theoretical [9] and experimental [2] losses in the mass 0.1-10MeV per one reaction, are significantly less than the mass of nuclides entering the reaction (>>1GeV). Thus, hypermultiple transmutation processes are executed in quasi-constant medium, which energy is decreasing. The obtained distribution will be, for this reason, in quasi-equilibrium state.

It should be noted that element group from sodium to zinc always appear in all experiments on transmutation, regardless of a medium where this process takes place. Evidently, some elements of this group are in the maximum of quasi-equilibrium distribution. In case of electron melting of zirconium such elements are magnesium and aluminum (Fig.2a), in some zones of transmutation products the maximum is formed by silicon and iron (10 - 45 mass. %) [6]. Paper [12] reports a significant concentration of Al, Si, Mn, Fe, Zn and Pb in transmutation products of the solution ^{137}Cs. For the last case it should be remembered that, due to presence of a large amount of water molecules and their constant involvement in transmutation process, the obtained element distribution for reaction products is far from quasi-equilibrium state.

As already mentioned, if transmutation proceeds without energy loss, then the end nuclide distribution would be in equilibrium state. Additionally, if coupling energy per nucleon is be equal for all elements, the quasi-equilibrium distribution would be the same, i.e. it would not depend on initial element composition of matter, where transmutation processes have started. Such distribution would characterize the transmutation process in its "pure" form. A distribution obtained for the case when transmutation process starts in hydrogen medium is most close to such hypothetical, "universal" distribution.

It is evident that transmutation process will not stop after quasi-equilibrium distribution is realized. Ultimately, it will result, due to exothermic feature, in prevalence of iron and nickel in distribution, as nuclides with maximal coupling energy. The transmutation process will end, when the number of isotopes ^{56,58}Fe, ^{62}Ni with maximal coupling energy per nucleon are substantially more than that of other isotopes.

It is clear that for cases, when transmutation process starts in element medium, say, from chromium to zinc, which are elements with approximately equal and close to maximal coupling energy, the quasi-equilibrium nuclide distribution will have its maximum, reasoning from phenomenological model, in the range of ^{56,58}Fe and ^{62}Ni. However, as stated above, atomic nuclei of all chemical elements (stable nuclides) will appear in transmutation products during transmutation process. At that, the distribution of these elements will presumably tend to become a "universal" distribution.

If this is true, then in any medium, regardless of its chemical composition, where hypermultiple transmutation processes take place, a "universal" distribution, connected exclusively with transmutation peculiarities will be realized. In addition to that, a maximum in the range of iron-nickel, connected with maximal coupling energy in isotopes of these elements, will be superimposed, with a certain degree of intensity, on the "universal" distribution. The intensity of Fe-Ni maximum will exactly depend on chemical composition of a medium, where transmutation process has started.

During data processing and analysis on electric explosions of metal foils in dielectric medium [9], we draw our attention to higher yield of some groups of elements in transmutation products. These groups are: Na-Si, K-Ca, Mn-Ni, Cu-Zn, Zr-Mo, Ag-Sb, Ta-W, Pb. It is interesting that similar element groups are found in spectra of transmutation products, caused by ultrasound cavitation and zirconium melting. Furthermore, we obtained a similar picture, when calculating yield of elements under involvement, in transmutation process, of N-molecules of water (Fig.6) and other elements (Fig.4c-e). Fig.6, gives, for better visual

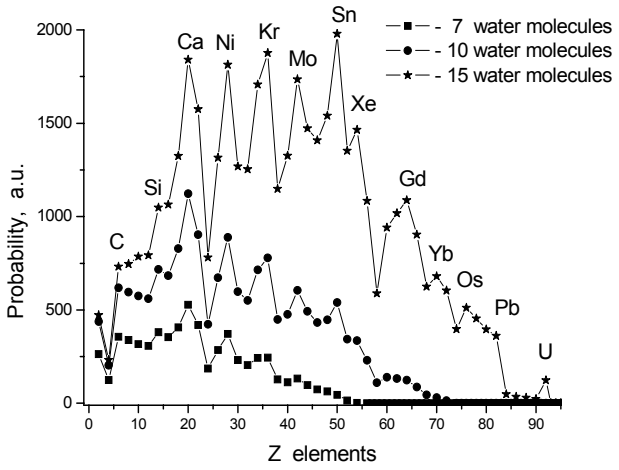

Fig.6 Calculation of yield of even-charge elements, at participation in transmutation process of 7, 10 and 15 – molecules of water. A sum of 2 and 3 nuclides is given in outlet channel.

understanding and to avoid sharp even-odd fluctuations (Fig.3d), the yields of even-charged elements. A decrease of element yield in the range of carbon-silicon with increased number of water molecules involved in the reaction is connected with the fact that calculation in outlet reaction channel allow for not more than three nuclides.

It is rather evident that increased probability of appearance of these elements in transmutation processes is connected to their proximity to maximums available depending on coupling energy of nucleons in atomic nuclei in virtue of their atomic number and a number of isotopes in these elements. These maximums are known to be caused by "magic" shells with a number of protons and neutron equal to: 2, 8, 20, 28, 50, 82 and 126. A higher yield of those elements was cited in the paper on ultrasound cavitation [12]. Really, in equal initial conditions in the inlet channel, presence of "magic" nuclides in the end spectrum increases a number of combinations of other nuclides in outlet channel. A large number of isotopes in a particular element increases the probability of its appearance statistically. Hence, the "universal" distribution will, in addition to Fe-Ni maximum, include peaks caused by "magic" shells.

Thus, *a "universal" distribution of nuclides with maximums connected to peculiarities of nuclide coupling energy versus mass number will be realized in transmutation products in any medium, regardless of its chemical composition, where hypermultiple transmutation processes take place. Intensity of Fe-Ni maximum depends on chemical composition of a medium, where the transmutation process has started.*

Strictly speaking, because element spectrum in transmutation products depends on energy density of excited medium, quasi-equilibrium distribution, at energy constantly applied to medium, will also depend on this parameter. We can talk about "universality" of

end distribution for transmuting systems only if they are not subject of action of external energy sources or their action is insignificant. And energy required for transmutation processes in such systems is supplied at the expense of transmutation reactions themselves. As mentioned above, the development of LEET process is limited by the Fe-Ni maximum.

The case of ultrasound processing of salt dissolved in water [12] is a multiple process and it is similar to Zr-melting. At ultrasound activation, element composition of salt dissolved in water transmutes into a nuclide distribution, which does not depend on this composition and which will not change due to a constant presence of water molecules in reactions. The same distribution will be obtained if transmutation process starts in clean water. As already mentioned above, the nuclide distribution in the process of transmutation will tend, under diminishing number of water molecules, to "universal" distribution of nuclides.

Certainly, all above reasonings require a strict theoretical justification and experimental check. Such experiments can be realized, using, in case of electron melting, various metals and their alloys, and in case of ultrasound processing and electric discharge in water-mineral medium – various chemical compounds.

6. Isotopic relationships in transmutation products

If hypermultiple transmutation processes lead to realization of "universal" nuclide distribution in its products, then the distribution will be "universal" both for elements and isotopes. We may rather evidently conclude from this circumstance that in a medium where nuclide distribution has not yet become "universal", elements should have isotope relationships, which differ from table values. It is especially true for cases of electron explosion and electric explosion, where single transmutation transitions take place.

Substantial isotopic shifts in transmutation products were observed in experiments with glow discharge in palladium and other metallic cathodes [2,4] and in experiments with electron explosion [7]. In other case, when mass distribution for zirconium melting (Fig.2a) was transformed in distribution of chemical elements (Fig.8a), a contribution of each isotope to a particular element had naturally to be taken into account. That is why an isotopic relationship, which is obtained in transmutation products as a result of zirconium melting, has been found at once for each element. If we compare these relationships with natural isotopic relationships (see Table), then it is evident, on the one hand, that their difference is significant, for example: for potassium, chromium, copper, zinc, germanium and barium (*). This circumstance evidences in favor of existence of transmutation phenomenon. On the other

Table. Comparison of natural isotope ratio (Nat.,%) with isotope ratio observed in zirconium transmutation products [7] (LEET, %).

Z	A	LEET	Nat.	Z	A	LEET	Nat..	Z	A	LEET	Nat.	Z	A	LEET	Nat.
Li	6	6	7.5	**Ti**	46	8	8.2	**Ga**	69	66	60	**Ba***	132	11	0.1
	7	94	92.5		47	8	7.4		71	34	40		134	29	2.4
B	10	22	20		48	74	73.8	**Ge***	70	73	20,5		135	11	6.6
	11	78	80		49	5	5.4		72	12	27,4		136	9	7.8
Mg	24	76	79		50	5	5.2		73	15	7,8		137	9	11.2
	25	11	10	**Cr***	52	70	83.8		74	2	36,5		138	29	71.7
	26	13	11		53	16	9.5	**Se**	77	15	7.6	**Eu**	151	56	47,8
Si	28	89	92.2		54	14	2.4		78	16	23.5		153	44	52,2
	29	7	4.7	**Cu***	63	48	69.2		80	54	44.6				
	30	4	3.1		65	52	30.8		82	6	9.4				
K*	39	76	93	**Zn***	64	49	48.6	**Sr**	86	24	9,9				
	41	24	7		66	17	27.9		87	7	7				
					67	14	4.1		88	69	82,6				
					68	20	18.8								

hand, a rather well match of their isotopic relationships with natural ones for the Earth is observed for the rest of elements [21]. The above mentioned difference in isotopic relationships for specified elements (K, Cr, Cu, Zn, Ge, Ba) can be explained by unfinished transmutation processes and, consequently, by distribution dependence, including isotopic distributions, on initial element, in this case, on zirconium.

7. Nucleosynthesis.

The fact that elements, which are zirconium transmutation products, have partly a natural isotopic relationship of the Earth, has lead us to the idea to compare distribution by mass numbers obtained as a result of zirconium melting with element occurrence by their masses in the Earth's crust [21].

Some difference in compared distributions (Fig.7), as already mentioned above, is likely to be connected with unfinished transmutation processes for the case of zirconium melting and distribution dependence on this element. Really, the "universal" distribution in case of zirconium transmutation was realized on the part of heavy masses relative to assumed distribution maximum in the range of Mg-Si. That is why heavy masses from M=60 to M=175 prevail in nuclide distribution at zirconium melting (M_{Zr} - 90÷92, 94, 96), if compared with the Earth's distribution, because heavy masses can be directly obtained from initial material, and simultaneously, the content of light masses is reduced from M=6 to M=30.

Furthermore, the distributions show a correlation by element groups. Same elements (Ti, Fe) and element groups (Na-Si, K-Ca, Cu-Zn, Cd-Sb) have maximums in both distributions (Fig.8a,b). The figure represented lacks, for convenience of comparison, lines at spots, which

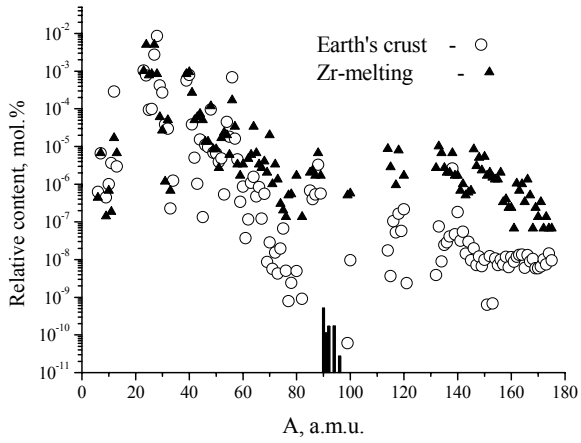

Fig.7 Comparison of element distribution in case of zirconium transmutation at its melting with element occurrence in the Earth's crust. For orientation, zirconium isotopes with their relative content are emphasized with bold lines.

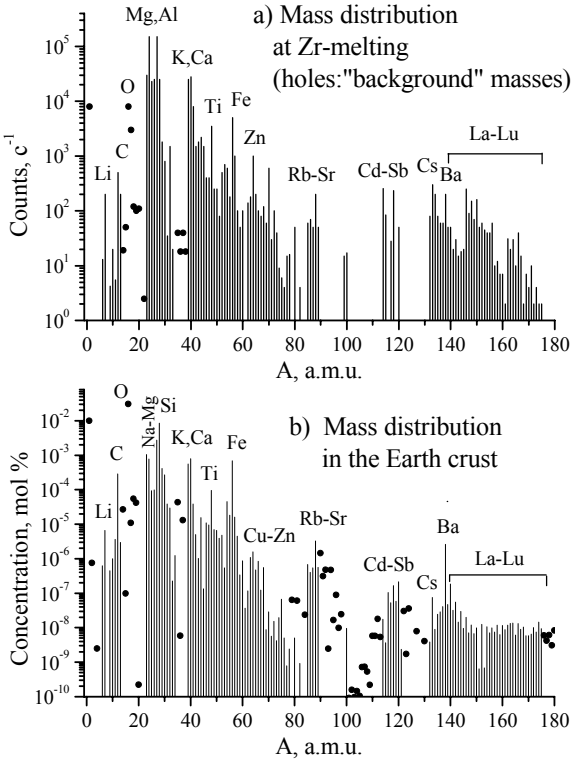

Fig.8 Comparison of element groups: a) case of zirconium transmutation at its melting; b) element occurrence in the Earth's crust.

correspond to "background" zirconium masses (Zr, ZrH, ZrO, ZrO_2, Zr_2, Zr_2O) and gas component, which is difficult to account for at the comparison. For gases, masses are given as dots.

Taking into account that low energy transmutation processes that occur under rather "soft" physical conditions (electric explosion, melting, ultrasound activation) and tend to reproduce "universal" distribution, the following conclusion can be drawn logically from above material.

Transmutation process is decisive at creation of chemical elements on the Earth. In other words, low energy transmutation process, along with nuclear reactions in stars, is responsible for nucleosynthesis. Furthermore, that nucleosynthesis can be realized directly on planets and form their element composition.

Transmutation process on the Earth was likely to occur at the time, when the Earth was a compressing, liquid, melted ball. It is quite possible that, deep in the Earth, transmutation processes are still going on and the huge energy released at that is observed by us as eruption of volcano. Specialist would know that intra-plate tectonic activity and volcanism can not be explained within plate tectonics. Most common hypothesis, which satisfactorily explains volcanism and tectonic activity within both oceanic and continental lithosphere, is associated with the idea of hot spots and mantle plumes [22]. Probably it is exactly in those hot spots and mantle plumes where transmutation processes take place.

Investigations in these hot spots and plumes demonstrated changes of isotopic relationships in such elements as helium, argon, strontium, neodymium, lead. For example, it was found that helium produced by subcortical layers of the Earth, has isotopic concentration relationship $^3He/^4He = (3\pm1)*10^{-5}$ [23-25]. This relationship is abnormally great and exceeds relationship in helium produced by the rocks of Earth's crust by hundreds and thousands times. The authors of this discovery put forward a supposition that subcortical helium is residual, primeval one, formed as a result of fusion reactions in stars, for which the relationship is $^3He/^4He = 3*10^{-4}$. But it is rather strange to believe that inert, easily mobile gas helium stayed in the interior of the Earth during its formation. Especially since the relationship $^3He/^4He$ should diminish at the expense of increased ^4He, obtained as a result of alpha-decay of thorium, uranium and their daughter products (protactinium-bismuth). That is why it was expected, before that discovery, that the increase of occurrence depth of rocks, the relation $^3He/^4He$ in them would diminish, because the relationship in the atmosphere is $^3He/^4He = 1.4*10^{-6}$. Thus, an increased isotopic relationship $^3He/^4He$ can be explained by transmutation processes occurring in subcortical layers of the Earth. It should be mentioned that the authors have fixed [11] in transmutation products an appearance of helium isotopes both in solid and liquid phase with abnormally high relationship $^3He/^4He = 0.2\text{-}1$.

Starting from general considerations, previous assumption on transmutation nature of nucleosynthesis is true for other planets too. An availability in many planets, including the Earth, of cores, which mainly consist of iron and similarity of element compositions are also evidences of this assumption.

Next general conclusion would be that transmutation processes should also occur on stars. Let us remember that transmutation processes are accompanied by release of energy. Then, if the energy generation by the Sun is determined (at least partly) by transmutation processes, the flow of Sun's neutrino should be different from that in case of thermonuclear

cycles, regardless of the fact that integrally, for all reactions, the number of neutrino per energy unit should be approximately equal, both for transmutation and fusion cycles. The difference is in the losses of gamma-ray quanta and neutrons for fusion cycles. It is probably for this reason that measured flow of Sun's neutrino is twice less than its calculated value (approximately by two times). Furthermore, the energetic neutrino spectrum for transmutation processes should differ from neutrino spectra of fusion cycles. For the first case, it should be shifted towards low energies. Last circumstance should also have an impact on registration of neutrino, because neutrino detectors are threshold detectors both in cases of chlorine-argon and gallium-germanium techniques.

Obviously, the application of transmutation mechanism to nucleosynthesis allows to understand, in easy way, the presence of heavy elements even on most old stars, because nucleosynthesis of all elements and their isotopes up to uranium becomes evident. For comparison, Fig.9 gives, in relative units: a) Element content in Solar atmosphere; b) Element occurrence in space; c) Element content in cosmic rays at the Earth; d) Calculation of element yield at 4 water molecules involved in transmutation process and e) Element composition of transmutation products in case of Zr-melting.

Thus, the processes of nucleosynthesis and energy release in the Universe can be realized, along with nuclear reactions, due to reactions of low energy transmutation. It is evident that as soon as transformation of some chemical elements into other elements is discovered, the question about nucleosynthesis emerges at once. That is why the problem on possible involvement of LEET mechanism in nucleosynthesis has been discussed by many scientists: S.E.Jones, T.Matsumoto, S.V.Adamenko, M.I.Solin, V.A.Krivitsky.

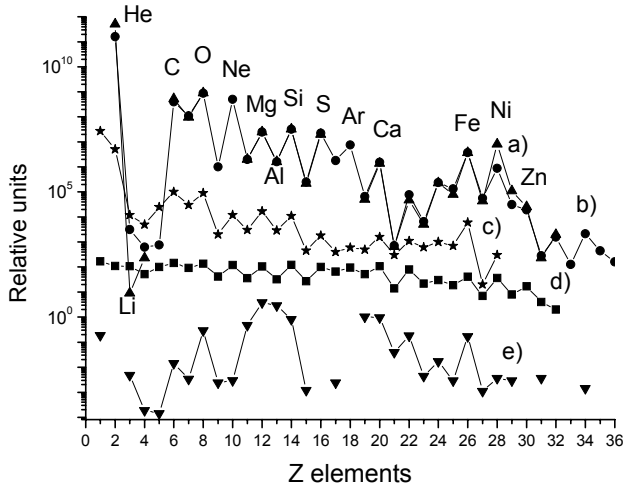

Fig.9 Comparison: a) content of elements in Solar atmosphere; b) element distribution in space; c) element content in cosmic rays at the Earth; d) calculation of element yield at participation of 4 molecules of water in transmutation process and e) element composition of transmutation products in case of Zr-melting.

Conclusion

Here, it is appropriate to emphasize that most new technologies can be developed in the following fields on the basis of transmutation phenomenon: generation of cheap and ecologically clean electricity and heat, production of precious and rare elements and isotopes from cheaper elements, recycling of radioactive waste – its transformation in stable isotopes, recycling of poison-gases and industrial toxic waste etc.

The authors express their gratitude to Penkov F.M.for useful scientific discussions and element yield calculations, to Gareev F.A., Dubovik V.M., Zhemenik V.I., Starkov V.V.and Arbuzov V.I. for useful discussions, critical remarks and support.

References

1. Karabut A.V., Kucherov Ya.R., Savvatimova I.B. Phys.Letters A170. 1992. P.265-272
2. Savvatimova I.B., Karabut A.B. Moscow. RAS. Surface. 1. 1996. P.63-75
3. Savvatimova I.B., Karabut A.B.. Moscow. RAS, Surface. 1. 1996. P.76-81
4. Karabut A.B. Proceedings of 7th Russian Conference on Cold Transmutation of Nuclei of Chemical Elements (RCCTNCE). Moscow. 2000. P.27-35
5. Karabut A.B. Proceedings of 9th RCCTNCE. Moscow. 2002. P.86-98
6. Solin M.I.. Physical Idea of Russia. 2001. No.1. P.43-58
7. Adamenko S.V.et al. http://www.proton21.com.ua/articles/Booklet_ru.pdf
8. Urutskoev L.I., Liksonov V.I., Tsinoev V.G.. Annales de la Fondation Louis de Broglie, 2002. V. 27. No 4. P. 701-726
9. Kuznetsov V.D., Mishinsky G.V., Penkov F.M., Arbuzov V.I., Zhemenik V.I. Annales de la Fondation Louis de Broglie, 2003. V. 28. No 2. P.173-214.
10. Krivitsky V.A. Geoinformatics, 2003, No.4, P. 50-53; Transmutation of chemical elements in evolution of Earth. Moscow. MPGU.2003
11. Vachaev A.V., Ivanov N.I., Pavlova G.V. Transformation of chemical elements. edited by Balakirev V.F., Ekaterinburg: Urals Branch of RAS. 2003. P.28-48
12. Kladov A. Cavitation destruction of matter. http://roslo.narod.ru/rao/rao1.htm
13. Vysotsky V.I., Kornilova A.A.. Nucleosynthesis and isotope transmutation in biological systems. 2003. Moscow. Mir.
14. Savvatimova I.B. Proc. 7th Int. Conf. On Cold Fusion. Canada. 1998. P.342-350. Proc. 8th Int. Conf. On Cold Fusion, Italy, 2000, P.277-283

15. Nesterovich A.V., Rodionov B.U., Savvatimova I.B. Proc. of 8th Russian Conference on Cold Transmutation of Nuclei of Chemical Elements. 2001. Moscow. P.211-215
16. Gareev F.A.,.Zhidkova I.E, Ratis Yu.L., Proceeding of the 11th International conference on cold fusion, Marseilles. France. 2004. P.459.
17. Gareev F.A., Zhidkova I.E., http://www.iacmns.org/iccf12/GareevF.pdf
18. Nemets O.F., Gofman Yu.V. Reference book on nuclear physics. Kiev. Naukova dumka. 1975
19. Landau L.D., Lifshits E.M. Quantum mechanics. Non-relativistic theory. M. Science. 1974
20. Kuni F.M. Statistical physics and thermodynamics. Moscow. Science. 1981
21. Kikoin I.K.. Tables of Physical Values. Reference book. Moscow. Atomizdat. 1976
22. Grachev A.F. Main problems of modern tectonics and geodynamics of Northern Eurasia . Physics of Earth. 1996. No. 12. p. 3-32.
23. Mamyrin B.A., Tolstikhin I.N., et al. DAN 1969. V.184 No.5, P.1197-1199
24. Clarke W.B., Beg M.A., et.al. Earth and Planet. Sci.Lett.1969, V.6. P.213-220
25. Mamyrin B.A., Tolstikhin I.N. Helium isotopes in nature. Moscow. Energoizdat. 1981. P.224

RATES FOR LOW ENERGY NUCLEAR REACTIONS AT SURFACES

David J. Nagel

The George Washington University, Washington DC, ***nagel@ gwu.edu***

Several requirements and features for LENR are known from experiments. Prime among them is the need for high loading, that is, ratios of protons or deuterons to lattice atoms that are near unity. One open basic question of both scientific and technological importance is the locations at which such reactions occur in heavily loaded materials. It matters greatly whether the reactions take place in the bulk of materials or at their surfaces. This paper examines the evidence for and implications of LENR occurring on or very near the surfaces of materials.

Experimentally, there are a few types of evidence for LENR taking place at the surfaces of materials. Such experimental results will be reviewed. Theoretically, Widom and Larsen published a concept that postulates the production of very slow neutrons on the surfaces of heavily loaded lattices and their subsequent reactions with nearby nuclei.

The rates for generation of heat and nuclear products are computed in this paper as a function of (1) the total area of the surfaces on which reactions can occur, (2) the fraction of the area that is active at any time, (3) the fundamental reaction rates, that is, the number of reactions per unit of active area per second and (4) the energy or number of products produced per reaction. Each of these factors and their limits are reviewed. A graphical means of relating the four factors over wide variations has been devised. It permits facile estimates of excess power and of the production rates of new elements for various combinations of the factors.

POWERS, MATERIALS AND RADIATIONS FROM LOW ENERGY NUCLEAR REACTIONS ON SURFACES

23 Oct 07

David J. Nagel

The George Washington University

1. Introduction.

The powers available from sources of energy determine their applications. This is true whether the energy comes from chemical or nuclear reactions. The power (energy per second, measured in watts or horsepower) is dependent on the energy per reaction, which is commonly constant, and the number of reactions per second. Hence, the rates of reactions are critically important for the potential uses of any energy source. This central role of reaction rates is also true for the production of materials or radiations from nuclear reactions.

In the field of LENR, solid lattices are common to almost all experiments. However, the phases from which hydrogen isotopes are introduced into lattices span the possibilities indicated in Figure 1. The ways with which lattices can be loaded with protons or deuterons fall into three broad categories. Initially and most commonly, electrochemical methods are used for loading protons from light water or deuterons from heavy water into an immersed lattice. In a few experiments, molten salts were the liquid source of the hydrogen isotopes. Many experiments have also been done with lattices placed within hydrogen or deuterium gases, often at elevated temperatures or pressures. The final large class of loading methods

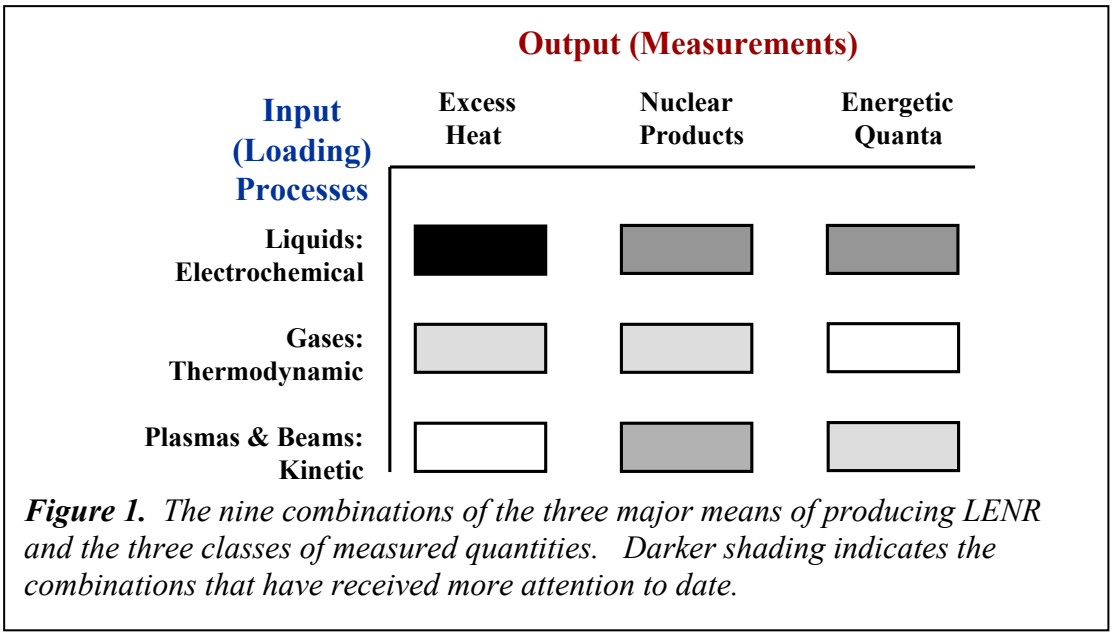

Figure 1. *The nine combinations of the three major means of producing LENR and the three classes of measured quantities. Darker shading indicates the combinations that have received more attention to date.*

involves plasmas, and sometimes low energy beams, as sources of energetic protons or deuterons.

No matter how the conditions to achieve LENR are produced, there are three major types of products from those reactions. The production of energy, called excess heat, is of greatest interest. However, the nuclei that result from the reactions, called nuclear ash, can also be significant. The production of desirable elements or destruction of unwanted isotopes could be very important. Finally, energetic quanta, both photons and particles, which are sometimes observed from LENR, are both diagnostically useful and possible concerns for radiation safety. Many other sources of radiation for applications ranging from medicine to security are now in use. However, any unwanted or wanted source of radiation inevitably comes with serious concerns over its possible degradation of the health of people or the environment.

In this paper, we are interested in all three of the means to produce LENR. However, because most of the research in the field has been on electrochemical experiments, such work is most commonly cited. Similarly, the production of energy, materials and radiation are all of interest. But, since the production of clean energy is probably the first, if not most important potential application of LENR, our focus is dominantly on the power available from such reactions.

The nuclear reactions that occur at ordinary energies can take place on the surface of a lattice, within its bulk, or in both locations. There is substantial experimental evidence for the first possibility, that is, reactions happening on or very near to the surface of a lattice. This evidence is briefly summarized in the next section. Then, we provide the simple equations that relate the rates of production of energy, nuclei or radiations to a few basic factors in the third section. The following four sections discuss each of these factors in additional detail. A simple, but very useful graphical means of relating surface areas to power production in LENR experiments constitutes section 8. The following section deals with maximization of the desired outputs. Implications for reproducibility, controllability and optimization of LENR for both research and applications are discussed in section 10. Then the relationships between LENR and nano-science and -technology are examined, prior to the concluding section. **Update this.**

2. Experimental Case for LENR Occurring on Surfaces

It is useful to begin by considering the possible locations on or near a surface or within the bulk at which LENR can occur. This can be done with the use of Figure 2. Clean surfaces can be classified as either smooth, if the shapes of the atoms and molecules that constitute the surface are ignored, or else structured with various geometries of different size scales. Surfaces usually are covered with diverse layers, which are generally complex in both their composition and structure. This is especially true of the environments in electrochemical cells. The layers on surfaces can be enabling or disabling of the chemical or nuclear reactions of interest.

The bulk of a material can be even more complex that the surface because of the various dimensionality and types of defects that are possible. Most of these are listed in Figure 2. We will next provide reasons for consideration of LENR on or very near to surfaces.

Later, after presentation and discussion of the analysis for LENR rates on surfaces, possibilities for bulk reactions will be considered in Section GG.

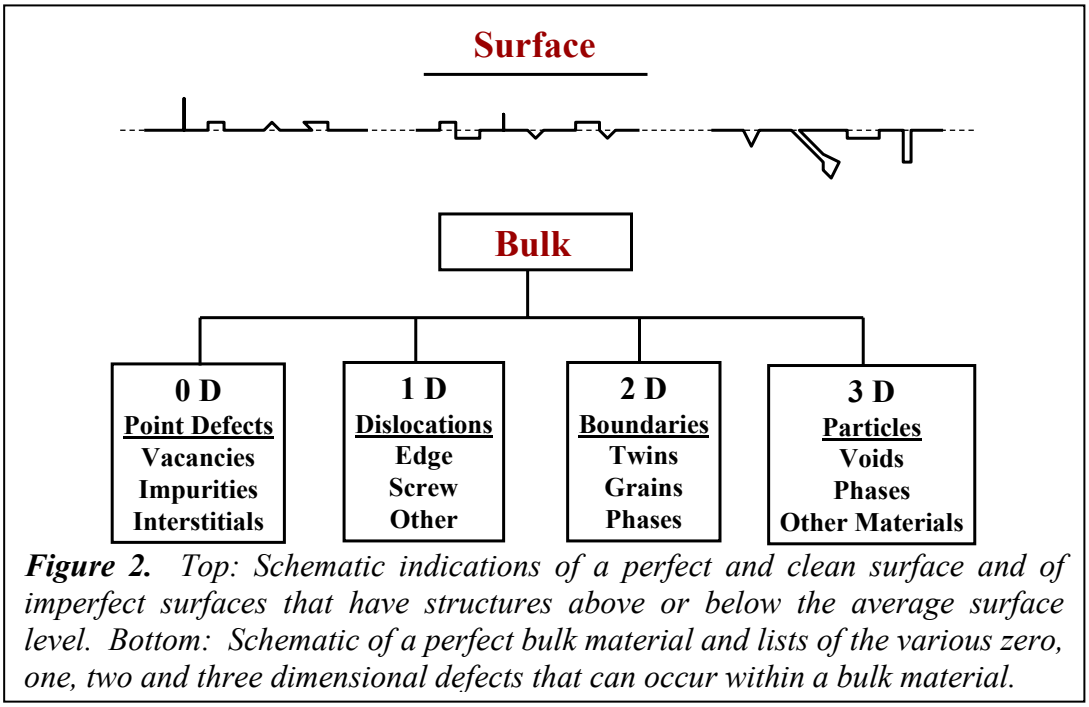

Figure 2. *Top: Schematic indications of a perfect and clean surface and of imperfect surfaces that have structures above or below the average surface level. Bottom: Schematic of a perfect bulk material and lists of the various zero, one, two and three dimensional defects that can occur within a bulk material.*

The definition of a surface or near-surface region can be complex, especially for contoured surfaces. Electronic structure calculations made for layers of atoms parallel to the clean surface of a crystal provide useful guidance on what constitutes a surface. They show that the band structure and density of states for the single surface layer of atoms is markedly different from those of bulk layers. This is due to the absence of bonds on one side of atoms in the surface layer. However, the second layer has an electronic structure that is very much like that of bulk layers. So, the surface and near-surface regions can be reasonably defined as just the top two layers of atoms on a surface. That is, the width of the surface and near-surface region is on the scale of one nanometer.

There is evidence from both electrochemical, and gas loading and permeation LENR experiments, that the reactions occur near the surface of the usually-ordered solid materials involved in the experiments. Many workers have found that excess power scales with the electrical current density through the surface of the cathode. A summary of such data is given in Figure 3. The Letts-Cravens Effect involves shining a laser on a cathode in an electrochemical cell, which increases the rate of power production. The skin depth for the laser-solid interaction is on the order of nanometers. Arata and Zhang used Pd black in their Double Structure Cathodes, which had a high pressure of deuterium gas inside of the hollow cathodes. In such finely-divided Pd, most of the atoms are near the surfaces of the nano-particles. The gas permeation transmutation experiments by Iwamura and his colleagues show the reaction products within about <10nm of the surface, as indicated in Figure 3. **Tritium data from Storms????**

Summary (and disclaimer????)

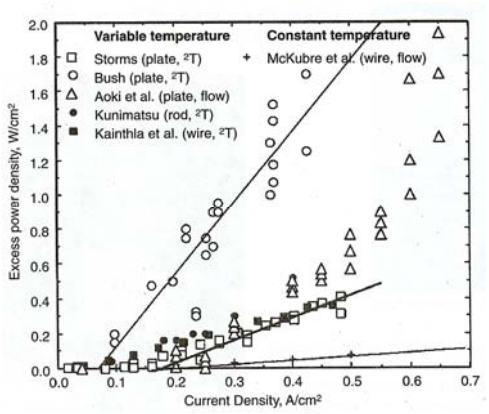

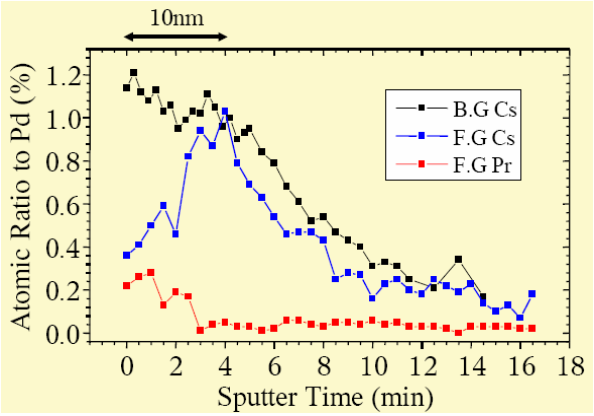

Figure 3. *Some of the experimental evidence that LENR occur on or very near surfaces. Left: A compilation by Storms of the dependence of excess power on the current density into the cathode in electrochemical experiments. Right: A profile into a complex Pd foil that had been permeated with deuterium gas, as measured by Iwamura et al.* ***Need 2 references***

3. Equations for Production of Power, Materials and Radiation

The equations that give the number (N) of reactions, the energy (E), the material (M) and the radiation (R) per unit time (T) are given, respectively, in equations (1) through (4). In all of these equations, A is the total surface area, F is the fraction of that area which is active in

$$N/T = A \times F \times [N/(A \times T)] \quad (1)$$

$$E/T = A \times F \times [N/(A \times T)] \times E = P \quad (2)$$

$$M/T = A \times F \times [N/(A \times T)] \times M \quad (3)$$

$$R/T = A \times F \times [N/(A \times T)] \times Q \quad (4)$$

producing nuclear reactions, and [N/(A x T)] is the reaction rate per unit of total area. *E* is the total emitted energy per reaction, *M* is the amount (mass) of a particular isotope of interest produced in each reaction and *Q* is the number of quanta of some electromagnetic or particulate radiation of interest. The energy of any quanta may be part of the total emitted reaction. The mass of particular quanta links their number and the production rate of materials.

In the rest of this paper, we will focus on the production of energy and power, that is, equation (2). If one wants the reaction, mass production or radiation production rates, then the other equations can be employed in a manner similar to the energy considerations that follow.

Figure 4 gives the energy production rate (power = P) equation again with labels. Values for each of the four terms in this equation are available with varying difficulty from different sources. They will be discussed in the following four sections.

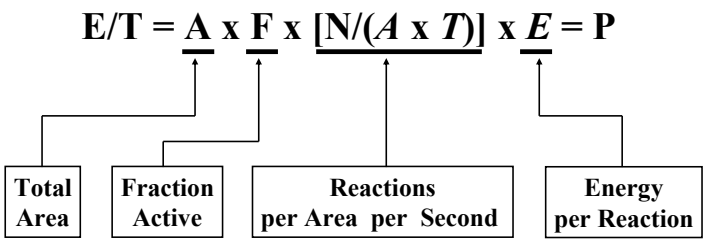

Figure 4. The equation governing energy production by LENR, with labels for the individual terms.

4. Total Surface Area (A)

The area of the surface of the cathode in an electrochemical loading experiment can vary widely on both an absolute basis and in relation to the volume of the cathode material. If the geometrical shape of the cathode is fixed, increasing the volume will increase the surface area. However, it is more effective to alter the geometry of the cathode for a fixed volume of material. This section will examine three varieties of geometries that have been used in LENR experiments, and then discuss the increase in surface area as the shape of a cathode with a fixed amount of material is varied.

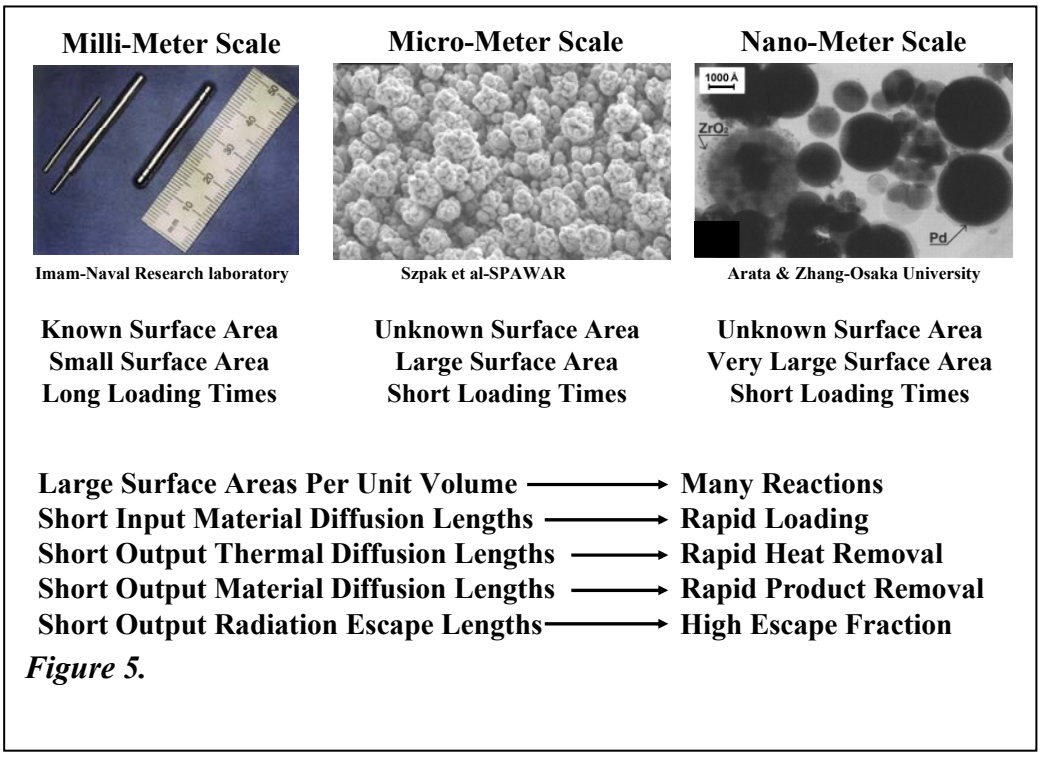

Figure 5.

Figure 5 shows photographs of LENR cathodes on three size scales. The classical electrode is a solid cylinder of Palladium or its alloys with a diameter on the scale of millimeters, such as that made by Imam (XX). Co-deposition of Palladium and deuterons leads to a material with

much higher surface area per cubic centimeter or gram, as found in the work of Szpak et al (XX). The largest surface area per volume is gotten for material with dimensions of nanometers, with the work of Arata and Zhang providing one of the few examples (XX). In going from the regular solid electrode form to progressively finer materials, there are both advantages and disadvantages, as noted in Figure 5. The increase in area, and possibly the number of nuclear reactions, and the decrease in loading times, are the major advantages. Rapid removal of heat, products and high escape rates for radiations can also be advantageous. However, unless particular assessment techniques are used, the actual surface area is not known for the micro- and nano-meter scale materials. This is not to say that the areas of the fine-scale materials cannot be measured. Catalysis scientists have developed an array of methods for measuring the surface areas of materials with very small particle sizes (XX). It seems that such techniques have not yet been used for the study of the dependence of the output of LENR experiments on the total areas of the cathodes.

Turning now to ways to increase the areas for a given volume of materials, there are conceptually two approaches. In the first, the material is cut into progressively smaller pieces, with each cut producing more surface area without the addition of any more volume. This is illustrated in Figure 6. Starting with a cube one centimeter on a side, regularly-spaced cuts

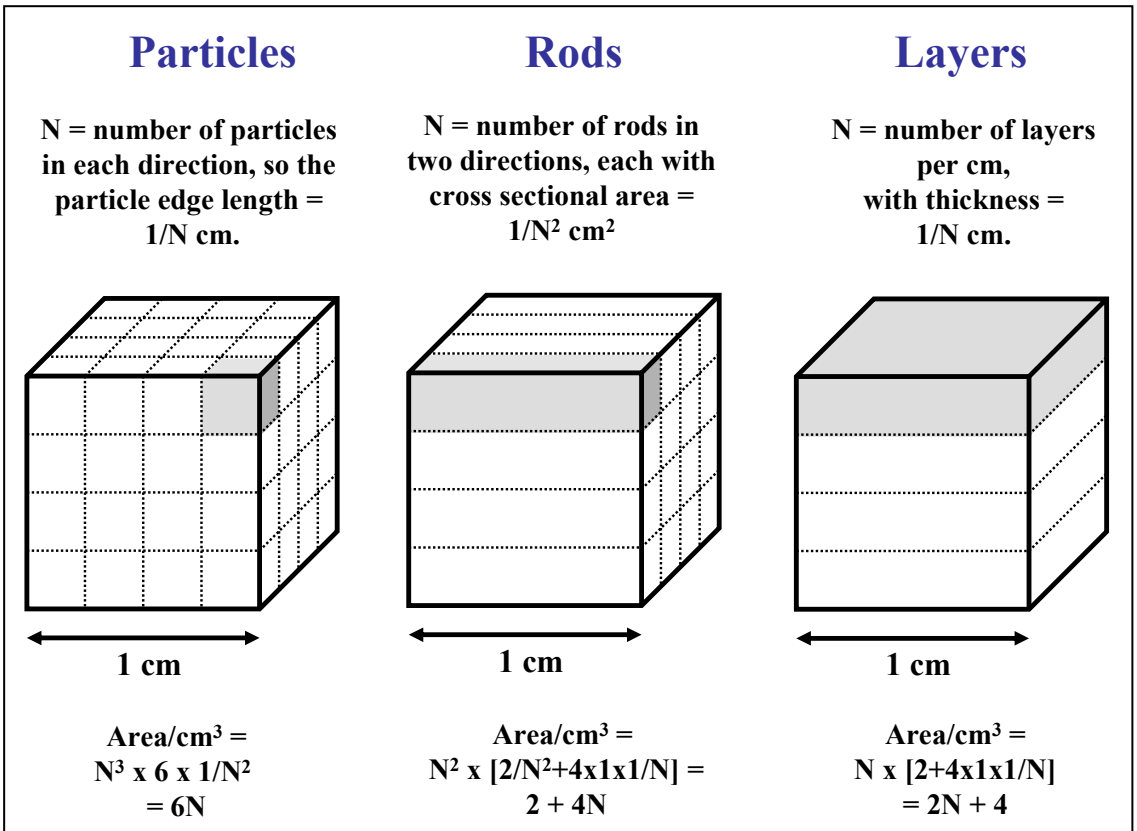

Figure 6. *Switch first and third diagrams*

parallel to one pair of sides will produce layers. Further cuts parallel to another pair of sides yields rods. Finally, cuts orthogonal to the first two sets of slices gives particles. The analytical expressions for the total surface areas of the layers, rods or particles are given in Figure 6 as a function of N, the number of entities in each case. It can be seen from the expressions that, for all three cases, the area per volume scales linearly with N. In the limit of large N, the scaling for layers is 2N, for rods 4N and for particles 6N. That is there is a gain of

a factor of a few (2 or 3) if the number of directions of the cuts is increased from one to two or three. The biggest gain is due to having large values of N, that is, by making numerous cuts. For example, in the case of particles, micrometer-sized particles have a value of N of 10^4, while nanometer-scale particle have an N = 10^7. In short, using particles with sizes of about 10 nanometers, gives a surface to area ratio of about 6 x 10^6 with units of cm^2/cm^3.

The second approach to increasing the surface area of a fixed volume of cathode material is to deform it, for example, by flattening it into a square sheet or pulling it into a wire with a square cross section. Flattening one cubic centimeter into a thin film with a thickness of 1 nm would give a square area with a side that is 300 m long. The area of the film would be about 10^5 square meters. Stretching the cubic centimeter into a wire that has a square cross section of 1 nm would yield a wire, which is 10^{13} km long with an area of 4 x 10^5 square meters. For comparison, gold leaf is 100-125 nanometers in thickness. It is clear that having one or two dimensions on the scale of nanometers results in very large total areas per cubic centimeter of material, whether the starting volume is cut up or deformed. http://hypertextbook.com/facts/1999/JeniferVilfranc.shtml

5. Active Area Fraction (F)

Even if the substrate material in an LENR experiment has a very large area, on either absolute or volumetric bases, only a small fraction of it may be active. The fraction of the overall area that can support LENR is critical to the effectiveness, total power output and cost of a power source based on LENR. This factor is not known now from either experiment or theory. It cannot be higher than 1.0 and is more likely to be low, maybe in the range 0.01 to 0.0001 or even lower. If it can be made high, say 0.1 or greater, then the substrate material will be used more effectively and the device output power relatively high. It is already clear that deposits and coatings of solid surfaces may render some regions inactive. Poisons could work by either simply covering the appropriate lattice sites or by reacting with them. It is also possible that deposits from the electrolyte, gas or plasma near the substrate might make some regions active by producing required conditions. A given small region of the substrate might alternatively be active and inactive, possibly due to the production and escape of nuclear reaction products from the region.

It is very important to devise experiments that can yield values for the fraction of the total surface that is active, both to make calculations of expected powers and for studies to control (increase!) the active fraction. Few of the large array of tools available for surface measurements in vacuo are operable in an electrochemical or even a gas cell. Even fewer instrumental analytical methods work under plasma conditions. In gas and plasma experiments, alternative operation and purging of the atmosphere will permit the use of many of the techniques from vacuum surface science.

Relatively simple imaging, with modern capture and analysis software tools, apply to liquid, gas and plasma loading experiments. Rather ordinary imaging in the visible range, with spatial resolution slightly below one micrometer and temporal resolution down to about one millisecond, is straightforward. Stroboscopic imaging with pulsed laser or other sources will yield images with temporal resolution down to nanoseconds and below. High spatial- and temporal-resolution infrared images of thin films on active cathodes might also yield useful information on the active fraction. Emission and fluorescent spectroscopy in both the visible

and the infrared regions, with both small spot sizes and short data acquisition times, should be done also. Other experimental probes that can operate under various ambient environments are also attractive. Focused x-ray synchrotron emission for both diffraction and, possibly, fluorescence, is an example. It is not guaranteed that any of these techniques offers sufficiently good spatial, temporal or spectral resolution to reveal the LENR activity on surfaces in operating devices. However, they should still be employed in an effort to determine the fraction of the surfaces that are usefully active.

6. Areal Reaction Rates (N/[A x T])

The number of reactions per second (Hz) per unit area is a parameter no less important than the total and fractionally active areas. This cannot even be guesstimated reasonably. Experimental values are hard to obtain because of all the other parameters that link this factor to the measured total power generation rate. Theoretical estimates are needed, but few are available. The theory due to Widom and Larsen involves concepts that are limited to the near surface region of materials. Their fourth paper gives estimates and an expression for areal reaction rates. The estimate of the areal reaction rates early in that paper is 10^{12} to 10^{14} reactions/second/cm^2, that is, about 10^{13} Hz/cm^2.

7. Energies per Reaction (E)

The energy released per nuclear reactions is known much better than the reaction rate per area. This fact is due to decades of experiments using accelerated ions. Energies released in exothermic nuclear reactions, or absorbed in endothermic nuclear reactions, are the energy equivalents of the mass differences between the initial and subsequent nuclei. The mass difference between the initial and final isotope after a reaction is called the Q value. It is commonly quoted in units of MeV/c^2. It was realized over 70 years ago that measured reactions energies would enable more precise determination of atomic weights.

Sources of data on isotopic masses and nuclear reaction rates.

In very general terms, most of the energies given off in nuclear reactions are in the MeV range. For example, for deuterium-deuterium fusion, the two main branches give 2.45 MeV (for the neutron and ^{3}He path) and 3.0 MeV (for the proton and triton branch). These occur with 50% probabilities. The third branch, production of a ^{4}He atom, has a very low fractional probability (10^{-7}) but yields 24 MeV per reaction. In several LENR experiments, both heat and ^{4}He were measured, and they were correlated. In general, the energy released per nuclear reaction (evidenced by the appearance of ^{4}He) is near 24 MeV. This correlation was first found by Miles (XX) and reviewed by Bressani (XX). McKubre and his colleagues found values for the MeV to ^{4}He ratio that were near 31+/-13 and 32 +/-13 MeV per helium atom in a gas loading experiment (XX). These relative high values might be due to the inability to capture and measure all of the He atoms produced in the experiments.

For the purposes of this study, it is convenient to consider reaction energies in LENR experiments to be in the range of 2 to 20 MeV. When all the parameters discussed in the last four sections are known with more precision, and the precise reaction paths are known, then

tabulated values for the specific reactions can be used in estimating the power output of a particular experiment.

8. Graphical Relations

The parameters discussed in the last four sections can be used sequentially to estimate the power available from a LENR experiment. The active fraction links the total surface area to the total active surface area. Then, the number of reactions per second per active area can be used to obtain the total number of nuclear reactions. Finally, the energy per reaction gives the energy per time, that is, the power. It is possible and convenient to use three related graphs to display the relevant parameters and the resultant power. The key observation is the fact that the two pairs of graphs (the first and second and the second and third) have one axis in common. This is illustrated in Figure 7. Importantly, log-log scales are employed in order to span the wide range of parametric variations and because it is easy to plot values for the key parameters.

In Figure 7, the first graph involves the total and active areas, with the active fraction being the key parameter. The second graph relates the active area to the number of reactions per second, with the areal reaction rate as the important parameter. Finally, the third graph links the reaction rate to the power, with the energy per reaction being the pivotal parameter. The utility of the linked graphs is due to the possibility of varying any of the parameters, and seeing simply and clearly the effect such variations will have on the excess power in a LENR experiment.

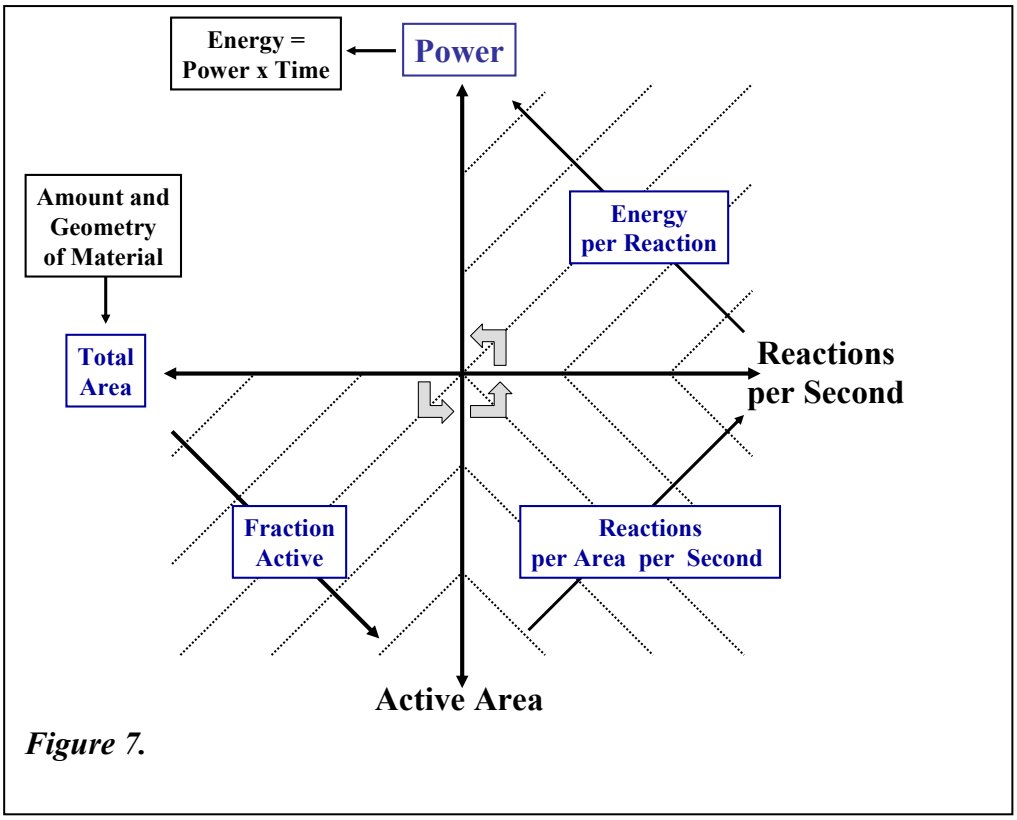

Figure 7.

We note that there are seven parameters in Figure 7, namely the values of the quantities on each of the four axes and of the three parameters, one on each graph. But, it is important to realize that four of the seven parameters suffice to fully determine the output power. This is because there are only four vertical or horizontal lines needed to fully define any case. The situation is illustrated in Figure 8. Note that any of the lines can be moved, which affects the values that depend on the two factors intersecting any of the lines, and thence, the power output. As one example, if the active fraction F is constant, increasing the total area will first increase the active area and, then both the reactions per second and the output power.

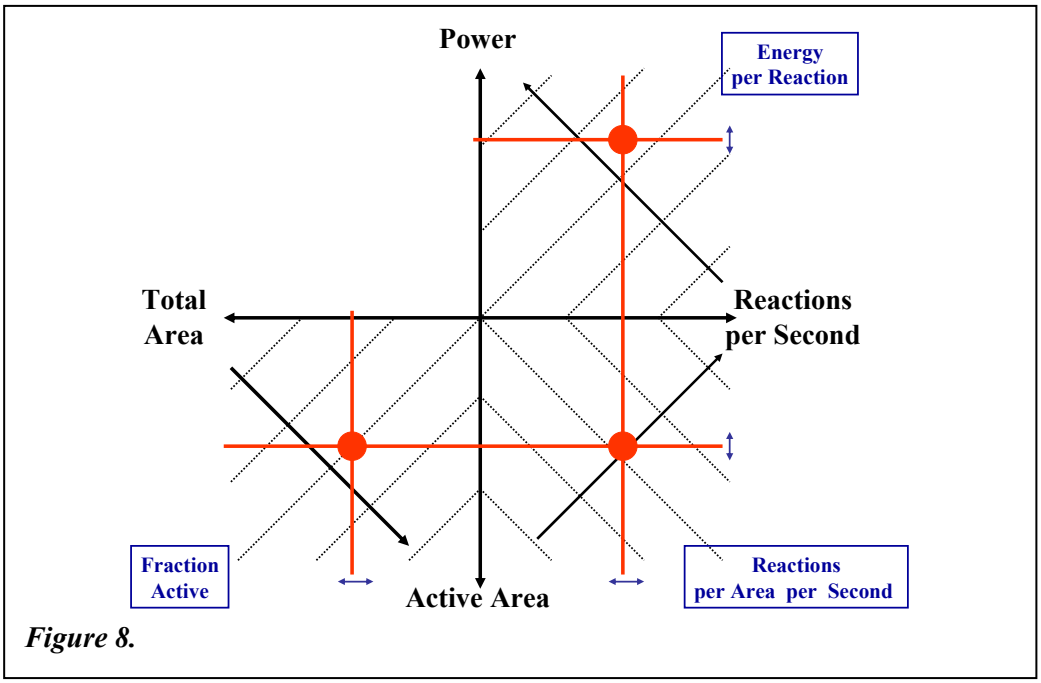

Figure 8.

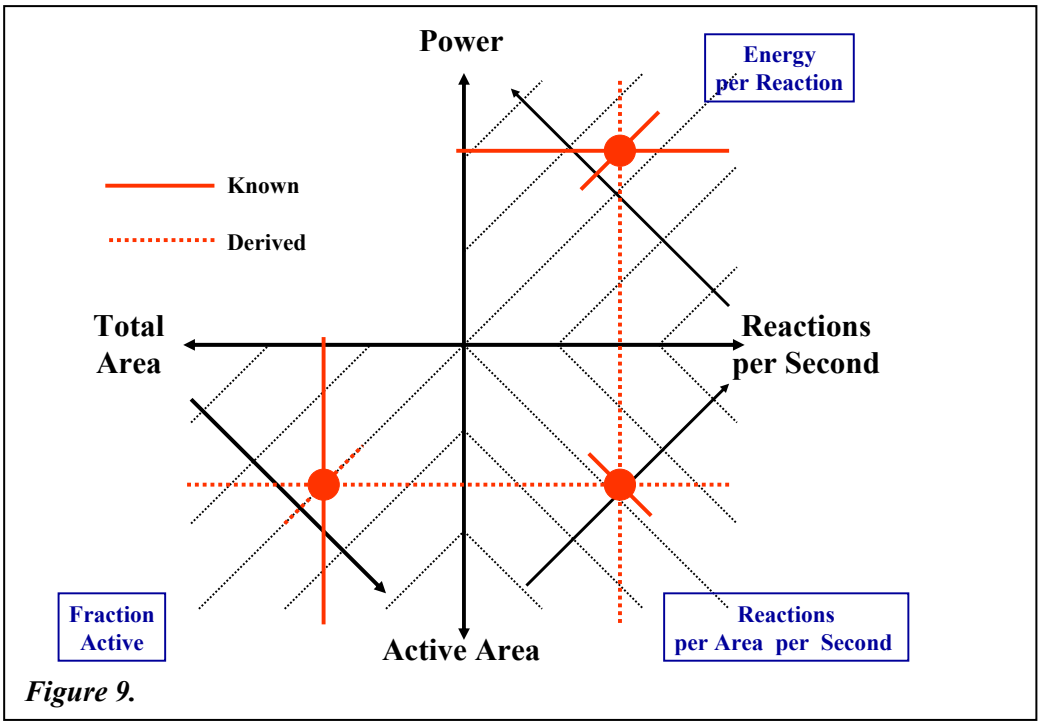

Figure 9.

There is another use of the linked graphs that makes it possible to estimate values of otherwise poorly known or unknown parameters in LENR experiments. The point is, since four parameters completely determine a particular situation, but there are seven total parameters, three can be derived in some cases. This is illustrated in Figure 9 for one set of circumstances. In the case shown, the power from an experiment and the reaction energy are known. This determines the position of two of the four lines and gives the reaction rate. If the areal reaction rate is known, the position of another line and another parameter is determined. That is, the active area is then known. Then, use of the total area sets the last line and the active fraction is then determined.

This exploitation of the linked graphs can be made quantitative using Figure 10. If an experiment gives an excess power of 10 W and the reaction rate is taken to be 24 MeV, then the reaction rate is close to 10^{12} Hz. Using an areal reaction rate from the theoretical estimate of Widom and Larsen, namely 10^{13} Hz per centimeter squared, indicates that the total active area is a few times 0.1 cm^2. It the total surface area is known to be 10 cm^2, then we have a value for the active fraction on the order of 10^{-2}, that is, a few percent. This is the initial estimate of a parameter that is key to power and energy production with LENR, but has yet to be either measured or calculated from theory. If the total area in the experiment were ten times less, than the active fraction would have to be ten times higher.

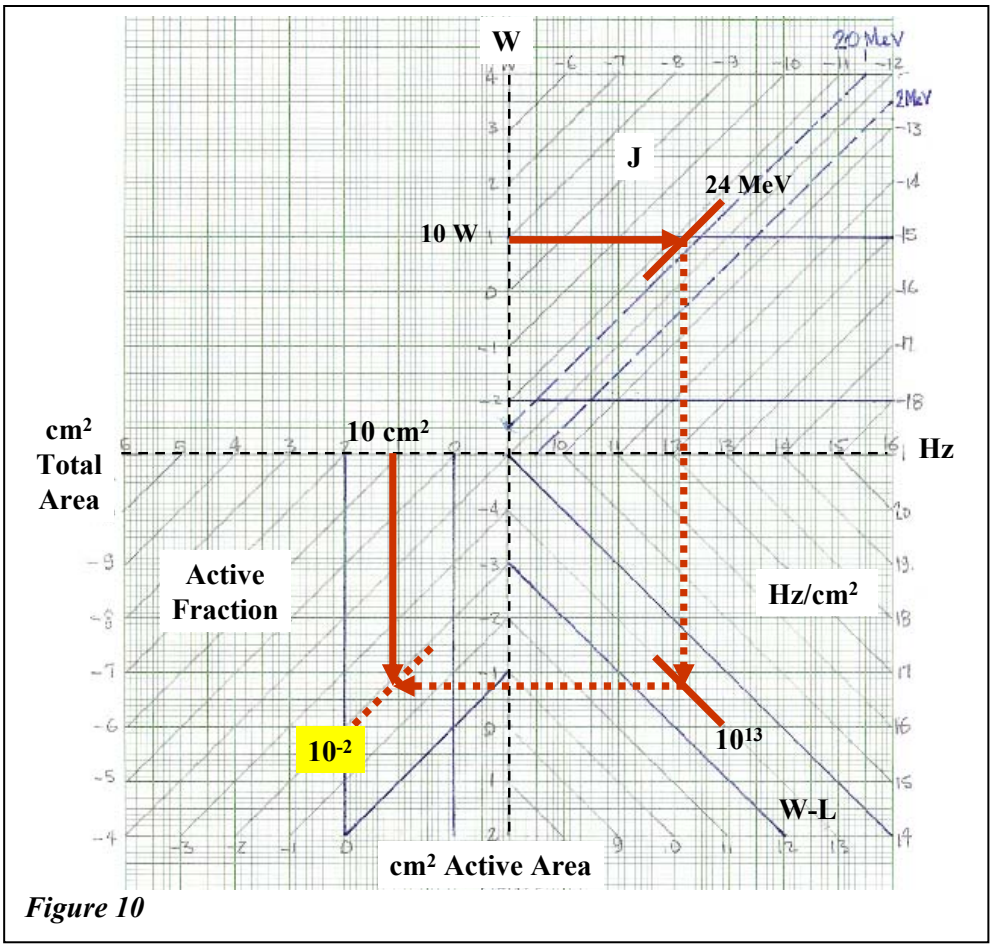

Figure 10

Two things should be noted about the set of liked graphs. First, the active fraction is 1.0 or less. That is, there is a part of the total and active area graph that is excluded. The second related to the common observation during a LENR experiment, namely the variation

of the excess power with time. It the horizontal line cutting the excess power axis moves up and down, and the reaction energy is fixed, then the reaction rate and the vertical line intersecting that axis must vary. If the total area is fixed, then either (or both) of the active fraction and the areal reaction rate must vary. This clearly points to the determination and control of these two parameters as being among the major challenges of the field, both for scientific understanding and engineering utility.

Finally, we note that the set of linked graphs can be overlaid to indicate the range of variations for each of the seven parameters. Observed powers in LENR experiments have usually fallen in the 10 mW to 10 W range. The lower value is set by calorimetric limit of detection in many cases. The upper limit has been exceeded in only a few cases. We already noted that reaction energies of 2 to 20 MeV are reasonable, and can be refined as more in known. There are no independent values for total reaction rates, but use of the two variations just cited gives reaction rates that can fall in the range of a few times 10^9 to a few times 10^{13} Hz. Areal reaction rates are not available from experiment, but have been estimated theoretically to be in the range 10^{12} to 10^{14} reactions/second/cm^2, as already noted. Total surface areas are known for simple electrode geometries, such as the rod shown in Figure 5. However, total areas for finer, more complex micro- and nano-scale materials are unknown. Their determination seems to be an experimental priority.

Certainly, the set of three graphs is not necessary to make estimates of the power or other four factors that appear in equation (2) and Figure 4. It the factors are known, computation of the power is trivial. For example, a total area of 100 cm^2, an active fraction of 10%, an areal reaction rate of 10^{13} Hz/cm^2 and a reaction energy of 24 MeV would yield a power output of XXXX, where the conversion factor of XXXX was used. In a similar fashion, it is possible to calculate the total area needed for a specific desired power output. MORE.

9. Maximization of Outputs

In almost all energy sources, the maximization of the output power is a serious consideration, because the highest available powers limit applications. This is expected to also be the case for energy sources based on LENR. Figure 11 indicates four parameters that can be increased to improve the power output of a LENR reactor.

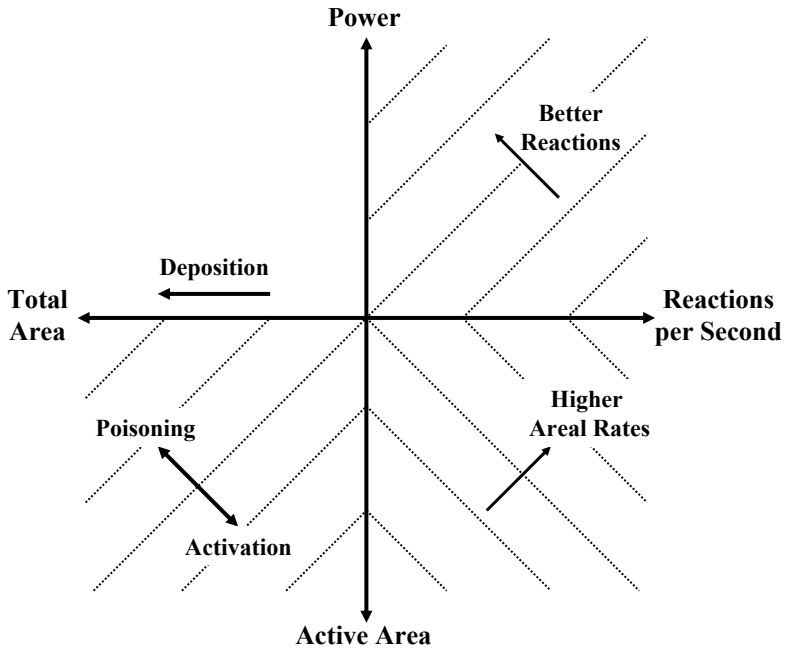

Figure 11. *Four parameters can be changed in order to maximize the power output from LENR. The first is to increase the surface available for LENR by addition or deposition of more solid substrate. The second is to improve the active fraction either by reducing poisoning or by activating new areas. The third is to increase the LENR areal reaction rate. Finally, the use of nuclear reactions that yield more energy per reaction may be possible.*

There are limits to the values for each of the four factors and, hence, to the maximum power that can be expected from a LENR reactor. The limits for each of these parameters will be discussed in turn.

Surface Area. This factor is the one that can be varied widely to scale up the power available from LENR. Catalysts can have areas exceeding 1000 meters squared per gram of material. If a kilogram of catalyst is used, one million square meters of surface area are available for LENR. Support of such a large amount of catalyst, and the transport of material to it, and heat and products away from it, will be major mechanical and thermal engineering challenges.

Active Fraction. This cannot exceed unity. It might not prove possible to achieve a high active fraction over all of the available area. The magnitude and willful control of the active fraction is one of the major scientific and engineering challenges in the field of LENR.

Areal Reaction Rate. Need number of lattice areas per unit surface area in Pd here. If there are on the order of 10^{15} reaction sites per square centimeter of surface area, and one reaction per second can occur at each, then 10^{15} reaction per second per square centimeter are possible. Again, this is a very high estimate, but it serves to permit an estimate of maximum power production rates.

Energy per Reaction. The output energies for nuclear reactions are on the order of 10 MeV, typically in or near the 2 to 20 Mev range, as noted above.

Taking the most optimistic values for each of the four factors yields energy production rate of 3 x 10^{13} watts. Check this. This is an unrealistically (unbelievably!) high number. Scaling the surface area back by 1000, making the active fraction 1% and reducing the areal reaction rate by 100 still gives a power of 3 megawatts. Realization of such a power seems unlikely in the foreseeable future. Besides the material transport challenges, the melting points of reactor materials will provide limits. However, the point of these estimates is that, in principle, very large powers are possible from LENR reactors. Further, the new field of LENR reactor design will be quite complex, as is the current design of fusion reactors.

10. Relations to Past Work

This is certainly not the first paper to discuss relations that give the output power from LENR in terms of various factors. McKubre's equation for excess power… Swartz OOP.

11. Reactions in the Bulk

It must be noted that the possibility of some LENR occurring within the bulk of solids is not entirely ruled out now. If this is clearly shown to happen, then a volumetric analysis similar to that above for surface reactions can be developed. In the volumetric case, the total volume of the solid in an LENR experiment and the fraction of that volume that is active would be relevant. The number of reactions per second per cubic centimeter would then apply. That is, the lower two graphic in Figures XXX and VVV would be replaced by their volumetric equivalents.

Paragraph on integration over depth and the limit as depth approaches zero. PLH 5-10 um

Because of the great complexity of the compositions and structures within materials, as indicated schematically in Figure NN, the analysis for bulk LENR would be more complicated than that for surface reactions. If LENR were occurring at both surface and bulk locations, a combination of the two analyses would be appropriate. Of course, the number of needed parameters would be roughly twice as great as for the surface case discussed in this paper.

From a practical viewpoint, there are two generally undesirable aspects of having LENR occur within materials. The first is the need to get reactants to and remove products from the reaction regions. In the surface case, this can be done partly or entirely by convection within a liquid or gas, or by particle transport within a plasma. In the bulk case, diffusion would inevitably be the rate limiting process. The second concern is the inability to quickly change conditions within a material for control purposes. For some applications, rapid control is not necessary. However, the range of applications of bulk LENR would seem to be less than that for surface LENR.

12. Control of LENR Power Sources

The graphical relationships presented and discussed in the last two sections have implications beyond those already discussed. It has already been emphasized that applications of LENR will require reproducible production of power or other desired factors (DJN Marseille Paper). Without causal relations between what goes into a LENR device and what comes out of the device, it is essentially impossible to use such reactions, except for research. Even if reproducibility of behavior is assured, the reactions must also be controllable. That is, applications demand the ability to turn on, turn up, turn down and turn off a source of power, materials or radiations. Finally, optimization of the performance has to be considered. Even if a power source is reliably reproducible and controllable, its economic value will depend on minimizing input costs for equipment and materials and maximizing the desired outputs.

The factors relevant to the presented graphs, which were discussed in sections 4 through 7, must have specific behaviors for a LENR experiment to be reproducible. Either all the factors must remain constant or there must be compensations in one or more factors as another of them changes, which is probably unlikely. It a single factor changes, even if the same equipment, materials and procedures are used, and there are not changes in any of the other factors, the output power will vary.

Triggering of LENR is the first step in their overall controllability. McKubre and XXXX have discussed changes in an experiment that can initiate production of excess power and heat. Also, Letts and Claytor are two examples. In the framework of this paper, triggering would result in one or more the factors in the graphs being increased to the point that the excess power exceeds the measurement threshold in a particular calorimetric experiment. The area and the energy per reaction are fixed in most experiments, so the active areal fraction and the areal reaction rates are candidates for increases to turn on energy, materials or radiation production. Since we do not know now what in an experiment controls either of the active fraction or the areal reaction rate, it is not currently possible to specify ways in which to control these factors.

We clearly know how to control the production of power by an internal combustion engine by varying the input rates of fuel and air. Control of nuclear fission reactors is also well established using neutron absorbing rods. There are no analogous fast control parameters for LENR now. However, we can anticipate their development and, also the appearance of longer-term effects somewhat similar to those in current engines and reactors. In hydrocarbon-burning motors, there can be gradual accumulations of deleterious materials, which have to be either prevented or cleaned away. In reactors, the fuel rods become depleted of fissionable materials over time and must be replaced. In seems likely that, even when LENR can be fully controlled on short time scales, there will still be some longer-term effects that must be considered. The delivery of reactants to the right sites and, especially, the removal of products, are inevitable challenges. It might be necessary to cycle the chemistry within an LENR reactor to remove products and refresh the surfaces on which reactions occur. This would be analogous to the manner in which ion-exchange water softeners were recharged periodically.

13. LENR Might be Part of Nano-Science and Nano-Technology

It is widely known that funding agencies in the America, Europe and Asia greatly increased support for nano-science and nano-technology in the past decade. Remarkable materials, whose properties are new and dependent on nano-meter scale effects, are under development or already commercialized. It is interesting that the independent development of a robust experimental case for the existence of LENR was contemporaneous with the explosive growth in nano-science and technology. This was accidental and not causal.

There are at least two reasons for LENR to be viewed as a part of nano-science and -technology. The first is simply the size scale of the materials that are and can be involved in the production of energy, materials or radiation by LENR. If LENR occur on or near the surfaces of materials, the maximum of surface area for a given amount (volume or weight) of the substrate material will be economically compelling. Section 4 presented the case for using nano-meter sized materials. As already noted, nano-meter scale particles have been used in very successful LENR experiments (Arata and Zhang).

The second reason why LENR can be viewed as a part of nano-science and -technology is less certain now. It is possible that the active areas on the surface of a LENR substrate have lateral dimensions below a micrometer. Storms called such areas NAE for Nuclear Active Environments (Storms Paper). The difficulty in understanding the essential parameters that determine the outcome of LENR experiments might be due to appropriate conditions existing in only very small regions for very short times. Such regions might turn on and off during an experiment, and might vary widely in size and duration. There is little direct experimental evidence for sub-micrometer active regions being important. Diagnostic equipment with the needed spatial and temporal resolution has not been brought to bear in LENR experiments. It is possible to immerse high power microscope objectives near cathodes in LENR experiments in order to obtain images with sub-micrometer spatial and sub-millisecond time resolution. The use of an Atomic Force Microscope (AFM) to examine the surfaces of cathodes within electrolytes during active LENR experiments would not be as simple, but should also be feasible. In short, the vast array of surface diagnostics, now of use in catalysis and other areas of science and technology, has not been employed in LENR experiments, primarily due to lack of financial support.

It is well known that the structures, including lattice constants of nanometer-scale materials are different than those of the bulk of the same materials. It is entirely unclear now whether such changes will improve or degrade the production of LENR. Similarly, it is well understood that the local order in amorphous materials is quite similar to the local order within ordered samples of the same materials. But, here again, it is not known now, either experimentally or theoretically, if the long range structure of a materials is relevant to the production of LENR.

Add two micrographs on Ni particles and forests of nanowires to this section.

14. Conclusion

Scientific and engineering parameters. Give examples, maybe from quantum, statistical and thermodynamic physics. Relate these to the graphic showing the new level.

Need ending

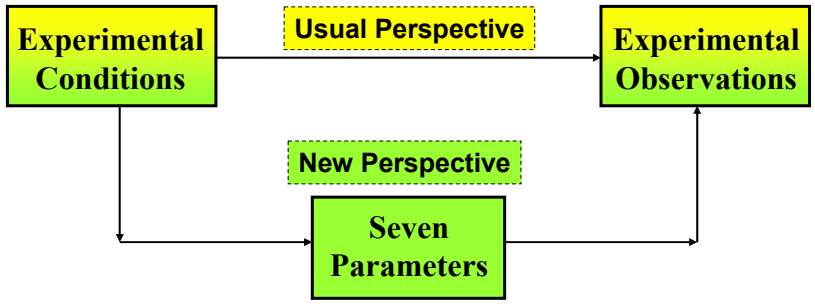

Figure NN. Frequently, scientists attempt to link directly the outputs of experiments to the input conditions. This approach has had some limited success for LENR to date, as discussed in the text. The new viewpoint of this paper is to define what are essentially engineering parameters, and to attempt to link them first to the experimental conditions and then to the experimental results. The linkage to conditions is challenging and still largely unknown. The linkages to the output energy, materials or radiation are quite simple, as discussed above.

Acknowledgements. Ashraf Imam provided part of Figure XX. …..provided references.

THE CONCEPTION OF NUCLEAR FORCES IN FIELD PHYSICS

O.N. Repchenko

PFU of Russia, Moscow

The field physics is a new scientific trend, which develops the idea of dynamical nature of mass. Thus in field physics the masses of all particles and objects, including the elementary particle masses of rest do not represent their internal properties (the quantity of matter), but are caused by external interactions (fields).

The conception of dynamical mass leads to traditional results in classic conditions, however at small distances it considerably changes the mechanical properties of the system. For instance, according to field physics, at the distances of the order of 10^{-15} m. the strong attraction of two identically charged particles (protons) converts into the adequately strong repulsion, and this behavior becomes possible because of the gravitational fields. This fact permits the construction of the new model of the nuclear interactions, and leads to better understanding of new approaches to the description of nuclear fusion and element transmutation.

The main ideas of this conception can be found in the book "**The field physics or how the World is arranged**" or at www.fieldphysics.ru

NUCLEAR TRANSMUTATIONS AT METEOROLOGY

B.U. Rodionov[1], O.G. Kudryavtzev[2], V.V. Botvinovsky[3]

1- Moscow Engg&Phys Inst (State University), 2- OLR «Alliance Holding», 3- SO «Department of Theoretical Problems»

The results of measurement of vertical current of non-ion nature on the coast and ice of Novosibirsk reservoir in January 2007 have shown that this unusual current is directed upwards over the water and downwards over the land (direction of the current is defined by the positive charge motion). We suppose the non-ion current (far from coast over the water it's about 10 mA/m^2 and at coastal line is close to zero) flows by dark matter. The dark matter consists of hypothetical long strings ("fluxes") with diameter about 60 femtometers on which being is cold nuclear transmutation in the water. It explains known effect of change of direction of horizontal component of the geomagnetic field along the coastal line and is possible reason of coastal squalls when the storm clouds are absence. Measurements of the non-ion current inside and near the large magnetic screens confirm a possible electromagnetic nature of squalls, tornados and hurricanes. These phenomena are believed to be produced by the non-ion currents induced by nuclear transmutations in the thread-like dark matter.

Fluxes Reality

We can see, that all substance like global cotton wool. Thus all forms of a matter are structured by invisible strings, on which atoms, molecule, micro- and macroparticles, stars and galaxies «thread» as beads in a necklace. Many facts about flux "Fibrous World" can be found at [2,3]. For example all matter, which we know, has string like form already externally or has string internal structure. All biological tissues are alike - internal structure of cell penetrated by thready channels. There are many forms of string or cotton wool like inorganic crystals (most known is asbestos). Three-dimensional lattice of crystalline solids atoms (molecules) located on almost ideal direct lines. The hurricanes are similar to huge spirals of fibrous chains of clouds. The spiral galaxies like terrestrial hurricanes. To examples also known for us we add new below.

A Reason of Tides Bisymmetry

At simple celestial and terrestrial mechanics in system Moon-Earth we must to have on Earth one bulge of atmosphere and oceans and one high tide and one low tide per day (fig.1). In reality we have two symmetric bulges, two high tides and two low tides per day.
Fig.1 and 2 explain this fact.

The change of water momentum dp_1 by one flux on shift vdt is given by

$$dp_1 \approx (Dd_f) \cdot n \cdot (mv) \cdot (vdt) = Dd_f n\, mv^2 dt,$$

in which n is a number density of water's molecules per cubic cm and m is mass of molecule of water. Frictional force of η fluxes per square cm creates in water the hydraulic pressure

$$p = \eta\, F_f \approx \eta\, Dd_f n\, mv^2 = (nm) \cdot gh,$$

in which g is free-fall acceleration near Earth's surface. Next we find

$$\eta \approx gh / Dd_f v^2 \approx 10^2 \text{ cm}^{-2}$$

Ocean currents and trade winds

Frictional forces of Moon- and Sun-Earth systems of flux can to move on Earth both – ocean water and atmospheric air. This simple mechanism explains the parallelism of trade winds and ocean currents under these winds near equator.

Fluxballs

The local fluxball formation and its motion explain (see fig.3 and fig.4):

- known effect of change of direction of horizontal component of the geomagnetic field B along the coast line - coastal field declination
- coastal squall when the storm clouds are absence.

Electron capture at strong magnetic field of flux produce flux current and set fluxball in moving (fig.3 and 4). So we have nuclear mechanism of meteorological energy for strong winds as jet stream, storms, hurricanes, tornadoes.

Thunderstorms and all types of lightning

Nuclear energy of mini fluxball and its movement explain many strange properties of Ball Lightning [1]. Thunderstorms formation and other lightning types may be explained by nuclear and electrical processes on fluxes.

Geomagnetism

Modern theoretical models of geomagnetism – magnetic dynamo at the Earth's center - is vary complexity and they did not explain the facts of sharp change magnetic field on small distances on Earth surface and on altitude. We suggest explaining the geomagnetism by electric currents along gigantic flux rings (cables) at ionosphere, atmosphere, on surface and in depth of Earth. Now we are measuring these currents by fammeter [2].

Aurora and magnetic storms

Flux model of geomagnetism will to explain, may be, the thin and strange peculiarities of Aurora (polar lights) types and influence of magnetic storms on man health and function of technical device.

Conclusion

1. Flux meteorological theory is *ordinary* academic physics with unusual conclusions.
2. The flux model of environment (active dark matter) can explain the many natural facts, which have now primitive or nonscientific explanations.
3. The flux model of environment and flux model of cold nuclear activity can explain the time-place instability meteorological phenomena.
4. We hope, that further elaboration of the electric currents measurements on the flux in near Cosmos and on Earth will make clear reasons of all meteorological factors and its function.

Nearest Objects of Flux Theory

- Tides and ocean currents (see here fig. 1 and fig. 2)
- Winds (trade winds, jet stream, cyclones and anticyclones, storms, hurricanes, tornadoes - see here figures 1 –3, our references here and below define problems more precisely only)
- Thunderstorms and all types of lightning [1]
- Geomagnetism [2]
- Aurora (polar lights). Magnetic storms [1-3]
- Nuclear composition of Earth‘s crust [2]
- Oil reproduction by cold nuclear synthesis [2,3]
- Thready (linear) structures in mineralogy, geology and in planetology (Jupiter’s Europe)[2,3]
- Earth history and dynamics. Earthquakes [2]
- Cold nuclear transmutations by all types electric discharges and cavitation [1-3]
- Astrological nuclear effects and control of radioactivity. Non-chance of catastrophes [1-3].
- Unusual methods of energy generation [1-3]
- Strange movement. Rotation and levitation [3]
- Unusual transform of matter [2]. Tracers [3]
- Thready (linear) structures and nuclear transmutation in biology [3]
- Life [3]

References

1. B.Rodionov “Flux Models of Ball Lightning” Proc. of Int. Symposium on Ball Lighting and Unconventional Plasmas, August 2006, Eindhoven University of Technology, Eindhoven, the Netherlands, and also “The Fire by Ball Lightning” in Problems of Cold Nuclear Transmutation of Chemical Elements and Ball Lightning, Proceedings of the10-th Russian Conference, Dagomys-Sochi,2002. Moscow, 2003, pp265-277 (Russian).
2. B.U.Rodionov, M.S.Godin, I.B. Savvatimova “Inspection Method to Check Quality of Nuclear Transmutation Media” see at this edition and B.U.Rodionov, M.V.Nemtzov and A.I.Zaitzev ‘Registration of Electrical Current in Physical Vacuum”. Proc. Asia-Pacific

Conf. On Environmental Electromagnetics – GEEM'2006, vol.2 of 2, Aug.1-4,2006 Dalian, China, pp.648-651; see also Proceedings Second International Symposium on Unconventional Plasmas, ISUP-06, 14-16 August 2006, Eindhoven, The Netherlands. Editors D.K. Callebaut, G. C. Dijkhuis & H. Kikuchi

3. B.Rodionov, I.Savvatimova "Unusual Structures on the Material Surfaces Irradiated by Low-Energy Ions" in Condensed matter nuclear science, Proc. of the 12-th Int. Conf. On Cold Fusion. Ed. Akito Takahashi, Ken-Ichiro ota Yosuhiro Iwamura, World Sc.Publ. Co.Pte Ltd. New Jersey-London-Singapore-Bejing-Shanghai-Hong Kong – Taipei-Chennai, 2006, pp 421-429S.

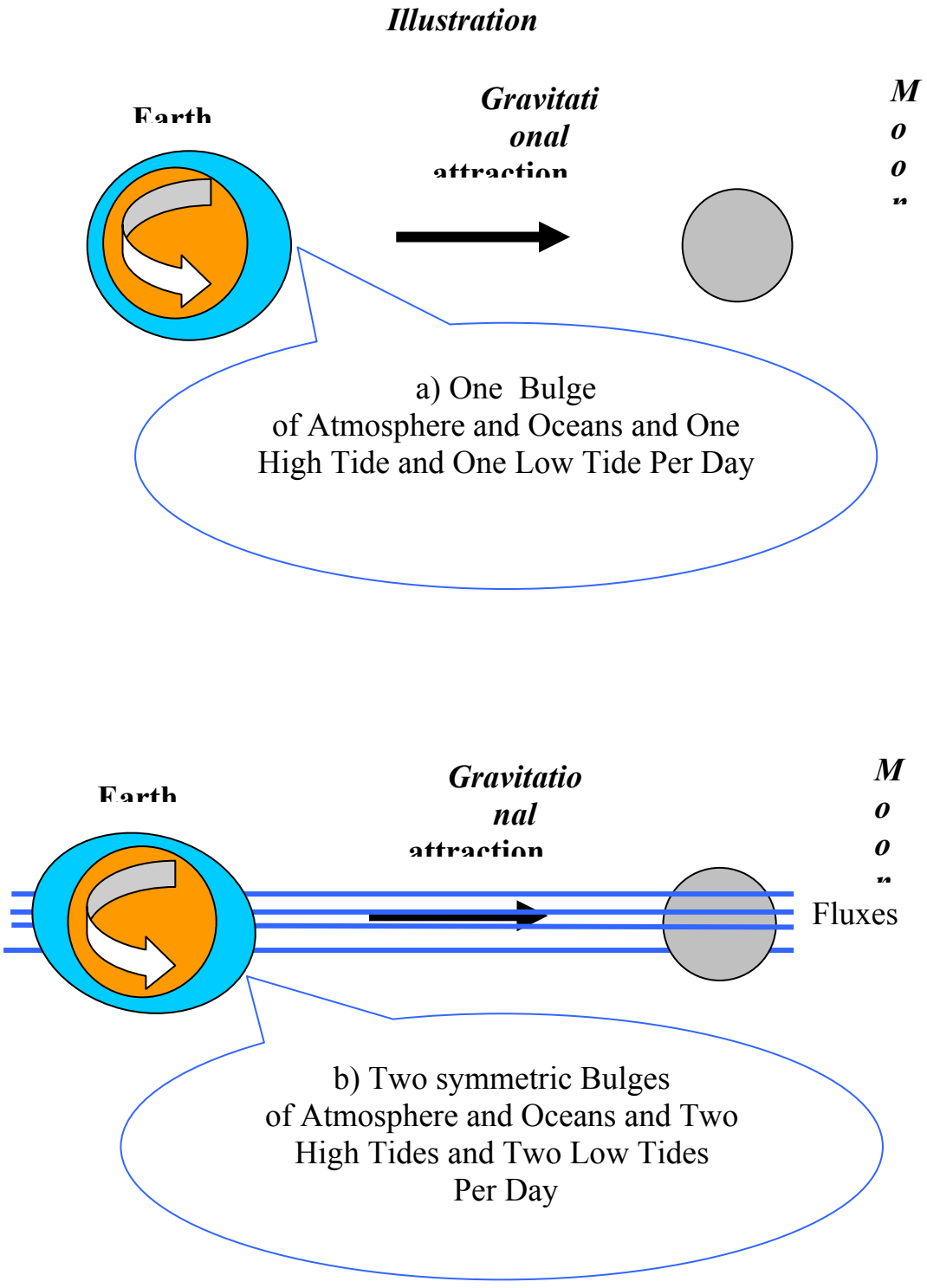

Fig.1. Fluxes as a Reason of Tides Bisymmetry

a. What we must to have at simple celestial and terrestrial mechanics - above

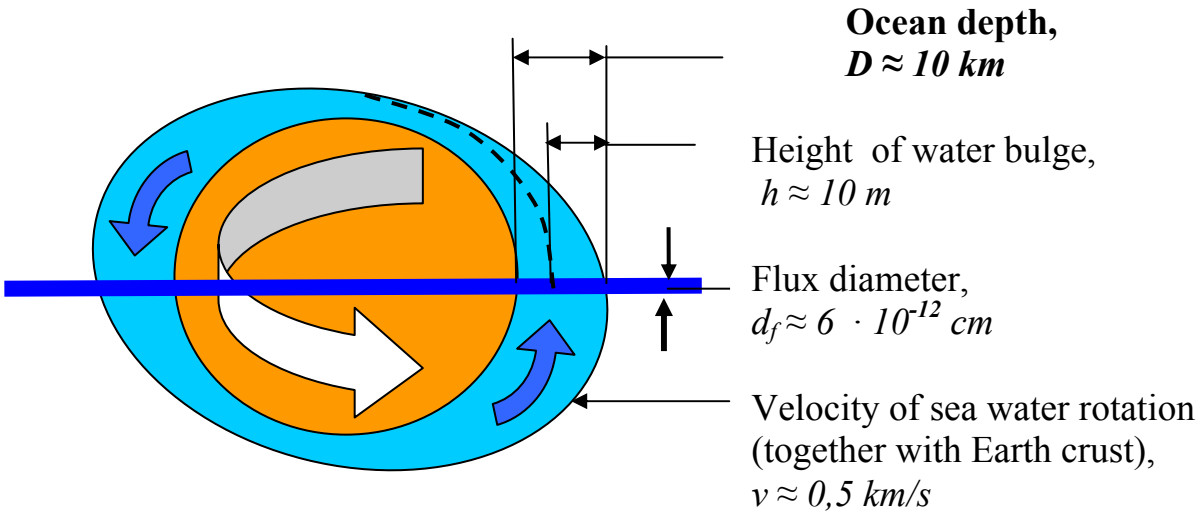

Fig.2. To Moon's Flux Density on the Earth Surface

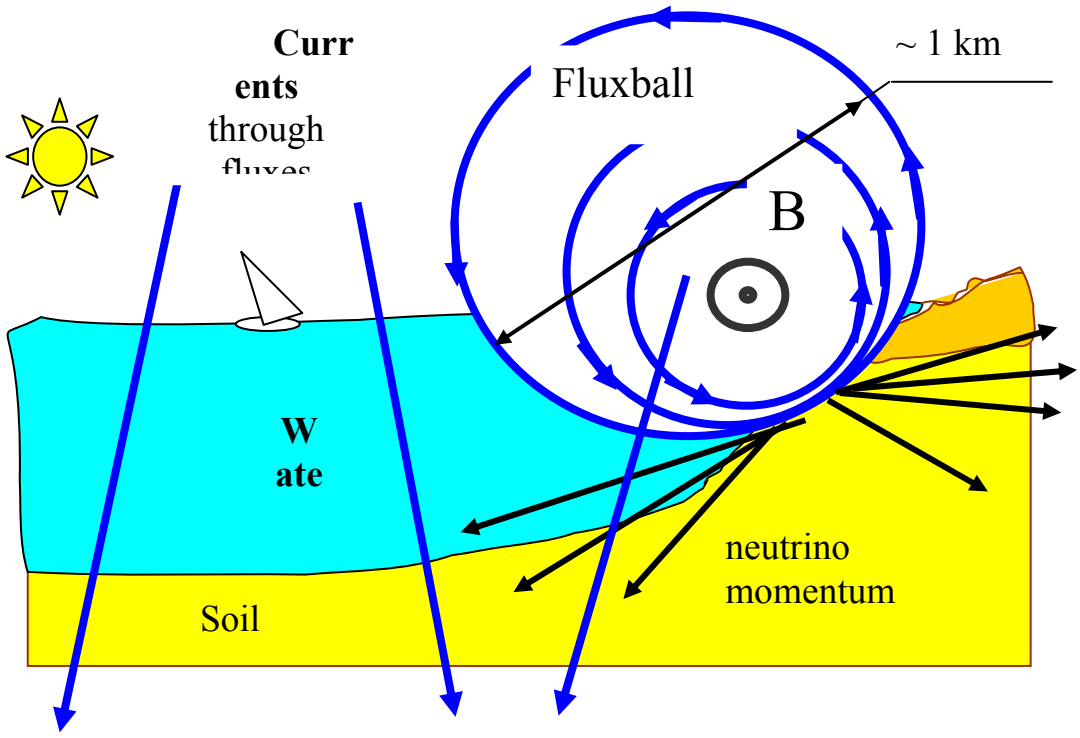

Fig.3 Fluxball

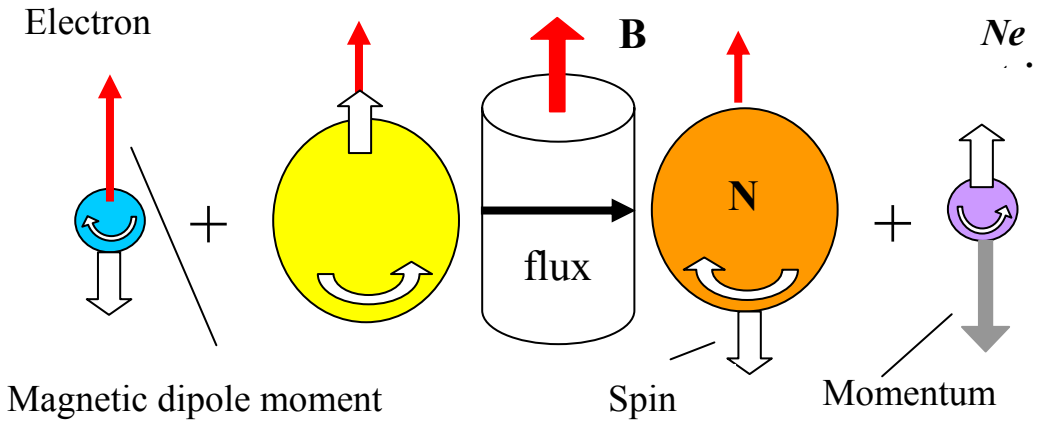

Fig.4. Electron capture at strong magnetic field set fluxball in moving by neutrino momentum

FUNDAMENTAL INTERACTIONS AND THEIR RELATIVE CONTRIBUTION TO THE NUCLEAR REACTIONS AT LOW ENERGIES.

N.V. Samsonenko

PFU of Russia, Moscow

The influence of the fundamental interactions (strong, week, electromagnetic and gravitational) on the low energy processes in condensed media is analyzed. It is shown that the gravitational interaction on the distances of atomic or nuclear order is negligibly small and can be ignored, but the electromagnetic interaction, under certain definite conditions can lead to the considerable increase of the probabilities of different reactions (including nuclear) and generate exotic bounded states, yet experimentally unobserved at present ("neutrino atoms", dineutrons, dineutrinos, "magnetic" hydrogen etc.). The existence of such states (including virtual) can explain the observable exotic phenomena of nuclear transmutation of elements in condensed media.

References

4. N.V.Samsonenko, D.V.Tahti, F.Ndahayo. On the Barut-Vigier model of the hydrogen atom. Phys. Lett. A220 (1996) 297-301.
5. N.V.Samsonenko, D.V.Tahti, F.Ndahayo. Reply to the comment on "On the Barut-Vigier model of the hydrogen atom". Phys. Lett. A229 (1997) 133-134.
6. N.V.Samsonenko, A.F.Gay, D.V.Tahti, F.Ndahayo. On electromagnetic structure of nuclear forces using deuteron as an example. Materials of the 6th Russian conference on CNF- Sochi, 1966. (in Russian).

ON THE POSSIBILITY OF THE DINEUTRON EXISTENCE AND THE DIFFICULTIES OF IT'S EXPERIMENTAL DETECTION

N.V. Samsonenko, S.L.Doubkov

PFU of Russia, Moscow

In the frames of nonrelativistic quantum mechanics with due regard for spin-spin and spin-orbital interactions the possibility of the bounded states (real and virtual) with negative (common nuclei), positive (resonances) and zero energies is investigated. The case with zero energy due to the limited lifetime (instability) despite of good localization should most likely be considered as resonances.

It is shown that proceeding from the general principles of quantum theory (ordinary Schrödinger equation with traditional insertion of electromagnetic interaction by extension of derivatives and inclusion of Pauli term is used) the Hamiltonian without free parameters which under certain condition permits the existence of exact solutions for bounded states of two neutrons (dineutron) can be obtained. The dineutron properties, the difficulties of it's detection and the effects of its existence on traditional nuclear physics including nuclear transmutation of elements at low energies are analyzed.

COLD NUCLEAR FUSION MECHANISM AT CRACK TIP SPEARHEAD LOCATED DEEP UNDER THE GROUND

A.V.Shestopalov

Research Institute of Comprehensive Exploitation of Mineral Resources RAS, Moscow, Russia, sinergo@mail.ru

Ore mines become deeper as mineral resources are extracted. At a depth of approximately 500 meters and more specific gas dynamics phenomena are observed, which are not typical at shallow depths. Power effects, e.g. on a bench coal, remain the same, while the response of the mining mass becomes inadequate to the effects (fig.1).

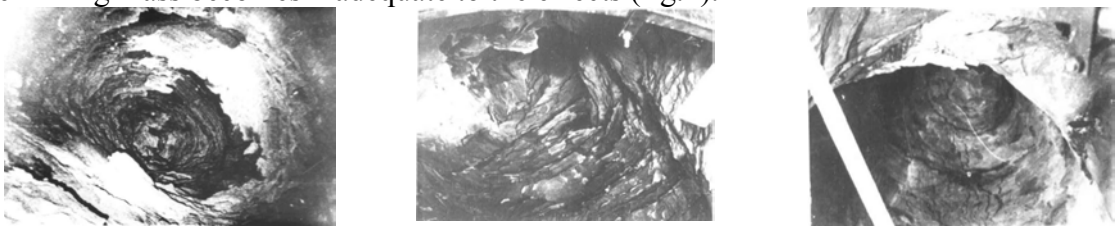

Fig.1

For example, once 14.5 thousand t of coal and 250 thousand cubic m of methane were thrown out from a 1-m bench coal (fig. 2). According to geologists' findings, amount of methane discharged at a coal outburst can be 10-times grater than that contained in the bench coal (fig. 2).

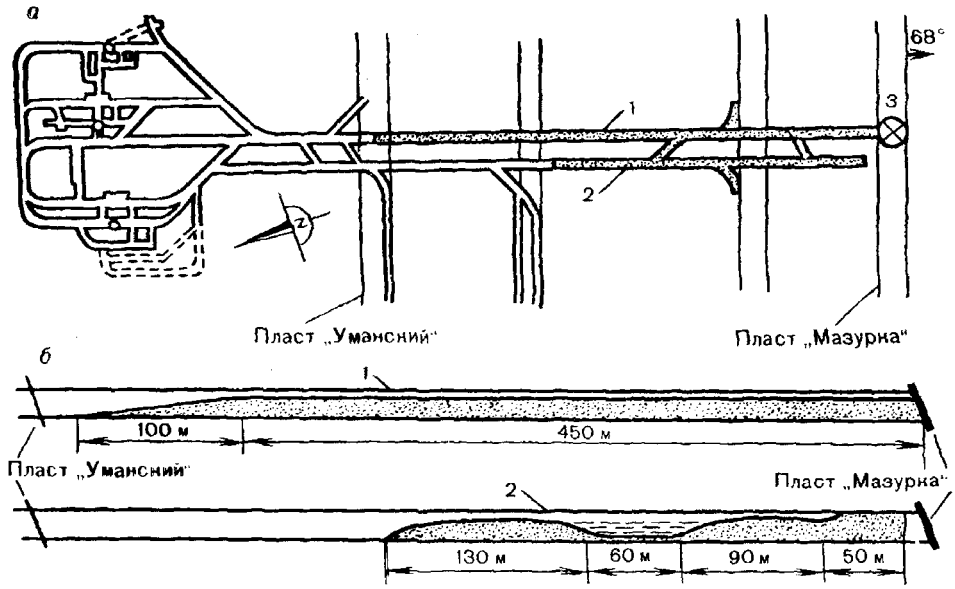

Fig. 2

The gas is discharged in a mode of filtration in the absence of permeability. The gas secrete volume is so great that one may speak about discontinuous diffusive superpermeability. The author proposes that the described phenomenon can occur under the effect of a mechanical energy flow through aligning of defects (conductive channels for this flow) along field force lines (fig. 3). A mechanism of discontinuous self-decomposition of geomaterial under the effect of rock pressure, i.e. external power source, was developed basing on these effects. The concrete material as a whole can be decomposed into the components which one were not before as a whole only by synthesis of components (products of decomposing). It is not thermodynamic decomposition of solid solution, i.e. a process due to internal power sources, like at heating.

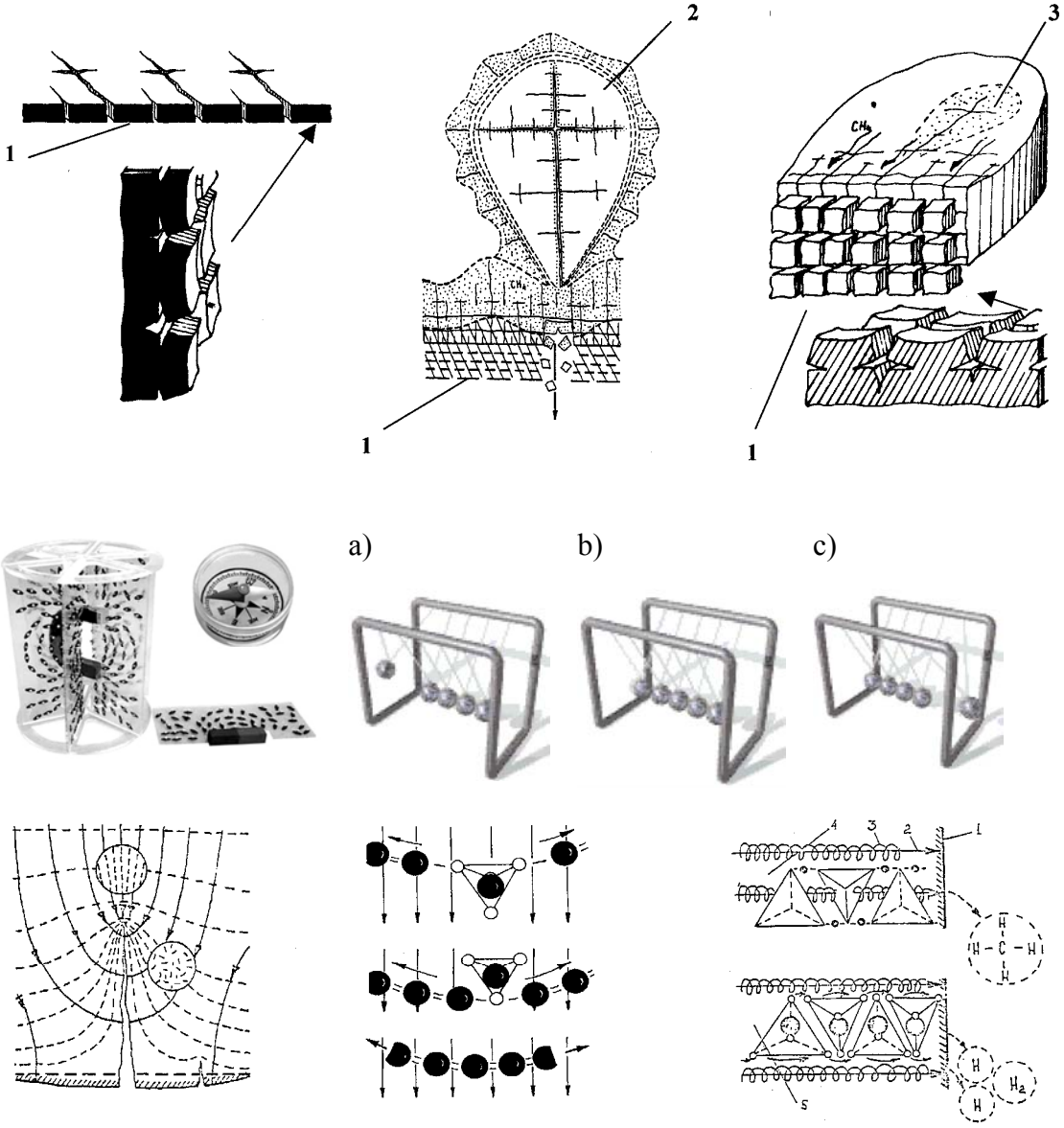

Fig.3

It is a mechanism of gas generation from a solid atomic solution (not molecular), when new elements and materials are synthesized as a result of nuclear reactions. The heaviest flow of rock pressure ("wind") appears at a crack tip spearhead. This “wind” “blows out" nuclei of different elements and free electrons, i.e. basic material for building atoms and molecules, into micro defect cavities. One may know that this type of synthesis is cold by touching the rock by a hand. For some time hydrogen and oxygen are in the form of atoms. As a result of interaction between them water and hydrogen dioxide are generated. If hydrogen is not enough, only water is generated (fig.4) [1], (fig5, 6).

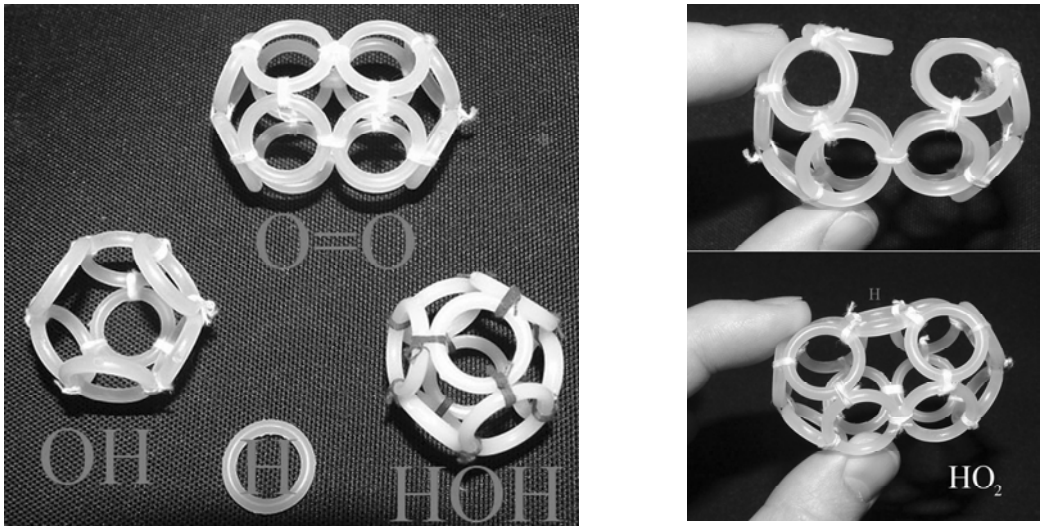

Fig. 4

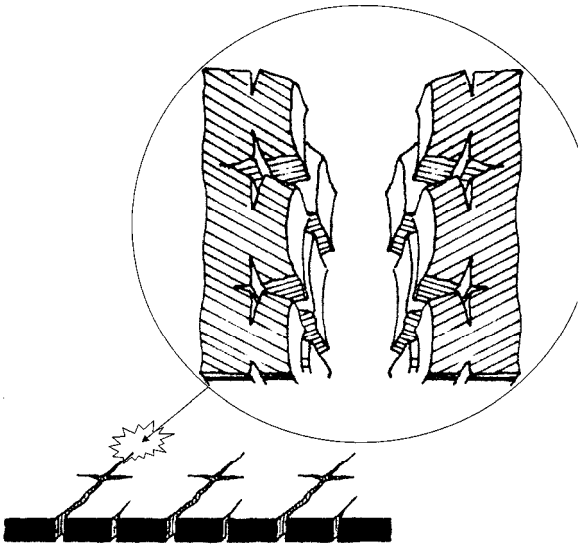

H_2 -> 2H

H + O_2 -> OH + O

O + H_2 -> HO + H

H + O_2 -> HO_2

HO_2 + H_2 -> H_2O + OH

Fig. 5

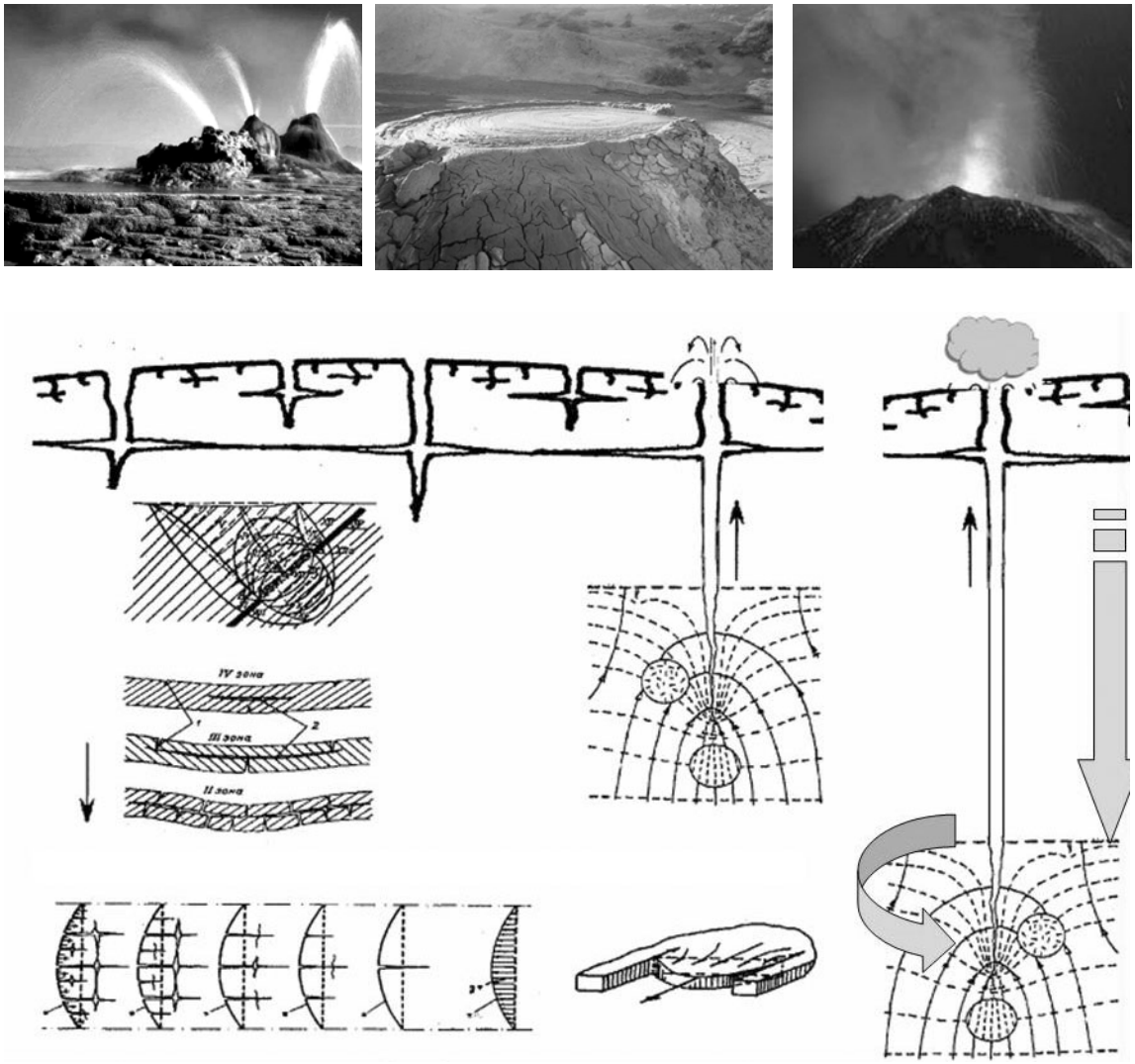

Fig. 6

The oxidation of hydrogen is a scintilla (chemical reaction of combustion). From a scintilla the flame can inflame. And then the coal mines blast out, flowing by heads oil-gas wells ignite, and in an asthenosphere the volcanoes bear. If hydrogen is not enough, only water is generated. The gas derivated by the CNF mechanism creates pressure in a crack which one invokes secondary emission of the same gas. In a system a return positive communication applies. The CNF process passes from a pseudo-steady mode in a mode with peaking – explosion.

The processes which possess efficiency coefficient > 1 are called "supersingle". As to supersingle geologic and geomechanical processes the following events are concerned: earthquakes, rock bumps mentioned above coal-and-gas outburst, as lets of rock and gas, lets of other firm mineral resources and gas. One of the supersingle processes is the grinding of

the rock up to a fraction of clay by a depth of 100 m at jumbo landslides in the mountains. The formation of such quantity of clay does not yield to explanation. Besides "air cushion" is necessary for explanation of a pathway of a landslide. Another example of the supersingle process is the formation of nanoparticles at mass explosions in opencasts (fig. 7). The energy of chemical explosions is not enough for formation nanoparticles from rock (fig. 8).

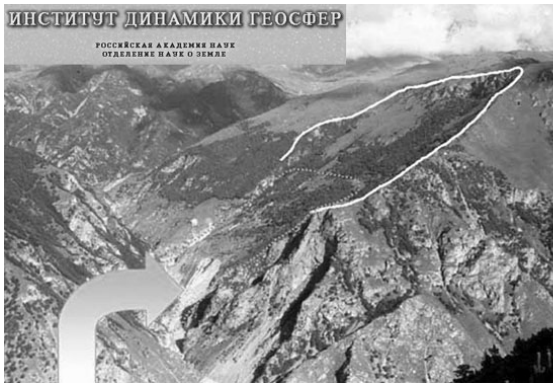

Fig. 7 ***Fig. 8***

Now there are multiple descriptions of experiments in which consumed power is not equal to power that is "produced" by a concrete device or natural phenomenon. The mechanism of cold nuclear fusion (CNF) for crack tip spearhead developed by the author is thought to fit all cases of CNF described in the scientific literature, e.g. in the fields of asymmetrical plasma electrolysis (fig. 9, 10) [2], sonofusion or sonoluminescence, produced by acoustic cavitation (fig. 11) [3], effect of powerful nanosecond electromagnetic pulses on aqueous solutions of salts and melts of metals, etc., for example, I.V.Zverev effect-“kollaps” hypothesis (fig. 12).

The common indispensable conditions for CNF are:

1) Pressure (flow of mechanical energy through a system);
2) Availability of a surface for a sink of energy;
3) Nano-second effects (not to superheat a system).

Reference CNF property is not a 100% repeatability of experiment or phenomenon in the nature. The thermodynamics was created for close systems. Close systems aren't in the nature. Theory of CNF (Cold Nuclear Fusion) needs other thermodynamics that bases on the stable balance of in and out flow of the energy but it don't bases on the low conservation of the energy. We have developed such a theory at a level of phenomenology for processed fractals.

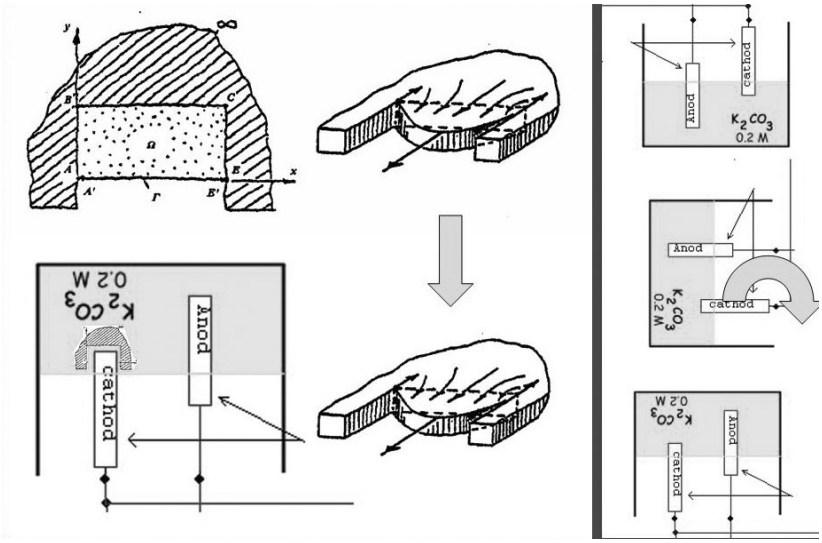

Fig. 9

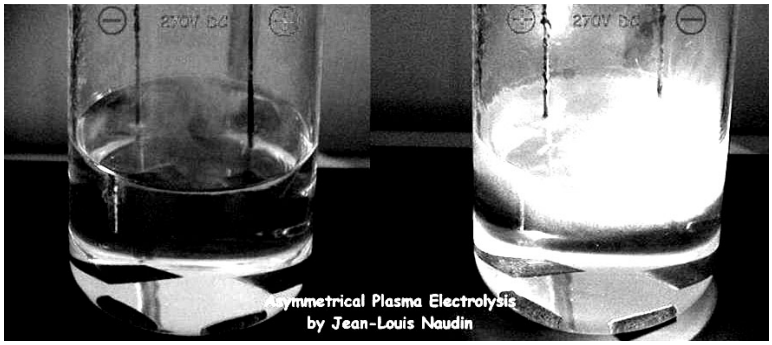

Fig. 10

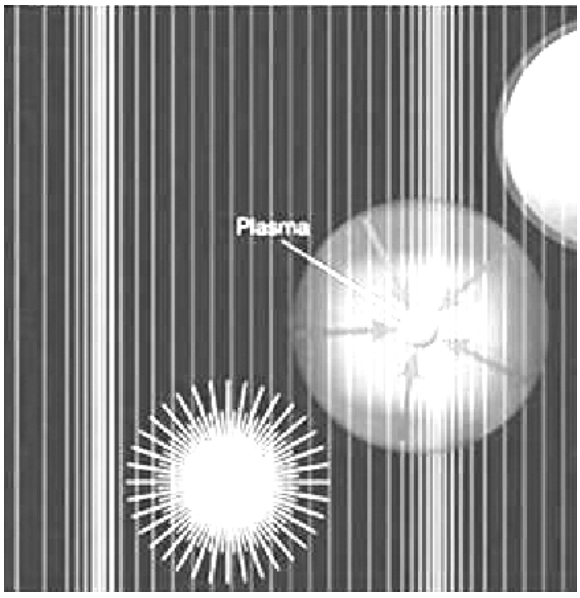

Fig. 11

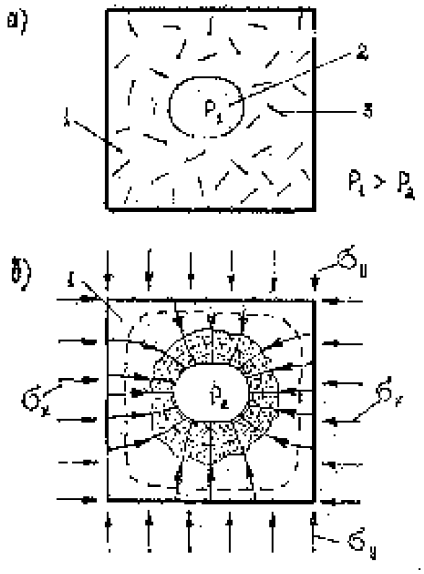

Fig. 12

Rock mechanics in depth where spontaneous failure of rockmass end part occurs is a new area of application of synergetics. We have called this theory "mechano-dynamics" and have expanded its field of application to all power sources of different nature whose flows are able to render mechanical pressure. The science about self-organization in not alive nature - synergetic by H.Haken (on West called "the theory of composite systems") creates alternative thermodynamics. The synergetics requires reorganization. It should be separated into two parts:

1) Synergetics of slowly flowing processes;
2) Synergetics of fast flowing processes.

"Fast" means by a discontinuity or explosion with localization and cumulations of process, with occurrence of return positive communication in a system. Both the scientific fields should contain subsections of quasiequilibrium and non-equilibrium thermodynamics and mechanodynamics, accordingly. I suggest that new scientific fields such as physical mesomechanics and synergetics of the rockmass end part that arose simultaneously and independently from each other should be united under a common name of mechanodynamics (as opposed to thermodynamics). The Journal of Physical Mezomechanics about a synergetics in materials technology is widely known as it is publicized simultaneously in Russian and English languages. The synergetics of a selvage of a mining massif has no the unified edition and consequently is poorly known.

The "rock mass - opening (cavity)" is an open system that may be far from mechanical equilibrium at big depth. Coal seam edge self-destruction is a typical problem of synergetic. The fact that mining science does not consider methane emission as a function of technogenous crack self-organization lead to crisis of conventional knowledge about coal methane. The alternative mechanism (CNF-mechanism) starts to lay the major role at big depth, i.e. below the gas erosion zone, where coal seam edge self-destruction may occur.

The self-destruction proceeds from the surface to the rock mass depth and lasts till mechanical equilibrium is restored due to generation of a post-failure coal zone. If this zone is reduced critically or eliminated, another self-destruction cycle starts and proceeds at sound rate till mechanical equilibrium is re-established. If the increase in mechanical energy flow density is caused by another event, it results in stepwise growth of the post-failure zone following a period of elastic resistance of the rock mass. Arising of a slip area in the coal seam edge is interpreted as generation of Prigozhyn dissipative structures (fig. 13).

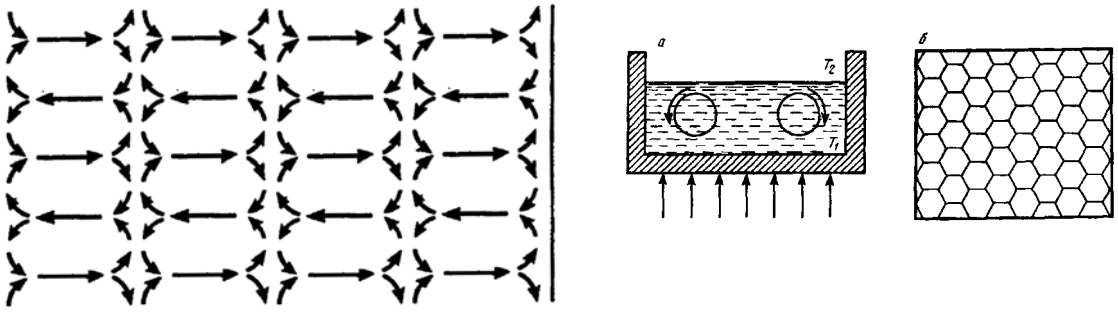

Fig. 13

Rock opening conditions cannot be simulated by laboratory experiments. Similarly, results of field experiments depend upon experimental methodology, e.g. technical means. The author demonstrates that the end part of a rockmass is a fractal, i.e. a multi-level self-organizing system for technogenic self-propelling fractures in which the loss of shear stability occurs in a self-consistent manner at micro-, meso-, macro- and mega-scale levels. This leads to emergence of Prigozhyn dissipative structures (geomaterial fragmentation) at the above-mentioned scale levels. Macro coal outburst in mine and micro coal outburst in crack. (fig. 14).

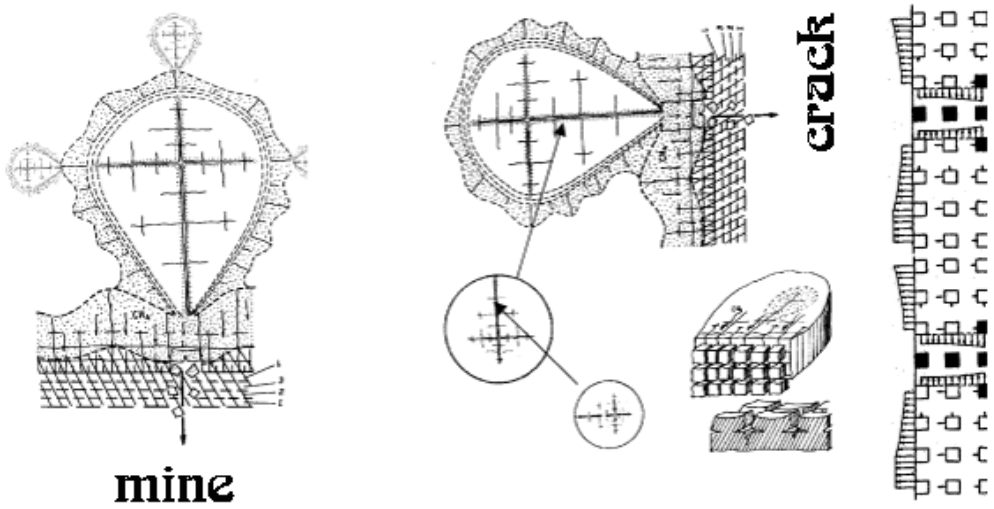

Fig.14.

It is practically impossible to describe in words the evolution of self organizing dissipative structure. Let us use the method of stationary (non-mobile) cell automata to visualize the process. We suggest that a system of 4 biharmonic differential equations should be substituted for the cell automaton. The equation are solved by numerical methods, e.g. method of end elements, but using a cell automaton algorithm. The area of solution continuity is a half-plane with an infinitely far border D=100% of pressure function and a border in the form of a straight line D=0% (fig. 15). Mathematical model for the "coal seam-opening" system is generally reduced to solution of problems of fragile failure under three energy fluxes, i.e. rock

pressure, filtrating gas pressure and loose mass weight pressure. Appearance of internal sources for the last two fluxes may be jump-like only. The solution algorithm says that function for the total pressure D(x,y) should be found at each iteration in the simulation area that satisfies the system of four biharmonic differential equations including an equation with pressure function D=F(Φ,P,G,x,y), where Φ, P and G are pressure functions of the remaining three equations in the above-mentioned system. Only one of the above listed functions may be present in one equation, x and y are space coordinates.

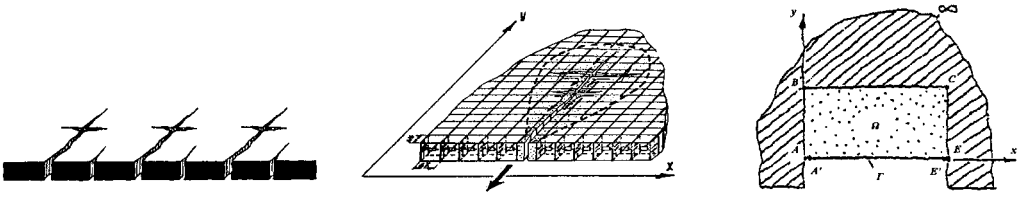

Fig. 15

$$\frac{\partial^4 D}{\partial x^4} + 2\frac{\partial^4 D}{\partial x^2 \partial y^2} + \frac{\partial^4 D}{\partial y^4} = F(\Phi, P, G, x, y)$$
$$\frac{\partial^4 \Phi}{\partial x^4} + 2\frac{\partial^4 \Phi}{\partial x^2 \partial y^2} + \frac{\partial^4 \Phi}{\partial y^4} = f(x, y)$$
$$\frac{\partial^4 P}{\partial x^4} + 2\frac{\partial^4 P}{\partial x^2 \partial y^2} + \frac{\partial^4 P}{\partial y^4} = v(x, y)$$
$$\frac{\partial^4 G}{\partial x^4} + 2\frac{\partial^4 G}{\partial x^2 \partial y^2} + \frac{\partial^4 G}{\partial y^4} = l(x, y)$$

$$D = \Phi + P + G$$
$$D|_{BC} = D|_{AA'} = D|_{E'E} = \text{const} = 100\%,$$
$$D|_{A'E'} = \text{const} = 0\%,$$
$$\frac{\partial D}{\partial n}|_{AB} = 0,$$
$$\frac{\partial D}{\partial n}|_{CE} = 0.$$

$$\frac{\partial}{\partial x}\left[A_{x(x,y)}\frac{\partial \Phi}{\partial x}\right] + \frac{\partial}{\partial y}\left[A_{y(x,y)}\frac{\partial \Phi}{\partial y}\right] = \alpha(x, y),$$
$$\frac{\partial}{\partial x}\left[A_{x(x,y)}\frac{\partial \alpha}{\partial x}\right] + \frac{\partial}{\partial y}\left[A_{y(x,y)}\frac{\partial \alpha}{\partial y}\right] = 0.$$
$$\frac{\partial}{\partial x}\left[\chi_{x(x,y)}\frac{\partial P}{\partial x}\right] + \frac{\partial}{\partial y}\left[\chi_{y(x,y)}\frac{\partial P}{\partial y}\right] = \beta(x, y),$$
$$\frac{\partial}{\partial x}\left[\chi_{x(x,y)}\frac{\partial \beta}{\partial x}\right] + \frac{\partial}{\partial y}\left[\chi_{y(x,y)}\frac{\partial \beta}{\partial y}\right] = 0.$$
$$\frac{\partial}{\partial x}\left[k_{x(x,y)}\frac{\partial G}{\partial x}\right] + \frac{\partial}{\partial y}\left[k_{y(x,y)}\frac{\partial G}{\partial y}\right] = \gamma(x, y),$$
$$\frac{\partial}{\partial x}\left[k_{x(x,y)}\frac{\partial \gamma}{\partial x}\right] + \frac{\partial}{\partial y}\left[k_{y(x,y)}\frac{\partial \gamma}{\partial y}\right] = 0.$$

$$A_{(x,y)} = \xi(\nabla D)$$
$$\nabla D < [\nabla D]_{1-2} \quad A_{(x,y)} = A_1,$$
$$\nabla D \geq [\nabla D]_{1-2} \quad A_{(x,y)} = A_2,, A_1 = a \cdot A_2;$$
$$\chi_{(x,y)} = \xi(\nabla D)$$
$$\nabla D < [\nabla D]_{2-3} \quad \chi_{(x,y)} = \chi_1,$$
$$\nabla D \geq [\nabla D]_{2-3} \quad \chi_{(x,y)} = \chi_2,, \chi_1 = a \cdot \chi_2;$$
$$k_{(x,y)} = \xi(\nabla D)$$
$$\nabla D < [\nabla D]_{2-3} \quad k_{(x,y)} = k_1,$$
$$\nabla D \geq [\nabla D]_{2-3} \quad k_{(x,y)} = k_2,, k_1 = a \cdot k_2;$$

Each solution of every biharmonic equation consists of solutions of 2 Poisson harmonic equations according the same algorithm. Final goal of the equation system solution analysis is to find coordinates of a cell (area) satisfying certain conditions that are the same for all cells. If the criterion is satisfied in some area, we change (e.g. decrease strength or increase gas permeability) properties of the medium and set internal sources for the respective pressure function. Changes of boundary conditions in solution continuity area for all the 4 biharmonic

equations precede solution of the mentioned equation system. Self-organization of the front of the process under simulation happens during the solution spontaneously (by previously unknown inertia) as a result of identical non-linear (jump-like) changes in the simulated medium between the solutions (fig. 16).

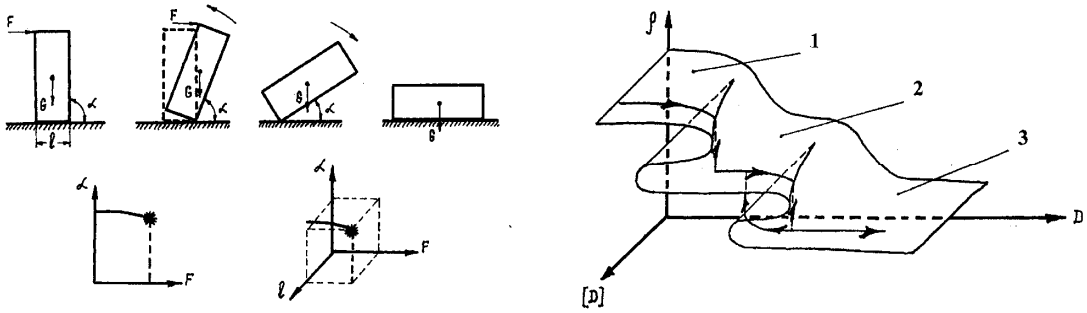

Fig. 16

Conclusion

Thermodynamics describes closed systems, which do not exist in nature. Another thermodynamics is needed to explain the CNF (cold nuclear fusion) phenomenon which would be based on balance of in- and out-flows of energies (balance of sinks and sources) rather than on conservation laws. The common indispensable conditions for CNF are: 1) Pressure (flow of mechanical energy through a system); 2) Availability of a surface for a sink of energy; 3) Nano-second effects (not to superheat a system). Reference CNF property is not a 100% repeatability of experiment or phenomenon in the nature.

References

1. Aleksander Yu. Kushelev “Nanoworld” Encyclopedia -

http://www.nanoworld.narod.ru/texteng.htm

2. Jean-Louis Naudin - http://jlnlabs.online.fr

3. Ken Suslik, David Flannigan –

http://www.c news.ru/cgi-bin/oranews/get_news.cgi?tmpl=top_print&news_id=175481

MANY-BODY EFFECTS OF BOSE PARTICLE SYSTEM IN SOLID

Ken-ichi Tsuchiya*, Shigeru Sasasbe and Masao Ozaki*****

** Tokyo National College of Technology,*
1220-2 Kunugida, Hachioji, Tokyo 193-0997, Japan, tsuchiya@tokyo-ct.ac.jp

*** Tokyo Metropolitan University,*
1-1 Minami-Ohsawa, Hachioji, Tokyo 192-0397, Japan, ssasabe@cc.tmit.ac.jp

**** Tokyo University of Agriculture,*
1-1-1 Sakuragaoka, Setagaya, Tokyo, 156-8502, Japan, m1ozaki@nodai.ac.jp

Abstract

Many-body effects strongly depended on the symmetry of the wave functions. And the screening effect by conduction electrons affects the interactions between charged particles in solids. In this study, the behaviors of charged Bose particles in solids are estimated by considering those two factors. Firstly, we introduce the pseudopotennsial, which acts on the Bose particles in the same way that symmetrization of the many-body wave functions will do. This is done by calculated the matrix elements of the density operator in the quantum statistical mechanics [1]. Secondly, screened interactions between charged Bose particles are introduced by using Hartree-Fock equation.

References

1. W.Greiner, “Thermodynamics and Statistical Mechanics”, Springer-Verlag (1995).

POSSIBLE CATALYSIS OF NUCLEAR TRANSMUTATIONS AT ELECTRONIC SCREENING OF NUCLEUS CHARGES IN THE DENSE LOW-TEMPERATURE PLASMA OF THE POWERFUL PULSING INDUCTION DISCHARGE

A.N. Vlasov

The Ryazan State Radio Engineering University, Russia
E-mail: anv@fulcra.ryazan.ru

Abstract

It is shown that the circuit solution based on fly-back pulsing schema is effective for input of energy in plasma of powerful induction discharge with pressure, close to atmospheric pressure. In this case at excess of a threshold level of amplitude of current impulse process of formation of a toroidal current layer inside the vortex ring is possible. Process of transition of the dense stream of electrons in an electronic layer is analyzed. It is demonstrated that toroidal current layer might be studying as quasi-superconductor. At a qualitative level the opportunity of electronic screening of the one-charging nucleus up to a level providing overcoming of a Coulomb barrier and course of nuclear fusion reactions is surveyed.

1. Introduction

As is known, controlled nuclear fusion (hot fusion) [1] at attempt of embodying of idea of magnetic isolation of plasma has met difficulties, the bound with instability magnetohydrodynamical configurations. If to use stable magnetohydrodynamical configurations that magnetic isolation of plasma becomes impossible, but there is an opportunity of formation of current layers. Examinations bounding with current layers are of interest from the point of view of studying plasma at super strong densities of a current when magnetic pressure in plasma is comparable with gas-dynamic pressure. Such currents may take place at discharges of the linear lightning, and also, possible, exist inside a ball lightning. It is possible that in ball lightning with very big internal energy the nuclear fusion may take place at low ion to temperature (cold fusion).

Current layers may be got at powerful pulsing induction discharges. Generators of such discharges are similar to single-stroke transformers of power electronics. Transferring of electrical energy to these devices occurs due to switching on and switching off of a power switch in a primary circuit that is inductive bounded with a secondary circuit. The transformer is designated as “forward” if energy in a loading transmits during a phase when the power switch is switched on. If energy in a loading transmits during a phase when the power switch is switched off then the transformer is designated as “fly-back”.

In the given article a toroidal current layer in vortex (TCV-layer) [2] formed according to the fly-back schema is considered and possible catalysis of nuclear transmutations at

electronic screening of nucleus charges in this magnetohydrodynamical configuration at low ion temperature is analyzed.

2. Fly-back pulsing schema for pumping energy into plasma

In fly-back schema of power electronics [3] shown on Fig. 1, the diode is closed during switching on of the power switch (PHASE 1), and energy into a loading does not transmit. It collects in the capacity of a magnetic field as the current of an initial winding of the transformer linearly accrues. The phase of transferring of this energy (PHASE 2) comes when the power switch is switching off. At this moment polarity of a voltage on the transformer varies, the diode is unclosed, and the current transmits into the loading.

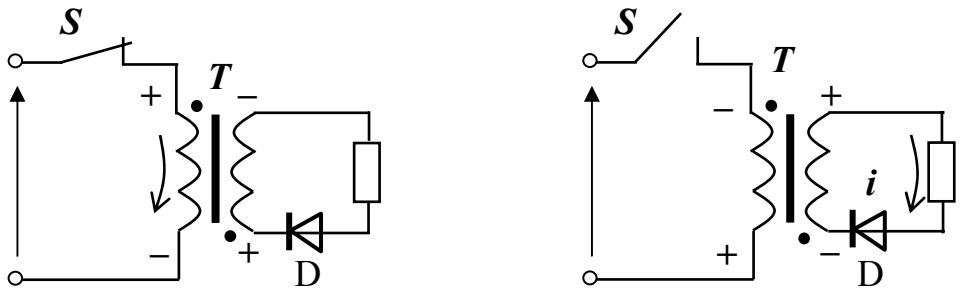

Fig. 1. Fly-back schema: ***U*** *is a voltage of feed;* ***S*** *is a power switch;* ***D*** *is the diode;* ***Z*** *is a loading;* ***T*** *is the transformer;* ***I*** *is a current of an initial winding (or a Ruhmkorff coil);* ***i*** *is a current of a secondary winding (or plasmas), signs «+» and «–» mean polarities of voltages*

Correspondingly the TCV-layer may be formed using the idea of fly-back schema as rotating θ-pinch ($R\theta$-pinch) [4] shown on Fig. 2. After switching on of a power switch (PHASE 1) the impulse of a current of primary coil has rather small steepness of forward front, energy in plasma practically does not transmit, and collects in the shape of a magnetic field. The phase of transferring of energy in plasma (PHASE 2) comes after moment when power switch is switched off. Thus plasma carrier gas is strongly ionized, and the strong current begins to flow in generated plasma. Distinctive feature of this expedient is that in central area of a formatted plasma filament the magnetic field is more strong, than on periphery, and inside a plasma filament there are forces ***F***, aspiring to push out plasma on walls of the chamber, but with this interferes circumrotate circulating plasma carrying gas. As result, in plasma filament the constriction is started up, and it receives the form of the TCV-layer.

3. Model of the TCV-layer as a toroidal metal shell

The substance of model of a toroidal metal shell consists that the toroidal plasma conductor assimilates to a toroidal metal shell which radius corresponds to radius most warmed up a stratum of plasma, as is shown on Fig. 2. A physical substantiation of model is that conductance of plasma $\sigma(\mathrm{r})$ has a steep temperature dependence therefore plasma sharply loses conductive properties there where its temperature begins reduced appreciably. Obviously, this temperature is peak at some radius r_0, which we shall count radius of a plasma filament. In a direction from radius r_0 to walls of the camber r_i the temperature is reduced because of a thermal conduction of plasma, and in a direction from r_0 to an axis of the camber ($r = 0$) the temperature is reduced because of radiation losses.

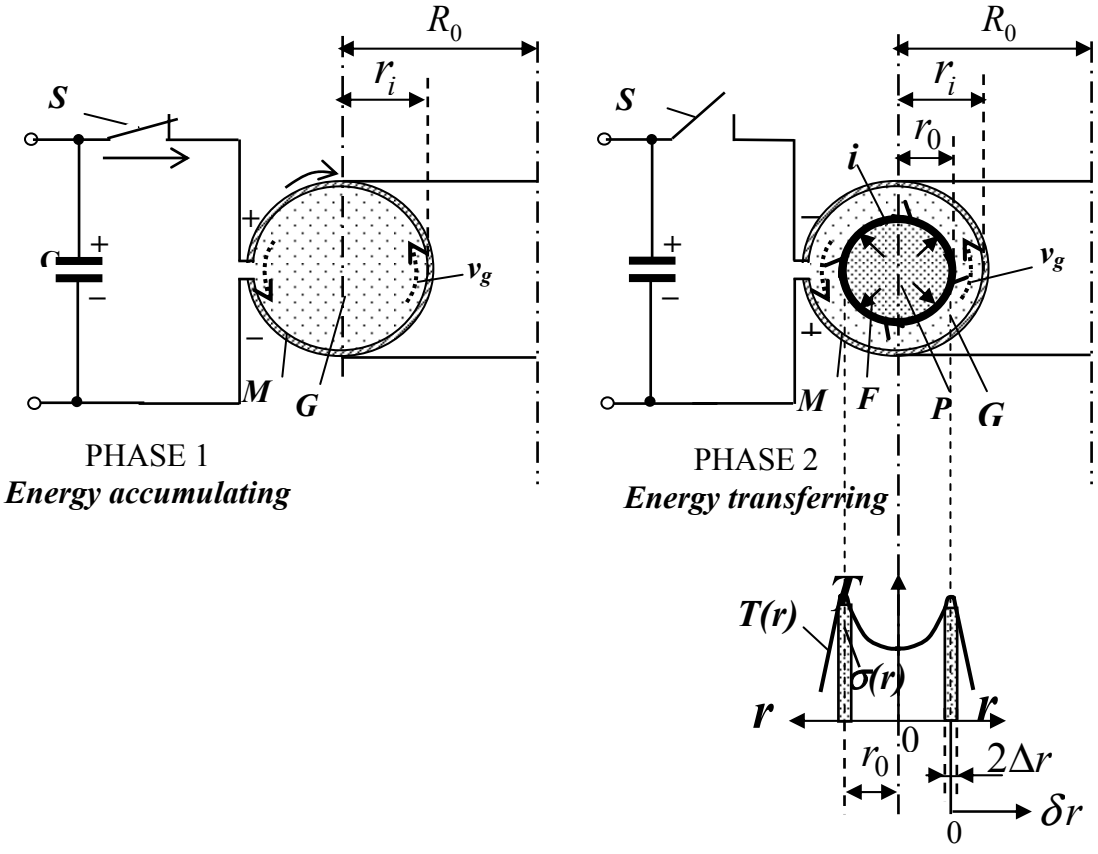

***Fig. 2. Pulsing gas discharge in toroidal camera (half of chamber is shown): C** is capacity; **M** is the metal coil covering the toroidal chamber in a plane of small radius; **S** is a power switch; **G** is plasma carrying gas; $\mathbf{v_g}$ is velocity plasma carrying gas at the vortex stabilization; **P** is plasma; **F** is the forces which are pushing out plasma from central area of the chamber; **I** is a current of an initial winding; **i** is a current of a plasmas; signs «+» and «–» mean polarities of voltages; r_0 is small radius of a plasma cord; R_0 is major radius of a plasma filament; r_i is small radius of a chamber; r is running radius; T is current temperature; T (r) is typical allocation of temperature of plasma on radius in induction discharges, σ (r) is the idealized allocation of conductance of plasma, Δr is a half-width of an electronic stream: δr is running coordinate.*

The shell conventionally is accepted as metallic, i.e. strong of those reasons that fly-back discharge develops for very short time (a share of micro second) when the gas dynamic processes have not time to prove appreciably. We shall figure also $R_0 >> r_0$, where R_0 and r_0 are according to major and small radiuses of a torus. It allows to view about enough major precision electromagnetic processes in a toroidal chamber as processes in a cylindrical chamber and at the specified assumptions the problem is reduced to viewing the idealized one-dimensional process.

The coefficient of entrapment of a magnetic field of primary coil a toroidal shell can be spotted under the formula:

$$\xi = i_m / I_m , \tag{1}$$

where i_m is amplitude of an impulse of a current in a shell; I_m is amplitude of an impulse of a current of primary coil. The electric field inside the chamber can be found from Maxwell equations

$$\oint_{(L)} \vec{E}\, d\vec{l} = -\int_{(S)} \frac{\partial \vec{B}}{\partial t} d\vec{S} , \tag{2}$$

where $\vec{E}$ is an electric intensity in the field of a vector $d\vec{l}$ contour of integration L with the area S, ($d\vec{S} = dS \cdot \vec{n}$, $\vec{n}$ is a normal line), $\vec{B}$ is an induction of a magnetic field.

As the medium is a plasma or plasma carrier gas, we accept $\mu = 1$ and $B = \mu_0 H$, where μ_0 is a permeability of vacuum, H is a magnetic intensity. Taking into account that time of formation the fly-back discharge is very little, it is possible to figure radius of a plasma cord the fixed, $r = r_0$. Then $L = 2\pi r_0$, $S = \pi r_0^2$ and a magnetic intensity H, created by a current of primary coil I it are possible within the framework of the accepted one-dimensional model $(r_0 << R_0)$ to present by relation $H = I/(2\pi R_0)$. Substitution of this relation in (2) after transformations allows receiving quantity of the induced electric field as

$$E(r_0) = -\frac{\mu_0 r_0}{4\pi R_0}(\partial I/\partial t), \tag{3}$$

where $(\partial I/\partial t)$ is velocity of change of a current of primary coil.

Further it permissible, that the current of primary coil wanes linearly:

$$\partial I/\partial t \approx -I_m/\tau_b , \tag{4}$$

where I_m is peak value of a current of primary coil, τ_b is time of wane.

Then from (3) with the account (4) it is possible to receive a voltage in a contour of formation of a plasma cord with radius r_0:

$$U_m = 2\pi r_0 \cdot E(r_0) \approx \frac{\mu_0 r_0^2}{2R_0} \cdot \frac{I_m}{\tau_b}. \qquad (5)$$

The equivalent circuitry of this contour represents current parallel connected a current source, inductance and resistance of a loading. The inductance of a toroidal shell equal to inductance of a toroidal choke:

$$L_0 = \frac{\mu_0 r_0^2}{2R_0}. \qquad (6)$$

During wane of a current of primary coil τ_b in a contour the voltage operates $U(t) = U_m$, therefore a current in a contour $i(t)$ grows up to the peak quantity i_m according to the differential equation

$$L_0 \frac{di}{dt} + i \cdot Z(i) = U_m \ . \qquad (7)$$

It permissible as a first approximation, that $Z(i) = Z = Const$, $U_m = Const$, then solving the equation (7) with boundary conditions $i(t=0) = 0$, $i(t=\tau_b) = i_m$ with the account (5) and (6) it is gained

$$i_m(\tau_b) \approx I_m \cdot \frac{1 - exp(-\tau_b/\tau_0)}{\tau_b/\tau_0}, \qquad (8)$$

where τ_0 is a stationary value of time of a toroidal metal shell:

$$\tau_0 = \frac{\mu_0 r_0^2}{2R_0 Z}. \qquad (9)$$

Having substituted (8) in (1) at $Z = Const$ and the linear wane of a current of primary coil we shall receive expression for coefficient of entrapment of a current of primary coil a toroidal shell:

$$\xi \approx \frac{1 - exp(-\tau_b/\tau_0)}{\tau_b/\tau_0}. \qquad (10)$$

Let's note, that resistance of losses Z at formation of the TCV-layer from the physical point of view represents the trebled average losses of energy $3\langle W_b \rangle$ in plasma for a period τ_b, Referred to a quadrate of an entrapped current $(\xi I_m)^2$, i.e. $Z = 3\langle W_b \rangle \tau_b^{-1} (\xi I_m)^{-2}$. Restlessly measured or designed value Z it is necessary to improve at direct experiments.

4. Dynamics of development of the discharge

In the further analysis it is convenient to yield the relevant estimations for a concrete example of performance of the device. Let the basic data will be the following: $R_0 = 0.1\,m$, $r_0 = 0.02\,m$; $r_i = 0.03\,m$, $\xi = 0.6$, plasma carrying gas is deuterium at atmospheric pressure $p_g = 1 \cdot 10^5\ Pa$ (mass of an ion is $m_i = 3.3 \cdot 10^{-27}\ kg$).

4. 1. Phase of an energy accumulation

Accumulation of energy is carried out in the shape of a magnetic field inside the toroidal cabinet as follows. At delivery on primary coil of a voltage $U_f(t)$ there is an increase of a current of primary coil I according to the formula

$$L_i \frac{dI}{dt} = U_f(t)\ , \tag{11}$$

L_i is inductance of primary coil (ohm losses in primary coil it is neglected).

At performance of primary coil as toroidal conductor its inductance L_i makes quantity by analogy with (6)

$$L_i = \frac{\mu_0 r_i^2}{2R_0}\ , \tag{12}$$

where r_i is radius of a coil of primary coil, fig. 2 (practically coincides with radius of the chamber).

Integrating the equation (11) with the account (12) it is gained

$$I_m = \frac{2R_0}{\mu_0 r_i^2} \int_0^{\tau_f} U_f(t) dt\ , \tag{13}$$

where τ_f is duration of forward front.

From (13) in approach $U_f(t) \approx U_f = Const$ we gain a relation for duration of forward front of an impulse of a current of primary coil

$$\tau_f \approx \mu_0 r_i^2 I_m / (2R_0 U_f)\,. \tag{14}$$

Quantity of an impulse of a current of primary coil I_m should be such, that the magnetic pressure created by a magnetic field of an entrapped current i_m it would be

approximately equal to pressure plasma carrier gas $p_m \equiv \mu_0 H_0^2/2 \approx p_g$, where $H_0 \cong i_m/(2\pi R_0)$. From told with the account (1) follows:

$$I_m \approx (2\pi R_0/\xi)\sqrt{2p_g/\mu_0}\ . \tag{15}$$

Numerical value of this current makes quantity

$$I_m \approx (2\pi\cdot 0.1/0.6)\sqrt{2\cdot 1\cdot 10^5/4\pi\cdot 10^{-7}} \approx 4.2\cdot 10^5\ A\ .$$

Period of activity of forward front of a pumping pulse, it is especial in a combination with HF-pumping, expediently to use for preparation of a working stratum of plasma for the subsequent perception it of the reserved energy of a magnetic field at activity of reverse motion. For this purpose it is necessary to create such intensity of an induced electric field E, which would be comparable to intensity E_0, sufficient for maintenance of the discharge which parameters are similar to parameters of the positive pole of an electric arc, i.e. $|E| \approx |E_0|$. From this with the account (3) and (5) it is possible to spot a voltage on primary coil during activity of a direct course:

$$U_f \cong 2\pi E_0 r_i^2/r_0\ . \tag{16}$$

According to available experimental dates $E_0 \approx 12\ V/cm = 1.2\cdot 10^3\ V/m$ and then the voltage at a direct course should make $U_f \approx 2\pi\cdot 1.2\cdot 10^3\cdot (0.03)^2/0.02 \approx 340\ V$.

Duration of a direct course according to (14) should make $\tau_f \approx 4\pi\cdot 10^{-7}(0.03)^2\cdot 4.2\cdot 10^5/(2\cdot 0.1\cdot 340) \approx 7\cdot 10^{-6}\ s$.

In this case starting resistance of losses of the toroidal shell, approximately equal is provided

$$Z_0 \approx r_0 E_0/(R_0 J_0), \tag{17}$$

where J_0 is density of a current on unity of length, A/m, proceeding in a toroidal shell before the beginning of back front of a pumping pulse.

According to experimental dates for maintenance of temperature of plasma near $T_i = 1\cdot 10^4\ K$ the density of a current on unity of length should make $J_0 \approx 80\ A/cm = 8\cdot 10^3\ A/m$. According to (17) starting resistance of losses it is possible to estimate quantity $Z_0 \approx 0.02\cdot 1.2\cdot 10^3/(0.1\cdot 8\cdot 10^3) = 0.03\ \Omega$.

4.2. Phase of an energy transferring

After achievement of a current of primary coil of a preset value I_m (15) the disrupter of a primary circuit is yielded. During wane of a current of primary coil τ_b, According to analytical model surveyed above the relation should be observed $\tau_b \le \tau_0$ And according to the formula (9) quantity τ_b should satisfy to a requirement

$$\tau_b \le \tau_0 = \mu_0 r_0^2 / (2R_0 Z_0) \ . \tag{18}$$

Duration of front of a disruptor according to (18) should be $\tau_b \le \tau_0 = 4\pi \cdot 10^{-7} (0.02)^2 / (2 \cdot 0.1 \cdot 0.03) \approx 84 \cdot 10^{-9}$ *s* .

The Amplitude of an impulse of a voltage on a primary coil at disrupting of a current with the account (12) will make quantity

$$U_b \approx L_i I_m / \tau_b = \mu_0 r_i^2 I_m / (2R_0 \tau_b) \ . \tag{19}$$

Here interaction of a magnetic field with a current shell, which reduces a voltage on primary coil, is not taken into account. Therefore (19) it is necessary to view as an upper bound of value of stress amplitude. From (19) follows that $U_b \approx 4\pi \cdot 10^{-7} \cdot (0.03)^2 \cdot 4.2 \cdot 10^5 / (2 \cdot 0.1 \cdot 84 \cdot 10^{-9}) \approx 28 \cdot 10^3$ *V* . In our case the power key unlocking a contour of a current with force should maintain such voltage $I_m \approx 420$ *kA* .

At observance of requirements of relations (15) and (18) inside the toroidal cabinet the strong vortex electric field, which in thin most warmed a stratum of plasma with radius is induced r_0 for rather short time near 84 *ns* induces a current of such quantity, that pressure of a magnetic field created by it is close to pressure of plasma carrier gas.

5. Forming of a monolayer of electrons

Within the framework of the simplified model in the beginning we shall consider the forces influencing an electron in an electronic stream of the TCV-layer after the termination of the second phase. Let the stream initiating has thickness $2\Delta r$ with a stationary value in density of a current (Fig. 2). Then inside a stream in limits $-\Delta r \le \delta r \le \Delta r$ the magnetic field has intensity

$$H(\delta r) = \frac{I_m \xi}{4\pi R_0} \left(1 - \frac{\delta r}{\Delta r} \right) \ . \tag{20}$$

On an electron having velocity v_e, force of Lorenz operates

$$F_m(\delta r) = ev_e\mu_0 H(\delta r). \tag{21}$$

The total of forces of Lorenz on an axis δr on an interval $-\Delta r \le \delta r \le \Delta r$ it is counterpoised effective on the part of ions of plasma by the total independent from δr Electrostatic forces F_g, equal to

$$F_g = \frac{1}{2\Delta r}\int_{-\Delta r}^{\Delta r} F_m(\delta r)\, d(\delta r). \tag{22}$$

The composite force effective on an electron in a stream with the account (20), (21), (22) is equal to

$$\delta F_m = F_m - F_g = -\frac{ev_e\mu_0 I_m\xi}{4\pi R_0\Delta r}\cdot\delta r\,. \tag{23}$$

This force is guided on squeezing of an electronic stream, and it the more at the given δr, than less thickness Δr stream. However with squeezing interfere perturbing force $|\delta F_c|$, the bound with a dispersion of electrons at collision with ions of plasma. Force $|\delta F_c|$ gives in fluctuations of thickness $|\delta r|$. If to enter restriction $|\delta r/\Delta r| \le 10$ that with the account (23) is possible to receive a requirement at which performance the opportunity of squeezing of a stream of electrons in the TCV-layer down to ultimate possible thickness in one electron is supposed:

$$|\delta F_c| \le \frac{ev_e\mu_0 I_m\xi}{40\pi R_0}. \tag{24}$$

At a dispersion of an electron on it the perturbing force on the average equal operates

$$|\delta F_c| = (\pi/2)\cdot\left(m_e v_e^2/L_{90}\right). \tag{25}$$

Here L_{90} is a medial path length in relation to a no single Coulomb scattering on a corner 90^0 [5], determined by the formula $1/nL_{90} \approx B_{90}/W_e^2$, which may be given in a view:

$$L_{90} \approx \kappa_c^2/(\sigma_0 n), \tag{26}$$

where $\sigma_0 = B_{90}/W_0^2 = 2.6\cdot 10^{-28}/(0.51)^2 \approx 1\cdot 10^{-27}\ m^2$ is coefficient, n is concentration of plasma, κ_c is critical value of the relative energy, having overcome which electronic stream may be squeezed down to the thickness in one electron.

From (26) with the account (24) and (25) it is gained:

$$\kappa_c > \pi\sqrt{\frac{40R_0\sigma_0 n v_e}{(e/m_e)\mu_0 I_m\xi}}. \tag{27}$$

For a rough numerical estimation ($v_e \approx 0.6c$) in conformity (27) we have $\kappa_c > \pi\sqrt{0.1\cdot 40\cdot 1\cdot 10^{-27}\cdot 7.3\cdot 10^{23}\cdot 1.8\cdot 10^8/\left(1.76\cdot 10^{11}\cdot 4\pi\cdot 10^{-7}\cdot 4.2\cdot 10^5\cdot 0.6\right)} \approx 0.01$, that corresponds to energy $W_c = W_0\kappa_c \approx 5\ keV$. It is achieved on the second phase, and, hence, the electronic stream in a composition of the TCV-layer may be squeezed up to thickness in one electron.

6. Parameters of electronic screening

In the TCV-layer electrons and ions are two thermodynamic equilibrium subsystems, it is feebly the bound with each other [6]. Therefore the temperature inside an electronic fluid depends on the ionic temperature a little. During diminution of thickness of a stream down to thickness in one electron inside a stream there is an alignment of energies of electrons as their relative travel becomes possible only in two measuring. It corresponds to an establishment inside an electronic fluid of ultra low temperature at which the motion of electrons is synchronized. But such current layer is not a superconductor; it may be called a quasi-superconductor. Here magnetic fluxes are not quantum, but application of some relations quite possible.

As the performance of a degree of sync the length of coherence serves Δx :

$$\Delta x \approx (\hbar/2)\cdot(1/\Delta k), \tag{28}$$

where Δk is indeterminacy of an impulse of an electron.

For a finding of indeterminacy of an electron impulse we shall take advantage of the formula

$$\Delta k \approx 2\overline{\Delta W}/v_e , \tag{29}$$

where $\overline{\Delta W}$ is medial energy of perturbation, v_e is medial velocity of an electron.

Figuring as energy of perturbations $\overline{\Delta W}$ interaction of the relativistic electrons with quasi-phonons of the plasma ionic oscillations having frequency ω_p, medial energy of perturbations can be presented as:

$$\overline{\Delta W} = \hbar\omega_p = \hbar e\sqrt{n_i/(m_i\varepsilon_0)}, \tag{30}$$

where n_i is an ion concentration in the field of a monolayer, which is determined by a depth of penetration of positively ionized atoms in the vacuum volume, occupied with a magnetic field. The quantity n_i it may be determined under the formula [2]

$$n_i = 2p_g\Big/\sqrt{3kT_i m_i c^2} . \tag{31}$$

Taking into account (29), (30) and (31) it is gained from (28) length of coherence as

$$\Delta x \approx v_e\tau_{ev}\sqrt[4]{T_i/T_{ev}}\Big/\sqrt{p_g/p_a} , \tag{32}$$

where $T_{ev} = 1.1\cdot 10^4\ K$, p_a is atmospheric pressure, τ_{ev} is a constant determined by the formula:

$$\tau_{ev} = \frac{\sqrt[4]{3kT_{ev}m_i c^2}}{4e\sqrt{2p_a/(\varepsilon_0 m_i)}} = \frac{\sqrt[4]{3\cdot 1.38\cdot 10^{-23}\cdot 1.1\cdot 10^4\cdot 3.3\cdot 10^{-27}\left(3\cdot 10^8\right)^2}}{4\cdot 1.6\cdot 10^{-19}\sqrt{2\cdot 10^5/\left(8.85\cdot 10^{-12}\cdot 3.3\cdot 10^{-27}\right)}} \approx 6.4\cdot 10^{-11}\ s .$$

Knowledge of length Δx allows estimating time of screening of charges of nucleus τ_{scr} in TCV-layer:

$$\tau_{scr} \approx \Delta x/v_e . \tag{33}$$

This time of screening with the account (32) and (33) can be presented as:

$$\tau_{scr} \approx \tau_{ev}\sqrt[4]{T_i/T_{ev}}\Big/\sqrt{p_g/p_a} . \tag{34}$$

According to a relation (49) we have $\tau_{scr} \approx 6.4 \cdot 10^{-11} \sqrt[4]{1 \cdot 10^4 / 1.1 \cdot 10^4} \Big/ \sqrt{1} \approx 6.25 \cdot 10^{-11}\ s$.

Let's find now the size of screening of charges of nucleus in the TCV-layer. We apply for this purpose connection between the size of a wave length of the negative particle and its impulse, guessing, that the size of screening $\sim 2a_{e,\mu}$, Provided by the negative particles (electron or muon), it is interlinked to an impulse of the relevant particle $P_{e,\mu}$ relation:

$$\sim 2a_{e,\mu} = 2\hbar / P_{e,\mu}\ . \tag{35}$$

We shall receive the justification of this guess by comparison of investigations from this formula about earlier known effects at realization below in the given operation of calculation of the size of muonic screening.

Using interrelation of an impulse of the relativistic particle with the relevant kinetic energy, and using the normalized energies $\kappa_{e,\mu} = W_{e,\mu} / W_{0(e,\mu)}$, where $W_{0e} = m_e c^2$, $W_{0\mu} = m_\mu c^2$, m_μ - Mass of muon, from (35) it is gained the generalized formula for evaluation of the size of screening of charges of nucleus by the negative particles (electrons or muon):

$$\sim 2a_{e,\mu} = 2\lambda\!\!\!^{-}_{e,\mu} \Big/ \sqrt{\kappa_{e,\mu}^2 + 2\kappa_{e,\mu}}\ , \tag{36}$$

where $\lambda\!\!\!^{-}_{e,\mu} = \hbar / \left(m_{e,\mu} c\right)$ is a Compton wavelength of the relevant particle.

Applying the formula (36) to evaluation of the size of muonic screening, we shall note, that the normalized energy of a muon in atom of an isotope of hydrogen is equal to

$$\kappa_\mu = \alpha^2 / \left(2n^2\right), \tag{37}$$

where α is a fine structure constant, n is a main quantum number. Then from the formula (36) with the account (37) we gain the size of screening of charges of nucleus in a mesonic molecule of an isotope of hydrogen in the basic state ($n = 1$):

$$\sim 2a_\mu \approx 2\lambda\!\!\!^{-}_{\mu} / \alpha\ . \tag{38}$$

Evaluations under the formula (38) give result $\sim 2a_\mu \approx 2 \cdot 1.867 \cdot 10^{-15} / \left(1/137\right) \approx 5 \cdot 10^{-13}\ m$, which completely coincides with the known data for muonic screening. It forms the basis of use of a relation (36) for electronic screening.

The basic question of process of electronic screening in the TCV-layer is to provide high enough velocity of fusion reactions, as time of screening in the TCV-layer is restricted. Effective process is possible only under condition of

$$\lambda_f \geq 1 / \tau_{scr}\ , \tag{39}$$

where λ_f is fusion velocity.

For estimating of the key opportunity of fusion we shall find values of the normalized kinetic energies κ_{dde}, at which the relevant (39) velocity of fusion in pure deuterium dd. For this purpose we shall take advantage of that circumstance that velocity of fusion depends on the sizes of screening and if at the particular sizes this velocity is known at other sizes of screening this velocity may be found under the approximate formula:

$$\lambda_f \approx \left(\frac{\sim 2a_\mu}{\sim 2a_{dde}} \right)^3 \lambda_{dd\mu}, \tag{40}$$

where $\sim 2a_{dde}$ are desired values of the sizes of electronic screening at fusion pure deuterium dd, $\lambda_{dd\mu} = 4.3 \cdot 10^8 \ s^{-1}$ are velocities of fusion at muonic screening.

Radiating from the generalized formula (36) with the account (38), (39) and (40) we gain the requirement for the normalized kinetic energies of electrons κ_{dte} and κ_{dde}:

$$\kappa_{dde} \geq \sqrt{1 + \left(m_\mu / m_e\right)^2 \left(\alpha \Big/ \sqrt[3]{\tau_{scr} \lambda_{dd\mu}}\right)^2} - 1. \tag{41}$$

Substitutions of values of parameters in (41) we yield the following result:

$$\kappa_{dde} \geq \sqrt{1 + (207)^2 \left(137^{-1} \Big/ \sqrt[3]{6.25 \cdot 10^{-11} \cdot 4.3 \cdot 10^8}\right)^2} - 1 \approx 4.1. \tag{42}$$

It is uneasy to show, that in process of the continuous acceleration surveyed above electrons may get a kinetic energy $W_{em} \approx 2.1 \quad MeV$. It corresponds to the normalized energy $\kappa_{em} = W_{em} / W_0 = 2.1 / 0.51 \approx 4.1$ that meets the requirements (42). It allows drawing a deduction that nuclear fusion in TCV-layer is possible.

7. Estimation of nuclear fusion energy at electronic screening

On the basis of the shown opportunity of fusion in TCV-layer it is possible to assume that the direction, the bound with generating of TCV-layer at pulsing induction discharges through vortexes may be used for an explanation of physical processes in ball lightning and appears perspective for the purposes of energy generating by means of nuclear fusion in cold matter. Perhaps, in this case may take place coherent electron catalyzed fusion (*ce*-catalyzed fusion) surveyed in [7].

From the formal point of view we can say that if deuteron d are exposed on influence of coherent electrons ce, then virtual atom D_{ce} (like hydrogen) are created and decomposed:

$$d + ce \rightarrow D_{ce} \rightarrow d + ce. \tag{43}$$

This atom (43) can enter nuclear reaction of synthesis resulting in liberation of coherent electrons ce and the latter may carry out *ce*-catalyzed fusion in reactions:

$$\begin{aligned} d + ce + d \rightarrow D_{ce} + d \quad &\rightarrow \quad {}^3He + n + ce + 3.3MeV, \\ &\rightarrow \quad t + p + ce + 4.0MeV. \end{aligned} \tag{44}$$

When the energy of the *ce*-catalyzed fusion is estimated, let us pay attention to a substantial feature: a process of catalysis may take place in a volume of a layer with the thickness equal to the size of effective shielding which, according to the formula (36) makes

$$2a_e \approx 2\lambda\!\!\!^{-}_e / \kappa_e . \tag{45}$$

The volume of a zone of reaction in this case in view of a ratio (45) will make size

$$V = 4\pi^2 r_0 R_0 \cdot 2a_e = 8\pi^2 r_0 R_0 \lambda\!\!\!^{-}_e / \kappa . \tag{46}$$

The number of the nuclear responses occurring in unity of volume for a time unit is defined by expression [1]

$$g = n_1 n_2 \langle v_z \sigma \rangle , \tag{47}$$

where n_1 is a concentration of reacting nucleus of the first grade; n_2 is a concentration of reacting nucleus of the second grade; $\langle v\sigma \rangle$ is an average product of the relative velocity of nucleus in a band of response to effective section of response

A concentration of deuterons is determined by a formula:

$$n_1 = n_2 = \frac{p_g}{kT_i} \cdot \eta , \tag{48}$$

where T_i is deuterium temperature, k is Boltzmann′s constant, η is a coefficient of content of hydrogen mixture in a reaction zone (for natural conditions $\eta \approx 8 \cdot 10^{-3}$).

Effective section of response we shall spot with the account (45) as the area of a circle in radius $\sim 2a_e$:

$$\sigma = \pi (2a_e)^2 = 4\pi \lambda\!\!\!^{-2}_e / \kappa_e^2 . \tag{49}$$

Velocity of deuterons in a band of response we shall find from a relation

$$\frac{m_i v_z^2}{2} = \int_{a_e}^{\infty} \frac{1}{4\pi\varepsilon_0} \cdot \frac{e^2}{r^2} dr ,$$

from which follows, that

$$v_z = \sqrt{\frac{e^2}{2\pi\varepsilon_0 m_i a_e}} . \tag{50}$$

Here it is necessary to pay attention to feature of a viewed band of response. In an operative range of an electronic stratum the strong electric field therefore the electrostatic lens which magnification makes is presumably formed operates very much:

$$\Gamma = v_z^2 / v_T^2 , \tag{51}$$

where v_T is the thermal velocity determined under the formula

$$v_T = \sqrt{3kT_i / m_i} . \tag{52}$$

The power oozed at nuclear synthesis, according to viewed model will make quantity $N = Q_{dd} g V \Gamma$, which in view of formulas (45-52) may be spotted under formulas

$$N = C_N \cdot \frac{R_0 r_0 p_g^2 \eta^2}{T_i^3 \kappa_e^{3/2}}, \tag{53}$$

where Q_{dd} is an energy, extracted during the elementary action of reaction (44), and C_N is coefficient

$$C_N = \frac{16\pi^{3/2} Q_{dd} e^3 \lambda_e^{3/2}}{3k^3 \sqrt{2m_i} \varepsilon_0^{3/2}} = \frac{16\pi^{3/2} \cdot 6 \cdot 10^{-13} \cdot \left(1.6 \cdot 10^{-19}\right)^3 \cdot \left(3.86 \cdot 10^{-13}\right)^{3/2}}{3\left(1.38 \cdot 10^{-23}\right)^3 \sqrt{2 \cdot 3.3 \cdot 10^{-27}} \left(8.85 \cdot 10^{-12}\right)^{3/2}} \approx 3 \cdot 10^{12}, \quad \frac{WK^3}{m^2 Pa^2}. \tag{54}$$

Presumably surveyed type transmutation nucleus is possible in ball lightning. Therefore we shall carry out an estimation of power for a configuration with parameters:

$R_0 = 0.1, \quad m$; $r_0 = 0.02, \quad m$; $p_g = 1 \cdot 10^5, \quad Pa$; $\eta = 8 \cdot 10^{-3}$; $T_i = 2 \cdot 10^4, \quad K$; $\kappa_e = 4.1$.

Substitution of these parameters in the formula (53) with the account (54) gives result:

$$N = 3 \cdot 10^{12} \cdot \frac{0.1 \cdot 0.02 \cdot \left(1 \cdot 10^5\right)^2 \cdot \left(8 \cdot 10^{-3}\right)^2}{\left(2 \cdot 10^4\right)^3 (4.1)^{3/2}} \approx 58, \quad W.$$

If to use intensive cooling and to reduce temperature of ions up to quantity of the order $T_{icool} = 1000$ K the generated power according to the formula (54) will make $W_{cool} \approx 4.6 \cdot 10^5, \quad W$. It explains energetics of ball lightning at sharp cooling, for example in a keg with water.

Thus on the basis of the shown opportunity of fusion in TCV-layer it is possible to assume that the direction, the bound with generating of TCV-layer at pulsing induction discharges through vortexes may be used for an explanation of physical processes in ball lightning and appears perspective for the purposes of energy generating.

References

1. Artsimovich L.A. *Controlled Thermonuclear Reaction*, Gordon and Breach, New York, 1964.
2. Vlasov A. N. *Possible formation of a toroidal current layer during a spark discharge* // Sov. Phys. JETP **70** (2), (1990) ©American Institute of Physics. P. 259-262.
3. Semionov B. Yu. *Power electronics*. Moscow: SOLON-R. 2001. [In Russian].

4. Vlasov A.N. *Possible creation and stabilization of a rotating θ-pinch* [In Russian], Dept. of Electronics Rep. No. 10296, TsNii, 1986.
5. Rrall N.A., and Trivelpiece A.W., *Principle of plasma physics,* McGraw Hill, New York, 1973.
6. Meierovich B.E. // *J. Plasma Phys.*, 1983, V. 29. P. 361.
7. Vlasov A.N., *Bose-Einstein condensed electron-catalyzed fusion as a possible mechanism of the ball lightning energy supply* // *In Proceedings 6th International Symposium on Ball Lightning (ISBL-99), 23-25 August 1999*. Antwerp Belgium: University of Antwerp. 1999. P. 133.

FORM OF NUCLEAR FUSION IN SOLID CRYSTALS*

Norio Yabuuchi†

High Scientific Research Laboratory, Marunouchi 24-16,
Tsu, Mie, 514-0033, Japanr

Akito Takahashi

High Scientific Research Laboratory, Marunouchi 24-16,
Tsu, Mie, 514-0033, Japan

Abstract

We discuss the electron orbital coupling between atoms by conceiving the structure (form) of atoms when we discuss about molecular binding.
In other way, it is like Prof. Linus Pauling who studied the atomic bonds conceiving, for instance, regular tetrahedral structure of methane molecule. In the same analogy, we can not study nuclear fusion without conceiving the structure (form) of nuclei. We study nuclear fusions in this paper, based on the concept of regular polyhedral forms (structures) of nuclei. It is our Ansatz that nuclei exist in similar structures as structures of Pythagoras-Platonic polyhedrons in universe, molecules and atomic clusters. Furthermore, there exists in the universe the *form* of self-organization to arrange these materials (from large one to small one) into regular polyhedrons in realizing stars, molecules, atoms and elementary particles. The natural selection should not be by chance, but formation of matter is inevitable. As a physical mechanism of enhanced nuclear fusion under self-organization, *bosonization* of electrons was required to overcome the difficulties of barrier penetration and electronic condensation. The Ansatz could develop unexpectedly the physical mechanisms to conclude the occurrence of cold fusion by 100% probability.

1. Introduction

Meta-Physics Background

Our Ansatz to study nuclear fusion is of two philosophical themes: one is *form*, and the other is *analogy*. First we argue on *form* [1-4].

The Platonic *idea* of regular polyhedrons has been playing a great role as *form* of self-organization in real material formation, in various strata of material arrangements in eras from Greek meta-physics, European medieval philosophies, astronomy in the early modern age, modern chemistry and modern physics. Especially we will explain that the Platonic

* This work is supported by High Scientific Research Laboratory.

polyhedral form appears topologically in nuclear structures, and its form of self-organization is applicable to study the mechanism of nuclear fusion.

Plato initiated the *idea* in his literature "Timaeus" that fundamental structures of all things are made of 5 regular polyhedrons. Based on the *idea*, Johanes Kepler explained the structure of the solar system by the combination of regular polyhedrons. In modern chemistry, many text books describe explanations that many molecular chemists revealed regular polyhedral arrangements of many stable molecules[5]. Linus Pauling explained the structure of stable-state methane with regular tetrahedral arrangement of atoms with quantum-mechanical orbits. In 1997, Prof. Brack (Germany) reported the experimental finding[6] that atomic clusters with regular polyhedral structures were formed when he spouted metal gas, made by heated small metal piece, from a nozzle into vacuum. In the analogy to this experimental result, he discussed that atomic cluster would be arranged in regular polyhedral structures[6]; for example, atomic cluster of sodium (Na) condenses to regular icosahedron and aluminum (Al) does regular octahedron.

One (NY) of authors felt the necessity of study on geometrical arrangement of nuclear structure, before explaining nuclear fusion. He proposed[7] that nuclear structures should be with Platonic polyhedrons, in the meta-physical analogy to the regular polyhedral structures for the solar system and the molecular systems. This is based on the *analogical ontology* by Aristotle. Yabuuchi considered first internally or externally touched regular polyhedrons with a sphere, put proton and neutron alternately on vertexes of each polyhedron and succeeded to explain atomic numbers and masses of nuclei. In this concept, ^{4}He is of regular tetrahedron. The nucleus of ^{16}O is made of regular tetrahedron
Inscribed and icosahedrons circumscribed with sphere of concentric circle . The nucleus of ^{40}Ca is of outer icosahedron, middle cube, outer icosahedron and outermost dodecahedron. For larger nuclei, he proposed horizontal chain of combinations by T(tetrahedron), O(octahedron), C(cube), I(icoshedron) and D(dodecahedron). The nucleus of ^{60}Ni is written by (C,D)(T)(C,D). The nucleus of ^{118}Sn is of (T,C,O,I,D)(T,C,O)(T,C,O,I,D). The ^{208}Pb nucleus is of (T,C,O,I,D)(C)(I,D)(C,D)(I,D)(C)(T,C,O,I,D). And these regular polyhedral structures contain magic numbers 2, 8, 20, 28, 50, 82 and 126 of nuclear shell structure. And nuclear-chemical explanation for fission yield ratios was successful; ^{238}U is of (C,O,I,D)(T)(C,O,I,D)!(C,O,I,D)(C,O,I,D)(T)(C,O,I,D), with neutron and proton composition of (23n,23p)(4n)(23n,23p)!(46n)(23n,23p)(4n)(23n,23p) where second fractions from both ends and the central fraction are made of purely neutrons. Since neutron and proton holds in a row vector with different propagation waves, there are no such states of all neutrons simultaneously, and neighboring peaks and valleys of waves for neutrons and protons are attracting (he assumed so). It was speculated that scission happens at a point of exclamation mark to produce mass=96 and mass=140 fission fragments and two neutrons (Fig.1). Thus, he proposed that helium-4 was regular tetrahedron, beryllium-8 was cube, and lithium-6 was regular octahedron[8]. Recently, researchers in France and Poland confirmed the existence of tetrahedral and octahedral nuclei in nuclear reaction experiments of rare earth nuclei[9]. In the same analogy, one (NY) of authors tried explanation on Iwamura's transmutation[10] in the ICCF12 meeting. However, no steady neutron or proton state exits in nucleus and he assumed geometrical structures at arbitrary moment. We need further study based on physical mechanisms, compared with experimental results.

Apart from the regular polyhedral forms of Platonic geometries, argued above, Aristotle conceived, as he made great influence to Hegel, that *form* in not merely structural situation, but it is the force to self-organize real existence of an individual. W. Heisenberg succeeded this idea in his universal equation. The philosophical concept of formation for real existence by *form* and *material* is not very new idea, but Heisenberg, Weizsaecker, Yabuuchi, and

others have used it frequently. In the past, Yabuuchi tried to apply the concept to geometrical structures of nuclei, and extended analogically to nuclear fusion. In this paper, we first extend meta-physics and then try to explain nuclear physics mechanism of fusion reactions.

Now, we argue on the *analogy*. The analogy means that existences in different strata are not completely different, although appearances are different, but there is mutual similarity in the forms of existence. According to the Platonic polyhedral structures, (discussing in this paper, as Kepler's planet by Platonic regular polyhedrons, molecular polyhedrons, Brack's polyhedral clusters and nuclear polyhedral structure in this paper) , all are regular polyhedrons but not same polyhedrons which are existing with correspondent formations. However, these structural formations are appearing in *analogy*. In the present case of nuclear fusion study, similarity in Platonic structures appears in condensation processes both in the external region of nuclear strong interaction and in the internal region of strong force, but transformation in *forms* happens.

In the case of atomic physics, Schroedinger's wave function plays a role of *form* for realizing an individual. Based on the meta-physical concept , we expand spherical atomic wave function in Schroedinger equation to select quantum number in order to correspond the wave form, and putting Pauli's principle to electrons as materials we realize self-organization of atoms as predicted by the periodical table in chemistry. According to Heisenberg, elementary particles are also self-organized from raw materials to various elementary particles, through the *forms* of waves. The *form* of nuclei is not the same one as those of atoms and elementary particles. However, there exists *analogy* in self-organization. For instance, we conceive that when helium and lithium nuclei are formed by fusion the self-organization for new nucleus appears, by the form of wave toward Platonic regular polyhedron, to make fusion with nucleons as *materials*. We start our discussions from hydrogen (deuterium) loaded metals since the condensed matter nuclear science emerged from experiments with H/D loaded metals.

2. Condensation Process in Coulombic Interaction

2.1 Condensation Process in the region out of strong interaction

We are going to show a Gedanken Experiment that 4 deuterium atoms in metal are transformed to a combination of 4 deuterons and 4 electrons in Cooper pair formation and condense to make 4D fusion associating with two He-4-particles emission by 100% probability. We conceive that deuteron wave functionsΨ_{t1}, Ψ_{t2}, Ψ_{t3}, Ψ_{t4} and Cooper pairs make regular tetrahedral arrangements in lattice to form a TSC (tetrahedral symmetric condensate) with double tetrahedral arrangement under orthogonal coupling. This double tetrahedral combination makes a cube (regular hexahedron) to induce a large condensation forces between 4 deuterons with electron-Cooper pairs[12].

2.2 Screening of d-d Coulombic repulsion by electron bosonization

According to molecular chemistry, methane with regular tetrahedral arrangement has low ground state energy and molecules are easy to condense. In the analogy, ^{4}He nucleus has similar tetrahedral structure with two neutrons and two protons. Deuteron is a boson and combines shortly with an electron to make a charge-neutral deuterium atom D. By collision, two deuterium-atoms combine to make a D_2 molecule with 74.1 pm d-d distance and its d-d fusion rate is on the order of 10^{-66} fusion/s/pair[12] to be negligibly small. It is known that when electron is replaced with a heavy fermion, namely muonic dd molecule has diminished d-d distance to be about 650 fm to make 100% d-d fusion in 200 ps. In analogy, if we have

diminished d-d distance by the condensation force of TSC (tetrahedral symmetric condensate) with the double Platonic symmetry of tetrahedron of 4 deuterons and bosonized electron pairs by combination of anti-parallel spins. See Fig.1, of Reference 12.
When there happens a cubic structure of 4 deuterons and 4 electrons (es+, es-, es+, es-) in PdD lattice, a regular tetrahedron of 4 deuterons and a regular tetrahedron of 4 electrons can combine orthogonally to make a cubic entity with total charge neutrality with all bosonized particles of double Platonic symmetry. Here s+ and s- denote spin. If we replace a bosonized electron pair with a single pseudo-particle of e*(2,2), d-d distance will diminish, according to our EQPET calculation[12)], to be 21.8 pm, the value of which is equivalent to that for mass-10 heavy fermion dd molecule, dde*(10,1). By our analysis with HMEQPET (Heavy Mass Electronic Quasi-Particle Expansion Theory) calculation [12)], muonic d-d molecule has d-d distance of 0.805pm which induce very high d-d fusion rate of the order of 10^{10} f/s/pair (namely about 100% fusion break-up in 200 ps). Analogously, our TSC Langevin calculation for molecular dynamics condensation motion of TSC gave 0.020 pm minimum d-d distance in the final condensation stage of about $2x10^{-20}$ s time interval with very high 4D fusion rate of the order of 10^{21} 4d-fusion/tsc/s (namely almost 100% 4d fusion break-up in $2x10^{-20}$ s of the time interval of final stage condensation)[12)]. Namely, 4D fusion yield is 100% per 4D/TSC generation and condensation (see Eqs.(35-39) in Section 6 of Reference 12). By 4D fusion, we conceive an intermediate compound state ^{8}Be*. Total TSC condensation time was calculated to be 1.4 fs, according to our standard model for the TSC condensation motion using non-linear Langevin equation. The great condensation force of TSC under Platonic symmetry may realize clean 4D fusion with high efficiency in low deuteron energy systems formed in condensed matter at room temperature.

2.3 Form in strong interaction

In the stage of strong interaction making 4d fusion (and with minor 2d fusion, 3d fusion, possibly), regular tetrahedron (or other regular polyhedron) can arrange largest number of particles in a unit volume to fill the regular polyhedron space. This means that regular polyhedral arrangement can condense nucleons with maximum efficiency to attain total energy minimum state of the system. Therefore, deuteron cluster condenses toward the regular polyhedral arrangement, according to Kepler's fill-up theory, to result in dominant 4D fusion.

From other point of view, sticking surface area between nucleons existing in the strong interaction range becomes maximum for regular tetrahedral and cubic arrangement. Since strong nuclear force is of very short range boson (charged pion) exchange force with about 2 fm range, the larger is the surface sticking area, the lager strong interaction is induced. Especially, the regular tetrahedral arrangement of 4 nucleons (namely alpha-cluster) realizes large binding force and induce stable α-cluster structure in larger nucleus.

Centripetal force works in atom system (positive nucleus plus negative electron). However, fusion of nucleons in deuterons by condensation is driven by ribbon-field force. In the case of atom, central proton with heavier mass and plus charge at center of spherical system makes a centripetal (attractive) force to negative electron. On the other way, ribbon force of strong interaction drives nucleons toward 4 vertexes of regular tetrahedron inside the internally touched sphere, with diminishing total size to smaller alpha-cluster, which is similar force when we tighten belt of trousers.

3. Condensation Process in the Strong Force Range

As physics will not be established only by experimental facts, we will extend recognition in space-time of Schroedinger equation.

3.1 Expansion of form Ψ by Schroedinger equation and fusion

First we describe about formed state and *form* Ψ for self-organization action. Here we pick up well-used formed states as regular tetrahedron to be ^{4}He and cube to be ^{8}Be* (compound excited state). The form Ψ which self-organizes to these formed states is illustrated by using Schroedinger presentation. Essentially, Schroedinger equation is written as EΨ=HΨ. Namely there are raw material E and its content H, and Ψ for self-organizing E and H. Therefore, by reflecting the Platonic symmetry in formed state of Ψ, eigenvalue E and operator H are defined. In classical mechanics, H depicts kinetic energy and position energy. In quantum mechanics, E and H depict not only particle itself, but also operator for mixed wave-functioned kinetics and position energy for self-organizing elements of wave *form* Ψ. According to Heisenberg's words, *formed* (wave-functioned) *materials* (fields of electrons and nucleons) are there. Mathematician Tetsu Toyama explained it as *acting quanta*.
Schroedinger equation for N nucleons is;

$$i\hbar\frac{\partial\Psi}{\partial t}=\left[\sum_{j=1}^{N}H(q_j)+\sum_{j\neq k}^{M}W(q_j,q_k)\right]\Psi \quad (1)$$

$$H(q_j)=(\hbar^2/2m)\nabla_j^2+U(q_j)$$

Helium-4 is shown in Fig.2. The compound excited state ^{8}Be* by 4D fusion is shown in Fig.3. By imaging these figures, we extend discussions.

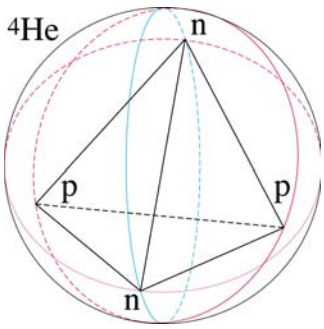

Figure 1. *Tetrahedral structure of helium*

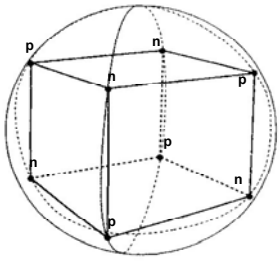

$_{8}$Be

Figure2. *Cubic structure of beryllium-8 as intermediate state*

As already discussed, 4 deuteron-atoms in TSC makes a regular tetrahedron of 4 deuterons, and mutual condensation force works between surrounding two bosonized electron pairs (two Cooper-like pairs). This double Platonic configuration provides media of self-organization to deuteron-cluster fusion. The wave function of four deuterons with tetrahedral form is written by,

$$\Psi_T = \Psi_T\,(q_{n_1 l_1 m_1 s_1}, q_{n_2 l_2 m_2 s_2}, o, o, t) \qquad (2)$$

Here T denotes tetrahedral, q is for nucleon positions and n,l,m,s are 4 kinds of quantum numbers.

Wave function which includes protons and neutrons at arbitrary time t_i is,

$$\Psi_{T1} = \Psi_{T1}(q_1 s\tfrac{1}{2}, q_2 s\tfrac{1}{2}, o, o, t_i),$$

$$\Psi_{T2} = (o, o, q_3 s{-}\tfrac{1}{2}, q_4 s{-}\tfrac{1}{2}, t_i) \qquad (3)$$

There are two wave functions for deuterons as given in Eq.(3). Here, q_1,q_3 denotes protons and q_2 and q_4 denotes neutrons. When 4D will condense into the final stage of condensation (TSC-min state) under the condition of bosonized 4 electrons, strong sticking force by nuclear fusion among 4 deuterons work by exchanging gauge charged bosons (pions) to create much diminished size compound nucleus ^{8}Be* and due to broken charge-neutrality, bosonized electrons will have to deviate from original orbits of condensed TSC to be scattered outward. There happens transition of regular tetrahedral arrangement from double tetrahedral arrangement of "dedededе" system (see Fig.1-1) of Reference-12) to two pairs of 2d systems, each of which acts toward the tetrahedral nuclear arrangement of ^{4}He (alpha-cluster). Consequently, two ^{4}He will be produced from ^{8}Be* of 4D fusion. Here, we can say that new condensation force by strong interaction works there by transformed form to the relation between 2 n and 2p for each of two 2d clusters. Here, same *analogy of form* holds keeping

tetrahedral symmetry, although exchange force field is changed from Coulombic force to nuclear force.
The process is written with wave functions, for guiding Ψ_{T1} andΨ_{T2} to form ^{4}He having tetrahedral form. For instance, acceptor operation of Ψ works for q_3 and q_4 of counter wave functions, respectively. This exchange is analogous to the chemical reactions with donors and acceptors. This self-organizing force of regular tetrahedron is written by,

$$\Psi_{T1+2} = a^*a^*\Psi_{T1}(q_1S\tfrac{1}{2}, q_2S\tfrac{1}{2}, o, o, t_i) + aa\Psi_{T2}(o, o, q_3S\text{-}\tfrac{1}{2}, q_4S\text{-}\tfrac{1}{2}, t_i) = \Psi_{T1+2}(q_1S\tfrac{1}{2}, q_2S\tfrac{1}{2}, q_3S\text{-}\tfrac{1}{2}, q_4S\text{-}\tfrac{1}{2}, t_i) \quad (4)$$

a * is acceptor operator and a is donor operator.

In this transition motion, condensation force by form works to form excited helium like nucleus, as shown in Fig.3.

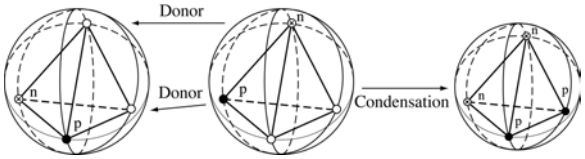

Figure 3. *Process by which two deuterium nuclei condense into a helium nucleus*

Polyhedral ^{4}He being produced by fusion is written by,

$$i\hbar\frac{\partial\Psi_{T1+2}}{\partial t} = \left\{\sum_{j=1}^{4}H_{(qj)} + \sum_{j\neq k}^{6}W_{(qj,\,qk)}\right\}\Psi_{T1+2} \quad (5)$$

$$H(qj) = \hbar^2\Delta_j^2/2m + U(qj) \qquad (Ex = 23.8\ MeV)$$

Referring Eq.(3), and using same expansion for q_3 and q_4, we get the following equation,

$$\Psi_{T3+4} = \Psi_{T3+4}(q_5S\tfrac{1}{2}, q_6S\,\tfrac{1}{2}, q_7S\text{-}\tfrac{1}{2}, q_8S\text{-}\tfrac{1}{2}, t_i) \qquad (x = 23.8\ MeV) \qquad (6)$$

However, as ^{4}He states in Eq.(4) and Eq.(6) are excited states, fusion product becomes a cubic ^{8}Be* with high excitation energy. In analogy to the process that deuterons fuse to ^{4}He, ^{4}He nuclei are going to fuse to ^{8}Be and wave functions are given as,

$$\Psi_{C1} = \Psi_{C1}(q_1S\tfrac{1}{2}, q_2S\tfrac{1}{2}, q_3S\text{-}\tfrac{1}{2}, q_4S\text{-}\tfrac{1}{2}, o, o, o, o, t_i) \quad (7)$$

$$\Psi_{C2} = \Psi_{C2}(o, o, o, o, q_5S\tfrac{1}{2}, q_6S\tfrac{1}{2}, q_7S\text{-}\tfrac{1}{2}, q_8S\text{-}\tfrac{1}{2}, t_i) \quad (8)$$

By using donor-acceptor operation, fusion going to a cubic ^{8}Be* is given by,

Ψ_{C1+2}= a*a* a*a*Ψc1 ($q_1S^{1}/_{2}$, $q_2S^{1}/_{2}$, $q_3S^{-1}/_{2}$, $q_4S^{-1}/_{2}$, o, o, o, o, t) + a a a aΨc2 (o, o, o, o, $q_5S^{1}/_{2}$, $q_6S^{1}/_{2}$, $q_7S^{-1}/_{2}$, $q_8S^{-1}/_{2}$, t_i) $= \Psi_{C1+2}(q_1So, q_2So, q_3So, q_4So, q_5So, q_6So, q_7So, q_8So, t_i)$ (9)

Ex = 47.6 MeV

Rewriting it using Schroedinger equation,

$$i\hbar\frac{\partial\Psi_{C1+2}}{\partial t}=[\sum_{j=1}^{8}H(q_j)+\sum_{j\neq k}^{12}W(q_j,q_k)]\Psi_{C1+2} \quad ,$$

$$H(q_j)=\hbar^2\nabla_j^2/(2m)+U(q_j) \tag{10}$$

Then ^{8}Be* as collectively excited cluster of two alpha-particles makes very quick transition to break-up of two ^{4}He particles.

$\Psi_{C1+2}\rightarrow\Psi_{T1+2}+\Psi_{T3+4}=$ Ψ_{T1+2} ($q_1S^{1}/_{2}$, $q_2S^{1}/_{2}$, $q_3S^{-1}/_{2}$, $q_4S^{-1}/_{2}$, t_i)
$+\Psi_{3+4}$ ($q_5S^{1}/_{2}$, $q_6S^{1}/_{2}$, $q_7S^{-1}/_{2}$, $q_8S^{-1}/_{2}$, t_i) (11)

For ^{4}He, kinetic energy is 23.8 MeV.

This is rewritten by Schroedinger equation by, (same as Eq.(5)),

$$i\hbar\frac{\partial\Psi_{T1+2}}{\partial t}=\left\{\sum_{j=1}^{4}H_{(qj)}+\sum_{j\neq k}^{6}W_{(qj,\,qk)}\right\}\Psi_{T1+2}$$

$$H_{(qj)}=\hbar^2\Delta_j^2/2_m+U_{(qj)} \tag{12}$$

3.2 Realization of Low Energy Fusion with Regular Tetrahedral Helium

As discussed in the previous section, absorbed deuterons in Pd-metal are trapped in crystal lattice or condensed in vacuum volumes of cracks, and induce further cluster condensation like TSC. In the final condensation stage of TSC, Kepler's fill-up law is satisfied to realize very large contact surface of pion-exchange force of strong interaction, and its activated form of wave function Ψ arranges 4 deuterons to form ^{4}He nuclei which are self-organized by donor and acceptor operation for neutrons and protons. However, due to the highly excited state (47.6 MeV, excited energy) of ^{8}Be* compound state, two self-organized ^{4}He clusters (α clusters) with wave function Ψ make further self-organization to ^{8}Be* state. With short life time (less than 1 fs), ^{8}Be* goes back (breaks up) to original two α-particles, namely transformed to stable helium-4 with magic number (2,2).

3.3 Initial Conditions in Metal and Fusion in Liquid Crystal State

Nature is akin to "dislike" vacuum and tries to fill up vacuum with matter. Therefore, there happens a trend of condensation of matter getting together in vacuum. In a self-analogy, gas molecules in denser region get together in "vacuum" to condense in phenomenon of Typhoon or Hurricane. In the higher temperature zone of atmosphere, gas density is diluted to drop pressure and approach to vacuum. In analogy, local temperature rise in metal by electric current will cause density difference in metal to generate vacuum-like holes in metal, where

deuterons with bosonized electrons are arranged to TSC and condense toward the central low density hole; we may conceive so. As minor final state interaction, TSC may produce so highly excited ^{4}He*, that due to its reaction an liquid crystal like ^{4}He with larger nuclear radius will be born to diverse its high excited energy to emitted particles. As is the case of uranium fission with fast neutrons which decrease fission rate, we need to consider the way to control 4D fusion rate in low reaction level. Anyway, technical ways to realize initiation conditions for condensation are of key for application to nuclear energy engineering.

4. Transmutation and Regular Polyhedral Structures

According to the work by Dr. Brack, all atomic clusters in vacuum make condensed forms in regular tetrahedrons. In analogy, the same form appears for nuclei. In a view of meta-physics, all nuclei are looking for stable states, namely wave function as *form* drives nuclei toward more stable states through nuclear fusion or fission reactions via the donor and acceptor interaction. From such consideration, one can conceive that unstable nuclei transform to stable state with regular polyhedral structures. In that case, nuclear transmutation happens through the nearest path to stable nuclei. Namely, wave function Ψ as *form* induces transmutation to stable isotopes via donor-fission or acceptor-fusion.

4.1 Transmutation via Condensed Acceptor is Fusion

When total number of nucleons is smaller than the total number of vertexes of regular polyhedron, wave function of self-organization plays a role of acceptor for fusion by filling nucleons onto vertexes of stable regular polyhedral structure. For example, fusion type transmutation happens in Iwamura experiments[10], since there are dominant acceptor-type condensation. The 3D (D+2D) reaction has 6 nucleons participated. The intermediate compound nucleus goes likely to ^{6}Li* which is supposed to be in octahedral arrangement (structure)[11]. However, ^{6}Li* is highly excited state and breaks up to t + ^{3}He + 9.5 MeV as one of main out-going channels. Tritium may accept one proton from deuteron to transform to ^{4}He.

4.2 Transmutation via Evaporating-Donor is Fission

As argued in Introduction, all nuclear structure may be described with combination of regular polyhedral structures. When total number of nucleons in nucleus is larger than the total number of vertexes of regular polyhedral structures, fission happens to emit nucleons toward stable regular polyhedral structures. Namely, transmutation takes place by donate nucleons to acceptor nuclei. Since total number of vertexes for regular polyhedral structures (Platonic structures) is always even number, the reason that odd mass nuclei may make more easily fission than even mass nuclei.

5. Conclusion

Fusion is the phenomenon that more than two nuclei fuse into one to transform excess *material* to energy. In other words, to diminish more materials to less materials transforms excess materials to free (kinetic) energy. In the diminishment of materials, thermo-nuclear fusion employs external means of atomic bomb or TOKAMAK type confinement for collision

processes. However, in a view of Boltzmann's thermo-dynamics, the more kinetic energy is put into material of particles, the more expansion happens against condensation. By this reason, thermo-nuclear fusion has difficult domain to escape, since the idea is against the law of materials. In contrast, cold fusion (condensed matter fusion) employs the way to condense materials by suppressing (screening or shielding) potential energy, that follows to the nature, to be able to realize clean fusion (^{4}He ash) with 100% yield per TSC generation according to our latest study[12].

The phenomenon of super-fluid of helium appears by *bosonized condensation* via phase transition from gas to liquid by decreasing temperature with cryogenic techniques. Water molecules condense to form regular polyhedral structures (tetrahedrons) by phase transition from liquid to solid (ice crystal). To realize self-sustainable systems on our planet, by overcoming with the global warming problem, is recognized to be appropriate way. We need some advanced clean energy sources as "condensed matter fusion" as studied by metal-physical Gedanken experiments in this work.

We hope new nuclear technology will emerge soon by the principle.

6 **References:**

1) Werner Heisenberg: *Physics and Philosophy*, Harper & Row, New York, 1958
2) C. F. Weizsaecker: *Die Einheit der Natur*, Carl Hanser Verlag, 1971
3)Ervin Schrodinger; MEIN LEBEN MEINE WELTA NSICHT Wien /Hamburg 1985
4) Norio Yabuuchi: *Meta Physics Founded on Atomic Physics*, Toshi-Kogyo Co., 1977
5) Brian C.Webster: *Chemical Bonding Theory,* (translation in Japanese) 1990
6) M. Brack: Metal clusters and magic numbers, *Sci.Am. (*1997)
7) W. Green: *Cold Fusion* 13 (1995)28-29
8) 1995Annual Meeting of the Atomic Energy Society of Japan –G8)
9) J. Dudek, et al: Island of Rare Earth Nuclei with Tetrahedral and Octahedral Symmetries : Possible Experimental Evidence, Phy.Rev.Lett.97,(2006) 072501
10) Norio Tabuuchi: Condensed Matter Nuclear Science., Proc. ICCF12, World Scietific Publ., (2006)564-570
11) Norio Yabuuchi: Trans. 1995 Annual Meeting of the Atomic Energy Society of Japan-G8The structure of nucleus and thermo nuclear fusion within solid)
12) A. Takahashi, N. Yabuuchi: Study on 4D/TSC condensation motion by non-linear Langevin Equation, submitted to Proc. New Energy Technologies, American Chemical Society, March, 2007, USA (to be published from Oxford Univ. Press)

ICCF-13 Participants List

Full name	Affiliation, position	Mail address	Tel/Fax	e-mail
Afonichev Vladimir	Research institute of Superplastic Metals, Russian Academy of Sciences, Senior Researcher	Apt. 78, 43/4 October Ave., city of Ufa, 450059, Russia	(7)3472253759	afon@imsp.mail.ru
Armanet Nicolas	Faculte des Scienceo de Lumini (Marseille), Research Assistant	Chambre 169-Bat E 171, Av. De Luminy, case 905, 13288 Marseille 9, France	(33)627411369	armanetnicolas@hotmail.com
Aubrice Shantal	LCD-SOLUTION s.a.r.l.	19, rue des Pruniers, F-57150 Creutzwald, France	(33)387827679	aubrice@lcd-solution.com
Bakumtsev Nikolay	International Foundation "Revision of Natural Sciences", President Volgodonsk Branch of Nuclear Society of Russia	P.O.B. 1264, Volgodonsk-20, Rostov Region, 347380, Russia	(7)8639265484	bakumtsev@vdonsk.ru
Bakumtseva Tatiana	International Foundation "Revision of Natural Sciences", Scientific Secretary	P.O.B. 1264, Volgodonsk-20, Rostov Region, 347380,Russia	(7)8639265484	bakumtseva@vdonsk.ru
Baranov Dmitri	Research Institute of High Temperatures, Russian Academy of Sciences, Leading Researcher	Apt. 8, 12 Tokarnaya st., Moscow, 107564, Russia	(7)9161385165	baranov@rambler.ru
Baranova Elena	Institute of High Temperatures, Russian Academy of Sciences	Apt. 8, 12 Tokarnaya st., Moscow, 107564, Russia	(7)9161385165	baranov@rambler.ru
Bazhutov Yuri	Pushkov Institute of Terrestrial Magnetism, Ionosphere & Radiowave Propagation, Russian Academy of Sciences, Town of Troitsk, Moscow region, Senior Researcher	Apt.129, 11 Bratislavskaya st., Moscow,109451, Russia	(7)4953340925 (7)4953340124	erzion@mail.ru bazhutov@izmiran.ru

Bychkov Vladimir	Moscow State University, Leading Research Scientist	apt.382, 24 Dm. Ulyanov Str., Moscow, 117036, Russia	(7)4951243036	bychvl@orc.ru
Bychkova Natalja	Scientific Foundation "Ball Lightning", Director, Moscow	apt.382, 24 Dm. Ulyanov Str., Moscow, 117036, Russia	(7)4951243036	bychvl@orc.ru
Castagna Emanuele	Universita' di Roma "La Sapienza", departimento di Energetica; ENEA C.R. Frascati	Via Enrico Fermi 45, 00044 Frascati (Rome)-Italy; Via Ponte Massorano 9, 00049 velletri, Rome, Italy	(39)3493765372 (39)0694009465	Emanuele.castagna@uniroma1.it
Celani Francesco	Instituto Nazionale Fisica Nucleare Lab. Naz. Frascati	INFN-LNF Via E.Fermi 40, 00044 Frascati Roma, Italy	(39)0694032201 (39)0694032548	francesco.celani@lnf.infn.it
Chernov Ivan	Tomsk Polytechnic University, Russia	apt.15, 15 Studencheskaya st., city of Tomsk, 634034, Russia	(7)3822418723	chernov@tpu.ru
Chubb Scott	Infinite Energy Magazine, Research Systems, Inc., USA; Naval Research Lab., Coastal and Ocean remote Sensing Branch, remote Sensing Division, Research Physicist	9035 Frederick st.,#6, Arlington, VA 22204, USA; Washington, DC 20375-5351	(1)2027675270 (1)3019755015 (1)5719704959	chubbscott@aol.com scott.chubb@nrl.navy.net
Chung David	Howard University, Physical Department, (Retired)	10508 Montrose, Ave. Rm.203 Bethesda, MD, 20814, USA	(1)3018979575	dchung@howard.edu
Clauzon Pierre	C.N.A.M. (Paris)	11 Rue Georges Bizet, 92330, Sceaux, France	(33)140272420 (33)146600605	Pierre.clauzon@wanadoo.fr

Collis William	ISCMNS, Hon. Secretary	Strada Sottopiazzo 18, 14055, Bogliatto, (AT), Italy	(39)0141968602	mr.collies@physics.org secretary@iscmns.org
Dash John	Portland State University, Physics Dept., Portland, USA Prof. Emeritus	313 N.Holman Str., Portland, OR, 97217, USA	(1)5037254222	dashj@pdx.edu
El-Boher Arie	Omer Energetics Technologies, Researcher	P.O.B. 3026, Omer Industrial Park, Israel	(972)86901114	arik@energetics.co.il
Fisher John	Physicist	600 Arbol Verde, Carpinteria, CA, 93013, USA	(1)8056841465	jcfisher@fisherstone.com
Fukuhara Mikio	Tohoku University, Laboratory of Nuclear Science, Mikamine 1-2-1, Taihaku, Sendai 982-0826, Japan	1-206, Tomisawa-Shukusha, 3T1,Mikamine, Taihaku, Sendai, 982-0826 Japan	(81)222152492	fukuhara@imr.tohoku.ac.jp
Gareev Fangil	Joint Institute of Nuclear Research, Lab. Of Theoretical Physics	JINR, town of Dubna, Moscow region, 141980, Russia	(7)4962165732	gareev@thsuni.jinr.ru
Godfrey Alison	Energetics Technologies, CEO, Co-owner	7 Fieldview Lane, Califon, NJ, 07830, USA	(1)9084399500	alison@energeticstechnologies.com
Goryachev Igor	Russian Research Center “Kurchatov Institute” Research Director Institute of High Technologies	1 Kurchatov sq. Moscow, 123182, Russia	(7)4991969476 (7)9104646101	goryachev@ivtem.kiae.ru goryachev37@mail.ru
Goryacheva Irina	Russian Research Center “Kurchatov Institute», Reviewer	apt.50, 15 Peschanaya st., Moscow, 125057, Russia	(7)4991987568	goryachev@ivtem.kiae.ru goryachev37@mail.ru

Greenspan Ehud	Omer Energetics Technologies, Researcher Dept. of Nuclear Engineering, Barkley University, USA	P.O.B. 3026, Omer Industrial Park, Israel	(972)86901114	gehud@uuc.berkeley.edu
Hioki Tatsumi	Energy-Conversion-Domain Frontier Research Center, TOYOTA Central, R&D Labs., Inc., Principal Researcher	Nagakute, Aichi-gun, Aichi-ken, 480-1192, Japan 1-4-24 Haruoka Chikusa-ku, Nagoya, 464-0848, Japan	(81)561717109 (81)527517515	hioki@mosk.tytlabs.jp
Karabut Alexander	SIA “LUTCH” Town of Podolsk, Moscow region, Russia Senior Researcher	apt.54, 13 Belaya Dacha, Kotelniky, Moscow region, Russia	(7)4955508129	7850.g23@g23.relcom.ru
Kasagi Jirohta	Tohoku University, Laboratory of Nuclear Science, Mikamine 1-2-1, Taihaku, Sendai 982-0826, Japan	Nachigaoka 4-11-4, Natori, Mivagi 981-1244, Japan	(81)227433420	kasagi@lns.tohoku.ac.jp
Kholodov Leonid	V.Barmin Design Bureau of General Machinery, Head Engineer	apt.11, bld.2, 16 Energeticheskaya st., Moscow, 111116, Russia	(7)4953625238	---
Kirkinskiy Vitaliy	Institute of Geology and Mineralogy, Siberian Branch Russian Academy of Sciences. Head researcher	44 Termikova st., apt.8 Novosibirsk, 630090, Russian Federation	(7)(383)3301503	kirkinsk@uiggm.nsc.ru

Koldomasov Alexander	Retired engineer	apt.25, 9 Molodezhnaya str., Town of Volgodonsk, Rostov region., Russia	(7)0843649483	----
Kornilova Alla	Moscow State University, Dept of Physics	Moscow State University, Dept of Physics, Moscow, Russia	(7)4959392391 (7)4959391313	prfnart@mail.ru
Kozima Hideo	Cold Fusion Research Laboratory	597-16 Yatsu, Aoi, Shizuoka 421-1202, Japan	(81)05011302376	hjrfq930@ybb.ne.jp cf-lab.kozima@pdx.edu
Krakov Vitaliy	Omer Energetics Technologies, Project manager	Omer Industrial Park, P.O.B. 3026 Haruv str., 9/6, Arad, 89055, Israel	(972)89959543 (972)86901114	vkrakov@energetics.co.il
Krivit Steven	New Energy Times Magazine, Editor	369-B Third Street, #556, San Rafael, CA, 94901, USA	(1)3107215919	steven1@newenergytimes.com
Laptev Yuri	Russian Peoples Friendship University, Dept. of Physics, Post graduate student; Moscow State Technical University, Dept of Physics, assistant tutor	6 Miklukho-Maklai str., 117198, Moscow, Russia		yplaptev@rambler.ru
Lipson Andrei	Research Institute of Physical Chemistry, Russian Academy of Sciences	31 Leninski Ave., 117915, Moscow, Russia	(7)4959554645	lipson@lmm.phyche.msk.ru
Macy Marianne	Infinite Energy Magazine	Apt. 3C, 440 West 24th St., New York, NY 10011, USA	(1)2127273816	mariannemacy@verizon.net

McKubre Michael	Energy Research SRI, Director	112 Durham St., Menlo Park, CA 94025, USA	(1)6505370516	mchael.mckubre@sri.com
Melich Michael	Naval Postgraduate School, Professor, Monterey, CA, USA	1224 Meigs Drive, Niceville, FL 32578-3018, USA	(1)8507291873 (1)8507293292	melich@alumni.rice.edu mmelich1@earthlink.net
Mobberley Peter	Advanced Energy Technologies, Director, Kidderminster, England	The Willows, Sladd Lane, Wolverley, Kidderminster, DY11 5ST, UK	(44)1562852622 (44)1562852753	petermobberley@hotmail.com
Mobberley Susan	Advanced Energy Technologies, Director, Kidderminster, England	The Willows, Sladd Lane, Wolverley, Kidderminster, DY11 5ST, UK	(44)1562852622 (44)1562852753	petermobberley@hotmail.com
Mozzhegorov Andrei	Center of Information Technologies, "Kubanecologia" Co, Ltd., Krasnodar region, Executive director	City of Armavir, Krasnodar region, Russia	(7)861559577 (7)9182148614	mozzhegorov@mail.ru
Motohiro Tomoyoshi	Energy-Conversion-Domain Frontier Research Center, TOYOTA Central, R&D Labs., Inc., Senior Fellow	Nagakute, Aichi-gun, Aichi-ken, 480-1192, Japan	(81)561635441	motohiro@mosk.tytlabs.co.jp
Nagel David	George Washington University, Research professor	3273 Rose Glen Court, Falls Church, VA 22042, USA	(1)2029945293 (1)7032418133	nagel@gwu.edu
Popov Vladimir	Research Institute of Applied Mechanics (IPRIM), Moscow Russian Academy of Sciences	10 Tsander st., apt.46 129515, Moscow, Russia	(7)4952574359 (7)9096215192	redluk@mail.ru

Rodionov Boris	Moscow Institute of Physical Engineering	31 Kashirskaya rd. 115409, Moscow, Russia	(7)4953239039	b.rodionov@ru.net
Roussetski Alexei	Lebedev Physical Institute, Russian Academy of Sciences, Senior Researcher	53 Lenin Ave., 119991, Moscow, Russia	(7)4951358718	rusets@x4u.lebedev.ru
Saiz Esperanza	Energy Research SRI, Materials Scientist	333 Ravenswood Ave., Menlo Park, CA, 94025, USA	(1)6508593114	Esperanza.alwarez@sri.com
Samsonenko Nikolai	Moscow Peoples Friendship university, Dept. of Theoretical Physics, Assistant Professor	117198, Moscow, 3 Ordzhonikidze, Moscow Peoples Friendship University	(7)4954344312 (7)4959522644 (7)9166274969	samson@mx.rudn.ru
Sarkisov Valery	SVITEX Co. Fellow-interpreter	123007, Moscow, 80,Khoroshovskoe rd., apt.211	(7)4953150419 (7)9161712712	valery.sarkisov@gmail.com
Savvatimova Irina	FSUE SIA “LUTCH”, Senior Researcher	24 Zheleznodorozhnaya, town of Podolsk, Moscow region, 142116, Russia	(7)9031877960	410492@dialup.podolsk.ru

Schelkunov Gennady	"Gamma", Ltd. Co. town of Fryazino, Moscow region, Senior engineer	Apt. 13, 7"A" Sovyetskaya st., Fryazino, Moscow region, 141195, Russia	(7)9055837022	gammaf@mail.ru
Sergeeva Elena	Russian Research Center "Kurchatov Institute", Manager International Relations	Apt. 228, 12 Rogova str., bld.2, Moscow, 123498, Russia	(7)9470336 (7)9104351341	elena_sergueeva@mail.ru
Shadrin Vladimir	Siberian Chemical Complex, Senior engineer	Apt.59, 33 Pushkin st., Tomsk, 634003, Russia	(7)3822)657343 (7)3823)557835 (7)9069495113	tomitch@nm.ru
Sharkov Victor	"Kurchatov Institute" Branch, Leading Researcher; Spiritual Culture Foundation, Vice president	Apt.52, 13 Shkolnaya st., town of Troitsk, Moscow region, 142190, Russia	(7)9104000782 (7)4967511705	Stones41@ttk.ru
Shestopalov Anatoli	IPKON, Russian Academy of Sciences, Researcher	Apt.16, 3 Vokzalnaya st., town of Podolsk, Moscow region, 142116, Russia	(7)4967631615	sinergo@mail.ru
Shestopalova Tatiana	"ZBSM" Co., town of Podolsk, power engineering engineer	Apt.16, 3 Vokzalnaya st., town of Podolsk, Moscow region, 142116, Russia	(7)4967631615	kadievka@mail.ru
Sinyapkin Dmitri	"Plasma technologies" Co., town of Novocherkask, Director general,	Apt.3, 211 Kavkaz st., town of Novocherkask, Rostov Region, 346430, Russia	(7)8632715596 (7)9185444733	plazmatec@yamdex.ru
Sinyapkin Yuri	Russian Research Institute of Experimental Physics, town of Sarov, Associated Researcher	Apt.57, 11 Nekrasov st., Nizhniy Novgorod Region, town of Sarov, 690183, Russia	(7)8313055346	mailbox@ntc.vniief.ru

Shabanov Gennady	Petersburg Institute of Nuclear Physics, Leading Engineer, Russia	Apt.128, 15 Roschinskaya str., town of Gatchina, Leningradskaya region, 188300, Russia	(7)8137130257 (7)8137119580	discharge@gtn.ru
Sokolovsky Boris	Petersburg Institute of Nuclear Physics, Russian academy of Sciences	Apt.92, 6 Seventh Army str., Gatchina Leningrad rgn., 188350, Russia	(7)8137130257 (7)9213495908	boris@pnpi.spb.ru
Srinivasan Mahadeva	Bhaba Atomic Research Center, Division of Physics Bombay, Associate (retired)	25/15,Rukmani Rd., Kalakshetra Colony, Besant Nagar, Chennai-600090, Tamil Nadu, India	(91)4424900572 (91)9380560672	chino37@gmail.com
Starostin Vladimir	Russian Research Center "Kurchatov Institute" Research scientist	Apt.3 , 28 Moldogulovoy str., bld.3, Moscow, 111086, Russia	(7)4991967616	vastarostin@mail.ru
Takahashi Akito	Osaka University, Dept. of Nuclear Engineering, Emeritus Professor	Shinashiyakami 19-10-606, Suita-shi, Osaka, 565-0804, Japan	(81)668761018	akito@sutv.zaq.ne.jp
Tarasenko Gennadi	University of Aktau city, Kazakhstan	Apt.58, 40 5th Microregion, City of Aktau, 130000, Kazakhstan	(7)3292429167 (7)7014207046	tarasenko-genadi@rambler.ru
Velikodny Vasili	Research Institute of applied Mechanics, Lab Leader	Apt.20, 10 Molodezhnaya st., Town of Dolgoprudny, Moscow Region, Russia	(7)4959461752 (7)4959461753	vvelikodny@mail.ru
Vlasov Alexander	Ryazan State Radiotechnical University, Professor	59/1 Gagarin st., city of Ryazan, 390005, Russia	(7)4912922512	anv@fulcra.ryazan.ru

Vysotskii Vladimir	Kiev National Shevchenko University, Head of Theoretical Radiophysics Dept., Ukraine	64 Vladimirskaya str., Kiev, 01033, Ukraine	(380)444581832	viv@vhome.kiev.ua
Wettin Uwe	LCD-SOLUTION s.a.r.l.	19, rue des Pruniers, F-57150 Creutzwald, France	(33)387827679	wettin@lcd-solution.com
Zilov Tatiana	Omer Energetics Technologies, Researcher	P.O.B. 3026; Omer Industrial Park, Shizaf str. 20/3, Arad, 80700, Israel	(972)86901114 (972)89971106	tanya@energetics.co.il

Author Index

A

Afonichev D.D.- 550
Alexandrov D.- 579
Andreassi V.- 181
Armanet Nicolas - 170

B

Bakumtsev N.J.- 237
Bazhutov Yu.N.- 26, 156, 534, 581, 585
Berkova M.D.- 399, 409
Biagio P. Di - 181
Bertolotti M.- 312
Bityurin V.A.- 127
Biberian Jean-Paul - 170
Botvinovsky V.V.- 757
Booth S.S.- 360
Bychkov D.V.- 76, 86, 94
Branover H.- 325
Bykov A.A.- 399, 409
Bychkov V.L.- 76, 86, 94, 139

C

Cantwell R.F.- 360
Cappuccio G.- 181
Castagna E.- 312, 439
Celani Francesco - 181
Chaudhary Irfan U.- 590
Chernov I.P.- 63
Chubb Scott R.- 607
Chubb Talbot A.- 390
Chung David Y.- 498, 628
Clauzon P.- 41
Collis William - 621

D

Dardik I.- 269, 312, 325
Dash J.- 202, 217, 348, 362
Dobrynetc Yu.V.- 409
Doubkov S.L.- 638, 766

E

El-Boher A.- 325
Eremeev A.V.- 156

F

Falcioni F.- 181
Fauvarque J.F.- 41
Filchenkov M.L.- 709
Fisher John C.- 666
Fontana F.- 181
Forsley Lawrence P.G.- 717
Fukuhara Mikio - 639
Fukutani K.- 476

G

Gamberale L.- 181
Garbelli D.- 181
Gareev F.A.- 361, 653
Gareeva G.F.- 653
Gavrilov S.V.- 48
Godin M.S.- 372
Goncharov A.I.- 661
Goryachev Igor V.- 53, 420, 534, 669
Goryacheva I.N.- 534
Grabowski K.- 312
Greenspan E.- 325

Grevtsov B.S.- 139
Grishin V.G.- 48, 156, 399, 409
Guo J.W.- 309

H

Hagelstein Peter L.- 590
Han Lijun - 665
Hioki Tatsumi – 518
Hora Heinz - 716
Hsieh Thomas K.T.- 628
Hubler G.- 312

I

Ishikawa T.- 476
Ishikawa Y.- 440
Itoh T.- 476
Iwamura Y.- 476

J

Jiang Songsheng – 47
Jiang Xingliu - 665
Jin L.H.- 309

K

Karabut A.B.- 73, 225
Karyaka V.I.- 53
Kasagi J.- 440, 476
Khachaturov B.- 325
Khmelnikov A.I.- 43
Khokhlov N.I.- 156
Kholodov L.I.- 669
Kirkinskii V.A.- 43, 661, 658
Kishida A.- 476
Knies D.- 312
Koldamasov A.I.- 237
Kolesnikov E.B.- 127
Kolesnikov S.A.- 147
Kolotilin B.I.- 147
Kopylov S.V.- 709
Kornilova Alla A.- 295, 477
Koroteev Yu.M.- 63
Koshelev A.P.- 156
Kozima Hideo - 348, 690
Kozlov Yu.V.- 26
Krakov V.- 325
Krivit Steven B.- 530
Krivitsky V.A.- 139, 361
Krivshich A.G.- 74, 75
Krychenko O.V.- 409
Kudryavtzev O.G.- 757
Kuhne Rainer W.- 704
Kuribayashi S.- 476
Kuzmin R.- 460
Kuznetsov V.D.- 718

L

Lalleve G.- 41
Laptev Yu. P.- 709
Leahu G.- 312
Le Buzit G.- 41
Lesin S.- 325
Li Xing Z.- 714
Lindesay James - 498
Lipson Andrei G.- 248, 446, 716
Liu Bin - 714
Luo Nie - 716
Lyakhov B.F.- 446

M

Mancini A.- 181
Manoshkin A.B.- 147
Marchesini M.- 181
Marini P.- 181
Marmigi A.- 181
Martemyanov V.P.- 26
Martynyuk M.M.- 53
Mastromatteo U.- 181
Matsumoto M.- 476
Matsuzaki H.- 476
Mcconnell M. L.- 360
McKubre M.C.H.- 312, 270

Meulenberg A.- 715
Mishinsky G.V.- 718
Mosier-Boss Pamela A.- 717
Motohiro Tomoyoshi - 518
Miley George H.- 248, 548, 716, 717

N

Nagao S.- 324
Nagel David J.- 738, 739
Nakamura M.- 181
Narusawa T.- 476
Nebiki T.- 476
Nikitenko L.K.- 409
Nikitin A.I.- 115
Nikitina T.F.- 115
Nizovtsev V.V.- 139

O

Ogura S.- 476
Okano T.- 476
Olikhov I.M.- 154
Ozaki Masao - 777

P

Panin V.V.- 147
Parkhomov A.G.- 279
Pinaev A.V.- 291
Pletnikov E.V.- 26
Popov Yu. A.- 48
Purchi E.- 181
Popov V.V.- 127, 156, 399, 409

Q

Quercia P.- 181

R

Repchenko O.N.- 756
Righi E.- 181
Rodionov B.U.- 372, 757
Roussetski A.S.- 248, 446
Rumyantsev A.D.- 156
Rychagov E.N.- 409

S

Sabelnikov A.A.- 26
Sakov D.M.- 446
Samovolik V.V.- 661
Samsonenko N.V.- 53, 637, 766, 765
Samuolis I.A.- 127
Sapozhnikov Yu.A.- 156
Sarto F.- 312, 439
Sasasbe Shigeru - 777
Saunin E.I.- 446
Savvatimova I.B.- 295, 372, 505
Savvatimov G.V.- 295
Schelkunov G.P.- 154
Sekiba D.- 476
Senftle Frank – 628
Serov P.- 460
Shabanov G.D.- 74, 75
Shapiro A.- 325
Shen B.J.- 217
Shestopalov A.V.- 767
Shrestha Prajakti Joshi - 716
Sibilia C.- 312, 439
Silkin V.M.- 63
Silver D.S.- 462
Sinha K.P.- 715
Sinyapkin D.Yu.- 153
Sinyapkin Yu.T.- 153
Sokolovsky B.Yu.- 74, 75
Sona P.G.- 181
Spallone A.- 181
Starostin V.A.- 26, 156
Stefano V. Di - 181

T

Takahashi Akito - 554, 569, 793
Takahashi Naoko - 518
Tanzella F.- 269
Tarasenko G.V.- 398
Tarasenkov V.G.- 26
Tashyrev Alexandr B.- 477
Terada Y.- 476
Tian J.- 309
Todarello F.- 181
Tolkunov B.N.- 409
Trenta G.- 181
Tsirlin M.- 325
Tsivadze A.Yu.- 446
Tsuchiya Ken-Ichi - 777
Tsvetkov S.A.- 311
Turbin E.V.- 26
Tyurin Yu.I.- 63

V

Velichko A. M.- 115
Velikodny V.Yu.- 48, 127, 156, 399, 409
Violante V.- 312, 439
Vorotilin V.P.- 409
Vlasov A.N.- 147, 778
Vyrodov V.N.- 26
Voti R. Li - 12
Vysotskii V.I.- 477

W

Wang C.Y.- 309
Wei Qing M.- 714
Wilde M.- 476

Y

Yabuuchi Norio - 793
Yamada H.- 324
Yamashita H.- 476
Yamazak N.- 476
Yonemura H.- 440, 476

Z

Zhang W.S.- 202, 348
Zherebtsov O.M.- 74, 75
Zhidkova I.E.- 653
Zilov T.- 312, 325